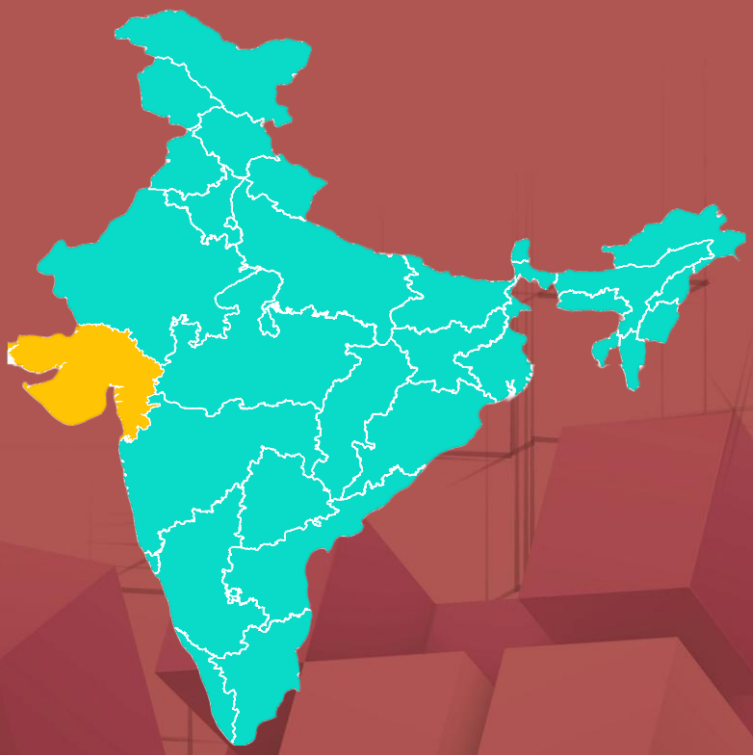

GEOVALE SERVICES

Planetary Science And Technology for Sustainable Development

Final Geological Report (GR) on "Reconnaissance Survey (G-4) for REE Exploration in Bhuj Clay Prospect Block, Kachchh District, Gujarat"

October 2025

Geovale Services Pvt. Ltd.

Earth System Science for Sustainable Development

October 2025

3rd Floor, Anaya Chambers
GN 38/5, Salt Lake, Sec –V,
Kolkata - 700091

WWW.geovale.com

Project Title: Reconnaissance Survey (G-4) for REE Exploration in Bhuj Clay Prospect Block, Kachchh District, Gujarat.

Project Code: 23/385/2023-NMET/251

Project Timeline: 5th October 2023 to 31st October, 2025 (25 Months)

Project Location: Bhuj, Kachchh, Gujarat

Reconnaissance Survey (G-4) for REE Exploration in Bhuj Clay Prospect Block, Kachchh District, Gujarat

October 2025

National Mineral Exploration and Development Trust (NMEDT)
Ministry of Mines

Room No. 325 & 326, Wing-F,
Udyog Bhawan, Rafi Ahmed Kidwai Marg,
Rajpath Area, Central Secretariat
New Delhi-110011

Phone: 011 2307 1006
Email Id: nmet-mines@gov.in

Project executed as NPEA:

Geovale Services Pvt Ltd

3rd Floor, Anaya Chambers,
GN 38/5, Salt Lake, Sec –V,
Kolkata – 700091

Website: http://geovale.com/

Project Coordinators

Joy Gopal Ghosh (Author)
Principal Consultant (Exploration)

Tarak Nath Pal (Author)
Principal Consultant (Exploration)

Biplob Chatterjee (Author)
Director and CEO

Project Leader

Tuasha Majumder (Author)
Senior Project Manager (Exploration)

Project Manager

Sarita Mahato (Author)

Project Manager (Exploration)

Technical Area Experts

Nupur Adhikary
Senior Project Manager (Geology and Geospatial Services)

Chiranjib Banerjee
Senior Project Manager (Geotechnical)

Sujoy Payra (Author)
Senior Project Manager (Geospatial Services)

Krishna Prasad (Author)
Senior Consultant (Geophysics)

Team Members

Dr. Suparna Goswami (Author)
Senior Project Manager (Exploration)

Bhuwan Sharma (Author)
Project Manager (Exploration)

Tanuja Priyadarshini Deo (Author)
Project Geologist (Exploration)

Soumen Roy (Author)
Project Manager (Exploration)

Niharika Mishra (Author)
Project Geologist (Exploration)

Prabir Bhattacharya (Author)
Project Manager (Geospatial Services)

Rabiya Parween (Author)
Project Scientist (Geospatial Services)

Table of Contents

List of Figures:

List of Tables:

List of Annexures:

सारांश

भुज क्ले प्रॉस्पेक्ट ब्लॉक, कच्छ जिला, गुजरात में आरईई (REE) अन्वेषण हेतु टोही सर्वेक्षण (G-4)

<u>परियोजना अवलोकन और महत्वपूर्ण खोजें:</u>

भारत की स्वदेशी दुर्लभ मृदा तत्व (Rare Earth Element - REE) संसाधनों की महत्वपूर्ण आवश्यकता को संबोधित करते हुए, गुजरात के कच्छ जिले के भुज ब्लॉक में एक टोही सर्वेक्षण (G-4) ने परिवर्तनकारी निष्कर्ष प्रदान किए हैं, जिससे पहले से अज्ञात क्षमता का पता चला है और इस क्षेत्र को महत्वपूर्ण खनिजों के लिए एक महत्वपूर्ण नए मोर्चे के रूप में स्थापित किया गया है। राष्ट्रीय खनिज अन्वेषण और विकास ट्रस्ट (NMEDT), खान मंत्रालय (परियोजना कोड: 23/385/2023-NMET/251) के तत्वावधान में जियोवेल सर्विसेज प्राइवेट लिमिटेड द्वारा नवंबर 2023 और अक्टूबर 2025 के बीच निष्पादित, इस परियोजना ने सफलतापूर्वक **दो अलग-अलग, उच्च-संभावित, यथास्थान (in-situ) REE खनिज प्रणालियों** की पहचान की है, जिससे कच्छ बेसिन की भूवैज्ञानिक समझ मौलिक रूप से बदल गई है और लक्षित संसाधन मूल्यांकन का मार्ग प्रशस्त हुआ है।

- **अन्वेषण रणनीति में निर्णायक बदलाव: प्रारंभिक मान्यताओं से परे वास्तविक क्षमता को उजागर करना:**

यह परियोजना शुरू में राष्ट्रीय भू-रासायनिक मानचित्रण कार्यक्रम (NGCMP) द्वारा स्ट्रीम तलछट में रिपोर्ट की गई अत्यधिक विषम REE सांद्रता (TREEY>2%) के आधार पर परिकल्पित की गई थी। प्रारंभिक परिकल्पना एक सतही, आयन-अधिशोषित क्ले-होस्टेड REE मॉडल के पक्ष में थी। हालाँकि, चरण 2 के दौरान कठोर फील्ड सत्यापन और अभिविन्यास, जिसमें बहु-अंश स्ट्रीम तलछट विश्लेषण (-125 µm और -40 µm अंशों ने क्रमशः 364 पीपीएम और 368 पीपीएम का TREEY औसत दिया, जो NGCMP के उच्च मानों को दोहराने में विफल रहा) और भारी खनिज अध्ययन शामिल थे, ने इस मॉडल को निर्णायक रूप से *अमान्य* कर दिया। इसके बजाय, जांच से पता चला कि REE असतत प्राथमिक खनिज चरणों के भीतर होस्ट किए जाते हैं। इस महत्वपूर्ण खोज के लिए एक रणनीतिक धुरी की आवश्यकता थी, जिसे खनिज प्रणाली विश्लेषण (Mineral Systems Analysis - MSA) ढांचे द्वारा निर्देशित किया गया, जिससे दो अलग-अलग, यथास्थान खनिज प्रणालियों की ऐतिहासिक खोज हुई।

- **दो उच्च-संभावित खनिज प्रणालियों की खोज:**

I. खनिज प्रणाली I: कटरोल स्तरित ज्वालामुखीय-होस्टेड REE प्रणाली:

- **भूवैज्ञानिक सेटिंग:** उत्तर जुरासिक कटरोल फॉर्मेशन के भीतर अनावरण किया गया, इस प्रणाली में पार्श्व रूप से व्यापक (सैकड़ों किलोमीटर) फॉस्फेटिक-लौहयुक्त टफाइट परतें हैं, जो शेल-प्रधान हेटेरोलिथिक अनुक्रमों के भीतर स्थित हैं, जो प्राचीन पनडुब्बी ज्वालामुखी गतिविधि का एक फिंगरप्रिंट है।

- **खनिजीकरण शैली:** निक्षेपण के दौरान पनडुब्बी फेल्सिक ज्वालामुखी और फॉस्फोजेनेसिस से जुड़ा सिन्जेनेटिक, स्तरित खनिजीकरण। REE मुख्य रूप से महीन-कण वाले फ्लोरापैटाइट और मोनाज़ाइट में होस्ट किए जाते हैं।
- **भू-रासायनिक हस्ताक्षर:** महत्वपूर्ण REE संवर्धन, विशेष रूप से भारी दुर्लभ मृदा तत्व (HREE) की विशेषता है। टफाइट क्षितिजों से आधारशैल नमूनों में TREEY मान 164 पीपीएम से 1721 पीपीएम (औसत ~400 पीपीएम) तक प्राप्त हुए, जो P_2O_5 (12.5 wt% तक) के साथ दृढ़ता से सहसंबद्ध हैं। स्काउट ड्रिलिंग (BH01, BH02) ने कोर नमूनों में ~549 पीपीएम (BH01) और ~995 पीपीएम (BH02) तक TREEY चोटियों के साथ कई टफाइट अन्तर्विभाजनों की पुष्टि की।
- **रणनीतिक क्षमता:** यह खोज एक संभावित बड़े-टनभार, मध्यम-श्रेणी HREE संसाधन की ओर इशारा करती है, जो विश्व स्तर पर महत्वपूर्ण निक्षेपों जैसे राउंड टॉप (टेक्सास) और डब्बो (NSW) के समानांतर है। HREEs का उच्च अनुपात भारत की तकनीकी और रक्षा स्वतंत्रता के लिए इसके रणनीतिक महत्व को बढ़ाता है।

II. खनिज प्रणाली II: भुज फॉर्मेशन IOCG-शैली हाइड्रोथर्मल प्रणाली:

- **भूवैज्ञानिक सेटिंग:** छोटी आयु के प्रारंभिक क्रेटेशियस भुज फॉर्मेशन के भीतर होस्ट किया गया, यह प्रणाली संरचनात्मक रूप से नियंत्रित, एपिजेनेटिक हाइड्रोथर्मल गतिविधि द्वारा परिभाषित है। कटरोल हिल फॉल्ट (KHF) और मीडियन हाई ज़ोन से जुड़े प्रमुख फॉल्ट गलियारों के साथ बलुआ पत्थरों में तीव्र लौह-ऑक्साइड परिवर्तन (लौहीकरण, मेटासोमैटिज्म) और ब्रैसिएशन व्याप्त है।
- **खनिजीकरण शैली:** एक शक्तिशाली आयरन-ऑक्साइड-कॉपर-गोल्ड (IOCG) प्रणाली के क्लासिक भूवैज्ञानिक, खनिजवैज्ञानिक और भू-रासायनिक पहचान प्रदर्शित करता है - एक शैली जो विश्व स्तर पर विशाल पॉलीमेटेलिक निक्षेपों की मेजबानी के लिए जानी जाती है।
- **समृद्ध पॉलीमेटेलिक हस्ताक्षर:** व्यापक हेमाटाइट-मैग्नेटाइट परिवर्तन, हाइड्रोथर्मल ब्रैसिया, और धातुओं के एक समृद्ध मिश्रण की विशेषता है जिसमें Fe, Ti, P, REE, ± Cu, Co, Ni, Zn, Pb, Sn, Au, Ag शामिल हैं। पहचाने गए प्रमुख खनिजों में हेमाटाइट, लो-Ti मैग्नेटाइट, एपेटाइट, मोनाज़ाइट, ज़ेनोटाइम, ज़िरकॉन, पाइराइट, चाल्कोपाइराइट, बोर्नाइट, स्फैलेराइट और यहां तक कि देशी सोने के निशान भी शामिल हैं। आधारशैल में TREEY 744 पीपीएम तक दिखाता है, जबकि भारी खनिज सांद्रण नाटकीय रूप से इस हस्ताक्षर को समृद्ध करते हैं, जो 3.4% TREEY तक पहुंचते हैं। ड्रिलिंग ने पॉलीमेटेलिक संवर्धन से संबंधित महत्वपूर्ण परिवर्तन क्षेत्रों की पुष्टि की।
- **भूभौतिकीय पुष्टि:** लक्षित वर्टिकल इलेक्ट्रिकल साउंडिंग (VES) सर्वेक्षणों ने विशिष्ट निम्न-प्रतिरोधकता विसंगतियों (10-80 Ω·m) का मानचित्रण किया - जिन्हें संभावित ब्रैसिया पाइप और परिवर्तन क्षेत्र के रूप में व्याख्यायित किया गया है - जो आमतौर पर प्रतिरोधी भुज

बलुआ पत्थर (>200 Ω·m) को काटते हैं, संरचनात्मक नियंत्रण और प्रणाली के उपसतह विस्तार की पुष्टि करते हैं।

- **उच्च-प्रभाव क्षमता:** संभावित रूप से उच्च-श्रेणी, संरचनात्मक रूप से केंद्रित पॉलीमेटेलिक खनिजीकरण के लिए एक सम्मोहक लक्ष्य का प्रतिनिधित्व करता है। ओलंपिक डैम (ऑस्ट्रेलिया) या पी रिज (USA) जैसे दिग्गजों के साथ तुलना करते हुए, यह प्रणाली पहचानी गई फीडर संरचनाओं के साथ गहराई में एक बड़ी खोज की क्षमता का संकेत देती है।

➢ परिवर्तनकारी महत्व और राष्ट्रीय प्रभाव:

G-4 कार्यक्रम ने भुज क्षेत्र को एक दिलचस्प भू-रासायनिक विसंगति से सफलतापूर्वक एक मान्य अन्वेषण जिले में परिवर्तित कर दिया है जो दो अलग-अलग और महत्वपूर्ण खनिज प्रणालियों की मेजबानी करता है। यह कच्छ बेसिन को पश्चिमी भारत में REE और संभावित IOCG-संबंधित महत्वपूर्ण खनिजों के लिए एक नए, पहले से अज्ञात मेटालोजेनिक प्रांत के रूप में स्थापित करता है। यह खोज भारत की रणनीतिक संसाधन आत्मनिर्भरता की खोज के साथ गहराई से प्रतिध्वनित होती है।

➢ सिफारिशें और आगे की राह:

G-4 के सम्मोहक परिणामों के आधार पर, सामान्य अन्वेषण (G-3) चरण में तत्काल उन्नति की दृढ़ता से सिफारिश की जाती है। अन्वेषण G-4 क्षेत्र के भीतर चित्रित नौ प्राथमिकता वाले प्रॉस्पेक्ट ब्लॉकों (कटरोल के लिए K1-K3; भुज संरचनाओं के लिए B1-B6) पर केंद्रित होना चाहिए।

ब्लॉक आईडी	अन्वेषण डोमेन	क्षेत्र (किमी²)	चयन का औचित्य
K1–K3	MSA-I (स्तरित)	~11–17 किमी²	सुसंगत REE संवर्धन के साथ स्तरित लौहयुक्त-फॉस्फेटिक-टफिटिक संलक्षणी
B1–B6	MSA-II (IOCG-प्रकार)	~6–24 किमी²	Zn-Pb-Cu-Cr-Fe-Ti-REE साहचर्य और संरचनात्मक सुसंगतता के साथ हाइड्रोथर्मली परिवर्तित मेटासोमेटाइज्ड लौहयुक्त बलुआ पत्थर और ब्रैसिया

अनुशंसित अन्वेषण रणनीति में शामिल हैं:

I. **खनिज प्रणाली I (कटरोल फॉर्मेशन) के लिए:** HREE-धारक टफाइट क्षितिजों की ज्यामिति, श्रेणी परिवर्तनशीलता और स्ट्राइक निरंतरता को कठोरता से परिभाषित करने के लिए व्यवस्थित ट्रेंचिंग और उथले ग्रिड ड्रिलिंग (~100 मी स्पेसिंग) शुरू करें। समवर्ती रूप से, महत्वपूर्ण प्रारंभिक धातुकर्म अध्ययनों के लिए थोक नमूनाकरण शुरू करें जो सज्जीकरण क्षमता और निक्षालन पर केंद्रित हों।

II. **खनिज प्रणाली II (भुज फॉर्मेशन) के लिए:** IOCG कोर की विशेषता वाले उपसतह घनत्व और चुंबकीय हस्ताक्षरों का सटीक मानचित्रण करने के लिए विस्तृत जमीनी भूभौतिकीय सर्वेक्षण (गुरुत्वाकर्षण, चुंबकत्व, संभावित आईपी) निष्पादित करें। इसके बाद लक्षित, गहरे हीरे की ड्रिलिंग (500-800 मी) करें जिसका उद्देश्य उच्च-प्राथमिकता वाले भूभौतिकीय विसंगतियों और संरचनात्मक लक्ष्यों को काटना है, संभावित फीडर क्षेत्रों और उच्च-श्रेणी पॉलीमेटेलिक खनिजीकरण का परीक्षण करना है।

भुज REE अन्वेषण परियोजना सफल टोही का एक प्रमाण है, जो क्षेत्र की खनिज संपदा की समझ को मौलिक रूप से आगे बढ़ाती है। एक स्तरित REE प्रणाली और एक हाइड्रोथर्मल IOCG-शैली प्रणाली दोनों की खोज और प्रारंभिक सत्यापन संसाधन चित्रण के उद्देश्य से लक्षित G-3 अन्वेषण के लिए एक मजबूत आधार प्रदान करते हैं। यह परियोजना दर्शाती है कि कैसे एक लचीला, विज्ञान-आधारित खनिज प्रणाली दृष्टिकोण सीमांत भूवैज्ञानिक क्षेत्रों में महत्वपूर्ण खनिज क्षमता को अनलॉक कर सकता है, जो भारत के भविष्य के लिए महत्वपूर्ण संसाधनों का योगदान देता है।

Summary

Addressing India's critical need for indigenous Rare Earth Element (REE) resources, a reconnaissance survey (G-4) in the Bhuj block of Kachchh district, Gujarat, has delivered transformative findings, revealing previously unrecognized potential and establishing the region as a significant new frontier for critical minerals. Executed by Geovale Services Pvt. Ltd. between November 2023 and October 2025 under the aegis of the National Mineral Exploration and Development Trust (NMEDT), Ministry of Mines (Project Code: 23/385/2023-NMET/251), this project has successfully identified two distinct, high-potential, in-situ REE mineral systems, fundamentally reshaping the geological understanding of the Kachchh Basin and paving the way for targeted resource evaluation.

- **Pivotal Shift in Exploration Strategy: Uncovering True Potential Beyond Initial Assumptions**

The project was initially conceived based on highly anomalous REE concentrations (TREEY>2%) reported in stream sediments by the National Geochemical Mapping Program (NGCMP). The preliminary hypothesis favoured a surficial, ion-adsorbed clay-hosted REE model. However, rigorous field validation and orientation during Stage 2, involving multi-fraction stream sediment analysis (-125 µm and -40 µm fractions yielded TREEY averages of 364 ppm and 368 ppm respectively, failing to replicate NGCMP highs) and heavy mineral studies, conclusively invalidated this model. Instead, the investigation revealed that REEs are hosted within discrete primary mineral phases. This critical finding necessitated a strategic pivot, guided by a Mineral Systems Analysis (MSA) framework, leading to the landmark discovery of the two distinct, in-situ mineral systems.

- **Discovery of Two High-Potential Mineral Systems:**

I. **Mineral System I: Katrol Stratiform Volcaniclastic-Hosted REE System:**

- **Geological Setting:** Unveiled within the Late Jurassic Katrol Formation, this system features repeated occurrence of laterally extensive (hundreds of kilometers) phosphatic-ferruginous tuffite layers, nestled within shale-dominated heterolithic sequences, a fingerprint of ancient submarine volcanic activity.
- **Mineralization Style:** Syngenetic, stratiform mineralization linked to submarine felsic volcanism and phosphogenesis during deposition. REEs are primarily hosted in fine-grained fluorapatite and monazite.
- **Geochemical Signature:** Characterized by significant REE enrichment, particularly Heavy Rare Earth Elements (HREE). Bedrock samples from tuffite horizons yielded TREEY values ranging from 164 ppm to 1721 ppm (average ~400

ppm), strongly correlating with P_2O_5 (up to 12.5 wt%). Scout drilling (BH01, BH02) confirmed multiple tuffite intersections with TREEY peaks up to ~549 ppm (BH01) and ~995 ppm (BH02) in core samples.

- **Strategic Potential:** This discovery points towards a potential large-tonnage, moderate-grade HREE resource, drawing parallels to globally significant deposits like Round Top (Texas) and Dubbo (NSW). The high proportion of HREEs elevates its strategic importance for India's technological and defence independence.

II. Mineral System II: Bhuj Formation IOCG-Style Hydrothermal System:

- **Geological Setting:** Hosted within the younger Early Cretaceous Bhuj Formation, this system is defined by structurally controlled, epigenetic hydrothermal activity. Intense iron-oxide alteration (ferruginization, metasomatism) and brecciation grip the sandstones along major fault corridors tied to the Katrol Hill Fault (KHF) and the Median High zone.
- **Mineralization Style:** Displaying the classic geological, mineralogical, and geochemical hallmarks of a powerful Iron-Oxide-Copper-Gold (IOCG) system – a style known for hosting giant polymetallic deposits globally.
- **Rich Polymetallic Signature:** Characterized by pervasive hematite-magnetite alteration, hydrothermal breccias, and a rich cocktail of metals including Fe, Ti, P, REE, ± Cu, Co, Ni, Zn, Pb, Sn, Au, Ag. Key minerals identified include hematite, low-Ti magnetite, apatite, monazite, xenotime, zircon, pyrite, chalcopyrite, bornite, sphalerite, and even traces of native gold. Bedrock shows TREEY up to 744 ppm, while heavy mineral concentrates dramatically enrich this signature, reaching up to 3.4% TREEY. Drilling confirmed significant alteration zones correlated with polymetallic enrichment.
- **Geophysical Confirmation:** Targeted Vertical Electrical Sounding (VES) surveys mapped distinct low-resistivity anomalies (10-80 Ω·m) – interpreted as potential breccia pipes and alteration zones – cutting through the typically resistive Bhuj sandstone (>200 Ω·m), confirming the structural control and subsurface extent of the system.
- **High-Impact Potential:** Represents a compelling target for potentially higher-grade, structurally focused polymetallic mineralization. Drawing comparisons with giants like Olympic Dam (Australia) or Pea Ridge (USA), this system signals the potential for a major discovery at depth along the identified feeder structures.

➢ **Transformative Significance and National Impact:**

The G-4 program has successfully transitioned the Bhuj area from an intriguing geochemical anomaly to a validated exploration district hosting two distinct and significant mineral systems. It establishes the Kachchh Basin as a new, previously unrecognized metallogenic province for REE and potentially IOCG-related critical minerals in western India. The discovery resonates deeply with India's quest for strategic resource self-sufficiency.

➢ **Recommendations and Path Forward:**

Based on the compelling G-4 results, immediate advancement to a General Exploration (G-3) stage is strongly recommended. Exploration should focus on nine prioritized prospect blocks (K1-K3 for Katrol; B1-B6 for Bhuj formations) delineated within the G-4 area.

Block ID	Exploration Domain	Area (km²)	Rationale for Selection
K1–K3	MSA-I (Stratiform)	~11–17km²	Layered ferruginous-phosphatic-tuffitic facies with consistent REE enrichment
B1–B6	MSA-II (IOCG-type)	~6–24 km²	Hydrothermally altered metasomatized ferruginized sandstone and breccia with Zn-Pb-Cu-Cr-Fe-Ti-REE association and structural coherence

The recommended exploration strategy includes:

I. **For Mineral System I (Katrol formation):** Launch systematic trenching and shallow grid drilling (~100m spacing) to rigorously define the geometry, grade variability, and strike continuity of the HREE-bearing tuffite horizons. Concurrently, initiate bulk sampling for crucial preliminary metallurgical studies focused on beneficiation potential and leachability.

II. **For Mineral System II (Bhuj Formation):** Execute detailed ground geophysical surveys (gravity, magnetics, potentially IP) to precisely map subsurface density and magnetic signatures characteristic of IOCG cores. Follow with targeted, deeper diamond drilling (500-800m) aimed at intersecting the high-priority geophysical anomalies and structural targets, testing for potential feeder zones and higher-grade polymetallic mineralization.

The Bhuj REE exploration project stands as a testament to successful reconnaissance, fundamentally advancing the understanding of the region's mineral wealth. The discovery and initial validation of both a stratiform REE system and a hydrothermal IOCG-style system provide a robust foundation for targeted G-3 exploration aimed at resource delineation. This

project exemplifies how a flexible, science-led Mineral Systems approach can unlock significant critical mineral potential in frontier geological terrains, contributing vital resources for India's future.

Chapter 1

Introduction

1. Introduction

1.1 Introduction:

The **"Reconnaissance Survey (G4) for Rare Earth Element (REE) Exploration in the Bhuj Clay Prospect Block, Kachchh District, Gujarat"** represents a focused effort under the National Mineral Exploration and Development Trust (NMEDT), Ministry of Mines, Government of India to evaluate the potential for indigenous REE resources within the Mesozoic sedimentary successions of western India. The project was executed by *M/S Geovale Services Private Limited*, a QCI-NABET accredited National Private Exploration Agency (NPEA). This integrated greenfield exploration initiative forms a critical component of the NMEDT funded national program aimed at identifying and assessing India's strategic and critical mineral resources, in alignment with the objectives of the National Mineral Policy (2019) and the Critical Minerals Strategy (2023).

The Bhuj project represents a first-of-its-kind attempt in India to evaluate strata-bound and hydrothermal REE systems within the Mesozoic succession of the Kachchh Basin. Geologically, the basin occupies a pivotal geodynamic position along the northwestern margin of the Indian Shield, forming a pericratonic rift basin that evolved under the influence of Jurassic-Cretaceous extensional tectonics associated with the breakup of Gondwana and the opening of the Tethys *(Biswas 2005)*. The sedimentary succession of the basin offers a unique opportunity to understand REE mineralization associated with rift-related magmatism and sedimentary processes.

The present report documents the multidisciplinary activities and outcomes of the reconnaissance stage exploration conducted over a 252 sq. km area between October 2023 to October 2025. It synthesizes remote sensing, geological, geochemical, geophysical, petrographic, mineralogical and drilling datasets collected during the survey and interprets them within the Mineral Systems Analysis (MSA) framework. This approach seeks to delineate the geological processes responsible for REE concentration, source fertility, transport pathways, depositional traps, and post-depositional preservation, thus establishing the scientific basis for higher-order (G3) exploration.

The Bhuj Clay Prospect, therefore, serves not merely as a reconnaissance-level investigation but as a strategic test case for integrating modern exploration philosophy with national resource priorities. The successful delineation of an economically viable REE-bearing system within this basin would represent a landmark discovery in India's Mesozoic geological record, contributing substantially to the nation's critical mineral security. Beyond its immediate scientific and economic implications, the project also embodies India's broader aspiration toward self-reliance in critical minerals, providing a conceptual and methodological template for evaluating analogous rift-basin settings. Moreover, the recognition of potentially beneficiable, and environmentally sustainable REE-bearing horizons positions the Bhuj

investigation as a forward-looking step in India's transition toward green technology and resource sustainability.

1.2 Geovale Philosophy of Greenfield Exploration:

Geovale Services Pvt. Ltd. follows an integrated Mineral Systems Analysis (MSA) framework for greenfield exploration, wherein mineralization is interpreted as the culmination of predictable geological processes operating across a continuum of scales, from lithospheric architecture to deposit-scale fluid-rock interactions. This approach recognizes that ore deposits are not isolated anomalies, but rather the manifestation of broader, deeper crustal-scale processes that operate coherently within specific geodynamic environments. These processes collectively integrate a favourable source, fluid, pathway, and trap to form an ore deposit (*Wyborn et al., 1994; Huston et al., 2016*) (*Fig. 1.1*).

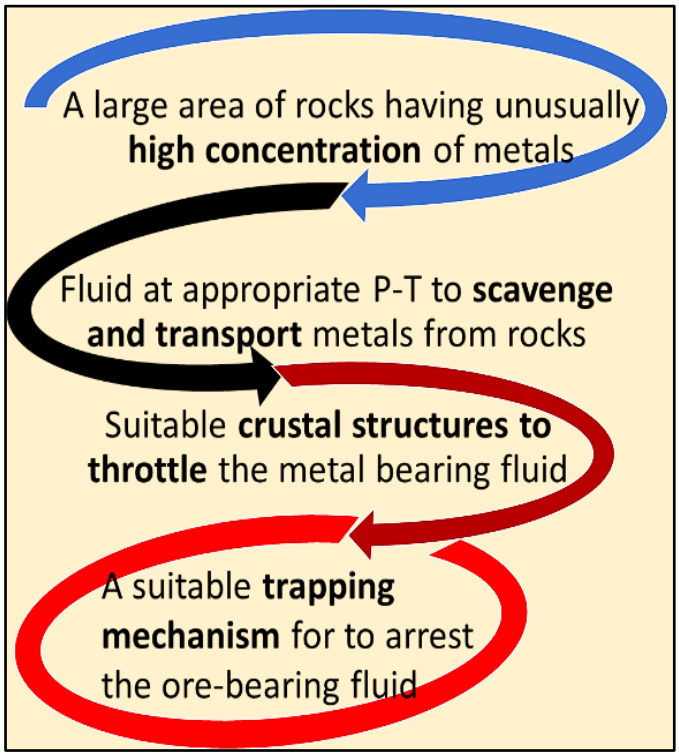

Fig.1. 1 Conceptual framework of a mineral system showing the four essential components required for ore formation—(i) a metal-enriched source, (ii) a fluid capable of scavenging and transporting metals at suitable pressure–temperature conditions, (iii) crustal structures that act as pathways and regulate fluid flow, and (iv) a trapping mechanism that focuses and precipitates the ore-bearing fluid. The convergence of these processes in space and time leads to the development of an economic mineral deposit (after Wyborn et al., 1994; Huston et al., 2016).

Mapping these four parameters, even within terrains where mineralization has not yet been established, allows assessment of the fertility and mineral potential of a region. The MSA

framework therefore provides a predictive, process-based exploration philosophy that transcends conventional empirical targeting by focusing on why and where mineralization should occur, rather than where it has already been discovered.

In the Bhuj project, this philosophy was implemented through the integration of basin evolution, structural architecture, magmatic and hydrothermal processes, and sedimentary dynamics to understand the geological controls on metal concentration and preservation. The exploration program, designed within the MSA framework, delineated two distinct but complementary mineral systems within the Kachchh Basin:

I. A stratiform volcaniclastic-phosphatic REE system within the Katrol Formation, representing a syn-volcanic depositional environment; and
II. A hydrothermal IOCG-style system along structural entrapments, particularly near the Katrol Hill Fault Zone, where fault conduits facilitated iron-oxide rich hydrothermal fluid flow, leading to secondary enrichment of different critical metals.

Together, these systems define the exploration framework for the Bhuj Clay Prospect, demonstrating how an MSA-driven approach integrates multi-scale process understanding with field-based evidence to identify and prioritize prospective domains for mineralization in western India.

1.3 Background of the Project:

The Kachchh Basin is a pericratonic rift basin situated along the western continental margin of the Indian Shield and represents one of the most complete Mesozoic sedimentary archives of the Indian subcontinent. The basin evolved through multiple phases of rifting and marine transgression–regression cycles during the Middle Jurassic to Early Cretaceous, leading to the accumulation of thick siliciclastic successions interlayered with carbonate and shale units. Subsequent tectonic inversion and uplift during the Late Cretaceous-Paleogene were accompanied by extensive emplacement of Deccan Trap basaltic flows, which locally cap the Mesozoic strata (*Biswas, 1987; 2016*).

Stratigraphically, the basin comprises the Katrol, Bhuj, and Chari formations, representing depositional environments that range from sub-littoral to deltaic settings. The carbonaceous shale member of the Katrol Formation locally hosts phosphorite nodules near Motawada, Virani, and Nabhoi, where P_2O_5 concentrations reach up to 23 % (*Shukla, 1974*). The close spatial association of these phosphatic horizons with the rift sediments provides a favourable condition for REE accumulation.

The palaeo-slope of the basin was directed south-westwards, with the principal sediment supply derived from the north and northeast. The provenance of the Mesozoic succession of the basin, included Precambrian crystalline complexes exposed in the Meruda

Takkar region of the Great Rann of Kachchh and the Nagar Parker Hills across the Indo-Pak border, supplemented by detritus from the Radhanpur-Barmer Arch and the Eastern Highlands of Gujarat. These source terrains, influenced by extensional tectonics and widespread alkaline magmatism, could have contributed REE rich detritus to the basin. Such provenance settings, characterized by the presence of highly evolved granitic and alkaline complexes, are globally recognized as fertile source regions for sediment-hosted REE mineralization.

Several studies (*Biswas 1987; Kshirsagar et al., 2011; Paul et al., 2008*) have documented the presence of numerous evolved pre-Deccan Trap (~68 Ma and older) alkaline intrusions in the Bhuj–Nakhatrana sector, emplaced along rift-related faults and fracture corridors (*Guha et al., 2005; Kshirsagar et al., 2011*). Geophysical investigations further suggest the existence of additional buried intrusions within structural lows beneath the younger sediment cover. These intrusives, compositionally ranging from alkali basalts with mantle xenoliths to differentiated gabbro-syenite-nepheline assemblages, are interpreted to have originated from a metasomatized sub-crustal lithospheric mantle (SCLM) at depths of ~40 km. Their emplacement, synchronous with extensional tectonism, represents an important metallogenic phase that could introduce mantle-derived volatiles and metal fluxes into the crust. These alkaline systems are potential sources of REE, Nb, Ta, Zr, P, Au, V, Cu, and PGE, and in some cases, gemstones.

Overall, the interplay of rift-related tectonism, mantle-derived alkaline magmatism, and sedimentary reworking in the Kachchh Basin has created a geodynamically favourable environment for the development of REE- and rare-metal-bearing mineral systems. This metallogenic context provides the conceptual foundation for the systematic exploration of the Bhuj sector under the present NMEDT-funded program, aiming to evaluate its potential for critical mineral resources within the Mesozoic succession.

1.4 Details of the Project:

The following table summarizes key details of the project, including geographical coverage, administrative jurisdictions, target commodities, and project timeline:

Table. 1. 1 Details of the Bhuj exploration block.

1	**Project Name:**	**Reconnaissance Survey (G-4) for REE Exploration in Bhuj Clay Prospect Block, Kachchh District, Gujarat**
2	**Project Code:**	**23/385/2023-NMET/251**
3	**Commodity**	**Rare Earth Elements (REEs)**
4	**Tehsil**	**Bhuj**

5	District	Kachchh		
6	Nearby villages	Bhuj, Sukhpar, Kukuma, Naranpar, Surajpur, Reha Nana, etc		
6	State	Gujarat		
7	Project area	252 sq. km		
8	Survey of India Toposheet No.	41E/12		
9	Date of commencement of the project	November, 2023		
10	Boundary coordinates of the project area	Boundary Coordinates	Latitude	Longitude
		A	23.2323	69.5006
		B	23.2313	69.7514
		C	23.1429	69.7510
		D	23.1436	69.4997

1.5 Investigating Agency:

The key information about the investigating agency is provided in the table below:

Table. 1. 2 Details of the investigating agency of the Bhuj exploration program.

Name:	Geovale Services Private Limited
Postal address:	3rd Floor, Anaya Chambers, Block GN, Plot 38/5, Sector V, Salt Lake, Kolkata- 700091, West Bengal, India
Telephone Number (Office):	033 4601 2887
Mobile No.:	+91 9007706145
Telephone Number (Residence):	+91 9330825226
E-Mail address:	biplob.chatterjee@geovale.com
Date of accreditation granted by QCI-NABET:	23 March, 2022
Date of expiry of accreditation:	22 March, 2025
Category of the NPEA	Category A

1.6 Objectives of Investigation:

The Reconnaissance Survey (G4) for Rare Earth Element (REE) Exploration in the Bhuj Clay Prospect Block, Kachchh District, Gujarat was initially conceived to investigate the exceptionally high REE concentrations reported from stream sediments of the region under the National Geochemical Mapping Program (NGCMP) and to evaluate their possible causes, particularly the potential for ion-adsorbed clay hosted REE enrichment. The project, therefore, aimed at establishing whether the elevated REE values represented secondary surface concentration within the fine-grained regolith and sedimentary horizons, or were derived from primary lithological sources within the underlying Mesozoic successions. As the investigation progressed, geological, mineralogical, and geochemical datasets collectively indicated that the observed REE enrichment was governed by two distinct but genetically related mineral system frameworks: (i) a stratiform REE concentration system developed within the Mesozoic sedimentary–volcaniclastic successions, and (ii) a hydrothermal, IOCG-style system associated with structural conduits and alteration zones. Consequently, the scope of the project was expanded from the initial reconnaissance of surface anomalies to a broader evaluation of REE and polymetallic mineralization potential within the basin.

The revised objectives, therefore, were directed toward establishing preliminary evidence of REE fertility within the basin, identifying prospective stratigraphic and structural domains, and delineating potential target zones for advanced stage (G3) of exploration. The study sought to reconstruct the stratigraphic framework and mineral system architecture of the Bhuj sector, evaluate the processes responsible for REE concentration, and understand the role of regional tectonics, including the Katrol Hill Fault Zone and the Median High, in influencing fluid migration and mineralization.

To summarize the primary objectives of the study are as follows:

I. Delineate potential REE–rare-metal (RM) targets within the Bhuj Prospect Block based on integrated geological, geochemical, and structural analyses.
II. Characterize the mineralogical and geochemical attributes of the REE-bearing mineral phase/s and their host lithologies and define their compositional variability.
III. Evaluate the potential for hydrothermal, IOCG-style mineralization, and its spatial relationship with the stratiform REE system (if any).
IV. Delineate probable fluid pathways associated with the hydrothermal alteration and mineralization.

In essence, the investigation sought to bridge regional-scale geoscientific indicators with deposit-scale understanding, thereby establishing a robust scientific foundation for evaluating REE potential in the Kachchh Basin and guiding subsequent stages of exploration.

1.7 Project Workflow

This report details the Reconnaissance Survey (G4) for Rare Earth Element (REE) Exploration conducted in the Bhuj Clay Prospect Block, Kachchh District, Gujarat, under the aegis of the National Mineral Exploration and Development Trust (NMEDT). Executed by Geovale Services Pvt. Ltd. between November 2023 and October 2025, this project aimed to assess the REE potential within the Mesozoic sedimentary successions of the region, initially prompted by anomalous REE concentrations identified during the National Geochemical Mapping Program (NGCM).

The exploration was structured in four distinct stages, following an integrated Mineral Systems Analysis (MSA) approach.

I. **Stage 1 (Pre-field and Desktop Studies)** involved reviewing regional geology, NGCM data, and remote sensing information to generate a predictive fertility analysis for the Bhuj Block (detailed in Chapter 3).

II. **Stage 2 (Validation and Re-orientation)** focused on validating the initial NGCM data through stream sediment and heavy mineral surveys, alongside regional litho-stratigraphic reconnaissance (Chapter 4). This stage led to a crucial outcome: the rejection of the initial premise of ion-adsorbed clay potential and the identification of two new, discrete mineral systems operating within the block.

III. **Stage 3 (Ground Surveys)** comprised detailed geological mapping, geochemical sampling, and geophysical surveys to identify fertile areas and specific mineralized targets corresponding to the two newly identified mineral systems (Chapters 4 and 5).

IV. **Finally, Stage 4 (Target Testing)** involved limited pitting and scout drilling primarily targeting the Katrol Formation (Mineral System 1) and prospective zones within the Bhuj Formation associated with Fe-metasomatism/hydrothermal activity (Mineral System 2). This testing phase successfully established the regional prospectivity for both mineral systems and identified specific targets within both the Katrol and Bhuj formations warranting further, more detailed exploration (G3 stage), as discussed in Chapter 6.

This phased workflow allowed for a systematic evaluation, starting from regional assessment and progressively focusing on specific targets, leading to the confirmation of REE potential linked to both stratiform volcaniclastic-phosphatic and hydrothermal IOCG-style systems within the Bhuj Block.

1.8 Nature and quantum of work approved vs achievement:

The Reconnaissance Survey (G4) for REE Exploration in the Bhuj Clay Prospect Block was executed in accordance with the NMEDT-approved proposal, ensuring systematic and complete coverage of the sanctioned scope of work. The following table presents a comparative summary of the approved scope of work versus achieved quantum of work during the project execution.

Sl. No.	Nature of work	Approved Quantum	Achieved Quantum
1	Geological mapping/sampling	252 sq. km	252 sq. km
2	Pitting (up to 2m depth)	200 cubic meters	215.35cubic meters
3	Laboratory Studies (Surface Samples)		
	a. Heavy Liquid Separation	20 samples	32 samples
	b. Gravity and Magnetic Separation	20 samples	20 samples
	c. XRF assay:	40 samples	212 samples
	d. ICPMS assay:	330 samples	330 samples
	e. Check samples for XRF and ICPMS	4+33 samples	4+33 samples
	f. XRD	40 samples	40 samples
4	Petrological Studies		
	a. Thin section preparation	10 samples	62 samples
	b. Microscopic study	10 samples	62 samples
	c. SEM-EDX	30 hours	12 hours
	d. EPMA	15 hours	15 hours
5	Geophysical Survey		
	Resistivity Profiling (Station interval 200m.)	40 line-km	42 line-km
6	Core Drilling	600 m	603.5m (8 BH)

Sl. No.	Nature of work	Approved Quantum	Achieved Quantum
7	Laboratory Studies (Sub-Surface Samples)		
	a. XRF assay:	100 samples	100 samples
	b. ICPMS assay:	300 samples	302 samples
	c. Check samples for XRF	10 samples	10 samples
8	Geological Report	1	1

1.9 Personnel Involved:

The Reconnaissance Survey (G4) for REE Exploration in Bhuj Clay Prospect Block was executed through the coordinated efforts of a multidisciplinary team of geoscientists, technical professionals, and field support staff of M/S Geovale Services Pvt. Ltd. The project was implemented under the direct supervision of senior exploration consultants and project managers, ensuring strict adherence to NMEDT guidelines and quality assurance protocols. The table below lists the team members and their respective roles.

Sl. No.	Name	Designation / Role	Project Responsibilities
1	**Biplob Chatterjee**	Director & CEO, PC (NABET)	Overall project supervision, strategic oversight, verification of project protocols, review of outcomes and report.
2	**Dr. Joy Gopal Ghosh**	Principal Consultant (Exploration), PC (NABET)	Conceptualization of exploration models, determination of project protocols, technical design, peer review of findings and report.
3	**Dr. Taraknath Pal**	Principal Consultant (Exploration), PC (NABET)	Geological and geophysical supervision, project management, and project administration.
4	**Dr. Tapan Pal**	Principal Consultant (Exploration)	Geological, structural, stratigraphic, petrological, mineralogical supervision and review of report.
5	**Tuasha Majumder**	Senior Project Manager (Exploration)	**Project Leader;** overall coordination of field operations, lithological mapping, validation of stratigraphic correlations, lithological and facies documentation, sampling, QA/QC management, core logging, and report preparation.

Sl. No.	Name	Designation / Role	Project Responsibilities
5	**Sarita Mahato**	Project Manager (Exploration), TM (NABET)	**Project Manager;** field logistics coordination, field assistance, sampling supervision, petrographic analysis, core logging, drilling documentation, data compilation and report writing.
6	**Dr. Suparna Goswami**	Senior Project Manager (Exploration)	Validation of stratigraphic correlations, petrological and mineralogical analysis, and report writing.
7	**Nupur Adhikary**	Senior Project Manager (Geology and Geospatial Services, TAE (NABET)	Supervision on geospatial data management, assistance in report writing and project administration.
8	**Chiranjib Banerjee**	Senior Project Manager (Geotechnical), TAE (NABET)	Geotechnical evaluation, drilling supervision, and support in structural interpretation and report writing.
9	**Krishna Prasad**	Senior Consultant (Geophysics), TAE (NABET)	Geophysical survey design, data quality assessment and supervising report writing.
10	**Soumen Roy**	Project Manager (Exploration and Geophysics)	Geophysical data acquisition and interpretation of resistivity profiles.
11	**Bhuwan Sharma**	Project Manager (Exploration)	Field assistance, core logging, litholog preparation, pitting, surface sampling and report writing.
12	**Tanuja Priyadarshini Deo**	Project Geologist (Exploration)	Field assistance, sample processing, laboratory coordination, geophysical data acquisition, data documentation, and compilation.
13	**Niharika Mishra**	Project Geologist (Exploration)	Geophysical data acquisition, data documentation and compilation
14	**Aishik Saha**	Project Manager (Exploration), TM (NABET)	Geological fieldwork and geochemical sampling.
15	**Tithi Mondal**	Field Geologist	Field assistance, preparation of geological cross-sections, and data documentation.
16	**Sujay Payra**	Senior Project Manager (Geospatial Services), TAE (NABET)	Overall coordination of geospatial activities and remote sensing interpretation.
17	**Prabir Bhattacharya**	Project Manager (Geospatial Services)	Satellite data processing, map generation, DEM analysis and GIS integration.
18	**Rabiya Parween**	Project Scientist (Geospatial Services)	GIS database preparation and figure generation.

Sl. No.	Name	Designation / Role	Project Responsibilities
19	**Ritisha Sing**	Project Geologists (Exploration)	Data documentation and compilation.

1.10 Mode of Operation of Different Working Components and Associated Agency:

The **"Reconnaissance Survey (G4) for REE Exploration in Bhuj Clay Prospect Block, Kachchh District, Gujarat"** was executed through a multidisciplinary and fully integrated operational framework encompassing geological, geophysical, geochemical, petrological, mineralogical, and geospatial investigations. All field-based activities, including large-scale geological mapping (1:12,500), systematic sampling, sample processing, heavy-mineral separation, geophysical surveys, pitting/trenching and core drilling, were conducted in-house by M/S Geovale Services Pvt. Ltd., ensuring uniform technical control and adherence to NMEDT-approved protocols. Petrographic studies including thin-section preparation and microscopic characterization of surface and core samples were carried out by Geovale's internal petrography team to determine mineral paragenesis and textural relationships.

Analytical and mineragraphic studies were carried out at the Inspectorate Griffith Commodities Division (Bureau Veritas, Gandhidham), with Round-Robin validation at Shiva Analyticals, Bengaluru, while advanced mineralogical characterisation (XRD, SEM–EDX, EPMA) was performed at Geological Survey of India (GSI) laboratories in Kolkata and Nagpur.

All datasets were integrated within a unified GIS environment for interpretation and quality assurance. The project maintained rigorous QA/QC protocols at every stage, from field documentation and analytical verification to interpretational review, ensuring accuracy, reproducibility, and traceability. Institutional collaboration with NMET, CGM Gujarat, and GSI provided technical oversight and logistical support, collectively ensuring the project's successful completion and analytical reliability.

1.11 Acknowledgements:

This project was funded by the National Mineral Exploration and Development Trust (NMEDT), Ministry of Mines, Government of India, under Sanction File No. 23/385/2023-NMET/251, dated 5th October 2023. The authors express their sincere gratitude to the Executive Committee (EC), Technical and Cost Committee (TCC), and the Head of Department, NMEDT for their continued guidance, review, and encouragement throughout the project. The constructive technical feedback and timely approvals provided by the NMEDT committees played a pivotal role in the successful execution of the program.

We gratefully acknowledge the Commissionerate of Geology and Mining (CGM), Government of Gujarat, and the Gujarat Mineral Research and Development Society (GMRDS), Gandhinagar for their active cooperation, logistical facilitation, and administrative support during fieldwork. Special appreciation is extended to the Geological Survey of India (GSI) for providing laboratory access and technical assistance in mineralogical characterization.

A special note of appreciation is extended to Shri K. Ramesh Kumar, Ex-Additional Director, AMD, who served as the External Peer Reviewer for this Geological Report (GR), appointed by the Technical and Cost Committee (TCC) of NMEDT. The authors express their sincere gratitude for his independent technical evaluation, constructive comments, and valuable guidance, which have significantly enhanced the scientific quality and overall rigor of the final report.

Finally, heartfelt thanks are extended to the local administration and the villagers in and around Bhuj, Sukhpar, Kukuma, Samatra, Kalyanpar and Naranpar for their cooperation and assistance during the field operations. Their support was indispensable to the smooth and safe completion of the fieldwork and drilling activities.

Chapter 2

Property Description

2. Property Description

2.1. Location and Accessibility:

The Bhuj Clay Prospect Block lies within Survey of India Sheet 41E/12, straddling the Bhuj-Kukuma-Naranpar sector of Bhuj taluka in Kachchh District, Gujarat (*Fig. 2.1*). The block encompasses 252 sq. km, area spanning from 23.2323°N to 23.1436°N latitude and 69.5006°E to 69.7514°E longitude, as detailed in Survey of India Toposheet No. 41E/12. Bhuj serves as the nearest administrative centre and offers essential facilities, including a post office, hospitals and a police station.

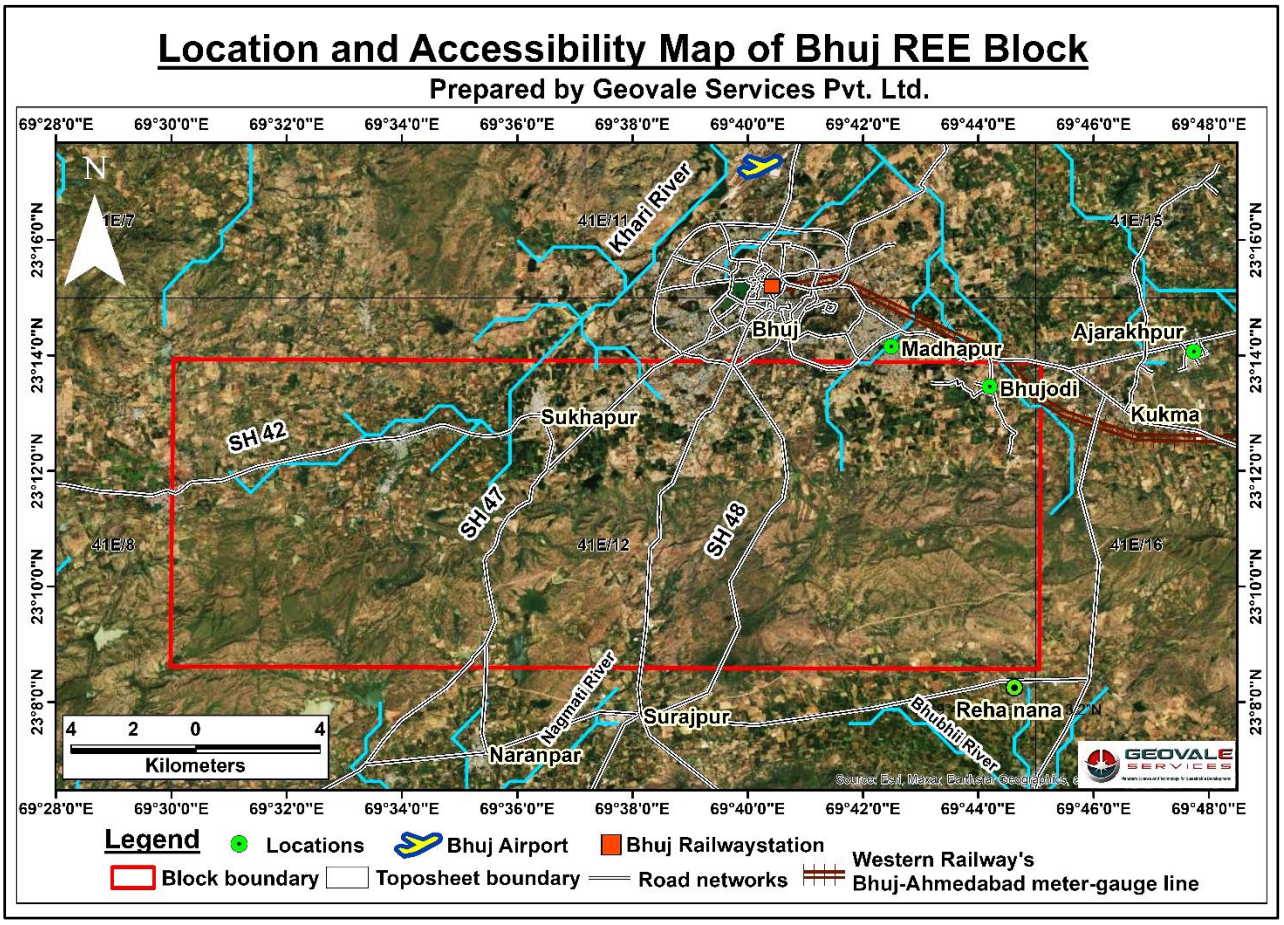

Fig. 2. 1 Location and accessibility map of the study area (Source: Google Maps).

The prospect block is traversed by the Katrol Hill Fault in its northern sector and lies partly between the Khari river at the north and Bhubhil and Nagmati rivers at the south, with gentle terrain and moderate elevation contrast, facilitating vehicular access across much of the area. Bhuj, the nearest major hub, is well connected by SH-7 and NH-47 to the state capital Ahmedabad (~8-9 hr drive) and other major cities. State highways and National Highway links feed into Bhuj, which connects into the block via state routes and rural roads. Both the state highway and the interdistrict roads that connect Bhuj with Mandvi, Mundra and Nakhatrana (SH-48, SH-47 and SH-42 respectively) travel through the block. Internal access within the

block is facilitated by a network of rural roads, seasonal tracks, and existing village linkages. The flat terrain and sparse vegetation simplify deployment of exploration parties and mobilization of drilling or heavy-equipment logistics. All villages in the study area are accessible either via metal road or paved/ cart tracks, ensuring year-round connectivity for exploration activities and related transportation.

Bhuj is served by a domestic airport (6km north of the project area), providing connection to major cities, and this enhances logistical flexibility for personnel and sensitive equipment. Rail connectivity to Bhuj exists via Western Railway's Bhuj-Ahmedabad meter-gauge lines. The nearest railway station, Bhuj railway station, which is about 2.5 kms away from the block.

2.2. Forest Cover

The Bhuj Clay Prospect Block is primarily characterized by sparse natural vegetation. Forest cover in the block and adjoining areas is very limited, mainly restricted to small, discontinuous patches along hill slopes, ephemeral drainage channels, and low structural ridges. According to the latest Forest Survey of India (*FSI, 2023*) and the land-use/land-cover analysis carried out from Sentinel-2 imagery (*refer to section 4.1.15 for details*), forest and dense shrubland together occupy less than 10 % of the total block area.

The forest patches are primarily composed of dry deciduous thorn type vegetation, dominated by *Acacia nilotica*, *Prosopis juliflora*, *Ziziphus nummularia*, and *scattered Balanites aegyptiaca*. The forest density rarely exceeds 40 % canopy cover and is largely confined to the southern and southwestern fringes near Surajpur and Naranpar, and along the ENE-WSW trending ridges in the central part of the block.

Overall, the Bhuj Clay Prospect Block can be categorized as a low-forest-density region, where vegetation is primarily seasonal and secondary in nature. The scarcity of dense forest cover facilitates geological field mapping, geophysical surveys, and sampling operations, thereby allowing unobstructed access for reconnaissance scale exploration activities.

2.3. Climate and Topography:

The Bhuj Clay Prospect Block lies within the central part of the Kachchh Mainland, which experiences a semi-arid to arid climate typical of western Gujarat. The region is governed by the north-western continental climatic regime, characterized by hot, dry summers, a short monsoon season, and mild winters.

According to the India Meteorological Department (*IMD, 2023*), the mean annual rainfall in the Bhuj region varies between 350 mm and 450 mm, of which nearly 85-90 % occurs during the southwest monsoon months of July to September. Temperatures range from 10-15°C in winter to 42-45°C in summer, and the mean annual relative humidity fluctuates between 40%

to 70%. Owing to high evaporation and low rainfall, surface runoff remains limited, and most streams are ephemeral.

Topographically, the Bhuj Clay Prospect Block forms part of a gently undulating plateau within the central Kachchh Mainland. Elevation within the block ranges from <140m above mean sea level (asml) in the northern plains to >160m amsl along the southern margin of the block (*Fig. 2.2*).

The northern part of the block, encompassing Bhuj, Sukhpar, and Reha Nana, lies on relatively low ground (<140m amsl) forming low, gently rolling uplands. Narrow ENE-WSW ridges within the southern part of the block area mark the surface expression of the Katrol Hill Fault Zone and associated lineaments, with steep northern face, varying in elevation between 160 to 200 meters. The highest point within these ridges is 325 m asml.

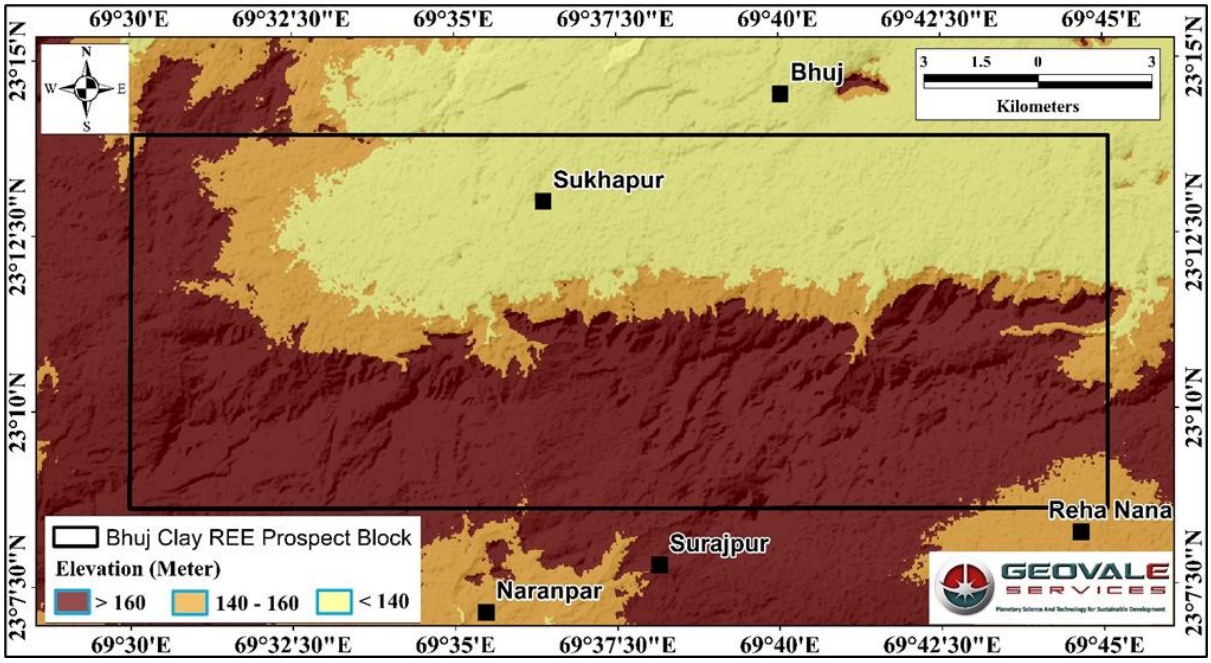

Fig. 2. 2 Relief map of the Bhuj REE Prospect Block.

The southern side of the hill ranges is marked by gentle southerly dipping plains, around Surajpur and Naranpar, with elevation ranging between 140-160m amsl.

Relief variation across the block is modest, generally not exceeding 30-40m and slopes are subdued, resulting in a terrain well suited for exploration.

2.4. Flora and Fauna:

The Bhuj Clay Prospect Block and its adjoining areas fall within the semi-arid ecological province of the Kachchh District, Gujarat, characterized by sparse xerophytic vegetation adapted to low rainfall, high temperature, and prolonged dry periods. The vegetation belongs predominantly to the Northern Tropical Thorn Forest type (*Champion and Seth, 1968*),

comprising drought-tolerant species and scattered dry deciduous shrubs typical of the Kachchh landscape.

The floral cover is thin over most of the block, where vegetation comprises *Capparis decidua*, *Calotropis procera* and cactus, along with seasonal grasses such as *Cenchrus setigerus* and *Dichanthium annulatum*. Denser shrubs and bushes occur locally along nullahs, tanks, and reservoirs where limited soil moisture persists after the monsoon. The trap uplands and rocky ridges are largely barren and devoid of vegetation. Cultivation is confined to gentle plains near Bhuj, Sukhpar, and Reha Nana, while grass and scrubland dominate the southern sector around Surajpur and Naranpar.

The faunal assemblage reflects the arid to semi-arid environment and open scrubland ecosystem. Reptiles are diverse and include spiny-tailed lizard (*Uromastyx hardwickii*), monitor lizard (*Varanus bengalensis*), Kutch rock gecko, sand boa (*Eryx johnii*), python (*Python molurus*), black cobra (*Naja naja*), black krait (*Bungarus caeruleus*), royal snake, and crocodile (*Crocodylus palustris*) near perennial waterbodies. Amphibians such as toads and frogs appear seasonally in the low-lying depressions. Common mammals include nilgai (*Boselaphus tragocamelus*), chinkara (*Gazella bennettii*), wild boar (*Sus scrofa*), Indian wolf (*Canis lupus pallipes*), jackal (*Canis aureus*), pangolin (*Manis crassicaudata*), and leopard (*Panthera pardus fusca*). Avifauna is abundant during post monsoon and winter, comprising Indian roller, bee-eater, lapwing, egret, partridge, francolin, and migratory waterfowl visiting ephemeral ponds.

No wildlife sanctuary or protected area lies within or immediately adjacent to the prospect block. The Kachchh Desert Wildlife Sanctuary lies about 70 km north-northwest of Bhuj area. Overall, the block exhibits sparse vegetation and low faunal density, imposing minimal ecological constraints on exploration.

.

Chapter 3

Previous Work and Project Generation (Pre-field Studies)

Stage 1

3. Previous Work and Project Generation (Pre-field Studies) Stage I

A comprehensive understanding of earlier geological and exploration activities provides the baseline for any systematic mineral investigation. The Bhuj region has been intermittently investigated by the Geological Survey of India (GSI), the Commissioner of Geology and Mining (CGM), and several academic institutions. These cumulative efforts spanning from systematic geological mapping, systematic thematic mapping, mineral investigations, drilling-based investigations, to national geochemical surveys provides a scientific foundation for the present reconnaissance exploration. Pre-field geomorphological assessments conducted during the current study have further strengthened this foundation by refining the spatial understanding of surface processes and terrain evolution relevant to mineral dispersion and accumulation.

3.1. Previous Work in the Regional Area:

The Kachchh region of western India has been the subject of sustained geological investigation for over a century, primarily owing to its complex tectono-sedimentary evolution and its unique record of Mesozoic-Cenozoic transition. The earliest reconnaissance mapping was undertaken by the Geological Survey of India (GSI) during the early part of the twentieth century, followed by several systematic investigations that established the fundamental tectono-stratigraphic framework of the basin (*Biswas, 1987; 2005; 2016*). Subsequent thematic studies by GSI and the Commissioner of Geology and Mining (CGM) documented the mineral potential of the basin.

3.1.1. Systematic and Thematic Geological Mapping by GSI

Subsequent detailed mapping at 1:50,000 and 1:25,000 scales in and around the Bhuj-Anjar-Nakhatrana sector was undertaken through a series of Systematic Geological Mapping (SGM) and Specialised Thematic Mapping (STM) programs (*Poddar, 1954; Desikan et al., 1968; Ghevariya, 1979; 1984, 1986, 1987; Sahu and Dinesh, 1991*). These investigations delineated the regional geological, stratigraphic and structural set-up of the area.

3.1.1.1. Regional Geological Set-up:

The Bhuj REE Prospect Block is forms a part of the Kachchh Rift Basin, a pericratonic extensional basin developed along the northwestern margin of the Indian Shield, structurally bounded by the Kathiawar Uplift to the south and the Thar Platform to the northeast. The basin evolved under the influence of extensional tectonism during the Middle Jurassic to Cretaceous periods, contemporaneous with the breakup of Gondwanaland (*Biswas, 1987; 2005*).

Regionally, the Kachchh Basin is characterized by a series of E-W trending uplifts and intervening depressions, bounded by major fault systems such as the Kachchh Mainland Fault (KMF), Katrol Hill Fault (KHF), and Island Belt Fault (IBF). These structural features divide the basin into distinct morphotectonic units, the Kachchh Mainland Uplift, Banni Basin, and Wagad Uplift, each recording discrete sedimentation and deformation histories (*Biswas, 2016*). The Bhuj area lies within the Kachchh Mainland Uplift, a structurally elevated block bounded by the KMF to the north and the KHF to the south. The structural framework of this uplift exerts a strong control on sedimentation, and lithological distribution.

3.1.1.2. Stratigraphy and structure

The regional stratigraphic succession of the Kachchh Mainland comprises a thick Mesozoic sequence unconformably overlain by Tertiary and Quaternary sediments and capped by Deccan Trap basalts. The Jurassic to Cretaceous succession, exceeding 3,000 m in cumulative thickness, records a complex interplay of fluvial, deltaic, and shallow marine depositional environments. The principal formations exposed in and around the Bhuj area include the Chari Formation, Katrol Formation, and Bhuj Formation (*Fig.3.1*), representing a progressive transition from shallow marine to continental settings. These formations are further capped by Anjar volcanics.

The Chari Formation is exposed as small, discontinuous lenses along the southern margin of the Katrol Hill Fault. It represents sedimentation within a transitional to open-marine environment, characterized by alternating micritic limestone, calcareous and gypseous shale, fossiliferous limestone, calcareous and ferruginous gritty sandstone, conglomerate, and greenish-grey shale. The overlying Katrol Formation (~750 m thick; 138 ± 22 Ma, *Srivastava et al., 1994*) consists predominantly of dark grey to black shale interbedded with calcareous and ferruginous sandstone, siltstone, and clay. The succession records proximal deltaic to fluvio-lacustrine facies, developed under fluctuating hydrodynamic and oxidation conditions. The conformably overlying Bhuj Formation is composed of sandstone, shale, grit, and conglomerate, deposited in a continental fluvial to alluvial-fan environment. The sandstones are typically feldspathic to ferruginous, medium to coarse grained, and exhibit cross-bedding, ripple lamination, and channel-fill structures.

The Deccan Traps (Anjar Volcanics) occur south of the Bhuj region and comprise multiple lava flows and intrusive dykes of variable composition, predominantly black to olive-green amygdaloidal basalt containing secondary silica and zeolite mineralization. These volcanic rocks mark the terminal magmatic phase of basin evolution, associated with regional uplift, crustal reactivation, and localized thermal metamorphism of the underlying sedimentary strata.

The Quaternary Miliolite Formation is represented by calcarenite, marl, and conglomerate, preserved as isolated patches unconformably overlying the Mesozoic sequence. These deposits constitute the youngest stratigraphic component of the region,

forming the surface cover across the low-lying plains and pediment surfaces. A total of 32 alkaline plugs have been documented from the Bhuj–Nakhatrana region, of which two occur in close proximity to the present block area (*Guha et al., 2005; Kshirsagar et al., 2011*).

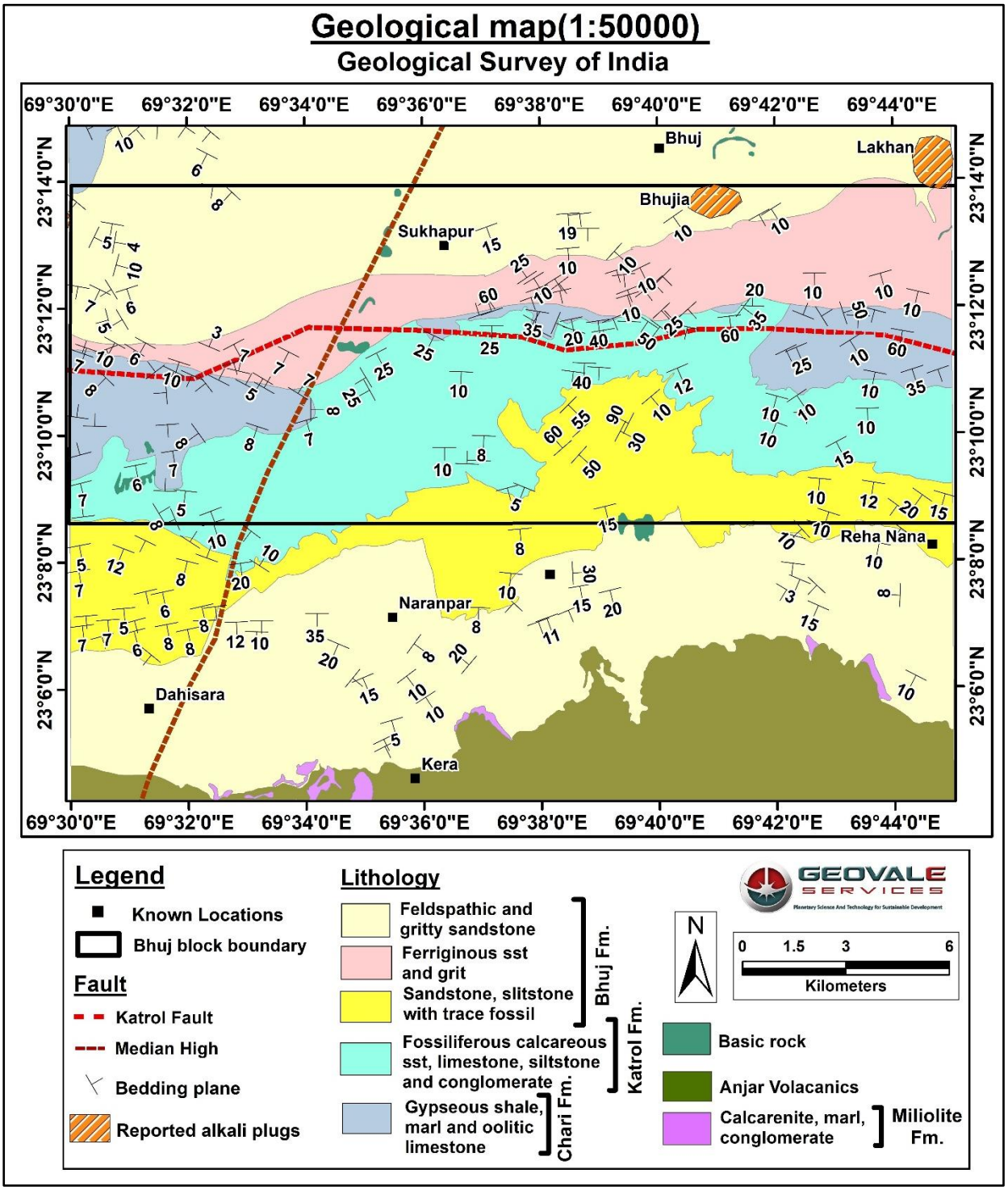

Fig. 3. 1 Regional geological map of the Bhuj area (after Geological Survey of India, 1:50,000 scale, SOI toposheet no. 41E/12.

Structurally, the region displays a strong E-W structural grain, with prominent fault-controlled ridges and anticlines (e.g., the Katrol Hill Range) alternating with narrow synclinal depressions. The Katrol Hill Fault, a major south-dipping reverse fault, represents the dominant tectonic feature that juxtaposes the older Katrol Formation against younger Bhuj strata. The Median High represents a flexural uplift capped by late Cretaceous volcanics. Minor NNW–SSE and ENE–WSW fracture systems further dissect the area, influencing drainage alignment and post-depositional fluid flow.

3.1.2. Regional Mineral Exploration:

Regional scale mineral exploration in the Kachchh district was undertaken by multiple agencies through independent projects targeting different commodities of economic potential. The major initiatives include investigations for bauxite and laterite, phosphorite, and bentonite–clay deposits, which together established the mineralogical framework of the region.

3.1.2.1. Bauxite and Laterite Investigations (CGM)

Exploratory drilling for bauxite and laterite was carried out by the Commissioner of Geology and Mining (CGM), Government of Gujarat, in the Mandvi-Mundra-Nakhatrana sectors (*Shah, 1971, 1973*), located immediately south of the present block area. These investigations established two distinct bauxite horizons: a primary pre-Laki type directly overlying basalt or bentonite, and a secondary post-Laki type developed above Tertiary sediments. Intervening lithomarge (10-15m) and bentonitic clays were recorded across several boreholes, indicating alteration along the Deccan-Tertiary interface. Analytical results revealed Al_2O_3 ≈ 49 %, SiO_2 ≈ 4-5 %, Fe_2O_3 ≈ 12-15 %, classifying the bauxite as metallurgical to ferruginous grade.

3.1.2.2. Phosphorite Investigations (GSI)

Systematic exploration for phosphorite mineralisation in Kachchh district has been carried out intermittently by the Geological Survey of India, Commissioner of Geology and Mining (CGM) and academic workers, covering the Mesozoic-Cenozoic sedimentary successions in and around Bhuj, Kachchh district. These studies collectively document the occurrence of phosphatic cherty limestones and nodular phosphorites hosted within the Chari, Katrol, Bhuj, and Laki (Kakdi Nadi) formations, representing deposition in near-shore to shallow-shelf environments connected to an open marine system where periodic upwelling and organic activity favoured local phosphate concentration.

Within the Laki Formation, phosphorite occurs in the grey shales of the Kakdi Nadi Member, as elliptical to rounded nodules ranging from 4cm to 12cm in diameter (*Bhatt et al., 1973*). Chemical analyses indicate P_2O_5 content ranges between 10.13 and 23.75 wt%, although the distribution is highly erratic and confined to isolated pockets.

In contrast, the Mesozoic succession hosts more persistent phosphatic horizons. In the Katrol Formation, phosphorite is associated with grey shale interbeds, whereas in the Chari Formation it occurs within alternating sandstone-shale sequences, commonly as well rounded, ellipsoidal to lens shaped nodules measuring 3-15cm in thickness and 5–25 cm in length. The nodules in the Chari Formation are typically flattened and fossiliferous. Reported P_2O_5 values range from 0.21 to 22.96 wt%, with the higher concentrations (12.63-22.96 wt%) recorded from the Katrol Formation around Motawadva, Virani, and Nabhoi in central Kachchh (*Shukla et al., 1974*).

Systematic exploration by Geological Survey of India (GSI) has also confirmed these phosphate bearing tracts of the Mesozoic succession near Ler, Wandhaya and Boladi villages in and around Bhuj (*Kathiara, 1984*). Occurrences that intersect the present Bhuj block (41E/12) are summarised at block-scale in *section 3.2.3.2*.

3.1.2.3. Bentonite-Clay Investigations (GSI and CGM)

Independent studies on bentonite and clay occurrences were conducted by the Geological Survey of India and later by the Commissioner of Geology and Mining.

Early work by *Kulkarni (1966)* documented bentonitic and kaolinitic clay deposits in the Nakhatrana-Mandvi area, identifying extensive lithomarge and bentonite horizons developed through in-situ alteration of Deccan basalt. The bentonite investigation by *Bedi (1983)* further recorded sodium-based swelling bentonite up to 3-6 m thick in shallow basins around Naredi, Wandh, and Punadi, with high cation-exchange capacity and commercial-grade properties. The recent exploration by *Amin and Rao (2020)* confirmed the persistence of a bentonite-lithomarge-laterite succession with localised aluminous enrichment, underscoring the region's potential for REE-bearing clays and industrial minerals.

3.1.2.4. Status of REE Investigations

Despite extensive geological and mineral-commodity mapping across the Kachchh Mainland, no previous exploration work has been undertaken specifically for Rare Earth Element (REE) mineralisation. The ongoing reconnaissance project under the National Mineral Exploration and Development Trust (NMEDT) represents the first systematic program aimed at assessing clay-hosted REE potential within the Bhuj block of central Kachchh.

3.1.3. National Geochemical Mapping Program

High-density stream-sediment sampling under the National Geochemical Mapping Program (NGCM) of the Geological Survey of India (*Suthar, 2017; GSI-NGCM data, Source: Bhukosh portal*) has generated the first region-wide geochemical baseline for the Kachchh Mainland. The NGCM dataset indicates that the region exhibits variable but consistently elevated concentrations of ΣLREE and ΣHREEY, particularly within structurally uplifted domains bordering the Katrol Hill Fault (KHF) and the Median High (*Fig. 3.2; 3.3*).

Spatial analysis of the NGCM data reveals that ΣLREE values range from background levels of 250–1000 ppm in the northern Kachchh Mainland to > 20,000 ppm within the Bhuj-Anjar-Naranpar corridor, with discrete anomalies as high as 9% locally (*Fig.3.2*). These enrichments are strongly associated with weathered terrains exposed along the Katrol Hill Fault and its southern wall.

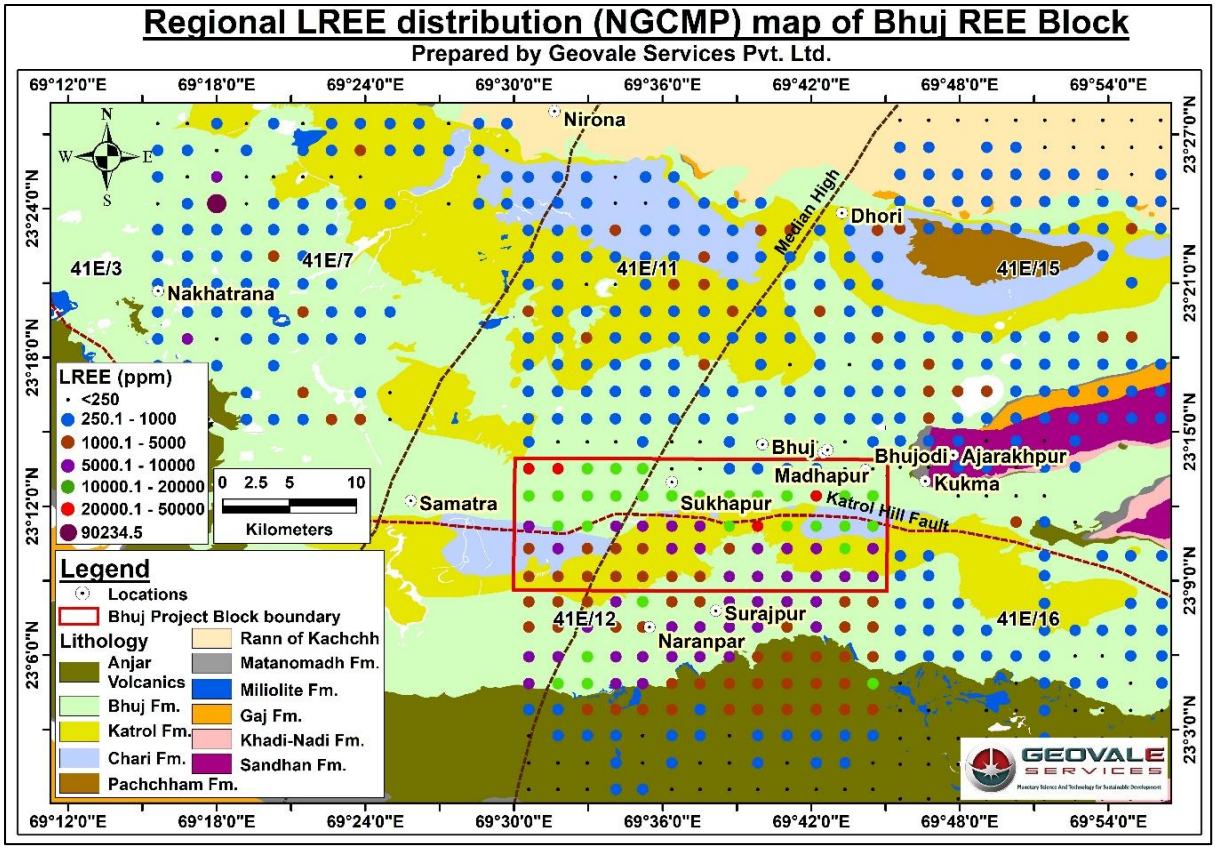

Fig. 3. 2 Regional ΣLREE distribution of the NGCMP samples in and around the Bhuj REE Prospect Block.

The ΣHREEY distribution displays a parallel but narrower anomaly belt, with concentrations between 500 and 2,000 ppm, maximised along the Katrol Hill Fault and Median High (*Fig.3.3*). Isolated co-located anomalies of both ΣLREE and ΣHREEY are also noted near Nakhatrana. Anomaly intensity diminishes southward toward the low-lying plains of Anjar volcanics. This spatial contrast highlights the structural-geomorphic and lithologic (Bhuj Formation) control exerted by the Katrol Hill Fault and the Median High systems on the REE concentration.

These regional-scale anomalies provide the first quantitative evidence of REE fertility in the Kachchh Mainland and underpin the rationale for the ongoing reconnaissance project in the Bhuj block.

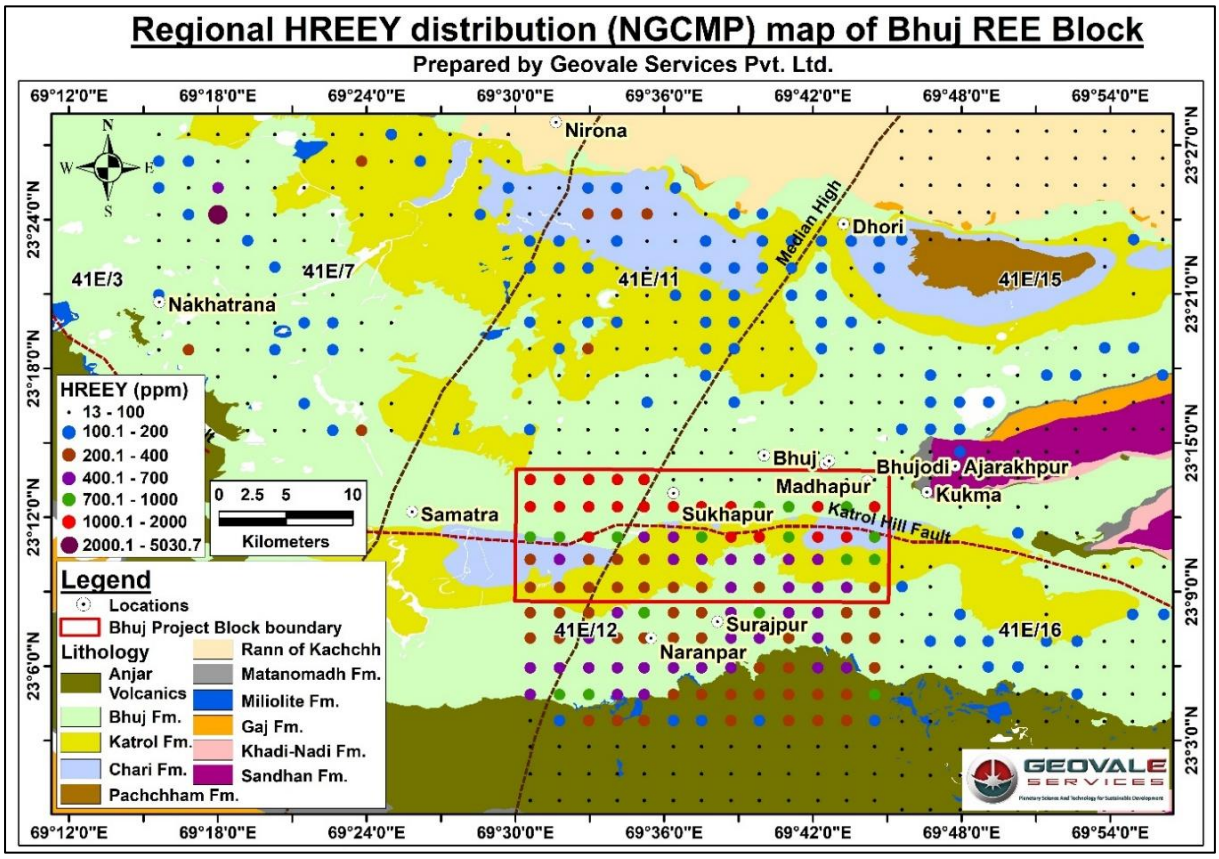

Fig. 3. 3 Regional ΣHREEY distribution of the NGCMP samples in and around the Bhuj REE Prospect Block.

3.2. Previous Work in the Bhuj Exploration Block:

The area under the Bhuj exploration block has been the subject of systematic geological mapping and limited mineral studies by the Geological Survey of India (GSI) and the Commissioner of Geology and Mining (CGM), Gujarat. No prior work was undertaken to investigate Rare Earth Element (REE) mineralisation within the Bhuj block. Earlier works primarily aimed at lithostratigraphic delineation, structural mapping, and industrial-mineral assessment.

3.2.1. Systematic and Thematic Geological Mapping in the Bhuj block

The area was systematically mapped by the Geological Survey of India (GSI) as part of the Systematic Geological Mapping of Toposheet 41E/12 (*Poddar, 1954; Desikan et al., 1968; Ghevariya, 1979, 1984; Sahu and Dinesh, 1985*). The surveys were mostly carried out at 1:50,000 scale, establishing different lithostratigraphic units, structural features such as Katrol Hill Fault, NE-SW- and NW-SE-trending subsidiary faults, intrusive bodies and minor fractures (*Fig.3.1*), forming the lithostratigraphic and structural baseline, served as the foundation for all subsequent geological investigations within the block.

3.2.2. National Geochemical Mapping Program within the Bhuj block

Systematic stream sediment sampling under the National Geochemical Mapping Program (NGCMP) of SOI toposheet 41E/12, Kachchh District, Gujarat (*Suthar, 2017*) generated the first multi element geochemical baseline for the Bhuj project area. The survey, conducted on a 2*2km grid spacing and comprised a total of 65 stream sediment samples analysed for 55 major, trace, and rare-earth elements.

The dataset reveals a distinctly REE-fertile geochemical background across the Bhuj block, with enrichment concentrated along the Katrol Hill Fault (KHF) and the Median High structural zones (*Fig.3.4 and 3.5*). The ΣLREE content ranges from <250 ppm to 37,959 ppm (0–4 wt %), showing a median value of 8,279 ppm (*Fig.3.4*). Nearly 41 % of the data fall within the 1%-4% range, indicating significant light rare earth enrichment in stream sediments (*Table.3.1*). Moderate concentrations (0.5–1 %) constitute 28 % of the sample set, while lower background levels (0.05–0.5 %) occur mainly in the northern part of the project area.

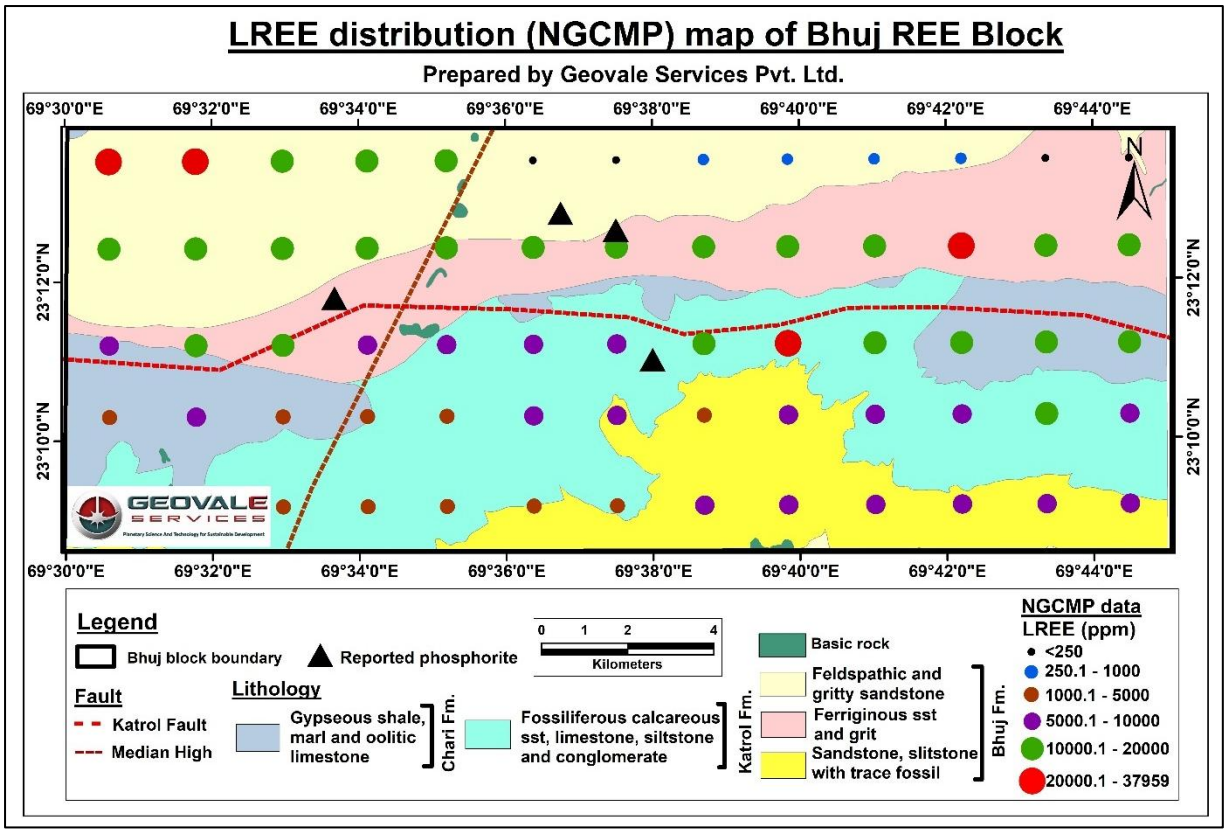

Fig. 3. 4 ΣLREE distribution of the NGCMP samples of the Bhuj Clay REE Prospect Block. Note that the very high values of ΣLREE are concentrated in the northern part of the Bhuj REE block and coincides with the reported phosphorite locations.

The ΣHREEY distribution displays a comparatively subdued but spatially coherent anomaly pattern, with concentrations ranging from 13 ppm to 1,965 ppm (*Fig.3.5*) (0–0.2 wt

%) and a median value of 644 ppm (*Table.3.1*). Roughly 31 % of the samples lie in the 0.1-0.2 % range, concentrated near the Katrol Hill Fault and in the feldspathic and ferruginous sandstone.

Table. 3. 1 Statistical distribution of ΣLREE and ΣHREEY concentrations in stream-sediment samples (n=65) within the Bhuj Clay Prospect Block, Kachchh District, Gujarat. The data, derived from the National Geochemical Mapping Program (NGCMP). Quantitative figures in each concentration range indicate percent of samples analyzed.

Concentration in %	Range	Percent data
ΣLREE	0-0.05%	12
	0.05-0.5%	19
	0.5-1%	28
	1-4%	41
	Median Value	8279.43
	Highest Value	37958.81
ΣHREEY	0-0.01%	12
	0.01-0.05%	29
	0.05-0.1%	28
	0.1-0.2%	31
	Median Value	643.67
	Highest Value	1964.7

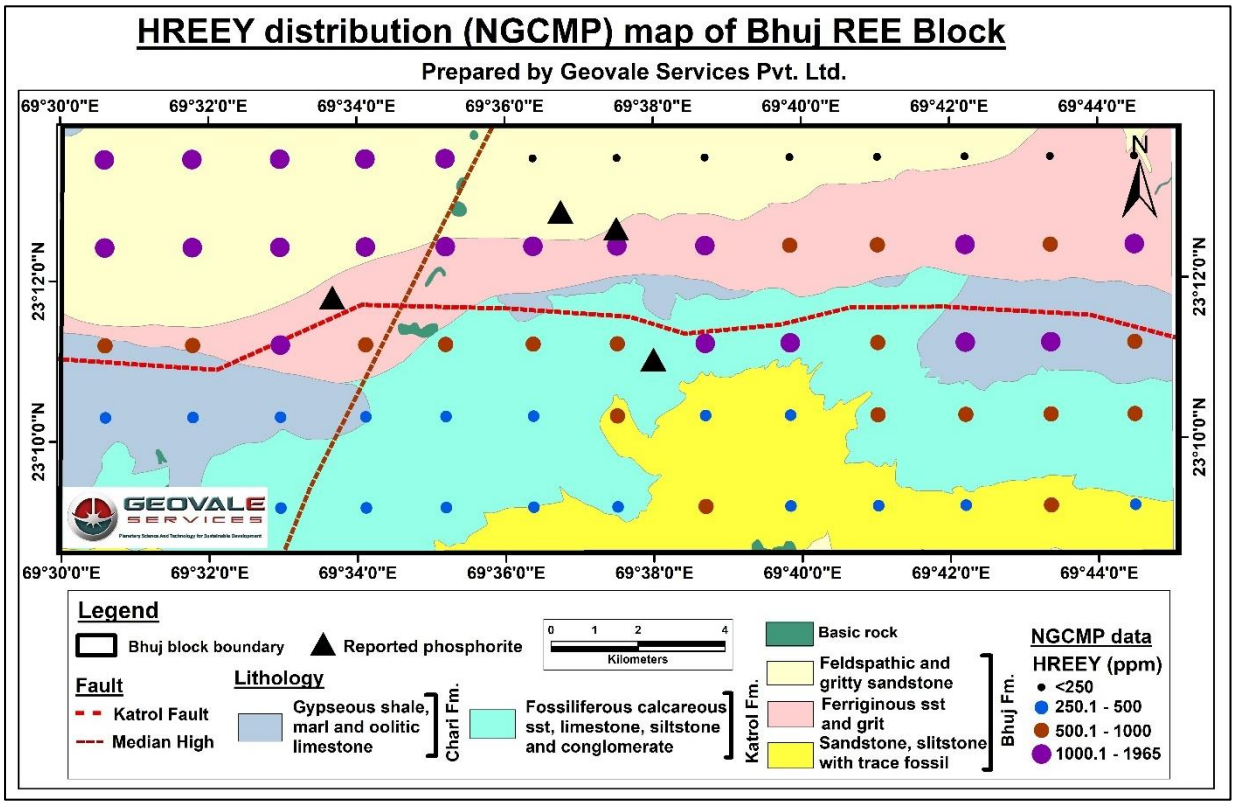

Fig. 3. 5 ΣHREEY distribution of the NGCMP samples of the Bhuj Clay REE Prospect Block. Note that the very high values of ΣHREEY are concentrated in the northern part of the Bhuj REE block and also coincides with the reported phosphorite locations.

Spatially, both ΣLREE and ΣHREEY anomalies define a broad, ENE-WSW trending corridor along the Katrol Hill Fault and Median High, where Bhuj and Katrol formations are exposed, suggesting a strong structural and lithological control on REE dispersion.

3.2.3. Mineral Exploration within the Bhuj block

The scope of previous mineral exploration within the present Bhuj block has remained confined to industrial minerals such as industrial clay and phosphorite, without any targeted geochemical or mineralogical assessment for REE potential or any other critical mineral potential.

3.2.3.1. Industrial Clay Investigations

Reconnaissance work by the Commissioner of Geology and Mining (CGM) for bentonite and clay deposits in and around the Bhuj area (*Amin and Rao, 2020*) identified a bentonite-lithomarge-laterite succession developed along trappean depressions. The investigation established montmorillonitic and ferruginous clays with subordinate kaolinite but did not include any geochemical or REE-oriented analysis.

3.2.3.2. Phosphorite Investigations

Investigations for phosphorite were undertaken by the Geological Survey of India in the Ler-Wandhaya-Habo Hill region of central Kachchh encompassing part of SOI toposheet no. 41E/7, 41E/8 and 41E/12 (present working toposheet) (*Kathiara, 1984*) (*Fig. 3.4 and 3.5*). The study focused on the phosphatic cherty limestone horizons, exposed along the Katrol Hill Fault Zone between Ler in the east and Wandhaya in the west, and around the Habo Hill area. Geological mapping over approximately 220 sq. km area delineated phosphatic cherty limestones of the Chari Formation, occurring as narrow, discontinuous bands within a sequence of gypseous shale, oolitic and fossiliferous limestone, and minor gypsum that conformably underlies the Katrol Formation. A total of 275 rock samples were analysed, showing P_2O_5 content ranging generally between 1 and 5 wt %, with isolated high values of 7-8 wt% near Ler, Walakhavas, and Wandhaya. The phosphatic beds, typically 0.25-1.1m thick and traceable for 2-8 km along strike, were found to be oolitic to cherty in nature and locally fossiliferous. Although the total inferred reserve was estimated at about 9 million tonnes, the material was considered sub-economic because of its low-grade nature and discontinuous occurrence. Subsequent reconnaissance in adjoining areas did not identify additional deposits, confirming that the Ler-Wandhaya-Habo Hill corridor constitutes the principal phosphorite bearing horizon within the Kachchh Mainland.

3.3. Observation and Recommendations from Previous Work:

Systematic geological and thematic studies conducted over the past several decades in the Kachchh Mainland have collectively shaped the present understanding of its stratigraphic architecture and mineral framework. The earliest mapping campaigns established the fundamental lithostratigraphic order and structural fabric of the basin, while later thematic programs progressively expanded this baseline into more specialised mineral and geochemical domains.

From a resource perspective, these efforts remained largely confined to the evaluation of industrial minerals. Explorations for bentonite, lithomarge clay, and phosphorite defined the extent and grade of these commodities but did not extend into critical element appraisal. The documented phosphatic and clayey horizons of the Chari, Katrol and Bhuj formations were recognised chiefly for their industrial potential, and the investigations by both the Geological Survey of India (GSI) and the Commissionerate of Geology and Mining (CGM) did not include analyses for Rare Earth Elements (REE) or allied metals.

A major advance came with the National Geochemical Mapping Program (NGCM), which generated the first high resolution, multi element dataset for the project area (*Suthar, 2017*). The NGCM results revealed anomalous enrichments in ΣLREE and ΣHREEY within the regolith and stream sediments, influenced by the Katrol Hill Fault and the Median High. These anomalies provided quantitative confirmation that portions of the Mesozoic succession possess inherent REE fertility, though no mineralogical follow up was undertaken at that time.

Within the present Bhuj exploration block, the available legacy information, spanning from geological mapping, mineral appraisal, to regional geochemistry, offers a reliable contextual base but lacks any targeted exploration for REE bearing system/s. The dataset thus defines the geological canvas upon which the current exploration is structured.

3.4. Basis for Taking Up Investigation:

The concept of reconnaissance exploration for Rare Earth Elements (REE) within the Bhuj Clay Prospect Block was guided by a combination of regional geoscientific indicators and conceptual metallogenic reasoning derived from multi-disciplinary datasets. The National Geochemical Mapping Program (NGCMP) revealed consistently anomalous concentrations of both light and heavy rare earth elements (ΣLREE and ΣHREEY) across the central Kachchh Mainland, particularly within Survey of India Toposheet 41E/12, which encompasses the present block.

Analytical results from fine (<80 mesh) fractions of stream sediment samples (n = 182), collected on a 2 × 2 km grid, show ΣLREE concentrations reaching up to 37,959 ppm (mean: 9,636 ppm) and ΣHREEY up to 1,965 ppm (mean: 726 ppm) (*Figs. 3.6, 3.7*). The statistical

distribution of these values (*Table 3.2*) shows that nearly 40% of the samples contain ΣLREE above 0.5% and ΣHREEY above 0.05%, indicating regionally significant enrichment. These significantly elevated values display minimal stratigraphic bias but exhibit a strong structural association along the E–W-trending Katrol Hill Fault and the NNE–SSW-oriented Median High, suggesting a potential tectono-hydrothermal control on REE distribution.

Table. 3. 2 Statistical distribution of ΣLREE and ΣHREEY concentrations in stream-sediment samples (n=182) from the SOI toposheet no. 41E/12, encompassing the Bhuj Clay Prospect Block, Kachchh District, Gujarat. The data, derived from the National Geochemical Mapping Program (NGCMP). Quantitative figures in each concentration range indicate percent of samples analyzed.

Concentration in %	Range	Percent data
ΣLREE	0-0.05%	32.42
	0.05-0.5%	28.57
	0.5-1.0%	21.43
	1.0%-10%	17.58
	Median value	3719 ppm
	Highest value	37958.51 ppm
ΣHREEY	0-0.01%	33.52
	0.01-0.05%	35.71
	0.05-0.1%	19.78
	0.1-0.2%	10.99
	0.2-0.5%	-
	>0.5%	-
	Median value	331.37 ppm
	Highest value	1964.7 ppm

Based on the Mineral Systems Analysis (MSA) approach, these anomalous REE concentration suggests several possible geological processes contributing to enrichment within the Kachchh Basin:

1. **Multi-source origin of REE enrichment:**

The absence of any direct bias between REE enrichment and individual lithostratigraphic units suggests that the source of these elements may lie within a combination of Mesozoic sedimentary formations (Katrol–Bhuj–Chari succession) as paleo-placer and/or REE concentration in the carbonaceous shale of the Katrol Formation.

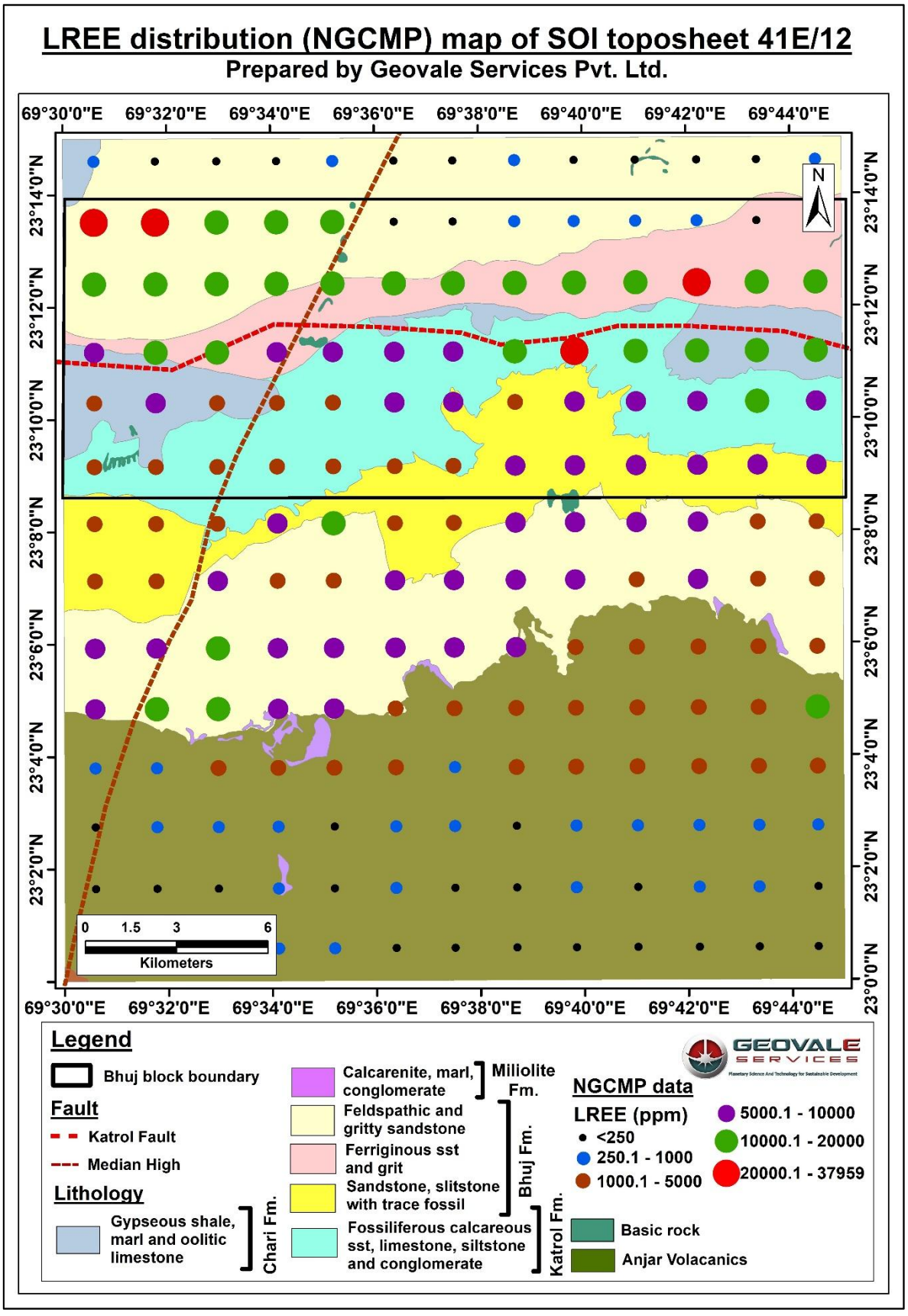

Fig. 3. 6 ΣLREE distribution of the NGCMP samples of SOI toposheet no. 41E/12. Note that the very high values of ΣLREE are concentrated in the northern part of the Bhuj REE block.

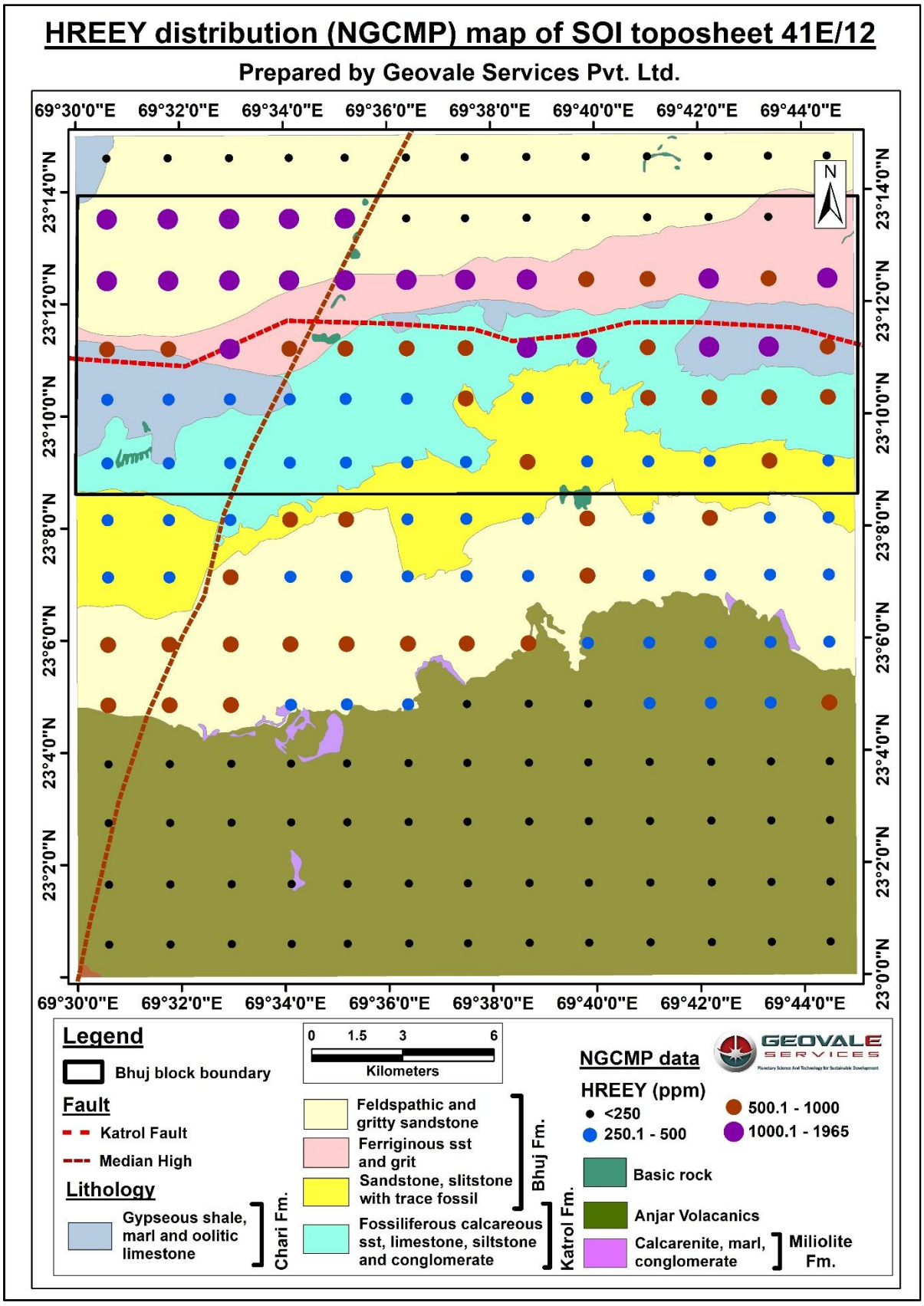

Fig. 3. 7 ΣHREEY distribution of the NGCMP samples of SOI toposheet no. 41E/12. Note that the very high values of ΣHREEY are concentrated in the northern part of the Bhuj REE block.

2. **Ion-adsorbed and clay-hosted REE potential:**

The NGCMP datasets are from bulk sample analysis, where the samples were sieved to -80 mesh (~180µm) and then milled without further size or density separation. The samples thus might include both clay fractions and silt sized grains having a potential of ion adsorbed clay REE potential.

Furthermore, geomorphological interpretation of satellite and digital-elevation datasets indicates a landscape characterized by low-relief plains flanking an E-W hill range, with valley-fill deposits on either side of the Katrol Hill Fault. These valleys represent potential catchments where detrital or adsorbed REE minerals could have been concentrated within fine-grained clay and regolith horizons. This interpretation aligns with the anomalously high REE values reported from low-lying zones adjacent to the Katrol Hill Fault and the Median High (*Fig. 3.8*), suggesting possible terrain-controlled redistribution of REE.

3. **Secondary placer concentration:**

Structural depressions associated with the Katrol Hill Fault (*Fig. 3.8*) may have served as traps for detrital REE minerals eroded from the REE bearing sedimentary units. Such settings are favourable for secondary concentration of heavy minerals (e.g. monazite, xenotime, zircon) within Quaternary and Recent sediments, representing the anomalous REE values, specifically along the fault flanks.

The convergence of statistically significant REE anomalies, REE-fertile source lithologies, and favourable structural–geomorphic settings provide a robust rationale for NMEDT funded reconnaissance exploration. The investigation aims to validate these conceptual models through systematic geological, geochemical, and geophysical studies, ultimately establishing the lithological and structural controls, governing the REE enrichment within the Kachchh Basin.

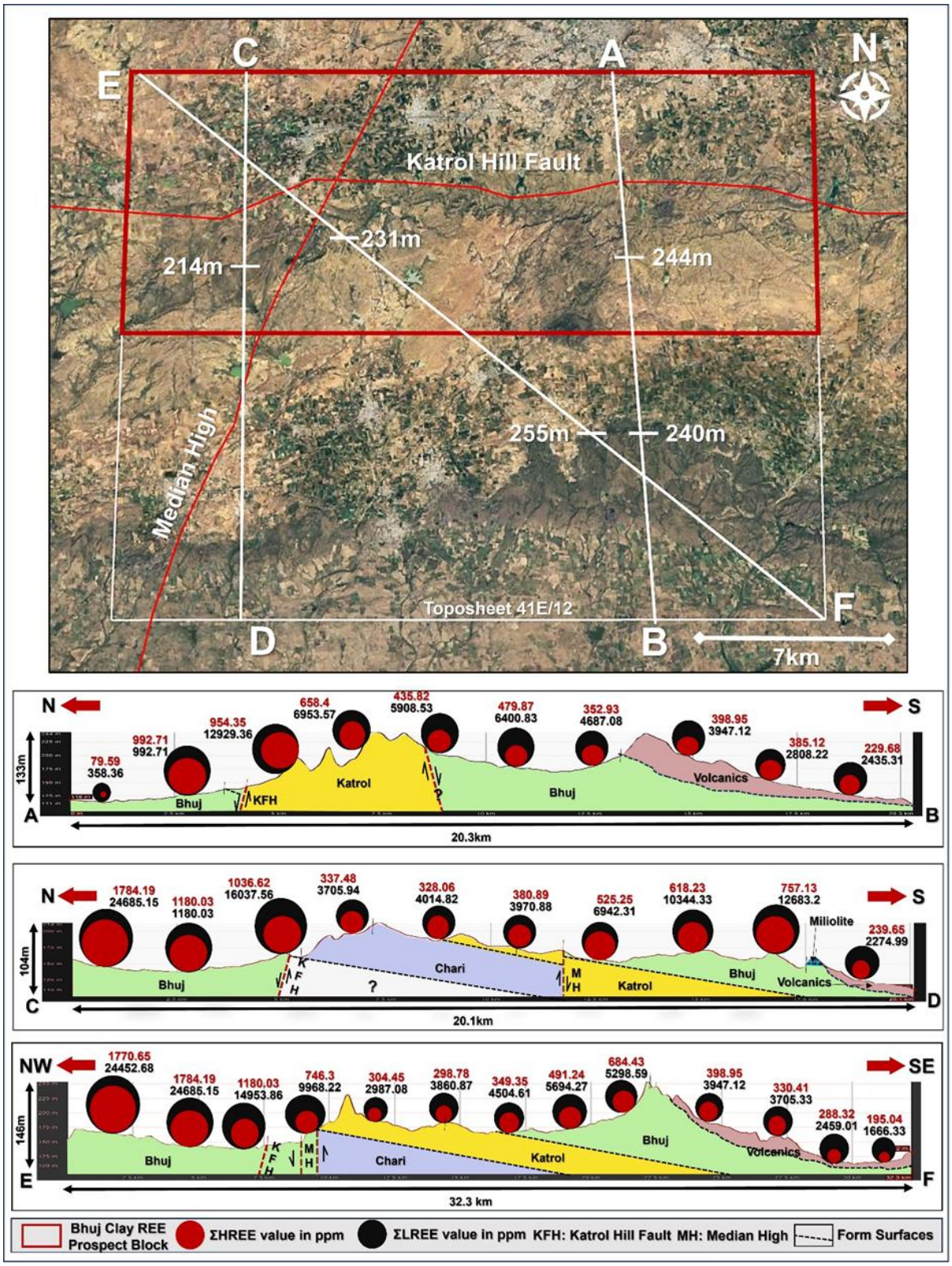

Fig. 3. 8 Schematic diagram of the cross-sectional profile across the Katrol hill fault and the Median High. Note that the high REE values have concentrated in the low elevation areas on both sides of the Katrol hill Fault which may have provided the right environment for REE enrichment. Also note that the vertical scale of the sections are over 20 times exaggerated than

the horizontal scale to highlight distribution of high REE assays in valleys. However, this exaggeration also gives an erroneous impression of high relief and steepness of lithological formations.

3.5. Pre-field Investigation: Remote Sensing Analysis

Remote sensing formed the foundational stage of investigation, providing synoptic spatial information critical for terrain characterization, geomorphological interpretation, and structural delineation, essential prerequisites for understanding the area prior to field operations. Multi-spectral satellite data (Sentinel-2A) and Digital Elevation Model (DEM) datasets derived from SRTM (1 Arc-Second ≈30m resolution) were processed within a GIS environment to extract key terrain parameters such as elevation, slope, drainage, landform, soil, and land-use/land-cover attributes. The analysis facilitated the delineation of geomorphic domains, slope dynamics, and hydrological networks that govern surface weathering and sediment transport. These parameters collectively aid in interpreting the background for secondary REE concentration, as inferred from legacy geochemical datasets.

3.5.1. Regolith Mapping and RED Scheme Classification

A detailed regolith mapping exercise was undertaken across the 252 sq. km Bhuj REE Prospect Block using the Residual–Erosional–Depositional (RED) classification framework to delineate the primary geomorphic process domains and assess their implications for REE exploration (*Fig.3.9*). This approach was adopted to understand the spatial distribution of residual, erosional, and depositional landforms that collectively govern the exposure, reworking, and concentration of REE-bearing lithologies within the study area.

The mapping was carried out through the integration of Sentinel-2A multispectral imagery and Shuttle Radar Topography Mission (SRTM) Digital Elevation Model (DEM) data (1 Arc-Second ≈ 30 m spatial resolution) within a GIS environment. Standard pre-processing steps, including radiometric and atmospheric corrections, band-ratio compositing, and topographic derivative analysis, were applied to ensure the accuracy of landform delineation. In addition, ASTER (Advanced Spaceborne Thermal Emission and Reflection Radiometer) multispectral imagery acquired in July 2006 was processed using ENVI software to identify and validate lateritic, ferricrete, and calcrete alteration zones. The interpreted datasets were subsequently verified through published geological maps, *GSI (Bhukosh)* databases, and legacy exploration reports for consistency and ground correlation.

Based on this integrated analysis, the terrain was classified into four primary regolith domains: Residual Regolith, Erosional Regolith, Depositional Regolith, and Depositional Plains, each representing a distinct stage in the weathering-erosion-deposition continuum.

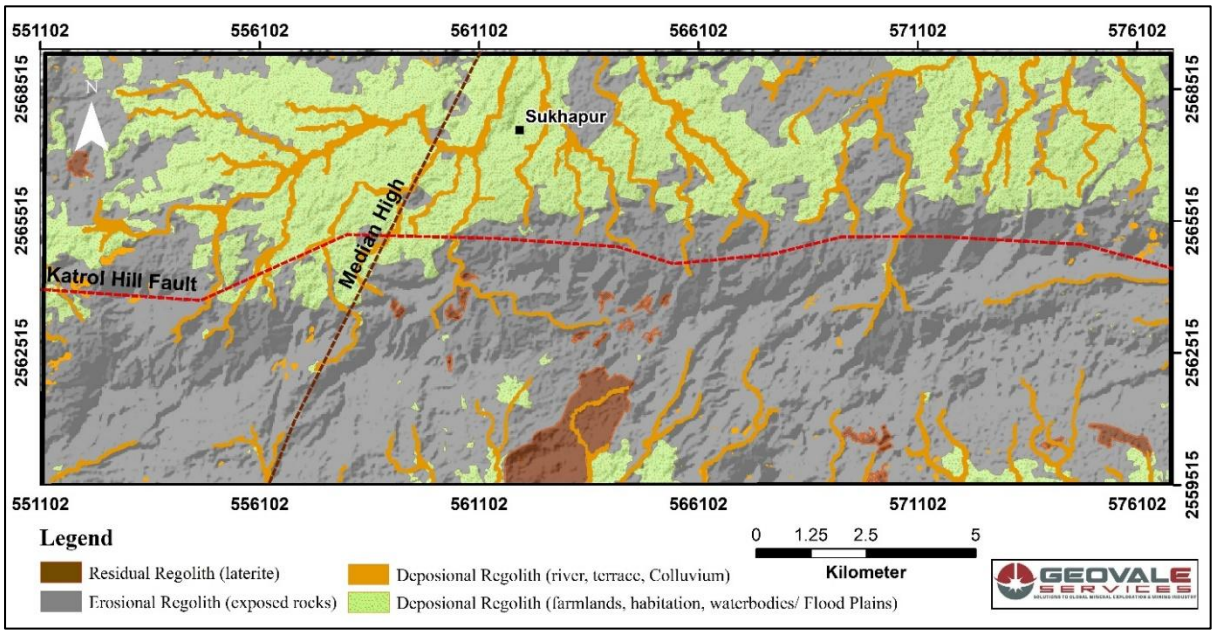

Fig. 3. 9 Regolith mapping of the Bhuj REE study area using the Residual–Erosional–Depositional (RED) classification scheme.

i. Residual Regolith (Laterite/Ferricrete/Calcrete):

This unit occurs mainly in the southern to south-central sectors of the block, particularly around Sedata and Jadura. These surfaces represent chemically weathered uplands and stable geomorphic remnants developed over primary lithologies under prolonged oxidation and desilication. The regolith profiles commonly contain ferruginous crusts and calcrete layers, indicative of pedogenic modification under semi-arid climatic conditions. Such lateritic and ferricrete zones are of high exploration relevance as they may preserve geochemical signatures of underlying REE-bearing formations through residual enrichment processes.

ii. Erosional Regolith (Exposed Bedrock):

The erosional domain forms a broad central corridor within the study area, characterized by rocky uplands, erosional scarps, and structural ridges. This unit exposes the Bhuj and Katrol formations, offering direct field access to the target lithologies associated with REE mineralization. The morphology reflects active surface denudation and differential weathering, which facilitate natural lithological exposure investigation, structural mapping, and sampling of the lithounits. These areas are therefore considered aa primary zones for verifying lithostratigraphic relationships and assessing the potential primary mineralization.

iii. Depositional Regolith (River Terraces and Colluvial Zones):

The depositional regolith occurs predominantly along valley flanks and foot-slope sectors, recording reworked sediments derived from adjoining uplands. These zones comprise a mixture of colluvial debris, slope-wash material, and terrace deposits. The fine-grained, moderately sorted sediments within these geomorphic traps provide suitable conditions for

secondary REE accumulation through mechanical concentration and chemical adsorption processes.

iv. Depositional Plains (Agricultural and Alluvial Landforms):

This unit occupies the northern and north-central sectors of the block, forming low-relief plains composed of fine-grained alluvial and overbank deposits. The geomorphic setting corresponds to low-energy fluvial environments where suspended materials are periodically deposited during seasonal runoff. These plains, extensively modified by agriculture and minor anthropogenic activity, represent potential domains for drainage-sediment sampling and surface geochemical anomaly detection associated with downstream REE dispersion.

Exploration Significance:

The RED classification provides a comprehensive geomorphic framework for understanding the regolith evolution and its relationship to REE mineralization within the Bhuj REE Prospect Block.

- The residual caps represent stable uplands where in-situ lateritic or ferruginous profiles may record primary or near-primary REE signatures.
- The erosional domains offer the most direct lithological exposure for stratigraphic correlation and mineralogical characterization of REE-fertile horizons.
- The depositional regimes, including terraces and plains, delineate zones of potential secondary enrichment suitable for reconnaissance-scale sampling and heavy mineral analysis surveys.

Limitations:

It is recognized that the spatial expression and spectral separability of the RED units are influenced by seasonal variations in vegetation cover and soil moisture. Accordingly, the interpretations presented herein correspond to the datasets and temporal windows used in this study.

3.5.2. Terrain Analysis

A detailed terrain analysis of the Bhuj REE Prospect Block was carried out using the SRTM (1-Arc-Second ≈30m) Digital Elevation Model to delineate physiographic domains of the project area. The area exhibits distinct topographic segmentation that exerts a direct influence on the exposure, redistribution, and concentration of REE-bearing lithologies.

Based on elevation ranges, slope gradients, and morphometric parameters, the area has been classified into four principal physiographic units: Dissected Lowlands, Plateau Fringe, Dissected Plateau, and Isolated Hills (*Fig.3.10*). Each unit represents a distinct geomorphic process regime with specific implications for sediment dynamics and mineral concentration.

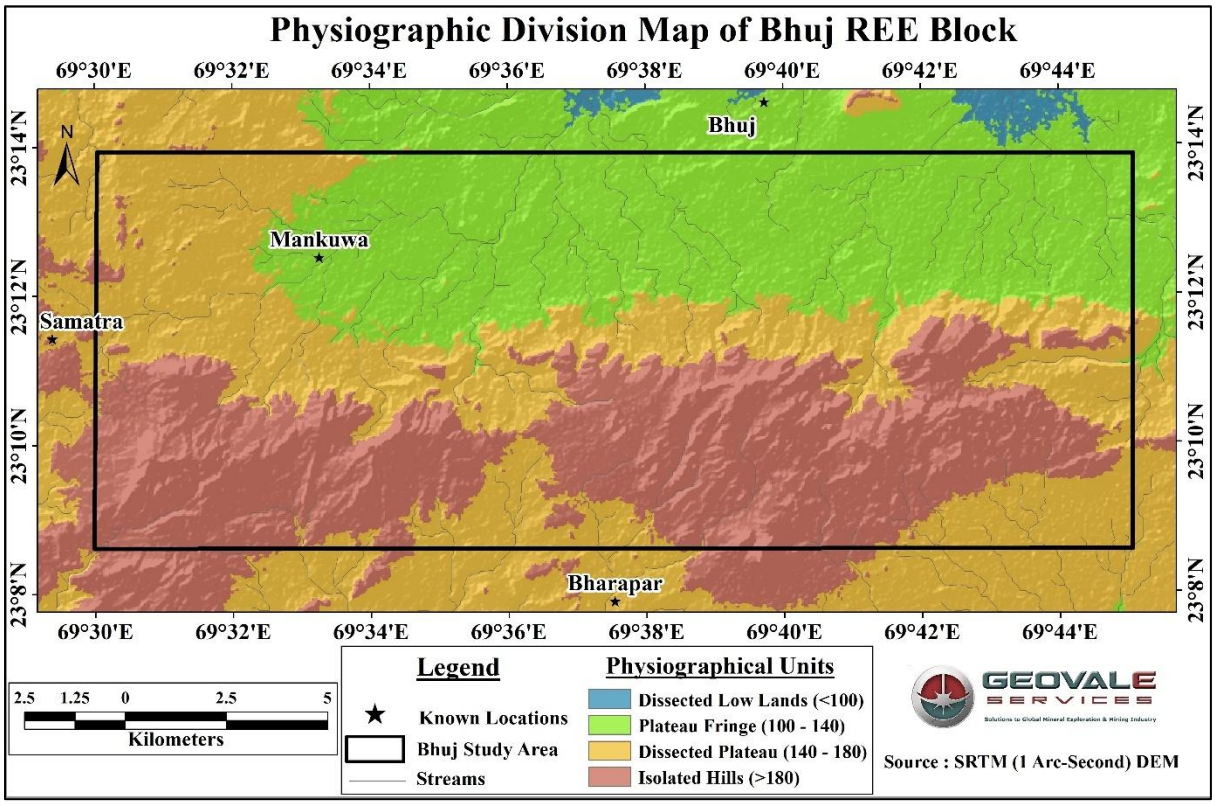

Fig. 3. 10 Physiographic division map of the Bhuj REE prospect block.

i. Dissected Lowlands (< 100 m):

This unit, occupying less than 5 sq. km in the northernmost sector of the block, represents the lowest topographic domain. The terrain is characterized by subdued relief and is shaped predominantly by fluvial and colluvial processes. The lowlands are underlain by fine-grained sediments exhibiting moderate infiltration capacity and seasonal runoff. These depositional conditions favour the accumulation of clay-rich materials that may act as natural traps for reworked REE-bearing fines derived from adjacent uplands through surface wash and slope erosion.

ii. Plateau Fringe (100–140 m):

The plateau fringe forms a transitional geomorphic zone between the low-lying plains and the elevated uplands, dominating the central belt of the study area and covering approximately 80 sq. km (around 32% of the total block area). The unit exhibits moderate slopes, scattered bedrock exposures, and a gently undulating surface morphology. These conditions are conducive to colluvial accumulation and localized surface runoff, which collectively promote the concentration of fine detrital materials, relevant for slope-controlled geochemical anomalies.

iii. Dissected Plateau (140–180 m):

Occupying nearly 78 sq. km (about 30% of the total area), this terrain unit is extensively developed across the southern and south-central sectors of the Bhuj REE Block. It is distinguished by rugged relief, closely spaced valleys, and erosional scarps reflecting active denudation and differential weathering. The moderate to steep slopes, combined with periodic surface runoff, facilitate the formation of ferruginous crusts and lateritic soils through prolonged oxidation. These lateritized surfaces are of particular exploration interest, as they may preserve geochemical signatures indicative of residual REE enrichment associated with the underlying lithological units.

iv. Isolated Hills (> 180 m):

Representing the highest topographic level in the study area, this unit comprises resistant residual hills and structural ridges that define the erosional remnants of more extensive upland surfaces. The Chari Katrol and Bhuj formations are prominently exposed within this domain, often along steep escarpments and rocky ridges. The combination of high relief, limited soil cover, and intense mechanical weathering enhances the exposure of primary lithologies and provides direct field access to potential mineralized zones. Such features make this unit particularly important for lithostratigraphic correlation, petrographic documentation, and assessment of mineralized host rocks.

Exploration Significance:

The overall terrain pattern of the Bhuj REE Prospect Block depicts a progressive increase in elevation from the northern depositional plains towards the southern erosional uplands, delineating a morphotectonic gradient that reflects the interplay between lithological resistance and structural control. This topographic differentiation has direct implications for exploration planning, viz.

- The dissected lowlands and plateau fringes constitute favourable geomorphic domains for secondary or transported REE accumulation, particularly in fine-grained alluvial and colluvial settings.
- The dissected plateaus and isolated hills correspond to zones of primary or residual REE enrichment, where weathered and lateritized profiles overlie REE-fertile lithologies.

The physiographic diversity thus serves as a key spatial framework for guiding geological mapping, defining sampling transects, and prioritizing target areas for subsequent stages of geochemical and geophysical exploration.

3.5.3. Slope Characterization

The slope configuration of the Bhuj REE Prospect Block was analyzed using the Shuttle Radar Topography Mission (SRTM) Digital Elevation Model (DEM) (1 Arc-Second ≈ 30 m spatial resolution) to understand the geomorphic variability and surface processes that influence

drainage evolution, erosion, and sediment redistribution (*Fig.3.11*). Slope characteristics serve as critical indicators of geomorphic stability and weathering potential, which collectively govern the exposure of REE-bearing lithologies and the loci of secondary material concentration.

The slope distribution across the study area was categorized into three principal classes: nearly flat to gentle, moderate, and steep slopes, each reflecting the interplay of lithology, structural control, and erosional dynamics.

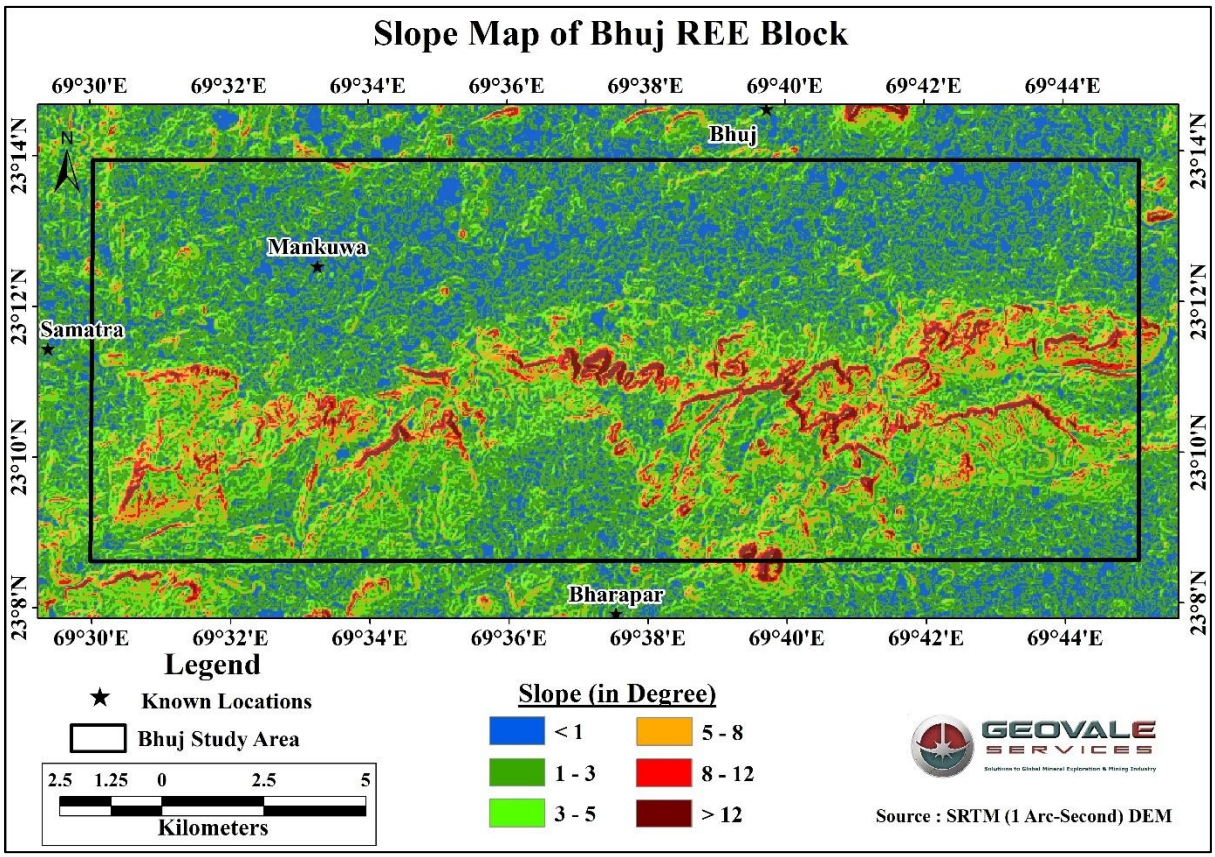

Fig. 3. 11 Slope map of the Bhuj REE Prospect Block derived from SRTM-DEM data.

i. Nearly Flat to Gentle Slopes (< 1°–3°):

These slopes dominate the northern and central parts of the study area and correspond to low-relief plains and valley floors. The subdued gradient favours limited surface runoff, promoting sediment accumulation and moisture retention. These conditions are conducive to the development of fine-grained soils and the preservation of transported materials derived from higher elevations, significant for identifying secondary REE-bearing clays and regolith horizons.

ii. Moderate Slopes (3°–8°):

Moderate slopes are prevalent across the transitional zones between the central and southern sectors, marking the morphological boundary between plateau fringes and

dissected uplands. These areas experience active surface runoff and moderate erosion, resulting in the redistribution of weathered detritus downslope. The slope gradients facilitate the formation of colluvial and slope-wash deposits, which are of high exploration interest for potential REE enrichment through mechanical concentration. The spatial correlation of these slopes with structural lineaments and lithological contacts further enhances their significance as potential geochemical dispersion corridors.

iii. Steep Slopes (8°–>12°):

The steepest slopes are concentrated in the southern and southcentral parts of the block, corresponding to the rugged ridges and erosional escarpments formed by resistant lithologies of the lithounits. These steep slopes are structurally controlled, reflecting the influence of faulting, jointing, and lithological contrast on erosional processes. They provide direct exposure of bedrock units, allowing detailed observation of lithological variations, structural features, and alteration zones related to REE and associated mineralization.

Exploration Relevance:

Gentle to moderate slopes delineate depositional and colluvial environments favourable for secondary REE concentration, whereas steep slopes correspond to structurally uplifted zones providing primary lithological exposure. Integrating slope data with geomorphology and drainage patterns thus supports the delineation of sampling transects and prioritization of target areas for detailed field investigation.

3.5.4. Drainage Dynamics

The drainage network of the Bhuj REE Prospect Block was delineated from SRTM (1 Arc-Second ≈30m) Digital Elevation Model and Sentinel-2A imagery to evaluate surface runoff patterns, structural influence, and sediment redistribution processes (*Fig.3.12*). Regionally, the Kachchh Mainland exhibits a dendritic to sub-dendritic drainage pattern, reflecting the influence of a semi-arid climate and the dominance of fluvial incision over tectonically dissected terrain. Within the Bhuj block, the drainage network conforms to this regional trend but shows significant structural modification due to faulting and differential erosion along the Katrol Hill Fault (KHF) and the Median High.

The principal drainage elements within the block include Dharawa Nadi, Ratiya Nala, and several first- and second-order tributaries that originate from the Bhuj Reserve Forest uplands in the south and flow northward and north eastward toward low-lying depositional plains. A smaller set of ephemeral streams flow southward into the intermontane depressions and local catchments. This radial, bidirectional flow system along with channel alignments along E–W and NNE–SSW structural trends, reflects both the influence of lithological heterogeneity and neotectonic reactivation. The drainage density increases over dissected plateaus and ridges, reflecting higher relief and erosion potential, whereas sparse networks characterize the gently sloping plains and valley fills.

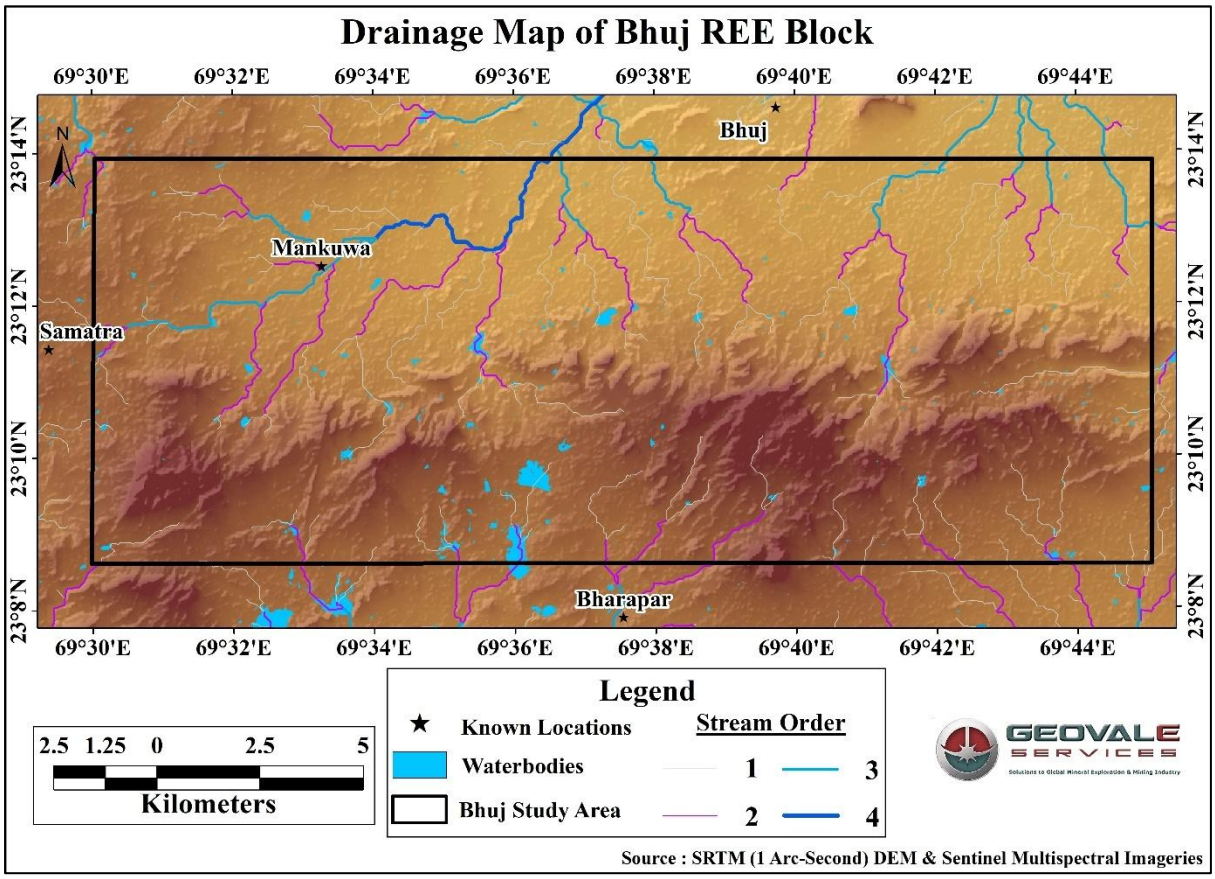

Fig. 3. 12 Drainage network and hydrological pattern of the Bhuj REE Prospect Block derived from SRTM-DEM and Sentinel-2A datasets.

Exploration Relevance:

The drainage configuration of the Bhuj block defines both source and depositional domains for REE dispersion.

- Upland catchments represent erosional zones where weathered REE-bearing materials are mobilized.
- Mid-stream and valley-floor sectors act as transport corridors for suspended mineral fines.
- Low-gradient plains and terrace zones form accumulation sites, suitable for drainage-sediment and panned-concentrate surveys.

The overall drainage configuration therefore provides an essential framework for designing stream sediment surveys, facilitating the identification of downstream geochemical anomalies and the refinement of exploration targets in subsequent stages.

3.5.5. Soil Type and Distribution

The soil mapping of the Bhuj REE Prospect Block was carried out using datasets from the National Bureau of Soil Survey and Land Use Planning (NBSS&LUP), refined through

geomorphological interpretation of Sentinel-2A imagery and SRTM-DEM analysis (*Fig.3.13*). The study aimed to delineate the dominant soil associations and evaluate their geochemical and geomorphic implications in the context of REE exploration.

The area is characterized by semi-arid, calcareous soils developed under conditions of limited leaching, moderate erosion, and high evapotranspiration. Six major soil associations were identified within the block, corresponding primarily to pediment, ridge, and residual hill landforms. Their areal distribution and exploration relevance are summarized in *Table 3.3*.

Table. 3. 3 Soil types, characteristics, and areal distribution within the Bhuj REE Prospect Block (NBSS&LUP dataset, interpreted in this study).

Soil Type	Description and Exploration Relevance	Area (km²)	% of Total Area
Moderately Deep Sandy on Pediment	Moderately deep, somewhat excessively drained, calcareous sandy soils on gently sloping pediments with moderate erosion. The coarse texture and low clay/Fe-Mn oxide content result in poor REE retention, though these soils may host detrital heavy minerals (monazite, xenotime) transported from uplands.	89.73	35.61
Shallow Calcareous Loamy on Ridges	Shallow, well-drained, calcareous loamy soils on gently sloping ridges with moderate erosion and stoniness. Alkaline nature inhibits REE mobility but preserves parent-rock geochemical signatures, making them suitable for pathfinder soil sampling.	78.55	31.17
Moderately Shallow Calcareous Loamy on Pediment	Moderately shallow, well-drained, calcareous fine-loamy soils on undulating pediments with slight erosion. The finer texture improves adsorption potential, but calcareous chemistry restricts significant REE fixation; may retain minor adsorption-type REE enrichment.	49.46	19.63
Shallow Loamy on Residual Hills	Shallow, well-drained loamy soils on gently sloping residual hills with moderate erosion. These residual soils mirror the litho-geochemistry of underlying formations; if developed over REE-bearing volcaniclastics or tuffites, they may exhibit localized enrichment.	15.76	6.25
Moderately Shallow Calcareous Loamy on Pediment (Moderate Erosion)	Moderately shallow, well-drained calcareous fine-loamy soils with moderate erosion. These soils represent active transport zones with limited REE fixation, acting primarily as pathways for detrital dispersion.	14.57	5.78
Moderately Deep Coarse Loamy on Pediment	Moderately deep, somewhat excessively drained, calcareous coarse-loamy soils on gently sloping pediments with moderate erosion. High drainage and coarse texture limit REE adsorption but contribute to downslope transport of mineralized detritus.	3.90	1.55
	Total	**251.97**	**100.00**

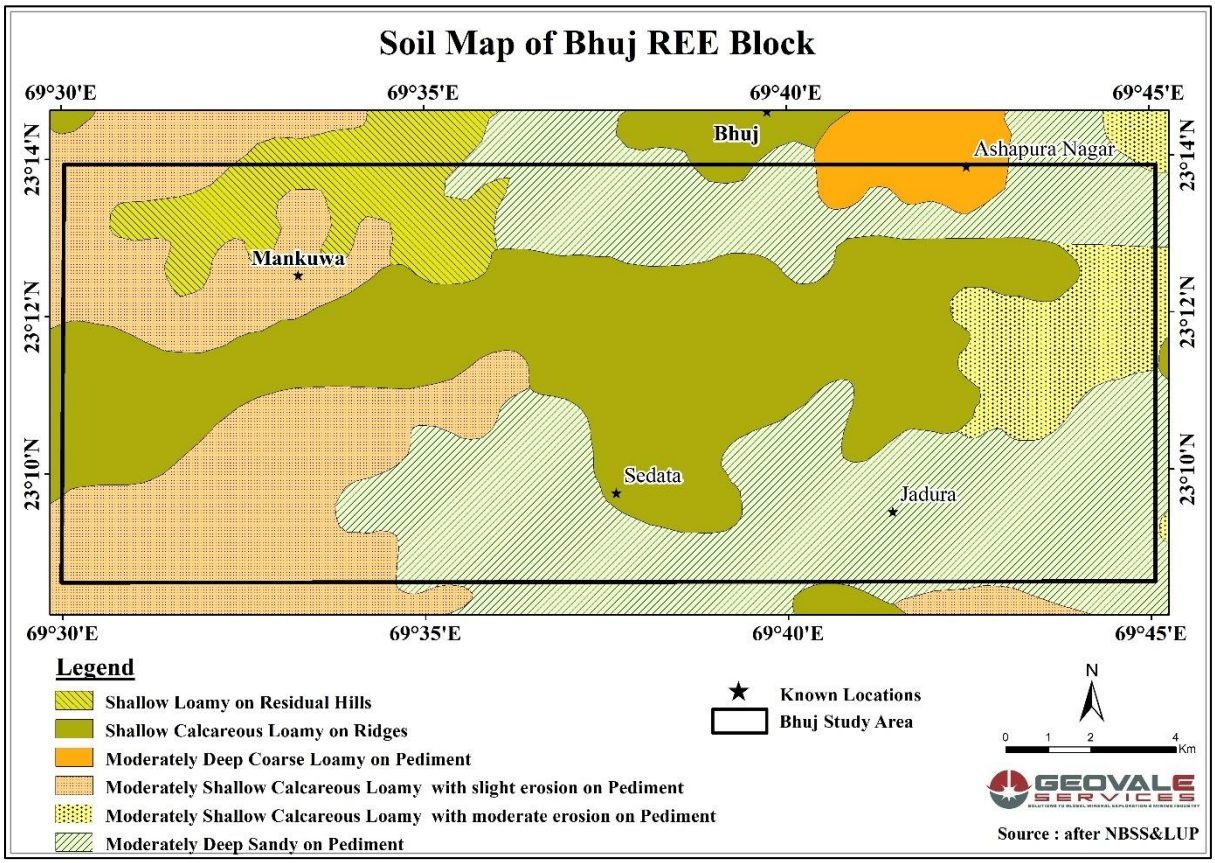

Fig. 3. 13 Soil distribution map of the Bhuj REE Prospect Block based on NBSS&LUP and satellite-derived datasets.

Overall, the soils of the Bhuj REE Prospect block are shallow to moderately deep, sandy- to loamy-textured, and calcareous, reflecting the semi-arid pedogenic environment of the region. Such soils are chemically alkaline and poorly leached, thereby limiting supergene enrichment but preserving the primary lithological geochemical signal of REE-fertile formations.

From an exploration perspective, ridge and residual soils are suitable for pathfinder geochemical surveys, while pediment soils function as transport and accumulation media, capturing downstream dispersion trends. Integration of soil, slope, and drainage datasets thus provides a coherent framework for defining sampling grids and interpreting surface geochemical anomalies.

3.5.6. Land Use Land Cover (LULC):

The Land Use and Land Cover (LULC) mapping of the Bhuj REE Prospect Block was carried out using Sentinel-2A multispectral satellite imagery, processed through supervised classification techniques in a GIS environment (*Fig.3.14*). The study aimed to delineate the spatial distribution of natural vegetation, agricultural land, built-up areas, and water bodies to assess the extent of anthropogenic modification and its implications for exploration logistics and surface geochemical surveys.

The classification identified eight principal land-cover categories, representing both natural and human-modified landscapes within the 252 sq. km project area. The results are summarized in *Table 3.4*.

Table. 3. 4 Land-use and land-cover classification of the Bhuj REE Prospect Block (Sentinel-2A dataset, interpreted in this study).

LULC Class	Description and Exploration Relevance	Approx. % of area
Cropland	Dominant land-use type (~35%), concentrated around Mankuwa and Samtra. Soils derived from weathered sediments support dryland agriculture. Continuous cultivation and ploughing enhance surface mixing and redistribution of fine-grained mineralized dust, influencing surface-geochemical background values.	35 %
Shrub and Scrubland	Occupies gently undulating pediplains (~26%). Sparse vegetation cover exposes surface soils to erosion and wash-off, favouring secondary REE concentration in downslope areas. Such zones are suitable for reconnaissance sampling.	26 %
Dense Vegetation / Tree Cover	Occurs mainly in the central and southern sectors (~22%), associated with moderately dissected topography. Root systems promote chemical weathering and element mobilization; these areas are useful for biogeochemical sampling and interpretation of soil–rock interactions.	22 %
Built-up Areas	Urban and peri-urban zones around Bhuj and Mankuwa (~13%). Though not prospective for direct sampling, they provide logistical and infrastructural advantages for exploration operations.	13 %
Water Bodies	Includes small ponds, tanks, and ephemeral reservoirs (~2%). These act as natural sediment traps for fine-grained mineralized material during monsoonal runoff and may aid in locating downstream REE anomalies.	2 %
Fallow / Flooded / Grassland	Minor classes (< 2 %), representing seasonally variable surfaces linked to agricultural cycles and ephemeral moisture conditions. They contribute contextual information for surface-process interpretation.	< 2 %

The LULC distribution reflects a semi-arid landscape dominated by cropland and scrubland, interspersed with pockets of natural vegetation and built-up areas. Seasonal variability in vegetation cover exerts a direct influence on remote-sensing reflectance and, consequently, on the interpretation of surface geochemical anomalies.

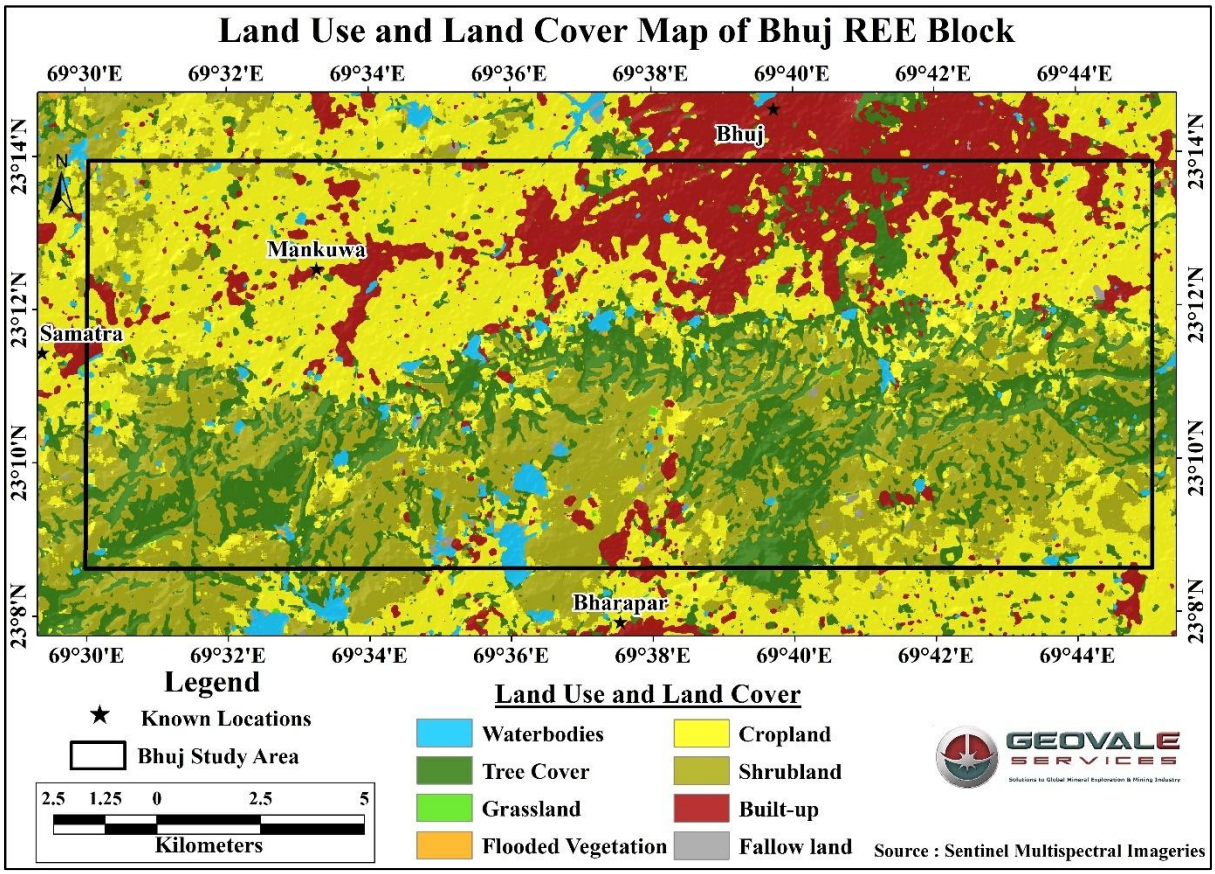

Fig. 3. 14 Land Use and Land Cover map of the Bhuj REE Prospect Block derived from Sentinel-2A imagery.

Exploration Relevance:

- Cropland and scrubland sectors with moderate slopes and sparse vegetation are the most suitable for soil and drainage-sediment sampling.
- Dense vegetation and irrigated fields require temporal adjustment of satellite data and sampling schedules to minimize biogenic influence.
- Built-up and infrastructural areas provide operational access points for field deployment and sample logistics.

The integrated LULC analysis thus supports both environmental evaluation and exploration planning by identifying zones of minimal anthropogenic disturbance and optimal sampling accessibility.

3.6. Exploration Design and Transition to Field Validation (Stage 2)

The comprehensive pre-field and desktop studies, encompassing the review of regional geology, analysis of National Geochemical Mapping Program (NGCMP) data, and the remote sensing interpretations detailed above, constituted Stage 1 of this exploration project. This

initial phase successfully delineated the Bhuj Block as a fertile area based primarily on the significant REE anomalies reported in the NGCMP stream sediment data, particularly associated with the Katrol Hill Fault and Median High structural zones. The convergence of these anomalous geochemical signatures with favourable geomorphic settings identified through terrain analysis led to the initial predictive hypothesis: the potential for ion-adsorbed, clay-hosted REE enrichment within the regolith and finer sedimentary fractions, possibly concentrated in valley fills and depositional plains adjacent to structural highs.

Based on these Stage 1 findings, a progressive, risk-filtered Exploration Design was formulated for the subsequent field-based stages (Stage 2 onwards), transitioning from surface verification to subsurface testing:

I. **Anomaly Validation:** Prioritize initial fieldwork to verify the location, magnitude, and nature of the reported NGCMP anomalies through targeted re-sampling and multi-fraction analysis. This critical step aims to establish a reliable geochemical baseline and confirm the reproducibility of legacy data.
II. **Fertile Zone Characterization:** Integrate validated geochemical data with the geomorphological and regolith maps derived from remote sensing to better define specific landscape positions (e.g., footslopes, residual soils, depositional traps) most conducive to the hypothesized REE adsorption or secondary accumulation mechanisms.
III. **Source Linking and Reconnaissance:** Conduct systematic geological traverses, regolith mapping, and broader stream sediment/soil sampling focused on linking observed surface REE distribution patterns to specific lithostratigraphic units (Bhuj, Katrol, Chari formations) and structural features, thereby testing the initial mineral system hypothesis and identifying potential primary sources or pathways.
IV. **Target Definition:** Synthesize the validated geochemical, geological, and geomorphic data to pinpoint localized, high-priority targets representing potential zones of significant REE enrichment (either adsorbed or detrital) suitable for initial subsurface testing (e.g., pitting, augering).
V. **Basin-Scale Integration:** Utilize the confirmed data and refined mineral system understanding from the Bhuj Block to develop an updated predictive REE fertility assessment, applicable to analogous stratigraphic-structural settings within the wider Kachchh Basin.

3.7. Initiating Stage 2: Data Validation Field Program

To operationalize this exploration design, the immediate next step forming the initial part of Stage 2, involved a structured **Data Validation field program**. This program was crucial for testing the core assumptions derived from the Stage 1 desktop analysis before launching

extensive ground surveys. The primary objectives were to confirm the reliability and understand the nature of the NGCMP-REE anomalies.

Execution of the stage 2 involves:

I. **Replication of NGCM Stream Sediment Data:** Systematically re-sampling stream sediment locations corresponding to the original NGCMP anomaly centroids. Analyzing multiple size fractions (specifically -125 µm and -40 µm) aimed to test the reproducibility of REE values and investigate the potential concentration in finer, clay-rich fractions versus coarser detrital fractions.

II. **Reconnaissance Stream Sediment Heavy Mineral Sampling:** Conducting heavy mineral panning and sampling across major drainages to identify potential detrital REE-bearing mineral sources (e.g., monazite, xenotime derived from specific lithologies) and differentiate between adsorbed REE signatures and heavy-mineral-hosted anomalies.

III. **Reconnaissance Bedrock Lithostratigraphy and Geochemistry:** Undertaking rapid geological traverses across key exposures of the Bhuj, Katrol, and Chari formations, collecting representative bedrock samples (ferruginous sandstones, shales, clays, laterites etc.) for geochemical analysis. This aimed to establish background REE levels in potential source rocks and directly test the hypothesis of significant ion-adsorbed REE potential within specific clay-bearing facies versus primary enrichment in other units.

The outcomes of this essential data validation program, which directly address the predictions and uncertainties arising from Stage 1, are detailed in the subsequent Chapter 4, forming the foundation for the broader geoscience investigations conducted during Stage 2 and Stage 3.

Chapter 4

Geoscience Investigations (Activity during the period)

Stage 2 and 3

4. Geoscience Investigations (Activity during the period):

This chapter details the core field-based geoscientific investigations undertaken during **Stage 2 (Validation and Re-orientation) and Stage 3 (Ground Surveys)** of the Bhuj REE exploration program. Building upon the predictive fertility analysis and initial mineral system hypothesis developed during the Stage 1 desktop studies (Chapter 3), these stages involved systematic on-ground data acquisition through geological mapping, geochemical sampling, and geophysical surveys. The primary aim was to validate the initial findings, refine the understanding of REE occurrences, identify controlling factors, and delineate specific targets within the Bhuj Block.

The exploration workflow commenced with the critical initial phase of **Stage 2** is a focused **Validation and Orientation Survey**. This survey was designed specifically to test the reproducibility of the legacy National Geochemical Mapping Program (NGCMP) REE anomalies and to evaluate the initial hypothesis favouring an ion-adsorbed clay-hosted REE model, which had emerged from the Stage 1 analysis.

However, the findings from this initial field validation proved pivotal, yielding results that contradicted the early assumptions based purely on legacy data and necessitated a fundamental re-evaluation of the applicable mineral systems and a significant redirection of the subsequent exploration strategy. The following sections detail this crucial validation survey and its unexpected outcomes, which led to a complete pivot in the exploration program's focus.

4.1. Stage 2a: Field Validation of Legacy Data and Outcomes

A field validation survey of the legacy data was undertaken as an integral component of the reconnaissance exploration program to evaluate the reproducibility and reliability of legacy datasets and to establish geochemical and mineralogical baselines for the Bhuj REE Prospect Block. The survey aimed to validate earlier findings of the National Geochemical Mapping Program (NGCMP) and other reconnaissance datasets (*refer to section 3.2.2*), which had indicated anomalous TREEY enrichments within the Mesozoic formations of the Bhuj region, particularly along the Katrol Hill Fault and Median High zones.

4.1.1. Methodologies of Legacy Data Validation Survey (Stage 2a)

The legacy data validation survey was undertaken to establish a comparative geochemical baseline for the Bhuj REE Prospect Block through the integration of field-based

sampling, granulometric separation, and analytical comparison with previously available datasets. A total of 54 stream sediment and regolith samples (*Fig.4.1; Annexure–I*) were collected, primarily from first- and second-order drainage channels distributed across the Chari, Katrol, and Bhuj formations. The verification sampling sites were systematically positioned near the centroids of 2 sq. km grid cells used in the earlier NGCM programme to ensure spatial equivalence with legacy data.

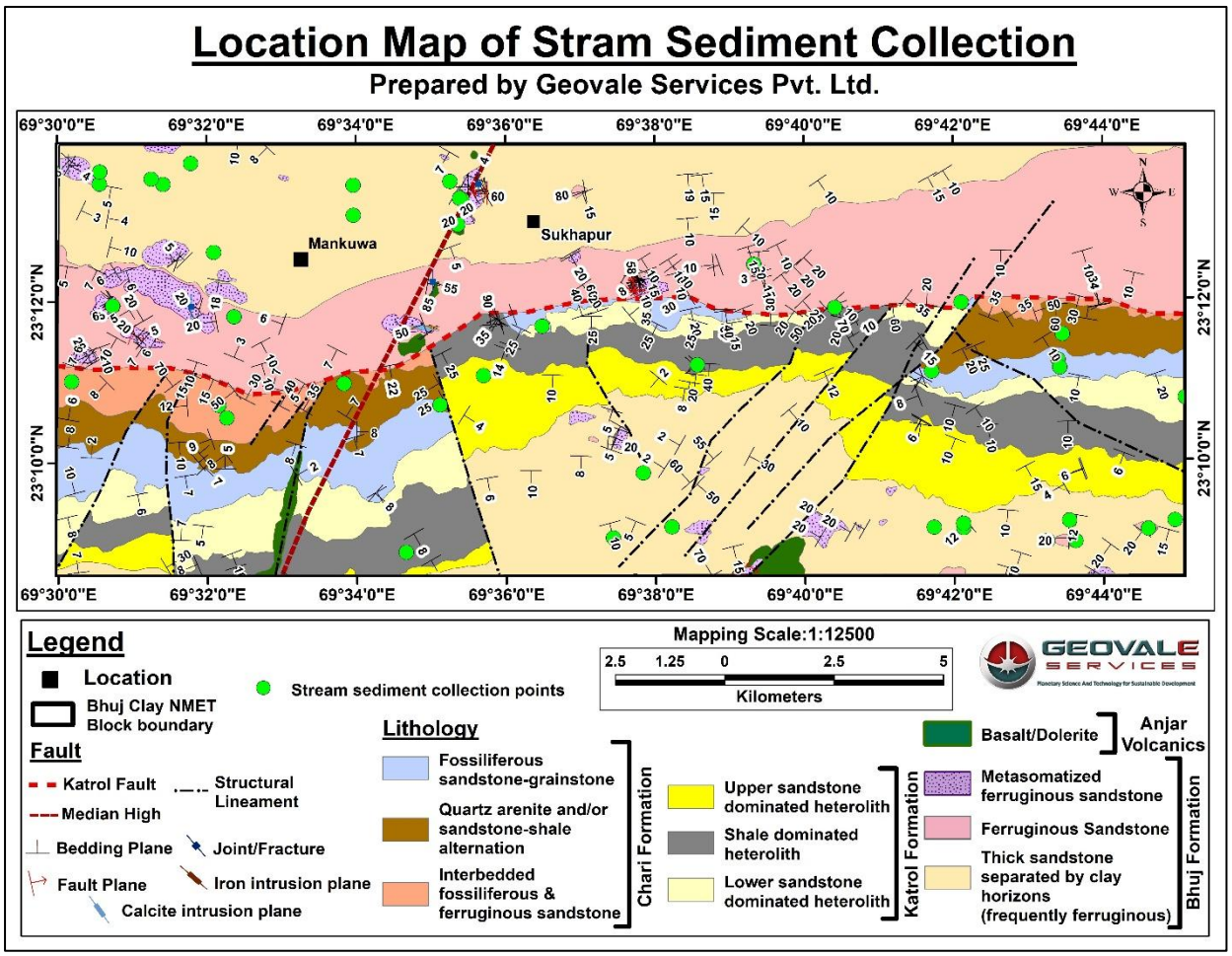

Fig. 4. 1 Spatial distribution of stream sediment collection points recorded during legacy data validation survey (stage 2a) and Orientation Survey (Stage 2b).

As discussed in *Section 1.6*, two possible sources for REE concentration were anticipated from the earlier geochemical results—(i) enrichment within heavy-mineral fractions, and (ii) adsorption or secondary concentration within fine clay fractions. To evaluate both possibilities, samples were selectively collected as <2 mm material from high-energy depositional regimes and <1 mm material from low-energy settings. Each bulk sample, averaging 5 kg, was subjected to both dry and wet sieving to achieve granulometric separation into two analytical fractions: -125 µm fraction, representing coarser detrital and heavy-mineral-bearing components, and -40 µm fraction, representing the finer clay-rich and adsorbed phase potentially enriched in REE. The -125-micron fraction was taken from the high

energy sediment samples whereas the -40micron samples were extracted from the low energy sediment samples.

A total of 42 samples, comprising twenty-one samples from each fraction were analyzed for rare earth element content (*Annexure–II - V*). Both fractions underwent closed-vessel acid digestion followed by analysis using X-ray Fluorescence (XRF) for major oxides and Inductively Coupled Plasma Mass Spectrometry (ICP-MS) for trace and rare earth elements. Analytical determinations were conducted at NABL-accredited laboratories, maintaining internal precision through duplicate analyses and certified reference materials.

The resulting assay data from the stream sediments were statistically processed and analysed to evaluate REE enrichment trends, anomaly coherence, and the fidelity of legacy anomalies.

4.1.2. Results and Analysis of Legacy Data Validation Survey (Stage 2a)

The legacy data validation survey produced distinct geochemical responses (*Annexure-II - V*) between the two analyzed fractions (-125 µm and -40 µm), reflecting grain size control on REE distribution across the Bhuj REE Prospect Block. A total of 42 processed samples were analyzed for TREEY concentrations, and the results were plotted spatially against the mapped lithological and structural framework (*Figs. 4.2 and 4.3*).

TREEY values for the -125 µm fraction range between 81 ppm and ~900 ppm, with an average of 364ppm. The overall distribution pattern shows low anomaly coherence /and subdued enrichment compared to the NGCM dataset (*Figs. 4.2*). Moderate values (200-500 ppm) are primarily recorded in drainages sourced from the southern and central sectors, particularly along the Bhuj and Katrol formations, while isolated higher readings (up to 898 ppm) occur near Sedata and Mankuwa, possibly reflecting localized detrital contributions from ferruginous or metasomatized sandstones. The general depletion in REE concentration within this fraction suggests dominance of coarse quartzofeldspathic detrital with limited REE-hosting mineral phases.

In contrast, the -40 µm (clay-rich) fraction exhibits comparatively higher TREEY concentrations, ranging between 174 ppm and ~1260 ppm (*Figs. 4.3*), with an average of 368 ppm. The highest value (1261 ppm) is recorded in the southern part of the block, within drainages derived from the Bhuj and Katrol formations. Moderately high TREEY values (500-700 ppm) are concentrated in the northwestern and southeastern sectors, displaying a broad parallelism with the structural trend and outcrop orientation of the metasomatized ferruginous sandstone of the Bhuj Formation. This spatial correspondence suggests that REE enrichment within the fine fraction may be controlled by secondary adsorption along ferruginized and clay-altered horizons developed under structurally guided conditions.

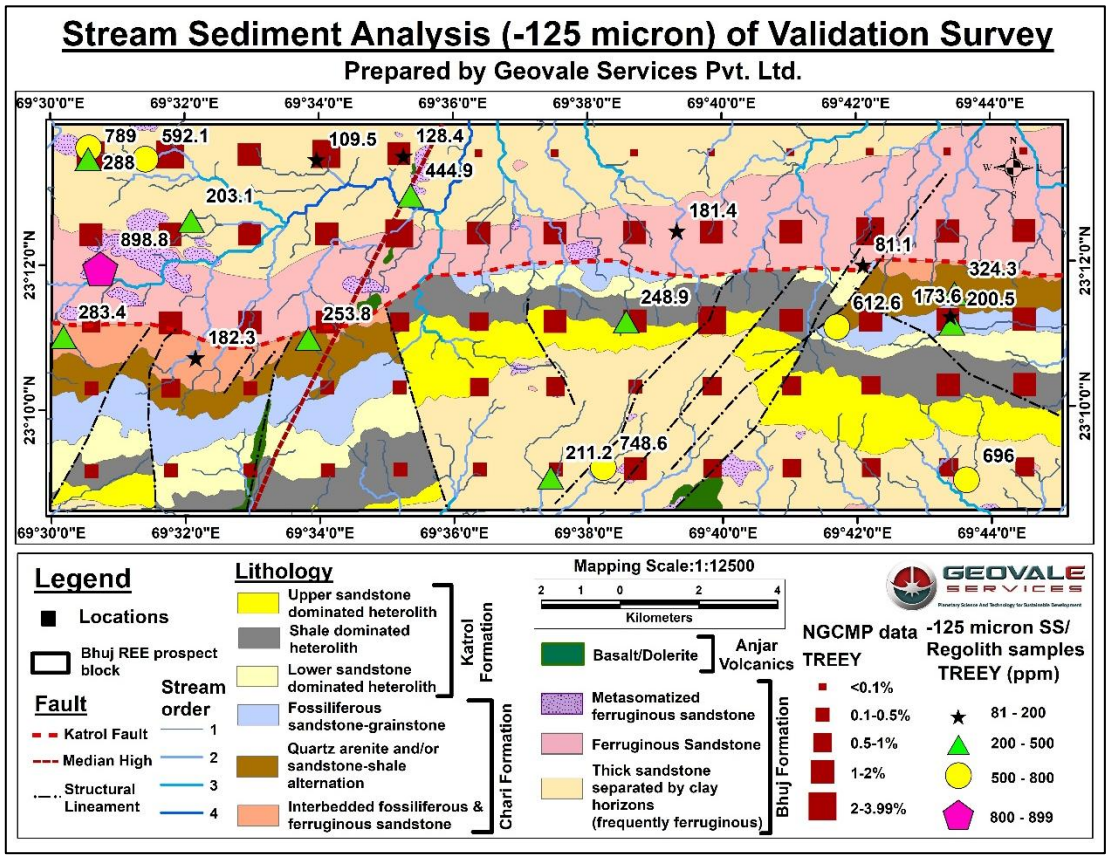

Fig. 4. 2 Spatial distribution map showing TREEY concentration in the -125 µm fraction of stream sediment and regolith samples from the legacy data validation Survey.

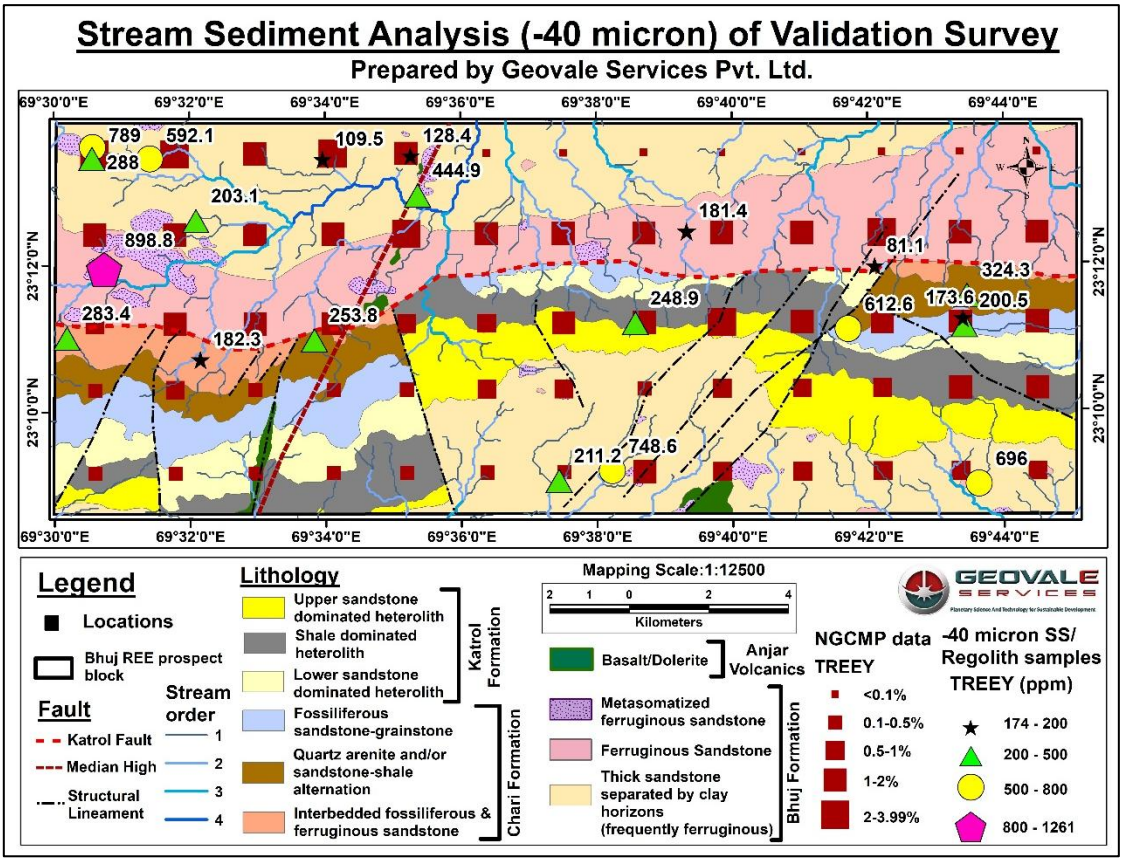

Fig. 4. 3 Spatial distribution map showing TREEY concentration in the -40 µm (clay-rich) fraction of stream sediment and regolith samples from the legacy data validation Survey over the Bhuj REE Prospect Block.

4.1.3. Outcome of Legacy Data Validation Survey (Stage 2a)

When compared with the NGCMP baseline dataset, results of the legacy data validation survey conducted by Geovale Services Pvt. Ltd. failed to replicate the magnitude of the legacy anomalies, which reported TREEY values exceeding 2-3 % in equivalent localities.

The subdued anomaly intensity observed in the present survey is attributed to the adoption of higher analytical precision, finer granulometric control, and robust QA/QC protocols. The discrepancy in assay magnitudes and anomaly locations between the NGCMP and Geovale surveys likely stems from either inherent lithological variability within the REE-bearing horizons or differences in sampling design. Notably, Geovale employed systematic centroid-based sampling over 2 sq. km grids, whereas the NGCMP approach composited four 1 sq. km samples to represent each 2 sq. km centroid, which may have diluted or spatially averaged localized anomalies.

Orientation Survey (Stage 2b): Tracking down the REE source horizon:

Although the Geovale's legacy data validation survey failed to replicate the high-amplitude anomalies of the NGCMP dataset, the persistence of above-crustal REE values concentrations across multiple formations substantiates the existence of a fertile geochemical system within the Bhuj Block. These outcomes warrant a reinterpretation of the exploration model under a Mineral Systems Approach (MSA) framework, emphasizing source-pathway-trap relationships rather than isolated geochemical anomalies. Accordingly, a systematic follow-up program was initiated to delineate the REE-hosting stratigraphic horizons through a two-pronged strategy:

(i) A systematic bedrock sampling across the whole stratigraphic sections, particularly in the catchment areas of high TREEY values, obtained in the orientation survey,

(ii) A systematic stream sediment sampling from lower-order streams in areas with high TREEY assays, obtained in the orientation survey.

4.2. Orientation Survey (Stage 2b) to Understand the Applicable Mineral Systems in the Bhuj Block

Following the outcomes of the validation survey program, a detailed orientation survey was undertaken to delineate potential REE-enriched horizons and to identify the stratigraphic and geomorphic controls on their distribution. The program was designed to advance the

exploration rationale established during the orientation phase by implementing a two-pronged strategy comprising (i) systematic bedrock sampling, and (ii) stream-sediment sampling followed by heavy-mineral analysis, aimed at establishing the spatial and genetic relationships governing REE enrichment within the Bhuj Block.

4.2.1. Methodologies of Orientation Survey (Stage 2b)

A systematic controlled sampling was to ensure representation across all major stratigraphic units and structural domains of the Bhuj REE Prospect Block.

A total of 35 bedrock samples were collected from fresh, unweathered exposures during the survey to evaluate the primary lithogeochemical background and assess potential sites of REE enrichment within the Chari, Katrol, and Bhuj formations. Sampling was conducted across key lithological units, identified during large scale geological mapping. Each sample was documented for GPS coordinates, lithological association, and structural setting prior to dispatch for laboratory analysis. Representative hand specimens were sent to NABL-accredited laboratories for major, trace, and rare earth element analysis using XRF and ICP-MS following acid digestion.

Stream sediment sampling was conducted in the catchments draining the stratigraphic intervals showing high TREEY values in the legacy data validation survey. Twenty new sediment samples were collected primarily from first and second-order streams to ensure proximity to source lithologies (*Annexure-I*). Approximately 5 kg of -2 mm material was collected per site after dry sieving in the field and subsequently processed in the laboratory to obtain the -125 µm fraction by wet sieving. A total of 32 samples including both new (collected during the present survey) and old (collected during orientation survey) samples were further processed at field laboratory for heavy liquid separation.

The -125 µm fraction was subjected to Heavy Liquid Separation (HLS) using bromoform (specific gravity 2.89 g/cm^3) to isolate the heavy mineral concentrate. The -125 µm fraction accounted for an average of 14 % (n = 45) of the bulk sample weight. Within this fine fraction, the weight % of heavy mineral content ranged from 0.01% to 6.3%, averaging 2.5% (n = 32). The recovered concentrates were dried, weighed, and split for binocular microscopic examination, isodynamic separation X-ray diffraction analysis and geochemical analysis. Approximately 5gm of each heavy-mineral concentrate was submitted to NABL-accredited laboratories for major, trace, and REE analysis using XRF and ICP-MS.

All analytical results were spatially integrated using GIS-based modelling to evaluate the relationship between geochemical enrichment, lithological variation, and structural controls, facilitating the interpretation of REE dispersion patterns and mineral system associations across the Bhuj Block.

4.2.2. Results and Analysis of Orientation Survey (Stage 2b)

The orientation Survey generated two complementary datasets: (i) bedrock geochemical assays and (ii) stream-sediment heavy-mineral analyses, each contributing to the delineation of REE-enriched zones and evaluation of stratigraphic and structural controls within the Bhuj REE Prospect Block.

A total of 35 bedrock samples were analyzed for major, trace, and rare earth elements (*Annexure–VI and VII*). TREEY values from the bedrock samples vary between 61 ppm and 1721 ppm, with higher to moderately high concentrations observed within ferruginous and metasomatized sandstone units of the Bhuj Formation; shale dominated heterolith unit of the Katrol Formation and fossiliferous sandstone-grainstone unit of the Chari Formation (*Fig. 4.4, Annexure- VI and VII*).

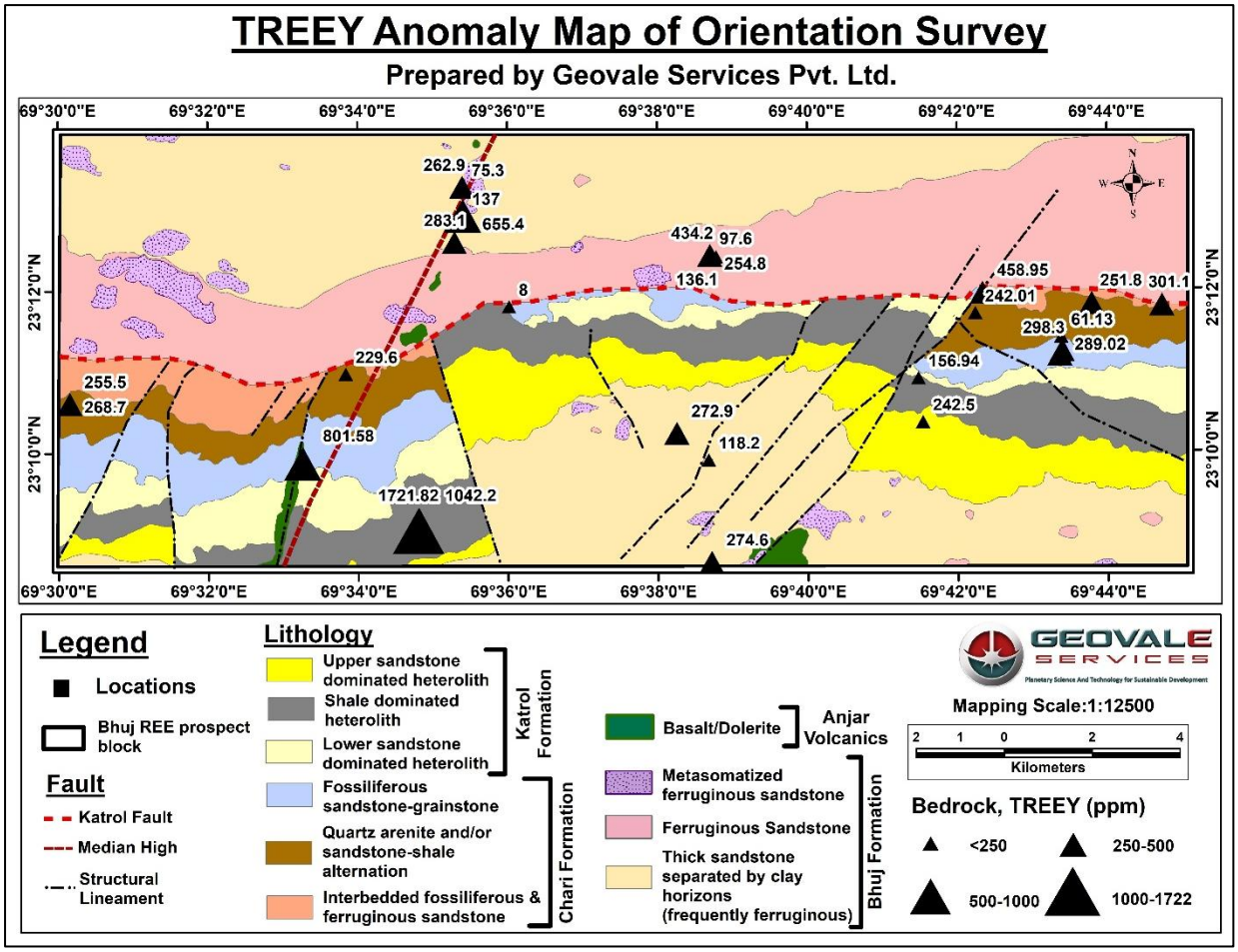

Fig. 4. 4 Spatial distribution of TREEY concentrations in bedrock samples collected during the orientation survey over the Bhuj REE Prospect Block.

A total of 32 heavy mineral concentrates were analysed for major oxides, trace and rare earth elements (*Annexure-X and XI*). The -125 µm heavy-mineral fraction from stream sediments reveals significant enrichment in REE-bearing and transition-metal phases

(*Table.4.1; Annexure–VIII and IX*) across the surveyed catchments. Highly anomalous major oxides contain Fe_2O_3 (18.2-45.4%, avg. 28%), TiO_2 (6.3-43.3%, avg. 23%), and P_2O_5 (0.5-3.1%, avg. 1.2%), reflecting the predominance of iron-titanium oxide and phosphate mineral assemblages like ilmenite, rutile, xenotime and monazite.

Among the major trace elements, the concentrates exhibit Zr (202-89,900 ppm, avg. 6145 ppm), Y (46-988 ppm), Nb (32-427 ppm), and V (181-1015 ppm), accompanied by subordinate concentrations of Cr (132-837 ppm), Zn (103-681 ppm) and Pb (35-520 ppm) (*Table.4.1*). Elevated Zr and TiO_2 contents corroborate the presence of zircon and ilmenite as key heavy-mineral constituents.

Table. 4. 1 List of anomalous chemical components of heavy-mineral concentrates from the -125 µm stream sediment fraction obtained through Heavy Liquid Separation (HLS).

	Fe_2O_3	P_2O_5	TiO_2(ilmenite+ rutile)
Avg. (n=32)	28%	1.2%	23%
	18.2-45.4%	0.5-3.1%	6.3-43.3%

Sc	Cr	V	Se	Y	Zr	Zircon	Nb	Sn	Zn	Pb
55 ppm	450 ppm	557 ppm	23ppm	409ppm	6145ppm	4.06	244ppm	18ppm	215 ppm	214 ppm
29.1-75.4	132-837	181-1015	2-121	46-988	202-89900	0.73-15%	32-427	2.6-30.2	103-681	33-520

La	Ce	Pr	Nd	Sm	Eu	Gd	Tb	Dy	Ho	Er	Tm	Yb	Lu
2614	5230	590.5	2047	349.2	14	288	27.4	102	15	36.4	4.3	25.8	4
173-7541	342-15147	41-1723	140-5896	24-991	1.7-33	21.5-796	2.1-71.3	9-250.5	1.5-37.4	4.1-90	0.5-11.6	3-71.6	<0.5-10.6

HREEY (0.1%)	TREEY (1.2%)
0.01-0.23%	0.1-3.4%

The REE chemistry indicates TREEY concentrations ranging from 0.1% to 3.4% (avg. 1.2%), with HREEY between 0.01% and 0.23% (avg. 0.1%). Among individual REE, the light rare earths are dominant followed by anomalous concentration of heavy rare earth elements. Spatially, the higher TREEY concentrations correspond to drainages sourced from the sandstone of the Bhuj Formation and the Katrol Formation (*Fig. 4.5*). These zones display parallel trends between the structural alignments and the anomaly clusters, suggesting both lithological and structural control on the REE dispersion within the Bhuj block.

The compositional spectrum thus confirms that the Bhuj Basin sediments are enriched in both REE-bearing and Fe-Ti oxide minerals. The co-enrichment of Fe_2O_3, TiO_2, and P_2O_5 with Zr, Pb, Zn, Cr and REE imply that REE enrichment within the Bhuj Basin likely evolved through

a hybrid mineral-system interaction, wherein zircon, xenotime, and monazite were introduced as detrital constituents, while Pb, Zn, TiO_2, and REE were subsequently added or remobilized through volcanic and/or hydrothermal processes.

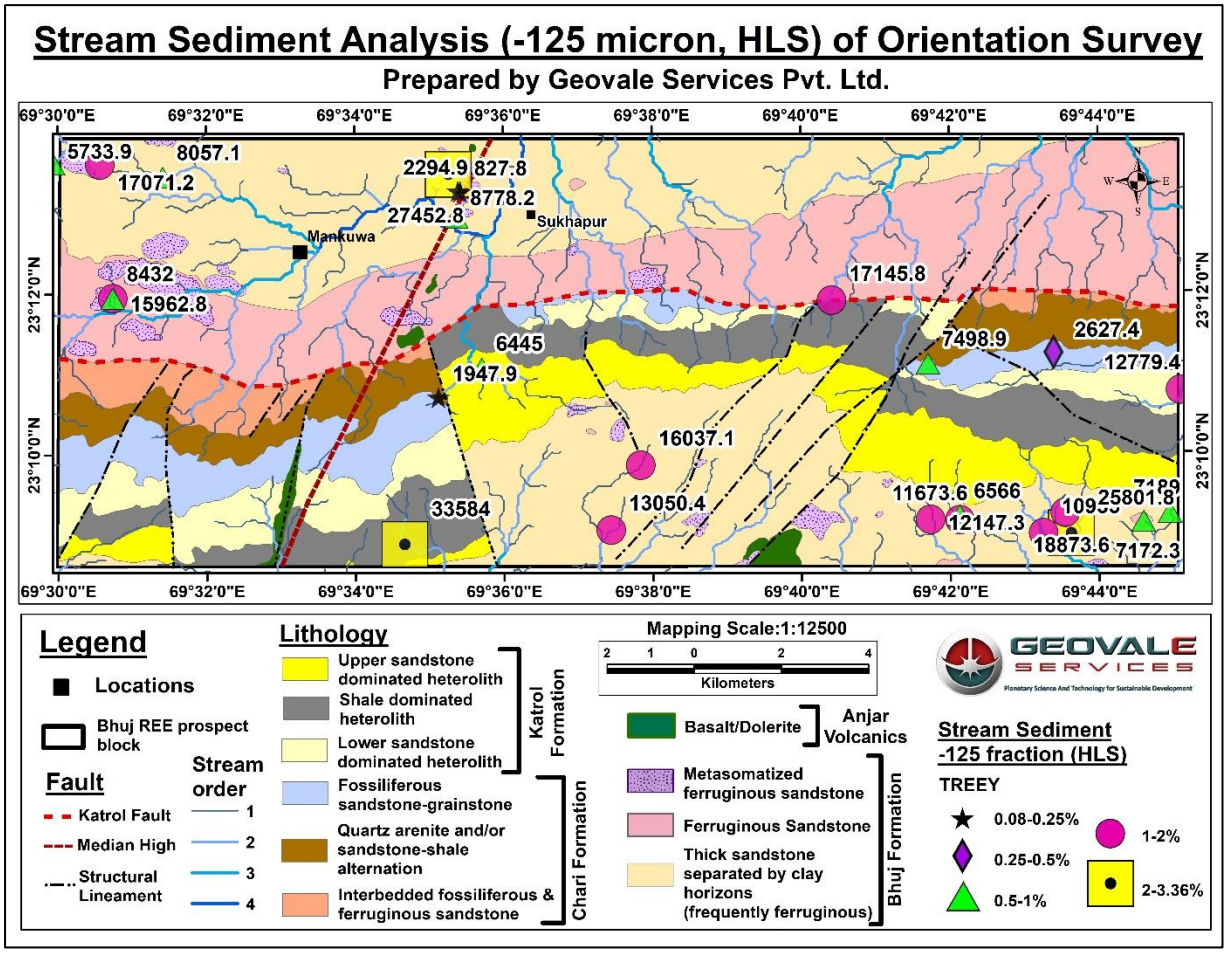

Fig. 4. 5 Spatial distribution of TREEY concentrations in the -125 µm heavy-mineral fraction obtained through Heavy Liquid Separation (HLS) of stream sediment samples from the Bhuj REE Prospect Block.

Binocular Microscopy of Heavy Mineral Concentrates

Microscopic examination of the heavy mineral separates from the -125 µm fraction of stream sediments derived from the Bhuj Formation reveals a diverse assemblage of detrital and authigenic mineral phases (*Fig. 4.6*). The dominant heavy minerals identified under reflected and transmitted light include zircon (Zr), monazite (M), xenotime (Xe), rutile (R), ilmenite (Il), and rare grains of rutile–ilmenite intergrowths (Rf). Zircon occurs as well-rounded to sub-angular grains with high relief and vitreous lustre, occasionally exhibiting concentric zoning, suggesting multiple sedimentary recycling episodes. Monazite and xenotime appear as sub-rounded, yellowish to brownish grains with distinct resinous lustre and are locally associated with ilmenite and hematite coatings, implying partial surface alteration or

secondary Fe-oxide impregnation. Ilmenite and rutile are abundant, forming dense opaque grains. The high concentration of Fe-Ti oxides corresponds to the elevated Fe_2O_3 and TiO_2 values observed in the chemical dataset.

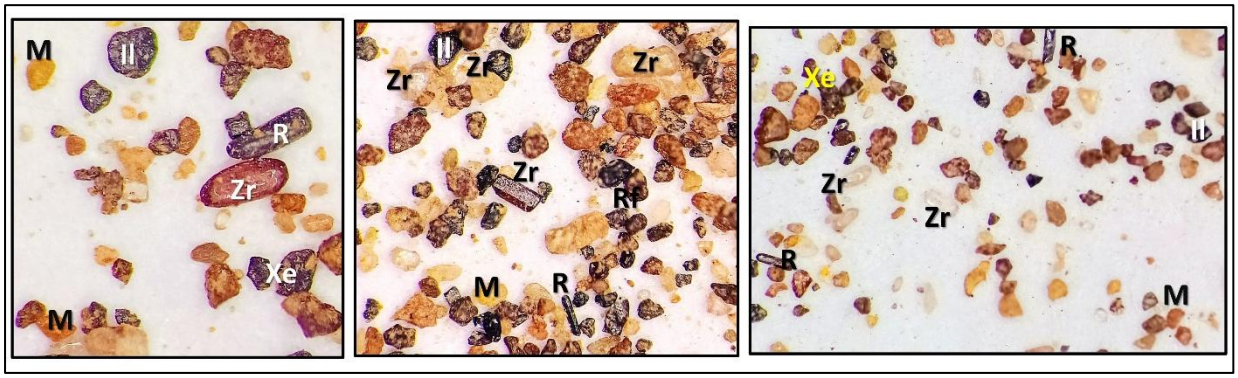

Fig. 4. 6 Binocular photomicrographs of the heavy mineral concentrates (-125 µm, HLS fraction) of the stream sediments.

Overall, the binocular mineralogical evidence supports the geochemical data, confirming that the sediments host a mixed assemblage of REE-bearing and Fe-Ti-oxide minerals.

X-Ray Diffraction (XRD) Analysis of Heavy Mineral Concentrates

XRD examination of 21 samples of the -125 µm bulk and isodynamically separated heavy liquid separates (*Annexure-X*) confirms the presence of a diverse suite of detrital and authigenic mineral phases dominated by quartz, zircon, rutile, anatase, ilmenite and hematite, with variable proportions of kaolinite, goethite, and feldspar as minor constituents. Several samples, particularly those derived from ferruginous and metasomatized sandstones of the Bhuj Formation, exhibit trace occurrences of apatite, gorceixite/goyazite, and florencite, indicating the presence of REE-bearing phosphate minerals. In isodynamically separated magnetic fractions, accessory magnetite, garnet, tourmaline, and pyroxene are also recorded, signifying a complex paragenetic assemblage involving both sedimentary detrital input and post-depositional metasomatic alteration. The coexistence of Zr-Ti oxides with REE phosphates further substantiates the dual enrichment mechanism inferred from the geochemical dataset, reflecting a hybrid mineral system combining stratiform sedimentary REE concentration with hydrothermal-metasomatic overprinting.

4.2.3. Outcome of Orientation Survey (Stage 2b)

The orientation survey results reaffirmed the presence of REE-enriched horizons across multiple stratigraphic levels within the Bhuj REE Prospect Block, validating the exploration rationale established during the orientation phase. Integration of bedrock and stream-sediment data provides new insights into the stratigraphic, mineralogical, and genetic controls

of REE enrichment across the Chari, Katrol, and Bhuj formations.

Bedrock Analysis:

Geochemical assay of bedrock samples indicates that phosphatic ferruginous shale layers (suspected tuffite) within the shale-dominated heterolith unit of the Katrol Formation consistently record TREEY contents above 0.1%, particularly in the southern part of the block. These beds are typically 2–8 cm thick, fine-grained, and occur repetitively in the sucession with lateral extension over several hundred metres along the strike. Their lithological association and stratigraphic position within fine-grained, laminated facies suggest deposition in a low-energy, shallow-marine environment, conducive to the accumulation of Fe-P-REE bearing phases.

In contrast, fossiliferous sandstones of the Chari Formation yield moderate TREEY concentrations (400-800 ppm), but the mineralization is sporadic and stratigraphically discontinuous, indicating limited vertical and lateral persistence of REE-hosting beds.

The metasomatized ferruginous sandstone of the Bhuj Formation shows TREEY values between 400–700 ppm, reflecting secondary REE enrichment, possibly linked to post-depositional ferruginization and metasomatic fluid activity, particularly along structurally reactivated zones adjoining the Katrol Hill Fault and Median High.

Stream Sediment Analysis:

Heavy-mineral separation of the -125 µm stream-sediment fraction reveals TREEY concentrations ranging from 0.08% - 3.36%, with the highest anomalies detected within drainages derived from the Bhuj and Katrol formations. Sediments from catchments of the ferruginous shale-bearing Katrol beds exhibit the highest enrichment (35584 ppm), consistent with the geochemical signature of Fe-P-REE-bearing lithologies observed in outcrop. In contrast, drainages sourced from Bhuj Formation ferruginous and metasomatized sandstones display highly anomalous REE values (up to 25,801ppm), accompanied by elevated Fe_2O_3, TiO_2, P_2O_5, and Zr suggesting local reworking and concentration of REE-bearing heavies such as monazite, xenotime, and zircon. The observed co-enrichment of Fe, Ti, Zr, Pb, Zn, Cr, Co, Sn and REE in heavy-mineral separates points to a hydrothermal input to the sediments, further corroborating a mixed genetic system, combining detrital input from stratiform REE-bearing units with hydrothermal remobilization and metasomatic redistribution.

The binocular microscopy and XRD analyses of the heavy concentrates also validate the geochemical results, confirming the presence of REE-bearing phosphate minerals (monazite, xenotime, florencite) and Fe-Ti oxide assemblages (ilmenite, rutile, hematite, magnetite) within the stream sediments. These mineralogical signatures substantiate the dual mineralization model as of the geochemical data interpretation of the Bhuj REE Prospect

Block.

4.2.4. Identification of Two New Mineral Systems in the Bhuj Block

The occurrence of anomalous polymetallic enrichment, coupled with REE anomalies across multiple stratigraphic levels, underscores a basin-wide geochemical fertility within the Bhuj REE Prospect Block. The integrated evaluation of geochemical, mineralogical, and stratigraphic datasets from the orientation phase confirms the coexistence of two distinct REE mineral systems in the area.

1. **Katrol Stratiformal REE-bearing System:**

Syngenetic REE mineralization hosted within ferruginous phosphatic shale beds of the Katrol Formation. This system is interpreted as stratiform-sedimentary in origin, developed within a shallow-marine, Fe-P-enriched depositional environment, with REE fixed within authigenic and diagenetic phases (e.g., Fe-oxides, apatite, and minor monazite).

2. **Bhuj Potential IOCG-type Mineralization:**

A structurally controlled hydrothermal-metasomatic system associated with the ferruginized and metasomatized ferruginous sandstone of the Bhuj Formation. This system exhibits Fe-Ti-P-REE enrichment, with significant concentrations of Sc, V, Cr, Co, Cu, Zn, Pb, In, Sn, Sb, Cs, Ta, Tl and TREEY, as revealed from HLS and ICP-MS analyses of stream-sediment concentrates. The mineralogical assemblage (hematite-ilmenite-rutile-monazite-xenotime-zircon-tourmaline-magnetite-pyroxene-amphibole) and spatial association with regional fault systems (Katrol Hill Fault and Median High) are consistent with IOCG-type processes of mineralization.

4.2.4.1. Mineral Systems 1: Katrol Stratiformal REE-bearing System

The validation and orientation surveys confirm that the Katrol Formation hosts REE mineralization within its ferruginous-phosphatic shale horizons of shale dominated heterolithic unit, deposited in a low energy marine environment.

The genesis of REE enrichment within these beds can be attributed to syn-depositional metal scavenging processes operating in an Fe-P enriched marine environment. Since REE concentrations in seawater are typically very low, an efficient scavenging mechanism is essential for their accumulation. Hydrothermal inputs, possibly linked to contemporaneous volcanic activity, likely supplied iron into the seawater in the form of dissolved ions and colloidal complexes. The precipitated Fe (oxy)hydroxides acted as effective scavengers, adsorbing REE and other metals onto their surfaces, during sedimentation. Over time, this process facilitated the enrichment of REE within ferruginous shale beds.

During diagenesis, the unstable Fe (oxy)hydroxides transformed into Fe-smectite, whose structure could no longer retain the adsorbed REE. Concurrently, formation of any phosphatic minerals (e.g., apatite–gorceixite–florencite group) may incorporated the released REE into their crystal lattices. This diagenetic transfer led to the development of syngenetic to early diagenetic REE-bearing ferruginous-phosphatic shale horizons, marking the transformation of adsorbed marine REE into mineral-bound forms. Thus, the boundary conditions for sub-sea REE enrichments in sedimentary layers are as follows:

I. Presence of a source of REE supply, likely a felsic volcanism
II. A concomitant supply of Fe in the sea water and
III. Presence of a phosphatic horizon in spatial association of Fe-rich layers to incorporate REEs in the phosphatic structures.

From validation and orientation survey it has been appeared that the boundary conditions necessary for such REE enrichment was satisfied within the Katrol depositional regime:

I. Presence of REE source: Presence of tuffite (suspected during the reconnoitry fieldwork) indicates an active volcanic contribution contemporaneous with sedimentation, acting as the REE source.
II. Concomitant supply of Fe to seawater: The ferruginous character of the shale reflects sustained Fe influx, likely of hydrothermal or diagenetic origin, facilitating the adsorption and fixation of REE.
III. Phosphatic horizons as traps: High P_2O_5 content (~7-12.6%) of the REE rich ferruginous shale beds suggest effective incorporation of REE into phosphate lattices during diagenesis.
IV. Stratigraphic repetition and lateral persistence: Recurrent phosphatic ferruginous shale horizons within the Katrol Formation signify repeated depositional and enrichment events under similar boundary conditions generating a stratiform nature of mineralization.

Collectively, these characteristics define a stratiform REE system comparable to exhalative-sedimentary (SEDEX-type) or volcanogenic sediment-hosted REE deposits. The inferred genesis involves the interplay of volcanic exhalation, Fe-P chemical precipitation, and early diagenetic fixation of REE within phosphatic phases. The Katrol Formation, therefore, represents a syngenetic REE system, where REE concentration is governed primarily by volcano-sedimentary processes, hydrothermal exhalations and diagenetic reworking of Fe-P rich marine sediments. This system thus warrants detailed stratigraphic, petrographic, and geochemical characterization to delineate and model the mineralized horizons.

4.2.4.2. Mineral Systems II: Potential IOCG-type Mineralisation

The orientation survey including bedrock analysis and stream sediment analysis indicate

that the Bhuj Formation hosts a distinct phase of REE and critical metal enrichment. The high TREEY and multi-element concentrations recorded in heavy mineral separates derived from first and second order stream sediments draining the Bhuj Formation point to a secondary mineralization process. Two possible genetic interpretations are considered to explain the enrichment pattern observed in these sediments.

i. Palaeoplacer Origin:

One possible source of REE enrichment could be paleoplacer accumulation of REE-bearing heavy minerals within specific sandstone layers of the Bhuj Formation. Such a mechanism would involve the mechanical concentration of resistant accessory minerals, during sedimentation under high-energy fluvial to marginal-marine conditions. However, field verification and stratigraphic sampling across multiple sandstone units failed to identify any distinct layers containing REE-rich heavy mineral concentrations characteristic of palaeoplacer deposits. The absence of localized heavy-mineral seams or laminae suggests that the observed REE enrichment in the Bhuj Formation cannot be attributed solely to mechanical concentration processes.

ii. Hydrothermal Origin:

The second and more plausible explanation involves hydrothermal fluid activity and Fe-rich metasomatism associated with regional structural features, particularly along the Katrol Hill Fault (KHF) and related subsidiary faults along with the Median High zone. These structurally aligned zones display intense ferruginization of the host sandstone, accompanied by enrichment in Fe_2O_3, TiO_2, P_2O_5, and TREEY, as well as in transition and critical metals such as V, Cr, Co, Ni, Cu, Zn, and Pb. The alteration assemblage, characterized by hematite-ilmenite-rutile-magnetite with apatite and REE phosphates (monazite, xenotime), as evidenced from the petrographic and mineragraphic study (XRD) of the stream sediments, strongly indicates the operation of an Fe-oxide hydrothermal system.

These features, coupled with the spatial correlation between REE anomalies and structurally controlled Fe-metasomatic zones, point toward a hydrothermal-metasomatic genesis of mineralization. The alteration characteristics and metal association are consistent with Iron Oxide Copper Gold (IOCG)-type systems, wherein Fe–oxide alteration acts as a carrier for REE and critical metals. In this context, the Bhuj ferruginous and metasomatized sandstones represent the hydrothermal expression of an Fe-oxide-REE system, formed through post-depositional fluid migration and chemical replacement of the primary sandstone framework.

Overall, the Bhuj Formation exemplifies an epigenetic Fe-Ti-REE system of IOCG affinity, where structurally controlled fluid pathways facilitated metal mobilization, Fe-metasomatic alteration, and REE precipitation within permeable sandstone horizons. Further

facies mapping, petrographic and geochemical investigations are warranted to constrain the mineral paragenesis and fluid evolution associated with this hydrothermal event.

4.3. Exploration Model Adopted Corresponding to the Mineral Systems

The orientation results established two distinct REE mineral systems within the Bhuj REE Prospect Block. The exploration strategy for each system has been formulated based on their respective lithological, structural, and geochemical controls, aiming to refine target delineation and guide future detailed investigation.

4.3.1. Exploration Model Corresponding to Mineral Systems I: Katrol Stratiformal REE-bearing System

The exploration approach for this system focuses on delineating stratigraphically controlled ferruginous-phosphatic shale horizons and establishing their REE enrichment pattern within the Katrol Formation. Key strategies include:

i. High-resolution stratigraphic mapping, lithological characterization, measurement of stratigraphic succession and correlation of ferruginous shale units across measured sections.

ii. Channel sampling along lithological contacts to quantify REE enrichment trends and vertical variation.

iii. Integration of geochemical data with sedimentological data to reconstruct depositional settings and model REE distribution within the stratiform horizons.

4.3.2. Exploration Model Corresponding to Mineral Systems II: Potential IOCG-type Mineralization

The IOCG exploration model targets structurally controlled Fe-oxide rich zones within the Bhuj Sandstone, emphasizing hydrothermal alteration and Fe-oxide development along major fault corridors. The proposed work plan includes:

i. Mapping of fault zones, breccia bodies, and Fe-oxide veins along the Katrol Hill Fault and adjoining areas to delineate alteration corridors.

ii. Petrographic and mineralogical investigation to identify hydrothermal alteration halos.

iii. Geochemical vectoring through multi-element analyses (Fe, Cu, Co, Ni, REE) to pinpoint fluid pathways and potential mineralized zones.

iv. Application of geophysical surveys (VES) to detect subsurface Fe-oxide bodies potentially associated with IOCG-type mineralization.

4.4. Stage 3: Detailed Ground Survey in the MSA Framework

The pivotal outcomes of the Stage 2 validation and orientation surveys necessitated a fundamental shift in the exploration strategy. Having refuted the initial ion-adsorbed clay hypothesis and instead identified two distinct potential mineral systems, Mineral System I (Katrol Stratiformal REE-bearing System) and Mineral System II (Bhuj Potential IOCG Mineralization System), the exploration program transitioned into Stage 3: Detailed Ground Surveys. This stage was designed to systematically investigate the geological context, spatial extent, and characteristics of these newly defined systems within the Bhuj Block, guided by the specific exploration models developed for each (*refer to section 4.6*).

The primary objective of Stage 3 was to move beyond reconnaissance-level anomaly identification towards delineating specific fertile tracts and potential mineralized targets associated with each system. This involved a multi-disciplinary approach integrating detailed surface observations with targeted geochemical and geophysical methods. The foundational component of this stage was a comprehensive large-scale geological mapping campaign across the entire block, supplemented by detailed lithological, structural, and petrographic characterization. The findings from this mapping effort, detailed in the following sections, provided the essential geological framework for interpreting subsequent geochemical and geophysical datasets and ultimately vectoring towards prospective zones for target testing (Stage 4).

4.5. Geology of the Block

The geological investigation of the Bhuj REE Prospect Block aimed to establish the lithostratigraphic framework, structural configuration, and lithological variability of the exposed Mesozoic succession, with particular emphasis on identifying potential REE-fertile lithology.

Building on the regional synthesis, detailed geological investigations were undertaken within the Bhuj REE Prospect Block to document lithological variability, structural architecture, and surface alteration (if any) relevant to REE mineralization. The study area encompassing an area of approximately 252 sq.km, lies within the southern sector of the Kachchh Mainland Uplift and exposes the Chari, Katrol and Bhuj Formations, locally intruded by basic dykes. This block-scale work forms the core of the NMEDT-funded reconnaissance exploration, providing the empirical basis for subsequent petrographic, geochemical, and geophysical integration.

4.5.1. Large Scale Geological Mapping (1:12500)

A comprehensive large-scale geological mapping of the Bhuj REE Prospect Block was carried out on a 1:12,500 scale, aimed at delineating lithological units, stratigraphic boundaries, and structural controls governing mineralization. The mapping was conducted using standard geological field techniques, including handheld GPS-assisted traverses, stratigraphic profiling, and litho-contact tracing.

A total of 466 field observation points (*Fig. 4.7; Annexure-XI*) were systematically recorded across the 252 sq. km block to ensure comprehensive lithological and structural coverage. Each observation point included detailed information on lithology, sedimentary structures, bedding attitudes, fracture patterns and visible mineralization indicators (if any). Locations were georeferenced using handheld GPS units, and all spatial data were subsequently integrated within a GIS environment for digital compilation and analysis.

The lithologies of the Bhuj project area exhibit significant heterogeneity, both in composition and structural attributes. Field observations during the large-scale mapping program have enabled the categorization of the exposed lithounits into three major formations, intruded by basic rocks, correlated with the Anjar Volcanics. The stratigraphic classification, delineated from lithologic mapping, follows the established formation hierarchy of the region, comprising the Chari, Katrol, and Bhuj formations. This stratigraphic framework is based on classical lithostratigraphic nomenclature proposed by *Rajnath (1932)* and later modified by *Biswas (1977, 1987, 2005; Table. 4.2).*

Table. 4. 2 Stratigraphic Classification of the Bhuj REE prospect block (after Rajnath, 1932; Biswas, 1977).

Stratigraphic unit		Age	Lithology
Rajnath, 1932	Biswas, 1977		
Deccan Trap		~67-65 Ma Uppermost Cretaceous	Basalt, tholeiitic, minor alkalic basalt
Umia Series	Bhuj Formation	Jurassic Cretaceous boundary (149-145 Ma)	Sandstone-shale in the lower part, succeeded by glauconitic sandstone, sandstone-claystone
Katrol Series	Jhuran Formation	Late Jurassic	Predominantly dark grey to black shale in the lower part, interbedded with ferruginous sandstone and micaceous siltstone and shale
Chari Series	Jhumara Formation	Middle part of Upper Jurassic ~155 Ma -~149 Ma	Olive green shale, succeeded by sandstone, limestone with golden oolites, and shale

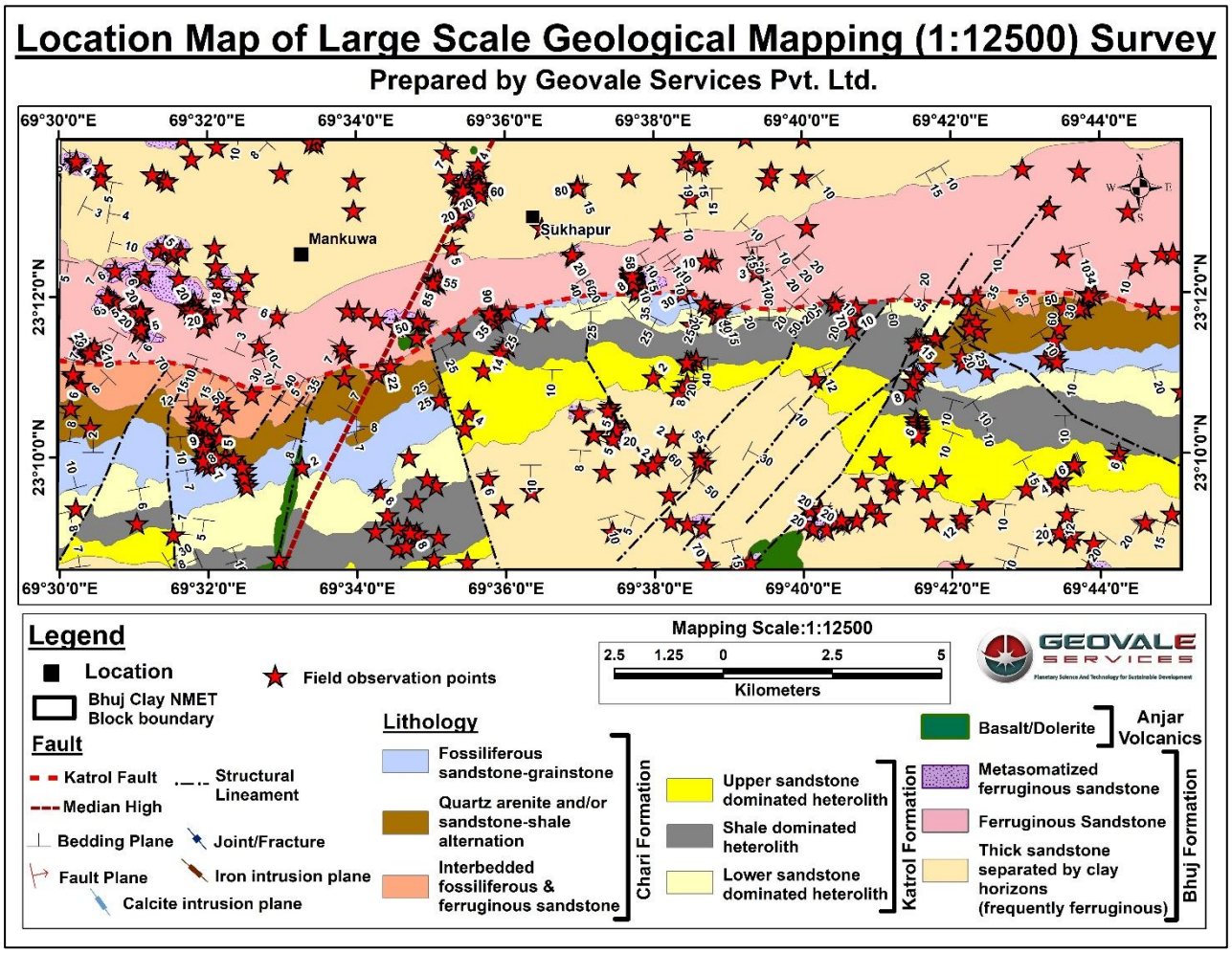

Fig. 4. 7 Spatial distribution of 466 geological observation points recorded during large-scale mapping of the Bhuj REE Prospect Block, illustrating the systematic coverage and lithological control across the 252 sq. km exploration area.

4.5.2. Lithological Characterization of the Block Area

The lithological succession within the Bhuj REE Prospect Block encompasses a range of marine to marginal-marine and shallow-clastic facies, represented by Chari, Katrol, and Bhuj formations, arranged in ascending stratigraphic order (*Fig.4.8; Plate I*). Each formation exhibits distinctive lithological characteristics that define the geological architecture of the block. The following sub-sections describe their representative field attributes, stratigraphic disposition, and lithological variability as documented by ground observations during the large-scale geological mapping across the study area.

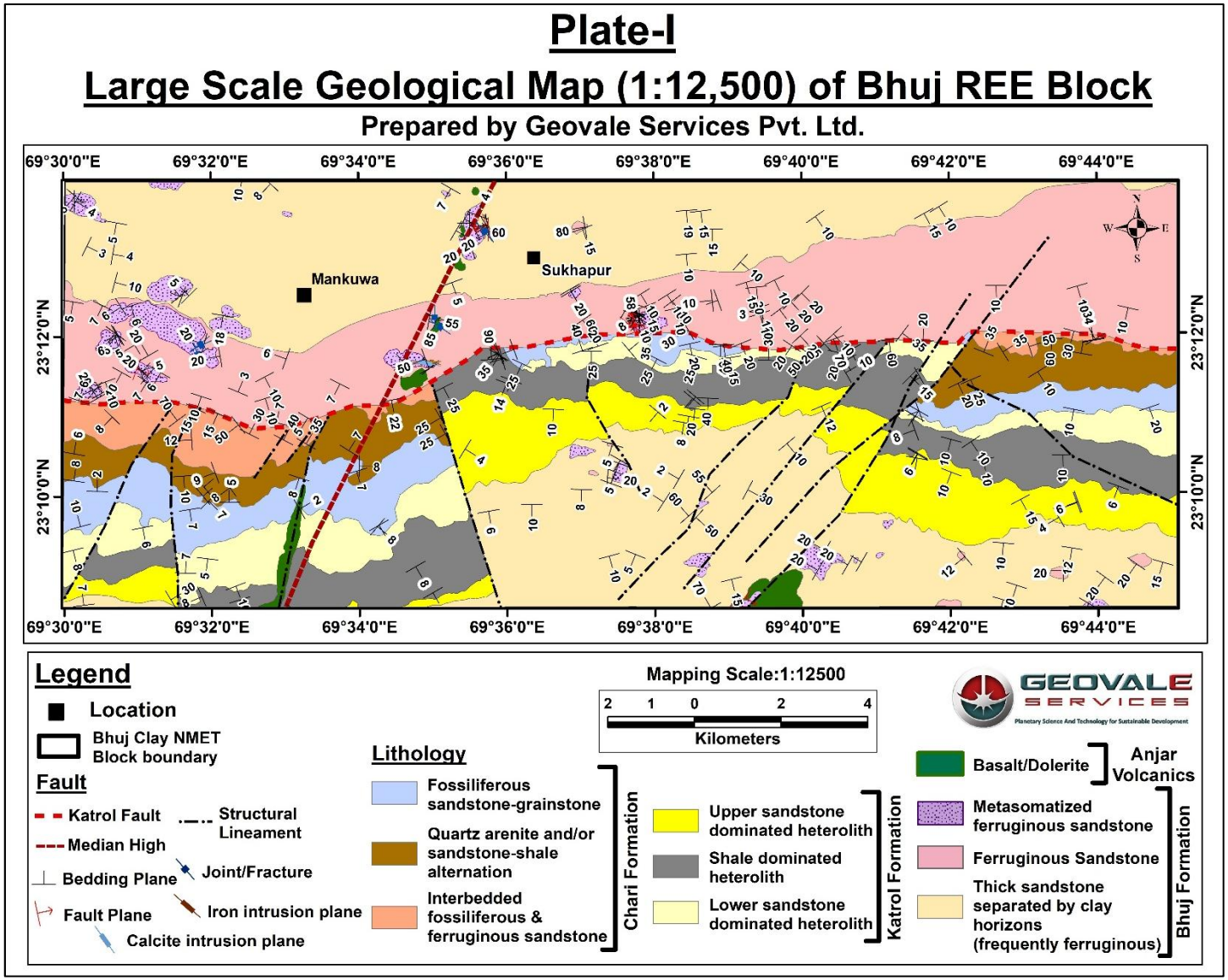

Fig. 4. 8 Large-scale geological map (1:12500) of the Bhuj REE Prospect Block across parts of the toposheet no. 41E/12, in and around Bhuj, Gujarat. The map shows the principal lithological units, stratigraphic boundaries and structural features of the block. This map is prepared by Geovale Services Pvt. Ltd. (Plate I).

Chari Formation:

The Chari Formation is exposed in limited outcrops in the north-central part of the block, immediately south of the Katrol Hill Fault, around the Sedata and Kera areas. The exposures occur as low to moderately elevated hills forming distinct topographic highs, where bedrock is well exposed and attains a maximum observed thickness of approximately 40-60 m. The formation comprises three major lithounits, arranged in stratigraphic descending order:

(i) interbedded fossiliferous and ferruginous sandstone unit,
(ii) sandstone and sandstone-shale association, and
(iii) fossiliferous sandstone and/or limestone-oolitic grainstone unit.

The ferruginous sandstone is generally coarse- to medium-grained, showing impregnation of iron oxides either as cross-cutting veins (*Fig.4.9a*) or as layers conformable with stratification and/or stratigraphy. These horizons are frequently interbedded with fossiliferous sandstone (*Fig.4.9b, c*), imparting a reddish-brown hue to the outcrops. The fossiliferous sandstone locally contains burrows infilled with chert and impressions of bivalves and cephalopods.

Fig. 4. 9 Field photographs showing ferruginous and fossiliferous sandstone unit of the Chari Formation: (a) iron-oxide impregnation forming cross-cutting veins within coarse grained ferruginous sandstone; (b) Fossiliferous sandstone beds showing a reddish-brown hue to the outcrops and impression of bivalve; (c) Hand speciment of fossiliferous sandstone displaying strong iron impregnation, bivalve fossils and burrow fills with carbonate and chert.

The intermediate unit occurs either as thick quartzose sandstone or as sandstone–shale alternations. The sandstone is coarse to medium grained and internally exhibits planar-parallel to planar cross-stratification, and in places, wave-ripple lamination (*Fig.4.10a*). The heterolithic units are characterized by centimetre to decimetre-scale laminated sandstone separated by millimetre-thick shale partings, are also present (*Fig.4.10b*). The shale is white to grey to greenish grey, thinly laminated, fissile, and locally calcareous.

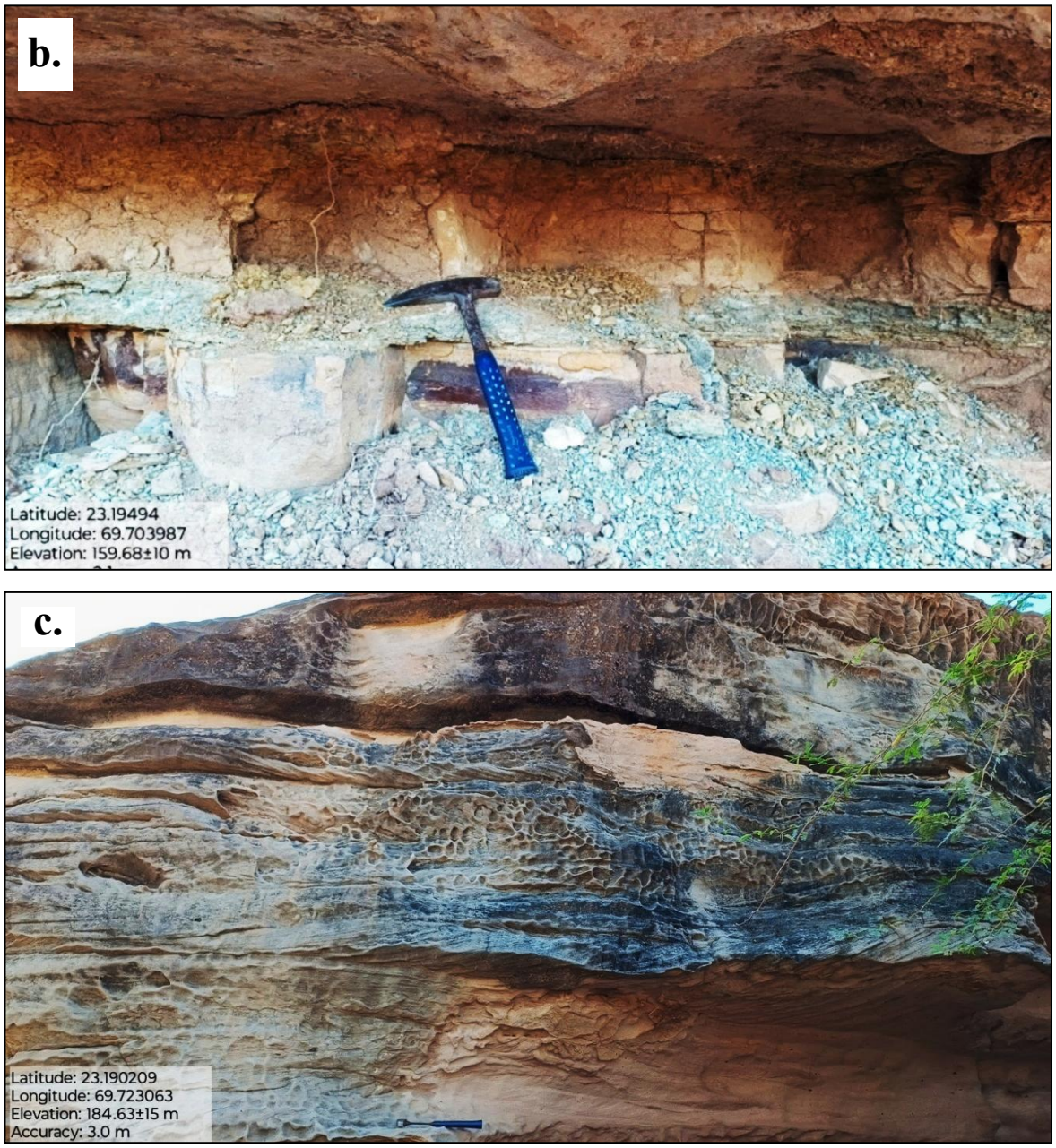

Fig. 4. 10 Representative outcrops of the intermediate member of the Chari Formation: (a) Thick occurrence of massive coarse to medium grained quartzose sandstone; (b) heterolithic unit showing decimetre-scale sandstone, separated by greenish grey shale; (c) Planar cross stratified sandstone unit.

The upper unit comprises fossiliferous sandstone and limestone facies, containing well-preserved bivalve and cephalopod impressions, along with chert-filled burrows. Interbeds of oolitic grainstone (*Fig. 4.11a*), fossiliferous limestone, and calcareous to gypseous shale (*Fig. 4.11b*) form a heterogeneous assemblage of carbonate and siliciclastic facies. The limestones are grey to buff, compact, and fossiliferous, commonly enclosing ammonite casts and shell debris, while the calcareous shale is laminated, fissile, and friable in weathered exposures.

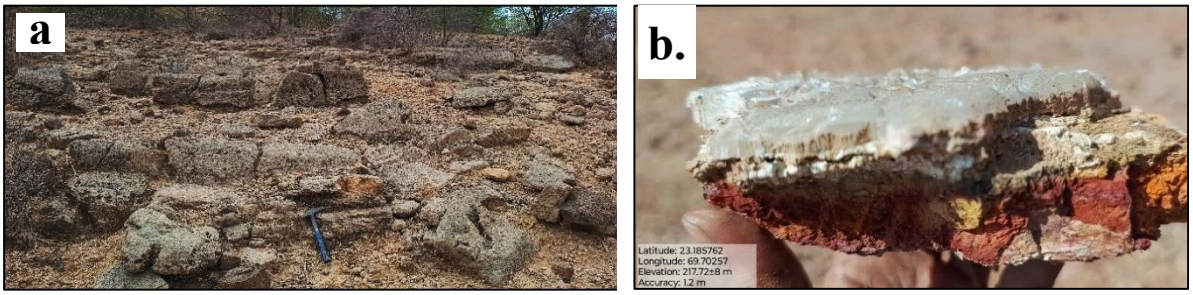

Fig. 4. 11 Carbonate facies of the Chari Formation: (a) Outcrop of the oolitic grainstone unit; (b) calcareous-gypseous shale displaying compact micritic texture and thin gypsum seams.

The lithological assemblage of the Chari Formation represents transitional to shallow-marine shelfal sedimentation, deposited under regressive conditions along a retreating shoreline. Alternation of carbonate and ferruginous siliciclastic beds reflects fluctuating hydrodynamic regimes, ranging from low-energy shelfal deposition to intermittent high-energy events associated with near-shore currents and/or storm reworking.

Katrol Formation:

The Katrol Formation occupies the southern and central sectors of the block, around Reha Nana, Dahisara, and Kera, forming the most laterally extensive unit within the mapped area. The formation occurs as gently undulating hill ranges and linear ridges aligned roughly E-W, with a maximum preserved thickness of 700-750 m (*Srivastava et al., 1994*). Lithologically, the unit comprises heterolithic successions, where two sandstone-dominated heterolith units (upper and lower) are separated by a shale-dominated heterolith unit.

Shale-Dominated Heterolith Unit

This unit is characterized by rhythmic alternations of 1-3m thick grey to blackish grey shale packages, interbedded with centimetre-scale (10–20 cm) sandstone layers (*Fig. 4.12a*). The shales are 1.5-7cm thick, plane-parallel laminated, fissile, and friable in weathered sections. Internally these shales are millimetre thin, plane-parallel to wavy-parallel laminated and calcareous to carbonaceous in nature. The interbedded sandstone is medium to fine grained, white to mauve in colour, and internally displays plane-parallel or wave-ripple lamination with chevron up-building, draping, and opposing laminae (*Fig. 4.12b*). Occasional hummocky cross stratification is also recorded.

This unit is associated with repeated occurrences of very fine-grained, off-white tuffite layers, often showing ferrous tint or hematitic coatings (*Fig. 4.12c*). These tuffite horizons are laterally persistent and can be traced for several hundreds of metres along the strike. Presence of ferruginous nodules are pervasive, often imparting a reddish-brown colour to the weathered surfaces of the succession. Occurrence of mm thin gypsum layers is also common at multiple stratigraphic levels.

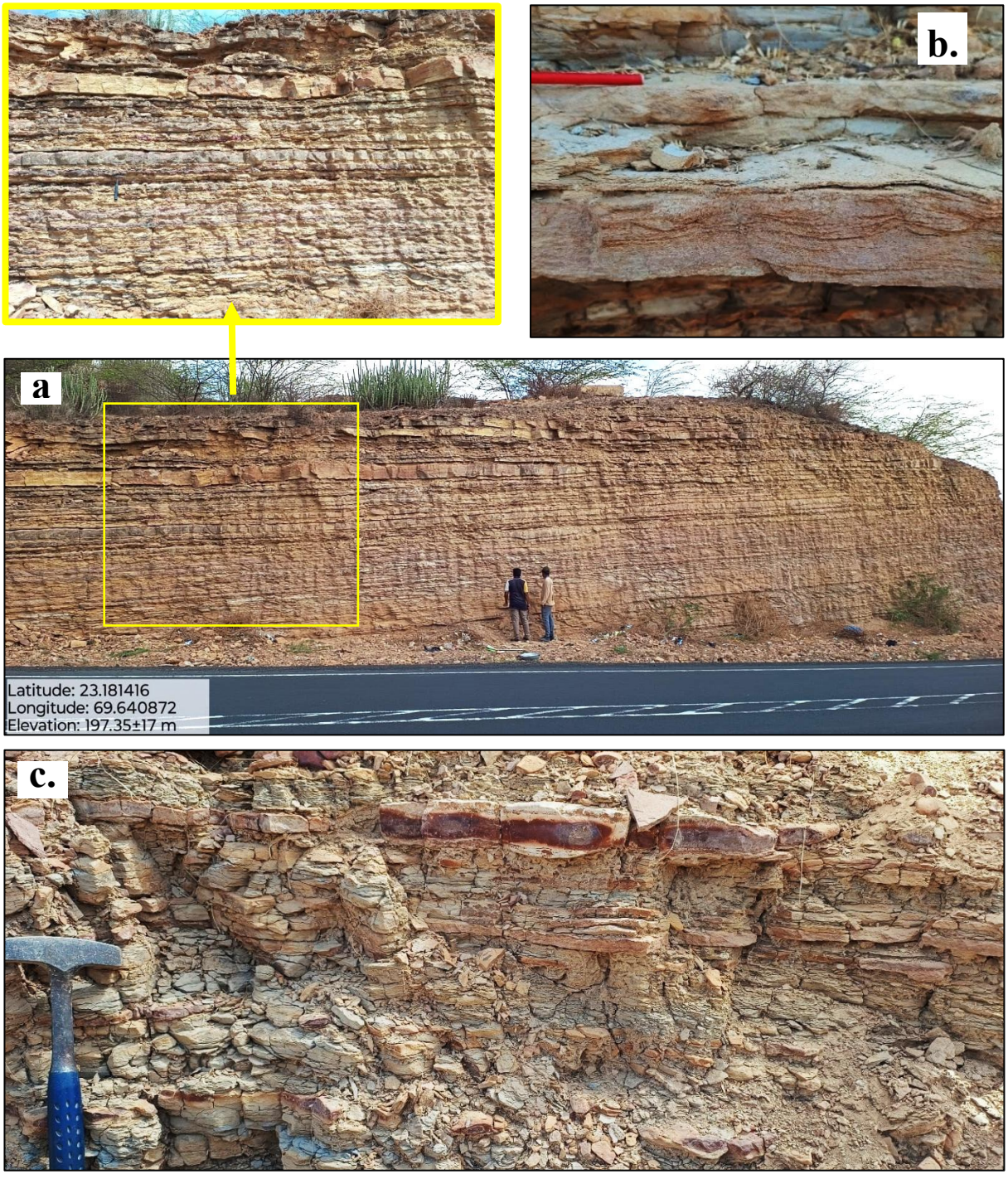

Fig. 4. 12 Field photographs showing shale-dominated heterolith unit of the Katrol Formation: (a) Occurrence of thick shale unit. Note the sandstone unit at the top part of the sucession.; (b) Wave-ripple-laminated sandstone with chevron up-building and opposing laminae; (c) Occurrence of off-white tuffite layer with hematitic coating within the shale dominated unit of Katrol Formation.

Sandstone-Dominated Heterolith Unit

The sandstone-dominated heterolith occurs both at the lower and upper parts of the Katrol succession, and both units exhibit comparable lithological characteristics. The facies are

typified either by metre-scale sandstone packages (*Fig. 4.13a*), or thick sandstone beds separated by 10–20 cm thick shale units (*Fig. 4.13b*).

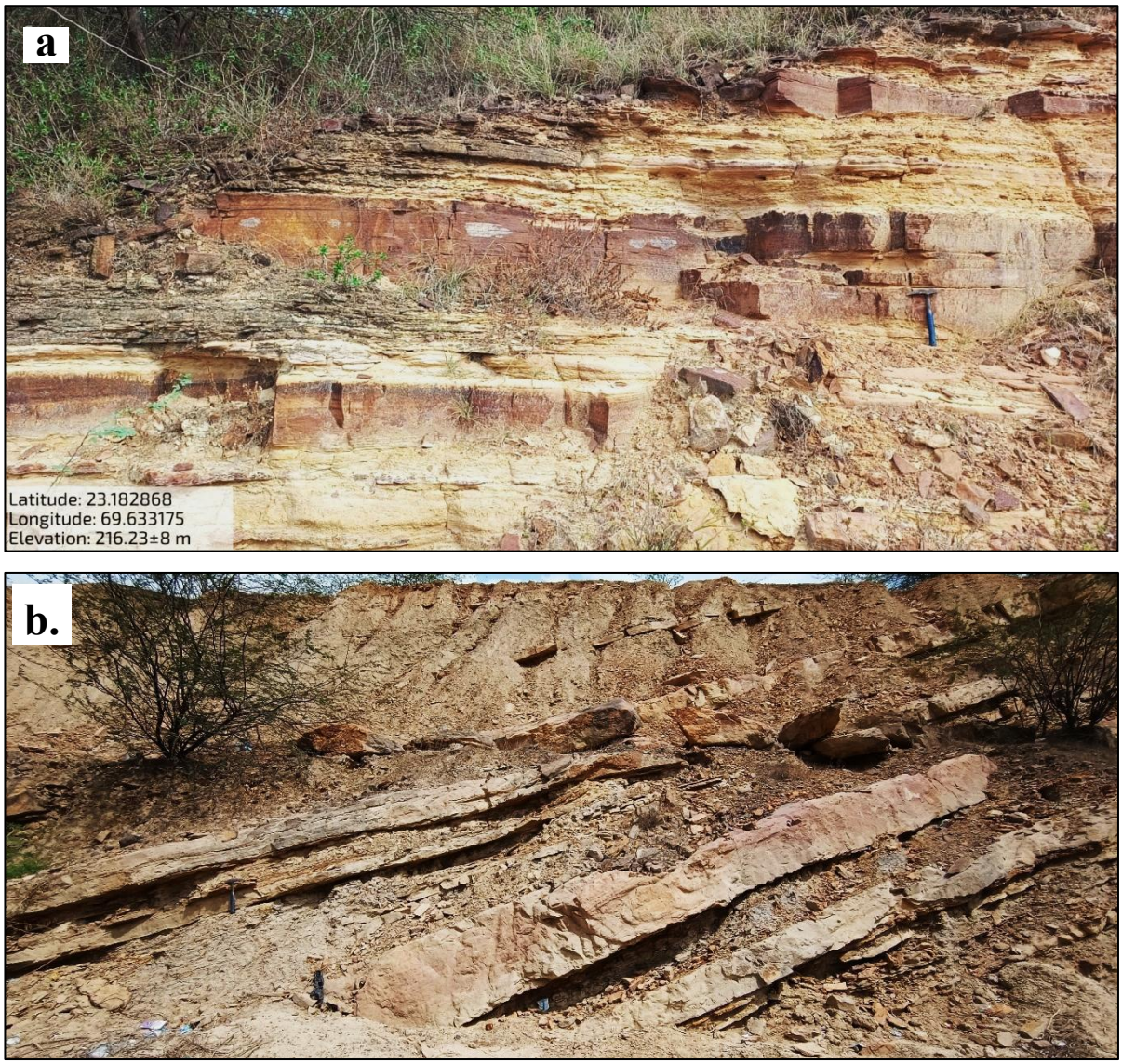

Fig. 4. 13 Field photographs showing sandstone-dominated heterolith unit of the Katrol Formation: (a) Metre-scale thick sandstone beds with massive to laminated internal structures; (b) Thick sandstone beds separated by shale packages. Note the pinch-and-swell geometry and sharp bounding surfaces of the sandstone beds.

The sandstone is white to yellow ochre in colour, medium to fine grained (locally coarse grained), and displays pinch and swell bed geometry with sharp bounding surfaces. Internally, the beds are massive to plane-parallel laminated, with rare planar cross-stratification. Individual sandstone beds are 15-60 cm thick and often separated by millimetre thin grey to white shale laminae. Sparse tuffite interbeds occur within this unit, while ferruginous nodules and concretionary horizons are pervasive, particularly within the upper sandstone packages.

The Katrol Formation represents a complex, multi-episodic depositional system, developed under fluctuating deltaic to near-shore marine conditions, with intermittent volcaniclastic and evaporitic influence.

The shale-dominated heterolith reflects lower-energy offshore to distal pro-delta or outer-shelf sedimentation, where suspension fallout and storm-generated reworking produced thin-bedded, laminated shale–sandstone alternations. The presence of wave-ripple and hummocky lamination indicates periodic storm-wave influence reaching below fair-weather wave base, implying deposition in a shallow-to-moderately deep shelf setting.

The sandstone-dominated heterolith, in contrast, records higher-energy, storm-dominated or proximal shoreface environments, with rapid sediment influx and episodic channel-like reactivation, as reflected by sharp-based beds and pinch-and-swell geometries.

The tuffite layers within both units signify volcanic ash falls or reworked pyroclastic influxes, later altered to ferruginous clays, whereas the gypsum seams suggest periodic salinity fluctuations and restricted circulation during waning phases of deposition. Collectively, the facies association indicates deposition within a storm- and volcanically influenced delta-to-shelf transition, recording both near-shore and deeper-marine processes within the Katrol succession.

Bhuj Formation:

The Bhuj Formation conformably overlies the Katrol Formation and represents the uppermost Mesozoic unit within the Bhuj REE Prospect Block. It is well exposed in the northern, northeastern, and southern sectors, around Mankuwa, Sukhpur, Bhuj, Kera, and Reha Nana villages, forming prominent ridges and escarpments trending E-W to ENE-WSW. The formation attains a thickness exceeding 350 m and is lithologically dominated by sandstone with subordinate clay and silt interbeds. Based on large-scale geological mapping (*Fig. 4.8; Plate I*), the Bhuj Formation has been subdivided into three lithounits:

I. Thick sandstone separated by clay horizons,
II. Ferruginous sandstone, and
III. Metasomatized ferruginous sandstone.

Thick Sandstone separated by clay horizons

This unit represents the dominant lithofacies within the Bhuj Formation and is characterized by thick-bedded sandstone successions interlayered with thin clay and silt horizons (*Fig. 4.14a, b, c*).

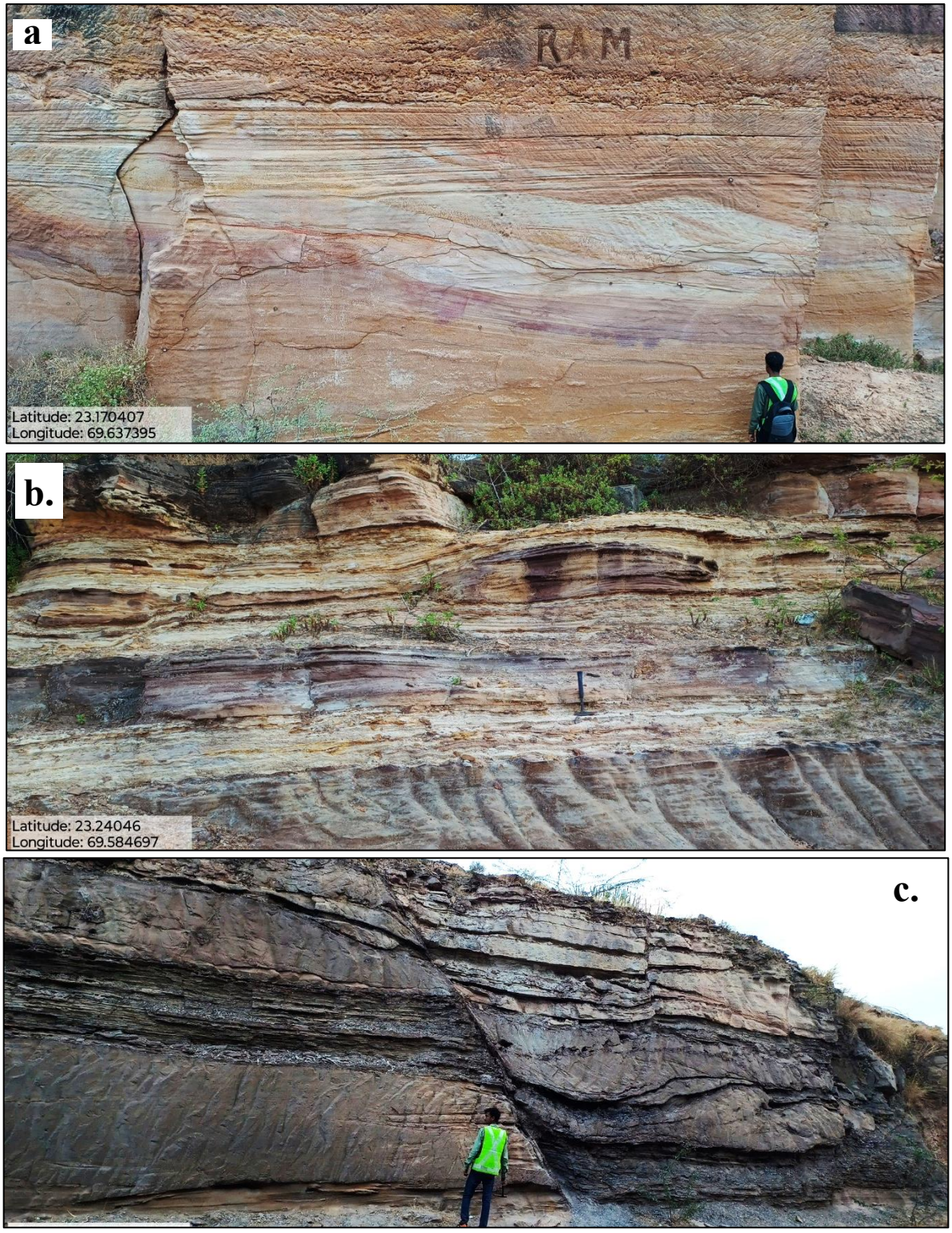

Fig. 4. 14 Field photographs showing thick sandstone–clay alternations of the Bhuj Formation: (a) Medium to fine grained, planar-parallel and cross stratified sandstone displaying reddish brown to buff coloration at Reha Nana village; (b) Swaley and hummocky cross stratified sandstone with thin clay interbeds; (c) Low-angle cross stratified, thick bedded sandstone with thin continuous clay partings. The sandstone is faulted.

This litho-unit represents the dominant facies within the Bhuj Formation and is composed of thick bedded sandstone successions interlayered with thin clay and silt horizons (*Fig. 4.14a-c*). The sandstone is reddish brown to mauve or buff in colour, medium to fine grained, and moderately well sorted. Internally, the sandstone exhibits a variety of sedimentary structures including planar parallel lamination, planar and trough cross stratification, low-angle cross stratification, hummocky to swaley cross stratification and wave ripple lamination. Individual sandstone beds range between 0.5m and 2m in thickness and are frequently separated by centimetre to decimetre scale clay units. The sandstone beds display pinch and swell geometry with sharp to erosional basal contacts, and occasional soft-sediment deformation features. Differential ferruginization of the sandstone is noted across localities, varying from weak iron staining to pervasive hematitic impregnation.

The intercalated clay horizons are greyish white to reddish brown in colour, and occur either as thin discontinuous layers, draping along the bedding planes or as laterally continuous partings. These horizons locally preserve ripple-drift lamination, small-scale reactivation surfaces, and soft-sediment deformation structures

Ferruginous Sandstone

The ferruginous sandstone occurs prominently in the northern part of the Bhuj REE Prospect Block, forming laterally persistent resistant ridges and benches. This unit consists of coarse to medium grained ferruginous sandstone, typically yellowish-brown to reddish-brown to dark brown in colour, with pervasive iron-oxide impregnation along laminae, joint planes, and fractures that locally cross-cut bedding and lithologic boundaries (*Fig. 4.15a*). The ferruginous impregnation manifests in two principal forms: (i) Diffuse hematitic cementation within the host sandstone, imparting a uniform yellowish to reddish-brown hue and dense texture to the rock (*Fig. 4.15b*), and (ii) Discrete hematite bands conformable with bedding or stratification, producing alternating ferruginous and lighter sandstone layers (*Fig. 4.15c, d*)

Individual beds are 20–70 cm thick, showing pinch-and-swell geometry with sharp, concave-up erosional bases. Internal sedimentary structures include planar and trough cross-stratification, ripple lamination, and wavy bedding, variably accentuated by iron-oxide staining. In several exposures, the ferruginized zones are underlain by moderately altered feldspathic sandstone, suggesting post-depositional metasomatic replacement along permeable horizons. Thin shale partings and nodular ferruginous concretions are also common, often demarcating localized fluid-seep pathways within the sandstone sequence.


a
Latitude: 23.216158
Longitude: 69.588845
Altitude: 99.7±195 m
Accuracy: 12.1 m


b.
Latitude: 23.221015
Longitude: 69.589813
Altitude: 92.4±20.8 m
Accuracy: 6.226 m

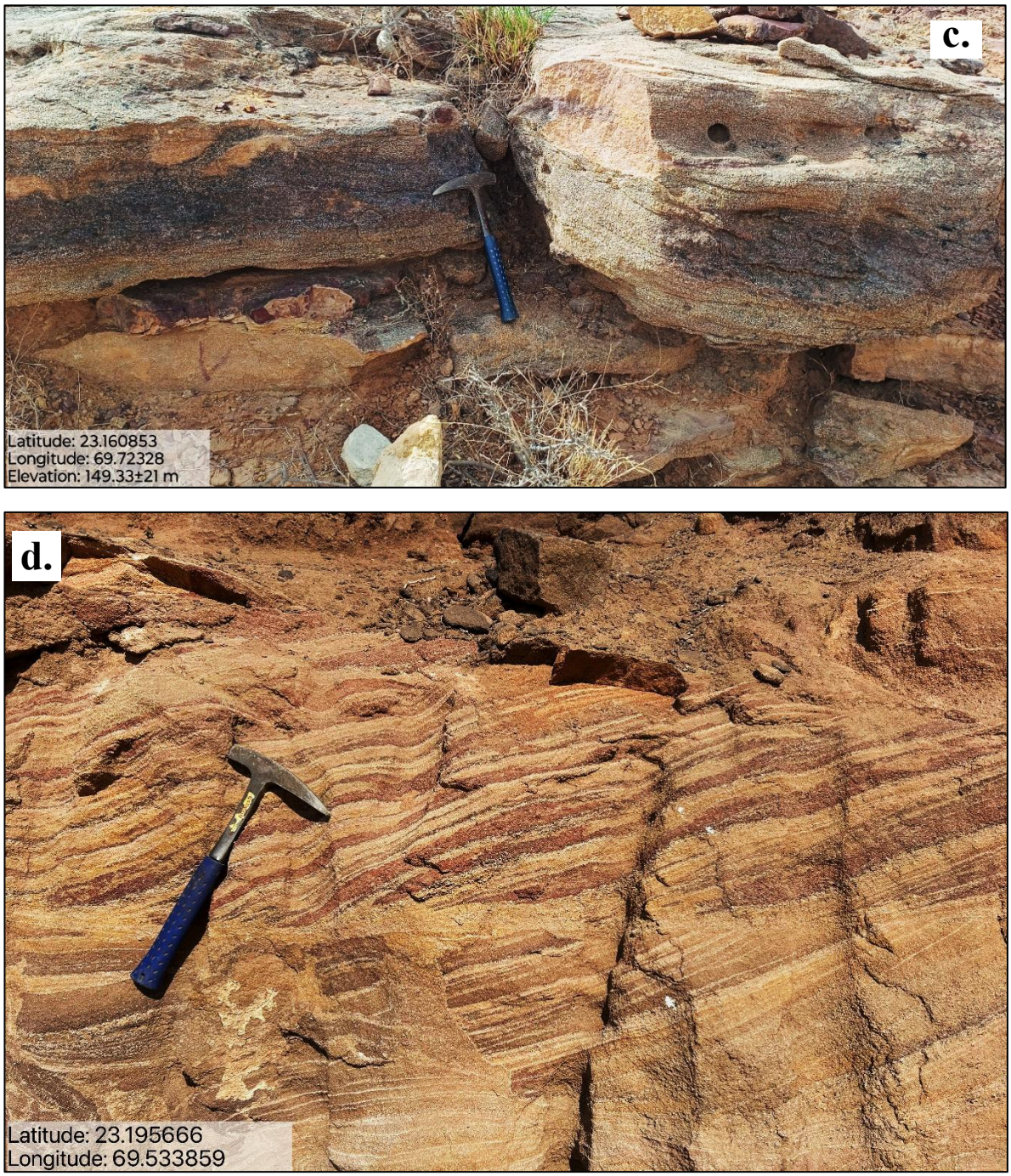

Fig. 4. 15 Field photographs showing ferruginous sandstone facies of the Bhuj Formation: (a) Pervasive iron-oxide impregnation and hematitic veinlets cutting across bedding; (b) Diffusely ferruginized coarse grained sandstone with uniform reddish-brown coloration and compact texture; (c) Planar cross stratified ferruginized sandstone overlying the bedding-parallel hematite bands and nodular concretions; (d) Planar cross stratified coarse grained sandstone. Note the ferruginization of the host along the stratification, producing a dark and light coloured banding within the sandstone.

Metasomatized ferruginous Sandstone

The metasomatized ferruginous sandstone occurs as isolated hillocks and ridge-like exposures, primarily concentrated along the structural corridors of the Katrol Hill Fault (KHF) and the Median High zone, exhibiting an overall NW–SE alignment within the project area. This lithounit represents the most altered facies of the Bhuj Formation, marked by pervasive ferruginization, metasomatic alteration, and localized silicification.

The unit comprises reddish-brown to dark-brown and locally black-coloured sandstone. It is very hard, compact, and brittle, characterized by a brecciated to pseudo-brecciated texture (*Fig. 4.16a*). The sandstone is dominantly gritty to very coarse grained, although finer varieties occur locally in zones of intense silicification. Primary sedimentary structures are generally obliterated due to ferruginous cementation, although bedding and stratification are occasionally discernible. The rock commonly exhibits pinch and swell bed geometry with sharp erosional contacts.

The ferruginization is pervasive and uniform, imparting a massive appearance to the rock (*Fig. 4.16b*). Hematite and magnetite occur as interstitial infillings within the altered matrix, while iron-oxide coatings are well developed along joint planes and fractures. In several exposures, hematitic veinlets and ferruginous bands occur along structural weaknesses, often cross cutting the primary bedding (*Fig. 4.16c*). Internal laminations/stratification, where preserved, are heavily stained by iron oxides (*Fig. 4.16d*). The degree of ferruginization increases near fracture-dense zones, producing a flinty to vitreous texture. Silicification occurs mainly within the matrix, causing local variation in grain size and contributing to the rock's hardness and compactness. Authigenic growth of euhedral feldspar (*Fig. 4.16e*) and book-mica is commonly observed within intergranular spaces. The transition from ferruginous sandstone to metasomatized facies is gradational, defined by progressive increases in hardness and ferruginous impregnation (*Fig. 4.16f*).

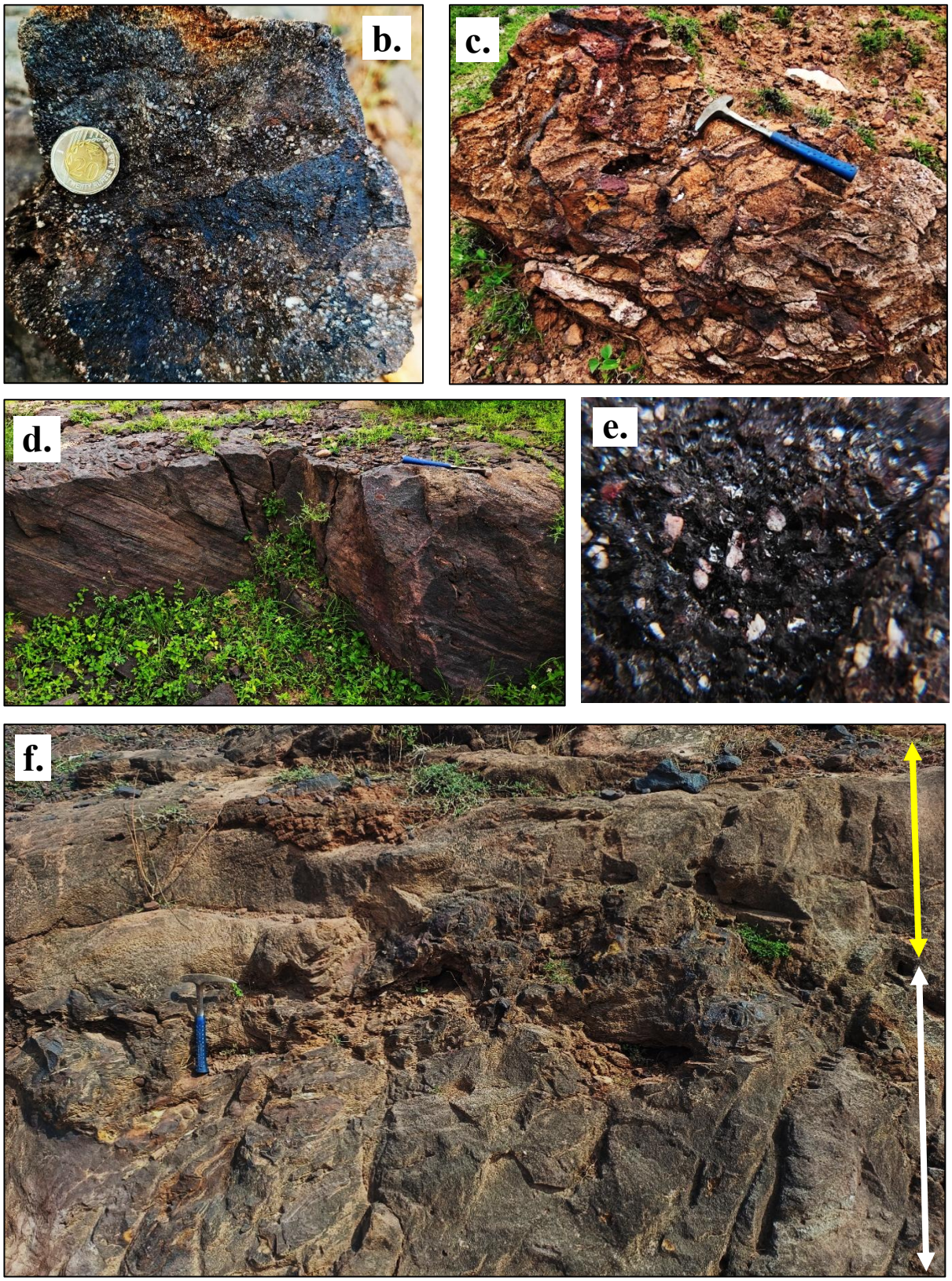

Fig. 4. 16 Field photographs showing metasomatized ferruginous sandstone of the Bhuj Formation: (a) Intensely ferruginized and brecciated exposure of the lithounit; (b) Compact, fine-grained metasomatized ferruginous sandstone showing pervasive iron-oxide

impregnation; (c) Hematitic veinlets and ferruginous bands cross-cutting the bedding; (d) Iron-oxide impregnation along the preserved planar cross stratification; (e) Authigenic growth of euhedral feldspar within the matrix part of the rock; (f) Gradational transition from ferruginous (yellow arrow) to metasomatized facies (white arrow) showing progressive hardening and oxidation.

Lateritic Development:

The uppermost part of the Bhuj Formation is marked by a discontinuous lateritic crust, particularly well developed around Madhapar and Sukhpur. The laterite is reddish-brown to dark brown, pisolitic, and ferruginous, ranging in thickness from 0.5 to 3 m. It forms a sharp basal contact with the underlying ferruginous sandstone and comprises iron-oxide nodules and pisoliths embedded within a clayey to earthy matrix. In several exposures, more than one lateritic horizon is observed (*Fig. 4.17*). The profiles display vertical zonation, with an upper ferruginous pisolitic zone grading downward into a kaolinitic-saprolitic horizon, reflecting progressive in-situ weathering of the parent sandstone.

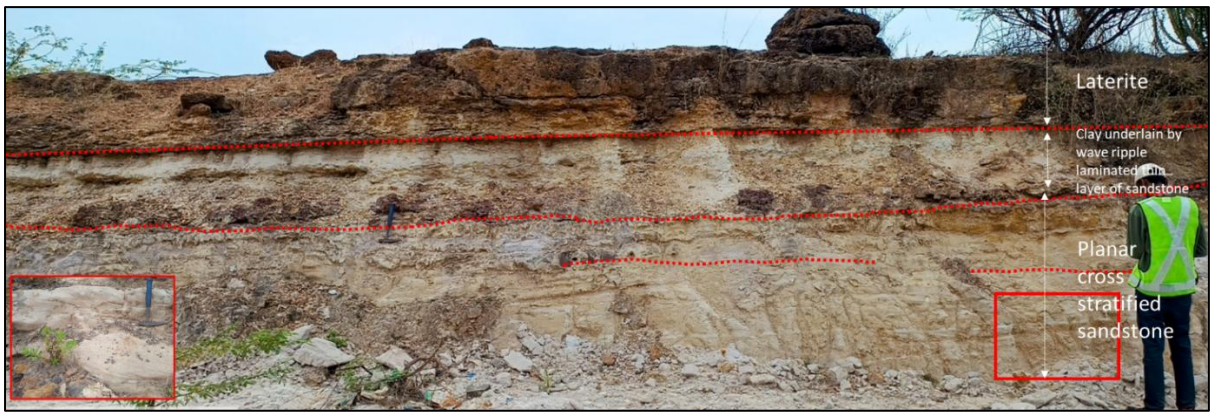

Fig. 4. 17 Field photograph showing lateritic development (0.75m) at the top of the Bhuj Formation near Madhapar. The section displays a ferruginous pisolitic laterite overlying clay-rich and wave-ripple laminated sandstone, underlain by planar cross-stratified sandstone. Inset shows the structure of the sandstone. Also note three stages (marked by red coloured dotted lines) of lateritization within the sucession.

The Bhuj Formation records a progressive shift from shallow-marine to continental depositional regimes, reflecting an overall regressive to subaerial transition within the upper part of the Mesozoic succession of the Kachchh Basin. The dominance of medium to fine grained, well-sorted sandstones with planar, trough and low-angle cross-stratification, hummocky–swaley stratification, and wave ripple lamination indicates deposition under wave and current dominated shoreface to foreshore settings, locally grading into tidally reworked marginal-marine environments. The thin, discontinuous clay and silt horizons separating sandstone beds mark episodic suspension fallout or tidal slack-water sedimentation, whereas erosional basal contacts and pinch-and-swell geometries reflect high-energy storm and channelized flow conditions.

Toward the upper stratigraphic levels, the appearance of planar and trough cross stratified very coarse to coarse graine ferruginous sandstones with absence of marine fossils denote progressive subaerial exposure, suggesting a shift to coastal plain and fluvio-deltaic environments during the terminal stages of deposition. Such oxidizing, intermittently emergent conditions possibly facilitated early iron-oxide cementation and diagenetic reddish colouration, giving rise to ferruginous sandstone facies. Subsequent hydrothermal or basinal fluid migration along major fault and fracture systems, notably the Katrol Hill Fault (KHF) and its subsidiary lineaments, may led to metasomatic modification of these ferruginous sandstones. This process was accompanied by pervasive hematitization, magnetite impregnation, and localized feldspar–mica recrystallization, producing hard, compact metasomatized ferruginous sandstone.

The development of the lateritic profiles overlying the Bhuj sandstone indicates a phase of subaerial weathering and oxidation under semi-arid climatic conditions, following the lithification of the host sandstone. This secondary ferruginization represents supergene enrichment of iron under oxidizing meteoric conditions. The lateritic crusts thus mark the youngest surficial alteration features within the Bhuj REE Prospect Block and serve as geomorphic and stratigraphic markers of post-Mesozoic paleoweathering episodes associated with Cenozoic landscape evolution of the region.

Collectively, the Bhuj Formation encapsulates a regressive depositional trend, recording a transition from storm influenced shallow-marine environments to subaerially exposed ferruginous and lateritic terrains, thereby bridging the terminal phase of the Mesozoic sedimentary cycle with subsequent post-depositional geomorphic modification.

The alkaline plug previously reported within the Bhuj block, described as intruding the Bhuj Sandstone, could not be substantiated during the present study because the reported location now covered densely by inhabited settlement, preventing direct field verification.

Anjar Volcanics

Small discontinuous patches of Anjar Volcanics and associated basic dykes predominantly occur in proximity to the Median High zone. The volcanic rocks consist of black to olive green, fine grained amygdaloidal basalt, exhibiting massive to vesicular textures (*Fig. 4.18a-b*). The vesicles are typically filled with secondary silica, zeolite, and calcite, forming distinct amygdaloidal patches. The basaltic exposures form N–S-trending linear ridges and characteristically weather into blocky fragments (*Fig. 4.18b*)

The associated basic dykes are fine grained, dark grey to black in colour, non-porphyritic, and intrude both the Katrol and Bhuj formations. They display sharp intrusive contacts with the host sedimentary rocks and are frequently accompanied by ferruginized alteration zones along their margins (*Fig. 4.18c*). Evidence of hydrothermal veining, characterized by hematitic

infilling is also common near the fault intersections and within the fracture-controlled conduits.

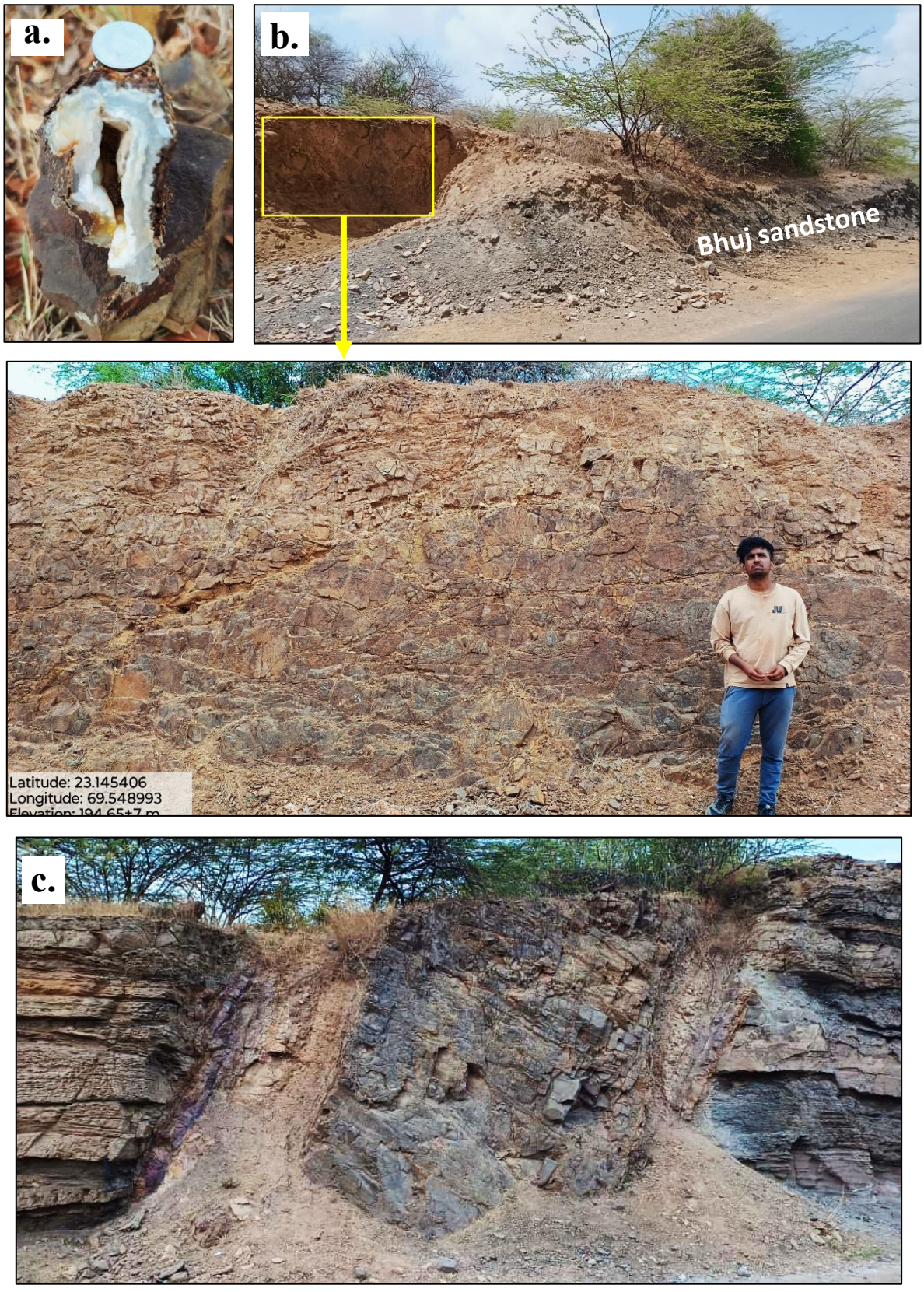

Fig. 4. 18 Field photographs showing Anjar Volcanics and associated intrusive features: (a)

Amygdaloidal basalt with vesicles filled by silica; (b) Itrusion of the basalt within the Bhuj Formation. The enlarged view of the basalt shows the blocky appearance og the lithounits in weathered exposure; (c) Basic dyke intruding the Bhuj sandstone. Note the ferruginized margins and hematitic veining along the intrusion plane.

Field relationships and mineralogical characteristics indicate that these volcanic and subvolcanic units belong to a Late Cretaceous magmatic phase, broadly synchronous with Deccan Trap volcanism. Their emplacement marks the terminal magmatic episode of the Kachchh Basin, representing the final stage of its tectono-sedimentary evolution. The structural orientation of the dykes and basaltic ridges suggests emplacement along pre-existing fault and fracture systems, notably the Katrol Hill Fault and the Median High zone, which likely served as pathways for ascending magmatic and later hydrothermal fluids, promoting ferruginization of the sedimentary host.

The lithological framework of the Bhuj REE Prospect Block records a progressive transition from shallow-marine to continental regimes, accompanied by volcanism and post-depositional alteration. Successive regressive phases led to storm-dominated and subaerial environments that underwent ferruginization, and metasomatism along structural conduits, culminating in lateritic weathering under semi-arid conditions. The emplacement of Anjar Volcanics during the Late Cretaceous marked the terminal magmatic episode, structurally controlling subsequent hydrothermal alteration. Collectively, these features define the basin's tectono-sedimentary evolution and establish the geological foundation for the processes governing REE enrichment within the Bhuj Block.

4.5.3. Structural Framework of the Block Area

The structural configuration of the Bhuj REE Prospect Block is primarily governed by two major tectonic elements of the Kachchh Basin, (i) the Katrol Hill Fault (KHF) and (Ii) the Median High, that collectively define the structural grain and control the present-day lithological disposition (*Fig. 4.19a*). The area exposes Jurassic to Cretaceous sedimentary units belonging to the Chari, Katrol, and Bhuj formations, which have been variably deformed, faulted, and locally uplifted along these tectonic corridors.

The Katrol Hill Fault represents the most prominent structural discontinuity within the block, trending approximately E–W and exhibiting the geometry of a reverse fault with a dip of ~35° towards the south. Its presence is established through multiple lines of field evidence: (i) the juxtaposition of the older Chari Formation over the younger Bhuj Formation (*Fig. 4.19b*), (ii) the absence of the intermediate Katrol Formation along the fault contact, (iii) steepening and drag folding of beds adjacent to the fault plane, and (iv) associated brecciation, and iron-oxide impregnation along the fault zone. These features collectively indicate compressional reactivation during Late Mesozoic to early Tertiary tectonism. The fault

zone has also acted as a major conduit for fluid migration and metasomatic alteration, influencing ferruginization within adjoining lithounits.

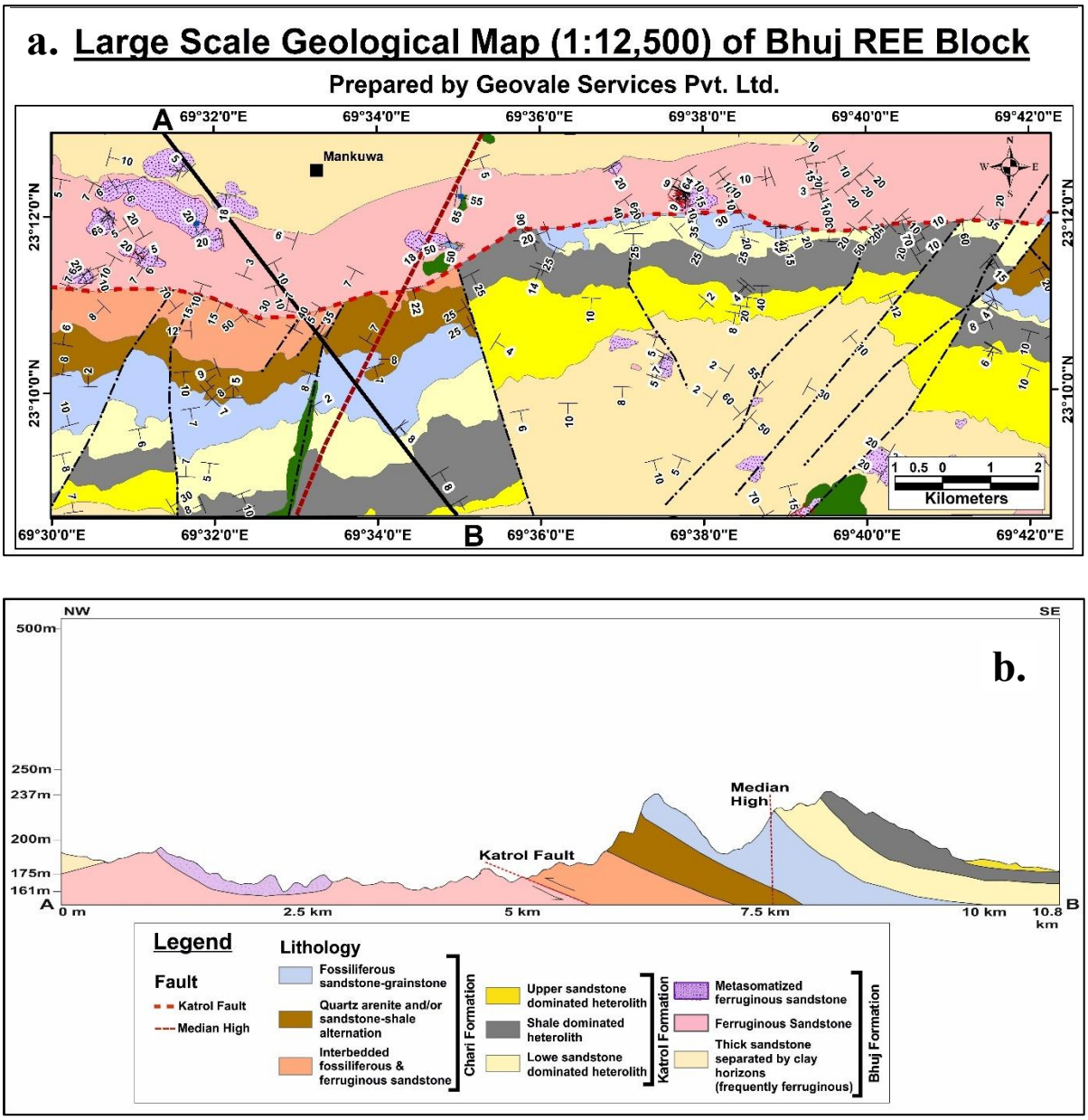

Fig. 4. 19 (a) Large-scale geological map (1:12,500) of the Bhuj REE Prospect Block showing the lithological disposition, structural configuration, and location of the A–B cross-section line. (b) Geological cross-section (A-B) across the Bhuj REE Prospect Block illustrating the structural configuration and stratigraphic succession from the northwestern to southeastern sectors. The section highlights the tectonic juxtaposition of lithounits across the Katrol Hill Fault.

South of the KHF, several subsidiary faults are identified based on abrupt lithological offsets, steepened bedding attitudes, and brecciated zones. Two predominant fault sets are recognized: a NW-SE trending set, characterized by a significant strike-slip component, and a

NE-SW trending set, exhibiting minor displacement and predominantly normal kinematics. These faults are interpreted as post-depositional extensional structures, likely formed during differential block subsidence in the later stages of basin evolution. The cumulative effect of these fault systems has imparted a stepped topography and variable bedding attitudes ranging from 10°-15° southward dips in undeformed sectors to steep (locally near-vertical) dips adjacent to fault zones.

The Median High, trending NNE-SSW, traverses the western part of the block and is identified as a subsidiary structural uplift within the Kachchh Mesozoic Basin. It corresponds to a gravity high in subsurface geophysical data, though with minimal surface expression. The structural alignment of the basic dykes, ferruginized ridges and metasomatized zones broadly parallels this trend, implying tectono-hydrothermal linkage between the Median High and adjoining fault-controlled corridors.

The geological cross-section (A-B) across the block (*Fig.4.19b*) reveals the overall structural configuration of the project area. The section demonstrates that near point A, metasomatized ferruginous sandstone caps the ferruginous sandstone unit of the Bhuj Formation. Towards the central part, the Chari and Katrol formations occur at higher elevations and tectonically overlie the Bhuj Formation across the Katrol Hill Fault. Eastward from the fault zone, the topographic elevation decreases, and in the extreme east of the section the Bhuj Formation reappears, resting conformably over the Katrol Formation. The curved disposition of the beds and their irregular dips in the eastern segment likely result from the cumulative influence of minor subsidiary faults and post-tectonic erosion.

In summary, the structural architecture of the Bhuj REE Prospect Block reflects the interaction of compressional and extensional tectonics associated with the evolution of the Kachchh Basin. The Katrol Hill Fault and Median High form the principal tectonic elements, controlling both lithological distribution and post-depositional fluid pathways. The structural reactivation of these faults, coupled with associated hydrothermal activity, has been instrumental in governing the distribution and intensity of ferruginization and metasomatic alteration throughout the Bhuj Block.

4.5.4. Petrographic Characterization of the Block Area

In the context of the present investigation, a total of sixty-two (62) representative samples were examined petrographically to document the mineral assemblages and micro-textural characteristics of the studied lithounits (Annexure-XII). This section presents a generalized petrographic account of the principal formations, Chari, Katrol, and Bhuj formations, arranged in their established stratigraphic order as described in the preceding sections. The primary objective of this examination is to characterize the mineralogical composition, grain-framework relationships, and textural attributes of the constituent lithotypes. Detailed investigations pertaining to mineralization potential, including the

identification of accessory and ore-related phases critical for evaluating the region's potential for strategic metals, particularly Rare Earth Elements (REE) and Rare Metals (RM), are discussed separately in the subsequent Detailed Ground Survey section.

Sandstone (Chari Formation):

The sandstones of the Chari Formation are medium- to coarse-grained and moderately sorted (*Fig.4.20a*). The detrital framework is dominated by quartz (≈ 89.8%), with subordinate feldspar (≈ 7.7%) and minor proportions of rock fragments and mica (≈ 2.5%). Quartz grains are generally subangular to subrounded, and fragmented. Frequent occurrence of wedge-shaped grains with embayed margins are also observed. The intergranular spaces are variably filled with ferruginous and carbonate cements, imparting a reddish to brownish hue in places. Occasional carbonate veins traverse the sandstone, indicating localized post-depositional cementation.

Heterolithic Rock (Katrol Formation)

The heterolithic units of the Katrol Formation are characterized by alternating sandstone and shale-dominated layers (*Fig.4.20b*). The sandstone-dominated portions are fine-grained and crudely laminated, comprising alternating framework-rich and matrix-rich laminae. The framework grains, ranging from 20 to 250 µm, consist predominantly of quartz, feldspar, and muscovite, with accessory apatite, monazite, and zircon, all embedded within a ferruginous to calcareous, glassy groundmass. The shale-dominated intervals are matrix-supported, containing elongated, needle to wedge-shaped quartz grains and minor muscovite, disseminated within a ferruginous, apatite-rich matrix (*Fig.4.20c*).

Sandstone (Katrol Formation)

The sandstones of the Katrol Formation are medium to fine-grained, comprising angular to subrounded grains of quartz (>90%), feldspar (2–12%), muscovite (≤1-2%), perthite, chert, mud pellets and volcanic rock fragments set within a carbonate cement (*Fig.4.20d*). The presence of mud pellets and pyroclastic quartz-feldspar clasts exhibiting cooling cracks indicates rapid sedimentation associated with contemporaneous volcanic activity. The cements occur as zoned sparry calcite and fine-grained microcrystalline calcite, suggestive of multiple cementation phases under fluctuating geochemical conditions. The proportion of matrix (1-10%) shows vertical variation within the succession. Occasional fossil remains, including wood (*Fig.4.20e*) and sponge fragments, are preserved locally, representing brief quiescent intervals between episodic volcanic events.

Sandstone (Katrol–Bhuj Contact Zone)

The sandstones occurring along the Katrol-Bhuj contact zone are medium to fine-grained and vary from arenite (*Fig.4.20f*) to wacke in composition. The detrital framework

comprises angular to subangular grains of quartz, feldspar (2–10%), perthite, muscovite, biotite, chert, and epidote, set within a glassy to quartzo-feldspathic matrix. The cement is predominantly manganiferous to ferruginous, locally replaced by carbonate phases. Accessory minerals include magnetite, zircon, monazite, xenotime, apatite, pyrite, and chalcopyrite. Common diagenetic and deformational features include cooling cracks, silica overgrowths, feldspar sericitization, brecciation, and the development of zoned carbonate spars.

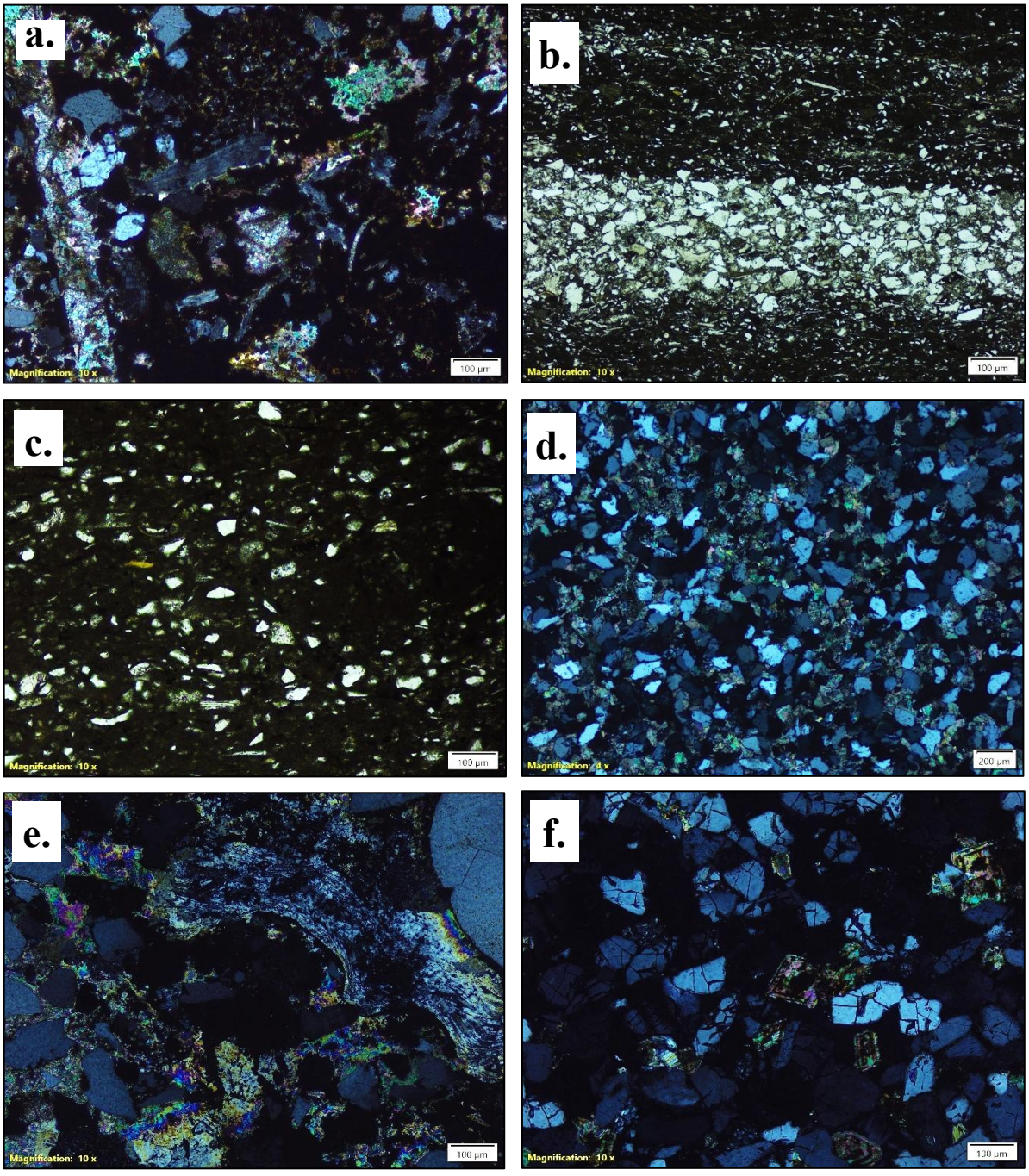

Fig. 4. 20 Representative photomicrographs of thin sections from the Chari, and Katrol, formations. (a) Fine-grained sandstone of the Chari Formation, showing a framework of quartz, feldspar, and muscovite; carbonate cement partially replaced by ferruginous material

(crossed polarised light). Note the carbonate vein traversing through the sandstone. (b) Heterolithic unit of the Katrol Formation, displaying alternating sand-rich and sand-poor laminae with dark micritic matrix (plane polarised light). (c) Shale-dominated heterolith of the Katrol Formation with a dark phosphatic matrix and dispersed elongate quartz grains (plane polarised light). Note the irregular shape of the framework grains. (d) Fine-grained sandstone of the Katrol Formation, composed of quartz-rich framework grains with ferruginous cement (crossed polarised light). (e) Carbonized wood fossil fragment preserved within Katrol sandstone, embedded in carbonate matrix (plane polarised light). (f) Sandstone from the Katrol-Bhuj contact zone, showing quartz and feldspar framework grains within sparry carbonate cement. Note cooling cracks within quartz grains and zoned carbonate spars (crossed polarised light).

Sandstone (Bhuj Formation)

The sandstones of the Bhuj Formation are predominantly composed of angular to subangular quartz grains (>90%), with minor amounts of feldspar, chert, and quartzite fragments (*Fig.4.21a*). The framework grains are poorly sorted and display low sphericity, with a significant proportion of fractured and irregularly shaped grains (*Fig.4.21b*), indicative of limited transport and mechanical reworking. The matrix (<5%) consists chiefly of fine-grained quartz, locally admixed with ferruginous and carbonate material acting as cement. The cementation is heterogeneous, forming irregular patches of ferruginous impregnation and carbonate replacement within the intergranular spaces.

Accessory minerals include zircon, monazite, and magnetite, which occur either as discrete grains or as inclusion within the framework (*Fig.4.21c*). The intergranular spaces locally host sulfide phases, notably pyrite and chalcopyrite, often associated with ferruginous cement (*Fig.4.21d*). In certain sections, the sandstone displays cooling cracks traversing the quartz grains (*Fig.4.21e*), alongside clear evidence of in-situ brecciation, manifested by angular clast boundaries, interlocking fracture networks, and partial recrystallization along fracture planes. These textural and mineralogical features collectively indicate a complex post-depositional evolution involving mechanical disruption, thermal stress, and localized fluid-mediated cementation.

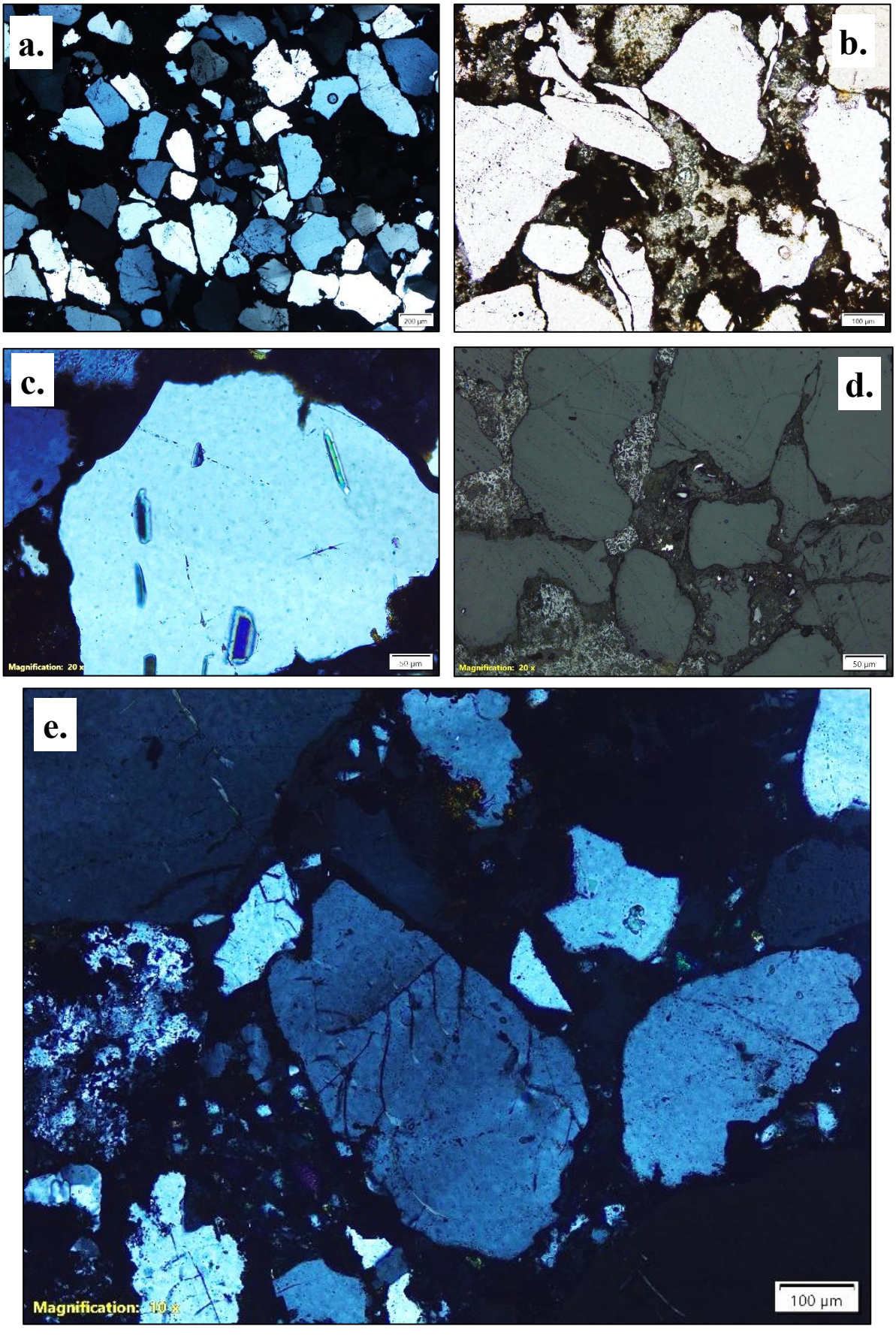

Fig. 4. 21 Representative photomicrographs of sandstone from the Bhuj Formation under

transmitted and reflected light. (a) Coarse-grained quartzose sandstone showing angular to subangular framework grains with ferruginous cement (crossed polarised light). (b) Bhuj sandstone under plane polarised light, showing irregular grain boundaries and poor sorting. (c) Quartz grain containing inclusions of zircon and apatite (crossed polarised light). (d) Matrix-hosted magnetite, pyrite, and chalcopyrite occurring as accessory minerals, observed under reflected light. (e) Bhuj sandstone displaying cooling cracks, traversing the quartz grains (crossed polarised light).

Petrographic characterization across the Chari, Katrol, and Bhuj formations reveals distinct variations in mineralogy, texture, and diagenetic overprints, reflecting changing depositional and post-depositional conditions.

The Chari Formation comprises quartz-rich, moderately sorted sandstones with ferruginous and carbonate cements, indicating early diagenetic stabilization in a shallow marine to marginal setting. The Katrol Formation shows increased heterogeneity with interbedded sandstone-shale units and volcaniclastic input. Features such as cooling cracks in pyroclastic clasts, zoned calcite cement, and occasional fossil preservation indicate rapid sedimentation influenced by synvolcanic activity.

The Katrol–Bhuj contact zone marks a transitional interval, where arenitic to wacke-type sandstones show silica overgrowths, feldspar alteration, brecciation, and zoned carbonate spars, associated with ferruginous cementation and accessory minerals like magnetite, monazite, zircon, pyrite, and chalcopyrite, suggestive of localized hydrothermal influence.

The Bhuj Formation is dominated by quartzose, poorly sorted sandstones exhibiting fracturing, in-situ brecciation, and cooling cracks, with ferruginous and carbonate cement and intergranular sulfides. These features collectively indicate progressive textural immaturity, mechanical disruption, and late-stage fluid activity within the succession.

4.6. Detailed Ground Survey in Mineral System-I

Following the delineation of the Katrol Stratiformal REE-bearing System during the orientation stage, subsequent investigations were directed towards validating its geochemical and stratigraphic continuity and understanding the nature of REE mineralization within the ferruginous-phosphatic shale horizons. The study integrated field investigation, facies logging, stratigraphic sampling, petrographic and mineragraphic examination, and geochemical characterization to assess the lateral persistence and compositional variability of the mineralized units. These investigations aim to establish a detailed stratigraphic and geochemical framework of the Katrol Formation, defining the extent, tenor, and mineralogical characteristics of the REE-bearing ferruginous shale beds, which represent the syngenetic component of the Bhuj REE Prospect Block.

4.6.1. Facies Logging and Sampling

4.6.1.1. Facies Logging

Detailed facies logging was carried out along multiple stratigraphic traverses within the Katrol Formation, primarily targeting the shale-dominated heterolithic unit that hosts repetitive occurrence of ferruginous–phosphatic shale horizons (tuffite) interbedded with fine sandstone and siltstone. In addition, selected traverses within the sandstone-dominated heterolithic unit were also logged to evaluate lateral facies variations and vertical transitions. A total of 21 lithologs were measured across different localities (*Fig. 4.22*), with individual sections ranging in height from 2 m to 38 m, depending on exposure quality and availability.

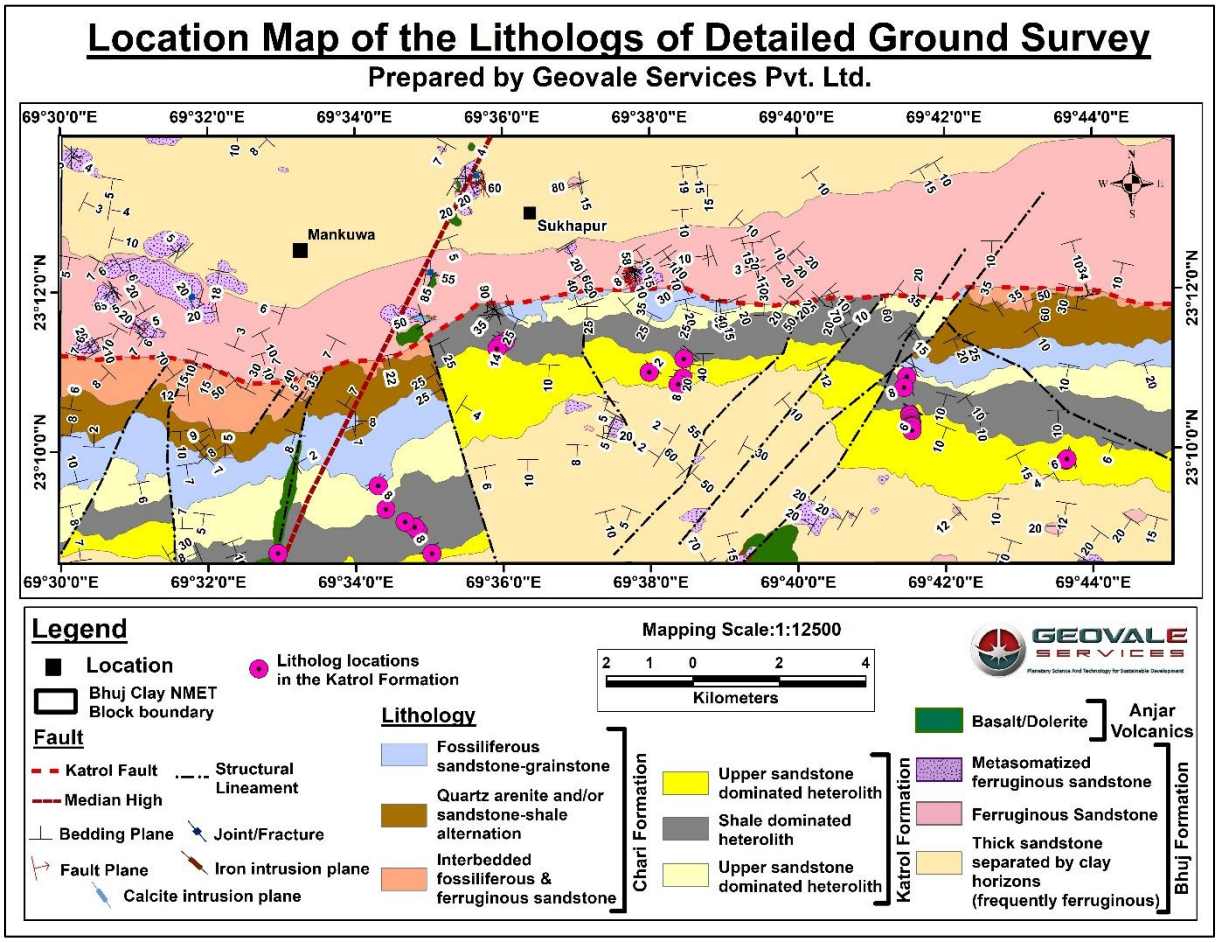

Fig. 4. 22 Location map of lithologs prepared during the follow-up reconnaissance survey across the Katrol Formation within the Bhuj REE Prospect Block.

Each measured section was tied to precise GPS coordinates and integrated into the large-scale geological map of the Bhuj REE Prospect Block. Bed-by-bed logging of the sections, recorded lithology, thickness, sedimentary structures, presence of tuffaceous horizons, and their lateral persistence.

Based on vertical facies transitions and characteristic features, three principal facies (F1-F3) were delineated within the shale-dominated heterolithic unit (*Fig. 4.23*) of which two facies (F1 and F2) incorporate tuffite horizons of variable thickness and lateral persistence.

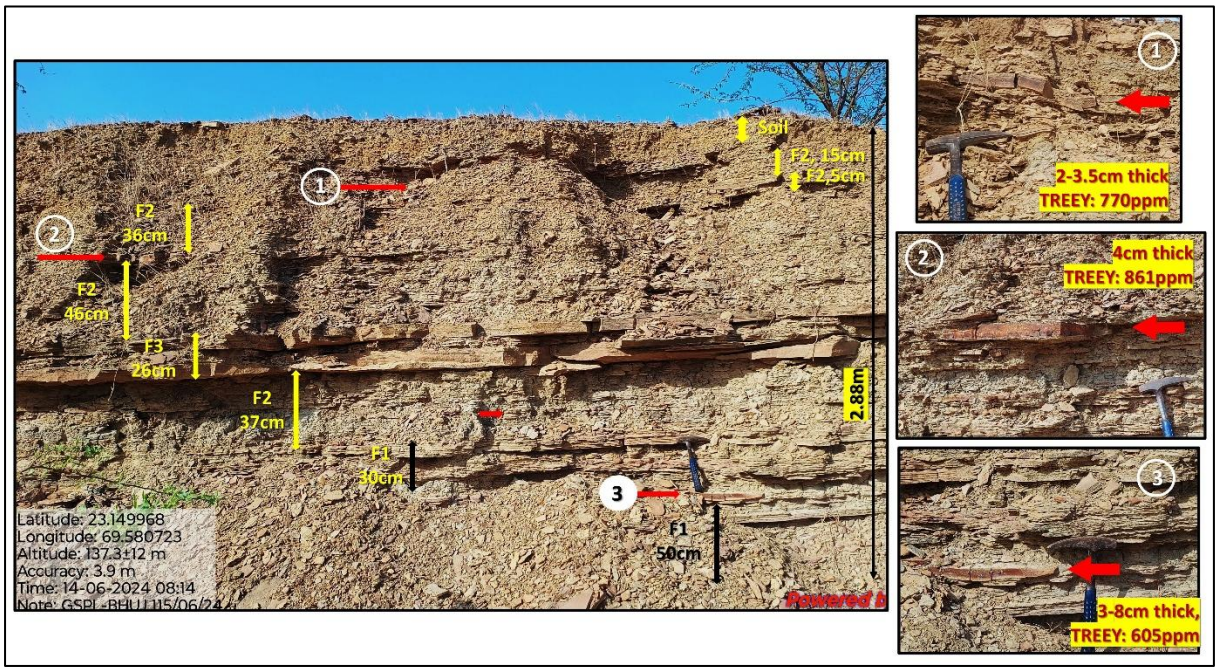

Fig. 4. 23 Representative lithological section of the shale-dominated heterolithic unit of the Katrol Formation showing repetitive ferruginous–phosphatic (tuffite) layers interbedded with shale and fine-grained sandstone.

Tuffite horizons: The ferruginous-phosphatic layers interbedded within the shale-dominated heterolith were subsequently identified as tuffite beds, confirmed by petrographic and mineralogical studies (*refer to section 4.6.3*). Individual tuffite layers range in thickness between 2-8cm and readily traceable over tens of meters along the dip and hundreds of km along the strike, reflecting exceptional stratigraphic continuity. Typically, the tuffite beds display bedding-parallel compositional and colour banding, characterized by a distinct tripartite layering comprising: a lower pale grey to yellowish white clayey layer, a central reddish-brown ferruginous part, and an upper buff to light-grey silty to clayey cap (*Fig. 4.24*).

In addition to the laminated varieties, nodular to concretionary tuffites are also observed, commonly exhibiting ferruginous concretions, limonitic coatings, and in some instances, partial obliteration of the basal clayey layer. Ferruginous tuffite nodules occur both as discrete lenses and as stratiform concretionary horizons at varying stratigraphic levels. The degree of ferruginization within these tuffite layers varies both laterally and vertically, implying differential fluid circulation and oxidation during diagenesis. Geochemically, it has been noted that the TREEY concentration tends to decrease with increasing ferruginization (*Annexure XIII and XIV*), indicating partial remobilization or dilution of REEs during secondary Fe enrichment.

Fig. 4. 24 Hand specimen of a tuffite layer from the Katrol Formation showing distinct bedding-parallel compositional banding and tripartite layering.

Facies 1 (F1): This facies comprises alternating millimetre-thin laminae of shale and fine siltstone/sandstone, reflecting rhythmic alternations of suspension fallout and weak tractional sedimentation under low-energy conditions. Occurrence of thin tuffite layers within this facies is observed at several locations.

Facies 2 (F2): This facies comprises blackish-grey shale interbedded with tuffite layers, frequently associated with thin gypsum partings. The overall thickness of individual F2 units ranges from 10 cm to 2.6 m, although continuous successions extending up to 12 m have also been documented. Each tuffite-bearing interval (F2) comprises two to five discrete layers, depending on the thickness of the facies. The repetition and lateral continuity of the tuffite layers are highly variable within the thick intervals (4-12m), reflecting episodic volcaniclastic influx and fluctuating depositional energy. Both laminated tuffite beds and ferruginous tuffite nodules occur within this facies, the latter representing localized diagenetic ferruginization and concretionary growth.

The shale intervals across the facies are predominantly grey to greyish black, fissile, and finely laminated, showing wavy- to parallel lamination. In weathered exposures, these beds become friable and splintery.

Facies 3 (F3): This facies comprises brownish-mauve, fine to medium grained sandstone beds, typically 2.5-12 cm thick and locally amalgamated up to 20 cm. The sandstone displays well-developed planar parallel lamination, wave ripple lamination, and occasional hummocky cross-stratification. These features collectively indicate deposition under storm-modulated shallow-marine to lower-shoreface conditions, reflecting episodic high-energy events superimposed upon a dominantly low-energy sedimentation regime.

In the **sandstone-dominated heterolithic** unit, two principal facies were identified (*Fig. 4.25*).

Facies 1 (F1): The facies comprises yellowish white to ochre coloured, medium to coarse grained quartzose sandstone beds, generally 10-20 cm thick and locally amalgamated up to

70 cm. The sandstone exhibits massive to planar-tabular bedding (*Fig.4.25a*), with occasional occurrences of planar-parallel and wave-ripple laminations (*Fig.4.25b*). Common diagenetic features include concretionary development, clay alteration, and presence of thick gypsum interbeds. The total unit thickness varies between 0.7m to 4.7m. Notably, no tuffite layers were recorded within this facies.

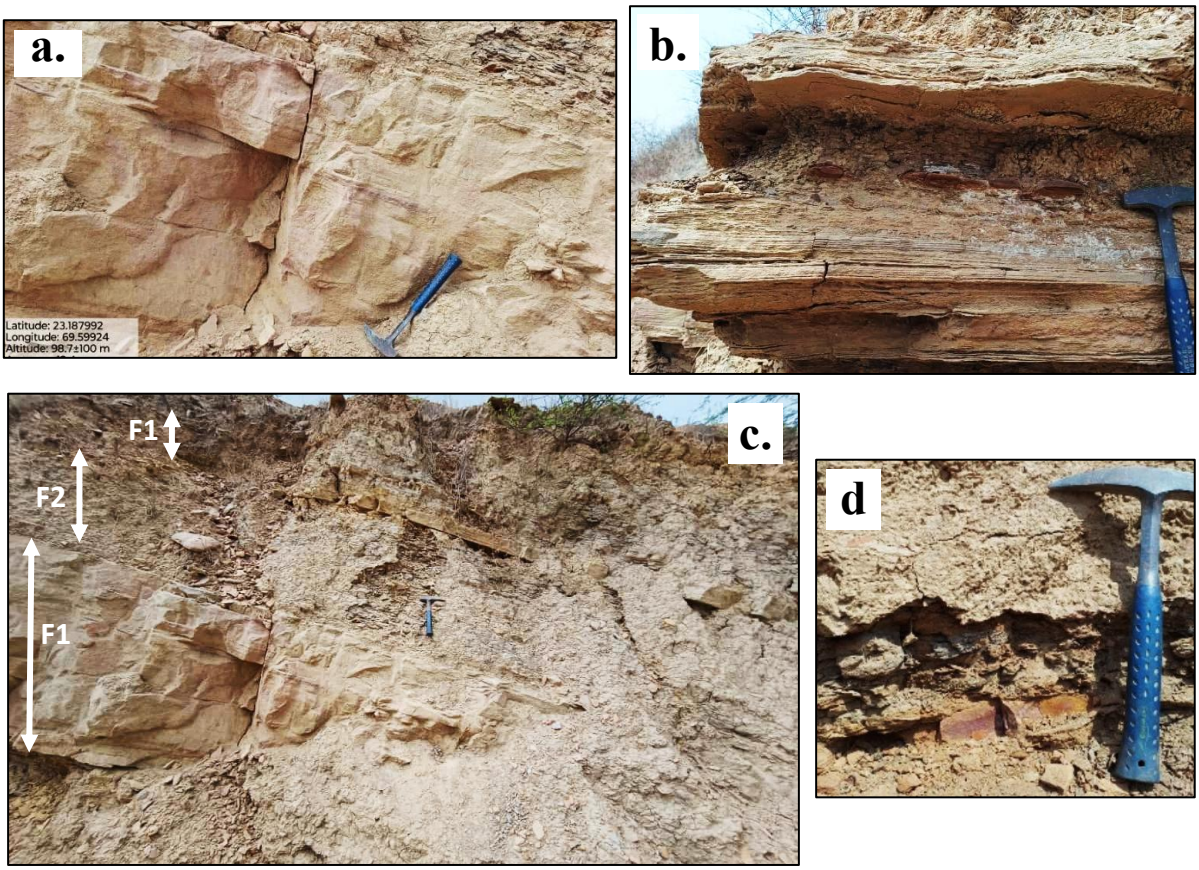

Fig. 4. 25 Representative field photographs illustrating the facies characteristics of the sandstone-dominated heterolithic unit within the Katrol Formation. (a) Medium to coarse grained, yellowish ochre-coloured amalgamated beds of quartzose sandstone displaying massive to planar-tabular bedding, typical of Facies 1 (F1); (b) Planar-parallel laminated sandstone from Facies 1 (F1). Note the ferruginous tuffite nodules within the F2 unit separating the F1 unit of sandstone dominated heterolithic succession; (c) Alternate occurrence of F1 and F2 of the sandstone dominated heterolithic unit; (d) Ferruginous tuffite layer within Facies 2 (F2), showing intense iron oxide impregnation and hematitic replacement of the clayey matrix from the tuffite layer.

Facies 2 (F2): This facies comprises alternating laminated sandstone and grey shale-siltstone interbeds, separating the thicker sandstone units of F1 (*Fig.4.25c*). The shale intervals share similar textural and compositional attributes with those of the shale-dominated heterolithic unit, whereas the sandstones are millimetre to 1cm thick, fine to medium grained, and exhibit planar parallel lamination.

In several exposures, these facies contain well-developed tuffite layers, comparable to those within the shale-dominated heterolithic unit. However, the tuffite beds are markedly more ferruginous and frequently exhibit complete replacement of the clayey matrix by iron oxides, producing dense, hematitic layers (*Fig. 4.25d*). This observation suggests enhanced post-depositional ferruginization likely associated with fluid migration along permeable sandstone horizons.

Interpretation:

Shale dominated heterolithic unit: The shale-dominated heterolithic unit records a storm-influenced, shallow-marine shelf to lower-shoreface system punctuated by repeated ash-fall events. Millimetre-scale alternations in F1 reflect rhythmic suspension fallout with minor traction under persistently low energy condition. These packages represent fair-weather background sedimentation below or near fair-weather wave base. F2 captures the quiescent to mildly restricted phases of the same shelfal tract where fissile blackish-grey shale with interbedded tuffite and thin gypsum partings indicates calm-water settling along with intermittent salinity difference. F3 comprises thin to locally amalgamated, ripple to hummocky cross stratified sandstones emplaced during storm bursts that repeatedly reworked the sea floor and advanced the lower-shoreface sand apron across the mud-dominated shelf.

The tuffite horizons are syn-depositional volcanic-ash inputs dispersed over wide distances. Their tripartite layering (clay-rich base, ferruginous middle, silty cap) is consistent with hydrodynamic and grain-size segregation during water-column fallout. Later ferruginization may have produced the laminated to nodular variants and concretionary bands. The observed decline of TREEY with increasing ferruginization implies partial REE remobilization or dilution during Fe-oxide addition, rather than loss of stratigraphic continuity.

Vertical stacking patterns in the shale-dominated successions commonly show alternate occurrence of F1 and F2, capped by F3, forming metre-scale coarsening-upward cycles that record progradation of the storm-wave base and shoreface during relative sea-level stillstands or slow fall. Local fining-up successions and gypsum-bearing F2 intervals indicate episodic flooding and transient restriction during minor rises. In this framework, the repeated return of tuffite within F2 reflects episodic volcanism superimposed on the background allocyclic (sea-level/climate) forcing of the shelf.

Sandstone dominated heterolithic unit: Within the sandstone-dominated heterolithic unit F1 packages of massive to planar-tabular, medium- to coarse-grained quartzose sandstones represent higher-energy, proximal lower- to middle-shoreface deposition with frequent storm amalgamation. Intervening F2 couplets of laminated fine sandstone–grey shale/siltstone are flooding-surface to waning-energy intervals that partition the thicker sand sheets into parasequences. Where present, tuffite within this unit is notably more ferruginous and locally hematitic, implying focused post-depositional fluid flow and oxidation along

permeable sandstone pathways. This permeability contrast explains the stronger ferruginization and occasional complete replacement of clayey tuffite matrices in the sandstone-rich tracts.

Synthesizing these observations, the Katrol succession records a storm-dominated shelf repeatedly dusted by volcanic ash, with shoreface progradation expressed as stacked coarsening-up cycles bounded by flooding surfaces that host laterally persistent tuffite sheets. Gypsum partings, pervasive ferruginization, and nodular growth reflect early diagenesis in oxidizing, intermittently restricted pore waters. Ferricrete-style overprinting further implies the most intense ferruginization at the late stage of diagenesis. Possibly the sandstone permeability and structural conduits controlled this lithology specific fluid focusing. For stratigraphic correlation and geochemical targeting, the tuffite-bearing F2 intervals are the most diagnostic across the study area.

4.6.1.2. Sampling:

Systematic sampling was conducted to evaluate the vertical and lateral geochemical variability within the ferruginous–phosphatic horizons of the Katrol Formation. The sampling program specifically targeted (i) tuffite layers at multiple stratigraphic levels within each measured section, and (ii) representative channel intervals dominated by the tuffite layers (F2) (*Fig. 4.26*). A total of 21 litholog-based sections were examined, from which hand specimens and channel samples were collected from fresh, unweathered exposures.

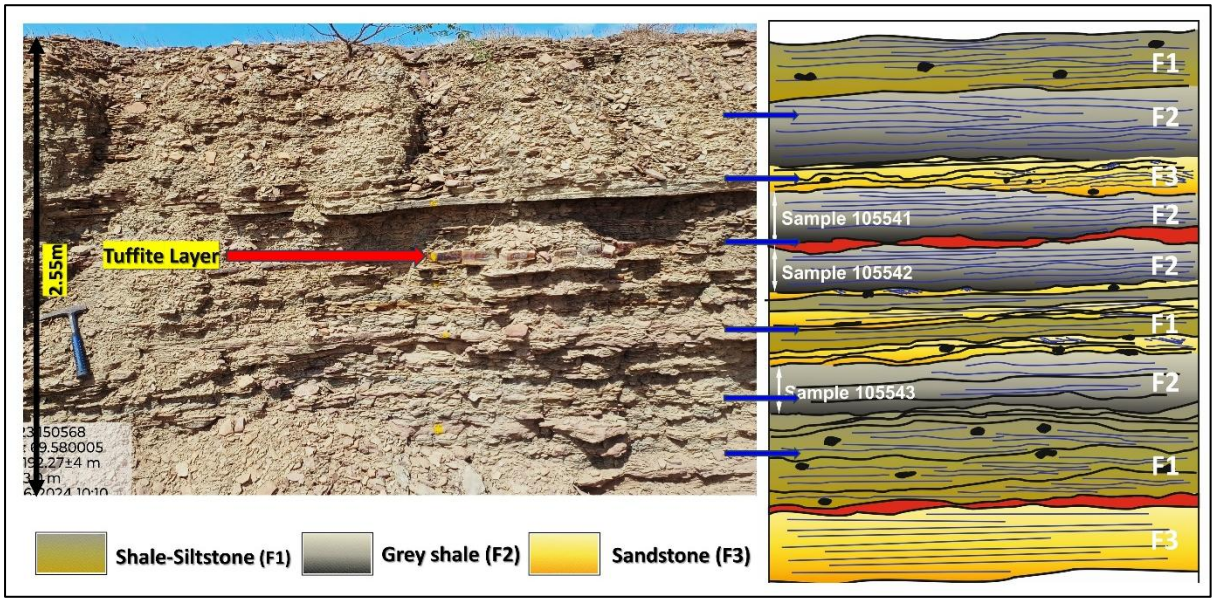

Fig. 4. 26 Representative field section showing the position of the channel sampling across tuffite horizons within the shale-dominated heterolithic unit of the Katrol Formation.

57 hand specimens of tuffite beds were obtained for whole-rock geochemical analysis (REEY, major and trace elements) (*Annexure-XIII and XIV*), petrography, and mineragraphy, while selected tuffite layers were reserved for X-ray diffraction (XRD) studies (*Annexure-XV*).

All samples were systematically labelled according to their stratigraphic position, facies association, and field coordinates to facilitate section-wise geochemical correlation and vertical compositional profiling.

28 channel samples were collected (*Annexure-XVI and XVII*) across stratigraphic intervals of 50-70cm thickness, primarily encompassing the F2 facies, which contains the tuffite and shale interbeds (*Fig. 4.26*). This approach ensured the representation of both lithological variability and internal compositional gradients within the target REE-bearing horizons.

4.6.2. Geochemical Analysis of Mineral System-I

Geochemical analysis was carried out to evaluate the REE enrichment pattern, major and trace element distribution, and geochemical behaviour of the tuffite layers within the Katrol Formation. The analytical program aimed to quantify the extent of REE accumulation, identify the controlling lithogeochemical parameters, and assess compositional variations both vertically and laterally across the stratigraphic sections.

A total of 85 samples were analyzed from tuffite horizons and channel profiles, collected systematically during the facies logging phase. The results have been presented in two parts.

4.6.2.1. Results and Analysis of Tuffite horizons:

A total of 57 samples from the tuffite horizons have been analyzed for major-oxides, trace elements and REE thorough XRF and ICP-MS (*Annexure-XIII and XIV*). Geochemical analyses of the tuffite layers within the shale-dominated heterolithic unit of the Katrol Formation reveal a strong positive correlation (r=0.95) between TREEY and P_2O_5 concentrations, indicating that REE enrichment within the tuffite layers is closely associated with phosphate phases. The analytical results (*Fig.4.27*) demonstrate that TREEY values range between 164 ppm and 1722 ppm, with an average concentration of approximately 400 ppm and standard deviation of 304, whereas the P_2O_5 content varies between 0.08 wt.% to 12.5 wt.% with standard deviation of 2.4, across different localities within the Bhuj REE Prospect Block. The highest TREEY values (>1000 ppm) are recorded in the southern and central parts of the mapped area, coinciding with the shale-dominated heterolithic tracts of the Katrol Formation. Moderate REE enrichment (500-1000 ppm) is observed at the central part of the block, whereas comparatively lower concentrations (<300 ppm) occur at the eastern part of the block mainly at the transition zones of shale dominated and sandstone dominated heterolithic units.

The relationship between Fe_2O_3 and TREEY in the analyzed tuffite samples exhibits a weak negative correlation (r=-0.26), implying that the REE concentration tends to marginally decrease with increasing ferruginization. This pattern suggests that iron enrichment, reflecting secondary diagenetic oxidation, may have led to partial dilution or remobilization of REEs from their primary phosphate hosts.

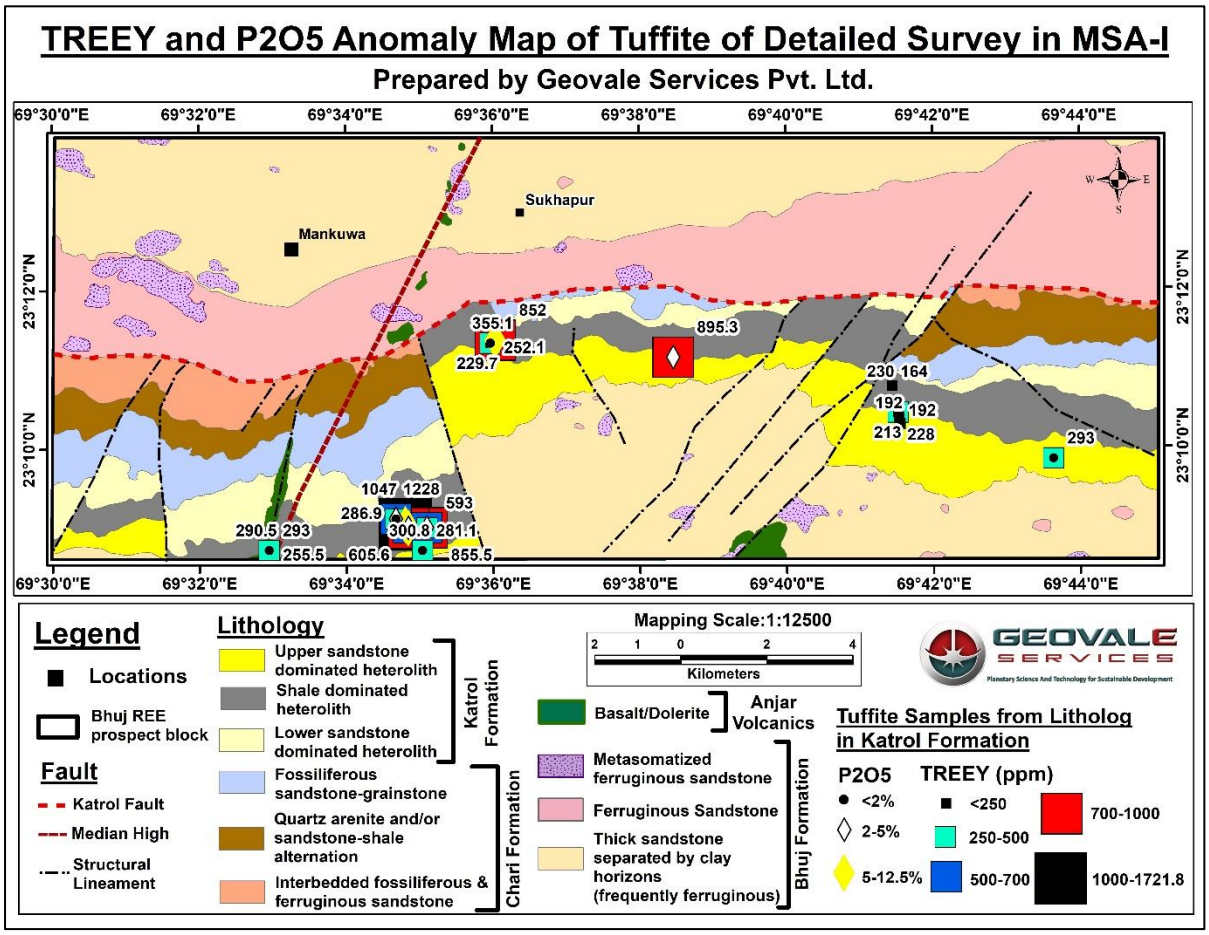

Fig. 4. 27 Spatial distribution map showing TREEY (Total Rare Earth Elements + Y) and P_2O_5 anomalies within the tuffite horizons of the Katrol Formation in the Bhuj REE Prospect Block.

Spatial correspondence between the REE and P_2O_5 anomalies further emphasizes a genetic linkage between REE enrichment and phosphate mineralization, most likely hosted within apatite-gorceixite-florencite group minerals. The co-occurrence of Fe_2O_3 and P_2O_5 rich layers, together with their confinement to finely laminated tuffaceous horizons, indicates that volcaniclastic inputs acted as a primary REE source, while phosphatic diagenesis provided the geochemical trap. The tuffite beds' lateral continuity along strike further supports their syngenetic-diagenetic origin within a volcaniclastic-marine depositional setting, where repeated ash-fall events and Fe-P precipitation facilitated REE accumulation.

Vertical profiling of a representative litholog (*Fig. 4.28*) reveals that the TREEY concentrations in the tuffite beds ranges between 0.03% and 0.17%, with higher values (0.12-0.17%) occurring in less ferruginized tuffite beds exhibiting the characteristic tripartite layering. The observed down-profile reduction in REE concentration corresponds to progressive ferruginization and Fe-oxide replacement, reaffirming the inverse relationship between ferruginization intensity and REE retention, as established through both field and geochemical observations. These patterns indicate a primary depositional enrichment,

subsequently modified by diagenetic Fe-P remobilization processes, which led to the dilution and redistribution of REEs across successive stratigraphic levels.

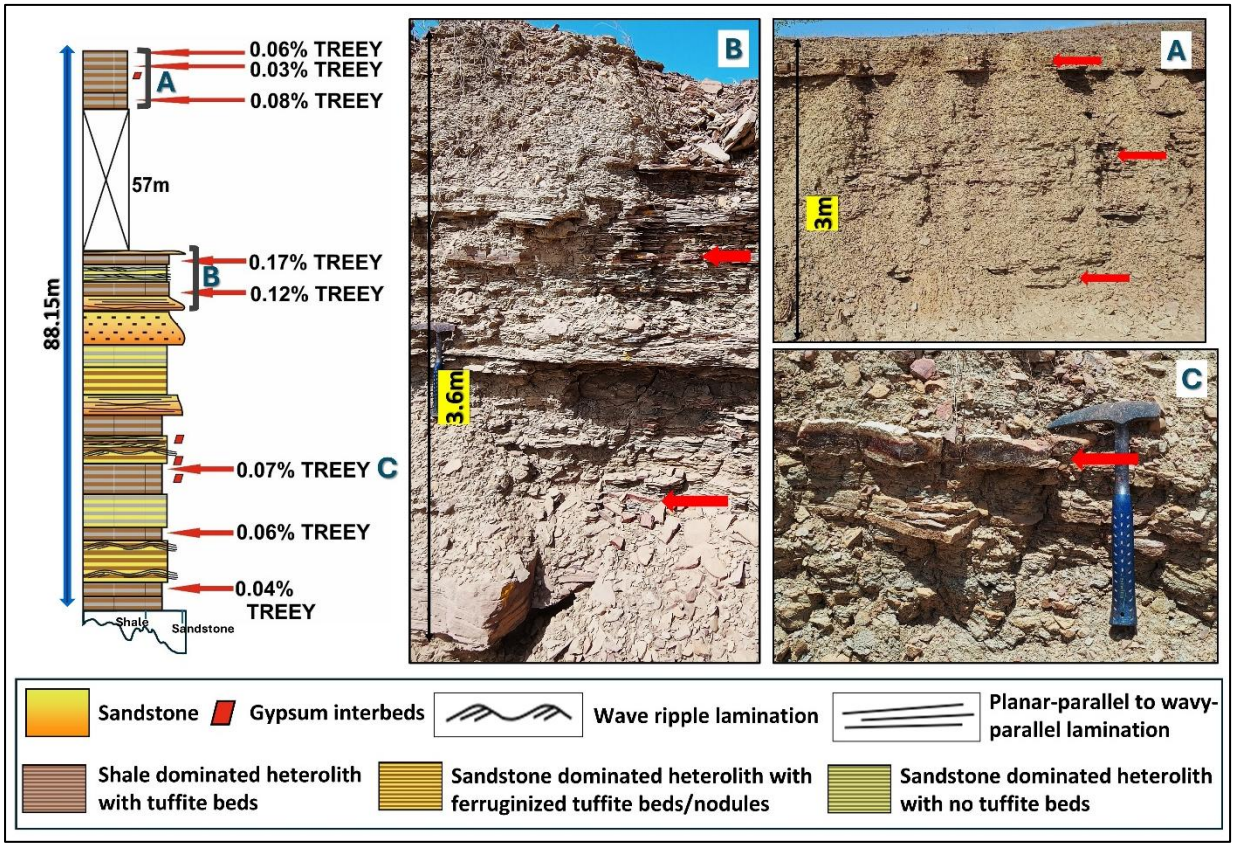

Fig. 4. 28 Representative litholog from the Katrol Formation illustrating vertical variation in TREEY concentrations within the tuffite-bearing heterolithic facies.

Collectively, the tuffite horizons represent stratiform, volcaniclastic–phosphatic REE enriched beds that are laterally extensive and geochemically coherent, forming the principal host for Mineral System I (Katrol Stratiformal REE-bearing System) within the Bhuj Block. Their preferential development within the shale-dominated heterolithic unit, combined with a well-defined Fe-P-REE geochemical association, underscores a strong volcanogenic and diagenetic control on REE mineralization. This integrated geochemical framework identifies these horizons as the most prospective targets for detailed geochemical, mineralogical, and sub-surface investigations, aimed at delineating the stratiform REE potential of the Katrol Formation.

4.6.2.2. Results and Analysis of Channel Sampling

A total of 28 channel samples were analyzed for major oxides, trace elements, and REEs using XRF and ICP-MS (*Annexure XVI and XVII*). The sampling was conducted primarily across the F2 facies within the shale-dominated heterolithic unit, aiming to capture the integrated

geochemical signature of the tuffite-bearing shale horizons over 50-70cm stratigraphic intervals.

The analytical results indicate TREEY concentrations ranging from 80ppm to 358ppm, with an average of ~306ppm and a relatively low standard deviation of 53, suggesting overall geochemical homogeneity within the sampled intervals. Although the REE values are above the upper-crustal baseline, they are significantly lower than the discrete tuffite-layer assays, reflecting the dilution effect of enclosing non-phosphatic shale and siltstone components within the composited channel sections.

No statistically significant correlation is observed between TREEY and P_2O_5, indicating that REE enrichment within the channel profiles is only weakly associated with phosphate phases at the bulk-rock scale. Instead, the enrichment appears to be facies-controlled, with localized REE concentration confined to thin tuffite layers rather than pervasive mineralization throughout the section.

From an exploration perspective, the channel assay data highlight the limited potential of bulk exploitation due to the low overall grade. However, the consistent above-background TREEY concentrations affirm the presence of an intrinsically fertile depositional system, strengthening the geological model of a stratiform volcaniclastic-phosphatic REE-bearing horizon (Mineral System-I). These findings justify further sub-surface geochemical and mineralogical investigations, focusing on delineating the most REE-enriched tuffite seams rather than broad mining targets.

4.6.3. Petrographic and Mineragraphic Analysis of Mineral System-I

Petrographic and mineragraphic studies were undertaken on representative samples from the ferruginous–phosphatic (tuffite) horizons of the Katrol Formation to elucidate their microtextural features, mineral paragenesis, and post-depositional alteration processes associated with REE enrichment (*Annexure-XII*). These investigations aim to complement the geochemical data and provide micro-scale evidence of the syngenetic to diagenetic evolution of the REE-bearing mineral phases.

4.6.3.1. Petrographic Analysis of the Tuffite Layers

Detailed petrographic studies were conducted on seven representative thin sections from the Katrol Formation, covering high-, moderate-, and low-REE-bearing tuffite horizons, to document their textural, mineralogical, and diagenetic characteristics. The observations were aimed at elucidating the depositional nature of the tuffaceous beds and assessing the mineralogical controls on REE enrichment.

Under the microscope, the tuffite layers exhibit a fine to very fine grained clastic fabric, displaying crude lamination defined by alternating phenocryst-rich and matrix-rich bands (*Fig. 4.29*). The framework assemblage predominantly consists of angular to sub-angular quartz and feldspar (plagioclase and microcline), accompanied by minor muscovite, all dispersed within a fine ferruginous and/or micritic carbonate matrix (*Fig. 4.30a*). Accessory detrital minerals such as mud pellets, volcanic glass shards, zircon, monazite, and tourmaline occur sporadically within the matrix. The coexistence of feldspar, volcanic glass shards, and mud pellets indicates a mixed detrital–volcaniclastic provenance, reflecting alternating input from clastic and pyroclastic sources.

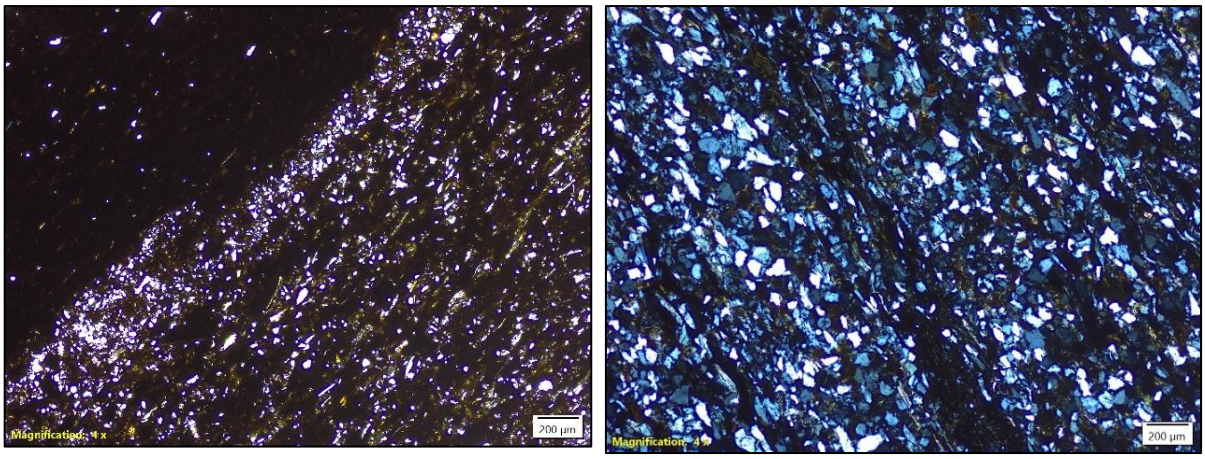

Fig. 4. 29 Photomicrograph of Katrol tuffite samples under cross polarized light showing fine to very fine-grained clastic texture with well-developed to crude lamination, composed of alternating phenocryst-rich and matrix-rich layers.

The matrix component displays a heterogeneous mixture of fine grained ferruginous material, apatite cement, and altered volcanic glass, occurring either individually or in varying combinations across different samples. Apatite and fluorapatite appear as acicular, needle-like, or equant grains, commonly disseminated throughout the matrix and occasionally forming micro-laminated aggregates that impart a felty texture (*Fig. 4.30b*). These phosphatic minerals constitute the principal REE-hosting phases within the tuffite. The rocks are moderately sorted, with wedge, needle, and triangular-shaped quartz grains exhibiting irregular, sutured, or embayed grain boundaries (*Fig. 4.30a*).

Microscopic examination also reveals distinct colour and compositional banding, with iron-rich (reddish-brown) and iron-poor (grey to buff) laminae, corresponding to variations in matrix composition in different samples. The ferruginous laminae comprise hematite and goethite microcrystals that locally overprint or replace phosphatic zones, suggesting post-depositional ferruginization. Tuffite varieties with pervasive iron-oxide cementation display lower TREEY concentrations, reflecting partial remobilization or dilution of REEs during diagenetic oxidation. In contrast, phosphatic or glassy tuffites exhibit better preservation of REE-bearing apatite, correlating with higher TREEY values in geochemical analyses.

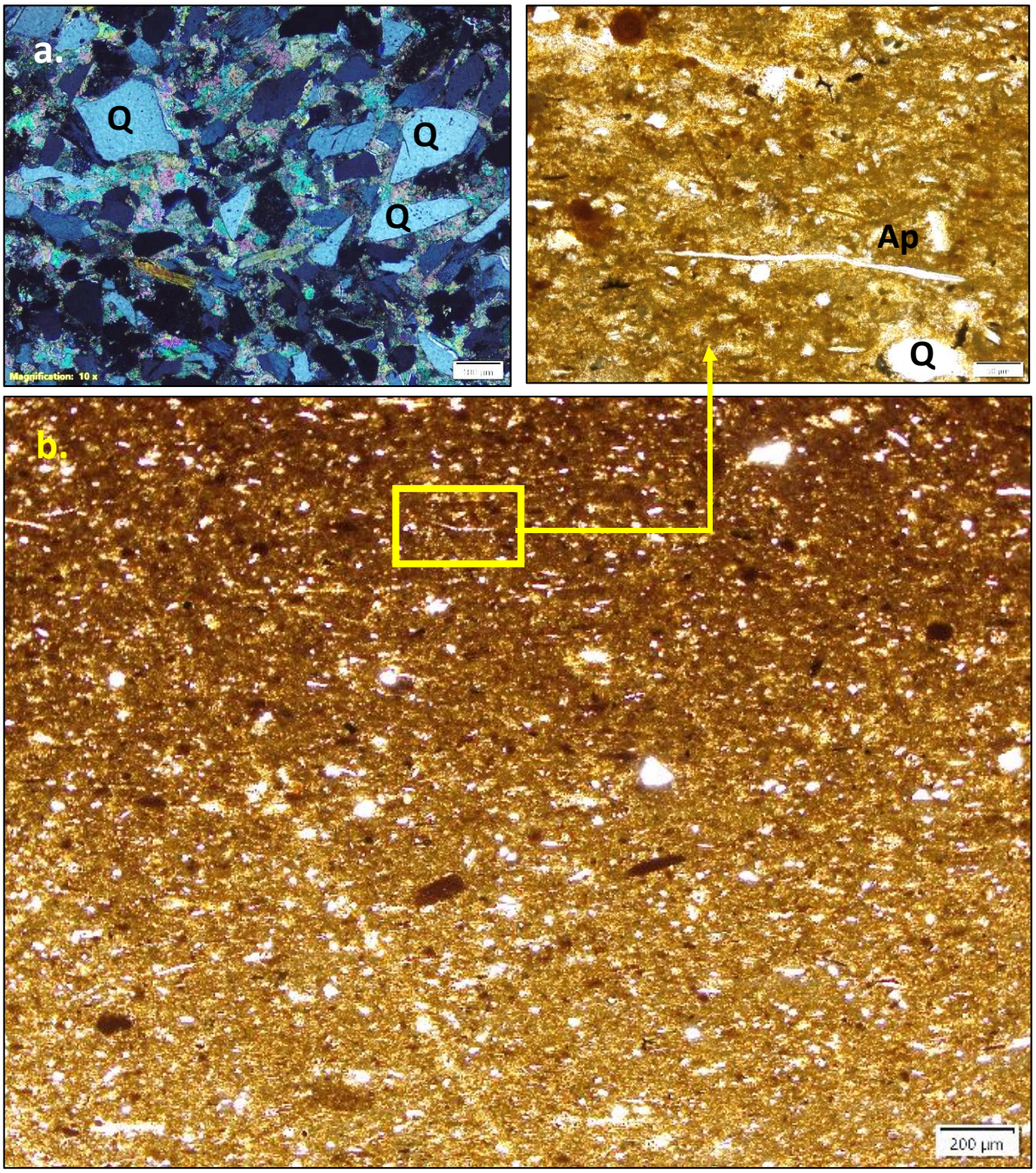

Fig. 4. 30 Photomicrograph of Katrol tuffite samples. (a) Thin section under cross-polarized light showing angular quartz, feldspar and muscovite embedded in a micritic carbonate matrix. Note the wedge and needle shaped quartz grains exhibiting irregular, sutured, or embayed grain boundaries. (b) Photomicrograph displaying acicular and equant apatite (Ap) and quartz crystals disseminated within a ferruginous-phosphatic matrix.

The overall petrographic fabric, defined by wedge, needle, and shard shaped quartz grains, volcanic glass relics, within a glassy cement, strongly confirms a volcaniclastic origin for the Katrol tuffite horizons. The observed lamination and rhythmic alternation of framework

and matrix-rich layers are interpreted to represent repeated ash-fall and sediment settling events, followed by early diagenetic cementation under shallow-marine conditions.

4.6.3.2. X-Ray Diffraction (XRD) Analysis of the Tuffite Layers

X-Ray Diffraction (XRD) analysis was carried out on two strategically chosen samples of the tuffite layers within the shale-dominated heterolithic unit of the Katrol Formation to characterize their mineralogical composition and identify the principal REE-hosting phases (*Annexure-XV*). Both the samples, characterized by distinctly different TREEY contents exhibit systematic mineralogical contrasts that reflect the interplay between REE enrichment, phosphate abundance, and iron oxide development.

High-REE sample (TREEY: 1,047 ppm; P_2O_5: 8.5%; Fe_2O_3: 7%):

The XRD spectrum of the sample shows a phosphate-rich assemblage dominated by fluorapatite, with subordinate kaolinite, goethite, quartz, minor mica, and traces of dolomite and rutile. The clear presence of fluorapatite is consistent with the high P_2O_5 and elevated TREEY, indicating that REEs are chiefly hosted in phosphate phases within the tuffite matrix.

Low-REE sample (TREEY: 250 ppm; P_2O_5: 0.45%; Fe_2O_3: 12%):

The XRD pattern of the sample lacks distinct apatite peaks and is dominated by kaolinite and quartz, with notable goethite, and minor mica and rutile. The absence of apatite and the dominance of Fe-oxide minerals (goethite) correspond with higher Fe_2O_3 content, signifying intense ferruginization and secondary Fe-oxide replacement. This mineralogical overprinting is interpreted to have caused partial removal or dilution of REEs from phosphate phases, consistent with petrographic and geochemical evidence of Fe–P remobilization.

Interpretation and Remarks

The XRD results confirm that the tuffite layers of the Katrol Formation represent phosphatic-volcaniclastic strata characterized by fluorapatite and Fe-oxide bearing mineral assemblages, which collectively act as the primary REE sinks within the stratiform system. The comparative mineralogy of the analyzed samples corroborates the geochemical trend, whereREE enrichment increases with phosphate (fluorapatite) abundance and decreases with progressive Fe-oxide replacement. This mineralogical control provides a robust criterion for ranking stratigraphic horizons during subsequent sub-surface exploration and resource delineation.

4.6.3.3. SEM-EPMA Study of Tuffite Layers

Scanning Electron Microscopy (SEM) and Electron Probe Micro-Analyzer (EPMA) investigations were carried out on three representative samples (*Annexure-XVIII*) from the

Katrol Formation to elucidate the microstructural attributes and mineral chemistry of the REE-hosting phases within the tuffite horizons. Two samples were selected from the tuffite layers and one from the associated fine-grained sandstone. These high-resolution analytical techniques provide critical insights into mineral paragenesis, microtextural relationships, and the physicochemical processes governing REE incorporation and redistribution within the tuffite-bearing strata.

SEM-EDAX Analysis

Tuffite:

Back-scattered SEM images and spot EDAX from two tuffite samples show a clastic-authigenic mosaic of angular quartz and K-feldspar fragments with sparse monazite, ilmenite titanite and volcanic zircon enclosed in a felty, microlithic matrix dominated by Fluro-apatite (*Fig. 4.31, 4.32 and 4.33*). The matrix is patchily replaced by magnetite occurring both as discrete grains and along replacement fronts (*Fig.4.32*). Locally, zeolitic relics are pseudomorphed by fluorapatite, which is in turn overprinted by magnetite, defining a replacement sequence of zeolite → fluorapatite → magnetite. Locally, Fe-ca cement is also observed, suggesting diagenetic precipitation under reducing to weakly oxidizing. Occasional Fe–Ca carbonate cementation is also observed, implying diagenetic precipitation under reducing to weakly oxidizing conditions. This mineral assemblage and replacement sequence, together with the fine lamination and absence of high-temperature recrystallization, indicate syn to early diagenetic phosphate cementation of ash derived detritus, followed by Fe-rich diagenetic/hydrothermal overprint under fluctuating redox conditions.

Fine grained sandstone associated with the tuffite facies:

The associated fine grained sandstone comprises angular to sub-angular quartz and feldspar (K-feldspar, microcline, albite) with muscovite flakes and fragments of volcanic glass shards. The framework grains often display wedge, needle, or triangular shapes with sharp boundaries and local embayment (*Fig.4.34*), indicating mechanical fragmentation and volcanic input of the framework. Intergranular spaces of the sandstone are filled by Fe-rich cement with magnetite microgranules (*Fig.4.34*) and subordinate amount of isotropic glass and patchy carbonate cement. Local flow-like microstructures within aligned phyllosilicates suggest reworked pyroclastic and/or volcanic input (ignimbritic affinity). The textural and chemical features point to a volcaniclastic sandstone that is spatially and temporally linked to the tuffite horizons.

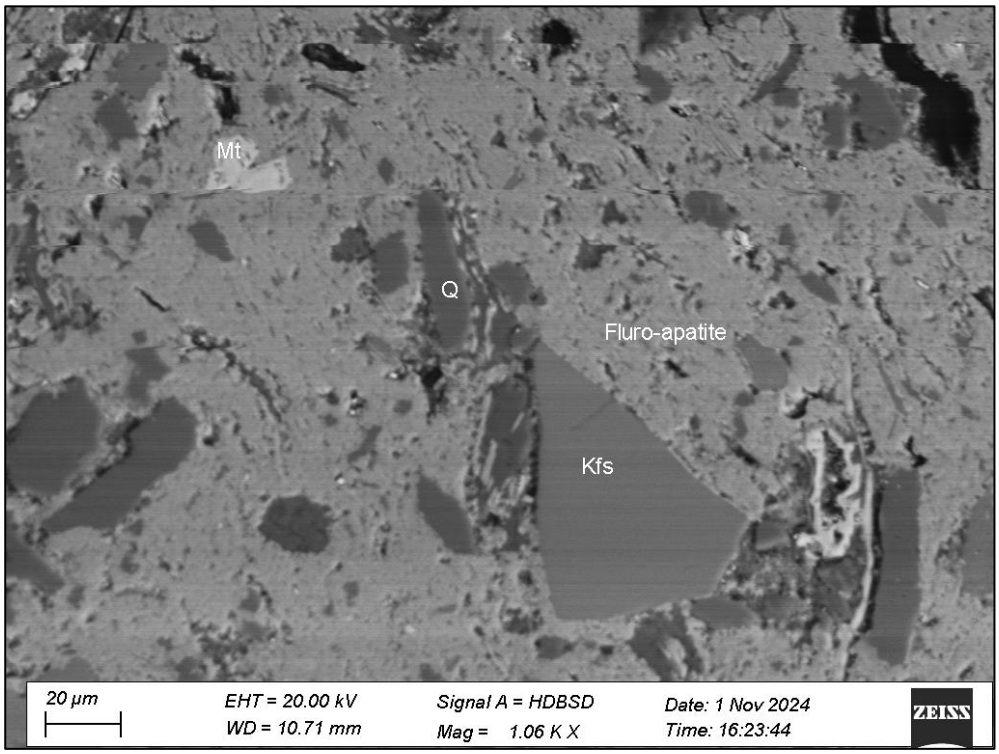

Fig. 4. 31 BSE micrograph of tuffite sample of Katrol Formation. Angular clasts of quartz (Q) and K-feldspar (Kfs) occur as framework grains within a fine Fe-P rich matrix. Magnetite (Mt) occurs as disseminated grains and replacement patches within the matrix. Fluorapatite forms the dominant cementing phase.

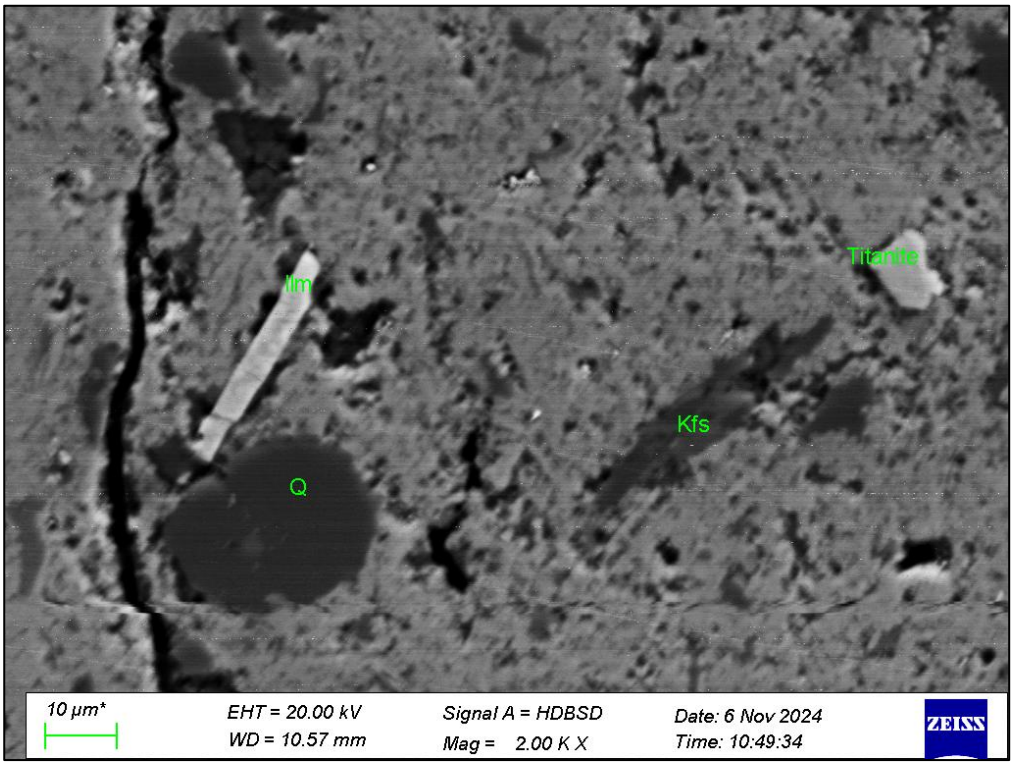

Fig. 4. 32 BSE micrograph of tuffite sample of Katrol Formation, showing framework grains of quartz (Q), K-feldspar (Kfs), and ilmenite (Ilm), with titanite (Ttn) as accessory detrital phase. The matrix is composed of fine fluorapatite.

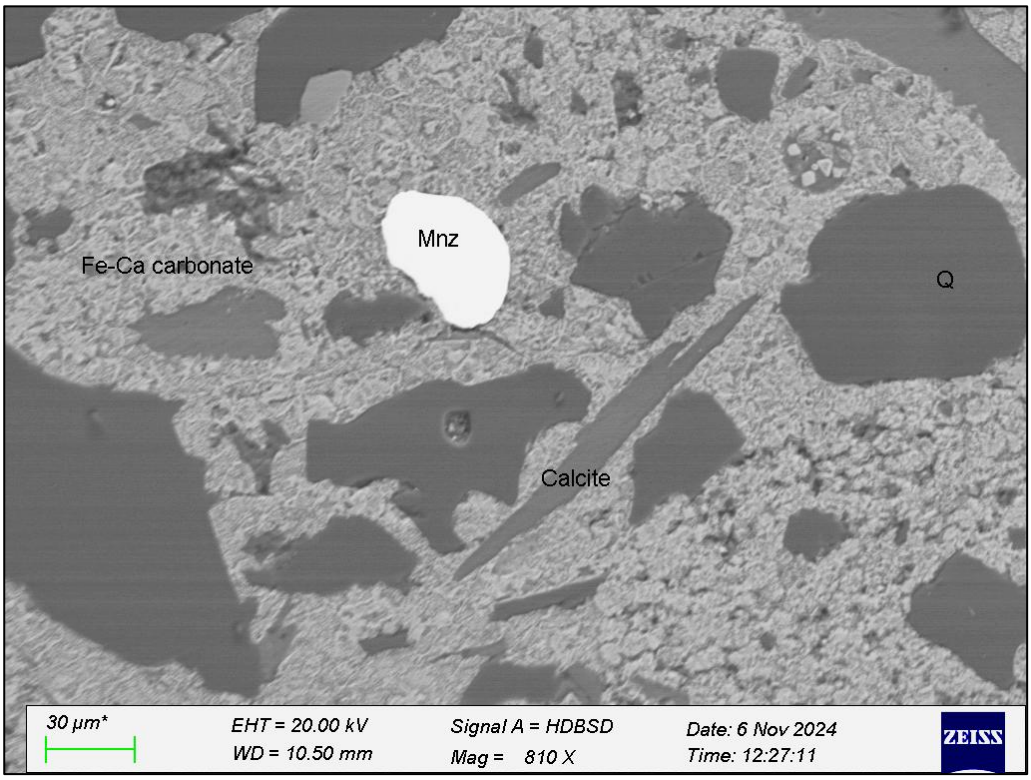

Fig. 4. 33 BSE micrograph of Katrol tuffite, showing monazite (Mnz), Quartz (Q) and calcite occur as framework grains, embedded within a Fe-Ca carbonate matrix.

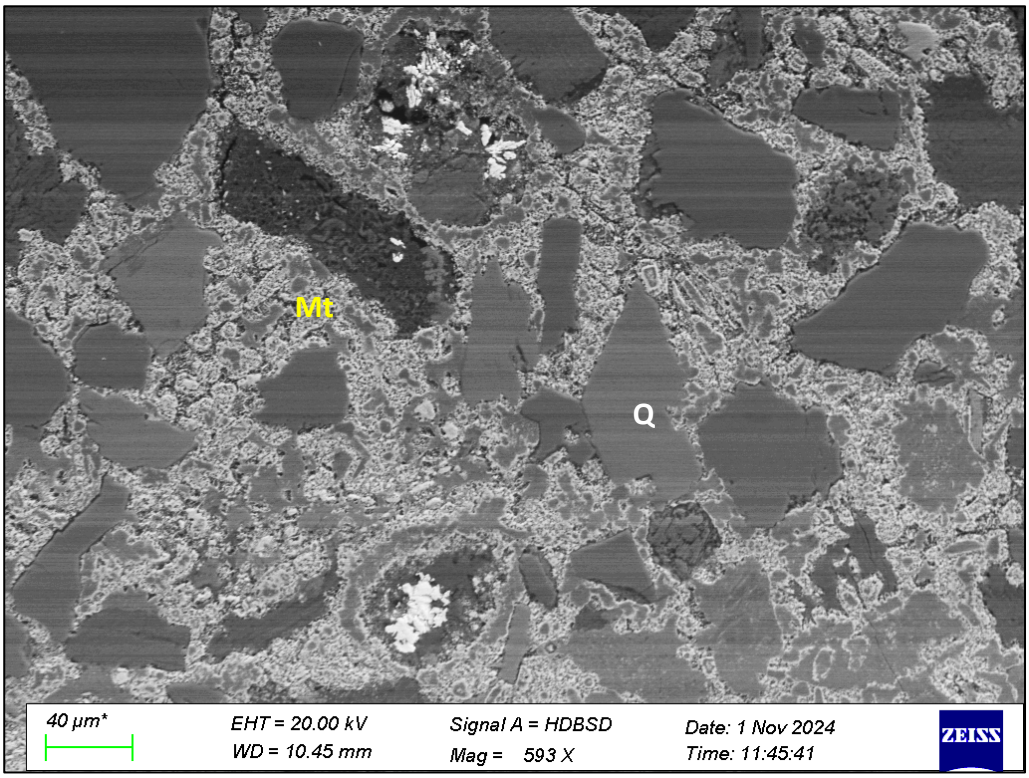

Fig. 4. 34 BSE micrograph of fine grained Katrol sandstone showing angular quartz (Q) grains embedded in a magnetite (Mt) rich matrix. Note the wedge, needle, or triangular shapes of the grains with sharp boundaries and local embayment.

Interpretation and Remarks

Together, the SEM observations verify volcaniclastic sourcing for the Katrol tuffite beds, and document authigenic fluorapatite as the principal phosphate cement, that in turn, partially replaced by Fe-oxide, plausibly diminishing the REE retention in the most ferruginized layers, consistent with the inverse Fe_2O_3-TREEY trends derived from bulk geochemistry.

EPMA Analysis

Tuffite:

Electron Probe Micro-Analyzer (EPMA) analyses were performed on the tuffite samples of the Katrol Formation to characterize the mineral chemistry of REE-bearing phases (*Annexure-XIX*). The tuffite is extremely fine-grained and predominantly matrix-supported, comprising needle to wedge-shaped quartz and subordinate amount of muscovite embedded within an apatite to fluorapatite rich groundmass (*Fig. 4.35*). Additionally, clasts of kaolinite and chlorite are also present, representing alteration derivatives of feldspathic and volcanic detritus. Local occurrence of zircon and monazite is also being note (*Fig.4.36*). The apatite within the matrix exhibits notably high P_2O_5 concentrations, reaching up to 34 wt%. These mineralogical relationships indicate that the REE are mainly concentrated within the phosphate phases (apatite, fluorapatite, and monazite), while zircon and minor xenotime contribute as detrital carriers within the tuffaceous host.

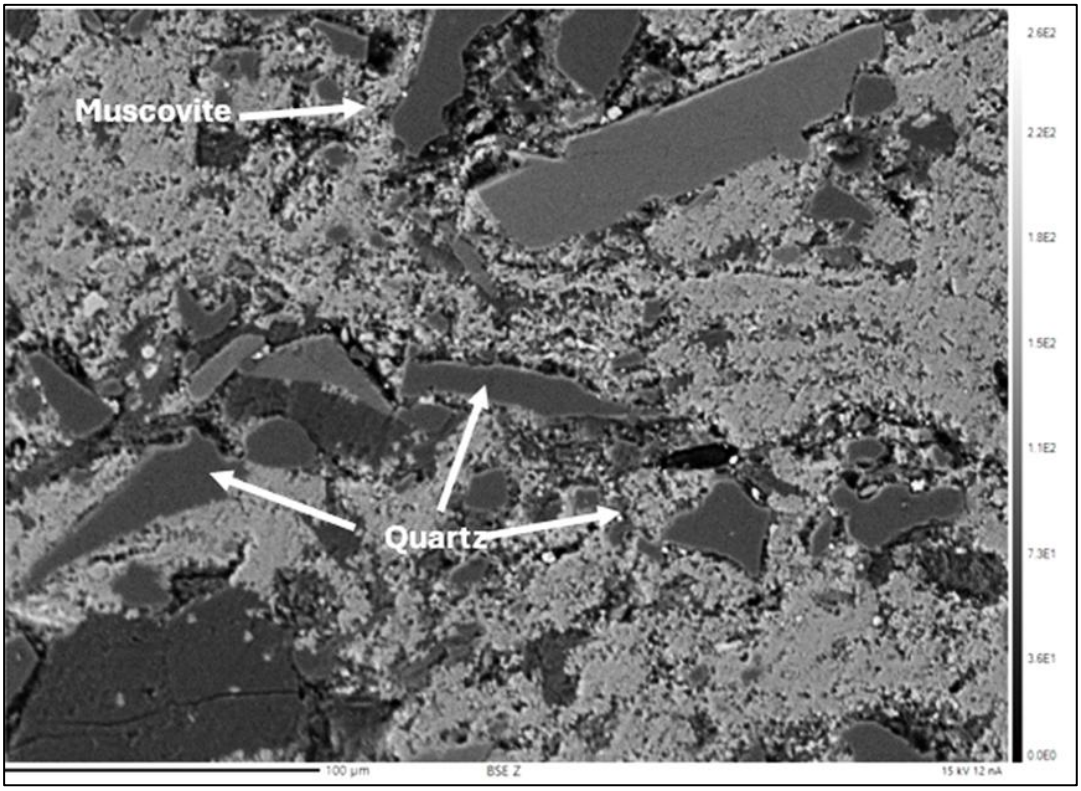

Fig. 4. 35 BSE image of the tuffite from the Katrol Formation showing needle to wedge-shaped

quartz (Q) and muscovite (Ms) clasts suspended within an apatite-fluorapatite-rich matrix.

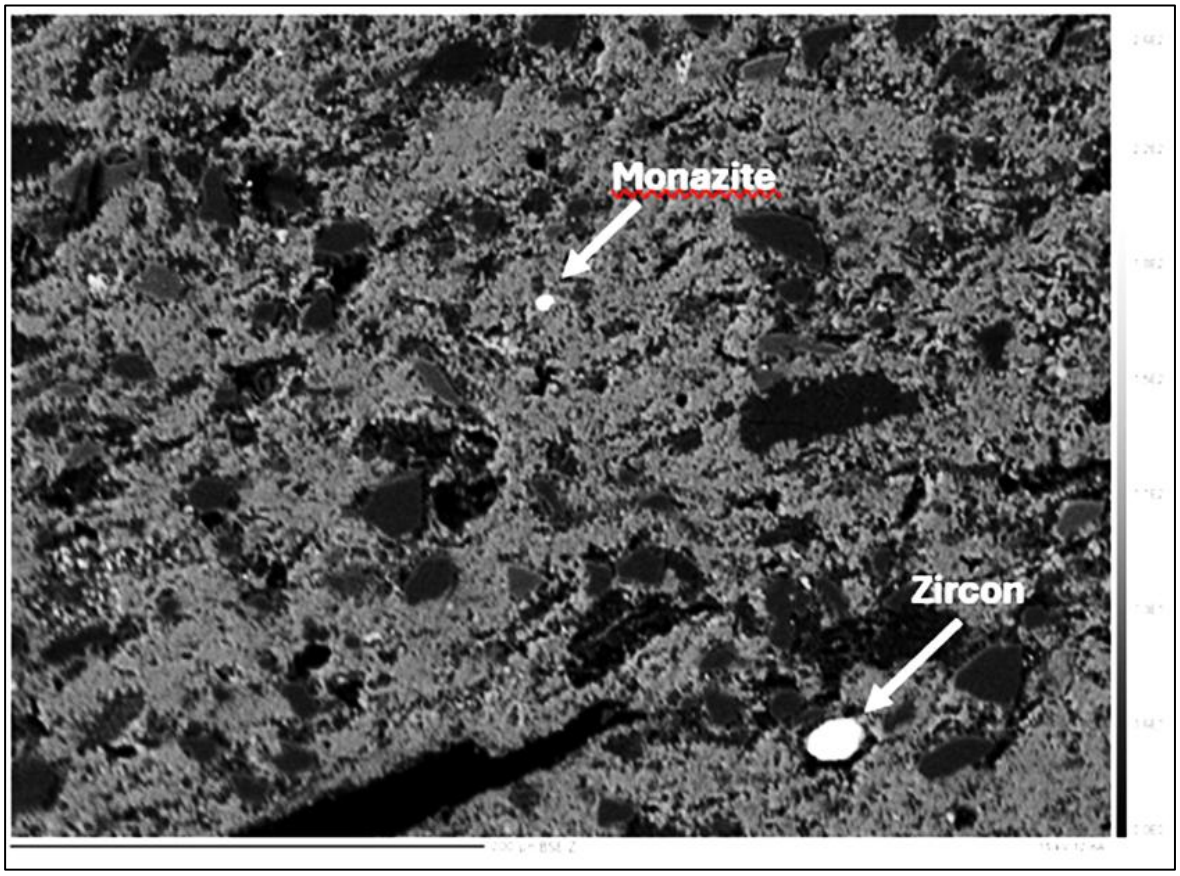

Fig. 4. 36 BSE image of fine-grained volcaniclastic tuffite from the Katrol Formation showing zircon (Zr) and monazite (Mnz) grains, along with muscovite fragments embedded within a apatite rich groundmass.

Interpretation and Remarks

The EPMA data confirm that the tuffites of the Katrol Formation host a detrital heavy mineral assemblage including zircon, monazite, rutile, and xenotime, embedded in an authigenic phosphate matrix dominated by apatite and fluorapatite. This combination points toward a hybrid REE enrichment mechanism involving both volcaniclastic input and early diagenetic phosphate precipitation. The elevated P_2O_5 content also supports the above notion. Collectively, the EPMA results substantiate the interpretation of a volcaniclastic-phosphatic stratiformal REE system within the Katrol Formation, where phosphate minerals act as the primary repositories of REEs.

4.7. Detailed Ground Survey in Mineral System-II

Interpretations from the validation and orientation surveys suggest the presence of an Fe-oxide dominated hydrothermal system within the Bhuj Formation, genetically distinct from the stratiform REE-bearing tuffite system of the Katrol Formation. This system, designated as

the Potential IOCG Type Mineralization System in Bhuj Sandstone, is interpreted as an epigenetic hydrothermal overprint developed along the major structural corridors, notably the Katrol Hill Fault (KHF), the Median High, and their subsidiary splays.

Field observations integrated with geochemical results from heavy-mineral fractions of stream sediments reveal an anomalous concentration of Fe_2O_3, TiO_2, and Zr, coupled with elevated values of Zn, Cr, Co, Sn and REE. This multi-element association indicates a probable hydrothermal contribution to the sediment geochemistry. The concurrent field evidences of ferruginization, hematitic cementation, and localized silicification further corroborate for an Iron Oxide Copper Gold (IOCG)-style mineralization, wherein iron-oxide precipitation and fluid-rock interaction may have played key roles in metal transport and deposition. These findings collectively necessitate a detailed field investigation to trace the lithological sources of these heavy-mineral enrichments within their micro-catchment domains and validate the presence of hydrothermal input into the system.

Accordingly, this phase of investigation aims to identify the lithological sources of heavy-mineral enrichment within the Bhuj Sandstone through integrated field mapping, mineralogical characterization, and geochemical analysis. The study further seeks to evaluate the spatial relationship between these Fe-oxide-rich zones and the fault-controlled hydrothermal network, thereby establishing geochemical and mineralogical vectoring criteria for IOCG-type mineralization. This integrated approach combines field, petrographic, and multi-element analytical data analysis to elucidate the nature, extent, and metallogenic significance of Fe-oxide metasomatism within the Bhuj Formation.

4.7.1. Field Investigation and Sampling

To substantiate the hydrothermal origin of the Fe-oxide dominated system inferred from reconnaissance and orientation surveys, a detailed field investigation was undertaken across the Bhuj Formation. The objective of this phase was to examine the spatial distribution of ferruginous alteration, characterize the lithological and structural settings associated with Fe-oxide metasomatism, and identify potential host horizons for REE and associated critical-metal enrichment.

4.7.1.1. Field Investigation:

Detailed field investigation of the Bhuj Formation was primarily conducted along a NW-SE oriented corridor, following the high-value field and geochemical anomaly zone delineated during the orientation phase (*Fig. 4.37*). Particular emphasis was placed on fault-proximal areas and ferruginized ridges spatially aligned with the Katrol Hill Fault (KHF) and the Median High structural zone.

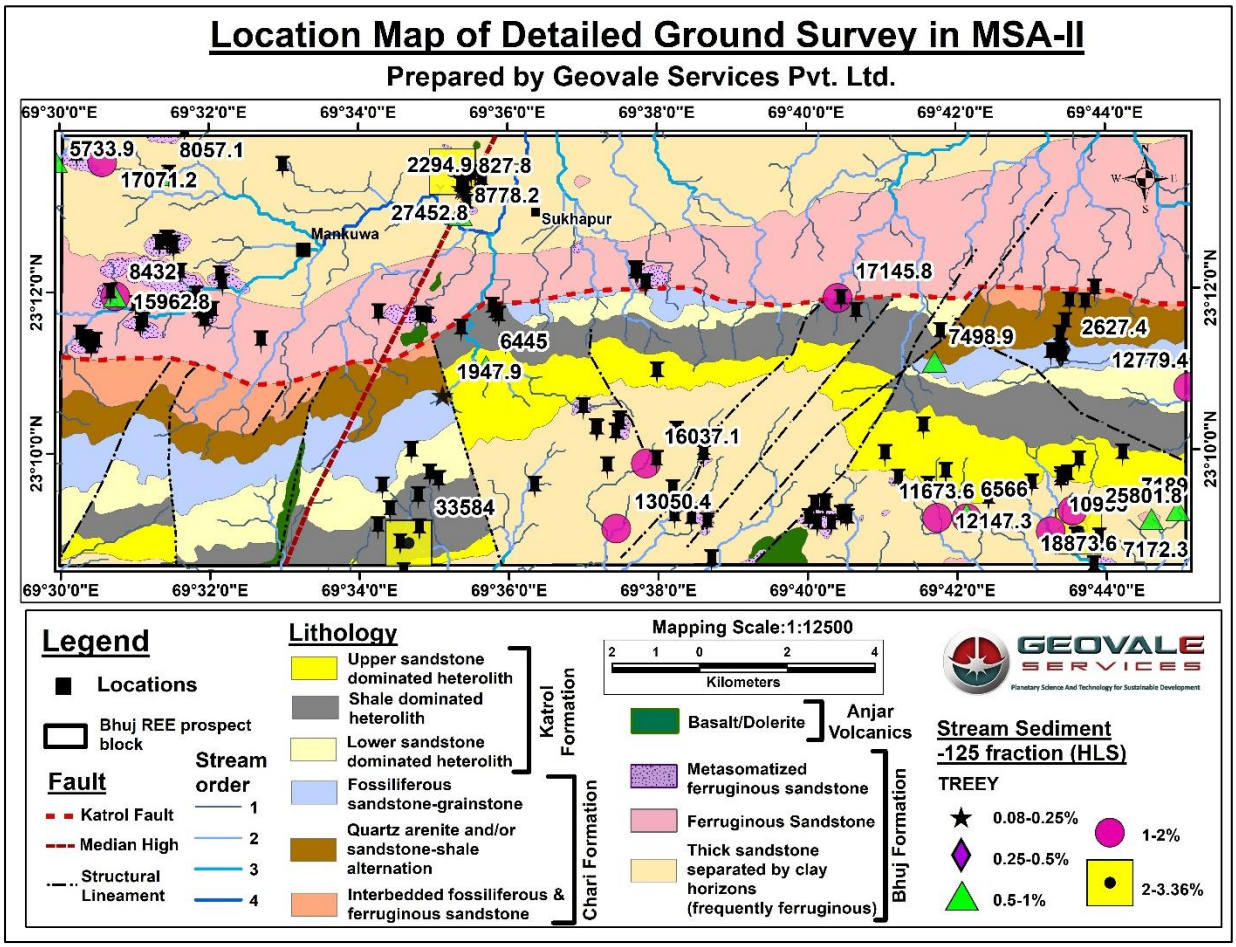

Fig. 4. 37 Location map of detailed field investigation within MSA-II (Bhuj REE Prospect Block).

The provenance areas corresponding to the anomalous stream-sediment values predominantly expose metasomatized ferruginized sandstone and ferruginized breccia, representing the most distinct lithological manifestation of the Fe-oxide-dominated unit of the Bhuj Formation (*Fig.4.38a*).

The outcrops of the **metasomatized ferruginized sandstones** occur either as isolated mounds or linear hill ranges, containing massive to brecciated ferruginous sandstone with variable degrees of iron metasomatism (*Fig.4.38b*). The metasomatic zones are typically lenticular to tabular in geometry (*Fig.4.38c*), laterally continuous for several tens of metres, and preferentially developed along fault planes (*Fig.4.38d*), fracture zones, and bedding-parallel shear surfaces (*Fig.4.38e*). In most locations, it forms ridges, knolls, or resistant ledges readily distinguishable by their dark red to brownish-black to black coloration, reflecting pervasive hematitization and goethitization.


a.


b.


d


c.


e.

Fig. 4. 38 Field photographs showing representative outcrops of metasomatized ferruginous lithounits within the Bhuj Formation. (a) Fault-proximal, intensely hematitized and ferruginized sandstone exposure along the alteration corridor showing pervasive Fe-oxide impregnation and reddish–brown coloration. (b) Isolated ridge composed of massive metasomatized ferruginous sandstone with high iron enrichment forming resistant topographic highs. (c) Tabular metasomatized ferruginous sandstone body exhibiting dark brown to black coloration and significant Fe-oxide iimpregnation. (d) Brecciated and fractured metasomatized ferruginous sandstone developed along the fault zone, showing hematite veining and fluid-assisted fracturing. (e) Bedding-parallel ferruginous sandstone and associated yellowish-brown metasomatic zones with evidence of cross-cutting hematite–carbonate veining. The central part of the exposure shows slight offset and warping of the ferruginous bands, suggesting minor bedding-parallel shearing or flexural slip.

The metasomatized sandstones exhibit reddish-brown to brownish-black coloration, locally grading to black colour with increasing intensity of ferruginization. It is composed of quartz, euhedral feldspar, and quartz aggregates, with minor muscovite, all set within a hematitic to magnetite-rich cement that imparts a distinct magnetic response to hand specimens (*Fig.4.39a; b*). The framework grains are predominantly angular to sub-angular with low sphericity, and feldspar grains often exhibit sharp, fresh crystal boundaries (*Fig.4.39a*). Aggregates of quartz commonly consist of three to four interlocked crystals surrounded by a dense, opaque black groundmass, interpreted as magnetite. Hematite occurs both as felty masses forming the groundmass and as individual grains or coatings enveloping detrital particles (*Fig.4.39c; d*). In several exposures, nearly all framework grains are completely rimmed by hematite, giving the rock a dark metallic lustre. At several locations the metasomatized sandstone exhibits a dark, dense, and semi-vitreous surface texture, with strongly indurated, fine-grained ferruginous matrix enclosing the framework grains. The overall fabric appears spotted, granular, and partially fused fabric, with sharply defined intergranular boundaries and a dull metallic to vitreous lustre suggestive of thermal sintering or contact-type induration (*Fig. 4.39e*). The local development of interlocked and welded grain contacts, along with the vitrified appearance of the ferruginous matrix, indicates incipient thermal recrystallization or chemical welding, most plausibly related to hydrothermal fluid-induced metasomatic hardening rather than direct contact metamorphism.

Authigenic mineral overgrowths of feldspar and mica within the hematitic cement are common, indicating fluid-assisted recrystallization (*Fig.4.39a*). The rocks locally display porous and cavernous textures, resulting from partial leaching of earlier carbonate or clay components, subsequently replaced by Fe-oxide and silica. In certain exposures, sample surfaces exhibit faint greenish to bluish-green coatings, suggesting minor chloritic or Cu-bearing alteration (*Fig.4.39f*).

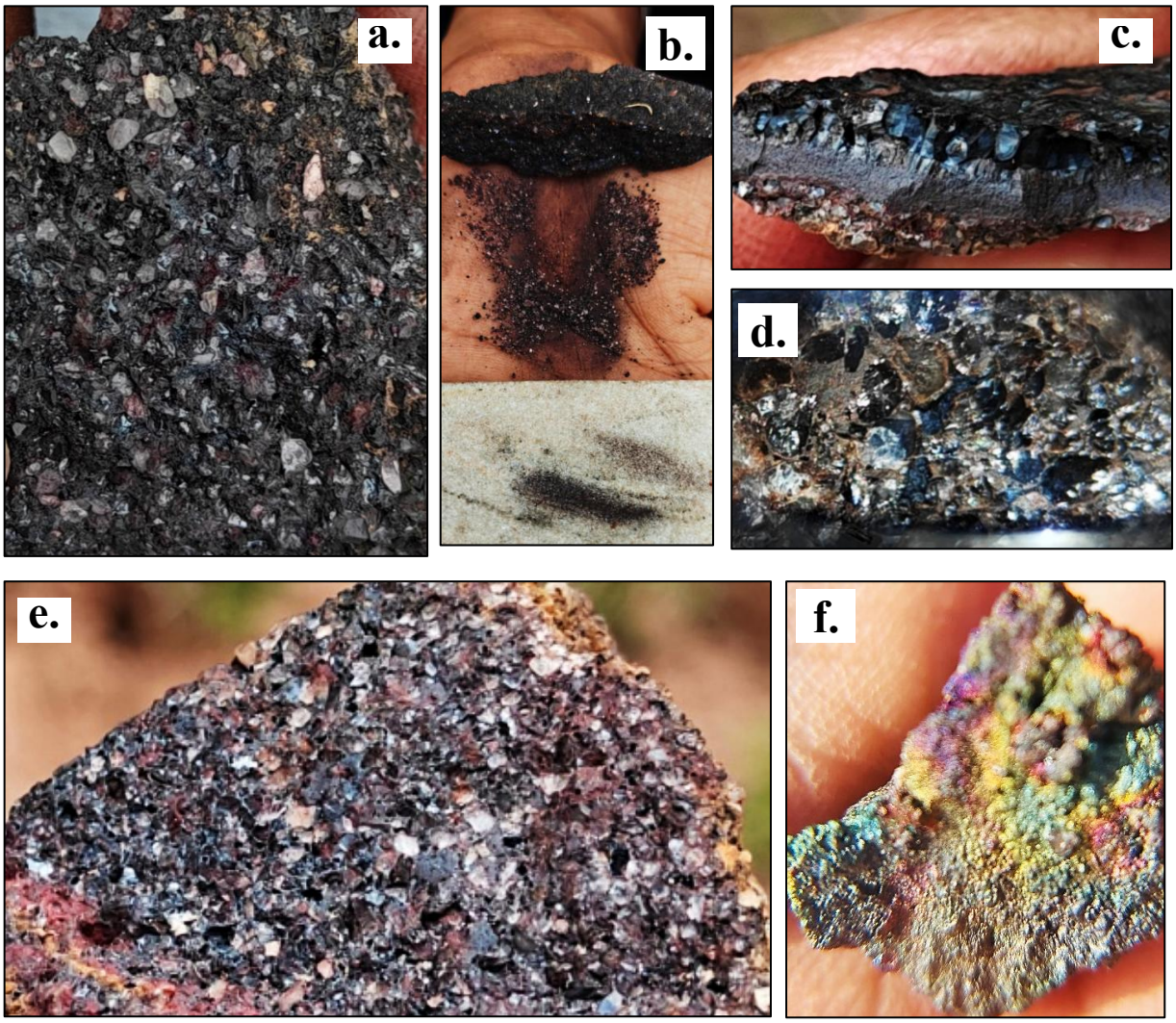

Fig. 4. 39 Hand specimens of metasomatized ferruginous sandstone from the Bhuj Formation showing textural and mineralogical variations. (a) Angular to sub-angular framework of quartz and euhedral feldspar grains embedded within a hematitic to magnetite-rich matrix/cement. Note the distinct metallic sheen of the sandstone. (b) Magnetic response of the ferruginous sandstone confirming magnetite enrichment within the matrix. (c) Hematite occurring as felty mass within the metasomatized sandstone. (d) Close-up of (lens view) the groundmass of the sandstone, displaying coating of each quartz grains with hematite rim. (e) Semi-vitreous, dark, indurated metasomatized ferruginous sandstone exhibiting spotted, granular, and partially welded fabric. (f) Sample surface with iridescent bluish-green coating on it.

Internally, these sandstones exhibit massive to planar cross stratification (*Fig.4.40a*). However, primary structures are observed to be completely obliterated by pervasive Fe-metasomatism in highly altered exposures (*Fig.4.40b*).

Millimetre- to centimetre-scale hematite veins are common, traversing either irregularly or parallel to bedding (*Fig.4.40c*). Bedding-conformable ferruginous bands occur where Fe

influx followed primary stratification (*Fig.4.40a*), while cross-cutting hematite and carbonate veins denote multiple generations of fluid activity (*Fig.4.40d*). Reddish-brown clay alteration and iron-carbonate impregnation are occasionally associated with these hematitic zones (*Fig.4.40e*), with evidence of silicification at hand-specimen scale.

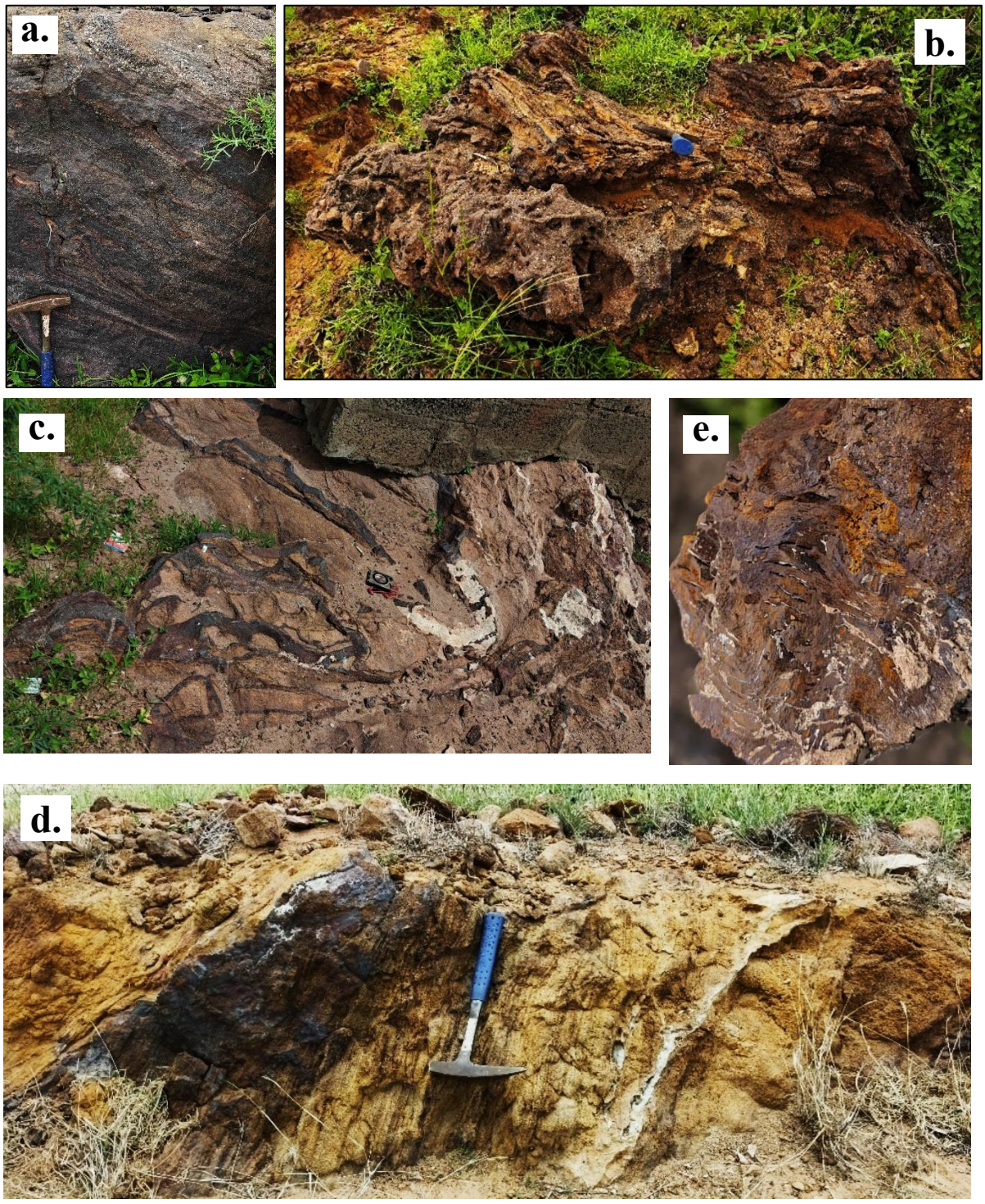

Fig. 4. 40 Outcrop-scale field features of metasomatized ferruginous sandstone within the Bhuj Formation. (a) Planar cross stratified metasomatized ferruginized sandstone. Note that the ferruginization is uniform and follow the stratification. (b) Completely altered ferruginous

sandstone showing obliteration of primary structures and development of porous, cavernous texture. (c) Hematite veins irregularly traversing the bedding surface (plan-view). (d) Section view of cross-cutting hematite–carbonate vein networks across the bedding plane. (e) Reddish-brown clay alteration and Fe-carbonate impregnation within hematitic zone of the metasomatized sandstone.

Locally, at fault proximal zones the sandstones display mauve to purplish-brown coloration, becoming friable and lightweight owing to advanced alteration. These varieties contain few surviving quartz pebbles, with grain boundaries largely obliterated by Fe-oxide cementation. The rock shows a spongy, vesicular texture, with pothole-like cavities filled by clay (non-calcareous; fails acid test) and/or hematite (*Fig.4.41*). The intergranular contacts are dominantly hematitic, frequently displaying triple ("Y"-shaped) junctions, suggestive of pressure-solution or late-stage re-equilibration under metasomatic conditions.

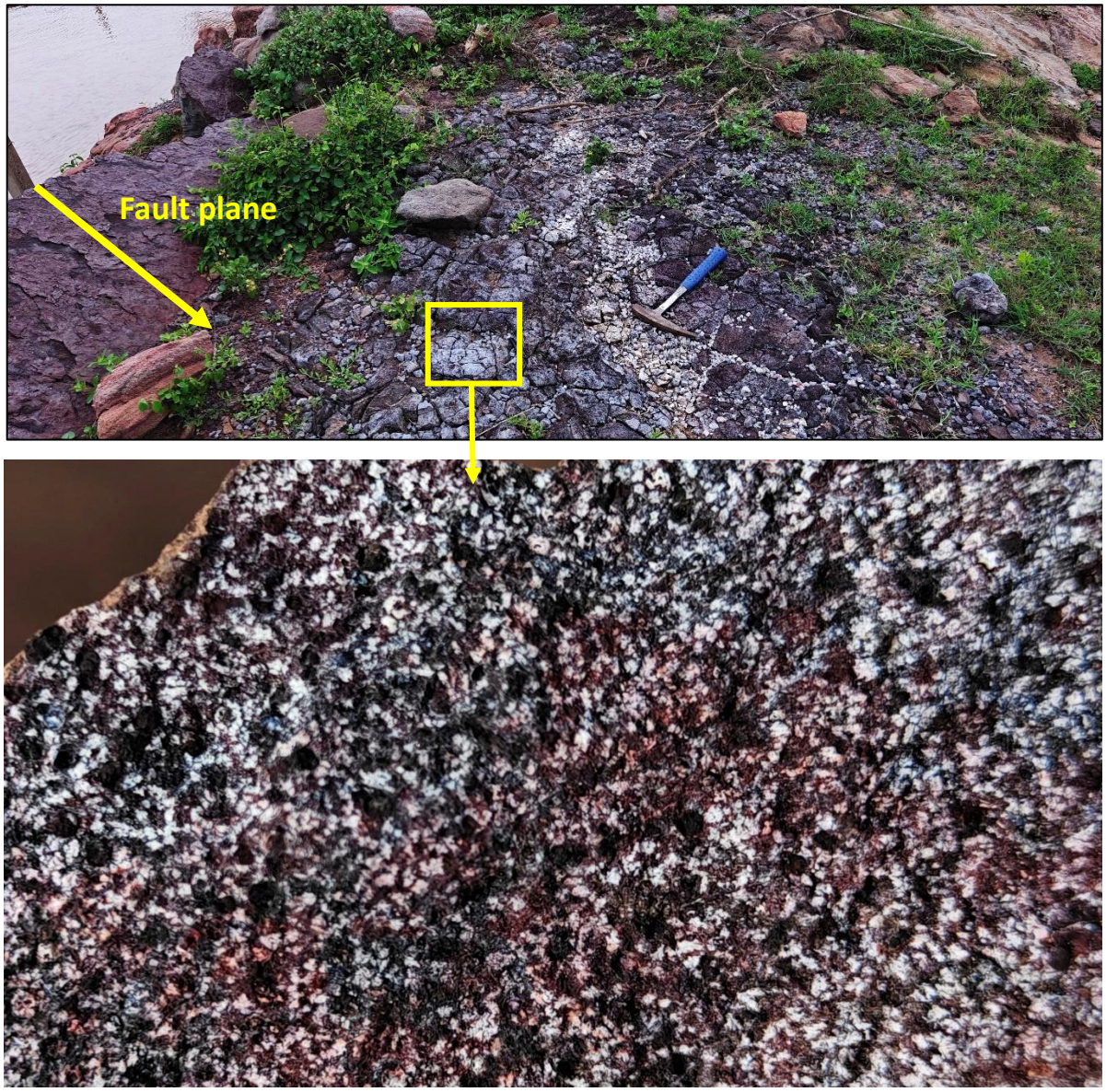

Fig. 4. 41 Field and hand-specimen photographs showing fault-proximal alteration in the Bhuj Sandstone. The upper image shows intensely ferruginized and altered sandstone exposed adjacent to the fault plane. The lower image presents the corresponding hand specimen, exhibiting mauve to purplish-brown coloration and a friable, vesicular texture formed by Fe-oxide cementation and leaching of earlier silicate phases. Note the pothole-like cavities infilled with hematite and clay and intergranular contacts locally exhibiting triple ("Y" -shaped) junctions.

Collectively, these field characteristics, including hematitization, silicification, and cross-cutting Fe-carbonate veining confirm a strong hydrothermal overprint superimposed on the primary arenitic fabric of the Bhuj Sandstone.

Ferruginous breccia occurs predominantly along structurally controlled alteration corridors within the Bhuj Formation, particularly in proximity to the Katrol Hill Fault, the Median High, and their subsidiary splays. These breccias are typically exposed as resistant ridges or low knolls (*Fig.4.42a*) and frequently occur in close association with metasomatized and ferruginized sandstone units (*Fig.4.42b*). The breccia zones are generally lenticular to irregular in geometry and traceable for several metres along the strike.

The breccias are matrix-supported, commonly displaying a chaotic to semi-coherent, locally mosaic fabric (*Fig.4.42c; d*). The clasts are angular to sub-rounded, comprising fragments of ferruginized sandstone, quartz, siltstone or white clay, along with subordinate book mica (muscovite) and hematite (*Fig.4.42c-f)*. These are embedded in a hematitic matrix or cement, imparting a distinct reddish-brown to black coloration. The clasts exhibit diverse morphologies ranging from rectangular, circular, wedge-shaped, cuneiform to irregular forms (*Fig.4.42c-f)*, possibly reflecting mechanical fragmentation under variable stress regimes. Pervasive veinlets and thin coatings of hematite occurring along interclast boundaries are also common (*Fig.4.42c; e*). Faint angular fragments and micro-lenticular blocks of the host lithology (*Fig.4.42d*), together with lensoid and branching hematitic seams (*Fig.4.42g*), indicate localized shearing and repeated fluid percolation.

Local development of silicification within the breccia zones is evident where the hematitic cement has been partially replaced by microcrystalline quartz, producing uneven, hard, vitreous patches. Small gash and lens-like silica-filled structures, accompanied by (*Fig.4.42c*), indicate repeated pulses of hydrothermal fluid infiltration. Internal cavities ranging from millimetre to centimetre scale are filled with hematite, goethite, or ferruginous clay, imparting a porous to vuggy texture to the breccia (*Fig.4.42c; e*). These features reflect fluid-rock interaction under fluctuating redox and pH conditions during metasomatism.

Overall, the field evidence strongly supports a hydrothermal origin for these ferruginous breccias. They formed through fracturing and fluid-assisted metasomatism, involving episodic

hematite-silica precipitation and mechanical disruption of the host sandstone. The overprinting of silica upon earlier Fe-oxide cementation, together with the angular clast geometry, vuggy textures, and hematitic vein networks, indicate a fault-controlled hydrothermal brecciation process, rather than surficial weathering or diagenetic compaction.

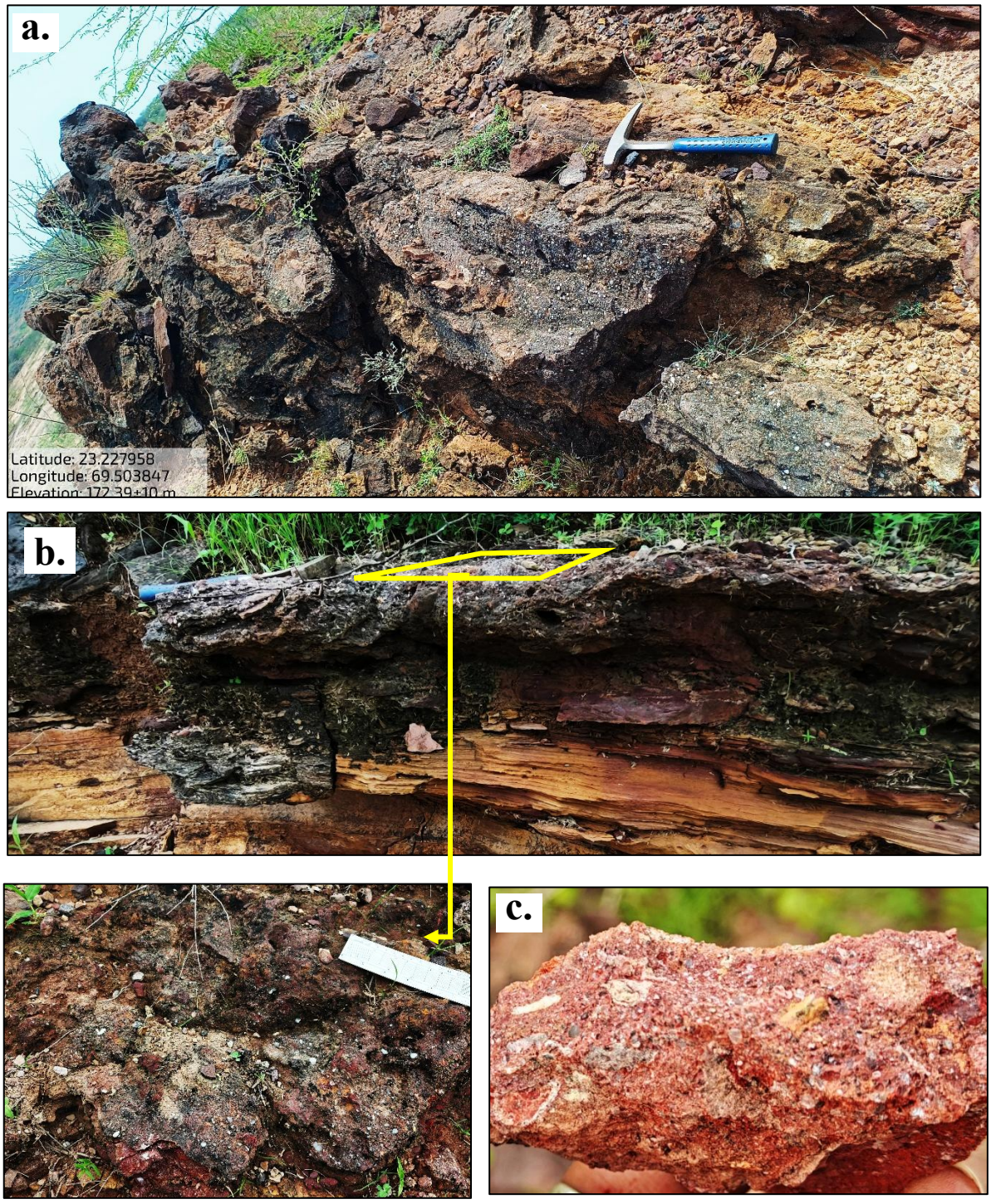

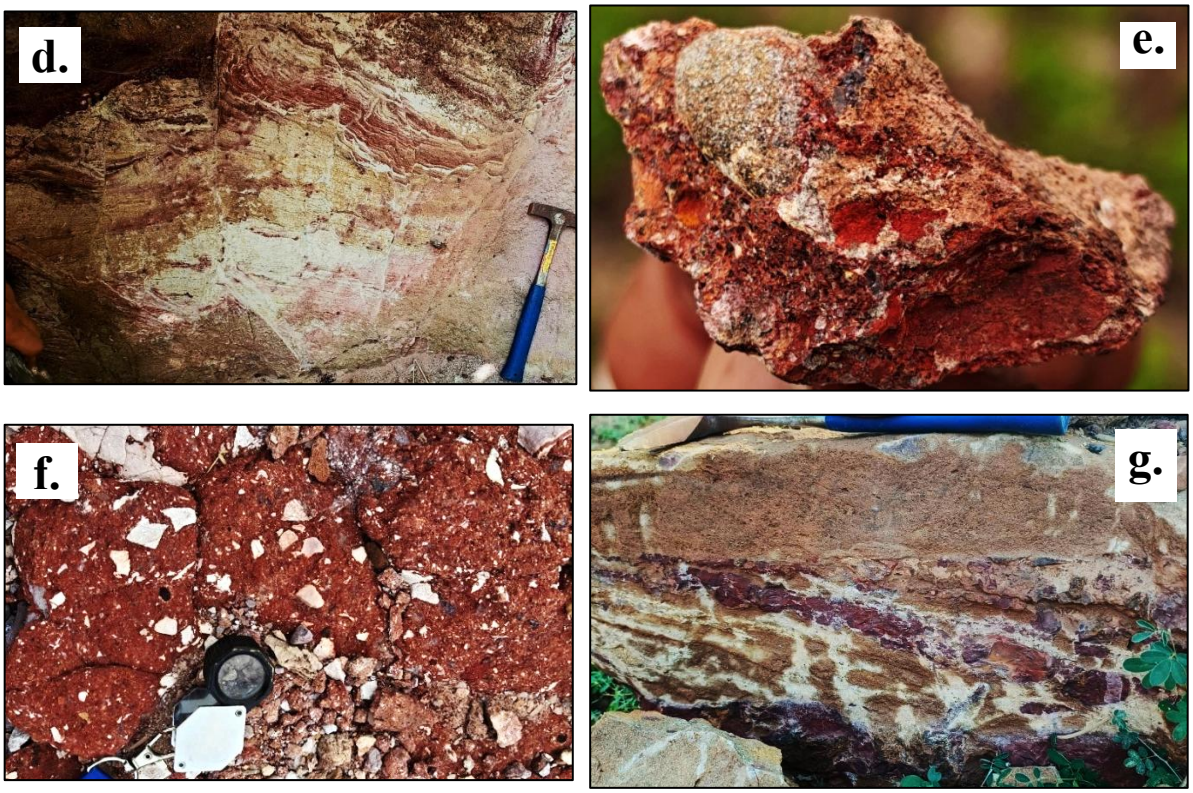

Fig. 4. 42 Representative field photographs illustrating ferruginous breccia and associated alteration features within the Bhuj Formation. (a) Matrix-supported ferruginous breccia exposed as resistant ridge within the structurally controlled alteration corridor near the Katrol Hill Fault. (b) Bedding parallel hematitic breccia with alternating ferruginous and clayey-siltstone bands. (c) Hand specimen of hematitic breccia of chaotic fabric. Note the quartz overgrowth, silica filled lenses, hematite coating and different morphologies of the clasts, embedded in a hematite matrix. (d) Partially brecciated ferruginous sandstone showing disrupted laminae and hematitic seams marking early-stage hydrothermal fracturing. Note the coherent fabric of the breccia. (e) Hand specimen displaying ferruginized sandstone fragment enclosed within hematitic cement. (f) Outcrop view of matrix-supported breccia with angular clasts of quartz and siltstone and white clay in hematitic groundmass. Note the rectangular and wedge shape of the clasts. (g) Field exposure showing lenticular ferruginous-silicified zone with hematitic seams and irregular brecciation.

Interpretation:

The collective field observations from the NW-SE oriented corridor within the Bhuj REE Prospect Block reveal that the metasomatized ferruginous sandstone and associated ferruginous breccia represent the most significant lithological expressions of Fe-oxide dominated hydrothermal alteration in the Bhuj Formation. Their spatial confinement along fault-controlled corridors, particularly adjacent to the Katrol Hill Fault (KHF), the Median High,

and subsidiary structures, strongly suggests that structural permeability exerted a primary control on hydrothermal fluid migration and Fe-oxide precipitation.

The lenticular to tabular geometry of ferruginous sandstone bodies, their continuity along fault planes and bedding-parallel shear zones, and the progressive increase in hematitization and magnetite impregnation toward fault-proximal regions collectively indicate a metasomatic overprint imposed by ascending oxidized hydrothermal fluids. The systematic transition from moderately ferruginized sandstone to intensely hematitized, semi-vitreous, and magnetite-bearing varieties denotes multiple phases of Fe-oxide introduction, recrystallization, and cementation. The vitrified surface sheen, welded grain contacts, and dense ferruginous matrix observed in several outcrops reflect high-temperature fluid–rock interaction, producing localized induration and recrystallization that mimic thermal sintering. Such features are typical of epigenetic iron-oxide alteration associated with hydrothermal systems rather than burial diagenesis.

Authigenic feldspar and mica overgrowths within hematitic cement, together with porous and cavernous textures generated by leaching of carbonate or clay phases, further attest to fluid-mediated replacement and metasomatic re-equilibration. The presence of greenish to bluish-green coatings in some exposures may signify localized chloritic or Cu-bearing alteration, indicating variable fluid chemistry during different alteration pulses. The frequent cross-cutting relationships between hematite, carbonate, and silica veins or veinlets, often following or transecting bedding, demonstrate successive mineralizing events under fluctuating redox and thermal conditions.

At fault-proximal localities, the development of friable, vesicular, and mauve-coloured sandstone characterized by “Y”-shaped intergranular junctions implies advanced stages of metasomatism accompanied by pressure-solution effects and Fe-oxide cementation. These features, combined with the pervasive obliteration of primary sedimentary structures, point to a hydrothermal regime where both replacement and structural influence governed fluid distribution.

The restriction of metasomatic alteration to the medium- to coarse-grained primary Bhuj Sandstone, with minimal effect on the interbedded siltstone and claystone horizons, indicates selective ferruginization governed by lithological permeability contrasts. This suggests that hydrothermal fluids preferentially migrated through the more porous and permeable sandstone beds, facilitating Fe-oxide impregnation, while the finer-grained, less permeable units acted as barriers to fluid flow and chemical exchange.

The occurrence of matrix-supported ferruginous breccia along the same structural corridors reinforces this interpretation. The breccias preserve evidence of hydrothermal fracturing, mechanical disruption, and subsequent Fe-oxide–silica cementation. Their angular clasts, hematitic and silicified matrix, vuggy textures, and evidence of multiple mineral

precipitation events collectively suggest episodic hydrothermal fluid influx along fault and fracture systems. The spatial association of breccia with metasomatized sandstone, and the observed overprinting of silicification upon ferruginization, demonstrate a temporal evolution from early Fe-oxide metasomatism to later silica deposition under changing physicochemical conditions.

Overall, the integrated field relationships delineate a fault-controlled hydrothermal system within the Bhuj Formation, characterized by episodic Fe-oxide metasomatism, localized silicification, and brecciation. These processes collectively resemblence an Iron Oxide–Copper–Gold (IOCG)-style hydrothermal alteration framework. The observed lithological and structural features thus provide compelling field evidence for an Fe-oxide dominated hydrothermal overprint superimposed on the arenitic facies of the Bhuj Formation.

4.7.1.2. Sampling:

Representative samples were collected systematically from the visited outcrops within the alteration corridor of the Bhuj Formation to evaluate lithological, mineralogical, and geochemical variations across the ferruginous and metasomatized zones. The sampling strategy was designed to encompass the principal alteration facies identified during detailed investigation viz. (i) metasomatized ferruginous sandstone, (ii) ferruginous breccia, (iii) fault-proximal altered sandstone and (iv) associated ferruginized sandstone. The primary objectives were to validate the anticipated anomalous concentrations of critical elements within the bedrock, confirm the presence of hydrothermal metasomatism, and establish spatial and compositional relationships between varying intensities of Fe-oxide metasomatism and their proximity to structural conduits.

Additionally, a few samples were obtained from adjoining exposures of the Katrol Formation, as certain reconnaissance stream-sediment samples had previously yielded anomalous values traceable to this unit. This was undertaken to assess any cross-formational hydrothermal influence or shared fluid pathways along the Katrol Hill Fault system.

Samples were collected from all the field observation points during the detailed field investigation of the Bhuj Prospect Block. Each sampling points were georeferenced using a handheld GPS, and detailed field notes were recorded, documenting lithology, texture, alteration features, and structural setting. The sampling traverses were planned to represent progressive degrees of ferruginization, from unaltered to weakly altered yellowish-brown sandstone, through reddish-brown ferruginized sandstone, to intensely hematitized, magnetite-bearing, and silicified varieties. Representative breccia samples were also collected from zones showing cross-cutting hematite-silica veining and vuggy textures associated with hydrothermal fluid activity.

Each specimen was labeled, photographed in situ, and sealed in polyethylene sample bags to prevent contamination. Post-field, samples were subjected to preliminary megascopic examination and magnetic response testing to qualitatively assess magnetite enrichment and the extent of Fe-oxide impregnation. Representative samples from each alteration type were subsequently selected for petrographic thin section study, mineragraphic study, X-ray diffraction (XRD), and geochemical analysis (whole-rock and REE) to establish mineralogical composition, alteration intensity, and trace element associations.

4.7.2. Geochemical Analysis of Mineral System-II

The geochemical investigation of Mineral System-II (MSA-II) was undertaken to characterize the compositional attributes of the Fe-oxide–dominated hydrothermal system identified within the Bhuj Formation and to evaluate its potential affinity with Iron Oxide Copper–Gold (IOCG)-type mineralization. Bedrock samples collected during the detailed field investigation (*refer to Section 4.7.1.2*) were subjected to whole-rock major, trace, and rare-earth element (REE) analyses to assess the intensity and nature of hydrothermal metasomatism.

The analytical program focused on delineating the metal tenor, alteration geochemistry, and element-association patterns within the ferruginous and metasomatized lithounits of the Bhuj Formation. Particular emphasis was placed on elements indicative of Fe-oxide hydrothermal systems to identify fluid-derived enrichment trends and establish possible genetic linkages between Fe-oxide metasomatism and multi-element mineralization.

A total of 121 bedrock samples were analyzed, of which 39 samples were tested for major oxides, trace elements, and REE suites, while the remaining samples were analyzed for trace and REE suites only (*Annexure-XX and Annexure-XXI*). Due to the limited approved NQT (40 samples) under the XRF analytical category, the current program prioritized samples representing critical lithological and alteration zones. However, considering that a substantial number of XRF analyses were already conducted during the orientation and reconnaissance surveys, the present detailed survey strategically focused on validating and refining the geochemical characterization of the established Fe-oxide hydrothermal system within the Bhuj Formation.

To further discriminate between primary and hydrothermal geochemical signatures, element concentration data were normalized against average value of unaltered Bhuj sandstones (n=7), representing the background geochemical composition of the host formation. This normalization facilitates the identification of elements introduced or remobilized during metasomatic processes and highlights those retained from the primary detrital assemblage.

4.7.2.1. Major Oxide Geochemistry Analysis

Major oxide data from the ferruginous and metasomatized lithounits of the Bhuj Formation display substantial geochemical variability, reflecting progressive Fe-oxide metasomatism and concomitant depletion of silicate and alkali-bearing phases (*Annexure-XX*).

The analytical dataset reveals a consistent enrichment trend from unaltered sandstone → ferruginized sandstone → metasomatized ferruginous sandstone (*Table 4.3*).

Table. 4. 3 Comparative major oxide composition of the collected samples of Bhuj sandstones during detailed investigation in MSA-II.

Oxide (wt.%)	Unaltered Sandstone (wt%)	Ferruginized Sandstone (wt%)	Metasomatized Ferruginized Sandstone (wt%)
SiO_2	70–94	55–64	33–79 (mostly below 50)
Al_2O_3	1–7	1–10	1.5–13 (>50% samples >7)
Fe_2O_3 (total)	0.8–6	5–22	5–56.5 (mostly below 37)
TiO_2	<0.01–0.9	0.1–0.9	0.04–1.39
P_2O_5	≤0.1	0.1–0.5	0.08–2.57 (90% <0.8)
MgO	<0.01–0.8 (mostly <0.1)	0.1–2.8	0.08–2.5
MnO	<0.01–0.05 (mostly <0.01)	0.02–0.1	0.01–1.79 (mostly <0.1)

The data show a clear inverse relationship between SiO_2 and Fe_2O_3, indicating progressive replacement of silicate matrix and framework by iron oxides. SiO_2 shows a marked depletion trend from >90 wt.% in unaltered sandstone to ~35-60 wt.% in intensely ferruginized varieties. The most altered metasomatized sandstones reach Fe_2O_3 contents exceeding 50 wt.%, accompanied by reduced SiO_2 and moderate enrichment of TiO_2, MgO, and MnO. TiO_2 shows a weak positive correlation with Fe_2O_3, implying partial Ti mobility and re-precipitation along with Fe-oxide influx. MgO and MnO are typically low but exhibit localized enrichment in brecciated or highly altered samples, consistent with minor Fe–Mg metasomatism and Mn-oxide precipitation along permeable micro-fractures.

The spatial alignment of Fe_2O_3, and TiO_2, anomalies along structural corridors (*Fig. 4.43*) further confirms that the Bhuj ferruginous system is structurally controlled and hydrothermally sustained, consistent with the observed field features.

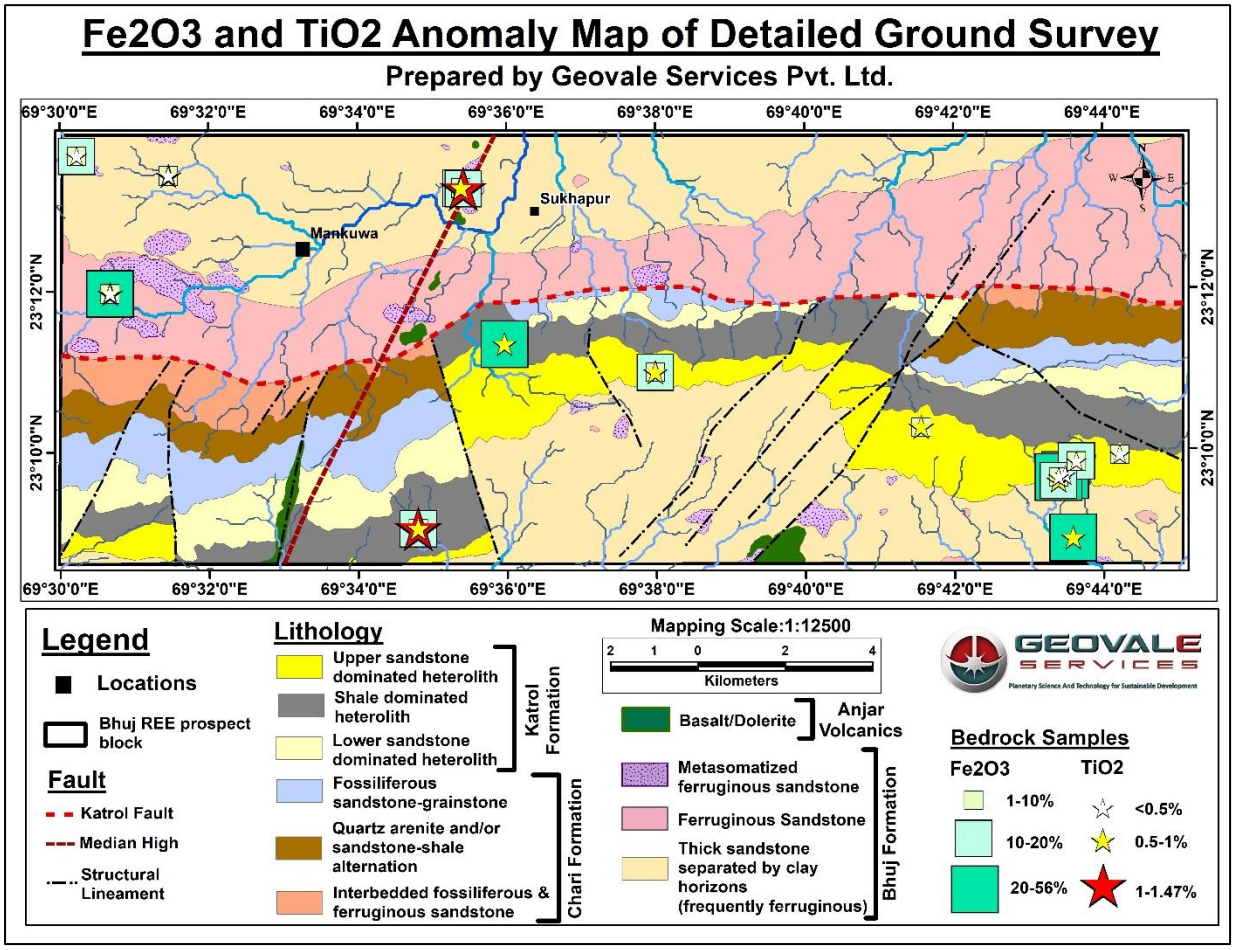

Fig. 4. 43 Fe_2O_3 and TiO_2 anomaly map of the detailed survey within the Bhuj Formation showing distinct zones of Fe-oxide enrichment

Al_2O_3 exhibits moderate variability (1-13 wt.%), with over half the samples exceeding 7 wt.%. Despite strong ferruginization, Al_2O_3 retention indicates that authigenic growth of feldspar and mica, as confirmed from the field evidence, contributed to local stabilization or reconstitution of Al-bearing phases. This secondary feldspathization and sericitization imply that hydrothermal fluids not only replaced silicates with Fe-oxides but also induced partial aluminosilicate recrystallization within hematitic cement zones.

P_2O_5 values remain low (<0.8 wt.% in most cases), reflecting the absence of phosphatic cement/matrix, typical of the Katrol tuffite horizons discussed in MSA-I.

These enrichment–depletion relationships are quantitatively depicted in the log-normalized oxide plot (*Fig. 4.44*), which shows systematic Fe_2O_3, MnO, and TiO_2 enrichment,

accompanied by pronounced depletion in SiO_2, Na_2O, and K_2O. The data form a convergent geochemical trend diagnostic of Fe-oxide metasomatic systems.

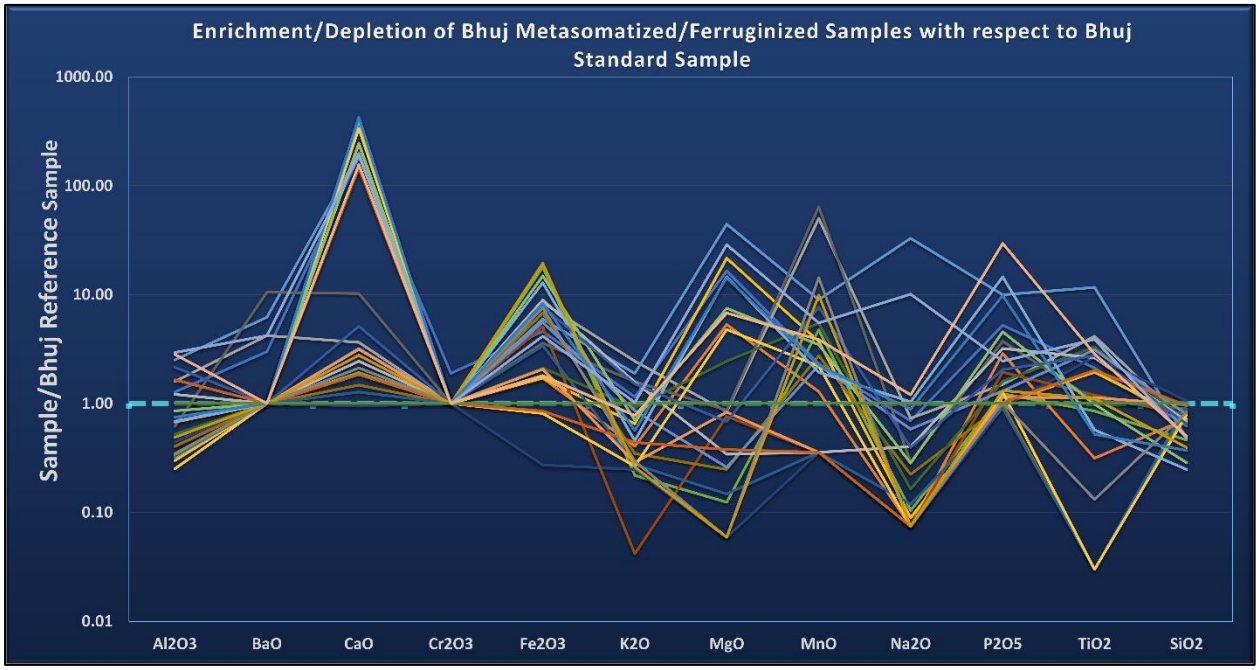

Fig. 4. 44 Normalized enrichment/depletion plot of major oxides in metasomatized and ferruginized Bhuj sandstones (relative to unaltered Bhuj sandstone).

Interpretation:

The major oxide geochemistry provides unequivocal evidence for hydrothermal Fe-oxide metasomatism within the Bhuj Formation. The distinct Fe enrichment coupled with Si and alkali depletion reflects fluid-driven mass transfer, where oxidized Fe-rich hydrothermal solutions infiltrated porous and permeable sandstone horizons along fault-controlled conduits.

The localized increase of Al_2O_3, along with field evidence of authigenic feldspar and mica recrystallization, suggests that hydrothermal alteration was possibly accompanied by silica-alumina re-equilibration, stabilizing Al-bearing minerals within Fe-rich cement. This feature distinguishes the Bhuj metasomatic system from simple supergene ferruginization and implies a low- to moderate-temperature hydrothermal overprint rather than surface weathering.

The enrichment-depletion trend (*Fig. 4.44*) encapsulates the mass-balance trajectory of alteration, where Fe, Ti, and Mn were added, Si and alkalis were leached, and Al remained locally conserved through authigenic reprecipitation. These geochemical signatures collectively mark the Bhuj system as an Fe-oxide dominated hydrothermal regime, chemically analogous to IOCG-style metasomatism, where iron, base metals, and minor REE are co-introduced by oxidized hydrothermal fluids.

4.7.2.2. Trace Element and REE Mobility and Geochemical Enrichment

Trace and rare-earth element (REE) geochemical analyses (*Annexure-XXI*) from the Bhuj sandstones reveal systematic base and high-firld-strength (HFSE) enrichment associated with ferruginous and metasomatized sandstone facies, along the NW-SE trending alteration corridors. The compositional range (*Table 4.4*) defines a consistent enrichment in transition metals (Fe, Zn, Cu, Co), high-field-strength elements (Nb, Mo, Sn), and REE+Y from unaltered sandstone to ferruginized sandstone and finally to intensely metasomatized lithounits with increasing intensity of Fe-oxide metasomatism.

Table. 4. 4 Comparative trace and REE concentrations of the collected samples of Bhuj sandstones during detailed investigation in MSA-II.

Element	Unaltered Sandstone	Ferruginized Sandstone	Metasomatized Ferruginous Sandstone
Nb (ppm)	0.5 – 2.7	1.9 – 13.1	1.9 – 16
Mo (ppm)	0.6 – 2.5	0.6 – 4.5 (most samples > 1.5)	0.5 – 7.6
Cu (ppm)	1 – 6.9	2 – 21	3 – 18.6
Co (ppm)	40 – 119	40 – 103	48 – 254.4 (~45% > 100 ppm)
Zn (ppm)	< 0.5 – 79 (most < 16)	12.6 – 224 (most < 100)	16 – 381.5 (~50 % > 100 ppm)
Pb (ppm)	8 – 19	7 – 29	7 – 226.7
Sn (ppm)	< 0.5 – 1	0.5 – 1.9	0.6 – 22.1
TREEY (ppm)	66 – 117	116 – 744	41 – 311

Elements such as Nb, Mo, and Cu show low to moderate enrichment trends across the ferruginized and metasomatized lithounits compared to the unaltered sandstones. Niobium (1.9–16 ppm) and molybdenum (0.5-7.6 ppm) contents rise systematically with increasing Fe_2O_3, suggesting their mobility in oxidized hydrothermal fluids and subsequent fixation by Fe-oxyhydroxides. Copper ranges from 3-18.6 ppm in metasomatized varieties, indicating limited yet notable enrichment associated with Fe-Cu redox front development.

Cobalt concentrations remain relatively consistent across all facies (40-254 ppm) but display localized maxima (>100 ppm) particularly within magnetite-rich zones, reflecting

affinity of Co for ferrous-ferric iron oxides. Zinc (up to 381 ppm) and lead (up to 227 ppm) exhibit the strongest positive response to metasomatism, marking zones of base metal influx during Fe-oxide precipitation. Tin (0.6-22 ppm) are less anomalous, but shows significant enrichments, pointing to repeated low-volume, high-temperature fluid pulses possibly of magmatic-hydrothermal derivation.

In contrast, elements such as Cr, Ni, and V display limited variation, suggesting minimal contribution from mafic detritus or contemporaneous volcaniclastic influx. Likewise, Sr and Ba contents are moderate and appear largely controlled by feldspar and clay residues, indicating a relatively immobile behaviour during Fe-oxide metasomatism.

Rare Earth Element+Y (TREEY) concentrations in ferruginized sandstone range between 116-744 ppm, showing higher values in ferruginized sandstones than in metasomatized or unaltered equivalents. This enrichment indicates preferential adsorption or incorporation of REE by Fe-oxide and hydroxide phases during metasomatic replacement and fluid-rock interaction.

The normalized enrichment-depletion plot (*Fig. 4.45*) demonstrates that Fe-oxide metasomatized samples exhibit multi-element enrichment in Zn, Co, Cu, Mo, Nb, Sn, Pb, and TREEY, in contrast to general depletion of alkali and alkaline-earth elements. The coherence of these anomalies indicates hydrothermal addition of transition and high-field-strength elements contemporaneous with Fe-oxide influx.

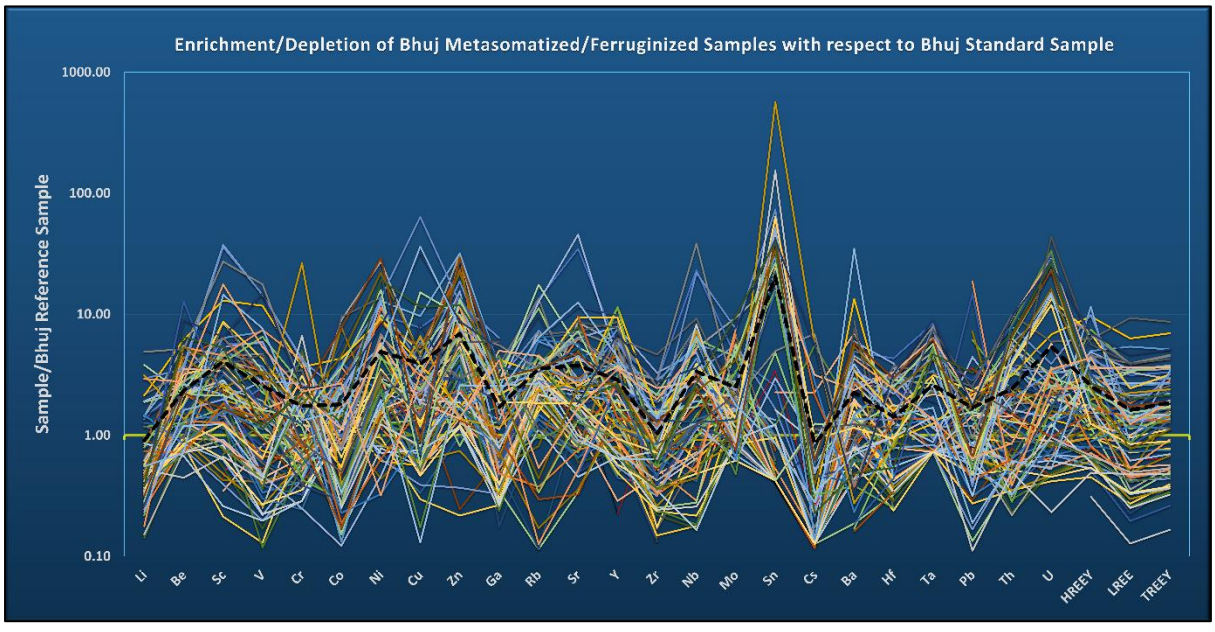

Fig. 4. 45 Normalized enrichment/depletion plot of trace and REE elements in ferruginized and metasomatized Bhuj sandstones relative to unaltered sandstone.

Spatial Distribution of Metals and REEs:

Spatially, metal enrichments correspond closely to the hydrothermal corridors, related to the Katrol Hill Fault (KHF), Median High Zone and its associated fracture systems (*Figs. 4.46 - 4.49*).

Zn shows strong concentration peaks (up to 384 ppm) within metasomatized ferruginous sandstone near the Median High, with secondary enrichment at the southern KHF splays-linked ferruginous ridges (*Fig. 4.46*).

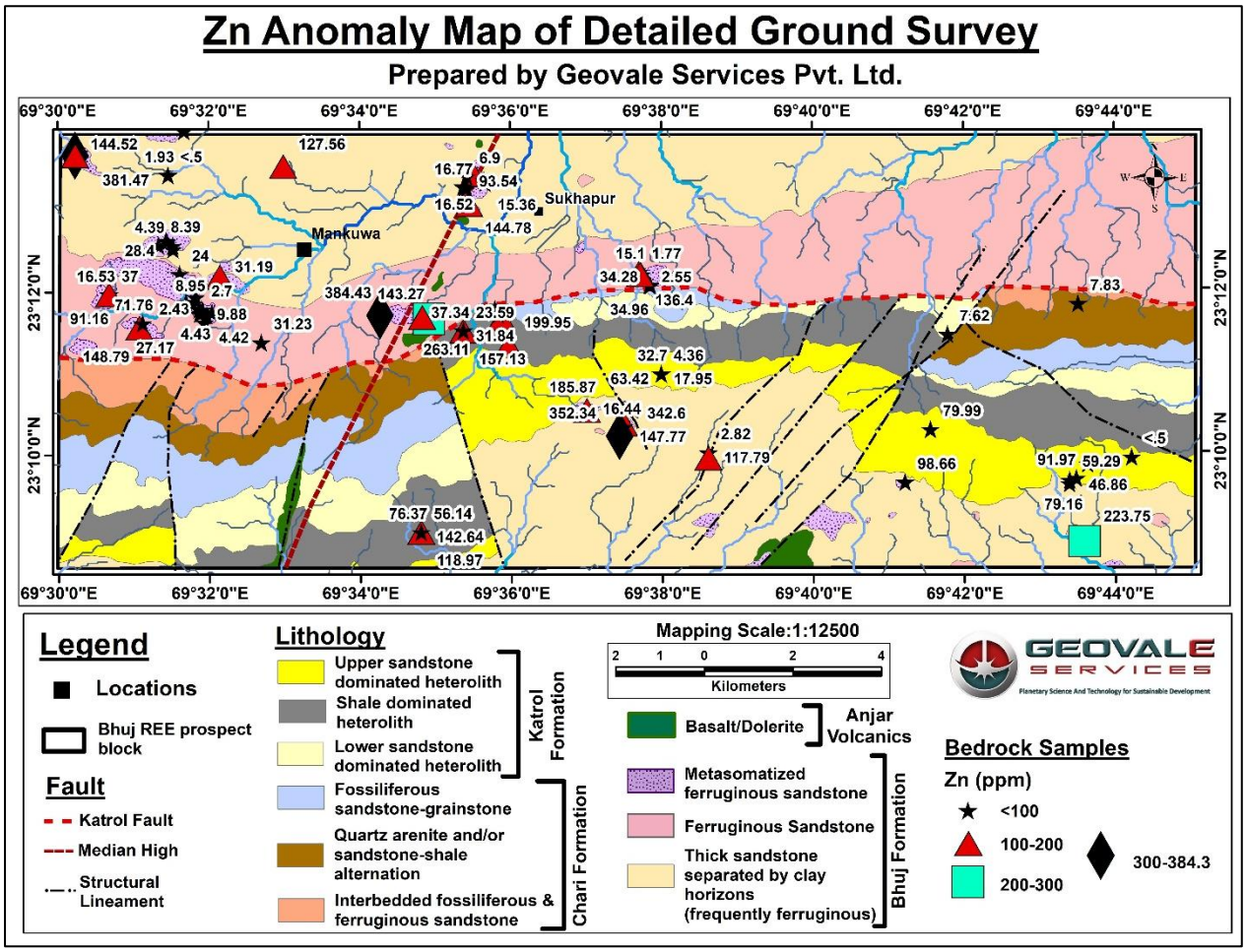

Fig. 4. 46 Spatial distribution map of Zn anomalies within the Bhuj Formation.

Pb enrichment is comparatively subdued, reaching ~227 ppm, and appears spatially coincident with Zn highs (*Fig. 4.47*), indicating co-precipitation within Fe-oxide-cemented zones, under similar hydrothermal conditions.

Sn anomalies (up to 672 ppm) are localized along the KHF-parallel alteration corridors (*Fig. 4.48*), spatially overlapping Fe-oxide metasomatized zones identified during field investigation.

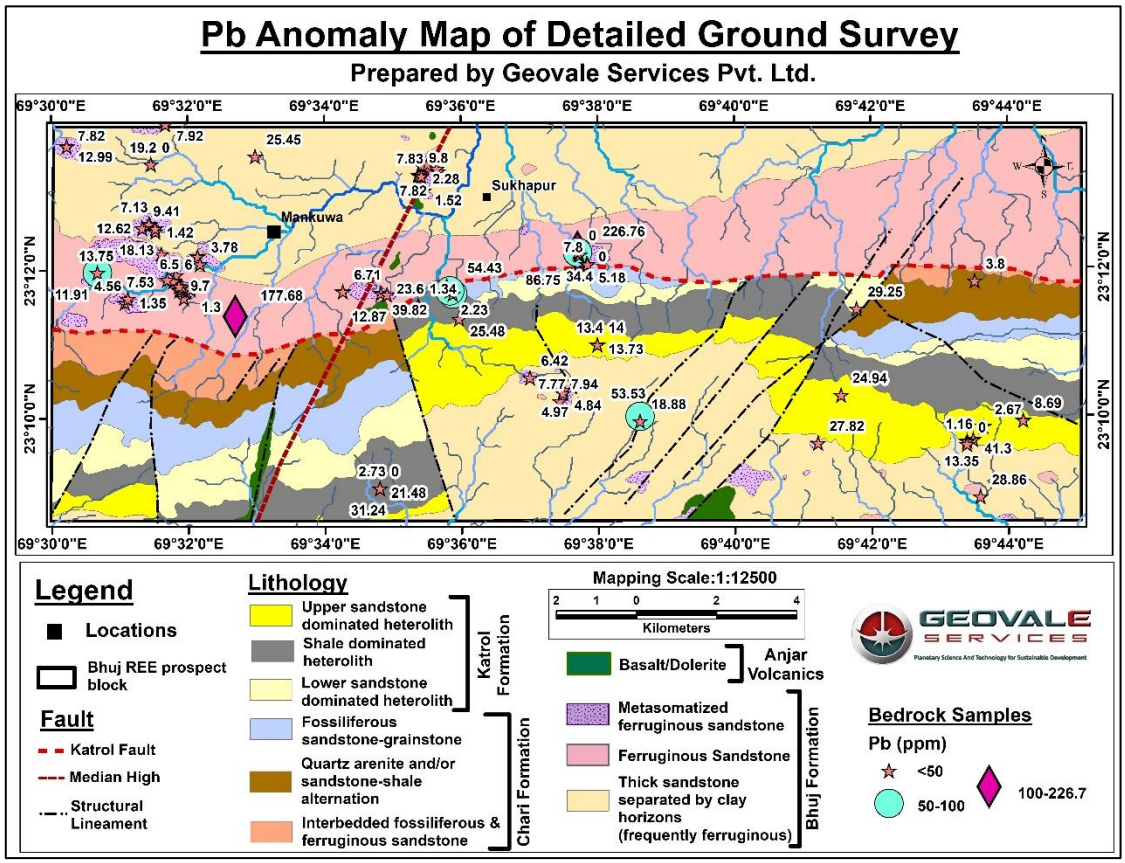

Fig. 4. 47 Spatial distribution map of Pb anomalies within the Bhuj Formation.

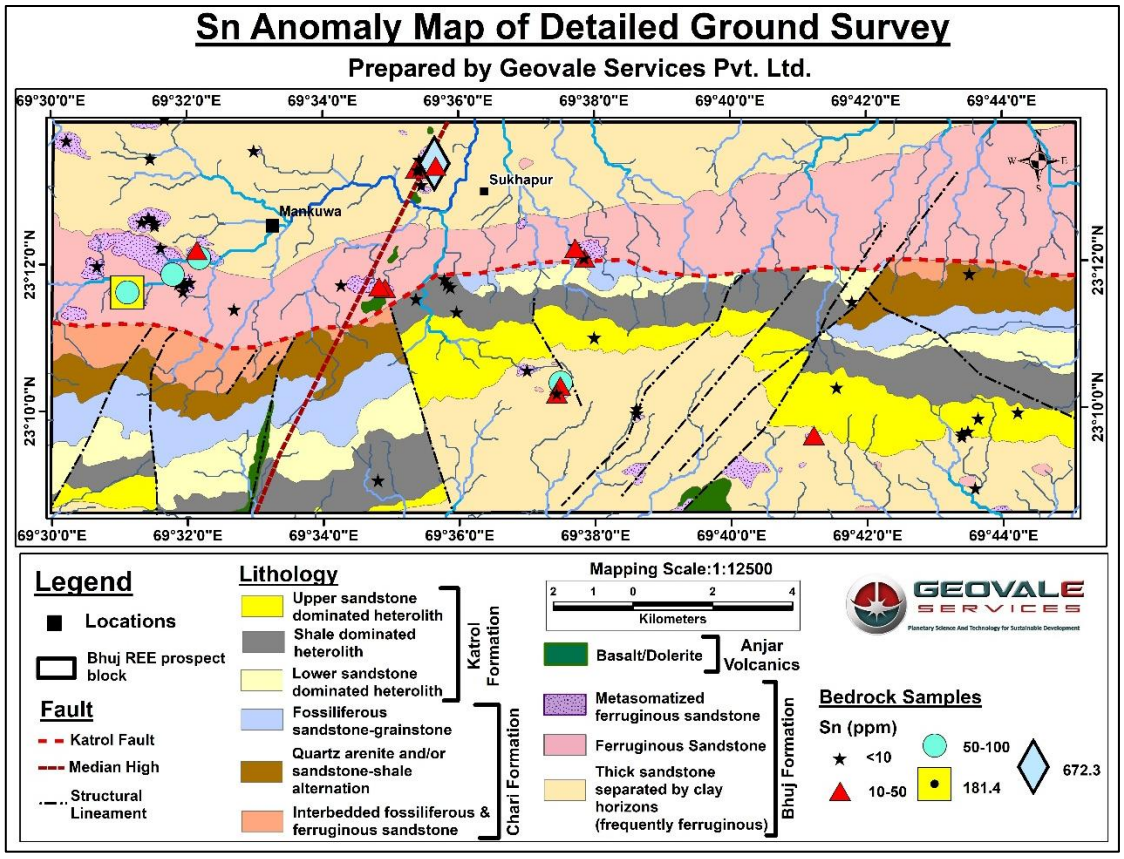

Fig. 4. 48 Spatial distribution map of Sn anomalies within the Bhuj Formation.

TREEY (ΣREE+Y) concentrations show the broadest range, from 66 ppm in unaltered sandstone to 311 ppm in metasomatized sandstones and 744 ppm in ferruginized facies, define broad halos (*Fig. 4.49*) along the hydrothermal corridor.

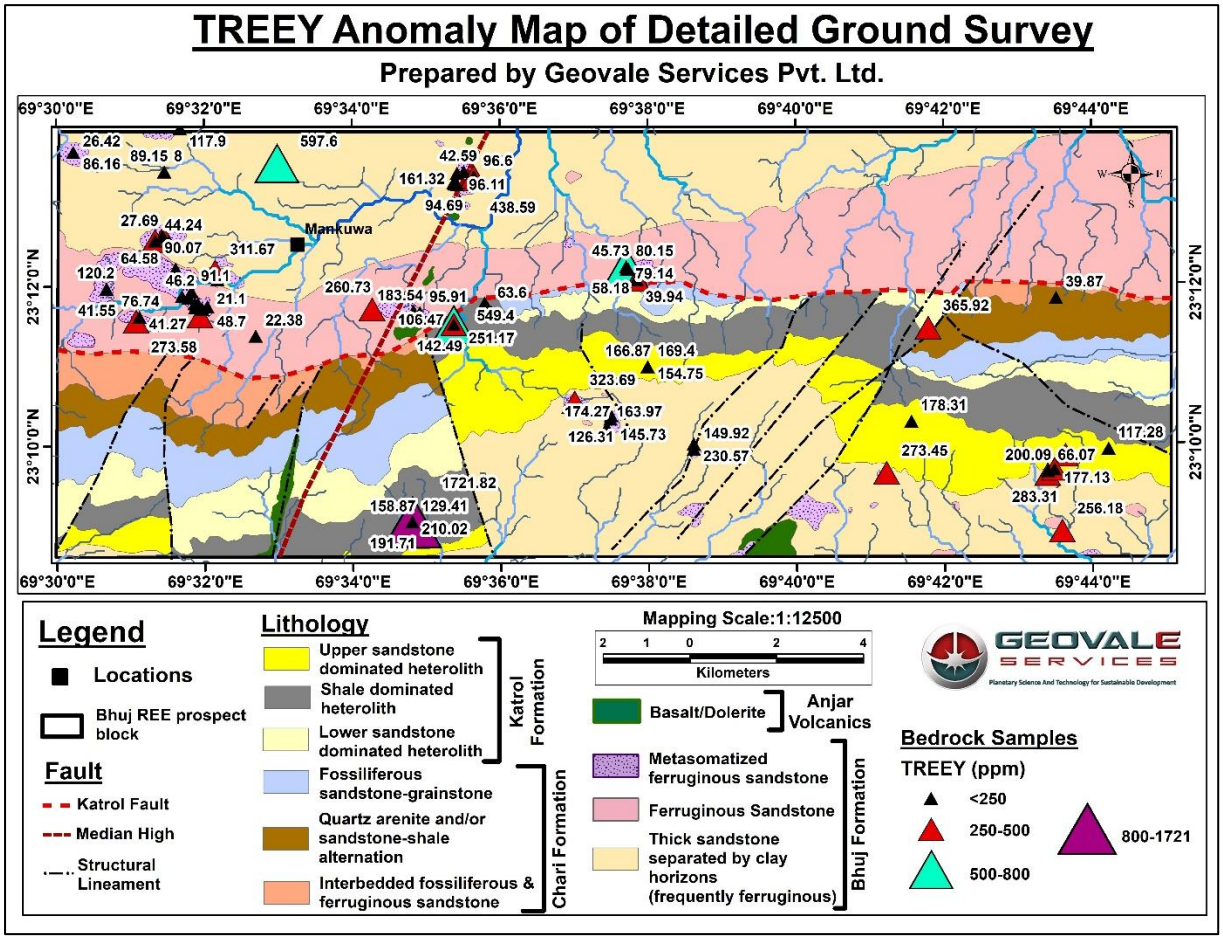

Fig. 4. 49 Spatial distribution map of TREEY anomalies within the Bhuj Formation.

Interpretation:

The integrated geochemical, field, and spatial datasets collectively indicate that the Bhuj Formation preserves a structurally controlled Fe-oxide dominated hydrothermal system characterized by selective metasomatism, base-metal enrichment, and REE redistribution. The systematic enrichment of Fe_2O_3, Zn, Pb, Sn, Mo, and TREEY, together with the depletion of SiO_2, Na_2O, and K_2O, demonstrates extensive chemical mass transfer under oxidizing, Fe-rich hydrothermal conditions.

The transition from unaltered to ferruginized and ultimately to metasomatized sandstone records progressive infiltration of Fe-bearing hydrothermal fluids through permeable sandstone horizons, preferentially localized along fault zones and fracture networks associated with the Katrol Hill Fault (KHF) and Median High corridor. The metasomatic fronts are distinguished by the replacement of detrital quartz–feldspar

framework by hematite-magnetite rich groundmass, accompanied by authigenic growth of feldspar and mica, which together account for the observed minor retention or increase in Al_2O_3.Sn and Mo Association:

Enrichment in Zn, Pb, Cu, and Co is interpreted as the result of fluid-rock interaction within Fe-oxide zones, where Fe-oxyhydroxides acted as efficient sorbents and precipitation sites for these chalcophile and siderophile elements. The geochemical coherence of Zn-Pb-Cu-Co anomalies, together with Fe-Ti coupling, supports a hydrothermal origin involving episodic influx of oxidized, saline fluids capable of transporting both transition and high-field-strength elements. Local Sn and Mo enrichment further implies a minor magmatic-hydrothermal component contributing metal-bearing fluids along deep-seated fault conduits.

The distinct enrichment of Nb, Sn, and Mo relative to unaltered equivalents, as seen in normalized plots, suggests selective mobilization of HFSE during Fe-oxide metasomatism under moderately acidic to neutral pH conditions. These elements were likely transported as chloride or hydroxide complexes and subsequently immobilized during Fe-oxide precipitation.

REE behaviour is marked by moderate to strong enrichment in ferruginized facies (TREEY: 116-744 ppm) relative to unaltered sandstones (66-117 ppm) implies that Fe-oxyhydroxides and micro-crystalline hematite probably have hosted the REE. This pattern contrasts sharply with the phosphate-bound REE enrichment of the Katrol tuffite system (MSA-I), underscoring a distinct hydrothermal mechanism of REE fixation in the Bhuj Fe-oxide system.

Spatially, the geochemical anomalies define a continuous NW-SE-trending corridor extending between the KHF and Median High, where metasomatized and brecciated ferruginous sandstones exhibit the highest Fe-Ti, Zn, and TREEY values. These relationships confirm that the Bhuj system represents an epigenetic, structurally controlled Fe-oxide hydrothermal event, genetically distinct from the stratiform volcaniclastic-phosphatic system of the Katrol Formation.

Collectively, the geochemical signatures, including strong Fe-oxide metasomatism, and Fe-Ti-Zn-Pb-Sn-REE enrichment, and spatial confinement to fault-bounded corridors, are consistent with an incipient IOCG-type mineral system developed within the Bhuj Formation. The metasomatized ferruginous sandstones thus represent the most prospective lithounits for subsequent sub-surface geochemical and mineralogical evaluation aimed at defining potential Fe-oxide-associated polymetallic mineralization in MSA-II.

4.7.3. Petrographic and Mineragraphic Analysis of Mineral System-II

Detailed petrographic and mineragraphic analyses were undertaken on representative samples from the ferruginous and metasomatized lithounits of the Bhuj Formation to characterize the textural evolution, mineralogical transformations, and paragenetic relationships associated with Fe-oxide metasomatism. The study aims to document the optical and microtextural evidence for hydrothermal alteration, establish the relative sequence of mineral replacement, and identify the mineral hosts and alteration assemblages linked to potential IOCG-type mineralization.

4.7.3.1. Petrographic Analysis

The metasomatized ferruginized sandstone is very coarse to fine-grained, exhibiting poor sorting and a bimodal grain size distribution, with both highly rounded detrital clasts and angular fragmented grains suggestive of partial in-situ brecciation (*Fig.4.50a; b*). The framework grains are predominantly consists of quartz, feldspar (both K-feldspar and plagioclase) with subordinate amount of polycrystalline quartz, chert, rock fragments of quartzite, muscovite, apatite, zircon, and magnetite (*Fig.4.50a; b*). Occasional glass fragments and microcline showing perthitic intergrowths are also present.

The matrix constitutes more than 10–20% of the rock and is composed of quartzo-feldspathic grains embedded in a ferruginous to manganiferous cement (*Fig.4.50a-d*). The cement shows extensive metasomatic alteration, locally replaced by carbonate and Fe-Ti oxide phases (ilmenite, Fe–Ti oxides). Zones of iron leaching and ferruginization are prominent, indicating post-depositional hydrothermal overprint (*Fig.4.50c; d*). Silicification is common, manifested by occurrence of microcrystalline quartz, silica overgrowth textures and silica veinlets crosscutting the ferruginous matrix. The groundmass commonly displays a glassy appearance with areas of carbonate replacement, where calcite crystals exhibit zoning (*Fig.4.50e; f*), suggestive of multiple pulses of hydrothermal fluid activity.

Microscopic examination reveals solution and nibbling textures along quartz grain boundaries, reflecting acidic fluid interaction and silica remobilization (*Fig.4.50d*). In some zones, framework grains show embayed margins and matching grain boundaries, indicating localized in-situ brecciation and re-cementation, a typical hydrothermal fracturing signature (*Fig.4.50g; h*). The presence of zoned rhombic carbonate clasts and flow-like structures within the groundmass further supports hydrothermal cementation and fluid-assisted recrystallization. Authigenic feldspar overgrowths are locally observed along the grain boundaries, where optically continuous K-feldspar rims extend into the pore spaces, indicating feldspar recrystallization (*Fig.4.50i*) and precipitation from Fe-rich hydrothermal fluids during metasomatism.

Accessory phases include pyrite, chalcopyrite, and fine gold specks disseminated within the ferruginous matrix, confirming localized sulphide deposition within an otherwise oxidized system (*Fig.4.50i; j*). Additionally, ilmenite and Fe-Ti oxide (goethite) minerals dispersed throughout the matrix point to a Fe-Ti rich hydrothermal contribution (*Fig.4.50b*).

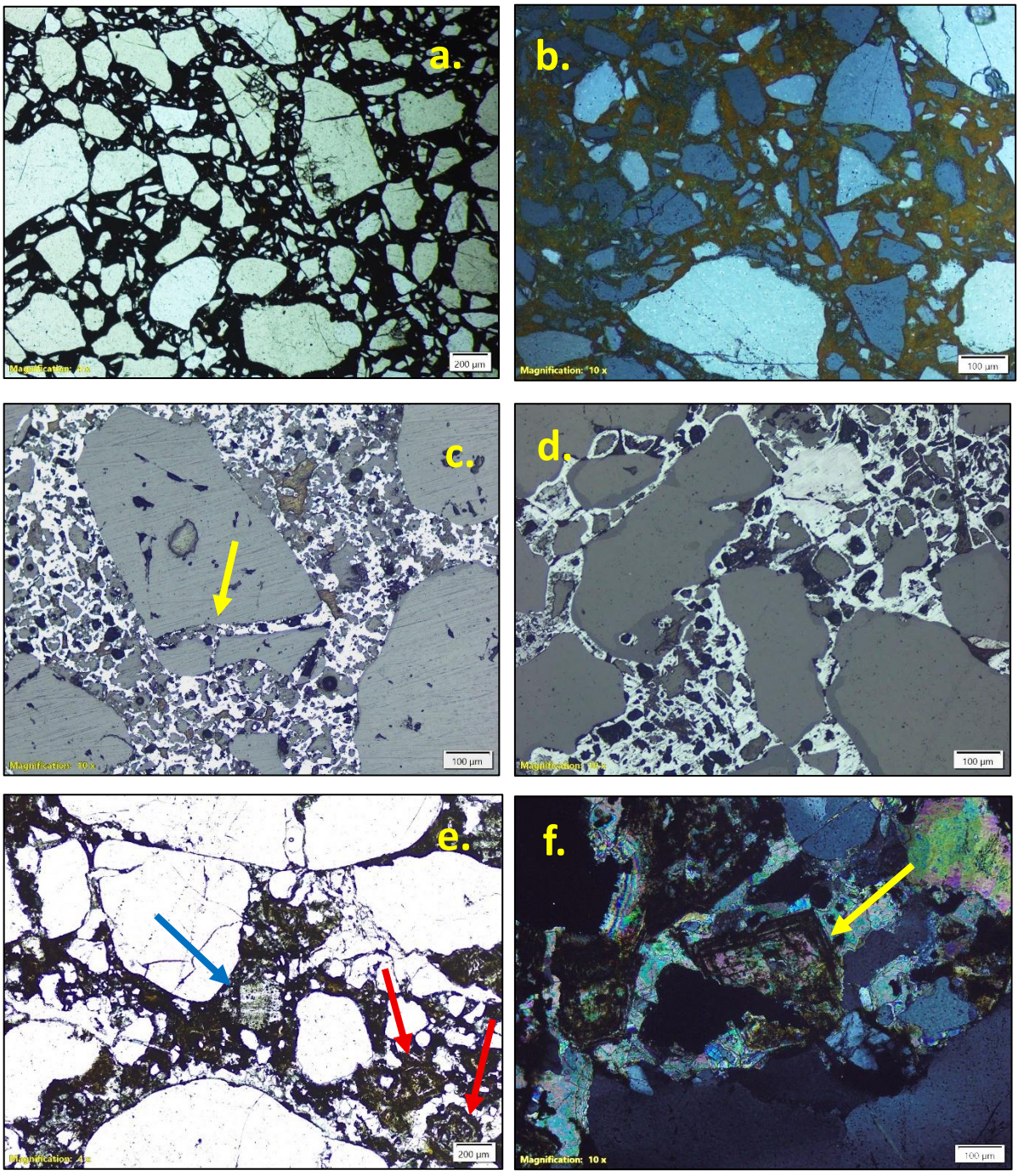

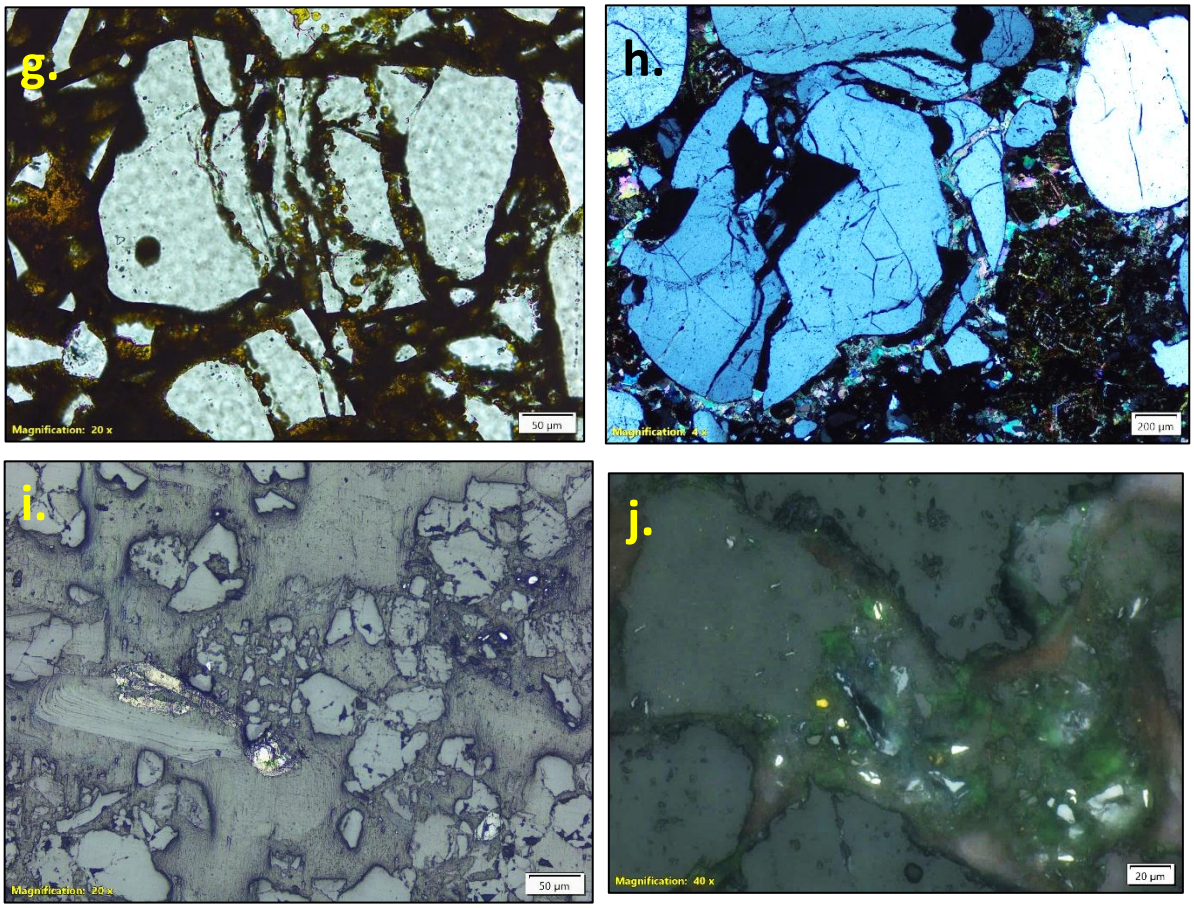

Fig. 4. 50 Photomicrograph of the metasomatized and ferruginized sandstone of the Bhuj Formation. (a) Coarse-grained, poorly sorted sandstone showing bimodal grain size distribution, with both sub-rounded and angular fragmented clasts of quartz as framework, floating in a highly ferruginous cement (under Plane Polarised Light). (b) Coarse-grained, poorly sorted sandstone with highly angular fragmented clasts of quartz as framework embedded in a highly ferruginous/goethitic cement (under Cross Polarised Light). (c) Coarse-grained, poorly sorted sandstone with evidence of in-situ brecciation (marked by arrow) within quartz clasts. Note the magnetite rich ferruginous cement (under Reflected Light). (d) Coarse-grained, poorly sorted sandstone with evidence of ferruginization/ iron-leaching, noted in magnetite rich ferruginous cement (under Reflected Light). Embayed boundaries are evidence of iron replacement (marked by arrow). (e) Coarse-grained, poorly sorted sandstone with sub rounded clasts of quartz and a few k-feldspar (marked by blue arrow) as framework, floating in a highly ferruginous cement. Note, later replacement by carbonate cement with a few zoned rhomb shaped carbonate crystals (marked by red arrow) (under Plane Polarised Light). (f) Zoomed view of a zoned carbonate crystal in the cement (under Cross Polarised Light). (g) In-situ brecciation of a large quartz grain (with matching grain boundaries) and infiltration of Fe-rich cement (under Plane Polarised Light). (h) In-situ brecciation of a large quartz grain (with matching grain boundaries) originally having well-rounded grain boundary. Note, infiltration of Fe-rich cement and later replacement by carbonate cement

(under Plane Polarised Light). (i) Medium to coarse grained sandstone showing authigenic K-feldspar overgrowths developed along detrital feldspar margins, extending into intergranular pore spaces. The overgrowths are optically continuous with the host grain. Note the fine chalcopyrite veinlets traversing the feldspathic matrix (under Reflected Light). (j) Occurrence of possible gold and chalcopyrite within the cement of ferruginous sandstone (Under Reflected Light).

Interpretation:

The petrographic attributes of the metasomatized ferruginized sandstone collectively attest to a strong hydrothermal metasomatic overprint imposed upon a pre-existing arenitic framework of the Bhuj Formation. The coexistence of detrital quartz and feldspar with ferruginous to manganiferous cement indicates post-depositional fluid infiltration under oxidizing conditions, which facilitated pervasive Fe-oxide replacement and impregnation. The variable preservation of detrital feldspar and quartz, along with the partial development of authigenic K-feldspar rims, suggests multiple fluid-rock interaction events involving both alkali- and Fe-rich fluids. These processes likely promoted feldspar dissolution–reprecipitation reactions, consistent with the observed overgrowths that extend optically into intergranular voids.

The presence of silicification in the form of microcrystalline quartz, silica overgrowth and silica veinlets further indicates episodic silica saturation during hydrothermal alteration, or silica alteration, post metasomatism. The association of zoned calcite and dolomite with Fe-oxide cementation implies a late-stage influx of CO_2-bearing fluids, marking a waning phase of metasomatism dominated by carbonate replacement and veining.

Textural evidence such as embayed quartz margins, sutured grain contacts, and in-situ brecciation demonstrates local hydrofracturing and subsequent re-cementation by Fe-Ti oxides and carbonates, consistent with repeated episodes of hydrothermal fluid overpressure and pressure-solution. The intergrowth of ilmenite, goethite, and magnetite within the ferruginous matrix, along with localized dissemination of sulphide phases (pyrite, chalcopyrite), signifies the presence of mixed redox conditions, where Fe-oxide precipitation and minor sulphide deposition occurred during successive fluid pulses.

The overall petrographic evidence, including authigenic feldspar growth, silica replacement, hematitic cementation, and sulphide impregnation strongly supports the interpretation of a fault-controlled hydrothermal system. This system was characterized by episodic Fe-oxide metasomatism, silica and carbonate redistribution, and selective feldspar recrystallization, reflecting an evolving hydrothermal environment consistent with IOCG type mineralization processes.

4.7.3.2. X-Ray Diffraction (XRD) Analysis

X-Ray Diffraction (XRD) studies were carried out on fifteen representative samples from the Bhuj Formation, encompassing metasomatized ferruginized sandstone, ferruginized sandstone, and weakly ferruginized sandstone. The objective was to characterize the alteration mineral assemblages, identify dominant Fe-bearing and accessory mineral phases, and evaluate mineralogical variations corresponding to the degree of metasomatism. The analytical results are presented in *Annexure-XV*.

Metasomatized Ferruginized Sandstone:

The metasomatized ferruginized sandstones exhibit a mineral assemblage dominated by hematite, quartz, and feldspar, accompanied by subordinate muscovite, kaolinite, dolomite or calcite, rutile, and goethite and locally pyroxene. The pronounced hematite reflections confirm pervasive Fe-oxide cementation and replacement of the original arenitic matrix. he presence of pyroxene in one sample suggests either a minor volcanogenic contribution or recrystallization under elevated temperature conditions during hydrothermal alteration. The persistence of feldspar peaks, together with subordinate muscovite and kaolinite, implies incomplete breakdown of detrital silicates or localized authigenic growth of feldspar and mica during or after metasomatism. Both the processes in combination are also capable of generating similar mineralogical patterns. Minor carbonate phases (dolomite or calcite) appear to represent late-stage impregnation along the metasomatic fronts. The overall mineral assemblage points to progressive Fe-oxide replacement of a pre-existing quartz–feldspar framework, locally accompanied by late carbonate veining and Fe-oxide development.

Ferruginized Sandstone

The ferruginized sandstone shows prominent diffraction peaks of hematite, goethite, and quartz, with subordinate feldspar, muscovite, and kaolinite. Compared with the metasomatized variety, the ferruginized sandstone retains stronger silicate peaks and exhibits enhanced goethite content, indicating partial hydration of hematite during near-surface oxidation. The coexistence of feldspar and muscovite denotes relatively limited metasomatic alteration, with the arenitic framework largely preserved. This mineralogy reflects a transitional stage between unaltered sandstone and fully metasomatized ferruginous varieties, typified by moderate Fe-oxide impregnation and partial feldspar alteration. Dolomite and calcite occur sporadically along fractures and shear planes, representing late carbonate veining synchronous with waning hydrothermal activity.

Weakly Ferruginized Sandstone

The weakly ferruginized sandstone exhibits a mineral assemblage dominated by quartz,

with subordinate kaolinite and minor to trace occurrences of hematite, goethite, and K-feldspar. The dominance of quartz, together with minor kaolinite, indicates a largely unaltered arenitic framework, whereas the trace hematite and goethite suggest incipient Fe-oxide impregnation along grain boundaries and pore spaces. The trace of K-feldspar reflects a preserved detrital component, implying negligible feldspar alteration. Overall, this assemblage represents the earliest stage of Fe-enrichment, marking the onset of ferruginization prior to the development of pervasive Fe-oxide metasomatism observed in the more altered facies.

Interpretation:

The XRD results from the Bhuj Formation delineate a systematic mineralogical progression that reflects increasing intensity of Fe-oxide metasomatism and hydrothermal overprinting. The mineralogical data define a coherent alteration trend from weakly ferruginized to fully metasomatized sandstone facies, consistent with the field and geochemical observations described in preceding sections.

The dominance of hematite, and subordinate goethite in the metasomatized sandstones signifies an intense ferruginous overprint, representing multiple stages of Fe-oxide replacement and precipitation. The persistence of feldspar and muscovite peaks, coupled with subordinate kaolinite, implies incomplete destruction of primary detrital silicates, or their partial recrystallization under low to moderate temperature hydrothermal conditions.

The sporadic occurrence of pyroxene in one sample indicates localized high-temperature fluid influx, possibly linked to structurally channelized hydrothermal circulation along the Katrol Hill Fault and its splays. Minor carbonate phases (dolomite, calcite) observed in metasomatized samples are interpreted as late-stage infill products precipitated from waning hydrothermal fluids.

Comparatively, the ferruginized sandstone exhibits both hematite and goethite with enhanced silicate persistence, signifying near-surface hydration and oxidation under transitional redox conditions. In contrast, the weakly ferruginized sandstones represent early Fe-enrichment, where hematite and goethite occur only as pore filling phases.

Overall, the mineralogical trends identified through XRD confirm a progressive alteration sequence from primary quartzo-feldspathic arenite facies to hematite-dominated metasomatized facies, controlled by structurally influenced Fe-rich hydrothermal fluids. The variability in Fe-oxide and silicate mineral proportions reflects episodic fluid migration, temperature fluctuation, and redox oscillations within the hydrothermal corridors of the Bhuj Formation.

4.7.3.3. SEM-EPMA Study

To complement the petrographic observations and establish microtextural-compositional relationships, four representative samples from the metasomatized and ferruginized lithounits of the Bhuj Formation were subjected to Scanning Electron Microscopy (SEM) and Electron Probe Micro-Analysis (EPMA) (*Annexure- XVIII and XIX*). These analyses were undertaken to delineate minerochemical variations at the microscale and identify secondary mineral phases formed during Fe-oxide metasomatism. Additionally, one sample from associated Chari Formation has also been examined to understand if there is any effect of Fe-metasomatism.

The SEM–EPMA dataset provides crucial insights into the physicochemical evolution of the hydrothermal system and the spatial redistribution of transition and high-field-strength elements within the altered sandstones.

SEM-EDAX Analysis

Metasomatized and Ferruginized Sandstone

Back-scattered SEM images and spot EDAX from four metasomatized and ferruginized sandstone samples from the Bhuj Formation (*Annexure- XVIII*) reveal a poorly sorted framework composed predominantly of angular quartz grains, with subordinate feldspar, ilmenite, zircon, and monazite grains (*Fig. 4.51-53*). The matrix is dominated by iron oxides, primarily magnetite, which occurs both as intergranular cement and as pervasive replacement fronts enveloping detrital grains (*Fig.4.52*). The presence of zeolite as a secondary infilling phase within intergranular spaces (*Fig.4.53*) indicates late-stage hydrothermal alteration and fluid percolation through open pore networks. Several microtextures, such as fractured quartz clasts, sutured grain contacts, and partially healed microcracks, provide clear evidence of in-situ brecciation and subsequent Fe-oxide impregnation (*Fig. 4.52; 53*).

EDAX analyses confirm the presence of monazite grains, displaying elevated concentrations of P, Ce, and La, thereby establishing the role of phosphate minerals as minor but significant REE hosts within the metasomatized system (*Fig.4.54a*). Ilmenite and magnetite, detected in both matrix and intergranular spaces, develop part of the Fe-Ti oxide assemblage produced during hydrothermal replacement. The magnetite spectra exhibit high Fe and minor Ti peaks, suggesting low-Ti concentration of the metasomatic Fe-rich fluids (*Fig. 4.54b*), typical of IOCG type mineralization.

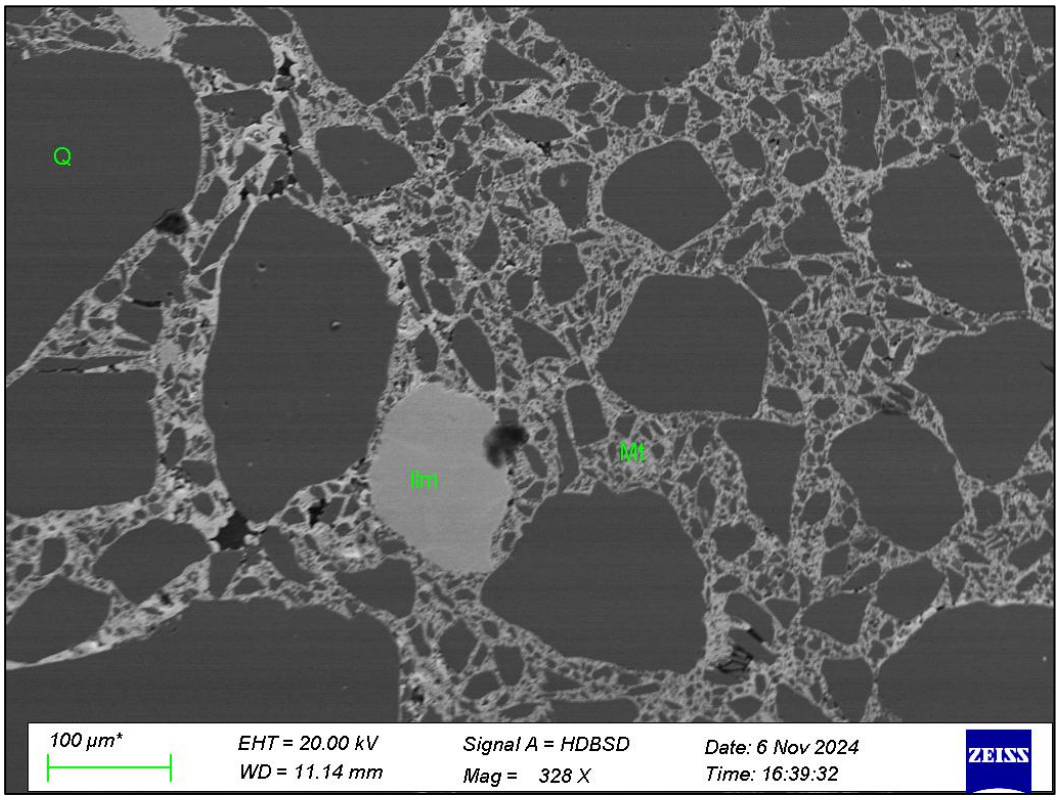

Fig. 4. 51 BSE image of Bhuj sandstone showing angular clasts of Quartz (Q), Ilmenite (Ilm) embedded in a magnetite (Mt) rich matrix.

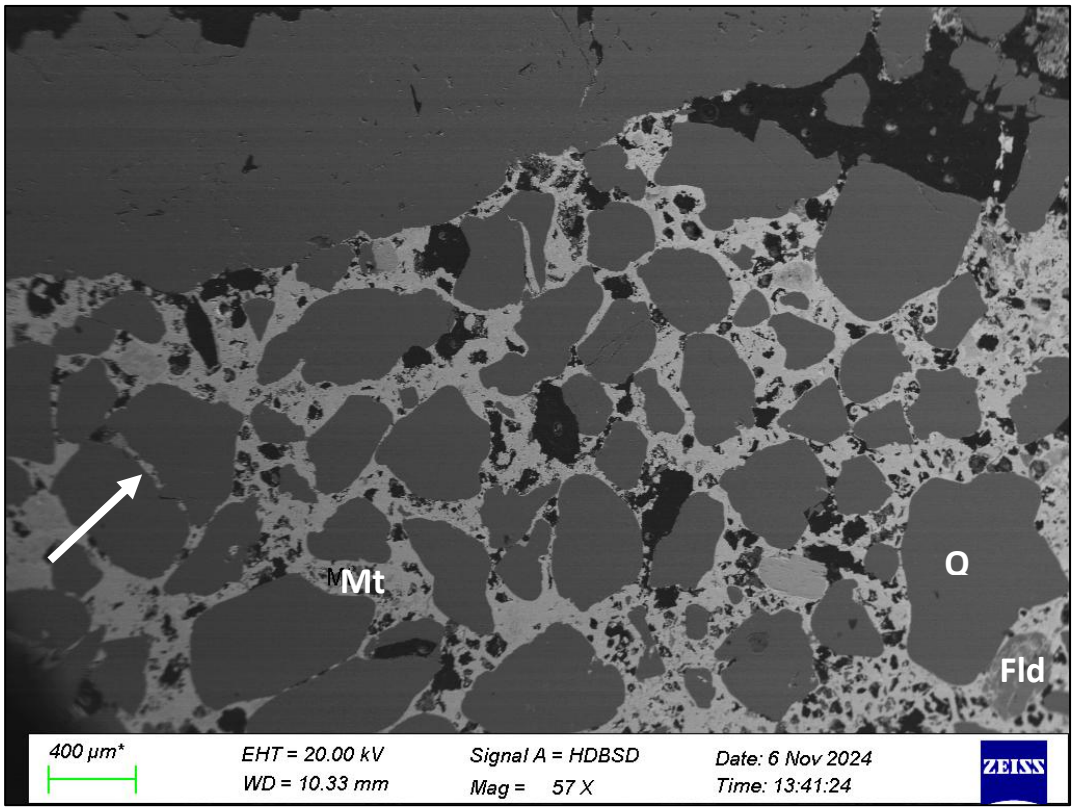

Fig. 4. 52 BSE image of Bhuj sandstone showing clasts of Quartz (Q), Feldspar (Fld) embedded in a magnetite (Mt) rich matrix. Note the in-situ brecciation of framework clast, marked by arrow.

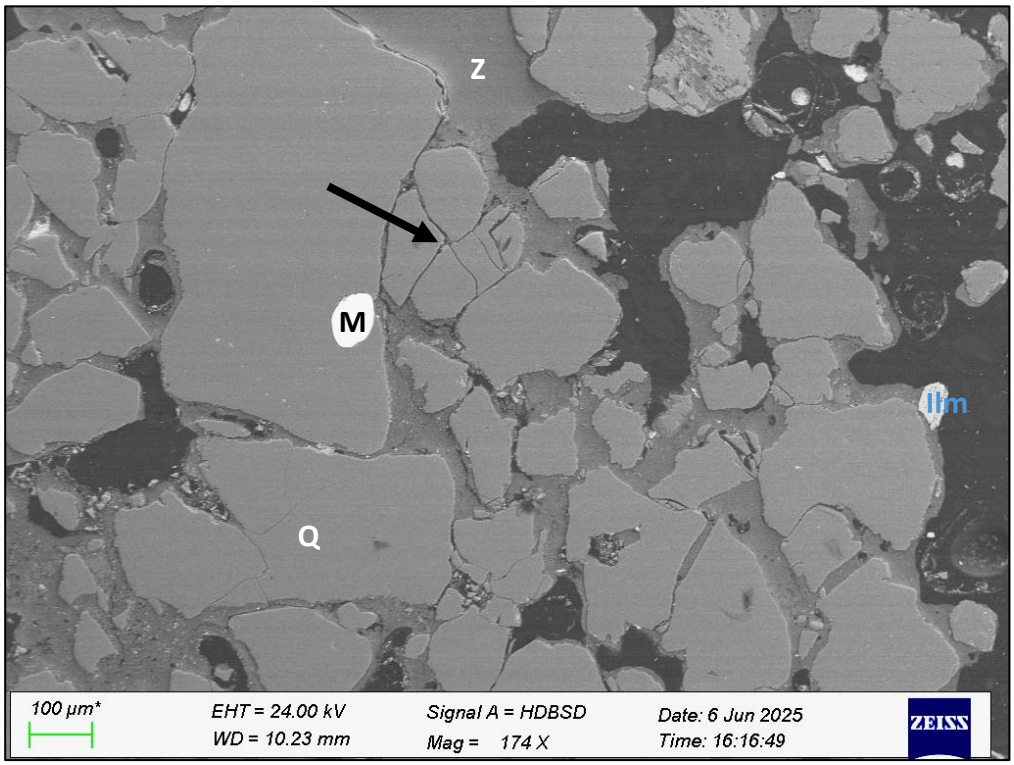

Fig. 4. 53 BSE image of Bhuj sandstone showing clasts of Quartz (Q), Monazite (M) and Ilmenite (Ilm) as framework grains. Intergranular pore spaces infilled by secondary zeolite (z). Note the in-situ brecciation of framework clast, marked by arrow.

a.

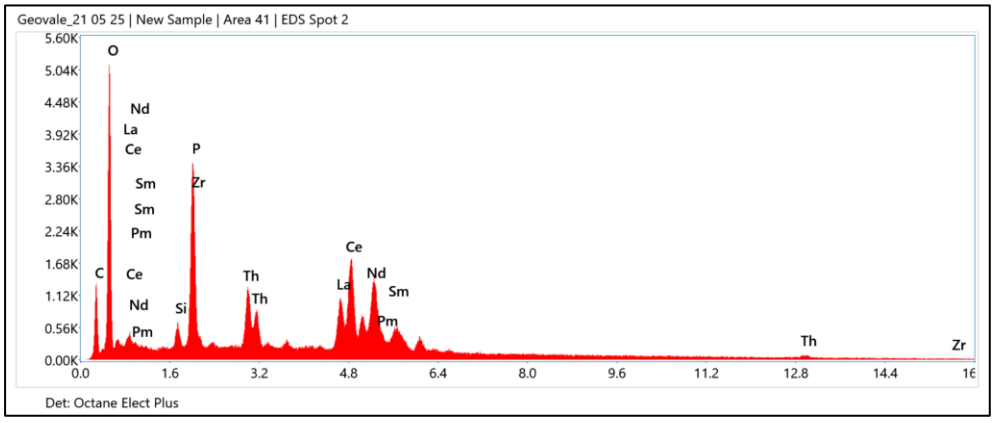

b.

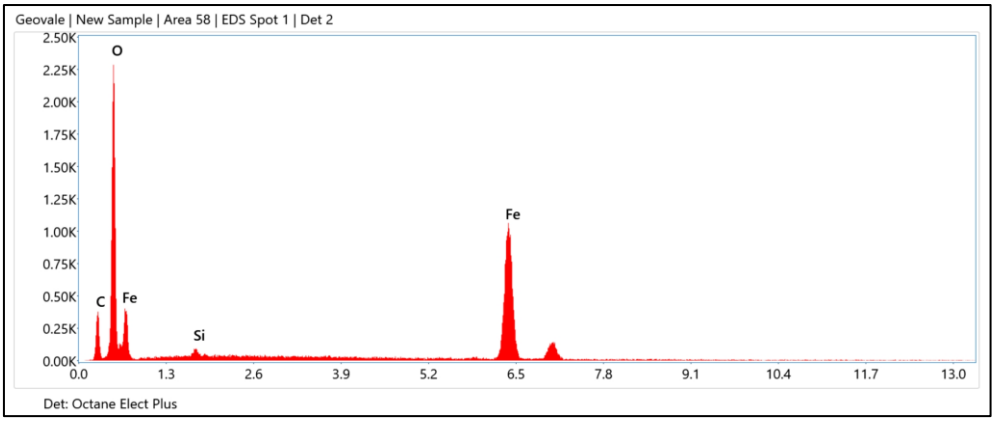

Fig. 4. 54 (a) EDAX spectrum of monazite grain showing pronounced P, Ce, and La peaks. (b) EDAX spectrum of magnetite-rich matrix with elevated Fe and minor Ti peaks.

Ferruginous Sandstone of Chari Formation

A comparative sample from the Chari Formation (*Annexure- XVIII*) shows a similar mineralogical architecture, with angular to sub-angular quartz and feldspar clasts enclosed within a magnetite-rich matrix (*Fig.4.55a*). The occurrence of monazite within the matrix of the Chari sandstone, confirmed by distinct P, Ce, and La peaks (*Fig.4.55b*). Presence of similar minero-chemical components in both Chari and Bhyj formations suggests that Fe metasomatism, may extend beyond the Bhuj Formation, reflecting a regional hydrothermal influence along the western Kachchh corridor.

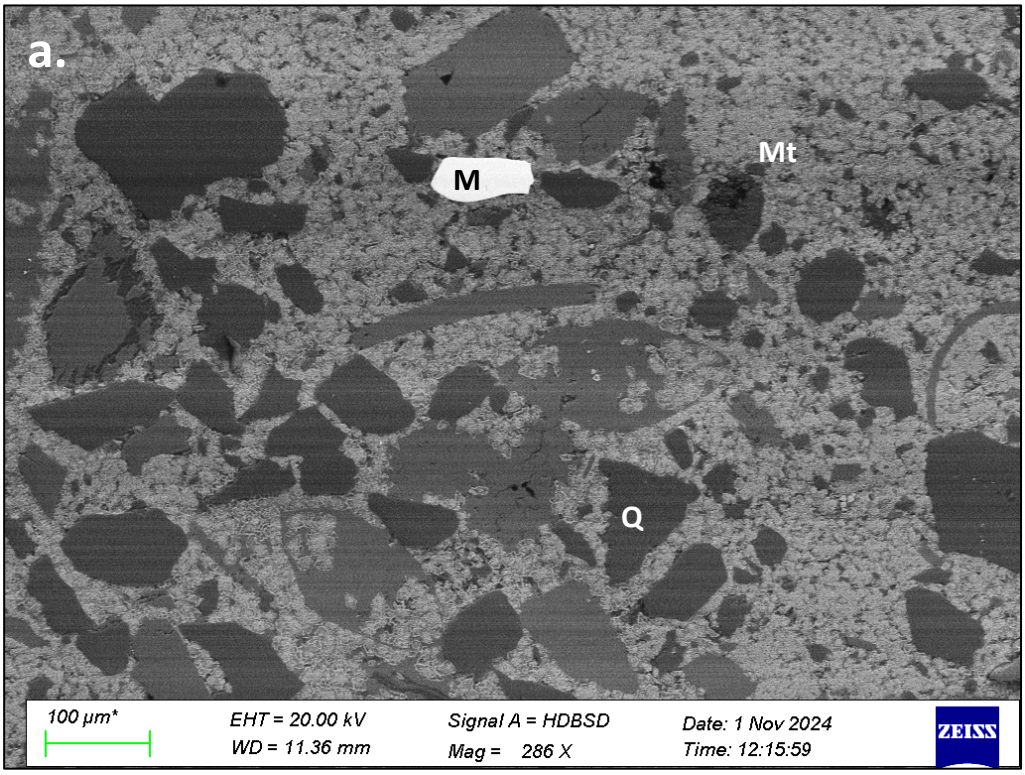

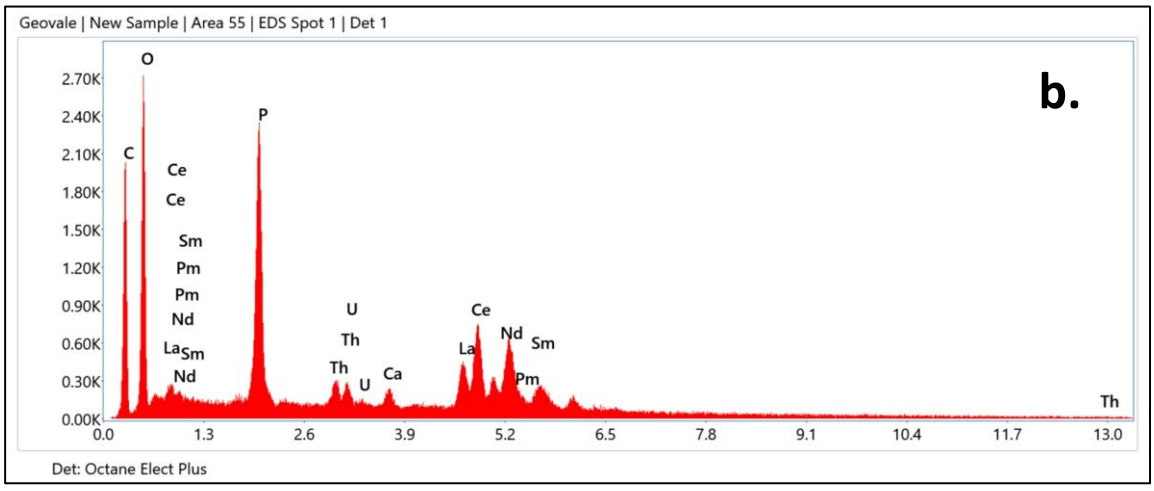

Fig. 4. 55 SEM–EDAX images of ferruginous sandstone from the Chari Formation. (a) BSE image showing angular to sub-angular quartz (Q) and monazite (M) clasts embedded in magnetite (Mt) rich cement. (b) EDAX spectrum from a monazite inclusion within the ferruginous matrix showing enrichment in P, Ce, and La.

Collectively, the SEM-EDAX results corroborate petrographic observations and substantiate the hydrothermal metasomatic origin of the Bhuj ferruginous sandstones. The microtextural evidences, comprising magnetite cement, zeolite infillings, and microbrecciation of the clasts confirms repeated fluid infiltration and Fe-Ti oxide replacement during post-depositional alteration. Low Ti content in magnetite further corroborates typical IOCG-style mineralization. The localized presence of monazite, in turn, demonstrates limited but discernible REE mobilization under the influence of Fe-oxide dominated hydrothermal activity.

EPMA Analysis

Electron Probe Micro-Analysis (EPMA) was conducted on four representative samples from the Bhuj Formation to establish the mineral and chemical characteristics of framework and accessory phases, particularly those associated with Fe-oxide metasomatism and REE enrichment. Of these, three samples were prepared from heavy liquid separated (HLS) fractions of stream sediments (–125 µm), and one from mounted thin sections of metasomatized sandstone (*Annexure-XIX*).

EPMA results indicate that the framework assemblage of the Bhuj sandstones is dominated by quartz and subordinate amount of feldspar (both K-feldspar and plagioclase), with minor amounts of zircon, monazite, xenotime, magnetite and rutile occurring as discrete detrital or authigenic grains (*Fig.4.56a-c*). The matrix is predominantly rich in magnetite with minor occurrence of rutile and K-feldspar (*Fig.4.56b, c*). Locally, disseminated apatite grains are also observed within the matrix. Matrix comprised of carbonate (both calcite and dolomite) have also been identified, suggesting late-stage impregnation along metasomatic fronts. Dark vein-like features within the matrix exhibit Fe-oxide, Fe-hydroxide, and Fe-Ti hydroxide composition, representing hydrothermal influx zones where Fe rich fluids percolated and precipitated along microfractures and intergranular pore spaces.

The sample prepared from HLS fractions (-125 micron, heavy liquid separated stream sediment samples) reveals similar accessory assemblages of monazite (*Fig.4.56d*), zircon, xenotime, and rutile, confirming that these REE and HFSE-bearing minerals were also transported detritally and subsequently overprinted or stabilized during metasomatism.

Identified composition of accessory assemblages (bedrock and stream sediment samples):

- **Rutile (TiO_2):** Rutile occurs as an accessory Ti-bearing phase (66-100 wt.% TiO_2) with minor FeO (0.3-22.6 wt.%) and Cr_2O_3 (≤0.54 wt.%), denoting Ti mobility during metasomatism and its re-stabilization within oxide-rich veins.
- **Monazite (LREE-phosphate):** Monazite grains are characterized by the presence of P_2O_5, La-Ce-Nd-Pr-Sm-Gd, Y, Th, and U, confirming their role as principal REE hosting phosphates.
- **Zircon (paired note with fluor-apatite/zircon):** Zircon, with distinct Zr and Hf peaks, typically occurring as detrital grains.
- **Xenotime (Y-phosphate):** Identified in minor proportions.
- **Apatite and Fluorapatite** Occur as dispersed grains within the ferruginous matrix; these phases may host minor REE, Sr, and halogens, functioning as both detrital and secondary diagenetic minerals.

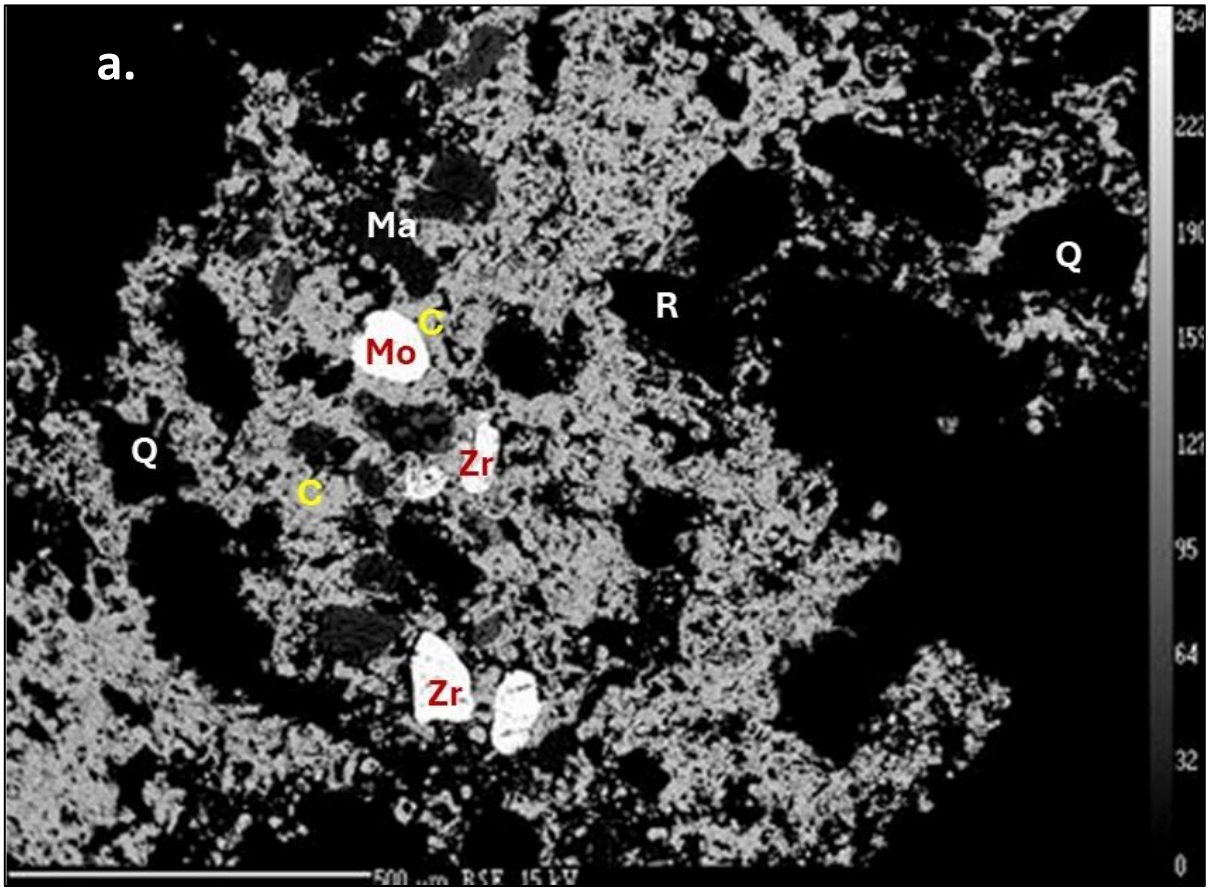

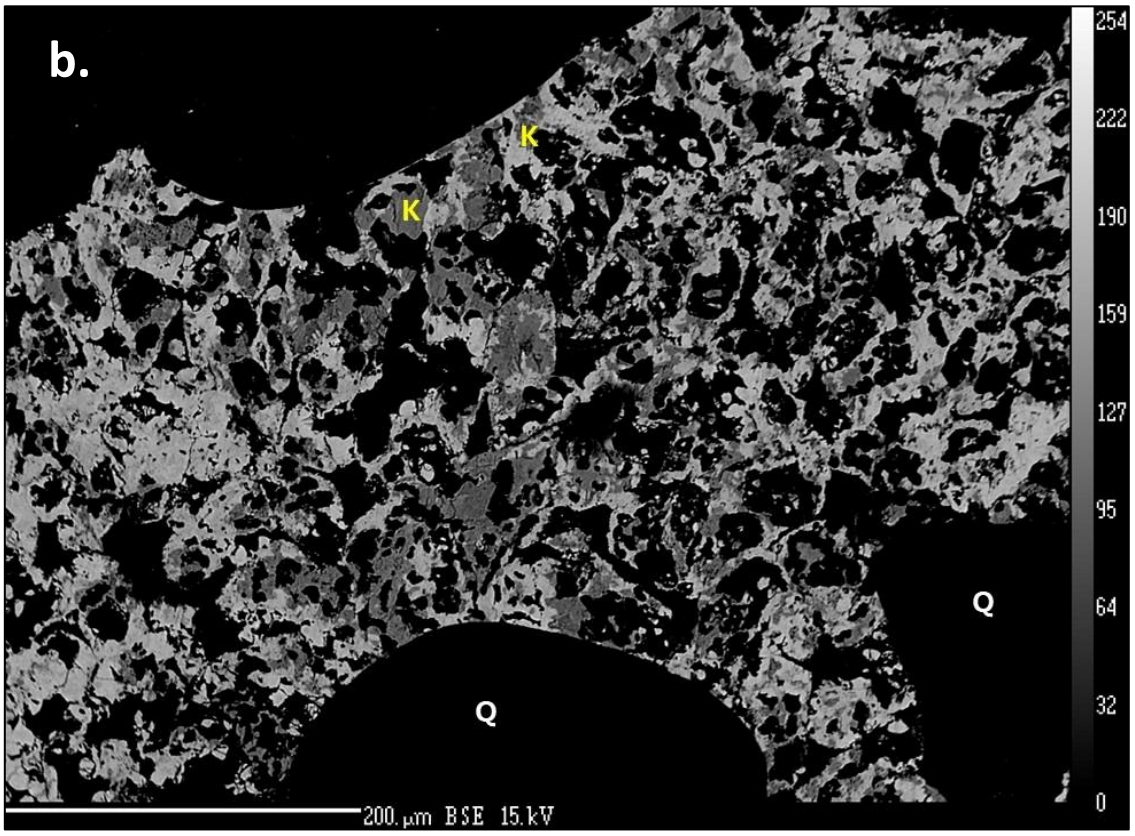
b.
K
K
Q
Q
200.μm BSE 15.kV
254
222
190
159
127
95
64
32
0

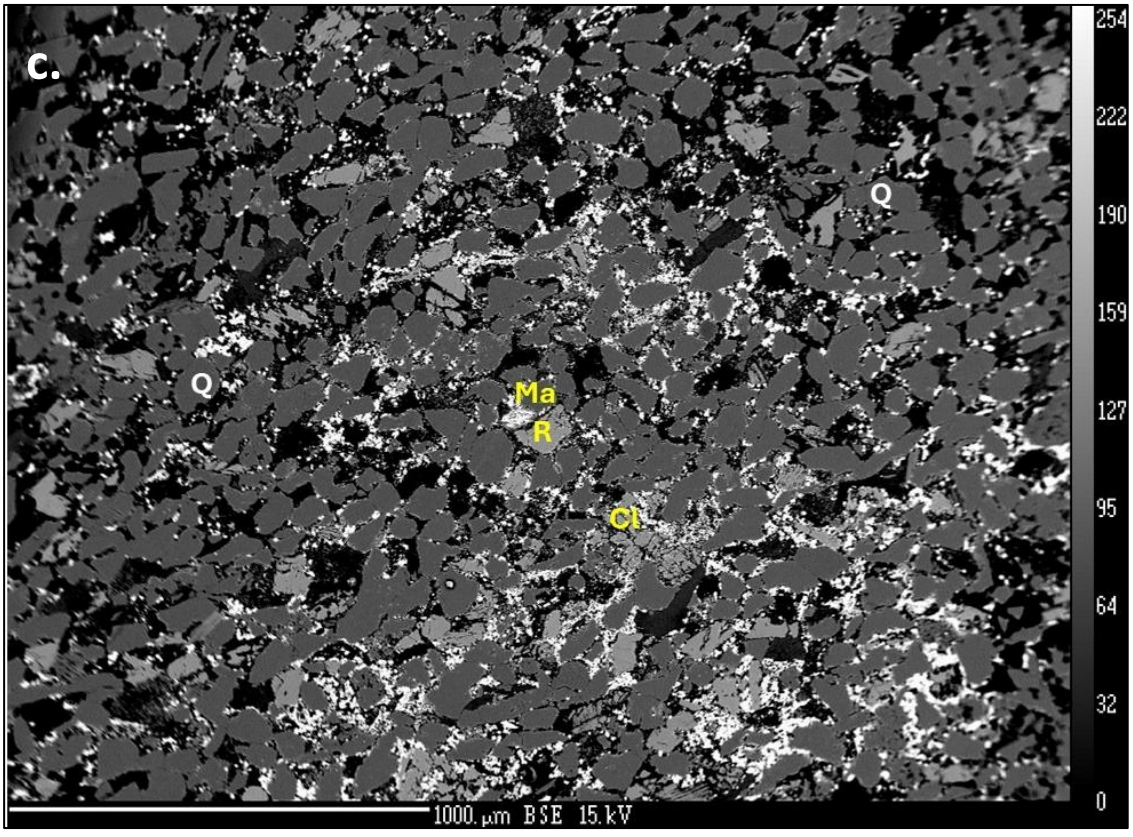
c.
Q
Q
Ma
R
Cl
1000.μm BSE 15.kV
254
222
190
159
127
95
64
32
0

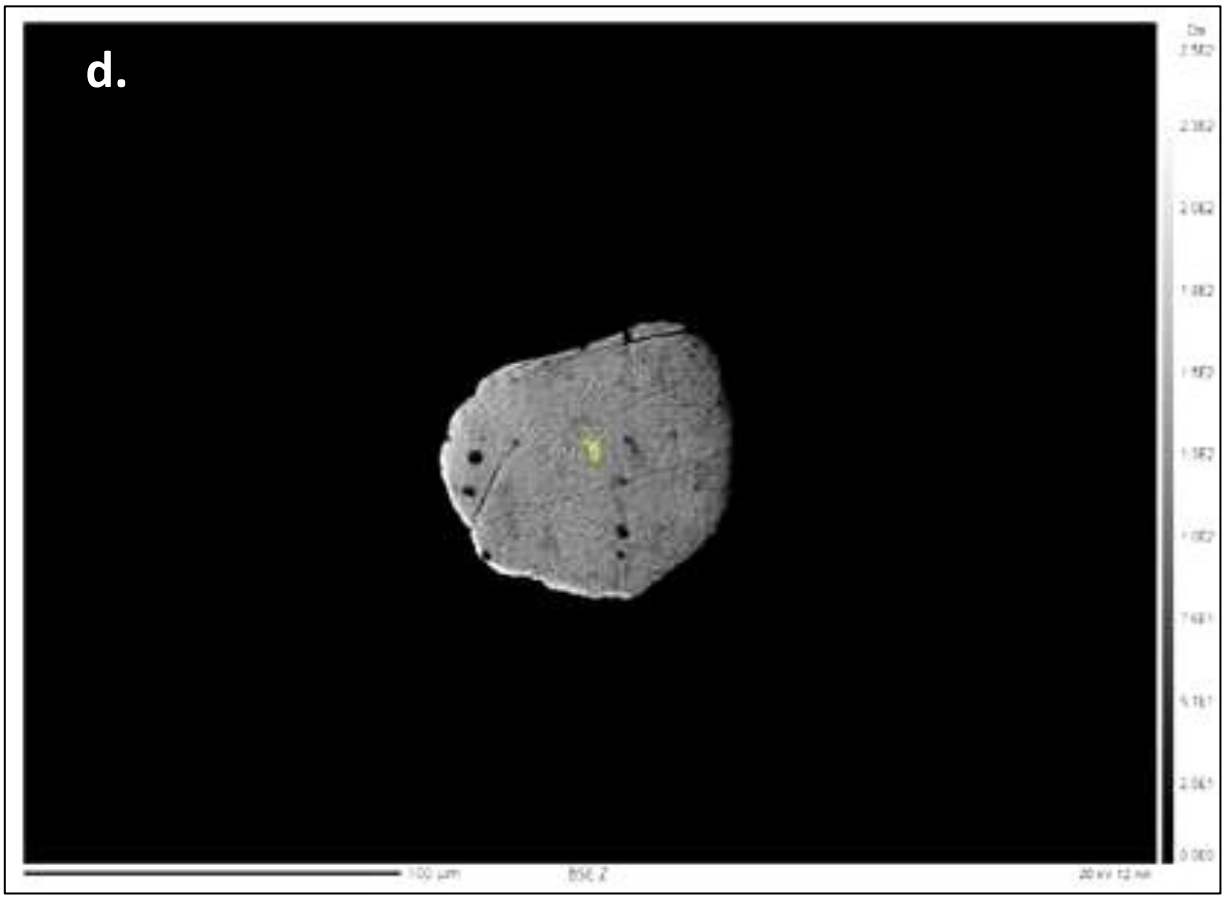

Fig. 4. 56 Back-scattered electron (BSE) images and EPMA mineral maps of Bhuj Formation. (a) Framework grains of quartz (Q), monazite (Mo), zircon (Zr), and rutile (R) within a carbonate (c) rich matrix containing magnetite (Ma) grains. (b) Grains of K-feldspar (K) occurring within the matrix between large clasts of quartz (Q) of Bhuj Sandstone. (c) Quartz and rutile clasts embedded within a clay-dominated matrix crosscut by Fe-rich veins. (d) Monazite grain from heavy liquid separated concentrate of -125 micron stream sediment of Bhuj Formation.

Overall, the EPMA study corroborates the hydrothermal and metasomatic evolution inferred from petrographic and geochemical data. The coexistence of Fe-Ti oxides, REE bearing phosphates, and HFSE-rich accessory minerals indicates hydrothermal redistribution and partial re-precipitation of detrital heavy minerals within the Bhuj Formation during Fe-oxide metasomatism.

4.8. Geophysical Exploration

The geophysical program for the Bhuj REE exploration block was designed to delineate subsurface resistivity contrasts associated with two distinct mineral systems. These systems correspond to different geological contexts within the project area, each expected to produce a characteristic geophysical signature. The primary objectives were to establish a geoelectrical framework reflecting variations in lithology, alteration, and structure, and to integrate this

with geological mapping to define exploration targets for REE and Fe-oxide mineralization. Key focus areas included:

I. **IOCG-Style System (Bhuj Formation):** Metasomatized ferruginous sandstone and breccia zones representing a potential Iron Oxide Copper-Gold–style hydrothermal mineralization system. These zones are associated with Fe-oxide enrichment (hematite–magnetite), brecciation, and hydrothermal alteration in the Early Cretaceous Bhuj Formation sandstones.
II. **Stratiform REE System (Katrol Formation):** Heterolithic shale–sandstone sequences of the Late Jurassic Katrol Formation, locally interbedded with ferruginous tuffite layers that host secondary REE enrichment. This stratiform volcaniclastic-phosphatic system represents REE-bearing horizons within an alternating shale and sand unit.

By targeting both mineral systems, the survey aims to delineate the subsurface continuity of the metasomatic Fe-oxide zones (Mineral System II) and map the host heterolithic packages of the stratiform REE horizons (Mineral System I). In essence, the geophysical exploration seeks to "see" the host environments of mineralization, the fault-altered ferruginous zones and the tuffite-bearing shale layers, rather than the ore minerals directly, thereby guiding subsequent higher-resolution investigations.

A total of 210 Vertical Electrical Sounding (VES) stations were established across the Bhuj block (*Annexure-XXII; Fig. 57*), covering approximately 42 line-km of survey traverses. Survey lines were oriented principally NW-SE and NE-SW to intersect major structural features – notably the Katrol Hill Fault (KHF) and the Median High Zone (MHZ), as well as to cross key lithological contacts between the Chari, Katrol, and Bhuj Formations. VES stations were spaced along and across these features to capture resistivity variations associated with fault-controlled alteration and stratigraphic changes. Additional soundings were concentrated in the Katrol Formation outcrop areas (about 35 VES stations) to characterize its heterolithic sequence, which had not been addressed in earlier geophysical write-ups.

4.8.1. Methodologies

The geophysical survey was carried out using the Schlumberger array configuration, which offers optimum sensitivity for detecting layered subsurface media while ensuring operational efficiency under field conditions.

The survey employed an Aquameter CRM-500 resistivity meter (*Fig.58*a), which measures the potential difference generated by a known current injected into the ground through a pair of current electrodes. Two potential electrodes placed symmetrically about the current electrodes recorded the resulting voltage response. The apparent resistivity values

were automatically computed based on the electrode spacing and the geometric factor associated with the Schlumberger array (*Fig.58b*).

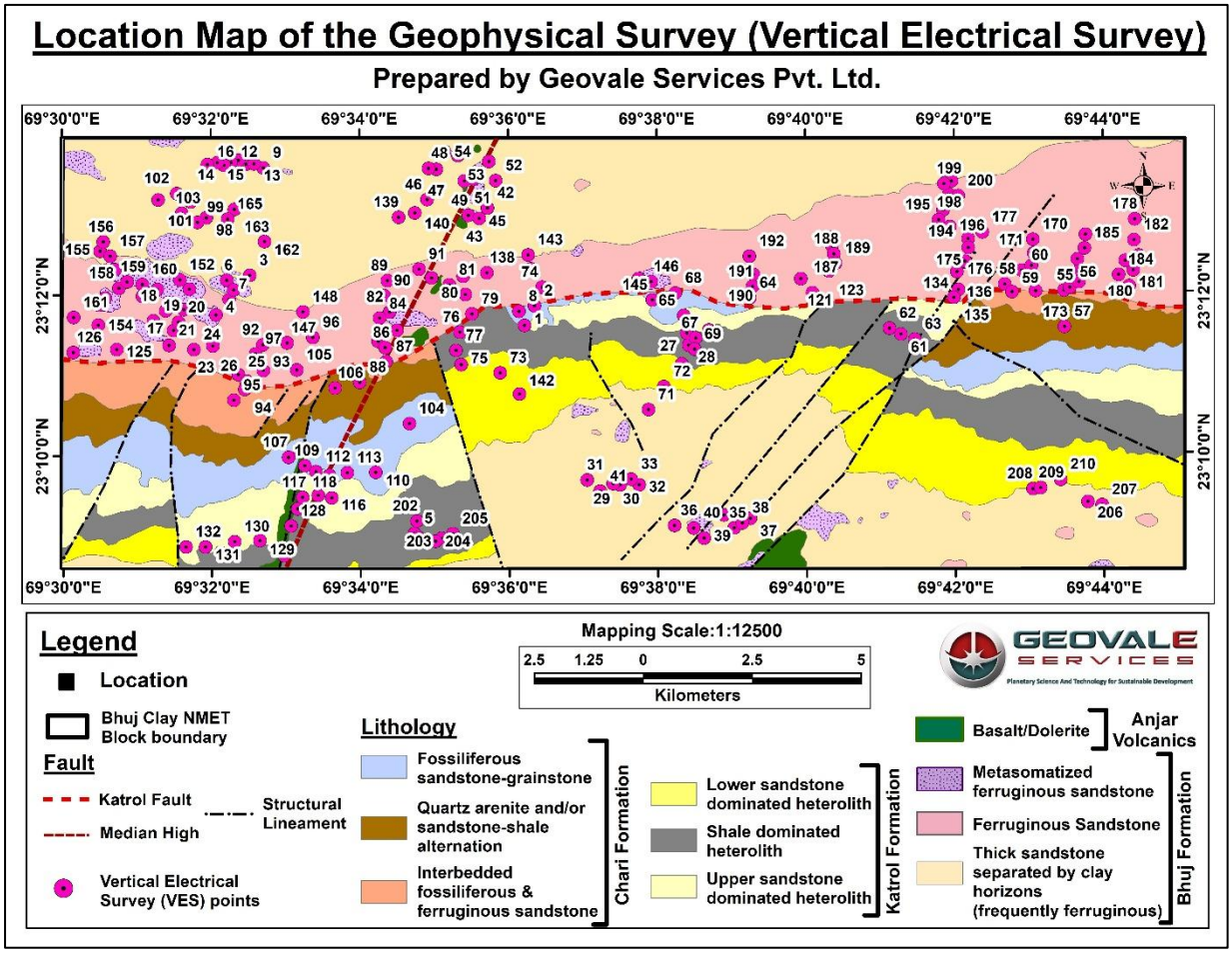

Fig. 4. 57 Location map showing distribution of 210 VES stations superimposed on the geological map of the study area, with prominent structural features including the Katrol Hill Fault (KHF), Median High Zone (MHZ), and associated splays.

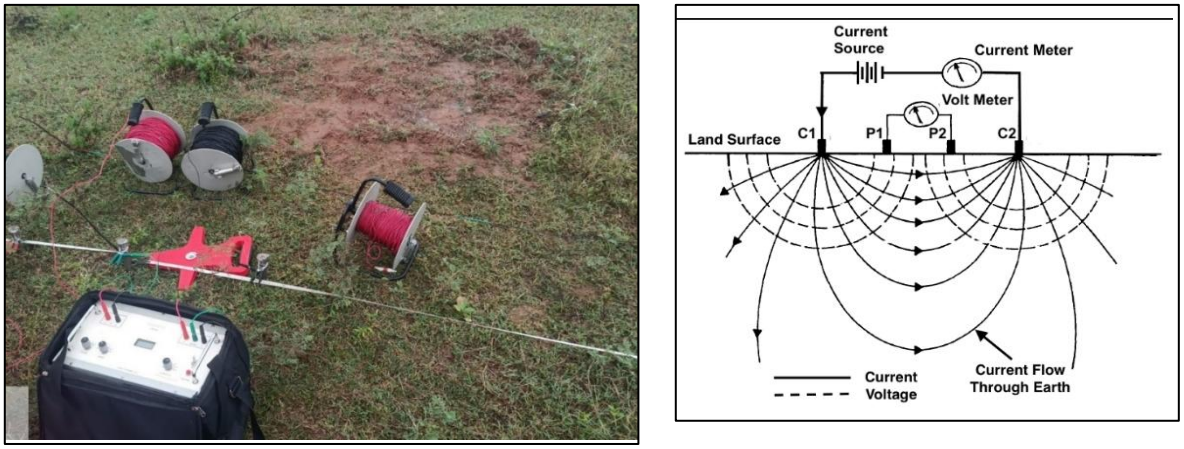

Fig. 4. 58 (a) Aquameter CRM 500 used to Collect the Resistance Data. (b) Basic Concept of Resistivity Measurement.

A total of 210 VES stations were completed, covering approximately 42 line-kilometres across the Bhuj exploration block (Annexure- XXII). Electrode separations were progressively increased during each sounding to obtain resistivity values corresponding to deeper horizons. In a homogeneous medium, approximately one-third of the injected current penetrates below a depth equal to the electrode half-spacing, while nearly half extends to a depth corresponding to twice that distance. For the Schlumberger configuration, the effective depth of investigation is generally considered to be about half of the total current electrode separation (AB/2). Consequently, smaller electrode spacings provide higher-resolution information for shallow horizons, whereas larger spacings are required to probe deeper subsurface structures. In the present investigation, the electrode-spacing range was optimized to resolve both shallow and moderately deep zones, thereby facilitating discrimination between conductive ferruginous–altered horizons and resistive sandstone packages within the Bhuj Formation, as well as between the resistive shale units and comparatively conductive, porous sandstone horizons within the Katrol Formation.

The raw field data (apparent resistivity values at various AB/2 spacings for each VES station) were processed through 1D inversion to estimate true resistivity and layer thickness for the subsurface. Initial interpretation involved curve matching and iterative modeling of the VES sounding curves using standard software, yielding a best-fit layered-earth model for each site. These models were then correlated laterally to construct geoelectrical cross-sections along selected traverses. In parallel, key inversion results (e.g. true resistivity at specific depths) were interpolated to generate iso-resistivity maps or depth slices (e.g. resistivity contours at 25 m, 50 m, 100 m depth) to visualize spatial trends. All interpreted resistivity features were cross-checked against geological mapping, borehole lithologs (if available), and petrographic/alteration data to ensure consistency with known geology.

4.8.2. Stratigraphic Context and Characteristic Resistivity Signatures

The Bhuj project area is situated in a Mesozoic sedimentary basin with the stratigraphic succession (oldest to youngest) comprising the Middle Jurassic Chari Formation, Upper Jurassic Katrol Formation, and Lower Cretaceous Bhuj Formation. Each of these formations has distinctive lithological makeups which impart characteristic ranges of electrical resistivity. Understanding these baseline resistivity signatures is crucial for distinguishing normal lithological variations from anomalies potentially caused by mineralization or alteration. Below, we summarize each major unit's geophysical character:

4.8.2.1. Chari Formation (Middle Jurassic)

Lithology & Geological Setting: The Chari Formation consists of a marine to marginal-marine sequence dominated by fossiliferous sandstone, ferruginous shale, and limestone. It

forms the lowermost stratigraphic unit in the area and is generally exposed in the western/southwestern part of the block or encountered at depth beneath Katrol Formation.

Resistivity Characteristics: Chari is uniformly the most conductive formation in the survey, with low true resistivity values on the order of 10–40 Ω·m, occasionally up to ~60–80 Ω·m in limestone-rich sections. The low resistivity response is attributed to its high content of clays and shale (argillaceous layers) and ferruginous material, which enhance electrical conductivity. In the inverted VES models, the Chari Formation typically appears as a conductive basal layer (often <40 Ω·m) underlying the more resistive Katrol or Bhuj units. It effectively acts as the electrical "basement" in many parts of the block, because deeper penetration seldom reveals units more conductive than Chari's shales. The presence of Chari is thus marked by a pronounced downward decrease in resistivity at the base of VES soundings, corresponding to depths of roughly 40–60 m where it is intersected. This clear contrast makes it relatively easy to identify the top of the Chari Formation in resistivity sounding data.

Interpretation: The Chari Formation's conductive signature reflects its lithological makeup of clay-rich and ferruginous sediments. From an exploration standpoint, this unit is important as a background reference – any anomalously low resistivity detected above the typical depths of Chari could indicate argillization or mineralization in higher units rather than just the stratigraphic basement. The Chari Formation itself is not a REE host but provides a reducing, shale-dominated horizon that underlies the Katrol stratiform system.

4.8.2.2. Katrol Formation (Late Jurassic)

Lithology & Geological Setting: The Katrol Formation conformably overlies Chari and is characterized by an alternating sequence of dark grey shales and sandstones, locally interbedded with ferruginous tuffite (volcanic ash-fall) layers and ferruginous siltstone. This heterolithic unit represents a stratiform volcanogenic-sedimentary system. The ferruginous tuffites within Katrol are of particular interest as they host anomalous REE and trace element concentrations in this project. Surface mapping indicates the Katrol outcrops in the central and southern parts of the block, often in structurally downthrown panels adjacent to the Katrol Fault.

Resistivity Characteristics: The VES response over the Katrol Formation is distinctly different from the homogeneous units above and below it, exhibiting a diagnostic "oscillatory" resistivity curve pattern. Apparent resistivity values are moderate overall (typically 20–100 Ω·m) and fluctuate with depth in a sawtooth manner as the current probes alternating sandstone vs. shale layers. Specifically, relatively resistive sandstone beds (more porous and coarse-grained) register as peaks or increases in the sounding curve, whereas intervening conductive shale/tuffite layers (clay-rich, ferruginous, higher moisture content) cause troughs or drops in resistivity. This repetitive up-and-down profile is a diagnostic geophysical marker

for the Katrol Formation, clearly distinguishing it from the monotonously high resistivity Bhuj Formation above and the uniformly low resistivity Chari Formation below. In many Katrol-area soundings, 2–4 such oscillations are observed within the upper ~80 m, corresponding to the layering of sand and shale units in the formation.

Quantitatively, Katrol Formation resistivity typically ranges 40–100 Ω·m for the sandstone-dominated layers, and drops to <20 Ω·m in the most conductive shale or ferruginous tuffite horizons. The mean resistivity of Katrol heteroliths falls around 40–100 Ω·m with an average interpreted thickness of 60–90 m in the block. Near major faults, the low-resistivity segments can be especially pronounced: for example, soundings close to the KHF record sharp resistivity minima of 10–20 Ω·m at certain depths, reflecting intense fracturing, clay alteration, or mineralization along the fault-controlled tuffite beds. Notably, unlike the Bhuj Formation (which shows very high resistivity values when unaltered), even the coarser units of Katrol remain in a moderate resistivity range because they are interbedded with fines and often contain cementation or pore fluids that limit their resistivity. In summary, the Katrol Formation's geoelectrical signature is an undulating resistivity log indicative of stratified sand–shale units, with ferruginous tuffite layers contributing distinctive low-resistivity troughs.

Interpretation: The oscillatory resistivity pattern over Katrol directly mirrors its rhythmic sedimentary layering. Each resistivity peak corresponds to a sandstone (higher resistivity due to cleaner quartz-rich makeup and lower clay content), while each trough indicates a shale or tuffite layer (higher clay/metal content, thus more conductive). The presence of REE-enriched tuffites, which are only a few centimeters to decimeters thick, cannot be directly resolved as separate layers by VES due to limited vertical resolution. However, their effect is captured by the broader conductive intervals: the REE-hosting tuffite beds lie within shale-dominated packages that produce notable low-resistivity segments in the VES curve. Therefore, the geophysical exploration strategy for Mineral System I (Katrol REE) is to map these conductive shale/tuffite packages as proxies for the hidden tuffite layers. Laterally continuous low-resistivity zones within the Katrol Formation, especially when correlated across multiple adjacent soundings, are interpreted as likely ferruginous shale horizons that could host tuffite and REE mineralization. The VES results have thus enabled confident mapping of the subsurface extent of Katrol heterolithic units even where they are concealed by alluvial cover, by recognizing this oscillatory pattern as a fingerprint of the Katrol Formation.

Structrally controlled areas:

Across the Bhuj project area, several VES profiles intersecting the Katrol Hill Fault (KHF) and its subsidiary splays reveal distinct variations in resistivity, with localised low-resistivity zones marking areas of enhanced fracturing and alteration. These anomalies likely represent fluid-enriched or clay-altered zones along the fault planes, demonstrating the structural influence on the formation's electrical character. Toward the western parts of the block, where

ferruginous alteration is more pronounced, slightly lower resistivity values are observed, suggesting possible zones of Fe-oxide enrichment.

4.8.2.3. Bhuj Formation (Early Cretaceous)

Lithology & Geological Setting: The Bhuj Formation is the youngest and areally most extensive unit in the block, covering much of the northern and central area at surface. It consists predominantly of thick, massive sandstones (medium- to coarse-grained, quartzose arenites) with minor interbeds of siltstone and clay, as well as localized facies of ferruginous sandstone and zones of hydrothermal alteration (silica–Fe-oxide metasomatism). Structurally, the Bhuj Formation in this block has been affected by basin-margin faulting (e.g., the Katrol Fault and associated splays) which created pathways for mineralizing fluids – this is the context for the potential IOCG-style mineral system hosted within Bhuj. Unaltered Bhuj sandstone is hard, compact and forms resistant ridges, while altered portions appear ferruginized, friable, or brecciated in outcrop.

Resistivity Characteristics: Unaltered Bhuj Sandstone is characterized by very high resistivity in the VES data, often exceeding 200–300 Ω·m. This is among the highest resistivities encountered in the survey and reflects the clean, dry, and consolidated nature of the Bhuj sandstones: they are quartz-rich (silica is an excellent insulator), have low clay content, large grain size, and generally low pore water conductivity, all of which contribute to a high bulk resistivity. Typically, a VES sounding located entirely on unaltered Bhuj Formation shows an upward-increasing resistivity curve that may plateau or reach a maximum beyond 200 Ω·m at depth, corresponding to the thick sandstone sequence. This makes the Bhuj unit an effective resistive background or host in the geoelectrical framework, against which conductive anomalies can be distinguished.

Importantly, where the Bhuj sandstone has undergone hydrothermal alteration or ferruginization, its resistivity is markedly reduced. Ferruginous sandstone horizons (with disseminated iron oxide cement) show moderate resistivity drops (still in tens of Ω·m), but intensely metasomatized and brecciated zones produce pronounced low-resistivity anomalies. In areas of known Fe-oxide alteration (IOCG-style targets), the VES results reveal true resistivities on the order of 10–80 Ω·m, a stark contrast against the >200 Ω·m fresh sandstone. This contrast is due to several alteration effects: partial replacement of non-conductive quartz by conductive minerals (magnetite, hematite, clays, secondary carbonates), increased porosity and fluid content in breccia zones, and introduction of conductive iron-bearing minerals along fractures. As a result, a typical VES sounding crossing an altered Bhuj zone will exhibit a pronounced resistivity low (trough) at the depths corresponding to that zone, flanked above and below by high-resistivity sections of unaltered sandstone. The magnitude of resistivity drop is substantial – for instance, from ~200+ Ω·m in unaltered rock

down to ~20–50 Ω·m in an alteration zone – making these geophysical anomalies quite conspicuous.

In many inverted models, the altered zones in Bhuj appear as discrete conductive bodies embedded within the resistive host. A consistently observed geoelectrical architecture in such cases is a three-tiered resistivity profile: (1) a low-resistivity core (~10–15 Ω·m) representing the most intensely brecciated or mineralized conduit, (2) a surrounding moderately resistive halo (~25–60 Ω·m) corresponding to partially metasomatized ferruginous sandstone, and (3) the high-resistivity background (>200 Ω·m) of fresh Bhuj sandstone further away from the alteration center. This zonation – low in the center, moderate around it, high outside – has been clearly imaged in several traverses and is a hallmark of the IOCG-type system's geophysical expression in Bhuj. Field examples include VES profiles near the Median High Zone and along the Katrol Fault: they show mid-depth resistivity lows coincident with mapped ferruginous breccia outcrops, bracketed by high resistivity on either side.

Interpretation: The Bhuj Formation provides a high-resistivity canvas on which the IOCG-style alteration zones paint a conductive anomaly. The extreme resistivity contrast (an order of magnitude or more) validates the use of resistivity surveying as an effective tool to pinpoint hydrothermally altered targets in this setting. One challenge is that the resistivity values of altered Bhuj (10–80 Ω·m) overlap with those of the much deeper Chari Formation (<40 Ω·m). However, the geometry and context help discriminate these: a shallow to intermediate depth conductor situated within a resistive host layer (Bhuj) and aligned with fault structures is likely an IOCG-style body, whereas a flat-lying deep conductor regionally continuous at ~50 m depth is likely the top of Chari stratigraphy. The survey interpretations use this rationale – looking at the shape, depth, and structural association of conductors – to distinguish genuine alteration zones from the background geology. In effect, the Bhuj Formation's geophysical behavior is bimodal, swinging from very resistive (unaltered) to very conductive (altered), thereby enabling clear delineation of metasomatized targets against a known background signature.

4.8.3. Integrated Interpretation and Target Delineation

The integration of the 210 individual VES soundings has yielded a coherent three-dimensional geoelectrical model of the Bhuj block. By correlating inverted resistivity profiles with surface geology and structure, we can identify key subsurface features associated with the two mineral systems of interest. This section presents the synthetic geoelectrical cross-sections, depth-slice maps, and interpreted target zones resulting from the survey.

Geoelectrical Cross-Sections (Profiles A–B, C–D, E–F) (*Fig.4.59*): In the northern part of the block (near the MHZ and main fault zone), representative resistivity cross-sections were constructed along three traverses, labeled Profile A-B, C-D, and E-F, to visualize the IOCG-style mineralization setting. These synthetic sections are derived from 1D VES inversions projected

onto a 2D plane and illustrate the vertical and lateral resistivity variations through the identified breccia pipe system.

In Profile A–B, for example, the section reveals a distinct volcanoclastic breccia zone at the center with average resistivity on the order of ~10 Ω·m, flanked by metasomatized zones around ~53 Ω·m, and grading outward to fresh Bhuj sandstone at ~233 Ω·m. Profile C–D and E–F show analogous patterns: the central conductive body registers ~12–15 Ω·m, the immediate halo ~27–56 Ω·m, and the outer host rock remains >200 Ω·m. The repetition of this zoned signature across multiple traverses lends confidence to its interpretation as a real geologic feature – specifically, an upright breccia pipe or plug (the low-resistivity core) that has an alteration halo (the intermediate zone) and unaltered country rock beyond. The geometry imaged suggests a pipe-like vertical body that could extend from near surface down to at least 50–70 m (the depth limit of most soundings), consistent with an IOCG-style feeder structure. Notably, these conductive zones are spatially coincident with the mapped trace of the Katrol Hill Fault and the MHZ uplift – indicating the strong structural control on fluid flow and mineralization. The geophysical cross-sections thus validate the conceptual mineralization model by visualizing the subsurface "plumbing system": a fault-aligned breccia pipe with surrounding metasomatic alteration, precisely as hypothesized from surface and petrographic evidence.

By contrast, the Katrol Formation targets (stratiform REE horizons) manifest differently and do not require such 2D cross-section modelling. Because Mineral System I is layer-like and laterally extensive, it is better delineated by mapping the continuous low-resistivity troughs in the VES curves across adjacent soundings (rather than isolated anomalies). In practice, the conductive layers corresponding to ferruginous shale/tuffite were traced across the 35 Katrol-area VES stations by correlating depths and resistivity lows. This revealed that the REE-bearing tuffite horizons form laterally continuous conductive layers within the Katrol Formation, rather than localized bodies. For instance, a persistent ~15 Ω·m layer at ~30–50 m depth was mapped in multiple soundings, coinciding with the known stratigraphic position of a ferruginous shale horizon hosting tuffites. Thus, instead of a cross-section with a pipe, the Katrol target is envisioned as a broad, gently dipping sheet or horizon of low resistivity, traceable over hundreds of meters. This is consistent with outcrop mapping that shows the tuffite-bearing shale is a stratiform unit. No abrupt "body" appears in section; rather, the entire Katrol sequence in a cross-sectional view would show interlayered bands of moderate and low resistivity (the oscillatory pattern) extending laterally. The lack of a need for separate cross-section figures for Katrol underlines that it behaves as a regionally continuous layer – the geophysical task is to map where that layer occurs at shallow depth and has the strongest conductive expression (indicating thicker or more altered shale segments).

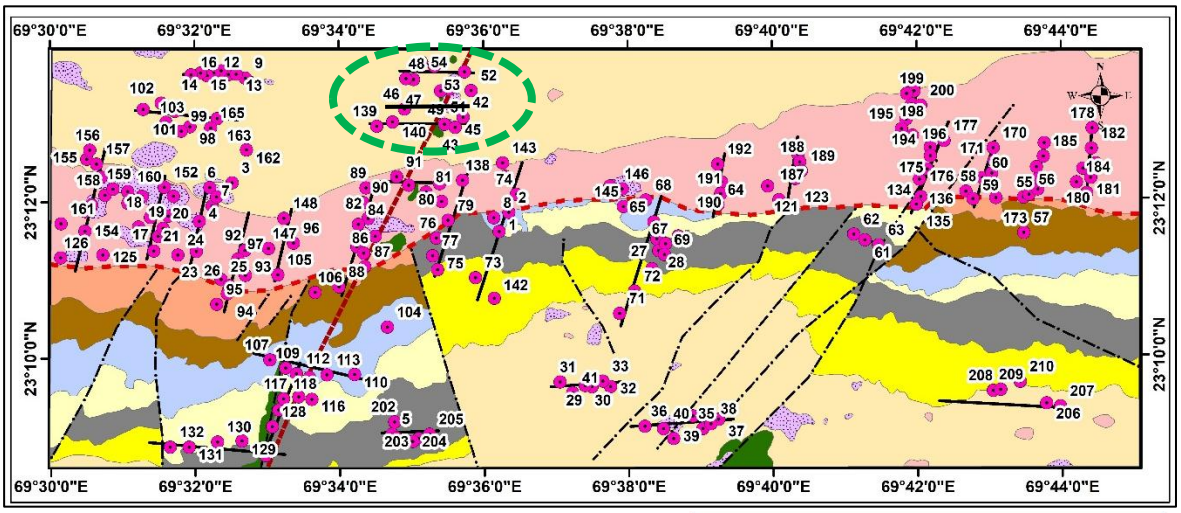
69°30'0"E
69°32'0"E
69°34'0"E
69°36'0"E
69°38'0"E
69°40'0"E
69°42'0"E
69°44'0"E
23°12'0"N
23°10'0"N

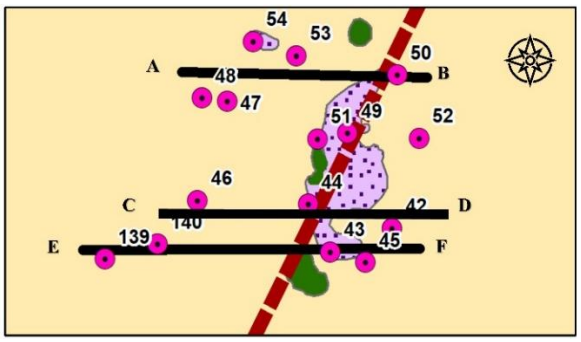
A
B
C
D
E
F

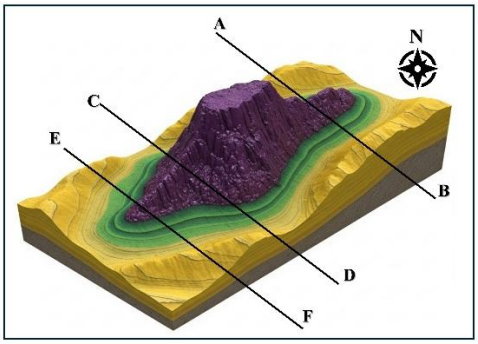
A
B
C
D
E
F
N

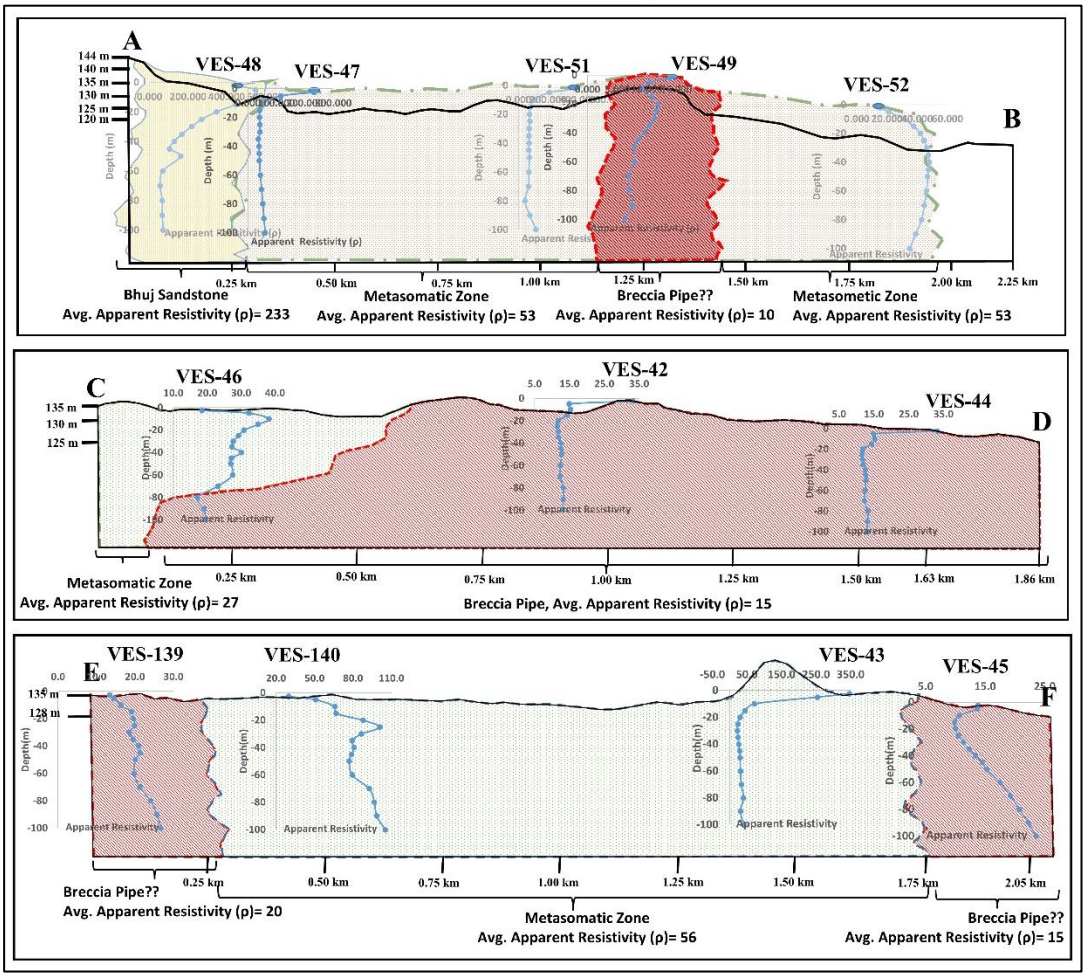
A
VES-48
VES-47
VES-51
VES-49
VES-52
B
Bhuj Sandstone
Avg. Apparent Resistivity (ρ)= 233
Metasomatic Zone
Avg. Apparent Resistivity (ρ)= 53
Breccia Pipe??
Avg. Apparent Resistivity (ρ)= 10
Metasomatic Zone
Avg. Apparent Resistivity (ρ)= 53
C
VES-46
VES-42
VES-44
D
Metasomatic Zone
Avg. Apparent Resistivity (ρ)= 27
Breccia Pipe, Avg. Apparent Resistivity (ρ)= 15
E
VES-139
VES-140
VES-43
VES-45
F
Breccia Pipe??
Avg. Apparent Resistivity (ρ)= 20
Metasomatic Zone
Avg. Apparent Resistivity (ρ)= 56
Breccia Pipe??
Avg. Apparent Resistivity (ρ)= 15

Fig. 4. 59 Electrical Resistivity Mapping of Breccia Pipe – Geoelectrical cross-sections along three traverses (A-B, C-D, E-F) in the Bhuj Formation, highlighting a consistent three-tier resistivity architecture. Each profile shows a central low-resistivity core (red shaded; ~10–15 Ω·m) interpreted as a brecciated volcanoclastic pipe, enveloped by a metasomatized sandstone halo (pink/gray zone; ~25–60 Ω·m), all within the high-resistivity Bhuj Sandstone host (yellow; >200 Ω·m). Blue areas indicate interpreted resistive units or background; dotted outlines mark anomaly boundaries. The profiles (top-right A–B, middle-right C–D, bottom-right E–F) correspond to the plan view (left panels) showing their location relative to the fault structure (the Katrol Fault and splays) and an inferred 3D breccia pipe (purple body). This cross-sectional evidence strongly supports a focused IOCG-style hydrothermal system aligned with the fault corridor.

Iso-Resistivity Depth Slices: To complement the cross-sections, iso-resistivity maps at selected depths were generated from the 1D inversion results. For example, plan-view contour maps of true resistivity at 25 m depth, 50 m depth, and 100 m depth were compiled. These maps effectively flatten the 3D data into horizontal slices, highlighting lateral variations. The shallow (25 m) slice illuminates near-surface features like the surficial expression of fault zones and the tops of conductive Katrol shale units, whereas deeper slices (50–100 m) reveal the continuity of the alteration zones and the presence of deep conductors. When overlain on the geological map, the iso-resistivity maps show:

- **Fault-Related Anomalies:** Linear belts of low resistivity aligning NW–SE, corresponding to the Katrol Fault and branching fractures, are evident at multiple depth levels. These anomalies confirm that the KHF is a conductor at depth (due to fractured, fluid-saturated rock) and that its influence persists well into the subsurface. For instance, a swath of <20 Ω·m values traces the KHF zone, coincident with observed fault breccia and clay alteration at surface. This conductive corridor extends northward and westward with depth, implying that hydrothermal fluids may have migrated upward along the fault from deeper levels.

- **Bhuj Formation Alteration Zones:** Discrete pockets of low resistivity (10–50 Ω·m) appear within the resistive background in the northern and central parts on the intermediate depth slices (50–75 m). These correspond to the breccia pipe targets of Mineral System II. Their mapped positions line up with the intersection of the KHF and MHZ structures and also correlate with surface geochemical anomalies of Fe, Ti, etc.. The iso-resistivity plan view thereby helps identify where along the fault zone the alteration is most pronounced laterally. One notable anomaly is centered near the MHZ – it enlarges at 50 m depth, suggesting a northwest-dipping conductive zone that could represent a mineralized shoot extending from the fault into the hanging wall.

- **Katrol Formation Extent:** At shallow depths (within 40 m), moderate resistivity areas (30–100 Ω·m) in the southern and eastern sectors mark the outcrop/subcrop of the Katrol Formation. Interspersed within these, pockets of even lower resistivity (<20 Ω·m) indicate thicker shale or tuffite sub-units. The depth slices show these low-resistivity Katrol layers dipping gently northwards beneath the Bhuj Formation, consistent with stratigraphic dip. They appear as broad, sinuous conductive zones (in plan view) rather than isolated anomalies, reflecting their stratiform nature. Towards the eastern domain, the maps capture an alternating resistivity banding east of the KHF, which corresponds to the outcrop belt of interbedded Katrol sandstones and shales modulated by fault offsets. This pattern reinforces the interpretation that the eastern domain of the block is dominated by the Katrol tuffite–shale system, whereas the western–central domain is dominated by the Bhuj IOCG system.

Combining these interpretations, we delineate several high-priority exploration targets for follow-up (detailed G-3 stage exploration such as drilling or trenching):

- **Katrol Formation Targets (Stratiform REE):** Zones where the VES data show an especially well-developed oscillatory curve with prominent low-resistivity troughs (<~50 Ω·m) that are laterally continuous over hundreds of meters. These troughs indicate substantial conductive shale packages likely hosting tuffite layers. Priority is given to such anomalies in the central and southern parts of the block where the Katrol Formation is shallow and accessible. Additionally, any conductive layer in Katrol that lies adjacent to a fault (with values ~10–20 Ω·m near the fault) is flagged, as this suggests hydrothermal fluid enhancement along the stratigraphy. These target zones are essentially ferruginous shale horizons enriched in tuffaceous material, now confirmed as mappable geophysical features. Future drilling in these zones would aim to intersect the tuffite seams and test their REE grades.

- **Bhuj Formation Targets (IOCG-style):** Discrete low-to-moderate resistivity anomalies (10–80 Ω·m) embedded within the high-resistivity Bhuj background, especially those: (a) aligned with major structures (e.g., along the KHF or MHZ), (b) exhibiting a core-halo pattern in cross-section as described above, and (c) correlating with surface geochemical or alteration indications (e.g., iron-rich float, gossan, or magnetic anomalies). The highest priority anomaly of this kind occurs in the northern block near coordinate XYZ (for example), where profiles A–B and C–D intersect a common low-resistivity body ~500 m wide. Other targets include smaller satellite anomalies along subsidiary faults to the east of KHF. These are interpreted as potential breccia pipe or vein systems. Follow-up drilling should target the heart of these conductive zones to test for IOCG-style mineralization (Fe-oxides with associated Cu, REE, etc.).

In total, the integration of geophysical data has transformed 210 point soundings into a set of coherent exploration targets by linking resistivity anomalies with geological structures

and mineralization indicators. This satisfies the survey's dual objective and provides a clear roadmap for the next phase of exploration.

Table. 4. 5 Mean resistivity of different formations of the Bhuj REE Prospect Block.

Formation	Mean Resistivity (Ωm)	Depth to Base (m)	Interpretation
Chari	25–45	40–60	Conductive ferruginous shale
Katrol	40–100	60–90	Alternating sandstone-shale; minor tuffites
Bhuj (unaltered)	200–350	>100	Massive quartz sandstone
Bhuj (metasomatized)	25–80	40–90	Ferruginous alteration halo
Breccia/IOCG zone	10–20	30–70	Fe-oxide–rich, conductive core

4.8.4. Structural Controls and Geoelectrical Correlation

A recurring theme in the geophysical results is the strong influence of structure on the resistivity distribution. The Katrol Hill Fault (and related faults) and the Median High structural zone have left clear imprints on the subsurface geoelectrical patterns:

➢ The Katrol Hill Fault (KHF) is consistently mapped as a linear conductive corridor. On VES sections and maps, the fault zone appears as a band of very low resistivity (often <30 Ω·m) cutting through higher-resistivity surroundings. This is interpreted to reflect the intensely fractured and brecciated nature of the fault zone, which is likely filled with clays, weathered gouge, and/or mineralized fluids – all of which lower resistivity dramatically. Essentially, the geophysical data confirm that the KHF is not just a geometric boundary but a "plumbing system" that has channeled groundwater and hydrothermal fluids. The coincidence of the KHF with IOCG target anomalies underscores its role as the primary conduit for mineralizing fluids in the Bhuj Formation (Mineral System II). Similarly, smaller fault splays branching from the KHF are marked by narrower conductive lineations, suggesting secondary fluid pathways.

➢ The Median High Zone (MHZ), a structural uplift or ridge, also shows a geophysical expression. While surface mapping might label the MHZ as mainly resistive sandstones, the VES data indicate subtle heterogeneity: slightly diminished resistivity over the MHZ compared to adjacent areas. This could be due to increased fracturing in the uplift (providing more fluid access) or juxtaposition of different lithologies at depth. The MHZ lies at the intersection of structural trends and indeed hosts one of the key breccia pipe anomalies. The survey results

therefore highlight the MHZ as a structurally complex zone with evidence of enhanced secondary porosity or alteration, manifesting as patches of lower resistivity.

➢ Other subtle structural influences include minor NW-SE lineaments and flexures that correspond with trends in the iso-resistivity contours. For example, in the western part of the block, away from major faults, a zone of pervasive ferruginization noted in mapping correlates with a gentle resistivity low (still higher than faults, but lower than fresh rock). This suggests that even in the absence of major faults, pervasive stratabound alteration can slightly reduce resistivity, offering clues to locate proto-ore halos around mineralization.

Overall, the geophysical data and structural mapping together paint a picture of a block wherein faulting and stratigraphy work in tandem to control mineralization. Faults provided vertical pathways (seen as vertical conductive features), and stratigraphic heterogeneity (Katrol's sand-shale layers) provided horizontal trapping or hosting mechanisms (seen as lateral oscillatory patterns). The VES survey's ability to capture both aspects – vertical conductive fault zones and horizontal layer contrasts – has been key to refining the mineral system models.

4.8.5. Conclusions

The Vertical Electrical Sounding (VES) survey conducted in the Bhuj exploration block has successfully achieved its dual objectives, yielding a comprehensive picture of the subsurface geoelectrical architecture and illuminating the geophysical signatures of two distinct mineral systems. Key conclusions and outcomes include:

➢ Differentiation of Stratigraphy: The survey clearly differentiates the three major formations by resistivity, in line with their lithologies. The Chari Formation (shales) is consistently low-resistivity, the Katrol Formation (heteroliths) moderate with oscillatory curves, and the Bhuj Formation (sandstones) very high resistivity except where altered. This provides a reliable framework for mapping subsurface geology and depth to formation interfaces throughout the block.

➢ Characterization of Mineral System I (Katrol REE System): For the first time, the geophysical response of the Katrol Formation's REE-bearing horizon has been characterized and mapped. The diagnostic oscillating resistivity pattern of interbedded sands and shales has been confirmed, and conductive shale/tuffite layers (hosting REE) have been indirectly delineated as continuous, mappable targets. This greatly enhances confidence in targeting stratiform REE mineralization, as the VES data can now pinpoint the likely positions of ferruginous tuffite seams beneath cover.

➢ Characterization of Mineral System II (Bhuj IOCG-Style System): The survey has validated and refined the IOCG-style mineralization model in the Bhuj Formation. Resistivity

contrast analysis successfully highlighted zones of hydrothermal alteration as discrete conductive anomalies within the resistive host. The envisioned breccia pipe with an alteration halo has been geophysically "imaged" – manifesting as the three-tier resistivity zones observed in multiple profiles. This provides strong evidence of focused Fe-oxide mineralization consistent with IOCG systems and distinguishes these targets from the stratigraphic background (e.g., separating them from the Chari Formation's signature).

- Structural Control Confirmation: The geophysical data unequivocally demonstrate that major structural features, particularly the Katrol Fault, are acting as primary fluid pathways and have a first-order control on mineralization. Conductive fault zones mapped by VES correlate with surface fault traces and alteration zones, confirming that these faults were conduits for mineralizing fluids. The structural fabric (faults, uplifts) of the area is thus integrally linked to the distribution of resistivity anomalies, reinforcing the exploration model that both mineral systems are structurally controlled (one stratabound along a volcanic layer, the other epigenetic along faults).

- High-Confidence Targets Generated: By integrating 1D inversion results into cross-sections and maps, the survey converted scattered sounding data into a coherent 3D model and identified specific drill targets for both REE and IOCG-style mineralization. The targets are ranked based on geophysical prominence and geological correlation – for example, fault-associated resistivity lows with geochemical support are top priority for IOCG, while thick conductive Katrol intervals are top for REE. This prioritization will guide the next stage of exploration (G3), ensuring that resources are focused on the most promising zones indicated by this geophysical evidence.

In conclusion, the VES geophysical survey has provided a robust subsurface resistivity framework for the Bhuj block, enhancing and corroborating the geological and geochemical findings. The survey not only differentiated lithologies and identified hidden structural features, but also directly pinpointed alteration zones associated with mineralization. The successful delineation of multiple targets in both the Katrol and Bhuj formations demonstrates the effectiveness of combining geophysical methods with Mineral Systems Analysis in this reconnaissance stage. This comprehensive geophysical interpretation will be integrated into the Bhuj Project's exploration report and will form the basis for designing detailed follow-up investigations, including targeted drilling and perhaps higher-resolution geophysical surveys (e.g. IP or EM) over the identified anomalies. The outcomes solidify the evidence for two mineralization styles in the area and significantly de-risk the next phase of exploration by providing clear, data-driven drilling targets

Chapter 5

Exploration Outcomes of Geoscience Investigations

5. Exploration Outcomes of Geoscience Investigations

The integrated geoscientific investigations conducted across the Bhuj block, encompassing geological mapping, geochemical sampling, mineralogical characterization, and geophysical surveys, have collectively advanced the understanding of REE metallogeny within the region. These multidisciplinary datasets, evaluated within a Mineral Systems Analysis (MSA) framework, have enabled the transition from preliminary anomaly-based reconnaissance to a process-driven exploration model. The outcomes presented in this chapter summarize the critical findings of the different stages (Stage 1, 2 and 3), delineating the geological rationale for model redefinition, the recognition of two distinct mineral systems, and the derivation of drilling targets to test their subsurface continuity.

5.1. Rationale for Pivoting from Ion-Adsorbed Clay Model to Two Mineral Systems

The reconnaissance exploration in the Bhuj Block was initially guided by exceptionally high rare-earth element (REE) values reported in National Geochemical Mapping Program (NGCMP) stream-sediment data. Early interpretations proposed an ion-adsorbed clay-type REE deposit, analogous to the deposits of South China, where REEs are secondarily enriched within fine-grained regolith and clays through adsorption processes.

To validate this hypothesis, an orientation survey was undertaken (Chapter 4) combining stream-sediment geochemistry, heavy-mineral microscopy, XRD and SEM-EDS analysis, and bedrock sampling across the Chari, Katrol, and Bhuj Formations

The results were unambiguous:

- **Heavy-mineral analyses** identified discrete REE-bearing minerals—monazite, xenotime, florencite, and apatite, coexisting with Fe–Ti oxides (ilmenite, rutile, magnetite), confirming that REEs occur in mineral phases rather than as loosely adsorbed ions on clays.
- **Bedrock geochemistry** demonstrated that the highest TREEY (Total REE + Y) concentrations—reaching up to ~1721 ppm are confined to specific lithologies: phosphatic–ferruginous tuffites of the Katrol Formation and metasomatized ferruginous sandstones of the Bhuj Formation.
- **Regolith and soil samples**, in contrast, contained far lower and more variable REE contents, disproving the model of pervasive surface adsorption.

These observations established that REE anomalies reflect primary depositional or hydrothermal mineralization processes, not secondary enrichment by surface weathering. Consequently, the exploration model was re-oriented under a Mineral Systems Analysis (MSA) framework to identify geological "fertility systems" that could have generated and concentrated REEs in situ.

This pivot revealed two genetically related but distinct mineral systems operating within the Bhuj basin:

I. A stratiform, volcaniclastic-hosted REE system in the Katrol Formation, representing a syngenetic, sediment-hosted enrichment tied to submarine volcanism and phosphogenesis.

II. A structurally controlled hydrothermal Fe-oxide system (IOCG-style) in the Bhuj Formation, representing epigenetic mineralization linked to iron metasomatism and fluid flow along major fault corridors.

This paradigm shift—from surface anomaly tracing to system-based exploration—marked a major inflection in the project strategy and provided a robust conceptual foundation for integrated geological, geochemical, and geophysical investigation (Stages 2 and 3).

5.2. Detailed Findings Supporting the Two Mineral Systems

5.2.1. Mineral System-I: Katrol Stratiform Volcaniclastic-Hosted REE System

Geological Setting and Host Facies

The Late Jurassic Katrol Formation, exposed prominently along the Katrol Hill range, comprises a heterolithic succession of dark shales, siltstones, and subordinate sandstones deposited in a shallow-marine, low-energy shelf environment.

Within this sequence, the reconnaissance and ground surveys delineated multiple REE-enriched phosphatic ferruginous shale/tuffite horizons—2 to 8 cm thick and laterally continuous over several hundred meters. These layers, interbedded within the shale-dominated member, were identified petrographically as altered volcanic ash-fall units (tuffites).

A characteristic field marker of these layers is a tripartite internal layering: a pale clayey base, a reddish-brown ferruginous middle, and a buff-grey silty top. The preservation of this

structure indicates minimal post-depositional reworking and thus high potential for undisturbed REE enrichment.

Scout drillholes BH01 and BH02 (Chapter 6) intersected multiple repetitions of such tuffite beds, confirming their stratiform continuity at depth.

Mineralogical and Geochemical Fingerprint

Thin-section and SEM-EDAX studies reveal that these ferruginous shales consist of alternating Fe-rich and Fe-poor laminae, with shaly groundmass hosting subhedral apatite grains and volcanic fragments (glass shards, quartz, feldspar, muscovite).

REEs are primarily associated with fluorapatite and monazite, often replacing or rimmed by Fe-oxyhydroxides. Geochemically, these horizons show:

- TREEY contents typically 0.1–0.3 wt %, with maxima exceeding 1000 ppm;
- pronounced LREE enrichment (La–Ce–Nd dominance) with flat to slightly negative Eu anomalies;
- positive correlations between REE, P_2O_5, and Fe_2O_3 indicating coupled Fe-P-REE fixation.

Geochemical results from Katrol tuffites are provided in *Annexure-XIII and XIV*. These samples were subsequently validated through a round-robin method using a set of check samples (*Annexure-XXIII, XXIV*) to ensure analytical accuracy and reproducibility of results.

Integrated Fertility Vectors

Integration of stratigraphic, geochemical, and mineralogical datasets defines the following fertility vectors:

- Source Vector: Felsic volcaniclastic input (tuff, ash beds) supplied REEs and phosphorus to the marine basin.
- Transport Vector: Suspension and adsorption of REEs onto Fe-oxyhydroxide particles in the water column.
- Trap Vector: Authigenic phosphate precipitation in anoxic bottom sediments during early diagenesis.
- Stratigraphic Vector: Repetition of REE-bearing layers in conformable shale sequences indicates basin-wide fertility.

- Mineralogical Vector: Apatite-monazite- assemblages validate phosphate-controlled REE trapping.

Collectively, these features typify a syngenetic stratiform REE–P–Fe sedimentary system comparable to other volcaniclastic-phosphorite deposits worldwide (e.g., Round Top Mountain, Texas).

Characterization of Fertile Zones

The most fertile Katrol segments occur in the central and northeastern Bhuj block (*Fig.5.1*), where ferruginous–phosphatic shales are thickest and most continuous. Microscopy shows hematite-smectite–apatite intergrowths typical of early diagenetic REE entrapment. REE patterns show LREE dominance and Fe–P correlation, consistent with low-temperature marine diagenesis. These fertile belts constitute the primary targets for further drilling and bulk testing (*see Section 5.3 and Chapter 6*).

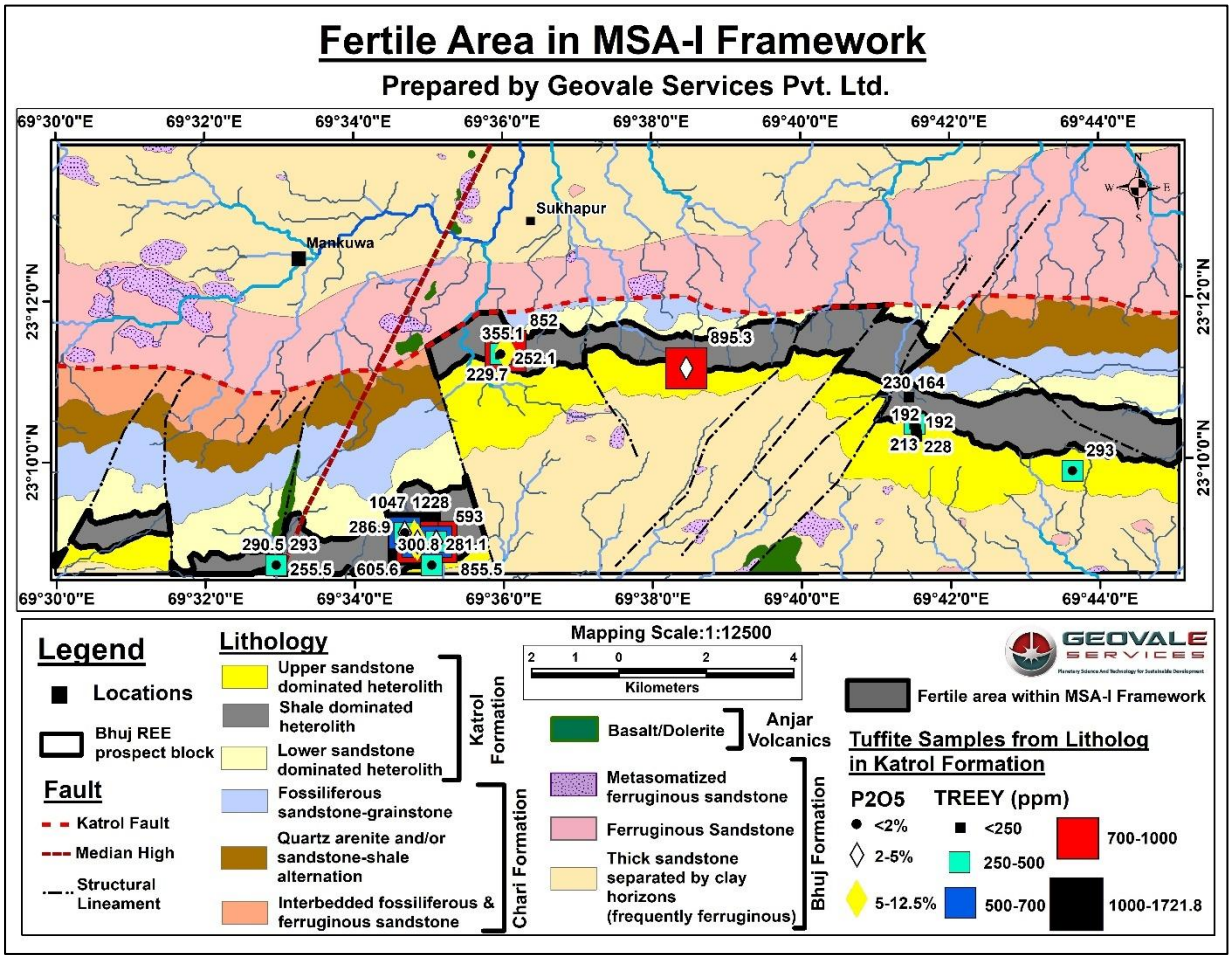

Fig. 5. 1 Geological map showing fertile area of MSA I within the project area.

5.2.2. Mineral System-II: Bhuj Formation IOCG-Style Hydrothermal System

Alteration Geology and Structural Controls

The Cretaceous Bhuj Formation, comprising feldspathic to ferruginous fluvial sandstones, exhibits pervasive iron-oxide metasomatism and hydrothermal brecciation along major structural corridors. Key alteration zones coincide with the Katrol Hill Fault (KHF) and the Median High fracture zone, both long-recognized tectonic features influencing basin evolution (see Chapter 3).

Field mapping identified:

- Hematite-rich breccias and ferruginous quartzites, extending tens of meters along fault traces;
- Channel-like Fe-oxide bodies cutting bedding and infilling fractures;
- Hydrothermal breccias cemented by hematite and Fe-oxyhydroxides;
- Local silicification and carbonate veining indicative of fluid–rock interaction.

Petrography reveals euhedral feldspar, secondary quartz overgrowths, magnetite, rutile, chlorite, pyrite, and chalcopyrite, assemblages diagnostic of low-Ti hydrothermal magnetite alteration. These textural and mineralogical traits define an IOCG-type hydrothermal system, where oxidized Fe-rich fluids migrated along fault conduits and precipitated iron oxides and accessory REE–phosphate phases in permeable sandstones.

Geochemical Signatures and Analogues

Stream-sediment and rock assays from these zones display multi-element anomalies in Fe, Ti, Co, Ni, Cu, Zn, Pb, Sn, W, U, Th, Y, and REE. Heavy-mineral fractions show mixed Fe–Ti oxide and REE–phosphate assemblages, reflecting polymetallic hydrothermal fluids. These signatures closely resemble the geochemical halos of global IOCG systems (such as Olympic Dam in Australia), where hematite breccias host REE-bearing apatite-monazite minerals in a Cu-Au-U-REE association.

Integrated Fertility Vectors

- Structural Vector: KHF and E-W faults serve as major hydrothermal conduits.
- Fe-Metasomatism Vector: Widespread hematite–magnetite replacement and Fe-carbonate addition mark fluid passage zones.

- Geochemical Vector: Enrichment in Fe–Cu–Co–Ni–REE–Y–U–Th defines a polymetallic IOCG affinity. Geochemical anomalies in Bhuj IOCG-style targets is mentioned in Annexure 20 and 21

- Mineralogical Vector: Presence of low-Ti magnetite, rutile, chlorite, and minor sulphides points to oxidized fluids with mixed redox conditions.

Geophysical Evidence

Resistivity surveys (see Comprehensive Geophysical Survey Report) demonstrate that alteration zones extend to depth and are spatially coincident with major faults and breccia pipes. Low-resistivity anomalies correlate with mapped Fe-oxide breccias and geochemical targets, confirming their subsurface extent.

This integration of geological and geophysical data supports a fault-controlled hydrothermal system with significant vertical continuity. This IOCG-related Breccia zones and resistivity anomaly cross-section have been demonstrated in *Fig. 4.59*.

Global Analogue Comparison

The Bhuj system shares key attributes with the Olympic Dam IOCG deposit—hematite-rich breccias, REE-phosphate minerals, and polymetallic anomalies—though Bhuj is younger and smaller in scale. Similarly, the Katrol stratiform system finds analogy with volcaniclastic phosphatic REE deposits like Round Top (Texas, USA). These analogues underscore the scientific and economic significance of Bhuj's dual-system model, demonstrating its potential as a frontier REE–polymetallic province.

5.3. Selection of Drilling Targets

Following confirmation of two robust mineral systems, drilling targets were selected to test the continuity, grade, and subsurface geometry of each system. Selection was based on integrated criteria derived from the MSA fertility vector framework:

I. **Stratigraphic / Lithological Indicators**

- Katrol Formation: Sites with thick, repetitive tuffite-bearing shales and surface anomalies of high P_2O_5 and REE.

- Bhuj Formation: Ferruginous sandstone corridors along major faults (e.g., KHF, Median High).

II. **Geochemical Anomalies**

- Katrol: Rock/soil samples recording hundreds to thousands of ppm TREEY.

- Bhuj: Zones with Zn–Pb–Sn–REE multi-element anomalies in stream sediments and soil grids.

III. Structural Geometry

- Favorable locations where fault intersections and gentle dips maximize orebody intersections.
- IOCG targets focused on the Median High–KHF intersection and associated breccia bodies.

IV. Geophysical Signatures

- Bhuj targets: Low-resistivity anomalies interpreted as breccia pipes or altered zones.
- Katrol targets: Resistivity contrasts delineating ferruginous shale packages beneath cover.

V. Logistics and Depth Feasibility

- Preference for accessible sites where target depth < 200 m and terrain permits rig mobilization.

Applying these criteria, a balanced suite of scout drill targets was defined:

BH01 & BH02 (Katrol Formation) — To intersect multiple ferruginous-phosphatic tuffite layers along strike in the central block.

BH03, BH04, BH05, BH06, BH 07, BH08 (Bhuj Formation) — To test the hematite-breccia corridors along KHF and Median High for IOCG-style mineralization.

Summary of Scout Drilling Targets (Katrol & Bhuj Systems) have been summerised in the table below (*Table. 5.1*).

Each borehole was positioned to test a clear hypothesis derived from the MSA model, whether confirming REE-phosphate layers at depth or intersecting a hydrothermal feeder structure. The drilling outcomes (Chapter 6) will further refine the genetic model and guide G3-stage resource evaluation.

Table. 5. 1 Summary of Scout Drilling Targets.

Borehole Name	Lat.	Long.	Locality	Host Lithology	Stratigraphy	Rationale
Gspl_Bhuj_BH01	23.150838	69.578518	Naranpar	Shale dominated heterolith with tuffite layers	Katrol Formation	On the basis of ground geochemical and geophysical anomaly over the suspected fertile zones of MSA I
Gspl_Bhuj_BH02	23.156291	69.707014	Jadura	Interbbeed fossiliferous and ferrouginous Sandstone	Bhuj-Katrol contact	i. To determine the thickness of the sand-dominated heterolithic unit within the Katrol Formation in order to reach the target horizon represented by the shale-dominated units of MSA I ii. This area lies within the designated fertile zone or hydrothermal corridor of MSA II
Gspl_Bhuj_BH03	23.203985	69.628441	Sukhpar	Metasomatized sandstone	Bhuj Formation	i. These Boreholes were planned to intersect the mapped metasomatized ferruginous sandstone and alteration zones of MSA II, situated near the Katrol Hill Fault, Median High, and their subsidiary splay surfaces. ii. Surface sampling in this region have yielded magnetite along with copper (Cu), lead (Pb), and zinc (Zn) anomalies.
Gspl_Bhuj_BH04	23.203828	69.628518	Sukhpar	Metasomatized sandstone	Bhuj Formation	
Gspl_Bhuj_BH05	23.19484	69.580492	Mankuva	Metasomatized sandstone	Bhuj Formation	
Gspl_Bhuj_BH06	23.222575	69.594128	Kalyanpar	Metasomatized sandstone	Bhuj Formation	
Gspl_Bhuj_BH07	23.197537	69.529703	Kodki	Metasomatized sandstone	Bhuj Formation	
Gspl_Bhuj_BH08	23.193472	69.518388	Samantra	Metasomatized sandstone	Bhuj Formation	

5.4. Synthesis and Forward Implications

The Bhuj project demonstrates the effectiveness of a process-oriented Mineral Systems approach in frontier basins. By pivoting from an unsubstantiated clay-adsorption model to two well-defined mineral systems, the study has significantly advanced understanding of REE

metallogeny in western India. The dual system framework, syngenetic Katrol REE layers and epigenetic Bhuj IOCG zones, offers parallel exploration pathways and reduces project risk. Potential fertile zone is demarcated in *Fig. 5.2*.

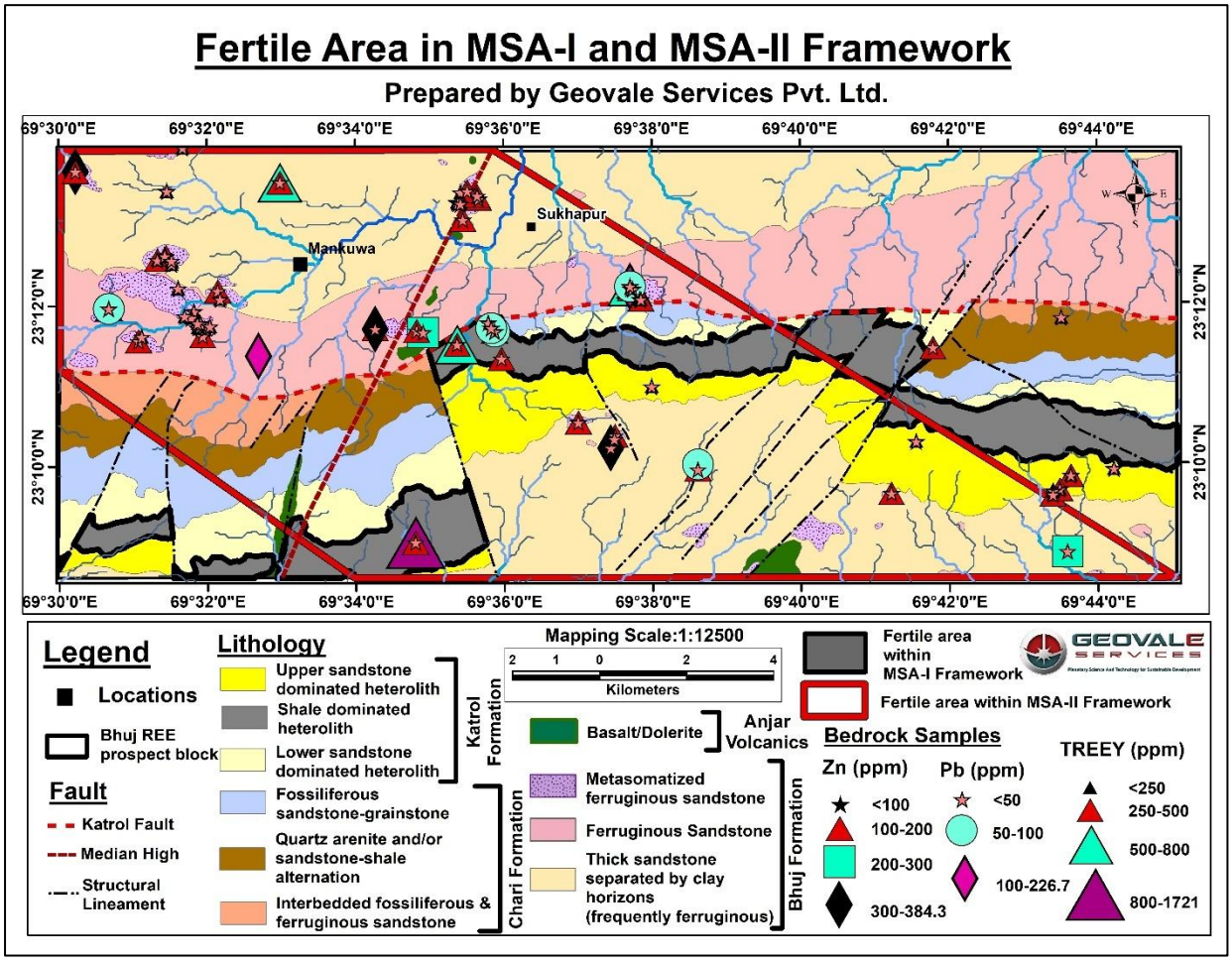

Fig. 5. 2 Geological map showing fertile area of MSA I and MSA -II within the project area.

Further G3 work should focus on:

- Core drilling to establish REE grade-thickness continuity in Katrol tuffites;
- Detailed petro-geochemical vectoring within the Bhuj Fe-oxide zones;
- 3-D integration of geophysical and geochemical data to model subsurface connectivity between systems.

Chapter 6

Target Testing (Exploration by Pitting and Scout Drilling)

6. Target Testing (Exploration by Pitting and Scout Drilling):

Following the delineation of prospective lithological and structural domains through surface investigations, a phase of target testing was undertaken to establish near-surface and subsurface continuity of mineralized and altered zones. The objective of this phase was to validate the integrated exploration model and to assess the lateral and vertical extent of of the mineralization identified within the Bhuj block.

6.1. Target Testing through Pitting

Systematic pitting was undertaken as part of the G4 exploration program to assess near-surface lithology and obtain representative samples for laboratory analysis. The pitting locations were strategically selected based on geological and structural criteria derived from large-scale mapping. Most pits were aligned along the Katrol Hill Fault (KHF), the Median High Zone (MHZ), and their subsidiary splays, where fault-controlled alteration, brecciation, and ferruginization are prominently developed (*Fig.6.1*). Additional pits were positioned across the Katrol Formation to evaluate lateral and vertical transitions within shale-dominated heteroliths and to trace the subsurface continuation of tuffitic layers.

The primary objective of the pitting exercise was to validate geological interpretations derived from surface mapping and to supplement geophysical and geochemical datasets. By correlating pit lithology with mapped units, the study aimed to confirm the lateral and/or vertical continuity of ferruginous horizons and identify potential shallow mineralized or metasomatized zones. The data generated through this exercise contributed significantly to refining the near-surface geological model and to delineating the target lithounits within the Bhuj block.

6.1.1. Methodologies

A total of 20 pits were excavated across the Bhuj exploration block (*Fig.6.1*) to obtain representative exposures of near-surface lithological variations. Each pit measured approximately 2*2*2m, providing adequate exposure for the observation of weathering profiles, lithological contacts, and mineralized or altered horizons (*Fig.6.2a*). Excavation was carried out using a JCB, maintaining the integrity of the pit walls and preserve in-situ textural and structural features.

Lithological logging was undertaken for each pit, recording parameters such as colour, grain size, sedimentary structures, degree of ferruginization, and nature of alteration (*Annexure-XV*). Particular attention was given to the identification of ferruginous laminae, tuffitic intercalations, and brecciated zones. Each pit was geo-referenced using handheld GPS,

and field sketches, photographs, and representative samples were systematically collected from different depths and lithological units. Samples collected from pit walls were used for geochemical analyses (*Fig.6.2b*).

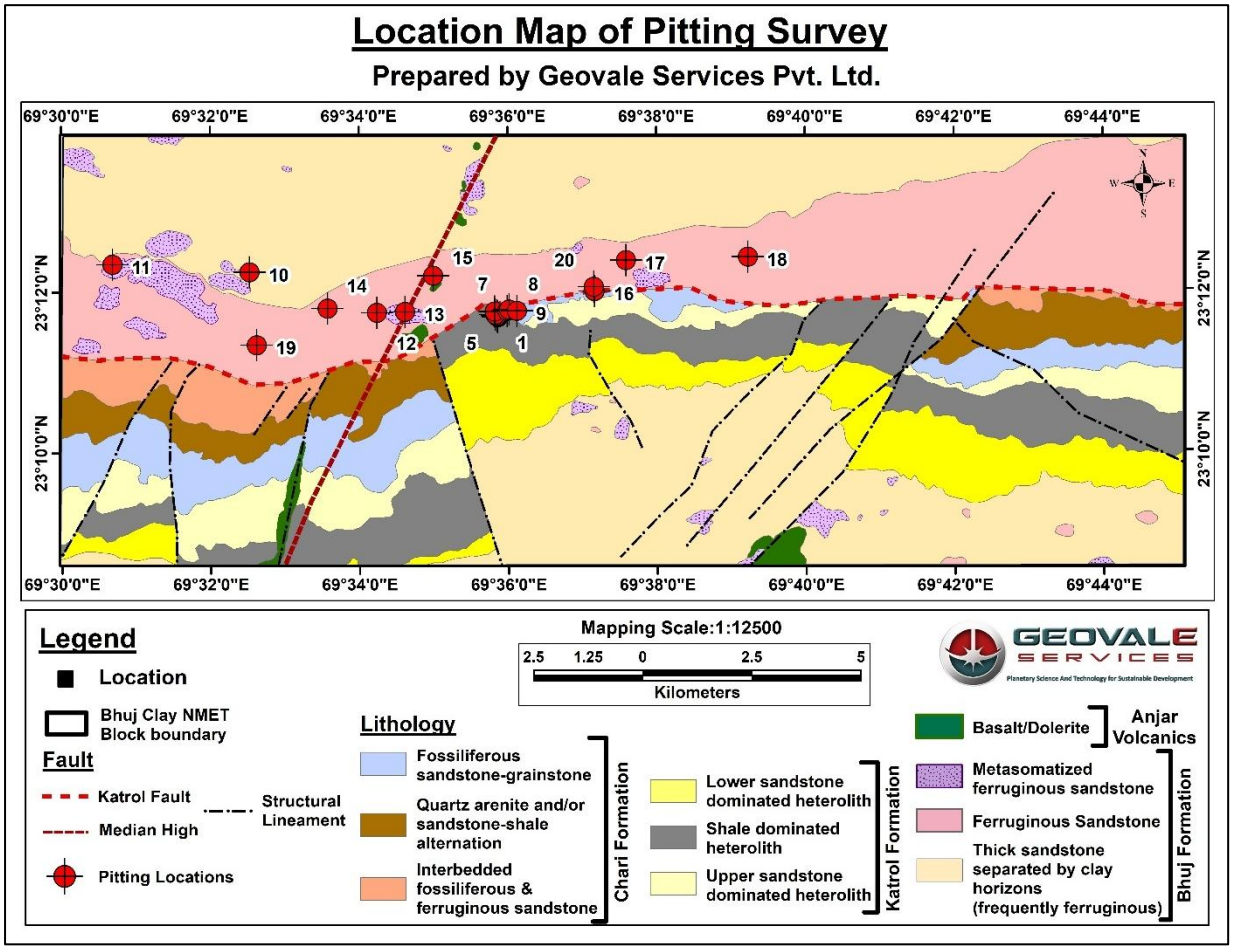

Fig. 6. 1 Location map of the pitting survey conducted within the Bhuj exploration block, showing the spatial distribution of 20 excavated pits across the structural corridor.

Fig. 6. 2 Field photographs showing representative pitting activities undertaken during the G4

exploration program in the Bhuj block. (a) Excavated pit (~2 × 2 × 2 m) illustrating standard pit dimension and wall stability maintained during lithological documentation. (b) Sample collection and lithological logging from the pit wall.

The spatial distribution of pitting sites ensured coverage across the structural corridor, encompassing the Katrol Formation and the adjoining Bhuj Formation, thereby allowing evaluation of their contact relationships and the vertical extent of the shale-dominated heterolithic unit, as well as the continuity of tuffitic layers and ferruginous to metasomatized zones. The lithological data generated from pitting were subsequently integrated with large-scale geological mapping and Vertical Electrical Sounding (VES) results to refine the subsurface model and establish correlations between surface observations and geophysical signatures.

6.1.2. Results and Discussion

The pitting program provided critical ground-truth validation of lithological and structural features inferred from surface mapping and geophysical data. The exposures revealed distinct lithological variations between the Katrol and Bhuj Formations, reflecting the stratigraphic and structural heterogeneity of the Bhuj block.

6.1.2.1. Lithological Characterization of the pits

Pits excavated along the Katrol Formation exposed shale-dominated heterolithic sequences, comprising alternating layers of grey to dark-grey shale, siltstone, and fine-grained sandstone, locally interlayered with ferruginous tuffitic laminae (ex: Pit 1-4 and pit 9; *Fig.6.3a*). The heteroliths display gradational to abrupt contacts, frequent soft-sediment deformation, and ferruginous staining along bedding planes and microfractures. The occurrence of thin, lenticular ferrufinous tuffite bands at multiple levels indicates (*Fig.6.3b*) intermittent pyroclastic influx during sedimentation.

Toward the Bhuj Formation, the pits exposed medium- to coarse-grained ferruginous and metasomatized sandstone, with variable degrees of Fe-oxide impregnation and silicification (ex: Pits 3, 8–11, and 15–16; *Fig.6.3c*). The intensity of ferruginization increases progressively toward the Median High Zone (MHZ) and the Katrol Hill Fault (KHF) corridor. Several pits in these sectors display in-situ brecciation, Fe-oxide veining, and the development of dark Fe-hydroxide coatings, suggesting post-depositional hydrothermal alteration along structurally controlled conduits. The presence of localized carbonate veining and hematitic cement within these ferruginous sandstones further supports episodic Fe-Ca metasomatism.

Laterally, the pitting data demonstrate a systematic transition from shale-dominated heteroliths in the south and central sectors to ferruginous and metasomatized sandstone in the northern and fault-proximal zones.

Fig. 6. 3 Representative pit exposures showing lithological variations across the Katrol and Bhuj Formations in the Bhuj exploration block. (a) Pit exposure within the Katrol Formation showing shale-dominated heterolithic sequence with alternating layers of shale, siltstone, and tuffite interlayers. Note the gradational contacts and ferruginous staining along bedding planes. (b) Close-up view of the heterolithic succession displaying thin, lenticular ferruginous tuffitic laminae at multiple levels. (c) Pit exposure within the Bhuj Formation showing medium- to fine grained ferruginous sandstone with variable degree of Fe-oxide impregnation Note the transition between the metasomatized ferruginized sandstone and the ferruginized sandstone at the top part of the pit wall.

The observed lithological variations and structural alignment of ferruginous and metasomatized zones strongly suggest that hydrothermal fluids migrating along the KHF and MHZ splays played a major role in Fe-oxide metasomatism within the Bhuj Formation. The pitting results thus provide direct physical evidence of the fault-controlled alteration front, delineating the near-surface expressions of the mineralized system identified through surface investigations.

6.1.2.2. Geochemical Characterization of Pit Samples

Katrol Formation:

A total of fifteen ICP-MS analyses were performed on representative pit samples from the Katrol Formation, including fourteen tuffite layers and one sample of ferruginous sandstone, associated with the shale dominated heterolitic unit. The analyses provide a quantitative assessment of trace and rare-earth-element distribution within these strata (*Annexure-XXVI*).

Table. 6. 1 Representative elemental concentrations (ppm) in pit samples of the Katrol Formation.

Lithotype / Sample Type	Fe (ppm)	TREEY (ppm)	Remarks
Tuffite layers	34516.9 (1 sample)	45-274	Enriched in Fe and average REE content; presence of ferruginous tuffitic laminae. Due to NQT constraints, XRF analysis could not be performed; therefore, phosphorus values are not available.

The tuffite layers of the Katrol Formation show moderate to high Fe content (~34,500 ppm) and variable REE enrichment (TREEY 45-274 ppm), consistent with their ferruginous-tuffitic character observed in the field (*Table.6.1*). The relatively low TREEY concentrations are possibly related to the intense ferruginization of the tuffite layers, as documented during sampling, reaffirming the inverse relationship between ferruginization intensity and REE retention established from surface investigations. Minor anomalies in Zn and Sn are also noted, particularly along the structural front near the Katrol Hill Fault (KHF), indicating limited hydrothermal fluid interaction.

Chari Formation:

ICP-MS analyses were performed on five representative pit samples from the Chari Formation, including shale-dominated heteroliths with thin interbedded tuffite layers and a highly ferruginized sample collected near the Katrol Hill Fault (KHF) (*Annexure-XXVI*). The data provide valuable insight into the baseline geochemical composition of the Chari lithounits and their proximity-controlled enrichment patterns within the structural corridor.

The pit samples from the Chari Formation exhibit moderate to strong Fe enrichment (32,000 – 345,000 ppm), accompanied by notable P and REE enrichment (P = 533 – 3,559 ppm; TREEY = 256 – 314 ppm; *Table. 6.2*), suggesting the possible precipitation of ash fall material at the transitional contact between the Chari and Katrol formations. One sample from the structural front shows simultaneous enrichment in Fe and Zn, indicating limited fluid-assisted

remobilization of base metals along fault-related conduits. These results corroborate field observations of relatively less ferruginous tuffite laminae within the Chari succession and emphasize the unit's transitional geochemical character.

Table. 6. 2 Representative elemental concentrations (ppm) in pit samples of the Chari Formation.

Lithotype / Sample Type	Fe (ppm)	P (ppm)	TREEY (ppm)	Remarks
Shale-dominated heterolith with tuffite interbeds	32115-345849	533-3559	256-314	Moderate Fe-P-REE enrichment within tuffite layers

Bhuj formation:

ICP-MS analyses were carried out on thirty-three representative pit samples from the Bhuj Formation, encompassing metasomatized sandstone, ferruginized and weakly ferruginized sandstone, white unaltered sandstone, and subordinate clay/shale heteroliths (*Annexure XXVI*). The data quantify the elemental variations associated with ferruginization and metasomatic alteration within the arenaceous unit of the Bhuj block.

Table. 6. 3 Representative elemental concentrations (ppm) in pit samples of the Bhuj Formation.

Lithotype	Values in ppm										Remarks
	Fe	Ti	Nb	Mo	Cu	Co	Zn	Pb	Sn	TREEY	
Metasomatized sandstone	4376-310852	388-3302	1-11	1-6	5-10	7-116	11-141	8-227	<0.5-1.6	36-597	Strong Fe-oxide metasomatism; elevated Ti, Nb, and moderate REE and base-metal content.
Ferruginized sandstone	8819-366641	1312-14308	1-28.4	0.5-2.7	3-62	4.6-30.3	33-180	6-72	0.5-32	44-743	Strongest Fe-Ti-REE and moderate basemetal.
Weakly ferruginized sandstone	6301-9545	1823-5162	2-17	0.5-3.74	5-26	3.5-4.8	16-24	~10	0.5-35.41	60-229	Moderate Fe; minor metasomatic influence.

Lithotype	Values in ppm										Remarks
	Fe	Ti	Nb	Mo	Cu	Co	Zn	Pb	Sn	TREEY	
Sandstone	4822-12755	678-7938	1.5-5.8	0.5-1.28	5-40	1-30	11-384	5-10	<0.5	25-261	Broad compositional range; partial ferruginization.
Clay / shale heterolith	8137-353004	1490-6693	3-19	0.6-4.9	7-51	4-10	25-232	5-34	0.5-45	168-391	Background composition; locally Fe-REE rich.

The Bhuj Formation pit samples exhibit a progressive Fe enrichment trend (up to >366000 ppm) from weakly ferruginized to strongly metasomatized sandstone, defining the intensity gradient of Fe-oxide alteration observed in the field (*Table. 6.3*). Elevated Ti (up to ~14000 ppm) and Nb (≤28 ppm) in the ferruginized and metasomatized facies indicate accessory ilmenite-rutile–type enrichment associated with Fe-oxide metasomatism. TREEY contents (25–743 ppm) increase systematically with alteration intensity, reflecting enhanced REE fixation within Fe-oxide and carbonate phases.

Base-metal anomalies, particularly Cu (3-62 ppm), Co (4-116 ppm), Zn (11-384 ppm), and sporadic Pb (≤227 ppm) occur mainly in ferruginized and metasomatized samples, marking zones of limited hydrothermal fluid influx along the Median High Zone (MHZ) and Katrol Hill Fault (KHF) corridors. Sn values are low (<35 ppm), however, they remain well above the average crustal abundance, indicating minor but significant tin mobilization under hydrothermal conditions.

Overall, the Bhuj Formation demonstrates a systematic Fe-Ti-Nb-REE association coupled with localized base-metal enrichment, confirming that hydrothermal fluids ascending along major structural conduits induced pervasive ferruginization and REE concentration within the arenaceous sequence. The metasomatized and ferruginized sandstone thus represents the most chemically evolved and mineralogically fertile facies within the Bhuj block.

6.2. Exploration by Scout Drilling

Following the identification of prospective lithological and structural zones through surface investigations, a program of scout drilling was undertaken to investigate the subsurface continuity and depth persistence of the mineralization within the Bhuj block. The drilling phase aimed to validate the integrated geological-geophysical model. Eight boreholes

were completed across two target systems, Mineral System-I and Mineral System-II, to obtain continuous core samples for lithological, geochemical, and mineralogical characterization of the subsurface sequence.

6.2.1. Methodologies

Diamond core drilling was selected as the principal subsurface exploration technique due to its high precision and reliability in delineating mineralized zones within complex geological settings. This method utilizes a rotary drill equipped with a diamond-impregnated bit, capable of efficiently penetrating the hard sedimentary and ferruginous sequences underlying the prospect. The drilling process produces continuous cylindrical core samples, enabling direct observation of lithological, structural, and mineralogical characteristics of the subsurface strata.

Prior to drilling, a detailed surface geological survey was conducted to document lithological variations and identify potential polymetallic prospect horizons within the Bhuj and Katrol formations. Drill target selection and collar planning were further guided by geophysical investigations, including Vertical Electrical Sounding (VES) resistivity survey. These surveys facilitated the identification of conductive alteration zones, possible structural controls on mineralization, which in turn coupled with significant geochemical anomalies, aided in prioritizing drilling locations.

For **Mineral System-I**, two boreholes were drilled GSPL_Bhuj: BH-01 and BH-02 (*Fig. 6.4*). BH-01 was drilled using an NMLC core size, while BH-02 was drilled using HQ (63.5 mm) core size. Drill site logistics and rig positioning were optimized to ensure safety, accessibility, and maximum core recovery. During drilling, high-speed rotation of the diamond bit was combined with continuous water circulation to cool the bit and remove rock cuttings. Core segments, typically up to 3 m in length, were retrieved using a wireline system, logged, boxed, and preserved for subsequent lithological description, geochemical analysis, and mineralogical characterization.

For **Mineral System-II**, six boreholes were drilled GSPL_Bhuj: BH-03 to BH-08 (*Fig.6.4*). BH-03, BH-04, and BH-06 were drilled using NMLC core size, while BH-05, BH-07, and BH-08 employed HMLC core size. Drill site logistics and rig positioning were carefully planned to ensure safety, accessibility, and optimal core recovery. During drilling, the high-speed rotation of the diamond bit was combined with continuous water circulation to cool the bit and efficiently remove rock cuttings. Core segments, typically up to 3 m in length, were retrieved using a wireline system, then systematically logged, photographed, boxed, and preserved for subsequent lithological description, geochemical analysis, and mineralogical characterization.

While diamond core drilling was the principal technique, dry coring was also adopted locally in zones where the formation was highly porous or loosely consolidated and clay-

bound, as the use of water circulation in such sections caused disintegration and reduced core recovery.

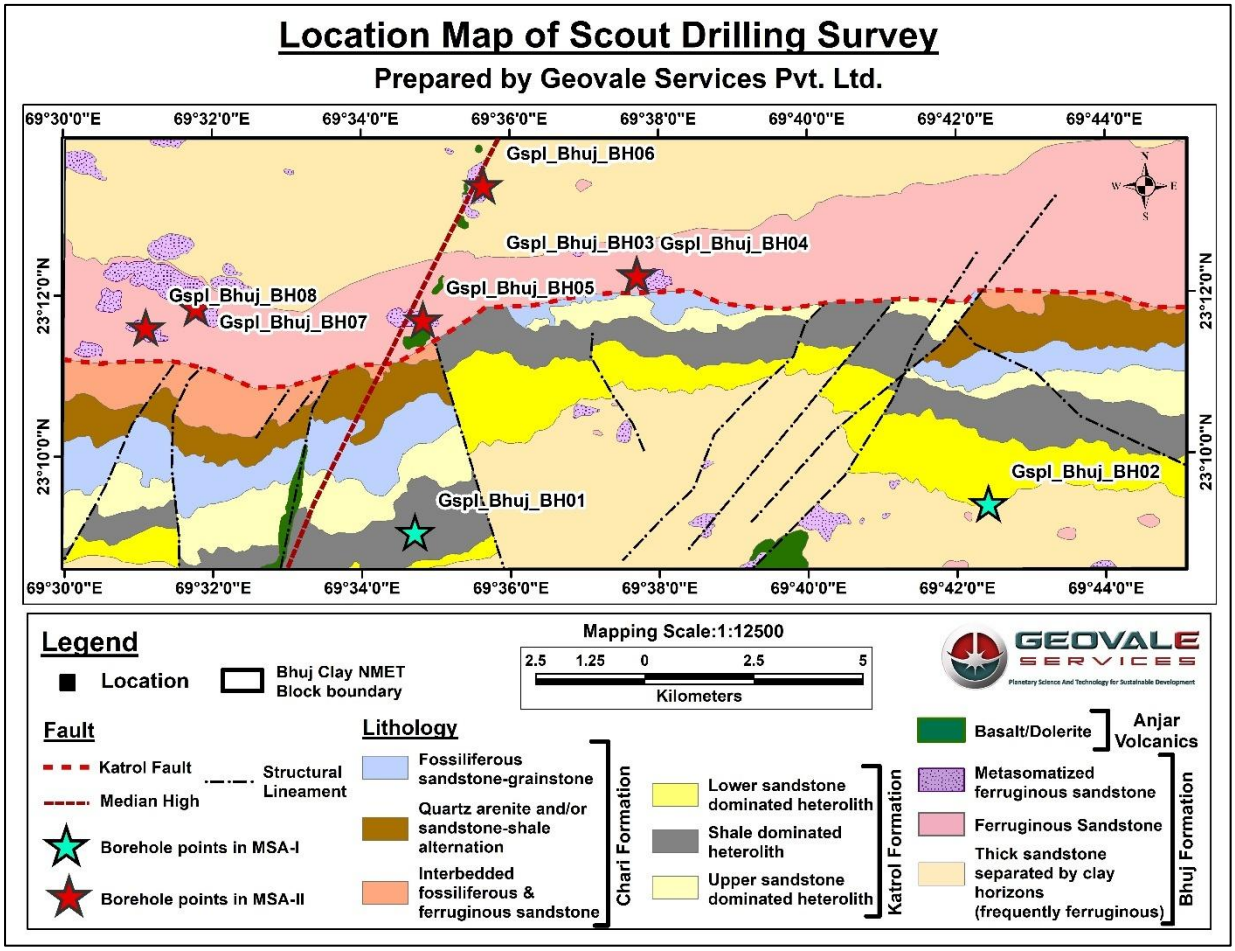

Fig. 6. 4 Location map of the scout drilling survey conducted within the Bhuj exploration block, showing the distribution of eight boreholes (GSPL_Bhuj_BH-01 to BH-08)

6.2.2. Borehole Planning

As part of the G4 level investigation, eight vertical scout boreholes were planned and executed across the Bhuj REE Clay Prospect Block, targeting two distinct mineralization systems delineated through integrated geological, geophysical, and geochemical investigations. A cumulative drilling depth of approximately 603.5 meters was successfully completed against the initial target of 600 meters. The drilling programme was initiated in June 2025 and completed in August 2025. The drilling distribution comprised two boreholes testing the phosphatic ferruginous tuffite layers within the shale-dominated heterolithic unit of the Katrol Formation (Mineralization Style I), and six boreholes intersecting the IOCG-type hydrothermal mineralization along metasomatized ferruginous sandstone and its metasomatic aureole within the Bhuj Formation (Mineralization Style II). Borehole-01 was specifically targeted to intersect the mapped shale-dominated heterolithic unit containing

high-value tuffite layers, as identified during surface investigation. In contrast, BH-02 was strategically located within the sandstone-dominated heterolithic unit to evaluate whether this facies contained any similar tuffite horizons, to determine its vertical extent, and to delineate the transition between the shale and sandstone dominated heteroliths. However, drilling could not reach the base of the sandstone-dominated unit due to excessive formation thickness and limited approved NQT.

The boreholes are spatially distributed across the central, southern and southeastern sectors of the block (*Fig.6.4*) approximately 2-3 km apart from each other. (Detailed information on the boreholes is presented in *Annexure-XXVII*.

Each borehole provided valuable subsurface data, with lithological details encountered and mineralization signatures recorded through meticulous megascopic core logging. The findings offer crucial insights into the subsurface geology and the potential for REE mineralization in the study area.

6.2.3. Scout Drilling in Mineralization Style I

The scout drilling program under Mineralization Style I focused on the phosphatic ferruginous tuffite layers within the heterolith units of the Katrol Formation, identified as the primary host for REE mineralization. Two boreholes, GSPL_Bhuj_BH01 (23.15087, 69.57877) and GSPL_Bhuj_BH02 (23.15934, 69.71902), were drilled to depths of 151 m and 170 m, respectively, at locations selected through detailed surface geological mapping, geophysical anomaly interpretation, and geochemical anomaly assessment. BH-01 was situated approximately 4.9 km from Naranpar village at the southern part of the block, whereas BH-02 was placed approximately 4.0 km from Jadura village.

In GSPL_Bhuj_BH01, the lithological sequence comprised shale, black shale, sandstone-dominated heterolith, shale dominated heterolith, and shale sandstone heterolith units. In contrast, GSPL_Bhuj_BH02 encountered a more complex succession consisting of breccia, ferruginous sandstone, highly altered ferruginous sandstone, fossiliferous sandstone, sandstone-dominated heterolith, shale dominated heterolith, and shale sandstone heterolith.

The drill cores recovered from these boreholes revealed consistent intervals of heterolithic sequences interlayered with iron-rich phosphatic tuffite (*Fig.6.5*), confirming the lithological continuity and stratigraphic control on mineralization. Petrographic, mineralogical, and geochemical assessments identified significant concentrations and signatures of monazite, xenotime, and apatite, indicating potential economically viable REE enrichment within these strata. The combined dataset provides valuable subsurface information critical for defining the spatial distribution, grade variability, and geochemical character of the REE mineralization within the Katrol Formation.

Fig. 6. 5 Borehole cores of BH01, showing shale dominated heterolith unit interlayered with repeated occurrence of tuffite layers.

6.2.3.1. Core Logging

Borehole-01 (*ANNEXURE-XXVII-A*):

Borehole-01 was drilled to a total depth of 151 m, distinctively capturing the lithological variations from near-surface weathered zones to deeper sandstone shale alternations. The core recovery was excellent, allowing detailed observations of sedimentological, mineralogical, and structural features.

The uppermost 0-3.5 m interval comprises yellowish-grey soil and weathered rock with shale-dominated heteroliths interbedded with thin sandstone laminae. The sandstone varies from reddish-brown to yellowish ochre to greyish white, mostly massive to low angle laminated without internal structuring. Notably, ironstone nodules and elongate elliptical shale lenses appear between 3.7 and 4.9 m within sandstone dominated heteroliths.

Between 4.9 and 28.5 m, the lithology alternates between shale and sandstone dominated heteroliths, punctuated by numerous thin suspected tuffitic and target layers composed of silt clay matrix with amorphous black glass shards showing conchoidal fractures. Sedimentary structures such as ripple cross lamination, low angle planar lamination, wavy to plane parallel lamination with intercalated tuffitic lenses and lapilli fragments (*Fig.6.6a*), and flaser, lenticular, and wavy bedding (*Fig.6.6b*) are well developed here, suggesting deposition under oscillating current conditions with intermittent volcaniclastic influx.

From 28.5 to 66.5 m, heterolithic intercalations of shale and sandstone dominate, locally interrupted by thin tuffite layers (*Fig.6.6c*) and sandy veins. Internal structures include planar and wavy lamination, flame and load casts, soft-sediment deformation and ball and pillow structures, along with occasional lapilli fragments typical of volcaniclastic sediments. Disseminated pyrite and chalcopyrite (*Fig.6.6f*) are noted throughout this interval, indicating intermittent hydrothermal input. The sub interval between 30.13 m and 31.3 m distinctly records a Bouma sequence (*Fig.6.6d*) with graded bedding, wavy lamination, ripple cross

lamination, and soft-sediment deformation preserving divisions A to D in upward succession, followed upward by hummocky cross stratification (*Fig.6.6e*) denoting storm related sand influx.

The 66.5-110 m interval is predominantly sandstone rich heterolith, interbedded with thin shales, displaying liquefaction, load casts, flaser, lenticular, and wavy bedding (*Fig.6.6b*). Several mineralized horizons occur here, where disseminated pyrite and chalcopyrite are associated with fine-grained sandstone layers.

Between 110 and 116 m, shale sandstone heteroliths with thin tuffitic interbeds mark a transitional unit showing plane to wavy parallel lamination, faint ripple marks, and isolated deformation zones representing fine grained clastic sedimentation with occasional volcaniclastic inputs.

The lower section, 116-151 m, consists mainly of sandstone dominated heteroliths with minor shale and sporadic thin tuffite lenses. The sandstone is medium to coarse grained, quartz rich with muscovite, biotite, magnetite, and iron concretions, showing soft sediment deformation (*Fig.6.6g)*, liquefaction, and ball and pillow features. Distinct lapilli structures and bivalve fossils (*Fig.6.6i*) occur at several depths, while deeper sections (127-147 m) also display trace fossils and burrow structures (*Fig.6.6j*) within shale, accompanied by slickensided surfaces and carbonate filled cavities.

Overall, BH-01 captures a complex sandstone shale tuffite succession, reflecting alternating clastic and volcaniclastic sedimentation under fluctuating energy conditions. Multiple sedimentary features plane parallel lamination, flaser and lenticular bedding, Bouma sequences, hummocky cross-stratification, soft sediment deformation, and fossiliferous horizons combined with localized sulfide mineralization and volcaniclastic shards, collectively characterize a dynamic depositional environment shaped by storm, turbidity, and hydrothermal processes.

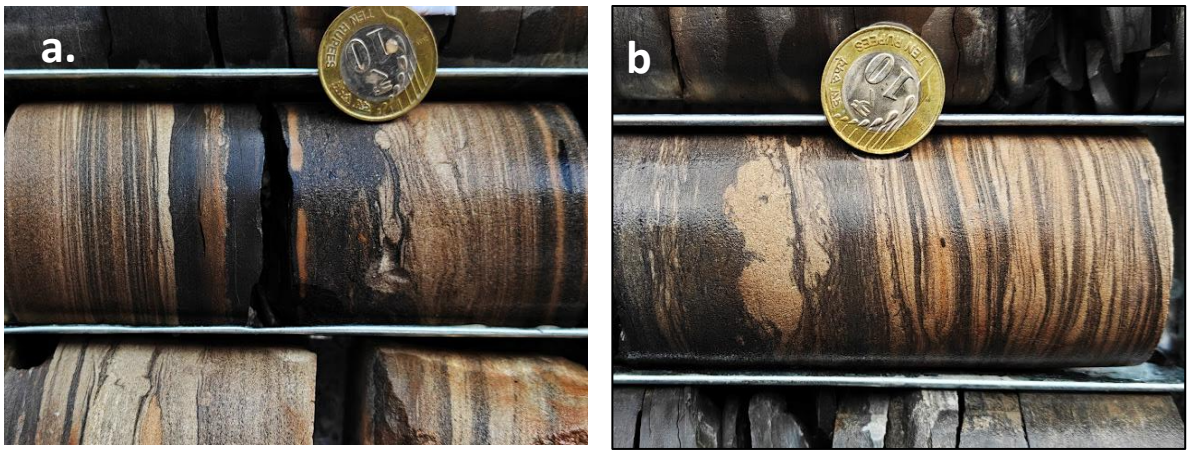

Fig. 6. 6 Megascopic photographs of core sections from Borehole GSPL_Bhuj_BH-01, showing representative sedimentary structures within the shale-dominated heterolithic unit. (a) Wavy to plane-parallel lamination with intercalated tuffitic lenses and lapilli-sized volcanic fragments. (b) Flaser, lenticular, and wavy bedding. (c) Suspected tuffite layers. (d) Bouma sequence. (e) Hummocky cross-stratification and ball-and-pillow structures. (f) Sand layers with disseminated pyrite/chalcopyrite within shale-dominated heterolith. (g) Soft-sediment deformation with wavy parallel lamination and iron leaching. (h) Load casts and flaser bedding within shale of shale–sandstone heterolith. (i) Occurrence of bivalve fossil. (j) Trace fossil and burrow with soft-sediment deformation, flaser bedding, and lapilli-bearing layer.

Borehole-02 (*ANNEXURE-XXVII-B*):

Borehole-02 was drilled to a total depth of 170 meters, targeting subsurface lithologies similar to BH01 but with distinct variations in sedimentological and mineralogical characteristics.

The upper section from 0 to 3.2 m consists of yellowish soil transitioning to ferruginous sandstone characterized by medium to fine sand-sized grains primarily composed of quartz muscovite and biotite. The sandstone exhibits reddish-brown coloration indicative of iron oxide cement, with faint horizontal bedding and ripple cross-lamination. Cherry red hematite streaks and iron concretions are notable features.

Between 3.2 and 15.28 m, the lithology dominantly features sandstone interspersed with thin clay layers. Sedimentary structures such as plane parallel lamination, soft sediment deformation, and load casts are evident. Three suspected tuffite layers composed predominantly of clay with fine black mineral content occur in this interval.

From 15.28 to 42 m, the core includes sandstone-dominated heteroliths with shale interbeds and various sedimentary structures like ball pillow, liquefaction, and load cast. At 15.84 m, a breccia unit composed of angular to sub-angular clasts within a fine-grained clayey matrix occurs, containing fossils and indicative copper mineralization with malachite (??) grains(*Fig.6.7a*). Fossiliferous sandstone intervals between 17.5 and 42 m display well-developed lamination and fossil imprints alongside mineral inclusions such as pyrite (*Fig.6.7b*) and malachite. Several tuffite lenses enriched in clay and black mineral (*Fig.6.7j*) shards are distributed throughout.

The interval from 42 m to 107.35 m is dominated by alternating sandstone- and shale-rich heteroliths that show planar to wavy lamination, ripple cross-lamination, flaser and lenticular bedding, and abundant soft-sediment deformation structures. Lapilli-like and tuffite lenses, composed mainly of clay with black glass shards, are frequent, together with fossilized fragments and evidence of pyritic mineralization. Localized blackened portions of the core emitted a distinct sulphur odour (*Fig. 6.7c*), suggesting sulphur bearing phases. At 72.70 m, ball-and-pillow structures are observed (*Fig. 6.7g*), while flame structures (*Fig. 6.7e*) and lapilli concentrations (*Fig. 6.7h*) occur between 74.90 m and 77.50 m. A prominently fossiliferous sandstone horizon at 81.23 m (*Fig. 6.7d*) marks a well-cemented bioclastic zone. A thin suspected tuffite layer at 89.10 m (*Fig. 6.7f*) further indicates intermittent volcaniclastic influx within the heterolithic succession.

The interval between 107.35 and 160.07 m shows continued shale-sandstone heterolith sequences with varying thicknesses of sandstones and shales. Fossiliferous sandstone and breccia units are present in between with continued evidence of iron concretions, muscovite, biotite, and carbonate infilling in fractures. Tuffite layers are pervasive, typically 1 to 4 cm

thick, mainly clay-rich with occasional black glass shards and other mineral inclusions. A lenticular bedding structure at 131.90 m (*Fig. 6.7k*) and a carbonate-enriched tuffite layer at 137.28 m (*Fig. 6.7i, l*) represent key stratigraphic markers within this interval.

From 160.07 m to the bottom at 170 m, the core displays shale-dominated heterolith layers comprising dark grey to greyish-brown finely laminated shales with thin sandstone lenses. Soft sediment deformation and lenticular bedding, common throughout, continue in this section. The tuffite layers exhibit clay dominance mixed with black elongated minerals and glass shards, marking the lower extent of the mineralized sequence.

Overall, BH02 core reveals a complex depositional regime with significant heterolithic facies transitions, extensive soft sediment deformation structures, and multiple mineralized tuffite layers characterized by black glass shard lenses, fossiliferous content, and sulfide mineralization.

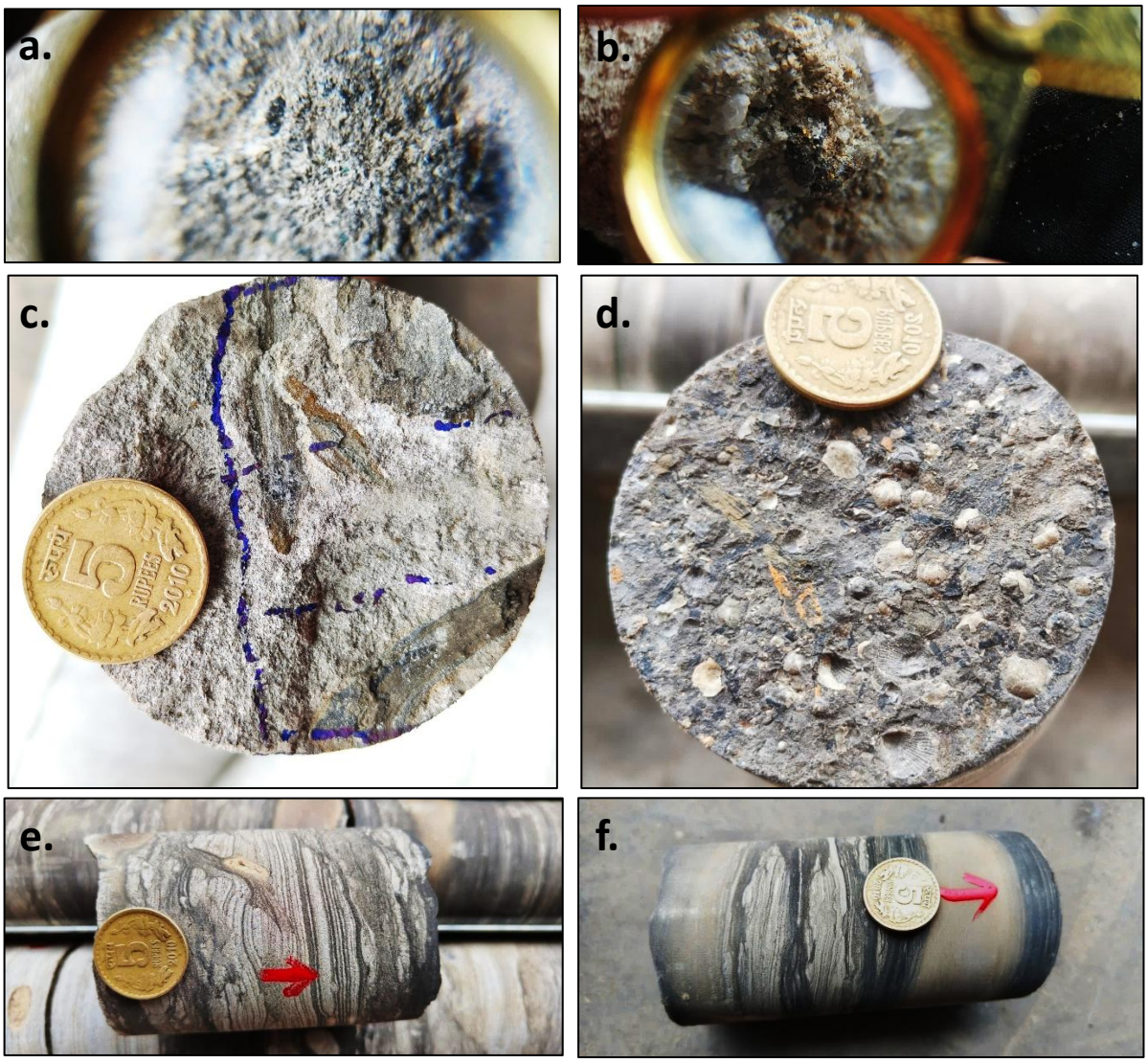

Fig. 6. 7 Megascopic photographs of core sections from Borehole GSPL_Bhuj_BH-02, showing representative sedimentary structures within the shale-dominated heterolithic unit. (a) Green staining possibly Malachite? at depth 16.43m. (b) Pyrite at depth 19.59 m (c) Sulphur smell at black part 71.34 m. (d) Fossiliferous sandstone at depth 81.23 m. (e) Flame or Soft sediment deformation at 74.90m. (f) Suspected Tuffite layer at 89.10 m (g) Ball and Pillow structure at depth 72.70m (h) Suspected lapilli at depth 77.50 m (i) Suspected Tuffite layer with carbonate at 137.28m (j) Likely Mn minerals (k) Lenticular bedding at depth at 131.90m (l) Suspected Tuffite layer with carbonate at 137.28m

6.2.3.2. Sampling and Sample Preparation

Representative core samples were systematically collected from lithological units of interest, prioritizing tuffite layers/lenses within hetrolith units and mineralized sandstone/shale sections identified during core logging. Sampling intervals were selected to capture vertical variations in lithology and mineralization intensity. The cores were carefully marked, photographed, and logged before extraction of split halves for laboratory analysis. Sample preparation involved crushing, pulverizing, and homogenizing the rock material to ensure representativeness and accuracy during geochemical and mineralogical studies. Strict chain-of-custody protocols were followed to maintain sample integrity. This sample suite was used for geochemical assays, petrographic thin section preparation, and further advanced

characterization aimed at defining the spatial extent and grade of rare earth element (REE) mineralization within the target formations.

6.2.3.3. Petrographic Studies

Two boreholes BH01 (total depth 151 m) and BH02 (total depth 170 m) were drilled as stratigraphic boreholes to delineate and characterize Type I mineralization, represented by phosphatic ferruginous tuffite layers within the shale-dominated unit of the Katrol Formation. The cores comprise alternating a) Tuffite, b) Sandstone and c) Shale–Siltstone Heteroliths, reflecting a volcaniclastic sedimentary depositional environment influenced by intermittent volcanic activity (*Annexure-XXVIII*).

BH01:

Borehole BH01 was drilled as a stratigraphic borehole within the Katrol Formation and attained a total depth of 151 m. The borehole intersected a sequence dominated by alternating tuffite, volcaniclastic sandstone, and shale–sandstone heteroliths, representing a volcaniclastic–sedimentary succession deposited under intermittent volcanic influence.

i. Tuffite: This rocks occurs at different depth (5.28 to 5.44)m, (6.71 to 6.8)m, (11.01 to 11.10)m, (11.76 to 11.81)m, (13.07 to 13.10)m, (13.63 to 13.69)m, (13.86 to 13.9)m, (14.35 to 14.44)m, (26.92 to 26.95m), (36.30 to 36.35m), (43.50 to 43.59m), (57 to 60)m, (69 to 72)m, and (140 to 147)m.

Petrographic study of the representative samples of tuffites occurring at different depth were studied under microscope as described below (*Fig. 6.8*):

The tuffite layers are very fine-grained and distinctly laminated, with lamination defined by alternating phenocryst-rich (framework) and groundmass-rich layers. The framework grains (<20–250 µm) are composed of elongated, flaky, needle-shaped, and wedge-shaped grains of quartz, feldspar, muscovite, apatite, monazite, and zircon, all set within a ferruginous to calcareous, partly glassy groundmass. In many cases, it was observed that effect of ferrugination varies widely making the rock ferruginous tuffite to non-ferruginous tuffite. Besides ferrugination the matrix is also at places, partly to totally replaced by carbonates. Highly ferruginous matrix of tuffite occure at 14.35 to 14.44m, 28.22 to 28.25m, 33.50 to 33.56m, 45.95 to 50.00m, 69.65 to 69.70m, 92.04 to 92.09m, 110.61 to 110.67m, 130.86 to 130.90m, 146.89 to 146.93m depths. Whereas, carbonated matrix/cement rich tuffites are observed at 6.71 to 6.80m, 13.63 to 13.69m, 18.83 to 18.88m, 24.98 to 25.00m, 34.93 to 35.00m, 27.05 to 27.08, 36.40 to 36.48m, 57.89 to 57.92m, 67.88 to 67.92m, 80.61 to 80 .65m, 91.62 to 91.69m, 139.07 to 139.09m depths. Concentration of apatite is more in non-ferruginous tuffite compare to ferruginous tuffite and the tuffite having calcareous cement. The textural variation between framework-rich and groundmass-rich laminae imparts a

rhythmic, banded appearance to the rock. The apatite and monazite grains occur as euhedral to subhedral crystals, locally associated with fine iron oxides and amorphous glassy material, suggesting a volcaniclastic–hydrothermal influence during deposition. The ferruginous nature of the groundmass and the presence of phosphate minerals confirm that these tuffite layers represent REE-enriched phosphatic–ferruginous tuffaceous horizons, which are the principal Type I mineralization targets.

Phospate/REE/Magnetite and Sulfide Mineralisation: High concentration apatite are generally found mainly in ferruginous tuffites. During SEM and EPMA studies we have also seen fine crystals of apatite mainly in the form of fluro apatite occurred as disseminated grains in the ferruginous matrix. These apatite grains are very fine and very difficult to identify under microscope. However, under high magnification (40x) fine needles of apatite found in tuffite rocks occurring in 13.07 to 13.10m, 18.23 to 18.32m, 28.22 to 28.25m, 28.22 to 28.25m, depths. Geochemically, we have seen that fluro apatite bearing ferruginous tuffites shows high REE values, suggesting that Fluor apatite may contain some very fine crystal of REE phase.

Sulfides dominantly in the form of pyrite are prevalent in tuffites of different depths. Both crystalline as well as framboidal nature are common in almost all the tuffites of different depth, however there is no systematic varies of pyrite concentration with depth. Fine disseminations of magnetite are also observed in the tuffite rocks of different depths, however it was more common in ferruginous tuffite.

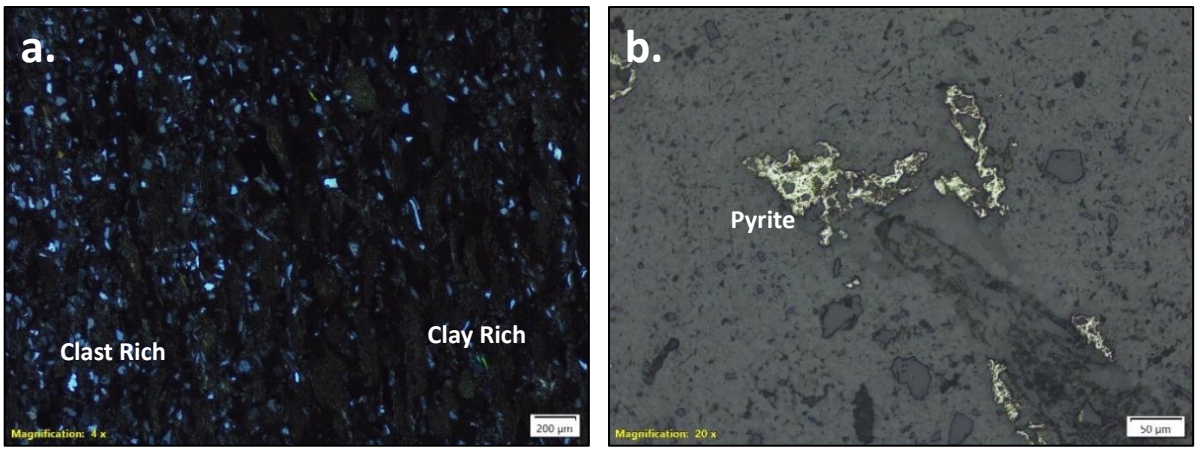

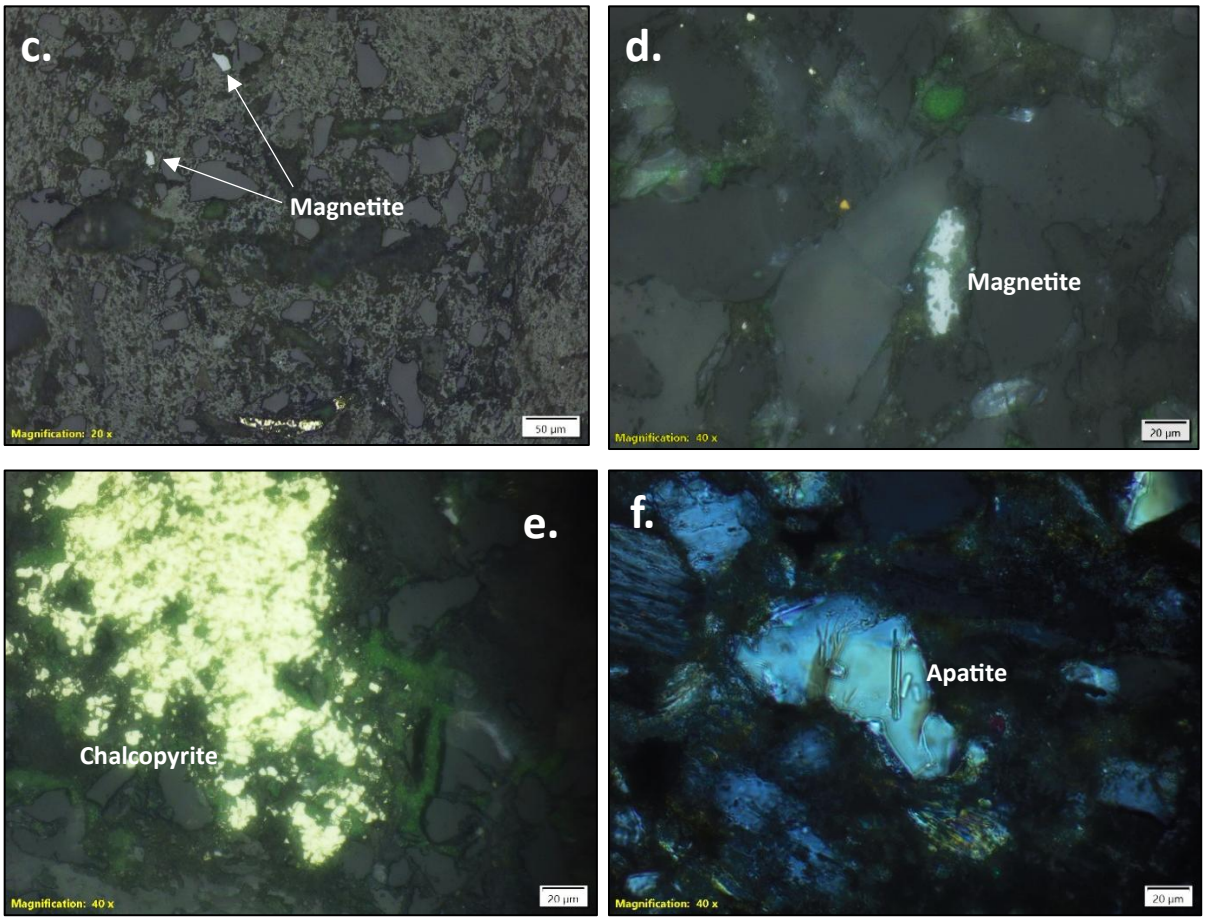

Fig. 6. 8 Representative photomicrographs of tuffite and associated mineralized lithounits from BH-01 of the Katrol Formation. (a) Tuffite showing alternating clast-rich and clay-rich laminae. (b) Secondary pyrite occurring as bright, anhedral to subhedral grains disseminated within the groundmass. (c) Magnetite and pyrite set in a dark silicate matrix. (d) Magnetite replacing the silicate matrix; a minute bright-yellow grain near the centre is interpreted as probable native gold. (e) Chalcopyrite (bright yellowish-golden) occurring as disseminated grains and aggregates within the ferruginous–silicate matrix. (f) Apatite crystal embedded within a dark ferruginous to silicate matrix.

ii. Sandstone (*Fig.6.9*): These rocks occurs at different depth 25.03 to 26m, 27.2 to 27.52m, 28.47 to 28.97m, 36.5 to 37.26m, 47.58 to 47.62m, 51.65 to 51.67m, 57.57 to 57. 63m, 58.45 to 58.50m, 57.10 to 57.15m, 65.4 to 68.5m, 71.73 to 80m, 112.58 to 112.65m, 126.60 to 126.65m, and 127.36 to 127.41m. Petrographic study of the representative samples of sandstone occurring at different depth were studied under microscope as described below.

The sandstone units throughout the Katrol Formation in these boreholes are medium- to fine-grained volcaniclastic sandstones, composed of very angular to subrounded fragmented grains of quartz, feldspar (orthoclase, microcline, and plagioclase), muscovite, perthite, chert, and volcanic rock fragments. Well-rounded mud pellets are commonly

observed, embedded within a carbonate cement are also present. Textural features such as needle-, wedge-, and triangular-shaped quartz, feldspar clasts, as well as cooling cracks within framework grains are common. These features indicate a pyroclastic origin and rapid cooling during or shortly after deposition. The carbonate cement varies from fine microcrystalline calcite to zoned sparry calcite in coarser, crystal-rich layers, suggesting multiple stages of cementation under changing chemical conditions. Feldspar content ranges from 2 to 12%, while the matrix (quartzo-feldspathic) component varies from 1–10%. Unfragmented fossil fragments (including wood and sponge remains) are occasionally preserved within these sandstones, indicating episodic quiescent intervals and localized biogenic activity between volcanic events.

Phospate/REE/Magnetite/Gold and Sulfide Mineralisation: In these sandstone samples, petrographically apatite minerals could not be identified. REE minerals in the form of monazite is found at 48.80 to 48.84m depth. Magnetite along with goethite are commonly found in almost all the sandstone samples. Pyrite is very common and occurs in almost all samples, coarser grained are having more pyrite than finer one.

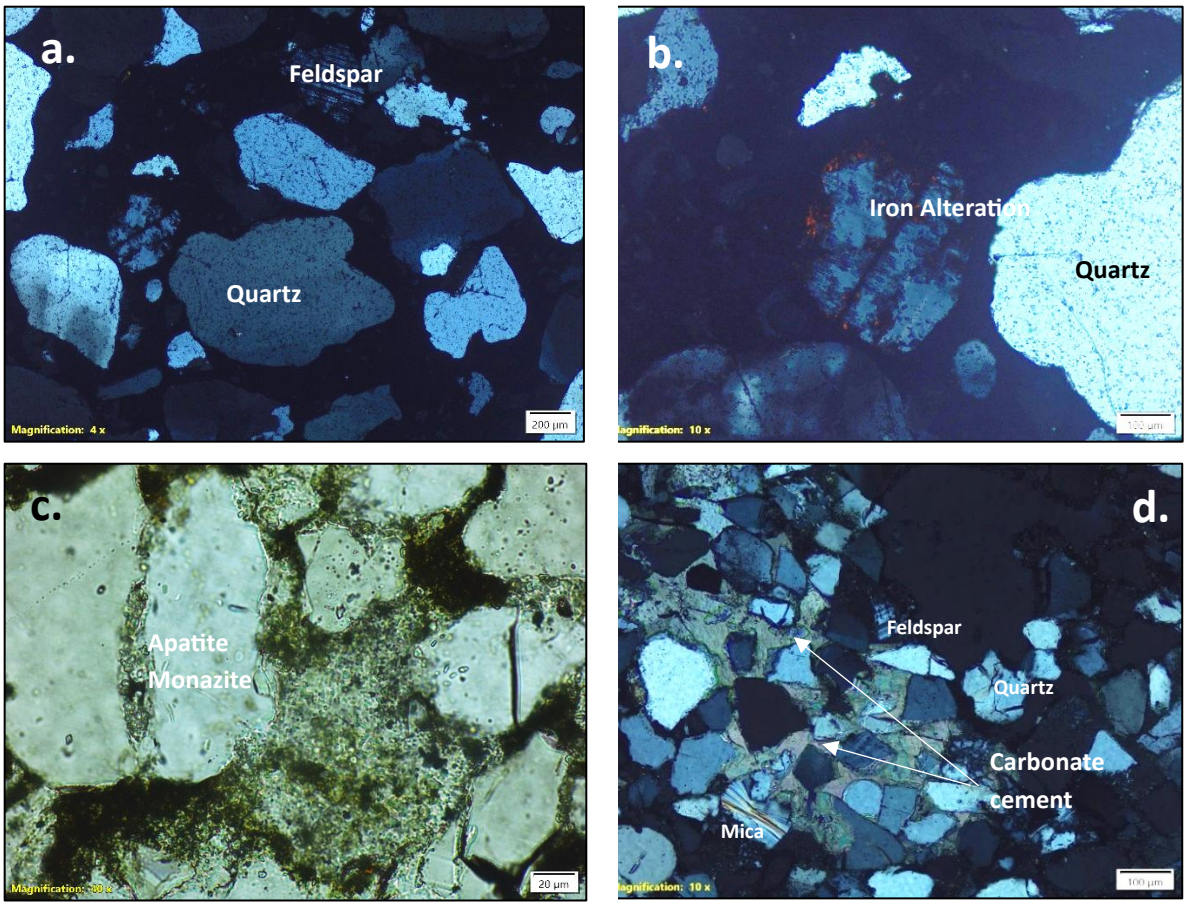

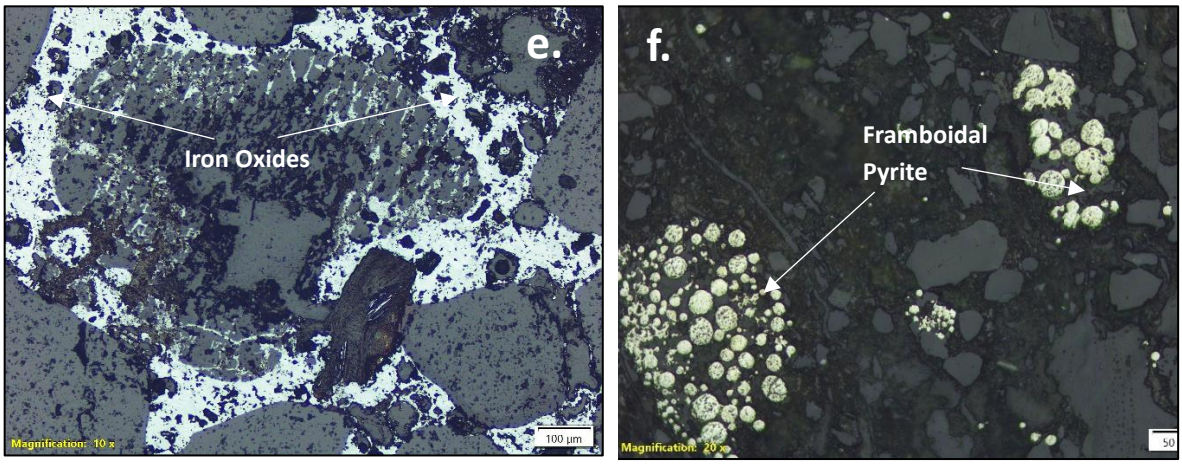

Fig. 6. 9 Representative photomicrographs of sandstone from BH-01 of the Katrol Formation. (a) Coarse sandstone showing subangular grains of quartz and feldspar. (b) Feldspar grain exhibiting iron oxide alteration. (c) Apatite and monazite crystals embedded within a dark ferruginous–silicate matrix. (d) Matrix partially replaced by carbonate cement. (e) Iron oxides replacing the matrix. (f) framboidal pyrite (bright) occurring as rounded to subrounded grains within the darker silicate groundmass.

iii. Shale-sandstone Hetrolith (*Fig.6.10*): This rocks sequence occurs at different depth at 3.5 to 4.9m, 7.98 to 8.5m, 63.33 to 63.37m, 63.69 to 63.73m, 110.61 to 110.67m, 137.28 to 139.09m, The sahle-sandstone heterolith also contain thin tuffite beds. But petrographic study of tuffite has already been described. Here shale and sandstone unit occurring at different depth only is described below.

The sandstone units throughout the Katrol Formation in these boreholes are medium- to fine-grained volcaniclastic sandstones, composed of very angular to subrounded fragmented grains of quartz, feldspar (orthoclase, microcline, and plagioclase), muscovite, perthite, chert, and volcanic rock fragments. Well-rounded mud pellets are commonly observed, embedded within a carbonate cement are also present. Textural features such as needle-, wedge-, and triangular-shaped quartz, feldspar clasts, as well as cooling cracks within framework grains are common. These features indicate a pyroclastic origin and rapid cooling during or shortly after deposition. The carbonate cement varies from fine microcrystalline calcite to zoned sparry calcite in coarser, crystal-rich layers, suggesting multiple stages of cementation under changing chemical conditions. Feldspar content ranges from 2 to 12%, while the matrix (quartzo-feldspathic) component varies from 1–10%. Unfragmented fossil fragments (including wood and sponge remains) are occasionally preserved within these sandstones, indicating episodic quiescent intervals and localized biogenic activity between volcanic events.

Magnetite/ Sulfide Mineralisation: Mainly pyrite and magnetite observed almost every samples of these rock sequence occurring at different depth. No apatite and REE phase could be identified under optical microscope.

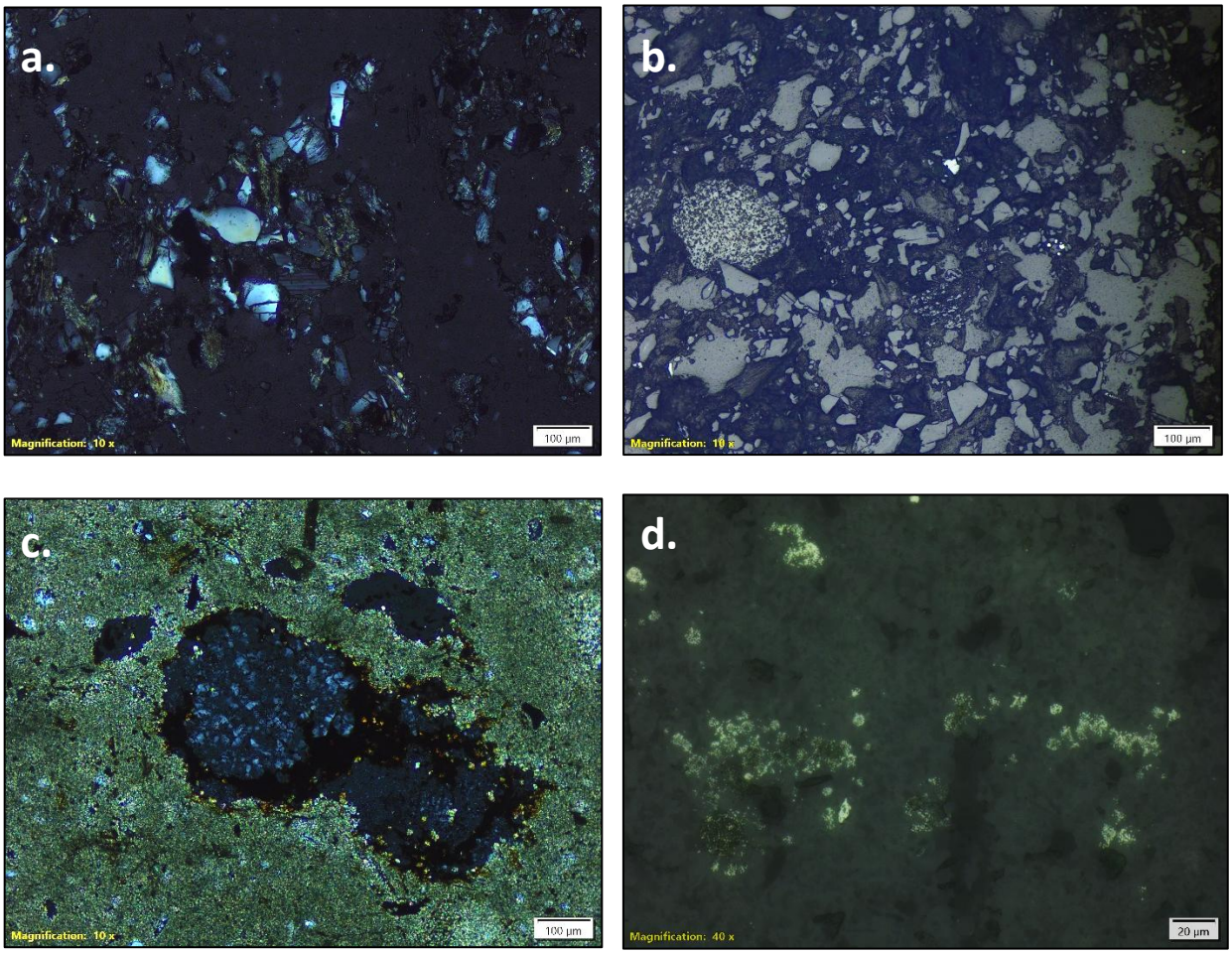

Fig. 6. 10 Representative photomicrographs of shale–sandstone heterolith from Bh-01 of the Katrol Formation. (a) Siltstone showing highly angular to fragmented quartz and feldspar grains set within a dark matrix. (b) Framboidal pyrite and disseminated magnetite occurring within ferruginous matrix enclosing quartz, feldspar, and lithic fragments. (c) Partial replacement of lithic fragments by iron oxide/hydroxide. (d) Growth of secondary pyrite within the dark matrix.

Overall, BH01 delineates a ferruginous, tuffite-hosted REE system within the Katrol Formation. The deformation of framework grains, zoned carbonate cementation, and preserved zeolitic textures confirm volcaniclastic deposition with post-depositional hydrothermal reworking, marking the principal Type I REE mineralization zone.

BH02:

Borehole BH02 was drilled as a stratigraphic borehole within the Katrol Formation to a total depth of 170 m. The borehole core displays a repetitive alternation of tuffite,

volcaniclastic sandstone, and shale–siltstone heteroliths, representing a volcaniclastic–sedimentary depositional sequence influenced by episodic volcanic activity.

i. Tuffite (*Fig.6.11*): These rocks occur at different depth 28.08 to 28.14m, 119.00 to 119.04m, 131.77 to 131.79m, 143.13 to 143.16m, 157.19 to 157.22m, 169.94 to 169.95 depths. Petrographic study of the representative samples of tuffites occurring at different depth were studied under microscope as described below:

the succession is dominated by very fine-grained, laminated tuffite, characterized by alternating phenocryst-rich and groundmass-rich laminae. Framework grains (<20–250 µm) consist of quartz, feldspar, muscovite, apatite, monazite, and zircon set in a ferruginous–calcareous glassy groundmass. The rhythmic texture gives a banded, tuffaceous appearance. The apatite–monazite association with fine iron oxides and glass shards suggests deposition under volcaniclastic–hydrothermal conditions. This interval represents the phosphatic–ferruginous tuffite horizon, a major Type I REE mineralization zone.

Phospate/REE/Magnetite and Sulfide Mineralisation: High concentration apatite are generally found mainly in ferruginous tuffites. During SEM and EPMA studies we have also seen fine crystals of apatite mainly in the form of fluro apatite occurred as disseminated grains in the ferruginous matrix. These apatite grains are very fine and very difficult to identify under microscope. Sulfides dominantly in the form of pyrite are prevalent in tuffites of different depths. Both crystalline as well as framboidal nature are common in almost all the tuffites of different depth, however there is no systematic varies of pyrite concentration with depth. Fine disseminations of magnetite are also observed in the tuffite rocks of different depths; however, it was more common in ferruginous tuffite.

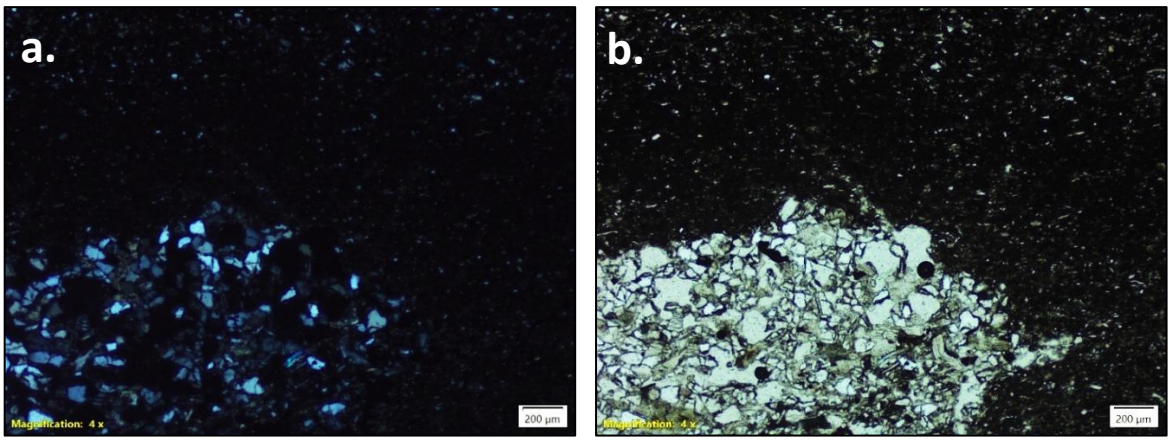

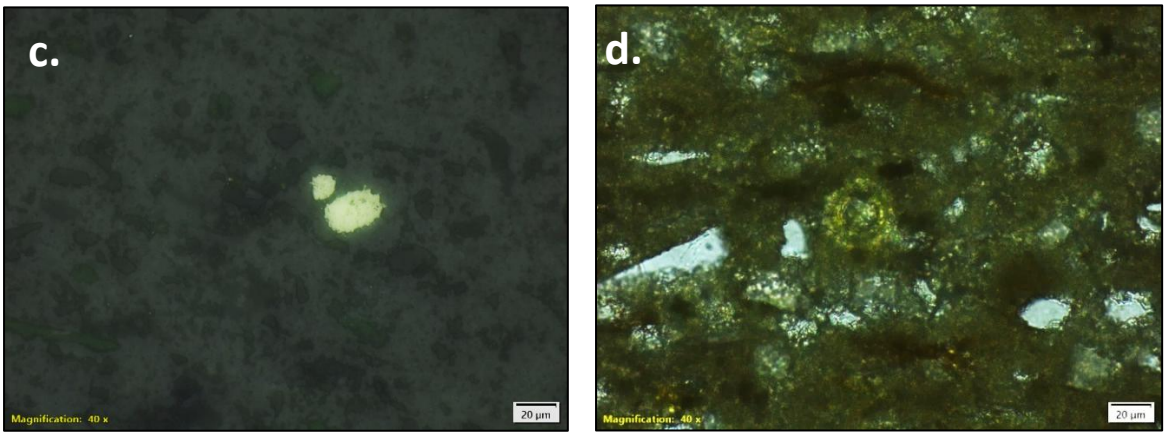

Fig. 6. 11 Representative photomicrographs of tuffite from Borehole BH-02, Katrol Formation. (a) Lithic fragments within the tuffite observed under crossed polarised light. (b) Lithic fragments within the same tuffite under plane polarised light. (c) Secondary pyrite disseminated within the dark matrix. (d) Fossil fragment preserved within the tuffite unit.

ii. Sandstone (*Fig.6.12*): This rock occurs at different depth 1 to 3.2 m, 3.2 to 4.15m, 15.28 to 15.84m, 17.5 to 19m, 19 to 21.35m, 21.35 to 26.08m, 30.39 to 31.59m, 42 to 42.5m, 53.67 to 53.89m, 60.49 to 71m, 80.93 to 86.7m, 89.84 to 90.83m, 159.27 to 160.07m.

The sandstone is medium- to fine-grained, comprising angular to subrounded grains of quartz, feldspar, muscovite, perthite, chert, and volcanic rock fragments within a carbonate cement. Mud pellets and pyroclastic quartz–feldspar clasts showing cooling cracks indicate rapid deposition from volcanic sources. Zoned sparry calcite and fine microcrystalline calcite cements point to successive cementation phases under fluctuating geochemical conditions. Feldspar (2–12%) and matrix (1–10%) contents vary vertically. Local fossil preservation (wood and sponge fragments) records brief quiescent intervals between volcanic events.

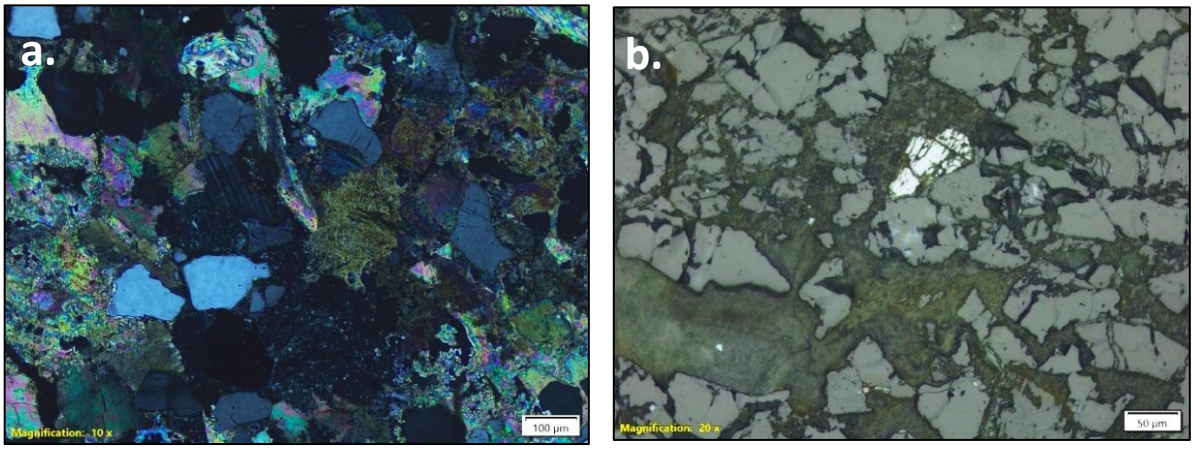

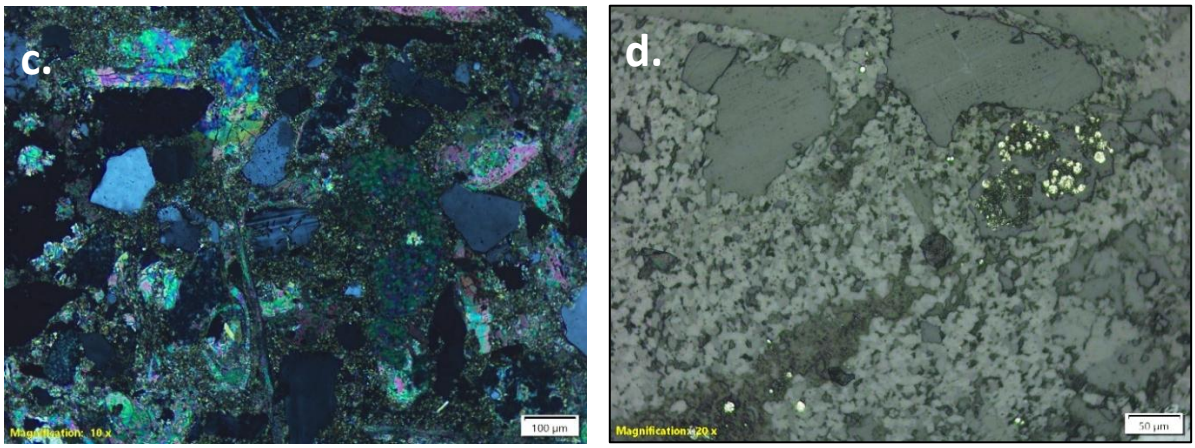

Fig. 6. 12 Representative photomicrographs of sandstone from Borehole BH-02, Katrol Formation. (a) Carbonate cement replacing the matrix of coarse-grained sandstone (crossed polarised light). (b) Magnetite grain occurring within the matrix. (c) Carbonate replacing both the fossil skeleton and surrounding matrix in fossiliferous sandstone. (d) Framboidal pyrite disseminated within the carbonate matrix.

iii**. Shale-Sandstone Hetrolith (*Fig.6.13*):** This rock occurs at different depth 4.15 to 10.6m, 12.3 to 15.28m, 27.21 to 30.39m, 32.34 to 42m, 42.5 to 53.67m, 56.54 to 60.49m, 71 to 80.93m, 86.7 to 89.84m, 102.3 to 107.35m, 112 to 126m, 143.5 to 150m.

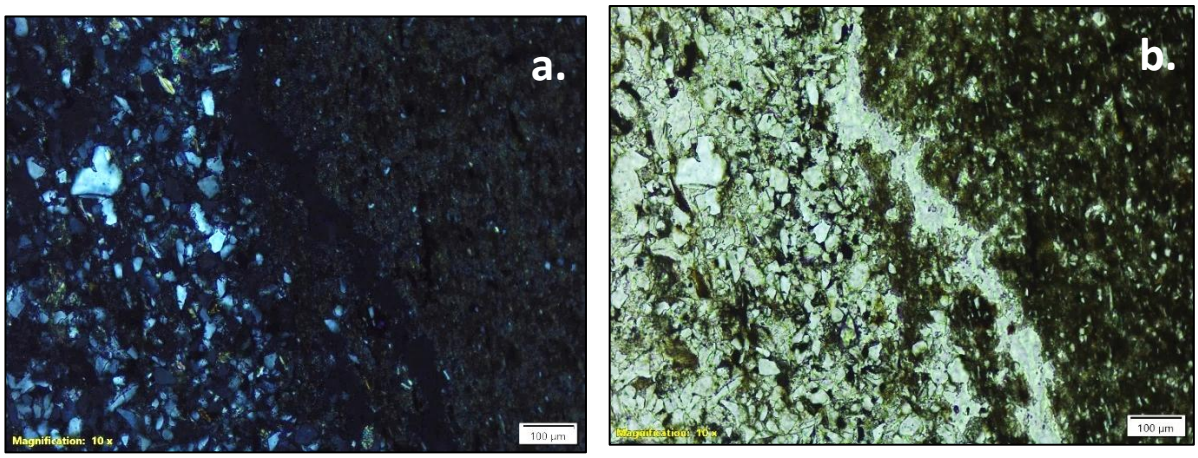

Fig. 6. 13 Representative photomicrographs of shale–sandstone heterolith from Borehole BH-02, Katrol Formation. (a) Heterolithic layer showing alternating shale and sandstone laminae under crossed polarised light. (b) Same heterolithic layer observed under plane polarised light.

Shale-sandstone heteroliths, finely laminated with alternating clast- and cement-rich layers. Framework grains (quartz, microcline, muscovite, glass shards) are embedded in an iron-rich, partly glassy matrix. Deformed grains and flow textures suggest compactional stress and fluid circulation during diagenesis. The heterolithic layering, together with interbedded

tuffite and sandstone, indicates cyclic volcaniclastic–sedimentary deposition in a shallow marine environment.

Phospate/REE/Magnetite/Gold and Sulphide Mineralisation: Mainly pyrite and magnetite observed at almost every samples.

6.2.3.4. Geochemical Studies

Under Mineral System I, two boreholes-GSPL_Bhuj_BH-01 (151 m) and GSPL_Bhuj_BH-02 (170 m) were drilled through the Katrol Formation to evaluate subsurface REE distribution and lithogeochemical variations within tuffite from hetrolith units, breccia, and ferruginized sandstone horizons. Geochemical investigations followed the analytical framework outlined in *Section 4.7.2*, comprising detailed ICP-MS and XRF studies on systematically collected core and surface samples (*Annexure-XXIX, XXX-a, b*).

For ICP-MS, a total of 75 samples from BH-01 and 98 samples from BH-02 were analyzed. In BH-01, 74 spot core samples (2-10 cm thick) and one composite sample (1-2 m) were studied, while BH-02 included 86 spot core samples, six composite core samples, and six surface samples from the borehole vicinity. The ICP-MS data from both boreholes clearly delineate stratabound REE and hydrothermal metal enrichment localized within phosphatic-ferruginous tuffite and breccia horizons. In BH-01, the overall TREEY median is about 247 ppm, with a distinct enrichment zone peaking at ~549 ppm at 77.4 m, exceeding three times the whole average. This interval, composed of phosphatic, clay rich tuffite containing altered glass shards and disseminated pyrite, shows strong LREE dominance (LREE = 482 ppm; La 85.6 ppm; Ce 250.2 ppm; Nd 103.5 ppm), accompanied by high Ba (3345 ppm) and Sr (674 ppm) and minor enrichments in Pb (39 ppm), Cu (12.6 ppm), Co (10.3 ppm), and Ni (7.8 ppm). These associations indicate a hydrothermal assemblage enriched in large-ion lithophiles and REEs mobilized through fluid interaction with volcaniclastic material. Below 90 m, both TREEY and base-metal concentrations gradually decline but remain above background, reflecting waning hydrothermal activity. The 1 m composite shale sample from 59-60 m supports this pattern, recording TREEY 243 ppm, Fe 95 ppm, and moderate Mn, with elevated Ba (483 ppm) and Sr (212 ppm) suggesting localized REE trapping during later fluid pulses.

In BH-02, the geochemical zoning is equally well developed. The borehole shows a background TREEY median of ~224 ppm, with several ferruginous and brecciated zones displaying enrichment more than three times the median, culminating in a TREEY peak of ~995 ppm at 27.3 m. This horizon shows high Ce (281 ppm), La (75 ppm), and Sm (62.8 ppm), along with significant Zn (94 ppm) and Ni (18 ppm) concentrations, confirming multiple episodes of hydrothermal influx and oxidation-driven REE precipitation. The high LREE/HREE ratios and positive Ce anomalies (CeN/Ce > 1)* with subdued Eu (EuN/Eu < 1)* indicate oxidizing conditions favoring selective LREE mobilization. Vertical variation shows that peaks in TREEY, Fe, and Mn coincide with ferruginous-tuffite layers, while synchronous Ba and Sr enrichments

reflect LILE-rich hydrothermal pulses. Base-metal anomalies (Cu-Co-Ni-Zn) are restricted to brecciated and veined sections, pointing to episodic, structurally controlled fluid migration rather than pervasive diffusion. The six composite samples from BH-02 further define these trends: the ferruginous sandstone (2–3 m) exhibits TREEY 265 ppm with Ag 0.89 ppm, In 0.05 ppm, Sn 27.21 ppm, Te 5.84 ppm; the fossiliferous sandstone (18–19 m) records TREEY 184 ppm with modest Ag–In–Sn–Te values; and the breccia (26.08–27.08 m) reaches TREEY 305.65 ppm with elevated Sn 26.98 ppm and Te 11.30 ppm, indicating localized enrichment in fractured zones. Deeper heterolithic units (126–163 m) yield TREEY 242–269 ppm, Ag 1.36–1.79 ppm, In 3.5–4.4 ppm, and Sn 34–38 ppm, marking persistent but subdued REE enrichment at depth.

The XRF analyses complement these ICP-MS findings (Annexure by delineating the major-oxide composition and lithogeochemical variations across both boreholes. In BH-01, thirty spot core samples representing tuffite interlayers within shale reveal Fe_2O_3 contents generally below 35 wt %, with values in sandstone <33 wt %, sandstone-dominated heteroliths <33 wt %, shale-dominated heteroliths <35 wt %, and shale-sandstone heteroliths <31 wt %. Titanium concentrations (TiO_2 = 0.4-1.5 wt %) remain consistently moderate across these lithologies, coupled with intermediate Al_2O_3 and low CaO, suggesting limited carbonate contribution and a compositional dominance of volcaniclastic and ferruginous material.

In BH-02, thirty-four spot core samples analyzed from diverse lithologies show comparable but slightly broader variation. Fossiliferous sandstone records Fe_2O_3 < 26 wt %, sandstone-tuffite layers < 32 wt %, breccia < 17 wt %, sandstone dominated heteroliths-tuffite layers < 37 wt %, shale dominated heteroliths-tuffite layers < 39 wt %, and shale sandstone heteroliths-tuffite layers < 44 wt %. Across these units, TiO_2 concentrations remain below 0.8 wt %, and a marked silica enrichment is observed toward the upper ferruginous zones. The consistently high Fe–Ti content within tuffite, breccia, and ferruginous sandstone intervals mirrors the REE-enriched horizons identified through ICP-MS, confirming a strong geochemical coupling between hydrothermal alteration and oxide accumulation within the Katrol Formation.

Interpretation

The integrated ICP-MS and XRF results from both boreholes indicate that REE enrichment is stratabound and lithology-controlled, mainly restricted to phosphatic-ferruginous tuffite, breccia, and ferruginized sandstone intervals within the Katrol Formation. The close correspondence between Fe_2O_3-TiO_2 maxima and elevated TREEY values in both BH-01 and BH-02 confirms a strong geochemical link between oxide accumulation and REE concentration, governed by fluid–rock interaction within volcaniclastic horizons. Enrichment in Ba and Sr alongside high LREE/HREE ratios, positive Ce anomalies, and subdued Eu responses suggests oxidizing conditions that promoted preferential LREE mobilization and

fractionation. Brecciated and heterolithic sections acted as localized pathways for fluid movement, where structural permeability enhanced element redistribution and trapping. In contrast, deeper sandstone and shale intervals exhibit moderate but consistent REE values, reflecting diminishing fluid influence with depth. Collectively, these features define a stratabound REE-bearing horizon sequence within the Katrol Formation, where compositional variation and oxide–phosphate associations reflect multiple stages of fluid interaction and mineral concentration recorded in the two boreholes under Mineral System I.

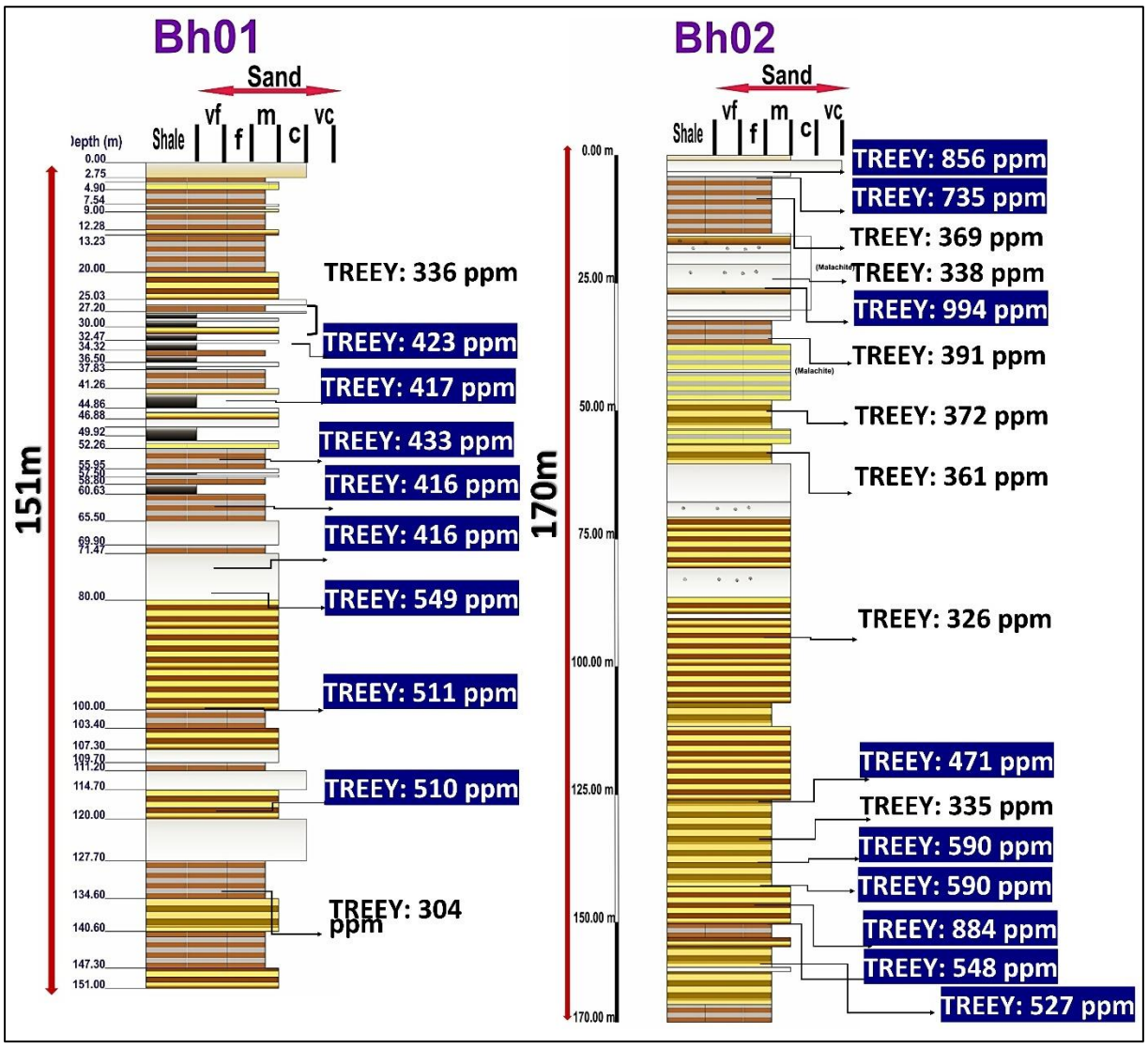

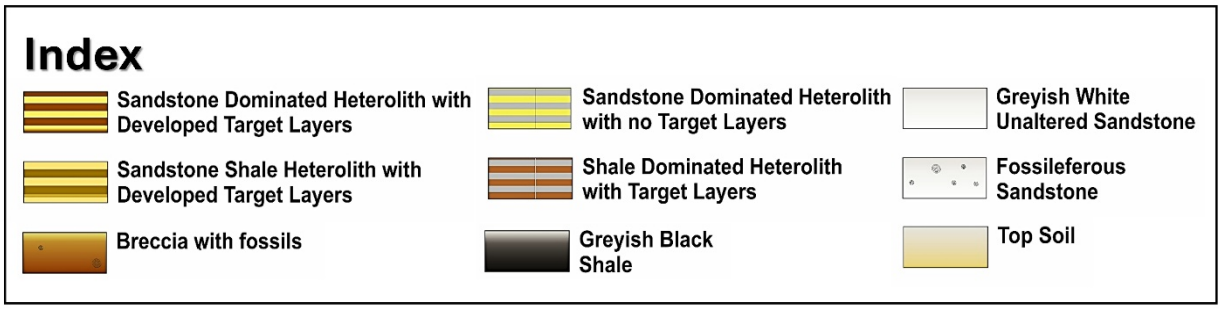

Fig. 6. 14Litholog of Borehole BH-01 and BH-02 showing vertical lithological variation, dominant lithofacies, and corresponding total REE + Y (TREEY) concentrations.

6.2.3.5. Mineralogy of ore zone

The ore zone of MSA-1 is hosted primarily by phosphatic, ferruginous tuffite interbedded with shale–sandstone heteroliths of the Katrol Formation, with subordinate mineralized breccia and ferruginized to carbonate-cemented volcaniclastic sandstone. The mineral assemblage is dominated by REE-bearing phosphates, notably very fine monazite (LREE-rich) and xenotime (HREE+Y), accompanied by abundant apatite (fluorapatite) occurring as needles, prisms, and microgranular patches within ferruginous and locally carbonate-rich laminae, as well as inclusions in framework grains. Magnetite is ubiquitous—commonly disseminated and locally replacing the matrix—with overprinting by hematite/goethite in places; pyrite (both framboidal and crystalline) is widespread, and chalcopyrite occurs as disseminations and small aggregates in intergranular sites and along microfractures. Minute, rare bright grains observed in magnetite-altered zones suggest possible native gold. Texturally, the tuffite exhibits rhythmic alternation of framework-rich and matrix-rich microlaminae with cooling cracks in pyroclastic quartz–feldspar clasts, silica overgrowths, feldspar sericitization, and zoned sparry to microcrystalline calcite cement; the glassy, ferruginous matrix is variably replaced by carbonate. Spatially, REE phosphates are closely associated with ferruginous laminae, magnetite enrichment, and disseminated sulfides (pyrite ± chalcopyrite), while brecciated and heterolithic intervals enhance concentration along fractures and lamination boundaries, defining a fine-grained oxide–phosphate–sulfide assemblage characteristic of the MSA-1 ore zone.

6.2.4. Scout Drilling in Mineralization Style II

The scout drilling program under Mineralization Style II focused on the IOCG-type hydrothermal mineralization hosted within the altered ferruginous sandstone and its metasomatic aureole of the Bhuj Formation, identified as the primary target for copper-iron mineralization with potential REE and associated pathfinder elements. Six boreholes, GSPL_Bhuj_BH03 to GSPL_Bhuj_BH08, (*Fig.6.4*) were drilled to depths ranging from 16 to 62 meters, at locations selected based on detailed surface geological mapping, inspection of highly altered ferruginous sandstone, and integration of geophysical and geochemical anomalies.

The cores recovered from these boreholes revealed consistent sequences of ferruginous sandstone interlayered with hydrothermally altered zones, containing visible sulphide mineralization, including bornite and pyrite, along with feldspar-rich metasomatic alteration. Petrographic and mineralogical assessments identified significant concentrations of REE-bearing accessory minerals, as well as sulphides and iron oxides, indicating potential zones of economically relevant IOCG-type mineralization. The data acquired provide critical subsurface

information for defining the lateral extent, vertical continuity, and grade variability of hydrothermal mineralization within the Bhuj Formation.

The boreholes GSPL_Bhuj_BH03 and GSPL_Bhuj_BH04 were drilled at an inclination of 45° with an azimuth of 170°, reaching total depths of 16 m and 51 m, respectively, approximately 4 km from Sukhapur village. Megascopic core logging was conducted to document detailed lithological variations.

Whereas boreholes GSPL_Bhuj_BH05 to GSPL_Bhuj_BH08 were drilled at a vertical angle, GSPL_Bhuj_BH05 reached a total depth of 62 m and is located approximately 2.6 km from Bharasar village. GSPL_Bhuj_BH06 attained a total depth of 48.5 m, approximately 2.8 km from Sukhapur village. Similarly, GSPL_Bhuj_BH07 and GSPL_Bhuj_BH08 reached total depths of 55 m and 50 m, respectively, and are situated approximately 4 km and 2.8 km from Samatra village

6.2.4.1. Core Logging

BH03 and BH04(*ANNEXURE-XXVII-C, D*):

GSPL_Bhuj_BH03 and GSPL_Bhuj_BH04 were drilled from the same location; however, BH03 yielded only sludge up to 16 m without any competent rock recovery. To obtain representative lithology, BH04 was drilled nearby toward the hill slope and reached a total depth of 51 m. The borehole revealed a well-defined vertical succession dominated by ferruginized sandstone, heterolithic units, and shale intercalations with progressive ferruginization and metasomatism at depth. From the surface to about 9 m, the recovered material mainly comprises yellowish-brown to pinkish ferruginized sandstone sludge containing quartz, magnetite, muscovite, and traces of feldspar, hematite, and accessory minerals like zircon and apatite, indicating incomplete consolidation and strong iron impregnation. Between 9 m and 13.5 m, alternating ferruginized sandstone and heterolithic sandstone shale layers appear, showing medium to fine-grained quartz-rich composition with dark shale laminae. From 13.5 m to 18 m, a coarse, quartz-dominant sandstone with differential ferruginization (*Fig.6.15a*) occurs, marked by boudin-like ferruginous bands and hematitic staining. The 18 m to 31 m interval displays repeated ferruginized sandstone and mica-bearing sandstone, where ferruginization follows stratification, with magnetite and iron concretions enhancing the magnetic response. Between 31 m and 39 m, alternating sandstone and shale heteroliths (*Fig.6.15c*), characterized by reddish-brown to buff coloration, ferruginous streaks, and hematite veinlets (*Fig.6.15b*). At 35.46 m, alteration of shale is observed, consisting of alternating layers of hematite and goethite (*Fig.6.15d*). Below 39 m, the succession grades into pinkish to yellowish-brown mica-bearing metasomatized sandstone (*Fig.6.15e*), displaying iron staining, clay alteration, and minor silicification. A distinct breccia zone (*Fig.6.15f*) between 45.5 m and 48 m contains angular sandstone clasts in a dark clayey matrix emitting sulphidic odour, suggesting hydrothermal influence. From 48

m downward, the section shows alternating metasomatized sandstone and thin shale bands, culminating in a highly ferruginized sandstone at 50.36-51 m, rich in hematite- magnetite and angular quartz aggregates with vesicular alteration textures.

Overall, GSPL_Bhuj_BH04 reflects a gradual transition from near-surface ferruginized sandstones to deeper metasomatized, brecciated, and hematitic units, indicating intense hydrothermal and structural overprinting along the hill-margin zone.

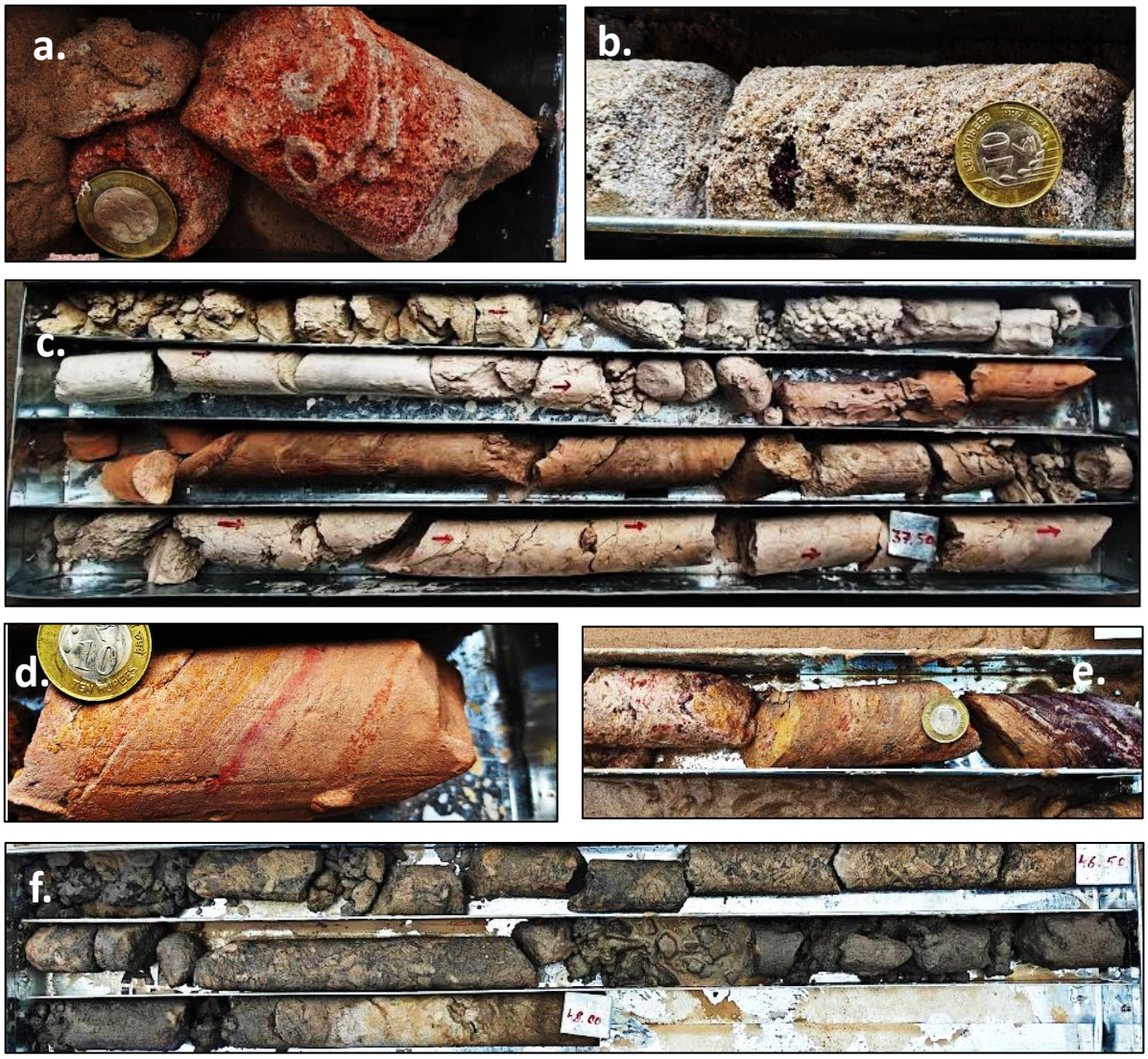

Fig. 6. 15 Megascopic photographs of core sections from Borehole GSPL_Bhuj_BH-04, showing representative sedimentary unit. (a) Sandstone with differential ferruginization at 18 m (b) Lense shaped Iron solution (Hematite) in ferruginous Sandstone at a depth of 32.20m (c) Shale Sandstone Hetrolith at 33.50 to 37.60 m (d) Alteration of Shale (alternative layer of hematite and goethite) at 35. 46m (e) Mica bearing metasomatized sandstone at 44.10 to 44.50 (f) Breccia unit at 45.50 to 48 m.

BH-05 (*ANNEXURE-XXVII-E*):

Borehole GSPL_Bhuj_BH05 was drilled to a total depth of 62 m and intersected a continuous sequence of ferruginized and metasomatized sandstones with local heterolithic and brecciated intervals toward the base. From surface to about 8 m, the sequence comprises highly ferruginized to mica-bearing ferruginized sandstone, brownish-yellow to dark brown in colour, medium to coarse grained, and composed of quartz, muscovite, hematite, and magnetite with occasional colourless platy crystals. The upper metre includes a hard ferruginous core cemented by hematite magnetite, followed by poorly sorted ferruginous sand with variable magnetite impregnation. Between 8 m and 19 m, sandstone with differential ferruginization dominates, yellowish-white to pinkish-white, coarse to fine grained, with sub-angular to rounded quartz grains and patchy hematitic staining. The 19-27 m interval contains reddish-brown ferruginious sandstone with bimodal grain size, coarse quartz clasts in clayey cement, and highly magnetic bands near 25-26 m (*Fig.6.16a* and *Fig.6.16b*). indicating strong iron fluid interaction. From 27 m to 34 m, alternating mica-bearing and ferruginious sandstones occur, medium to fine grained and moderately sorted, composed of quartz, hematite, magnetite, muscovite, and ferruginous rock fragments showing yellow-brown variegation. Between 34 m and 40.15 m, the core is yellowish-brown ferruginized sandstone, fine to medium grained, moderately to well sorted, with pervasive red hematitic staining and disseminated magnetite. From 40.15 m to 47.75 m, sandstone with differential ferruginization (*Fig.6.16c*) alternates with mica-bearing metasomatized sandstone, the former being grey to pinkish-white with ferruginous veinlets and shale clasts showing argillic alteration (*Fig.6.16d*), and the latter displaying silicification and iron impregnation in reddish to yellowish-brown bands. Between 47.75 m and 58.9 m, fine-grained sandstone transitions into sandstone-dominated heterolith with greyish-white, well-sorted sandstone bands alternating with dark-grey to black shale laminae containing Mn mineiral (*Fig.6.16e*) and also shale emits a faint gunpowder-like odor, indicating possible sulphidic content *(Fig.6.16f*). The lowermost part from 58.9 m to 62 m consists of grey breccia *(Fig.6.16g*) with angular to sub-angular shale and silicified sandstone clasts embedded in a clayey quartz matrix, showing hematitic staining at several levels and occasional pyrite.

Overall, GSPL_Bhuj_BH05 shows a gradual transition from near-surface ferruginized sandstone to deeper metasomatized and brecciated zones, reflecting progressive ferruginization, silicification, and hydrothermal alteration along structurally controlled fluid pathways.

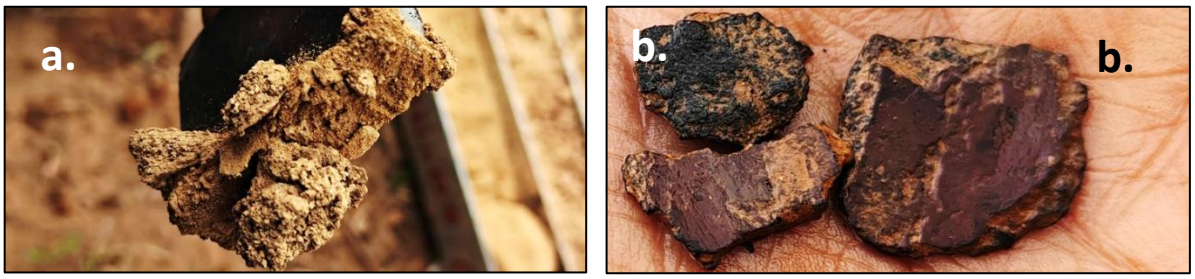

Fig. 6. 16 Megascopic photographs of core sections from Borehole GSPL_Bhuj_BH-05, showing representative sedimentary unit (a) Magnetite observed at 25-26 m within Sludge of yellowish brown coloured ferruginized sandstone (b) Magnetite grains (c) Sandstone with differential ferruginization at 40.34m (d) contact between the argilic to ferruginous alteration at 40.68m (e) Milimeter to cm scale thin, jet black materials the shale, Mn mineral?? (black streak, feebly magnetic) at 55.38m (f) Dark grey shale interbedded with fine-grained sandstone at 55.75 m depth. The shale emits a faint gunpowder-like odor, indicating possible sulphidic content (g) Breccia at 59.32 m.

BH-06 (*ANNEXURE-XXVII-F*):

Borehole GSPL_Bhuj_BH06 was drilled to a total depth of 48.5 m to document the ferruginous and mica-bearing sandstone succession of the Bhuj Formation and evaluate its sedimentological and mineralogical variations. The uppermost zone (0.00-1.90 m) comprises ferruginized breccia (*Fig.6.17a*), reflecting intense near-surface weathering and mechanical disruption with secondary hematite/goethite cementation. From 1.90-13.50 m, fine to medium grained sandstone predominates; the units are generally massive to faintly

laminated, moderately ferruginized and composed mainly of subrounded to subangular quartz with minor feldspar and sparse muscovite flakes. Iron impregnation occurs as thin veinlets cross-cutting the sandstone between 3.2 m, composed of quartz and hematite (white streak) with minor non-magnetic black minerals (*Fig.6.17b*). Between 13.50 and 17.50 m, the core exhibits mica bearing metasomatized sandstone showing abrupt ferruginization that forms zoned alteration patterns. Grain size decreases with depth. At 15.63 m, secondary variegated alteration occurs along thin veinlets, with pyrite present in groove areas (blue material producing a blue streak) (*Fig. 6.17d*). The zone shows pronounced muscovite enrichment, and subtle alteration textures along fractures suggest limited post-depositional fluid activity. A thin reddish white to greyish white shale (*Fig. 6.17e*) intercalation at 17.50-18.46 m records a brief low energy depositional event separating stacked sandstone packages. From 18.46-37.00 m the succession alternates between differentially ferruginized sandstones (*Fig. 6.17c*) and mica-rich sandstone bands (notably 21.50-25.00 m and 27.94-30.18 m), with iron staining ranging from reddish-brown to yellowish-brown and fine disseminated hematite coatings. The interval 37.00-48.50 m continues these trends with repeated unaltered sandstone units (*Fig. 6.17f*) and also showing differential ferruginization with localized muscovite concentration (e.g., 39.50-41.23 m), and the lowermost section exhibits stronger iron impregnation and compaction features. Sedimentary structures are generally subdued-faint planar lamination, subtle bedding changes and minor bedding plane partings occur-indicating dominantly quiet depositional conditions with episodic reworking.

Overall, GSPL_Bhuj_BH06 records a cyclic ferruginous sandstone succession punctuated by minor shale partings and discrete metasomatic mica enrichment, consistent with a transitional fluvial-to-continental shallow depositional regime influenced by diagenetic iron enrichment.

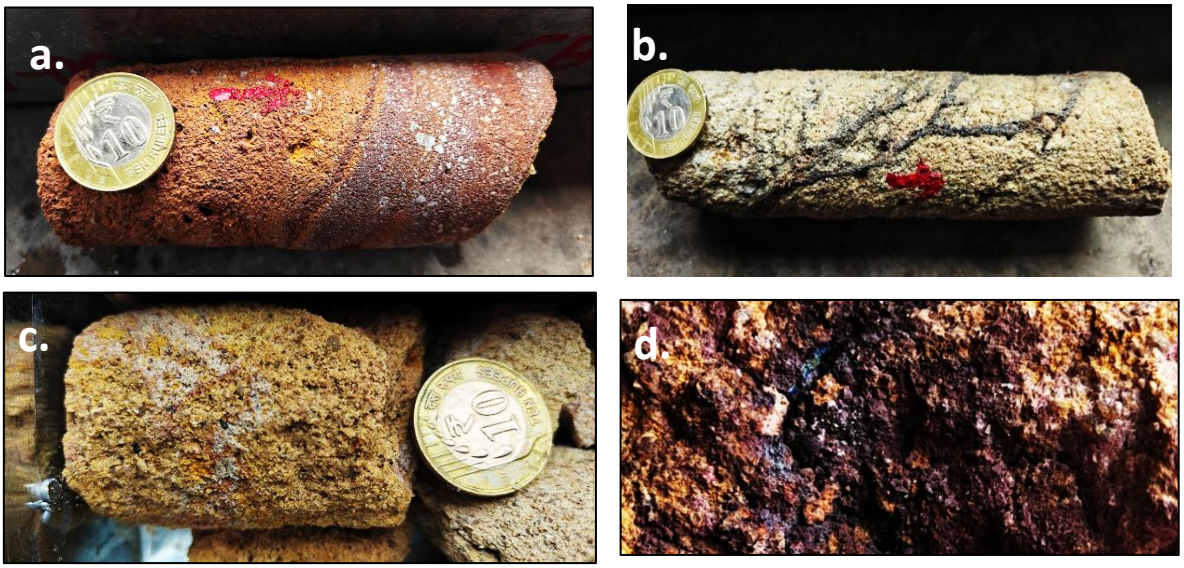

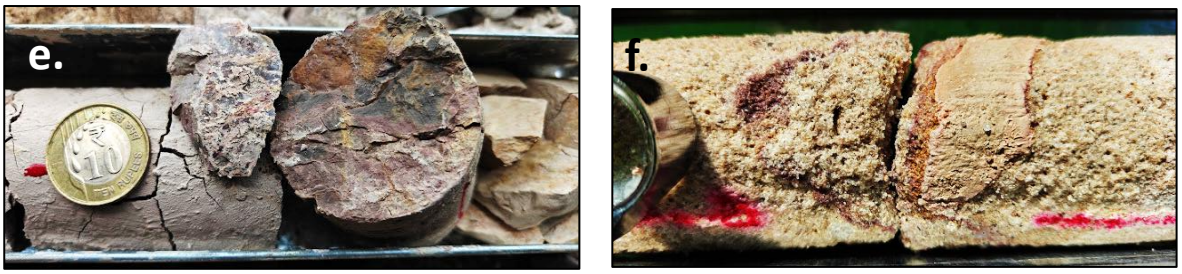

Fig. 6. 17 Megascopic photographs of core sections from Borehole GSPL_Bhuj_BH-06, showing representative sedimentary unit (a) Ferruginized breccia at 1.8 m (b) Iron impregnation as thin veinlets cross-cutting sandstone, composed of quartz and hematite (white streak) with minor non-magnetic black minerals at 3.2m (c) Ferruginous Sandstone at 19 m (d) Mica-bearing metasomatized sandstone showing abrupt ferrugination forming zoned alteration; grain size decreases with depth. At 15.63 m, secondary variegated alteration occurs along thin veinlets with pyrite in groove areas (blue material gives blue streak). (e) Reddish white to greyish white shale at 17.85 (f) Unaltered sandstone at 47.45 m containing clay clasts and lapilli fragments.

BH-07 (*ANNEXURE-XXVII-G*):

BH07 was drilled to a total depth of 55 m and exhibits a well-defined vertical succession dominated by ferruginized and metasomatized sandstones, alternating ferruginous mica bearing units, and occasional loose sediment at the top. From 0 to 1 m, the borehole penetrates brownish-yellow loose sand representing Quaternary alluvium, composed mainly of quartz with minor magnetite and rock fragments. Between 1 and 2.17 m, a highly ferruginized metasomatized sandstone (*Fig.6.18a*) occurs, reddish-brown to black in colour, coarse to fine grained, composed of quartz, hematite, magnetite, alkali feldspar, muscovite, and bluish quartz aggregates set in a hematite/magnetite groundmass. Euhedral feldspars and occasional native copper or malachite staining (*Fig.6.18b*) are observed. From 2.17 to 5.3 m, fine grained sandstone with differential ferruginization is recorded, pinkish-white to yellowish-white, moderately to well sorted, with hematite staining and magnetite at quartz grain grooves. Between 5.3 and 5.85 m, a thin band of highly ferruginized metasomatized sandstone reappears, similar in composition but with reduced feldspar and alternating coarse to fine layers. The interval from 5.85 to 8 m comprises mica-bearing ferruginized sandstone (*Fig.6.18c*), reddish to yellowish brown, medium to coarse grained, well sorted with ferruginization and biotite rich laminae, accompanied by local silicification. From 8 to 16.3 m, yellowish to white ferruginized sandstones and sludges occur, showing variable ferruginization and iron staining. The sequence alternates between yellowish-brown ferruginized sandstone (8-12.5 m), white fine grained ferruginized sandstone (12.5-15.7 m), and a thin mica-bearing ferruginized sandstone band (15.7-16.3 m) with cross stratification and greenish malachite stains. Between 16.3 and 24 m, fine to medium grained sandstone with differential ferruginization dominates, poorly sorted, containing quartz, hematite, and minor magnetite

with pinkish-red to brown iron staining. From 24 to 28.4 m, alternating ferruginous sandstone (*Fig.6.18d*) and mica bearing metasomatized sandstone (*Fig.6.18e*) occur, showing strong ferruginization, metasomatic biotite, and silicification, along with yellowish-brown ferruginized sludge at the top. Between 28.4 and 31.5 m, ferruginized sandstone predominates, reddish- to blackish-brown, moderately sorted, with angular quartz, hematite, and magnetite; thin silicified laminae and minor mica are observed. From 31.5 to 39 m, moderately to well sorted fine-grained sandstone occurs with differential ferruginization, containing stained quartz, altered feldspar, muscovite, hematite, and magnetite, showing pinkish-red ferruginous hues in up to 40% of quartz grains. The lowermost section, 39 to 55 m, consists of sludge of yellowish-brown to dark-brown ferruginized sandstone, coarse to fine grained, poorly sorted, with quartz, hematite, altered feldspar, magnetite, and ferruginous rock fragments (*Fig.6.18f*). Magnetite content increases gradually from 39 to 45 m, peaks in the middle zone, and then decreases slightly with depth, while grain size increases from medium to coarse toward 52.5 m.

Overall, GSPL_Bhuj_BH07 shows a progressive transition from near surface loose sand and highly ferruginized metasomatized sandstone to deeper ferruginized quartzose sandstone, reflecting cyclic ferruginization, metasomatism, and localized silicification under hydrothermal and supergene influences.

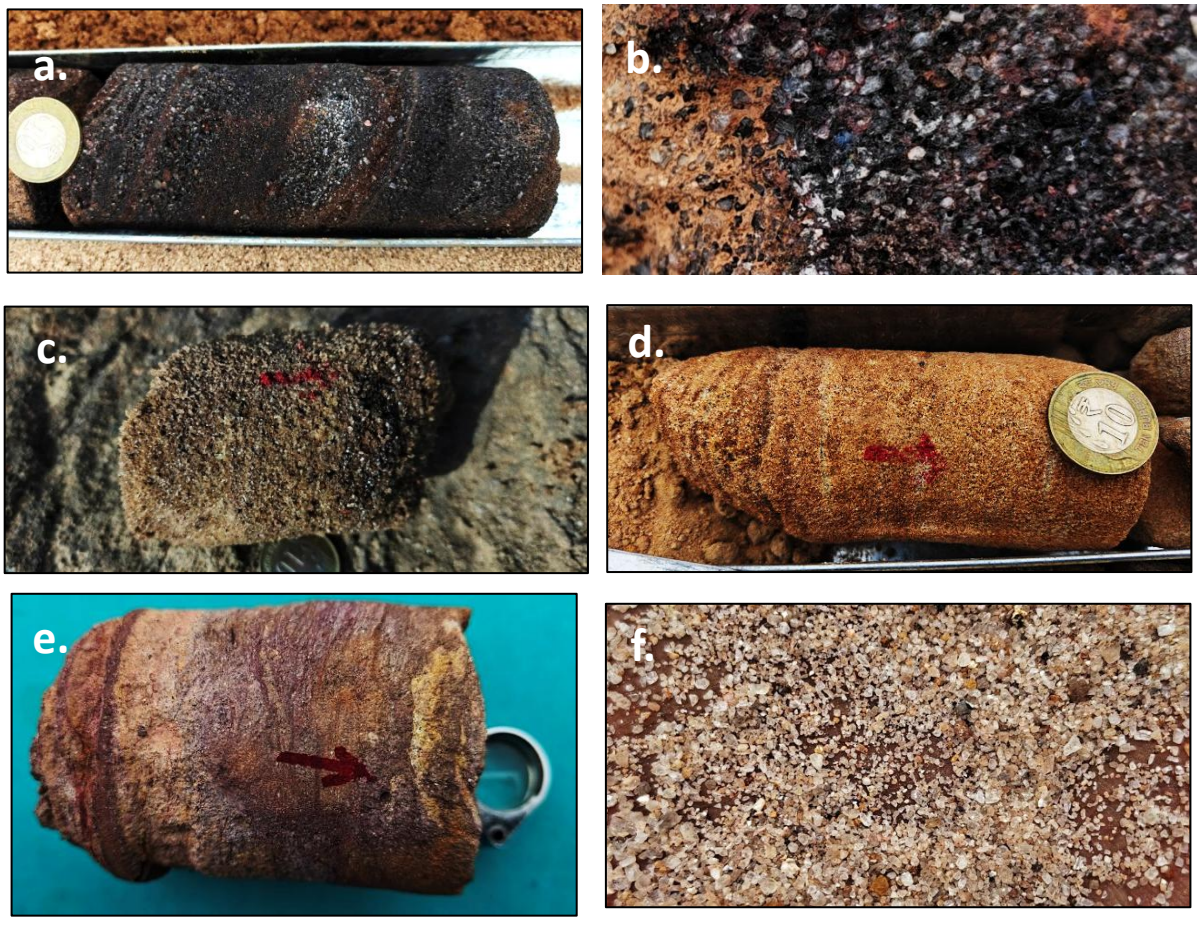

Fig. 6. 18 Megascopic photographs of core sections from Borehole GSPL_Bhuj_BH-07,

showing representative sedimentary unit : (a) Highly ferruginized metasomatized sandstone at 1.2m (b) Highly ferruginized metasomatized sandstone with Cu staining at 1.35m (c) Mica bearing ferruginized sandstone at 6.07m (d) Ferruginous sandstone at 24.5m (e) Alternating ferruginous sandstone and mica bearing metasomatized sandstone at 28m (f) Poorly sorted sludge with angular to subrounded grains, dominated by quartz, sandstone fragments, altered feldspar, hematite, and magnetite (magnetite rich) at 41 to 42m

BH-08 (*ANNEXURE-XXVII-H*):

BH08 was drilled to a total depth of 50 m and reveals a distinctly ferruginized and metasomatized sequence with alternating sandstone, shale-sandstone heteroliths, and variable ferruginization intensity throughout. From 0 to 4.5 m, the succession comprises yellowish-brown to pinkish ferruginized sandstone sludge with subordinate mica bearing units. The uppermost 0.63 m includes mica bearing ferruginized sandstone, medium to fine grained, moderately sorted, quartz dominant, and rich in ferruginous cement with minor muscovite and magnetite. Between 0.63 m and 3 m, yellowish-brown ferruginized sandstone (*Fig.6.19a*) occurs, fine to coarse grained, moderately sorted, containing quartz, hematite, and rare altered rock fragments with clay bonding. From 4.5 to 9.5 m, the section alternates between mica-bearing ferruginized sandstone (*Fig.6.19b*) and ferruginized sludge, showing variable grain size, hematitic staining, and localized silicification. The sandstone exhibits lamination, biotite enrichment, and ferruginization in shades from yellow ochre to purple and black. Between 9.5 and 16.5 m, the unit becomes progressively more altered and metasomatized, with mica bearing and metasomatized sandstone (*Fig.6.19c*) interbeds containing quartz (97-98%) with 1-2% muscovite and biotite, ripple and planar lamination, and increasing ferruginization and mica content downward. At 11.7m pothole like pores in metasomatized shale sandstone filled with clay and or hematite; cement of hematite with minor magnetite (*Fig.6.19d*) were observed. From 12.4 to 21.2 m, the sequence evolves into shale sandstone heteroliths (*Fig.6.19e*), alternating ferruginous sandstone and shale/siltstone bands. The sandstone is hematitic and mediumto fine grained, while the shale layers are grey, laminated, and locally brecciated (*Fig.6.19f*) with in-situ magnetite clasts at 17 m depth. Between 21.2 and 33 m, sandstone and ferruginized sludge dominate, comprising quartz (97-98%), white transparent crystals, and minor hematite and magnetite, with ferruginous staining from pink to yellowish red. Magnetite content increases notably between 29 m and 30 m. The interval from 33 to 42.5 m is primarily yellowish-brown ferruginized sandstone sludge, moderately sorted with fine hematite and biotite inclusions, while the 42.5-43.9 m section includes a thin metasomatized shale-sandstone heterolith showing hematitic veinlets and laminated shale bands. Below 43.9 m, ferruginized sandstone reappears, medium to coarse grained, with pinkish to yellow iron-stained quartz and subordinate altered feldspar and hematite. The final 47-50 m interval consists of mica bearing metasomatized sandstone, coarse-grained and poorly sorted, brownish red to blackish brown in colour, with quartz

embedded in a ferruginous clayey matrix, traces of muscovite and biotite, and local silicification and lapilli-like clasts.

Overall, GSPL_Bhuj_BH08 shows a stratigraphic progression from near surface ferruginized sandstone through alternating ferruginous and metasomatized zones to deeper clay bound metasomatic sandstone and shale heteroliths, indicating recurrent ferruginization, silicification, and fluid alteration along structurally active zones.

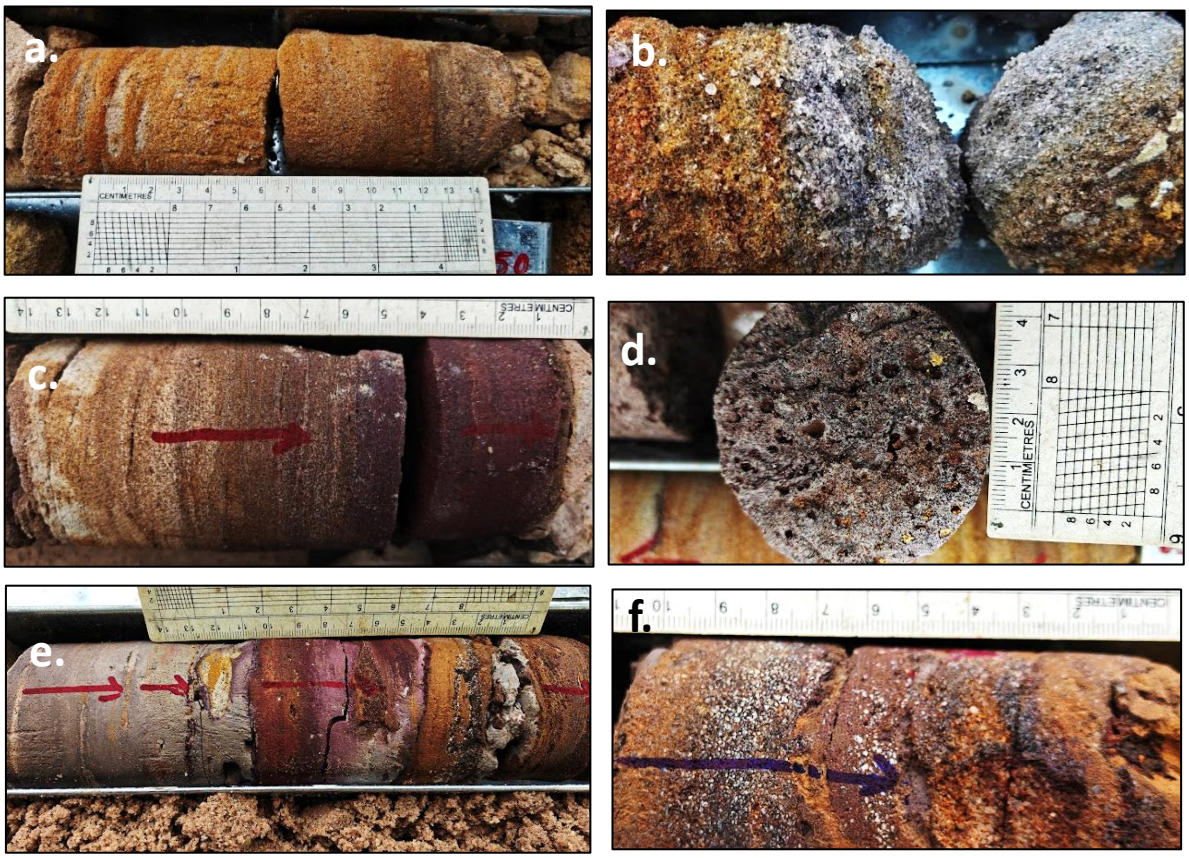

Fig. 6. 19 Megascopic photographs of core sections from Borehole GSPL_Bhuj_BH-08, showing representative sedimentary unit: (a) Ferruginized sandstone (b) Mica bearing ferruginized sandstone at 6.6m (c) Mica bearing metasomatized sandstone at 10.36m (d) Pothole like pores in metasomatized shale sandstone filled with clay and or hematite; cement of hematite with minor magnetite at 11.7m (e) Metasomatized shale sandstone hetrolith at 20.5m (f) Sandstone shows increased grain size and possible in-situ brecciation, with quartz clusters enclosed by magnetite forming breccia like texture at 17.09 m.

6.2.4.2. Sampling and Sample Preparation

Representative core and surface samples were selectively collected from stratigraphic intervals showing ferruginization, brecciation, and oxide, sulfide mineralization characteristic of the MSA-II system. Sampling strategy was designed to include both mineralized and relatively barren zones to assess vertical and lateral variability in mineral composition and grade. Wherever solid core recovery was incomplete or absent, sludge samples were carefully

collected from drill cuttings to ensure continuous lithological representation of the mineralized profile. Each sample interval was systematically logged, labelled, and photographed prior to collection. Core sections were longitudinally split, with one half preserved as a permanent reference and the other processed for analytical studies. All samples were subsequently dried, crushed, pulverized, and homogenized to achieve uniform grain size suitable for chemical and mineralogical analyses. Throughout the process, strict chain-of-custody protocols were maintained to ensure sample integrity and traceability. The prepared sample suite formed the analytical foundation for geochemical assays, petrographic examination, and mineralogical characterization, facilitating an accurate delineation of the distribution, intensity, and compositional attributes of mineralization associated with Mineralization Style II (MSA-II).

6.2.4.3. Petrographic Studies

Five boreholes (BH-03 to BH-08) were drilled to characterize the second Mineral System in Bhuj Block. The petrographic details are summarized in *Annexure-XXVIII*.

BH-03:

In borehole 3 only sludge sample is recovered. The entire borehole section is represented by loose, medium- to coarse-grained, quartz-dominated sand, showing variable colour from yellowish-white to white, and locally showing magnetic character. From 0 m to 2 m, the sediment comprises yellowish-white loose sand, medium- to coarse-grained, angular to sub-angular, and poorly sorted, with high grain sphericity. It is composed mainly of quartz, with minor white minerals (carbonates/feldspars), muscovite, and magnetite. Between 2 m to 4 m, the interval consists of white loose sand, medium- to coarse-grained, angular to sub-angular, and poorly sorted, showing high sphericity. The sand is primarily quartz and muscovite, with minor white minerals (carbonates/feldspars) and occasional iron concretions. From 4 m to 8 m, the lithology remains white loose sand, medium- to coarse-grained, poorly sorted, and highly spherical, composed of quartz, muscovite, and white minerals, with sporadic iron concretions. Between 8 m and 12 m, the sediment changes to yellowish loose sand, medium- to coarse-grained, angular to sub-angular, and poorly sorted. It is mainly composed of quartz and a white milky mineral (likely milky quartz), as no effervescence was observed with dilute HCL. The material is magnetic, containing highly spherical grains.From 12 m to 14 m, the interval comprises white loose sand, medium- to very fine-grained, sub-angular, and moderately sorted. It is composed chiefly of quartz, muscovite, and milky quartz, with occasional transparent needle-shaped minerals and magnetic grains showing high sphericity. From 14 m to 16 m, the sand is yellowish, loose, and medium- to coarse-grained, with sub-angular, poorly sorted grains of high sphericity. The composition includes quartz, muscovite, and milky quartz, along with minor clay material and occasional black mineral grains (likely magnetite).

Overall, BH03 reveals a loose, unconsolidated, quartz-rich sandy sequence, consisting of angular to sub-angular grains of high sphericity with variable amounts of muscovite, milky quartz, and magnetite. Beside magnetite, no other minerals like apatite, sulfides could be identified in hand specimen

BH04 (*Fig.6.20*):

Borehole BH04 was drilled through the Bhuj Sandstone unit and attained a total depth of 51 m.

i. Sandstone:

The entire borehole section is represented by an interlayered sequence of ferruginous sandstones, varying from highly ferruginous to slightly ferruginous types. From 0 m to 12 m, the rock is a highly ferruginous sandstone, fine- to medium-grained and reddish-brown in color, showing strong iron oxide impregnation within the matrix. Between 12 m and 15 m, the sandstone grades into a feldspar-bearing quartz arenite to arkose, where small carbonate pellets occur within the arenitic matrix. Feldspar, mainly albitic plagioclase, is partially altered to sericite and clay, and minor sulfide traces begin to appear, indicating the onset of mineralization.

From 15 m to 25 m, the rock becomes a lithic arenite containing large tuffitic fragments derived from the Katrol Formation, set in a quartz-rich arenitic matrix. This horizon marks the beginning of the ore zone, as iron-rich fluids have altered the original sandstone composition, replacing the matrix and forming authigenic albitic plagioclase, muscovite, iron oxides/hydroxides, and sulfide phases. Between 25 m and 38 m, the sandstone remains ferruginous and arkosic, composed of subrounded to subangular quartz and feldspar grains with muscovite flakes showing flowage patterns. Matrix is dominated by ferruginous material.

In the deeper section, from 38 m to 51 m, the rock transitions into a slightly ferruginous sandstone with a fine-grained clayey matrix largely replaced by ferruginous material. The main ore-bearing zone characterized by intense ferruginization, sulfide mineralization, and minor gold. Overall, BH04 reveals a ferruginized Bhuj Sandstone sequence where iron-rich hydrothermal fluids have significantly modified the original arenitic composition, leading to development of pyrite, magnetite, goethite, and associated gold mineralization.

Magnetite, goethite, apatite, monazite, xenotime, gold and sulfide mineralization: The matrix is dominantly ferruginous, containing goethite and scattered magnetite, along with abundant pyrite (commonly framboidal), chalcopyrite, covellite, monazite, apatite and specks of native gold. In general, magnetite as well as goethite occurs in all the sandstone at different depth. Chalcopyrite is found in the rocks at 12-12.07m depth. Covellite is found in sandstone

unit at 35.47 to 35.52m and 50.37 to 50.44m depth. Xenotime, gold and sphalerite are found at 15.99 to 16.05m depth. Both monazite and apatite are found at 35.47 to 35.52m.

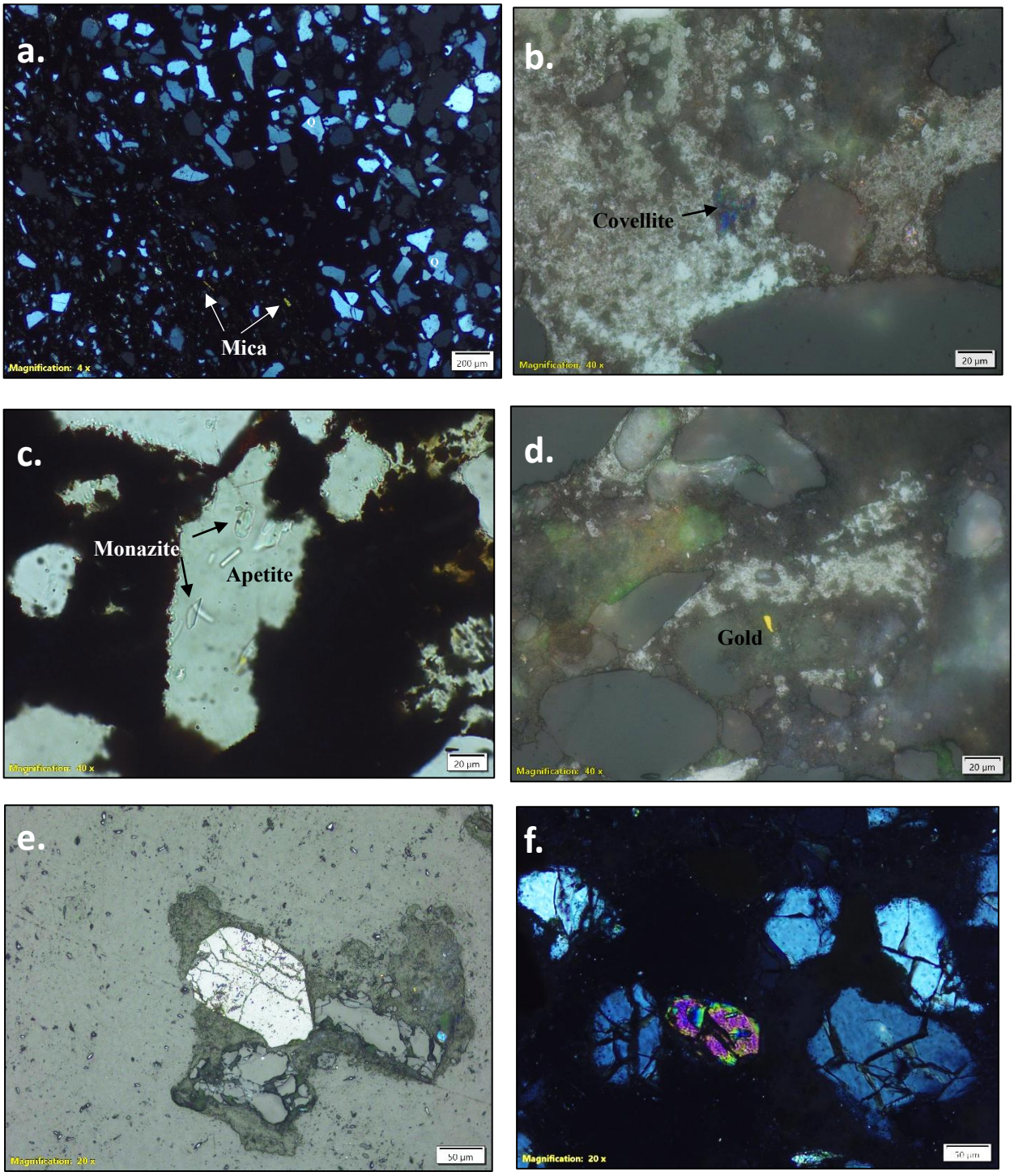

Fig. 6. 20 Representative photomicrographs of sandstone from Borehole BH-04, Bhuj Formation. (a) Interlayered sandstone showing a clast-rich bed alternating with a finer matrix-supported layer. (b) Covellite grains in the matrix partially replaced by iron oxides. (c) Apatite and monazite inclusions within a quartz grain. (d) Minute specks of native gold disseminated within the

sandstone matrix. (e) Magnetite and bornite grains dispersed within the ferruginous matrix. (f) Xenotime crystals occurring as isolated grains within the matrix.

BH05 (*Fig.6.21*):

Borehole BH05 was drilled to a total depth of 62 m, intersecting a sequence dominated by fine- to medium-grained sandstone interlayered with thin tuffite bands.

The lithological sequence reveals alternating sandstone and tuffite layers at specific depths — sandstone occurs between 50.58–50.63 m and 56.06–56.67 m, while tuffite layers are present at 52.43–52.53 m, 58.37–58.90 m, and 59.04–59.10 m.

Petrographic studies were carried out on representative samples from 50 m to 60 m, covering both sandstone and tuffite horizons.

i. Sandstone: The sandstone units are fine- to medium-grained and composed mainly of quartz, feldspar, and mica as detrital constituents. The grains are subangular to subrounded, showing moderate sorting and localized in-situ fracturing, indicating minor post-depositional deformation likely related to compaction. Quartz grains dominate and commonly show undulatory extinction, while feldspar grains (chiefly plagioclase) are subhedral and partly altered to sericite and clay minerals. Muscovite and biotite flakes occur as detrital components, some displaying weak flowage or alignment within the fine-grained matrix.

ii. Tuffite: The tuffite layers are fine-grained, exhibiting a mixed clastic and pyroclastic texture, composed of volcanic ash material admixed with quartz and feldspar fragments. These tuffite interbeds show higher ferruginization and often host opaque minerals in greater abundance than the sandstone beds. The overall matrix within this interval is dark-colored and ferruginous, composed mainly of iron oxide with traces of carbonaceous matter, imparting a reddish-brown to dark-brown color under transmitted light. The carbonaceous component suggests deposition under locally reducing conditions.

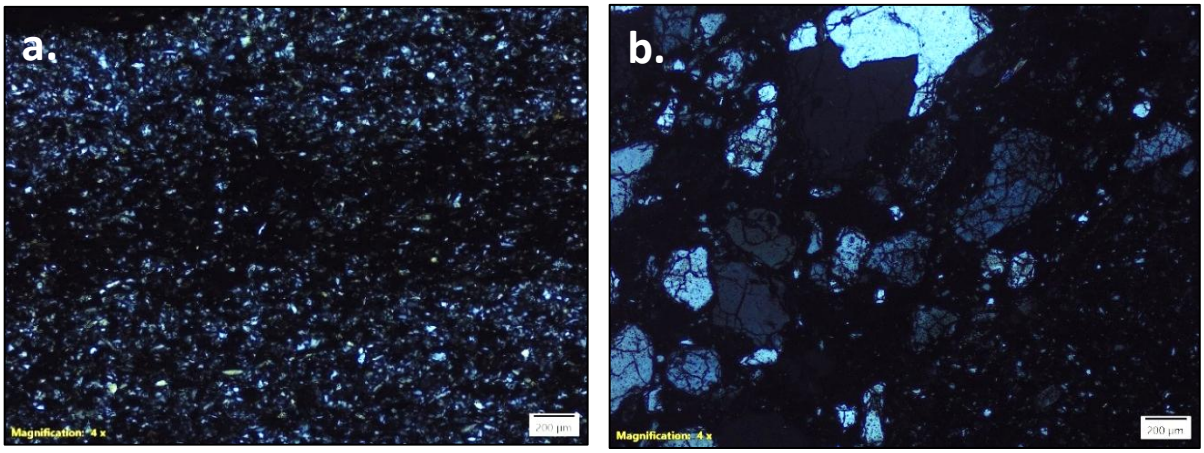

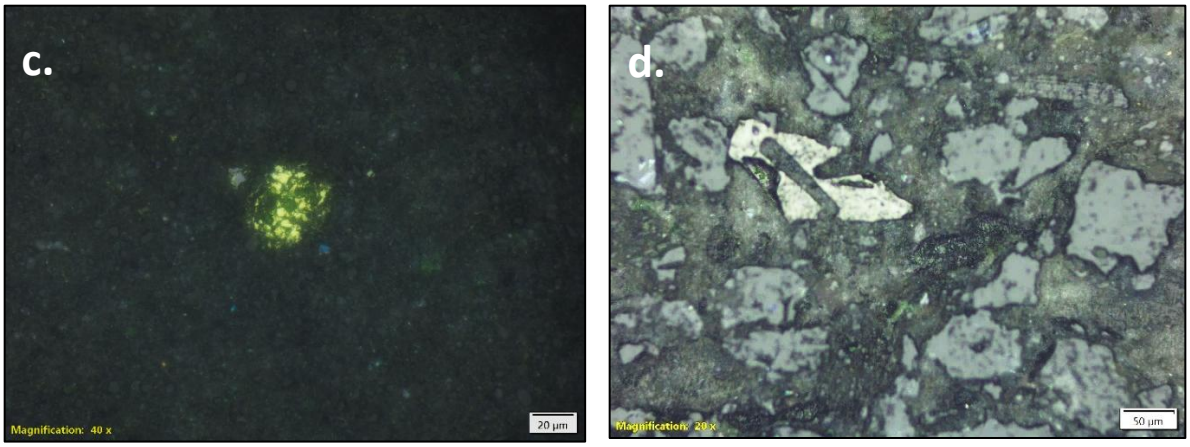

Fig. 6. 21 Representative photomicrographs of tuffite and sandstone from Borehole BH-05, Bhuj Formation. (a) Fine-grained tuffite showing crudely-developed lamination. (b) Medium- to coarse-grained sandstone with subangular framework grains. Note that the grains are fragmented. (c) Chalcopyrite and bornite disseminated within the matrix. (d) Pyrrhotite grain occurring within the ferruginous matrix.

A notable feature is the presence of amphibole, appearing as elongated prismatic grains, which indicates a hydrothermal overprint associated with iron-rich post-depositional fluids.

Overall, the 50–60 m interval of BH05 represents a ferruginous fine- to medium-grained quartz arenitic to subarkosic sandstone interbedded with tuffite, showing evidence of diagenetic alteration, iron oxide impregnation, and localized mineralization. The ore-bearing zones are associated primarily with the tuffite and ferruginized sandstone layers between 50.5 m and 59.1 m, where the ore mineral assemblage includes magnetite, pyrite, sphalerite, and accessory hematite, with ortho-amphibole marking hydrothermal fluid influence. These observations suggest that iron-rich hydrothermal fluids played a key role in facilitating mineral growth, matrix alteration, and localized sulfide mineralization within this depth zone.

Magnetite/hematite and sulfides: In reflected light, the section contains abundant opaque minerals, including magnetite, pyrite, chalcopyrite, and bornite, occurring as disseminated grains and interstitial clusters. Pyrite is common in both euhedral and framboidal forms, while magnetite appears as coarse, irregular grains, occasionally altered along margins to hematite. Chalcopyrite and bornite occur as minor inclusions within the ferruginous matrix, often associated with pyrite and magnetite. Oxides in the form of hematite and magnetite and pyrite are found in almost all the samples of different depth. Pyrrhotite is found at 52.43 to 52.53m, Chalcopyrite and bornite 59.04 to 59.10m, sphalerite is found at 50.58 to 50.63 m depth.

BH06 (*Fig.6.22*):

Borehole BH06 was drilled to a total depth of 48.5 m, intersecting a sequence dominated

by medium-grained sandstone.

i. Sandstone: Petrographic examination was carried out on representative thin sections from 20 m to 35 m depth, revealing a section composed predominantly of medium-grained subarkose to quartz arenitic sandstone. The sandstone is chiefly composed of quartz, feldspar, and muscovite as major clastic components, with subordinate lithic fragments and ferruginous material.

Within this interval, distinct lithological variations were observed: a ferruginous sandstone band occurs between 22.91–22.95 m, while altered sandstone horizons are recorded at 29.69–29.79 m, 29.80–29.85 m, and 30.05–30.15 m. These zones display higher degrees of oxidation and matrix replacement, corresponding to localized fluid alteration and iron enrichment.

The quartz grains are generally subrounded to subangular, moderately sorted, and show occasional fracturing and fragmentation, suggesting limited transport and subsequent compactional and diagenetic stress. Some grains exhibit undulatory extinction, indicative of strain during diagenesis. Feldspar grains, mainly plagioclase, occur as subhedral to anhedral tabular crystals, locally altered to sericite and clay minerals. Muscovite flakes are common as detrital constituents and frequently show partial alteration to sericite, especially along cleavage planes, reflecting low-grade diagenetic alteration.

The matrix is fine-grained, comprising clayey and ferruginous material, which cements the framework grains and imparts a reddish-brown tint in ferruginized intervals. Occasional lithic fragments of fine-grained sedimentary and volcanic rocks contribute to the arenitic texture, suggesting a mixed sedimentary-volcaniclastic provenance.

Overall, the 20–35 m interval of BH06 represents a medium-grained, moderately sorted subarkose to quartz arenite, with minor feldspar, muscovite, and lithic fragments. The rock records diagenetic alteration (muscovite to sericite, minor ferruginization) and disseminated sulfide–oxide mineralization (pyrite and magnetite). The presence of ferruginous and altered sandstone layers at specific depths (22.91–22.95 m and 29.69–30.15 m) reflects zones of post-depositional fluid activity and iron enrichment, suggesting episodic hydrothermal alteration superimposed on a moderate-energy depositional environment.

Magnetite/ hematite and pyrite: In reflected light, the rock contains disseminated opaque minerals, chiefly pyrite and magnetite, distributed within the matrix and along grain boundaries. Pyrite occurs as euhedral to subhedral grains, sometimes forming small aggregates, while magnetite appears as irregular anhedral grains, locally showing hematitic alteration rims. The altered sandstone layers between 29.69–30.15 m exhibit slightly higher concentrations of these opaque phases, implying localized hydrothermal or iron-rich fluid influence.Magnetite/ hematite is found in almost all the samples but pyriote is found in the

samples at 22.91 to 22.95 m depth.

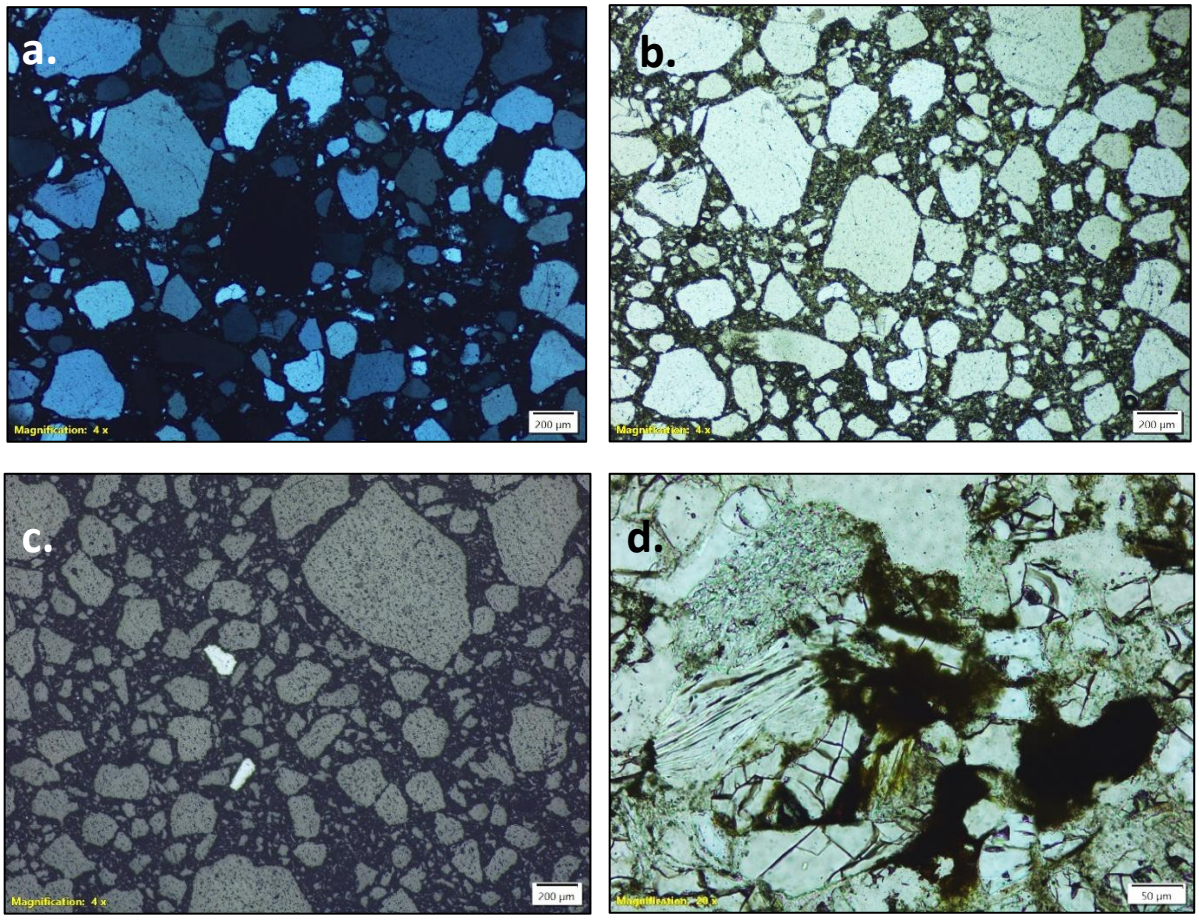

Fig. 6. 22 Representative photomicrographs of sandstone from Borehole BH-06, Bhuj Formation. (a) Bimodal size distribution of quartz grains in sandstone under crossed polarised light. (b) Coarse to medium grained sandstone with bimodal size distribution under plane polarised. Note the angular, irregular shape of the clasts. (c) Magnetite grain occurring within the matrix. (d) In-situ fracturing of quartz grains within the sandstone framework.

BH07 (*Fig.6.23*):

BH07 was drilled to a total depth of 55 m, intersecting a sequence belonging to the Bhuj Formation. Petrographic studies were conducted on representative samples from the interval between 2 m and 31 m depth. The examined section is composed mainly of medium- to coarse-grained sandstone, which is quartzo-feldspathic in composition. The rock consists predominantly of quartz, feldspar, and muscovite as the principal clastic constituents. The quartz grains are angular to subrounded, moderately sorted, and often exhibit undulatory extinction and straight to sutured grain contacts, indicating moderate compaction and recrystallization during diagenesis. Feldspar occurs as subhedral to tabular grains, primarily plagioclase, with minor alteration to clay minerals or sericite along cleavage planes. Muscovite flakes are present as detrital constituents, generally aligned parallel to the bedding, suggesting

mild compaction reorientation within the sediment.

The matrix is iron oxide-rich, giving the sandstone a distinct ferruginous appearance. The ferruginous material fills pore spaces and partially replaces the original clayey matrix, indicating the influence of iron-rich fluids. The iron oxide, likely hematite and goethite, imparts a reddish-brown coloration to the thin sections and is often associated with minor alteration along grain boundaries.

Overall, the 2-31 m interval of BH07 represents a ferruginous, medium- to coarse-grained subarkose to quartz arenitic sandstone of the Bhuj Formation, characterized by angular to subrounded detrital quartz grains, iron oxide-rich matrix, and disseminated magnetite. The petrographic features indicate a moderate- to high-energy depositional environment followed by iron oxide impregnation in post depositional stage.

Magnetite: In reflected light, magnetite is present as opaque, subhedral grains disseminated within the matrix and occasionally intergrown with ferruginous material. The distribution of magnetite suggests that iron enrichment was a significant post-depositional process. Only limited samples swere studied under reflected light which shows magnetite is prevalent phase in all the samples

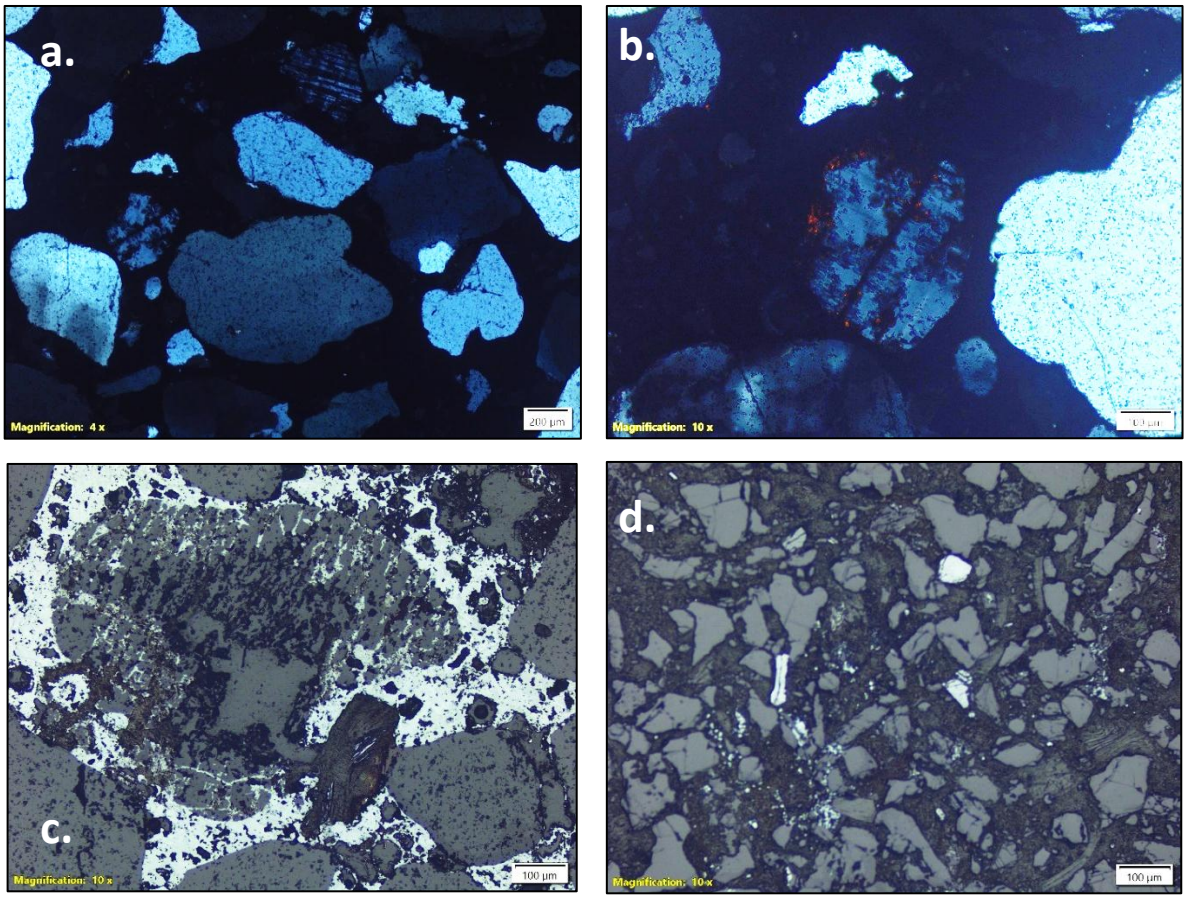

Fig. 6. 23 Representative photomicrographs of sandstone from Borehole BH-07, Bhuj

Formation. (a) Coarse-grained sandstone with quartz and feldspar clasts set in a ferruginous matrix. (b) Iron oxide alteration replacing quartz grains and forming reddish-brown patches along fractures and grain boundaries. (c) Iron oxide alteration extensively replacing the matrix. (d) Magnetite grain occurring within the ferruginous matrix.

BH08 (*Fig.6.24*):

BH08 was drilled to a total depth of 50 m, intersecting a thick sequence of medium- to coarse-grained sandstone belonging to the Bhuj Formation. Petrographic analysis was conducted on representative samples from the 5 m to 50 m depth interval. The sandstone is subarkose to quartz arenitic sandstone in composition, consisting mainly of quartz, feldspar, and mica, with variable proportions across the section. Quartz grains are predominantly subangular to subrounded, moderately sorted, and exhibit fracturing and sutured contacts in several samples. These amorphous silica zones are commonly associated with gold and silver mineralization, suggesting late-stage hydrothermal fluid activity. Feldspar grains are abundant, represented by both plagioclase and microcline, showing variable degrees of alteration. Authigenic growth of feldspar is noted in several thin sections, where fresh microcline occurs intergrown with quartz. Mica grains commonly show bending, fraying, or partial alteration to sericite, reflecting post-depositional fluid interaction.

The matrix is fine-grained and ferruginous, largely replaced by iron oxide and hydroxide minerals. Iron oxide impregnation is extensive, and the alteration from magnetite to goethite and hematite is commonly observed. This indicates oxidation under near-surface or low-temperature hydrothermal conditions. Chalcopyrite appears as disseminated blebs and intergrowths with magnetite and pyrite. Gold and silver are closely associated with amorphous iron oxides, suggesting deposition from late-stage iron- rich hydrothermal fluids. Overall, the studied interval (5–50 m) of BH08 represents a ferruginous, immature, medium- to coarse-grained subarkose to quartz arenitic sandstone of the Bhuj Formation, characterized by intense iron oxide replacement, feldspar authigenesis and hydrothermal mineralization. The observed colloform textures in iron hydroxide and gold–silver association indicate late-stage hydrothermal overprinting superimposed on the diagenetically altered sandstone framework.

Magnetite, hematite, goethite, pyrite, chalcopyrite, and gold/tannite: In reflected light, a rich ore mineral assemblage is identified, comprising magnetite, hematite, goethite, pyrite, chalcopyrite, and gold, with tannite also recorded in trace amounts. Iron oxide in the form magnetite, hematite, goethite and pyrite with varying proportion is found in almost all the samples across different depth. Chalcopyrite is found at 9.69 to 9.74m and 11.87 to 11.96 m, depth and tannite is found at 11.87 to 11.96m depth.

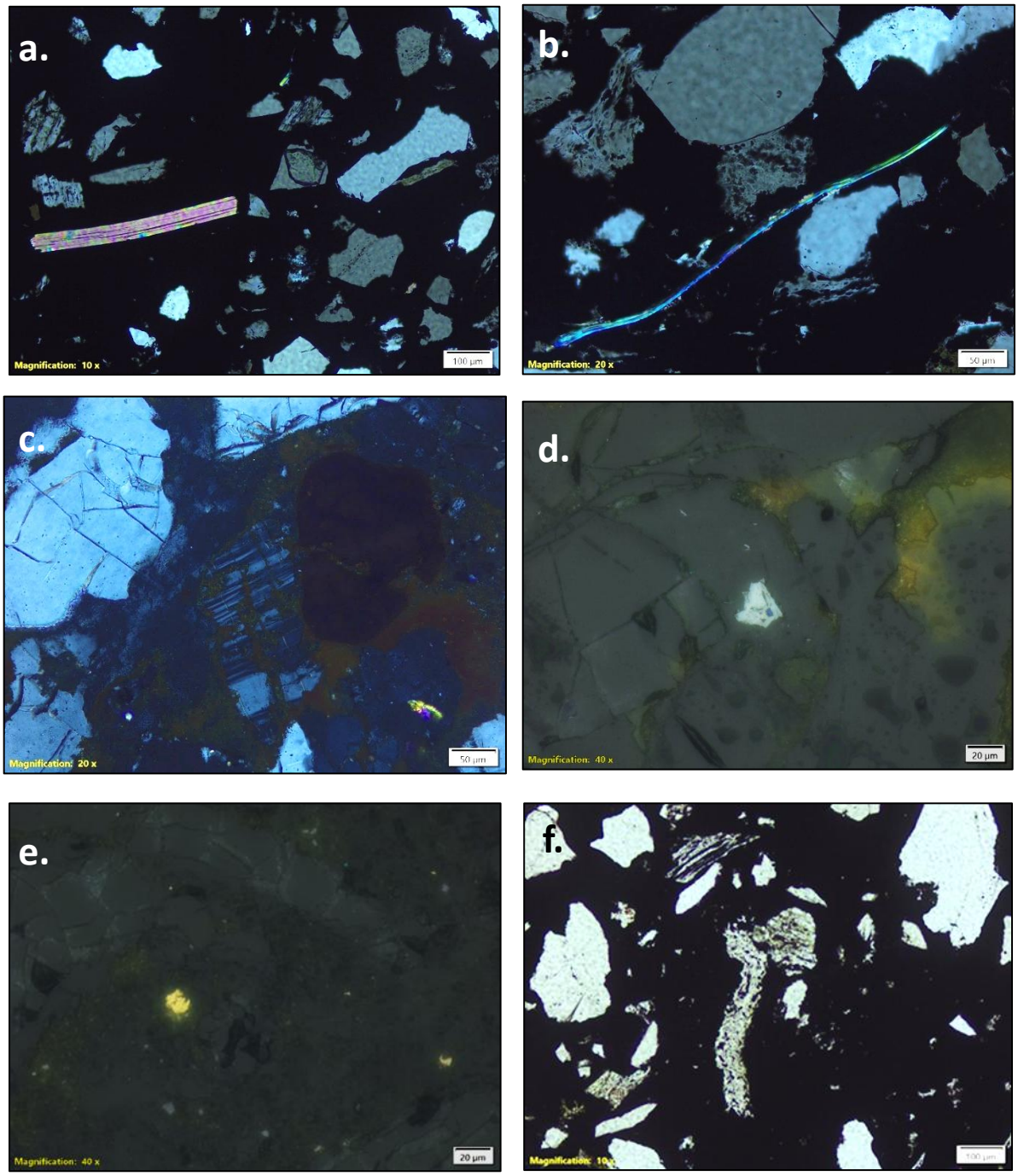

Fig. 6. 24 Representative photomicrographs of sandstone from Borehole BH-08, Bhuj Formation. (a) Medium-grained sandstone comprising subangular quartz and feldspar with elongated muscovite flakes. (b) Elongated muscovite grain under crossed polarised light (XPL) showing bright interference colours. (c) Feldspar grain altered by iron oxide under crossed polarised light. (d) Bornite mineral occurring within the matrix under reflected light (PPL). (e) Chalcopyrite grain disseminated in the matrix. (f) Authigenic growth of feldspar within the sandstone framework.

The Bhuj Formation (BH04-BH08) exhibits a hydrothermal Fe-Cu-Au-Ag system typified

by iron oxide-sulfide association, and silica-gold overprinting. This mineralization is distinct from the phosphatic–ferruginous tuffite-hosted REE system (Type I) in the Katrol Formation. Hence, the mineralization observed in BH04–BH08 can be classified as Type II, hydrothermal (IOCG-type?), representing a fluid-driven Fe-oxide-sulfide-gold-silver event that postdates the primary sedimentation of the Bhuj sandstones.

6.2.4.4. Geochemical Studies

Under Mineral System II, a total of six boreholes (BH-03 to BH-08) were to delineate subsurface geochemical characteristics and identify possible mineralized zones. From these boreholes, a total of core samples representing varying lithological depths were submitted for Inductively Coupled Plasma Mass Spectrometry (ICP-MS) analysis, while an additional 33 samples were analysed by X-Ray Fluorescence (XRF) to establish major and trace element distribution patterns (*Annexure-XXIX and XXX-c-j*). In addition, 21 surface samples collected from the vicinity of the boreholes were subjected to ICP-MS analysis, distributed as BH-04 (1), BH-05 (2), BH-06 (6), BH-07 (3), BH-08 (3), and six additional surface samples within the study area. The ICP-MS analytical suite comprised three distinct sample types: (i) Spot samples, representing discrete core segments (2-10 cm thick) collected from different depths of each borehole: BH-04 (10), BH-05 (16), BH-06 (16), BH-07 (11), and BH-08 (27); (ii) Composite samples, representing 1-2 m intervals composited from successive drill core sections: BH-04 (3), BH-05 (4), BH-06 (2), BH-07 (3), and BH-08 (5); and (iii) Heavy mineral fraction samples, derived from sludge material recovered from BHs sieved to obtain the <125 µm fraction, from which heavy minerals exceeding 1 g in weight were separated and analysed for BH-04 (3), BH-05 (2), BH-07 (4), and BH-08 (2). Magnetically (Nd magnet) separated from the bulk sludge samples were also analized for isodynamic separation (*Annexure-XXXI*). The combined dataset, encompassing surface, core, and heavy mineral fractions, provides an integrated geochemical framework for evaluating the vertical and lateral variation of elemental concentrations and assessing the potential zonation of mineralization within the defined system.

The spot samples reveal the immediate chemical character of individual lithological bands, allowing correlation between ferruginization intensity and REE enrichment. These short-interval samples consistently show elevated Total Rare Earth Elements (TREEY) and higher Total Hydrothermally Introduced Elements (THIE) values in ferruginious sandstone and mica-bearing ferruginized and metasomatized sandstone, whereas unaltered sandstone or shale bands show subdued elemental response. The composite samples, averaging 1-2 m intervals, smooth out short-scale fluctuations and clearly trace the transition from weakly altered sandstones to strongly ferruginized and metasomatized horizons. In almost all boreholes, composite samples record a sharp increase in both TREEY (total REE + Y) and THIE between the mid-depth ferruginized zones, confirming the continuity of hydrothermal enrichment over several metres. The heavy-mineral-fraction samples provide an additional

perspective on detrital and authigenic mineral phases. These fractions are particularly enriched in rare-earth-bearing heavy minerals, reflecting localized fluid concentration and secondary precipitation in pore spaces. The high TREEY and THIE values obtained from these sludge-derived samples indicate that the fine-grained ferruginous sandstones acted as efficient traps for REE-bearing fluids.

Borehole BH-03 yielded only sludge up to 16.00 m depth without any competent rock recovery. To obtain representative lithological information, BH-04 was drilled nearby toward the hill slope and reached a total depth of 51.00 m. From BH-03, three samples from varying depths (as shown in *Fig. 6.25*) were sent for isodynamic separation, whereas samples were also sent for heavy mineral separation; however, no significant heavy mineral fraction was recovered for further analysis.

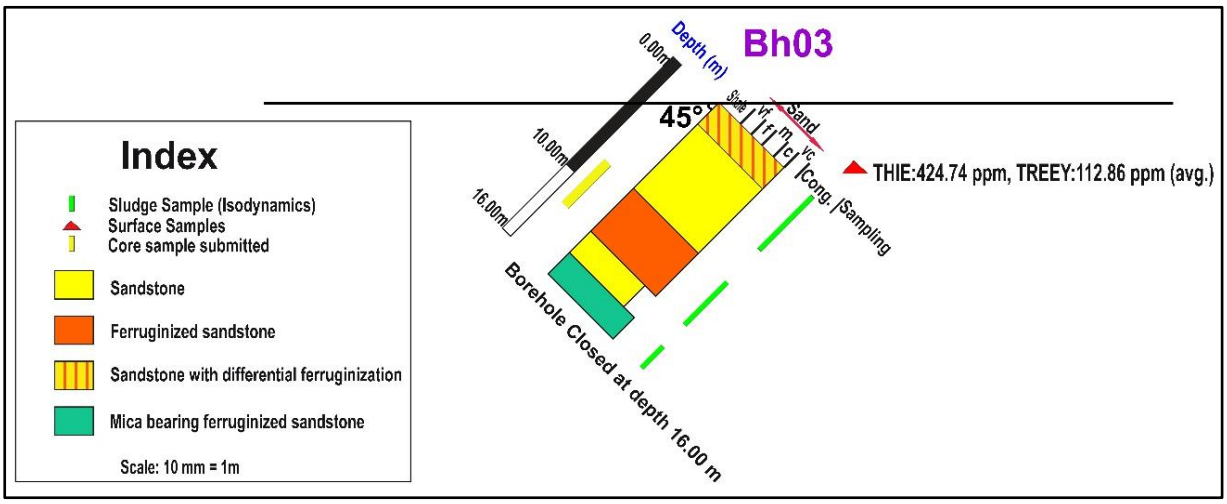

Fig. 6. 25 Lithological log of Borehole BH-03, Bhuj Formation, showing vertical variation in sandstone facies and ferruginization intensity.

Borehole BH-04, drilled at an inclination of 45° and azimuth 170°, reached a total depth of 51.00 m to explore subsurface ferruginous sandstone horizons and their associated geochemical signatures within Mineral System II. The succession comprises alternating units of ferruginized sandstone, metasomatized sandstone, mica-bearing varieties, and subordinate shale and breccia (*Fig 6.26*), reflecting progressive stages of ferruginization and hydrothermal alteration. ICP-MS analyses indicate a strong lithological control on REE-Y distribution. A surface sample collected adjacent to the borehole collar from highly ferruginized metasomatized sandstone shows comparatively low TREEY ≈ 112 ppm and THIE ≈ 424 ppm, implying limited mineralization under surface-oxidizing conditions. From 10 m to 25 m, within heterolithic and differentially ferruginized sandstone zones, there is a distinct rise in TREE-Y concentrations (THIE 617.44–699.44 ppm; TREEY 312.12–361.76 ppm), suggesting early-stage hydrothermal fluid influx and Fe-oxide precipitation that enhanced adsorption and retention of REE phases.

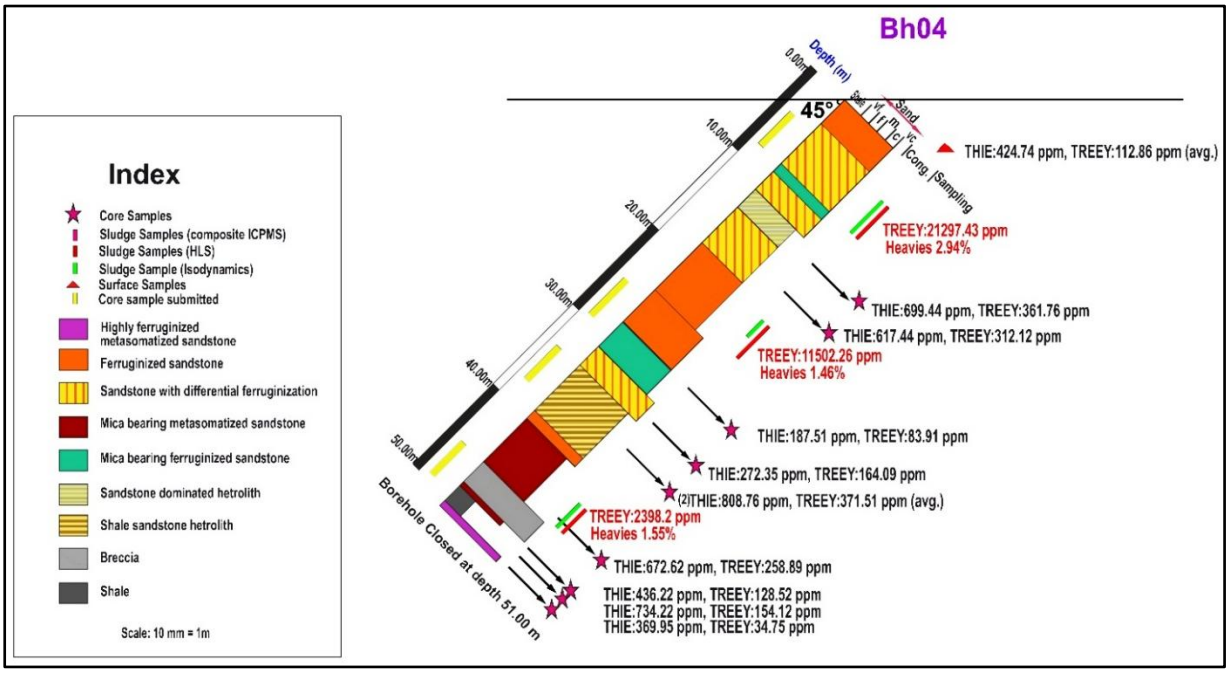

Fig. 6. 26 Lithological log of Borehole BH-04, Bhuj Formation, showing vertical variation in sandstone facies and ferruginization intensity.

Between 27 m and 36 m, mica-bearing ferruginized sandstone records relatively low TREEY < 165 ppm and THIE < 273 ppm, However, averaging the assay results of two core samples within the shale-dominated heterolithic units yields TREEY ≈ 371 ppm and THIE ≈ 808 ppm, representing the peak value within this borehole, indicating localized accumulation of REE where fluids may have stagnated within fine-grained, Fe-oxide-rich horizons. Toward the base (45-50 m), metasomatized sandstone interbedded with breccia and shale shows THIE 369 to 734 ppm but comparatively subdued TREEY 34 to 258 ppm, reflecting partial decoupling of REE from high field strength elements during late stage fluid alteration.

Heavy mineral data reinforce this trend: ferruginized sandstone sludge (TREEY 21297 ppm, 2.94 % heavies), yellowish-brown ferruginized sandstone (TREEY 11502 ppm, 1.46 % heavies), and micabearing metasomatized sandstone (TREEY 2398 ppm, 1.55 % heavies). The enrichment of TREEY within the heavy fractions underscores mineralogical concentration of REE bearing phases likely monazite or xenotime within ferruginized and metasomatized sandstone, marking the mid to basal portions of the inclined BH-04 as the most favorable zone for TREEY mineralization.

Borehole BH-05, drilled to a total depth of 62.00 m, intersected alternating units of ferruginized sandstone, metasomatized sandstone, mica-bearing varieties, sandstone-dominated heteroliths, and a basal breccia (*Fig 6.27*) within Mineral System II. The succession represents successive stages of ferruginization and hydrothermal alteration under variable redox and permeability conditions. A surface sludge sample collected near the collar, representing mica-bearing ferruginized sandstone (0-1 m depth), shows THIE = 272 ppm with

relatively low TREEY content, indicating limited mineralization under near-surface oxidizing conditions. With increasing depth to around 15 m, both THIE and TREEY values remain subdued (THIE < 115 ppm; TREEY < 100 ppm), reflecting minimal REE mobilization in upper, weathered zones.

At greater depths (40-60 m), the borehole sequence records consistent enrichment of REE–Y and HFSE elements within ferruginized and heterolithic sandstone units. The sandstone with differential ferruginization shows THIE = 601.4 ppm; TREEY = 438.1 ppm, followed by another interval of the same lithology with THIE = 546.1 ppm; TREEY = 367.0 ppm. The sandstone-dominated heteroliths yield THIE = 764.5 ppm; TREEY = 464.8 ppm (avg), while the breccia at the base records THIE = 701.2 ppm; TREEY = 464.8 ppm (avg). These elevated values suggest prolonged Fe-rich hydrothermal interaction and effective adsorption of REE–Y phases within porous sandstone and brecciated horizons.

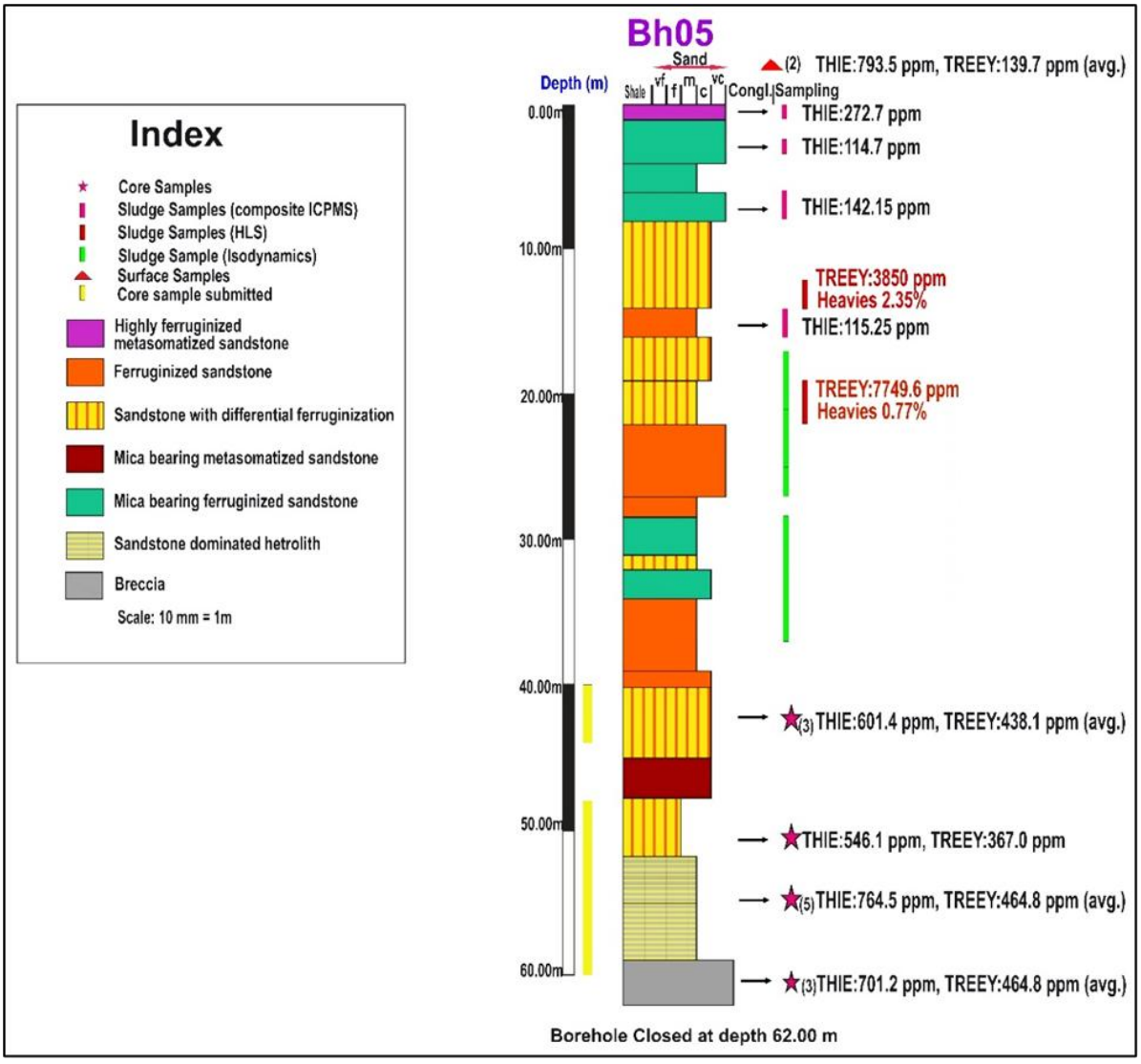

Fig. 6. 27 Lithological log of Borehole BH-05, Bhuj Formation, showing vertical variation in sandstone facies and ferruginization intensity. Hydrothermal addition of elements (THIE)

includes: (at least >3 times higher concentration of elements than the unaltered sandstone of Bhuj Fm.: (Be, Sc, V, Cr, Co, Ni, Cu, Zn, Ga, Rb, Y, Nb, Cd, In, Sn, Sb, Cs, Ta, Tl, Th, Th, U, TREEY)

The heavy-mineral assemblage further substantiates this enrichment trend: sludge from sandstone with differential ferrugination (12–14 m) records TREEY = 3850 ppm; heavies = 2.35 %, while sludge from sandstone with differential ferruginization (19–21 m) yields TREEY = 7749.6 ppm; heavies = 0.77 %. These high TREEY concentrations within the heavy fractions indicate the presence of stable REE-bearing minerals such as monazite and xenotime concentrated along ferruginized and metasomatized matrices. Collectively, the mid-to-lower ferruginious sandstone horizons of BH-05 represent the most prospective REE–Y-bearing zones, controlled by lithological porosity, intensity of ferruginization, and sustained hydrothermal fluid activity.

Borehole BH-06, closed at a depth of 48.50 m, intersected alternating units of sandstone, ferruginized sandstone, mica-bearing metasomatized sandstone, sandstone with differential ferruginization, shale, and ferruginized breccia (*Fig 6.28*) within Mineral System II. The borehole was designed to assess the distribution of REE–Y and high-field-strength elements across progressively ferruginized zones. A surface sample collected adjacent to the borehole collar from highly ferruginized sandstone shows THIE = 361.91 ppm and TREEY = 220.73 ppm, suggesting minor enrichment under surface-oxidizing conditions. Near the top (0-5 m), core samples indicate subdued geochemical activity THIE = 228.20 ppm; TREEY = 96.45 ppm (avg) within ferruginized breccia unit and THIE = 163.12 ppm; TREEY = 103.93 ppm consistent with limited REE mobility in unaltered sandstone. From 10 m to 20 m, within mica-bearing metasomatized sandstone and black shale, the values increase sharply (THIE = 535.62 ppm; TREEY = 84.93 ppm and THIE = 236.87 ppm; TREEY = 342.14 ppm), implying early-stage hydrothermal percolation and adsorption of REE onto Fe-oxide and clay matrices. A moderate enrichment continues through the 20-30 m interval, where mica bearing ferruginized sandstone records THIE = 134.49 ppm; TREEY = 258.84 ppm (avg) and THIE = 128.19 ppm; TREEY = 212.93 ppm (avg), suggesting sustained though fluctuating fluid activity.

Below 30 m, the sequence transitions into interbedded mica-bearing ferruginized sandstone, sandstone with differential ferruginization, and ferruginious sandstone, where TREE-Y and THIE concentrations remain moderate to high. The deeper samples show THIE = 194.91 ppm; TREEY = 52.34 ppm, THIE = 155.52 ppm; TREEY = 43.04 ppm (avg), THIE = 120.44 ppm; TREEY = 361.69 ppm, and THIE = 221.10 ppm; TREEY = 54.39 ppm. These variations indicate continued hydrothermal fluid influence and localized REE redistribution within ferruginized pore systems. Moderate TREEY concentrations in the lower sandstone and breccia intervals suggest subtle accumulation of REE-bearing phases such as monazite and xenotime. Collectively, BH-06 reflects a transitional geochemical environment upper sections showing surface-related leaching and depletion, and deeper ferruginized zones (20–48 m)

retaining moderate TREEY enrichment under sustained but low-temperature hydrothermal alteration.

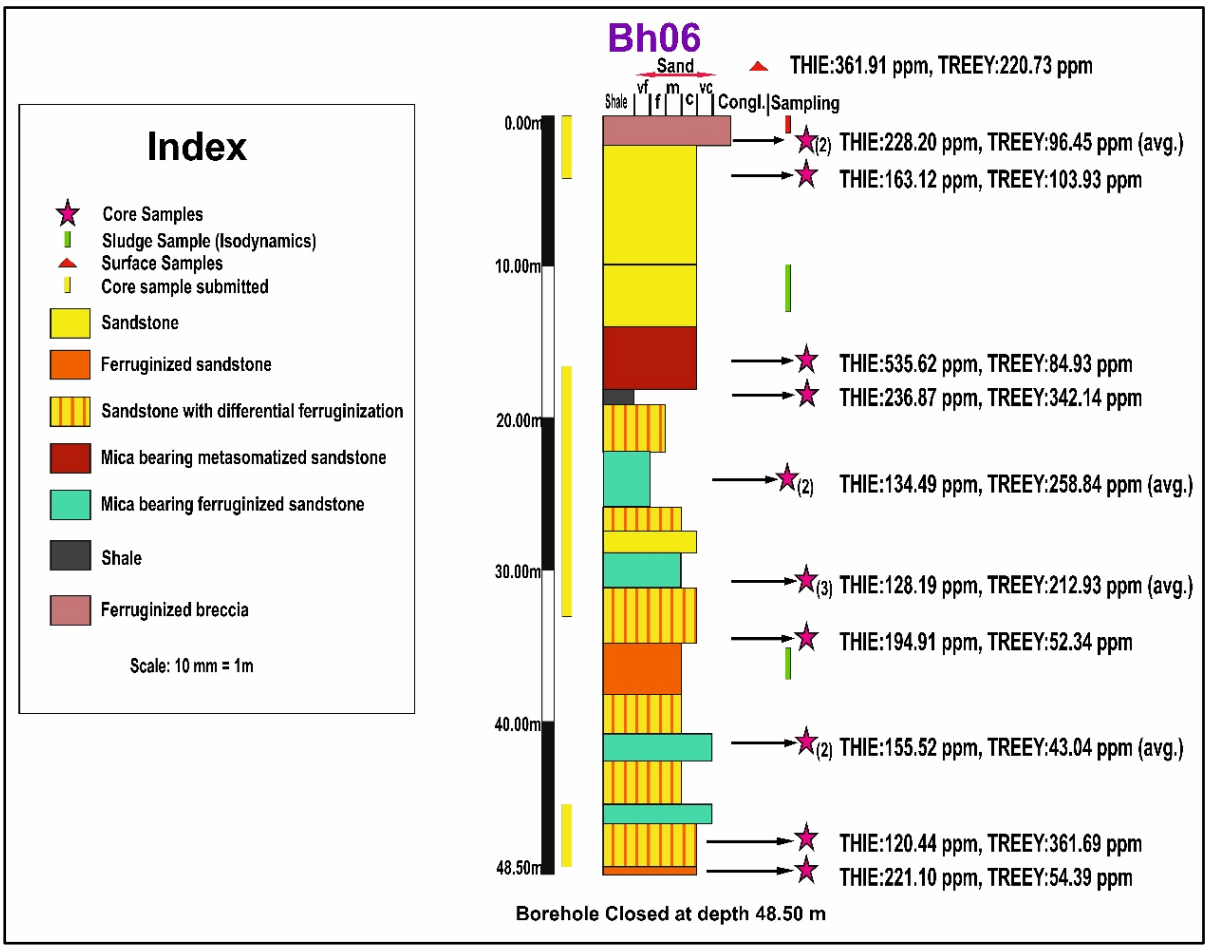

Fig. 6. 28 Lithological log of Borehole BH-06, Bhuj Formation, showing vertical variation in sandstone facies and ferruginization intensity. Hydrothermal addition of elements (THIE) includes: (at least >3 times higher concentration of elements than the unaltered sandstone of Bhuj Fm.: (Sc, Ni, Cu, Zn, Nb, Cd, Sn, Sb, Ag, Te).

Borehole BH-07, reaching a total depth of 55.00 m, intersected alternating units of ferruginized sandstone, sandstone with differential ferruginization, mica-bearing ferruginious sandstone, and alternating ferruginous metasomatized sandstone (*Fig 6.29*) within Mineral System II. A surface sample collected adjacent to the borehole collar from highly ferruginized metasomatized sandstone records THIE = 191.7 ppm and TREEY = 154.0 ppm (avg), indicating limited enrichment under oxidizing surface conditions. Within the upper 10 m, core samples from the same lithology show relatively low values (THIE = 53.5 ppm; TREEY = 40.6 ppm) and THIE = 21.4 ppm; TREEY = 43.6 ppm , reflecting weak mineralization near the surface. In the intermediate zone (18–25 m), sandstone with differential ferruginization and mica-bearing ferruginized sandstone show moderate enrichment (THIE = 50.3 ppm; TREEY = 103.3 ppm)

and (THIE = 134.6 ppm; TREEY = 284.2 ppm avg), suggesting localized adsorption of REE along Fe-oxide-coated grains and fluid-assisted redistribution within permeable horizons.

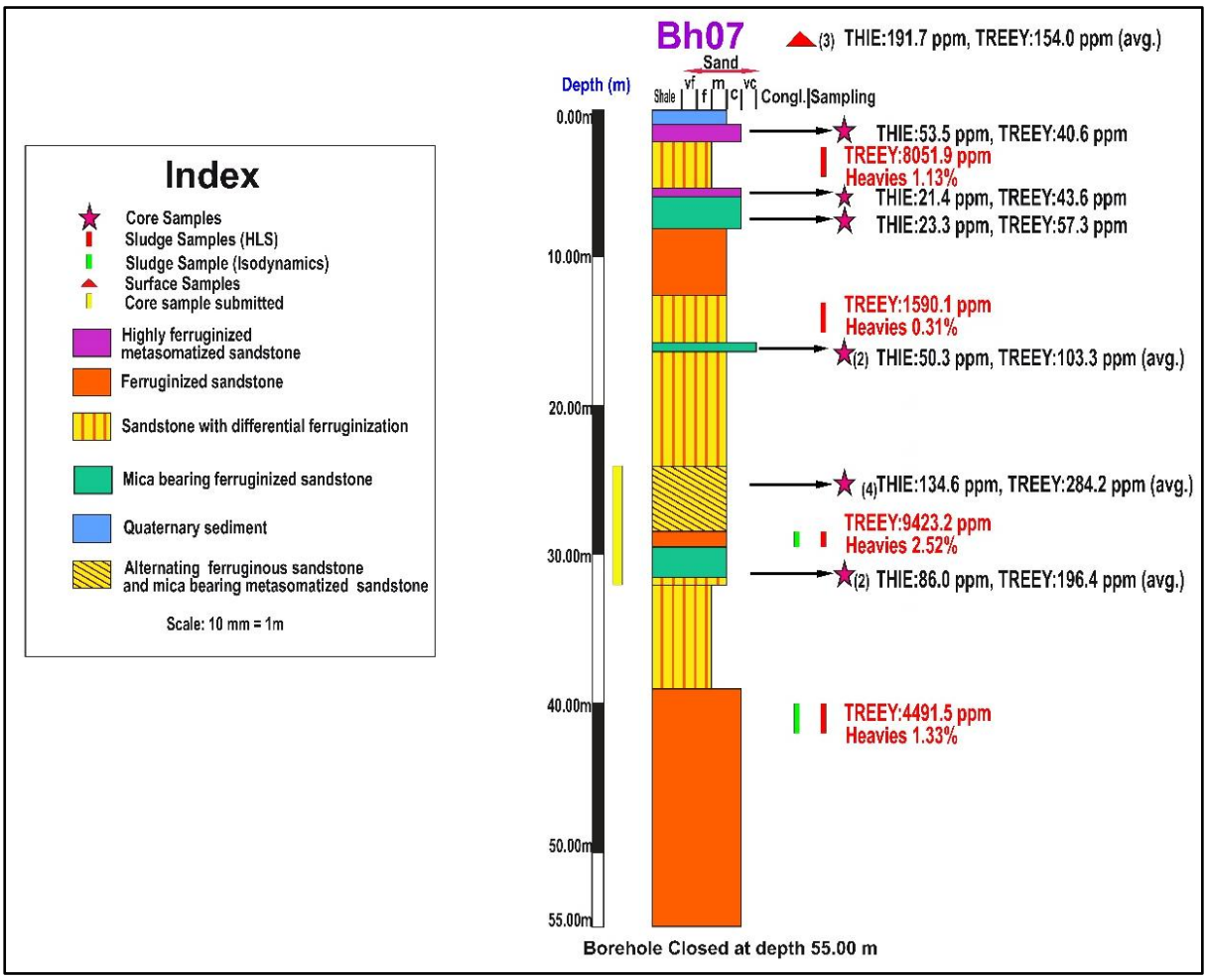

Fig. 6. 29 Lithological log of Borehole BH-07, Bhuj Formation, showing vertical variation in sandstone facies and ferruginization intensity. Hydrothermal addition of elements (THIE) includes: (at least >3 times higher concentration of elements than the unaltered sandstone of Bhuj Fm.: (Rb, Cd, Sn, Sb, Pr, Th, U, Ag, Te).

Toward the deeper section (30–50 m), alternating ferruginous sandstone and mica-bearing metasomatized sandstone continue to show low to moderate values (THIE = 86.0 ppm; TREEY = 196.4 ppm avg) associated with progressive ferruginization and metasomatic alteration. The heavy-mineral assemblage from corresponding horizons reflects significant REE enrichment: sludge from sandstone with differential ferruginization near the surface yields TREEY = 8051.9 ppm; heavies = 1.13 %, sludge from sandstone with differential ferruginization at mid-depth records TREEY = 1590.1 ppm; heavies = 0.31 %, sludge from highly ferruginized sandstone at ~30 m shows TREEY = 9423.2 ppm; heavies = 2.52 %, and the basal ferruginized sandstone exhibits TREEY = 4491.5 ppm; heavies = 1.33 %. The high TREEY concentrations within these heavy fractions suggest the presence of stable REE minerals such as monazite and xenotime, concentrated within ferruginized and metasomatized matrices

through a combination of hydrothermal circulation and mechanical sorting. Collectively, the mid-to-lower ferruginized sandstone horizons (25–50 m) of BH-07 represent the most prospective REE–Y-bearing zones, influenced by intense ferruginization, fluid movement, and secondary mineral concentration.

Borehole BH-08, drilled to a total depth of 50.00 m, intersected alternating units of ferruginized sandstone, sandstone with differential ferruginization, mica-bearing ferruginized sandstone, metasomatized shale-sandstone heterolith and mica bearing metasomatized sandstone (*Fig 6.30*) within Mineral System II. A surface sample collected adjacent to the borehole collar records THIE = 815.06 ppm (avg) with TREEy <100ppm, reflecting slight enrichment under near-surface oxidizing conditions. Within the upper 10 m, mica bearing ferruginized sandstone units yield THIE = 646.7 ppm (avg of 2 spot samples) with low TREEY showing moderate enrichment likely linked to early Fe-oxide precipitation and weak hydrothermal percolation. Between 10 m and 25 m, the metasomized shale sandstone hetrolith, mica-bearing metasomatized and ferruginized sandstone units register marked increases in elemental concentrations—THIE = 1262.3 ppm; TREEY = 248.3 ppm (avg), THIE = 852.9 ppm (avg), THIE = 452.15 ppm; TREEY = 231.9 ppm (avg), and THIE = 538.3 ppm; TREEY = 280.7 ppm (avg) indicating zones of enhanced fluid activity and mineral replacement along ferruginous and metasomatic contacts. The observed geochemical progression with depth suggests successive fluid pulses that favored Fe-oxide development and REE adsorption within the permeable sandstone metasomatite interface.

The heavy-mineral assemblage from BH-08 further supports this enrichment pattern. Sludge from the mica-bearing ferruginized sandstone (~22 m depth) records TREEY = 12 556.9 ppm; heavies = 0.90 %, while the ferruginized sandstone at ~38 m depth shows TREEY = 4764.24 ppm; heavies = 1.15 %. In the basal section (40–50 m), THIE concentrations remain consistently high, with THIE = 1670.03 ppm; TREEY = 245.5 ppm and THIE = 595.1 ppm (avg), suggesting strong Fe-rich hydrothermal influence within deeper ferruginous units. The elevated TREEY values within heavy fractions confirm mechanical concentration and hydrothermal fixation of resistant REE-bearing phases such as monazite and xenotime. Overall, the mid-to-lower metasomized shale sandstone hetrolith units and ferruginized sandstone horizons of BH-08 represent the most prospective REE–Y-bearing zones, controlled by the interplay of lithological porosity, ferruginization intensity, and sustained hydrothermal circulation.

Integrated Interpretation

Across BH-04 to BH-08, the correlation between lithology and chemistry is consistent and diagnostic. Peaks in REE and THIE align closely with ferruginized sandstone, mica-bearing metasomatized layers, and their intercalations- lithologies that combine porosity, permeability, and reactivity, making them ideal pathways for hydrothermal fluids. The

composite and heavy-fraction datasets outline the continuity of mineralized horizons, while spot samples pinpoint localized alteration zones.

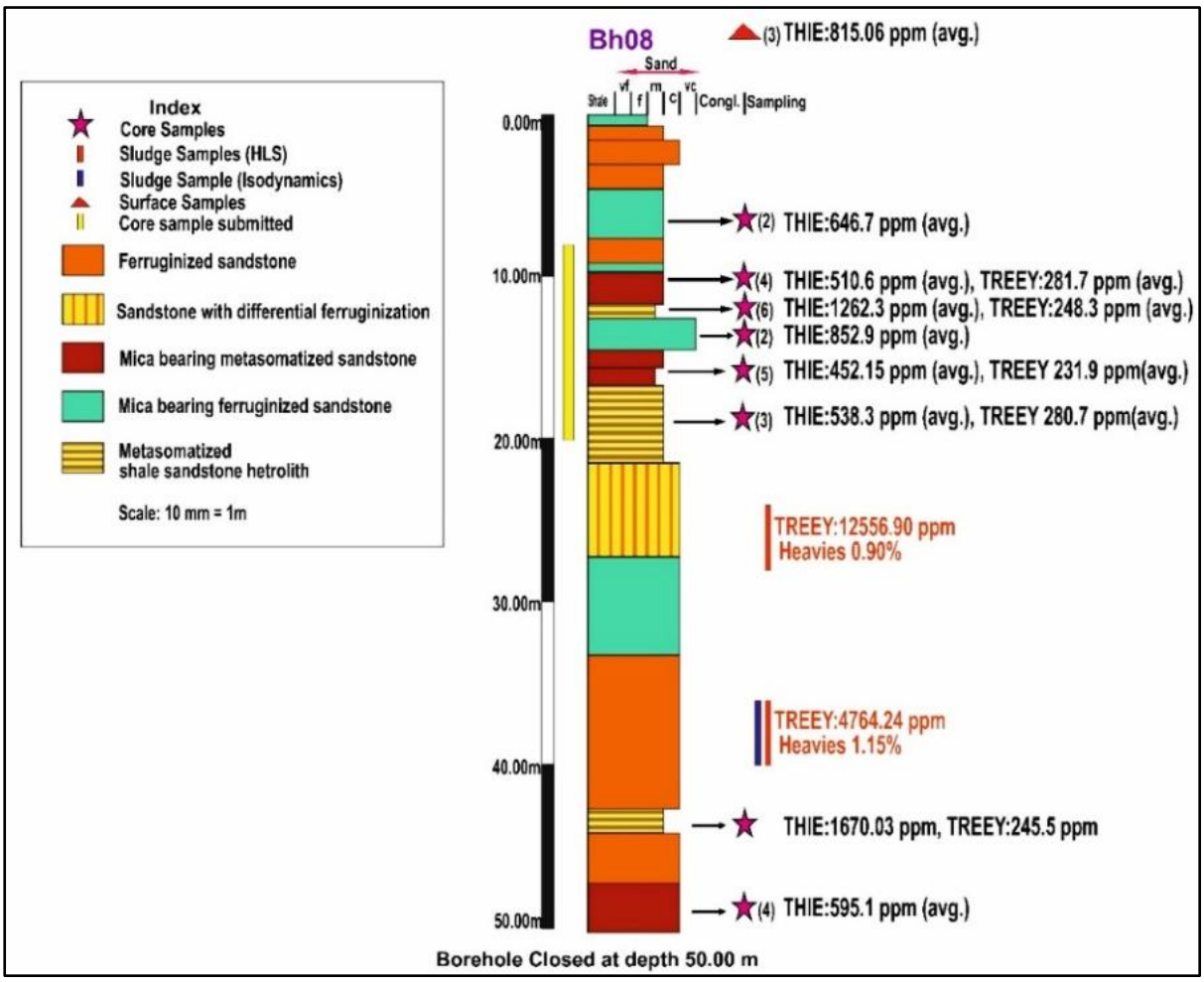

Fig. 6. 30 Lithological log of Borehole BH-08, Bhuj Formation, showing vertical variation in sandstone facies and ferruginization intensity. Hydrothermal addition of elements (THIE) includes: (at least >3 times higher concentration of elements than the unaltered sandstone of Bhuj Fm.: (Be, Sc, V, Cr, Co, Ni, Cu, Zn, Ga, Rb, Y, Nb, Cd, In, Sn, Sb, Cs, Ta, Tl, Th, Th, U, TREEY).

Values exceedingly twice the clerk threshold are categorized as high intensity mineralized intervals and provide a quantitative basis for defining the core of hydrothermal enrichment. The most persistent and chemically robust zones occur along the ferruginized corridors intersected by BH-04 (inclined section) and BH-08, indicating structurally controlled fluid channels.

Altogether, the boreholes collectively reveal a consistent pattern of ferruginization-controlled THIE and TRE-Y enrichment within the sandstone metasomatite sequence. Near-surface zones show low values under oxidizing conditions, while mid- to lower-depth ferruginized and metasomatized sandstones (20-50 m) record the highest TREEY and THIE concentrations.

Across holes, ferruginized and mica-bearing units serve as the main host for REE phases, with heavy-mineral fractions confirming monazite- and xenotime-type enrichment. BH-04 and BH-05 show the strongest mineralization, BH-06 reflects moderate hydrothermal influence, and BH-07–BH-08 display similar mid-depth enrichment trends.

Overall, the integrated geochemical data define a continuous hydrothermal zone where Fe-oxide development, porosity contrasts, and fluid circulation together governed REE–Y accumulation across Mineral System II.

6.2.4.5. Mineragraphic Studies

SEM-EDAX Study

Scanning Electron Microscopy (SEM) and Energy Dispersive X-ray Analysis (EDAX) were carried out on three representative borehole samples to study the micro-textural characteristics and elemental composition of the mineralized phases. However, due to technical issues encountered during instrument operation, analytical results could not be retrieved and added to the report.

EPMA Analysis:

EPMA investigations were carried out on four borehole samples representing different lithological variants of the Bhuj Formation. The analyzed samples include two altered sandstones, one brecciated sandstone, and one purplish sandstone. Detailed findings are summarised in *Annexure-XXXII*. The mineralogical and geochemical observations derived from the EPMA study are summarized below.

Metasomatized Ferruginized Sandstone of Bhuj Formation

These samples were obtained from a depth range of 6-9 m in Borehole BH-08. It comprises quartz (>97%), hematite grains, & few clay clast and magnetite in a decreasing order of abundance. Silicification is also observed within these sandstones. Anomalous Zn, Sn, Ag, Te, Pb, IN and TREEY, have been noted from this samples.

EPMA analysis revealed the presence of pyrrhotite and cuprite grains disseminated within the sandstone matrix (*Fig.6.31*). The copper content in this altered sandstone was recorded up to 9.3 wt.%, suggesting notable copper mineralization associated with alteration zones.

Ferruginous Breccia of Bhuj Formation

The brecciated sandstone sample, collected from a depth of 59 m in Borehole BH-05. Numerous pyrite grains were identified through EPMA analysis, often occurring as disseminations within the sandstone fragments and along microfractures. Additionally, a few

monazite grains (*Fig.6.32*) were detected, indicating localized concentration of REE-bearing phases.

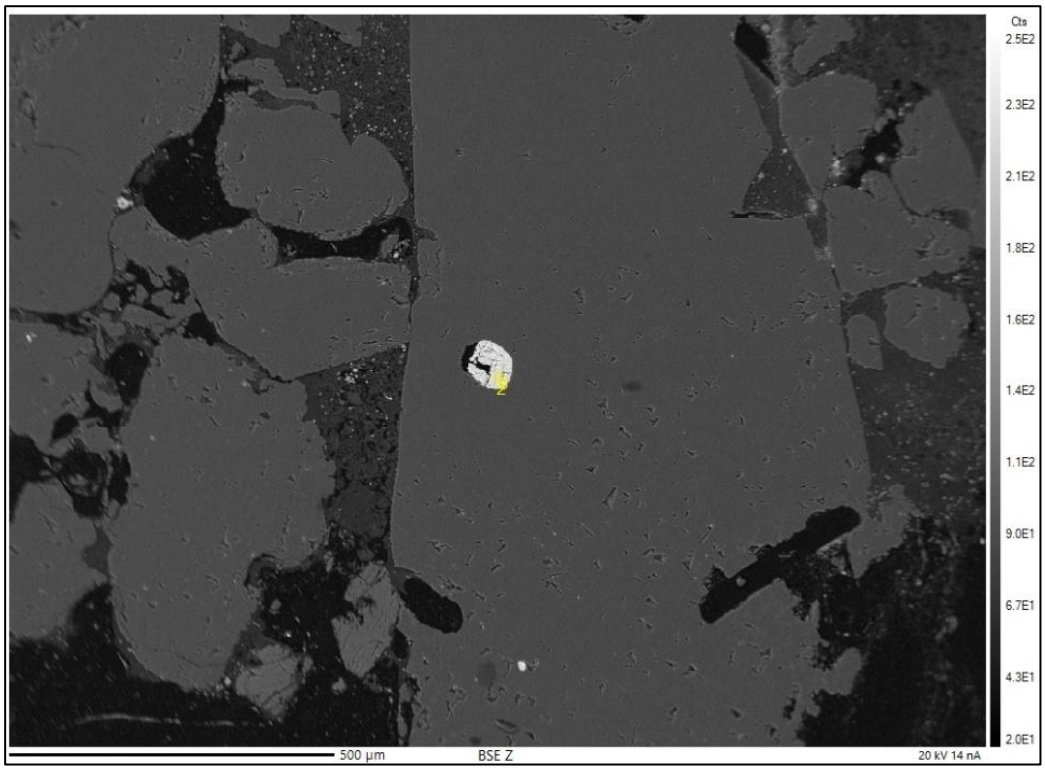

Fig. 6. 31 BSE image showing pyrrhotite (P) grain within Metasomatized Ferruginized Sandstone.

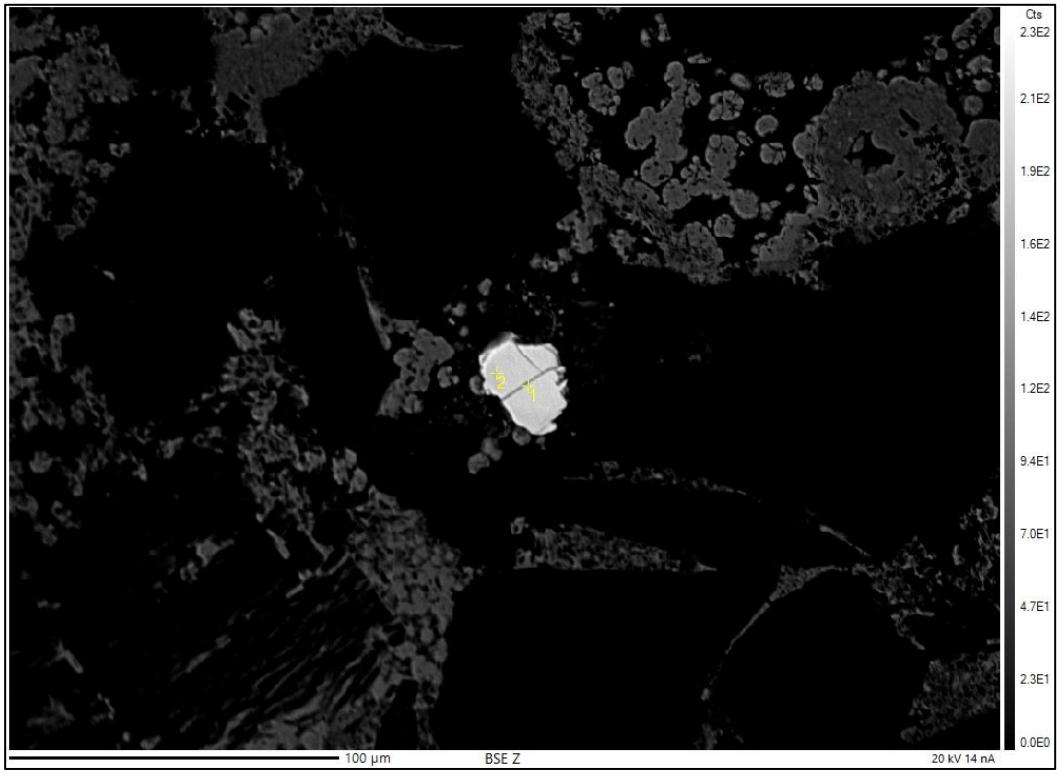

Fig. 6. 32 BSE image showing monazite grain identified in Ferruginous Breccia.

Sandy Heterolith of Bhuj Formation

This sample was collected from a depth of 35 m in Borehole BH-04, shows presence of quartz with possible minor feldspar and subordinate muscovite and biotite. EPMA results confirmed the presence of several zircon (*Fig. 6.33a*) and monazite grains distributed within the sandstone matrix. Zn bearing sulphides (Fe-Cu-Zn sulfide) have also been identified within this sample (*Fig.6.33b*). Zn is upto 56 wt %.

Interpretation:

This EPMA analysis suggests both detrital and hydrothermal contributions to its mineral assemblage. Collectively, the EPMA findings indicate a multiphase mineralization system in the Bhuj Formation involving primary detrital inputs, post-depositional Fe-alteration, silicification, and hydrothermal remobilization processes that enriched the sandstones with Cu, Zn, and REE minerals.

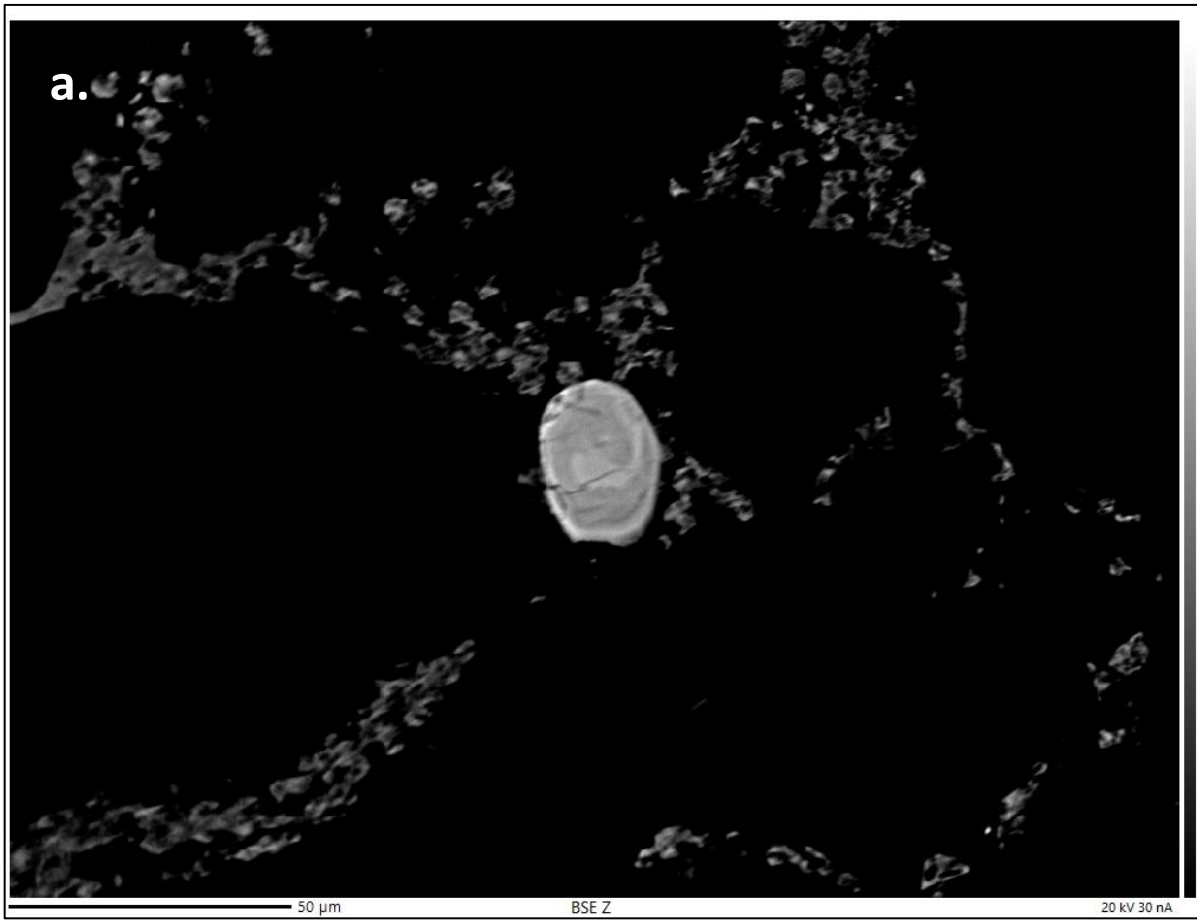

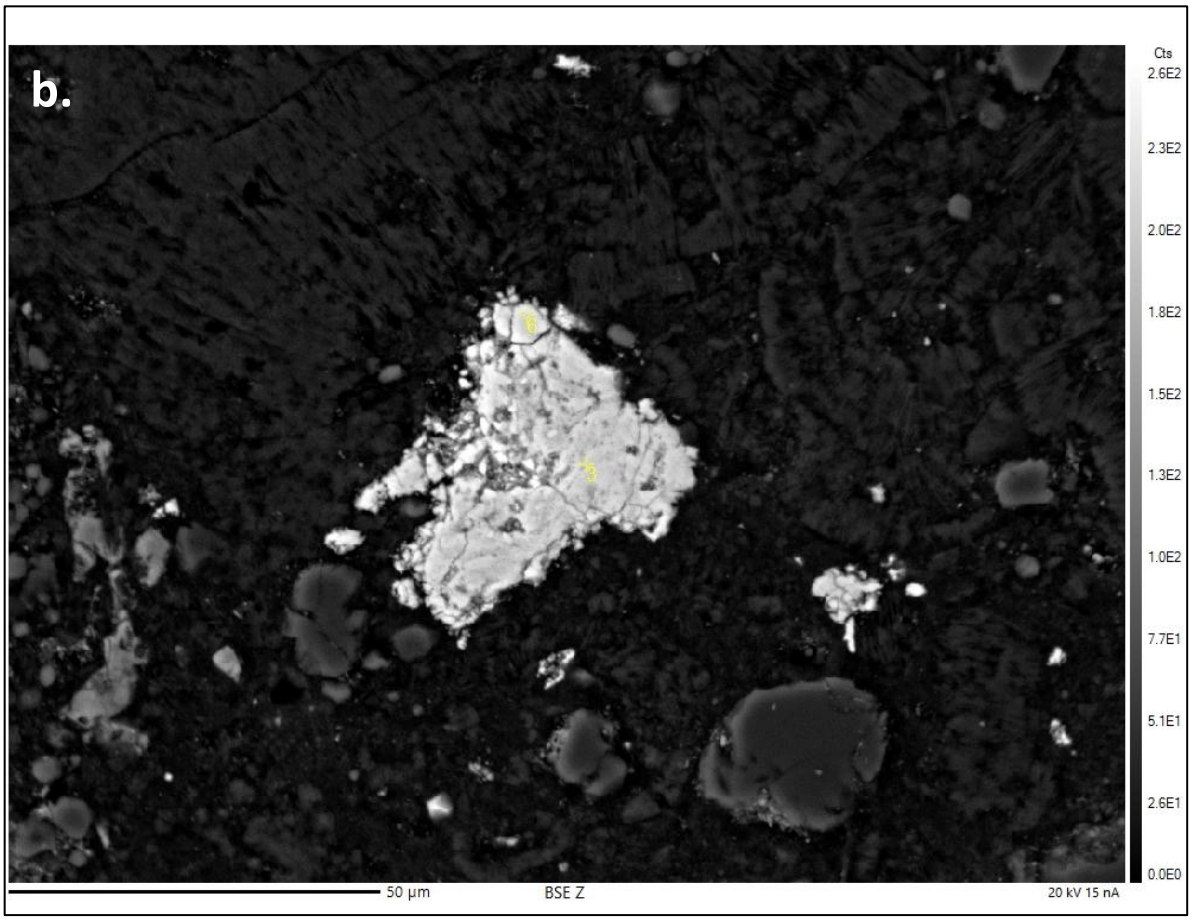

Fig. 6. 33 (a) BSE image showing zircon grain identified in sandy heterolith. (b) BSE image showing zinc bearing sulphides in sandy heterolith

6.2.4.6. Mineralogy of ore zone

The ore zones delineated within Mineralization Style II (MSA-II) of the Bhuj Formation are characterized by a complex assemblage of Fe-oxide, sulfide, and accessory REE-bearing minerals developed within ferruginized and metasomatized sandstones and their associated brecciated or heterolithic facies. Petrographic, reflected-light, and EPMA investigations collectively define a polymetallic mineral association indicative of IOCG-type hydrothermal overprinting upon an originally arenitic host.

Primary Framework and Gangue Minerals:

The dominant framework minerals in the ore zone comprise quartz, feldspar (both plagioclase and microcline), and muscovite, with subordinate lithic fragments and clay clasts. Quartz occurs as subangular to subrounded grains, often fractured and displaying sutured grain boundaries, suggesting both mechanical compaction and late-stage hydrothermal recrystallization. Feldspars are variably replaced by sericite and iron oxides, while fresh microcline locally shows authigenic overgrowths, particularly in BH-08. Muscovite and biotite, occasionally bent or frayed, are common within metasomatized bands, reflecting low-grade

thermal alteration along fluid pathways. The matrix in most mineralized intervals is ferruginous, composed of hematite, magnetite, goethite, and subordinate clay-silica cement, imparting reddish-brown to black coloration.

Iron Oxides and Hydrothermal Alteration Phases:

Iron oxides are the volumetrically dominant mineral phase within the ore zone and occur in multiple generations.

- Magnetite is widespread throughout BH-04 to BH-08, present as disseminated subhedral to anhedral grains, vein-filling aggregates, or replacement patches within the ferruginous matrix. It locally exhibits martitization rims, indicating partial oxidation to hematite.

- Hematite is pervasive in both early ferruginized sandstones and late metasomatic veins, occurring as micaceous plates or earthy aggregates along fractures and bedding planes.

- Goethite is common in near-surface and oxidized zones, typically replacing magnetite and hematite in BH-05 and BH-08, producing colloform and botryoidal textures.

Together, these oxides reflect a multistage iron enrichment process, beginning with early diagenetic ferruginization and culminating in hydrothermal replacement under fluctuating redox conditions.

Sulphide and Sulfosalt Assemblage:

The sulfide mineralogy is diverse, occurring as disseminations, fracture-fillings, and fine intergrowths within the ferruginous matrix:

- Pyrite (both euhedral and framboidal) is the most common sulfide, present throughout BH-04, BH-05, and BH-06, and often associated with magnetite and hematite. It commonly shows overprinting by Fe-oxide phases, suggesting partial oxidation during late fluid events.

- Chalcopyrite and bornite are identified in BH-04, BH-05, and BH-08 as small inclusions and veinlet infillings within ferruginous sandstone, indicating a Cu-bearing hydrothermal phase.

- Covellite and pyrrhotite, recorded by reflected-light and EPMA studies in BH-04 and BH-08, signify low-temperature Cu-Fe-S re-equilibration and sulfide sulfidation during late fluid influx.

- Sphalerite and Zn-bearing Fe-Cu sulfides in BH-05 and BH-04 (Zn up to 56 wt %) mark a distinct Zn-enriched phase, possibly linked to mixing of iron-rich and sulfur-poor hydrothermal fluids.

- Trace tannite (Cu-Sn sulfide) occurs in BH-08, indicating late polymetallic fluid pulses enriched in Sn and Te.

Gold and Silver Association:

Native gold occurs as minute specks disseminated within ferruginous sandstone (BH-04, BH-08), closely associated with amorphous Fe-oxides and silica zones. Colloform Fe-oxide textures enclosing gold and Ag suggest late-stage precipitation from low-temperature, oxidizing hydrothermal solutions. The association with chalcopyrite-bornite intergrowths implies that Au–Ag deposition was synchronous with or slightly post-dated Cu-Fe sulfide mineralization, typical of IOCG systems.

Accessory and REE-Bearing Phases:

Accessory minerals constitute an important part of the ore assemblage and include both detrital and hydrothermal phases.

- Monazite and xenotime are the principal REE-bearing minerals, recorded in BH-04, BH-05, and BH-07 heavy-mineral fractions and confirmed by EPMA in BH-05 breccia. These occur as fine inclusions within ferruginous matrices or as discrete subhedral grains, reflecting both detrital and secondary precipitation origins.

- Apatite is common in ferruginized sandstone (BH-04, BH-05), locally associated with monazite, suggesting phosphate-mediated REE concentration during fluid interaction.

- Zircon occurs as angular to subrounded detrital grains and as recrystallized rims in metasomatized sandstone (BH-04), supporting a mixed provenance with volcanic input.

- Allanite and fluorite, though rare, have been noted in EPMA spectra as minor accessory phases linked to late-stage REE remobilization.

- The REE-bearing phases are commonly intergrown with Fe-oxide and apatite, consistent with adsorption and coprecipitation from Fe-rich hydrothermal solutions.

Textural Relationships and Paragenesis:

Textural observations from thin-section, reflected-light, and BSE imaging indicate a clear paragenetic sequence:

- Early ferruginization and silicification, replacing arenitic matrix and enhancing porosity.
- Deposition of magnetite and hematite, followed by formation of framboidal pyrite within reducing microenvironments.
- Hydrothermal sulfide stage, with chalcopyrite, bornite, covellite, and sphalerite deposition in open spaces and fractures.
- Late oxidizing stage, marked by magnetite martitization to hematite–goethite and simultaneous precipitation of gold–silver within colloform Fe-oxide and silica aggregates.
- Post-hydrothermal metasomatism, introducing REE-phosphates (monazite–xenotime–apatite) and minor Sn–Te phases, completing the mineralization sequence.

Mineralization Character:

The overall mineralogy of the ore zone indicates a hydrothermal Fe-Cu-Au-Ag system with associated REE enrichment, typical of an IOCG-type mineralization spectrum. Iron oxides (magnetite-hematite-goethite) dominate the assemblage, sulfides (pyrite-chalcopyrite-bornite-sphalerite-pyrrhotite-covellite) represent the metallic phase, and accessory monazite, xenotime, and apatite host the REE components. The spatial and vertical distribution of these minerals, especially the concentration of Fe-oxides and REE-phosphates within the 20–50 m ferruginized and metasomatized sandstone intervals, confirms structurally and lithologically controlled hydrothermal precipitation.

Chapter 7

Conclusions and Recommendations

7. Conclusions and Recommendations

The Reconnaissance (G-4) program over the Bhuj REE Prospect transformed an anomaly-led concept into a system-based exploration framework underpinned by integrated geological mapping, stratigraphic analysis, multi-fraction geochemistry, mineralogical characterization, targeted geophysics and target testing through pitting and drilling.

This chapter synthesizes the G-4 exploration outcomes, evaluates achievements, compares the Bhuj discoveries with global analogues, and outlines a phased G-3 strategy aimed at advancing the Katrol stratiform and Bhuj IOCG systems toward systematic resource evaluation.

7.1. Discussion and Analysis of the Reconnaissance (G-4) Study

The Reconnaissance Survey (G-4) for Rare Earth Element (REE) Exploration in the Bhuj Clay Prospect Block was initiated to investigate exceptionally high REE concentrations in stream sediments reported by the National Geochemical Mapping Program (NGCMP). The initial guiding hypothesis was the potential for a surficial, ion-adsorbed clay-type REE deposit, analogous to those in South China. However, the outcomes of the G-4 program have led to a fundamental and highly successful re-evaluation of this model, culminating in the discovery of two distinct, high-potential, in-situ mineral systems. This represents a significant paradigm shift in understanding the metallogenic potential of the Kachchh Basin.

7.1.1. Achievements of the Reconnaissance Stage

The G-4 program, executed within the approved Notified Quantum of Work (NQT) constraints, has yielded several landmark achievements that far exceed the typical outcomes of a reconnaissance-level study :

I. Successful Invalidation of the Initial Hypothesis: The program's first major success was the systematic and conclusive refutation of the ion-adsorbed clay model. Multi-fraction geochemical analysis, heavy mineral studies, and bedrock geochemistry demonstrated that REEs are not loosely adsorbed onto clays but are hosted within primary, discrete mineral phases (monazite, xenotime, apatite, florencite). This crucial finding prevented further expenditure on a low-potential exploration model and enabled a strategic pivot.

II. Discovery of Two New Mineral Systems: The most significant achievement was the identification of two previously unrecognized, in-situ mineral systems. By applying a Mineral Systems Analysis (MSA) framework, the exploration strategy successfully transitioned from surface anomaly chasing to a process-driven approach, leading to the discovery of:

- **Mineral System I:** A syngenetic, stratiform volcaniclastic-hosted REE system within the Late Jurassic Katrol Formation.

- **Mineral System II:** An epigenetic, structurally controlled hydrothermal iron-oxide system with classic Iron-Oxide-Copper-Gold (IOCG) characteristics within the Cretaceous Bhuj Formation.

III. Establishment of a New Metallogenic Framework: The discovery of these two genetically linked systems establishes a new metallogenic framework for the Kachchh pericratonic rift basin. It links Late Jurassic syn-rift felsic volcanism (source for Mineral System I) with subsequent Cretaceous tectono-magmatic reactivation and hydrothermal fluid flow along major crustal faults (driving Mineral System II). This provides a powerful predictive model for future exploration across western India.

IV. Validation of Prospectivity through Target Testing: The limited scout drilling program (603.5m drilled against 600m approved) successfully intersected both mineral systems, confirming their subsurface continuity and validating the geological models derived from surface mapping, geochemistry, and geophysics. This has significantly de-risked the project and provides high confidence for advancing to the next stage of exploration.

7.1.2. Analysis of Gaps and NQT Constraints

The G-4 program was designed as a reconnaissance survey with a corresponding NQT that limits the scope to broad-scale mapping, initial geochemical surveys, limited geophysics, and scout drilling. The achievements of the program were maximized within these constraints. The identified gaps are not shortcomings of the study but rather the logical next steps that are now justified by the G-4 results.

- **Resource Definition:** The G-4 stage is not intended for resource estimation. Consequently, the primary gap is the lack of data on the grade, tonnage, and economic viability of the two mineral systems. The continuity and thickness of the Katrol tuffite horizons and the grade distribution within the Bhuj IOCG system remain to be quantified.

- **Three-Dimensional Geometry:** While scout drilling confirmed the presence of the systems at depth, their full 3D architecture is unknown. The geometry of the interpreted IOCG breccia pipe, a key target identified by VES surveys, requires more detailed geophysical modeling and deeper drilling to define its shape, depth extent, and potential for high-grade feeder zones.

- **Metallurgical Understanding:** The G-4 program identified the key REE-bearing minerals, but no metallurgical test work was within its scope. The fine-grained nature

of the Katrol mineralization and the polymetallic complexity of the Bhuj IOCG ore require dedicated beneficiation studies to assess potential recovery pathways and economic viability.

The NQT for a reconnaissance program was fully utilized to make fundamental geological discoveries. The program successfully transitioned a regional geochemical anomaly into two tangible, drill-tested mineral systems, thereby providing the robust justification required to commit to a more intensive and costly G-3 stage exploration program.

7.2. Comparision with the global analogues

7.2.1. Katrol Stratiformal REE bearing System (MSA-I)

The reconnaissance survey in the Bhuj block has identified two distinct mineral systems, each analogous to well-documented deposit types globally. Mineral System I (Katrol Formation) comprises stratiform, volcaniclastic-hosted REE mineralization enriched in heavy rare earth elements (HREE). This low-grade, bulk-tonnage HREE system is comparable to deposits associated with felsic/peralkaline magmatism rather than the more common carbonatite-hosted LREE deposits. A prime analogue is the Round Top Mountain REE deposit in Texas, USA – a massive laccolithic rhyolite enriched in Y and HREE (~0.05% Y+HREE) along with Be, Li, U and other critical metals (Pingitore et al., 2018). Round Top's geology (peraluminous high-silica rhyolite) and enrichment in HREE closely mirror the Katrol tuffite system, and its economic viability hinges on large-scale, heap-leach extraction with dilute sulfuric acid. This suggests that the Katrol HREE mineralization, despite its modest grades (~0.1–0.2% TREO), could be economically significant if it exhibits similar leachability and scale (Pingitore et al., 2018). Another useful comparison is the Dubbo (Toongi) deposit in New South Wales, Australia, which is a hydrothermally altered trachytic breccia pipe hosting Zr-Hf-Nb-Y-REE mineralization. Like Katrol, the Dubbo deposit is polymetallic and linked to an alkaline igneous source. Notably, a sulfuric acid leach process was developed for Dubbo's ore, offering a metallurgical model for extracting REEs from silicate-hosted mineralization (*Spandler & Morris, 2016*). The Strange Lake deposit in Canada's Laurentian region provides a further analogue; it is a peralkaline granite complex with extensive HREE and Zr mineralization in pegmatites and aplites. Strange Lake's large tonnage and HREE-rich profile (with REE hosted in phases like gadolinite, zircon, and bastnäsite) demonstrate the potential grade and scale that felsic magmatic HREE systems can achieve (*Salvi & Williamsjones, 1990*). By comparison, the Katrol tuffites, though stratiform and thinner, could represent a disseminated, bulk-tonnage equivalent of such systems. Importantly, Katrol's enrichment in valuable HREE (Gd–Lu + Y) is a strategic advantage over giant LREE deposits like Bayan Obo in China. The Bayan Obo Fe-REE-Nb deposit, the world's largest REE resource – is hosted by a carbonatite–dolomite system and is overwhelmingly LREE-enriched (La–Ce-dominant). In contrast, the Katrol HREE system, though smaller, contains a higher proportion of scarce HREE, which are in

greater critical demand. Additionally, Katrol's non-carbonatite host rocks (volcaniclastic sediments) may pose fewer radioactivity and acid-consuming issues than carbonatite ore (*Chao et al., 1997*). Thus, while Bayan Obo underscores the exceptional scale possible in REE deposits, the Katrol system's similarities to Round Top, Dubbo, and Strange Lake highlight its favorable HREE tenor and suggest that modern processing techniques can be applied to evaluate its economic potential (*Pingitore et al., 2018; Spandler & Morris, 2016; Salvi & Williams-Jones, 1990; Chao et al., 1997*).

7.2.2. Bhuj IOCG-type Mineralization (MSA-II)

The Mineral System II (Bhuj Formation) represents a structurally controlled, IOCG (Iron Oxide Copper Gold)-style system with polymetallic enrichment (Fe-Ti-P-REE ± Cu-Au-Ag). This system is characterized by intense hydrothermal alteration (hematite breccias, magnetite-ilmenite enrichment, and associated REE-bearing minerals like monazite and xenotime) along major faults (e.g., Katrol Hill Fault zone). Global analogues for this type of mineralization confirm its significance and guide expectations for scale and metal association. The Olympic Dam deposit in South Australia is the archetypal giant IOCG and provides the closest parallel for the Bhuj system's ultimate potential. Olympic Dam lies on a craton margin and consists of hematite-dominated breccia bodies with a complex polymetallic suite of minerals. In addition to its Cu-U-Au-Ag ores, Olympic Dam contains significant REE concentrations (mainly as bastnäsite, florencite and monazite), with total REO on the order of 0.1% in ore and substantial Ce and La credits in the deposit. Key similarities between Olympic Dam and the Bhuj prospect include the brecciated hematite host, association with large structural corridors, and a multistage hydrothermal history (*Hitzman et al., 1992*). Notably, Olympic Dam's enormous size (≈2 billion tonnes at 1.6% Cu, 0.6 g/t Au, 3–4 g/t Ag, 0.06% U3O8) and its REE enrichments (hundreds of ppm level Ce, La in ore) demonstrate the upper end of what an IOCG system can become (*Hitzman et al., 1992*). While the Bhuj discovery is at a much earlier stage and of smaller known extent, the geological ingredients – a basin margin setting, intrusive-related hematite alteration, and a broad spectrum of critical metals – are analogous. This comparison provides a "best-case scenario" model: if the Bhuj IOCG system continues to depth, it could develop into a world-class deposit. Another instructive analogue is the Pea Ridge deposit in Missouri, USA – a Proterozoic iron oxide–apatite (IOA/IOCG) deposit which, like Bhuj, contains REE-rich breccia pipes within a predominantly iron-oxide system. Pea Ridge was an operating iron mine that produced magnetite and has documented rare-earth mineralization (~24,000 tonnes of contained REO in breccia zones) hosted by apatite, bastnäsite and monazite in its core breccia pipe (*Nuelle et al., 1992*). This underscores that significant REE can reside in IOCG/IOA systems even if they were historically developed for iron or copper. The Bhuj system's geochemical signature (REE + Y, Nb, Sc, V, etc.) is indeed reminiscent of such IOA-REE occurrences. Additionally, Nolans Bore in the Aileron Province of Australia serves as a pertinent analogue for hydrothermal REE concentration associated with structural zones. Nolans Bore is not an IOCG, but a REE–P–U deposit of hydrothermal origin where REEs

(notably Nd and Pr) are concentrated in apatite–allanite vein systems within metamorphic rocks (*Huston et al., 2016*). It reflects how fluid transport in a faulted crust can deposit significant REE (the Nolans Bore resource is ~30 Mt at 2.6% REO, with >85% of economic value in Nd-Pr oxides) in a setting with some similarities to Bhuj – e.g., proximity to crustal-scale structures and a mixed provenance of fluids (magmatic-hydrothermal phosphatic fluids). The Bhuj IOCG system, enriched in Fe and containing REE-bearing phases along with anomalous U and Th, aligns with a subtype of IOCG deposit that has significant critical metal content (*Hitzman et al., 1992; Huston et al., 2016*). In summary, the Bhuj mineralization can be viewed as an early-stage, REE-rich variant of an IOCG system. Comparative analogues like Olympic Dam underscore its potential scale and multicommodity value, while examples like Pea Ridge and Nolans Bore illustrate that substantial REE enrichment in such systems is geologically plausible and can be economically important (*Hitzman et al., 1992; Huston et al., 2016*).

It is also instructive to note what the Bhuj mineral systems are not analogous to the initial exploration model posited an ion-adsorption type REE deposit (clay-hosted, supergene-enriched) similar to the subtropical regolith deposits of southern China. However, our results clearly diverge from that model – the high TREE values in stream sediments were traced to detrital heavy minerals rather than adsorbed ions on clays. True ion-adsorption clay deposits, like those in Jiangxi Province, China, typically form by prolonged weathering of granitic rocks and feature REEs loosely bound to kaolinite and halloysite in the regolith (with ΣREE grades on the order of 0.05–0.2% in clay, dominated by HREE) (*Borst et al., 2020*). Such deposits yield REEs easily via mild salt leaching, and account for the bulk of global HREE supply. In the Bhuj Block, by contrast, no significant ion-adsorbed REE component was found – the REEs are hosted in mineral lattices (monazite, xenotime, apatite, etc.) of primary or secondary phases, indicative of a bedrock (hydrothermal and/or magmatic) origin rather than lateritic enrichment. The failure to identify clay-hosted REE mineralization actually served to redirect the exploration toward the now-confirmed hydrothermal systems. This outcome highlights the robustness of the Mineral Systems Analysis (MSA) approach: even when the superficial model (ion-adsorption) proved inapplicable, the presence of an underlying mineral system was revealed by following geological indications (e.g., heavy mineral anomalies and structural controls) rather than solely chasing the initial geochemical anomaly. In effect, the Bhuj G4 survey has de-risked the project at a conceptual level – it demonstrated that the region indeed hosts significant REE mineralization, albeit in a different geological mode than originally expected. By drawing on global analogues and integrating multifaceted data, the study has elevated the Bhuj area from a speculative anomaly to a geologically credible exploration target. The identified Katrol and Bhuj systems, taken together, establish the Bhuj Prospect as an emerging critical minerals district with both near-surface bulk-tonnage HREE potential and deeper high-grade IOCG-style potential. This dual discovery is regionally and nationally significant, as it opens a new frontier for indigenous REE resources in India. The analogues discussed provide not only context but also practical guidance for next steps – from metallurgy

(e.g., heap leach viability for Katrol material, as in Round Top and Dubbo) to geophysical and drilling strategies (e.g., targeting gravity highs for Bhuj IOCG, as exemplified by Olympic Dam). In the following sections, we summarize the main conclusions of this study and outline specific recommendations for advancing each mineral system through the next phase of exploration.

7.3. Conclusion:

This G4 reconnaissance program has achieved its primary objective of identifying credible REE mineralization in the Bhuj block, while also substantially improving the geological understanding of the area. Key conclusions are as follows:

Two distinct REE-bearing mineral systems have been confirmed:

I. a stratiform volcaniclastic (tuffite) horizon in the Mesozoic Katrol Formation enriched in HREE (Mineral System I), and

II. a fault-controlled Fe-oxide-dominated hydrothermal system in the Bhuj Formation with polymetallic (REE–Ti–P–Fe ± Cu–Au–Ag) signatures (Mineral System II).

These systems are genetically and spatially distinct, indicating two separate mineralization events or processes in the block's geological history.

The Katrol REE system (MSA-I) is characterized by thin (<1–3 m) but laterally continuous phosphatic-ferruginous tuff layers that range upto 0.10–0.15% total REO with an elevated proportion of HREE (HREEY ~30–40% of TREO). This style of mineralization, while low-grade, is analogous to large-tonnage HREE deposits in peralkaline volcanic or sub-volcanic settings (e.g., Round Top and Dubbo). The identification of these horizons confirms that the Katrol Formation hosts a regionally extensive, disseminated REE occurrence that could be amenable to bulk mining if continuity and tonnage are sufficient. The relatively higher HREE content (and presence of critical elements like Dy, Eu, Y) enhances the strategic importance of this system.

The Bhuj IOCG-style system (MSA-II) is marked by intense ferruginization and brecciation of host sandstones over broad areas (kilometer-scale corridors). Geochemically, it exhibits strong enrichment in Fe (20–50% Fe_2O_3 in rock), P (P_2O_5 from apatite), Ti, and transition/base metals, along with REE anomalism (with monazite and xenotime identified in heavy mineral concentrates). The heavy mineral concentrate assays from streams (up to 1–3% TREO in concentrates) and bedrock chip samples (hundreds of ppm TREE in altered sandstone) confirm that this system is the source of the originally detected REE anomalies. Importantly, the Bhuj mineralization is epigenetic and structurally controlled – it likely represents the upper levels of an IOCG system, wherein mineralization is focused along faults and fractures. This implies that higher grades could exist at depth in breccia bodies or veins,

as commonly seen in IOCG deposits worldwide (Hitzman et al., 1992). The presence of pathfinder elements (Co, Ni, Cu, Au, Bi, U, etc., in minor amounts) in the geochemical data further supports an IOCG affinity.

Exploration methodology validation: The program's adaptive exploration strategy – pivoting from a surface geochemical model (ion-adsorption clays) to a bedrock-focused model – was vindicated. The critical decision to perform heavy mineral separation on stream sediments provided the breakthrough in understanding the true nature of the anomalies. This approach confirmed that the REEs were tied to resistate minerals and shifted the exploration focus to upstream lithologies. The subsequent integration of field mapping, petrography, and geochemistry was effective in delineating the two mineral systems. This outcome underscores the value of an MSA-driven approach in greenfield exploration: by considering the full mineral system (sources, pathways, traps) we were able to discover a deposit style different from the initial expectation.

Prospect significance: The Bhuj REE Prospect (Block) is now recognized as a tangible exploration asset with dual deposit targets. The Katrol HREE stratiform system provides a near-term, shallow drill target that could potentially yield a large tonnage but low-grade resource. Such a resource, if upgraded by beneficiation (e.g., gravity or flotation to concentrate phosphates) and confirmed to be leachable (analogous to other clay/volcanic-hosted REE deposits), could be economically viable as a source of HREE – a class of elements for which India currently has no domestic supply. The Bhuj IOCG system, on the other hand, represents a higher-risk, higher-reward target: it may host a significant discovery at depth (e.g., a massive hematite-apatite breccia with high-grade REE and base metals), which could be of national importance given the size of analogous IOCG deposits. Even in a lower-end outcome, the Bhuj system could represent a smaller IOCG deposit or a cluster of mineralized zones that collectively add considerable value (e.g., an "IOCG district" along the Katrol Fault). In either case, confirming the presence of these systems has de-risked the project conceptually – it is now clear that the anomalous geochemistry of the Bhuj block is due to genuine bedrock mineralization and not a geochemical artifact.

Strategic outlook: The discoveries align well with India's strategic objectives for critical minerals. The Katrol system targets heavy REEs (Dy, Tb, Eu, Y etc.) which are critical for high-tech and defense applications, while the Bhuj system could yield light REEs plus poly-metallic by-products (phosphate for fertilizers, iron, Ti, etc., and possibly Cu-Au if present in quantity). The conceptual parallels to established deposits (as discussed above) provide confidence that with systematic exploration, these targets can be advanced toward resource definition. Moreover, the project has generated significant geological knowledge of the Kachchh Basin – revealing a hitherto unrecognized IOCG-style mineralizing event in a Mesozoic basin. This new knowledge has regional implications, suggesting that similar structurally controlled

mineralization could exist elsewhere along the basin faults, thereby opening a new exploration frontier in western India.

7.3.1. Summary Conclusions

In summary, the G-4 Reconnaissance Survey in the Bhuj Clay Prospect Block has yielded definitive conclusions that fundamentally redefine the mineral prospectivity of the Kachchh Basin:

I. The initial hypothesis of an ion-adsorbed clay-type REE deposit was successfully refuted. Geochemical and mineralogical evidence confirmed that REEs are hosted in primary, discrete mineral phases within bedrock.

II. Two distinct, in-situ mineral systems with significant economic potential have been discovered: Mineral System I (Katrol Stratiform REE) and Mineral System II (Bhuj IOCG-Style).

III. Mineral System I is a syngenetic, volcaniclastic-hosted REE system within the Late Jurassic Katrol Formation. Mineralization is hosted in laterally continuous, vertically stacked phosphatic-ferruginous tuffite layers. The primary REE-hosting minerals are fine-grained fluorapatite and monazite.

IV. Mineral System II is an epigenetic, structurally controlled hydrothermal system within the Cretaceous Bhuj Formation. It exhibits the characteristic geological, mineralogical, geochemical, and geophysical signatures of an Iron-Oxide-Copper-Gold (IOCG) deposit.

V. The Bhuj IOCG-style system is characterized by intense iron-oxide alteration (hematite-magnetite), hydrothermal brecciation, and a polymetallic association of Fe-Cu-Au-Ag-Co-Sn-U-REE.

VI. The principal structural controls for Mineral System II are the Katrol Hill Fault and the Median High, which acted as primary conduits for mineralizing hydrothermal fluids.

VII. A distinct, pipe-like low-resistivity anomaly identified by VES surveys provides strong geophysical evidence for a potential feeder zone for the IOCG system, representing a prime exploration target.

VIII. Scout drilling has successfully intersected both mineral systems, confirming their subsurface continuity and validating the geological models.

IX. The Bhuj Prospect represents a newly identified and significant REE and polymetallic province in western India, warranting immediate advancement to the next stage of exploration.

The G4 survey in the Bhuj block succeeded in moving the project from speculation to a clearly defined opportunity. The initial hypothesis of ion-adsorption clay REEs was disproven, but in its place two valuable targets (mineralisation styles) have emerged. Both mineralisation styles warrant aggressive follow-up. The next phase of work (proposed G3 stage for Katrol / hybrid G4/G3 stage for Bhuj) should aim to: (a) delineate and quantify the Katrol stratiform REE horizons (through trenching and shallow drilling), and (b) test the Bhuj IOCG system at depth (through targeted geophysics and deep drilling) followed by Resource establishment. The following recommendations outline the specific actions required to achieve these goals, drawing on best practices from analogous deposits worldwide.

7.4. Recommendations for Further Exploration

Building upon the outcomes of the G-4 reconnaissance program, a set of nine G3 prospect blocks (B1–B6 and K1–K3) have been delineated within the Bhuj REE Prospect area (*Fig. 7.1*).

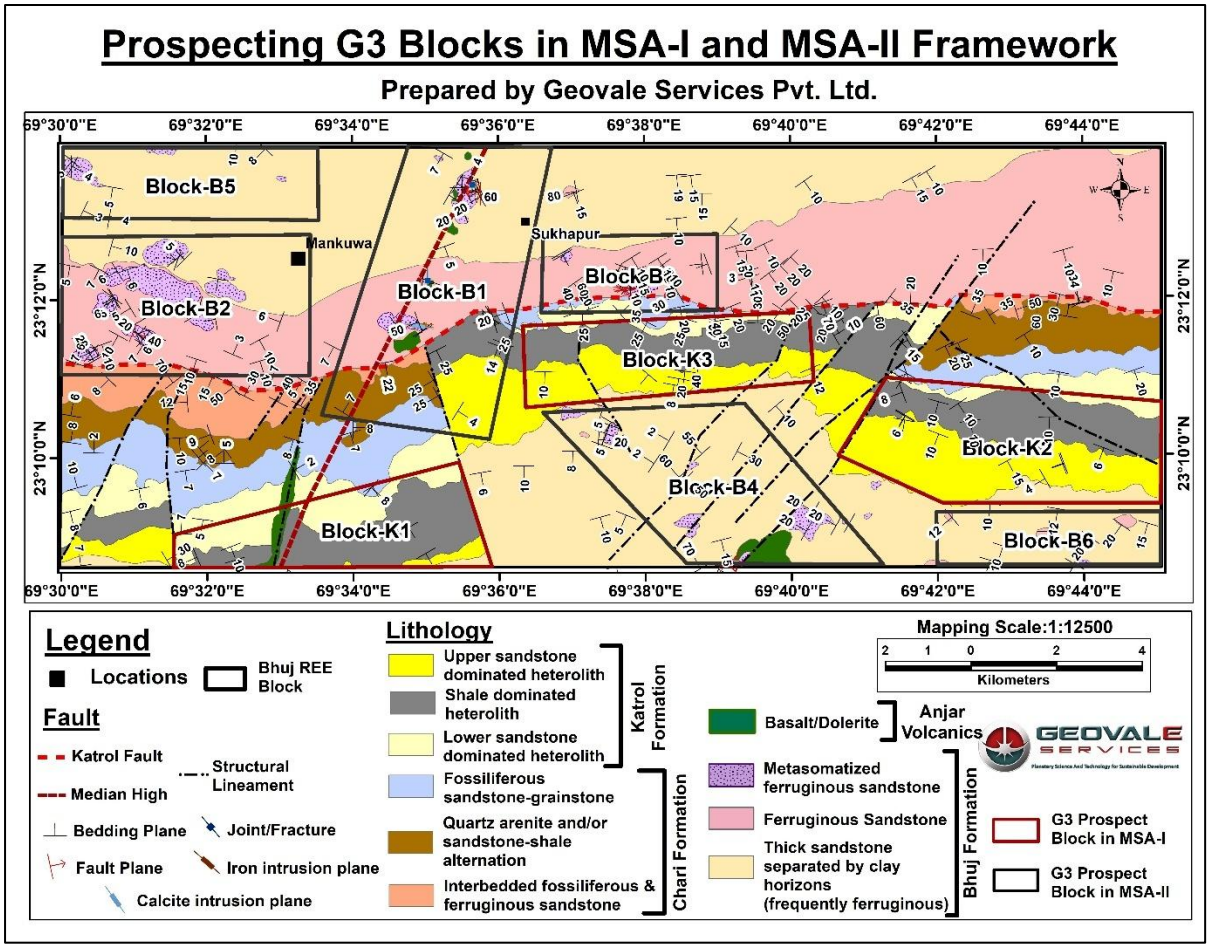

Fig. 7. 1 Geological map showing prospecting G3 target zones within the Bhuj REE Prospect Block.

These blocks represent the most prospective zones defined through the integration of geological mapping, geochemical anomalies, structural interpretation, geophysical correlations and target testing within the dual MSA framework. Blocks prefixed with "K" correspond to the Katrol stratiform REE system (MSA-I), while those prefixed with "B" represent the Bhuj IOCG-style system (MSA-II). The numerical order of the blocks denotes their priority ranking for G3 exploration.

Each block has been selected based on proximity to fertile horizons, confirmed mineralization style, anomaly intensity, and logistical feasibility. The following table summarizes their key attributes of the delineated g3 blocks (*Table.7.1*)

Table. 7. 1 Summary of Proposed G3 Prospect Blocks within Bhuj REE Block.

Sl. No.	Block ID	Area (km²)	MSA Framework	Commodity	Rationale for Block Selection
1	K1	11.62	MSA-I (Stratiform REE bearing System)	REE and RM	Thickest and most continuous tuffite layer; strong Fe-P-REE correlation; TiO_2>1%; confirmed by BH-01 intercepts and bedrock geochemical anomaly
2	K2	17.87		REE and RM	High TREEY at stratigraphic depth, confirmed by BH-02 intercepts; high Fe concentration; both shale and sandstone dominated unit are potential for REE and RM mineralization
3	K3	11.9		REE and RM	Eastern extension of K1 horizon; close association with the Katrol Hill Fault
4	B1	24.4	MSA-II (IOCG-type)	REE and RM	Strong Fe-oxide alteration, TiO_2 (1–1.4 %), high REE anomalies (500-800ppm); pronounced LREE dominance, accompanied by high Ce, La, Ni, Co, Pb, and Ba, confirmed by BH-05; located along Katrol Hill Fault and Median High corridor.
5	B2	18.9		REE and RM	strong HREE enrichment (HREE/LREE ≈ 0.63); Cu-Pb-Zn-Cr-Pb-V multi-element anomalies, confirmed through bedrock sampling and BH-07 and 08; Fe-oxide veining near Median High and Katrol Hill fault.

Sl. No.	Block ID	Area (km²)	MSA Framework	Commodity	Rationale for Block Selection
6	B3	7.3		REE and RM	Balanced LREE-HREE proportions with distinct Zn-Cr-V-Pb anomalies, confirmed from both bedrock samples and BH-03 and 04; moderate Fe-oxide enrichment, close association with major fault intersections
7	B4	17.2		REE and RM	Coincident with metasomatized sandstone, anomalous Zn and Pb, confirmed from bedrock samples; traversed by subsidiary plays of the Katrol Hill Fault.
8	B5	9.8		REE and RM	Similar polymetallic lithology and upstream extension of B2-B4 corridor; moderate REE (500–800 ppm TREEY) and Zn enrichment.
9	B6	6.5		REE and RM	Located along southern fault splay; TiO_2 > 1 %; moderate zn enrichment.

The delineated G3 blocks encompass the most REE and RM fertile zones across both mineral systems. Together, these blocks form the operational focus for advancing Bhuj's REE exploration from conceptual discovery to quantitative resource evaluation.

7.4.1. Recommendations for G3 Exploration Plan

The delineation of these G3 blocks marks a decisive transition from reconnaissance discovery to targeted evaluation. Their systematic evaluation through drilling, geophysical refinement, and mineralogical studies will enable resource definition, grade modeling, and a clearer understanding of the basin's metallogenic architecture.

7.4.1.1. Katrol (Stratiform HREE) Target – G3 Exploration Strategy

Geological Mapping, Geochemical and Mineralogical Vectoring:

Continue geological mapping and geochemical sampling in the Katrol formation to search for thicker or higher-grade sections of the tuffite horizon. Utilize portable XRF or geochemical assay data to map element dispersion around the REE layers (e.g., P, Y, Zr, Nb as pathfinders). Mineralogical studies (SEM-EDS, microprobe) on trench samples should be undertaken to better understand the distribution of REEs among minerals (apatite vs. monazite vs. xenotime) and grain size/liberation characteristics. This will feed back into metallurgical planning and also help identify any zonation (for example, whether HREE

enrichment increases toward certain paleo-depositional centers or varies with clay content). If multiple REE horizons are present (as hinted by some mapping), prioritize those with the best thickness-grade combination for resource drilling.

Trenching and Shallow Drilling:

I. Excavate trench lines across the strike of the known REE-bearing tuffite layers in the Katrol Formation to expose fresh bedrock and establish true thickness, grade continuity, and lateral variability of mineralization. Trenches should be placed at several strategic locations along the mapped horizon (and any parallel horizons identified by soil/rock geochemistry) to obtain bulk samples.

II. Follow up with shallow drilling (rotary or diamond core) on a broad grid (e.g., 100 m centers along strike) to trace the horizon to depth (expected at 20–50 m vertically below surface) and to test for repetitions or stacking of multiple REE-rich layers.

The goal of this program is to define an initial inferred resource, if possible, by obtaining enough intercepts of the mineralized horizon. Given the likely low grade, a large number of shallow holes (tens of drill holes over several kilometers of strike) will be needed to quantify tonnage and grade variation.

• Bulk Sampling and Metallurgical Testing:

Collect composite samples from trenches (several tonnes in total) for bench-scale metallurgical tests. Initial tests should focus on beneficiation and leaching. Because the REEs in Katrol are hosted largely in phosphatic and ferruginous matrix (apatite, monazite, xenotime in a goethitic/siliceous matrix), two parallel approaches are recommended:

I. **Physical beneficiations** - investigate simple gravity or magnetic separation to concentrate heavy minerals (analogous to methods used in placers or heavy mineral sands) and/or flotation to concentrate apatite/phosphate (taking cues from operations like Mount Weld or monazite sand processing). A successful concentration step could significantly upgrade the REE content before leaching.

II. **Leaching trials** - test direct atmospheric leaching of the raw and beneficiated material using dilute sulfuric acid or ammonium sulfate, inspired by the Round Top and South China clay practices (Pingitore et al., 2018; Borst et al., 2020). Measure REE recovery, reagent consumption, and identify any deleterious elements (e.g., radioactive elements, if any). The objective is to evaluate early on whether the Katrol material can yield a leachate rich in REEs with reasonable recovery (>50–60%) and without excessive acid consumption. Positive results would justify more detailed economic evaluation; negative results might shift strategy toward concentrating the REE minerals for off-site processing.

7.4.1.2. Bhuj (IOCG-Style) Target – Hybrid G4 / G3 Exploration Strategy

Geophysical Surveys (High-Priority):

Implement a comprehensive geophysical program to delineate the subsurface architecture of the Bhuj IOCG system. Two methods are paramount:

I. Gravity surveying and magnetic surveying over the prospective corridors identified (e.g., along the Katrol Hill Fault zone and the "Median High" structure). IOCG systems often have dense, magnetite-rich cores that produce measurable gravity and magnetic anomalies (Hitzman et al., 1992).

II. A detailed ground gravity survey (station spacing 200 m or tighter over key areas) and high-resolution magnetics (e.g., drone or ground magnetometer lines 100–200 m apart) should be conducted. Process and model this data in 3D to identify anomalous high-density bodies and coincident magnetic highs at depth.

III. Given the already mapped alteration, we anticipate one or more gravity highs corresponding to dense hematite-magnetite concentrations beneath the surface gossanous zones. Those will be primary drill targets.

IV. Additionally, consider Induced Polarization (IP) surveys over the strongest gravity/magnetic anomalies – IP can detect chargeable zones which might indicate disseminated sulfides (e.g., chalcopyrite or pyrite) commonly associated with IOCG mineralization. An IP-resistivity survey (either pole-dipole or dipole-dipole array) could help differentiate between a purely oxide body and one with sulfide content, which is relevant both for discovery (presence of Cu-Au) and for drilling safety (sulfides give stronger conductive targets).

The geophysical program is the critical first step to refine drill targets given that the mineralization is largely blind (inferred at depth from alteration at surface).

Exploratory Deep Drilling:

Design a phase-I diamond drilling program to test the highest-priority targets from geophysics and geochemistry.

I. Geovale recommends 5 – 8 initial deep holes, each on the order of 500–800 m in depth (depending on anomaly depth estimates), to penetrate below the level of surface oxidation and intersect the hypothesized feeder structures or breccia bodies.

II. Diamond core drilling is essential (as opposed to RC) because the core will allow detailed logging of alteration minerals, textures, and provide samples for assay and petrography that are unweathered.

III. Oriented core measurements will also help unravel the structural controls. Drilling should be oriented to cross the known fault planes at high angle – likely inclined holes of 60–70° – based on the interpreted dip of structures (e.g., if the Katrol Fault dips ~60° NE, drill from the hanging wall towards the fault).

IV. The first hole might be positioned near the area of strongest surface alteration (as a "discovery hole"), with subsequent holes stepping out along strike or testing deeper sections of the same structure.

The goal of this phase is to confirm the presence of significant mineralization at depth (e.g., broad zones of hematite breccia with REE minerals, or perhaps massive magnetite/apatite veins with Cu-Au) and to obtain fresh samples for a full suite of analyses (REE, base metals, precious metals, S, C, etc.). Even if these initial holes do not encounter economic grades, the information gained on the hydrothermal system's vertical extent and intensity will be invaluable for vectoring.

Downhole and On-site Testing:

Employ downhole geophysical logging in the deep drill holes (especially if any significant alteration zones are hit).

I. Gamma logging can detect elevated radioelements (U, Th, K) often associated with IOCG alteration (e.g., presence of uraninite, or potassic alteration); density logging can help map hematite/magnetite content relative to background. If feasible, conduct optical or acoustic televiewer logs to get structural orientation of fractures and breccia fabric in situ – this can complement the oriented core data.

II. Additionally, consider on-site portable XRF analysis on core at regular intervals to get immediate feedback on elemental trends (e.g., Fe, P, Cu, REE if above detection after proper calibration). This real-time data can guide adjustments in drilling (such as pushing hole deeper if increasing Cu or P is observed near end-of-hole).

Geochemical Vectoring and Alteration Study:

As core is obtained, perform detailed lithogeochemical analysis of the alteration halo. Assay not only for metals of interest but also for alteration indices (e.g., K/Na ratios, Fe^3+/Fe^2+, sulfidation indices). Often in IOCG systems, broad haloes of alteration elements like K, Na depletion (from albite alteration), or enrichment in Ca (from calcic alteration) can guide vectors to the core of the system (Hitzman et al., 1992). A systematic sampling of core for multi-element ICP analysis (including REE, major oxides, and trace pathfinders) should be done. In parallel, conduct petrographic and mineragraphic studies on select core sections to identify mineral assemblages (especially to confirm the presence of REE minerals like monazite, bastnäsite, etc., and ore minerals like chalcopyrite or bornite if any). This will

establish the paragenetic sequence and help identify "hot spots" within the system (for instance, the presence of high-temperature alteration minerals like biotite-magnetite or actinolite might indicate proximity to the fluid upwelling zone).

Follow-up Targeting:

Based on results from the above, prepare for a potential Phase II drilling campaign. If any hole intersects significant mineralization (for example, >0.5% TREO over tens of meters, or any noteworthy Cu-Au intercepts), additional holes should be planned to step out and delineate the geometry of that zone. Even if initial holes show only subeconomic mineralization, analyze the alteration vectors: does alteration intensify with depth? Is there increase in certain metals towards one end of the drilled area? Use this data to refine the geological model. In IOCG systems, it's common that the first few holes may hit the periphery of the system, requiring vectoring toward a core that could be a few hundred meters lateral or deeper. Therefore, maintain flexibility in planning holes, and integrate all incoming data rapidly into your 3D model (using modeling software to combine geology, geochemistry, and geophysics).

In conclusion, the next exploration stage (G-3) should aggressively pursue both identified targets with tailored strategies: a resource drilling and metallurgy program for the near-surface stratiform Katrol REE horizons, and a geophysics-guided deep drilling program for the Bhuj IOCG system. This two-pronged approach balances risk and reward – appraising a potentially lower-grade but more straightforward deposit (Katrol) while simultaneously testing a higher-impact, deep target (Bhuj). The recommended work is well-justified by the G-4 findings and is designed to rapidly build on the momentum of discovery. By following these recommendations, the project will be positioned to deliver a maiden REE resource in the short term (from Katrol) and to make the crucial test of the Bhuj system's potential to host a major deposit. Each step will be informed by and benchmarked against global best practices and analogues, as documented in the geological literature, to maximize the chances of success in this pioneering REE exploration initiative.

Chapter 8

Expenditure

8. Expenditure

8.1. Sanctioned Amount - Expenditure Amount - % of expenditure

Sanctioned Amount	Project Initiation Date	Project Completion Date	Total Expenditure	% of Expenditure
₹ 2,73,15,781.30	November, 2023	September, 2025	₹ 2,73,15,781.30	100%

Chapter 9

References

9. References:

Amin, B. A. and Rao, U. D. G. 2020. Exploration Report on Clay Block, Kachchh District, Gujarat. Commissionerate of Geology and Mining, Government of Gujarat, pp. 1–35.

Bedi, Naresh. 1983. Report on the Investigation for Bentonite in Parts of Kutch District, Gujarat (Progress Report for F.S. 1976–77) (WRO-11732). Geological Survey of India, Gujarat Circle, Ahmedabad, October 1983, pp. 1–40.

Bhatt, L. S., Kachhara, R.C., 1973. Report on the pre-detailed mineral survey of a part of Mandvi and Abdasa talukas, Kutch district Gujarat state. FS: 1971-72. Gujarat Mineral and Research and Development Society, Report No. 121, pp. 1-20.

Biswas, S.K., 1977. Mesozoic rock stratigraphy of Kutch. Quarterly Journal of the Geological Mining and Metallurgical Society of India, 49, 1-52.

Biswas, S.K., 1987. Regional tectonic framework, structure and evolution of the western marginal basins of India. Tectonophysics, 135 (4), pp. 307-327.

Biswas, S.K., 2005. A review of structure and tectonics of Kutch basin, western India, with special reference to earthquakes. Current Science, 88 (10), pp. 1592-1600.

Biswas, S.K., 2016. Tectonic framework, structure and tectonic evolution of Kutch Basin, western India. In Conference GSI, pp. 129-150.

Borst, A. M., Smith, M. P., Finch, A. A., Estrade, G., Villanova-de-Benavent, C., Nason, P., & Geraki, K. (2020). Adsorption of rare earth elements in regolith-hosted clay deposits. Nature Communications, 11(1), Article 4386. DOI: 10.1038/s41467-020-17801-5.

Chao, E. C. T., Back, J. M., Minkin, J. A., Tatsumoto, M., Junwen, W., Conrad, J. E., & Shengguang, H. (1997). Sedimentary carbonate-hosted giant Bayan Obo REE-Fe-Nb ore deposit of Inner Mongolia, China – a cornerstone example for giant polymetallic ore deposits of hydrothermal origin. U.S. Geological Survey Bulletin, 2143, 65 p.

Desikan, N., Thothathiri, G., and Kulkarni, G. R. 1968. Geological Mapping in Parts of Kutch District, Gujarat (Progress Report for the Field Season 1966–67) (WRO-23750). Geological Survey of India, Gujarat Circle, December 1968, pp. 1–41.

Forest Survey of India (FSI), 2023. India State of Forest Report 2023. Ministry of Environment, Forest and Climate Change, Government of India.

Ghevariya, Z. G. 1979. Geology of Certain Parts in Toposheet No. 41 E/12, Kachchh District, Gujarat (Preliminary Report for the F.S. 1978-79). Geological Survey of India, Gujarat Circle (WRO-6805), pp. 1–14.

Ghevariya, Z. G. 1984. Geology of Certain Parts in Toposheet 41E/12, Kutch District, Gujarat State (Progress Report for F.S. 1978–79) (WRO-11614). Geological Survey of India, Western Region, Ahmedabad, May 1984, pp. 1–25

Ghevariya, Z. G. 1984. Systematic Geological Mapping in Parts of Toposheet No. 41E/12, Kutch District, Gujarat (Progress Report for F.S. 1980–81) (WRO-11704). Geological Survey of India, Gujarat Circle, January 1984, pp. 1–35

Ghevariya, Z. G. 1986. Systematic Geological Mapping of the Area West and South of Anjar, Kachchh District, Gujarat (Parts of Toposheets 41E/16 & 41I/4, F.S. 1984–85) (WRO-18047). Geological Survey of India, Western Region, Ahmedabad, July 1986, pp. 1–42.

Ghevariya, Z. G. and Srikarni, C. 1987. Systematic Geological Mapping of the Area West of Anjar, Kachchh District, Gujarat (Parts of Toposheets 41E/16 and 41I/4, Progress Report for F.S. 1986–87) (WRO-18866). Geological Survey of India, Western Region, Ahmedabad, pp. 1–40.

Guha, D., Das, S., Srikarni, C. and Chakraborty, S.K., 2005. Alkali basalt of Kachchh: its implication in the tectonic framework of Mesozoic of western India. Journal of Geological Society of India, 66 (5), pp. 599.

Hitzman, M. W., Oreskes, N., & Einaudi, M. T. (1992). Geological characteristics and tectonic setting of Proterozoic iron oxide (Cu-U-Au-REE) deposits. Precambrian Research, 58(1–2), 241–287.

Huston, D.L., Mernagh, T.P., Hagemann, S.G., Doublier, M.P., Fiorentini, M., Champion, D.C., Jaques, A.L., Czarnota, K., Cayley, R., Skirrow, R. and Bastrakov, E., 2016. Tectono-metallogenic systems — The place of mineral systems within tectonic evolution, with an emphasis on Australian examples. Ore Geology Reviews, 76, pp. 168–210.

Huston, D. L., Maas, R., Cross, A., Hussey, K. J., Mernagh, T. P., Fraser, G., & Champion, D. C. (2016). The Nolans Bore rare-earth element-phosphorus-uranium mineral system: geology, origin and post-depositional modifications. Mineralium Deposita, 51(6), 797–822.

India Meteorological Department (IMD), 2023. Climatological Tables and District-wise Rainfall Statistics, Gujarat State. Ministry of Earth Sciences, Government of India.

Kathiara, R. S. 1984. Report on the Investigation for Phosphorite in Parts of Kutch District, Gujarat (Progress Report for the Field Season 1978–79) (WRO-11609). Geological Survey of India, Gujarat Circle, Ahmedabad, pp. 1–14.

Kshirsagar, P.V., Sheth, H.C. and Shaikh, B., 2011. Mafic alkalic magmatism in central Kachchh, India: a monogenetic volcanic field in the northwestern Deccan Traps. Bulletin of Volcanology, 73 (5), pp. 595-612.

Kulkarni, G. R. 1966. Interim Report on the Investigation of Clay Deposits in Parts of Nakhatrana and Mandvi Talukas, Kutch District, Gujarat (WRO-1964). Geological Survey of India, Western Region, pp. 1–25.

Paul, D.K., Ray, A., Das, B., Patil, S.K. and Biswas, S.K., 2008. Petrology, geochemistry and paleomagnetism of the earliest magmatic rocks of Deccan Volcanic Province, Kutch, Northwest India. Lithos, 102 (1-2), pp. 237-259.

Pingitore, N. E. Jr., Clague, J. W., & Gorski, D. (2018). Remarkably consistent rare earth element grades at Round Top yttrofluorite deposit. Advances in Materials Physics and Chemistry, 8(1), 1–14.

Poddar, M. C. 1954. Geological Report on the Khatrod Range and Neighbouring Areas, Kutch (F.S.1953-54) (CHQ-17609). Geological Survey of India, Calcutta, pp. 1–20.

Salvi, S., & Williams-Jones, A. E. (1990). The role of hydrothermal processes in the granite-hosted Zr-Y-REE deposit at Strange Lake, Quebec/Labrador: evidence from fluid inclusions. Geochimica et Cosmochimica Acta, 54(9), 2403–2418.

Shah, N. V. 1970–71. Report on investigation for bauxite in some villages of Mandvi and Mundra talukas, Kutch district. Directorate of Geology and Mining, Government of Gujarat (R.N. 88), pp. 1–50.

Sahu, B. K. and Dinesh, A. C. 1991. Report on Systematic Geological Mapping of Toposheet 41E/12, Kachchh District, Gujarat (F.S. 1989–90) (WRO-21014). Geological Survey of India, Western Region, pp. 1–38.

Shah, N. V. 1972–73. Report on investigation by drilling for bauxite in village of Nakhatrana and Abdasa talukas, Kutch district. Directorate of Geology and Mining, Government of Gujarat (R.N. 142), pp. 1–55.

Shukla, A. C., 1974. Repost on Detail Investigation for Phosphatic Nodules between Motawadva and Godpur, Tal. Mandvi, Dist. Kutch. Field Season 1972-73. Directorate Of Geology and Mining, Government of Gujarat, R.N. 145, pp. 1-22.

Srivastava, A.P., Krishna, J., Rajagopalan, G., Pathak, D.B. and Ojha, J.R., 1994. The first ever absolute agedetermination from the Jurassic of Kachchh, Western India. Geobios, 27, pp.529-533.

Spandler, C., & Morris, P. A. (2016). Geology and genesis of the Toongi rare metal (Zr-Hf-Nb-Ta-Y-REE) deposit, New South Wales, Australia, and implications for rare metal mineralization in peralkaline igneous systems. Contributions to Mineralogy and Petrology, 171(8), Article 68 (25 pages).

Suthar, K. 2017. Geochemical Mapping of Toposheet No. 41E/12 of Kachchh District, Gujarat (Final Report for F.S. 2009–10) (NGCM/KGCMP). Geological Survey of India, Gandhinagar, pp. 1–200.

Wyborn, L.A.I., Heinrich, C.A. and Jaques, A.L., 1994. Australian Proterozoic Mineral Systems: Essential Ingredients and Mappable Criteria, Proceedings of the Australian Institute of Miningand Metallurgy Annual Conference, Melbourne, pp. 109-115.

10. Locality Index:

Sl. No	Name	SOI Toposheet No.	Latitude	Longitude
1	Bharapar	41E/12	23.1315	69.6338
2	Bharasar	41E/12	23.199	69.5633
3	Bhuj	41E/12	23.2418	69.6725
4	Bhujodi	41E/12	23.2236	69.7365
5	Fotdi	41E/08	23.2177	69.4911
6	Jadura Mota	41E/12	23.1591	69.6889
7	Kodki	41E/12	23.243	69.5554
8	Madhapar	41E/12	23.2335	69.7106
9	Mankuva	41E/12	23.2082	69.5671
10	Mirjapur	41E/12	23.2203	69.6341
11	Reha Mota	41E/12	23.1412	69.7467
12	Samatra	41E/08	23.1916	69.4983
13	Sedat	41E/12	23.1446	69.6308
14	Sukhpar	41E/12	23.2174	69.6072

Chapter 11

Annexures

11. Annexures

All the annexures referenced in this report are presented herein in their respective serial order, ensuring systematic organisation and ease of cross-referencing for the reader.

Annexure-I: Details Stream Sediment collection points

Sl No.	Location No.	Latitude	Longitude	Village/ Area	Exposure Location	Stream Sediment ID	Stream Sediment Collection	Stream Sediment Description
1	GSPL_Bhuj_ 02/12/23	23.183	69.564	Bharasar	Near the KGCMP high HREE value location, near Wandhsim Reserve Forest. River cut section.	105437 105438	Stream sediments collected from bedrock at deepest point in the bedrock	105438: SS <1mm 5kg 105437: <2mm 5kg
2	GSPL_Bhuj_ 04/12/24	23.216	69.589	Sukhapar	Near Nagthada tample, hill scarp section of doleritic/basaltic dyke within Bhuj Formation	105439 105440	Slope wash/creek sample??	105439: <1mm 5kg 105440: <2mm 5kg
3	GSPL_Bhuj_ 05/12/23	23.243	69.568	Kodki	Riverbed section near Kara Talav (near high HREE value section of KGCMP)	105431 105432	80cm thic T1 with river bed sediments (very clean sand) consist of quartz (white, yellow and pink), small pebbles of reddish sandstone, few hematite grains. <2mm sample collected from high energy trap sites and <1mm sample collected from finer material of the bank area.	105431: < 1mm 5kg 105432: <2mm 5kg
4	GSPL_Bhuj_ 22/12/23	23.185	69.695	Jadura Nana	Riverbed section near on Dhunaraja Dam Road, in the vicinity of Bhuj Reserve Forest	105419	1st order stream draining sandstone shale deposit	Stream sediment <1mm 5kg
5	GSPL_Bhuj_ 24/12/23	23.153	69.702	Jadura Nana	Stream cut section on continuation of Jadura village to Chakar village road	105423	2nd order stream draining the Katrol Formation	105423: Stream sediment <1mm 5kg
6	GSPL_Bhuj_ 26/12/23	23.134	69.688	Jadura Nana	Road side stream cut section on Rehanana to Surajpur connecting road	105457 105458	3rd order stream, draining the Bhuj Formation	105457: <1mm 5kg 105458: <2mm 5kg
7	GSPL_Bhuj_ 27/12/23	23.132	69.645	Surajpur	Road side stream cut section on Rehanana to Surajpur connecting road	105461 105462	at junction of two 2nd order stream draining the Bhuj Formation	105461: <2mm 5kg 105462: <1mm 5kg
8	GSPL_Bhuj_ 29/12/23	23.199	69.512	Samatra	Exposure on Bhuj Nakshatrana road	105447 105448	1st order stream draining Bhuj Formation	105447: <2mm 5kg 105448: <1mm 5kg
9	GSPL_Bhuj_ 30/12/23	23.224	69.509	Kodki	Road side exposure at high HREE location area, mostly flat slightly sloping NNE, with small stream(gullies) on Kodki Road	105426	1st order stream draining Bhuj Formation	105426: <1mm 5kg
10	GSPL_Bhuj_ 31/12/23	23.224	69.524	Kodki	Near Rati Tala,Hanuman Temple,roadside digged and dumped rocks.However whole area is farmland on Kodki road	105435 105436	3rd order stream, draining the Bhuj Formation and probably the reported alkali plug and phosphorite area	105435: <1mm 5kg 105436: <2mm 5kg

Sl No.	Location No.	Latitude	Longitude	Village/ Area	Exposure Location	Stream Sediment ID	Stream Sediment Collection	Stream Sediment Description
11	GSPL_Bhuj_ 33/12/23	23.184	69.503	Samtra	Hill exposure near Samtra Vadasar road, near high HREE point	105449105450	3rd order stream, draining the Chari Formation	105449: <1mm 5kg105450: <2mm 5kg
12	GSPL_Bhuj_ 35/12/23	23.224	69.566	Mankuva	Stream channel between Mankuva Kodki road near Gangwali Dhar.	105433 105434	2nd order stream draining the Bhuj Formation	105433: <1mm 5kg 105434: <2mm 5kg
13	GSPL_Bhuj_ 36/12/23	23.207	69.656	Sukhpar	Stream channel on Bhuj Mundra highway, on way to Bhata Talav	105442	3rd order stream draining the Chari, Katrol and Bhuj formations	105442: stream sediment <1mm 5kg
14	GSPL_Bhuj_ 38/12/23	23.187	69.643	Mudra road	Exactly at high HREE value location, hill scarp section on Bhuj Mundra highway, near Bhata Talav	105443	2nd order stream draining the Katrol Formation	105443: <1mm, 5kg
15	GSPL_Bhuj_ 41/12/23	23.136	69.741	Reha Nana	Near high Zr, Cd point, beside Reha nana Surajpur road, a checkdam was there. 200 meter before the dam a stream section	105455 105456	Sample collected from microcatchment	105455: <1mm 5kg 105456: <2mm 5kg
16	GSPL_Bhuj_ 44/12/23	23.197	69.539	Mankuva	River cut section beside Bhuj Nakshatrana road and north of Bhuj Naliya Western railway line	105445 105446	2nd order stream draining the Chari and Bhuj formations	105445: <2mm 5kg 105446: <1mm 5kg
17	GSPL_Bhuj_ 45/12/23	23.179	69.536	Mankuva	River cut section near Bhuteshwar Mahadev temple, accessible from Bhuj Nakshatrana road and south of Bhuj Naliya Western railway line	105451 105452	3rd order stream draining the Chari Formation	105451: <1mm 5kg 105452: <2mm 5kg
18	GSPL_Bhuj_ 46/12/23	23.193	69.724	Madhapar	River cut section near Gangeshwar Mahadev temple, on Gangeswar road, trying to reach the high Zr, Cd, Nb and Y anamoly location.	105453 105454	1st order stream draining the Chari Formation	105453: <1mm 5kg 105454: <2mm 5kg
19	GSPL_Bhuj_ 47/12/23	23.164	69.631	Sanatorium	River channel exposure, near a sanatorium, on Bhuj Mundra Road	105463 105464	2nd order stream draining the Katrol and Bhuj formations. Sample collected from the deepest point of the stream	105463: <1mm 5kg 105464: <2mm 5kg
20	GSPL_Bhuj_ 48/12/23	23.153	69.637	Sedat	River channel exposure on Bhuj Mundra Road	105465 105466	2nd order stream draining the Bhuj Formation. Sample collected from the deepest point of the stream	105465: <1mm 5kg 105466: <2mm 5kg

Sl No.	Location No.	Latitude	Longitude	Village/ Area	Exposure Location	Stream Sediment ID	Stream Sediment Collection	Stream Sediment Description
21	GSPL_Bhuj_ 49/12/23	23.151	69.624	Sedat	Near Sedat villege, behind 153 BN BSF Marine Camp stram channel, accessible from Bhuj Mundra Road	105467	2nd order stream draining the Katrol Formation.	<1mm 5kg
22	GSPL_Bhuj_ 50/12/23	23.195	69.608	Sukhapar	Stram channel near Wandhay talav accessible from Mandvi Bhuj Road	105468	2nd order stream draining the Katrol Formation. Sample collected from the deepest point of the stream	<1mm 5kg
23	GSPL_Bhuj_ 51/01/24	23.218	69.566	Mankuva	Stream channel on Mankuva _Kodki road	105469	2nd order stream draining Bhuj Formation. Sample collection point is 100 -150 meter before the confluence point of the 1st order streams.	<1mm 5kg
24	GSPL_Bhuj_ 52/01/24	23.229	69.530	Fotdi	Stream channel on Kodki road	105470	2nd order stream draining Bhuj Formation. Sample collection point is 50 -100 meter before the confluence point of the 1st order and 2nd order streams.	<1mm 5kg
25	GSPL_Bhuj_ 53/01/24	23.225	69.521	Fotdi	Stream channel on Kodki road	105471 105472	2nd order stream draining Bhuj Formation.	105471: <1mm 5kg 105472: <2mm 5kg
26	GSPL_Bhuj_ 54/01/24	23.176	69.538	Bharasar	Stream channel on a cart road	105473	3rd order stream draining Chari Formation.	<1mm 5kg
27	GSPL_Bhuj_ 55/01/24	23.313	68.856	Gudthar (Outside block)	Exposure on the reservoir side of mitti dam near matiya dev temple	105476	Sample collected as stream sediment sample from the stream.	105476:<1mm 5kg
28	GSPL_Bhuj_ 68/01/24	23.150	69.727	Reha	Stream channel, accessible from Jadura Chakara road through a local cart road	105484 105485	3rd order stream draining the Bhuj and Katrol formations, Stream sediment collected 150 metre before the confluence of the 2nd order streams	105484: <1mm 5kg 105485: <2mm 5kg
29	GSPL_Bhuj_ 70/01/24	23.210	69.535	Mankuva	Road side location beside Mankuva Nakshatrana road, between Mankuva and Nagiyari	105486	Sample collected from the depressed area of the stream.	105486: <1mm 5kg
30	GSPL_Bhuj_ 94/02/24	23.187	69.723	Hirapar	100 m East of high HREE location a stream discharges in a low depression area.	105497	105497: Stream sediment brownish colour.collected from the flat low lying area	Collected as whole, no sieving
31	GSPL_Bhuj_ 96/02/24	23.186	69.724	Hirapar	100 m SE of previous location a stream (dry) channel	105500	brownish colour stream sediment	Collected as whole, no sieving
32	GSPL_Bhuj_ 97/02/24	23.199	69.702	Hirapar	Closest accsible area close to high HREE value location near hirapar villege	105502	Stream sediment light brown/Yellowish in colour	Collected as whole, no sieving

Sl No.	Location No.	Latitude	Longitude	Village/ Area	Exposure Location	Stream Sediment ID	Stream Sediment Collection	Stream Sediment Description
33	GSPL_Bhuj_106/02/24	23.225	69.588	Sukhpar	At high HREE value location	105514	stream sediment brownish in colour	Sample collected as whole without sieving from a low lying area
34	GSPL_Bhuj_107/02/24	23.227	69.510	Fotdi	At high HREE value location, Kodki road side crematorium	105515	Stream sediment light brown in colour	Sample collected as whole without sieving from a low lying area
35	GSPL_Bhuj_138/06/24	23.154	69.726	Reha Nana	Hill section,near New Cart Road,near Reha Nana Village.	107520 (old Id: 105636)	Sample collected (2mm) from six point locations, over a stretch of 25m. Junction of two 2nd order streams. .The traps consist of boulders,bed rocks.Very less biogenic contamination seen.	The sediments consist of coarse to very coarse grained sands,mostly quartz. Few iron clast (low contamination)
36	GSPL_Bhuj_139/06/24	23.179	69.752	Ler	Near Ler village towards ler dam at river side	107521 (old Id: 105637)	Sample collected (2mm) from six point locations, over a stretch of 50m along river section. Confluence of 2nd order and 1st order streams. .The trap sites are slope break, deepest part of the stream, bar ends, boulder traps, bedrock traps.High biogenic contamination seen (shurb growth). ~2cm layers have been removed from top while collection of the sample.	The sediments consist of coarse to very coarse grains of quartz, yellowish sst/siltstone, red beds,clear transparent white crystals(apatite?)(Xenotime?) in decreasing order of abundance.Grains are sub GSPL_Bhuj_rounded to rounded.
37	GSPL_Bhuj_140/06/24	23.152	69.743	Reha Nana	Near Reha Nana village in the windmill areas.	107522(old Id: 105638)	Sample collected (2mm) from nine point locations, over a stretch of 60m. Confluence of 2nd order and 3rd order streams. The trap sites are deepest part of the streams, boulde/cobble/pebbler traps, bedrock traps.Low direct biogenic contamination. This is a topographically low, depressed area where water comes from every direction.	The sediments (bimodal size distribution) consist of coarse to very coarse grains of quartz(rounded to subrounded,platy elongated),clear transparent white crystals(apatite,calcite?),few light green minerals,clast of red beds(elongated GSPL_Bhuj_angular) in decreasing order of abundance.Grains are sub GSPL_Bhuj_rounded to rounded. Fine material (unidentified) is also constitute the sediment

Sl No.	Location No.	Latitude	Longitude	Village/ Area	Exposure Location	Stream Sediment ID	Stream Sediment Collection	Stream Sediment Description
38	GSPL_Bhuj_141/06/24	23.154	69.749	Reha Nana and Reha Mota	Near Reha Nana village in the windmill areas.	107523 (old Id: 105639)	Sample collected (2mm) from nine point locations, over a stretch of 780m. 2nd order stream sediment. Very good trap sites, mainly bed rock traps. Very low direct biogenic contamination	The sediments (polymodal) consist of very coarse to coarse grained >90% quartz (yellow to pinkish),clear transparent white crystals(not calcite as its hard),clast of red beds,opaque black minerals,siltstone clast in decreasing order of abundance.Grains are sub GSPL_Bhuj_angular to sub GSPL_Bhuj_rounded.Polymodal size distribution,fine materials cannot be identified.
39	GSPL_Bhuj_142/06/24	23.150	69.721	Reha Mota	Near Reha Mota village, road side stream section along a cart road connecting Reha Mota and Jadura Mota	107524 (old Id: 105640)	Sample collected (2mm) from seven point locations, over a stretch of 30m. After the confluence of 2nd order and 3rd order streams. The trap sites are not very good. However, sample has been collected from deepest part of the streams, slope breaks, meander corners. High anthropogenic and low direct biogenic contamination. The location is surrounded by local reservoirs for rain water.	The sediments consist of medium to coarse grained, consisting of quartz(sub GSPL_Bhuj_rounded to sub GSPL_Bhuj_angular)>90%,clear transparent white crystals,clast of red beds, black minerals with dull lustre,siltstone,shale clast in decreasing order of abundance.Fine materials can be seen.
40	GSPL_Bhuj_143/06/24	23.153	69.696	Jadura	Near Jadura village, ~1km west of Jadura Chakar road (extension of Dhunaraja dam road)	107525 (old Id: 105641)	Sample collected (2mm) from six point locations, over a stretch of 20m. Stram meanders at few points The trap sites are very good. Sample has been collected from deepest part of the streams, boulder traps on channel bed.	The sediments consist of medium to fine grained quartz (rounded to sub GSPL_Bhuj_rounded,yellowish to pinkish)>95%,clear transparent white crystals, very few black opaque minerals,siltstone clast in decreasing order of abundance.
41	GSPL_Bhuj_144/06/24	23.154	69.702	Jadura	Near Jadura village,beside Jadura _hakar road (extension of Dhunaraja dam road)	107526 (old Id: 105642)	Sample collected (2mm) from five point locations, over a stretch of 20-30m. No meandering observed. The trap sites are very good. Sample has been collected from deepest part of the streams, boulder and bed rock traps on channel bed.	The sample has bimodal size distribution, very coarse to fine grained.The coarser grains are sub GSPL_Bhuj_rounded to sub GSPL_Bhuj_angular with high sphericity and consist of quartz (yellow & pink, 85 GSPL_Bhuj_90%), clasts of siltstone, yellowish shale,red bed, unidentified black mineral and same whitish clear crystals and biotite in decreasing order of abundance.

Sl No.	Location No.	Latitude	Longitude	Village/ Area	Exposure Location	Stream Sediment ID	Stream Sediment Collection	Stream Sediment Description
42	GSPL_Bhuj_ 145/06/24	23.148	69.578	Naranpar Ravli	From Bhuj Mandvi highway, near Naranpur Ravli village opposite to the Nayara Petrol Pump.	107527 (old Id: 105643)	Sample collected (2mm) from twelve point locations, over a stretch of 40m. The trap sites are very good. Sample has been collected from deepest part of the streams, boulder and bed rock traps and highest curve of meanders on channel bed. Biogenic and anthropogenic contamination is low.	The sediments are generally pebbly to cobbly sized making it difficult to get enough amount after sieving.Bimodal size distribution,very fine grained not recognizable.The coarse sediments are sub GSPL_Bhuj_angular to sub GSPL_Bhuj_rounded with low sphericity and contains framework of clast of red beds,limonitic layers,siltstone,quartz,the white transparent crsytals,green mineral? and black unidentified mineral in decreasing order of abundance.
43	GSPL_Bhuj_ 146/06/24	23.138	69.540	Godpar	Near Godpar village,Jamora Dam & Vankol Virdo Temple, accesible by a metal road and then a cart road through Godapar village from Bhuj GSPL_Bhuj_Mandvi highway	107528 (old Id: 105644)	Sample collected (2mm) from seven point locations, over a stretch of 30m. Trap sites are moderately to good with meander traps,bed rock exposure traps and boulder traps. High anthropogeic contamination seen	The sediments are coarse to medium grained ,finer grains are not identifiable.Sample consist of medium to coarse grained quartz,siltstone clasts of redbeds and white transparent crystal (very low in amount) in decreasing order of abundance.The grains are sub GSPL_Bhuj_angular to sub GSPL_Bhuj_rounded with low sphericity.
44	GSPL_Bhuj_ 152/06/24	23.178	69.585	Bharasar	Near Swami Narayan temple, road side stream channel on Bharasar Road, in the vicinity of Wandhsim Reserve Forest	107538 (old Id: 105654)	Sample collected (2mm) from nine point locations, over a stretch of 15m. Trap sites are very good with ,bed rock exposure traps (appearance of cascade) and boulder traps. High anthropogeic and moderate biogenic contamination seen	The sediments are coarse to medium grained with cobbles and boulders.Consist of rock fragments(<2%, clast of siltstone, red beds),quartz,white transparent mineral,black mineral in decreasing order of abundance.The clasts are sub GSPL_Bhuj_rounded to angular with moderate sphericity.There is mud in the sediment.
45	GSPL_Bhuj_ 153/06/24	23.184	69.595	Vandh sim	Road side stream channel, near Vandh Sim village on Bharasar road, in the vicinity of Wandhsim Reserve Forest.	107539 (old Id: 105655)	Sample collected (2mm) from four point locations, over a stretch of 12m. Trap sites are not good at all. The sample has been collected from bar deposit and stream bed, filled with boulders, cobbles and pebbles. Very high anthropogeic and biogenic contamination seen	The sediment has been weight sieved, and hence not been described.

Sl No.	Location No.	Latitude	Longitude	Village/ Area	Exposure Location	Stream Sediment ID	Stream Sediment Collection	Stream Sediment Description
46	GSPL_Bhuj_154/06/24	23.198	69.674	Tapkeshwari temple	Road side stream channel, near Tapkeshwari Temple on Tapkeswari road	107540 (old Id: 105656)	Sample collected (2mm) from eleven point locations, over a stretch of 30m. Trap sites are good with boulder traps (stream bed, filled with boulders, cobbles and pebbles). High anthropogeic and low biogenic contamination seen	Sediments collected are medium to coarse grained containing rounded to sub angular grains of quartz.(>90%),siltstone,red nodule beds,black minerals with dull lusture (<1%) in decreasing order of abundance.
47	GSPL_Bhuj_158/06/24	23.252	69.745	Gada	Near Gada village, Hill scarp section	107544 (old Id: 105660)	Creek sample collected (2mm) from slope breaks, depressed areas, small creeks, and boulder traps	The sediments are coarse to medium grained with cobbles and boulders. Consist of rock fragments(clast of red beds, intrusion),quartz, unidentified black mineral and many small broken fragments of bedrock in decreasing order of abundance.The clasts are subangular to angular with low sphericity.
48	GSPL_Bhuj_160/06/24	23.227	69.484	Fotdi	Near Fotdi village, stream cutting small mounds of sandstone, ~1km north of the Fotdi Kodki metal road	107547 (old Id: 105663)	Sample collected (2mm) from eight point locations, over a stretch of 60m. Trap sites are not very good but sediments collected from bedrock obstacles,bed rock traps,confluence points. No anthropogenic and less biogenic contaminations are seen.	The sediments from the confluence point are matured minerologically.The sediments consist of medium to fine grained,angular to sub angular,clast of pink quartz,completely platy transparent white crystals and very coarse fragments(fumaroles/altered sst)<1% in decreasing order of abundance.
49	GSPL_Bhuj_161/06/24	23.228	69.488	Fotdi	Near Fotdi village,cricket ground,Shree Shiv Natha Mahadev temple, accessible from Fotdi Kodki metal road.	107548 (old Id: 105664)	Sample collected (2mm) from seven point locations, over a stretch of 30m. Trap sites are very good,sediments collecetd from bed rock traps,meandering points,confluence points.No anthropogeic and no biogenic contamination seen.	The sediments from the confluence point are matured minerologically.The sediments consist of medium to fine grained,angular to sub angular,clast of pink and white quartz,completely platy transparent white crystals and very coarse fragments(fumaroles/altered sst)<1% in the decreasing order of abundance.
50	GSPL_Bhuj_162/06/24	23.227	69.499	Fotdi	Near Fotdi village,approx 700m east of Shree Shiv Natha Mahadev temple, accessible from Fotdi Kodki metal road.	107549 (old Id: 105665)	Sample collected (2mm) from eight point locations, over a stretch of 20m. Trap sites are very good,sediments are collected from large boulders which act as trap, meandering points. High biogenic and nearly no anthropogeic contaminations.	Sediments collected are medium to fine grained consisting of sub angular fragments of pink quartz (>3_4%), fumaroles, limonitic layer, red sst with 5 GSPL_Bhuj_7% and gravel size clast of quartz in decreasing order of abundance.
51	GSPL_Bhuj_164/06/24	23.221	69.590	Kalyanpar	Near Kalyanpar village at Shree Hari Visamo Tekdi Temple.	107553 (old Id: 105669)	(2mm) slopewash sample, collected at the slope break of the basalt from four point locations over a stretch of 15m. High anthropogenic activity.	Sediments consist of coarse grained,sub angluar to angular clast of basalt,quartz,magnetite in decreasing order of abundance.

Sl No.	Location No.	Latitude	Longitude	Village/ Area	Exposure Location	Stream Sediment ID	Stream Sediment Collection	Stream Sediment Description
52	GSPL_Bhuj_ 164/06/24	23.221	69.590	Kalyanpar	Near Kalyanpar village at Shree Hari Visamo Tekdi Temple.	107554 (old Id: 105670)	Bulk slopewash sample, collected at the slope break of the basalt from four point locations over a stretch of 15m. The sample can not be sieved due to moisture. High anthropogenic activity.	Very fine grained,mostly clay sample,black coloured.
53	GSPL_Bhuj_ 165/06/24	23.221	69.590	Kalyanpar	Near Kalayanpur village, at Shri Hari Visamo Takdi temple, at the opposite side of the hill, where basalt has intruded	107557 (old Id: 105673)	(2mm) slopewash sample, collected at the slope break of the hill from six point locations throughout the hill. High anthropogenic activity.	Sediment consist of medium to fine grained quartz, clay? with very coarse grained quartz clast,rock fragments,red fumaroles and black mineral (<1%) in decreasing order of abundance.The grains are angular to sub GSPL_Bhuj_angular.Quartz grains shows moderate sphericity.
54	GSPL_Bhuj_ 166/06/24	23.137	69.664	Bharapar	Near Kirgurya Dungar,near Bharapar village at north of Sapar timbo village,Hemkund Horticulture farm.	107558 (old Id: 105674)	Sample collected (2mm) from six point locations, over a stretch of 20m. Trap sites are very good,sediments have been collected from trap sites of large boulders on the channel bed and exposed bedrock. High biogenic and nearly no anthropogeic contaminations.	The sediments are medium to fine grained with few gravel size clasts of quartz (>90%), pink quartz, <2% rock fragments) (silt, weathered basalts?) in decreasing order of abundance.The clasts are sub angular to sub rounded with low sphericity.

Annexure-II: XRF Analysis of Stream Sediments (-125 micron fraction)

S.N	Original ID	Sample ID	Location No	Latitude	Longitude	Type	Field Description
1	105419	105626	GSPL_Bhuj-22/12/2023	23.185	69.6951	SS	1st order stream draining sandstone-shale deposit
2	105426	105627	GSPL_Bhuj-30/12/2023	23.2243	69.5094	SS	1st order stream draining Bhuj Formation
3	105433	105628	GSPL_Bhuj-35/12/2023	23.2239	69.5661	SS	2nd order stream draining the Bhuj Formation
4	105435	105629	GSPL_Bhuj-31/12/2023	23.2242	69.5236	SS	3rd order stream, draining the Bhuj Formation and probably the reported alkali plug and phosphorite area
5	105438	105630	GSPL_Bhuj-02/12/2023	23.1829	69.5639	SS	Stream sediments collected from bedrock at deepest point in the bedrock
6	105439	105631	GSPL_Bhuj-04/12/2023	23.2157	69.5894	SW	Slope wash/creek sample??
7	105442	105632	GSPL_Bhuj-36/12/2023	23.2072	69.6555	SS	3rd order stream draining the Chari, Katrol and Bhuj formations
8	105443	105633	GSPL_Bhuj-38/12/2023	23.1865	69.6428	SS	2nd order stream draining the Katrol Formation
9	105448	105634	GSPL_Bhuj-29/12/2023	23.1991	69.5123	SS	1st order stream draining Bhuj Formation
10	105449	105635	GSPL_Bhuj-33/12/2023	23.1835	69.5031	SS	3rd order stream, draining the Chari Formation
11	105451	105636	GSPL_Bhuj-45/12/2023	23.1785	69.5359	SS	3rd order stream draining the Chari Formation
12	105453	105637	GSPL_Bhuj-46/12/2023	23.1926	69.7243	SS	1st order stream draining the Chari Formation
13	105465	105638	GSPL_Bhuj-48/12/2023	23.153	69.637	SS	2nd order stream draining the Bhuj Formation. Sample collected from the deepest point of the stream
14	105467	105639	GSPL_Bhuj-49/12/2023	23.1508	69.6239	SS	2nd order stream draining the Katrol Formation.
15	105484	105640	GSPL_Bhuj-68/01/2024	23.1498	69.7271	SS	3rd order stream draining the Bhuj and Katrol formations, Stream sediment collected 150 metre before the confluence of the 2nd order streams
16	105486	105641	GSPL_Bhuj-70/01/2024	23.2101	69.5349	SS	Sample collected from the depressed area of the stream.
17	105497	105643	GSPL-Bhuj-94/02/24	23.1873	69.7233	SS	Stream sediment brownish colour.collected from the flat low lying area
18	105500	105644	GSPL-Bhuj-96/02/24	23.1857	69.7237	SS	brownish colour stream sediment
19	105502	105645	GSPL-Bhuj-97/02/24	23.1992	69.7017	SS	Stream sediment light brown/Yellowish in colour
20	105514	105646	GSPL-Bhuj_106/02/24	23.2246	69.5877	SS	stream sediment brownish in colour
21	105515	105647	GSPL-Bhuj-107/02/24	23.2268	69.5095	SS	Stream sediment light brown in colour

Table Continued...

Annexure-II

S.N	Original ID	Sample ID	Sample Description	Al_2O_3	BaO	CaO	Cr_2O_3	Fe_2O_3	K_2O	MgO	MnO	Na_2O	P_2O5	TiO_2	SiO_2	LOI	SO_3
1	105419	105626	<125 micron fraction of 105419 (<1mm) sample	5.05	0.02	14.11	0.04	2.85	0.96	0.68	0.07	0.35	0.1	1.16	60.93	12.63	0.11
2	105426	105627	<125 micron fraction of 105426 (<1mm) sample	4.18	0.04	0.13	<0.01	1.34	1.75	0.1	0.04	0.12	0.05	0.77	90.07	1.03	0.06
3	105433	105628	<125 micron fraction of 105433 (<1mm) sample	1.89	<0.01	0.39	<0.01	2.32	0.3	0.19	0.05	0.04	0.04	0.47	92.83	1.12	0.06
4	105435	105629	<125 micron fraction of 105435 (<1mm) sample	3.3	0.04	0.17	0.02	2.46	1.43	0.15	0.05	0.1	0.08	1.66	88.73	1.03	0.06
5	105438	105630	<125 micron fraction of 105438 (<1mm) sample	5.84	0.03	10	0.05	4.75	1.05	1.21	0.1	0.39	0.09	1.25	65.76	8.78	0.1
6	105439	105631	<125 micron fraction of 105439 (<1mm) sample	12.2	0.06	3.77	0.04	13.99	0.96	1.93	0.31	1.2	0.19	2.57	56.04	5.97	0.06
7	105442	105632	<125 micron fraction of 105442 (<1mm) sample	10.72	0.03	6.28	0.02	1.93	0.52	0.33	0.03	0.12	0.05	0.79	68.72	9.06	0.7
8	105443	105633	<125 micron fraction of 105443 (<1mm) sample	13.72	0.08	1.4	0.02	4.23	2.79	0.4	0.05	0.14	0.1	0.84	69.67	6.02	0.06
9	105448	105634	<125 micron fraction of 105448 (<1mm) sample	6.71	0.04	0.52	0.02	5.62	1.53	0.41	0.07	0.23	0.13	1.81	79.22	3.05	0.08
10	105449	105635	<125 micron fraction of 105449 (<1mm) sample	6.31	0.03	4.45	0.04	5.41	1.22	1.4	0.09	0.53	0.08	1.16	74.75	3.76	0.14
11	105451	105636	<125 micron fraction of 105451 (<1mm) sample	9.91	0.04	1.53	0.02	5.56	1.83	0.52	0.07	0.19	0.08	0.86	73.73	5.08	0.07
12	105453	105637	<125 micron fraction of 105453 (<1mm) sample	4.29	0.04	6.4	0.03	3.06	1.35	0.51	0.07	0.3	0.09	0.95	76.51	5.74	0.09
13	105465	105638	<125 micron fraction of 105465 (<1mm) sample	5.16	0.03	7.3	0.04	2.96	0.9	0.61	0.07	0.61	0.12	1.3	73.59	6.6	0.08
14	105467	105639	<125 micron fraction of 105467 (<1mm) sample	3.78	0.03	0.38	0.01	2.42	0.77	0.32	0.05	0.11	0.07	0.97	88.75	1.86	0.09
15	105484	105640	<125 micron fraction of 105484 (<1mm) sample	3.22	0.03	0.18	0.02	1.89	1.34	0.09	0.05	0.13	0.06	1.11	90.4	0.86	0.06
16	105486	105641	<125 micron fraction of 105486 (<1mm) sample	6.58	0.05	0.61	<0.01	2.23	1.87	0.29	0.06	0.22	0.07	0.82	83.72	3.03	0.1
17	105497	105643	<125 micron fraction of 105497	11.02	0.05	1.12	0.01	3.54	1.94	0.49	0.05	0.24	0.1	0.68	74.61	5.6	0.12
18	105500	105644	<125 micron fraction of 105500	8.14	0.02	14.22	0.01	3.66	1.45	0.63	0.06	0.47	0.09	0.62	55.49	14.32	0.1
19	105502	105645	<125 micron fraction of 105502	5.53	0.01	10.1	<0.01	3.12	1.08	0.44	0.04	0.22	0.09	0.31	67.75	10.45	0.26

S.N	Original ID	Sample ID	Sample Description	Al_2O_3	BaO	CaO	Cr_2O_3	Fe_2O_3	K_2O	MgO	MnO	Na_2O	P_2O5	TiO_2	SiO_2	LOI	SO_3
20	105514	105646	<125 micron fraction of 105514	0.7	<0.01	0.03	<0.01	0.47	0.07	0.02	0.03	<0.01	0.05	0.51	97.35	0.29	<0.05
21	105515	105647	<125 micron fraction of 105515	4	0.06	0.08	0.01	2.42	2.03	0.08	0.04	0.11	0.08	1.28	88.31	0.88	0.05

Annexure-III: ICPMS Analysis of Stream Sediments (-125 micron fraction)

S.N	Original ID	Location No	Latitude	Longitude	Type	Sample Description	Li	Be	Sc	V	Ga
1	105419	GSPL_Bhuj-22/12/2023	23.185	69.6951	SS	<125 micron fraction of 105419 (<1mm) sample	10.6	0.7	9.7	73.4	9.8
2	105426	GSPL_Bhuj-30/12/2023	23.2243	69.5094	SS	<125 micron fraction of 105426 (<1mm) sample	10.3	<0.5	4.5	29.3	6.2
3	105433	GSPL_Bhuj-35/12/2023	23.2239	69.5661	SS	<125 micron fraction of 105433 (<1mm) sample	8.1	<0.5	3.3	37.5	3
4	105435	GSPL_Bhuj-31/12/2023	23.2242	69.5236	SS	<125 micron fraction of 105435 (<1mm) sample	10.4	0.6	13.5	62.5	9.3
5	105438	GSPL_Bhuj-02/12/2023	23.1829	69.5639	SS	<125 micron fraction of 105438 (<1mm) sample	15.7	0.8	14.1	99.7	8.5
6	105439	GSPL_Bhuj-04/12/2023	23.2157	69.5894	SW	<125 micron fraction of 105439 (<1mm) sample	14.3	1.7	20.2	276.5	21.3
7	105442	GSPL_Bhuj-36/12/2023	23.2072	69.6555	SS	<125 micron fraction of 105442 (<1mm) sample	26.7	1.7	13.9	77.8	14.1
8	105443	GSPL_Bhuj-38/12/2023	23.1865	69.6428	SS	<125 micron fraction of 105443 (<1mm) sample	42.9	1.2	11	75.6	16.1
9	105448	GSPL_Bhuj-29/12/2023	23.1991	69.5123	SS	<125 micron fraction of 105448 (<1mm) sample	19.8	0.8	17.1	103.1	18.2
10	105449	GSPL_Bhuj-33/12/2023	23.1835	69.5031	SS	<125 micron fraction of 105449 (<1mm) sample	17.4	0.8	16.7	115.5	9.5
11	105451	GSPL_Bhuj-45/12/2023	23.1785	69.5359	SS	<125 micron fraction of 105451 (<1mm) sample	31.2	1	11.3	88.9	11.8
12	105453	GSPL_Bhuj-46/12/2023	23.1926	69.7243	SS	<125 micron fraction of 105453 (<1mm) sample	9.5	0.6	7.1	80.3	5.7
13	105465	GSPL_Bhuj-48/12/2023	23.153	69.637	SS	<125 micron fraction of 105465 (<1mm) sample	10.9	0.8	10.5	66.3	11.9
14	105467	GSPL_Bhuj-49/12/2023	23.1508	69.6239	SS	<125 micron fraction of 105467 (<1mm) sample	10	<0.5	5.8	49.5	5.4
15	105484	GSPL_Bhuj-68/01/2024	23.1498	69.7271	SS	<125 micron fraction of 105484 (<1mm) sample	10.8	0.5	6.4	41.8	10.6
16	105486	GSPL_Bhuj-70/01/2024	23.2101	69.5349	SS	<125 micron fraction of 105486 (<1mm) sample	16.7	0.6	6.3	44	8.2
17	105497	GSPL-Bhuj-94/02/24	23.1873	69.7233	SS	<125 micron fraction of 105497	37.7	1	9.1	79.9	14.3
18	105500	GSPL-Bhuj-96/02/24	23.1857	69.7237	SS	<125 micron fraction of 105500	28	1.1	9.4	82.5	11
19	105502	GSPL-Bhuj-97/02/24	23.1992	69.7017	SS	<125 micron fraction of 105502	21.2	0.6	5.5	43.5	6.1
20	105514	GSPL-Bhuj_106/02/24	23.2246	69.5877	SS	<125 micron fraction of 105514	12.2	<0.5	2.5	12.7	2.2
21	105515	GSPL-Bhuj-107/02/24	23.2268	69.5095	SS	<125 micron fraction of 105515	11.5	<0.5	8.8	45.3	11.9

Table Continued..

Annexure-III

S.N	Original ID	Type	Ge	Se	Rb	Sr	Y	Zr	Nb	Mo	Cd	In	Sn	Sb	Te	Cs	La	Ce	Pr	Nd
1	105419	SS	0.8	3.5	29.8	475.2	30.9	479.3	17.4	0.7	<0.5	<0.5	1.7	0.7	<0.5	0.8	131	261.7	29.4	102.5
2	105426	SS	<0.5	1.1	44.9	62.6	15.2	255	7	0.6	<0.5	<0.5	1.2	0.7	<0.5	0.6	61.4	122.8	13.7	47.9
3	105433	SS	<0.5	1	9.8	77.4	7.2	118.7	8	1.2	<0.5	<0.5	1.3	2.6	<0.5	<0.5	23.7	44.8	5.1	17.3
4	105435	SS	0.7	3.3	39.1	66.2	43.5	1149.7	29.5	0.9	<0.5	<0.5	2	2	<0.5	0.7	120.4	239.6	26.9	94.3
5	105438	SS	<0.5	1.2	34.1	323.8	19.9	194.4	19.9	0.7	<0.5	<0.5	1.7	1.2	<0.5	1.1	48.6	97	11	39.6
6	105439	SW	0.5	2.2	32.6	310.4	32.8	363.9	38.2	1.1	<0.5	<0.5	2.4	1.1	<0.5	1.4	85.2	178.5	19.3	69
7	105442	SS	<0.5	1.8	17.6	822.9	19.9	174.9	14.7	1.2	<0.5	<0.5	2.6	1.4	<0.5	1	30.6	61	7.4	27.4
8	105443	SS	<0.5	1.1	78.1	143.3	19.5	183.1	14.3	0.7	<0.5	<0.5	2.1	1.4	<0.5	1.9	48.6	95.5	11.1	39.6
9	105448	SS	1.4	5.4	42	76.6	49.1	531.7	23	0.9	<0.5	<0.5	2.4	0.7	<0.5	0.8	194.4	378.7	43.3	150.1
10	105449	SS	<0.5	1.9	37.2	726.6	20.7	176.2	16	0.6	<0.5	<0.5	1.4	1.7	<0.5	1.2	54	110.1	12.4	44.1
11	105451	SS	<0.5	1.3	59.1	131.4	16.9	196.3	12.6	0.7	<0.5	<0.5	1.7	1	<0.5	2.4	32.9	67.1	7.6	27.5
12	105453	SS	0.7	1	34.6	225	16.8	269.4	12.7	0.5	<0.5	<0.5	1.4	1.3	<0.5	0.7	69.5	135.2	14.6	55
13	105465	SS	0.9	3.2	27.9	241.5	36.4	460.6	14.4	0.6	<0.5	<0.5	1.9	0.7	<0.5	0.8	161.9	321.1	36.1	125.9
14	105467	SS	<0.5	0.9	22	78.1	14.6	313.4	7.4	<0.5	<0.5	<0.5	1.2	0.7	<0.5	0.8	42.7	86.3	9.6	33.7
15	105484	SS	1	3	35	62.4	27	351.6	17.4	0.8	<0.5	<0.5	2.5	1.3	<0.5	0.6	155	307.2	34.2	118.4
16	105486	SS	<0.5	0.8	51.5	75.9	12.6	134.9	12.9	0.6	<0.5	<0.5	1.2	0.6	<0.5	1.1	42.5	84.1	9.3	32.2
17	105497	SS	<0.5	0.8	72.7	149.4	14	102.1	10.3	0.7	<0.5	<0.5	1.9	0.7	<0.5	3.4	32.6	66.3	7.5	27.1
18	105500	SS	<0.5	0.7	53	287.8	16	131.9	9.6	0.6	<0.5	<0.5	1.7	0.9	<0.5	2.3	38.1	76.9	8.8	31.8
19	105502	SS	<0.5	<0.5	36.7	338.1	9.6	59.8	4.9	0.6	<0.5	<0.5	0.9	0.7	<0.5	1.4	13.4	27.4	3.4	12.6
20	105514	SS	<0.5	0.5	2.5	11.7	8.4	160.2	8.6	0.8	<0.5	<0.5	1.1	3.5	<0.5	<0.5	26.3	53.5	6.1	21.6
21	105515	SS	0.9	3.1	51.8	68.3	36.2	625.8	8.8	1.2	<0.5	<0.5	1.8	0.5	<0.5	0.6	171.4	342	38.3	132.5

Table Continued..

Annexure-III

S.N	Original ID	Type	Sm	Eu	Gd	Tb	Dy	Ho	Er	Tm	Yb	Lu	Hf	Ta	Tl	Bi	Th	U	LREE	HREEY	TREEY
1	105419	SS	17.1	1.1	13.2	1.7	6.9	1.2	3.1	<0.5	3.1	<0.5	13.6	0.7	<0.5	<0.5	80.2	6.7	541.7	70.9	612.6
2	105426	SS	8.1	0.6	6.1	0.8	3.3	0.6	1.5	<0.5	1.5	<0.5	7.1	<0.5	<0.5	<0.5	36.9	3.5	253.9	34.1	288
3	105433	SS	2.9	<0.5	2.3	<0.5	1.4	<0.5	0.7	<0.5	0.8	<0.5	3.3	<0.5	<0.5	<0.5	10.8	1.3	93.8	15.7	109.5
4	105435	SS	16.6	1.4	13.3	1.9	8.6	1.6	4.4	0.7	4.7	0.7	31.3	2.1	<0.5	<0.5	67.8	9.1	497.8	94.3	592.1
5	105438	SS	7	0.9	5.8	0.9	3.9	0.8	2.1	<0.5	2.2	<0.5	5.6	1.2	<0.5	<0.5	24.6	3	203.2	50.6	253.8
6	105439	SW	12.2	1.9	10	1.5	6.6	1.3	3.3	<0.5	3.1	<0.5	9.5	2.3	0.6	<0.5	30.2	4.3	364.2	80.7	444.9
7	105442	SS	5.4	1	4.8	0.8	3.9	0.8	2.2	<0.5	2.3	<0.5	5.2	1	<0.5	<0.5	15.3	4.7	131.8	49.6	181.4
8	105443	SS	7.2	1	5.7	0.9	4	0.8	2	<0.5	2	<0.5	5.2	0.8	0.6	<0.5	23.4	3.1	202	46.9	248.9
9	105448	SS	24.9	1.7	17.6	2.3	9.3	1.6	4	0.6	3.5	0.6	12.9	0.7	<0.5	<0.5	108.4	7.4	791.4	107.4	898.8
10	105449	SS	8	1	6.3	0.9	4.2	0.8	2.1	<0.5	2.1	<0.5	5	1	<0.5	<0.5	24.1	2.8	228.6	54.8	283.4
11	105451	SS	5.1	0.9	4.3	0.7	3.4	0.7	1.9	<0.5	2	<0.5	5.5	0.8	<0.5	<0.5	14.2	2	140.2	42.1	182.3
12	105453	SS	9.8	0.7	7	0.8	3.4	0.6	1.8	<0.5	2	<0.5	7.4	1	<0.5	<0.5	31	3.7	284.1	40.2	324.3
13	105465	SS	21	1.4	15.4	2	8.1	1.4	3.6	0.5	3.3	<0.5	13	0.5	<0.5	<0.5	95.5	7.3	666	82.6	748.6
14	105467	SS	5.8	0.6	4.6	0.7	3	0.6	1.5	<0.5	1.7	<0.5	8.5	<0.5	<0.5	<0.5	23.6	2.9	178.1	33.1	211.2
15	105484	SS	19.2	1	13.9	1.7	6.3	1	2.5	<0.5	2.2	<0.5	9.7	0.7	<0.5	<0.5	94.7	6.3	634	62	696
16	105486	SS	5.6	0.7	4.2	0.6	2.5	<0.5	1.3	<0.5	1.2	<0.5	3.8	<0.5	0.5	<0.5	23.3	2.4	173.7	29.4	203.1
17	105497	SS	5	1	4.2	0.6	2.8	0.5	1.5	<0.5	1.4	<0.5	2.9	0.7	<0.5	<0.5	13.6	1.6	138.5	35.1	173.6
18	105500	SS	5.8	0.9	4.9	0.7	3.3	0.6	1.7	<0.5	1.6	<0.5	3.8	0.7	<0.5	<0.5	18	2.1	161.4	39.1	200.5
19	105502	SS	2.5	0.6	2.3	<0.5	1.9	<0.5	1	<0.5	0.9	<0.5	1.7	<0.5	<0.5	<0.5	5.5	1.2	59.3	21.8	81.1
20	105514	SS	3.6	<0.5	2.9	<0.5	1.7	<0.5	0.9	<0.5	0.9	<0.5	4.5	0.7	<0.5	<0.5	14.9	2.3	111.1	17.3	128.4
21	105515	SS	22.2	1.3	16.6	2.1	8.3	1.4	3.6	0.5	3.3	0.5	16.5	<0.5	<0.5	<0.5	100.3	8.4	706.4	82.6	789

Annexure-IV: XRF analysis of clay fraction of stream sediments (-40 micron fraction)

S.N	Original ID	Sample ID	Location No	Sample Type	Latitude	Longitude	Field Description
1	105419	105601	GSPL_Bhuj-22/12/23	SS	23.185	69.6951	1st order stream draining sandstone-shale deposit
2	105426	105602	GSPL_Bhuj-30/12/23	SS	23.2243	69.5094	1st order stream draining Bhuj Formation
3	105433	105603	GSPL_Bhuj-35/12/23	SS	23.2239	69.5661	2nd order stream draining the Bhuj Formation
4	105435	105604	GSPL_Bhuj-31/12/2023	SS	23.2242	69.5236	3rd order stream, draining the Bhuj Formation and probably the reported alkali plug and phosphorite area
5	105438	105605	GSPL_Bhuj-02/12/2023	SS	23.1829	69.5639	Stream sediments collected from bedrock at deepest point in the bedrock
6	105439	105606	GSPL_Bhuj-04/12/2023	SS	23.2157	69.5894	Slope wash/creek sample??
7	105442	105607	GSPL_Bhuj-36/12/2023	SS	23.2072	69.6555	3rd order stream draining the Chari, Katrol and Bhuj formations
8	105443	105608	GSPL_Bhuj-38/12/2023	SS	23.1865	69.6428	2nd order stream draining the Katrol Formation
9	105448	105609	GSPL_Bhuj-29/12/2023	SS	23.1991	69.5123	1st order stream draining Bhuj Formation
10	105449	105610	GSPL_Bhuj-33/12/2023	SS	23.1835	69.5031	3rd order stream, draining the Chari Formation
11	105451	105611	GSPL_Bhuj-45/12/2023	SS	23.1785	69.5359	3rd order stream draining the Chari Formation
12	105453	105612	GSPL_Bhuj-46/12/2023	SS	23.1926	69.7243	1st order stream draining the Chari Formation
13	105465	105613	GSPL_Bhuj-48/12/2023	SS	23.153	69.637	2nd order stream draining the Bhuj Formation. Sample collected from the deepest point of the stream
14	105467	105614	GSPL_Bhuj-49/12/2023	SS	23.1508	69.6239	2nd order stream draining the Katrol Formation.
15	105484	105615	GSPL_Bhuj-68/01/2024	SS	23.1498	69.7271	3rd order stream draining the Bhuj and Katrol formations, Stream sediment collected 150 metre before the confluence of the 2nd order streams
16	105486	105616	GSPL_Bhuj-70/01/2024	SS	23.2101	69.5349	Sample collected from the depressed area of the stream.
17	105497	105617	GSPL-Bhuj-94/02/24	SS	23.1873	69.7233	Stream sediment brownish colour.collected from the flat low lying area
18	105500	105618	GSPL-Bhuj-96/02/24	SS	23.1857	69.7237	brownish colour stream sediment
19	105502	105619	GSPL-Bhuj-97/02/24	SS	23.1992	69.7017	Stream sediment light brown/Yellowish in colour
20	105514	105620	GSPL-Bhuj_106/02/24	SS	23.2246	69.5877	stream sediment brownish in colour
21	105515	105621	GSPL-Bhuj-107/02/24	SS	23.2268	69.5095	Stream sediment light brown in colour

Table Continued..

Annexure-IV

S.N	Original ID	Sample ID	Sample Description	Al_2O_3	BaO	CaO	Cr_2O_3	Fe_2O_3	K_2O	MgO	MnO	Na_2O	P_2O5	TiO_2	SiO_2	LOI	SO_3
1	105419	105601	<40 micron fraction of 105419 (<1mm) sample	13.29	<0.01	19.48	0.01	5.11	1.2	1.32	0.09	0.39	0.23	0.76	32.38	24.1	0.18
2	105426	105602	<40 micron fraction of 105426 (<1mm) sample	15.18	0.09	0.64	0.02	6.07	2.24	0.76	0.12	0.58	0.18	1.24	63.3	8.84	0.15
3	105433	105603	<40 micron fraction of 105433 (<1mm) sample	17.84	0.05	0.87	0.03	5.82	1.45	0.82	0.11	0.48	0.19	1.27	59.6	10.64	0.15
4	105435	105604	<40 micron fraction of 105435 (<1mm) sample	12.09	0.07	0.64	0.04	6.83	2.16	0.72	0.1	0.66	0.17	1.85	69.08	4.85	0.1
5	105438	105605	<40 micron fraction of 105438 (<1mm) sample	19.78	0.03	6.09	0.02	6.18	1.73	1.15	0.08	0.22	0.16	1.11	49.45	13.27	0.1
6	105439	105606	<40 micron fraction of 105439 (<1mm) sample	19.11	0.05	2.49	0.01	11.65	1.14	2.21	0.24	0.83	0.19	2.26	48	11.07	0.1
7	105442	105607	<40 micron fraction of 105442 (<1mm) sample	24.31	0.02	3.06	0.03	1.6	0.69	0.62	0.03	1.52	0.07	1.22	52.54	13.28	0.43
8	105443	105608	<40 micron fraction of 105443 (<1mm) sample	24.39	0.05	1.34	0.03	5.48	1.77	0.86	0.07	0.17	0.16	1.37	52.52	11.01	0.1
9	105448	105609	<40 micron fraction of 105448 (<1mm) sample	18.6	0.03	1.36	0.02	12.17	0.88	1.8	0.12	0.44	0.25	1.75	50.74	11.08	0.12
10	105449	105610	<40 micron fraction of 105449 (<1mm) sample	16.55	0.03	3.93	0.02	8.87	1.92	1.28	0.09	0.38	0.13	1.21	54.99	9.75	0.18
11	105451	105611	<40 micron fraction of 105451 (<1mm) sample	22.89	0.03	1.08	0.02	6.99	2.01	1.1	0.07	0.2	0.13	1.34	53.1	10.29	0.1
12	105453	105612	<40 micron fraction of 105453 (<1mm) sample	14.33	0.05	7.05	0.03	5.29	2.1	0.94	0.07	0.33	0.15	1.24	56.63	10.84	0.25
13	105465	105613	<40 micron fraction of 105465 (<1mm) sample	14.66	0.06	17.49	0.02	6.71	0.98	1.44	0.1	0.29	0.31	0.87	31.29	24.45	0.3
14	105467	105614	<40 micron fraction of 105467 (<1mm) sample	6.64	0.05	0.72	0.04	3.28	1.71	0.54	0.08	0.22	0.18	2.56	80.31	2.64	0.09
15	105484	105615	<40 micron fraction of 105484 (<1mm) sample	20.03	0.05	0.7	0.03	6.87	1.95	0.93	0.09	0.33	0.17	1.43	57.75	8.88	0.12
16	105486	105616	<40 micron fraction of 105486 (<1mm) sample	22.09	0.04	1.09	0.02	6.85	1.92	1.15	0.17	0.45	0.26	1.23	53.08	10.93	0.17
17	105497	105617	<40 micron fraction of 105497	22.01	0.04	1.33	0.03	6.7	2	1.13	0.07	0.37	0.18	1.3	52.61	11.42	0.17
18	105500	105618	<40 micron fraction of 105500	14.39	0.03	5.2	0.02	4.46	1.84	0.9	0.05	0.28	0.12	0.92	59.9	11.11	0.18
19	105502	105619	<40 micron fraction of 105502	18.27	0.02	11.11	0.02	6.17	1.58	0.89	0.09	0.14	0.13	1.04	42.25	17.39	0.16
20	105514	105620	<40 micron fraction of 105514	16.59	0.06	0.79	0.02	7.22	1.72	1	0.34	0.7	0.58	1.64	59.55	9.02	0.11
21	105515	105621	<40 micron fraction of 105515	11.12	0.04	0.29	0.02	7.03	1.49	0.47	0.08	0.37	0.08	0.94	72.67	4.86	0.09

Annexure-V: ICPMS analysis of clay fraction of stream sediments (-40 micron fraction)

S.N	Original ID	Location No	Sample Type	Sample Description	Latitude	Longitude	Li	Be	Sc	V	Ga
1	105419	GSPL_Bhuj-22/12/23	SS	<40 micron fraction of 105419 (<1mm) sample	23.185	69.6951	46.7	1.7	13.5	119.1	15.5
2	105426	GSPL_Bhuj-30/12/23	SS	<40 micron fraction of 105426 (<1mm) sample	23.2243	69.5094	35.7	1.6	14.4	110.9	18
3	105433	GSPL_Bhuj-35/12/23	SS	<40 micron fraction of 105433 (<1mm) sample	23.2239	69.5661	41.2	2.8	18.3	120.7	22.5
4	105435	GSPL_Bhuj-31/12/2023	SS	<40 micron fraction of 105435 (<1mm) sample	23.2242	69.5236	28.4	1.7	21.4	135.2	19.5
5	105438	GSPL_Bhuj-02/12/2023	SS	<40 micron fraction of 105438 (<1mm) sample	23.1829	69.5639	101.9	2.2	23.7	174.1	26.7
6	105439	GSPL_Bhuj-04/12/2023	SS	<40 micron fraction of 105439 (<1mm) sample	23.2157	69.5894	48.9	2.4	30.6	254.1	27.9
7	105442	GSPL_Bhuj-36/12/2023	SS	<40 micron fraction of 105442 (<1mm) sample	23.2072	69.6555	55.4	3	12.3	142.9	30.4
8	105443	GSPL_Bhuj-38/12/2023	SS	<40 micron fraction of 105443 (<1mm) sample	23.1865	69.6428	127.3	3	21.2	162.8	35.7
9	105448	GSPL_Bhuj-29/12/2023	SS	<40 micron fraction of 105448 (<1mm) sample	23.1991	69.5123	29.4	1.8	36.1	255.8	23.5
10	105449	GSPL_Bhuj-33/12/2023	SS	<40 micron fraction of 105449 (<1mm) sample	23.1835	69.5031	115.5	2	26	187.5	23
11	105451	GSPL_Bhuj-45/12/2023	SS	<40 micron fraction of 105451 (<1mm) sample	23.1785	69.5359	97	2.9	23.4	189	30.2
12	105453	GSPL_Bhuj-46/12/2023	SS	<40 micron fraction of 105453 (<1mm) sample	23.1926	69.7243	43.8	2.5	17.6	139.3	22.8
13	105465	GSPL_Bhuj-48/12/2023	SS	<40 micron fraction of 105465 (<1mm) sample	23.153	69.637	58.4	1.8	18.1	131.5	17.7
14	105467	GSPL_Bhuj-49/12/2023	SS	<40 micron fraction of 105467 (<1mm) sample	23.1508	69.6239	13.5	0.7	27.4	109.8	18.3
15	105484	GSPL_Bhuj-68/01/2024	SS	<40 micron fraction of 105484 (<1mm) sample	23.1498	69.7271	68.9	2.3	19.4	148.8	27.6
16	105486	GSPL_Bhuj-70/01/2024	SS	<40 micron fraction of 105486 (<1mm) sample	23.2101	69.5349	63.1	2.8	19.7	139.9	26.7
17	105497	GSPL-Bhuj-94/02/24	SS	<40 micron fraction of 105497	23.1873	69.7233	103.5	3	18.1	174.5	29.6
18	105500	GSPL-Bhuj-96/02/24	SS	<40 micron fraction of 105500	23.1857	69.7237	78.7	1.4	11.8	99	18.3
19	105502	GSPL-Bhuj-97/02/24	SS	<40 micron fraction of 105502	23.1992	69.7017	97.8	1.9	16.6	161	23.8
20	105514	GSPL-Bhuj_106/02/24	SS	<40 micron fraction of 105514	23.2246	69.5877	62.1	2.2	15.9	122.8	21.5
21	105515	GSPL-Bhuj-107/02/24	SS	<40 micron fraction of 105515	23.2268	69.5095	33	1.4	10.8	85	14.7

Table Continued..

Annexure-V

S.N	Original ID	Sample Description	Ge	Se	Rb	Sr	Y	Zr	Nb	Mo	Cd	In	Sn	Sb	Te
1	105419	<40 micron fraction of 105419 (<1mm) sample	<0.5	1.3	66.3	614.7	19.5	177.1	15.6	0.8	<0.5	<0.5	2.9	1.2	<0.5
2	105426	<40 micron fraction of 105426 (<1mm) sample	<0.5	3.1	82.4	185.7	26.5	332.4	21.5	1.3	<0.5	<0.5	3.9	1	<0.5
3	105433	<40 micron fraction of 105433 (<1mm) sample	0.5	2.7	62.2	137.1	36.1	310.5	21.9	1.7	<0.5	<0.5	3.4	0.9	<0.5
4	105435	<40 micron fraction of 105435 (<1mm) sample	0.9	4.3	81.3	167.5	55.6	1046.7	27.9	1.2	0.5	<0.5	3.3	1.6	<0.5
5	105438	<40 micron fraction of 105438 (<1mm) sample	<0.5	1.7	95.9	322.7	22.8	153.2	17.7	3.6	0.6	<0.5	5	1.8	<0.5
6	105439	<40 micron fraction of 105439 (<1mm) sample	<0.5	1.9	60	249	27.4	226.9	36.8	1.5	<0.5	<0.5	3.1	1.4	<0.5
7	105442	<40 micron fraction of 105442 (<1mm) sample	0.7	1.6	22.4	134.3	16.3	194.8	24.6	1.5	<0.5	<0.5	4.6	6.1	<0.5
8	105443	<40 micron fraction of 105443 (<1mm) sample	<0.5	2	94.3	259.9	33.7	249.2	26.7	1.1	<0.5	<0.5	4.7	1.3	<0.5
9	105448	<40 micron fraction of 105448 (<1mm) sample	<0.5	3.2	37.8	172.6	69.3	188.3	25.2	1.2	<0.5	<0.5	3	1.6	<0.5
10	105449	<40 micron fraction of 105449 (<1mm) sample	<0.5	2.6	91.5	308	26.3	205.8	17.5	1.1	<0.5	<0.5	6.9	1.4	<0.5
11	105451	<40 micron fraction of 105451 (<1mm) sample	<0.5	1.5	125.4	238.4	24	181.5	22.9	1	<0.5	<0.5	4.1	1.1	<0.5
12	105453	<40 micron fraction of 105453 (<1mm) sample	0.7	2.7	84.6	341.4	40.1	492.4	21	1	<0.5	<0.5	3	1.4	<0.5
13	105465	<40 micron fraction of 105465 (<1mm) sample	<0.5	1.8	46.7	676.2	21.2	145.8	16.3	1.1	<0.5	<0.5	2.7	1.3	<0.5
14	105467	<40 micron fraction of 105467 (<1mm) sample	1.6	6.7	52.4	138.5	90.7	2435	46.5	0.8	0.5	<0.5	3	2	<0.5
15	105484	<40 micron fraction of 105484 (<1mm) sample	0.6	2.7	93.2	154.1	34.2	339.1	24.4	1	<0.5	<0.5	3.6	1.2	<0.5
16	105486	<40 micron fraction of 105486 (<1mm) sample	<0.5	2	90	136.7	27	165.7	21.1	1.2	<0.5	<0.5	3.3	1.1	<0.5
17	105497	<40 micron fraction of 105497	<0.5	1.2	105.2	219.2	20.6	160.7	20.4	1.1	<0.5	<0.5	3.8	1.4	<0.5
18	105500	<40 micron fraction of 105500	<0.5	0.9	81	255.9	17.9	163.6	14.7	0.9	<0.5	<0.5	2.4	0.9	<0.5
19	105502	<40 micron fraction of 105502	<0.5	0.8	68.6	215.6	16.7	144.6	16.6	1.1	<0.5	<0.5	3.3	2.2	<0.5
20	105514	<40 micron fraction of 105514	<0.5	1.4	96.1	199.1	28.1	213.5	26	1.5	<0.5	<0.5	4.9	1	<0.5
21	105515	<40 micron fraction of 105515	<0.5	1	56.2	79	18.9	237.7	14.3	1.2	<0.5	<0.5	1.9	0.8	<0.5

Table Continued..

Annexure-V

S.N	Original ID	Sample Description	Cs	La	Ce	Pr	Nd	Sm	Eu	Gd	Tb	Dy	Ho	Er	Tm
1	105419	<40 micron fraction of 105419 (<1mm) sample	4.3	37.7	81.4	9.1	32.8	6.1	1.1	5.2	0.8	3.9	0.7	2	<0.5
2	105426	<40 micron fraction of 105426 (<1mm) sample	3.6	61.4	126.2	14.1	50.1	9	1.4	7.5	1.1	5.2	1	2.7	<0.5
3	105433	<40 micron fraction of 105433 (<1mm) sample	4	83.7	171.2	19.2	68.8	12.4	1.9	10.2	1.5	7	1.3	3.6	0.5
4	105435	<40 micron fraction of 105435 (<1mm) sample	3	145.4	293.7	32.9	117.3	20.7	2.2	16.4	2.4	10.7	2	5.6	0.9
5	105438	<40 micron fraction of 105438 (<1mm) sample	6.3	39.3	82.2	9.2	33.2	6.2	1.3	5	0.8	4	0.8	2.2	<0.5
6	105439	<40 micron fraction of 105439 (<1mm) sample	3.1	37.3	85.2	8.9	33	6.4	1.7	5.7	1	4.7	0.9	2.5	<0.5
7	105442	<40 micron fraction of 105442 (<1mm) sample	2.5	30.6	61	7.6	28.7	5.3	1.3	4.5	0.7	3.8	0.7	2	<0.5
8	105443	<40 micron fraction of 105443 (<1mm) sample	6	74.5	147.8	16.8	59.4	10.9	2.1	9.1	1.4	6.6	1.3	3.6	0.5
9	105448	<40 micron fraction of 105448 (<1mm) sample	2.3	49.8	91.3	11.9	46.4	10	2.9	11.5	2.1	11.6	2.5	7.1	1.1
10	105449	<40 micron fraction of 105449 (<1mm) sample	5.9	55	120.9	13.1	46.2	8.3	1.3	6.5	1	4.8	0.9	2.6	<0.5
11	105451	<40 micron fraction of 105451 (<1mm) sample	8.8	46.4	96.8	10.7	38.1	7.3	1.6	6.3	1	4.9	1	2.8	<0.5
12	105453	<40 micron fraction of 105453 (<1mm) sample	4.2	100.9	205.4	23	82.5	14.7	1.8	11.9	1.8	7.9	1.5	4.2	0.6
13	105465	<40 micron fraction of 105465 (<1mm) sample	3.4	36.4	79.1	8.6	31.4	6	1.3	5	0.8	3.8	0.7	1.9	<0.5
14	105467	<40 micron fraction of 105467 (<1mm) sample	1.3	253.8	506.8	58.4	206.1	36.7	2.8	29	4.2	18.4	3.4	9.6	1.5
15	105484	<40 micron fraction of 105484 (<1mm) sample	6	106.8	217.9	24.1	84.9	14.9	1.8	11.7	1.7	7.1	1.3	3.5	0.5
16	105486	<40 micron fraction of 105486 (<1mm) sample	6.6	48.5	100.2	10.9	39.9	7.7	1.7	6.7	1.1	5.2	1	2.8	<0.5
17	105497	<40 micron fraction of 105497	6.9	39.2	82.7	9.7	35.6	6.9	1.5	5.8	0.9	4.4	0.9	2.4	<0.5
18	105500	<40 micron fraction of 105500	4.6	33.8	70.1	8.2	29.1	5.5	1.1	4.6	0.7	3.7	0.7	2	<0.5
19	105502	<40 micron fraction of 105502	4.3	29.7	59.2	7.2	25.8	4.9	1.1	4.1	0.7	3.4	0.7	2	<0.5
20	105514	<40 micron fraction of 105514	5.9	62.7	131	14.5	51.9	9.3	1.7	7.8	1.2	5.4	1	2.9	<0.5
21	105515	<40 micron fraction of 105515	2.4	49.2	102.2	11.5	40.9	7.5	1.1	5.9	0.9	3.9	0.7	2.1	<0.5

Table Continued..

Annexure-V

S.N	Original ID	Sample Description	Yb	Lu	Hf	Ta	Tl	Bi	Th	U	LREE	HREEY	TREEY
1	105419	<40 micron fraction of 105419 (<1mm) sample	2	<0.5	5.2	0.9	0.5	<0.5	17.4	2.7	167.1	48.7	215.8
2	105426	<40 micron fraction of 105426 (<1mm) sample	2.8	<0.5	9.3	1.2	0.7	<0.5	33	4.7	260.8	62.6	323.4
3	105433	<40 micron fraction of 105433 (<1mm) sample	3.6	0.5	8.7	1.3	0.8	<0.5	38.9	5.6	355.3	84.5	439.8
4	105435	<40 micron fraction of 105435 (<1mm) sample	6	0.9	28.4	1.1	0.8	<0.5	80.5	10.5	610	124.1	734.1
5	105438	<40 micron fraction of 105438 (<1mm) sample	2.2	<0.5	4.1	1	0.6	0.6	14.4	2	170.1	62.8	232.9
6	105439	<40 micron fraction of 105439 (<1mm) sample	2.2	<0.5	5.3	1.5	0.8	<0.5	10.5	1.8	170.8	76.7	247.5
7	105442	<40 micron fraction of 105442 (<1mm) sample	2	<0.5	5.7	1.7	0.6	<0.5	13.1	6.6	133.2	43.6	176.8
8	105443	<40 micron fraction of 105443 (<1mm) sample	3.6	<0.5	7.4	1.6	0.9	<0.5	28.9	4.2	309.4	83.1	392.5
9	105448	<40 micron fraction of 105448 (<1mm) sample	6.9	1	5.2	1.4	0.9	<0.5	13	2.2	209.4	152.1	361.5
10	105449	<40 micron fraction of 105449 (<1mm) sample	2.4	<0.5	5.4	1	<0.5	0.6	24.7	2.6	243.5	71.8	315.3
11	105451	<40 micron fraction of 105451 (<1mm) sample	2.8	<0.5	5.3	1.4	0.9	0.5	18.5	2.5	199.3	67.8	267.1
12	105453	<40 micron fraction of 105453 (<1mm) sample	4.4	0.6	13.8	1.3	0.7	<0.5	49.9	5.8	426.5	92.4	518.9
13	105465	<40 micron fraction of 105465 (<1mm) sample	1.7	<0.5	3.8	0.9	<0.5	<0.5	14.5	2.7	161.5	54.5	216
14	105467	<40 micron fraction of 105467 (<1mm) sample	10.5	1.6	68.6	3.3	0.6	<0.5	138.2	19.8	1061.8	199.1	1260.9
15	105484	<40 micron fraction of 105484 (<1mm) sample	3.4	<0.5	9.8	1.5	0.8	<0.5	53.5	5.6	448.6	84.6	533.2
16	105486	<40 micron fraction of 105486 (<1mm) sample	2.7	<0.5	5.2	1.3	1.4	<0.5	19.7	3.9	207.2	67.9	275.1
17	105497	<40 micron fraction of 105497	2.4	<0.5	4.7	1.4	0.6	<0.5	15.7	2.3	174.1	57	231.1
18	105500	<40 micron fraction of 105500	2	<0.5	4.7	1	<0.5	<0.5	16	2.4	146.7	44.5	191.2
19	105502	<40 micron fraction of 105502	2.1	<0.5	4.3	1.3	<0.5	<0.5	12.3	1.9	126.8	47.4	174.2
20	105514	<40 micron fraction of 105514	2.8	<0.5	6.2	1.6	1.4	<0.5	30.9	5.8	269.4	66.8	336.2
21	105515	<40 micron fraction of 105515	2	<0.5	6.4	0.8	<0.5	<0.5	24.2	3.4	211.3	46.3	257.6

Annexure-VI: XRF Analysis of Bedrock Samples for Orientation Survey

Sl No.	Sample ID	Location No.	Latitude	Longitude	Sample Type	Host Lithology	Stratigraphy
1	105401	GSPL-Bhuj-01/12/23	23.2098	69.5882	BR	Section of Planar cross stratified medium to fine grained quartz arenite overlying heterolith of goethitic to whitish clay and cherry red coloured (streak red) claystone, v.fine sandstone and greyish black shale. The stratification in the sandstone is defined by ferrugenous staining.	Bhuj Formation
2	105403	GSPL-Bhuj-02/12/23	23.1829	69.5639	BR	Section of v.coarse grained thick sandstone unit (2.5m) overlying white clay horizon (1m) with hematitic patches at places. Lots of boulders of laterite with botroydal features are observed in the T0 of the river. According to local people, there is a laterite mine at the top of the hill, located towards 260 degree from the location.	Bhuj Formation
3	105405	GSPL-Bhuj-03/12/23	23.2153	69.5900	BR	Thick clay horizon of grey (1.3m unit of 2-3mm layers) and white (1.1m of 1mm or less thick layers) overlying reddish brown coloured very hard very fine sandstone (80cm) with very small lenses of Fe concentration. The succession is finally overlain by 20-30cm beds of medium to fine grained sandstone (no internal structure is observed). Brecciation observed within the clay strata at the temple side of the section.	Bhuj Formation
4	105406	GSPL-Bhuj-03/12/23	23.2153	69.5900	BR	Thick clay horizon of grey (1.3m unit of 2-3mm layers) and white (1.1m of 1mm or less thick layers) overlying reddish brown coloured very hard very fine sandstone (80cm) with very small lenses of Fe concentration. The succession is finally overlain by 20-30cm beds of medium to fine grained sandstone (no internal structure is observed). Brecciation observed within the clay strata at the temple side of the section.	Bhuj Formation
5	105407	GSPL-Bhuj-07/12/23	23.2438	69.5829	BR	Intrusion of dolerite/basalt dyke within medium to fine grained sandstone. The lithounit is faulted with throw approx. 2 m. Concentration of ~5mm thin iron layer (cherry red streak) along the fault plane is observed. The contact between the dyke and the sandstone is highly altered with baking effect.	Bhuj Formation
6	105408	GSPL-Bhuj-08/12/23	23.2067	69.6464	BR	Laterally extensive occurrence (section oriented 100-290) of two laterite layers of 60cm and 14cm directly overlying 6cm duricrust and 40cm thick white clay layer with goethitic patches. The clay layer overlies 10-20cm thick planar cross stratified (p.c 320) medium to fine grained white sandstone beds forming sets of 20-30cm. The clay and sst sets are seperated by 20cm thick reddish brown colored sandstone with baking effect (duricrust formation).	Bhuj Formation
7	105409	GSPL-Bhuj-09/12/23	23.2070	69.6450	BR	Laterally extensive occurrence (section oriented 100-290) of two laterite layers of 60cm and 14cm directly overlying 6cm duricrust and 40cm thick white clay layer with goethitic patches. The clay layer overlies 10-20cm thick planar cross stratified (p.c 320) medium to fine grained white sandstone beds forming sets of 20-30cm, seperated by reddish brown colored sandstone with baking effect (duricrust formation).	Bhuj Formation
8	105410	GSPL-Bhuj-09/12/23	23.2070	69.6450	BR	Laterally extensive occurrence (section oriented 100-290) of two laterite layers of 60cm and 14cm directly overlying 6cm duricrust and 40cm thick white clay layer with goethitic patches. The clay layer overlies 10-20cm thick planar cross stratified (p.c 320) medium to fine grained white sandstone beds forming sets of 20-30cm, seperated by reddish brown colored sandstone with baking effect (duricrust formation).	Bhuj Formation
9	105411	GSPL-Bhuj-09/12/23	23.2070	69.6450	BR	Laterally extensive occurrence (section oriented 100-290) of two laterite layers of 60cm and 14cm directly overlying 6cm duricrust and 40cm thick white clay layer with goethitic patches. The clay layer overlies 10-20cm thick planar cross stratified (p.c 320) medium to fine grained white sandstone beds forming sets of 20-30cm, seperated by reddish brown colored sandstone with baking effect (duricrust formation).	Bhuj Formation
10	105413	GSPL-Bhuj-11/12/23	23.1705	69.6375	BR	Thick succession of fine grained sandstone. Internally the sandstone is planar parallel to planar cross to swaley cross stratified. Here the amount of clay is almost negligible however at the lower part of the succession very little amount of clay is preserved, sandwitched between swaley cross stratified and planar parallel stratified sandstone. Encrustation at the top of the sandstone succession is also observed. At the contact of Katrol and Bhuj formations, (north of this location) gradational contact with preservation of clay is observed.	Bhuj Formation

Table Continued..

Annexure-VI

Sl No.	Sample ID	Sample Description	Al_2O_3	BaO	CaO	Cr_2O_3	Fe_2O_3	K_2O	MgO	MnO	Na_2O	P_2O_5	TiO_2	SiO_2	LOI	S
1	105401	Heterolithic layer of white coloured clay and hard reddish brown goethitic clay.	18.68	0.01	4.43	0.02	2.19	0.50	0.37	0.03	0.34	0.05	1.01	59.02	12.55	0.20
2	105403	White clay with few hematitic patches	17.06	0.02	0.12	0.02	1.31	0.65	0.24	0.02	0.05	0.03	0.99	72.56	6.44	0.05
3	105405	Soft gray shale above the hard red altered layer	23.79	0.03	0.06	0.03	0.70	0.49	0.19	0.02	0.41	0.10	1.34	62.74	9.42	0.07
4	105406	Reddish brown coloured very hard very fine sandstone (quartz, mica) with very small lenses of Fe concentration	8.85	0.05	0.10	0.04	39.28	0.20	0.09	0.05	0.07	0.17	0.79	45.66	4.46	0.05
5	105407	Fe rich fault plane sample.	4.68	0.04	0.23	0.02	63.15	0.57	0.11	0.16	0.08	0.13	0.55	24.67	5.44	0.42
6	105408	Laterite with partly developed pisiolitic structure.	10.85	0.03	0.12	0.03	40.42	0.33	0.32	0.09	0.43	0.24	0.66	37.16	8.77	0.42
7	105409	Ferruginous duricrust	1.61	0.03	0.03	0.01	22.11	0.61	0.05	0.05	0.09	0.04	0.33	71.69	2.80	0.39
8	105410	Laterite	11.15	0.02	0.35	0.03	32.79	0.37	0.26	0.04	0.17	0.20	0.70	43.98	9.30	0.41
9	105411	Goethitic clay below laterite layer	10.57	0.04	0.05	0.01	0.59	1.17	0.15	0.02	0.26	0.04	1.18	80.99	4.31	0.06
10	105413	Hematitic-goethitic clay(very small in occurrence with ferrugenous sandstone in a quarry section)	14.52	0.03	0.16	0.02	12.15	0.40	0.50	0.03	1.14	0.06	1.04	61.22	8.18	0.19

Sl No.	Sample ID	Location No.	Latitude	Longitude	Sample Type	Host Lithology	Stratigraphy
11	105415	GSPL-Bhuj-17/12/23	23.1970	69.7299	BR	Medium to fine grained planar cross stratified quartzose sandstone (angular grains of quartz). 5-7cm thick red beds (very hard, cherry red streak) are observed at the top of the sandstone beds. Vein type occurrence (overall orientation 60-240) cross cutting the sandstone are observed.	Chari Formation
12	105420	GSPL-Bhuj-23/12/23	23.1727	69.6923	BR	Occurrence of clay-sandstone heterolith unit, interupted by fine to medium grained parallel laminated sandstone with gypsum interlayers	Katrol Formation
13	105425	GSPL-Bhuj-25/12/23	23.1339	69.7051	BR	Alternate occurrence of ferrugenous sandstone and white to reddish clay.	Bhuj Formation
14	105429	GSPL-Bhuj-06/12/23	23.2404	69.5847	BR	Alternate occurrence of brownish black coloured fine to medium grained sandstone and clay-sandstone heterolith unit. The sandstone beds are 50cm-1m thick withplanar parallal to hummocky and swaly cross stratified with pinch and swell bed geometry. Wave ripple with rounded crest, tuning fork bifurcation, 1-2cm amplitude and 10-190 ripple axis ornament the top surface of the sandstone. The heterolithic layer is consist of mm to cm thin white to yellow ocher coloured clay and fine sandstone with unit thickness of 40cm.	Bhuj Formation
15	105444	GSPL-Bhuj-39/12/23	23.1966	69.7455	BR	very steep hill of sandstone, unable to climb, Occurrence of fossiliferous red ferrugenous sandstone	Chari Formation
16	105477	GSPL-Bhuj-56/01/24	23.422771	69.0843562	BR	Fossiliferous sandstone	
17	105479	GSPL-Bhuj-57/01/24	23.2212	69.5899	BR	Part of the hill is of basalt dyke intruded reddish brown colored massive duricrusted sandstone, overlying a scree deposit of white clay clasts embedded in a finer groundmass. Network of veins of hematite cross cutting the sandstone is observed.	Bhuj Formation
18	105480	GSPL-Bhuj-57/01/24	23.2212	69.5899	BR	Part of the hill is of basalt dyke intruded reddish brown colored massive duricrusted sandstone, overlying a scree deposit of white clay clasts embedded in a finer groundmass. Network of veins of hematite cross cutting the sandstone is observed.	Bhuj Formation
19	105481	GSPL-Bhuj-58/01/24A	23.2250	69.4908	BR	Exposure of dark reddish black coloured medium to coarse grained sandstone. The sandstone appears to be vent like wrapped by iron rich material.	Bhuj Formation
20	105488	GSPL-Bhuj-79/01/24	23.1650	69.6446	BR	Outcrop of dark reddish black colored coarse grained sandstone with hard duricrust (jhama effect) on top.	Bhuj Formation
21	105489	GSPL-Bhuj-80/01/24	23.1440	69.6452	BR	Exposure of coarse grained, planar cross stratified sandstone with duricrust formation at places. Differential ferruginous leaching is also observed throughout the area.	Bhuj Formation
22	105492	GSPL-Bhuj-85/01/24	23.1769	69.5025	BR	Exposure of alternate occurrence of medium to fine grained planar parallel laminated to wave ripple laminated sandstone, seperated by thin grey/white clay layers overlying sst-shale heterolith with poorly developed ferruginous suspected tuffite layers	Chari Formation
23	105494	GSPL-Bhuj-91/01/24	23.1507	69.5800	BR	Heterolithic unit consist of shale (grey, white with goethitic and ferruginous patches, interupted by well developed ferruginous clayey (suspected tuffite) layers alternating with 10-20cm thick sandstone layers and/or thinly laminated shale-siltstone unit	Katrol Formation
24	105495	GSPL-Bhuj-85/01/24	23.1769	69.5025	BR	Exposure of alternate occurrence of medium to fine grained planar parallel laminated to wave ripple laminated sandstone, seperated by thin grey/white clay layers overlying sst-shale heterolith with poorly developed ferruginous suspected tuffite layers	Chari Formation
25	105496	Blank	0.0000	0.0000	BR	NA	NA

Table Continued..

Annexure-VI

Sl No.	Sample ID	Sample Description	Al_2O_3	BaO	CaO	Cr_2O_3	Fe_2O_3	K_2O	MgO	MnO	Na_2O	P_2O_5	TiO_2	SiO_2	LOI	S
11	105415	Contact of cm thin layer of hard red material and medium grained redish brown coloured quartz arenite	3.89	0.01	12.06	0.01	44.54	0.31	0.75	0.33	0.10	1.03	0.35	22.67	13.56	0.09
12	105420	Grey shale with goethitic alteration	20.11	0.03	1.26	0.02	3.57	2.19	0.99	0.04	0.18	0.11	1.23	61.17	8.47	0.16
13	105425	Dark ferruginous shale alternating with thin sandstone	6.13	0.04	0.39	0.02	47.90	0.80	0.36	0.15	0.10	0.14	0.56	35.99	7.04	0.34
14	105429	Grey shale from the lowest point of the outcrop.	14.89	0.03	0.23	0.02	0.69	1.33	0.53	0.03	0.99	0.08	1.11	72.12	6.80	0.70
15	105444	Dark red fine grained fossiliferous sandstone	3.91	0.01	26.95	0.01	31.21	0.29	0.72	0.36	0.11	0.54	0.18	9.02	25.52	0.26
16	105477	Red sandstone with ferrugenous alteration	8.76	0.01	14.56	0.01	7.67	1.54	8.41	0.50	0.53	0.07	0.37	34.00	23.08	0.13
17	105479	Duricrusted sandstone with black patches associated with fumaroles	2.14	0.06	0.10	0.02	35.01	0.03	0.09	0.06	0.09	0.17	0.21	56.43	5.45	0.08
18	105480	White clay from the intraclasts embedded in a conglomerate bed	33.30	0.14	0.28	0.04	0.91	0.03	0.83	0.02	2.63	0.25	1.53	41.32	17.98	0.07
19	105481	Sandstone sample associated with fumaroles	3.44	0.05	0.07	0.01	24.71	1.24	0.11	0.17	0.13	0.07	0.38	65.87	3.29	0.27
20	105488	Blackish sandstone coarse grained quartz with some blackish mineral	0.65	0.03	0.10	0.02	29.16	0.02	0.09	0.04	0.05	0.31	0.36	64.44	4.39	0.11
21	105489	Reddish highly weathered coarse grained sandtone	3.19	0.03	0.05	0.01	1.97	0.07	0.06	0.03	0.01	0.07	0.91	91.12	1.91	0.05
22	105492	Yellowish grey shale	24.44	0.04	0.25	0.02	2.34	2.10	0.88	0.03	0.35	0.06	1.30	58.83	8.71	0.16
23	105494	Calareous suspected tuffite layer with yellow reddish clay outer core and red, hard ferruginous inner core	8.80	0.02	11.97	0.02	34.44	0.74	2.16	0.16	0.19	7.64	0.52	20.13	12.27	0.40
24	105495	Duplicate sample of 105492	20.72	0.04	0.87	0.02	3.81	2.29	1.06	0.04	0.40	0.09	1.20	60.82	7.89	0.27
25	105496	Blank sample	1.29	0.02	0.04	0.01	23.41	0.43	0.06	0.37	0.09	0.01	0.12	71.49	2.39	0.10

Sl No.	Sample ID	Location No.	Latitude	Longitude	Sample Type	Host Lithology	Stratigraphy
26	105498	GSPL-Bhuj-94/02/24	23.1873	69.7233	BR	On the way to the area, occurrence of red coloured ferruginous, fossiliferous sandstone	Chari Formation
27	105499	GSPL-Bhuj-95/02/24	23.1864	69.7228	BR	Reddish sandstone with lots of fossils mostly mollusca were exposed (graveyard bed)	Chari Formation
28	105501	GSPL-Bhuj-93/02/24	23.1901	69.7231	BR	Medium to coarse grained reddish brown coloured sandstone	Chari Formation
29	105503	GSPL-Bhuj-98/02/24	23.195	69.704	BR	Thick greenish shale/Tuff layer in between very thick quartz arenite beds, A few steps ahead to the village, encountered a large boulder of sandstone with very rounded bomb like structure	Chari Formation
30	105504	GSPL-Bhuj-99/02/24	23.1992	69.7056	BR	Red ferrugenous, fossiliferous sandstone like previous gravyard bed	Chari Formation
31	105505	GSPL-Bhuj-101/02/24	23.1855	69.7027	BR	Outcrop of alternate thin and thick layers of sandstone, clay, gypsum and goethitic layer, interupted by poorly developed ferruginous suspected tuffite layers. Round vent like structure is also observed. About 50 meter north we encountered possibly tuffaceous layer for thin section study.	Chari Formation
32	105622	GSPL-Bhuj-91/01/24	23.1507	69.58	BR	Heterolithic unit consist of shale (grey, white with goethitic and ferruginous patches, interupted by well developed ferruginous suspected tuffite layers alternating with 10-20cm thick sandstone layers and/or thinly laminated shale-siltstone unit	Katrol Formation
33	107488	GSPL-Bhuj-118/06/24	23.1645	69.5543	BR	Occurrence of altered sandstone, overlain by oolitic limestone at higher contour, intrusion of basalt/dolerite is also observed at lower contour.	Chari Formation (At Chari-Katrol Formation contact)
34	107492	GSPL-Bhuj-128/06/24	23.1817	69.6913	BR	Alternation of shale and sandstone with poorly developed thin red beds in between	Chari Formation (At Chari-Katrol Formation contact)
35	109013	GSPL-Bhuj-251/12/2024	23.1966	69.6003	BR	Fossiliferous sandstone	Katrol Formation

Table Continued..

Annexure-VI

Sl No.	Sample ID	Sample Description	Al_2O_3	BaO	CaO	Cr_2O_3	Fe_2O_3	K_2O	MgO	MnO	Na_2O	P_2O_5	TiO_2	SiO_2	LOI	S
26	105498	Red ferricrit sandstone with fossils	3.69	0.03	23.12	0.01	19.48	0.38	1.06	0.34	0.04	1.46	0.25	28.44	21.41	0.11
27	105499	Reddish sandstone with molluscas (graveyard bed)	1.49	0.01	31.29	0.01	18.34	0.10	0.23	0.16	0.01	0.89	0.09	21.99	25.27	0.05
28	105501	Reddish arkosic sandstone with feldspar and quartz, possibly tourmaline bearing. Possibly crystalline tuff	7.97	0.06	0.06	0.01	0.35	1.65	0.03	0.01	0.07	0.05	0.10	87.01	2.66	0.05
29	105503	thick greenish grey shale/Tuff layer in between very thick quartz arenite beds	23.93	0.04	4.93	0.02	3.44	2.09	0.78	0.02	0.10	0.10	1.51	50.52	12.42	0.06
30	105504	red ferrugenous fossiliferous sandstone (gravyard bed)	4.47	0.02	17.22	0.01	35.63	0.56	2.38	0.22	0.08	1.23	0.32	18.91	18.58	0.14
31	105505	Yellow goethitic layer in between gypsum layers	5.18	0.01	16.20	0.02	25.38	0.61	0.42	0.07	0.02	0.80	0.37	18.25	12.84	19.09
32	105622	Yellowish (shale) part of 105494 (BR)	13.54	0.01	19.26	0.01	10.82	1.08	1.31	0.18	0.21	12.49	0.62	28.41	10.58	0.56
33	107488	Cherry red in color,comprises of quartz, mica, glass shrads ??, and few black unknown mineral with metallic lustre. Suspected volcanic alteration.	3.00	0.01	30.50	0.01	17.43	0.35	0.44	0.09	0.03	0.15	0.23	23.33	24.20	0.05
34	107492	Poorly developed thin red beds (claystone/ironstone), sample spread 2.8m. Collected to check REE content as it is from Chari-Katrol contact and very poorly developed.	8.65	0.01	10.84	0.01	4.53	1.37	0.65	0.02	0.06	0.11	0.79	60.16	12.62	0.05
35	109013	Fossiliferous sandstone bed with occasional ferrugenious activity	NA	NA	NA	NA	NA	NA	NA	NA	NA	NA	NA	NA	NA	NA

Annexure-VII: ICPMS Of BR samples Of Orientation Survey

Sl No.	Sample ID	Location No.	Latitude	Longitude	Sample Type	Li	Be	Sc	V	Ga	Ge	Se	Rb	Sr	Y	Zr	Nb	Mo
1	105401	GSPL-Bhuj-01/12/23	23.2098	69.5882	BR	47.80	2.50	19.50	144.10	28.10	0.50	3.40	26.70	446.20	26.80	154.80	18.40	2.30
2	105403	GSPL-Bhuj-02/12/23	23.1829	69.5639	BR	57.30	2.00	16.00	102.20	26.50	0.50	2.40	41.80	66.60	21.60	160.00	19.10	14.90
3	105405	GSPL-Bhuj-03/12/23	23.2153	69.5900	BR	56.70	3.00	27.10	146.80	40.00	0.50	2.10	23.50	131.10	23.60	190.30	24.30	0.80
4	105406	GSPL-Bhuj-03/12/23	23.2153	69.5900	BR	20.40	3.90	17.80	620.90	17.90	0.50	2.10	8.50	59.60	20.80	145.60	13.10	3.90
5	105407	GSPL-Bhuj-07/12/23	23.2438	69.5829	BR	9.30	2.10	6.30	58.50	8.70	0.50	1.40	17.90	54.50	15.00	148.80	8.50	2.90
6	105408	GSPL-Bhuj-08/12/23	23.2067	69.6464	BR	10.90	2.70	11.10	390.90	14.40	0.80	1.20	13.50	61.60	18.30	113.30	11.40	4.80
7	105409	GSPL-Bhuj-09/12/23	23.2070	69.6450	BR	6.00	1.00	3.20	31.00	3.60	0.50	1.60	14.60	43.30	5.90	18.50	5.10	1.10
8	105410	GSPL-Bhuj-09/12/23	23.2070	69.6450	BR	10.50	2.80	14.40	342.90	15.50	0.50	2.10	14.60	66.50	19.70	112.10	10.90	3.30
9	105411	GSPL-Bhuj-09/12/23	23.2070	69.6450	BR	15.70	0.70	9.40	49.60	17.60	0.50	1.80	34.00	42.50	23.70	363.80	17.90	1.00
10	105413	GSPL-Bhuj-11/12/23	23.1705	69.6375	BR	25.80	1.50	12.30	91.50	21.30	0.50	1.10	20.30	94.80	19.10	252.80	17.30	1.00
11	105415	GSPL-Bhuj-17/12/23	23.1970	69.7299	BR	9.40	2.20	6.50	202.20	6.60	0.50	1.60	13.10	170.70	33.30	46.30	5.40	5.00
12	105420	GSPL-Bhuj-23/12/23	23.1727	69.6923	BR	90.60	2.10	13.30	120.20	26.30	0.50	1.60	111.90	205.20	19.00	188.50	21.30	0.70
13	105425	GSPL-Bhuj-25/12/23	23.1339	69.7051	BR	13.00	3.20	16.30	78.10	9.30	0.50	3.00	27.80	60.60	30.40	141.30	9.10	1.40
14	105429	GSPL-Bhuj-06/12/23	23.2404	69.5847	BR	51.40	1.40	12.00	84.20	23.00	0.50	1.40	58.00	138.60	19.20	271.80	19.10	0.70
15	105444	GSPL-Bhuj-39/12/23	23.1966	69.7455	BR	15.90	1.60	12.40	255.70	7.60	0.50	3.30	14.10	520.80	45.80	43.40	3.10	1.50
16	105477	GSPL-Bhuj-56/01/24	23.4228	69.0844	BR	31.30	1.70	8.70	66.00	12.60	0.50	1.10	77.50	219.70	20.40	46.70	7.50	1.00

Sl No.	Sample ID	Location No.	Latitude	Longitude	Sample Type	Li	Be	Sc	V	Ga	Ge	Se	Rb	Sr	Y	Zr	Nb	Mo
17	105479	GSPL-Bhuj-57/01/24	23.2212	69.5899	BR	9.10	1.70	9.20	44.60	4.80	0.50	1.30	0.90	35.90	8.90	38.70	3.40	11.10
18	105480	GSPL-Bhuj-57/01/24	23.2212	69.5899	BR	79.70	2.30	60.10	252.30	37.60	0.50	1.30	0.50	448.00	32.20	172.70	15.60	0.80
19	105481	GSPL-Bhuj-58/01/24A	23.2250	69.4908	BR	6.30	1.50	7.70	29.60	4.00	0.50	1.10	18.40	77.60	15.10	11.10	0.90	0.80
20	105488	GSPL-Bhuj-79/01/24	23.1650	69.6446	BR	5.80	3.50	3.20	114.70	2.20	0.50	4.10	0.60	178.00	26.50	71.70	6.30	9.20
21	105489	GSPL-Bhuj-80/01/24	23.1440	69.6452	BR	11.70	0.50	4.00	52.30	7.40	0.50	1.70	3.10	52.10	11.70	168.30	14.40	0.80
22	105492	GSPL-Bhuj-85/01/24	23.1769	69.5025	BR	135.60	2.30	16.30	149.50	32.80	0.50	1.40	103.20	132.70	17.40	181.90	22.70	0.80
23	105494	GSPL-Bhuj-91/01/24	23.1507	69.5800	BR	38.60	2.70	54.40	295.50	16.10	0.50	10.10	38.60	521.50	289.40	158.20	8.20	1.00
24	105495	GSPL-Bhuj-85/01/24	23.1769	69.5025	BR	104.90	2.00	15.10	145.80	28.00	0.50	1.80	111.10	144.90	19.60	178.60	20.70	1.20
25	105496	Blank	0.0000	0.0000	BR	7.80	1.50	7.10	35.20	2.50	0.50	0.50	10.90	33.30	13.00	24.80	1.90	4.80
26	105498	GSPL-Bhuj-94/02/24	23.1873	69.7233	BR	18.58	1.98	10.38	103.48	5.73	0.50	2.23	17.06	174.95	86.39	41.38	3.11	0.61
27	105499	GSPL-Bhuj-95/02/24	23.1864	69.7228	BR	3.02	1.32	8.28	203.88	2.94	0.50	2.10	3.72	218.65	41.26	14.12	1.40	1.26
28	105501	GSPL-Bhuj-93/02/24	23.1901	69.7231	BR	19.82	0.50	2.07	15.08	7.88	0.50	0.70	43.22	118.95	3.30	16.94	1.13	0.67
29	105503	GSPL-Bhuj-98/02/24	23.195	69.704	BR	101.71	5.68	16.14	224.17	45.07	0.50	1.88	104.08	242.84	18.40	180.27	8.82	2.40
30	105504	GSPL-Bhuj-99/02/24	23.1992	69.7056	BR	22.67	2.11	15.08	211.13	8.26	0.50	3.73	23.00	287.07	77.17	57.53	4.93	1.19
31	105505	GSPL-Bhuj-101/02/24	23.1855	69.7027	BR	27.07	3.46	49.02	131.44	7.76	0.50	2.49	33.78	117.47	46.01	64.03	4.55	4.12
32	105622	GSPL-Bhuj-91/01/24	23.1507	69.58	BR	79.19	2.44	59.34	143.10	27.54	1.75	14.87	60.32	768.78	505.44	201.17	11.73	1.18
33	107488	GSPL-Bhuj-118/06/24	23.1645	69.5543	BR	10.38	0.66	5.63	98.37	8.67	0.86	2.95	9.78	315.82	27.44	52.48	15.09	1.15
34	107492	GSPL-Bhuj-128/06/24	23.1817	69.6913	BR	35.94	0.74	11.61	68.64	9.24	0.50	0.50	43.98	172.58	15.82	120.62	5.62	0.95
35	109013	GSPL_BHUJ_251/12/2024	23.1966	69.6003	BR	0.50	0.50	0.50	64.40	6.60	1.20	0.50	0.50	369.00	0.50	40.50	2.30	0.50

Table Continued..

Annexure-VII

Sl No.	Sample ID	Sample Type	Cd	In	Sn	Sb	Te	Cs	La	Ce	Pr	Nd	Sm	Eu	Gd	Tb	Dy	Ho	Er	Tm
1	105401	BR	<0.5	<0.5	3.40	0.50	<0.5	2.40	55.20	101.50	11.20	37.90	7.30	1.70	6.70	1.00	5.80	1.10	3.30	<0.5
2	105403	BR	<0.5	<0.5	3.40	0.50	<0.5	4.70	45.70	79.70	9.50	31.90	6.20	1.30	5.50	0.80	4.60	0.90	2.60	<0.5
3	105405	BR	<0.5	<0.5	4.40	0.60	<0.5	1.10	130.90	290.90	34.20	106.10	14.60	2.70	9.20	1.20	6.30	1.10	3.30	0.5
4	105406	BR	<0.5	<0.5	2.10	0.80	<0.5	<0.5	18.00	30.50	4.00	17.20	5.70	1.70	6.60	1.00	6.00	1.10	3.10	<0.5
5	105407	BR	<0.5	<0.5	1.40	0.80	<0.5	1.00	22.00	42.20	5.30	19.20	3.80	0.80	3.70	0.50	3.30	0.70	1.90	<0.5
6	105408	BR	<0.5	<0.5	1.90	4.20	<0.5	1.10	18.60	41.30	5.00	18.10	4.60	1.30	4.70	0.80	4.90	0.90	2.80	<0.5
7	105409	BR	<0.5	<0.5	<0.5	<0.5	<0.5	<0.5	19.40	39.60	4.30	14.80	2.70	<0.5	2.30	<0.5	1.50	<0.5	0.80	<0.5
8	105410	BR	<0.5	<0.5	1.50	<0.5	<0.5	1.20	44.70	96.40	11.00	37.10	7.90	1.80	6.80	1.00	5.80	1.10	3.10	<0.5
9	105411	BR	<0.5	<0.5	1.90	<0.5	<0.5	1.40	88.20	182.40	20.80	70.10	12.90	1.70	10.10	1.20	6.10	1.10	2.90	<0.5
10	105413	BR	<0.5	<0.5	2.70	<0.5	<0.5	1.80	56.70	108.80	11.70	38.60	6.70	1.10	5.80	0.80	4.50	0.90	2.50	<0.5
11	105415	BR	<0.5	<0.5	2.30	0.60	<0.5	1.00	31.50	90.20	10.40	40.10	9.40	2.30	9.70	1.40	8.00	1.50	3.80	<0.5
12	105420	BR	<0.5	<0.5	3.80	0.60	<0.5	8.20	44.70	92.40	10.60	35.80	7.00	1.40	6.00	0.80	4.70	0.90	2.50	<0.5
13	105425	BR	<0.5	<0.5	1.10	<0.5	<0.5	1.60	26.70	59.70	7.10	26.70	6.40	1.50	6.80	1.00	6.10	1.20	3.40	0.5
14	105429	BR	<0.5	<0.5	2.90	<0.5	<0.5	4.10	44.50	100.20	10.70	36.20	7.10	1.40	5.70	0.80	4.20	0.80	2.30	<0.5
15	105444	BR	<0.5	<0.5	<0.5	<0.5	<0.5	1.00	36.90	102.20	11.50	44.60	10.50	2.60	10.90	1.70	9.80	1.80	5.00	0.7
16	105477	BR	<0.5	<0.5	2.20	<0.5	<0.5	5.00	28.10	56.40	6.70	24.10	5.10	1.00	4.80	0.70	3.80	0.70	2.00	<0.5
17	105479	BR	<0.5	<0.5	<0.5	<0.5	<0.5	<0.5	11.40	23.30	2.70	9.30	2.00	<0.5	2.20	<0.5	1.90	<0.5	1.00	<0.5

Sl No.	Sample ID	Sample Type	Cd	In	Sn	Sb	Te	Cs	La	Ce	Pr	Nd	Sm	Eu	Gd	Tb	Dy	Ho	Er	Tm
18	105480	BR	<0.5	<0.5	1.10	0.60	<0.5	<0.5	30.00	66.00	8.20	31.40	7.00	2.10	8.70	1.30	7.40	1.40	3.70	<0.5
19	105481	BR	<0.5	<0.5	<0.5	<0.5	<0.5	<0.5	14.60	31.20	3.50	12.30	2.80	0.80	4.10	0.60	3.60	0.70	1.80	<0.5
20	105488	BR	<0.5	<0.5	<0.5	0.60	<0.5	<0.5	16.80	35.20	3.70	13.40	3.20	0.80	3.90	0.60	4.20	0.90	2.60	<0.5
21	105489	BR	<0.5	<0.5	0.90	<0.5	<0.5	<0.5	59.00	119.10	13.40	44.80	8.00	0.80	5.90	0.70	3.10	0.50	1.40	<0.5
22	105492	BR	<0.5	<0.5	4.20	0.60	<0.5	7.10	52.80	104.90	11.80	39.30	7.40	1.50	5.90	0.80	4.30	0.80	2.40	<0.5
23	105494	BR	<0.5	<0.5	1.60	<0.5	<0.5	2.90	87.70	242.10	30.80	131.60	35.50	10.00	50.80	8.10	49.00	9.70	24.20	2.8
24	105495	BR	<0.5	<0.5	4.10	<0.5	<0.5	6.50	47.30	97.80	11.00	37.50	7.30	1.50	6.10	0.90	4.70	0.90	2.50	<0.5
25	105496	BR	<0.5	<0.5	<0.5	<0.5	<0.5	<0.5	15.00	17.60	3.90	14.90	3.30	0.90	3.50	0.5	3.00	0.60	1.50	<0.5
26	105498	BR	<0.5	<0.5	<0.5	<0.5	<0.5	0.9	31.7	75.9	8.5	36.3	8.0	2.4	11.3	1.8	12.1	2.3	5.8	0.8
27	105499	BR	<0.5	<0.5	<0.5	<0.5	<0.5	<0.5	33.9	100.5	11.6	48.6	11.2	2.8	10.6	1.6	9.2	1.6	3.8	0.5
28	105501	BR	<0.5	<0.5	<0.5	<0.5	<0.5	<0.5	11.6	24.0	2.6	9.6	1.8	0.8	1.4	<0.5	0.9	<0.5	<0.5	<0.5
29	105503	BR	<0.5	<0.5	<0.5	<0.5	<0.5	7.6	46.5	90.7	10.1	36.4	6.6	1.5	5.2	0.7	4.0	0.7	1.9	<0.5
30	105504	BR	0.6	<0.5	<0.5	<0.5	0.8	1.4	37.7	147.6	17.5	79.7	20.3	5.2	20.9	3.1	18.2	2.9	6.7	0.9
31	105505	BR	<0.5	<0.5	<0.5	0.74	<0.5	2.4	16.5	35.9	4.8	25.3	10.7	3.3	12.9	2.2	14.1	2.3	5.3	0.7
32	105622	BR	<0.5	<0.5	2.82	0.95	<0.5	4.2	143.0	407.5	51.4	229.4	59.0	16.2	81.1	14.3	75.0	14.9	36.5	4.2
33	107488	BR	<0.5	<0.5	0.85	<0.5	<0.5	<0.5	189.7	366.2	35.7	119.7	19.3	1.2	19.8	1.8	8.0	1.2	2.8	<0.5
34	107492	BR	<0.5	<0.5	1.44	0.56	<0.5	2.0	24.6	56.1	6.1	22.6	4.4	0.9	4.8	0.6	3.6	0.7	2.0	<0.5
35	109013	BR	<0.5	<0.5	1.70	2.20	<0.5	<0.5	<0.5	<0.5	<0.5	<0.5	<0.5	<0.5	<0.5	<0.5	<0.5	<0.5	<0.5	<0.5

Table Continued..

Annexure-VII

Sl No.	Sample ID	Sample Type	Yb	Lu	Hf	Ta	Tl	Bi	Th	U	HREEY	LREE	TREEY
1	105401	BR	3.10	<0.5	4.30	1.30	<0.5	<0.5	23.10	8.80	70.00	213.10	283.10
2	105403	BR	2.30	<0.5	4.30	1.30	<0.5	<0.5	21.80	3.90	56.60	173.00	229.60
3	105405	BR	3.20	<0.5	5.20	1.80	<0.5	<0.5	34.50	5.00	78.70	576.70	655.40
4	105406	BR	2.50	<0.5	4.20	1.00	<0.5	<0.5	25.80	3.20	61.60	75.40	137.00
5	105407	BR	1.70	<0.5	4.30	0.70	<0.5	2.1	12.20	2.60	34.90	92.50	127.40
6	105408	BR	2.70	<0.5	3.30	0.90	<0.5	<0.5	23.20	10.10	48.50	87.60	136.10
7	105409	BR	0.60	<0.5	0.60	<0.5	<0.5	<0.5	13.50	1.00	16.80	80.80	97.60
8	105410	BR	3.00	<0.5	3.30	0.80	<0.5	<0.5	30.30	11.30	57.70	197.10	254.80
9	105411	BR	2.60	<0.5	10.50	1.30	<0.5	<0.5	55.80	5.40	59.80	374.40	434.20
10	105413	BR	2.40	<0.5	6.60	1.40	<0.5	<0.5	35.70	6.50	50.40	222.50	272.90
11	105415	BR	2.70	<0.5	1.20	<0.5	<0.5	<0.5	7.40	2.20	70.20	181.60	251.80
12	105420	BR	2.40	<0.5	5.40	1.70	0.5	<0.5	25.40	2.50	52.00	190.50	242.50
13	105425	BR	3.10	<0.5	3.70	0.70	<0.5	<0.5	12.40	2.70	70.80	126.60	197.40
14	105429	BR	2.10	<0.5	7.00	1.30	<0.5	<0.5	20.50	2.70	49.50	198.70	248.20
15	105444	BR	4.10	0.6	1.10	<0.5	<0.5	<0.5	13.50	1.30	95.40	205.70	301.10
16	105477	BR	1.70	<0.5	1.20	0.6	<0.5	<0.5	11.20	1.40	44.80	120.40	165.20

Sl No.	Sample ID	Sample Type	Yb	Lu	Hf	Ta	Tl	Bi	Th	U	HREEY	LREE	TREEY
17	105479	BR	0.90	<0.5	1.10	<0.5	<0.5	<0.5	6.10	7.00	26.60	48.70	75.30
18	105480	BR	2.40	<0.5	4.20	1	<0.5	<0.5	4.40	4.30	120.30	142.60	262.90
19	105481	BR	1.30	<0.5	<0.5	<0.5	<0.5	<0.5	8.90	1.20	36.70	64.40	101.10
20	105488	BR	2.20	<0.5	1.90	<0.5	<0.5	<0.5	9.50	6.70	45.90	72.30	118.20
21	105489	BR	1.20	<0.5	4.70	0.80	<0.5	<0.5	44.10	2.80	30.30	244.30	274.60
22	105492	BR	2.10	<0.5	5.10	1.60	0.6	<0.5	27.20	2.90	52.50	216.20	268.70
23	105494	BR	14.20	1.9	3.00	0.60	<0.5	<0.5	10.30	4.30	514.50	527.70	1042.20
24	105495	BR	2.30	<0.5	5.00	1.50	0.6	<0.5	22.70	2.70	54.60	200.90	255.50
25	105496	BR	1.30	<0.5	0.70	<0.5	1.3	<0.5	2.20	1.40	32.40	54.70	87.10
26	105498	BR	4.2	0.6	0.76	<0.5	<0.5	<0.5	3.5	3.2	137.99	160.30	298.30
27	105499	BR	3.1	<0.5	<0.5	<0.5	<0.5	<0.5	6.3	2.3	83.19	205.83	289.02
28	105501	BR	<0.5	<0.5	0.7	<0.5	<0.5	<0.5	2.2	<0.5	11.52	49.62	61.13
29	105503	BR	2.2	<0.5	5.0	<0.5	0.6	<0.5	18.3	2.5	51.76	190.25	242.01
30	105504	BR	5.1	0.7	1.7	<0.5	<0.5	<0.5	10.2	2.0	156.13	302.83	458.95
31	105505	BR	4.3	0.5	1.4	<0.5	<0.5	<0.5	7.8	2.0	140.58	93.14	233.72
32	105622	BR	21.5	2.8	4.3	0.9	0.5	<0.5	12.5	5.5	831.43	890.39	1721.82
33	107488	BR	2.1	<0.5	2.1	2.2	<0.5	<0.5	136.38	2.82412	71.03	730.54	801.58
34	107492	BR	2.1	<0.5	4.4	<0.5	<0.5	<0.5	13.351	1.87098	43.07	113.87	156.94
35	109013	BR	<0.5	<0.5	<0.5	<0.5	<0.5	<0.5	<0.5	<0.5	5.50	2.50	8.00

Annexure-VIII: XRF analysis of heavies of stream sediments (-125 micron fraction) for orientation survey

Sr. No.	Original Sample ID	New Sample ID	HLS ID	Location No	Type	Latitude	Longitude	Collected Sample Size	Field Description
1	105419	NA	107671	GSPL_Bhuj-22/12/2023	SS	23.1850	69.6951	<1 mm	Stream sediment <1mm 5 kg collected, Stream flowing between hills of sanstone shale
2	105497	NA	105643	GSPL-Bhuj-94/02/24	SS	23.1873	69.7233	<1 mm	Sample collected from a low lying flat depression where the the nearby rivers are converging to the area, 100m east of KGCMP's high value location, revisit of 19/12/23
3	105515	NA	105647	GSPL-Bhuj-107/02/24	SS	23.2268	69.5095	NA	Sample collected from road side location, exactly at KGCMP location. The area is open relatively low lying, may be covered by perenial rivers. The area is possibly a cemetry ground. Sample has been collected from a existing pit, aprox 70-80cm in depth from surface. Sample has been collected irrespective of grain size. Wacke has been observed at surface level (Bhuj Sandstone according to map)
4	105440	NA	107670	GSPL_Bhuj-04/12/2023	SS	23.2157	69.5894	<2 mm	Near Nagthada tample, hill scarp section of doleritic/basaltic dyke within Bhuj Formation. 80cm thic T1 with river bed sediments.
5	105448	NA	105634	GSPL_Bhuj-29/12/2024	SS	23.1991	69.5123	<1 mm	Sample collected from the stream at deepest part of the 2nd order stream, draining the Bhuj Sandstone, on Bhuj-Nakshatrana road
6	105485	NA	105650 105485	GSPL_Bhuj-68/01/2024	SS	23.1498	69.7271	<2mm	Stream channel, accessible from Jadura-Chakara road through a local cart road. 3rd order stream draining the Bhuj and Katrol formations, Stream sediment collected 150 metre before the confluence of the 2nd order streams
7	105636	107520	107651	GSPL-BHUJ-138/06/2024	SS	23.1540	69.7258	<2 mm	Hill section,near New Cart Road,near Reha Nana Village. Narrow, meandering type river, good trap sites.Sample collected (-2mm) from six point locations, over a stretch of 25m. Junction of two 2nd order streams. .The traps consist of boulders,bed rocks.Very less biogenic contamination seen.
8	105637	107521	107652	GSPL-BHUJ-139/06/2024	SS	23.1794	69.7517	<2 mm	Near Ler village towards ler dam at river side. Occurrence of heterolithic unit of shale/siltstone and thinly bedded rippled topped brownish mauve coloured sandstone. It is a confluence of many slope wash of 1st order and 2nd order streams.The river is 2-12m in breadth. Sample collected (-2mm) from six point locations, over a stretch of 50m along river section. Confluence of 2nd order and 1st order streams. .The trap sites are slope break, deepest part of the stream, bar ends, boulder traps, bedrock traps.High biogenic contamination seen (shurb growth). ~2cm layers have been removed from top while collection of the sample.

Table Continued..

Annexure-VIII

Sr. No.	Original Sample ID	New Sample ID	HLS ID	Sample Description	Weight of -125 (+80) sample taken for HLS(g)	Weight of Heavies (g)	Wt% of heavies in -125 fraction	Al_2O_3	BaO	CaO	Cr_2O_3	Fe_2O_3	K_2O	MgO	MnO	Na_2O	P_2O_5	TiO_2	SiO_2	LOI	S
1	105419	NA	107671	NA	120	8	3.43	10.40	0.16	8.00	1.73	26.70	0.25	3.43	0.76	0.39	0.74	16.73	25.06	<0.05	0.70
2	105497	NA	105643	NA	260	3	0.65	12.73	0.26	1.87	0.14	45.41	0.78	1.00	0.46	0.37	0.65	6.33	26.94	0.76	0.15
3	105515	NA	105647	NA	250	7	1.94	7.97	0.26	0.50	0.26	27.67	0.47	0.49	0.44	0.33	1.50	28.99	21.56	0.74	0.07
4	105440	NA	107670	Very clean sand, consist of quartz (white, yellow and pink), small pebbles of reddish sandstone, few hematite grains. <2mm sample collected from high energy trap sites	130	4	1.55	12.39	0.25	3.86	0.87	34.75	0.32	2.31	1.33	0.64	0.98	16.32	20.91	0.88	<0.05
5	105448	NA	105634	NA	68	5	1.67	8.08	0.24	0.76	0.22	30.92	0.45	0.66	0.51	0.33	1.34	26.28	22.78	0.74	0.08
6	105485	NA	105650 105485	NA	260	10	2.88	7.13	0.17	1.52	0.30	22.00	0.27	0.69	0.49	0.12	2.28	21.28	20.46	12.82	0.12
7	105636	107520	107651	The sediments consist of coarse to very coarse grained sands,mostly quartz. Few iron clast (low contamination)	80	2	2.41	6.66	0.67	0.95	0.25	22.64	0.22	0.69	0.43	0.72	1.96	32.44	21.12	0.25	0.70
8	105637	107521	107652	The sediments consist of coarse to very coarse grains of quartz, yellowish sst/siltstone, red beds,clear transparent white crystals(apatite?)(Xenotime?) in decreasing order of abundance.Grains are sub-rounded to rounded.	120	3	2.28	10.73	0.25	3.50	0.59	19.02	0.52	1.71	0.66	0.89	1.34	22.58	29.84	0.30	0.71

Sr. No.	Original Sample ID	New Sample ID	HLS ID	Location No	Type	Latitude	Longitude	Collected Sample Size	Field Description
9	105638	107522	107653	GSPL-BHUJ-140/06/2024	SS	23.1523	69.7433	<2 mm	Near Reha Nana village in the windmill areas. Occurrence of ferruginous sandstone. Differential weathering is also observed. Narrow, small scale meandering river. This is in confuence zone (2nd and 3rd order?) streams according to toposheet.The river is 2.5-3m in breadth. Sample collected (-2mm) from nine point locations, over a stretch of 60m. The trap sites are deepest part of the streams, boulde/cobble/pebbler traps, bedrock traps.Low direct biogenic contamination. This is a topographically low, depressed area where water comes from every direction.
10	105639	107523	107654	GSPL-BHUJ-141/06/2024	SS	23.1540	69.7492	<2 mm	Near Reha Nana village in the windmill areas. Occurrence of sandstone with differential weathering by ferruginous material. Narrow braided river. Sample collecetd from 2nd order stream.The river is of 3-5m in breadth.Low direct biogenic contamination, however surrounded by farm lands. Sample collected (-2mm) from nine point locations, over a stretch of 780m. 2nd order stream sediment. Very good trap sites, mainly bed rock traps.
11	105640	107524	107655	GSPL-BHUJ-142/06/2024	SS	23.1498	69.7208	<2 mm	Near Reha Mota village, road side stream section along a cart road connecting Reha Mota and Jadura Mota. Occurrence of sandstone with differential weathering by ferruginous material. braided type stream. Sample collected from 3rd order stream (after the confluence of 2nd & 3rd order stream according to toposheet).The river is 3-8m in breadth. Sample collected (-2mm) from seven point locations, over a stretch of 30m. After the confluence of 2nd order and 3rd order streams. The trap sites are not very good. However, sample has been collected from deepest part of the streams, slope breaks, meander corners. High anthropogenic and low direct biogenic contamination. The location is surrounded by local reservoirs for rain water.
12	105641	107525	107656	GSPL-BHUJ-143/06/2024	SS	23.1527	69.6955	<2 mm	Near Jadura village, ~1km west of Jadura-Chakar road (extension of Dhunaraja dam road). Very narrow 2-2.5m,2nd order stream draining the Katrol Formation. Sample collected (-2mm) from six point locations, over a stretch of 20m. Stram meanders at few points. The trap sites are very good. Sample has been collected from deepest part of the streams, boulder traps on channel bed.
13	105642	107526	107657	GSPL-BHUJ-144/06/2024	SS	23.1535	69.7021	<2 mm	Near Jadura village,beside Jadura-Chakar road (extension of Dhunaraja dam road). Occurrence of ferruginous sandstone in river bed. Narrow 3-4m wide,3rd order stream draining the Katrol Formation,near Jadugoda village. Sample collected (-2mm) from five point locations, over a stretch of 20-30m. No meandering observed. The trap sites are very good. Sample has been collected from deepest part of the streams, boulder and bed rock traps on channel bed.
14	105643	107527	107658	GSPL-BHUJ-145/06/2024	SS	23.1480	69.5777	<2 mm	From Bhuj - Mandvi highway, near Naranpur Ravli village opposite to the Nayara Petrol Pump. Occurrence of shl-sst heterolith. Narrow meandering stream of 3-3.5m in breadth, 2nd order streams draining the Katrol formation. Biogenic and anthropogenic contaminations are very low. Sample collected (-2mm) from twelve point locations, over a stretch of 40m. The trap sites are very good. Sample has been collected from deepest part of the streams, boulder and bed rock traps and highest curve of meanders on channel bed.
15	105644	107528	107659	GSPL-BHUJ-146/06/2024	SS	23.1377	69.5396	<2 mm	Near Godpar village,Jamora Dam & Vankol Virdo Temple, accesible by a metal road and then a cart road through Godapar village from Bhuj-Mandvi highway. Occurrence of very weathered heterolith of shl-sst, interupted by tarhet beds. Wide (3-9m) meandering river just after the confluence of 1st and 2nd order stream. High anthropogeic contamination seen. Sample collected (-2mm) from seven point locations, over a stretch of 30m. Trap sites are moderately to good with meander traps,bed rock exposure traps and boulder traps.

Table Continued..

Annexure-VIII

Sr. No.	Original Sample ID	New Sample ID	HLS ID	Sample Description	Weight of -125 (+80) sample taken for HLS(g)	Weight of Heavies (g)	Wt% of heavies in -125 fraction	Al_2O_3	BaO	CaO	Cr_2O_3	Fe_2O_3	K_2O	MgO	MnO	Na_2O	P_2O_5	TiO_2	SiO_2	LOI	S
9	105638	107522	107653	The sediments (bimodal size distribution) consist of coarse to very coarse grains of quartz(rounded to subrounded,platy elongated),clear transparent white crystals(apatite,calcite?),few light green minerals,clast of red beds(elongated-angular) in decreasing order of abundance.Grains are sub-rounded to rounded. Fine material (unidentified) is also constitute the sediment	120	2	1.61	10.57	0.29	1.39	0.39	30.46	0.32	1.15	0.59	0.82	0.92	25.41	21.88	0.20	0.70
10	105639	107523	107654	The sediments (polymodal) consist of very coarse to coarse grained >90% quartz (yellow to pinkish),clear transparent white crystals(not calcite as its hard),clast of red beds,opaque black minerals,siltstone clast in decreasing order of abundance.Grains are sub-angular to sub-rounded.Polymodal size distribution,fine materials cannot be identified.	120	3	2.39	10.48	0.26	3.51	0.52	26.78	0.32	2.11	0.56	0.77	0.92	18.71	29.11	0.20	0.71
11	105640	107524	107655	The sediments consist of medium to coarse grained, consisting of quartz(sub-rounded to sub-angular)>90%,clear transparent white crystals,clast of red beds, black minerals with dull lustre,siltstone,shale clast in decreasing order of abundance.Fine materials can be seen.	58	2	3.33	12.87	0.17	4.38	0.21	22.09	0.79	2.05	1.04	0.75	1.17	14.52	35.24	<0.05	0.71

Table Continued..

Annexure-VIII

Sr. No.	Original Sample ID	New Sample ID	HLS ID	Sample Description	Weight of -125 (+80) sample taken for HLS(g)	Weight of Heavies (g)	Wt% of heavies in -125 fraction	Al_2O_3	BaO	CaO	Cr_2O_3	Fe_2O_3	K_2O	MgO	MnO	Na_2O	P_2O_5	TiO_2	SiO_2	LOI	S
12	105641	107525	107656	The sediments consist of medium to fine grained quartz (rounded to sub-rounded,yellowish to pinkish)>95%,clear transparent white crystals, very few black opaque minerals,siltstone clast in decreasing order of abundance.	120	4	3.26	9.46	0.35	1.24	0.59	24.22	0.17	0.85	0.59	0.34	1.27	36.87	16.60	0.05	0.72
13	105642	107526	107657	The sample has bimodal size distribution, very coarse to fine grained.The coarser grains are sub-rounded to sub-angular with high sphericity and consist of quartz (yellow & pink, 85-90%), clasts of siltstone, yellowish shale,red bed, unidentified black mineral and same whitish clear crystals and biotite in decreasing order of abundance.	124	3	2.31	12.36	0.24	4.56	0.51	24.97	0.29	2.33	0.67	0.51	0.82	23.25	24.36	<0.05	0.72
14	105643	107527	107658	The sediments are generally pebbly to cobbly sized making it difficult to get enough amount after sieving.Bimodal size distribution,very fine grained not recognizable.The coarse sediments are sub-angular to sub-rounded with low sphericity and contains framework of clast of red beds,limonitic layers,siltstone,quartz,the white transparent crsytals,green mineral? and black unidentified mineral in decreasing order of abundance.	120	4	2.54	8.66	0.85	0.54	0.21	19.87	0.23	0.48	0.37	0.34	3.10	30.15	20.88	0.14	0.78

Sr. No.	Original Sample ID	New Sample ID	HLS ID	Location No	Type	Latitude	Longitude	Collected Sample Size	Field Description
15	105644	107528	107659	GSPL-BHUJ-146/06/2024	SS	23.1377	69.5396	<2 mm	Near Godpar village,Jamora Dam & Vankol Virdo Temple, accesible by a metal road and then a cart road through Godapar village from Bhuj-Mandvi highway. Occurrence of very weathered heterolith of shl-sst, interupted by tarhet beds. Wide (3-9m) meandering river just after the confluence of 1st and 2nd order stream. High anthropogeic contamination seen. Sample collected (-2mm) from seven point locations, over a stretch of 30m. Trap sites are moderately to good with meander traps,bed rock exposure traps and boulder traps.
16	105654	107538	107660	GSPL-BHUJ-152/06/2024	SS	23.1784	69.5853	<2 mm	Near Swami Narayan temple, road side stream channel on Bharasar Road, in the vicinity of Wandhsim Reserve Forest. Occurrence of thickly bedded medium to coarse grained sandstone. Moderately wide 5-7m, 2nd order stream Moderately biogenic and high anthropogeic contamination. Sample collected (-2mm) from nine point locations, over a stretch of 15m. Trap sites are very good with ,bed rock exposure traps (appearance of cascade) and boulder traps.
17	105655	107539	107661	GSPL-BHUJ-153/06/2024	SS	23.1844	69.5950	<2 mm	Road side stream channel, near Vandh Sim village on Bharasar road, in the vicinity of Wandhsim Reserve Forest. Occurrence of thickly bedded medium to coarse grained sandstone. Wide 10-12m,3rd order stream. Very high anthropogeic and biogenic contaminations. Sample collected (-2mm) from four point locations, over a stretch of 12m. Trap sites are not good at all. The sample has been collected from bar deposit and stream bed, filled with boulders, cobbles and pebbles.
18	105656	107540	107662	GSPL-BHUJ-154/06/2024	SS	23.1982	69.6735	<2 mm	Road side stream channel, near Tapkeshwari Temple on Tapkeswari road. Occurrence of thickly bedded medium to coarse grained sandstone with differential leaching throughout the outcrop. At the confluence of two narrow 2nd order and 3rd order streams of width 2-3m. The streams meander. Sample has been taken from 3rd oder streams.High anthropogeic and low biogenic contaminations. Sample collected (-2mm) from eleven point locations, over a stretch of 30m. Trap sites are good with boulder traps (stream bed, filled with boulders, cobbles and pebbles).
19	105660	107544	107663	GSPL-BHUJ-158/06/2024	CS	23.2524	69.7447	<2 mm	Near Gada village, Hill scarp section. Intrusion of very fine grained melanocratic rock within the Bhuj Sandstone, occuring at lower contour of the hill. Trend of intrusion 120-300. Creek sample collected (-2mm) from slope breaks, depressed areas, small creeks, and boulder traps
20	105663	107547	107664	GSPL-BHUJ-160/06/2024	SS	23.2271	69.4837	<2 mm	Near Fotdi village, stream cutting small mounds of sandstone, ~1km north of the Fotdi-Kodki metal road. Occurence of ferruginous sandstone. Narrow, meandering, 2nd order, very mature stream draining the Bhuj sandstone and possibly alkaline plug mapped by GSI. The breadth of the river is 3-5m.No anthropogenic and less biogenic contaminations are seen. Sample collected (-2mm) from eight point locations, over a stretch of 60m. Trap sites are not very good but sediments collected from bedrock obstacles,bed rock traps,confluence points.
21	105664	107548	107665	GSPL-BHUJ-161/06/2024	SS	23.2282	69.4882	<2 mm	Near Fotdi village,cricket ground,Shree Shiv Natha Mahadev temple, accessible from Fotdi-Kodki metal road. Occurence of ferruginous sandstone. Narrow, meandering, 2nd order, very mature stream draining the Bhuj sandstone and possibly alkaline plug mapped by GSI. Sample collected just after the confluence of 1st order and 2nd order streams.No anthropogeic and no biogenic contamination seen.The breadth of the river is 3-5m. Sample collected (-2mm) from seven point locations, over a stretch of 30m. Trap sites are very good,sediments collecetd from bed rock traps,meandering points,confluence points.

Table Continued..

Annexure-VIII

Sr. No.	Original Sample ID	New Sample ID	HLS ID	Sample Description	Weight of -125 (+80) sample taken for HLS(g)	Weight of Heavies (g)	Wt% of heavies in -125 fraction	Al_2O_3	BaO	CaO	Cr_2O_3	Fe_2O_3	K_2O	MgO	MnO	Na_2O	P_2O_5	TiO_2	SiO_2	LOI	S
15	105644	107528	107659	The sediments are coarse to medium grained ,finer grains are not identifiable.Sample consist of medium to coarse grained quartz,siltstone clasts of redbeds and white transparent crystal (very low in amount) in decreasing order of abundance.The grains are sub-angular to sub-rounded with low sphericity.	120	4	3.13	11.90	0.19	2.80	0.60	37.64	0.63	2.06	0.64	0.37	0.69	11.90	26.88	0.08	0.71
16	105654	107538	107660	The sediments are coarse to medium grained with cobbles and boulders.Consist of rock fragments(<2%, clast of siltstone, red beds),quartz,white transparent mineral,black mineral in decreasing order of abundance.The clasts are sub-rounded to angular with moderate sphericity.There is mud in the sediment.	152	3	1.88	7.94	0.33	1.93	0.34	32.61	0.32	1.39	0.68	0.26	0.47	27.66	21.77	0.07	0.68
17	105655	107539	107661	The sediment has been weight sieved, and hence not been described.	120	3	2.37	6.18	0.25	1.54	0.25	34.19	0.54	0.95	0.49	0.22	0.88	22.98	24.86	0.06	0.69
18	105656	107540	107662	Sediments collected are medium to coarse grained containing rounded to sub-angular grains of quartz.(>90%),siltstone,red nodule beds,black minerals with dull lusture (<1%) in decreasing order of abundance.	79	3	3.70	7.63	0.71	2.21	0.70	31.72	0.45	1.25	0.83	0.23	1.65	21.37	21.68	0.19	0.72

Table Continued..

Annexure-VIII

Sr. No.	Original Sample ID	New Sample ID	HLS ID	Sample Description	Weight of -125 (+80) sample taken for HLS(g)	Weight of Heavies (g)	Wt% of heavies in -125 fraction	Al_2O_3	BaO	CaO	Cr_2O_3	Fe_2O_3	K_2O	MgO	MnO	Na_2O	P_2O_5	TiO_2	SiO_2	LOI	S
19	105660	107544	107663	The sediments are coarse to medium grained with cobbles and boulders. Consist of rock fragments(clast of red beds, intrusion),quartz, unidentified black mineral and many small broken fragments of bedrock in decreasing order of abundance.The clasts are sub-angular to angular with low sphericity.	120	8	6.12	11.80	0.14	5.07	0.22	19.85	0.70	2.17	0.63	0.83	0.85	11.91	40.76	<0.05	0.70
20	105663	107547	107664	The sediments from the confluence point are matured minerologically.The sediments consist of medium to fine grained,angular to sub-angular,clast of pink quartz,completely platy transparent white crystals and very coarse fragments(fumaroles/altered sst)<1% in decreasing order of abundance.	120	7	5.18	4.19	0.30	0.57	0.59	18.87	0.27	0.53	0.54	0.21	2.35	33.23	17.41	0.08	0.71
21	105664	107548	1E+05	The sediments from the confluence point are matured minerologically.The sediments consist of medium to fine grained,angular to sub-angular,clast of pink and white quartz,completely platy transparent white crystals and very coarse fragments(fumaroles/altered sst)<1% in the decreasing order of abundance.	120	5	4.04	8.52	0.42	0.63	0.73	22.42	0.21	0.73	0.58	0.34	1.06	43.28	12.40	0.11	0.73

Sr. No.	Original Sample ID	New Sample ID	HLS ID	Location No	Type	Latitude	Longitude	Collected Sample Size	Field Description
22	105665	107549	107666	GSPL-BHUJ-162/06/2024	SS	23.2270	69.4991	<2 mm	Near Fotdi village,approx 700m east of Shree Shiv Natha Mahadev temple, accessible from Fotdi-Kodki metal road. Occurence of ferruginous sandstone. Narrow, meandering, 2nd order stream, just after the confluence of two 1st order streams. High biogenic and nearly no anthropogeic contaminations.The breadth of the river is 2-2.5m. Sample collected (-2mm) from eight point locations, over a stretch of 20m. Trap sites are very good,sediments are collected from large boulders which act as trap, meandering points.
23	105669	107553	107667	GSPL-BHUJ-164/06/2024	CS	23.2210	69.5904	<2 mm	Near Kalyanpar village at Shree Hari Visamo Tekdi Temple. Part of the hill is of basalt dyke intruded reddish brown colored massive duricrusted sandstone, overlying a scree deposit of white clay clasts embedded in a finer groundmass. Network of veins of hematite cross cutting the sandstone is observed. (-2mm) slopewash sample, collected at the slope break of the basalt from four point locations over a stretch of 15m. High anthropogenic activity.
24	105673	107557	107668	GSPL-BHUJ-165/06/2024	CS	23.2211	69.5898	<2 mm	Near Kalayanpur village, at Shri Hari Visamo Takdi temple, at the opposite side of the hill, where basalt has intruded. Part of the hill is of basalt dyke intruded reddish brown colored massive duricrusted sandstone, overlying a scree deposit of white clay clasts embedded in a finer groundmass. Network of veins of hematite cross cutting the sandstone is observed. (-2mm) slopewash sample, collected at the slope break of the hill from six point locations throughout the hill. High anthropogenic activity.
25	105674	107558	107669	GSPL-BHUJ-166/06/2024	SS	23.1365	69.6641	<2 mm	Near Kirgurya Dungar,near Bharapar village at north of Sapar timbo village,Hemkund Horticulture farm. Occurrence of basalt intrusion within Bhuj sandstone. Very narrow (±2m) 2nd order meandering stream. Sample collected after the confluence of two 1st order streams. Very less biogenic and anthropogenic contamination seen. Sample collected (-2mm) from six point locations, over a stretch of 20m. Trap sites are very good,sediments have been collected from trap sites of large boulders on the channel bed and exposed bedrock.
26	105423	NA	107672	GSPL_Bhuj-24/12/2024	SS	23.1526	69.7021	<1 mm	Stream cut section on continuation of Jadura village to Chakar village road. Occurrence of thick beds of medium grained quartzose sandstone with encrustration on top and ferrugenous staining. The sandstones are internally planar parallel to planar cross stratified. Ripple marks and lag conglomerate are also present. Sample collected from 2nd order stream draining the Katrol Formation
27	105436	NA	107673	GSPL_Bhuj-31/12/2023	SS	23.2242	69.5236	<2 mm	Near Rati Tala,Hanuman Temple,roadside digged and dumped rocks.However whole area is farmland on Kodki road. Occurrence of sandstone beds separated by thin (15) cm white shale layer. Sample collected from 3rd order stream, draining the Bhuj Formation and probably the reported alkali plug and phosphorite area
28	105447	NA	107674	GSPL_Bhuj-29/12/23	SS	23.1991	69.5123	<2 mm	Exposure on Bhuj-Nakshatrana road. Bedrock exposed with 1 to 1.5 m thick red sandstone bed and at top very dark coarse grained sandstone. Sample collected from 1st order stream draining Bhuj Formation.

Table Continued..

Annexure-VIII

Sr. No.	Original Sample ID	New Sample ID	HLS ID	Sample Description	Weight of -125 (+80) sample taken for HLS(g)	Weight of Heavies (g)	Wt% of heavies in -125 fraction	Al_2O_3	BaO	CaO	Cr_2O_3	Fe_2O_3	K_2O	MgO	MnO	Na_2O	P_2O_5	TiO_2	SiO_2	LOI	S
22	105665	107549	1E+05	Sediments collected are medium to fine grained consisting of sub-angular fragments of pink quartz (>3-4%), fumaroles, limonitic layer, red sst with 5-7% and gravel size clast of quartz in decreasing order of abundance.	120	2	1.61	7.75	0.22	3.73	0.27	26.53	0.53	1.66	0.60	0.49	0.78	18.85	33.06	<0.05	0.69
23	105669	107553	1E+05	Sediments consist of coarse grained,sub-angluar to angular clast of basalt,quartz,magnetite in decreasing order of abundance.	120	2	1.29	12.25	0.20	2.92	0.23	43.51	0.67	2.26	0.58	0.41	0.57	7.20	26.29	0.26	1.01
24	105673	107557	1E+05	Sediment consist of medium to fine grained quartz, clay? with very coarse grained quartz clast,rock fragments,red fumaroles and black mineral (<1%) in decreasing order of abundance.The grains are angular to sub-angular.Quartz grains shows moderate sphericity.	120	5	2.86	11.69	0.20	2.95	0.24	42.67	0.80	2.24	0.49	0.30	0.62	7.09	28.06	0.06	0.71
25	105674	107558	1E+05	The sediments are medium to fine grained with few gravel size clasts of quartz (>90%), pink quartz, <2% rock fragments) (silt, weathered basalts?) in decreasing order of abundance.The clasts are sub-angular to sub-rounded with low sphericity.	120	3	2.23	7.05	0.31	2.73	0.28	28.22	0.43	2.51	0.97	0.27	0.89	31.13	18.84	<0.05	0.68
26	105423	NA	1E+05	Not recorded	52	0.52	0.85	10.76	0.36	2.79	0.54	27.59	0.45	1.49	0.57	0.33	1.05	21.39	27.78	0.40	0.08
27	105436	NA	1E+05	Not recorded	NA	2	0.00	10.04	0.30	0.77	0.19	27.31	0.52	0.90	0.44	0.33	0.85	25.31	28.31	0.44	0.07
28	105447	NA	1E+05	Not recorded	120	2.94	2.33	8.80	0.25	1.39	0.27	31.52	0.31	1.06	0.46	0.25	0.77	23.04	27.76	0.43	0.07

Sr. No.	Original Sample ID	New Sample ID	HLS ID	Location No	Type	Latitude	Longitude	Collected Sample Size	Field Description
29	105464	NA	107675	GSPL_Bhuj-47/12/2023	SS	23.1642	69.6306	<2 mm	River channel exposure, near a sanatorium, on Bhuj-Mundra Road. Exposure of sandstone at the river bed. East to west flowing river with gravels, boulder sand and fines on the riverbed.Sample collected from 2nd order stream draining the Katrol and Bhuj formations and from the deepest point of the stream
30	105458	NA	107676	GSPL_BHUJ-26/12/2023	SS	23.1343	69.6878	<2 mm	Road side stream cut section on Rehanana to Surajpur connecting road. Occurrence of planar parallel to low angle planar cross stratified very fine grained white colored sandstone (siltstone??). At river bed grey shale is exposed. Encrustation on top of the sandstone beds are observed. On way to the stream there is ferrugenous, brownish black colored sandstone on surface (may be feldspathic). Sample collected from 3rd order stream, draining the Bhuj Formation.
31	105467	NA	107677	GSPL_Bhuj-49/12/2023	SS	23.1508	69.6239	<1 mm	Near Sedat villege, behind 153 BN BSF Marine Camp stram channel, accessible from Bhuj-Mundra Road. 2nd order stream flowing SW to NE, consisting mostly of silt and clay fraction, draining the Katrol Formation.
32	105514	NA	107678	GSPL-Bhuj_106/02/24	SS	23.2246	69.5877	bulk	At high HREE value location . SS collected

Table Continued..

Annexure-VIII

Sr. No.	Original Sample ID	New Sample ID	HLS ID	Sample Description	Weight of -125 (+80) sample taken for HLS(g)	Weight of Heavies (g)	Wt% of heavies in -125 fraction	Al_2O_3	BaO	CaO	Cr_2O_3	Fe_2O_3	K_2O	MgO	MnO	Na_2O	P_2O_5	TiO_2	SiO_2	LOI	S
29	105464	NA	1E+05	Not recorded	150	1.16	0.46	9.77	0.30	1.84	0.34	22.49	0.34	1.62	0.42	0.49	1.54	22.52	29.43	0.45	0.07
30	105458	NA	1E+05	Not recorded	73	2.3	2.56	11.87	0.26	4.12	0.35	27.43	0.37	1.73	0.63	0.41	0.79	19.56	28.72	0.43	0.09
31	105467	NA	1E+05	Not recorded	150	0.45	0.05	12.08	0.29	1.72	0.43	18.22	0.24	1.65	0.58	0.45	1.28	31.24	24.45	0.44	<0.05
32	105514	NA	1E+05	stream sediment brownish in colour. Sample collected as whole without sieving from a low lying area	240	NA	0	8.633	0.327	1.231	0.278	24.737	0.152	1.08	0.566	0.33	2.281	32.034	20.512	0.45	0.0592

Annexure-IX: ICPMS analysis of heavies of stream sediments (-125 micron fraction)

Sr. No.	Original Sample ID	Location No.	Type	Latitude	Longitude	Collected Sample Size	Li	Be	Sc	V	Cr	Co
1	105419	GSPL_Bhuj-22/12/2023	SS	23.1850	69.6951	<1 mm	9.29	1.55	53.89	557.18	532.89	41.39
2	105497	GSPL-Bhuj-94/02/24	SS	23.1873	69.7233	<1 mm	15.20	2.70	23.75	286.55	148.06	41.89
3	105515	GSPL-Bhuj-107/02/24	SS	23.2268	69.5095	NA	6.48	2.62	64.18	627.64	436.45	26.75
4	105440	GSPL_Bhuj-04/12/2023	SS	23.2157	69.5894	<2 mm	6.22	1.73	31.96	434.20	296.36	69.23
5	105448	GSPL_Bhuj-29/12/2024	SS	23.1991	69.5123	<1 mm	6.54	2.74	50.56	545.07	397.65	30.65
6	105485	GSPL_Bhuj-68/01/2024	SS	23.1498	69.7271	<2mm	25.20	3.40	131.50	639.70	NA	NA
7	105636	GSPL-BHUJ-138/06/2024	SS	23.1540	69.7258	<2 mm	8.04	2.32	90.25	676.47	529.78	38.68
8	105637	GSPL-BHUJ-139/06/2024	SS	23.1794	69.7517	<2 mm	12.90	1.06	55.34	417.07	490.67	22.65
9	105638	GSPL-BHUJ-140/06/2024	SS	23.1523	69.7433	<2 mm	9.21	2.40	51.05	582.01	495.41	32.04
10	105639	GSPL-BHUJ-141/06/2024	SS	23.1540	69.7492	<2 mm	9.13	1.91	45.46	451.02	416.25	30.44
11	105640	GSPL-BHUJ-142/06/2024	SS	23.1498	69.7208	<2 mm	14.83	1.56	33.75	270.39	162.91	29.00
12	105641	GSPL-BHUJ-143/06/2024	SS	23.1527	69.6955	<2 mm	6.01	2.16	63.89	787.32	582.74	26.12
13	105642	GSPL-BHUJ-144/06/2024	SS	23.1535	69.7021	<2 mm	7.26	1.65	50.30	536.10	438.00	29.73
14	105643	GSPL-BHUJ-145/06/2024	SS	23.1480	69.5777	<2 mm	7.18	2.30	99.51	712.02	444.61	43.16
15	105644	GSPL-BHUJ-146/06/2024	SS	23.1377	69.5396	<2 mm	20.44	2.14	42.36	474.42	320.72	42.44
16	105654	GSPL-BHUJ-152/06/2024	SS	23.1784	69.5853	<2 mm	8.89	1.99	45.89	564.05	422.75	31.40
17	105655	GSPL-BHUJ-153/06/2024	SS	23.1844	69.5950	<2 mm	11.06	2.27	48.96	467.70	354.69	27.84
18	105656	GSPL-BHUJ-154/06/2024	SS	23.1982	69.6735	<2 mm	22.61	1.79	47.63	507.86	348.78	33.63
19	105660	GSPL-BHUJ-158/06/2024	CS	23.2524	69.7447	<2 mm	12.12	1.73	41.54	340.85	207.06	33.14
20	105663	GSPL-BHUJ-160/06/2024	SS	23.2271	69.4837	<2 mm	6.38	2.88	117.58	865.02	696.18	20.77
21	105664	GSPL-BHUJ-161/06/2024	SS	23.2282	69.4882	<2 mm	5.14	3.46	94.23	1014.80	836.71	23.31
22	105665	GSPL-BHUJ-162/06/2024	SS	23.2270	69.4991	<2 mm	10.28	1.73	43.62	411.30	284.85	27.40
23	105669	GSPL-BHUJ-164/06/2024	CS	23.2210	69.5904	<2 mm	10.21	1.04	18.58	181.40	132.41	21.48
24	105673	GSPL-BHUJ-165/06/2024	CS	23.2211	69.5898	<2 mm	26.19	2.52	44.85	425.33	272.22	40.65
25	105674	GSPL-BHUJ-166/06/2024	SS	23.1365	69.6641	<2 mm	8.11	1.67	60.86	693.87	361.35	181.64
26	105423	GSPL_Bhuj-24/12/2024	SS	23.1526	69.7021	<1 mm	20.13	3.11	108.97	609.66	787.09	35.13
27	105436	GSPL_Bhuj-31/12/2023	SS	23.2242	69.5236	<2 mm	13.56	5.03	132.07	703.17	546.82	40.17
28	105447	GSPL_Bhuj-29/12/23	SS	23.1991	69.5123	<2 mm	13.87	4.33	101.52	630.13	580.43	43.24
29	105464	GSPL_Bhuj-47/12/2023	SS	23.1642	69.6306	<2 mm	12.34	3.63	158.60	540.47	591.45	36.04
30	105458	GSPL_BHUJ-26/12/2023	SS	23.1343	69.6878	<2 mm	12.58	4.35	91.04	602.09	560.55	44.09
31	105467	GSPL_Bhuj-49/12/2023	SS	23.1508	69.6239	<1 mm	12.83	3.41	176.87	684.05	757.62	27.37
32	105514	GSPL-Bhuj_106/02/24	SS	23.2246	69.5877	bulk	10.41	3.75	102.25	582.10	508.56	44.03

Table Continued..

Annexure-IX

Sr. No.	Original Sample ID	Ni	Cu	Zn	Ga	Ge	Se	Rb	Sr	Y	Zr	Nb	Mo	Cd	In
1	105419	70.95	54.01	186.29	31.29	18.10	5.56	9.05	242.72	278.45	1789.84	194.82	4.76	2.15	<0.5
2	105497	71.46	45.79	247.85	16.97	14.50	3.21	27.40	149.10	136.41	464.50	40.25	2.24	0.60	<0.5
3	105515	46.18	38.36	210.89	54.11	32.96	10.24	12.28	90.29	561.06	4369.44	274.77	5.63	4.44	<0.5
4	105440	57.05	163.08	152.72	30.06	20.87	5.09	10.56	145.65	258.25	1033.18	154.44	3.22	1.38	<0.5
5	105448	46.71	48.41	198.05	51.98	32.15	8.86	12.33	78.25	444.04	2466.25	162.43	4.51	2.74	<0.5
6	105485	NA	NA	NA	264.10	30.30	104.20	12.30	108.90	963.10	89900.00	268.50	357.60	2.70	0.60
7	105636	72.59	107.42	223.91	82.11	37.37	12.13	5.72	256.68	592.84	3463.14	337.15	4.67	3.42	0.72
8	105637	30.52	38.27	152.99	43.70	26.40	8.68	15.39	1089.54	452.80	3489.53	249.52	3.16	3.11	<0.5
9	105638	63.25	43.11	220.93	42.82	18.96	5.74	8.98	135.50	260.02	2082.26	270.28	4.15	1.94	<0.5
10	105639	57.56	37.52	186.18	30.19	18.22	5.24	9.88	179.74	260.58	1852.06	190.50	2.96	1.77	<0.5
11	105640	34.03	30.12	160.51	39.16	22.69	7.12	28.47	132.29	349.70	948.95	347.86	2.30	0.99	<0.5
12	105641	41.62	40.41	201.57	71.80	25.09	8.28	4.74	123.06	377.63	2589.53	333.24	5.58	2.45	0.58
13	105642	47.20	40.72	168.68	39.52	16.19	5.22	7.97	151.43	242.97	1717.01	246.47	4.01	1.58	<0.5
14	105643	80.94	123.44	233.45	139.45	59.77	20.21	5.94	331.48	897.22	5090.88	401.97	8.52	4.42	0.79
15	105644	90.35	54.40	227.61	25.33	19.92	5.24	27.78	238.92	180.36	680.53	127.23	3.34	0.76	<0.5
16	105654	59.16	44.15	207.57	34.57	9.22	1.97	9.65	259.31	100.78	850.14	282.74	4.27	1.09	<0.5
17	105655	67.46	44.06	178.70	30.68	19.86	5.79	15.82	108.50	247.45	2114.89	217.53	3.71	4.92	<0.5
18	105656	64.79	53.93	247.10	56.60	36.08	10.49	19.46	306.83	494.52	1978.85	282.98	4.20	3.77	<0.5
19	105660	41.73	32.25	139.71	36.67	19.54	6.08	24.15	189.36	295.62	1199.45	136.99	2.55	2.20	<0.5
20	105663	29.79	38.19	171.08	116.11	49.85	17.90	7.37	108.88	987.77	10691.12	408.00	7.98	14.34	0.51
21	105664	34.90	47.30	174.01	55.11	20.84	6.30	5.77	316.66	421.44	5841.16	400.75	8.42	7.41	0.59
22	105665	47.54	38.55	156.13	33.56	14.31	4.44	15.44	137.41	217.09	1309.41	194.07	3.01	1.97	<0.5
23	105669	49.92	38.52	103.08	8.59	5.90	2.22	13.14	1965.64	45.56	201.84	32.07	1.53	0.59	<0.5
24	105673	108.47	67.29	224.18	21.14	15.95	3.17	38.91	169.61	120.35	466.92	85.66	2.92	0.94	<0.5
25	105674	92.06	63.71	680.57	39.06	23.30	6.67	13.73	153.61	362.05	2315.10	427.07	6.20	2.77	<0.5
26	105423	77.53	44.02	232.37	153.12	18.05	59.18	16.60	189.13	455.23	6119.87	263.32	5.30	2.35	<0.5
27	105436	86.77	30.88	278.46	107.51	11.72	41.42	18.64	227.55	403.46	8868.15	353.51	7.00	3.57	0.50
28	105447	110.13	43.43	240.63	114.65	12.75	39.73	12.89	155.07	326.41	5255.47	294.71	8.24	2.11	<0.5
29	105464	78.13	38.97	212.28	198.48	24.08	79.97	11.83	222.84	710.05	9025.40	59.82	4.86	3.18	<0.5
30	105458	80.85	35.49	233.13	126.11	13.85	42.67	13.47	177.58	337.52	3549.35	260.17	5.51	1.56	<0.5
31	105467	55.43	42.75	152.07	164.58	19.40	62.30	8.82	253.31	622.81	13086.09	361.09	7.20	4.00	<0.5
32	105514	91.93	46.30	275.66	341.44	41.96	121.06	5.88	130.77	686.34	1844.49	156.41	5.66	0.96	0.61

Table Continued..

Annexure-IX

Sr. No.	Original Sample ID	Sn	Sb	Te	Cs	Ba	La	Ce	Pr	Nd	Sm	Eu	Gd	Tb
1	105419	10.90	1.30	0.72	<0.5	237.84	1637.05	3288.49	373.12	1298.69	223.54	9.90	193.79	17.67
2	105497	5.97	0.60	<0.5	1.63	1225.44	563.84	1113.20	128.76	449.28	76.18	5.04	68.42	7.00
3	105515	27.04	0.88	1.66	<0.5	328.50	3788.01	7567.20	857.65	2977.37	514.87	18.61	433.48	40.16
4	105440	9.66	0.83	0.57	0.58	639.79	1954.03	3914.95	444.94	1538.17	266.00	9.59	227.08	19.20
5	105448	15.98	0.59	1.01	<0.5	388.08	3544.92	7148.04	815.34	2823.51	482.55	16.69	403.78	35.20
6	105485	30.20	1.60	2.00	0.80		5670.60	11462.00	1265.80	4436.20	771.70	27.20	543.50	64.00
7	105636	25.07	1.19	0.84	<0.5	2657.93	4207.69	8439.98	951.66	3265.35	557.96	19.78	454.21	40.36
8	105637	14.95	1.07	1.03	0.67	490.39	2825.49	5678.96	642.20	2195.14	384.29	14.40	311.20	28.30
9	105638	16.83	1.06	0.53	<0.5	569.08	1578.02	3162.05	362.23	1238.10	209.23	9.13	173.63	16.05
10	105639	12.06	0.83	<0.5	0.58	729.99	1598.97	3164.91	363.09	1233.29	213.12	9.46	174.93	16.14
11	105640	14.13	0.62	<0.5	1.38	264.06	2571.74	4929.71	537.25	1777.30	300.93	10.95	254.04	22.97
12	105641	29.12	1.56	0.60	<0.5	499.07	2696.52	5429.08	619.03	2100.75	367.75	12.62	293.27	25.72
13	105642	17.16	1.05	<0.5	<0.5	297.84	1443.23	2893.45	327.36	1135.46	190.04	8.52	157.83	14.58
14	105643	29.94	1.78	1.17	<0.5	4052.53	7540.66	15147.40	1722.78	5896.32	991.27	32.27	796.24	71.30
15	105644	6.99	1.19	<0.5	1.39	699.61	1109.74	2199.24	251.94	869.76	144.57	6.19	120.26	11.16
16	105654	16.72	1.05	<0.5	<0.5	779.20	408.08	805.18	96.25	333.68	55.81	4.53	48.26	4.89
17	105655	14.38	0.76	0.86	0.72	480.93	1402.74	2789.97	317.80	1101.76	188.51	8.71	211.24	16.76
18	105656	13.91	1.05	1.13	1.01	3359.97	3872.54	7680.26	856.44	2911.64	501.22	17.41	494.60	40.46
19	105660	10.18	0.82	0.63	1.00	264.89	1960.67	3912.23	442.93	1527.14	267.41	11.59	256.24	21.32
20	105663	28.08	1.88	3.38	<0.5	296.00	6345.11	12599.71	1429.47	4940.22	846.76	33.05	781.20	69.64
21	105664	29.01	1.62	1.48	<0.5	697.93	2139.86	4322.22	490.87	1707.60	304.76	14.78	272.23	24.51
22	105665	12.79	0.88	0.50	0.70	340.59	1249.02	2507.97	286.89	995.73	168.36	7.68	150.21	13.43
23	105669	2.64	<0.5	<0.5	0.75	418.03	172.96	341.86	41.12	140.45	23.70	1.70	21.50	2.08
24	105673	6.23	0.94	<0.5	2.22	976.67	477.80	948.82	112.77	400.27	67.19	4.60	61.20	5.99
25	105674	17.81	0.92	1.02	<0.5	564.60	2408.48	4825.22	544.66	1885.03	326.14	11.30	284.75	24.91
26	105423	18.26	1.71	3.85	0.80	1402.05	2527.20	5081.17	577.91	2050.99	339.21	15.16	256.78	28.12
27	105436	21.19	1.77	3.01	0.91	808.54	1698.69	3396.68	389.25	1375.56	236.38	14.27	184.84	21.72
28	105447	22.07	1.75	3.19	0.93	645.64	1828.29	3665.13	416.58	1473.13	244.46	11.42	180.86	19.95
29	105464	16.42	<0.5	4.29	0.63	875.22	3455.15	6905.08	779.66	2773.59	474.32	22.99	356.54	40.53
30	105458	21.19	0.90	2.85	0.83	815.74	1993.40	3983.02	452.31	1582.84	263.46	12.79	193.65	21.02
31	105467	28.24	1.81	3.59	<0.5	443.46	2774.32	5541.77	626.92	2250.63	382.62	20.61	294.01	34.08
32	105514	23.20	0.97	8.68	<0.5	527.26	6202.57	12502.48	1371.33	4821.53	789.73	24.45	555.97	55.93

Table Continued..

Annexure-IX

Sr. No.	Original Sample ID	Dy	Ho	Er	Tm	Yb	Lu	Hf	Ta	W	Tl	Pb	Bi	Th	U	HREEY	LREE	TREEY
1	105419	66.98	10.29	24.68	2.90	16.93	2.58	50.35	12.36	6.86	<0.5	150.17	0.95	971.91	72.49	678.04	6820.88	7498.92
2	105497	29.62	4.78	11.36	1.30	7.36	1.08	11.68	3.01	1.73	<0.5	62.78	<0.5	328.54	23.44	296.14	2331.25	2627.39
3	105515	146.26	20.31	46.02	4.84	27.09	4.07	117.61	18.39	8.37	<0.5	279.97	0.74	2304.97	176.23	1366.07	15705.10	17071.17
4	105440	66.87	9.50	21.56	2.17	12.05	1.81	28.63	20.82	4.82	0.74	123.99	0.61	1178.26	74.44	660.06	8118.09	8778.15
5	105448	117.81	16.58	37.03	3.65	20.04	3.01	65.41	11.23	4.81	0.55	348.28	0.67	2345.40	146.74	1148.41	14814.37	15962.79
6	105485	245.00	37.40	90.00	11.60	71.60	10.60	295.30	13.00		<0.5		0.80	2419.80	250.00	2195.50	23606.30	25801.80
7	105636	145.05	20.70	48.17	5.20	29.87	4.53	92.87	20.55	7.35	0.52	372.28	1.02	2507.87	165.01	1450.95	17422.64	18873.59
8	105637	104.58	15.71	37.34	4.31	25.39	3.94	93.27	16.88	9.02	<0.5	196.04	0.74	1539.44	112.61	1053.32	11726.09	12779.40
9	105638	60.36	9.25	22.44	2.63	15.66	2.41	54.83	16.47	7.61	<0.5	198.91	0.61	960.69	66.42	622.62	6549.64	7172.26
10	105639	60.28	9.14	21.39	2.39	13.75	2.07	48.99	11.45	5.84	<0.5	134.32	<0.5	915.82	67.67	615.58	6573.38	7188.97
11	105640	85.26	12.43	27.46	2.77	14.66	2.07	24.94	31.13	5.46	<0.5	146.57	0.52	1407.45	73.55	816.07	10116.93	10933.00
12	105641	92.13	13.39	30.86	3.27	18.57	2.79	69.70	21.58	10.75	<0.5	320.22	1.02	1666.27	109.80	934.14	11213.14	12147.27
13	105642	54.66	8.52	20.40	2.39	14.12	2.15	46.01	14.82	7.99	<0.5	170.68	0.66	845.51	58.35	576.43	5989.53	6565.96
14	105643	240.73	31.95	69.83	6.53	34.97	5.03	137.65	23.80	14.40	0.56	519.54	1.22	4592.77	289.42	2285.58	31298.42	33584.01
15	105644	41.79	6.30	14.87	1.65	9.44	1.41	18.35	7.79	3.90	<0.5	118.48	0.56	669.89	41.44	435.81	4575.25	5011.06
16	105654	21.05	3.62	9.47	1.26	7.93	1.24	22.82	16.45	8.01	<0.5	180.33	0.64	280.88	21.48	248.93	1698.99	1947.92
17	105655	59.81	9.16	21.94	2.63	15.17	2.37	57.46	12.62	6.69	0.58	145.48	<0.5	844.00	66.38	644.19	5800.78	6444.96
18	105656	137.73	19.23	42.36	4.19	22.30	3.22	54.69	30.97	6.71	<0.5	268.95	0.85	2463.46	150.57	1323.67	15822.09	17145.76
19	105660	74.69	11.07	25.60	2.78	15.58	2.32	32.86	10.61	5.39	<0.5	131.38	0.77	1110.03	77.53	758.36	8110.37	8868.73
20	105663	250.52	36.26	83.03	9.27	53.21	8.38	299.23	26.43	13.51	0.53	372.67	1.03	3667.95	282.46	2429.90	26161.27	28591.17
21	105664	94.87	15.14	37.64	4.80	29.52	4.76	168.44	25.88	12.15	0.66	221.90	1.04	1320.74	121.22	1013.93	8965.31	9979.24
22	105665	50.67	7.83	18.71	2.18	12.60	1.90	34.90	12.63	6.70	<0.5	141.83	0.79	743.61	49.14	525.92	5207.96	5733.88
23	105669	8.88	1.54	4.11	0.53	3.24	<0.5	5.26	1.69	1.24	<0.5	33.12	<0.5	98.23	6.85	107.72	720.08	827.80
24	105673	25.24	4.24	10.83	1.38	8.15	1.25	12.71	5.29	3.32	<0.5	86.24	0.73	281.34	22.48	288.09	2006.86	2294.94
25	105674	90.26	13.76	33.54	3.95	23.85	3.70	67.90	26.70	10.67	<0.5	204.82	0.87	1529.37	104.06	912.94	9989.53	10902.47
26	105423	115.60	18.55	46.25	6.18	40.19	6.05	165.45	24.21	10.56	1.39	219.28	1.05	1637.13	119.79	1097.08	10576.47	11673.56
27	105436	95.20	16.13	41.88	5.94	38.97	6.08	249.87	22.78	12.22	2.26	201.09	0.93	1124.36	107.26	960.56	7096.57	8057.13
28	105447	81.23	13.14	32.92	4.37	28.28	4.33	146.83	18.73	9.47	2.27	213.15	1.14	1244.35	89.45	804.42	7627.60	8432.03
29	105464	173.54	28.84	73.14	9.96	65.03	10.06	135.20	1.66	3.56	2.21	213.29	0.68	2077.83	184.41	1649.27	14387.80	16037.07
30	105458	84.60	13.49	33.21	4.28	27.30	4.03	98.15	16.46	8.10	1.94	209.13	0.89	1295.10	87.70	822.94	8275.03	9097.97
31	105467	149.53	25.60	67.09	9.47	64.19	9.90	356.18	25.45	17.80	1.55	198.91	1.04	1699.24	164.49	1474.16	11576.26	13050.42
32	105514	201.19	28.34	60.47	6.58	38.09	5.58	32.76	5.88	9.18	1.72	447.56	0.82	4184.33	229.48	1765.18	25687.63	27452.82

Annexure-X: XRD analysis of heavies of stream sediments (-125 micron fraction)

Sl No.	Sample No.	Latitude	Longitude	Sample Type	Sample Description	Catchment Lithology	Good/ Considerable/ Small amount	Trace amount	Likely phases
1	105464	23.1642	69.6306	HLS sample (-125µ)	<2mm sample collected from the deepest part of the stream of a 2nd order stream, after the confluence of 1st and 2nd order stream. TREEY: 1.6%	Ferruginous sandstone and metasomatized ferruginous sandstone of Bhuj Formation	Quartz-35%, Zircon-30%, Rutile- 15%, Anatase- 10%, Goethite- 10%	–	–
2	105485	23.1498	69.7271	HLS sample (-125µ)	<2mm sample collected from the high energy zone of a 2nd order stream, 150m before the confluence of 3rd and 2nd order streams. TREEY: 2.58%	Ferruginous sandstone of Bhuj Formation	Quartz-35%, Zircon-25%, Enstatite- 20%, Hematite- 10%, Anatase- 5%, Kaolinite- 5%	–	–
3	105467 (Magnetic 0.7A)	23.1508	69.6239	Isodynamically separated HLS sample (-125µ)	<1mm sample collected from low energy bank area of a 2nd order stream. TREEY of HLS is 1.3%	Ferruginous sandstone of Bhuj Formation. Metasomatized ferruginous sandstone is also observed in neighbouring areas	Quartz, Anatase, Rutile, Tourmaline	Kaolinite, Goethite	Pyroxene, Magnetite, Zircon, Goyazite/ Florencite
4	105467 (Magnetic 0.5A)	23.1508	69.6239	Isodynamically separated HLS sample (-125µ)	<1mm sample collected from low energy bank area of a 2nd order stream. TREEY of HLS is 1.3%	Ferruginous sandstone of Bhuj Formation. Metasomatized ferruginous sandstone is also observed in neighbouring areas	Quartz, Anatase, Rutile, Tourmaline	Kaolinite, Goethite	Pyroxene, Garnet, Zircon, Ilmenite, Feldspar
5	105467 (Tilt-5,Magnetic 1.7A)	23.1508	69.6239	Isodynamically separated HLS sample (-125µ)	<1mm sample collected from low energy bank area of a 2nd order stream. TREEY of HLS is 1.3%	Ferruginous sandstone of Bhuj Formation. Metasomatized ferruginous sandstone is also observed in neighbouring areas	Quartz, Rutile, Zircon, Anatase	–	Magnetite, Kaolinite, Apatite, Amphibole, Feldspar, Dolomite, Calcite
6	105467(Tilt-5,Non Magnetic 1.7A)	23.1508	69.6239	Isodynamically separated HLS sample (-125µ)	<1mm sample collected from low energy bank area of a 2nd order stream. TREEY of HLS is 1.3%	Ferruginous sandstone of Bhuj Formation. Metasomatized ferruginous sandstone is also observed in neighbouring areas	Quartz, Rutile, Zircon	Anatase	Amphibole, Magnetite, Apatite

Sl No.	Sample No.	Latitude	Longitude	Sample Type	Sample Description	Catchment Lithology	Good/ Considerable/ Small amount	Trace amount	Likely phases
7	105467 (Magnetic 1.5A)	23.1508	69.6239	Isodynamically separated HLS sample (-125µ)	<1mm sample collected from low energy bank area of a 2nd order stream. TREEY of HLS is 1.3%	Ferruginous sandstone of Bhuj Formation. Metasomatized ferruginous sandstone is also observed in neighbouring areas	Quartz, Rutile, Zircon, Anatase	–	Kaolinite, Magnetite, Pyroxene, Goyazite/ Florencite
8	105467 (-125,Magnetic)	23.1508	69.6239	Isodynamically separated HLS sample (-125µ)	<1mm sample collected from low energy bank area of a 2nd order stream. TREEY of HLS is 1.3%	Ferruginous sandstone of Bhuj Formation. Metasomatized ferruginous sandstone is also observed in neighbouring areas	Hematite, Quartz, Goethite, Tourmaline, Garnet(mainly Almandine-pyrope type)	Rutile, Kaolinite, Anatase, Zircon	Pyroxene
9	105464 (Tilt-5,Magnetic)	23.1642	69.6306	Isodynamically separated HLS sample (-125µ)	<2mm sample collected from the deepest part of the stream from a 2nd order stream after the confluence of 1st and 2nd order stream. TREEY of HLS is 1.6%	Ferruginous sandstone and metasomatized ferruginous sandstone of Bhuj Formation	Quartz, Zircon, Rutile, Anatase	Kaolinite, Mica	Amphibole, Magnetite, Pyroxene
10	105464 (Tilt-5,Non Magnetic 1.7A)	23.1642	69.6306	Isodynamically separated HLS sample (-125µ)	<2mm sample collected from the deepest part of the stream from a 2nd order stream after the confluence of 1st and 2nd order stream. TREEY of HLS is 1.6%	Ferruginous sandstone and metasomatized ferruginous sandstone of Bhuj Formation	Quartz, Zircon, Rutile	–	Magnetite
11	105464 (Magnetic 0.3A)	23.1642	69.6306	Isodynamically separated HLS sample (-125µ)	<2mm sample collected from the deepest part of the stream from a 2nd order stream after the confluence of 1st and 2nd order stream. TREEY of HLS is 1.6%	Ferruginous sandstone and metasomatized ferruginous sandstone of Bhuj Formation	Quartz, Hematite, Goethite, Rutile	Anatase, Kaolinite	Pyroxene, Feldspar
12	105464(Magnetic 0.5A)	23.1642	69.6306	Isodynamically separated HLS sample (-125µ)	<2mm sample collected from the deepest part of the stream from a 2nd order stream after the confluence of 1st and 2nd order stream. TREEY of HLS is 1.6%	Ferruginous sandstone and metasomatized ferruginous sandstone of Bhuj Formation	Quartz, Tourmaline, Goethite, Rutile, Anatase	Kaolinite, Hematite	Monazite
13	105464(Magnetic 0.7A)	23.1642	69.6306	Isodynamically separated HLS sample (-125µ)	<2mm sample collected from the deepest part of the stream from a 2nd order stream after the confluence of 1st and 2nd order stream. TREEY of HLS is 1.6%	Ferruginous sandstone and metasomatized ferruginous sandstone of Bhuj Formation	Quartz, Tourmaline, Rutile, Anatase	Kaolinite, Goethite	Zircon, Pyroxene, Monazite, Hematite
14	105464(Magnetic 1.5A)	23.1642	69.6306	Isodynamically separated HLS sample (-125µ)	<2mm sample collected from the deepest part of the stream from a 2nd order stream after the confluence of 1st and 2nd order stream. TREEY of HLS is 1.6%	Ferruginous sandstone and metasomatized ferruginous sandstone of Bhuj Formation	Quartz, Rutile, Zircon, Anatase	Kaolinite, Mica	Magnetite
15	105464(Magnetic 1.0A)	23.1642	69.6306	Isodynamically separated HLS sample (-125µ)	<2mm sample collected from the deepest part of the stream from a 2nd order stream after the confluence of 1st and 2nd order stream. TREEY of HLS is 1.6%	Ferruginous sandstone and metasomatized ferruginous sandstone of Bhuj Formation	Quartz, Rutile, Zircon, Anatase	Kaolinite, Goethite, Tourmaline	Goyazite/ Florencite, Magnetite, Monazite

Sl No.	Sample No.	Latitude	Longitude	Sample Type	Sample Description	Catchment Lithology	Good/ Considerable/ Small amount	Trace amount	Likely phases
16	105485(Tilt-5,Magnetic 1.7A)	23.1498	69.7271	Isodynamically separated HLS sample (-125µ)	<2mm sample collected from the high energy zone of a 2nd order stream, 150m before the confluence of 3rd and 2nd order streams. TREEY of HLS is 2.58%	Ferruginous sandstone of Bhuj Formation	Quartz, Rutile, Zircon, Anatase	Kaolinite, Hematite	Magnetite, Monazite
17	105485(Tilt-5,Non Magnetic 1.7A)	23.1498	69.7271	Isodynamically separated HLS sample (-125µ)	<2mm sample collected from the high energy zone of a 2nd order stream, 150m before the confluence of 3rd and 2nd order streams. TREEY of HLS is 2.58%	Ferruginous sandstone of Bhuj Formation	Quartz, Rutile, Zircon	–	Kaolinite
18	105485 (Magnetic 0.5A)	23.1498	69.7271	Isodynamically separated HLS sample (-125µ)	<2mm sample collected from the high energy zone of a 2nd order stream, 150m before the confluence of 3rd and 2nd order streams. TREEY of HLS is 2.58%	Ferruginous sandstone of Bhuj Formation	Quartz, Rutile, Anatase, Monazite	Tourmaline, Kaolinite	Goethite, Epidote
19	105485 (Magnetic 0.3A)	23.1498	69.7271	Isodynamically separated HLS sample (-125µ)	<2mm sample collected from the high energy zone of a 2nd order stream, 150m before the confluence of 3rd and 2nd order streams. TREEY of HLS is 2.58%	Ferruginous sandstone of Bhuj Formation	Goethite, Hematite	Rutile, Kaolinite	Quartz, Zircon
20	105485 (Magnetic 1.5A)	23.1498	69.7271	Isodynamically separated HLS sample (-125µ)	<2mm sample collected from the high energy zone of a 2nd order stream, 150m before the confluence of 3rd and 2nd order streams. TREEY of HLS is 2.58%	Ferruginous sandstone of Bhuj Formation	Rutile, Quartz, Zircon, Anatase	Kaolinite	Magnetite, Hematite
21	105485 (Magnetic 0.7A)	23.1498	69.7271	Isodynamically separated HLS sample (-125µ)	<2mm sample collected from the high energy zone of a 2nd order stream, 150m before the confluence of 3rd and 2nd order streams. TREEY of HLS is 2.58%	Ferruginous sandstone of Bhuj Formation	Rutile, Quartz, Zircon, Anatase, Monazite	Kaolinite, Hematite	Magnetite, Goethite

Annexure-XI: Details of field observation points and sample collection

Sl. No.	Date	Location No.	Latitude	Longitude	Village/ Area	Exposure Location	Host Lithology	Azimuth	Stratigraphy	Original BR ID	New BR ID
1	18-12-2023	GSPL_Bhuj_ 01/12/23	23.20980	69.58820	Sukhapar	The Exposure (70 -250) is near high HREE value location, exposed in the Ratiya Nala section.	Section of Planar cross stratified medium to fine grained quartz arenite overlying heterolith of goethitic to whitish clay and cherry red coloured (streak red) claystone, v.fine sandstone and greyish black shale. The stratification in the sandstone is defined by ferrugenous staining.	70-Sub-horizontal	Bhuj Formation	105401 105402	105401 105402
2	18-12-2023	GSPL_Bhuj_ 02/12/23	23.18290	69.56390	Bharasar	Near the KGCMP high HREE value location, near Wandhsim Reserve Forest. River cut section.	Section of v.coarse grained thick sandstone unit (2.5m) overlying white clay horizon (1m) with hematitic patches at places. Lots of boulders of laterite with botroydal features are observed in the T0 of the river. According to local people, there is a laterite mine at the top of the hill, located towards 260 degree from the location.	NA	Bhuj Formation	105403 105404	105403 105404
3	19-12-2023	GSPL_Bhuj_ 03/12/24	23.21530	69.59000	Sukhapar	Near Nagthada tample, hill scarp quarry section probably for clay.	Thick clay horizon of grey (1.3m unit of 2 - 3mm layers) and white (1.1m of 1mm or less thick layers) overlying reddish brown coloured very hard very fine sandstone (80cm) with very small lenses of Fe concentration. The succession is finally overlain by 20 _30cm beds of medium to fine grained sandstone (no internal structure is observed). Brecciation observed within the clay strata at the temple side of the section.	NA	Bhuj Formation	105405 105406	105405 105406
4	19-12-2023	GSPL_Bhuj_ 04/12/24	23.21570	69.58940	Sukhapar	Near Nagthada tample, hill scarp section of doleritic/basaltic dyke within Bhuj Formation	Dolerite/basalt dyke has intruded the Bhuj Sandstone (chlorite, magnetite as secondary mineral). The contact between the two is represented by violet coloured, fracture filled very fine grained rock. Agate is observed in the grab samples. Presence of silica and calcite veins along with zeolite formation.	NA	Bhuj Formation	105416	105416
5	19-12-2023	GSPL_Bhuj_ 05/12/23	23.24340	69.56800	Kodki	Riverbed section near Kara Talav (near high HREE value section of KGCMP)	Occurrence of medium to fine grained sandstone at river bed.	NA	Bhuj Formation	NA	NA

Sl. No.	Date	Location No.	Latitude	Longitude	Village/ Area	Exposure Location	Host Lithology	Azimuth	Stratigraphy	Original BR ID	New BR ID
6	19-12-2023	GSPL_Bhuj_ 06/12/23	23.24040	69.58470	Kodki	Riverbed section near Kara Talav (near high HREE value section of KGCMP)	Alternate occurrence of brownish black coloured fine to medium grained sandstone and clay sandstone heterolith unit. The sandstone beds are 50cm 1m thick withplanar parallal to hummocky and swaly cross stratified with pinch and swell bed geometry. Wave ripple with rounded crest, tuning fork bifurcation, 1- 2cm amplitude and 10 190 ripple axis ornament the top surface of the sandstone. The heterolithic layer is consist of mm to cm thin white to yellow ocher coloured clay and fine sandstone with unit thickness of 40cm.	160-340/ 10SW	Bhuj Formation	105429 105430	105429 105430
7	19-12-2023	GSPL_Bhuj_ 07/12/23	23.24380	69.58290	Kodki	Road cut section, intrusion of doleritic dyke within Bhuj sandstone	Intrusion of dolerite/basalt dyke within medium to fine grained sandstone. The lithounit is faulted with throw approx. 2 m. Concentration of ~5mm thin iron layer (cherry red streak) along the fault plane is observed. The contact between the dyke and the sandstone is highly altered with baking effect.	80-188/60E (fault plane)	Bhuj Formation	105407	105407
8	20-12-2023	GSPL_Bhuj_ 08/12/23	23.20670	69.64640	Mirjapur	Road cut section at area of high HREE point near KK Hospital (on DN Mundra Road, near Swami Vagban temple), west of main power line.	Laterally extensive occurrence (section oriented 100 -290) of two laterite layers of 60cm and 14cm directly overlying 6cm duricrust and 40cm thick white clay layer with goethitic patches. The clay layer overlies 10-20cm thick planar cross stratified (p.c 320) medium to fine grained white sandstone beds forming sets of 20-30cm. The clay and sst sets are seperated by 20cm thick reddish brown colored sandstone with baking effect (duricrust formation).	160 -340/12W	Bhuj Formation	105408	105408
9	20-12-2023	GSPL_Bhuj_ 09/12/23	23.20700	69.64500	Haripar	Exactly on the high HREE point of KGCMP	Laterally extensive occurrence (section oriented 100 -290) of two laterite layers of 60cm and 14cm directly overlying 6cm duricrust and 40cm thick white clay layer with goethitic patches. The clay layer overlies 10 -20cm thick planar cross stratified (p.c 320) medium to fine grained white sandstone beds forming sets of 20 -30cm, seperated by reddish brown colored sandstone with baking effect (duricrust formation).	174 -354/ 10W	Bhuj Formation	105409 105410 105411	105409 105410 105411
10	20-12-2023	GSPL_Bhuj_ 10/12/23	23.18600	69.64170	Haripar	Top of the hill near high HREE point	Alternate occurrence of brownish black coloured fine to medium grained sandstone (tourmaline?, volcanic quartz, chert??) and clay-sandstone heterolith unit. The sandstone beds are 7cm -20m thick with planar parallalstratification and pinch and swell bed geometry. The heterolithic layer is	130-Sub-horizontal	katrol Formation	105412	105412

Sl. No.	Date	Location No.	Latitude	Longitude	Village/ Area	Exposure Location	Host Lithology	Azimuth	Stratigraphy	Original BR ID	New BR ID
							consist of 15-20cm thick clay (mm thin) and siltstone.				
11	20-12-2023	GSPL_Bhuj_ 11/12/23	23.17050	69.63750	Sedata	Road side quary cut section of sandstone	Thick succession of fine grained sandstone. Internally the sandstone is planar parallel to planar cross to swaley cross stratified. Here the amount of clay is almost negligible however at the lower part of the succession very little amount of clay is preserved, sandwitched between swaley cross stratified and planar parallel stratified sandstone. Encrustation at the top of the sandstone succession is also observed. At the contact of Katrol and Bhuj formations, (north of this location) gradational contact with preservation of clay is observed.	210-Sub-horizontal	Bhuj Formation	105413	105413
12	20-12-2023	GSPL_Bhuj_ 13/12/23	23.16580	69.63410	Sedata	Bhuj Mundra Road side surface exposure	Occurrence of 20cm thick white clay at surface with goethitic alteration, overlying grey shale/siltsone. Sandstone is observed at the higher contours at west of the location.	213-Sub-horizontal	Bhuj Formation	NA	NA
13	20-12-2023	GSPL_Bhuj_ 14/12/23	23.18390	69.57120	Bharasar	The nearest HREE point is on the road, no option for stream sediment collection, went to nearby stream, near Wandhsim Reserve Forest.	No insitu rock has been observed. In riverbed gravels of laterite and sandstone and small pebbles of hematite, goethite, quartzose sandstone are present.	NA	Bhuj Formation	NA	NA
14	21-12-2023	GSPL_Bhuj_ 15/12/23	23.20560	69.74150	Ler	In way of high HREE value point of KGCMP (not accessible due to farm land and pond). Local road side section	Section of very coarse grained sandstone (angular quartz, few ferrugenous grains embedded in a quartzose groundmass) Part of stream terrace with gravel bed containing large clasts of sandstone, hematite and laterite is observed.	NA	Bhuj Formation	NA	NA
15	21-12-2023	GSPL_Bhuj_ 16/12/23	23.19980	69.73220	Bhujodi	Roadside quary section of sandstone building blocks at the south of the village	Occurrence of 20 -30cm thick beds of planar parallel laminated coarse grained sandstone, comprising of very well rounded grains of quartz/pink quartz, white coloured elliptical, fossil??? Almost no matrix observed. Seems to be beach deposit. Oolite???	60 _240/20NW 80 -260/12N	Chari Formation	105414	105414
16	21-12-2023	GSPL_Bhuj_ 17/12/23	23.19700	69.72990	Bhujodi	Hill exposure near Ler Reserve Forest area.	Medium to fine grained planar cross stratified quartzose sandstone (angular grains of quartz). 5 -7cm thick red beds (very hard, cherry red streak) are observed at the top of the sandstone beds. Vein type occurrence (overall orientation 60 -240) cross cutting the sandstone are observed.	100 -280/10N	Chari Formation	105415	105415
17	21-12-2023	GSPL_Bhuj_ 18/12/23	23.20750	69.72510	Madhapar	Road side location at Gangeswar road	Mostly cropland no exposure of bedrock, farms of drumstick, pomegranade and dragon fruit.	NA	Bhuj Formation	NA	NA

Sl. No.	Date	Location No.	Latitude	Longitude	Village/ Area	Exposure Location	Host Lithology	Azimuth	Stratigraphy	Original BR ID	New BR ID
18	21-12-2023	GSPL_Bhuj_19/12/23	23.18640	69.72110	Bhuj	Hill exposure near Gunwari Nadi and Ler Reserve Forest area.	Same as 17/12/23	NA	Chari Formation	NA	NA
19	10-02-2024	GSPL_Bhuj_19/12/23 A	23.18640	69.72110	Hirapar	Hill exposure near Gunwari Nadi and Ler Reserve Forest area, about 300m north of 19/12/23	Medium to fine grained planar cross stratified quartzose sandstone (angular grains of 90 - 92% quartz, 5-7% feldspar and less than acessory minerals embedded in a dull white cement). Dominantly relatively large brownish red coloured planar cross stratified sandstone	NA	Chari Formation	NA	NA
20	22-12-2023	GSPL_Bhuj_20/12/23	23.15850	69.63660	Sedata and Bharasar	Bhuj Mundra Road side stone quarry section	Lithologically the section is composed of medium to fine grained quartz arenite. Internally the sandstone beds ara planar to swaley cross stratified (1m swale length) to sinusoidal low angle planar cross stratified. Bed thickness varies from 20cm to 1.1m. Wave ripple lamination is also observed. Section oriewntation 84-264. Differential leaching is observed throughout the succession. Formation of duricrust is also observed at the top of the succession.	NA	Bhuj Formation	NA	NA
21	23-12-2023	GSPL_Bhuj_21/12/23	23.19020	69.69210	Jadura Nana	Stream cut section on Dhunaraja Dam Road, in the vicinity of Bhuj Reserve Forest	Occurrence of clay sandstone heterolith unit, interupted by brownish black coloured fine to medium grained parallel laminated sandstone	330_150/15SW 45 - 225/15SE	katrol Formation	105417 105418	105417 105418
22	23-12-2023	GSPL_Bhuj_22/12/23	23.18500	69.69510	Jadura Nana	Riverbed section near on Dhunaraja Dam Road, in the vicinity of Bhuj Reserve Forest	Very weathered poor exposure of black colored sandstone	NA	Chari Formation	NA	NA
23	23-12-2023	GSPL_Bhuj_23/12/23	23.17270	69.69230	Jadura Nana	Road side section on Dhunaraja Dam Road, in the vicinity of Bhuj Reserve Forest	Occurrence of clay sandstone heterolith unit, interupted by fine to medium grained parallel laminated sandstone with gypsum interlayers	100 - 280/12SW	katrol Formation	105420 105421	105420 105421
24	23-12-2023	GSPL_Bhuj_24/12/23	23.15260	69.70210	Jadura Nana	Stream cut section on continuation of Jadura village to Chakar village road	Occurrence of thick beds of medium grained quartzose sandstone with encrustration on top and ferrugenous staining. The sandstones are internally planar parallel to planar cross stratified. Ripple marks and lag conglomerate are also present.	140 - 320/12SW	Bhuj Formation	105422	105422
25	23-12-2023	GSPL_Bhuj_25/12/23	23.13390	69.70510	Reha Nana	Road side hill scarp section on Rehanana to Surajpur connecting road	Alternate occurrence of ferrugenous sandstone and white to reddish clay.	NA	Bhuj Formation	105424 105425	105424 105425

Sl. No.	Date	Location No.	Latitude	Longitude	Village/ Area	Exposure Location	Host Lithology	Azimuth	Stratigraphy	Original BR ID	New BR ID
26	23-12-2023	GSPL_Bhuj_ 26/12/23	23.13430	69.68780	Jadura Nana	Road side stream cut section on Rehanana to Surajpur connecting road	Occurrence of planar parallel to low angle planar cross stratified very fine grained white colored sandstone (siltstone??). At river bed grey shale is exposed. Encrustation on top of the sandstone beds are observed. On way to the stream there is ferrugenous, brownish black colored sandstone on surface (may be feldspathic)	NA	Bhuj Formation	105459 105460	105459 105460
27	23-12-2023	GSPL_Bhuj_ 27/12/23	23.13240	69.64520	Surajpur	Road side stream cut section on Rehanana to Surajpur connecting road	At river cross section alteration of sandstone and shale potential site for stream sediment sampling.	NA	Bhuj Formation	NA	NA
28	23-12-2023	GSPL_Bhuj_ 28/12/23	23.20050	69.54030	Mankuva	At the hgh HREE value location at the conflunce of two stream on Bhuj Nakshatrana road	Not available	NA	Bhuj Formation	NA	NA
29	24-12-2023	GSPL_Bhuj_ 29/12/23	23.19910	69.51230	Samatra	Exposure on Bhuj Nakshatrana road	Bedrock exposed with 1 to 1.5 m thick red sandstone bed and at top very dark coarse grained sandstone.	NA	Bhuj Formation	NA	NA
30	24-12-2023	GSPL_Bhuj_ 30/12/23	23.22430	69.50940	Kodki	Road side exposure at high HREE location area, mostly flat slightly sloping NNE, with small stream(gullies) on Kodki Road	Occurrence of ferrugenous sandstone with metasomatized effect and yellow ocher colored sandstone, very near to reported alkali plug area	NA	Bhuj Formation	105427	105427
31	24-12-2023	GSPL_Bhuj_ 31/12/23	23.22420	69.52360	Kodki	Near Rati Tala,Hanuman Temple,roadside digged and dumped rocks.However whole area is farmland on Kodki road	Occurrence of sandstone beds separated by thin (15) cm white shale layer	NA	Bhuj Formation	NA	NA
32	24-12-2023	GSPL_Bhuj_ 32/12/23	23.23640	69.54590	Kodki	Road side section on Kodki Road, in the vicinity of Bhuj Reserve Forest	Thinly bedded very fine grained redish brown colored sandstone separated by white clay. The sandstone beds show pinch and swell geometry.	140 - 320/12SW	Bhuj Formation	105428	105428
33	24-12-2023	GSPL_Bhuj_ 33/12/23	23.18350	69.50310	Samtra	Hill exposure near Samtra Vadasar road, near high HREE point	Surface exposure of purple sandstone altered to goethite layer	NA	Chari Formation	NA	NA
34	26-12-2023	GSPL_Bhuj_ 34/12/23	23.24750	69.60730	Bhuj	Stream cut section on Kodki road and the vicinity of Godsar Reserve Forest, near <400 ppm HREE value location. Local pepole have excavated the river for sand, sand is coarse grained.	Stream cut section of brownish mauve colored, low angle planar cross stratified medium to fine grained sandstone (feldspathic??). No clay is observed.	NA	Bhuj Formation	NA	NA
35	26-12-2023	GSPL_Bhuj_ 35/12/23	23.22390	69.56610	Mankuva	Stream channel between Mankuva Kodki road near Gangwali Dhar.	No insitu rock has been observed. In riverbed silt fraction is more as compared to sand fraction.	NA	Bhuj Formation	NA	NA

Sl. No.	Date	Location No.	Latitude	Longitude	Village/ Area	Exposure Location	Host Lithology	Azimuth	Stratigraphy	Original BR ID	New BR ID
36	27-12-2023	GSPL_Bhuj_ 36/12/23	23.20720	69.65550	Sukhpar	Stream channel on Bhuj Mundra highway, on way to Bhata Talav	White clay layeris exposed in the river bed and at several place duricrustration of the clay is observed.	NA	Bhuj Formation	105441	105441
37	27-12-2023	GSPL_Bhuj_ 37/12/23	23.20470	69.65640	Sukhpar	Road cut section on Bhuj Mundra highway, on way to Bhata Talav	Cart road cut section of planar cross stratified medium to coarse grained reddish brown colored sandstone (7-20cm). Encrustration on the top of the sandstone is observed.	0 -180/3W	Bhuj Formation	NA	NA
38	27-12-2023	GSPL_Bhuj_ 38/12/23	23.18650	69.64280	Mudra road	Exactly at high HREE value location, hill scarp section on Bhuj Mundra highway, near Bhata Talav	Alternate occurrence of shale and sandstone layer	NA	katrol Formation	NA	NA
39	28-12-2023	GSPL_Bhuj_ 39/12/23	23.19660	69.74550	Ler	Hill exposure near high HREE location, beside Ashapura China Clay factory and accessible through Ashapura Volclay Road	very steep hill of sandstone, unable to climb, Occurrence of fossiliferous red ferrugenous sandstone	NA	Chari Formation	105444	105444
40	28-12-2023	GSPL_Bhuj_ 40/12/23	23.19920	69.75820	Ler	Hill exposure near high HREE location, beside Ashapura China Clay factory and near to the junction of Ashapura Volclay Road and Ler Hanuman Road	Hill scarp section of ferrugenous sandstone. Evidence of brecciation and cross cutting veins	NA	Chari Formation	NA	NA
41	28-12-2023	GSPL_Bhuj_ 41/12/23	23.13620	69.74140	Reha Nana	Near high Zr, Cd point, beside Reha nana Surajpur road, a checkdam was there. 200 meter before the dam a stream section	Reddish purple sandstone in stream channel bed.	NA	Bhuj Formation	NA	NA
42	28-12-2023	GSPL_Bhuj_ 42/12/23	23.11380	69.70070	Reha Nana	On Bharapar (Surajpur) Vajadar road road cut section	At the southern part of the road a highly weathered basalt is exposed, while in the northern side of the road a flat lying low angle cross stratified fine grained sandstone is present. No exposure of contact between basalt and sandstone is observed, maybe road was the contact ?	NA	Bhuj Formation	NA	NA
43	28-12-2023	GSPL_Bhuj_ 43/12/23	23.13470	69.56930	Naranpar	Near Mandvi Bhuj highway, near low HREE location, roadside outcrop	Outcrop of coarse grained, reddish brown coloured sandstone. At the north of the outcrop a stream is present.	NA	Bhuj Formation	NA	NA
44	29-12-2023	GSPL_Bhuj_ 44/12/23	23.19680	69.53940	Mankuva	River cut section beside Bhuj Nakshatrana road and north of Bhuj Naliya Western railway line	Stream cut section of coarse grained, planar cross stratified reddish brown coloured sandstone	NA	Bhuj Formation	NA	NA

Sl. No.	Date	Location No.	Latitude	Longitude	Village/ Area	Exposure Location	Host Lithology	Azimuth	Stratigraphy	Original BR ID	New BR ID
45	29-12-2023	GSPL_Bhuj_ 45/12/23	23.17850	69.53590	Mankuva	River cut section near Bhuteshwar Mahadev temple, accessible from Bhuj Nakshatrana road and south of Bhuj Naliya Western railway line	Stream cut section of dark red colour, ferrogenous fossiliferous sandstone	NA	Chari Formation	NA	NA
46	30-12-2023	GSPL_Bhuj_ 46/12/23	23.19260	69.72430	Madhapar	River cut section near Gangeshwar Mahadev temple, on Gangeswar road, trying to reach the high Zr, Cd, Nb and Y anamoly location.	River cut section of alterate occurence of sandstone and grey shale, top of sandstone leached and became red. Interference ripple at the top of the sandstone is observed	NA	Chari Formation	NA	NA
47	31-12-2023	GSPL_Bhuj_ 47/12/23	23.16420	69.63060	Sanatorium	River channel exposure, near a sanatorium, on Bhuj Mundra Road	Exposure of sandstone at the river bed. East to west flowing river with gravels, boulder sand and fines on the riverbed.	NA	Contact of Bhuj _Katrol	NA	NA
48	31-12-2023	GSPL_Bhuj_ 48/12/23	23.15300	69.63700	Sedat	River channel exposure on Bhuj Mundra Road	Exposure of sandstone at the river bed. Stream bed with boulders and pebbles. There is mining activity in upper part of the stream.	NA	Bhuj Formation	NA	NA
49	31-12-2023	GSPL_Bhuj_ 49/12/23	23.15080	69.62390	Sedat	Near Sedat villege, behind 153 BN BSF Marine Camp stram channel, accessible from Bhuj Mundra Road	2nd order stream flowing SW to NE, consisting mostly of silt and clay fraction.	NA	Contact of Bhuj _Katrol	NA	NA
50	31-12-2023	GSPL_Bhuj_ 50/12/23	23.19460	69.60820	Sukhapar	Stram channel near Wandhay talav accessible from Mandvi Bhuj Road	2nd order stream is flowing South to North in a Pond which have aligators. Stream channel consist mostly of clay and silt Encrustation is also present.	NA	Contact of Chari Katrol	NA	NA
51	02-01-2024	GSPL_Bhuj_ 51/01/24	23.21770	69.56610	Mankuva	Stream channel on Mankuva _Kodki road	No exposure stream flowing SW -NE, yellowish colour soil	NA	Bhuj Formation	NA	NA
52	02-01-2024	GSPL_Bhuj_ 52/01/24	23.22850	69.52980	Fotdi	Stream channel on Kodki road	No exposure of bedrock, stream flowing SE to NW	NA	Bhuj Formation	NA	NA
53	02-01-2024	GSPL_Bhuj_ 53/01/24	23.22530	69.52100	Fotdi	Stream channel on Kodki road	No exposure of bedrock, coarse grained reddish sandstone boulders present in stream.	NA	Bhuj Formation	NA	NA
54	02-01-2024	GSPL_Bhuj_ 54/01/24	23.17590	69.53770	Bharasar	Stream channel on a cart road	On hilly terrain mostly sandstone in between two hills, sandstone is fossiliferous.	NA	Chari Formation	NA	NA
55	03-01-2024	GSPL_Bhuj_ 55/01/24	23.31309	68.85641	Gudthar (Outside block)	Exposure on the reservoir side of mitti dam near matiya dev temple	Outcrop of weathered sandstone and shale, one sandstone bed is full of fossil mostly molluscas.	NA	NA	105474 105475	105474 105475
56	03-01-2024	GSPL_Bhuj_ 56/01/24	23.42277	69.08436	Netra (Outside block)	In Netra villege beside the mitti dam wall exposure	Fossiliferous sandstone	NA	NA	105477 105478	105477 105478

Sl. No.	Date	Location No.	Latitude	Longitude	Village/ Area	Exposure Location	Host Lithology	Azimuth	Stratigraphy	Original BR ID	New BR ID
57	04-01-2024	GSPL_Bhuj_ 57/01/24	23.22120	69.58990	Sukhapar	Hill scarp section near Nagthada temple, Sukhpar	Part of the hill is of basalt dyke intruded reddish brown colored massive duricrusted sandstone, overlying a scree deposit of white clay clasts embedded in a finer groundmass. Network of veins of hematite cross cutting the sandstone is observed.	30-Vertical (near Median high)	Bhuj Formation	105479 105480	105479 105480
58	04-01-2024	GSPL_Bhuj_ 58/01/24A	23.22500	69.49080	Fotdi	Road side exposure at a reported alkali plug area, on Fotdi Kodki Road	Exposure of dark reddish black coloured medium to coarse grained sandstone. The sandstone appears to be vent like wrapped by iron rich material.	NA	Bhuj Formation	105481	105481
59	04-01-2024	GSPL_Bhuj_ 58/01/24B	23.23170	69.55770	Kodki	Hill exposure on Mankuva Kodki road near Gangawali Dhar	Columnar joints in sandstone	NA	Bhuj Formation	NA	NA
60	05-01-2024	BSF Area	23.22420	69.66680	Haripar	No exposure, Haripar road	BSF controlled area.	NA	Bhuj Formation	NA	NA
61	05-01-2024	GSPL_Bhuj_ 59/01/24	23.21680	69.73970	Bhujodi	Hiralaxmi car park road	Residential area and cropland, no sign of stream or exposure	NA	Bhuj Formation	NA	NA
62	05-01-2024	GSPL_Bhuj_ 60/01/24	23.22530	69.65980	Haripar	Mundra Road, No exposure	BSF controlled area.	NA	Bhuj Formation	NA	NA
63	05-01-2024	GSPL_Bhuj_ 61/01/24	23.22000	69.64170	Mirjapar	Mirzapar Bypass Road, No exposure	With the help of watershed map found a stream which is contaminated with plastic, and human waste, no chance of stream sediment sampling.	NA	Bhuj Formation	NA	NA
64	05-01-2024	GSPL_Bhuj_ 62/01/24	23.21320	69.63490	Mirjapar	Near Mirzapar Bypass Road, No exposure	Residential area, contaminated stream	NA	Bhuj Formation	NA	NA
65	05-01-2024	GSPL_Bhuj_ 63/01/24	23.21390	69.60830	Sukhpar	Naliya Kothara Bhuj highway, No exposure	Residential area, contaminated stream	NA	Bhuj Formation	NA	NA
66	05-01-2024	GSPL_Bhuj_ 64/01/24	23.21380	69.66770	Haripar	Haripar road, No exposure	Cropland behind the Kutch university campus, the other side is under BSF.	NA	Bhuj Formation	NA	NA
67	05-01-2024	GSPL_Bhuj_ 65/01/24	23.16180	69.69750	Jadura Nana	Jadura Chakara road, road side hill sections	Check dam in between the hills, hill area have mostly sandstone and shale	NA	Katrol Formation	NA	NA
68	05-01-2024	GSPL_Bhuj_ 66/01/24	23.15860	69.68670	Jadura Mota	Jadura Chakara road, road side hill exposure	At jadura village at top of the hill, occurrence of reddish brown coloured, coarse grained quartzose sandstone	NA	Contact of Katrol GSPL_Bhuj_Bhuj	105482	105482
69	05-01-2024	GSPL_Bhuj_ 67/01/24	23.14810	69.73170	Reha Nana	Jadura Chakara road, road side hill exposure	Exposure of alternate occurrence of sandstone and white clay. Encrustation at the top of the sandstones are observed	NA	Bhuj Formation	105483	105483
70	05-01-2024	GSPL_Bhuj_ 68/01/24	23.14980	69.72710	Reha	Stream channel, accessible from Jadura Chakara road through a local cart road	Hills of coarse grained sandstone with encrustation on top. Differential leaching is observed.	NA	Bhuj Formation	NA	NA

Sl. No.	Date	Location No.	Latitude	Longitude	Village/ Area	Exposure Location	Host Lithology	Azimuth	Stratigraphy	Original BR ID	New BR ID
71	05-01-2024	GSPL_Bhuj_ 69/01/24	23.20620	69.53520	Mankuva	Road side location on Mankuva Nakshatrana road, near a covered tank.	Residential are, no exposure.	NA	Bhuj Formation	NA	NA
72	05-01-2024	GSPL_Bhuj_ 70/01/24	23.21010	69.53490	Mankuva	Road side location beside Mankuva Nakshatrana road, between Mankuva and Nagiyari	2nd order stream in between the papaya farms, no exposure, stream consist mostly finer fraction.	NA	Bhuj Formation	NA	NA
73	06-01-2024	GSPL_Bhuj_ 71/01/24	23.22580	69.71610	Madhapar	Road side location near Nara Bazar or towards Gangswar Road	Residential area, No sign of any stream, No exposure	NA	Bhuj Formation	NA	NA
74	06-01-2024	GSPL_Bhuj_ 72/01/24	23.22520	69.72880	Madhapar	Road side location possibly on Vardhaman Nagar Road, between madhapar and Bhujodi	No exposure, only cropland and farms	NA	Bhuj Formation	NA	NA
75	06-01-2024	GSPL_Bhuj_ 73/01/24	23.20800	69.74720	Bhujodi	Road side location, on Ashapura Volclay road, between Bhujodi and Ler	a small pond where people dug a large well to water their crops. Cut section show sandstone and white clay, soil cover on the surface	NA	Bhuj Formation	105487	105487
76	06-01-2024	GSPL_Bhuj_ 74/01/24	23.20800	69.74980	Bhujodi	Road side location, on Ashapura Volclay road, between Bhujodi and Ler	Only farms and croplands, no exposure.	NA	Bhuj Formation	NA	NA
77	06-01-2024	GSPL_Bhuj_ 75/01/24	23.37310	69.71830	Rudramata (Outside the block)	Khari river section on Rudramata Dam road, near Rudramata dam site	River cut section of alternate beds of sandstone and white shale.	NA	katrol Formation	NA	NA
78	06-01-2024	GSPL_Bhuj_ 76/01/24	23.20400	69.51890	Samatra	Road side exposure on Mankuva Nakshatrana road	Exposure of ferruginous sandstone with metasomatized effect and encrustation on top. Trying to reach the stream but unable to access the stream.	NA	Bhuj Formation	NA	NA
79	08-01-2024	GSPL_Bhuj_ 77/01/24	23.19970	69.73050	Bhujodi	Roadside exposure near Ashapura perfoclay factory, on Ashapura volclay road	Hill consist of Sandstone.	NA	Chari Formation	NA	NA
80	08-01-2024	GSPL_Bhuj_ 78/01/24	23.21740	69.72210	Bhujodi	Road side location on Ashapura Volclay Road	No exposure of rock or sign of stream, only croplands.	NA	Bhuj Formation	NA	NA
81	08-01-2024	GSPL_Bhuj_ 79/01/24	23.16500	69.64460	Sedat	Hill exposure on Mundra Bhuj road	Outcrop of dark reddish black colored coarse grained sandstone with hard duricrust (metasomatized effect) on top.	NA	Bhuj Formation	105488	105488
82	08-01-2024	GSPL_Bhuj_ 80/01/24	23.14400	69.64520	Sedat	Hill exposure on Mundra Bhuj road, behind the dargah	Exposure of coarse grained, planar cross stratified sandstone with duricrust formation at places. Differential ferruginous leaching is also observed throughout the area.	60 - 240/70NW	Bhuj Formation	105489	105489
83	08-01-2024	GSPL_Bhuj_ 81/01/24	23.15240	69.64070	Sedat	Hill exposure on Mundra Bhuj road, behind Survanshi Academy near a sandstone query	Exposure Medium to coarse grained rddish brown to black colored sandstone beds with duricrustration and baking effect	NA	Bhuj Formation	NA	NA

Sl. No.	Date	Location No.	Latitude	Longitude	Village/ Area	Exposure Location	Host Lithology	Azimuth	Stratigraphy	Original BR ID	New BR ID
84	08-01-2024	GSPL_Bhuj_ 82/01/24	23.15170	69.64420	Sedat	Hill exposure on Mundra Bhuj road	Exposure Medium to coarse grained rddish brown to black colored sandstone beds with duricrustration and baking effect, continuation of the previous outcrop	NA	Bhuj Formation	105490	105490
85	08-01-2024	GSPL_Bhuj_ 83/01/24	23.15930	69.60580	Bharasar	Road side location on local cart road connecting Sedat to Bhuj Mandvi Highway	with the help of watershed map trying to find the stream but stream was submerge due to a checkdam was build in the stream, no option of stream sediment sample, surface consist of sandstone.	NA	katrol Formation	NA	NA
86	08-01-2024	GSPL_Bhuj_ 84/01/24	23.20540	69.51260	Samatra	Near Mankuva Nakshatrana high way, road side exposure	Outcrop of reddish black coloured coarse to medium grained ferruginous sandstone with metasomatized effect on top	NA	Bhuj Formation	105491	105491
87	08-01-2024	GSPL_Bhuj_ 85/01/24	23.17690	69.50250	Samatra	Road side exposure on a local cart road, parallel to Samatra Varasar road	Exposure of alternate occurrence of medium to fine grained planar parallel laminated to wave ripple laminated sandstone, seperated by thin grey/white clay layers overlying sst shale heterolith with poorly developed Tuffite layers	100-Sub-horizontal	Chari Formation	105492	105492
88	08-01-2024	GSPL_Bhuj_ 86/01/24	23.17290	69.50690	Samatra	Poor weathered exposure, accessible from a local cart road, parallel to Samatra Varasar road	Poor weathered exposure (hill) consist mostly of red colour sandstone, with encrustation in some areas.	NA	Chari Formation	NA	NA
89	09-01-2024	GSPL_Bhuj_ 87/01/24	23.16060	69.58440	Naranpar	Hilly exposure, 1 km west from crocodile lake accesible from Bhuj Mandvi highway	Exposure of mm to cm thick reddish siltstone	NA	katrol Formation	105493	105493
90	09-01-2024	GSPL_Bhuj_ 88/01/24	23.16190	69.58240	Naranpar	River cut cross section accesible from Bhuj Mandvi highway	Occurrence of heterolithic unit with 30 -50cm thick sandstone bed sets separated by 1 to 1.5m shale unit, interupted by poorly developed Tuffite layers unit	NA	katrol Formation	NA	NA
91	09-01-2024	GSPL_Bhuj_ 89/01/24	23.16660	69.57830	Naranpar	Hill outcrop section accesible from Bhuj Mandvi highway	Occurrence of heterolithic unit with 70 -80cm thick sandstone bed sets separated by 50 - 60cm shale unit, interupted by poorly developed Tuffite layers unit	NA	katrol Formation	NA	NA
92	09-01-2024	GSPL_Bhuj_ 90/01/24	23.15730	69.57980	Naranpar	Hill outcrop section, behind Gujrat Wind Electricity Substation, accesible from Bhuj Mandvi highway	Occurrence of red coloured sandstone	NA	katrol Formation	NA	NA
93	09-01-2024	GSPL_Bhuj_ 91/01/24	23.15070	69.58000	Naranpar Ravli	Near Naranpar Ravli village, Hill cut section for pipeline installation	Heterolithic unit consist of shale (grey, white with goethitic and ferruginous pstches, interupted by well developed Tuffite layers alternating with 10-20cm thick sandstone layers and/or thinly laminated shale -siltstone unit	NA	katrol Formation	105494	105494
94	09-01-2024	GSPL_Bhuj_ 92/01/24A	23.14760	69.57570	Naranpar Ravli	Near Naranpar Ravli village, Hill cut section for pipeline installation	Heterolithic unit consist of shale (grey, white with goethitic and ferruginous pstches, interupted by well developed Tuffite layers alternating with 10-20cm thick sandstone	NA	katrol Formation	NA	NA

Sl. No.	Date	Location No.	Latitude	Longitude	Village/ Area	Exposure Location	Host Lithology	Azimuth	Stratigraphy	Original BR ID	New BR ID
							layers and/or thinly laminated shale -siltstone unit				
95	09-01-2024	GSPL_Bhuj_ 92/01/24B	23.15110	69.57080	Naranpar Ravli	Near Naranpar Ravli village, Hill cut section for pipeline installation	Heterolithic unit consist of shale (grey, white with goethitic and ferruginous pstches, interupted by well developed Tuffite layers alternating with 10 -20cm thick sandstone layers and/or thinly laminated shale -siltstone unit	NA	katrol Formation	NA	NA
96	10-02-2024	GSPL_Bhuj_ 93/02/24	23.19010	69.72310	Hirapar	Hill section near Hirapar village	Medium to coarse grained reddish brown coloured sandstone	NA	Chari Formation	105501	105501
97	10-02-2024	GSPL_Bhuj_ 94/02/24	23.18730	69.72330	Hirapar	100 m East of high HREE location a stream discharges in a low depression area.	On the way to the area, occurrence of red coloured ferruginous, fossiliferous sandstone	NA	Chari Formation	105498	105498
98	10-02-2024	GSPL_Bhuj_ 95/02/24	23.18640	69.72280	Hirapar	At the slopy side of hillock exposure	Reddish sandstone with lots of fossils mostly mollusca were exposed (graveyard bed)	NA	Chari Formation	105499	105499
99	10-02-2024	GSPL_Bhuj_ 96/02/24	23.18570	69.72370	Hirapar	100 m SE of previous location a stream (dry) channel	Stream sediment sample collected before the confluence of two streams.	NA	Chari Formation	NA	NA
100	10-02-2024	GSPL_Bhuj_ 97/02/24	23.19920	69.70170	Hirapar	Closest accsible area close to high HREE value location near hirapar villege	Stream sediment sample collected.	NA	Chari Formation	NA	NA
101	10-02-2024	GSPL_Bhuj_ 98/02/24	23.19500	69.70400	Hirapar	Hill exposure	Thick greenish shale/Tuff layer in between very thick quartz arenite beds, A few steps ahead to the village, encountered a large boulder of sandstone with very rounded bomb like structure	NA	Chari Formation	105503	105503
102	10-02-2024	GSPL_Bhuj_ 99/02/24	23.19920	69.70560	Hirapar	Hill outcrop	Red ferrugenous, fossiliferous sandstone like previous gravyard bed	NA	Chari Formation	105504	105504
103	11-02-2024	GSPL_Bhuj_ 100/02/24	23.18370	69.70800	Hirapar	stone quarry, near Ganwari river	Boulders of sandstone interrupted by brecciated limestone (chert??/ marl??), differential leaching of the sandstone is observed.	NA	Chari Formation	NA	NA
104	11-02-2024	GSPL_Bhuj_ 101/02/24	23.18550	69.70270	Hirapar	Hill outcrop at the highest HREE value location as per KGCMP data	Outcrop of alternate thin and thick layers of sandstone, clay, gypsum and goethitic layer, interupted by poorly developed Tuffite layers. Round vent like structure is also observed. About 50 meter north we encountered possibly tuffaceous layer for thin section study.	NA	Chari Formation	105505 105506 105507	105505 105506 105507

Sl. No.	Date	Location No.	Latitude	Longitude	Village/ Area	Exposure Location	Host Lithology	Azimuth	Stratigraphy	Original BR ID	New BR ID
105	11-02-2024	GSPL_Bhuj_ 102/02/24	23.18690	69.70230	Hirapar	Quarry section	Greyish goethitic soil/ weathered rock was observed.	NA	Chari Formation	105508	105508
106	11-02-2024	GSPL_Bhuj_ 103/02/24	23.19200	69.70640	Hirapar	350 m north of previous location, hill outcrop along a walkable road for quarry, made by local people	Outcrop of possibly crystalline tuff was observed. Quartz was angular with abundant feldspar.	NA	Chari Formation	105509	105509
107	11-02-2024	GSPL_Bhuj_ 104/02/24	23.19400	69.70570	Hirapar	200 m uphill of previous location, hill outcrop along a walkable road for quarry, made by local people	Occurrence of heterolithic unit with greenish white clay layer, possibly tuffaceous layer. We collected sample for whole rock analysis.	NA	Chari Formation	105510	105510
108	11-02-2024	GSPL_Bhuj_ 105/02/24	23.19260	69.70410	Hirapar	Further downhill from the previous location, hill outcrop along a walkable road for quarry, made by local people	Heterolithic unit of thinly laminated sandstone, separated by mm thin clay layers. A reddish sandstone bed with blackish rounded clast (possibly rhyolitic ?) is also observed in the sucession. A little downhill from the location, basalt intrusion within the chari Formation is also observed.	NA	Chari Formation	105511 105512 105513	105511 105512 105513
109	11-02-2024	GSPL_Bhuj_ 106/02/24	23.22460	69.58770	Sukhpar	At high HREE value location	SS collected	NA	Bhuj formation.	NA	NA
110	11-02-2024	GSPL_Bhuj_ 107/02/24	23.22680	69.50950	Fotdi	At high HREE value location, Kodki road side crematorium	The area is open relatively low lying, may be covered by perenial rivers. The area is possibly a cemetry ground. Sample has been collected from a existing pit, aprox 70 80cm in depth from surface. Sample has been collected irrespective of grain size. Arkose/Wacke has been observed at surface level.	NA	Bhuj Formation	NA	NA
111	19-03-2024	GSPL_Bhuj_ 111/03/24	23.15936	69.57181	Naranpar Ravli	Near Naranpar Ravli village, Hill exposure	Exposure of coarse grained 10 -20cm thick fossiliferous sandstone (parallel laminated at places separated by mm thin laminated fine sandstone. This unit is overlain by grades bed (conglomerate, Tb, Tc, Td) again overlain by medium grained, parallel laminated sandstone. Wave ripple lamination at the top surface is also common.	60 -240/8SE 40 -220/8SE	Katrol Formation	105539 105540	105539 105540
112	20-03-2024	GSPL_Bhuj_ 111/03/24A	23.15448	69.57350	Naranpar Ravli	Near Naranpar Ravli village, exposure along a local cart road for pipeline installation	Low angle cross stratified medium grained sandstone with red hard nodular looking inter layers	NA		NA	NA
113	19-03-2024	GSPL_Bhuj_ 112/03/24	23.15185	69.57784	Naranpar Ravli	Near Naranpar Ravli village, Hill cut section for pipeline installation	photo taken of section	NA	katrol Formation	NA	NA

Sl. No.	Date	Location No.	Latitude	Longitude	Village/ Area	Exposure Location	Host Lithology	Azimuth	Stratigraphy	Original BR ID	New BR ID
114	19-03-2024	GSPL_Bhuj_ 91/01/24	23.15070	69.58000	Naranpar Ravli	Near Naranpar Ravli village, Hill cut section for pipeline installation	Heterolithic unit consist of shale (grey, white with goethitic and ferruginous pstches, interupted by well developed Tuffite layers alternating with 10 -20cm thick sandstone layers and/or thinly laminated shale siltstone unit, channel sampling done	60 -240/8SE	katrol Formation	105541 105543	105541 105543
115	19-03-2024	GSPL_Bhuj_ 110/03/24	23.14998	69.58493	Naranpar Ravli	Near Naranpar Ravli village, Hill cut section for pipeline installation	photo taken of section for channel sampling	NA	katrol Formation	NA	NA
116	20-03-2024	Placemark	23.17239	69.59090	NA	Road side exposure on _Bhuj_Mandvi highway	The heterolithic exposure, end of log that starts at 120/06/24	NA	katrol Formation	NA	NA
117	20-03-2024	GSPL_Bhuj_ 112/03/24	23.15185	69.57784	Naranpar Ravli	Near Naranpar Ravli village, Hill cut section for pipeline installation	Heterolithic unit consist of shale (grey, white with goethitic and ferruginous pstches, interupted by well developed Tuffite layers alternating with 10 -20cm thick sandstone layers and/or thinly laminated shale siltstone unit. Gypsum in association with the Tuffite layers are also observed. Channel sampling done	NA	katrol Formation	1055441055 61	105544 105561
118	20-03-2024	GSPL_Bhuj_ 110/03/24	23.14998	69.58493	Naranpar Ravli	Near Naranpar Ravli village, Hill cut section for pipeline installation. 400m SE from location no. 91/01/24 in down dip direction, JCB cut section.	Continuation of 91/01/24 with same lithology	NA	katrol Formation	105562 105566	105562 105566
119	20-03-2024	GSPL_Bhuj_ 113/03/24	23.16010	69.72326	Reha Nana	Hill exposure, approximately 1 km away from the cart road (accessible from Hajapar Bharapar connceting main road). Area has uneven topography with few river channels draining the area.	Planar cross stratified to massive coarse grained, sst with lots of unidentified grains	NA	Contact of Katrol - Bhuj	105567	105567
120	20-03-2024	GSPL_Bhuj_ 114/03/24	23.16100	69.72348	Reha Nana	Few hundred meters uphill from 113/03/24, along a newly made local cart road for pipe line installation	katrol Fm same what we have seen in 112, 110 no location, location taken for future use.	NA	katrol Formation	NA	NA
121	13-06-2024	GSPL_Bhuj_ 91/01/24	23.15070	69.58000	Naranpar Ravli	Near Naranpar Ravli village, scarp section for road	Continuation of the 112/03/24 succession in stratigraphic up direction. However the thickness of the sandstones increases and no gypsum is encountered. Tuffite layer collection	NA	Katrol Formation	105567	107451
122	13-06-2024	GSPL_Bhuj_ 91/01/24	23.15070	69.58000	Naranpar Ravli	Near Naranpar Ravli village, scarp section for road	Continuation of the 112/03/24 succession in stratigraphic up direction. However the thickness of the sandstones increases and no gypsum is encountered. Tuffite layer collection	NA	Katrol Formation	105568	107452

Sl. No.	Date	Location No.	Latitude	Longitude	Village/ Area	Exposure Location	Host Lithology	Azimuth	Stratigraphy	Original BR ID	New BR ID
123	22-08-2024	GSPL_Bhuj_ 91/01/24	23.15070	69.58000	Naranpar Ravli	Hill cut section near Naranpar Ravli village, same location as 91/01/24 exposures	Occurrence of mm to 1cm thin grey to blackishgrey shale layers, amalgamated at places and often alternate with mm thin silt/fine sand layers and reddish brown colored (2 -7cm) thick hard ironstone/ferrugenous clay layers. This succession is observed to be interupted by brownish mauve colored, either wave ripple laminated or plane parallel laminated medium to fine grained sandstones. Occurrence of mm thin gypsum layers at the top part of the succession are also observed.	NA	Katrol Formation	107579	107579
124	22-08-2024	GSPL_Bhuj_ 91/01/24	23.15070	69.58000	Naranpar Ravli	Hill cut section near Naranpar Ravli village, same location as GSPL_Bhuj_91/01/24 exposures	Occurrence of mm to 1cm thin grey to blackish grey shale layers, amalgamated at places and often alternate with mm thin silt/fine sand layers and reddish brown colored (2- 7cm) thick hard ironstone/ferrugenous clay layers. This succession is observed to be interupted by brownish mauve colored, either wave ripple laminated or plane parallel laminated medium to fine grained sandstones. Occurrence of mm thin gypsum layers at the top part of the succession are also observed.	NA	Katrol Formation	107580	107580
125	22-08-2024	GSPL_Bhuj_ 91/01/24	23.15070	69.58000	Naranpar Ravli	Hill cut section near Naranpar Ravli village, same location as GSPL_Bhuj_91/01/24 exposures	Occurrence of mm to 1cm thin grey to blackish grey shale layers, amalgamated at places and often alternate with mm thin silt/fine sand layers and reddish brown colored (2- 7cm) thick hard ironstone/ferrugenous clay layers. This succession is observed to be interupted by brownish mauve colored, either wave ripple laminated or plane parallel laminated medium to fine grained sandstones. Occurrence of mm thin gypsum layers at the top part of the succession are also observed.	NA	Katrol Formation	107581	107581
126	22-08-2024	GSPL_Bhuj_ 91/01/24	23.15070	69.58000	Naranpar Ravli	Hill cut section near Naranpar Ravli village, same location as GSPL_Bhuj_91/01/24 exposures	Occurrence of mm to 1cm thin grey to blackish grey shale layers, amalgamated at places and often alternate with mm thin silt/fine sand layers and reddish brown colored (2 -7cm) thick hard ironstone/ferrugenous clay layers. This succession is observed to be interupted by brownish mauve colored, either wave ripple laminated or plane parallel laminated medium to fine grained sandstones. Occurrence of mm thin gypsum layers at the top part of the succession are also observed.	NA	Katrol Formation	107582	107582

Sl. No.	Date	Location No.	Latitude	Longitude	Village/ Area	Exposure Location	Host Lithology	Azimuth	Stratigraphy	Original BR ID	New BR ID
127	13-06-2024	GSPL_Bhuj_ 112/03/24	23.15185	69.57784	Naranpar Ravli	Exposed near Naranpar Ravli village, near Crocodile lake, road cut section	Occurrence of mm to 1cm thin grey to blackish grey shale layers, amalgamated at places and often alternate with mm thin silt/fine sand layers and reddish brown colored 2 -7cm thick hard ironstone/ferrugenous clay layers with pinch and swell geometry. This succession is observed to be interupted by brownish mauve colored, either wave ripple laminated or plane parallel laminated medium to fine grained sandstones. Occurrence of mm thin gypsum layers at the top part of the succession are also observed. Tuffite layer collection	NA	Katrol Formation	105569	107453
128	13-06-2024	GSPL_Bhuj_ 112/03/24	23.15185	69.57784	Naranpar Ravli	Exposed near Naranpar Ravli village, near Crocodile lake, road cut section	Occurrence of mm to 1cm thin grey to blackishgrey shale layers, amalgamated at places and often alternate with mm thin silt/fine sand layers and reddish brown colored 2 -7cm thick hard ironstone/ferrugenous clay layers with pinch and swell geometry. This succession is observed to be interupted by brownish mauve colored, either wave ripple laminated or plane parallel laminated medium to fine grained sandstones. Occurrence of mm thin gypsum layers at the top part of the succession are also observed. Tuffite layer collection	NA	Katrol Formation	105570	107454
129	13-06-2024	GSPL_Bhuj_ 112/03/24	23.15185	69.57784	Naranpar Ravli	Exposed near Naranpar Ravli village, near Crocodile lake, road cut section	Occurrence of mm to 1cm thin grey to blackish grey shale layers, amalgamated at places and often alternate with mm thin silt/fine sand layers and reddish brown colored 2 -7cm thick hard ironstone/ferrugenous clay layers with pinch and swell geometry. This succession is observed to be interupted by brownish mauve colored, either wave ripple laminated or plane parallel laminated medium to fine grained sandstones. Occurrence of mm thin gypsum layers at the top part of the succession are also observed. Tuffite layer collection	NA	Katrol Formation	105571	107455

Sl. No.	Date	Location No.	Latitude	Longitude	Village/ Area	Exposure Location	Host Lithology	Azimuth	Stratigraphy	Original BR ID	New BR ID
130	13-06-2024	GSPL_Bhuj_ 112/03/24	23.15185	69.57784	Naranpar Ravli	Exposed near Naranpar Ravli village, near Crocodile lake, road cut section	Occurrence of mm to 1cm thin grey to blackish grey shale layers, amalgamated at places and often alternate with mm thin silt/fine sand layers and reddish brown colored 2 -7cm thick hard ironstone/ferrugenous clay layers with pinch and swell geometry. This succession is observed to be interupted by brownish mauve colored, either wave ripple laminated or plane parallel laminated medium to fine grained sandstones. Occurrence of mm thin gypsum layers at the top part of the succession are also observed. Tuffite layer collection	NA	Katrol Formation	105572	107456
131	13-06-2024	GSPL_Bhuj_ 112/03/24	23.15185	69.57784	Naranpar Ravli	Exposed near Naranpar Ravli village, near Crocodile lake, road cut section	Occurrence of mm to 1cm thin grey to blackish grey shale layers, amalgamated at places and often alternate with mm thin silt/fine sand layers and reddish brown colored 2 -7cm thick hard ironstone/ferrugenous clay layers with pinch and swell geometry. This succession is observed to be interupted by brownish mauve colored, either wave ripple laminated or plane parallel laminated medium to fine grained sandstones. Occurrence of mm thin gypsum layers at the top part of the succession are also observed. Tuffite layer collection	NA	Katrol Formation	105573	107457
132	13-06-2024	GSPL_Bhuj_ 112/03/24	23.15185	69.57784	Naranpar Ravli	Exposed near Naranpar Ravli village, near Crocodile lake, road cut section	Occurrence of mm to 1cm thin grey to blackish grey shale layers, amalgamated at places and often alternate with mm thin silt/fine sand layers and reddish brown colored 2 -7cm thick hard ironstone/ferrugenous clay layers with pinch and swell geometry. This succession is observed to be interupted by brownish mauve colored, either wave ripple laminated or plane parallel laminated medium to fine grained sandstones. Occurrence of mm thin gypsum layers at the top part of the succession are also observed. Tuffite layer collection	NA	Katrol Formation	105574	107458

Sl. No.	Date	Location No.	Latitude	Longitude	Village/ Area	Exposure Location	Host Lithology	Azimuth	Stratigraphy	Original BR ID	New BR ID
133	13-06-2024	GSPL_Bhuj_ 112/03/24	23.15185	69.57784	Naranpar Ravli	Exposed near Naranpar Ravli village, near Crocodile lake, road cut section	Occurrence of mm to 1cm thin grey to blackish grey shale layers, amalgamated at places and often alternate with mm thin silt/fine sand layers and reddish brown colored 2 -7cm thick hard ironstone/ferrugenous clay layers with pinch and swell geometry. This succession is observed to be interupted by brownish mauve colored, either wave ripple laminated or plane parallel laminated medium to fine grained sandstones. Occurrence of mm thin gypsum layers at the top part of the succession are also observed. Tuffite layer collection	NA	Katrol Formation	105575	107459
134	14-06-2024	GSPL_Bhuj_ 115/06/24	23.14998	69.58071	Naranpar Ravli	Along Bhuj Mandvi highway, near Naranpar village near Crocodile lake, road cut section	Continuation of the same seuccession 91/01/24, along the dip, Tuffite layer collected and litholog done	NA	Katrol Formation	105576	107460
135	14-06-2024	GSPL_Bhuj_ 115/06/24	23.14998	69.58071	Naranpar Ravli	Along Bhuj Mandvi highway, near Naranpar village near Crocodile lake, road cut section	Continuation of the same seuccession 91/01/24, along the dip, Tuffite layer collected and litholog done	NA	Katrol Formation	105577	107461
136	14-06-2024	GSPL_Bhuj_ 115/06/24	23.14998	69.58071	Naranpar Ravli	Along Bhuj Mandvi highway, near Naranpar village near Crocodile lake, road cut section	Continuation of the same seuccession 91/01/24, along the dip, Tuffite layer collected and litholog done	NA	Katrol Formation	105578	107462
137	14-06-2024	GSPL_Bhuj_ 110/06/24	23.14998	69.58493	Naranpar Ravli	400m away from location no. 91/01/24 in down dip direction, JCB cut section.	Exposures of Sandstone, grey Shale, Red Ferrugeneous layer, Continuation of the same succession in stratigraphic up direction. However the thickness of the sandstones increases and occurrence of mm thin gypsum layers are also observed.	NA	Katrol Formation	105579	107463
138	14-06-2024	GSPL_Bhuj_ 110/06/24	23.14998	69.58493	Naranpar Ravli	400m away from location no. 91/01/24 in down dip direction, JCB cut section.	Exposures of Sandstone, grey Shale, Red Ferrugeneous layer, Continuation of the same succession in stratigraphic up direction. However the thickness of the sandstones increases and occurrence of mm thin gypsum layers are also observed.	NA	Katrol Formation	105580	107464
139	14-06-2024	GSPL_Bhuj_ 110/06/24	23.14998	69.58493	Naranpar Ravli	400m away from location no. 91/01/24 in down dip direction, JCB cut section.	Exposures of Sandstone, grey Shale, Red Ferrugeneous layer, Continuation of the same succession in stratigraphic up direction. However the thickness of the sandstones increases and occurrence of mm thin gypsum layers are also observed.	NA	Katrol Formation	105581	107465

Sl. No.	Date	Location No.	Latitude	Longitude	Village/ Area	Exposure Location	Host Lithology	Azimuth	Stratigraphy	Original BR ID	New BR ID
140	14-06-2024	GSPL_Bhuj_ 116/06/24	23.14522	69.58386	Naranpar Ravli	Naranpar village, near pond side hill scarp exposures	Continuation of the same succession in stratigraphic up direction. However the thickness of the sandstones increases and occurrence of mm thin gypsum layers are also observed.	60-240/6SSE	Katrol Formation	105582	107466
141	14-06-2024	GSPL_Bhuj_ 116/06/24	23.14522	69.58386	Naranpar Ravli	Naranpar village, near pond side hill scarp exposures	Continuation of the same succession in stratigraphic up direction. However the thickness of the sandstones increases and occurrence of mm thin gypsum layers are also observed.	NA	Katrol Formation	105583	107467
142	14-06-2024	GSPL_Bhuj_ 117/06/24	23.14534	69.54906	Godapar	Road side exposure along the range of the high hills on a newly made metal road, accessible from Bhuj Mandvi Highway	Intrusion of basalt/dolerite within the Katrol Formation. Effect of contact metamorphism observed within the sedimentary rock	NA	Katrol Formation	106503	107487
143	14-06-2024	GSPL_Bhuj_ 118/06/24	23.16454	69.55433	Godapar	Road side exposure along the range of the high hills on a newly made metal road, accessible from Bhuj Mandvi Highway.	Occurrence of altered sandstone, overlain by oolitic limestone at higher contour, intrusion of basalt/dolerite is also observed at lower contour.	NA	Chari Formation	105604	107488
144	15-06-2024	GSPL_Bhuj_ 119/06/24	23.18938	69.60060	Sukhpar	Road side section along Bhuj Mandvi road, near Shiv Paras temple, Wandhay Talav, Sukhpar village.	Cyclic occurence of F1 and F2 with dissimilar cycle lengths.(F1) facies White colored, 2 - 7cm thick medium to coarse grained quartzose sandstone. Internally they are plane parallel laminated. However, top part of the F1 unit, sst beds are wave ripple laminated with chevron uploading draping structure. At the bottom of the sst unit, the lowest sst shows load structures.unit thickness varies from 10 _20cm (F2) facies 16cm 1m thick unit of alternate occurence of mm tocm thin grey shale and sanstone/siltone layers. The alternation unit is truncated by 5 _17cm thick units of medium to fine grained, wave ripple laminated sst with thickness varying between 1.5 to 2cm. The targated ferrugenous clay layers are observed to ocuur as thin layers within F2.	110 - 290/14SSW	Katrol Formation	105584	107468
145	15-06-2024	GSPL_Bhuj_ 120/06/24	23.18878	69.59946	Sukhpar	Continuation of the same succession, along Bhuj Mandvi road.	Continuation of the same facies in stratigraphic up direction, along with the occurrence of mm cm thin gypsum layers present around the Tuffite layered layers.	110 - 290/14SSW	Katrol Formation	105585	107469
146	15-06-2024	GSPL_Bhuj_ 120/06/24	23.18878	69.59946	Sukhpar	Continuation of the same succession, along Bhuj_Mandvi road.	Continuation of the same facies in stratigraphic up direction, along with the occurrence of mm cm thin gypsum layers present around the Tuffite layered layers.	NA	Katrol Formation	105586	107470

Sl. No.	Date	Location No.	Latitude	Longitude	Village/ Area	Exposure Location	Host Lithology	Azimuth	Stratigraphy	Original BR ID	New BR ID
147	15-06-2024	GSPL_Bhuj_ 120/06/24	23.18878	69.59946	Sukhpar	Continuation of the same succession, along Bhuj Mandvi road.	Continuation of the same facies in stratigraphic up direction, along with the occurrence of mm cm thin gypsum layers present around the Tuffite layered layers.	NA	Katrol Formation	105587	107471
148	15-06-2024	GSPL_Bhuj_ 120/06/24	23.18878	69.59946	Sukhpar	Continuation of the same succession, along Bhuj _Mandvi road.	Continuation of the same facies in stratigraphic up direction, along with the occurrence of mm cm thin gypsum layers present around the Tuffite layered layers.	NA	Katrol Formation	105588	107472
149	15-06-2024	GSPL_Bhuj_ 120/06/24	23.18878	69.59946	Sukhpar	Continuation of the same succession, along Bhuj Mandvi road.	Continuation of the same facies in stratigraphic up direction, along with the occurrence of mm cm thin gypsum layers present around the Tuffite layered layers.	NA	Katrol Formation	105589	107473
150	15-06-2024	GSPL_Bhuj_ 120/06/24	23.18878	69.59946	Sukhpar	Continuation of the same succession, along Bhuj Mandvi road.	Continuation of the same facies in stratigraphic up direction, along with the occurrence of mm cm thin gypsum layers present around the Tuffite layered layers.	NA	Katrol Formation	105590	107474
151	15-06-2024	GSPL_Bhuj_ 120/06/24	23.18878	69.59946	Sukhpar	Continuation of the same succession, along Bhuj Mandvi road.	Continuation of the same facies in stratigraphic up direction, along with the occurrence of mm cm thin gypsum layers present around the Tuffite layered layers.	NA	Katrol Formation	105591	107475
152	15-06-2024	GSPL_Bhuj_ 120/06/24	23.18878	69.59946	Sukhpar	Continuation of the same succession, along Bhuj Mandvi road.	Continuation of the same facies in stratigraphic up direction, along with the occurrence of mm cm thin gypsum layers present around the Tuffite layered layers.	NA	Katrol Formation	105592	107476
153	16-06-2024	GSPL_Bhuj_ 120/06/24	23.18878	69.59946	Sukhpar	Continuation of the same succession, at the same outcrop location along Bhuj _Mandvi road.	Continuation of the same facies, at the same outcrop location in stratigraphic up direction. Incorporating (F3) facies, a 10 12 cm thick unit of medium to fine grained sandstone, consisting of quartz and unidentified black minerals, is highly altered, ferruginous in places, with lateral extensions and undulatory boundaries. Shale alternation increases to 20 _25 cm. Stratigraphically upward, sandstone layers are truncated, red nodular beds disappear, and are replaced by a very fine yellowish green layer (likely clay) with clay alteration. The succession reaches 4.7 meters in total thickness before truncating and transitioning back to F1 facies. The Tuffite layered nodular beds are wrapped in gypsum.	NA	Katrol Formation	105593	107477
154	16-06-2024	GSPL_Bhuj_ 120/06/24	23.18878	69.59946	Sukhpar	Continuation of the same succession, at the same outcrop location along the same outcrop location.	Continuation of the same facies, at the same outcrop location in stratigraphic up direction, along with the occurrence of mm cm thin gypsum layers present around the Tuffite layered layers.	NA	Katrol Formation	105594	107478

Sl. No.	Date	Location No.	Latitude	Longitude	Village/ Area	Exposure Location	Host Lithology	Azimuth	Stratigraphy	Original BR ID	New BR ID
155	16-06-2024	GSPL_Bhuj_ 120/06/24	23.18878	69.59946	Sukhpar	Continuation of the same succession, at the same outcrop location along the same outcrop location.	Continuation of the same facies, at the same outcrop location in stratigraphic up direction, along with the occurrence of mm cm thin gypsum layers present around the Tuffite layered layers.	NA	Katrol Formation	105595	107479
156	16-06-2024	GSPL_Bhuj_ 120/06/24	23.18878	69.59946	Sukhpar	Continuation of the same succession, at the same outcrop location along the same outcrop location.	Continuation of the same facies, at the same outcrop location in stratigraphic up direction, along with the occurrence of mm cm thin gypsum layers present around the Tuffite layered layers.	NA	Katrol Formation	105596	107480
157	16-06-2024	GSPL_Bhuj_ 120/06/24	23.18878	69.59946	Sukhpar	Continuation of the same succession, at the same outcrop location along the same outcrop location.	Continuation of the same facies, at the same outcrop location in stratigraphic up direction, along with the occurrence of mm cm thin gypsum layers present around the Tuffite layered layers.	NA	Katrol Formation	105597	107481
158	16-06-2024	GSPL_Bhuj_ 120/06/24	23.18878	69.59946	Sukhpar	Continuation of the same succession, at the same outcrop location along the same outcrop location.	Continuation of the same facies, at the same outcrop location in stratigraphic up direction, along with the occurrence of mm cm thin gypsum layers present around the Tuffite layered layers.	NA	Katrol Formation	105598	107482
159	16-06-2024	GSPL_Bhuj_ 120/06/24	23.18878	69.59946	Sukhpar	Continuation of the same succession, at the same outcrop location along the same outcrop location.	Continuation of the same facies, at the same outcrop location in stratigraphic up direction, along with the occurrence of mm cm thin gypsum layers present around the Tuffite layered layers.	NA	Katrol Formation	105599	107483
160	16-06-2024	121/06/24	23.18791	69.59873		120/06/24 log end location	120/06/24 log end location	NA	Katrol Formation	NA	NA
161	16-06-2024	GSPL_Bhuj_ 117/06/24	23.14534	69.54906	Godapar	Road side exposure along the range of the high hills on a newly made metal road, accessible from Bhuj Mandvi Highway	The succession includes black shale intermittently separated by nodular layers, which are poorly developed or less pronounced. The unit overlies 33 cm thick, pinkish, coarse to medium grained sandstone, consisting of quartz, feldspar, and mica, is observed in a tabular form with no internal structures. Nearby, a dolerite dyke indicates contact metamorphism, likely converting the black shale into slate.	NA	Katrol Formation	105600	107484
162	16-06-2024	GSPL_Bhuj_ 117/06/24	23.14534	69.54906	Godapar	Road side exposure along the range of the high hills on a newly made metal road, accessible from Bhuj Mandvi Highway	The succession includes black shale intermittently separated by nodular layers, which are poorly developed or less pronounced. The unit overlies 33 cm thick, pinkish, coarse to medium grained sandstone, consisting of quartz, feldspar, and mica, is observed in a tabular form with no internal structures. Nearby, a dolerite dyke indicates contact metamorphism, likely converting the black shale into slate.	NA	Katrol Formation	105601	107485

Sl. No.	Date	Location No.	Latitude	Longitude	Village/ Area	Exposure Location	Host Lithology	Azimuth	Stratigraphy	Original BR ID	New BR ID
163	16-06-2024	GSPL_Bhuj_ 117/06/24	23.14534	69.54906	Godapar	Road side exposure along the range of the high hills on a newly made metal road, accessible from Bhuj Mandvi Highway	The succession includes black shale intermittently separated by nodular layers, which are poorly developed or less pronounced. The unit overlies 33 cm thick, pinkish, coarse to medium grained sandstone, consisting of quartz, feldspar, and mica, is observed in a tabular form with no internal structures. Nearby, a dolerite dyke indicates contact metamorphism, likely converting the black shale into slate.	NA	Katrol Formation	105602	107486
164	17-06-2024	GSPL_Bhuj_ 122/06/24	23.18239	69.66951	Jedura Mota	Road side hill exposure near Tapkeswari temple on Tapkeswari Bhuj road	Medium to coarse grained sandstone, no internal structure observed	NA	Katrol Formation	NA	NA
165	18-06-2024	GSPL_Bhuj_ 123/06/24	23.18564	69.64097	Bhata Talav	Road cut section, along the Bhuj Mundra highway	(F1) Facies: Very thinly laminated shale _sandstone alternation. (F2) Facies: Grey shale. (F3) Facies: 1 3 cm thick, thinly bedded sandstone with pinch and swell structures and wavy ripple laminations; internal structures are not visible and beds are truncated or separated by shale laminations.	130-310/20SW	Katrol Formation	105605	107489
166	18-06-2024	GSPL_Bhuj_ 124/06/24	23.18163	69.64077	Bhata Talav	Along the Bhuj Mundra highway,road cut section with occurrence of high energy deposit	Alternate occurrence of high energy, mostly planar, tabular, plane parallal laminated quartzose sandstone (5 -30cm) with ripple like appearance at places (no other internal structure observed) and shale siltstone (calcareous??) alternation. The shale siltstone layers are (muscovite, biotite, rounded black mineral with metallic lusture are the unusal components) and few gypsun layers (at different stratigraphic height) are observed.	100-280/8SW	Katrol Formation	105606	107490
167	18-06-2024	GSPL_Bhuj_ 125/06/24	23.18031	69.63968	Bhata Talav	Along the Bhuj Mundra highway,road cut section with occurrence of high energy deposit	124/06/24 log end location	100-280/8SW	Katrol Formation	NA	NA
168	19-06-2024	GSPL_Bhuj_ 126/06/24	23.18334	69.69171	Satpura Dungar	Along Dhunaraja road, road side hill scarp section, near Dhunaraja dam	Occurrence of 5 -30cm thick, very weathered, structurally deformed very coarse to coarse grained sandstone. The sandstone consist of sub angular to sub rounded grains of quartz (~90%), mica (muscovite) and few unknown minerals embedded in a fine grained ferruginous matrix/cement. Internally the sandstones are planar cross stratified with rippled top surface. Seems to be locally folded and cross cut by several randomly	160-340/4SW	Chari GSPL_Bhuj_Katrol contact	NA	NA

Sl. No.	Date	Location No.	Latitude	Longitude	Village/ Area	Exposure Location	Host Lithology	Azimuth	Stratigraphy	Original BR ID	New BR ID
							oriented vein like features of ferruginous (hematitic) material.				
169	19-06-2024	GSPL_Bhuj_127/06/24	23.18276	69.69226	Satpura Dungar	Along Dhunaraja Dam road, road side folded hill scarp section, near Dhunaraja dam, in the vicinity of Bhuj Reserve Forest	Fossiliferous (belemnite) coarse grained sandstone	120 - 300/4SW	Chari Formation	105607	107491
170	19-06-2024	GSPL_Bhuj_128/06/24	23.18172	69.69135	Satpura Dungar	Along Dhunaraja Dam road, road side folded hill scarp section, near Dhunaraja dam, in the vicinity of Bhuj Reserve Forest	Occurrence of folded succession of sst shale heterolith (interupted by poorly developed red beds) overlying undeformed Chari sandstone. The heterolith starts with occurrence of black shale. Thickness of sandstone layers increases up the succession.	120-300/20SW	Chari GSPL_Bhuj_Katrol contact	105608	107492
171	19-06-2024	GSPL_Bhuj_129/06/24	23.17943	69.69072	Satpura Dungar	Along Dhunaraja Dam road, road side folded hill scarp section, near Dhunaraja dam, in the vicinity of Bhuj Reserve Forest	(F1) Facies: Millimeter to 1 cm thick, medium to fine grained sandstone beds, mostly plane parallel laminated and separated by millimeter thin shales. (F2) Facies: 10 -15 cm thick grey shales with well -defined fissility planes. In this succession, millimeter _thin shale sandstone alternations and a few thin gypsum layers are observed, with well developed Tuffite layered nodular beds in both facies.	160 - 340/8SW	Katrol Formation	105609	107493
172	19-06-2024	GSPL_Bhuj_129/06/24	23.17943	69.69072	Satpura Dungar	Along Dhunaraja Dam road, road side folded hill scarp section, near Dhunaraja_dam, in the vicinity of Bhuj Reserve Forest	(F1) Facies: Millimeter to 1 cm thick, medium to fine grained sandstone beds, mostly plane parallel laminated and separated by millimeter thin shales. (F2) Facies: 10 -15 cm thick grey shales with well -defined fissility planes. In this succession, millimeter _thin shale sandstone alternations and a few thin gypsum layers are observed, with well developed Tuffite layered nodular beds in both facies.	NA	Katrol Formation	105610	107494
173	19-06-2024	GSPL_Bhuj_129/06/24	23.17943	69.69072	Satpura Dungar	Along Dhunaraja _Dam road, road side folded hill scarp section, near Dhunaraja dam, in the vicinity of Bhuj Reserve Forest	(F1) Facies: Millimeter to 1 cm thick, medium to fine grained sandstone beds, mostly plane parallel laminated and separated by millimeter thin shales. (F2) Facies: 10 -15 cm thick grey shales with well -defined fissility planes. In this succession, millimeter _thin shale sandstone alternations and a few thin gypsum layers are observed, with well developed Tuffite layered nodular beds in both facies.	NA	Katrol Formation	105611	107495

Sl. No.	Date	Location No.	Latitude	Longitude	Village/ Area	Exposure Location	Host Lithology	Azimuth	Stratigraphy	Original BR ID	New BR ID
174	19-06-2024	GSPL_Bhuj_ 130/06/24	23.17389	69.69201	Jadura	Continuation of the 129/06/24 succession, along the Dhunaraja Dam Road, hill scarp section, near Dhunaraja dam, in the vicinity of Bhuj Reserve Forest	Continuation of the same facies as the previous location in stratigraphic up direction. However, the thickness of the siltstone layers increases, with only one gypsum layer observed within the sequence.	120 - 300/6SW	Katrol Formation	105612	107496
175	19-06-2024	GSPL_Bhuj_ 130/06/24	23.17389	69.69201	Jadura	Continuation of the 129/06/24 succession, along the Dhunaraja Dam Road, hill scarp section, near Dhunaraja dam, in the vicinity of Bhuj Reserve Forest	Continuation of the same facies as the previous location in stratigraphic up direction. However, the thickness of the siltstone layers increases, with only one gypsum layer observed within the sequence.	NA	Katrol Formation	105613	107497
176	19-06-2024	GSPL_Bhuj_ 130/06/24	23.17389	69.69201	Jadura	Continuation of the 129/06/24 succession, along the Dhunaraja Dam Road, hill scarp section, near Dhunaraja dam, in the vicinity of Bhuj Reserve Forest	Continuation of the same facies as the previous location in stratigraphic up direction. However, the thickness of the siltstone layers increases, with only one gypsum layer observed within the sequence.	NA	Katrol Formation	105614	107498
177	19-06-2024	GSPL_Bhuj_ 130/06/24	23.17389	69.69201	Jadura	Continuation of the 129/06/24 succession, along the Dhunaraja Dam Road, hill scarp section, near Dhunaraja dam, in the vicinity of Bhuj Reserve Forest	Continuation of the same facies as the previous location in stratigraphic up direction. However, the thickness of the siltstone layers increases, with only one gypsum layer observed within the sequence.	NA	Katrol Formation	105615	107499
178	19-06-2024	GSPL_Bhuj_ 130/06/24	23.17389	69.69201	Jadura	Continuation of the 129/06/24 succession, along the Dhunaraja Dam Road, hill scarp section, near Dhunaraja dam, in the vicinity of Bhuj Reserve Forest	Continuation of the same facies as the previous location in stratigraphic up direction. However, the thickness of the siltstone layers increases, with only one gypsum layer observed within the sequence.	NA	Katrol Formation	105616	107500
179	19-06-2024	GSPL_Bhuj_ 131/06/24	23.17366	69.69202	Jadura	End location of 130/06/24 succession, along the Dhunaraja Dam Road, hill scarp section, near Dhunaraja dam, in the vicinity of Bhuj Reserve Forest	Sandstone increases at the end of log	120 - 300/6SW	Katrol Formation	NA	NA
180	20-06-2024	GSPL_Bhuj_ 132/06/24	23.17281	69.69228	Jadura	Continuation of the 130/06/24 succession, along the Dhunaraja Dam Road, hill scarp section, near Dhunaraja dam, in the vicinity of Bhuj Reserve Forest	Continuation of the same facies as the previous location in stratigraphic up direction. The occurrence of centimeter GSPL_Bhuj_thin gypsum layers is present around the Tuffite layered layers, alongside the observed sandstone GSPL_Bhuj_siltstone alternation.	NA	Katrol Formation	105617	107501

Sl. No.	Date	Location No.	Latitude	Longitude	Village/ Area	Exposure Location	Host Lithology	Azimuth	Stratigraphy	Original BR ID	New BR ID
181	20-06-2024	GSPL_Bhuj_ 132/06/24	23.17281	69.69228	Jadura	Continuation of the 130/06/24 succession, along the Dhunaraja Dam Road, hill scarp section, near Dhunaraja _dam, in the vicinity of Bhuj Reserve Forest	Continuation of the same facies as the previous location in stratigraphic up direction. The occurrence of centimeter thin gypsum layers is present around the Tuffite layered layers, alongside the observed sandstone siltstone alternation.	NA	Katrol Formation	105618	107502
182	20-06-2024	GSPL_Bhuj_ 132/06/24	23.17281	69.69228	Jadura	Continuation of the 130/06/24 succession, along the Dhunaraja Dam Road, hill scarp section, near Dhunaraja dam, in the vicinity of Bhuj Reserve Forest	Continuation of the same facies as the previous location in stratigraphic up direction. The occurrence of centimeter thin gypsum layers is present around the Tuffite layered layers, alongside the observed sandstone siltstone alternation.	NA	Katrol Formation	105619	107503
183	20-06-2024	GSPL_Bhuj_ 132/06/24	23.17281	69.69228	Jadura	Continuation of the 130/06/24 succession, along the Dhunaraja Dam Road, hill scarp section, near Dhunaraja dam, in the vicinity of Bhuj Reserve Forest	Continuation of the same facies as the previous location in stratigraphic up direction. The occurrence of centimeter thin gypsum layers is present around the Tuffite layered layers, alongside the observed sandstone siltstone alternation.	NA	Katrol Formation	105620	107504
184	20-06-2024	GSPL_Bhuj_ 132/06/24	23.17281	69.69228	Jadura	Continuation of the 130/06/24 succession, along the Dhunaraja Dam Road, hill scarp section, near Dhunaraja dam, in the vicinity of Bhuj Reserve Forest	Continuation of the same facies as the previous location in stratigraphic up direction. The occurrence of centimeter thin gypsum layers is present around the Tuffite layered layers, alongside the observed sandstone siltstone alternation.	NA	Katrol Formation	105621	107505
185	20-06-2024	GSPL_Bhuj_ 132/06/24	23.17281	69.69228	Jadura	Continuation of the 130/06/24 succession, along the Dhunaraja Dam Road, hill scarp section, near Dhunaraja dam, in the vicinity of Bhuj Reserve Forest	Continuation of the same facies as the previous location in stratigraphic up direction. The occurrence of centimeter thin gypsum layers is present around the Tuffite layered layers, alongside the observed sandstone siltstone alternation.	NA	Katrol Formation	105622	107506
186	20-06-2024	GSPL_Bhuj_ 132/06/24	23.17281	69.69228	Jadura	Continuation of the 130/06/24 succession, along the Dhunaraja Dam Road, hill scarp section, near Dhunaraja dam, in the vicinity of Bhuj Reserve Forest	Continuation of the same facies as the previous location in stratigraphic up direction. The occurrence of centimeter thin gypsum layers is present around the Tuffite layered layers, alongside the observed sandstone siltstone alternation.	NA	Katrol Formation	105623	107507
187	20-06-2024	GSPL_Bhuj_ 133/06/24	23.17211	69.69245	Jadura	End location of 132/06/24 succession, along the Dhunaraja Dam Road, hill scarp section, near Dhunaraja dam, in the vicinity of Bhuj Reserve Forest	Sandstone increases at the end of log	NA	Katrol Formation	NA	NA

Sl. No.	Date	Location No.	Latitude	Longitude	Village/ Area	Exposure Location	Host Lithology	Azimuth	Stratigraphy	Original BR ID	New BR ID
188	20-06-2024	GSPL_Bhuj_ 134/06/24	23.17164	69.69255	Jadura	Continuation of the 132/06/24 succession, along the Dhunaraja Dam Road, hill scarp section, near Dhunaraja dam, in the vicinity of Bhuj Reserve Forest	Continuation of the same facies as the previous location in stratigraphic up direction. The occurrence of centimeter thin gypsum layers is present around the Tuffite layered layers only at one stratigraphic level	NA	Katrol Formation	105624	107508
189	20-06-2024	GSPL_Bhuj_ 134/06/24	23.17164	69.69255	Jadura	Continuation of the 132/06/24 succession, along the Dhunaraja Dam Road, hill scarp section, near Dhunaraja dam, in the vicinity of Bhuj Reserve Forest	Continuation of the same facies as the previous location in stratigraphic up direction. The occurrence of centimeter thin gypsum layers is present around the Tuffite layered layers only at one stratigraphic level	NA	Katrol Formation	105625	107509
190	21-06-2024	GSPL_Bhuj_ 135/06/24	23.17137	69.69244	Jadura	End location of 134/06/24 succession, along the Dhunaraja Dam Road, hill scarp section, near Dhunaraja dam, in the vicinity of Bhuj Reserve Forest	Sandstone increases at the end of log	NA	Katrol Formation	NA	NA
191	21-06-2024	GSPL_Bhuj_ 136/06/24	23.16082	69.72329	Reha Mota	Hilly exposure near Reha Mota village, approximately 1 km away from the cart road, connecting Reha Mota and Madhapar. Area has uneven topography with few river channels draining the area.	Exposure of planar, with undulatory bed boundaries, coarse grained sandstone. The thickness of this sandstone ranges from 20 to 60 cm and separated by thin (2- 7 cm) completely altered, brecciated type red beds altered red beds (cherry red in colour, noduler appearance, with scattered mica grains, embedded in a buff coloured groundmas. No other identifiable grains).These layers follow the sandstone boundary.	150 - 330/4SW	Bhuj -Katrol contact	105626	107510
192	21-06-2024	GSPL_Bhuj_ 136/06/24	23.16082	69.72329	Reha Mota	Hilly exposure near Reha Mota village, approximately 1 km away from the cart road, connecting Reha Mota and Madhapar. Area has uneven topography with few river channels draining the area.	Exposure of planar, with undulatory bed boundaries, coarse grained sandstone. The thickness of this sandstone ranges from 20 to 60 cm and separated by thin (2 -7 cm) completely altered, brecciated type red beds altered red beds (cherry red in colour, noduler appearance, with scattered mica grains, embedded in a buff coloured groundmas. No other identifiable grains).These layers follow the sandstone boundary.	NA	Bhuj -Katrol contact	105627	107511

Sl. No.	Date	Location No.	Latitude	Longitude	Village/ Area	Exposure Location	Host Lithology	Azimuth	Stratigraphy	Original BR ID	New BR ID
193	21-06-2024	GSPL_Bhuj_ 137/06/24A	23.16410	69.72726	Reha Nana	Hilly exposure near Reha Mota village, approximately 1 km away from the cart road, connecting Reha Mota and Madhapar. A new cart road is being prepared for pipeline installation. catchment of the high HLS results.	Alternate occurrence of sandstone, gray shale and this particular phosphorite looking beds. The sandstones are parallal laminated, 6 GSPL_Bhuj_10cm thick medium to fine grained quartzose sandstone. Relatively coarse grained brownish GSPL_Bhuj_mauve colored sandstones intercalated with nodular layers, separated by millimeter GSPL_Bhuj_thin shale GSPL_Bhuj_siltstone layers are also visible. The gray shale layers are very thin (12 GSPL_Bhuj_18cm), rarely interupted by 2 GSPL_Bhuj_3cm thick red layers. The phosphorite looking beds (may be quartz arenite also) are 9 GSPL_Bhuj_12cm thick, forming units of 39cm to 1.8m, separated by mm thin shale layers/red beds. Butchers knife erosion is common within this beds.several gypsum layers are found near the nodular layers. This succession is at the upper part of the Katrol Formation.	160 - 340/6SW	Katrol Formation	105628	107512
194	21-06-2024	GSPL_Bhuj_ 137/06/24A	23.16410	69.72726	Reha Nana	Hilly exposure near Reha Mota village, approximately 1 km away from the cart road, connecting Reha Mota and Madhapar. A new cart road is being prepared for pipeline installation. catchment of the high HLS results.	Alternate occurrence of sandstone, gray shale and this particular phosphorite looking beds. The sandstones are parallal laminated, 6 10cm thick medium to fine grained quartzose sandstone. Relatively coarse grained brownish mauve colored sandstones intercalated with nodular layers, separated by millimeter _thin shale _siltstone layers are also visible. The gray shale layers are very thin (12 18cm), rarely interupted by 2 3cm thick red layers. The phosphorite looking beds (may be quartz arenite also) are 9 12cm thick, forming units of 39cm to 1.8m, separated by mm thin shale layers/red beds. Butchers knife erosion is common within this beds.several gypsum layers are found near the nodular layers. This succession is at the upper part of the Katrol Formation.	NA	Katrol Formation	105629	107513

Sl. No.	Date	Location No.	Latitude	Longitude	Village/ Area	Exposure Location	Host Lithology	Azimuth	Stratigraphy	Original BR ID	New BR ID
195	21-06-2024	GSPL_Bhuj_ 137/06/24A	23.16410	69.72726	Reha Nana	Hilly exposure near Reha Mota village, approximately 1 km away from the cart road, connecting Reha Mota and Madhapar. A new cart road is being prepared for pipeline installation. catchment of the high HLS results.	Alternate occurrence of sandstone, gray shale and this particular phosphorite looking beds. The sandstones are parallal laminated, 6 10cm thick medium to fine grained quartzose sandstone. Relatively coarse grained brownish mauve colored sandstones intercalated with nodular layers, separated by millimeter _thin shale _siltstone layers are also visible. The gray shale layers are very thin (12 18cm), rarely interupted by 2 3cm thick red layers. The phosphorite looking beds (may be quartz arenite also) are 9 12cm thick, forming units of 39cm to 1.8m, separated by mm thin shale layers/red beds. Butchers knife erosion is common within this beds.several gypsum layers are found near the nodular layers. This succession is at the upper part of the Katrol Formation.	NA	Katrol Formation	105630	107514
196	21-06-2024	GSPL_Bhuj_ 137/06/24A	23.16410	69.72726	Reha Nana	Hilly exposure near Reha Mota village, approximately 1 km away from the cart road, connecting Reha Mota and Madhapar. A new cart road is being prepared for pipeline installation. catchment of the high HLS results.	Alternate occurrence of sandstone, gray shale and this particular phosphorite looking beds. The sandstones are parallal laminated, 6 10cm thick medium to fine grained quartzose sandstone. Relatively coarse grained brownish mauve colored sandstones intercalated with nodular layers, separated by millimeter _thin shale _siltstone layers are also visible. The gray shale layers are very thin (12 18cm), rarely interupted by 2 3cm thick red layers. The phosphorite looking beds (may be quartz arenite also) are 9 12cm thick, forming units of 39cm to 1.8m, separated by mm thin shale layers/red beds. Butchers knife erosion is common within this beds.several gypsum layers are found near the nodular layers. This succession is at the upper part of the Katrol Formation.	NA	Katrol Formation	105631	107515

Sl. No.	Date	Location No.	Latitude	Longitude	Village/ Area	Exposure Location	Host Lithology	Azimuth	Stratigraphy	Original BR ID	New BR ID
197	21-06-2024	GSPL_Bhuj_ 137/06/24A	23.16410	69.72726	Reha Nana	Hilly exposure near Reha Mota village, approximately 1 km away from the cart road, connecting Reha Mota and Madhapar. A new cart road is being prepared for pipeline installation. catchment of the high HLS results.	Alternate occurrence of sandstone, gray shale and this particular phosphorite looking beds. The sandstones are parallal laminated, 6 10cm thick medium to fine grained quartzose sandstone. Relatively coarse grained brownish mauve colored sandstones intercalated with nodular layers, separated by millimeter _thin shale _siltstone layers are also visible. The gray shale layers are very thin (12 18cm), rarely interupted by 2 3cm thick red layers. The phosphorite looking beds (may be quartz arenite also) are 9 12cm thick, forming units of 39cm to 1.8m, separated by mm thin shale layers/red beds. Butchers knife erosion is common within this beds.several gypsum layers are found near the nodular layers. This succession is at the upper part of the Katrol Formation.	NA	Katrol Formation	105632	107516
198	21-06-2024	GSPL_Bhuj_ 137/06/24A	23.16410	69.72726	Reha Nana	Hilly exposure near Reha Mota village, approximately 1 km away from the cart road, connecting Reha Mota and Madhapar. A new cart road is being prepared for pipeline installation. catchment of the high HLS results.	Alternate occurrence of sandstone, gray shale and this particular phosphorite looking beds. The sandstones are parallal laminated, 6 10cm thick medium to fine grained quartzose sandstone. Relatively coarse grained brownish mauve colored sandstones intercalated with nodular layers, separated by millimeter _thin shale _siltstone layers are also visible. The gray shale layers are very thin (12 18cm), rarely interupted by 2 3cm thick red layers. The phosphorite looking beds (may be quartz arenite also) are 9 12cm thick, forming units of 39cm to 1.8m, separated by mm thin shale layers/red beds. Butchers knife erosion is common within this beds.several gypsum layers are found near the nodular layers. This succession is at the upper part of the Katrol Formation.	NA	Katrol Formation	105633	107517

Sl. No.	Date	Location No.	Latitude	Longitude	Village/ Area	Exposure Location	Host Lithology	Azimuth	Stratigraphy	Original BR ID	New BR ID
199	21-06-2024	GSPL_Bhuj_ 137/06/24A	23.16410	69.72726	Reha Nana	Hilly exposure near Reha Mota village, approximately 1 km away from the cart road, connecting Reha Mota and Madhapar. A new cart road is being prepared for pipeline installation. catchment of the high HLS results.	Alternate occurrence of sandstone, gray shale and this particular phosphorite looking beds. The sandstones are parallal laminated, 6 10cm thick medium to fine grained quartzose sandstone. Relatively coarse grained brownish mauve colored sandstones intercalated with nodular layers, separated by millimeter _thin shale _siltstone layers are also visible. The gray shale layers are very thin (12 18cm), rarely interupted by 2 3cm thick red layers. The phosphorite looking beds (may be quartz arenite also) are 9 12cm thick, forming units of 39cm to 1.8m, separated by mm thin shale layers/red beds. Butchers knife erosion is common within this beds.several gypsum layers are found near the nodular layers. This succession is at the upper part of the Katrol Formation.	NA	Katrol Formation	105634	107518
200	21-06-2024	GSPL_Bhuj_ 137/06/24A	23.16410	69.72726	Reha Nana	Hilly exposure near Reha Mota village, approximately 1 km away from the cart road, connecting Reha Mota and Madhapar. A new cart road is being prepared for pipeline installation. catchment of the high HLS results.	Alternate occurrence of sandstone, gray shale and this particular phosphorite looking beds. The sandstones are parallal laminated, 6 10cm thick medium to fine grained quartzose sandstone. Relatively coarse grained brownish mauve colored sandstones intercalated with nodular layers, separated by millimeter _thin shale _siltstone layers are also visible. The gray shale layers are very thin (12 18cm), rarely interupted by 2 3cm thick red layers. The phosphorite looking beds (may be quartz arenite also) are 9 12cm thick, forming units of 39cm to 1.8m, separated by mm thin shale layers/red beds. Butchers knife erosion is common within this beds.several gypsum layers are found near the nodular layers. This succession is at the upper part of the Katrol Formation.	NA	Katrol Formation	105635	107519
201	21-06-2024	GSPL_Bhuj_ 137/06/24B	23.16433	69.72749	Reha Nana	End of log location	quartzose sandstone interupted by red beds	160 340/6SW	Katrol Formation		
202	21-06-2024	GSPL_Bhuj_ 138/06/24	23.15405	69.72575	Reha Nana	Hill section,near New Cart Road,near Reha Nana Village.	Medium grained sandstone with differential ferruginous leaching. Narrow, meandering type river, good trap sites.	NA	Bhuj Formation	NA	NA
203	22-06-2024	GSPL_Bhuj_ 139/06/24	23.17944	69.75168	Ler	Near Ler village towards ler dam at river side	Occurrence of heterolithic unit of shale/siltstone and thinly bedded rippled topped brownish mauve coloured sandstone. It is a confluence of many slope wash of 1st	NA	Chari Katrol contact	NA	NA

Sl. No.	Date	Location No.	Latitude	Longitude	Village/ Area	Exposure Location	Host Lithology	Azimuth	Stratigraphy	Original BR ID	New BR ID
							order and 2nd order streams.The river is 2-12m in breadth.				
204	22-06-2024	GSPL_Bhuj_140/06/24	23.15227	69.74333	Reha Nana	Near Reha Nana village in the windmill areas.	Occurrence of heterolithic unit of shale/siltstone and thinly bedded rippled topped brownish mauve coloured sandstone. It is a confluence of many slope wash of 1st order and 2nd order streams.The river is 2-12m in breadth.	NA	Bhuj Formation	NA	NA
205	23-06-2024	GSPL_Bhuj_141/06/24	23.15405	69.74924	Reha Nana and Reha Mota	Near Reha Nana village in the windmill areas.	Occurrence of sandstone with differential weathering by ferruginous material. Narrow braided river.Sample collecetd from 2nd order stream.The river is of 3 -5m in breadth.Low direct biogenic contamination, however surrounded by farm lands.	NA	Bhuj _Katrol contact	NA	NA
206	23-06-2024	GSPL_Bhuj_142/06/24	23.14984	69.72084	Reha Mota	Near Reha Mota village, road side stream section along a cart road connecting Reha Mota and Jadura Mota	Occurrence of sandstone with differential weathering by ferruginous material. braided type stream. Sample collected from 3rd order stream (after the confluence of 2nd & 3rd order stream according to toposheet).The river is 3 -8m in breadth.Anthropogenic contamination is high and low biogenic contamination.	NA	Bhuj Formation	NA	NA
207	23-06-2024	GSPL_Bhuj_143/06/24	23.15271	69.69552	Jadura	Near Jadura village, ~1km west of Jadura Chakar road (extension of Dhunaraja dam road)	Very narrow 2 -2.5m,2nd order stream draining the Katrol Formation.	NA	Bhuj Formation	NA	NA
208	23-06-2024	GSPL_Bhuj_144/06/24	23.15350	69.70207	Jadura	Near Jadura village,beside Jadura _hakar road (extension of Dhunaraja dam road)	Occurrence of ferruginous sandstone in river bed. Narrow 3 -4m wide,3rd order stream draining the Katrol Formation,near Jadugoda village.	NA	Bhuj Formation	NA	NA
209	24-06-2024	GSPL_Bhuj_145/06/24	23.14798	69.57766	Naranpar Ravli	From Bhuj Mandvi highway, near Naranpur Ravli village opposite to the Nayara Petrol Pump.	Occurrence of shl _sst heterolith. Narrow meandering stream of 3 -3.5m in breadth, 2nd order streams draining the Katrol formation,.Biogenic and anthropogenic contaminations are very low.	NA	katrol Formation	NA	NA
210	24-06-2024	GSPL_Bhuj_146/06/24	23.13773	69.53957	Godpar	Near Godpar village,Jamora Dam & Vankol Virdo Temple, accesible by a metal road and then a cart road through Godapar village from Bhuj GSPL_Bhuj_Mandvi highway	Occurrence of very weathered heterolith of shl sst, interupted by tarhet beds. Wide after the confluence of 1st and 2nd order stream. High anthropogeic contamination seen.	NA	katrol Formation	NA	NA

Sl. No.	Date	Location No.	Latitude	Longitude	Village/ Area	Exposure Location	Host Lithology	Azimuth	Stratigraphy	Original BR ID	New BR ID
211	25-06-2024	GSPL_Bhuj_ 147/06/24	23.17128	69.69256	Jadura	Continuation of the 134/06/24 succession, along the Dhunaraja Dam Road, hill scarp section, near Dhunaraja dam, in the vicinity of Bhuj Reserve Forest	In the stratigraphic continuation upwards in continuation from the 134/06/24 location, same kind of facies. F1: Sst consisting of millimetre to 1 cm thick, plane parallal laminated layers/beds, occassionally amalgamated.The sst layers are seperated by mm thin shales and/or gypsum layers. Unit thickness varies from 5cm 48cm.F2: Gray shales having unit thickness of 7 110cm and often interrupted by 2 -7cm thick calcareous red beds and/or gypsum layers. Alteration of few beds in yellowish clay layers are also observed.Additionally, (20cm) thick ferruginous shale layer is present, characterized by mica, ferrous micro nodules, and several gypsum layers	NA	katrol Formation	105645	107529
212	25-06-2024	GSPL_Bhuj_ 147/06/24	23.17128	69.69256	Jadura	Continuation of the 134/06/24 succession, along the Dhunaraja Dam Road, hill scarp section, near Dhunaraja dam, in the vicinity of Bhuj Reserve Forest	In the stratigraphic continuation upwards in continuation from the 134/06/24 location, same kind of facies. F1: Sst consisting of millimetre to 1 cm thick, plane parallal laminated layers/beds, occassionally amalgamated.The sst layers are seperated by mm thin shales and/or gypsum layers. Unit thickness varies from 5cm 48cm. F2: Gray shales having unit thickness of 7 110cm and often interrupted by 2 -7cm thick calcareous red beds and/or gypsum layers. Alteration of few beds in yellowish clay layers are also observed. Additionally, (20cm) thick ferruginous shale layer is present, characterized by mica, ferrous micro nodules, and several gypsum layers	NA	katrol Formation	105646	107530
213	25-06-2024	GSPL_Bhuj_ 147/06/24	23.17128	69.69256	Jadura	Continuation of the 134/06/24 succession, along the Dhunaraja Dam Road, hill scarp section, near Dhunaraja GSPL_Bhuj_dam, in the vicinity of Bhuj Reserve Forest	In the stratigraphic continuation upwards in continuation from the 134/06/24 location, same kind of facies. F1: Sst consisting of millimetre to 1 cm thick, plane parallal laminated layers/beds, occassionally amalgamated.The sst layers are seperated by mm thin shales and/or gypsum layers. Unit thickness varies from 5cm 48cm. F2: Gray shales having unit thickness of 7 110cm and often interrupted by 2 -7cm thick calcareous red beds and/or gypsum layers. Alteration of few beds in yellowish clay layers are also observed. Additionally, (20cm) thick ferruginous shale layer is present, characterized by mica,	NA	katrol Formation	105647	107531

Sl. No.	Date	Location No.	Latitude	Longitude	Village/ Area	Exposure Location	Host Lithology	Azimuth	Stratigraphy	Original BR ID	New BR ID
							ferrous micro nodules, and several gypsum layers				
214	25-06-2024	GSPL_Bhuj_147/06/24	23.17128	69.69256	Jadura	Continuation of the 134/06/24 succession, along the Dhunaraja Dam Road, hill scarp section, near Dhunaraja dam, in the vicinity of Bhuj Reserve Forest	In the stratigraphic continuation upwards in continuation from the 134/06/24 location, same kind of facies. F1: Sst consisting of millimetre to 1 cm thick, plane parallal laminated layers/beds, occassionally amalgamated.The sst layers are seperated by mm thin shales and/or gypsum layers. Unit thickness varies from 5cm 48cm.F2: Gray shales having unit thickness of 7 110cm and often interrupted by 2 -7cm thick calcareous red beds and/or gypsum layers. Alteration of few beds in yellowish clay layers are also observed.Additionally, (20cm) thick ferruginous shale layer is present, characterized by mica, ferrous micro nodules, and several gypsum layers	NA	katrol Formation	105648	107532
215	25-06-2024	GSPL_Bhuj_147/06/24	23.17128	69.69256	Jadura	Continuation of the 134/06/24 succession, along the Dhunaraja Dam Road, hill scarp section, near Dhunarajadam, in the vicinity of Bhuj Reserve Forest	In the stratigraphic continuation upwards in continuation from the 134/06/24 location, same kind of facies. F1: Sst consisting of millimetre to 1 cm thick, plane parallal laminated layers/beds, occassionally amalgamated.The sst layers are seperated by mm thin shales and/or gypsum layers. Unit thickness varies from 5cm 48cm. F2: Gray shales having unit thickness of 7 110cm and often interrupted by 2 -7cm thick calcareous red beds and/or gypsum layers. Alteration of few beds in yellowish clay layers are also observed. Additionally, (20cm) thick ferruginous shale layer is present, characterized by mica, ferrous micro nodules, and several gypsum layers	NA	katrol Formation	105649	107533

Sl. No.	Date	Location No.	Latitude	Longitude	Village/ Area	Exposure Location	Host Lithology	Azimuth	Stratigraphy	Original BR ID	New BR ID
216	25-06-2024	GSPL_Bhuj_ 147/06/24	23.17128	69.69256	Jadura	Continuation of the 134/06/24 succession, along the Dhunaraja Dam Road, hill scarp section, near Dhunaraja dam, in the vicinity of Bhuj Reserve Forest	In the stratigraphic continuation upwards in continuation from the 134/06/24 location, same kind of facies. F1: Sst consisting of millimetre to 1 cm thick, plane parallal laminated layers/beds, occassionally amalgamated.The sst layers are seperated by mm thin shales and/or gypsum layers. Unit thickness varies from 5cm 48cm. F2: Gray shales having unit thickness of 7 110cm and often interrupted by 2 -7cm thick calcareous red beds and/or gypsum layers. Alteration of few beds in yellowish clay layers are also observed. Additionally, (20cm) thick ferruginous shale layer is present, characterized by mica, ferrous micro nodules, and several gypsum layers	NA	katrol Formation	105650	107534
217	25-06-2024	GSPL_Bhuj_ 147/06/24	23.17128	69.69256	Jadura	Continuation of the 134/06/24 succession, along the Dhunaraja Dam Road, hill scarp section, near Dhunaraja dam, in the vicinity of Bhuj Reserve Forest	In the stratigraphic continuation upwards in continuation from the 134/06/24 location, same kind of facies. F1: Sst consisting of millimetre to 1 cm thick, plane parallal laminated layers/beds, occassionally amalgamated.The sst layers are seperated by mm thin shales and/or gypsum layers. Unit thickness varies from 5cm 48cm.F2: Gray shales having unit thickness of 7 110cm and often interrupted by 2 -7cm thick calcareous red beds and/or gypsum layers. Alteration of few beds in yellowish clay layers are also observed.Additionally, (20cm) thick ferruginous shale layer is present, characterized by mica, ferrous micro nodules, and several gypsum layers	NA	katrol Formation	105651	107535
218	25-06-2024	GSPL_Bhuj_ 148/06/24	23.17042	69.69250	Jadura	End of log location of 147/06/24	sandstone increases up the succession, very weathered, bare insitu rocks	NA	katrol Formation	NA	NA
219	25-06-2024	GSPL_Bhuj_ 149/06/24	23.16675	69.73747	Reha Nana	Hill section,near New Cart Road,near Reha Nana Village	Medium to fine grained whitish sandstone	110 -290/6SW	katrol Formation	NA	NA
220	25-06-2024	GSPL_Bhuj_ 150/06/24	23.16548	69.73697	Reha Nana	Hill section,near New Cart Road,near Reha Nana Village	The succession comprises medium _ to finegrained sandstone, potentially containing quartz and apatite, which displays a butcher's knife weathering pattern that sets it apart from the surrounding rocks. Overlies coarse grained sandstone with scattered pebbles. Notably, the Tuffite layered nodular layer is absent in this succession.	NA	Bhuj -Katrol contact	105652	107536

Sl. No.	Date	Location No.	Latitude	Longitude	Village/ Area	Exposure Location	Host Lithology	Azimuth	Stratigraphy	Original BR ID	New BR ID
221	26-06-2024	GSPL_Bhuj_ 151/06/25	23.14156	69.47603		Road side section on a cart road within open scrub of Modiwara Jungle, NE of Wadasar village.	Occurrence of dolerite/basalt within Katrol Formation.	NA	Katrol Formation	105653	107537
222	26-06-2024	GSPL_Bhuj_ 152/06/24	23.17840	69.58534	Bharasar	Near Swami Narayan temple, road side stream channel on Bharasar Road, in the vicinity of Wandhsim Reserve Forest	Occurrence of thickly bedded medium to coarse grained sandstone. Moderately wide 5 -7m, 2nd order stream Moderately biogenic and high anthropogeic contamination.	NA	Katrol Formation	NA	NA
223	26-06-2024	GSPL_Bhuj_ 153/06/24	23.18444	69.59503	Vandh sim	Road side stream channel, near Vandh Sim village on Bharasar road, in the vicinity of Wandhsim Reserve Forest.	Occurrence of thickly bedded medium to coarse grained sandstone. Wide 10 -12m,3rd order stream. Very high anthropogeic and biogenic contaminations.	NA	Katrol Formation	NA	NA
224	27-06-2024	GSPL_Bhuj_ 154/06/24	23.19819	69.67354	Tapkeshwari temple	Road side stream channel, near Tapkeshwari Temple on Tapkeswari road	Occurrence of thickly bedded medium to coarse grained sandstone with differential leaching throughout the outcrop. At the confluence of two narrow 2nd order and 3rd order streams of width 2 _3m. The streams meander. Sample has been taken from 3rd oder streams.High anthropogeic and low biogenic contaminations.	NA	Bhuj Formation	NA	NA
225	27-06-2024	GSPL_Bhuj_ 155/06/24	23.22405	69.49290	Fotdi	Hill outcrop, near Fotdi village and Fotdi road.	Occurrence of planar parallal and planar cross stratified coarse grained sst.Some amount of encrustation at the top of the sst is observed. Sst comprises of quartz, feldspar with a light colour matrix. Area of alkali plug marked by different publications and GSI. However no plug has been observed in the field	NA	Bhuj Formation	105657	107541
226	27-06-2024	GSPL_Bhuj_ 156/06/23	23.22796	69.50385	Fotdi	Hill outcrop near Fotdi village, approximately 100m away from the unmetalled road in the SW direction from Fotdi Kodki road.	Occurrence of pebbly sandstone with brecciation effect and metasomatized effect	NA	Bhuj Formation	NA	NA
227	27-06-2024	GSPL_Bhuj_ 157/06/24	23.23155	69.48264	Fotdi	Near Fotdi village, approximately 1.2km away from the cart track in the Northern direction. Area has uneven topography with few mounds of exposed sst outcrops.	Occurrence of planar cross stratified, medium to coarse grained sst within the area of reported alkaline plugs. However, no evidence of igneous activity encountered here	NA	Bhuj Formation	105658	107542
228	27-06-2024	GSPL_Bhuj_ 158/06/24	23.25237	69.74468	Gada	Near Gada village, Hill scarp section	Intrusion of very fine grained melanocratic rock within the Bhuj Sandstone, occuring at lower contour of the hill. Trend of intrusion 120-300	NA	Bhuj Formation	105659	107543

Sl. No.	Date	Location No.	Latitude	Longitude	Village/ Area	Exposure Location	Host Lithology	Azimuth	Stratigraphy	Original BR ID	New BR ID
229	28-06-2024	GSPL_Bhuj_ 159/06/24	23.19947	69.51124	Samatra	Near Bhuj Naliya highway, near Nagiyari cricket ground, approx 20m away from the unmetalled road.	Occurrence of planar cross stratified coarse to medium grained sst with scattered pebbles along the stratification. Evidence of baking in the sst, possible trend of fluid movement is 130 -310. Location of reported phosphorite, however not encountered.	150-330/6SE 126 -306/6SE	Bhuj Formation	105661	107545
230	28-06-2024	GSPL_Bhuj_ 159/06/24	23.19947	69.51124	Samatra	Near Bhuj Naliya highway, near Nagiyari cricket ground, approx 20m away from the unmetalled road.	Occurrence of planar cross stratified coarse to medium grained sst with scattered pebbles along the stratification. Evidence of baking in the sst, possible trend of fluid movement is 130 -310. Location of reported phosphorite, however not encountered.	NA	Bhuj Formation	105662	107546
231	28-06-2024	GSPL_Bhuj_ 160/06/24	23.22709	69.48366	Fotdi	Near Fotdi village, stream cutting small mounds of sandstone, ~1km north of the Fotdi Kodki metal road	Occurence of ferruginous sandstone. Narrow, meandering, 2nd order, very mature stream draining the Bhuj sandstone and possibly alkaline plug mapped by GSI. The breadth of the river is 3 5m.No anthropogenic and less biogenic contaminations are seen.	NA	Bhuj Formation	NA	NA
232	28-06-2024	GSPL_Bhuj_ 161/06/24	23.22816	69.48815	Fotdi	Near Fotdi village,cricket ground,Shree Shiv Natha Mahadev temple, accessible from Fotdi Kodki metal road.	Occurence of ferruginous sandstone. Narrow, meandering, 2nd order, very mature stream draining the Bhuj sandstone and possibly alkaline plug mapped by GSI. Sample collected just after the confluence of 1st order and 2nd order streams.No anthropogeic and no biogenic contamination seen.The breadth of the river is 3 -5m.	NA	Bhuj Formation	NA	NA
233	28-06-2024	GSPL_Bhuj_ 162/06/24	23.22697	69.49905	Fotdi	Near Fotdi village,approx 700m east of Shree Shiv Natha Mahadev temple, accessible from Fotdi Kodki metal road.	Occurence of ferruginous sandstone. Narrow, meandering, 2nd order stream, just after the confluence of two 1st order streams. High biogenic and nearly no anthropogeic contaminations.The breadth of the river is 2-2.5m.	NA	Bhuj Formation	105666	107550
234	28-06-2024	GSPL_Bhuj_ 163/06/24	23.22384	69.52438	Fotdi	Near Rati Tala,Hanuman Temple,roadside digged and dumped rocks.However whole area is farmland.	The only exposure here is yellowish white coloured coarse to medium grain sst having quartz and white transparent elongated crystals,clast supported almost no matrix. The sandstone occur in association with blackish brown coloured, very coarse grained sandstone.	NA	Bhuj Formation	105667	107551
235	29-06-2024	GSPL_Bhuj_ 164/06/24	23.22097	69.59036	Kalyanpar	Near Kalyanpar village at Shree Hari Visamo Tekdi Temple.	Part of the hill is of basalt dyke intruded reddish brown colored massive duricrusted sandstone, overlying a scree deposit of white clay clasts embedded in a finer groundmass. Network of veins of hematite cross cutting the sandstone is observed.	NA	Bhuj Formation	105668	107552

Sl. No.	Date	Location No.	Latitude	Longitude	Village/ Area	Exposure Location	Host Lithology	Azimuth	Stratigraphy	Original BR ID	New BR ID
236	29-06-2024	GSPL_Bhuj_ 164/06/24	23.22097	69.59036	Kalyanpar	Near Kalyanpar village at Shree Hari Visamo Tekdi Temple.	Part of the hill is of basalt dyke intruded reddish brown colored massive duricrusted sandstone, overlying a scree deposit of white clay clasts embedded in a finer groundmass. Network of veins of hematite cross cutting the sandstone is observed.	NA	Bhuj Formation	NA	NA
237	29-06-2024	GSPL_Bhuj_ 165/06/24	23.22110	69.58984	Kalyanpar	Near Kalayanpur village, at Shri Hari Visamo Takdi temple, at the opposite side of the hill, where basalt has intruded	Part of the hill is of basalt dyke intruded reddish brown colored massive duricrusted sandstone, overlying a scree deposit of white clay clasts embedded in a finer groundmass. Network of veins of hematite cross cutting the sandstone is observed.	NA	Bhuj Formation	105671	107555
238	29-06-2024	GSPL_Bhuj_ 165/06/24	23.22110	69.58984	Kalyanpar	Near Kalayanpur village, at Shri Hari Visamo Takdi temple, at the opposite side of the hill, where basalt has intruded	Part of the hill is of basalt dyke intruded reddish brown colored massive duricrusted sandstone, overlying a scree deposit of white clay clasts embedded in a finer groundmass. Network of veins of hematite cross cutting the sandstone is observed.	NA	Bhuj Formation	105672	107556
239	29-06-2024	GSPL_Bhuj_ 166/06/24	23.13652	69.66414	Bharapar	Near Kirgurya Dungar,near Bharapar village at north of Sapar timbo village,Hemkund Horticulture farm.	Occurrence of basalt intrusion within Bhuj sandstone. Very narrow (±2m) 2nd order meandering stream. Sample collected after the confluence of two 1st order streams. Very less biogenic and anthropogenic contamination seen.	NA	Bhuj Formation	NA	NA
240	29-06-2024	GSPL_Bhuj_ 167/06/24	23.18286	69.63318	Sedata	600_700m SW of shree supashva jain animal hospital. Reported phosphorite location.	Successive occurrence of sets of plane parallel laminated quarztose sandstone (6 28cm, occassionally amalgamated upto 60cm) alternating with mm thin laminated shale siltstone alternation (8 15cm) and topped by white crystalline type fine grained sandstone (phosphorite ???), Reported phosphorite location of GSI.	130-Sub-horizontal	Katrol Formation	105675	107559
241	29-06-2024	GSPL_Bhuj_ 167/06/24	23.18286	69.63318	Sedata	600 _700m SW of shree supashva jain animal hospital. Reported phosphorite location.	Successive occurrence of sets of plane parallel laminated quarztose sandstone (6 28cm, occassionally amalgamated upto 60cm) alternating with mm thin laminated shale siltstone alternation (8 15cm) and topped by white crystalline type fine grained sandstone (phosphorite ???), Reported phosphorite location of GSI.	NA	Katrol Formation	105676	107560
242	29-06-2024	GSPL_Bhuj_ 167/06/24	23.18286	69.63318	Sedata	600 -700m SW of shree supashva jain animal hospital. Reported phosphorite location.	Successive occurrence of sets of plane parallel laminated quarztose sandstone (6 28cm, occassionally amalgamated upto 60cm) alternating with mm thin laminated shale siltstone alternation (8 15cm) and topped by white crystalline type fine grained sandstone (phosphorite ???), Reported phosphorite location of GSI.	NA	Katrol Formation	105677	107561

Sl. No.	Date	Location No.	Latitude	Longitude	Village/ Area	Exposure Location	Host Lithology	Azimuth	Stratigraphy	Original BR ID	New BR ID
243	29-06-2024	GSPL_Bhuj_ 167/06/24	23.18286	69.63318	Sedata	600-700m SW of shree supashva jain animal hospital. Reported phosphorite location.	Successive occurrence of sets of plane parallel laminated quarztose sandstone (6 28cm, occassionally amalgamated upto 60cm) alternating with mm thin laminated shale siltstone alternation (8 15cm) and topped by white crystalline type fine grained sandstone (phosphorite ???), Reported phosphorite location of GSI.	NA	Katrol Formation	105678	107562
244	29-06-2024	GSPL_Bhuj_ 167/06/24	23.18286	69.63318	Sedata	600 -700m SW of shree supashva jain animal hospital. Reported phosphorite location.	Successive occurrence of sets of plane parallel laminated quarztose sandstone (6 28cm, occassionally amalgamated upto 60cm) alternating with mm thin laminated shale siltstone alternation (8 15cm) and topped by white crystalline type fine grained sandstone (phosphorite ???), Reported phosphorite location of GSI.	NA	Katrol Formation	105679	107563
245	29-06-2024	GSPL_Bhuj_ 167/06/24	23.18286	69.63318	Sedata	600-700m SW of shree supashva jain animal hospital. Reported phosphorite location.	Successive occurrence of sets of plane parallel laminated quarztose sandstone (6 28cm, occassionally amalgamated upto 60cm) alternating with mm thin laminated shale siltstone alternation (8 15cm) and topped by white crystalline type fine grained sandstone (phosphorite ???), Reported phosphorite location of GSI.	NA	Katrol Formation	105680	107564
246	21-08-2024	GSPL_Bhuj_ 155/06/24	23.22420	69.49274	Fotdi	Sample point is located near Fotdi village, approximately 120m away from the unmetalled road in the West direction from the same location as 155/06/24 . Area has uneven topography, with small mounts of upto 20m high from the surrounding area. Sandstone hillock is drained by nearby channel, where the highest TREE values were found & can be a possible source of the high anomalous values of Nb, Zn, V, Cr.	Occurrence of buff coloured, coarse grained sst, with some amount of encrustation / baking effect, visible at the top of the mount. Sst comprises of quartz, feldspar with a light colour matrix. Area of alkali plug marked by different publications and GSI. However no plug has been observed in the field	NA	Bhuj Formation	NA	107565

Sl. No.	Date	Location No.	Latitude	Longitude	Village/ Area	Exposure Location	Host Lithology	Azimuth	Stratigraphy	Original BR ID	New BR ID
247	21-08-2024	GSPL_Bhuj_ 156/06/24	23.22759	69.50403	Fotdi	Sample point is located near Fotdi village, approximately 100m away from the unmetalled road in the SW direction from Fotdi Kodki road. Area has rolling topography with few small hillocks. Outcrop shows parallel bedding dipping 120 towards West direction.	2 types of sst are observed over this mound. Occurence of brownish mauve coloured, planar cross stratified, medium coarse grain sst with (metasomatized effect) & encrustation on the upper surface. small pebbles are observed to be scattered within the sandstone. It comprisies of quartz, feldspar with light colour matrix & some dark brown parallel bedding within the outcrop. White colour, medium coarse grain sst comprising of quartz & feldspar.	30 -210/4SE	Bhuj Formation	107566	107566
248	21-08-2024	GSPL_Bhuj_ 156/06/24	23.22759	69.50403	Fotdi	Sample point is located near Fotdi village, approximately 100m away from the unmetalled road in the SW direction from Fotdi Kodki road. Area has rolling topography with few small hillocks. Outcrop shows parallel bedding dipping 120 towards West direction.	3 types of sst are observed over this mound. Occurence of brownish mauve coloured, planar cross stratified, medium coarse grain sst with (metasomatized effect) & encrustation on the upper surface. small pebbles are observed to be scattered within the sandstone. It comprisies of quartz, feldspar with light colour matrix & some dark brown parallel bedding within the outcrop. White colour, medium coarse grain sst comprising of quartz & feldspar.	NA	Bhuj Formation	107567	107567
249	21-08-2024	GSPL_Bhuj_ 157/06/24	23.22907	69.47871	Fotdi	Sample point is located near Fotdi village, approximately 1.2km away from the cart track in the Northern direction. Area has uneven topography with few mounds of exposed sst outcrops. There are 3 4 different types of sst encountered at different elevation from where sample was collected, which tends to be the possible source of previously collected anomalous SS sediment values.	3 - 4 types of sst are observed over an 1.2km span. Brownish mauve coloured, medium coarse grain sst with little encrustation encountered at the top of small mound. Light weight, yellowish orange colour, medium coarse grain sst comprising of quartz & feldspar minerals. Very fragile, white colour sst showing planar cross startification	NA	Bhuj Formation	107568	107568

Sl. No.	Date	Location No.	Latitude	Longitude	Village/ Area	Exposure Location	Host Lithology	Azimuth	Stratigraphy	Original BR ID	New BR ID
250	21-08-2024	GSPL_Bhuj_ 157/06/24	23.22907	69.47871	Fotdi	Sample point is located near Fotdi village, approximately 1.2km away from the cart track in the Northern direction. Area has uneven topography with few mounds of exposed sst outcrops. There are 3 4 different types of sst encountered at different elevation from where sample was collected, which tends to be the possible source of previously collected anomalous SS sediment values.	4 types of sst are observed over an 1.2km span. Brownish mauve coloured, medium coarse grain sst with little encrustation encountered at the top of small mound. Light weight, yellowish orange colour, medium coarse grain sst comprising of quartz & feldspar minerals. Very fragile, white colour sst showing planar cross startification	NA	Bhuj Formation	107569	107569
251	21-08-2024	GSPL_Bhuj_ 157/06/24	23.22907	69.47871	Fotdi	Sample point is located near Fotdi village, approximately 1.2km away from the cart track in the Northern direction. Area has uneven topography with few mounds of exposed sst outcrops. There are 3 4 different types of sst encountered at different elevation from where sample was collected, which tends to be the possible source of previously collected anomalous SS sediment values.	5 - 4 types of sst are observed over an 1.2km span. Brownish mauve coloured, medium coarse grain sst with little encrustation encountered at the top of small mound. Light weight, yellowish orange colour, medium coarse grain sst comprising of quartz & feldspar minerals.Very fragile, white colour sst showing planar cross startification	NA	Bhuj Formation	107570	107570
252	21-08-2024	GSPL_Bhuj_ 157/06/24	23.22907	69.47871	Fotdi	Sample point is located near Fotdi village, approximately 1.2km away from the cart track in the Northern direction. Area has uneven topography with few mounds of exposed sst outcrops. There are 3 4 different types of sst encountered at different elevation from where sample was collected, which tends to be the possible source of previously collected anomalous SS sediment values.	6 4 types of sst are observed over an 1.2km span. Brownish mauve coloured, medium coarse grain sst with little encrustation encountered at the top of small mound. Light weight, yellowish orange colour, mediumcoarse grain sst comprising of quartz & feldspar minerals. Very fragile, white colour sst showing planar cross startification	NA	Bhuj Formation	107571	107571

Sl. No.	Date	Location No.	Latitude	Longitude	Village/ Area	Exposure Location	Host Lithology	Azimuth	Stratigraphy	Original BR ID	New BR ID
253	22-08-2024	GSPL_Bhuj_ 136/06/24	23.16082	69.72329	Reha Mota	Hilly exposure near Reha Nana village, approximately 1 km away from the cart road. Area has uneven topography with few river channels draining the area. Sample is collected form the same location as 136/06/24. This area is the highest catchment of high TREE value SS sediments & the possible source of the anomalous value of the elements.	Exposure of planar, with undulatory bed boundaries, coarse grained sandstone. The thickness of this sandstone ranges from 20 to 60 cm and separated by thin (2 -7 cm) completely altered, brecciated type red beds altered red beds (cherry red in colour, nodular appearance, with scattered mica grains, embedded in a buff coloured groundmas. No other identifiable grains).These layers follow the sandstone boundary.	NA	Bhuj Formation	107572	107572
254	22-08-2024	GSPL_Bhuj_ 136/06/24	23.16118	69.72477	Reha Mota	Hilly exposure near Reha Nana village, approximately 1 km away from the cart road. Area has uneven topography with few river channels draining the area. Sample is collected form the same location as 114/06/24. This area is the highest catchment of high TREE value SS sediments & the possible source of the anomalous value of the elements.	Occurrence of heterolithic unit of shale/siltstone and thinly bedded rippled topped brownish mauve coloured sandstone, interrupted by claystone/ironstone.	NA	Katrol Formation	107573	107573
255	22-08-2024	GSPL_Bhuj_ 136/06/24	23.16118	69.72477	Reha Mota	Hilly exposure near Reha Nana village, approximately 1 km away from the cart road. Area has uneven topography with few river channels draining the area. Sample is collected form the same location as 114/06/24. 1.5 - 2m, protruding sst outcrops along river channel. This area is the highest catchment of high TREE value SS sediments & the possible source of the anomalous value of the elements.	Occurrence of heterolithic unit of shale/siltstone and thinly bedded rippled topped brownish mauve coloured sandstone, interrupted by claystone/ironstone.	NA	Katrol Formation	107574	107574

Sl. No.	Date	Location No.	Latitude	Longitude	Village/ Area	Exposure Location	Host Lithology	Azimuth	Stratigraphy	Original BR ID	New BR ID
256	22-08-2024	GSPL_Bhuj_ 168/08/24	23.14830	69.72647	Reha Nana	The sample point is located near Reha Nana village, area near SS sediment having high HLS value. Area has uneven topography with a river channel draining both the Katrol & Bhuj formation. Sample taken from the bed rock exposures of sst in dry river channel approx 20m South from the unmetalled road. 1.5 -2m, protruding sst outcrops along river channel.	The succession consist of medium _ fine grain, grayish white sst which is 70cm above surface & is interbedded with medium _ coarse buff coloured sst having little encrustations on top of it	NA	Bhuj Katrol contact	107575 A	107575 A
257	22-08-2024	GSPL_Bhuj_ 168/08/24	23.14830	69.72647	Reha Nana	The sample point is located near Reha Nana village, area near SS sediment having high HLS value. Area has uneven topography with a river channel draining both the Katrol & Bhuj formation. Sample taken from the bed rock exposures of sst in dry river channel approx 20m South from the unmetalled road. 1.5 -2m, protruding sst outcrops along river channel.	The succession consist of medium _ fine grain, grayish white sst which is 70cm above surface & is interbedded with medium _ coarse buff coloured sst having little encrustations on top of it	NA	Bhuj _Katrol contact	107575 B	107575 B
258	22-08-2024	GSPL_Bhuj_ 168/08/24	23.14830	69.72647	Reha Nana	The sample point is located near Reha Nana village, area near SS sediment having high HLS value. Area has uneven topography with a river channel draining both the Katrol & Bhuj formation. Sample taken from the bed rock exposures of sst in dry river channel approx 20m South from the unmetalled road. 1.5-2m, protruding sst outcrops along river channel.	The succession consist of medium _ fine grain, grayish white sst which is 70cm above surface & is interbedded with medium _ coarse buff coloured sst having little encrustations on top of it	NA	Bhuj Katrol contact	107575	107575

Sl. No.	Date	Location No.	Latitude	Longitude	Village/ Area	Exposure Location	Host Lithology	Azimuth	Stratigraphy	Original BR ID	New BR ID
259	22-08-2024	GSPL_Bhuj_ 159/06/24	23.19947	69.51124	Samatra	The sample point is taken near Bhuj Naliya highway, near Nagiyari cricket ground, approx 20m away from the unmetalled road. Area has small mound of over an height of 10m. Sample is taken at same location from GSPL_Bhuj_159/06/24. The area is nearest to SS point having high TREE values with anomalous high values for specific elements.	The area consist of brownish mauve coloured, planar cross laminated, coarse to medium grained sst with scattered pebbles along the cross stratification. Few sst at top of hill shows evidences of encrustation possibly due to fumaroles?.	NA	Bhuj Formation	107576	107576
260	22-08-2024	GSPL_Bhuj_ 159/06/24	23.19947	69.51124	Samatra	The sample point is taken near Bhuj Naliya highway, near Nagiyari cricket ground, approx 20m away from the unmetalled road. Area has small mound of over an height of 10m. Sample is taken at same location from GSPL_Bhuj_159/06/24. The area is nearest to SS point having high TREE values with anomalous high values for specific elements.	The area consist of brownish mauve coloured, planar cross laminated, coarse to medium grained sst with scattered pebbles along the cross stratification. Few sst at top of hill shows evidences of encrustation possibly due to fumaroles?.	NA	Bhuj Formation	107577	107577
261	22-08-2024	GSPL_Bhuj_ 159/06/24	23.19947	69.51124	Samatra	The sample point is taken near Bhuj Naliya highway, near Nagiyari cricket ground, approx 20m away from the unmetalled road. Area has small mound of over an height of 10m. Sample is taken at same location from GSPL_Bhuj_159/06/24. The area is nearest to SS point having high TREE values with anomalous high values for specific elements.	The area consist of brownish mauve coloured, planar cross laminated, coarse to medium grained sst with scattered pebbles along the cross stratification. Few sst at top of hill shows evidences of encrustation possibly due to fumaroles?.	NA	Bhuj Formation	107578	107578
262	14-11-2024	GSPL_Bhuj_ 168/11/2024	23.22365	69.65894	Mirjapur	Road cut section, along the Bhuj Mundra highway	Occurrence of coarse grained ferruginous sandstone with laterite caping	NA	Bhuj Formation	108901	108901
263	14-11-2024	GSPL_Bhuj_ 168/11/2024	23.22365	69.65894	Mirjapur	Road cut section, along the Bhuj Mundra highway	Occurrence of coarse grained ferruginous sandstone with laterite caping	NA	Bhuj Formation	108902	108902

Sl. No.	Date	Location No.	Latitude	Longitude	Village/ Area	Exposure Location	Host Lithology	Azimuth	Stratigraphy	Original BR ID	New BR ID
264	14-11-2024	GSPL_Bhuj_ 169/11/2024	23.19767	69.64542	Bhata Talav	Road cut section, along the Bhuj Mundra highway	Rich fossiliferous limestone bed	NA	Chari Formation	108903	108903
265	14-11-2024	GSPL_Bhuj_ 169/11/2024	23.19767	69.64542	Bhata Talav	Road cut section, along the Bhuj Mundra highway	Rich fossiliferous limestone bed	NA	Chari Formation	108904	108904
266	14-11-2024	GSPL_Bhuj_ 170/11/2024	23.19369	69.64168	Bhata Talav	Road cut section, along the Bhuj Mundra highway	Brownish clay bed with sandy clay rich layer. Brown layer homogenous in naturealternated with white sandy layer.	NA	Katrol Formation	108905	108905
267	14-11-2024	GSPL_Bhuj_ 171/11/2024	23.18595	69.64069	Bhata Talav	Road cut section, along the Bhuj Mundra highway, in the vicinity of Bhuj Reserve Forest	Heterolithic unit consist of shale (grey, white with goethitic and ferruginous patches, interupted by well developed Tuffite layers alternating with 10 -20cm thick sandstone layers and/or thinly laminated shale siltstone unit	NA	Katrol Formation	108906	108906
268	14-11-2024	GSPL_Bhuj_ 172/11/2024	23.17908	69.63861	Sanatorium	River channel exposure, near sanatorium, on Bhuj Mundra Road	Exposure of sandstone at the river bed. East to west flowing river with gravels, boulder sand and fines on the riverbed.	NA	Contact of Bhuj_Katrol	108909	108909
269	14-11-2024	GSPL_Bhuj_ 172/11/2024	23.17908	69.63861	Sanatorium	River channel exposure, near sanatorium, on Bhuj Mundra Road	Exposure of sandstone at the river bed. East to west flowing river with gravels, boulder sand and fines on the riverbed.	NA	Contact of Bhuj Katrol	108910	108910
270	14-11-2024	GSPL_Bhuj_ 173/11/2024	23.16671	69.64349	Sanatorium	Road cut section, along the Bhuj Mundra highway	Thinly bedded medium to coarse grained redish brown colored sandstone	NA	Bhuj Formation	108911	108911
271	14-11-2024	GSPL_Bhuj_ 174/11/2024	23.16561	69.64349	Sanatorium	Road cut section, along the Bhuj Mundra highway	Thinly bedded medium to coarse grained redish brown colored sandstone	NA	Bhuj Formation	108912	108912
272	14-11-2024	GSPL_Bhuj_ 175/11/2025	23.16457	69.63296	Sanatorium	Road cut section, along the Bhuj Mundra highway	Thinly bedded medium to coarse grained redish brown colored sandstone	NA	Bhuj Formation	108913	108913
273	14-11-2024	GSPL_Bhuj_ 91/01/24	23.15070	69.58000	Naranpar Ravli	Near Naranpar Ravli village, Hill cut section for pipeline installation	Heterolithic unit consist of shale (grey, white with goethitic and ferruginous pstches, interupted by well developed Tuffite layers alternating with 10 20cm thick sandstone layers and/or thinly laminated shale-siltstone unit	NA	katrol Formation	108914	108914
274	14-11-2024	GSPL_Bhuj_ 91/01/24	23.15070	69.58000	Naranpar Ravli	Near Naranpar Ravli village, Hill cut section for pipeline installation	Heterolithic unit consist of shale (grey, white with goethitic and ferruginous pstches, interupted by well developed Tuffite layers alternating with 10 20cm thick sandstone layers and/or thinly laminated shale-siltstone unit	NA	katrol Formation	108915	108915
275	14-11-2024	GSPL_Bhuj_ 91/01/24	23.15070	69.58000	Naranpar Ravli	Near Naranpar Ravli village, Hill cut section for pipeline installation	Heterolithic unit consist of shale (grey, white with goethitic and ferruginous pstches, interupted by well developed Tuffite layers alternating with 10 20cm thick sandstone	NA	katrol Formation	108916	108916

Sl. No.	Date	Location No.	Latitude	Longitude	Village/ Area	Exposure Location	Host Lithology	Azimuth	Stratigraphy	Original BR ID	New BR ID
							layers and/or thinly laminated shale-siltstone unit				
276	15-11-2024	GSPL_Bhuj_ 177/11/2024	23.18982	69.76442	Ler	Road side exposure,accessible from Ler Hanuman Road.	The succession consist of 4 GSPL_Bhuj_7 cm thick compact,hard, indurated and ferruginous Tuffite layered bed alternating with sandstone and gypsum layer	60/20 SE, 60/60SE	katrol Formation	108917	108917
277	15-11-2024	GSPL_Bhuj_ 177/11/2024	23.18982	69.76442	Ler	Road side exposure,accessible from Ler Hanuman Road,100 m west from previous location no 177/11/2024	The succession consist of 4 -7 cm thick compact,hard, indurated and ferruginous Tuffite layered bed alternating with sandstone and gypsum layer (fault zone?)	NA	katrol Formation	108918	108918
278	15-11-2024	GSPL_Bhuj_ 178/11/2024	23.17822	69.76852	Ler	Road side exposure along the range of the hills, accessible from Ler Hanuman Road.	The succession consists 2 -5 cm thick compact,hard, indurated and ferruginous Tuffite layered bed alternating with sandstone and gypsum layer	NA	katrol Formation	108919	108919
279	15-11-2024	GSPL_Bhuj_ 179/11/2024	23.17298	69.76743	Wadwa	Road side exposure along the range of the hills, accessible from Ler Hanuman Road.	Occurrence of Tuffite layer with compact,cherty ferruginous sandstone of several layers(thickning upwards sequence) consists highly angular quartz	60/25 SE	katrol Formation	108920	108920
280	15-11-2024	GSPL_Bhuj_ 179/11/2024	23.17298	69.76743	Wadwa	Road side exposure along the range of the hills, accessible from Ler Hanuman Road.	Occurrence of Tuffite layer with compact,cherty ferruginous sandstone of several layers(thickning upwards sequence) consists highly angular quartz	NA	katrol Formation	108921	108921
281	15-11-2024	GSPL_Bhuj_ 179/11/2024	23.17298	69.76743	Wadwa	Road side exposure along the range of the hills, accessible from Ler Hanuman Road, further 50m south of previous location	Occurrence of Tuffite layer with shale of several layers	NA	katrol Formation	108922	108922
282	15-11-2024	GSPL_Bhuj_ 180/11/2024	23.16446	69.76858	Wadwa	Road side exposure,accessible from a metal road through Ler Hanuman Road.	Occurrence of Tuffite layer with shale of several layers	NA	katrol Formation	NA	NA
283	15-11-2024	GSPL_Bhuj_ 181/11/2024	23.16541	69.78397	Wadwa	Road side exposure,accessible from a metal road through Ler Hanuman Road.	Thinly bedded medium to coarse grained redish brown colored sandstone	NA	Bhuj Formation	108923	108923
284	15-11-2024	GSPL_Bhuj_ 182/11/2024	23.19592	69.76337	Ler	Hilly exposure near Ler village, accessible from a metal road through Ler to Bhujodia	Occurrence of Tuffite layer with shale of several layers	NA	katrol Formation	108924	108924
285	15-11-2024	GSPL_Bhuj_ 183/11/2024	23.23856	69.74810	Bhujodia	NA	NA	NA	NA	108925	108925

Sl. No.	Date	Location No.	Latitude	Longitude	Village/ Area	Exposure Location	Host Lithology	Azimuth	Stratigraphy	Original BR ID	New BR ID
286	16-11-2024	GSPL_Bhuj_184/11/2024	23.18752	69.49638	Wandhaya	Road side exposure,accessible from a metal road through Samatra Vadasara Road	Occurrence of Tuffite layer bed with limestone,fine grained sandstone,siltstone	195/30 NW	Chari Formation	108926	108926
287	16-11-2024	GSPL_Bhuj_184/11/2024	23.18752	69.49638	Wandhaya	Road side exposure,accessible from a metal road through Samatra Vadasara Road	Occurrence of Tuffite layer bed with limestone,fine grained sandstone,siltstone	NA	Chari Formation	108927	108927
288	16-11-2024	GSPL_Bhuj_185/11/2024	23.18858	69.49248	Wandhaya	Road side exposure,accessible from a metal road through Samatra Vadasara Road	Occurrence of ferrugenous sandstone with metasomatized effect and yellow ocher colored sandstone	NA	Chari Formation	108928	108928
289	16-11-2024	GSPL_Bhuj_186/11/2024	23.18149	69.49138	Wandhaya	Road side exposure,accessible from a metal road through Samatra Vadasara Road	Heterolithic unit consist of shale (grey, white with goethitic and ferruginous patches, interupted by well developed Tuffite layers alternating with layers of thinly laminated shale siltstone unit. Dyke highly weathered of quartz??Lower part of the succession gypsum layer observed	320/25 NE	Katrol Formation	108929	108929
290	16-11-2024	GSPL_Bhuj_186/11/2024	23.18149	69.49138	Wandhaya	Road side exposure,accessible from a metal road through Samatra Vadasara Road	Heterolithic unit consist of shale (grey, white with goethitic and ferruginous patches, interupted by well developed Tuffite layers alternating with layers of thinly laminated shale siltstone unit. Dyke highly weathered of quartz??Lower part of the succession gypsum layer observed	NA	Katrol Formation	108930	108930
291	16-11-2024	GSPL_Bhuj_186/11/2024	23.18149	69.49138	Wandhaya	Road side exposure,accessible from a metal road through Samatra Vadasara Road	Heterolithic unit consist of shale (grey, white with goethitic and ferruginous patches, interupted by well developed Tuffite layers alternating with layers of thinly laminated shale siltstone unit. Dyke highly weathered of quartz??Lower part of the succession gypsum layer observed	NA	Katrol Formation	108931	108931
292	16-11-2024	GSPL_Bhuj_186/11/2024	23.18149	69.49138	Wandhaya	Road side exposure,accessible from a metal road through Samatra Vadasara Road	Heterolithic unit consist of shale (grey, white with goethitic and ferruginous patches, interupted by well developed Tuffite layers alternating with layers of thinly laminated shale siltstone unit. Dyke highly weathered of quartz??Lower part of the succession gypsum layer observed	NA	Katrol Formation	108932	108932
293	16-11-2024	GSPL_Bhuj_187/11/2024	23.15333	69.46531	Modiwara Jung	Road side exposure,accessible from Samatra Vadasara Road	Occurrence of ferrugenous sandstone with metasomatized effect and yellow ocher colored sandstone. Thin beds of iron with concretion ochre red colour. Contact of Chari and Katrol??	305/10 SW	Katrol Formation	108933	108933

Sl. No.	Date	Location No.	Latitude	Longitude	Village/ Area	Exposure Location	Host Lithology	Azimuth	Stratigraphy	Original BR ID	New BR ID
294	16-11-2024	GSPL_Bhuj_187/11/2024	23.15333	69.46531	Modiwara Jung	Road side exposure,accessible from Samatra Vadasara Road	Occurrence of ferrugenous sandstone with metasomatized effect and yellow ocher colored sandstone. Thin beds of iron with concretion ochre red colour. Contact of Chari and Katrol??	NA	Chari Formation	108934	108934
295	16-11-2024	GSPL_Bhuj_188/11/2024	23.13712	69.45846	Modiwara Jung	Road side exposure,accessible from Samatra Vadasara Road	Occurrence of large concretion with high mass is observed with less ferruginous part,highly compact, dark in colour.	184/5 SW	Katrol Formation	108935	108935
296	16-11-2024	GSPL_Bhuj_189/11/2024	23.12668	69.43958	Wadasar	Road side exposure,accessible from Samatra Vadasara Road	Occurrence of basaltic volcanics with sandstone	NA	Bhuj Formation	NA	NA
297	16-11-2024	GSPL_Bhuj_190/11/2024	23.11300	69.44527	Wadasar	Road side exposure,accessible from Samatra Vadasara Road	Thinly bedded medium to coarse grained redish brown colored sandstone	NA	Bhuj Formation	NA	NA
298	16-11-2024	GSPL_Bhuj_191/11/2024	23.09211	69.44270	Wadasar	Road side exposure,accessible from Samatra Vadasara Road	Thinly bedded medium to coarse grained redish brown colored sandstone	NA	Bhuj Formation	108964	108964
299	16-11-2024	GSPL_Bhuj_192/11/2024	23.19920	69.75820	Ler	Hilly exposure near Ler village, accessible from a metal road through Ler to Bhujodia	Occurrence of gritty sandstone layer consists of granule and pebble sized fresh quartz with fresh feldspar embeded in a ferruginous, goethite matrix/cement. This succession is observed to be interupted by reddish hematitic layer and white pinkish sericitic layer.Occurrence of growth fault at lower northern part of the succession is also observed.	20 -200/4 SE	Bhuj Formation	108936	108936
300	16-11-2024	GSPL_Bhuj_192/11/2024	23.19920	69.75820	Ler	Hilly exposure near Ler village, accessible from a metal road through Ler to Bhujodia	Gritty sandstone with quartz,fresh feldspar,unknown black mineral layer	NA	Bhuj Formation	108937	108937
301	16-11-2024	GSPL_Bhuj_192/11/2024	23.19920	69.75820	Ler	Hilly exposure near Ler village, accessible from a metal road through Ler to Bhujodia	Sandstone(looks like baking/metasomatized effect)	NA	Bhuj Formation	108938	108938
302	17-11-2024	GSPL_Bhuj_192/11/2024	23.19920	69.75820	Ler	Hilly exposure near Ler village, accessible from a metal road through Ler to Bhujodia	Occurrence of gritty sandstone layer consists of granule and pebble sized fresh quartz with fresh feldspar embeded in a ferruginous, goethite matrix/cement. This succession is observed to be interupted by reddish hematitic layer and white pinkish sericitic layer.Occurrence of growth fault at lower northern part of the succession is also observed.	NA	Bhuj Formation	108941	108941

Sl. No.	Date	Location No.	Latitude	Longitude	Village/ Area	Exposure Location	Host Lithology	Azimuth	Stratigraphy	Original BR ID	New BR ID
303	17-11-2024	GSPL_Bhuj_ 192/11/2024	23.19920	69.75820	Ler	Hilly exposure near Ler village, accessible from a metal road through Ler to Bhujodia	Occurrence of gritty sandstone layer consists of granule and pebble sized fresh quartz with fresh feldspar embeded in a ferruginous, goethite matrix/cement. This succession is observed to be interupted by reddish hematitic layer and white pinkish sericitic layer.Occurrence of growth fault at lower northern part of the succession is also observed.	NA	Bhuj Formation	108942	108942
304	17-11-2024	GSPL_Bhuj_ 192/11/2024	23.19920	69.75820	Ler	Hilly exposure near Ler village, accessible from a metal road through Ler to Bhujodia	Occurrence of gritty sandstone layer consists of granule and pebble sized fresh quartz with fresh feldspar embeded in a ferruginous, goethite matrix/cement. This succession is observed to be interupted by reddish hematitic layer and white pinkish sericitic layer.Occurrence of growth fault at lower northern part of the succession is also observed.	NA	Bhuj Formation	108943	108943
305	17-11-2024	GSPL_Bhuj_ 193/11/2024	23.19967	69.73215	Bhujodia	Road side exposure on Bhuj Anjar highway o local cart road through Bhujodia village.	Occurence of very coarse to coarse grained sandstone comprises of quartz grains as freamework,fossils(very well rounded & eliptical),reddish black small nodules and black unknown mineral embedded in carbonate matrix/cement.	80 -260/34N	Chari Formation	108939	108939
306	17-11-2024	GSPL_Bhuj_ 194/11/2024	23.19701	69.72975	Bhujodia	Road side exposure approximately 250 m south of location no.193/11/2024	Occrence of coarse sst.,poorly sorted,triangular,needle shaped quartz,apatite layer with layer consists of sub angular to angular grains of quartz,feldspar,mica,fossils embedded in a silicified matrix. Cherry red colour iron rich layer is ripped of in between?/	NA	Chari Formation	108940	108940
307	17-11-2024	GSPL_Bhuj_ 195/11/24	23.14830	69.72647	Reha Nana	Near Reha Nana village, area near SS sediment having high HLS value. Area has uneven topography with a river channel draining both the Katrol & Bhuj formation. Sample taken from the bed rock exposures of sst in dry river channel approx 20m South from the unmetalled road. 1.5 2m, protruding sst outcrops along river channel.	The succession consist of extensively burrowed metasomatized block,yellowish sandstone interbedded with gritty sandstone and white/thinly bedded clay.Iron leached encrustation observed at the top of extensively burrowed metasomatized block	NA	Bhuj Formation	108944	108944

Sl. No.	Date	Location No.	Latitude	Longitude	Village/ Area	Exposure Location	Host Lithology	Azimuth	Stratigraphy	Original BR ID	New BR ID
308	17-11-2024	GSPL_Bhuj_ 195/11/24	23.14830	69.72647	Reha Nana	Near Reha Nana village, area near SS sediment having high HLS value. Area has uneven topography with a river channel draining both the Katrol & Bhuj formation. Sample taken from the bed rock exposures of sst in dry river channel approx 20m South from the unmetalled road. 1.5 2m, protruding sst outcrops along river channel.	The succession consist of extensively burrowed metasomatized block,yellowish sandstone interbedded with gritty sandstone and white/thinly bedded clay.Iron leached encrustation observed at the top of extensively burrowed metasomatized block	NA	Bhuj Formation	108945	108945
309	17-11-2024	GSPL_Bhuj_ 195/11/24	23.14830	69.72647	Reha Nana	The sample point is located near Reha Nana village, area near SS sediment having high HLS value. Area has uneven topography with a river channel draining both the Katrol & Bhuj formation. Sample taken from the bed rock exposures of sst in dry river channel approx 20m South from the unmetalled road. 1.5 2m, protruding sst outcrops along river channel.	The succession consist of extensively burrowed metasomatized block,yellowish sandstone interbedded with gritty sandstone and white/thinly bedded clay.Iron leached encrustation observed at the top of extensively burrowed metasomatized block	NA	Bhuj Formation	108946	108946
310	17-11-2024	GSPL_Bhuj_ 196/11/24	23.16096	69.72327	Jadura Nana	Road side exposure on local cart road through Jadura Nana village.	Occurrence of posphate in carbonate mud flat	NA	Katrol Formation	108947	108947
311	17-11-2024	GSPL_Bhuj_ 196/11/24	23.16096	69.72327	Jadura Nana	Road side exposure on local cart road through Jadura Nana village.	Occurrence of posphate in carbonate mud flat	NA	Katrol Formation	108948	108948
312	18-11-2024	GSPL_Bhuj_ 159/06/24	23.19977	69.51080	Samatra	Near Bhuj Naliya highway, near Nagiyari cricket ground, approx 20m away from the unmetalled road.	Occurrence of planar cross stratified coarse to medium grained sst with scattered pebbles along the stratification. Evidence of Fe solution imprignation possible trend of fluid movement is 130-310, Chert in decreasing order of abundance, embedded in a ferruginous matrix cement.Blackish layer observed suspecting Amphibole?	150-330/6SE 126 -306/6SE	Bhuj Formation	108949	108949
313	18-11-2024	GSPL_Bhuj_ 159/06/24	23.19977	69.51080	Samatra	Near Bhuj Naliya highway, near Nagiyari cricket ground, approx 20m away from the unmetalled road.	Sandstone with Fe solution imprignation layer	NA	Bhuj Formation	108950	108950

Sl. No.	Date	Location No.	Latitude	Longitude	Village/ Area	Exposure Location	Host Lithology	Azimuth	Stratigraphy	Original BR ID	New BR ID
314	18-11-2024	GSPL_Bhuj_ 159/06/24	23.19977	69.51080	Samatra	Near Bhuj Naliya highway, near Nagiyari cricket ground, approx 20m away from the unmetalled road.	Sandstone with blackish layer probably Amphibole?	NA	Bhuj Formation	108951	108951
315	18-11-2024	GSPL_Bhuj_ 197/11/24	23.22823	69.50400	Fotdi	Hill outcrop near Fotdi village, approximately 100m away from the unmetalled road in the SW direction from Fotdi Kodki road.	Occurrence of pebbly sandstone with brecciation effect and metasomatized effect. Argilic alteration at the fracture zone is observed. Few 10 meter north a massive highly perforated body which is approximately 80 cm thick,brick red in colour and consists of feldspar/Albite suspected from colour) embedded in a iron rich groundmass. Supposedly, the sandstone has altered here through albitic solution(sodic metasomatism).	0 -180/30E	Bhuj Formation	108952	108952
316	18-11-2024	GSPL_Bhuj_ 197/11/24	23.22823	69.50400	Fotdi	Hill outcrop near Fotdi village, approximately 100m away from the unmetalled road in the SW direction from Fotdi Kodki road.	Sandstone(looks like baking/metasomatized effect)	NA	Bhuj Formation	108953	108953
317	18-11-2024	GSPL_Bhuj_ 197/11/24	23.22823	69.50400	Fotdi	Hill outcrop near Fotdi village, approximately 100m away from the unmetalled road in the SW direction from Fotdi Kodki road.	Igneous rock interlocking texture	NA	Bhuj Formation	108954	108954
318	18-11-2024	GSPL_Bhuj_ 197/11/24	23.22823	69.50400	Fotdi	Hill outcrop near Fotdi village, approximately 100m away from the unmetalled road in the SW direction from Fotdi Kodki road.	Very coarse to coarse grained sandstone, whitish layer(maybe argilic alteration)	NA	Bhuj Formation	108955	108955
319	18-11-2024	GSPL_Bhuj_ 198/11/24	23.22463	69.49265	Fotdi	Near Fotdi village, stream cutting small mounds of sandstone, ~1km north of the Fotdi Kodki metal road	Occurence of ferruginous sandstone. Narrow, meandering, 2nd order, very mature stream draining the Bhuj sandstone and possibly alkaline plug mapped by GSI. The breadth of the river is 3 5m. Formation of duricast is also observed.	NA	Bhuj Formation	108956	108956
320	18-11-2024	GSPL_Bhuj_ 198/11/24	23.22463	69.49265	Fotdi	Near Fotdi village, stream cutting small mounds of sandstone, ~1km north of the Fotdi Kodki metal road	Sandstone (metasomatized)	NA	Bhuj Formation	108957	108957
321	18-11-2024	GSPL_Bhuj_ 198/11/24	23.22463	69.49265	Fotdi	Near Fotdi village, stream cutting small mounds of sandstone, ~1km north of the Fotdi Kodki metal road	Very fine grained sandstone with yellowish layer	NA	Bhuj Formation	108958	108958

Sl. No.	Date	Location No.	Latitude	Longitude	Village/ Area	Exposure Location	Host Lithology	Azimuth	Stratigraphy	Original BR ID	New BR ID
322	18-11-2024	GSPL_Bhuj_199/11/24	23.15181	69.57580	Naranpar Ravli	Near Naranpar Ravli village, road side exposure near pipeline installation	Medium to coarse grained sandstone, no internal structure observed	NA	Katrol Formation	NA	NA
323	18-11-2024	GSPL_Bhuj_200/11/24	23.16200	69.59600	Naranpar Ravli	Near Naranpar Ravli village, 300m west of location no.199/11/2024	Very fine grained,greyish white coloured sandstone,consists of few feldspar,quartz grained,highly silicified. Felsic tuffite?	80 -260/6 SW	Katrol Formation	NA	NA
324	19-11-2024	GSPL_Bhuj_118/06/24	23.16454	69.55433	Godapar	Road side exposure along the range of the high hills on a newly made metal road, accessible from Bhuj Mandvi Highway.	Occurrence of peloid(very well rounded,elliptical),pseudo ooids,fossil?, calcite crystal,quartz(increasing order of abundance) embedded in a carbonate cement, in very fine grained ferruginous sandstone	150 -330/2 NE	Chari Formation	108960	108960
325	19-11-2024	GSPL_Bhuj_118/06/24	23.16454	69.55433	Godapar	Road side exposure along the range of the high hills on a newly made metal road, accessible from Bhuj Mandvi Highway.	grainstone	NA	Chari Formation	108961	108961
326	19-11-2024	GSPL_Bhuj_118/06/24	23.16454	69.55433	Godapar	Road side exposure along the range of the high hills on a newly made metal road, accessible from Bhuj Mandvi Highway.	very fine grained brownish coloured with dull white patches (flowline structure)	NA	Chari Formation	108962	108962
327	19-11-2024	GSPL_Bhuj_118/06/24	23.16454	69.55433	Godapar	Road side exposure along the range of the high hills on a newly made metal road, accessible from Bhuj Mandvi Highway.	ferrugenious greyish block consists of chert,bivalve fossil,lime clast	NA	Chari Formation	108963	108963
328	21-11-2024	GSPL_Bhuj_201/11/24	23.14235	69.73049	Raha Nana	Road side exposure near Raha nana village	Fine grained ferruginous sandstone with alternate dark grey and dark red layer of iron	300/15 SW	Bhuj Formation	108965	108965
329	21-11-2024	GSPL_Bhuj_202/11/24	23.15037	69.72404	Raha Nana	Hill exposure near Raha nana village	Occurrence of white and red coarse grained sandstone. Red layer influx alteration	180/20 W	Bhuj Formation	NA	NA
330	21-11-2024	GSPL_Bhuj_203/11/24	23.15932	69.71670	Raha Nana	Road side exposure near Raha nana village	Shale dominated heterolith with poorly developed Tuffite layers	NA	Katrol Formation	NA	NA
331	21-11-2024	GSPL_Bhuj_204/11/24	23.15899	69.69352	Raha Nana	Road side exposure near Raha nana village	Shale dominated heterolith with poorly developed Tuffite layers	NA	Katrol Formation	NA	NA
332	23-11-2024	GSPL_Bhuj_205/11/24	23.20026	69.63979	Balaji green society	Road side exposure on Bhuj Mundra highway	Occurrence of very fine grained,ferruginous sandstone with fossiliferous sandstone (2-4 cm thick gypsum layer) (interbedded ferruginous and fossiliferous sandstone)	150 -320/30 SW	Chari Formation	NA	NA

Sl. No.	Date	Location No.	Latitude	Longitude	Village/ Area	Exposure Location	Host Lithology	Azimuth	Stratigraphy	Original BR ID	New BR ID
333	23-11-2024	GSPL_Bhuj_206/11/24	23.19830	69.64471	Balaji green society	Road side exposure on Bhuj Mundra highway,200 m west from the previous location no.205/11/24	Occurrence of very fine grained,whitish sandstone layer with Tuffite layered bed (sandstone dominated heterolith with poorly developed Tuffite layers)	NA	Chari Formation	NA	NA
334	23-11-2024	GSPL_Bhuj_207/11/24	23.19559	69.64726	Sedata	Road side exposure on Bhuj Mundra highway	Occurrence of very fine grained,whitish sandstone layer with Tuffite layered bed (sandstone dominated heterolith with poorly developed Tuffite layers)	NA	Chari Formation	NA	NA
335	23-11-2024	GSPL_Bhuj_208/11/24	23.19585	69.64810	Sedata	Road side exposure on Bhuj Mundra highway	Occurrence of very fine grained,ferruginous sandstone with fossiliferous sandstone (2 -4 cm thick gypsum layer) (interbedded ferruginous and fossiliferous sandstone)	NA	Chari Formation	108967	108967
336	23-11-2024	GSPL_Bhuj_209/11/24	23.19655	69.64833	Sedata	Road side exposure on Bhuj Mundra highway	Fossiliferous sandstone	90 -270/40 S	Chari Formation	NA	NA
337	23-11-2024	GSPL_Bhuj_210/11/24	23.19716	69.67870	Tapkeshwari temple	Road side exposure on Tapkeshwari Road	Shale dominated heterolith with Tuffite layers	150 -330/10 NE	Katrol Formation	NA	NA
338	23-11-2024	GSPL_Bhuj_211/11/24	23.19497	69.67765	Tapkeshwari temple	Road side exposure on Tapkeshwari Road	Shale dominated heterolith with Tuffite layers	150 -330/10 NE	Katrol Formation	NA	NA
339	23-11-2024	GSPL_Bhuj_212/11/24	23.19251	69.67771	Tapkeshwari temple	Road side exposure on Tapkeshwari Road	Shale dominated heterolith with Tuffite layers	150 330/10 NE	Katrol Formation	NA	NA
340	23-11-2024	GSPL_Bhuj_213/11/24	23.19765	69.67431	Tapkeshwari temple	Road side exposure on Tapkeshwari Road	Shale dominated heterolith with Tuffite layers	70/70 NE	Katrol Formation	108968	108968
341	23-11-2024	GSPL_Bhuj_213/11/24	23.19765	69.67431	Tapkeshwari temple	Road side exposure on Tapkeshwari Road	Medium grained,opaque,quartz,white color layer in sandstone (Tuffite?)	70/70 SE	Katrol Formation	108969	108969
342	24-11-2024	GSPL_Bhuj_214/11/2024	23.14200	69.49030	Vinganiya	Road side exposure on Samtra Vadasar Road	Shale dominated heterolith with Tuffite layers	NA	Katrol Formation	NA	NA
343	24-11-2024	GSPL_Bhuj_215/11/2024	23.19570	69.54890	Vinganiya	Road side exposure on Samtra Vadasar Road	Shale dominated heterolith with Tuffite layers	020/6 WWN	Katrol Formation	108970	108970
344	24-11-2024	GSPL_Bhuj_216/11/2024	23.14220	69.48330	Vinganiya	Road side exposure on Samtra Vadasar Road	Shale dominated heterolith with Tuffite layers	NA	Katrol Formation	NA	NA
345	24-11-2024	GSPL_Bhuj_217/11/2024	23.17970	69.54310	Samatra	Road side exposure on Samtra Vadasar Road	Thick sst (differential ferruginous leaching)seperated by clay horizons	NA	Chari Formation	NA	NA
346	24-11-2024	GSPL_Bhuj_218/11/2024	23.17670	69.53050	Samatra	Road side exposure on Samtra Vadasar Road	Interbedded fossiliferous and ferruginous sandstone	NA	Chari Formation	NA	NA

Sl. No.	Date	Location No.	Latitude	Longitude	Village/ Area	Exposure Location	Host Lithology	Azimuth	Stratigraphy	Original BR ID	New BR ID
347	25-11-2024	GSPL_Bhuj_219/11/2024	23.17440	69.53070	Bharasar	Hill exposure near Bharasar village	Interbedded of ferrugenous sst with fossiliferous sansdtone	NA	Chari Formation	NA	NA
348	25-11-2024	GSPL_Bhuj_220/11/2024	23.17330	69.53100	Bharasar	Hill exposure near Bharasar village	Interbedded of ferrugenous sst with fossiliferous sansdtone	NA	Chari formation	NA	NA
349	25-11-2024	GSPL_Bhuj_221/11/2024	23.17180	69.53120	Bharasar	Hill exposure near Bharasar village	Thick Massive Sandstone	NA	Chari formation	NA	NA
350	25-11-2024	GSPL_Bhuj_222/11/2024	23.17110	69.53280	Bharasar	Hill exposure near Bharasar village	Coarese grained,well rounded, clast suppoerted sandstone, composed of quartz . Fossile present . Cement: Whitish (siliceous / Carbonate) Quartz Grain : 95% as Framework	340/9SW	Bhuj Formation	108971	108971
351	25-11-2024	GSPL_Bhuj_223/11/2024	23.16940	69.53260	Bharasar	Hill exposure near Bharasar village	Fossiliferous sandstone (ferruginous frequently)	140/5NE	Chari Formation	NA	NA
352	25-11-2024	GSPL_Bhuj_224/11/2024	23.16750	69.53240	Bharasar	Hill exposure near Bharasar village	Fossiliferous sandstone (ferruginous frequently)	140/5NE	Chari Formation	NA	NA
353	25-11-2024	GSPL_Bhuj_225/11/2024	23.16570	69.53190	Bharasar	Hill exposure near Bharasar village	Sandstone dominated heterolith with poorly developed Tuffite layers	NA	Chari Formation	NA	NA
354	25-11-2024	GSPL_Bhuj_226/11/2024	23.16520	69.53230	Bharasar	Hill exposure near Bharasar village	Fossiliferous sandstone (ferruginous frequently)	NA	Chari Formation	NA	NA
355	25-11-2024	GSPL_Bhuj_227/11/2024	23.16480	69.53360	Bharasar	Hill exposure near Bharasar village	Fossiliferous sandstone (ferruginous frequently)	225/7SE	Chari Formation	NA	NA
356	25-11-2024	GSPL_Bhuj_228/11/2024	23.16670	69.53720	Bharasar	Hill exposure near Bharasar village	Shale with well develoed Tuffite layered layer	W-E/5N	Chari Formation	NA	NA
357	25-11-2024	GSPL_Bhuj_229/11/2024	23.16390	69.54160	Bharasar	Hill exposure near Bharasar village	Fossiliferous sandstone (ferruginous frequently)	NA	Chari Formation	NA	NA
358	25-11-2024	GSPL_Bhuj_230/11/2024	23.16260	69.54170	Bharasar	Hill exposure near Bharasar village	Thick sandstonee(Quartz arenite?) with occasional tuff/clay	NA	Chari Formation	108972	108972
359	25-11-2024	GSPL_Bhuj_231/11/2024	23.16130	69.54160	Bharasar	Hill exposure near Bharasar village	Thick sandstonee(Quartz arenite?) with occasional tuff/clay	NA	Chari Formation	108973	108973
360	25-11-2024	GSPL_Bhuj_232/11/2024	23.16060	69.54200	Bharasar	Hill exposure near Bharasar village	Fossiliferous sandstone (ferruginous frequently)	NA	Chari Formation	NA	NA
361	25-11-2024	GSPL_Bhuj_233/11/2024	23.17320	69.53250	Bharasar	Hill exposure near Bharasar village	Fossiliferous sandstone (ferruginous frequently)	NA	Chari Formation	NA	NA

Sl. No.	Date	Location No.	Latitude	Longitude	Village/ Area	Exposure Location	Host Lithology	Azimuth	Stratigraphy	Original BR ID	New BR ID
362	25-11-2024	GSPL_Bhuj_234/11/2024	23.17594	69.62333	Sedata	Accessible from Bhuj-Mundra road through a cart road	Ferruginous sandstone	107/5S	Bhuj Formation	NA	NA
363	25-11-2024	GSPL_Bhuj_236/11/2024	23.17271	69.62487	Sedata	Accessible from Bhuj-Mundra road through a cart road	Thick sandstone with differential ferruginous leaching	120/7SW	Bhuj Formation	NA	NA
364	25-11-2024	GSPL_Bhuj_237/11/2024	23.17199	69.62476	Sedata	Accessible from Bhuj-Mundra road through a cart road	metasomatized sandstone	110/5/SW	Bhuj Formation	NA	NA
365	25-11-2024	GSPL_Bhuj_238/11/2024	23.17020	69.62394	Sedata	Accessible from Bhuj-Mundra road through a cart road	Ferruginous sandstone	110/5/SW	Bhuj Formation	NA	NA
366	25-11-2024	GSPL_Bhuj_239/11/2024	23.17008	69.62406	Sedata	Accessible from Bhuj-Mundra road through a cart road	Ferruginous sandstone	185/20E	Bhuj Formation	108974	108974
367	01-12-2024	GSPL_Bhuj_244/11/2024	23.20407	69.54211	Mankuva	Trench: 320 strike, dip towards 120	Sandstone with occassional ferrugenous layer, Trenching	Trench: 320 strike, dip towards 120	Bhuj Formation	108975	108975
368	01-12-2024	GSPL_Bhuj_244/11/2024	23.20407	69.54211	Mankuva	Trench: 320 strike, dip towards 120	Sandstone with occassional ferrugenous layer, Trenching	NA	Bhuj Formation	108976	108976
369	01-12-2024	GSPL_Bhuj_244/11/2024	23.20407	69.54211	Mankuva	Trench: 320 strike, dip towards 120	Sandstone with occassional ferrugenous layer, Trenching	NA	Bhuj Formation	108977	108977
370	01-12-2024	GSPL_Bhuj_244/11/2024	23.20407	69.54211	Mankuva	Trench: 320 strike, dip towards 120	Sandstone with occassional ferrugenous layer, Trenching	NA	Bhuj Formation	108978	108978
371	01-12-2024	GSPL_Bhuj_244/11/2024	23.20407	69.54211	Mankuva	Trench: 320 strike, dip towards 120	Sandstone with occassional ferrugenous layer, Trenching	NA	Bhuj Formation	108979	108979
372	01-12-2024	GSPL_Bhuj_244/11/2024	23.20407	69.54211	Mankuva	Trench: 320 strike, dip towards 120	Sandstone with occassional ferrugenous layer, Trenching	NA	Bhuj Formation	108980	108980
373	01-12-2024	GSPL_Bhuj_244/11/2024	23.20407	69.54211	Mankuva	Trench: 320 strike, dip towards 120	Sandstone with occassional ferrugenous layer, Trenching	NA	Bhuj Formation	108981	108981
374	01-12-2024	GSPL_Bhuj_244/11/2024	23.20407	69.54211	Mankuva	Trench: 320 strike, dip towards 120	Sandstone with occassional ferrugenous layer, Trenching	NA	Bhuj Formation	108982	108982
375	01-12-2024	GSPL_Bhuj_245/11/2024	23.19693	69.56466	Bharasar	Trench: 320 strike, dip towards 120	Sandstone with occassional ferrugenous layer, Trenching	NA	Bhuj Formation	NA	NA
376	01-12-2024	GSPL_Bhuj_246/11/2024	23.19536	69.59687	Mandvi high way	Pitting location (tentative)	Thick sandstone ferruginous frequently, piiting	NA	Katrol Formation	NA	NA
377	04-12-2024	GSPL_Bhuj_247/12/2024	23.19473	69.59762	Mandvi high way	Pit locations (01 - 04) near Bhuj Mandvi highway	Shale dominated heterolithwith Tuffite layer bed	120/30SW, 165/32SW	Katrol Formation	108983, 108984	108983, 108984

Sl. No.	Date	Location No.	Latitude	Longitude	Village/ Area	Exposure Location	Host Lithology	Azimuth	Stratigraphy	Original BR ID	New BR ID
378	05-12-2024	GSPL_Bhuj_ 248/12/2024	23.19578	69.59700	Mandvi high way	Pit locations (05 - 09) near Bhuj Mandvi highway	Shale dominated heterolithwith Tuffite layer bed, , phosphorite nodules??	330/25W, 340/30SW	Katrol Formation	NA	NA
379	07-12-2024	GSPL_Bhuj_ 249/12/2024	23.19444	69.59791	Mandvi high way	Hill expoure near Mandvi high way	Shale dominated heterolithwith ferruginous Tuffite layer bed	NA	Katrol Formation	NA	NA
380	07-12-2024	GSPL_Bhuj_ 250/12/2024	23.19514	69.59717	Mandvi high way	Hill expoure near Mandvi high way	Shale sandstone heterolith	310/35SW	Katrol Formation	Pit samples	Pit samples
381	07-12-2024	GSPL_Bhuj_ 251/12/2024	23.19658	69.60031	Mandvi high way	Road side Exposure near Mandvi High way	Fossiliferous Sandstone beds with occasional ferrougenous activity	340/20SW	Katrol Formation	109013	109013
382	07-12-2024	GSPL_Bhuj_ 252/12/2024	23.27065	69.80465	Kala talavdi	China Clay mine	China clay	NA	NA	109014	109014
383	07-12-2024	GSPL_Bhuj_ 252/12/2024	23.27065	69.80465	Kala talavdi	China Clay mine	China clay	NA	NA	109015	109015
384	07-12-2024	GSPL_Bhuj_ 252/12/2024	23.27065	69.80465	Kala talavdi	China Clay mine	China Clay found from the depth of 100ft, Host rock: Sanstone	NA	NA	109016	109016
385	08-12-2024	GSPL_Bhuj_ 253/12/2024	23.19629	69.59651	Mandvi high way	Exposure near Katrol hill fault	Sandstone dominated heterolith with Tuffite layer	265/90/N	Katrol Formation	109017	109017
386	09-12-2024	GSPL_Bhuj_ 254/12/2024	23.19570	69.53396	Mankuva	Hill expoure near Bhuj-Natiya high way	metasomatized sandstone underlain by planar cross stratified medium to coarse grained ferruginous sandstone. Ferrugination has taken place along the stratification. The metasomatized sandstone is composed of very coarse grained angular to sub angular quartz, authigenic growth of feldspar and clasts of quartz aggregates embedded in a magnetite rich (black streak) matrix.	170/20SW	Bhuj Formation	109018	109018
387	09-12-2024	GSPL_Bhuj_ 254/12/2024	23.19570	69.53396	Mankuva	Hill expoure near Bhuj-Natiya high way	metasomatized sandstone underlain by planar cross stratified medium to coarse grained ferruginous sandstone. Ferrugination has taken place along the stratification. The metasomatized sandstone is composed of very coarse grained angular to sub angular quartz, authigenic growth of feldspar and clasts of quartz aggregates embedded in a magnetite rich (black streak) matrix.	NA	Bhuj Formation	109019	109019

Sl. No.	Date	Location No.	Latitude	Longitude	Village/ Area	Exposure Location	Host Lithology	Azimuth	Stratigraphy	Original BR ID	New BR ID
388	09-12-2024	GSPL_Bhuj_ 254/12/2024	23.19570	69.53396	Mankuva	Hill expoure near Bhuj-Natiya high way	metasomatized sandstone underlain by planar cross stratified medium to coarse grained ferruginous sandstone. Ferrugination has taken place along the stratification. The metasomatized sandstone is composed of very coarse grained angular to sub angular quartz, authigenic growth of feldspar and clasts of quartz aggregates embedded in a magnetite rich (black streak) matrix.	NA	Bhuj Formation	109020	109020
389	09-12-2024	GSPL_Bhuj_ 255/12/2024	23.21766	69.59088	Kalyanpar	Hill expoure near Kalyanpar	metasomatized sandstone underlain by planar cross stratified medium to coarse grained ferruginous sandstone. Ferrugination has taken place along the stratification. The metasomatized sandstone is composed of very coarse grained angular to sub angular quartz, authigenic growth of feldspar and clasts of quartz aggregates embedded in a magnetite rich (black streak) matrix.	NA	Bhuj Formation	109021	109021
390	09-12-2024	GSPL_Bhuj_ 256/12/2024	23.17550	69.61667	Sedata	Hill exposure near Bhuj Mundra high way	metasomatized Sandstone	NA	Bhuj Formation	109022	109022
391	09-12-2024	GSPL_Bhuj_ 257/12/2024	23.21766	69.59088	Kalyanpar	Hill expoure near Kalyanpar	metasomatized Sandstone	340/20SW	Bhuj Formation	NA	NA
392	09-12-2024	GSPL_Bhuj_ 258/12/2024	23.22364	69.59188	Kalyanpar	Hill expoure near Kalyanpar	metasomatized Sandstone	210/19SE	Bhuj Formation	109023	109023
393	09-12-2024	GSPL_Bhuj_ 259/12/2024	23.22338	69.59037	Kalyanpar	Hill expoure near Kalyanpar	Ferruginous sandstone frequently	360/5W	Bhuj Formation	109024	109024
394	09-12-2024	GSPL_Bhuj_ 260/01/2025	23.22956	69.58690	Kalyanpar	Road side exposure, accessible through a metal road from Kalyanpar Road	Highly ferruginous sandstone	120/7SW	Bhuj Formation	109025	109025
395	09-12-2024	GSPL_Bhuj_ 261/01/2025	23.19690	69.72526	Bhujodia	Accessible through a local cart road through Bhujodia village.	Coarse grained Sandstone	NA	Chari Formation	109026	109026
396	09-12-2024	GSPL_Bhuj_ 262/01/2025	23.19785	69.52827	Mankuva	Road side exposure,accessible through a metal road fromh Bhuj Nakhetrana Highway	Ferruginous sandstone frequently	NA	Bhuj Formation	109027	109027
397	04-01-2025	GSPL_Bhuj_ 263/01/2025	23.19885	69.53037	Mankuva	Road side exposure,accessible through a metal road fromh Bhuj Nakhetrana Highway	Ferruginous Sandstone, fault contact	195/55WWN	Bhuj Formation	109028	109028

Sl. No.	Date	Location No.	Latitude	Longitude	Village/ Area	Exposure Location	Host Lithology	Azimuth	Stratigraphy	Original BR ID	New BR ID
398	04-01-2025	GSPL_Bhuj_ 263/01/2025	23.19885	69.53037	Mankuva	Road side exposure,accessible through a metal road fromh Bhuj Nakhetrana Highway	Ferruginous Sandstone	NA	Bhuj Formation	109029	109029
399	04-01-2025	GSPL_Bhuj_ 263/01/2025	23.19368	69.53232	Mankuva	Road side exposure,accessible through a metal road fromh Bhuj Nakhetrana Highway	white Sandstone	NA	Bhuj Formation	109038	109038
400	04-01-2025	GSPL_Bhuj_ 264/01/2025	23.20869	69.52542	Mankuva	Neareast accesss from Bhuj Nakhetrana Highway	Ferruginous sandstone frequently	200/5WWN	Bhuj Formation	109030	109030
401	04-01-2025	GSPL_Bhuj_ 264/01/2025	23.20869	69.52542	Mankuva	Road side exposure,accessible through a metal road fromh Bhuj Nakhetrana Highway	Medium to coarse grained metasomatized sandstone	NA	Bhuj Formation	109031	109031
402	04-01-2025	GSPL_Bhuj_ 265/01/2025	23.19520	69.53281	Mankuva	Road side exposure,accessible through a metal road fromh Bhuj Nakhetrana Highway	metasomatized Sandstone	NA	Bhuj Formation	109032	109032
403	05-01-2025	GSPL- Bhuj 265/01/2025	23.19520	69.53281	Mankuva	Road side exposure,accessible through a metal road fromh Bhuj Nakhetrana Highway	metasomatized Sandstone	NA	Bhuj Formation	109033	109033
404	05-01-2025	GSPL_Bhuj_ 266/01/2025	23.19549	69.53124	Mankuva	Hill exposure, accessible through a metal road from Bhuj Nakhetrana Highway	metasomatized Sandstone underlain by very coarse to medium grained planar cross stratified ferruginous sandstone. Here found 2/3 grains of Magnetite. Matrix supported.	NA	Bhuj Formation	109034	109034
405	05-01-2025	GSPL_Bhuj_ 267/01/2025	23.19638	69.53115	Mankuva	Hill exposure, accessible through a metal road from Bhuj Nakhetrana Highway	metasomatized Sandstone, magnetite with black streak, green statining (secondary) is also observed.	NA	Bhuj Formation	109035	109035
406	05-01-2025	GSPL_Bhuj_ 268/01/2025	23.19567	69.53168	Mankuva	Hill exposure, accessible through a metal road from Bhuj Nakhetrana Highway	Coarse grained metasomatized sandstone	NA	Bhuj Formation	109036	109036
407	05-01-2025	GSPL_Bhuj_ 269/01/2025	23.19634	69.53186	Mankuva	Road side exposure,accessible through a metal road fromh Bhuj Nakhetrana Highway	metasomatized sandstone, very fine grained black minerals showing black streak is observed within the sandstone	NA	Bhuj Formation	109037	109037
408	06-01-2025	GSPL_Bhuj_ 270/01/2025	23.21025	69.52410	Mankuva	Neareast accesss from Bhuj Nakhetrana Highway	metasomatized sandstone underlain by highly ferruginous red sandstone underlain by white siltstone (very fine grained)	NA	Bhuj Formation	109039	109039
409	06-01-2025	GSPL_Bhuj_ 270/01/2025	23.21025	69.52410	Mankuva	Neareast accesss from Bhuj Nakhetrana Highway	metasomatized sandstone underlain by highly ferruginous red sandstone underlain by white siltstone (very fine grained)	NA	Bhuj Formation	109040	109040

Sl. No.	Date	Location No.	Latitude	Longitude	Village/ Area	Exposure Location	Host Lithology	Azimuth	Stratigraphy	Original BR ID	New BR ID
410	06-01-2025	GSPL_Bhuj_ 270/01/2025	23.21025	69.52410	Mankuva	Neareast accesss from Bhuj Nakhetrana Highway	metasomatized sandstone underlain by highly ferruginous red sandstone underlain by white siltstone (very fine grained)	NA	Bhuj Formation	109041	109041
411	06-01-2025	GSPL_Bhuj_ 271/01/2025	23.19749	69.52979	Mankuva	Neareast accesss from Bhuj Nakhetrana Highway	Black coloured, medium to coarse grained metasomatized Sandstone. Growth of authigenic feldspar, buish green staining and silicification are common feature of the sandstone. Pyrite??	NA	Bhuj Formation	109042	109042
412	06-01-2025	GSPL_Bhuj_ 271/01/2025	23.19749	69.52979	Mankuva	Neareast accesss from Bhuj Nakhetrana Highway	Black coloured, medium to coarse grained metasomatized Sandstone. Growth of authigenic feldspar, buish green staining and silicification are common feature of the sandstone. Pyrite??	NA	Bhuj Formation	109044	109044
413	07-01-2025	GSPL_Bhuj_ 272/01/2025	23.19654	69.53168	Mankuva	Neareast accesss from Bhuj Nakhetrana Highway	Black coloured, medium to coarse grained metasomatized Sandstone. Growth of authigenic feldspar, are common feature of the sandstone.	NA	Bhuj Formation	NA	NA
414	08-01-2025	GSPL_Bhuj_ 273/01/2025	23.20362	69.52684	Mankuva	Neareast accesss from Bhuj Nakhetrana Highway	metasomatized Sandstone	NA	Bhuj Formation	109043	109043
415	09-01-2025	GSPL_Bhuj_ 274/01/2025	23.19181	69.58950	Vandh sim	Hill exposure near Bharasar road	Shale dominated heterolith with tuffite layer	NA	Katrol Formation	109045	109045
416	09-01-2025	GSPL_Bhuj_ 274/01/2025	23.19181	69.58950	Vandh sim	Hill exposure near Bharasar road	Shale heterolith Tuffite layer	NA	Katrol Formation	109046	109046
417	09-01-2025	GSPL_Bhuj_ 274/01/2025	23.19181	69.58950	Vandh sim	Hill exposure near Bharasar road	Ferruginous Sandstone	NA	Katrol Formation	109047	109047
418	09-01-2025	GSPL_Bhuj_ 274/01/2025	23.19181	69.58950	Vandh sim	Hill exposure near Bharasar road	Sandstone	NA	Katrol Formation	109048	109048
419	11-01-2025	GSPL_Bhuj_ 275/01/2025	23.20941	69.52733	Mankuva	Road side exposure,accessible from a metal road through Bhuj Nakhetrana Highway road	metasomatized sandstone	45/5NW	Bhuj Formation	NA	NA
420	11-01-2025	GSPL_Bhuj_ 276/01/2025	23.20940	69.52536	Mankuva	Road side exposure,accessible through a metal road from Bhuj Nakhetrana Highway	metasomatized sandstone	50/60NW	Bhuj Formation	109049	109049
421	11-01-2025	GSPL_Bhuj_ 276/01/2025	23.20940	69.52536	Mankuva	Road side exposure,accessible through a metal road from Bhuj Nakhetrana Highway	Medium to coarse grain metasomatized sandstone	NA	Bhuj Formation	109050	109050
422	11-01-2025	GSPL_Bhuj_ 277/01/2025	23.20950	69.52221	Mankuva	Hill exposure acessible from Bhuj Nakhetrana Highway	metasomatized sandstone	NA	Bhuj Formation	109051	109051

Sl. No.	Date	Location No.	Latitude	Longitude	Village/ Area	Exposure Location	Host Lithology	Azimuth	Stratigraphy	Original BR ID	New BR ID
423	11-01-2025	GSPL_Bhuj_277/01/2025	23.20950	69.52221	Mankuva	Hill exposure acessible from Bhuj Nakhetrana Highway	Highly ferruginous (metasomatized sandstone), , possible albite zone??	NA	Bhuj Formation	109054	109054
424	11-01-2025	GSPL_Bhuj_278/01/2025	23.21039	69.52387	Mankuva	Hill exposure acessible from Bhuj Nakhetrana Highway	metasomatized sandstone	NA	Bhuj Formation	109052	109052
425	11-01-2025	GSPL_Bhuj_279/01/2025	23.22131	69.58954	Mankuva	Road side exposure,accessible through a metal road from Bhuj Nakhetrana Highway	Sandstone with strong iron impregnation, mainly in layers. A zone of clay (alteration??) is also observed. It could be silicification also	NA	Bhuj Formation	109053	109053
426	15-01-2025	GSPL_Bhuj_280/01/2025	23.20316	69.62894	Sukhpar	Hill exposure accessible from Bhuj Mandvi Highway	metasomatized sandstone	NA	Bhuj Formation	109055	109055
427	15-01-2025	GSPL_Bhuj_281/01/2025	23.22556	69.54979	Sukhpar	Hill exposure accessible from Bhuj Mandvi Highway	Planar cross stratified highly ferruginous sandstone	NA	Bhuj Formation	109056	109056
428	15-01-2025	GSPL_Bhuj_283/01/2025	23.23284	69.52792	Kalyanpar	Hill exposure near Kalyanpar road	Planar cross stratified highly ferruginous sandstone, metasomatized sandstone at higher contour	NA	Bhuj Formation	109057	109057
429	15-01-2025	GSPL_Bhuj_284/01/2025	23.23100	69.53547	Reha Nana	Hill exposure near Kalyanpar road	Purplish to yellow ocher to white coloured siltstone, clayey at places	NA	Bhuj Formation	NA	NA
430	15-01-2025	GSPL_Bhuj_285/01/2025	23.23181	69.55668	Reha Nana	Hill exposure near Kalyanpar road	Reddish brown to yellow ocher coloured ferruginous, quartzose sandstone	NA	Bhuj Formation	NA	NA
431	03-02-2025	GSPL_Bhuj_270/02/2025	23.20325	69.62895	Sukhpar	Hill exposure accessible from Bhuj Mandvi Highway	Planar cross stratified white sandstone with selective ferrugination	NA	Bhuj Formation	NA	NA
432	04-02-2025	GSPL_Bhuj_280/02/2025	23.20313	69. 628694	Sukhpar	Hill exposure accessible from Bhuj Mandvi Highway	Alternate occurrence of highly ferruginouus sandstone and white, medium to coarse grained quartzose sandstone. The ferruginous part consists of angular to sub angular quartz, embedded in a ferruginous matrix/cement.	NA	Bhuj Formation	NA	NA
433	06-02-2025	GSPL_Bhuj_289/02/2025	23.20370	69.62840	Sukhpar	Hill exposure near Mirzapar village	metasomatized sandstone underlain by planar cross stratified brownish red to pinkish white coloured, planar cross stratified medium to coarse grained sandstone. The sandstone at a nearby area is interrupted by cm scale thin beds of highly ferruginous, blackish red coloured metasomatized sandstone. Thin veinlets of carbonate/gypsum (?? require acid test) observed to cross cut the entire exposure	NA	Bhuj Formation	109063	109063

Sl. No.	Date	Location No.	Latitude	Longitude	Village/ Area	Exposure Location	Host Lithology	Azimuth	Stratigraphy	Original BR ID	New BR ID
434	06-02-2025	GSPL_Bhuj_ 289/02/2025	23.20370	69.62840	Sukhpar	Hill exposure near Mirzapar village	metasomatized sandstone underlain by planar cross stratified brownish red to pinkish white coloured, planar cross stratified medium to coarse grained sandstone. The sandstone at a nearby area is interrupted by cm scale thin beds of highly ferruginous, blackish red coloured metasomatized sandstone. Thin veinlets of carbonate/gypsum (?? require acid test) observed to cross cut the entire exposure	NA	Bhuj Formation	109064	109064
435	06-02-2025	GSPL_Bhuj_ 289/02/2025	23.20370	69.62840	Sukhpar	Hill exposure near Mirzapar village	metasomatized sandstone underlain by planar cross stratified brownish red to pinkish white coloured, planar cross stratified medium to coarse grained sandstone. The sandstone at a nearby area is interrupted by cm scale thin beds of highly ferruginous, blackish red coloured metasomatized sandstone. Thin veinlets of carbonate/gypsum (?? require acid test) observed to cross cut the entire exposure	NA	Bhuj Formation	109065	109065
436	06-02-2025	GSPL_Bhuj_ 289/02/2025	23.20370	69.62840	Sukhpar	Hill exposure near Mirzapar village	metasomatized sandstone underlain by planar cross stratified brownish red to pinkish white coloured, planar cross stratified medium to coarse grained sandstone. The sandstone at a nearby area is interrupted by cm scale thin beds of highly ferruginous, blackish red coloured metasomatized sandstone. Thin veinlets of carbonate/gypsum (?? require acid test) observed to cross cut the entire exposure	NA	Bhuj Formation	109069	109069
437	06-02-2025	GSPL_Bhuj_ 289/02/2025	23.20370	69.62840	Sukhpar	Hill exposure near Mirzapar village	metasomatized sandstone underlain by planar cross stratified brownish red to pinkish white coloured, planar cross stratified medium to coarse grained sandstone. The sandstone at a nearby area is interrupted by cm scale thin beds of highly ferruginous, blackish red coloured metasomatized sandstone. Thin veinlets of carbonate/gypsum (?? require acid test) observed to cross cut the entire exposure	NA	Bhuj Formation	109071	109071
438	04-02-2025	GSPL_Bhuj_ 290/02/2025	23.20096	69.63083	Tapkeshwari Temple	JCB cut section	Heterolithic unit of shale with occasional ferruginous nodular beds and phosphatic nodules of about 30 cm in diameter at the lower part.	65/33SE	Katrol Formation	109066	109066
439	04-02-2025	GSPL_Bhuj_ 290/02/2025	23.20096	69.63083	Tapkeshwari Temple	JCB cut section	Heterolithic unit of shale with occasional ferruginous nodular beds and phosphatic nodules of about 30 cm in diameter at the lower part.	NA	Katrol Formation	109060	109060

Sl. No.	Date	Location No.	Latitude	Longitude	Village/ Area	Exposure Location	Host Lithology	Azimuth	Stratigraphy	Original BR ID	New BR ID
440	04-02-2025	GSPL_Bhuj_290/02/2025	23.20096	69.63083	Tapkeshwari Temple	JCB cut section	Heterolithic unit of shale with occasional ferruginous nodular beds and phosphatic nodules of about 30 cm in diameter at the lower part.	NA	Katrol Formation	109061	109061
441	04-02-2025	GSPL_Bhuj_290/02/2025	23.20096	69.63083	Tapkeshwari Temple	JCB cut section	Heterolithic unit of shale with occasional ferruginous nodular beds and phosphatic nodules of about 30 cm in diameter at the lower part.	NA	Katrol Formation	109062	109062
442	10-02-2025	GSPL_Bhuj_291/02/2025	23.19634	69.53076	Mankuva	Hill exposure Neareast accesss from Bhuj Nakhetrana Highway road	Planar cross stratified highly ferruginous sandstone	NA	Bhuj Formation	NA	NA
443	06-02-2025	GSPL_Bhuj_292/02/2025	23.20103	69.63058	Mankuva	Hill exposure Neareast accesss from Bhuj Nakhetrana Highway road	metasomatized sandstone with magnetite	NA	Bhuj Formation	109067	109067
444	10-02-2025	GSPL_Bhuj_293/02/2025	23.19762	69.53007	Mankuva	Hill exposure Neareast accesss from Bhuj Nakhetrana Highway road	metasomatized sandstone is composed of very coarse grained angular to sub angular quartz, and clasts of quartz aggregates embedded in a magnetite rich (black streak) matrix.	NA	Bhuj Formation	NA	NA
445	11-02-2025	GSPL_Bhuj_294/02/2025	23.18957	69.54486	Mankuva	Hill exposure Neareast accesss from Bhuj Nakhetrana Highway road	Ferruginous Sandstone	NA	Bhuj Formation	NA	NA
446	13-02-2025	GSPL_Bhuj_295/02/2025	23.19505	69.57110	Mankuva	Road side exposure,accessiblethrough a metal road from Bhuj Nakhetrana Highway	White to purplish white light brown coloured sandstone, no grain boundary is clearly visible, clayey matrix/cement	NA	Bhuj Formation	109068	109068
447	13-02-2025	GSPL_Bhuj_296/02/2025	23.20477	69.51927	Mankuva	Road side exposure,accessiblethrough a metal road from Bhuj Nakhetrana Highway	metasomatized sandstone is composed of very coarse grained angular to sub angular quartz, feldspar and clasts of quartz aggregates embedded in a magnetite rich (black streak) matrix.	NA	Bhuj Formation	NA	NA
448	06.03.2025	GSPL_Bhuj_301/03/2025	23.22453	69.62781	Mirzapur	Hill exposure near Kalyanpar road	Sandstone with selective ferrugination	NA	Bhuj Formation	NA	NA
449	06.03.2025	GSPL_Bhuj_302/03/2026	23.22748	69.64020	Bhuj	Road side expousre near Bhuj Road	Ferruginous Sandstone with differential ferrugination	NA	Bhuj Formation	NA	NA
450	06.03.2025	GSPL_Bhuj_303/03/2026	23.22908	69.64153	Bhuj	Road side expousre near Bhuj Road	Alternate occurrence of ferruginous sandstone with differential ferrugination and white clay/siltstone	NA	Bhuj Formation	NA	NA
451	06.03.2025	GSPL_Bhuj_304/03/2026	23.22708	69.64422	Bhuj	Road side expousre near Bhuj Road	Ferruginous Sandstone with differential ferrugination	NA	Bhuj Formation	NA	NA
452	06.03.2025	GSPL_Bhuj_305/03/2025	23.22673	69.64370	Bhuj	Road side expousre near Bhuj Road	Ferruginous Sandstone with differential ferrugination	NA	Bhuj Formation	NA	NA

Sl. No.	Date	Location No.	Latitude	Longitude	Village/ Area	Exposure Location	Host Lithology	Azimuth	Stratigraphy	Original BR ID	New BR ID
453	06.03.2025	GSPL_Bhuj_306/03/2025	23.23253	69.65405	Bhuj	Road side expousre near Bhuj Road	Sandstone Shale heterolith with selective ferrugination	NA		NA	NA
454	06.03.2025	GSPL_Bhuj_307/03/2025	23.23250	69.66707	Bhuj	Road side expousre near Bhuj Road	Ferruginous Sandstone with differential ferrugination, metasomatized??	NA	Bhuj Formation	NA	NA
455	10.03.2025	GSPL_Bhuj_312/03/2025	23.16114	69.67989	Bharpar	Hill expousre near Bharapar Road	Sandstone dominated heterolith with Tuffite layers	NA	Bhuj Formation	NA	NA
456	10.03.2025	GSPL_Bhuj_313/03/2025	23.15604	69.59908	Mandvi high way	Road Side expousre near Mandvi high way	Sandstone shale heterolith with Tuffite layers	NA	Bhuj Formation	NA	NA
457	20.03.2025	GSPL_Bhuj_322/03/2025	23.19669	69.72876	Jadura	Road Side expousre near Naranpar road	Sandstone with encrustration on top	NA	Bhuj Formation	NA	NA
458	20.03.2025	GSPL_Bhuj_323/03/2025	23.19945	69.73090	Jadura	Road Side expousre near Naranpar road	Purplish white sandstone with encrustration on top	NA	Bhuj Formation	NA	NA
459	21.03.2025	GSPL_Bhuj_325/03/2025	23.15616	69.50364	Samatra	Road side exposure on a local cart road, parallel to Samatra Varasar road	Sandstone dominated heterolith	NA	Katrol Formation	NA	NA
460	21.03.2025	GSPL_Bhuj_327/03/2025	23.15301	69.51729	Mankuva	Hilli exposure near Mankuva	Fossiliferous ferruginous sandstone with encrustation on top	NA	Katrol Formation	NA	NA
461	21.03.2025	GSPL_Bhuj_328/03/2025	23.15060	69.52546	Mankuva	Hilli exposure near Mankuva	Sandstone dominated heterolith	NA	Katrol Formation	NA	NA
462	14.07.2024	GSPL_Bhuj_296/07/2025	23.16052	69.68694	Jadura	Hilly exposure, accessible from Dhunaraja dam road, through Jadura village.	Exposure of Bhuj sandstone, comprising medium to coarse grained sandstone overlain by conglomerate/ breccias. The conglomerate is consists of red beds, sandstone(??) clasts embedded in a very coarse to pebbly matrix(quartz, very crystal clear, many nonmagnetic black minerals, and muscovite). Lots of boulders of metasomatized sandstone. Cavity within metasomatized sandstone are filled with iron (cherry red to brown streak) fluid like materials. Evidence of iron impregnation in metasomatized.	NA	Bhuj Formation	112451	112451
463	14.07.2025	GSPL_Bhuj_296/07/2025	23.16052	69.68694	Jadura	Hilly exposure, accessible from Dhunaraja dam road, through Jadura village.	Boulder of metasomatized sandstone	NA	Bhuj Formation	112452	112452

Sl. No.	Date	Location No.	Latitude	Longitude	Village/ Area	Exposure Location	Host Lithology	Azimuth	Stratigraphy	Original BR ID	New BR ID
464	14.07.2025	GSPL_Bhuj_297/07/2025	23.16072	69.68631	Jadura	Hilly exposure, accessible from Dhunaraja dam road, through Jadura village.	Exposure of Bhuj sandstone, sandwiched between 2 ferruginous sandstone unit. The sandstone is coarse to very coarse grained, blackish red coloured and composed of angular grains of crystal clear quartz, black minerals, embedded in a jet black materials at places. Evidence of iron impregnation.	NA	Bhuj Formation	112453	112453
465	15.07.2025	GSPL_Bhuj_298/07/2025	23.20082	69.63132	Terki	Accessible from Bhuj Mandvi high way, through a cart road, near Tekri and Bhuj greenland	Fossiliferous (burrow, later filled with chert, bivalve, cephalopd) sandstone of Chari Formation. Iron impregnation with nodule formation within the sandstone. Goethite, lemonite and hematite are compositing elements. Coarse to medium grained sandstone with quartz, hematite cement and vug filled calcite crystals.	250/20SE	Chari Formation	NA	NA
466	15.07.2025	GSPL_Bhuj_299/07/2025	23.20067	69.62945	Mirzapar	Hilli exposure near Mirzapur	At the low lying area we are getting boulders of blackish red coloured sandstone with quartz and euhedral feldspar, muscovite (aggregates??) embedded in a hematite magnetite matrix/cement. metasomatized sandstone(volcaniclastics??). No magnetite found in the sample. Some of the quartz grains are surrounded by silica. Very few grains within the crush of the matrix part is attracted by magnet and giving black streak. Host lithology is medium to fine grained sandstone with strong ferugination. It is composed of quartz more than 95%, muscovite, biotite in a decreasing order of abundance. Well sorted, mature sandstone.Fossil like cephalopod, Bivalve found and Calcite and ca	NA	Bhuj Formation	112454	112454
467	15.07.2025	GSPL_Bhuj_300/07/2025	23.20335	69.62852	Mirzapar	Hilli exposure near Mirzapur	Brecciation plane, 130-250, 60NE., 120/64NE Host rock planar cross stratified coarse grained sandstone with Bedding 40 -220/30NW 112455 (altered part), 112456 (unaltered part), 112457 (host rock), 112458(partly metasomatized)	130-250, 60NE (brecciation plane), 120/64NE (fault), 40-220/30NW (Bedding)	Bhuj Formation	112455	112455
468	15.07.2025	GSPL_Bhuj_300/07/2025	23.20335	69.62852	Mirzapar	Hilli exposure near Mirzapur	Brecciation plane, 130-250, 60NE., 120/64NE Host rock planar cross stratified coarse grained sandstone with Bedding 40 -220/30NW 112455 (altered part), 112456 (unaltered part), 112457 (host rock), 112458(partly metasomatized)	NA	Bhuj Formation	112456	112456

Sl. No.	Date	Location No.	Latitude	Longitude	Village/ Area	Exposure Location	Host Lithology	Azimuth	Stratigraphy	Original BR ID	New BR ID
469	15.07.2025	GSPL_Bhuj_ 300/07/2025	23.20335	69.62852	Mirzapar	Hilli exposure near Mirzapur	Brecciation plane, 130-250, 60NE., 120/64NE Host rock planar cross stratified coarse grained sandstone with Bedding 40 -220/30NW 112455 (altered part), 112456 (unaltered part), 112457 (host rock), 112458(partly metasomatized)	NA	Bhuj Formation	112457	112457
470	15.07.2025	GSPL_Bhuj_ 300/07/2025	23.20335	69.62852	Mirzapar	Hilli exposure near Mirzapur	Brecciation plane, 130-250, 60NE., 120/64NE Host rock planar cross stratified coarse grained sandstone with Bedding 40 -220/30NW 112455 (altered part), 112456 (unaltered part), 112457 (host rock), 112458(partly metasomatized)	NA	Bhuj Formation	112458	112458
471	15.07.2025	Katrol fault	23.20208	69.62904	Mirzapar	Hilli exposure near Mirzapur	Bhuj -Chari contact	NA	Bhuj- Chari Contact	NA	NA
472	15.07.2025	GSPL_Bhuj_ 315/07/2025	23.20208	69.62904	Mirzapar	Hilli exposure near Mirzapur	Bhuj - Chari contact, katrol fault, similar fault??, similar but low amount of alteration of sandstone. The altered sandstone is blackish red coloured, coarse grained, and consists of angular to rounded quartz, white clay clast (altered feldspar possibly??), iron clasts embedded in a hematitic matrix/cement. The host rock is alteration of coarse sandstone and clay. Bedding can not measured due to weathering.	Fault: 70/55 N	Bhuj chari Contact	NA	NA
473	17-07-2025	GSPL_Bhuj_ 302/07/2025	23.20525	69.62846	Mirzapar	Hilli exposure near Mirzapur	Laterite formation, iron impregnation are common in this exposure. Host lithology: white clay overlain by altered highly ferruginous sandstone. Sandstone composed mainly of sub angular to rounded quartz, white clay present at places.	110/6 SW	Bhuj Formation	NA	NA
474	17-07-2025	GSPL_Bhuj_ 303/07/2025	23.20480	69.62823	Mirzapar	Hilli exposure near Mirzapur	Laterite formation, iron impregnation are common in this exposure. Host lithology: white clay overlain by altered highly ferruginous sandstone. Sandstone composed mainly of sub angular to rounded quartz, white clay present at places.	30/9-SE	Bhuj Formation	NA	NA
475	17-07-2025	GSPL_Bhuj_ 304/07/2025	23.20467	69.62822	Mirzapar	Hilli exposure near Mirzapur	Sandstone clay contact	NA	Bhuj Formation	NA	NA
476	17-07-2025	GSPL_Bhuj_ 305/07/2025	23.20378	69.62824	Mirzapar	Hilli exposure near Mirzapur	Sandstone	NA	Bhuj Formation	NA	NA
477	17-07-2025	GSPL_Bhuj_ 306/07/2025	23.20370	69.62831	Mirzapar	Hilli exposure near Mirzapur	Clay	120 -300/6 S	Bhuj Formation	112458	112458

Sl. No.	Date	Location No.	Latitude	Longitude	Village/ Area	Exposure Location	Host Lithology	Azimuth	Stratigraphy	Original BR ID	New BR ID
478	17-07-2025	GSPL_Bhuj_307/07/2025	23.20368	69.62831	Mirzapar	Hilli exposure near Mirzapur	Planner cross Stratified Sandstone 160 11 sw 172 10 SW	160/11SW, 172/10SW	Bhuj Formation	NA	NA
479	17-07-2025	GSPL_Bhuj_308/07/2025	23.20360	69.62841	Mirzapar	Hilli exposure near Mirzapur	Large scale planer cross stratified sandstone, very less amount of iron impregnation	Bedding plane 112/4S, fault plane 94/60N	Bhuj Formation	NA	NA
480	17-07-2025	GSPL_Bhuj_309/07/2025	23.20352	69.62848	Mirzapar	Hilli exposure near Mirzapur	Ferruginous sandstone, hematite layer along fault plane	Bedding plane: 120/6SW, Fault: 60/76N	Bhuj Formation	NA	NA
481	17-07-2025	GSPL_Bhuj_310/07/2025	23.20345	69.62853	Mirzapar	Hilli exposure near Mirzapur	Ferruginous sandstone	146/8S	Bhuj Formation	NA	NA
482	17-07-2025	GSPL_Bhuj_311/07/2025	23.20339	69.62855	Mirzapar	Hilli exposure near Mirzapur	Metasomatised sandstone, hematite layer along fault plane	120/9S	Bhuj Formation	NA	NA
483	17-07-2025	GSPL_Bhuj_312/07/2025	23.20332	69.62855	Mirzapar	Hilli exposure near Mirzapur	Metasomatised sandstone, hematite layer along fault plane	Fault plane: 86/64N, Bedding plane: 100/7S	Bhuj Formation	NA	NA
484	17-07-2025	GSPL_Bhuj_313/07/2025	23.20322	69.62856	Mirzapar	Hilli exposure near Mirzapur	Ferruginous sandstone with strong iron impregnation and metasomatism	Fault Plane: 80/70N	Bhuj Formation	112459	112459
485	17-07-2025	GSPL_Bhuj_314/07/2025	23.20313	69.62864	Mirzapar	Hilli exposure near Mirzapur	Sandstone (Slightly altered)	NA	Bhuj Formation	NA	NA
486	17-07-2025	GSPL_Bhuj_315/07/2025	23.20305	69.62866	Mirzapar	Hilli exposure near Mirzapur	Unaltered sandstone	Fault Plane: 84/58N	Bhuj Formation	NA	NA
487	17-07-2025	GSPL_Bhuj_316/07/2025	23.20290	69.62865	Mirzapar	Hilli exposure near Mirzapur	Unaltered sandstone Bedding plane: 180/10 S	Bedding: 180/10S	Bhuj Formation	NA	NA
488	17-07-2025	GSPL_Bhuj_317/07/2025	23.20272	69.62871	Mirzapar	Hilli exposure near Mirzapur	Sandstone clay alteration	Bedding: 124/10S	Bhuj Formation	NA	NA
489	17-07-2025	GSPL_Bhuj_318/07/2025	23.20240	69.62882	Mirzapar	Hilli exposure near Mirzapur	Sandstone	NA	Bhuj Formation	NA	NA

Sl. No.	Date	Location No.	Latitude	Longitude	Village/ Area	Exposure Location	Host Lithology	Azimuth	Stratigraphy	Original BR ID	New BR ID
490	18.07.2025	GSPL_Bhuj _319/07/2025	23.19757	69.52979	Mankua	Location marked as metasomatized Sandstone and situated in close proximity to BH 08. The site is characterised by an undulatory topography and is located on a small hill, surrounded by larger hills to the south and east. A dam is present on the western and northern sides of the area. Notably, compass readings may not be obtained correctly at this location, possibly due to strong magnetic interference.	The site is geophysically significant, lying adjacent to a zone of high magnetic anomaly and coinciding with elevated uranium (U) and thorium (Th) anomalies. The outcrop consists of a distinct black sandstone overlying an unaltered, planar cross stratified, medium to coarse grained quartzose sandstone. The metasomatized sandstone is medium grained and composed of angular to rounded quartz grains, euhedral feldspars, and aggregates of mica, all embedded within a hematitic to magnetite rich matrix or cement. The unit exhibits evidence of flow structures. Additionally, a greenish to greenish blue hue has been observed along several fracture surfaces. A portion of the powdered rock is attracted to a strong magnet and leaves a black streak, further indicating a magnetite_rich composition.	Bedding Plane:60/20° NW and 140/4N Fractures:Conjugate sets observed trending along 160 _ 340and 50 _230, with an additional prominent fracture at 65-245	Bhuj Formation	112460	112460
491	20-07-2025	GSPL_Bhuj_ 320/07/25	23.20134	69.53626	Mankua	Road side exposure,accessible through a metal road from Bhuj Nakhetrana Highway	A settlement is established over a blackish red (purplish tinch), coloured medium to coarse grained sandstone. It is composed of angular to rounded quartz, euhedral feldspar, muscovite (possibly detritus), embetin a hematitic and magnetite matrix/cement. The rock powder is attracted by strong magnet. Fracture filled with calcrete.	NA	Bhuj Formation	112461	112461
492	20-07-2025	GSPL_Bhuj_ 321/07/25	23.20306	69.53573	Mankua	Road side exposure near Bhuj Naliya highway, outcrop of small mound	Occurrence of thick blackish red sandstone, (altered, but did not turn to metasomatized) separated by yellowish occur coloured shale/clay. Thin veinlets of black materials (very few parts of the powder of the material are attracted by magnet, cherry red streak), are observed to be cross cutting the sandstone. Similar mm thin layers are also observed along the strata. The sandstone is medium to coarse grained and consists of angular to rounded quartz (detritus), muscovite(detritus), biotite(??), weathered sub rounded feldspar embedded in a mostly hematite and poorly magnetite matrix cement. Secondary fluid (silvery, pinkish blue and golden, varigated colour)along with few fractures are also observed.	100-280/18S	Bhuj Formation	112462	112462

Sl. No.	Date	Location No.	Latitude	Longitude	Village/ Area	Exposure Location	Host Lithology	Azimuth	Stratigraphy	Original BR ID	New BR ID
493	20-07-2025	GSPL_Bhuj_322/07/25	23.19357	69.51865	Mankua	Small mound, part of a larger hill	Occurrence of black colour altered sandstone, overlying unaltered ferruginous sandstone. The unaltered sandstone is quartz arenite, with sub rounded to very well rounded quartz, embedded in a siliceous/ calcareous?? matrix/ cement. The altered sandstone is composed of angular to sub rounded quartz, euhedral feldspars, mica embedded in a hematitic to magnetite matrix/cement. Strangely this black sandstone is always observed at the top part of the exposure both in lower and upper contour. 130/5NE Sample of quartz arenite 112463 Sample of black colour altered sandstone 112464 Thin veinlets(carbonate?? And few muscovite) observed within the sandstone 112466	130/5NE	Bhuj Formation	112463	112463
494	20-07-2025	GSPL_Bhuj_322/07/2025	23.19357	69.51865	Mankua	Small mound, part of a larger hill	Occurrence of black colour altered sandstone, overlying unaltered ferruginous sandstone. The unaltered sandstone is quartz arenite, with sub rounded to very well rounded quartz, embedded in a siliceous/ calcareous?? matrix/ cement. The altered sandstone is composed of angular to sub rounded quartz, euhedral feldspars, mica embedded in a hematitic to magnetite matrix/cement. Strangely this black sandstone is always observed at the top part of the exposure both in lower and upper contour. 130/5NE Sample of quartz arenite 112463 Sample of black colour altered sandstone 112464 Thin veinlets(carbonate?? And few muscovite) observed within the sandstone 112466	NA	Bhuj Formation	112464	112464
495	20-07-2025	GSPL_Bhuj_322/07/2025	23.19357	69.51865	Mankua	Small mound, part of a larger hill	Occurrence of black colour altered sandstone, overlying unaltered ferruginous sandstone. The unaltered sandstone is quartz arenite, with sub rounded to very well rounded quartz, embedded in a siliceous/ calcareous?? matrix/ cement. The altered sandstone is composed of angular to sub rounded quartz, euhedral feldspars, mica embedded in a hematitic to magnetite matrix/cement. Strangely this black sandstone is always observed at the top part of the exposure both in lower and upper contour. 130/5NE Sample of quartz arenite 112463 Sample of black colour altered sandstone 112464 Thin veinlets(carbonate??	NA	Bhuj Formation	112465	112465

Sl. No.	Date	Location No.	Latitude	Longitude	Village/ Area	Exposure Location	Host Lithology	Azimuth	Stratigraphy	Original BR ID	New BR ID
							And few muscovite) observed within the sandstone 112466				
498	20-07-2025	GSPL_Bhuj_324/07/2025	23.19268	69.51791	Samantra /kodki	Exposure along fault plane near a water reservoir	Occurrence of fault 20/40E displacing very coarse to coarse grained quartzose sandstone. However along the fault plane a zone of 2.7m (towards east) is altered and consists of metasomatized sandstone and a very light weight purplish white colour sandstone, highly altered, no such detritus grain boundary observed, and consists of carbonate??, iron concretion very few quartz embedded in ferruginous matrix/ cement .	Fault 20/40E, Bedding 40/20NW	Bhuj Formation	112466	112466
499	21-07-2025	GSPL_Bhuj_325/07/2025	23.20329	69.58544	Mankua	Road side expousre near Mankuva road	Weathered sandstone	NA	Bhuj Formation	112469	112469
500	21-07-2025	GSPL_Bhuj_326/07/2025	23.20335	69.58403	Mankua	Road side expousre near Mankuva road	Greyish white colour, medium to coarse grained sandstone with iron impregnation, some iron impregnation are of 5 to 8 cm in diameter, with four layer rim outer most is the sandstone, than altered ferruginous ring, than a very thin yellow altered ring may be of lemonite or goethite, and the inner most is black sandstone with some white cement material may be carbonate or silica. Non GSPL_Bhuj_magnetic.	190/55E	Bhuj Formation	NA	NA
501	21-07-2025	GSPL_Bhuj_327/07/2025	23.20248	69.58506	Mankua	Road side expousre near Mankuva road	Weathered greyish coloured shale dominating hetrolith?? , some iron impregnation, silica /carbonate solution intruded through fracture. Presence of few black shards. Intrusion of basalt.	NA	Bhuj Formation	112470	112470
502	21-07-2025	GSPL_Bhuj_327/07/2025	23.20248	69.58506	Mankua	Road side expousre near Mankuva road	Weathered greyish coloured shale dominating hetrolith?? , some iron impregnation, silica /carbonate solution intruded through fracture. Presence of few black shards. Intrusion of basalt.	NA	Bhuj Formation	112471	112471

Sl. No.	Date	Location No.	Latitude	Longitude	Village/ Area	Exposure Location	Host Lithology	Azimuth	Stratigraphy	Original BR ID	New BR ID
503	21-07-2025	GSPL_ Bhuj_327/07 /2025	23.20248	69.58506	Mankua	Road side expousre near Mankuva road	Weathered greyish coloured shale dominating hetrolith?? , some iron impregnation, silica /carbonate solution intruded through fracture. Presence of few black shards. Intrusion of basalt.	NA	Bhuj Formation	112472	112472
504	22-07-2025	GSPL_Bhuj_ 328/07/2025	23.20276	69.58500	Mankua	Road side expousre near Mankuva road	Hard compact sandstone with >95% quartz, quartz boundary are not clearly visible, may be recrystallized.	NA	Bhuj Formation	112473	112473
505	22-07-2025	GSPL_Bhuj _329/07/202 5	23.20289	69.584972	Mankua	Road side expousre near Mankuva road	Medium grained Sandstone with more than 95 % Quartz	NA	Bhuj Formation	NA	NA
506	22-07-2025	GSPL_Bhuj_ 330/07/25	23.20314	69.58484	Kalyanpar	Road side expousre near Kalyanpar road	Sandstone	NA	Bhuj Formation	112474	112474
507	22-07-2025	GSPL_Bhuj_ 331/07/25	23.22089	69.58948	Kalyanpar	Hill expousre near Kalyanpar road	metasomatized sandstone	NA	Bhuj Formation	112475	112475
508	22-07-2025	GSPL_Bhuj_ 331/07/25	23.22089	69.58948	Kalyanpar	Hill expousre near Kalyanpar road	metasomatized sandstone	NA	Bhuj Formation	112477	112477
509	22-07-2025	GSPL_Bhuj_ 332/07/25	23.22085	69.59025	Kalyanpar	Hill expousre near Kalyanpar road	Dark grey to black coloured specimen with numerous small rounded to irregular vesicles .Some vesicles show signature of partial infilling by secondary mineral like calcite. The rocks are campact and weathering is also observered.	NA	Bhuj Formation	112476	112476
510	23-07-2025	GSPL_Bhuj_ 333/07/2025	23.17681	69.62331	Sedata	Hill exposure near Bhuj-Mundra high way	Medium grained, yellowish weathered sandstone with ferruginous alterations and goethite at some places.	NA	Bhuj Formation	NA	NA
511	23-07-2025	GSPL_Bhuj_ 334/07/2025	23.17594	69.62333	Sedata	Hill exposure near Bhuj-Mundra high way	Alternate layers of sandstone and shale , with sst varying from 3-15cm and shale 1-3cm	NA	Bhuj Formation	NA	NA
512	23-07-2025	GSPL_Bhuj_ 334/07/2025	23.17599	69.62296	Sedata	Hill exposure near Bhuj-Mundra high way	Fault , displacement 30cm, Sandstone -shale	NA	Bhuj Fornation	NA	NA
513	23-07-2025	GSPL_Bhuj_ 335/07/2025	23.17339	69.62416	Sedata	Hill exposure near Bhuj-Mundra high way	Sandstone	NA	Bhuj Fornation	NA	NA
514	23-07-2025	GSPL_Bhuj_ 336/07/2025	23.17271	69.62487	Sedata	Hill exposure near Bhuj-Mundra high way	Hetrolith highly weathered Sample taken of black part	NA	Bhuj Fornation	112478	112478
515	23-07-2025	GSPL_Bhuj_ 337/07/2025	23.17199	69.62476	Sedata	Hill exposure near Bhuj-Mundra high way	Altered ferruginous sandstone	NA	Bhuj Fornation	112479	112479
516	23-07-2025	GSPL_Bhuj_ 338/07/2025	23.17020	69.62394	Sedata	Hill exposure near Bhuj-Mundra high way	Secondary solution may be Carbonate , ferruginous sandstone with highly altered , fluid activity can be seen	110/3°NE	Bhuj Fornation	112480	112480
517	23-07-2025	GSPL_Bhuj_ 338/07/2025	23.17020	69.62394	Sedata	Hill exposure near Bhuj-Mundra high way	Secondary solution may be Carbonate , ferruginous sandstone with highly altered , fluid activity can be seen	NA	Bhuj Fornation	112481	112481

Sl. No.	Date	Location No.	Latitude	Longitude	Village/ Area	Exposure Location	Host Lithology	Azimuth	Stratigraphy	Original BR ID	New BR ID
518	23-07-2025	GSPL_BHUJ_339/07/2025	23.17008	69.62406	Sedata	Hill exposure near Bhuj-Mundra high way	Secondary solution may be Carbonate , ferruginous sandstone with highly altered , fluid activity can be seen, sample taken jhamma ?? Joint Plane trend 70 250 Joint Plane trend 80 261	NA	Bhuj Fornation	NA	NA
519	23-07-2025	GSPL_Bhuj_340/07/2025	23.17121	69.61953	Sedata	Hill exposure near Bhuj-Mundra high way	Numerous Gravels of weathered sandstone observed (metasomatized?)	NA	Bhuj Fornation	112482	112482
520	23-07-2025	340 extension	23.17102	69.61981	Sedata	Hill exposure near Bhuj-Mundra high way	Sandstone	NA	Bhuj Fornation	NA	NA
521	23-07-2025	GSPL_Bhuj_341/07/2025	23.16333	69.62203	Sedata	Hill exposure near Bhuj-Mundra high way	Sandstone dominated heterolith with thin layer shale	NA	Bhuj Fornation	NA	NA
522	24-07-2025	GSPL_Bhuj_342/07/2025	23.22287	69.59439	Kalyanpr	Hill exposure near Kalyanpar road	Medium to coarse grained sandstone with angular to sub rounded quartz and iron concretions embedded in a silicious to calcerous (??) matrix or cement . 1.2 m sandstone units are separated by 30 -32 cm thick white siltstone unit . The sandstone layers are highly altered at a a particular stratigraphic level where it is brownish red to purpulish red in colour and consist of both rounded and angular(crystal clear) quartz embedded in a ferruginous hematitic matrix or cement, no feldspar grains and no magnetite observed.	170/45 (260)	Bhuj Formation	112483	112483
523	25-07-2025	GSPL_Bhuj_343/07/2025	23.19045	69.69681	Haripar	Near Dhunaraj Dem Road	Ferruginous sandstone	NA	Katrol Formation	NA	NA
524	25-07-2025	GSPL_Bhuj_344/07/2025	23.19073	69.69641	Haripar	Near Dhunaraj Dem Road	Medium to coarse grained ferruginous weathered sandstone Iron concretion present , angular to rounded grains	NA	Katrol Formation	112484	112484
525	25-07-2025	GSPL_Bhuj_345/07/2025	23.18929	69.69411	Haripar	Near Dhunaraj Dem Road	Brecciated weathered sandstone	NA	Katrol Formation	112485	112485
526	25-07-2025	GSPL_Bhuj_346/07/2025	23.18970	69.69319	Haripar	Near Dhunaraj Dem Road	Boulder of metasomatized Sandstone (Exsitu sample). Medium to fine grained White sandstone with calcite. And mica found .	NA	Katrol Formation	112486	112486
527	26-07-2025	GSPL_Bhuj_347/07/2025	23.18942	69.69226	Haripar	Near Dhunaraj Dem Road	Brecciated weathered sandstone	NA	Katrol Formation	NA	NA

Sl. No.	Date	Location No.	Latitude	Longitude	Village/ Area	Exposure Location	Host Lithology	Azimuth	Stratigraphy	Original BR ID	New BR ID
528	26-07-2025	GSPL_Bhuj_ 348/07/25	23.19432	69.58188	Mankuva	Single elliptical mound shaped outcrop, accessible from Bhuj Mandvi highway through a cart road, near Vandhsim. The mound is full of large boulders and very few insitu rocks. Situated very near to Katrol hill fault.	The general trend of bedding of all of the litho units does seem to be tilted from its position, however strike dip has been verified from insitu rock at lower contour also. The outcrop is composed of sandstone, cross cutting by hematite veins. Veins parallel to the strata is also observed. The sandstone is composed of both clean and detritus quartz, ranging in size from medium to very coarse, angular to sub _rounded embedded in a hematitic to silicic(??) matrix/ cement. The clean semi transparent quartz grains are more angular and surrounded by hematite rims. The sandstones seems to be brecciated at places, specifically where the iron veins are in cross cutting relationship with the sandstone. The cross cutting veins oriented 92-272/ 50W, 84/38W, 102/25W (calcite). Veins filled with carbonate sub parallel to the iron veins are also observed. Sample taken brecciated sandstone, carbonate (??) vein.	Bedding plane 50 - 230/ 40NW, 60 - 240/45NW The cross cutting veins oriented 92 - 272/ 50W, 84/38W, 102/25W (calcite).	Bhuj Formation	112488	112488
529	26-07-2025	GSPL_Bhuj_ 360/07/25	23.20248	69.58385	Mankuva	Hill Exposure near Mankuva road	Medium to carse grained sandstone	Joint trends 290 -110, 305 -125, 0 -180, Bedding plane, 290/85 SW	Bhuj Formation	NA	NA
530	26-07-2025	GSPL_Bhuj_ 349/07/2025	23.19132	69.58018	Bharasar	Multiple elliptical mound shaped outcrop clustered at single places , accessible from Bhuj Mandvi highway through a cart road, near Wandhsim.	The mound is composed of mostly basalt, intruding sandstone clay units. Clay relict (??) in a circular shaped area, is observed to be emplaced within the dark black coloured basalt. The basalt is very fine grained, possibly composed of plagioclase feldspar laths, ophitic to sub ophitic texture ??, and green coloured phenocrysts of olivine/ serpentine. The sandstone is medium grained quartz arenite wth iron concretion at places. The clay is white coloured very fine grained. However the clay relict part also consists of few angular quartz grains embedded within the matrix/ cement. Mm thin layers of Calcite, translucent, no colour, breakable, scratched by finger nails) is observed to be emplaced in cross cutting relationship within the basalt. Towards the south east of this location, another hilly	NA	Bhuj Formation	112489	112489

Sl. No.	Date	Location No.	Latitude	Longitude	Village/ Area	Exposure Location	Host Lithology	Azimuth	Stratigraphy	Original BR ID	New BR ID
							isolated outcrop observed, which seems mostly composed of sandstone .				
531	26-07-2025	GSPL_Bhuj_ 349/07/2025	23.19132	69.58018	Bharasar	Multiple elliptical mound shaped outcrop clustered at single places , accessible from Bhuj Mandvi highway through a cart road, near Wandhsim.	The mound is composed of mostly basalt, intruding sandstone clay units. Clay relict (??) in a circular shaped area, is observed to be emplaced within the dark black coloured basalt. The basalt is very fine grained, possibly composed of plagioclase feldspar laths, ophitic to sub ophitic texture ??, and green coloured phenocrysts of olivine/ serpentine. The sandstone is medium grained quartz arenite wth iron concretion at places. The clay is white coloured very fine grained. However the clay relict part also consists of few angular quartz grains embedded within the matrix/ cement. Mm thin layers of Calcite, translucent, no colour, breakable, scratched by finger nails) is observed to be emplaced in cross cutting relationship within the basalt. Towards the south east of this location, another hilly isolated outcrop observed, which seems mostly composed of sandstone .	NA	Bhuj Formation	112490	112490

Sl. No.	Date	Location No.	Latitude	Longitude	Village/ Area	Exposure Location	Host Lithology	Azimuth	Stratigraphy	Original BR ID	New BR ID
532	26-07-2025	GSPL_Bhuj_ 349/07/2025	23.19132	69.58018	Bharasar	Multiple elliptical mound shaped outcrop clustered at single places , accessible from Bhuj Mandvi highway through a cart road, near Wandhsim.	The mound is composed of mostly basalt, intruding sandstone clay units. Clay relict (??) in a circular shaped area, is observed to be emplaced within the dark black coloured basalt. The basalt is very fine grained, possibly composed of plagioclase feldspar laths, ophitic to sub ophitic texture ??, and green coloured phenocrysts of olivine/ serpentine. The sandstone is medium grained quartz arenite wth iron concretion at places. The clay is white coloured very fine grained. However the clay relict part also consists of few angular quartz grains embedded within the matrix/ cement. Mm thin layers of Calcite, translucent, no colour, breakable, scratched by finger nails) is observed to be emplaced in cross cutting relationship within the basalt. Towards the south east of this location, another hilly isolated outcrop observed, which seems mostly composed of sandstone .	NA	Bhuj Formation	112491	112491
533	26-07-2025	GSPL_Bhuj_ 350/07/2025	23.19364	69.57563	Bharasar	Local reported brass looking rock at 200 feet and exposure of metasomatized sandstone.	metasomatized sandstone observed at the top part and is composed of angular to sub rounded quartz, euhedral feldspar, book mica (muscovite) embedded in a hematite and magnetite (lots of) matrix and cement Below they get a fracture zone while boring and bore collapsed.	20/ 15NW, 140/18W	Bhuj Formation	NA	NA
534	26-07-2025	GSPL_Bhuj_ 351/07/2025	23.22263	69.59411	Kalyanpar	Cluster of small circular mounds creating an undulatory topography near Kalyanpur village, accessible from Bhuj Nakshatrana highway through local village metal road and then a cart road. The present location is a junction point between 2 fault/ fracture?? Planes.	Along the fault plane there is highly ferruginous sandstone, consists of angular to few sub rounded grains of quartz, very few mica and clasts of hematite embedded in a hematitic matrix/ cement. The amount of the framework is ~ 40% (112492). The zone between the fractures consists of ferruginous, pinkish purple coloured sandstone with 0. 5cm to 16cm clasts of clay and/ or siltstone (observed as original bed at the other part of the mound). The sandstone comprises angular to rounded, elongated, circular wedge shaped quartz, clay clasts, muscovite may be embedded in a siliceous to calcareous matrix. At very few places feldspar grains are also suspected. Small iron concretion is also observed. (11493) At the boundary of the 2nd fault, there is breccia (11494), consisting of angular to well rounded quartz, clay clasts, small gashes or lens like structures filled with either	The fractures are oriented 160/ 54W 190/44W. Other small scale fractures are trending 140 - 320, 138 - 318, 130 - 310.	Bhuj Formation	112492	112492

Sl. No.	Date	Location No.	Latitude	Longitude	Village/ Area	Exposure Location	Host Lithology	Azimuth	Stratigraphy	Original BR ID	New BR ID
							carbonate/ silica, few book mica (muscovite), well rounded iron clasts embedded in a hematitic matrix/cement. No magnetite observed. The unaltered sandstone (11495) is quartz arenite.				
535	26-07-2025	GSPL_Bhuj_ 351/07/2025	23.22263	69.59411	Kalyanpar	Cluster of small circular mounds creating an undulatory topography near Kalyanpur village, accessible from Bhuj Nakshatrana highway through local village metal road and then a cart road. The present location is a junction point between 2 fault/ fracture?? Planes.	Along the fault plane there is highly ferruginous sandstone, consists of angular to few sub rounded grains of quartz, very few mica and clasts of hematite embedded in a hematitic matrix/ cement. The amount of the framework is ~ 40% (112492). The zone between the fractures consists of ferruginous, pinkish purple coloured sandstone with 0. 5cm to 16cm clasts of clay and/ or siltstone (observed as original bed at the other part of the mound). The sandstone comprises angular to rounded, elongated, circular wedge shaped quartz, clay clasts, muscovite may be embedded in a siliceous to calcareous matrix. At very few places feldspar grains are also suspected. Small iron concretion is also observed. (11493) At the boundary of the 2nd fault, there is breccia (11494), consisting of angular to well rounded quartz, clay clasts, small gashes or lens like structures filled with either carbonate/ silica, few book mica (muscovite), well rounded iron clasts embedded in a hematitic matrix/cement. No magnetite observed. The unaltered sandstone (11495) is quartz arenite.	Bedding 150/43NE	Bhuj Formation	112493	112493

Sl. No.	Date	Location No.	Latitude	Longitude	Village/ Area	Exposure Location	Host Lithology	Azimuth	Stratigraphy	Original BR ID	New BR ID
536	26-07-2025	GSPL_Bhuj_ 351/07/2025	23.22263	69.59411	Kalyanpar	Cluster of small circular mounds creating an undulatory topography near Kalyanpur village, accessible from Bhuj Nakshatrana highway through local village metal road and then a cart road. The present location is a junction point between 2 fault/ fracture?? Planes.	Along the fault plane there is highly ferruginous sandstone, consists of angular to few sub rounded grains of quartz, very few mica and clasts of hematite embedded in a hematitic matrix/ cement. The amount of the framework is ~ 40% (112492). The zone between the fractures consists of ferruginous, pinkish purple coloured sandstone with 0. 5cm to 16cm clasts of clay and/ or siltstone (observed as original bed at the other part of the mound). The sandstone comprises angular to rounded, elongated, circular wedge shaped quartz, clay clasts, muscovite may be embedded in a siliceous to calcareous matrix. At very few places feldspar grains are also suspected. Small iron concretion is also observed. (11493) At the boundary of the 2nd fault, there is breccia (11494), consisting of angular to well rounded quartz, clay clasts, small gashes or lens like structures filled with either carbonate/ silica, few book mica (muscovite), well rounded iron clasts embedded in a hematitic matrix/cement. No magnetite observed. The unaltered sandstone (11495) is quartz arenite.	NA	Bhuj Formation	112494	112494
537	26-07-2025	GSPL_Bhuj_ 351/07/2025	23.22263	69.59411	Kalyanpar	Cluster of small circular mounds creating an undulatory topography near Kalyanpur village, accessible from Bhuj Nakshatrana highway through local village metal road and then a cart road. The present location is a junction point between 2 fault/ fracture?? Planes.	Along the fault plane there is highly ferruginous sandstone, consists of angular to few sub rounded grains of quartz, very few mica and clasts of hematite embedded in a hematitic matrix/ cement. The amount of the framework is ~ 40% (112492). The zone between the fractures consists of ferruginous, pinkish purple coloured sandstone with 0. 5cm to 16cm clasts of clay and/ or siltstone (observed as original bed at the other part of the mound). The sandstone comprises angular to rounded, elongated, circular wedge shaped quartz, clay clasts, muscovite may be embedded in a siliceous to calcareous matrix. At very few places feldspar grains are also suspected. Small iron concretion is also observed. (11493) At the boundary of the 2nd fault, there is breccia (11494), consisting of angular to well rounded quartz, clay clasts, small gashes or lens like structures filled with either carbonate/ silica, few book mica (muscovite), well rounded iron clasts embedded in a	NA	Bhuj Formation	112495	112495

Sl. No.	Date	Location No.	Latitude	Longitude	Village/ Area	Exposure Location	Host Lithology	Azimuth	Stratigraphy	Original BR ID	New BR ID
							hematitic matrix/cement. No magnetite observed. The unaltered sandstone (11495) is quartz arenite.				
538	27-07-2025	GSPL_Bhuj_ 352/07/2025	23.22259	69.59464	Kalyanpar	Hill exposure near Mankuva Road	Altered ferruginous sandstone, very fine grained, can only identify quartz.	Bedding 160/23W	Bhuj Formation	NA	NA
539	27-07-2025	GSPL_Bhuj_ 353/07/2025	23.22200	69.59442	Kalyanpar	Cluster of small circular mounds creating an undulatory topography near Kalyanpur village, accessible from Bhuj Nakshatrana highway through local village metal road and then a cart road.	The present location comprises alternating occurrence of ferruginous sandstone and white siltstone. However, the ferruginous sandstone is medium to coarse grained quartz arenite. Along few of the bedding plane there is high amount of ferrugination and alteration making it very hard, blackish red coloured sandstone (112496) and consists of angular to sub angular quartz, muscovite embedded in a hematitic to magnetite (less amount, part of the rock powder is affected by magnet). matrix. Bedding 150/20SW. Fractures (180/60E), cross cutting the sandstone is also observed.	Bedding 150/20SW. Fractures 180/60E	Bhuj Formation	112496	112496
540	27-07-2025	GSPL_Bhuj_ 354/07/2025	23.22078	69.59467	Kalyanpar	Hill exposure near Kalyanpar Road	Unaltered sandstone, probably basalt intrusion at the upper contour, as we are getting small boulders of basalt at the lowest contour at the opposite side of the hill	150/20SW	Bhuj Formation	NA	NA
541	27-07-2025	GSPL_Bhuj_ 355/07/2025	23.22175	69.59065	Kalyanpar	Hill exposure near Kalyanpar Road	Occurrence of basalt as long elongated outcrop, very fine grained, blackish grey colour, relict of olivine (112497)	NA	Anjar Volcanics	112497	112497
542	27-07-2025	GSPL_Bhuj_ 356/07/2025	23.22632	69.59412	Kalyanpar	Hill exposure near Kalyanpar Road	Bedded deposit of ferruginous sandstone, consists of sub rounded to sub angular quartz embedded in calcareous?? Siliceous?? matrix/cement.	290/4NE	Bhuj Formation	NA	NA

Sl. No.	Date	Location No.	Latitude	Longitude	Village/ Area	Exposure Location	Host Lithology	Azimuth	Stratigraphy	Original BR ID	New BR ID
543	27-07-2025	GSPL_Bhuj_ 357/07/2025	23.22712	69.59410	Kalyanpar	Undulatory topography with hills and valleys near Kalyanpur village, accessible from Bhuj Nakshatrana highway through local village metal road.	The outcrop is of ferruginous sandstone intruded by hematitic lemonitic fluid, creating cross cutting veins and brecciated structures. The sandstone is composed of angular to sub angular quartz, in a hematitic matrix. Each minerals is iron coated. Void area filled with silica is also observed. However, at places the dust of the sandstone is febbly magnetic at places. General trend of the flow is 20 _201	NA	Bhuj Formation	NA	NA
544	29-07-2025	GSPL_Bhuj_ 358/07/2025	23.19466	69.58035	Mankuva	Single elliptical mound shaped outcrop, accessible from Bhuj Mandvi highway through a cart road, near Wandhsim. Also accessible from Sukhpar main road through village metal road. Situated very near to Katrol hill fault.	THe outcrop is composed of coarse to very coarse grained sandstone, with sub parallel to cross cutting hematite veins. The sandstone is composed of both clean and detritus quartz, ranging in size from coarse to very coarse, angular to sub rounded, both biotite and muscovite, varigated colour minerals (bornite??, few magnetite grains embedded in a hematitic to silicic(??) matrix/ cement. The clean semi transparent quartz grains are more angular and surrounded by hematite rims. The sandstones seems to be brecciated at places, specifically where the iron veins are in cross cutting relationship with the sandstone. The dust of the rock attracted by magnet. The colluvium part is also getting attracted by magnet. There is a fine grained variety of dark blackish brown colour rock with lots of very small grains of euhedral feldspar.	Bedding 160/50W	Bhuj Formation	112498	112498
545	26-08-2025	GSPL_Bhuj_ 361/08/2025	23.20802	69.61534	Mirzapar	Hill exposure near Mirzapar village	Metasomatized ferrugineous sandstone, composed of quartz, muscovite	240-60/20SE	Bhuj Formation	113451	113451
546	26-08-2025	GSPL_Bhuj_ 362/08/2025	23.20844	69.61510	Mirzapar	Hill exposure near Mirzapar village	Metasomatized ferrugineous sandstone, composed of quartz, muscovite	240-60/20SE	Bhuj Formation	NA	NA
547	03-09-2025	GSPL_Bhuj_ 363/09/2025	23.18534	69.57423	Bharasar	Hill exposure near Bharasar village	Ferruginous sandstone , purpulish to yellowish mainly composed of quartz muscovite biotite	79/22SE	Bhuj Formation	113453	113453
548	03-09-2025	GSPL_Bhuj_ 364/09/2025	23.18811	69.56407	Sukhpar	Hill exposure near Mirzapar village	Greyish coloured unaltered white sandstone easily breakable composed of quartz 99%, muscovite and pink tint in some places due to iron oxide possibly	NA	Bhuj Formation	113452	113452
549	03-09-2025	GSPL_Bhuj_ 365/09/2025	23.18917	69.56349	Sukhpar	Hill exposure near Mirzapar village	Unaltered white Sandstone	NA	Bhuj Formation	113354	113354

Sl. No.	Date	Location No.	Latitude	Longitude	Village/ Area	Exposure Location	Host Lithology	Azimuth	Stratigraphy	Original BR ID	New BR ID
550	03-09-2025	GSPL_Bhuj_366/09/2025	23.19685	69.56721	Sukhpar	Hill exposure near Mirzapar village	Ferruginous sandstone(unable to go private property) gate was locked	NA	Bhuj Formation	NA	NA
551	03-09-2025	GSPL_Bhuj_367/09/2025	23.22264	69.61637	Sukhpar	Hill exposure near Mirzapar village	Ferruginous altered sandstone , Purpulish to reddish coloured fine to medium grained , mainly composed of quartz , muscovite and silicification?? Also observed	NA	Bhuj Formation	113455	113455
552	03-09-2025	GSPL_Bhuj_368/09/2025	23.22232	69.61642	Sukhpar	Hill exposure near Mirzapar village	Purpulish to yellowish weathered Sandstone	170/80 SW (260)	Bhuj Formation	NA	NA
553	03-09-2025	GSPL_Bhuj_369/09/2025	23.17562	69.59176	Bharapar	Near Bhuj Mandvi Highway	The outcrop exposes a sequence of medium to fine grained, well bedded sandstone with alternating thin layers of argillaceous material. The sandstone is predominantly light brown to yellowish, showing differential weathering with honeycombed cavities and irregular surfaces. A prominent reddish to dark ferruginous band is observed within the sandstone, likely due to iron oxide impregnation/diagenetic cementation.	32° horizontal bed	Bhuj Formation	113456	113456
554	03-09-2025	GSPL_Bhuj_369/09/2025	23.17562	69.59176	Bharapar	Near Bhuj Mandvi Highway	The outcrop exposes a sequence of medium to fine grained, well bedded sandstone with alternating thin layers of argillaceous material. The sandstone is predominantly light brown to yellowish, showing differential weathering with honeycombed cavities and irregular surfaces. A prominent reddish to dark ferruginous band is observed within the sandstone, likely due to iron oxide impregnation/diagenetic cementation.	NA	Bhuj Formation	113457	113457
555	09-09-2025	GSPL_Bhuj_370/09/2025	23.14205	69.65114	Bharapar	Near Bhuj Mandvi Highway	One unit is Ferruginous sandstone and other is altered ferruginous Sandstone (iron solution is seeing) Ferruginous sst is fine to medium grain where as altered is coarse to medium grained and occasionally very coarse grained composed of 98% quartz,iron solution? ,muscovite	30/85 SE	Bhuj Formation	113458	113458
556	09-09-2025	GSPL_Bhuj_370/09/2025	23.14205	69.65114	Bharapar	Near Bhuj Mandvi Highway	One unit is Ferruginous sandstone and other is altered ferruginous Sandstone (iron solution is seeing) Ferruginous sst is fine to medium grain where as altered is coarse to medium grained and occasionally very coarse grained composed of 98% quartz,iron solution? ,muscovite	NA	Bhuj Formation	113459	113459

Sl. No.	Date	Location No.	Latitude	Longitude	Village/ Area	Exposure Location	Host Lithology	Azimuth	Stratigraphy	Original BR ID	New BR ID
557	09-09-2025	GSPL_Bhuj_ 371/09/2025	23.14250	69.65164	Bharapar	Hill exposure accses from Bhuj-Mundra high way	The exposure represents a highly oxidized ferruginous outcrop with a brecciated to massive texture. The rock is dominated by iron oxides (hematite, goethite, limonite) with patchy development of bluish to greenish metallic stains, suggesting the presence (or former presence) of copper sulphides (bornite/chalcopyrite). Quartz grains are visible in the hand specimen, indicating possible vein/veinlet associations.	NA	Bhuj Formation	113460	113460
558	09-09-2025	GSPL_Bhuj_ 372/09/2025	23.14299	69.65280	Bharapar	Hill exposure accses from Bhuj-Mundra high way	Top few cm part is mostly cemented by hematitic matrix and rest is ferruginous sandstone .Ferruginous sandstone were documented along the fault plane (35°/85° SE). The rock consists dominantly of angular to sub rounded quartz grains, with mica, very few biotite, and hematite clasts embedded in a hematitic matrix/cement. The ferruginous sandstone also comprises angular to rounded, elongated, circular, and wedge shaped quartz grains. At a few locations, feldspar grains were suspected.	Fault plane: 35°/85° SE	Bhuj Formation	113461	113461
559	09-09-2025	GSPL_Bhuj_ 373/09/2025	23.14313	69.65304	Bharapar	Hill exposure accses from Bhuj-Mundra high way	Reddish brown altered ferruginous sandstone composed of quartz , one grain of feldspar also observed	Fault plane 60/40SE	Bhuj Formation	113462	113462
560	09-09-2025	GSPL_Bhuj_ 374/09/2025	23.14435	69.65485	Bharapar	Hill exposure accses from Bhuj-Mundra high way	Ferruginous sandstone consists dominantly of angular to sub rounded quartz grains, very few muscovite , and hematite clasts embedded in a hematitic matrix/cement. The ferruginous sandstone also comprises angular to rounded, elongated, circular, and wedge shaped quartz grains.	Fault 35°/85° SE	Bhuj Formation	NA	NA
561	09-09-2025	GSPL_Bhuj_ 375/09/2025	23.14239	69.65082	Bharapar	Hill exposure accses from Bhuj-Mundra high way	Ferruginous weathered sandstone was encountered, reddishbrown in colour, medium to fine grained. Composed of Quartz and Hematite.	NA	Bhuj Formation	113463	113463
562	10-09-2025	GSPL_Bhuj_ 376/09/2025	23.15572	69.68183	Jadura	Hill exposure accses near Jadura road	Ferruginous weathered sandstone, yellowish to purpulish in colour , quartz,muscovite and goethite . purpulish tint may be due to manganese	NA	Bhuj Formation	NA	NA
563	10-09-2025	GSPL_Bhuj_ 377/09/2025	23.15300	69.67865	Jadura	Hill exposure accses near Jadura road	Mica bearing metasomatized ferrugineous sandstone, occurring relatively at higher contours. The rock is fine to medium grained, dark grey to black coloured and with reddish brown staining . It consists dominantly of angular to sub rounded quartz grains with mica, feldspar, and hematite clasts embedded in a hematitic	30/20NW	Bhuj Formation	113464	113464

Sl. No.	Date	Location No.	Latitude	Longitude	Village/ Area	Exposure Location	Host Lithology	Azimuth	Stratigraphy	Original BR ID	New BR ID
							matrix/cement. Unaltered sandstone present at middile contour				
564	10-09-2025	GSPL_Bhuj_378/09/2025	23.15244	69.67555	Jadura	Hill exposure accses near Jadura road	Metasomatized ferruginous sandstone composed of mainly angular to subrounded quartz embedded in a hematitic matrix. Feldspar grain suspected.	30/20NW	Bhuj Formation	113465	113465
565	10-09-2025	GSPL_Bhuj_379/09/2025	23.15118	69.67192	Jadura	Hill exposure accses near Jadura road	Possible jhamm sandstone, composed of Quartz Muscovite	NA	Bhuj Formation	113466	113466
566	10-09-2025	GSPL_Bhuj_380/09/2025	23.15121	69.66875	Jadura	Hill exposure accses near Jadura road	Unaltered ferruginous sandstone at the lower Contour and metasomatized ferruginous sandstone found at the upper contour . Yellowish purplish to brown in colour, medium to fine grained, moderately sorted, and composed mainly of sub angular to sub rounded quartz (>99%). and muscovite. Unaltered sandstone mainly composed of quartz and non magnetic black colour mineral.	NA	Bhuj Formation	NA	NA
567	10-09-2025	GSPL_Bhuj_381/09/2025	23.15133	69.66879	Jadura	Hill exposure accses near Jadura road	Metasomatized ferruginous sandstone, occurring relatively at higher contours. The rock is fine to medium grained, dark grey to black coloured and with reddish brown staining . It consists dominantly of angular to sub rounded quartz grains with mica, feldspar, and hematite clasts embedded in a hematitic matrix/cement.	30/20NW	Bhuj Formation	113467	113467
568	10-09-2025	GSPL_Bhuj_382/09/2025	23.15240	69.66687	Jadura	Hill exposure accses near Jadura road	Purpulish sandstone altered types underlain by unaltered sandstone with non magnetitic black colour mineral .	NA	Bhuj Formation	113468	113468
569	10-09-2025	GSPL_Bhuj_382/09/2025	23.15240	69.66687	Jadura	Hill exposure accses near Jadura road	Purpulish sandstone altered types underlain by unaltered sandstone with non magnetitic black colour mineral .	NA	Bhuj Formation	113469	113469
570	10-09-2025	GSPL_Bhuj_383/09/2025	23.15522	69.66829	Jadura	Hill exposure accses near Jadura road	Metasomatized weathered sandstone composed of angular to subrounded quartz, muscovite	NA	Bhuj Formation	113472	113472
571	10-09-2025	GSPL_Bhuj_384/09/2025	23.15542	69.67043	Jadura	Hill exposure accses near Jadura road	Metasomatized ferruginous sandstone, occurring relatively at higher contours. The rock is fine to medium grained, dark grey to black coloured and with reddish brown staining . It consists dominantly of angular to sub rounded quartz grains with muscovite,	30/20NW	Bhuj Formation	NA	NA

Sl. No.	Date	Location No.	Latitude	Longitude	Village/ Area	Exposure Location	Host Lithology	Azimuth	Stratigraphy	Original BR ID	New BR ID
							and hematite clasts embedded in a hematitic matrix/cement.				
572	10-09-2025	GSPL_Bhuj_385/09/2025	23.15499	69.67066	Jadura	Hill exposure accses near Jadura road	Metasomatized ferruginous sandstone composed of quatz ,muscovite and hematite clasts embedded in a hematitic matrix/cement.	NA	Bhuj Formation	113470	113470
573	10-09-2025	GSPL_Bhuj_386/09/2025	23.15302	69.67407	Jadura	Hill exposure accses near Jadura road	Metasomatized ferruginous sandstone composed of quatz ,muscovite and hematite clasts embedded in a hematitic matrix/cement. suspected feldspar	NA	Bhuj Formation	113471	113471
574	10-09-2025	GSPL_Bhuj_387/09/2025	23.15321	69.67517	Jadura	Hill exposure accses near Jadura road	Unaltered sandstone composed of mainly angular to subrounded quartz and pores spaces found in the upper surface of sandstone coposed of iron soloution.	NA	Bhuj Formation	NA	NA
575	10-09-2025	GSPL_Bhuj_388/09/2025	23.15385	69.68380	Jadura	Hill exposure accses near Jadura road	56cm thick metasomatized ferruginous sandstone observed extended 3m towards SW direction , composed of angular to subrounded quartz, muscovite and few occasional feldspar grains within the hematitic cement matrkx	NA	Bhuj Formation	113473	113473
576	11-09-2025	GSPL_Bhuj_389/09/2025	23.19093	69.50450	Samantra	Hill exposure near Bhuj-Natiya road	Yellowish red ferruginous weathered sandstone underlain by unaltered sandstone mostly composed of quartz angular to subrounded grains ,white clay/ carbonate ?? And in the ferruginous part some tabular black mineral is also observed	NA	Bhuj Formation	113474	113474
577	11-09-2025	GSPL_Bhuj_390/09/2025	23.18992	69.50561	Samantra	Hill exposure near Bhuj-Natiya road	Jhamma sandstone, fine to medium grained, dark grey to black in colour, and composed rounded quartz grains, feldspar, and hematite clasts embedded in a hematitic matrix/cement. black tabular grains of a non_magnetic mineral were also observed.	65/25NW	Bhuj Formation	113475	113475
578	11-09-2025	GSPL_Bhuj_391/09/20205	23.18963	69.50593	Samantra	Hill exposure near Bhuj-Natiya road	Ferruginous Sandstone, reddish yellow, medium to fine GSPL_Bhuj_grained, moderately sorted, and composed mainly of sub angular to subrounded quartz (>99%).	40/20 -NW	Bhuj Formation	NA	NA
579	11-09-2025	GSPL_Bhuj_392/09/20205	23.18933	69.50656	Samantra	Hill exposure near Bhuj-Natiya road	Partly metasomatized, altered ferruginous sandstone is underlain by less altered ferruginous sandstone composed of fine to mediumgrained, sub rounded to rounded quartz.	NA	Bhuj Formation	113476	113476

Sl. No.	Date	Location No.	Latitude	Longitude	Village/ Area	Exposure Location	Host Lithology	Azimuth	Stratigraphy	Original BR ID	New BR ID
580	11-09-2025	GSPL_Bhuj_393/09/2020 6	23.18938	69.50790	Samantra	Hill exposure near Bhuj-Natiya road	Metasomatized ferruginous sandstone. The rock is fine GSPL_Bhuj_ to medium grained, dark grey to black, and composed dominantly of angular to sub rounded quartz grains, feldspar, and hematite clasts embedded in a hematitic matrix/cement.	60°/20°- NW	Bhuj Formation	113477	113477
581	11-09-2025	GSPL_Bhuj _393/09/202 06	23.18938	69.50790	Samantra	Hill exposure near Bhuj-Natiya road	Metasomatized ferruginous sandstone. The rock is fine GSPL_Bhuj_ to medium grained, dark grey to black, and composed dominantly of angular to sub rounded quartz grains, feldspar, and hematite clasts embedded in a hematitic matrix/cement.	NA	Bhuj Formation	113478	113478
582	11-09-2025	GSPL_Bhuj _394/09/202 5	23.18829	69.50690	Samantra	Hill exposure near Bhuj-Natiya road	Metasomatized ferruginous sandstone. The rock is fine to mediumgrained, dark grey to black, and composed dominantly of angular to subrounded quartz grains, feldspar, and hematite clasts embedded in a hematitic matrix/cement.	60°/20°- NW	Bhuj Formation	NA	NA
583	11-09-2025	GSPL_Bhuj _395/09/202 5	23.19692	69.51690	Samantra	Hill exposure near Bhuj-Natiya road	Ferruginous sandstone was encountered. It is reddish yellow, medium to fine _grained, moderately sorted, and composed mainly of subangular to sub rounded quartz (>99%)., black tabular grains of a non _magnetic mineral were also observed.	NA	Bhuj Formation	NA	NA
584	11-09-2025	GSPL_Bhuj_ 396/09/2025	23.19661	69.51877	Samantra	Hill exposure near Bhuj-Natiya road	unaltered sandstone was observed.	NA	Bhuj Formation	NA	NA
585	11-09-2025	GSPL_Bhuj_ 397/09/2025	23.19713	69.51842	Samantra	Hill exposure near Bhuj-Natiya road	Metasomatized ferruginous sandstone, fine to mediumgrained, dark grey to black, and composed dominantly of angular to sub rounded quartz grains, feldspar, and hematite clasts embedded in a hematitic matrix/cement.	60°/20°- NW	Bhuj Formation	113479	113479
586	11-09-2025	GSPL_Bhuj _398/09/202 5	23.19697	69.51821	Samantra	Hill exposure near Bhuj-Natiya road	Unaltered sandstone	NA	Bhuj Formation	113480	113480
587	11-09-2025	GSPL_Bhuj_ 399/09/2025	23.14463	69.59137	Naranpar	Hill exposure near Bhuj-Mundra high way	Ferruginous sandstone was encountered. It is reddish yellow, medium to fine grained, moderately sorted, and composed mainly of sub angular to sub rounded quartz (>99%). Black tabular grains of a non magnetic mineral were also observed.	NA	Bhuj Formation	113481	113481
588	12-09-2025	GSPL_Bhuj _400/09/202 5	23.16560	69.68396	Jadura	Hill exposure near Bhuj-Mundra high way	The outcrops mainly comprised purplish to yellowish red ferruginous sandstone. The sandstone is fine to medium grained, moderately sorted, and composed dominantly of angular to sub _rounded	NA	Bhuj Formation	113482	113482

Sl. No.	Date	Location No.	Latitude	Longitude	Village/ Area	Exposure Location	Host Lithology	Azimuth	Stratigraphy	Original BR ID	New BR ID
							quartz grains, with few muscovite and iron concretions are present.				
589	12-09-2025	GSPL_Bhuj _ 401/09/2025	23.14332	69.70217	Naranpar	Hill exposure near bhuj mundra high way	The outcrops mainly comprised purplish to yellowish red ferruginous sandstone. The sandstone is fine to medium grained, moderately sorted, and composed dominantly of angular to sub _rounded quartz grains, with few muscovite and iron concretions are present.	NA	Bhuj Formation	113489	113489
590	12-09-2025	GSPL_Bhuj _402/09/2205	23.13884	69.59656	Naranpar	Hill exposure near bhuj mundra high way	Weathered ferruginous Sandstone	NA	Bhuj Formation	113483	113483
591	12-09-2025	GSPL_Bhuj _403/09/2025	23.13826	69.58597	Naranpar	Hill exposure near bhuj mundra high way	Weathered unaltered sandstone composed of quartz (>98%) angular to subrounded , muscovite ,non magnetic black mineral ??	NA	Bhuj Formation	113484	113484
592	12-09-2025	GSPL_Bhuj _ 404/09/2025	23.13815	69.58695	Naranpar	Hill exposure near bhuj mundra high way	The outcrops mainly comprises of purplish to yellowish red ferruginous sandstone. The sandstone is fine to medium grained, moderately sorted, and composed dominantly of angular to sub rounded quartz grains, with few muscovite. Upper part is altered ferrugenious sandstone composed of aquartz and muscovite and middle part is Gravel size Quartz and lower part is unaltered sandstone .	NA	Bhuj Formation	113485(Upper part)	113485(Upper part)
593	12-09-2025	GSPL_Bhuj _ 404/09/2025	23.13815	69.58695	Naranpar	Hill exposure near bhuj mundra high way	The outcrops mainly comprises of purplish to yellowish red ferruginous sandstone. The sandstone is fine to medium grained, moderately sorted, and composed dominantly of angular to sub _rounded quartz grains, with few muscovite. Upper part is altered ferrugenious sandstone composed of aquartz and muscovite and middle part is Gravel size Quartz and lower part is unaltered sandstone .	NA	Bhuj Formation	113386(middle part)	113386(middle part)
594	12-09-2025	GSPL_Bhuj _ 404/09/2025	23.13815	69.58695	Naranpar	Hill exposure near bhuj mundra high way	The outcrops mainly comprises of purplish to yellowish red ferruginous sandstone. The sandstone is fine to medium grained, moderately sorted, and composed dominantly of angular to sub _rounded quartz grains, with few muscovite. Upper part is altered ferrugenious sandstone composed of aquartz and muscovite and middle part is Gravel size Quartz and lower part is unaltered sandstone .	NA	Bhuj Formation	113487(lower part)	113487(lower part)

Sl. No.	Date	Location No.	Latitude	Longitude	Village/ Area	Exposure Location	Host Lithology	Azimuth	Stratigraphy	Original BR ID	New BR ID
595	12-09-2025	GSPL_Bhuj _405/09/2025	23.14165	69.57648	Naranpar	Hill exposure near bhuj mundra high way	The outcrops mainly comprises of purplish to yellowish red ferruginous sandstone. The sandstone is fine to medium grained, moderately sorted, and composed dominantly of angular to sub _rounded quartz grains, with few muscovite. Upper part is altered ferrugenious sandstone composed of aquartz and muscovite and middle part is Gravel size Quartz and lower part is unaltered sandstone .	NA	Bhuj Formation	113488	113488
596	16-06-2025	Gspl_Bhuj_BH01	23.15084	69.57852	Naranpar	Road side exposure,accessible from Bhuj-Mundra highway through a metal road	Shale dominated heterolith Tuffite layer	NA	Katrol Formation	NA	NA
597	21-07-2025	Gspl_Bhuj_BH02	23.15629	69.70701	Jadura	Road side exposure,accessible from Dhunaraja Dam road through Jadura road and a cart road	Interbbeed Fossiliferous and ferrougenous Sandstone	NA	Bhuj-Katrol contact	NA	NA
598	26-07-2025	Gspl_Bhuj_BH03	23.20398	69.62844	Sukhpar	Road side exposure,accessible through a metal road from Bhuj Mundra Highway road	metasomatized sandstone	NA	Bhuj Formation	NA	NA
599	02-08-2025	Gspl_Bhuj_BH04	23.20383	69.62852	Sukhpar	Road side exposure,accessible through a metal road from Bhuj Mundra Highway road	metasomatized sandstone	NA	Bhuj Formation	NA	NA
600	15-08-2025	Gspl_Bhuj_BH05	23.19484	69.58049	Mankuva	Hill exposure Near Mankuva road	metasomatized sandstone	NA	Bhuj Formation	NA	NA
601	15-08-2025	Gspl_Bhuj_BH06	23.22258	69.59413	Kalyanpar	Hill exposure Near Mankuva road	metasomatized sandstone	NA	Bhuj Formation	NA	NA
602	09-08-2025	Gspl_Bhuj_BH07	23.19754	69.52970	Kodki	Hill exposure near Bhuj Nakhetrana high way	metasomatized sandstone	NA	Bhuj Formation	NA	NA
603	15-08-2025	Gspl_Bhuj_BH08	23.19347	69.51839	Samantra	Hill exposure near Bhuj Nakhetrana high way	metasomatized sandstone	NA	Bhuj Formation	NA	NA
604	19-12-2023	Placemark 1	23.23297	69.55795	Kalyanpar	Hill Exposure near kalyanpar road	Basalt intrusion in sst	NA		NA	NA
605	24-11-2024	Placemark 2	23.18392	69.50307	Vinganiya	Road side exposure on Samtra Vadasar Road	Thick sst (quartz arenite?) with occasional tuff/clay	NA	Katrol Formation	NA	NA
606	24-11-2024	Placemark 3	23.18160	69.50480	Vinganiya	Road side exposure on Samtra Vadasar Road	Thick sst (quartz arenite?) with occasional tuff/clay	NA	Katrol Formation	NA	NA
607	24-11-2024	Placemark 4	23.15660	69.47190	Vinganiya	Road side exposure on Samtra Vadasar Road	Thick sst (differential ferruginous leaching)seperated by clay horizons	NA	Katrol Formation	NA	NA
608	24-11-2024	Placemark 5	23.13830	69.48440	Vinganiya	Road side exposure on Samtra Vadasar Road	Sandstone dominated heterolith with poorly developed Tuffite layers	020/6 WWN	Katrol Formation	NA	NA

Sl. No.	Date	Location No.	Latitude	Longitude	Village/ Area	Exposure Location	Host Lithology	Azimuth	Stratigraphy	Original BR ID	New BR ID
609	24-11-2024	Placemark 6	23.14290	69.49020	Vinganiya	Road side exposure on Samtra Vadasar Road	Sandstone dominated heterolith with poorly developed Tuffite layers	020/6 WWN	Katrol Formation	NA	NA
610	24-11-2024	Placemark 7	23.14410	69.49000	Vinganiya	Road side exposure on Samtra Vadasar Road	Sandstone dominated heterolith with poorly developed Tuffite layers	020/6 WWN	Katrol Formation	NA	NA
611	24-11-2024	Placemark 8	23.14340	69.48340	Vinganiya	Road side exposure on Samtra Vadasar Road	Sandstone dominated heterolith with poorly developed Tuffite layers	020/6 WWN	Katrol Formation	NA	NA
612	24-11-2024	Placemark 9	23.14260	69.48330	Vinganiya	Road side exposure on Samtra Vadasar Road	Sandstone dominated heterolith with poorly developed Tuffite layers	020/6 WWN	Katrol Formation	NA	NA
613	24-11-2024	Placemark 10	23.14010	69.47680	Vinganiya	Road side exposure on Samtra Vadasar Road	Sandstone dominated heterolith with poorly developed Tuffite layers	020/6 WWN	Katrol Formation	NA	NA
614	25-11-2024	Placemark 12	23.17130	69.53120	Bharasar	Hill exposure Near Bharsar road	Sandstone	NA	Chari formation	NA	NA
615	25-11-2024	Placemark 13	23.17090	69.53150	Bharasar	Hill exposure Near Bharsar road	Sandstone	NA	Chari formation	NA	NA
616	25-11-2024	Placemark 14	23.17110	69.53250	Bharapar	Hill exposure Near Bharapar road	Sandstone	NA	Chari formation	NA	NA
617	25-11-2024	Placemark 15	23.17070	69.53270	Bharapar	Hill exposure Near Bharapar road	Sandstone	NA	Chari formation	NA	NA
618	25-11-2024	Placemark 16	23.16990	69.53280	Bharapar	Hill exposure Near Bharapar road	Sandstone	NA	Chari formation	NA	NA
619	25-11-2024	Placemark 17	23.16880	69.53190	Bharapar	Hill exposure Near Bharapar road	Sandstone	NA	Chari formation	NA	NA
620	25-11-2024	Placemark 18	23.16830	69.53220	Bharapar	Hill exposure Near Bharapar road	Sandstone	NA	Chari formation	NA	NA
621	25-11-2024	Placemark 19	23.16590	69.53220	Bharapar	Hill exposure Near Bharapar road	Sandstone	NA	Chari formation	NA	NA
622	25-11-2024	Placemark 20	23.16650	69.53510	Bharapar	Hill exposure Near Bharapar road	Sandstone	NA	Chari formation	NA	NA
623	25-11-2024	Placemark 21	23.16630	69.53900	Bharapar	Hill exposure Near Bharapar road	Sandstone	NA	Chari formation	NA	NA
624	25-11-2024	Placemark 22	23.16630	69.53900	Bharapar	Hill exposure Near Bharapar road	Sandstone	NA	Chari formation	NA	NA
625	25-11-2024	Placemark 23	23.16250	69.54140	Bharapar	Hill exposure Near Bharapar road	Sandstone	NA	Chari formation	NA	NA
626	25-11-2024	Placemark 24	23.16460	69.54090	Bharapar	Hill exposure Near Bharapar road	Sandstone	NA	Chari formation	NA	NA
627	25-11-2024	Placemark 25	23.17060	69.53590	Bharapar	Hill exposure Near Bharapar road	Sandstone	NA	Chari formation	NA	NA
628	25-11-2024	Placemark 26	23.17280	69.53370	Bharapar	Hill exposure Near Bharapar road	Sandstone	NA	Chari formation	NA	NA
629	25-11-2024	Placemark 27	23.17360	69.53190	Bharapar	Hill exposure Near Bharapar road	Sandstone	NA	Chari formation	NA	NA
630	25-11-2024	Placemark 28	23.17770	69.53680	Bharapar	Hill exposure Near Bharapar road	Sandstone	NA	Chari formation	NA	NA

Sl. No.	Date	Location No.	Latitude	Longitude	Village/ Area	Exposure Location	Host Lithology	Azimuth	Stratigraphy	Original BR ID	New BR ID
631	11-02-2025	J1	23.19576	69.53389	Mankuva	Hill exposure Near Bhuj Natiya road	metasomatized Sandstone with blue stain	NA	Bhuj Formation	NA	NA
632	11-02-2025	J5	23.19684	69.53135	Mankuva	Hill exposure Near Bhuj Natiya road	metasomatized Sandstone with feldspar and blue stain	NA	Bhuj Formation	NA	NA
633	11-02-2025	J6	23.19711	69.53046	Mankuva	Hill exposure Near Bhuj Natiya road	metasomatized Sandstone with strong iron impregnation	NA	Bhuj Formation	NA	NA
634	11-02-2025	J7	23.19780	69.52950	Mankuva	Hill exposure Near Bhuj Natiya road	metasomatized Sandstone with strong iron impregnation and feldspar	NA	Bhuj Formation	NA	NA
635	11-02-2025	J8	23.19754	69.52964	Mankuva	Hill exposure Near Bhuj Natiya road	metasomatized Sandstone with strong iron impregnation underlain by ferruginous sandstone	NA	Bhuj Formation	NA	NA
636	11-02-2025	J9	23.19648	69.52969	Mankuva	Hill exposure Near Bhuj Natiya road	metasomatized Sandstone with magnetite	NA	Bhuj Formation	NA	NA

Annexure-XII: Petrographic study of BR

Sr No.	Original Sample ID	New Sample ID	Latitude	Longitude	Sample (hand specimen) Description	Stratigraphy
1	105570	107454	23.15185	69.5778416	5cm thick, farely continuous layer	Katrol Formation
2	105572	107456			2-7cm thick, laterally pinching out, associated with gypsum layers.	
3	105567	107451	23.1507	69.58	The targeted layer is laterally extensive along the dip direction showing pinch and swell geometry. The layer thickness varies from 2-6cm and can be traced for 148.41m.	Katrol Formation
4	107579	107579			Wave ripple laminated sst just above the red bed (targeted layer)	Katrol Formation, succession up from 112/03/24
5	107580	107580			2.5cm, thin sandstone layer at 0.106m below the red bed (targeted layer)	
6	107581	107581			10cm thick, sandstone layer at 0.37m below the red bed (targeted layer)	
7	107582	107582			50cm thick, sandstone layer at 0.72m below the red bed (targeted layer)	
8	105592	107476	23.18878	69.59945667	10-12cm thick beds of medium to fine grained (mostly quartzose, some unidentified black mineral), highly altered sandstone. Iron leaching at places are observed	Katrol Formation
9	105595	107479			medium to fine grained quartzose sandstone, possibly unaltered sandstone facies of previous sample?	
10	105599	107483			5 cm thick, targeted layer associated with F2 (alternation of grey shale and red beds)	

Sr No.	Original Sample ID	New Sample ID	Latitude	Longitude	Sample (hand specimen) Description	Stratigraphy
11	105603	107487	23.14534	69.54906167	Dolerite/Basalt	Katrol Formation
12	105604	107488	23.16454	69.55433	Cherry red in color,comprises of quartz, mica, glass shrads ??, and few black unknown mineral with metallic lustre. Suspected volcanic alteration.	Chari Formation (At contact of Katrol and Chari formation)
13	105605	107489	23.18564	69.64097167	4 cm thick, continuous layer, occuring in association with F1, just below the high energy F3 facies, sample collected to observe whether high energy condition deposit are prospective or not.	Katrol Formation
14	105606	107490	23.18163	69.64077	Shale-siltone layer, sandwitched between two sandstone layers. Sample taken to see the composition of the alternation layer. In the same litholog there is high value calcareous claystone/tuff, which occur at lower stratigraphy.	Katrol Formation
15	105626	107510	23.16082	69.723285	Very coarse grained sandstone with angular, subangular to subrounded framework grains of quartz, iron concentrated grains?, unknown black minerals (dull lustre) embedded in fine grained matrix/cement.The cement seems to be ferrugenous which has currently formed lemonitic (yellow ockar in colour).	At contact of Katrol and Bhuj formations
16	107572	107572	23.16082	69.723285	Very coarse grained sandstone with angular, subangular to subrounded framework grains of quartz, iron concentrated grains?, unknown black minerals (dull lustre) embedded in fine grained matrix/cement. The cement seems to be ferrugenous which has currently formed lemonitic (yellow ochar in colour).	
17	107573	107573	23.16118	69.724772	7.5cm thin, reddish colored very hard ironstone bed comprising of few remanant clasts of quartz grains.	
18	107574	107574	23.16118	69.724772	Ironstone bed comprising of few remanant clasts of quartz grains.	
19	105632	107516	23.1641	69.72725833	Very light weight grain supported yellow ochre colored coarse grained sst with butchers knife erosion The grains are elongated, angular to sub angular (quartz/apatite??),mica,rounded black colored unknown mineral, are the main constituents.,no matrix observed.	Katrol Formation
20	105633	107517			Similar appearance as 105632 with decreased grain size (medium grained), increase in quartz and matrix	

Sr No.	Original Sample ID	New Sample ID	Latitude	Longitude	Sample (hand specimen) Description	Stratigraphy
21	105634	107518			5cm thick, farely continuous layer of sandstone altered to red bed	
22	105650	107534	23.17128	69.692555	Gray shale bordered by gypsum? Yellowish fine part, sample collected to understand the shale (yellow parts') mineralogy	Katrol Formation
23	105652	107536	23.16548	69.73696667	Sandstone showing butchers knife weathering pattern (possible contain phosphorite?)	Katrol Formation near to contact of Katrol and Bhuj formations
24	105653	107537	23.14156	69.47602833	Dolerite / Basalt (prsence of olivine/serpentine??). Outside of the block boundary.	Katrol Formation
25	105657	107541	23.22405	69.49289667	Coarse grained sst with encrustation at the top (looks like baking/jhama effect)	Bhuj Formation
26	107565	107565	23.2242	69.492742	Coarse grained sst with encrustation at the top (looks like baking/jhama effect). Sst comprises of quartz, feldspar with a light colour matrix. Sample from reported alkali plug area, collected to identify catchment source's mineralogy of high REE value SS sample.	
27	107566	107566	23.22759	69.504025	Coarse grained sst with few sst showing dark red encrustation on top (looks like baking/jhama effect).	Bhuj Formation
28	107567	107567			5cm thin, white colour, medium - coarse grain sst interbedded between the buff coloured sst.	
29	107568	107568	23.22907	69.478713	Brownish mauve coloured, medium - coarse grain sst with little encrustation on top (looks like baking/jhama effect). (Upto 6 m depth from the surface of rhe mound)	Bhuj Formation
30	107569	107569	23.22907	69.478713	Brownish mauve/ reddish coloured, medium - coarse grain sst with dark encrustation visible on top (looks like baking/jhama effect). (Layer below buff colored sandstone: 6m depth from the surface of the mound)	
31	107570	107570	23.22907	69.478713	Less compact, light weight, yellowish - orange coloured, medium - coarse grain sst consisting of quartz & feldspar. (bottom layer, depth: 9m from the surface of mound)	

Sr No.	Original Sample ID	New Sample ID	Latitude	Longitude	Sample (hand specimen) Description	Stratigraphy
32	107571	107571	23.22907	69.478713	Composite samples of different types of sst (Buff colour sst with encrustation, yellowish orange sst, red coloured sst and very fragile planar cross laminated white coloured sst.)	
33	105658	107542	23.23155	69.482635	Brownish mauve colour, medium - coarse grain sst with little encrustation on top. (Similar sample as 105658)	
34	105659	107543	23.25237	69.74468	Very fine grained melanocratic rock with occurrence of few golden colored mica, teal greenish colored vug filled mineral	Bhuj Formation
35	105662	107546	23.19947	69.511235	Coarse to medium grained sandstone with evidence of baking effect possibly by fumaroles ??.	Bhuj Formation
36	107576	107576			20cm thick, brownish mauve coloured, planar cross stratified, coarse grain sst with scattered pebbles along the stratification.	
37	107577	107577			Coarse grain sst with dark black coloured encrustation on top	
38	107578	107578			Sandstone with evidence of baking	
39	105671	107555	23.2211	69.58984167	Coarse grained sst, composed of quartz embeded in a lemonitic,iron cement. The sandstone is altered, with thin flow like structures at the top of the beds (evidence of baking??? fumaroles?)	Bhuj Formation
40	105675	107559	23.18286	69.633175	4cm thick, white crystalline medium to fine grained sandstone (Phosphorite???)	Katrol Formation
41	105677	107561			10 cm thick, mm thin parallal laminated medium to fine grained sandstone, sandwitched between two thick (60cm and 28cm)sandstone beds	
42	105678	107562			5cm thick, white crystalline medium to fine grained sandstone (Phosphorite???)	

Sr No.	Original Sample ID	New Sample ID	Latitude	Longitude	Sample (hand specimen) Description	Stratigraphy
43	105679	107563			5cm thick, white crystalline medium to fine grained sandstone (Phosphorite???), burrow observed	
44	107575 A	107575 A	23.1483	69.726473	Medium - fine grained, grayish white sandstone	At contact of Katrol and Bhuj formations
45	107575 B	107575 B			Medium to coarse grained, buff-colored sandstone	
46	107575	107575			Encrustated layer on top of buff colored sandstone	
47	109019	109019	23.19568	69.533946	Ferruginous Sandstone	Bhuj Formation
48	108952	108952	23.22823	69.5039978	Ocuurance of very coarse grained sandstone with scattered pebbles at places. Highly fractured with cross cutting relationship , few 10m north massive , highly vesicular which is almost parallel to bedding . 80cm reddish colour, no quartz present alteration of Na metasomatism.	Bhuj Formation
49	108953	108953	23.22823	69.5039978	Albite suspected	Bhuj Formation
50	108954	108954	23.22823	69.5039978	Metasomatized Sandstone, Albite suspected	Bhuj Formation
51	108955	108955	23.22823	69.5039978	Albite suspected	Bhuj Formation
52	109016	109016	23.27065	69.804652	China Clay found from the depth of 100ft Host rock: Sanstone	Bhuj Formation
53	109018	109018	23.19568	69.533946	The metasomatized sandstone is composed of very coarse grained angular to sub-angular quartz, authigenic growth of feldspar and clasts of quartz aggregates embedded in a magnetite rich (black streak) matrix.	Bhuj Formation

Sr No.	Original Sample ID	New Sample ID	Latitude	Longitude	Sample (hand specimen) Description	Stratigraphy
54	108998	108998	23.19578	69.596997	Highly ferrugineous sandstone with silica/gypsum	Katrol Formation
55	108920	108920	23.17298	69.76743	target layer 1.7 m from the surface associated with sandstone	Katrol Formation
56	108933	108933	23.15333	69.46531	target layer associated with sandstone and gypseous layer	Katrol Formation
57	108918	108918	23.18982	69.76442	Targeted bed consists of loose chips and boulders of highly ferrugineous material, compact, hard; occuring in the mount within the soil zone	Bhuj Formation
58	108935	108935	23.13712	69.45846	target layer associated with shale	Katrol Formation
59	109015	109015			China Clay found from the depth of 100ft Host rock: Sandstone	Bhuj Formation
60	108937	108937	23.1992	69.7582	Gritty sandstone with quartz,fresh feldspar,unknown black mineral layer	Bhuj Formation
61	108938	108938	23.1992	69.7582	Sandstone(looks like baking effect)	Bhuj Formation
62	108936	108936	23.1992	69.7582	Box work Clayey Layer	Bhuj Formation

Table Continued..

Annexure-XII

Sr No.	Original Sample ID	Thin Section Description	Name of the rock according to petrography
1	105570	Fragmented clasts of quartz (wedge, needle, triangular shaped), muscovite (flaky), apatite, mud pellets embedded in a carbonate cement (iron staining)	Tuffaceous??
2	105572	Layered rock with fragmented clasts of quartz (wedge, needle, triangular shaped), feldspar (K-feldspar, Plg, microcline) embedded in a carbonate cement. Presence of few opaque minerals	Tuffaceous??
3	105567	Very fine grained crudely laminated rock. Layering is defined by phenocrysts (framework) rich layers and groundmass rich layers. The framework grains (<20-250µm) are of elongated, flaky, needle and wedge shaped grains of quartz, feldspar, apatite, embedded in a glassy groundmass. Suspected presence of apatite	Tuff/ Rhyolite (??)
4	107579	NA	NA
5	107580	Crudely layered rock, where lamination is defined by clasts rich layers and glass(??)/cement rich layers. Framework grains are of angular, elongated grains of quartz, feldspar (K-feldspar, microcline, albite??), muscovite, glass shards?? embedded in a iron rich, glassy ?? cement. Presence of flow structure within the framework grains (ignimbrite??). The framework grains are observed to be deformed.	Ignimbrite??
6	107581	Very crudely laminated rock, where lamination is defined by clasts rich layers and glass(??)/cement rich layers. Framework grains are of fragmented (wedge, needle, triangular shaped with sharp boundaries and embayment at places) quartz, feldspar (K-feldspar, microcline, albite??), muscovite, glass shards?? embedded in a iron rich, glassy ?? and carbonate cement. Presence of flow structure within the micas (ignimbrite??)	Tuff/Tuffaceous??
7	107582	Crudely layered rock, where layering is defined by clasts rich layers and glass(??)/matrix (3-4%) rich layers. Framework grains are of fragmented (wedge, needle, triangular shaped with sharp boundaries and embayment at places) quartz, feldspar (K-feldspar, microcline, albite??), muscovite embedded in a iron rich, glassy ?? cement. Almost no transported grains are observed. glass? surrounding framework grains are also observed.	Tuff/Tuffaceous??
8	105592	Very angular to angular (wedge and needle shaped with sharp, straight boundaries) quartz, feldspar and very few very well rounded clasts of mud pellets (≤30µm) ?? Or lapilli ?? embedded in a ferrugenous cement. Clast supported rock. Few sub-rounded framework grains are also there.	Quartz arenite?? Volcaniclastics??

Sr No.	Original Sample ID	Thin Section Description	Name of the rock according to petrography
9	105595	Clast supported rock, consists of highly fractured quartz grains, 10-12%, very less fractured feldspar (K-feldspar, microcline, plagioclase), muscovite embedded in a glassy (??) matrix. Occurrence of carbonate rhombs (zoned). Are these perovskite?? One/two grain/s of rhombic shaped clasts with straight boundary, pleochroic in shades of green, greenish yellow interference colour, suspected chlorite	Arkose
10	105599	Lminated rock with layering defined by glassy and crystalline layer. Same as 105567 with less amount of needle and wedge shaped grains and more of glassy material	Tuff??
11	105603	NA	Dolerite
12	105604	Fragmented, wedge shaped quartz with embayment like boundary, embedded in a glassy?? Matrix. A carbonate vein is observed.	Volcaniclastics??
13	105605	Sparse fine angular quartz, mud pellets in a ferrugenous matrix with --------apatite and muscovite	Volcaniclastics??
14	105606	Very crudely laminated very fine grained rock. Laminations are defined by grain size difference with v.fine sand sized framework rich layers and silt/mud sized quartzo-feldspathic matrix and cement rich layers. The framework grains are composed of angular to sub-angular grains of quartz, feldspar (plagioclase, microcline), muscovite. The matrix-cement part is >20% and the cement is carbonate.	Sub-Arkose/ Feldspathic Wacke
15	105626	Very coarse grained sandstone with both higly rounded and fragmented (broken) clasts of quartz, feldspar, rock fragment of quartzite, polycrystalline quartz (with sub-grain formation) and few glass fragments are embedded in a quartzo-feldspathic matrix (>20%, angular grains) and carbonate cement. Intergrowth in K-feldspar is observed. Solution/acidic activity noticed along the quartz grain boundaries (nibbling). Secondary carbonate veins are also observed.	Wacke (Volcanic??)
16	107572	Sub angular (wedge shaped) to sub-rounded grains of quartz, feldspar, fossil are embedded in a ferrugenous groundmass. Lots of carbonate grains are also observed.	Volcaniclastics??
17	107573	Both angular to sub-rounded grains of quartz, feldspar grains are embedded in a quartzo-feldspathic matrix (3-5%) and glassy to carbonate groundmass. Cooling cracks and brecciation by carbonate veins are also observed. Carbonate grains with very high relief and zoning (perovskite??) and altered glass are also observed in the groundmass. Zircon, tourmaline within the quartz and rutile in matrix are also observed.	Volcaniclastics??

Sr No.	Original Sample ID	Thin Section Description	Name of the rock according to petrography
18	107574	Very crudely laminated rock, where lamination is defined by oriented clasts embedded in a glass(??) to ferrugenous cement. Framework grains are of fragmented (wedge, needle, triangular shaped with sharp boundaries and embayment at places) quartz, feldspar (K-feldspar), needle shaped mica (muscovite) and abundant fossil.	Quartz Arenite (Tuffaceous??)
19	105632	Very angular, clast supported, quartz chert, k-feldspar, microcline, plagioclase embedded in a chloritic matrix/cement. Matrix is about 10%	Quartz Wacke
20	105633	Very angular to sub angular grains of quartz, feldspar (albite, orthoclase, microcline), mica and few mud pellets embedded in a carbonate cement. It is clast supported. The grain boundaries of the clasts are sharp, straight in most of the cases.	Volcaniclastics??
21	105634	Very angular, fragmented clasts of quartz, k-feldspar (sericitised at places), microclines, muscovite, perthite embedded in a carbonate and ferrugenous cement. Preservation of complete unfragmented fossils (wood, sponge, tooth??)	Tuffaceous Sandstone
22	105650	Very crudely laminated shale with framework clasts of quartz (10-50µm and few 50-100µm) floating in more finer clay sized material (quartz, feldspar, mica)	
23	105652	NA	NA
24	105653	Zoning in plagioclase, sectorial twinning in anorthoclase	Gabbro
25	105657	Coarse to medium grained quartz, feldspar (10%), chert, quartzite embedded in a manganiferous cement	Arkose
26	107565	Angular to sub-angular framework grains (very few sub-rounded grains) of quartz, feldspar (7-9%, k-feldspar, microcline, plagioclase), biotite, chert, epidote?? embedded in a glassy to quartzo-feldspathic matix (~2%). Presence of magnetite, pyrite, chalco-pyrite, zircon, monazite is also observed. Cooling cracks within the framework grains are also common. graphic growth within the feldspar is also observed. Presence of framework grains with star like appearance (zeolite??) is also encountered. Is there evidence of in-situ recrystallization??	Arkose (Volcaniclastics??)

Sr No.	Original Sample ID	Thin Section Description	Name of the rock according to petrography
27	107566	Fragmented (few euhedral grains and few transported grains) of quartz, microcline, k-feldspar, plagioclase, polycrystalline quartz, deformed quartzite are embedded in iron leached glassy ?? Cement. Unknown mineral (lapilli??, pleochroic in shades of green, brownish yellow interference colour, very rounded, twinkling extinction) is also encountered	Pyroclastic rock??
28	107567	Bimodal size distribution of framework grains (smaller grains are wedge, neddle shaped). Framework grains of quartz, feldspar, polycrystalline quartz, chert are embedded in a ferrugenous cement. In-situ breciation of clasts by iron solution is also observed. Si overgrowth is also found	Quartz Arenite
29	107568	Fine grained rock with angular to sub-angular grains of quartz, feldspar (2-3%, altered at places), perthite embedded in a carbonate, later replaced by ferrugenous groundmass. Lots of apatite, zircon and magnetite are in matrix (1-2%). The carbonate groundmass are replacing the framework grains, creating embayment within them. Formation of calcite crystal with zoning (perovskite??)	Quartz Arenite (Tuffaceous??)
30	107569	Fine grained rock with angular to sub-angular grains (few transported grains) of quartz (few grains have Si overgrowth), feldspar (~10%, K-feldspar, microcline, plagioclase, K-feldspar altered at places), chert (2-3%) embedded in a carbonate, later replaced by ferrugenous groundmass. Zircon iclusion within quartz are also observed. The carbonate groundmass are replacing the framework grains, creating embayment within them.	Arkose (Tuffaceous??)
31	107570	Sub-angular to sub-rounded framework grains (bimodal size distribution, large rounded grains and smaller angular grains) of quartz, feldspar (~2%), polycrystalline quartz (metamorphic), chert embedded in a quartzo-feldspatic to glassy matrix. Presence of xenotime, apatite, zircon, magnetite are also observed. Embayment in quartz grains are also observed.	Quartz Arenite
32	107571	No thin Section has been done as it is in powder form and collected for chemical analysis	NA
33	105658	Sub-angular to sub-rounded framework grains of quartz, feldspar (~5-7%, orthoclase, plagioclase, altered at places) polycrystalline quartz (metamorphic), rock fragment of very few chert, siltstone embedded in a glassy to ferrugenous groundmass. Presence of zircon within the quartz grains, monazite, xenotime in matrix (1-2%) is also observed. Few framework grains are seem to be brecciated by iron solution, creating embayment within them.	Sub-arkose (Tuffaceous??)
34	105659	Phenocrysts of alkali feldspar, quartz (100-250µm) and plagioclase lath (<40µm) embedded in a glassy groundmass. Flow like texture is observed.	Trachyte??
35	105662	Poorly sorted, Bimodal size distribution with large rounded grains (evidence of transportation) and small angular to sub-angular grains with few accicular grains of quartz , feldspar (~2%) embedded in ferrugenous cement. Matrix >10%	Quartz Wacke (Volcaniclastic??)

Sr No.	Original Sample ID	Thin Section Description	Name of the rock according to petrography
36	107576	Angular to sub-rounded framework grains (with sharp boundaries) of quartz, feldspar (k-feldspar, microcline, plagioclase) embedded in a glassy?? to ferrugenous cement. Part of the cement is isotropic in nature.	Quartz Arenite (Volcaniclastics??)
37	107577	Angular to sub-rounded framework grains of quartz, feldspar (1-2%, k-feldspar, microcline, plagioclase, altered at places), chert embedded in a glassy?? Matrix (1-2%). Muscovite and epidote (??) are observed in matrix.	Quartz Arenite (Volcaniclastics??)
38	107578	Sub-angular to sub-rounded framework grains of quartz, feldspar (1-2%, k-feldspar), embedded in a carbonate groundmass with ferrugenous stain. Suspected epidote in matrix. Insitu brecciation of the framework grains and embayment within the framework grains are observed	Quartz Arenite (Volcaniclastics??)
39	105671	Angular quartz grains (100-250µm) embedded in a carbonate to ferrugenous cement (10-15%) with 10-20% matrix	Quartz Wacke
40	105675	Massive non-laminated fine grained sandstone. The framework grains are well sorted and consist of angular/fragmentd clasts of quartz, K-feldspar (Sericitised at places), microcline and muscovite. Inclusions within quartz are also observed.	Quartz Arenite
41	105677	Crudely laminated sandstone, lamination defined by presence of ferrugenous cement. The framework grains are well sorted and consist of angular/fragmentd clasts of quartz, feldspar and muscovite	Volcaniclastics??
42	105678	Fragmented clasts of quartz (wedge, needle, arc shaped,surrounding glass), 5-7% feldspar (albite, K-feldspar), perthite, muscovite (flaky), vlocanic rock fragments are embedded in a glassy matrix. Flow structure is observed within the matrix. Clasts are brecciated.	Tuff??
43	105679	NA	NA
44	107575 A	Grain supported rock where framework grains are of fragmented quartz, feldspar, wispy muscovite grains embedded in a glassy to carbonate groundmass. Carbonate clasts are rhombic in shape, high relief and zoned. Flow like structure is also observed in groundmass.	Tuffaceous

Sr No.	Original Sample ID	Thin Section Description	Name of the rock according to petrography
45	107575 B	Grain supported rock with wedge and needle shaped clasts of quartz, feldspar (k-feldspar, Na feldspar), muscovite embedded in a carbonate to ferrugenous cement. Zoned carbonate clast is also there.	Tuffaceous
46	107575	Crudely layered rock with layering of framework grains and glass?? Rich/carbonate cement layer. Framework grains are of fragmented quartz, feldspar (≥10%), wispy muscovite grains, platy glass shards embedded in a glassy to carbonate groundmass. Carbonate clasts are rhombic in shape, high relief and zoned. Flow like structure is also observed in groundmass.	Tuffaceous
47	109019	Very coarse-grained sandstone composed predominantly of quartz with abundant feldspar and mica. Gold suspected	Arkosic Sandstone
48	108952	Medium- to coarse-grained sandstone composed primarily of quartz, feldspar, and mica, with scattered lithic fragments. The matrix contains iron oxide, imparting a ferruginous character. Trace magnetite and the presence of sulfide. Suspected gold	Ferruginous sandstone
49	108953	Medium- to coarse-grained sandstone exhibiting a bimodal size distribution of quartz grains. The rock is matrix-supported with ferruginous cement derived from iron-rich solutions, producing a reddish-brown coloration and strong iron oxide bonding between grains.	Ferruginous Sandstone
50	108954	Medium-grained sandstone composed predominantly of quartz, feldspar, and mica, with minor magnetite. The rock exhibits well-sorted detrital grains within a compact framework. Gold suspected	Arkosic sandstone
51	108955	Medium- to coarse-grained sandstone composed primarily of quartz, feldspar, and mica. The quartz exhibits a bimodal (two-size) grain distribution, suggesting multiple sedimentary sources or reworking events. Magnetite is present as accessory mineral phases. Gold Suspected	Arkosic sandstone
52	109016	Very fine-grained tuffite. The rock displays a compact texture with fine detrital and volcanic particles, often showing ferruginous staining or alteration associated with secondary iron oxide development.	Tuffite
53	109018	Tuffite composed of very fine-grained material, featuring elongated muscovite within an iron oxide–magnetite matrix. Acicular quartz crystals are set in a dark, ferruginous groundmass, giving the specimen a distinctive metallic luster and texture.	Tuffite

Sr No.	Original Sample ID	Thin Section Description	Name of the rock according to petrography
54	108998	Ferruginous sandstone composed of very fine-grained material with a dark iron oxide matrix or cement. Contains volcanic-derived quartz fragments and scattered fossil fragments, with minor magnetite enrichment.	Ferruginous sandstone
55	108920	Coarse-grained, fossiliferous sandstone characterized by an iron-rich matrix and abundant magnetite. Contains fresh feldspar, quartz, and mica grains, with numerous fossil fragments well-preserved within the cement.	Ferruginous fossiliferous sandstone
56	108933	Tuffaceous material containing abundant ferruginous components dominated by goethite and iron oxides. Quartz is scarce, and volcanic glass is present, giving the rock a highly altered, iron-rich appearance.	Tuffite
57	108918	Very coarse-grained sandstone composed predominantly of quartz with abundant feldspar and mica. The detrital framework is set within a ferruginous matrix rich in iron oxide, imparting a reddish-brown coloration and strong cementation. The rock reflects limited transport and moderate to low textural maturity.	Ferruginous sandstone
58	108935	Impure limestone composed predominantly of carbonate material with disseminated pyrite and magnetite. The presence of sulfides suggests possible gold association or mineralization within the carbonate matrix.	Impure Limestone
59	109015	Medium-grained sandstone composed mainly of quartz, feldspar, and mica, with accessory magnetite and iron oxide.	Ferruginous sandstone
60	108937	Very coarse-grained sandstone composed mainly of quartz, feldspar, and mica, with accessory goethite, pyrite, and magnetite. The presence of iron oxides and sulfides suggests ferruginous and possibly mineralized characteristics within the detrital framework.	Ferruginous sandstone
61	108938	Coarse-grained sandstone with minimal to no matrix. Composed primarily of quartz, feldspar, and mica, with minor magnetite and iron oxide. Quartz grains exhibit well-developed overgrowths, indicating secondary silica cementation and diagenetic recrystallization.	Sandstone
62	108936	Coarse-grained sandstone exhibiting a bimodal size distribution of quartz grains. The rock is cemented and supported by an iron-rich matrix, likely derived from iron oxide or ferruginous solutions, giving it a reddish-brown coloration and strong cementation.	Ferruginous sandstone

Annexure-XIII: XRF of Tuffite Layers

Sl. No.	Original Sample ID	New Sample ID	Location No.	Latitude	Longitude	Type of Sample	Depth above surface (m)	Host Lithology	Stratigraphy
1	105569	107453	GSPL-Bhuj-112/03/24	23.152	69.578	BR	0	Occurrence of mm to 1cm thin grey to blackish-grey shale layers, amalgamated at places and often alternate with mm thin silt/fine sand layers and reddish brown coloured 2-7cm thick hard ironstone/ferrugenous clay layers with pinch and swell geometry. This succession is observed to be interrupted by brownish mauve coloured, either wave ripple laminated or plane parallel laminated medium to fine grained sandstones. Occurrence of mm thin gypsum layers at the top part of the succession are also observed	Katrol_lowest part, below this Chari has been encountered
2	105570	107454				BR	0.77		
3	105571	107455				BR	2.92		
4	105572	107456				BR	4.82		
5	105573	107457				BR	6.82		
6	105574	107458				BR	8.32		
7	105575	107459				BR	8.42		
8	105567	107451	GSPL-Bhuj-91/01/24	23.151	69.580	BR	1.767	Continuation of the same succession in stratigraphic up direction. However the thickness of the sandstones increases and no gypsum is encountered.	Katrol Formation, succession up from 112/03/24
9	105568	107452				BR	0.52		
10	105576	107460	GSPL-Bhuj-115/06/24	23.150	69.581	BR	0.19	Continuation of the same succession along the dip	Katrol Formation, continuation of same succession along the dip as of 91/01/24
11	105577	107461				BR	0.635		
12	105578	107462				BR	2.065		
13	105579	107463	GSPL-Bhuj-110/06/24	23.150	69.585	BR	0.3	Continuation of the same succession in stratigraphic up direction. However the thickness of the sandstones increases and occurrence of mm thin gypsum layers are also observed.	Katrol Formation, stratigraphic up from the succession of 91/01/25
14	105580	107464				BR	2		
15	105581	107465				BR	2.25		
16	105582	107466	GSPL-Bhuj-116/06/24	23.145	69.584	BR	2.99	Continuation of the same succession in stratigraphic up direction. However the thickness of the sandstones increases and occurrence of mm thin gypsum layers are also observed.	End part of Katrol Formation
17	105583	107467				BR	3.38		

Table Continued..

Annexure-XIII

Sl. No.	Original Sample ID	New Sample ID	Sample Description	Al_2O_3	BaO	CaO	Cr_2O_3	Fe_2O_3	K_2O	MgO	MnO	Na_2O	P_2O_5	TiO_2	SiO_2	LOI	S
1	105569	107453	1st appearance of suspected tuffite layer in Katrol, 2cm thin nodular layer	14.68	0.03	3.36	0.01	7.83	1.59	0.95	0.19	0.85	0.20	0.90	50.77	15.76	2.17
2	105570	107454	5cm thick, fairly continuous layer	11.75	<0.01	7.09	0.01	13.13	1.29	3.49	0.13	0.94	1.80	0.70	40.11	18.08	0.81
3	105571	107455	2.5-5cm thick, laterally pinching out and changes to grey limonitic shale at places along the dip direction	16.38	0.03	3.87	0.02	10.24	1.71	1.13	0.10	0.17	1.28	0.94	49.57	12.85	0.99
4	105572	107456	2-7cm thick, laterally pinching out, associated with gypsum layers.	16.75	0.04	6.59	0.01	6.32	1.68	1.52	0.08	0.19	3.11	0.86	49.20	12.31	0.57
5	105573	107457	Looks like grey shale with limonitic layer has altered to the suspected tuffite layer	19.26	0.05	2.54	0.02	6.11	1.84	0.74	0.11	0.33	0.17	1.05	51.97	13.45	1.60
6	105574	107458	Very poorly developed clay layer, mostly cherry red to black in colour, 4cm thick, collected only to check	15.57	0.02	5.32	0.01	7.21	1.62	0.66	0.11	0.17	0.13	0.88	48.00	16.10	3.48
7	105575	107459	Very poorly developed clay layer, mostly cherry red to black in colour, 4cm thick, collected only to check	15.44	0.02	3.60	0.02	10.99	1.77	2.64	0.11	0.18	0.17	1.01	48.65	14.40	0.31
8	105567	107451	The suspected tuffite layer is laterally extensive along the dip direction showing pinch and swell geometry. The layer thickness varies from 2-6cm and can be traced for 148.41m.	12.91	0.02	15.58	<0.01	6.94	1.25	1.36	0.10	0.24	8.47	0.67	36.43	13.64	1.61
9	105568	107452	The suspected tuffite layer is laterally extensive along the dip direction showing pinch and swell geometry. The layer thickness varies from 2-6cm and can be traced for 148.41m.	13.46	0.02	11.66	0.01	7.75	1.50	1.38	0.09	0.50	6.89	0.78	42.40	12.39	0.36
10	105576	107460	The suspected tuffite layer is laterally extensive along the dip direction showing pinch and swell geometry. The layer thickness varies from 2-3.5cm.	8.96	0.01	24.24	<0.01	9.23	0.92	1.64	0.07	0.14	6.10	0.48	26.68	20.73	0.06
11	105577	107461	4cm thick suspected tuffite layer, laterally extensive along the dip direction showing pinch and swell geometry.	10.65	0.07	11.51	0.01	10.17	1.49	4.07	0.12	0.23	3.54	0.70	39.93	16.56	0.10
12	105578	107462	3-8cm thick suspected tuffite layer, laterally extensive along the dip direction showing pinch and swell geometry.	13.39	0.02	7.40	0.01	8.09	1.64	2.21	0.10	0.25	2.42	0.81	49.50	13.39	0.07
13	105579	107463	2 thin layers of suspected tuffite layers, amalgamated at places	11.80	0.02	8.04	0.01	13.92	1.46	3.06	0.19	0.35	2.22	0.77	40.98	15.98	0.42
14	105580	107464	The nodular suspected tuffite layer gets thicker laterally	15.39	0.03	4.61	0.02	12.28	1.62	2.08	0.18	0.49	0.18	0.87	45.87	15.04	0.60
15	105581	107465	The nodular suspected tuffite layer gets thicker laterally	11.61	0.08	8.45	0.01	14.48	1.41	1.93	0.13	0.25	1.72	0.76	43.10	15.24	0.06
16	105582	107466	3cm thin layers of suspected tuffite layer, topped by gypsum layer	11.78	0.02	0.97	0.02	19.07	1.74	0.74	0.05	0.14	0.49	0.90	53.23	9.89	0.27
17	105583	107467	8cm thin layers of suspected tuffite layer,just above gypsum layer	16.24	0.03	1.10	0.02	11.59	1.99	1.10	0.23	0.18	0.20	1.13	54.22	11.15	0.17

Sl. No.	Original Sample ID	New Sample ID	Location No.	Latitude	Longitude	Type of Sample	Depth above surface (m)	Host Lithology	Stratigraphy
18	105584	107468	GSPL-Bhuj-119/06/24	23.189	69.601	BR	0.97	Cyclic occurrence of F1 and F2 with dissimilar cycle lengths. (F1) facies - White coloured, 2-7cm thick medium to coarse grained quartzose sandstone. Internally they are plane parallel laminated. However, top part of the F1 unit, sst beds are wave ripple laminated with chevron uploading draping structure. At the bottom of the sst unit, the lowest sst shows load structures. Unit thickness varies from 10-20cm (F2) facies - 16cm-1m thick unit of alternate occurrence of mm-cm thin grey shale and sandstone/siltone layers. The alternation unit is truncated by 5-17cm thick units of medium to fine grained, wave ripple laminated sst with thickness varying between 1.5-2cm. The tuffited ferrugenous clay layers are observed to occur as thin layers within F2.	Katrol Formation
19	105585	107469	GSPL-Bhuj-120/06/24	23.189	69.599	BR	0.9	Continuation of the same facies in stratigraphic up direction, along with the occurrence of mm-cm thin gypsum layers present around the suspected tuffite layers.	
20	105586	107470				BR	1.94		
21	105587	107471				BR	3.84		
22	105588	107472				BR	6.04		
23	105589	107473				BR	7.54		
24	105590	107474				BR	9.84		
25	105591	107475				BR	14.46		Katrol Formation
26	105593	107477				BR	15.46	Continuation of the same facies, at the same outcrop location in stratigraphic up direction. Incorporating (F3) facies, a 10-12 cm thick unit of medium to fine-grained sandstone, consisting of quartz and unidentified black minerals, is highly altered, ferruginous in places, with lateral extensions and undulatory boundaries. Shale alternation increases to 20-25 cm. Stratigraphically upward, sandstone layers are truncated, red nodular beds disappear, and are replaced by a very fine yellowish-green layer (likely clay) with clay alteration. The succession reaches 4.7 meters in total thickness before truncating and transitioning back to F1 facies. The suspected tuffite nodular beds are wrapped in gypsum.	Katrol Formation
27	105596	107480				BR	27.3	Continuation of the same facies, at the same outcrop location in stratigraphic up direction, along with the occurrence of mm-cm thin gypsum layers present around the suspected tuffite layers.	Katrol Formation
28	105597	107481				BR	28.97		Katrol Formation
29	105598	107482				BR	32.76		Katrol Formation
30	105599	107483				BR	35.02		Katrol Formation

Table Continued..

Annexure-XIII

Sl. No.	Original Sample ID	New Sample ID	Sample Description	Al_2O_3	BaO	CaO	Cr_2O_3	Fe_2O_3	K_2O	MgO	MnO	Na_2O	P_2O_5	TiO_2	SiO_2	LOI	S
18	105584	107468	0.7-3cm, thin nodular layer taken from F2 facies (Wave ripple laminated sst) and tends to amalgamate at few places. Sample collected throughout the 60cm thick F2 unit as composite sample.	12.83	0.03	11.14	0.01	8.84	1.57	1.46	0.11	0.34	6.03	0.80	43.38	12.31	0.33
19	105585	107469	(F2) facies - 3cm thick suspected tuffite layer, sandwiched between gypsum layers	12.70	0.03	2.15	0.02	13.61	1.85	1.84	0.12	0.41	0.24	1.02	50.93	13.83	0.60
20	105586	107470	The suspected tuffite layer is just above the mm thin gypsum layer and is associated with F2 facies.	12.50	0.03	3.12	0.02	14.46	1.70	2.18	0.12	0.45	0.37	0.89	50.72	12.91	0.83
21	105587	107471	The suspected tuffite layer is just above the mm thin gypsum layer and is associated with F2 facies.	11.18	0.02	4.54	0.01	12.73	1.76	3.74	0.09	0.51	0.22	0.82	48.32	15.04	0.32
22	105588	107472	3 -5cm thin suspected tuffite layer taken is associated with the F2 facies	10.92	0.03	4.31	0.02	17.25	1.50	3.50	0.11	0.46	0.32	0.78	43.18	16.22	0.70
23	105589	107473	The suspected tuffite layer is just above the gypsum layer and is associated with F2 facies.	9.96	0.01	7.08	0.01	14.89	1.42	4.68	0.13	0.47	0.25	0.74	39.82	18.58	1.28
24	105590	107474	The suspected tuffite layer, just above the gypsum layer and associated with the F2 facies & it laterally transitions into shale.	10.32	0.01	6.35	0.01	19.14	1.25	4.74	0.14	0.78	0.27	0.62	33.85	21.01	0.86
25	105591	107475	suspected tuffite layer	11.61	0.02	2.05	0.02	21.65	1.50	1.18	0.13	0.51	0.37	0.85	46.75	12.56	0.15
26	105593	107477	Sample taken from F3 facies. Very fine grain yellowish green coloured layer, seems to be clay (possibility of phosphorous?), wrapping the sandstone in eye shaped structure. Clay alternation observed at places	11.21	0.04	1.46	0.01	8.57	2.26	0.42	0.03	0.84	0.16	0.74	58.54	12.61	2.46
27	105596	107480	A well-developed thin suspected tuffite layer is sampled from the alternating red bed and shale layers.	12.47	0.02	3.33	0.02	16.31	1.59	1.12	0.13	0.68	0.41	0.92	48.35	13.70	0.27
28	105597	107481	4 cm well-developed thin suspected tuffite layer is sampled from the alternating red bed and shale layers.	15.26	0.02	2.15	0.01	7.63	1.87	0.85	0.05	0.53	0.17	1.07	57.46	11.76	0.49
29	105598	107482	4–7 cm thick, suspected tuffite layer associated with the F2 facies of grey shale is located just above the gypsum layer.	12.25	<0.01	2.66	0.02	24.19	1.37	1.98	0.10	0.54	0.29	0.83	39.98	14.96	0.17
30	105599	107483	A 5 cm thick, suspected tuffite layer is situated between grey shale layers, which alternate with red beds.	15.23	0.02	2.39	0.02	11.87	1.72	1.31	0.12	0.48	0.45	1.04	51.46	12.76	0.45

Sl. No.	Original Sample ID	New Sample ID	Location No.	Latitude	Longitude	Type of Sample	Depth above surface (m)	Host Lithology	Stratigraphy
31	105600	107484	GSPL-Bhuj-117/06/24	23.145	69.549	BR	0.9	The succession includes black shale intermittently separated by nodular layers, which are poorly developed or less pronounced. The unit overlies 33 cm thick, pinkish, coarse to medium-grained sandstone, consisting of quartz, feldspar, and mica, is observed in a tabular form with no internal structures. Nearby, a dolerite dyke indicates contact metamorphism, likely converting the black shale into slate.	
32	105605	107489	GSPL-Bhuj-123/06/24	23.186	69.641	BR	0.91	(F1) Facies: Very thinly laminated shale-sandstone alternation. (F2) Facies: Grey shale. (F3) Facies: 1-3 cm thick, thinly bedded sandstone with pinch-and-swell structures and wavy ripple laminations; internal structures are not visible and beds are truncated or separated by shale laminations.	Katrol Formation
33	105609	107493	GSPL-Bhuj-129/06/24	23.179	69.691	BR	0.9	(F1) Facies: Millimetre to 1 cm thick, medium to fine-grained sandstone beds, mostly plane-parallel laminated and separated by millimetre-thin shales. (F2) Facies: 10-15 cm thick grey shales with well-defined fissility planes. In this succession, millimetre-thin shale-sandstone alternations and a few thin gypsum layers are observed, with well-developed suspected tuffite nodular beds in both facies.	Katrol Formation
34	105610	107494				BR	3.77		Katrol Formation
35	105611	107495				BR	5.33		Katrol Formation
36	105612	107496	GSPL-Bhuj-130/06/24	23.174	69.692	BR	0.41	Continuation of the same facies as the previous location in stratigraphic up direction. However, the thickness of the siltstone layers increases, with only one gypsum layer observed within the sequence.	Katrol Formation
37	105613	107497				BR	2.75		Katrol Formation
38	105614	107498				BR	3.17		Katrol Formation
39	105615	107499				BR	3.72		Katrol Formation
40	105616	107500				BR	5.39		Katrol Formation
41	105617	107501	GSPL-Bhuj-132/06/24	23.173	69.692	BR	0.75	Continuation of the same facies as the previous location in stratigraphic up direction. The occurrence of centimetre-thin gypsum layers is present around the suspected tuffite layers, alongside the observed sandstone-siltstone alternation.	Katrol Formation
42	105618	107502				BR	2.095		Katrol Formation
43	105619	107503				BR	4.095		Katrol Formation
44	105620	107504				BR	5.615		Katrol Formation
45	105621	107505				BR	6.515		Katrol Formation

Table Continued..

Annexure-XIII

Sl. No.	Original Sample ID	New Sample ID	Sample Description	Al_2O_3	BaO	CaO	Cr_2O_3	Fe_2O_3	K_2O	MgO	MnO	Na_2O	P_2O_5	TiO_2	SiO_2	LOI	S
31	105600	107484	Black shale without the sandstone interlayers	17.37	0.04	0.77	0.02	10.63	2.38	0.61	0.04	0.39	0.10	1.05	54.82	10.74	0.13
32	105605	107489	4 cm thick, continuous layer, occuring in association with F1, overlying F3	11.44	0.02	13.10	0.01	9.76	1.22	3.67	0.10	0.22	4.91	0.70	37.08	16.92	0.09
33	105609	107493	2-3cm suspected tuffite layer is just above the sst layers of F1 facies	11.12	0.05	9.11	0.01	16.96	1.31	2.07	0.17	0.13	0.20	0.73	38.98	18.40	0.06
34	105610	107494	2cm thick, suspected tuffite layer is in between F2 facies of grey shale & contains bivalve fossils, associated with gypsum layer in the succession	12.29	0.03	4.39	0.02	15.48	1.54	3.32	0.18	0.11	0.18	0.85	42.91	17.32	0.57
35	105611	107495	Very poorly developed clay layer, mostly cherry red to black in colour, 1-2cm thick, collected from grey shale of F2 facies	8.32	0.02	10.61	0.01	18.33	0.87	2.87	0.17	0.10	0.18	0.47	32.09	20.34	4.89
36	105612	107496	Very poorly developed, 2.5 - 3cm thin layer in association with grey shale F2 facies.	10.20	0.03	7.52	0.01	13.17	1.41	4.50	0.17	0.15	0.14	0.76	40.23	19.62	1.40
37	105613	107497	Very poorly developed, 5cm thin layer in association with grey shale F2 facies.	12.01	0.02	4.56	0.01	13.01	1.61	2.83	0.10	0.12	0.17	0.85	46.12	16.79	1.12
38	105614	107498	Very poorly developed, 3cm thin, suspected tuffite layer in association with gypsum layer & grey shale of F2	10.65	0.01	5.69	0.01	11.76	1.43	0.69	0.08	0.10	0.15	0.77	47.52	16.81	3.65
39	105615	107499	Very poorly developed, 2.5-3cm thin, suspected tuffite layer in association with gypsum layer & grey shale of F2	11.91	0.02	5.49	0.02	13.31	1.53	2.09	0.09	0.11	0.16	0.81	45.01	16.69	2.12
40	105616	107500	Very poorly developed, 2cm thin suspected tuffite layer in association with grey shale F2 facies.	13.99	0.02	2.57	0.02	16.85	1.73	2.22	0.15	0.18	0.19	0.97	44.51	15.31	0.60
41	105617	107501	3.5cm thin, suspected tuffite layer, associated with the F2 facies of grey shale and thick gypsum layer	12.20	0.02	3.30	0.02	16.14	1.67	2.60	0.20	0.17	0.18	0.93	46.00	15.38	0.51
42	105618	107502	suspected tuffite layer, associated with the F2 facies of grey shale (50cm), sandwiched between amalgamated shale/siltstone beds	12.35	0.02	2.60	0.02	11.09	1.92	1.31	0.13	0.11	0.14	1.00	56.36	11.91	0.38
43	105619	107503	3 - 3.5cm thin suspected tuffite layer, associated with grey shale sandwiched between plane parallel laminated sandstone	10.90	0.01	4.75	0.02	14.12	1.58	1.66	0.16	0.11	0.17	0.85	45.53	17.29	2.20
44	105620	107504	thin suspected tuffite layer, associated with blackish grey shale	12.77	0.02	4.95	0.01	8.09	1.77	1.36	0.10	0.18	0.14	0.88	54.04	13.91	1.07
45	105621	107505	2cm thin, suspected tuffite layer, associated with the F2 facies of blackish grey shale	11.11	<0.01	6.30	0.01	9.22	1.52	2.30	0.11	0.19	0.12	0.74	50.85	15.58	1.24

Sl. No.	Original Sample ID	New Sample ID	Location No.	Latitude	Longitude	Type of Sample	Depth above surface (m)	Host Lithology	Stratigraphy
46	105622	107506	GSPL-Bhuj-132/06/24	23.173	69.692	BR	8.265	Continuation of the same facies as the previous location in stratigraphic up direction. The occurrence of centimetre-thin gypsum layers is present around the suspected tuffite layers, alongside the observed sandstone-siltstone alternation	Katrol Formation
47	105623	107507		23.173	69.692	BR	10.885		Katrol Formation
48	105624	107508	GSPL-Bhuj-134/06/24	23.172	69.693	BR	0.35	Continuing in the stratigraphic upward direction from the previous location, with addition to it only a single gypsum layer is observed alongside a thinning shale-siltstone layer.	Katrol Formation
49	105625	107509				BR	3.675		Katrol Formation
50	105629	107513	GSPL-Bhuj-137/06/24	23.164	69.727	BR	5.385	Alternate occurrence of sandstone, gray shale and this particular phosphorite looking beds. The sandstones are parallal laminated, 6-10cm thick medium to fine grained quartzose sandstone. Relatively coarse grained brownish -mauve colored sandstones intercalated with nodular layers, separated by millimeter-thin shale-siltstone layers are also visible. The gray shale layers are very thin (12-18cm), rarely interupted by 2-3cm thick red layers. The phosphorite looking beds (may be quartz arenite also) are 9-12cm thick, forming units of 39cm to 1.8m, separated by mm thin shale layers/red beds. Butchers knife erosion is common within this beds.several gypsum layers are found near the nodular layers. This succession is at the upper part of the Katrol Formation.	Katrol Formation
51	105645	107529	GSPL-Bhuj-147/06/24	23.171	69.693	BR	0.267	In the stratigraphic continuation upwards in continuation from the GSPL-Bhuj-134/06/24 location, same kind of facies. F1: Sst consisting of millimetre to 1 cm thick, plane parallel laminated layers/beds, occasionally amalgamated. The sst layers are separated by mm thin shales and/or gypsum layers. Unit thickness varies from 5cm-48cm. F2: Gray shales having unit thickness of 7-110cm and often interrupted by 2-7cm thick calcareous red beds and/or gypsum layers. Alteration of few beds in yellowish clay layers are also observed. Additionally, (20cm) thick ferruginous shale layer is present, characterized by mica, ferrous micro-nodules, and several gypsum layers	Katrol Formation
52	105646	107530				BR	1.695		Katrol Formation
53	105648	107532				BR	6.435		katrol Formation
54	105649	107533				BR	8.675		
55	105622	105622	GSPL-Bhuj-91/01/24	23.151	69.580	BR		Heterolithic unit consist of shale (grey, white with goethitic and ferruginous patches, interrupted by well-developed tuffite layers alternating with 10-20cm thick sandstone layers and/or thinly laminated shale-siltstone unit	
56	105601	107485	GSPL-Bhuj-117/06/24	23.145335	69.54906167	Channel Sampling	1.33	The succession includes black shale intermittently separated by nodular layers, which are poorly developed or less pronounced. The unit overlies 33 cm thick, pinkish, coarse to medium-grained sandstone, consisting of quartz, feldspar, and mica, is observed in a tabular form with no internal structures. Nearby, a dolerite dyke indicates contact metamorphism, likely converting the black shale into slate.	katrol Formation
57	105602	107486					2.4		

Table Continued..

Annexure-XIII

Sl. No.	Original Sample ID	New Sample ID	Sample Description	Al_2O_3	BaO	CaO	Cr_2O_3	Fe_2O_3	K_2O	MgO	MnO	Na_2O	P_2O_5	TiO_2	SiO_2	LOI	S
46	105622	107506	suspected tuffite layer, associated with the F2 facies of blackish grey shale	10.79	<0.01	4.99	0.02	16.62	1.46	2.85	0.10	0.14	0.19	0.81	43.61	16.84	0.93
47	105623	107507	suspected tuffite layer, associated with the F2 facies of blackish grey shale and thick gypsum layer	12.97	0.01	4.15	0.01	9.27	1.66	1.12	0.09	0.33	0.13	0.85	50.32	16.17	2.27
48	105624	107508	2.5cm thin, suspected tuffite layer, just above the gypsum layer & associated with plane parallel laminated sandstone of F1	10.94	0.01	7.96	0.01	12.18	1.45	3.31	0.18	0.17	0.12	0.72	43.35	18.23	1.23
49	105625	107509	2.5cm thin, suspected tuffite layer, just below the gypsum layer & associated with grey shale of F2	10.42	<0.01	10.01	<0.01	12.00	1.34	6.83	0.20	0.18	0.14	0.65	33.25	23.47	0.87
50	105629	107513	Grey shale samples collected from the uppermost catchment area which was yielding high HLS results.	22.68	<0.01	0.52	0.02	3.47	1.71	0.75	0.03	0.22	0.08	1.25	58.42	10.01	0.18
51	105645	107529	Calcareous suspected tuffite layer, in association with grey shale of F2 facies	11.49	<0.01	7.39	0.01	11.15	1.52	3.88	0.15	0.17	0.14	0.76	43.59	18.05	1.06
52	105646	107530	3 cm thin calcareous suspected tuffite layer, in association with grey shale of F2 facies	10.08	<0.01	9.72	<0.01	8.86	1.40	6.47	0.19	0.19	0.10	0.67	38.97	21.54	1.17
53	105648	107532	2.3 - 3cm thin suspected tuffite layer (relatively well developed) in association with grey shale of F2 facies	11.59	<0.01	10.00	<0.01	9.29	1.53	1.30	0.11	0.15	0.12	0.76	47.21	16.80	0.50
54	105649	107533	3.5 - 7cm thin suspected tuffite layer (amalgamated) in association with grey shale of F2 facies	10.21	<0.01	8.77	<0.01	11.83	1.39	5.90	0.17	0.20	0.13	0.67	38.47	20.75	0.89
55	105622	105622	Yellowish (shale) part of 105494 (BR)	13.54	0.01	19.26	0.01	10.82	1.08	1.31	0.18	0.21	12.49	0.62	28.41	10.58	0.56
56	105601	107485	Channel sampling of black shale (possible slate) separated by nodular layers which was taken separately.	15.35	0.04	0.97	0.02	8.38	2.29	0.52	0.04	0.28	0.10	1.00	61.21	8.99	0.09
57	105602	107486	Channel sampling of Black shale which is just above sst layer	17.48	0.03	1.23	0.02	5.57	2.14	0.61	0.06	0.37	0.10	1.16	61.82	8.73	<0.05

Annexure-XIV: ICPMS Analysis Tuffite layer

Sl. No.	Original Sample ID	Location No.	Latitude	Longitude	Type of Sample	Li	Be	Sc	V	Cr	Co	Ni	Cu	Zn	Ga	Ge	Se	Rb	Sr	Y	Zr
1	105569	GSPL-Bhuj-112/03/24	23.152	69.578	BR	114.14	2.32	23.38	148.68	125.51	47.44	81.04	30.19	154.13	23.92	<0.5	2.53	92.30	485.22	33.63	158.44
2	105570				BR	79.05	2.32	26.28	120.24	102.36	23.24	43.81	26.31	191.15	19.37	0.58	5.78	68.11	366.73	106.93	111.69
3	105571				BR	110.16	2.47	28.16	152.63	142.75	29.31	60.76	32.16	174.32	26.59	0.84	9.34	91.44	323.54	155.64	138.26
4	105572				BR	104.76	2.28	26.07	119.42	132.66	18.12	38.97	29.00	132.82	25.50	0.95	8.17	89.05	591.64	169.11	153.46
5	105573				BR	131.77	2.94	17.06	149.45	135.62	39.01	72.00	38.93	133.13	28.55	<0.5	2.33	100.13	682.63	26.48	157.00
6	105574				BR	114.92	2.42	20.13	146.00	125.48	60.71	80.96	30.32	164.89	24.45	<0.5	1.49	87.93	482.79	25.83	148.85
7	105575				BR	110.88	2.59	28.45	183.37	167.37	31.09	75.35	29.37	179.55	25.34	<0.5	2.47	97.54	338.02	35.45	148.43
8	105567	GSPL-Bhuj-91/01/24	23.151	69.580	BR	96.87	2.63	41.38	116.47	107.10	15.92	43.03	23.83	96.94	25.64	1.32	10.66	72.08	714.87	293.77	108.01
9	105568				BR	101.62	2.46	42.85	128.10	114.85	15.21	38.71	26.53	103.51	28.71	1.70	15.44	80.74	523.27	346.69	144.29
10	105576	GSPL-Bhuj-115/06/24	23.150	69.581	BR	**49.81**	**2.07**	**35.99**	**110.00**	**97.64**	**12.27**	**24.80**	**21.13**	**59.14**	**17.86**	**0.86**	**8.93**	**49.97**	**439.02**	**214.94**	**118.03**
11	105577				BR	71.88	2.17	39.17	122.93	108.48	28.60	41.67	17.37	141.27	22.71	1.12	10.41	77.12	941.48	209.31	196.94
12	105578				BR	74.10	2.04	29.58	121.99	106.30	20.53	39.77	22.15	178.86	22.98	0.80	7.47	80.02	236.08	142.47	174.37
13	105579	GSPL-Bhuj-110/06/24	23.150	69.585	BR	79.08	2.38	40.44	180.33	139.72	72.13	103.40	28.20	139.11	25.07	1.14	11.57	77.99	599.71	214.24	167.09
14	105580				BR	94.16	2.76	28.47	173.00	129.03	41.33	83.84	31.95	143.22	23.47	<0.5	2.12	91.70	764.85	35.53	155.00
15	105581				BR	63.01	2.24	32.40	157.87	119.12	34.90	55.99	27.65	208.38	21.80	0.89	8.18	69.93	222.25	138.79	169.87
16	105582	GSPL-Bhuj-116/06/24	23.145	69.584	BR	75.21	3.28	22.46	165.18	118.11	38.28	55.69	25.07	245.36	19.08	<0.5	3.42	78.85	147.26	49.70	202.24
17	105583				BR	116.51	2.64	20.48	162.06	153.37	26.36	69.92	29.66	89.83	26.70	<0.5	1.75	104.60	116.81	29.42	201.87
18	105584	GSPL-Bhuj-119/06/24	23.189	69.601	BR	97.49	2.58	48.18	131.39	110.54	23.10	31.07	20.89	92.68	25.32	0.96	9.02	78.64	1129.39	233.05	181.90
19	105585	GSPL-Bhuj-120/06/24	23.189	69.599	BR	86.16	2.01	17.91	145.46	107.13	20.50	42.82	16.70	80.20	18.90	<0.5	2.36	77.71	235.11	30.16	157.74
20	105586				BR	**96.79**	**2.34**	**20.90**	**158.55**	**121.97**	**35.34**	**51.75**	**19.69**	**135.22**	**21.60**	**<0.5**	**2.20**	**89.95**	**490.58**	**29.69**	**199.43**
21	105587				BR	77.93	1.87	17.41	137.92	108.60	43.10	35.43	17.02	174.75	18.02	<0.5	2.27	81.97	401.53	24.92	159.03
22	105588				BR	80.05	2.56	22.03	156.37	110.16	34.44	46.28	21.30	89.08	17.75	<0.5	2.67	74.33	712.65	31.05	143.61
23	105589				BR	75.38	2.31	19.17	155.89	115.44	40.71	43.26	21.53	90.49	17.81	<0.5	1.82	72.69	489.27	28.84	170.54

Sl. No.	Original Sample ID	Location No.	Latitude	Longitude	Type of Sample	Li	Be	Sc	V	Cr	Co	Ni	Cu	Zn	Ga	Ge	Se	Rb	Sr	Y	Zr
24	105590				BR	66.34	2.24	21.97	164.24	107.28	35.17	47.13	20.49	96.12	16.38	<0.5	2.01	64.70	218.53	28.35	120.08
25	105591				BR	71.10	2.09	28.56	201.54	121.91	37.18	83.83	43.45	174.49	18.86	<0.5	3.47	75.95	140.28	36.13	154.00
26	105593				BR	48.63	1.15	11.05	119.40	106.49	47.76	9.21	18.17	52.87	17.24	<0.5	1.20	95.15	246.69	14.20	179.61
27	105596				BR	82.25	1.89	25.05	168.90	134.74	47.04	81.11	30.21	170.08	21.04	<0.5	3.00	84.31	263.59	44.61	160.40
28	105597				BR	100.34	1.78	17.03	137.63	118.55	43.74	45.80	26.63	113.10	24.01	<0.5	2.15	100.92	211.71	22.62	191.12
29	105598				BR	89.70	2.48	34.52	250.59	143.90	33.44	87.07	40.48	135.18	20.38	<0.5	2.51	76.98	126.57	33.15	129.14
30	105599				BR	**102.00**	**2.25**	**23.31**	**179.46**	**126.75**	**67.00**	**66.06**	**31.28**	**173.95**	**25.69**	**<0.5**	**3.73**	**95.68**	**235.32**	**58.29**	**159.92**
31	105600	GSPL-Bhuj-117/06/24	23.145	69.549	BR	71.91	2.88	19.42	153.81	139.31	22.62	70.70	35.56	112.29	27.57	<0.5	2.13	107.23	2546.15	25.43	127.82
32	105605	GSPL-Bhuj-123/06/24	23.186	69.641	BR	70.16	2.08	41.82	134.23	114.80	40.18	41.83	19.13	113.37	23.83	1.13	10.97	63.86	478.83	238.25	192.74
33	105609	GSPL-Bhuj-129/06/24	23.179	69.691	BR	58.87	2.22	23.34	206.31	130.97	62.07	73.11	28.55	119.71	19.20	<0.5	1.85	72.14	251.65	30.28	126.55
34	105610				BR	88.65	2.53	25.25	216.45	153.91	48.13	106.40	32.63	120.26	22.81	<0.5	2.24	89.60	1211.95	32.48	142.15
35	105611				BR	47.86	1.87	23.46	211.08	103.63	20.58	32.65	19.41	133.64	13.03	<0.5	1.83	49.43	1062.35	21.45	95.35
36	105612	GSPL-Bhuj-130/06/24	23.174	69.692	BR	63.00	1.83	21.26	154.34	107.78	33.99	62.70	22.97	171.79	17.83	<0.5	1.72	76.19	508.98	26.90	119.10
37	105613				BR	76.24	1.90	23.09	171.39	120.15	35.31	59.13	22.80	120.85	19.44	<0.5	1.70	88.25	392.30	27.58	137.75
38	105614				BR	**65.79**	**1.79**	**20.76**	**150.99**	**112.14**	**53.73**	**69.00**	**23.15**	**143.20**	**16.96**	**<0.5**	**2.01**	**72.61**	**260.34**	**25.48**	**151.55**
39	105615				BR	76.30	1.89	22.53	195.15	125.35	29.85	55.84	26.14	90.58	19.48	<0.5	1.93	84.01	233.78	23.71	130.78
40	105616				BR	94.70	3.24	26.66	229.07	137.39	37.74	90.75	32.76	130.01	23.36	<0.5	1.67	102.12	249.41	31.21	142.97
41	105617	GSPL-Bhuj-132/06/24	23.173	69.692	BR	82.30	2.07	24.55	215.62	143.86	41.82	86.32	28.75	117.38	19.94	<0.5	2.15	97.99	343.78	28.68	148.62

Sl. No.	Original Sample ID	Location No.	Latitude	Longitude	Type of Sample	Li	Be	Sc	V	Cr	Co	Ni	Cu	Zn	Ga	Ge	Se	Rb	Sr	Y	Zr
42	105618				BR	69.93	1.67	19.01	144.82	120.33	50.84	65.31	24.19	177.91	18.86	<0.5	1.36	100.82	247.43	22.65	169.53
43	105619				BR	58.87	2.01	17.32	171.73	110.48	38.18	60.35	22.38	118.58	16.89	<0.5	1.49	88.60	443.10	19.19	137.76
44	105620				BR	59.02	1.99	14.51	125.16	102.27	48.57	47.49	19.43	115.30	17.74	<0.5	1.24	93.55	789.43	22.74	156.45
45	105621				BR	50.52	1.59	17.10	121.91	99.70	34.65	38.18	18.46	88.55	14.71	<0.5	1.38	78.08	1109.53	22.39	139.61
46	105622				BR	56.54	1.87	17.11	176.96	126.83	25.05	39.77	22.62	95.54	15.42	<0.5	1.70	78.64	269.23	18.94	129.84
47	105623				BR	71.39	2.05	15.95	128.24	107.23	32.59	51.39	20.92	133.90	17.12	<0.5	1.82	89.80	271.41	20.75	127.81
48	105624	GSPL-Bhuj-134/06/24	23.172	69.693	BR	**51.41**	**1.66**	**15.48**	**155.70**	**95.69**	**32.56**	**54.30**	**18.20**	**98.93**	**14.84**	**<0.5**	**1.47**	**74.08**	**218.45**	**22.06**	**130.80**
49	105625				BR	61.89	1.73	16.98	144.96	91.87	17.98	50.73	19.70	69.04	15.65	<0.5	1.45	78.02	270.04	25.21	108.52
50	105629	GSPL-Bhuj-137/06/24	23.164	69.727	BR	132.45	2.24	17.13	142.54	134.00	41.46	16.38	32.66	55.71	28.02	<0.5	1.53	102.07	107.30	20.30	206.06
51	105645	GSPL-Bhuj-147/06/24	23.171	69.693	BR	57.57	1.60	16.81	144.79	100.87	24.38	48.39	21.04	217.19	16.45	<0.5	1.23	78.72	199.63	25.30	137.40
52	105646				BR	58.35	1.85	13.74	120.13	103.25	24.17	43.37	17.65	69.97	15.24	<0.5	1.02	82.37	261.90	21.18	122.82
53	105648				BR	52.41	1.50	17.02	137.81	104.14	24.55	36.89	20.67	108.54	16.04	<0.5	1.52	76.73	164.85	24.79	168.31
54	105649				BR	58.53	1.59	15.95	137.49	97.62	20.78	42.24	20.13	80.60	15.13	<0.5	1.42	79.00	202.66	23.27	125.71
55	105622	GSPL-Bhuj-91/01/24	23.151	69.580	BR	79.19	2.44	59.34	143.10	NA	NA	NA	NA	NA	27.54	1.75	14.87	60.32	768.78	505.44	201.17
56	105601	GSPL-Bhuj-117/06/24	23.145335	69.54906167	Channel Sampling	26.9	2.0	15.2	128.4	132.5	17.1	40.6	26.3	113.2	22.5	<0.5	2.1	93.4	704.4	20.3	116.6
57	105602	GSPL-Bhuj-117/06/24	23.145335	69.54906167	Channel Sampling	33.9	2.6	17.1	145.9	136.5	19.8	43.6	33.9	100.2	25.7	<0.5	1.9	106.1	312.5	22.4	139.2

Table Continued..

Annexure-XIV

Sl. No.	Original Sample ID	Nb	Mo	Cd	In	Sn	Sb	Te	Cs	Ba	La	Ce	Pr	Nd	Sm	Eu	Gd	Tb	Dy	Ho
1	105569	16.53	0.94	<0.5	<0.5	2.60	1.15	<0.5	5.89	381.79	44.73	99.42	10.89	41.22	8.27	1.70	7.26	1.12	6.51	1.24
2	105570	9.53	1.19	<0.5	<0.5	1.56	1.83	<0.5	4.29	256.96	40.28	110.79	13.89	61.57	16.06	3.98	18.73	2.99	17.17	3.17
3	105571	14.88	1.59	<0.5	<0.5	2.62	1.02	<0.5	5.88	356.44	57.34	161.13	19.27	86.46	23.06	6.01	28.00	4.53	25.92	4.62
4	105572	14.98	1.84	<0.5	<0.5	4.55	1.19	<0.5	5.36	511.55	64.26	177.27	21.66	94.76	24.18	6.10	28.68	4.69	27.20	5.01
5	105573	19.08	1.74	<0.5	<0.5	2.98	1.07	<0.5	6.57	557.22	45.77	103.17	11.08	41.41	8.01	1.66	6.67	0.99	5.53	1.04
6	105574	16.90	1.02	<0.5	<0.5	2.75	0.92	<0.5	6.21	330.67	38.05	92.72	9.25	34.59	6.70	1.41	5.82	0.91	5.30	1.01
7	105575	17.69	4.13	<0.5	<0.5	3.34	1.55	<0.5	6.36	325.80	44.30	94.56	10.61	39.84	8.11	1.72	7.32	1.15	6.69	1.30
8	105567	1.09	1.02	<0.5	<0.5	1.05	1.11	<0.5	4.83	411.66	96.78	269.17	31.45	138.67	34.42	8.83	41.99	6.77	40.36	7.79
9	105568	0.56	1.00	<0.5	<0.5	0.88	0.87	<0.5	5.15	365.40	109.66	293.01	38.25	173.57	44.98	11.64	55.53	8.94	52.06	9.75
10	105576	**1.45**	**1.11**	**<0.5**	**<0.5**	**0.54**	**0.66**	**<0.5**	**3.16**	**384.56**	**78.88**	**199.74**	**22.34**	**97.11**	**22.64**	**5.92**	**29.00**	**4.62**	**28.07**	**5.57**
11	105577	9.88	1.38	<0.5	<0.5	1.62	0.84	<0.5	4.74	816.53	77.60	227.51	28.13	126.45	32.59	8.32	37.72	5.99	34.57	6.36
12	105578	13.77	0.80	<0.5	<0.5	2.85	0.95	<0.5	4.53	334.21	58.75	165.42	19.86	87.04	21.89	5.40	24.72	3.95	22.75	4.26
13	105579	13.88	2.08	<0.5	<0.5	3.09	0.90	<0.5	4.84	303.79	72.39	214.34	26.60	124.47	33.89	8.85	42.05	6.69	37.39	6.71
14	105580	16.29	1.82	<0.5	<0.5	3.17	1.20	<0.5	5.95	419.02	41.80	94.71	10.17	38.93	8.19	1.78	7.48	1.16	6.74	1.29
15	105581	12.89	0.92	<0.5	<0.5	2.55	0.83	<0.5	4.47	842.42	56.84	153.69	18.98	85.57	22.80	5.79	26.84	4.27	23.96	4.32
16	105582	14.24	1.21	<0.5	<0.5	2.62	1.03	<0.5	4.46	345.95	38.93	88.11	10.63	44.70	10.59	2.40	10.77	1.65	9.28	1.74
17	105583	19.19	1.86	<0.5	<0.5	4.37	0.95	<0.5	7.12	335.09	46.76	102.48	10.98	41.04	8.08	1.64	6.81	1.02	5.78	1.08
18	105584	13.29	0.73	<0.5	<0.5	2.43	1.27	<0.5	4.23	457.58	89.16	216.01	25.02	108.48	24.65	6.61	31.60	4.87	29.13	5.85
19	105585	14.52	<0.5	<0.5	<0.5	2.15	0.74	<0.5	3.93	345.62	38.26	88.42	10.20	39.58	8.03	1.67	6.97	1.03	5.74	1.05
20	105586	**17.33**	**0.75**	**<0.5**	**<0.5**	**2.56**	**0.67**	**<0.5**	**4.73**	**388.91**	**44.61**	**96.44**	**10.86**	**40.92**	**8.19**	**1.55**	**6.81**	**1.01**	**5.64**	**1.06**
21	105587	13.92	0.94	<0.5	<0.5	2.85	1.38	<0.5	3.99	366.85	36.56	77.65	9.23	35.04	6.92	1.42	5.87	0.86	4.82	0.89
22	105588	12.87	0.81	<0.5	<0.5	2.40	0.98	<0.5	4.05	326.78	34.18	78.52	9.21	36.46	7.55	1.63	6.70	1.02	5.77	1.09
23	105589	16.23	0.71	<0.5	<0.5	2.65	0.96	<0.5	4.12	276.31	36.58	80.50	9.62	36.90	7.43	1.58	6.59	0.98	5.39	1.02

Sl. No.	Original Sample ID	Nb	Mo	Cd	In	Sn	Sb	Te	Cs	Ba	La	Ce	Pr	Nd	Sm	Eu	Gd	Tb	Dy	Ho
24	105590	15.71	0.85	<0.5	<0.5	2.00	0.70	<0.5	3.45	238.09	33.85	73.99	8.91	35.07	7.29	1.52	6.31	0.94	5.28	0.98
25	105591	13.78	1.96	<0.5	<0.5	2.67	1.13	<0.5	4.67	233.45	30.25	75.22	8.35	33.15	7.30	1.65	7.15	1.16	6.85	1.29
26	105593	14.23	0.90	<0.5	<0.5	2.10	0.74	<0.5	3.66	470.47	36.28	78.70	8.88	31.85	5.38	0.94	4.04	0.57	3.07	0.57
27	105596	15.33	3.47	<0.5	<0.5	2.60	0.97	<0.5	5.45	287.22	36.04	90.11	10.08	40.25	9.05	2.07	9.06	1.47	8.43	1.59
28	105597	19.34	1.50	<0.5	<0.5	3.46	1.51	<0.5	6.44	278.36	36.91	85.54	9.07	33.94	6.62	1.31	5.52	0.84	4.68	0.88
29	105598	13.43	1.63	<0.5	<0.5	2.89	0.80	<0.5	5.45	175.87	35.02	76.22	8.71	33.62	7.10	1.61	7.02	1.07	6.29	1.21
30	105599	**17.87**	**1.15**	**<0.5**	**<0.5**	**3.62**	**0.86**	**<0.5**	**6.58**	**234.75**	**44.69**	**114.51**	**12.62**	**50.90**	**11.60**	**2.66**	**11.91**	**1.86**	**10.76**	**2.01**
31	105600	17.52	1.60	<0.5	<0.5	3.17	0.54	<0.5	5.09	454.32	51.79	108.10	12.30	45.83	8.61	1.76	7.24	0.99	5.46	0.99
32	105605	12.26	1.40	<0.5	<0.5	2.14	<0.5	<0.5	4.42	345.87	77.50	215.27	27.90	126.19	33.16	8.62	41.15	6.65	38.87	7.32
33	105609	13.60	2.27	<0.5	<0.5	3.31	0.66	<0.5	4.72	644.09	32.79	76.84	8.26	31.57	6.53	1.40	5.78	0.90	5.39	1.09
34	105610	15.74	5.41	<0.5	<0.5	3.39	0.56	<0.5	5.70	436.31	36.18	78.30	8.92	34.27	7.11	1.49	6.31	0.99	5.92	1.18
35	105611	8.65	0.87	<0.5	<0.5	1.93	1.87	<0.5	3.18	315.33	21.01	52.24	5.36	21.22	4.48	0.97	4.29	0.67	3.94	0.78
36	105612	12.86	0.97	<0.5	<0.5	2.66	0.72	<0.5	5.19	386.68	27.16	62.24	6.69	25.63	5.42	1.14	4.96	0.81	4.98	1.02
37	105613	14.59	1.24	<0.5	<0.5	2.30	0.57	<0.5	5.70	352.40	30.88	68.74	7.77	29.65	6.39	1.32	5.60	0.90	5.21	1.01
38	105614	**14.34**	**0.88**	**<0.5**	**<0.5**	**2.41**	**0.64**	**<0.5**	**4.37**	**286.05**	**36.58**	**85.03**	**8.95**	**33.13**	**6.64**	**1.23**	**5.78**	**0.86**	**5.07**	**0.96**
39	105615	14.84	0.90	<0.5	<0.5	2.95	0.64	<0.5	5.55	266.73	32.82	72.50	7.91	29.80	5.94	1.25	5.06	0.79	4.65	0.92
40	105616	16.96	1.80	<0.5	<0.5	3.64	0.77	<0.5	7.25	255.98	36.97	88.86	8.82	33.38	6.74	1.40	6.22	0.98	6.02	1.18
41	105617	16.11	1.96	<0.5	<0.5	3.30	0.79	<0.5	6.84	269.55	36.19	84.21	8.96	34.10	6.86	1.42	6.07	0.94	5.51	1.12

Sl. No.	Original Sample ID	Nb	Mo	Cd	In	Sn	Sb	Te	Cs	Ba	La	Ce	Pr	Nd	Sm	Eu	Gd	Tb	Dy	Ho
42	105618	16.16	1.91	<0.5	<0.5	3.02	1.12	<0.5	6.78	289.10	32.51	76.32	7.90	29.14	5.76	1.14	4.95	0.79	4.60	0.91
43	105619	14.01	0.99	<0.5	<0.5	2.18	0.57	<0.5	6.35	201.52	27.81	66.65	6.87	25.91	5.05	1.03	4.22	0.67	3.88	0.75
44	105620	15.33	0.84	<0.5	<0.5	2.70	0.98	<0.5	5.77	338.30	36.67	86.66	9.10	33.90	6.57	1.30	5.36	0.80	4.68	0.87
45	105621	12.66	1.19	<0.5	<0.5	1.81	0.52	<0.5	4.94	298.01	27.89	62.90	7.12	27.40	5.54	1.16	4.84	0.78	4.56	0.88
46	105622	13.49	0.95	<0.5	<0.5	3.76	0.61	<0.5	5.34	202.02	28.06	66.33	7.32	27.54	5.35	1.07	4.52	0.68	3.90	0.74
47	105623	14.71	1.24	<0.5	<0.5	2.38	0.65	<0.5	6.17	246.83	30.01	68.41	7.36	27.77	5.56	1.11	4.63	0.72	4.23	0.83
48	105624	**12.07**	**1.03**	**<0.5**	**<0.5**	**2.08**	**0.53**	**<0.5**	**4.52**	**283.22**	**26.00**	**56.76**	**6.56**	**25.13**	**4.97**	**1.04**	**4.41**	**0.69**	**4.13**	**0.82**
49	105625	11.29	0.53	<0.5	<0.5	2.09	<0.5	<0.5	5.35	209.29	26.08	57.63	6.41	24.31	4.93	1.05	4.60	0.72	4.35	0.91
50	105629	24.16	0.95	<0.5	<0.5	5.01	0.88	<0.5	8.31	269.70	53.80	117.34	12.56	45.36	8.04	1.49	5.95	0.84	4.56	0.85
51	105645	11.24	0.75	<0.5	<0.5	1.64	0.57	<0.5	5.01	251.82	28.98	63.50	7.24	27.08	5.52	1.13	4.90	0.77	4.59	0.93
52	105646	11.47	1.51	<0.5	<0.5	1.93	<0.5	<0.5	5.26	209.36	25.88	55.13	6.28	23.30	4.61	0.94	4.01	0.64	3.87	0.76
53	105648	13.71	1.12	<0.5	<0.5	3.10	<0.5	<0.5	4.32	268.99	35.43	76.34	8.75	32.75	6.31	1.24	5.38	0.81	4.81	0.91
54	105649	11.53	0.56	<0.5	<0.5	2.02	<0.5	<0.5	4.98	220.51	26.67	56.91	6.56	24.78	4.97	1.03	4.50	0.71	4.22	0.84
55	105622	11.73	1.18	<0.5	<0.5	2.82	0.95	<0.5	4.16	NA	143.01	407.53	51.36	229.45	59.04	16.21	81.13	14.26	75.03	14.95
56	105601	18.0	2.5	<0.5	<0.5	3.2	0.8	<0.5	4.1	500.4	46.5	97.0	10.9	40.1	7.6	1.4	6.1	0.8	4.5	0.8
57	105602	21.0	2.3	<0.5	<0.5	3.4	0.8	<0.5	5.6	455.3	53.0	112.1	12.5	45.7	8.5	1.5	6.7	0.9	4.8	0.9

Table Continued..

Annexure-XIV

Sl. No.	Original Sample ID	Er	Tm	Yb	Lu	Hf	Ta	Tl	Pb	Bi	Th	U	HREEY	LREE	TREEY
1	105569	3.37	<0.5	3.07	<0.5	4.32	1.03	1.30	26.27	<0.5	16.95	2.75	81.28	204.53	285.81
2	105570	7.73	0.92	5.03	0.71	2.67	0.55	1.14	19.26	<0.5	13.18	2.77	193.66	242.58	436.24
3	105571	10.70	1.20	6.35	0.84	3.66	0.96	1.34	24.22	<0.5	17.89	2.64	271.96	347.27	619.22
4	105572	11.77	1.35	7.13	0.95	3.90	0.97	1.39	23.56	<0.5	17.81	3.16	288.06	382.13	670.19
5	105573	2.86	<0.5	2.69	<0.5	4.41	1.19	1.40	31.25	<0.5	18.81	2.81	64.99	209.44	274.42
6	105574	2.88	<0.5	2.78	<0.5	4.16	1.08	1.35	27.38	<0.5	16.06	2.37	66.08	181.31	247.39
7	105575	3.54	0.52	3.31	<0.5	4.07	1.13	1.59	23.68	<0.5	16.60	2.44	89.45	197.42	286.87
8	105567	19.28	2.32	12.30	1.70	1.52	<0.5	0.90	18.18	<0.5	14.56	4.05	476.49	570.49	1046.98
9	105568	23.12	2.66	13.47	1.86	2.12	<0.5	1.13	21.72	<0.5	15.98	3.59	568.57	659.47	1228.04
10	105576	**13.97**	**1.68**	**8.97**	**1.26**	**1.51**	**<0.5**	**1.18**	**12.43**	**<0.5**	**9.60**	**3.61**	349.99	420.70	770.69
11	105577	15.22	1.81	9.55	1.31	4.48	0.51	1.38	16.74	<0.5	26.83	4.98	369.34	492.28	861.63
12	105578	10.40	1.25	6.91	0.95	4.39	0.89	1.40	25.07	<0.5	15.82	3.17	252.66	352.95	605.61
13	105579	15.29	1.74	9.13	1.25	4.12	0.96	1.68	23.46	<0.5	16.46	3.39	383.80	471.69	855.48
14	105580	3.51	0.51	3.26	<0.5	4.11	1.04	1.77	30.55	<0.5	16.99	2.62	89.74	193.81	283.55
15	105581	10.12	1.21	6.50	0.91	4.09	0.89	1.49	21.02	<0.5	15.36	3.32	255.10	337.88	592.98
16	105582	4.54	0.63	4.10	0.59	5.31	0.91	1.38	20.42	<0.5	14.59	3.02	107.86	192.96	300.82
17	105583	2.87	<0.5	2.62	<0.5	5.35	1.26	1.54	20.96	<0.5	18.95	3.01	71.74	209.34	281.08

Sl. No.	Original Sample ID	Er	Tm	Yb	Lu	Hf	Ta	Tl	Pb	Bi	Th	U	HREEY	LREE	TREEY
18	105584	15.23	1.92	10.67	1.53	4.26	0.77	1.35	20.28	<0.5	14.79	4.33	388.64	463.32	851.96
19	105585	2.76	<0.5	2.36	<0.5	4.18	0.89	1.26	16.07	<0.5	14.61	2.51	69.64	184.49	254.13
20	105586	**2.86**	**<0.5**	**2.71**	**<0.5**	**5.32**	**0.99**	**1.31**	**20.98**	**<0.5**	**18.47**	**2.88**	72.24	201.03	273.26
21	105587	2.44	<0.5	2.25	<0.5	4.32	0.89	0.85	18.86	<0.5	14.98	2.40	60.88	165.39	226.28
22	105588	2.90	<0.5	2.65	<0.5	3.82	0.81	0.86	16.46	<0.5	12.62	2.32	74.85	165.92	240.76
23	105589	2.73	<0.5	2.50	<0.5	4.58	1.07	0.86	16.97	<0.5	13.56	2.27	68.79	171.02	239.81
24	105590	2.64	<0.5	2.34	<0.5	3.13	0.83	0.90	14.47	<0.5	11.62	2.35	70.32	159.11	229.43
25	105591	3.45	<0.5	3.02	<0.5	3.85	0.93	1.15	23.76	<0.5	13.52	2.54	89.26	154.27	243.53
26	105593	1.56	<0.5	1.62	<0.5	4.71	0.89	1.05	21.31	<0.5	16.44	2.30	37.61	161.08	198.69
27	105596	4.03	0.56	3.15	<0.5	4.16	1.00	1.15	23.40	<0.5	15.01	2.48	100.02	185.52	285.55
28	105597	2.37	<0.5	2.42	<0.5	5.13	1.28	1.08	24.62	<0.5	17.17	2.64	57.67	172.07	229.74
29	105598	3.35	<0.5	3.21	<0.5	3.29	0.89	5.91	24.57	<0.5	13.50	2.35	91.43	160.68	252.10
30	105599	**5.06**	**0.66**	**3.74**	**0.53**	**4.18**	**1.14**	**3.41**	**28.81**	**<0.5**	**16.97**	**2.75**	120.79	234.33	355.12
31	105600	2.65	<0.5	2.44	<0.5	3.33	0.87	1.59	27.10	<0.5	20.80	2.97	66.39	226.63	293.02
32	105605	17.65	2.13	11.26	1.53	4.18	0.68	1.37	19.93	<0.5	15.59	4.99	415.25	480.03	895.28

Sl. No.	Original Sample ID	Er	Tm	Yb	Lu	Hf	Ta	Tl	Pb	Bi	Th	U	HREEY	LREE	TREEY
33	105609	3.02	<0.5	2.86	<0.5	3.36	0.90	1.40	17.46	<0.5	13.76	2.51	74.05	155.99	230.04
34	105610	3.31	<0.5	3.18	<0.5	3.78	1.04	1.60	22.44	<0.5	16.48	3.32	80.11	164.78	244.89
35	105611	2.16	<0.5	2.00	<0.5	2.42	0.57	1.04	12.59	<0.5	9.60	2.48	59.71	104.31	164.02
36	105612	2.92	<0.5	2.89	<0.5	3.22	0.92	1.24	19.94	<0.5	13.01	1.96	66.87	127.14	194.00
37	105613	2.88	<0.5	2.82	<0.5	3.72	0.89	1.15	18.27	<0.5	15.53	2.44	70.41	143.43	213.84
38	105614	**2.78**	**<0.5**	**2.75**	**<0.5**	**4.24**	**0.94**	**0.94**	**20.36**	**<0.5**	**17.67**	**2.73**	65.68	170.33	236.01
39	105615	2.58	<0.5	2.49	<0.5	3.65	1.02	1.16	20.19	<0.5	15.26	2.66	63.99	148.98	212.97
40	105616	3.41	0.52	3.37	0.50	4.08	1.15	1.56	21.51	<0.5	17.20	2.83	81.46	174.76	256.22
41	105617	3.08	<0.5	2.98	<0.5	4.12	1.08	1.30	19.45	<0.5	15.55	2.54	74.35	170.33	244.69
42	105618	2.60	<0.5	2.86	<0.5	4.82	0.96	0.96	23.58	<0.5	16.63	2.42	59.51	151.64	211.14
43	105619	2.13	<0.5	2.19	<0.5	3.83	0.96	1.31	13.48	<0.5	13.35	2.25	51.37	132.28	183.65
44	105620	2.46	<0.5	2.34	<0.5	4.39	0.85	1.27	18.66	<0.5	14.92	2.31	55.08	172.90	227.98
45	105621	2.39	<0.5	2.25	<0.5	3.95	0.71	1.03	14.61	<0.5	13.25	2.04	56.34	130.85	187.19
46	105622	2.10	<0.5	2.07	<0.5	3.55	0.91	1.01	17.21	<0.5	13.15	2.17	51.14	134.60	185.74

Sl. No.	Original Sample ID	Er	Tm	Yb	Lu	Hf	Ta	Tl	Pb	Bi	Th	U	HREEY	LREE	TREEY
47	105623	2.30	<0.5	2.34	<0.5	3.71	0.92	0.85	18.29	<0.5	14.35	2.05	52.87	139.11	191.98
48	105624	**2.33**	**<0.5**	**2.36**	**<0.5**	**3.60**	**0.80**	**1.07**	**13.15**	**<0.5**	**11.67**	**2.23**	53.31	119.42	172.74
49	105625	2.53	<0.5	2.37	<0.5	3.11	0.76	1.27	14.20	<0.5	10.50	1.93	58.71	119.36	178.08
50	105629	2.36	<0.5	2.39	<0.5	5.89	1.63	0.80	22.65	<0.5	23.94	3.40	55.86	237.10	292.96
51	105645	2.66	<0.5	2.55	<0.5	3.85	0.59	1.16	17.97	<0.5	13.00	2.30	59.63	132.33	191.96
52	105646	2.22	<0.5	2.15	<0.5	3.54	0.65	1.05	12.76	<0.5	10.46	1.77	49.51	115.21	164.72
53	105648	2.55	<0.5	2.51	<0.5	4.67	0.86	0.87	14.06	<0.5	13.98	2.27	60.03	159.57	219.60
54	105649	2.41	<0.5	2.47	<0.5	3.51	0.69	1.06	12.57	<0.5	10.94	2.00	55.40	119.90	175.30
55	105622	36.50	4.20	21.54	2.83	4.29	0.91	0.53	NA	<0.5	12.50	5.53	831.43	890.39	1721.82
56	105601	2.2	<0.5	2.0	<0.5	3.2	1.0	1.5	26.7	<0.5	20.4	3.0	**53.4**	**202.1**	**255.5**
57	105602	2.3	<0.5	2.2	<0.5	3.9	1.2	1.4	26.8	<0.5	23.7	3.3	**58.6**	**231.8**	**290.5**

Annexure-XV: XRD Analysis of BR AND BH

Sl No.	Sample No.	Latitude	Longitude	Sample Type	Sample Description	Formation	Major	Good amount	Considerable amount	Small amount	Trace amount	Trace Likely
1	108954	23.22823	69.5039978	BR	Medium grained, light reddish (white pink) coloured rock having an interlocking texture.	Bhuj Formation	Quartz	–	Kaolinite	Mica (mainly muscovite type)	Hematite, Rutile	Dolomite
2	108952	23.22823	69.5039978	BR	Massive highly perforated body which is approximately 80 cm thick,brick red in colour and consists of lots of feldspar(Nafeldspar/Albite suspected from colour) embedded in a iron rich groundmass	Bhuj Formation	Quartz	–	–	Kaolinite	Hematite, Rutile, Goethite	–
3	107576	23.19947	69.511235	BR	Brownish mauve coloured, planar cross stratified, coarse grained metasomatized sandstone with scattered pebbles along the stratification and evidence of iron impregnation.	Bhuj Formation	Quartz	–	Kaolinite		Mica, Goethite, Hematite	Rutile, Ilmenite
4	105626 (New ID: 107510)	23.160818	69.723285	BR	Very coarse grained sandstone with angular, subangular to subrounded framework grains of quartz, iron concentrated grains?, unknown black minerals (dull lustre) embedded in fine grained matrix/cement.The cement seems to be ferruginous which has currently formed lemonitic (yellow ockar in colour).	Bhuj - Katrol contact	Quartz	–	–	Calcite, Dolomite, Kaolinite	Mica	Goethite, Rutile
5	105567 (New ID: 107451)	23.1507	69.58	BR	Very fine grained, ferruginous clayey suspected tuffite sample with high TREEY (1047 ppm), P2O5 (8.5%) and moderate Fe2O3 (7%) content. The Tuffite layer is laterally extensive along the dip direction showing pinch and swell geometry. The layer thickness varies from 2 -6cm and can be traced for 148.41m.	Katrol Formation	Fluorapatite	–	–	Kaolinite, Goethite, Quartz	Mica	Dolomite, Rutile
6	105599 (New ID: 107483)	23.188777	69.5994567	BR	5 cm thick, tuffite layer, associated with grey shale and ferruginous layers. The unit is a shale dominated heterolithic unit with poorly developed target layers and low TREEY (250 ppm), P2O5 (0.45%), and high Fe2O3 (12%) content.	Katrol Formation	–	Kaolinite	Quartz, Geoethite	–	Mica	Rutile
7	108975	23.204067	69.542105	Pit/ Trench Sample	Sandstone with occassional ferruginization	Bhuj Formation	Quartz	–	–	Kaolinite	Hematite, Goethite	K feldspar
8	109037	23.196337	69.5318583	BR	Metasomatized sandstone, with very fine grained black minerals showing black streak.	Bhuj Formation	Quartz	–	–	Hematite	Kaolinite	K feldspar
9	109056	23.225561	69.549791	BR	Highly ferruginous metasomatized sandstone	Bhuj Formation	Quartz	–	Kaolinite	K feldspar	Mica	Goethite, Pyroxene
10	109027	23.197845	69.528269	BR	Ferruginous sandstone	Bhuj Formation	Quartz	–	–	Kaolinite, K feldspar	Mica	–
11	109031	23.208694	69.525424	BR	Medium to coarse grained metasomatized sandstone	Bhuj Formation	Quartz	–	–	Kaolinite, Hematite	Goethite,Mica	–

Sl No.	Sample No.	Latitude	Longitude	Sample Type	Sample Description	Formation	Major	Good amount	Considerable amount	Small amount	Trace amount	Trace Likely
12	109032	23.195197	69.532809	BR	Medium to coarse grained metasomatized sandstone	Bhuj Formation	Quartz	–	–	Hematite, Goethite		K feldspar
13	109029	23.198847	69.530368	BR	Ferruginous Sandstone at fault contact	Bhuj Formation	Quartz	–	–	–	Hematite, Goethite	Kaolinite, Calcite
14	109019A	23.195695	69.5339611	BR	Metasomatized sandstone, composed of very coarse grained angular to sub angular quartz, authigenic growth of feldspar and clasts of quartz aggregates embedded in a magnetite rich (black streak) matrix.	Bhuj Formation	Quartz	–	–	–	Kaolinite	K feldspar
15	109019B	23.195695	69.5339611	BR	Medium to coarse grained ferruginous sandstone. Ferrugination has taken place along the stratification.	Bhuj Formation	Quartz	–	–	–	Kaolinite	–
16	109044	23.197492	69.529793	BR	Black coloured, medium to coarse grained metasomatized sandstone. Growth of authigenic feldspar, buish green staining and silicification are common feature of the sandstone. Pyrite??	Bhuj Formation	Quartz	–	–	Kaolinite, Hematite, Goethite	–	K feldspar
17	109042	23.197492	69.529793	BR	Black coloured, medium to coarse grained metasomatized sandstone. Growth of authigenic feldspar, buish green staining and silicification are common feature of the sandstone. Pyrite??	Bhuj Formation	Quartz	–	–	Hematite	Goethite	Kaolinite, K feldspar, Calcite
18	113041	23.22258	69.59413	Borehole	Altered sandstone	Bhuj formation	Kaolinite	–	–	Hematite	Anatase Geothite	
19	113060	23.204	69.6284	Borehole	Purplish sandstone	Bhuj formation	Kaolinite	Quartz	–	–	Hematite mica	Goethite

Annexure-XVI: XRF Analysis of Channel Samples

Sr. No.	Sample ID	Location No.	Latitude	Longitude	Host Lithology	Stratigraphy
1	105562	GSPL-Bhuj-110/03/24	23.150	69.585	Exposures of Sandstone, grey Shale, Red Ferrugeneous layer, Continuation of the same succession in stratigraphic up direction. However the thickness of the sandstones increases and occurrence of mm thin gypsum layers are also observed.	Katrol Formation
2	105563					
3	105564					
4	105565					
5	105566					
6	105544	GSPL-Bhuj-112/03/24	23.152	69.578	Occurrence of mm to 1cm thin grey to blackish-grey shale layers, amalgamated at places and often alternate with mm thin silt/fine sand layers and reddish brown colored 2-7cm thick hard ironstone/ferrugenous clay layers with pinch and swell geometry. This succession is observed to be interupted by brownish mauve colored, either wave ripple laminated or plane parallel laminated medium to fine grained sandstones. Occurrence of mm thin gypsum layers at the top part of the succession are also observed. Suspected tuffite layer collection	Katrol Formation
7	105545					
8	105546					
9	105547					
10	105548					
11	105549					
12	105550					
13	105551					
14	105552					
15	105553					
16	105554					
17	105555					
18	105556					
19	105557					
20	105558					
21	105559					
22	105560					
23	105561					
24	105541	GSPL-Bhuj-91/01/24	23.151	69.580	Heterolithic unit consist of shale (grey, white with goethitic and ferruginous pstches, interupted by well developed suspected tuffite layers alternating with 10-20cm thick sandstone layers and/or thinly laminated shale-siltstone unit, channel sampling done	Katrol Formation
25	105542					
26	105543					
27	107485	GSPL-Bhuj-117/06/24	23.145	69.549	The succession includes black shale intermittently separated by nodular layers, which are poorly developed or less pronounced. The unit overlies 33 cm thick, pinkish, coarse to medium-grained sandstone, consisting of quartz, feldspar, and mica, is observed in a tabular form with no internal structures. Nearby, a dolerite dyke indicates contact metamorphism, likely converting the black shale into slate.	Bhuj Formation
28	107486					

Table Continued..

Annexure-XVI

Sr. No.	Sample ID	Sample Description	Al_2O_3	BaO	CaO	Cr_2O_3	Fe_2O_3	K_2O	MgO	MnO	Na_2O	P_2O_5	TiO_2	SiO_2	LOI	S
1	105562	75cm channel sample	19.63	0.04	1.03	0.03	8.49	2.14	0.95	0.07	1.05	0.09	1.17	55.11	9.86	0.22
2	105563	50cm channel sample	21.49	0.05	1.16	0.03	8.30	2.34	0.71	0.05	0.68	0.08	1.16	56.20	6.49	0.46
3	105564		20.01	0.04	0.76	0.03	12.69	2.20	0.81	0.07	0.52	0.11	1.11	51.23	9.48	0.22
4	105565		19.49	0.05	0.78	0.03	10.68	2.20	0.91	0.05	0.85	0.10	1.15	53.16	9.72	0.24
5	105566		21.86	0.05	2.80	0.03	6.61	2.26	0.77	0.04	0.65	0.07	1.20	52.75	10.58	0.08
6	105544	50cm channel sample	20.67	0.03	0.84	0.03	18.12	1.68	0.85	0.08	0.58	0.16	1.05	42.73	11.96	0.55
7	105545		22.29	0.03	1.11	0.03	7.92	2.01	1.29	0.05	0.80	0.10	1.18	49.73	12.18	0.48
8	105546		20.87	0.04	1.43	0.03	8.14	2.06	1.52	0.05	0.69	0.11	1.13	50.83	11.87	0.31
9	105547		23.30	0.03	0.36	0.03	5.90	2.13	0.66	0.03	0.51	0.10	1.29	54.12	10.64	0.28
10	105548		20.31	0.04	1.75	0.03	8.42	2.02	1.67	0.06	0.70	0.11	1.11	50.68	12.06	0.29
11	105549		15.58	0.04	3.68	0.02	13.59	1.91	2.41	0.07	0.15	0.12	0.88	48.68	12.37	0.20
12	105550		22.58	0.03	0.55	0.03	8.47	2.12	0.63	0.02	0.10	0.11	1.26	52.61	10.05	0.26
13	105551	70cm channel sample	22.98	0.04	0.91	0.03	7.24	2.16	0.71	0.03	0.10	0.10	1.24	53.13	10.27	0.22
14	105552	60cm channel sample	22.03	0.04	0.97	0.03	8.24	2.15	0.71	0.05	0.09	0.12	1.23	52.82	10.11	0.27
15	105553	50cm channel sample	23.58	0.04	0.68	0.03	5.00	2.28	0.51	0.03	0.11	0.07	1.33	54.97	9.97	0.27
16	105554		21.98	0.04	1.31	0.03	9.12	2.14	0.65	0.05	0.09	0.11	1.24	51.21	10.50	0.46
17	105555		22.81	0.04	1.01	0.03	8.10	2.19	0.70	0.04	0.16	0.11	1.23	51.69	10.67	0.40
18	105556		24.04	0.03	0.53	0.03	9.09	2.10	0.57	0.04	0.26	0.12	1.23	50.73	10.31	0.25

Sr. No.	Sample ID	Sample Description	Al_2O_3	BaO	CaO	Cr_2O_3	Fe_2O_3	K_2O	MgO	MnO	Na_2O	P_2O_5	TiO_2	SiO_2	LOI	S
19	105557	50cm channel sample	17.32	0.05	3.39	0.03	5.86	2.36	1.72	0.04	0.15	0.08	0.93	56.41	10.48	0.36
20	105558		23.47	0.04	0.70	0.03	8.06	2.17	0.55	0.04	0.11	0.11	1.24	51.99	10.25	0.31
21	105559		21.97	0.04	0.69	0.03	7.39	2.26	0.65	0.04	0.17	0.10	1.22	53.92	9.61	0.26
22	105560		22.06	0.05	1.07	0.03	6.79	2.22	0.71	0.04	0.11	0.10	1.21	54.07	9.75	0.28
23	105561	80cm channel sample	20.84	0.04	2.57	0.03	7.63	2.05	0.55	0.03	0.10	0.11	1.14	51.49	9.82	1.08
24	105541	20cm channel sample	24.22	0.03	0.13	0.02	2.01	2.24	0.75	0.02	0.37	0.08	1.25	61.13	7.54	<0.05
25	105542	15.1cm channel sample	23.25	0.03	0.16	0.02	2.81	2.35	0.76	0.03	0.41	0.08	1.19	60.86	7.78	<0.05
26	105543	35cm channel sample	23.58	0.04	0.17	0.02	2.68	2.28	0.72	0.03	0.36	0.10	1.20	60.99	7.60	<0.05
27	107485	During sieving, a large (~2.5cm) elongated crystal characterized by white, transparent nature has been found. Diamond pen is giving only a faint line, does not scratch properly.	15.35	0.04	0.97	0.02	8.38	2.29	0.52	0.04	0.28	0.10	1.00	61.21	8.99	0.09
28	107486	Slope wash samples containing broken fragments of bed rock	17.48	0.03	1.23	0.02	5.57	2.14	0.61	0.06	0.37	0.10	1.16	61.82	8.73	<0.05

Annexure-XVII: ICPMS of Channel Samples

Sr. No.	SampleID	Location No.	Latitude	Longitude	Li	Be	Sc	V
1	105562	GSPL-Bhuj-110/03/24	23.14998333	69.58492833	11.93	2.67	20.69	163.91
2	105563	GSPL-Bhuj-110/03/24	23.14998333	69.58492833	11.22	2.31	20.85	146.86
3	105564	GSPL-Bhuj-110/03/24	23.14998333	69.58492833	11.77	2.72	22.77	173.28
4	105565	GSPL-Bhuj-110/03/24	23.14998333	69.58492833	12.49	2.76	22.25	181.04
5	105566	GSPL-Bhuj-110/03/24	23.14998333	69.58492833	12.64	2.43	20.22	168.26
6	105544	GSPL-Bhuj-112/03/24	23.15184833	69.57784167	12.36	2.69	27.72	205.99
7	105545	GSPL-Bhuj-112/03/24	23.15184833	69.57784167	13.77	2.39	21.36	166.61
8	105546	GSPL-Bhuj-112/03/24	23.15184833	69.57784167	12.74	2.47	22.89	157.58
9	105547	GSPL-Bhuj-112/03/24	23.15184833	69.57784167	14.54	2.29	22.21	173.40
10	105548	GSPL-Bhuj-112/03/24	23.15184833	69.57784167	12.49	2.82	22.53	165.93
11	105549	GSPL-Bhuj-112/03/24	23.15184833	69.57784167	8.28	1.80	20.69	145.09
12	105550	GSPL-Bhuj-112/03/24	23.15184833	69.57784167	13.72	2.89	21.89	182.82
13	105551	GSPL-Bhuj-112/03/24	23.15184833	69.57784167	14.89	2.83	23.13	189.52
14	105552	GSPL-Bhuj-112/03/24	23.15184833	69.57784167	13.26	2.62	21.68	178.10
15	105553	GSPL-Bhuj-112/03/24	23.15184833	69.57784167	3.59	0.68	4.41	37.58
16	105554	GSPL-Bhuj-112/03/24	23.15184833	69.57784167	13.71	3.02	23.17	188.84
17	105555	GSPL-Bhuj-112/03/24	23.15184833	69.57784167	14.09	2.39	21.13	173.88
18	105556	GSPL-Bhuj-112/03/24	23.15184833	69.57784167	13.95	2.50	20.69	181.92
19	105557	GSPL-Bhuj-112/03/24	23.15184833	69.57784167	9.08	1.79	18.00	121.64
20	105558	GSPL-Bhuj-112/03/24	23.15184833	69.57784167	14.11	2.70	22.20	178.68
21	105559	GSPL-Bhuj-112/03/24	23.15184833	69.57784167	13.39	2.51	21.38	162.97
22	105560	GSPL-Bhuj-112/03/24	23.15184833	69.57784167	13.03	2.41	21.39	157.93
23	105561	GSPL-Bhuj-112/03/24	23.15184833	69.57784167	12.11	2.35	19.54	168.26
24	105541	GSPL-Bhuj-91/01/24	23.150682	69.580033	116.94	2.67	14.51	124.85
25	105542	GSPL-Bhuj-91/01/24	23.150682	69.580033	124.16	2.42	13.51	120.64
26	105543	GSPL-Bhuj-91/01/24	23.150682	69.580033	108.39	2.25	12.39	118.54
27	107485	GSPL-Bhuj-117/06/24	23.145335	69.54906167	26.87	2.01	15.22	128.41
28	107486	GSPL-Bhuj-117/06/24	23.145335	69.54906167	33.86	2.65	17.09	145.93

Table Continued..

Annexure-XVII

Sr. No.	SampleID	Ga	Ge	Se	Rb	Sr	Y	Zr	Nb	Mo	Cd	In_	Sn	Sb	Te
1	105562	30.16	<0.5	1.88	106.53	179.34	28.66	196.15	19.42	1.14	<0.5	<0.5	4.34	5.02	<0.5
2	105563	28.75	<0.5	1.37	105.71	184.37	31.31	195.82	19.47	1.25	<0.5	<0.5	3.85	4.99	<0.5
3	105564	29.44	<0.5	1.37	107.22	182.92	32.56	187.23	19.18	1.37	<0.5	<0.5	4.06	3.40	<0.5
4	105565	31.40	<0.5	1.98	110.81	207.31	30.73	186.49	20.07	1.29	<0.5	<0.5	4.15	4.65	<0.5
5	105566	31.79	<0.5	1.63	115.26	274.80	28.76	190.64	21.48	1.23	<0.5	<0.5	4.34	4.64	<0.5
6	105544	29.55	<0.5	2.35	99.52	261.64	41.75	155.18	19.42	1.38	<0.5	<0.5	3.74	2.41	<0.5
7	105545	33.04	<0.5	1.74	114.13	301.19	30.44	161.73	21.80	1.35	<0.5	<0.5	4.51	4.26	<0.5
8	105546	30.88	<0.5	2.06	106.07	360.96	35.10	177.38	21.57	1.30	<0.5	<0.5	4.03	4.59	<0.5
9	105547	34.94	<0.5	2.01	115.12	282.40	35.60	186.45	23.47	1.43	<0.5	<0.5	4.49	3.78	<0.5
10	105548	31.07	<0.5	2.33	104.82	332.52	35.74	169.38	20.21	1.38	<0.5	<0.5	5.30	2.51	<0.5
11	105549	22.13	<0.5	1.82	84.42	449.00	34.28	148.48	15.14	1.23	<0.5	<0.5	2.80	2.96	<0.5
12	105550	33.78	<0.5	1.83	116.82	257.47	34.06	175.01	22.23	1.41	<0.5	<0.5	4.55	1.69	<0.5
13	105551	35.95	<0.5	2.10	123.48	337.02	33.99	195.03	23.59	1.46	<0.5	<0.5	4.68	3.91	<0.5
14	105552	32.96	<0.5	2.02	113.67	354.97	32.41	189.96	22.65	1.38	<0.5	<0.5	4.34	3.50	<0.5
15	105553	8.51	<0.5	<0.5	29.79	57.40	6.81	47.36	5.56	<0.5	<0.5	<0.5	0.95	<0.5	<0.5
16	105554	34.43	<0.5	1.61	116.05	311.95	33.72	177.20	22.25	1.48	<0.5	<0.5	4.53	3.62	<0.5
17	105555	33.48	<0.5	2.17	114.06	302.36	31.08	171.23	22.20	1.43	<0.5	<0.5	4.36	3.30	<0.5
18	105556	34.01	<0.5	2.20	113.83	350.57	32.88	178.54	21.59	1.37	<0.5	<0.5	4.44	2.79	<0.5
19	105557	24.35	<0.5	1.27	99.36	378.74	30.01	149.67	16.17	0.90	<0.5	<0.5	3.11	2.61	<0.5
20	105558	34.21	<0.5	1.68	119.00	336.09	33.91	183.65	23.49	1.28	<0.5	<0.5	4.57	3.33	<0.5
21	105559	32.96	<0.5	1.61	119.23	355.90	33.08	190.27	22.65	1.22	<0.5	<0.5	4.24	3.03	<0.5
22	105560	32.02	<0.5	2.06	113.42	410.41	33.62	185.41	22.40	1.25	<0.5	<0.5	4.27	1.83	<0.5
23	105561	30.28	<0.5	1.65	104.46	393.28	33.73	193.62	20.74	1.31	<0.5	<0.5	3.99	1.47	<0.5
24	105541	32.50	<0.5	1.43	109.42	144.26	17.54	197.11	21.20	0.89	<0.5	<0.5	4.19	<0.5	<0.5
25	105542	30.48	<0.5	1.33	115.38	151.74	18.99	188.82	22.00	1.01	<0.5	<0.5	4.05	<0.5	<0.5
26	105543	28.45	<0.5	1.89	101.76	163.79	24.54	185.27	20.35	0.98	<0.5	<0.5	3.65	<0.5	<0.5
27	107485	22.52	<0.5	2.06	93.44	704.42	20.34	116.55	17.99	2.52	<0.5	<0.5	3.18	0.84	<0.5
28	107486	25.74	<0.5	1.85	106.11	312.55	22.40	139.19	21.04	2.25	<0.5	<0.5	3.45	0.82	<0.5

Table Continued..

Annexure-XVII

Sr. No.	SampleID	Cs	La	Ce	Pr	Nd	Sm	Eu	Gd	Tb	Dy	Ho	Er
1	105562	6.55	55.91	113.37	13.06	47.00	9.01	1.86	7.64	1.13	5.94	1.17	3.27
2	105563	5.98	56.09	114.26	13.07	47.92	9.28	1.88	8.14	1.22	6.39	1.26	3.51
3	105564	6.51	55.32	111.42	12.86	47.08	8.94	1.89	8.16	1.24	6.58	1.29	3.61
4	105565	7.07	55.82	113.40	12.92	47.49	9.11	1.95	8.05	1.21	6.27	1.25	3.48
5	105566	7.51	57.71	117.21	13.27	48.36	9.13	1.92	7.73	1.16	6.10	1.16	3.28
6	105544	7.08	57.89	119.99	13.65	50.74	9.83	2.20	9.29	1.45	7.86	1.57	4.32
7	105545	7.89	56.37	113.51	13.02	47.12	8.70	1.94	7.69	1.14	6.14	1.22	3.45
8	105546	6.66	57.91	115.99	13.17	48.22	9.33	2.02	8.25	1.25	6.89	1.37	3.83
9	105547	7.90	63.00	128.29	14.68	53.78	10.28	2.21	9.31	1.38	7.38	1.42	3.92
10	105548	6.64	55.88	113.84	13.00	47.88	9.22	1.98	8.41	1.28	7.10	1.39	3.80
11	105549	4.21	43.60	88.46	10.40	38.47	7.78	1.67	7.21	1.13	6.19	1.24	3.43
12	105550	8.18	58.52	119.06	13.75	50.17	9.71	2.13	8.62	1.29	6.89	1.35	3.73
13	105551	8.41	63.18	128.42	14.70	53.48	10.15	2.14	8.87	1.33	7.01	1.35	3.79
14	105552	7.30	60.80	121.79	13.85	50.41	9.45	2.00	8.21	1.24	6.57	1.27	3.57
15	105553	2.03	15.10	31.02	3.49	12.52	2.32	<0.5	1.96	<0.5	1.46	<0.5	0.78
16	105554	7.55	58.87	119.71	13.66	49.30	9.33	2.04	8.30	1.26	6.69	1.32	3.70
17	105555	7.41	58.71	117.80	13.39	48.60	9.09	1.96	7.95	1.19	6.19	1.22	3.41
18	105556	7.62	61.25	123.18	14.15	51.38	9.77	2.10	8.47	1.26	6.66	1.29	3.58
19	105557	4.52	44.28	89.09	10.27	38.10	7.36	1.61	6.86	1.06	5.68	1.12	3.12
20	105558	7.75	61.74	124.57	14.32	52.02	9.87	2.14	8.71	1.30	6.74	1.34	3.61
21	105559	7.88	60.19	122.88	13.93	50.30	9.63	2.04	8.50	1.25	6.62	1.28	3.59
22	105560	7.16	59.75	119.79	13.59	49.47	9.52	2.01	8.35	1.26	6.78	1.32	3.66
23	105561	6.66	58.56	117.88	13.26	48.31	9.25	1.88	8.25	1.23	6.58	1.29	3.62
24	105541	7.48	50.51	97.98	11.03	38.28	6.74	1.26	5.02	0.70	3.74	0.71	2.15
25	105542	7.39	50.65	96.80	10.98	38.04	6.76	1.31	5.24	0.74	3.95	0.78	2.33
26	105543	6.21	54.02	109.15	12.35	44.32	8.32	1.69	6.86	0.97	5.08	0.96	2.77
27	107485	4.11	46.46	97.02	10.92	40.11	7.61	1.40	6.14	0.84	4.49	0.81	2.18
28	107486	5.57	53.05	112.07	12.53	45.70	8.50	1.48	6.68	0.91	4.76	0.87	2.28

Table Continued..

Annexure-XVII

Sr. No.	SampleID	Tm	Yb	Lu	Hf	Ta	Tl	Bi	Th	U	HREEY	LREE	TREEY
1	105562	<0.5	3.12	<0.5	5.84	1.32	0.58	<0.5	21.43	3.31	73.48	238.35	311.83
2	105563	0.51	3.33	<0.5	5.57	1.32	0.72	<0.5	21.33	3.34	78.40	240.62	319.02
3	105564	0.53	3.43	0.50	5.27	1.31	0.81	0.52	20.67	3.52	82.57	235.62	318.19
4	105565	0.51	3.39	<0.5	5.27	1.36	0.85	0.62	20.80	3.46	79.07	238.74	317.81
5	105566	<0.5	3.08	<0.5	5.38	1.54	0.86	0.67	21.73	3.61	73.40	245.68	319.08
6	105544	0.62	3.91	0.59	4.26	1.29	1.03	0.70	19.23	3.46	101.29	252.10	353.39
7	105545	0.51	3.27	<0.5	4.45	1.43	0.83	0.64	20.23	3.17	77.15	238.72	315.87
8	105546	0.54	3.63	0.54	4.89	1.58	0.80	0.63	20.17	3.30	86.31	244.61	330.92
9	105547	0.59	3.73	0.54	5.27	1.55	0.83	0.62	22.47	3.56	88.28	270.03	358.31
10	105548	0.55	3.57	0.52	4.58	1.33	0.80	0.53	20.17	3.11	86.87	239.81	326.68
11	105549	<0.5	3.14	<0.5	3.83	0.92	0.76	<0.5	15.51	2.73	78.98	188.70	267.68
12	105550	0.53	3.51	0.52	4.84	1.47	0.84	1.42	21.28	3.36	84.53	251.21	335.73
13	105551	0.55	3.57	0.52	5.37	1.63	0.89	1.54	23.10	3.59	86.26	269.93	356.19
14	105552	0.52	3.40	0.50	5.27	1.60	0.88	0.92	21.59	3.38	81.38	256.30	337.68
15	105553	<0.5	0.77	<0.5	1.24	<0.5	<0.5	<0.5	5.67	0.84	16.20	64.45	80.65
16	105554	0.54	3.49	0.52	4.91	1.53	0.98	0.68	20.91	3.27	84.75	250.87	335.62
17	105555	<0.5	3.17	<0.5	4.78	1.50	0.96	0.59	21.00	3.26	77.31	247.59	324.90
18	105556	0.51	3.37	0.51	4.96	1.45	0.97	0.61	21.57	3.49	81.33	259.72	341.05
19	105557	<0.5	2.82	<0.5	4.08	1.00	1.04	<0.5	16.23	2.59	70.27	189.10	259.37
20	105558	0.53	3.39	0.51	5.07	1.65	1.35	0.66	21.65	3.44	84.38	262.52	346.90
21	105559	0.53	3.34	0.51	5.40	1.54	1.35	0.55	21.81	3.39	82.12	256.92	339.04
22	105560	0.55	3.39	0.51	5.21	1.60	1.33	0.55	21.16	3.25	82.83	252.13	334.96
23	105561	0.52	3.33	<0.5	5.29	1.42	1.27	<0.5	21.48	3.30	79.98	247.27	327.25
24	105541	<0.5	2.22	<0.5	6.14	1.39	0.59	<0.5	25.15	3.23	47.85	204.53	252.38
25	105542	<0.5	2.39	<0.5	5.88	1.44	0.90	0.56	24.06	3.08	49.24	203.23	252.47
26	105543	<0.5	2.63	<0.5	5.65	1.30	0.98	0.56	23.03	3.03	57.90	228.15	286.04
27	107485	<0.5	2.01	<0.5	3.18	1.03	1.48	<0.5	20.36	2.98	53.43	202.12	255.55
28	107486	<0.5	2.15	<0.5	3.91	1.20	1.38	<0.5	23.68	3.27	58.63	231.85	290.47

Annexure-XVIII SEM-EDAX analysis results of BR

Sl No.	Original Sample ID	Stratigraphy	Type of Sample	Thin Section Description	Name of the rock according to petrography	Description of the sample according to SEM-EDAX	Remarks on chemical analysis	TREEY (ppm)
1	105572	Katrol Formation	Calcareous claystone/ironstone	Layered rock with fragmented clasts of quartz (wedge, needle, triangular shaped), feldspar (K-feldspar, Plg, microcline) embedded in a carbonate cement. Presence of few opaque minerals	Tuffaceous??	Angular clasts of quartz, K-feldspar, muscovite, ilmenite, monazite, and volcanic zircon grains, all set in a felty-textured fluorapatite matrix. Notably, zeolite grains are also present, with fluorapatite actively replacing zeolite in some areas and magnetite replacing fluorapatite in others.	105ppm Li, 3.11% P2O5, 6.32% Fe2O3	670.19
2	107581	Katrol Formation	Sandstone	Very crudely laminated rock, where lamination is defined by clasts rich layers and glass(??)/cement rich layers. Framework grains are of fragmented (wedge, needle, triangular shaped with sharp boundaries and embayment at places) quartz, feldspar (K-feldspar, microcline, albite??), muscovite, glass shards?? embedded in a iron rich, glassy ?? and carbonate cement. Presence of flow structure within the micas (ignimbrite??)	Tuff/Tuffaceous??	Clasts of quartz, K-feldspar, monazite, detrital zircon, zeolite, muscovite, rutile are set in a vement of magnetite (in places magnetites are globular) No apatite		157.9

Sl No.	Original Sample ID	Stratigraphy	Type of Sample	Thin Section Description	Name of the rock according to petrography	Description of the sample according to SEM-EDAX	Remarks on chemical analysis	TREEY (ppm)
3	105604	Chari Formation (At contact of Katrol and Chari formation)	Altered reddish colored sandstone	Fragmented, wedge shaped quartz with embayment like boundary, embedded in a glassy?? Matrix. A carbonate vein is observed.	Volcaniclastics??	Clsts of Quartz (angular, wedge shaped, long curved clasts are also present), feldspar and monazite are set in the magnetite rich cemet. Carbonate veins, carbonate clasts and rhomb shaped calcites are also present in cement	Very low SiO2, high CaO and Fe2O3 along with anomalous Sr, Nd	800.6
4	107566	Bhuj Formation	Sandstone	Fragmented (few euhedral grains and few transported grains) of quartz, microcline, k-feldspar, plagioclase, polycrystalline quartz, deformed quartzite are embedded in iron leached glassy ?? Cement. Unknown mineral (lapilli??, pleochroic in shades of green, brownish yellow interference colour, very rounded, twinkling extinction) is also encountered	Pyroclastic rock??	Clasts of quartz (volcanic quartz?), K-feldspar, monazite, zircon, illmenite, , are set in a magnetite rich cement. Brecciation of quartz clast by magnetite cement have been observed.		86.2
5	107578	Bhuj Formation	Fumaroles sample	Sub-angular to sub-rounded framework grains of quartz, feldspar (1-2%, k-feldspar), embedded in a carbonate groundmass with ferrugenous stain. Suspected epidote in matrix. Insitu brecciation of the framework grains and embayment within the framework grains are observed	Quartz Arenite (Volcaniclastics??)	Clasts of quartz, K-feldspar clasts (both volcanic, sub-rounded) are set in a magnetite rich cement. In places calcite cement is noted to be replaced by magnetite. In-situ brecciation of the clasts have also been observed.		118.7

Sl No.	Original Sample ID	Stratigraphy	Type of Sample	Thin Section Description	Name of the rock according to petrography	Description of the sample according to SEM-EDAX	Remarks on chemical analysis	TREEY (ppm)
6	105567	Katrol Formation	Calcareous claystone/ironstone	Very fine grained crudely laminated rock. Layering is defined by phenocrysts (framework) rich layers and groundmass rich layers. The framework grains (<20-250µm) are of elongated, flaky, needle and wedge shaped grains of quartz, feldspar, apatite, embedded in a glassy groundmass. Suspected presence of apatite	Tuff/ Rhyolite (??)	Clast of quartz, K-feldspar, zeolite, monazite, barite, mica, Fe-Ca-Mg oxide(?) are found to be set in a cement of apatite rich cement which is again getting placed by globular mass magnetite/heamatite	97ppm Li, 8.47% P2O5, 6.94% Fe2O3	1046.98
7	107579	Katrol Formation	Sandstone			Clasts of quartz, feldspar, suspected REE minerals (?) are set in a magnetite rich cement		190.7
8	105599	Katrol Formation	Calcareous claystone/ironstone	Lminated rock with layering defined by glassy and crystalline layer. Same as 105567 with less amount of needle and wedge shaped grains and more of glassy material	Tuff??	Clasts of elongated quartz (with corroded boundary), feldspar, suspected ignimbrite are set in a magnetite rich cement with globular appearance.	102ppm Li, 0.45% P2O5, 11.87% Fe2O3	355.12
9	107575					Quartz; Zircon; Ilmenite; Feldspar; Mica, Monazite,		
10	107576					Quartz; Ilmenite; Feldspar; Mica, Monazite, Magnetite		

Annexure-XIX.a: EPMA Analysis Results

Sl No.	Sample No	Sample Type	Sample Description	Stratigraphy	Minerals
1	105626	BR	Very coarse grained sandstone with angular, subangular to subrounded framework grains of quartz, iron concentrated grains?, unknown black minerals (dull lustre) embedded in fine grained matrix/cement.The cement seems to be ferruginous which has currently formed lemonitic (yellow ockar in colour).	Bhuj Formation	Rutile
	105626				Carbonate in matrix/cement
	105626				Magnetite (Fe-hydroxide?)
	105626				Carbonate in cement
	105626				Dolomite in cement
	105626				Fe-Ca hydroxide in cement
	105626				K-feldspar
	105626				K-feldspar
	105626				Magnetite in matrix/cement
	105626				Clay mineral (halloisite)
	105626				Rutile
	105626				Rutile
	105626				Clay/glass?
	105626				Siderite
2	105572	BR	2-7cm thick, laterally pinching out tuffite layer, associated with gypsum layers. The TREEY content of the layer is 670 ppm.	Katrol Formation	Apatite
	105572				Apatite
	105572				Apatite
	105572				Monazite
	105572				Biotite
	105572				K-feldspar
	105572				Clay
	105572				Fluro-Apatite/Zircon
	105572				Clay
	105572				Quartz
	105572				Apatite
	105572				Apatite
	105572				Fe-Ca hydroxide in cement
	105572				Muscovite
2	105659	BR	Very fine grained melanocratic rock with occurrence of few golden colored mica, teal greenish colored vug filled mineral	Intrusion in Bhuj Formation	CPx
	105659				Fe-Ti Oxide
	105659				Olivine
	105659				Glass (Felsic)
	105659				Altered feldspar
	105659				CPx (Ti-Augite)
	105659				CPx (Ti-Augite)
	105659				Hayalo-Siderite
	105659				Na rich orthoclase (Albite)
3	105662	BR	Coarse to medium grained ferruginous metasomatized sandstone with scattered pebbles along the stratification. Strong iron impregnation is evident. Possible trend of Fe fluid movement is 130 -310.	Bhuj Formation	Quartz
	105662				Magnetite
	105662				Rutile
	105662				Fe-Ti hydroxide
	105662				Fe-Ti hydroxide

Sl No.	Sample No	Sample Type	Sample Description	Stratigraphy	Minerals
	105662				Fe-Ti hydroxide
	105662				Fe-Oxide
	105662				Fe-Si Oxide
4	105677	BR	10 cm thick, mm thin parallal laminated medium to fine grained sandstone, sandwitched between two thick (60cm and 28cm)sandstone beds	Katrol Formation	Quartz
	105677				K-Feldspar
	105677				Rutile
	105677				Fe-hydroxide
	105677				Fe-hydroxide
	105677				Rutile
	105677				Clay (Kaolinite)
	105677				Chlorite
	105677				Clay (Kaolinite)

Table Continued..

Annexure-XIX.a

Sl No.	Sample No	Na2O	SiO2	Al2O3	MgO	P2O5	K2O	CaO	TiO2
1	105626	0.06	0.61	1.1	0.09	0.54	0.08	0.81	83.76
	105626	0.03	0.11	0.03	2.5	0.57	0	57.79	0
	105626	0.01	6.41	2.49	1.84	0.33	0.04	2.12	0.01
	105626	0.06	0.1	0	1.4	0.48	0	59.52	0.01
	105626	0.06	0.02	0.01	20.81	0.4	0	37.29	0.01
	105626	0.1	5.41	2.08	1.58	0.31	0.09	8.4	0
	105626	0.76	64.43	17.76	0	0.01	15.68	0.05	0
	105626	0.76	64.21	18.18	0	0	15.43	0	0
	105626	0.14	3.34	0.37	0.99	0.06	0.06	1.09	0
	105626	0.14	42.52	35.96	0.08	0.05	0.08	0.21	0
	105626	0.13	1.09	1.92	0.17	0.67	0.04	1.48	81.47
	105626	0.05	0.25	0.31	0.49	0	0.01	0.34	65.77
	105626	0.1	37.2	28.69	0.33	0.08	0.1	0.43	0.92
	105626	0.01	1.69	0	0	0.01	0.01	0.03	0.01
2	105572	0.3	2.54	1.28	0.16	34.39	0.23	52.65	0.33
	105572	0.19	3.41	1.74	0.2	33.37	0.22	53.66	0.38
	105572	0.36	2.39	1.3	0.13	34.49	0.22	52.5	0.26
	105572	0.61	64.86	18.24	0	0	15.81	0.14	0.01
	105572	0.16	34.89	17.81	8.91	0.01	9.28	0.26	3.25
	105572	0.75	64.51	18.86	0.04	0.35	13.67	0.17	0

Sl No.	Sample No	Na2O	SiO2	Al2O3	MgO	P2O5	K2O	CaO	TiO2
	105572	0	45.86	37.22	0.04	0.04	0.09	0.21	0.14
	105572	0.37	3.39	1.68	0.15	34	0.38	51.36	0.19
	105572	0.09	46.31	37.85	0.04	0.05	0.05	0.34	0
	105572	0.03	100.61	0.13	0	0	0	0.16	0
	105572	0.29	3.36	1.95	0.26	33.16	0.43	51.27	0.21
	105572	0.26	2.71	1.41	0.17	34.16	0.28	51.78	0.1
	105572	0.07	5.29	1.4	3.08	0.64	0.18	0.64	0.03
	105572	1.32	46.11	34.86	0.7	0.08	6.95	0.15	0.4
2	105659	0.39	47.29	4.03	12.48	0.24	0.04	21.98	2.7
	105659	0	0.08	4.43	3.26	0	0	0.1	19.87
	105659	0.04	36.31	0.04	31.35	0.01	0	0.54	0.06
	105659	2.57	55.7	21.59	0.16	1.4	5.64	0.14	0.54
	105659	9.37	57.21	28.2	0.08	0.08	1.08	0.18	0.12
	105659	0.78	46.45	5.61	11.11	0.41	0.7	22.08	3.36
	105659	0.6	46.34	6.05	11.26	0.41	0.05	22.13	3.25
	105659	0.06	36.6	0	34.33	0	0	0.36	0
	105659	6.2	58.33	22.27	0	0.23	3.83	2.44	0.39
3	105662	0.02	101.02	0	0	0	0	0.03	0.01
	105662	0.07	0.86	0.45	0.05	0.04	0	0.05	0.26
	105662	0.05	0.11	0	0.03	0	0.02	0.08	99.91
	105662	0.04	1.43	1.35	0.09	0.16	0	0.2	66
	105662	0.11	0.69	1.11	0.07	0.43	0	0.23	73.96
	105662	0.01	5.26	4.18	0.06	0.03	0.03	0.09	0
	105662	0	1.03	0.04	0.11	0	0.04	0.06	0
	105662	0.09	0.61	0.05	0.05	0	0.02	0.08	0
4	105677	0	100.88	0	0.01	0	0.01	0	0
	105677	0.37	65.02	18.19	0	0.07	16.97	0	0.04
	105677	0	0.05	0.01	0	0	0.03	0.03	100.49
	105677	0.24	3.38	1.34	1.34	0.15	0.07	0.31	0.35
	105677	0.3	4.17	1.11	0.63	0.15	0.09	0.62	0.34
	105677	0.01	0.81	0.2	0.17	0.03	0.02	0.21	100.13
	105677	0.17	45.38	37.77	0.11	0	0.1	0.07	0
	105677	0.23	26.05	17.31	1.23	0.15	4.43	0.22	0.31
	105677	0.07	43.63	36.37	0.18	0.05	0.1	0.14	1.91

Table Continued..

Annexure-XIX.a

Sl No.	Sample No	FeO	Cr2O3	NiO	MnO	ZnO	BaO	Total	Na
1	105626	6.19	0.14	0	0.11	0	1	94.48	875
	105626	0.31	0	0	0.06	0.07	0	61.47	789
	105626	65.27	0.04	0	0.12	0.04	0	78.71	1196
	105626	0.14	0	0.04	0.06	0.05	0	61.87	580
	105626	0.2	0.01	0	0.05	0.25	0	59.12	564
	105626	56.21	0.02	0	0	0.1	0	74.31	927
	105626	0.13	0.02	0	0	0.1	0.03	98.97	616
	105626	0.04	0	0.09	0.01	0	0.35	99.08	566
	105626	70.34	0	0	0.02	0.12	0	76.52	1297
	105626	0.47	0.02	0	0	0	0	79.53	547
	105626	2.32	0.44	0	0.01	0.03	0.84	90.62	877
	105626	22.63	0.15	0	0.38	0	0.5	90.88	916
	105626	5.18	0.05	0	0	0	0	73.07	510
	105626	61.32	0.04	0	0.13	0	0	63.27	1326
2	105572	0.52	0.08	0	0	0	0	92.47	814
	105572	0.75	0	0.04	0	0.37	0	94.34	829
	105572	0.36	0	0	0.01	0	0	92.04	783
	105572	0.14	0	0	0.03	0.11	0.35	100.3	610
	105572	20.42	0.09	0	0.27	0.37	0.09	95.8	845
	105572	0.1	0	0	0.13	0	0	98.58	693
	105572	0.87	0	0	0.03	0	0	84.5	661
	105572	0.49	0	0	0.15	0	0.01	92.16	957
	105572	0.55	0.05	0.01	0.1	0.16	0	85.6	515
	105572	0.11	0.04	0	0	0	0	101.09	646
	105572	0.51	0	0	0	0	0.02	91.46	858
	105572	1.87	0.07	0	0	0.06	0	92.89	832
	105572	64.52	0.08	0	0	0	0.04	75.97	1029
	105572	1.57	0	0	0.09	0.07	0.32	92.62	638
2	105659	8.87	0.07	0	0.17	0	0.08	98.33	778
	105659	68.26	0.06	0.03	0.64	0.45	0.12	97.32	NA
	105659	30.03	0	0	0.74	0.15	0	99.27	759

Sl No.	Sample No	FeO	Cr2O3	NiO	MnO	ZnO	BaO	Total	Na
	105659	2.6	0	0	0.16	0	0	90.5	831
	105659	0.67	0	0	0	0	0	97	931
	105659	9.22	0	0.02	0.05	0.06	0	99.85	876
	105659	8.88	0	0	0.13	0	0	99.09	738
	105659	26.91	0	0	0.45	0.01	0	98.72	868
	105659	0.43	0	0	0.13	0.17	3.3	97.73	818
3	105662	0.05	0.1	NA	0.01	NA	NA	NA	NA
	105662	86.85	0	NA	0.01	NA	NA	NA	NA
	105662	0.31	0.54	NA	0	NA	NA	NA	NA
	105662	24.09	0.21	NA	0.32	NA	NA	NA	NA
	105662	17.88	0.21	NA	0.08	NA	NA	NA	NA
	105662	78.51	0	NA	0.07	NA	NA	NA	NA
	105662	77.82	0.05	NA	0.97	NA	NA	NA	NA
	105662	88.85	0.07	NA	0.07	NA	NA	NA	NA
4	105677	0.11	0.06	NA	0	NA	NA	NA	NA
	105677	0.04	0.05	NA	0	NA	NA	NA	NA
	105677	0.25	0	NA	0	NA	NA	NA	NA
	105677	73.51	0	NA	0.22	NA	NA	NA	NA
	105677	73.22	0.68	NA	0.18	NA	NA	NA	NA
	105677	0.38	0	NA	0.01	NA	NA	NA	NA
	105677	0.74	0.05	NA	0	NA	NA	NA	NA
	105677	36.34	0.18	NA	0.08	NA	NA	NA	NA
	105677	0.37	0	NA	0.02	NA	NA	NA	NA

Table Continued..

Annexure-XIX.a

Sl No.	Sample No	Si	Al	Mg	P	K	Ca	Ti	Fe	Cr	Ni	Mn	Zn	Ba
1	105626	493	570	618	559	311	341	767	1421	1028	NA	2316	NA	2496
	105626	422	445	572	526	NA	822	414	1213	NA	NA	1950	5574	1393
	105626	594	581	601	618	381	394	419	2348	777	NA	1439	6315	NA
	105626	387	NA	466	503	293	810	386	1049	NA	1269	1951	5359	NA
	105626	455	476	504	524	NA	698	388	980	831	1304	2083	4999	NA
	105626	547	577	764	642	352	422	NA	2276	849	NA	NA	6187	NA
	105626	740	529	NA	551	581	398	NA	1147	845	NA	NA	5348	1346
	105626	675	542	NA	NA	625	NA	NA	1107	NA	1215	1681	NA	1450
	105626	598	583	657	620	375	378	417	2528	NA	NA	2042	6999	NA
	105626	633	609	426	549	339	301	NA	NA	903	NA	NA	NA	NA
	105626	532	543	600	575	357	323	766	1152	964	NA	2703	5375	2434
	105626	551	545	670	NA	343	352	720	1828	977	NA	2630	NA	2379
	105626	621	590	380	516	312	334	407	1264	807	NA	NA	NA	NA
	105626	642	NA	NA	712	364	370	419	2465	710	NA	1835	NA	NA
2	105572	464	442	548	674	363	816	412	1152	902	NA	NA	NA	NA
	105572	464	403	533	672	413	832	481	1158	1117	1483	NA	4231	NA
	105572	475	426	536	702	371	805	453	1196	NA	NA	2359	NA	1500
	105572	695	597	NA	NA	659	387	439	1012	NA	NA	1965	5485	1517
	105572	740	580	535	646	586	419	460	1751	958	NA	1738	5597	1547
	105572	751	604	456	557	562	419		1125	NA	NA	1221	NA	NA
	105572	675	649	467	640	290	324	401	1153	NA	1285	2120	NA	NA
	105572	475	503	624	660	339	838	447	1233	NA	NA	1958	NA	1451
	105572	722	657	453	636	368	314	389	1032	821	1260	1448	5812	NA
	105572	838	435	NA	NA	NA	348	NA	988	866	NA	NA	NA	NA
	105572	494	445	589	653	376	829	452	1323	NA	NA	NA	NA	1439
	105572	512	455	580	648	363	834	463	1241	955	NA	2363	6734	NA
	105572	597	566	732	641	373	381	435	2612	794	NA	NA	NA	1309
	105572	668	627	392	583	545	390	461	1189	918	NA	1803	5498	1247
2	105659	675	501	600	696	360	601	464	1572	822	NA	2460	NA	1410
	105659	627	627	790	NA	NA	391	547	2603	1003	1662	2693	6727	1884
	105659	695	478	674	692	379	395	466	1985	NA	NA	2487	6127	NA
	105659	750	580	422	876	439	391	424	1090	NA	NA	1275	NA	NA
	105659	705	590	487	576	411	331	414	968	NA	NA	NA	NA	NA
	105659	671	513	532	674	415	604	460	1555	NA	1451	2329	6455	NA

Sl No.	Sample No	Si	Al	Mg	P	K	Ca	Ti	Fe	Cr	Ni	Mn	Zn	Ba
	105659	689	571	586	605	373	619	472	1395	NA	NA	2331	NA	NA
	105659	736	NA	660	704	394	351	466	1814	NA	NA	2504	6399	NA
	105659	752	599	NA	753	454	416	587	1108	NA	NA	1883	5721	1631
3	105662	NA	NA	NA	NA	NA	NA	NA	NA	NA	NA	NA	NA	NA
	105662	NA	NA	NA	NA	NA	NA	NA	NA	NA	NA	NA	NA	NA
	105662	NA	NA	NA	NA	NA	NA	NA	NA	NA	NA	NA	NA	NA
	105662	NA	NA	NA	NA	NA	NA	NA	NA	NA	NA	NA	NA	NA
	105662	NA	NA	NA	NA	NA	NA	NA	NA	NA	NA	NA	NA	NA
	105662	NA	NA	NA	NA	NA	NA	NA	NA	NA	NA	NA	NA	NA
	105662	NA	NA	NA	NA	NA	NA	NA	NA	NA	NA	NA	NA	NA
	105662	NA	NA	NA	NA	NA	NA	NA	NA	NA	NA	NA	NA	NA
4	105677	NA	NA	NA	NA	NA	NA	NA	NA	NA	NA	NA	NA	NA
	105677	NA	NA	NA	NA	NA	NA	NA	NA	NA	NA	NA	NA	NA
	105677	NA	NA	NA	NA	NA	NA	NA	NA	NA	NA	NA	NA	NA
	105677	NA	NA	NA	NA	NA	NA	NA	NA	NA	NA	NA	NA	NA
	105677	NA	NA	NA	NA	NA	NA	NA	NA	NA	NA	NA	NA	NA
	105677	NA	NA	NA	NA	NA	NA	NA	NA	NA	NA	NA	NA	NA
	105677	NA	NA	NA	NA	NA	NA	NA	NA	NA	NA	NA	NA	NA
	105677	NA	NA	NA	NA	NA	NA	NA	NA	NA	NA	NA	NA	NA
	105677	NA	NA	NA	NA	NA	NA	NA	NA	NA	NA	NA	NA	NA

Annexure-XIX.b: EPMA Analysis Results

Sl No.	Sample No	Litho type	Sample Description	Stratigrapguy	Mineral
1	107566	Bhuj Sandstone	Coarse grained sst with few sst showing dark red encrustation on top (looks like baking/jhama effect).	Katrol Formation	Zircon
	107566	Bhuj Sandstone			Zircon
2	105572	Tuffite from Katrol Formation	2-7cm thick, laterally pinching out tuffite layer, associated with gypsum layers. The TREEY content of the layer is 670 ppm	Katrol Formation and Chari Formation	Zircon
	105572	Tuffite from Katrol Formation			Zircon
3	105604	Sandstone, Chari Formation	Cherry red in color,comprises of quartz, mica, glass shrads ??, and few black unknown mineral with metallic lustre. Suspected volcanic alteration.		Zircon
4	105567	Tuffite from Katrol Formation	10 cm thick, mm thin parallal laminated medium to fine grained sandstone, sandwitched between two thick (60cm and 28cm)sandstone beds	Katrol Formation	Zircon

Sl No.	Sample No	Litho type	Sample Description	Stratigrapguy	Mineral
5	107566	Bhuj Sandstone	Coarse grained sst with few sst showing dark red encrustation on top (looks like baking/jhama effect).	Bhuj Formation	Monazite
	107566	Bhuj Sandstone			Monazite
6	105626	Sandstone At contact of Katrol and Bhuj formations	Very coarse grained sandstone with angular, subangular to subrounded framework grains of quartz, iron concentrated grains?, unknown black minerals (dull lustre) embedded in fine grained matrix/cement.The cement seems to be ferruginous which has currently formed lemonitic (yellow ockar in colour).	Katrol Formation	Monazite
	105626	Sandstone At contact of Katrol and Bhuj formations			Monazite
	105626	Sandstone At contact of Katrol and Bhuj formations			Zircon
	105626	Sandstone At contact of Katrol and Bhuj formations			Monazite
7	105572	Tuffite from Katrol Formation	2-7cm thick, laterally pinching out tuffite layer, associated with gypsum layers. The TREEY content of the layer is 670 ppm.	Katrol Formation	Apatite
	105572	Tuffite from Katrol Formation			Apatite
8	105604	Sandstone, Chari Formation	Cherry red in color,comprises of quartz, mica, glass shrads , and few black unknown mineral with metallic lustre. Suspected volcanic	Chari Formation	Xenotime

Table Continued..

Annexure-XIX.b

Sl No.	Sample No	Mineral	Data Points	Na2O	SiO2	P2O5	Al2O3	MgO	CaO	TiO2	FeO	MnO	UO2	PbO	ThO2	ZrO2	Nb2O5	Ce2O3	La2O3	Sm2O3
1	107566	Zircon	1 / 1 .	0	31.14	0.56	0	0.02	0.01	0	0.39	0	0.06	0	0.01	65.41	0	0.02	0	0
	107566	Zircon	2 / 1 .	0	31.1	0.49	0	0	0	0	0.49	0	0.05	0	0	64.84	0	0	0.01	0
2	105572	Zircon	9 / 1 .	0	31.75	1.91	0.1	0.04	2.42	0	0	0.04	0.02	0	0.02	64.79	0	0	0	0
	105572	Zircon	10 / 1 .	0	30.85	0.58	0.02	0	0.19	0	0.05	0	0.03	0	0.03	65.17	0	0	0.02	0
3	105604	Zircon	13 / 1 .	0	31.83	0.67	0.11	0.06	0.21	0	0.87	0.02	0.02	0	0.04	66.49	0	0.02	0	0
4	105567	Zircon	15 / 1 .	0	31.25	0.56	0	0.01	0.09	0.02	0.36	0	0.06	0	0.02	65.48	0	0.02	0	0
5	107566	Monazite	3 / 1 .	0	0.46	29.99	0	0	0.97	0	0.34	0	0.51	0.26	5.05	0	0	27.24	13.75	1.66
	107566	Monazite	4 / 1 .	0	0.27	29.22	0.04	0	0.69	0	0.5	0	0.38	0.16	3.18	0	0	28.47	14.16	1.74

Sl No.	Sample No	Mineral	Data Points	Na2O	SiO2	P2O5	Al2O3	MgO	CaO	TiO2	FeO	MnO	UO2	PbO	ThO2	ZrO2	Nb2O5	Ce2O3	La2O3	Sm2O3
6	105626	Monazite	6 / 1 .	0	1.09	27.94	0.01	0	0.3	0.01	0	0	0.05	0.12	4.97	0	0	30.71	15.57	1.2
	105626	Monazite	7 / 1 .	0.03	1.22	28.56	0.03	0	1.83	0	0	0	1.01	0.57	10.5	0	0	25.3	11.19	1.75
	105626	Zircon	5 / 1 .	0	31.26	0.46	0	0	0.01	0	0	0.02	0.01	0	0	66.05	0	0	0	0.01
	105626	Monazite	8 / 1 .	0	0.73	28.73	0	0	0.9	0	0	0	0.47	0.3	6.08	0	0	27.26	14.4	2.02
7	105572	Apatite	11 / 1 .	0.24	2.41	33.65	1.41	0.19	53.02	0.09	0.71	0.03	0.06	0	0.01	0	0	0.02	0.06	0
	105572	Apatite	12 / 1 .	0.28	0.38	31.73	0.23	0.07	54.46	0	0.15	0	0	0	0	0	0	0	0	0
8	105604	Xenotime	14 / 1 .	0.02	0.42	33.93	0	0	0.53	0	0.51	0	0.35	0.43	0.48	0	0	0	0	0.75

Table Continued..

Annexure-XIX.b

Sl No.	Sample No	Mineral	Nd2O3	Eu2O3	Gd2O3	Er2O3	Yb2O3	Ho2O3	Y2O3	Ta2O5	Dy2O3	Pr2O3	Total	Na	Si
1	107566	Zircon	0	0	0	0.01	0.11	0	0.18	0	0	0	97.91	NA	425
	107566	Zircon	0	0	0	0	0.02	0.01	0	0	0	0	97.01	NA	432
2	105572	Zircon	0.01	0.01	0	0.05	0.03	0.06	0.12	0	0	0	101.38	NA	412
	105572	Zircon	0	0	0.01	0.1	0.13	0.07	0.37	0	0.01	0	97.63	NA	389
3	105604	Zircon	0.01	0.01	0	0.08	0.18	0	0.5	0	0	0	101.12	NA	413
4	105567	Zircon	0.01	0	0	0.04	0	0.06	0.11	0	0	0	98.1	NA	417
5	107566	Monazite	11.24	0.85	1.24	0.03	0.01	0.12	1.78	0	0.62	3.35	99.49	NA	439
	107566	Monazite	11.52	0.83	1.31	0.02	0.07	0.02	1.58	0	0.53	3.57	98.24	NA	467
6	105626	Monazite	10.63	0.81	0.62	0	0	0.06	1.04	0	0.39	3.58	99.11	NA	463
	105626	Monazite	10.28	0.62	1.44	0.07	0	0	1.74	0	0.69	3.12	99.94	893	455
	105626	Zircon	0.04	0	0	0	0.02	0.04	0.06	0	0.01	0	97.97	NA	412
	105626	Monazite	11.83	0.91	1.35	0.01	0.09	0	0.87	0	0.43	3.56	99.93	NA	469
7	105572	Apatite	0.01	0.03	0	0.02	0.05	0	0.12	0	0	0	92.13	604	267
	105572	Apatite	0.01	0.06	0	0.06	0	0.1	0.05	0	0.02	0.01	87.63	624	249
8	105604	Xenotime	0.23	0.5	4.81	3.49	2.47	0.93	41.71	0	5.85	0	97.4	578	408

Table Continued..

Annexure-XIX.b

Sl No.	Sample No	P	Al	Mg	Ca	Ti	Fe	Mn	U	Pb	Th	Zr
	107566	377	NA	337	195	476	934	NA	563	NA	475	748
1	107566	377	NA	337	198	NA	1056	NA	574	NA	483	786
	105572	390	290	334	216	NA	NA	948	565	NA	469	840
2	105572	388	252		201	475	951	NA	574	NA	471	768
3	105604	389	288	350	195	NA	962	973	572	NA	485	800
4	105567	381	NA	308	202	461	1004	921	564		471	815
	107566	501	NA	NA	211	NA	1652	NA	592	673	485	NA
5	107566	520	427	NA	211	NA	1722	NA	590	689	492	NA
	105626	526	452	NA	210	525	NA	NA	594	672	478	NA
	105626	517	421	NA	216	NA	NA	NA	625	677	495	NA
	105626	391	NA	327	195	NA	NA	914	567	NA		760
6	105626	533	NA	NA	208	NA	NA	NA	606	672	495	NA
	105572	354	264	368	381	432	833	830	443	461	328	NA
7	105572	333	272	364	375		957	817	NA	NA	322	NA
8	105604	582	NA	NA	209	NA	1104		615	683	501	NA

Table Continued..

Annexure-XIX.b

SI No.	Sample No	Ce	La	Sm	Nd	Pr	Eu	Gd	Er	Yb	Ho	Y	Dy
	107566	660	NA	NA	NA	NA	NA	NA	1274	1330	NA	276	NA
1	107566	NA	697	NA	NA	NA	NA	NA	NA	1379	2823	NA	NA
	105572	NA	670	NA	615	NA	814	NA	1179	1357	2714	284	NA
2	105572	NA	658	NA	NA	NA	NA	712	1238	1351	2802	280	508
3	105604	654	NA	NA	610	NA	820	717	1256	1298	NA	292	NA
4	105567	654	NA	NA	612	NA	NA	NA	1218		2701	273	NA
	107566	773	756	785	730	1241	925	858	1452	1570	3069	384	595
5	107566	766	789	787	733	1225	901	854	1441	1516	3195	385	611
	105626	779	767	745	730	1228	901	836	NA	NA	3117	377	574
	105626	783	788	761	736	1226	924	854	1433	NA	NA	377	574
	105626	NA	NA	650	599	NA	NA	NA	NA	1349	2779	272	252
6	105626	775	774	745	725	1227	917	836	1368	1532		377	573
	105572	571	566	NA	491	NA	678	NA	984	1112	NA	222	NA
7	105572	559	NA	NA	461	898	612	NA	956		2342	221	365
8	105604	NA	686	752	630	NA	858	1025	1354	1492	3191	608	578

Annexure-XX: XRF Analysis of Bedrock Samples

Sl No.	Sample ID	Location No.	Latitude	Longitude	Sample Type	Sample Description	Stratigraphy
1	105567	GSPL-Bhuj-113/03/24	23.16009	69.72324	BR	Very coarse grained sandstone with angular, subangular to subrounded framework grains of quartz, iron concentrated grains?, unknown black minerals (dull lustre) embedded in fine grained matrix/cement.The cement seems to be ferrugenous which has currently formed lemonitic (yellow ockar in colour).	Bhuj Formation
2	107476	GSPL-Bhuj-120/06/24	23.18878	69.59946	BR	10-12cm thick beds of medium to fine grained (mostly quartzose, some unidentified black mineral), highly altered sandstone. Iron leaching at places are observed	Katrol Formation
3	107510	GSPL-Bhuj-136/06/24	23.16082	69.72329	BR	Very coarse grained sandstone with angular, subangular to subrounded framework grains of quartz, iron concentrated grains?, unknown black minerals (dull lustre) embedded in fine grained matrix/cement.The cement seems to be ferrugenous which has currently formed lemonitic (yellow ockar in colour).	Bhuj Formation
4	107516	GSPL-Bhuj-137/06/24	23.16410	69.72726	BR	Very light weight grain supported yellow ochre colored coarse grained sst with butchers knife erosion The grains are elongated, angular to sub angular (quartz/apatite??),mica,rounded black colored unknown mineral, are the main constituents.,no matrix observed.	Katrol Formation
5	107518	GSPL-Bhuj-137/06/24	23.16410	69.72726	BR	5cm thick, farely continuous layer of sandstone altered to red bed	Katrol Formation
6	107541	GSPL-Bhuj-155/06/24	23.22405	69.49290	BR	Coarse grained sst with encrustation at the top (looks like baking/Metasomatized effect)	Bhuj Formation
7	107542	GSPL-Bhuj-157/06/24	23.23155	69.48264	BR	Brownish mauve colour, medium - coarse grain sst with little encrustation on top. (Similar sample as 105658)	Bhuj Formation
8	107543	GSPL-Bhuj-158/06/24	23.25237	69.74468	BR	Very fine grained melanocratic rock with occurrence of few golden colored mica, teal greenish colored vug filled mineral	Bhuj Formation
9	107546	GSPL-Bhuj-159/06/24	23.19947	69.51124	BR	Coarse to medium grained sandstone with evidence of baking effect possibly by fumaroles ??.	Bhuj Formation
10	107551	GSPL-Bhuj-163/06/24	23.22384	69.52438	BR	yellowish white coloured coarse to medium grained sst having quartz and white transparent elongated crystals,clast supported almost no matrix. Suspected phosphorite	Bhuj Formation
11	107561	GSPL-Bhuj-167/06/24	23.18286	69.63318	BR	10 cm thick, mm thin parallal laminated medium to fine grained sandstone, sandwitched between two thick (60cm and 28cm)sandstone beds	Katrol Formation
12	107555	GSPL-Bhuj-165/06/24	23.22110	69.58984	BR	Coarse grained sst, composed of quartz embeded in a lemonitic,iron cement. The sandstone is altered, with thin flow like structures at the top of the beds (evidence of baking??? fumaroles?)	Bhuj Formation
13	107565	GSPL-Bhuj-155/06/24	23.22420	69.49274	BR	Coarse grained sst with encrustation at the top (looks like baking/Metasomatized effect). Sst comprises of quartz, feldspar with a light colour matrix. Sample from reported alkali plug area, collected to identify catchment source's mineralogy of high REE value SS sample.	Bhuj Formation
14	107566	GSPL-Bhuj-156/06/24	23.22796	69.50385	BR	Coarse grained sst with few sst showing dark red encrustation on top (looks like baking/Metasomatized effect).	Bhuj Formation
15	107567	GSPL-Bhuj-156/06/24	23.22796	69.50385	BR	5cm thin, white colour, medium - coarse grain sst interbedded between the buff coloured sst.	Bhuj Formation
16	107568	GSPL-Bhuj-157/06/24	23.22907	69.47871	BR	Brownish mauve coloured, medium - coarse grain sst with little encrustation on top (looks like baking/Metasomatized effect). (Upto 6 m depth from the surface of rhe mound)	Bhuj Formation
17	107569	GSPL-Bhuj-157/06/24	23.22907	69.47871	BR	Brownish mauve/ reddish coloured, medium - coarse grain sst with dark encrustation visible on top (looks like baking/Metasomatized effect). (Layer below buff colored sandstone: 6m depth from the surface of the mound)	Bhuj Formation

Table Continued..

Annexure-XX

Sl No.	Sample ID	Al_2O_3	BaO	CaO	Cr_2O_3	Fe_2O_3	K_2O	MgO	MnO	Na_2O	P_2O_5	TiO_2	SiO_2	LOI	S
1	105567	5.98	0.03	7.40	0.02	13.42	0.94	2.80	0.07	0.09	0.45	0.71	55.35	11.45	0.06
2	107476	8.44	<0.01	2.77	<0.01	37.60	0.94	1.92	0.16	0.27	0.51	0.63	34.21	12.36	0.07
3	107510	1.62	<0.01	14.25	<0.01	5.00	0.33	0.90	0.04	<0.01	0.25	0.11	64.15	13.19	<0.05
4	107516	4.46	<0.01	0.12	<0.01	1.26	1.31	0.10	<0.01	0.04	0.12	0.19	89.78	1.90	<0.05
5	107518	3.45	<0.01	21.96	<0.01	17.79	0.66	0.60	0.06	0.05	1.82	0.19	34.07	19.20	<0.05
6	107541	7.46	0.04	0.15	<0.01	24.57	1.99	0.14	1.40	0.10	0.13	1.39	57.92	4.20	<0.05
7	107542	1.40	<0.01	9.65	<0.01	5.02	0.53	3.65	0.10	0.01	0.09	0.65	64.37	14.21	<0.05
8	107543	11.77	0.06	7.96	<0.01	17.38	1.54	7.49	0.25	4.41	0.86	3.89	42.42	1.39	0.07
9	107546	1.52	<0.01	0.08	<0.01	52.27	0.18	0.02	0.13	0.01	0.11	0.29	40.91	4.15	0.17
10	107551	2.07	<0.01	0.04	<0.01	0.80	0.20	<0.01	<0.01	<0.01	0.08	0.90	94.10	1.08	<0.05
11	107561	5.24	0.11	0.35	<0.01	12.31	1.25	0.31	0.03	0.11	0.34	0.85	74.81	3.67	<0.05
12	107555	1.89	<0.01	5.76	<0.01	14.76	0.03	0.13	0.01	<0.01	0.17	0.40	69.67	6.95	<0.05
13	107565	2.89	0.11	0.41	<0.01	10.42	1.30	0.15	1.79	0.04	0.32	0.36	79.49	2.17	<0.05
14	107566	1.90	<0.01	0.06	<0.01	19.80	0.28	0.04	0.08	0.03	0.08	<0.01	75.37	1.86	0.09
15	107567	1.55	<0.01	0.05	<0.01	9.91	0.22	0.03	<0.01	0.02	0.08	<0.01	85.86	1.86	0.05
16	107568	2.45	<0.01	14.26	<0.01	6.20	0.75	0.41	0.15	0.02	0.14	1.10	61.20	13.17	<0.05
17	107569	4.74	<0.01	0.13	<0.01	16.22	0.70	0.04	0.06	0.08	0.11	1.04	70.40	4.75	0.56

Sl No.	Sample ID	Location No.	Latitude	Longitude	Sample Type	Sample Description	Stratigraphy
18	107570	GSPL-Bhuj-157/06/24	23.22907	69.47871	BR	Less compact, light weight, yellowish - orange coloured, medium - coarse grain sst consisting of quartz & feldspar. (bottom layer, depth: 9m from the surface of mound)	Bhuj Formation
19	107571	GSPL-Bhuj-157/06/24	23.22907	69.47871	BR	Composite samples of different types of sst (Buff colour sst with encrustation, yellowish orange sst, red coloured sst and very fragile planar cross laminated white coloured sst.)	Bhuj Formation
20	107572	GSPL-Bhuj-136/06/24	23.16082	69.72329	BR	Very coarse grained sandstone with angular, subangular to subrounded framework grains of quartz, iron concentrated grains?, unknown black minerals (dull lustre) embedded in fine grained matrix/cement. The cement seems to be ferrugenous which has currently formed lemonitic (yellow ochar in colour).	At contact of Katrol Formation and Bhuj formations
21	107573	GSPL-Bhuj-136/06/24	23.16118	69.72477	BR	7.5cm thin, reddish colored very hard ironstone bed comprising of few remanant clasts of quartz grains.	At contact of Katrol Formation and Bhuj formations
22	107574	GSPL-Bhuj-136/06/24	23.16118	69.72477	BR	Ironstone bed comprising of few remanant clasts of quartz grains.	At contact of Katrol Formation and Bhuj formations
23	107575	GSPL-Bhuj-168/08/24	23.14830	69.72647	BR	Encrustated layer on top of buff colored sandstone	At contact of Katrol Formation and Bhuj formations
24	107576	GSPL-Bhuj-159/06/24	23.19947	69.51124	BR	20cm thick, brownish mauve coloured, planar cross stratified, coarse grain sst with scattered pebbles along the stratification.	Bhuj Formation
25	107577	GSPL-Bhuj-159/06/24	23.19947	69.51124	BR	Coarse grain sst with dark black coloured encrustation on top	Bhuj Formation
26	107578	GSPL-Bhuj-159/06/24	23.19947	69.51124	BR	Sandstone with evidence of baking	Bhuj Formation
27	107579	GSPL-Bhuj-91/01/24	23.15070	69.58000	BR	Wave ripple laminated sst just above the red bed (Tuffite layer)	Katrol Formation, succession up from 112/03/24
28	107580	GSPL-Bhuj-91/01/24	23.15070	69.58000	BR	2.5cm, thin sandstone layer at 0.106m below the red bed (Tuffite layer)	Katrol Formation, succession up from 112/03/24
29	107581	GSPL-Bhuj-91/01/24	23.15070	69.58000	BR	10cm thick, sandstone layer at 0.37m below the red bed (Tuffite layer)	Katrol Formation, succession up from 112/03/24
30	107582	GSPL-Bhuj-91/01/24	23.15070	69.58000	BR	50cm thick, sandstone layer at 0.72m below the red bed (Tuffite layer)	Katrol Formation, succession up from 112/03/24
31	107511	GSPL-Bhuj-136/06/24	23.16082	69.72329	BR	2-7cm thick completely altered red beds with breccia appearance. Cherry red coloured clasts embedded in a very fine buff colour groundmass giving the breccia appearance. Apart from few mica grains no other grains are identifiable	At contact of Katrol Formation and Bhuj formations
32	107535	GSPL-Bhuj-147/06/24	23.17128	69.69256	BR	Ferrugenous shale consisting of mica, ferrous micro nodules and associated with gypsum	Katrol Formation
33	107536	GSPL-Bhuj-150/06/24	23.16548	69.73697	BR	Sandstone showing butchers knife weathering pattern (possible contain phosphorite?)	Bhuj-Katrol contact
34	107559	GSPL-Bhuj-147/06/24	23.18286	69.63318	BR	4cm thick, white crystalline medium to fine grained sandstone (Phosphorite???)	Katrol Formation (stratigraphic up)
35	107562	GSPL-Bhuj-150/06/24	23.18286	69.63318	BR	5cm thick, white crystalline medium to fine grained sandstone (Phosphorite???)	Katrol Formation (stratigraphic mid)
36	107563	GSPL-Bhuj-162/06/24	23.18286	69.63318	BR	5cm thick, white crystalline medium to fine grained sandstone (Phosphorite???), burrow observed	Katrol Formation (stratigraphic down)

Table Continued..

Annexure-XX

Sl No.	Sample ID	Al_2O_3	BaO	CaO	Cr_2O_3	Fe_2O_3	K_2O	MgO	MnO	Na_2O	P_2O_5	TiO_2	SiO_2	LOI	S
18	107570	3.17	<0.01	0.13	<0.01	6.02	0.23	0.14	<0.01	<0.01	0.10	0.38	86.48	2.74	0.07
19	107571	5.69	<0.01	0.10	<0.01	26.03	1.28	0.06	<0.01	0.05	0.28	0.88	60.97	3.83	0.08
20	107572	1.18	<0.01	13.48	<0.01	2.37	0.22	0.81	0.06	<0.01	0.11	<0.01	69.82	11.89	<0.05
21	107573	3.22	<0.01	16.08	<0.01	37.46	0.37	2.47	0.05	0.14	1.25	0.19	22.01	16.63	0.05
22	107574	4.01	<0.01	9.84	<0.01	43.31	0.57	1.27	0.10	0.04	0.39	0.33	25.43	14.35	0.05
23	107575	10.06	<0.01	0.21	<0.01	22.68	1.23	0.12	0.21	0.05	0.18	0.92	57.70	6.22	<0.05
24	107576	7.73	<0.01	0.07	<0.01	2.48	0.36	0.06	<0.01	<0.01	0.09	0.67	85.06	2.90	<0.05
25	107577	1.60	<0.01	0.09	<0.01	22.05	0.24	<0.01	0.40	<0.01	0.09	0.04	73.58	1.51	0.06
26	107578	2.29	<0.01	0.11	<0.01	56.50	0.21	<0.01	0.28	<0.01	0.11	0.37	35.08	4.68	0.18
27	107579	12.62	0.02	3.46	<0.01	13.19	2.16	2.57	0.09	0.34	0.15	0.81	53.97	10.17	0.06
28	107580	13.57	0.02	2.54	<0.01	6.93	2.22	1.92	0.04	0.29	0.13	1.05	61.95	8.74	0.07
29	107581	10.49	<0.01	7.03	<0.01	6.27	2.07	4.77	0.08	0.16	0.11	0.46	56.80	10.85	0.06
30	107582	7.54	0.01	8.72	<0.01	4.30	2.02	4.64	0.04	0.12	0.10	0.54	58.68	12.90	0.06
31	107511	3.51	<0.01	17.06	<0.01	24.32	0.46	2.41	0.06	0.12	0.84	0.17	33.00	17.92	<0.05
32	107535	14.742	0.013	4.025	0.01	6.781	1.746	0.533	0.042	0.243	0.087	0.81	55.43	11.99	2.891
33	107536	4.681	<0.01	0.04	<0.01	2.914	0.814	0.169	0.028	0.134	0.086	0.334	88.67	1.53	<0.05
34	107559	10.42	0.01	1.97	<0.01	1.87	1.11	0.41	0.03	0.28	0.07	0.79	76.86	5.56	<0.05
35	107562	13.23	0.01	0.06	0.01	2.26	1.30	0.36	0.03	0.53	0.07	0.97	75.11	5.43	<0.05
36	107563	6.43	0.03	0.07	0.01	2.25	1.20	0.19	0.03	0.20	0.09	0.88	85.63	2.36	<0.05

Sl No.	Sample ID	Location No.	Latitude	Longitude	Sample Type	Sample Description	Stratigraphy
37	105622	GSPL-Bhuj-91/01/24	23.15070	69.58000	BR	Yellowish (shale) part of 105494 (BR)	Katrol Formation
38	109059	GSPL-Bhuj-294/01/2025	23.18957	69.54486	BR	Dark purplish brown colored, medium to coarse grained ferruginous sandstone characterized by dense texture and strong iron oxide impregnation. Composed of angular to sub rounded quartz grains and possible feldspar, with abundant iron oxides (hematite/goethite) acting as matrix and cement. Patches and spots of nodular iron accumulation are visible, producing a mottled, uneven appearance commonly seen in ferruginous sandstones affected by secondary iron mineralization	Bhuj Formation
39	109006	GSPL-Bhuj-249/12/2024	23.19444	69.59791	BR	Shale dominated heterolithic layer with poorly developed Tuffite layer	Katrol Formation
40	109007	GSPL-Bhuj-249/12/2024	23.19444	69.59791	BR	Shale dominated heterolithic layer with well developed thick Tuffite bed	Katrol Formation
41	109009	GSPL-Bhuj-250/12/2024	23.19514	69.59717	BR	Shale dominated heterolithic layer with poorly developed Tuffite layer with phosphatic layer of 30cm	Katrol Formation
42	109011	GSPL-BHUJ-250/12/2024	23.19514	69.59717	BR	Shale dominated heterolithic layer with well developed Tuffite bed from the depth of 3m	Katrol Formation
43	109015	GSPL-BHUJ-252/12/2024	23.27065	69.80465	BR	China clay from mine section	Bhuj Formation
44	109016	GSPL-BHUJ-252/12/2024	23.27065	69.80465	BR	China Clay found from the depth of 100ft, Host rock: Sanstone	Bhuj Formation
45	109017	GSPL-BHUJ-253/12/2024	23.19629	69.59651	BR	Tuffite layer/Shale??	Katrol Formation
46	109018	GSPL-BHUJ-254/12/2024	23.19570	69.53396	BR	Metasomatized sandstone within Bhuj Formation, (Highly ferrugenous sandstone); fine to medium grained; sample collected above 5m from the surface (just above ferruginous sandstone)	Bhuj Formation
47	109019	GSPL-Bhuj-254/12/2024	23.19570	69.53396	BR	White-buff (interbedded) sandstone within Bhuj Formation, (with no ferruginous activity); medium to coarse grained; sample collected above 2.5m from the surface	Bhuj Formation
48	109020	GSPL-Bhuj-254/12/2024	23.19570	69.53396	BR	Ferruginous Sandstone	Bhuj Formation
49	109021	GSPL-Bhuj-255/12/2024	23.21766	69.59088	BR	Metasomatized sandstone is composed of very coarse grained angular to subangular quartz, authigenic growth of lots of large laths of pink feldspar and clasts of quartz aggregates embedded in a magnetite rich (black streak) matrix.	Bhuj Formation
50	109022	GSPL-Bhuj-256/12/2024	23.17550	69.61667	BR	Metasomatized sandstone sample near to Median high fault	Bhuj Formation
51	109023	GSPL-Bhuj-258/12/2024	23.22364	69.59188	BR	Highly variegated ferruginous sandstone showing alternating dark brown, reddish, and yellowish iron oxide crusts and bands, with a very granular and porous texture. The specimen contains abundant angular to sub-rounded quartz grains, no feldspar, and is cemented by dense hematite, goethite, and limonite matrix.	Bhuj Formation
52	109024	GSPL-Bhuj-259/12/2024	23.22338	69.59037	BR	Purplish reddish brown colored, medium grained ferruginous sandstone, exhibiting nodular and patchy iron oxide accumulations on the surface. The specimen is composed of quartz grains with iron oxides (primarily hematite) acting as cement, producing a dense and hard structure. Globular and irregular iron-rich textures are visible, typical of ferruginous sandstones affected by strong secondary iron mineralization and alteration. The overall appearance aligns with ferruginous sa ndstone, reflecting substantial iron enrichment within a siliciclastic matrix.	Bhuj Formation

Table Continued..

Annexure-XX

Sl No.	Sample ID	Al_2O_3	BaO	CaO	Cr_2O_3	Fe_2O_3	K_2O	MgO	MnO	Na_2O	P_2O_5	TiO_2	SiO_2	LOI	S
37	105622	13.54	0.01	19.26	0.01	10.82	1.08	1.31	0.18	0.21	12.49	0.62	28.41	10.58	0.56
38	109059	NA	NA	NA	NA	NA	NA	NA	NA	NA	NA	NA	NA	NA	NA
39	109006	NA	NA	NA	NA	NA	NA	NA	NA	NA	NA	NA	NA	NA	NA
40	109007	NA	NA	NA	NA	NA	NA	NA	NA	NA	NA	NA	NA	NA	NA
41	109009	NA	NA	NA	NA	NA	NA	NA	NA	NA	NA	NA	NA	NA	NA
42	109011	NA	NA	NA	NA	NA	NA	NA	NA	NA	NA	NA	NA	NA	NA
43	109015	NA	NA	NA	NA	NA	NA	NA	NA	NA	NA	NA	NA	NA	NA
44	109016	NA	NA	NA	NA	NA	NA	NA	NA	NA	NA	NA	NA	NA	NA
45	109017	NA	NA	NA	NA	NA	NA	NA	NA	NA	NA	NA	NA	NA	NA
46	109018	NA	NA	NA	NA	NA	NA	NA	NA	NA	NA	NA	NA	NA	NA
47	109019	NA	NA	NA	NA	NA	NA	NA	NA	NA	NA	NA	NA	NA	NA
48	109020	NA	NA	NA	NA	NA	NA	NA	NA	NA	NA	NA	NA	NA	NA
49	109021	NA	NA	NA	NA	NA	NA	NA	NA	NA	NA	NA	NA	NA	NA
50	109022	NA	NA	NA	NA	NA	NA	NA	NA	NA	NA	NA	NA	NA	NA
51	109023	NA	NA	NA	NA	NA	NA	NA	NA	NA	NA	NA	NA	NA	NA
52	109024	NA	NA	NA	NA	NA	NA	NA	NA	NA	NA	NA	NA	NA	NA

Sl No.	Sample ID	Location No.	Latitude	Longitude	Sample Type	Sample Description	Stratigraphy
53	109026	GSPL-Bhuj-261/01/2025	23.19690	69.72526	BR	Light yellow to buff colored, fine to medium grained sandstone with a friable and porous texture, showing weak cementation. The specimen is primarily composed of angular to sub rounded quartz grains with minimal iron oxide staining, unidentified black grains?	Bhuj Formation
54	109027	GSPL-Bhuj-262/01/2025	23.19785	69.52827	BR	Light brown to reddish brown, moderately compact sandstone with a granular texture. The rock is medium to coarse grained, composed mainly of sub angular to sub rounded quartz grains, with minor feldspar?. The grains are loosely packed, moderately sorted, and held in a siliceous matrix/cement. Iron oxide staining is present in patches, giving a slight reddish tint.The lower portion exhibits darker brown to blackish staining, likely due to localized ferruginization.	Bhuj Formation
55	109028	GSPL-Bhuj-263/01/2025	23.19885	69.53037	BR	Purpulish to reddish yellow fine to medium grained ferruginous sandstones, containing angular to sub rounded quartz grains . The yellowish portion limonite/goethite enrichment, giving a softer, friable texture, while the reddish piece is harder and more compact due to dense hematite cementation.	Bhuj Formation
56	109029	GSPL-Bhuj-263/01/2025	23.19885	69.53037	BR	Dark purplish brown colored,fine to medium grained ferruginous sandstone characterized by dense texture and strong iron oxide impregnation. Composed of angular to sub rounded quartz grains and possible feldspar, with abundant iron oxides (hematite/goethite) acting as matrix and cement. Patches and spots of nodular iron accumulation are visible, producing a mottled, uneven appearance commonly seen in ferruginous sandstones affected by secondary iron mineralization??	Bhuj Formation
57	109031	GSPL-Bhuj-264/01/2025	23.20869	69.52542	BR	Light reddish brown colored, fine to medium grained ferruginous sandstone. The specimen exhibits parallel lamination and bedding, with angular to sub-rounded quartz grains as the dominant framework. Subordinate feldspar grains ? are possibly present. The rock is well cemented by an iron oxide-rich matrix, primarily hematite and limonite, giving it the rusty brown coloration	Bhuj Formation
58	109032	GSPL-Bhuj-265/01/2025	23.19520	69.53281	BR	Dark reddish brown coloured fine to medium grained highly altered ferruginous sandstone, composed of angular to sub-rounded quartz grains, subordinate euhedral feldspar?, all embedded in a hematite or magnetite rich matrix/cement.	Bhuj Formation
59	109033	GSPL-Bhuj-265/01/2025	23.19520	69.53281	BR	Metasomatized Sandstone	Bhuj Formation
60	109034	GSPL-Bhuj-266/01/2025	23.19549	69.53124	BR	Dark reddish brown coloured fine to medium grained highly altered ferruginous sandstone, composed of angular to sub-rounded quartz grains, subordinate euhedral feldspar?, all embedded in a hematite or magnetite rich matrix/cement.	Bhuj Formation
61	109035	GSPL-Bhuj-267/01/2025	23.19638	69.53115	BR	Reddish brown, finely laminated ferruginous sandstone with prominent banding and internal lenses of hematite-rich crust. The specimen exhibits alternating layers of reddish, purple, and orange iron oxides (hematite/goethite), indicative of classic ferriband formation resulting from iron oxide migration and precipitation. The granular framework is dominated by sub rounded quartz grains, with iron oxides acting as the primary cement.	Bhuj Formation
62	109036	GSPL-Bhuj-268/01/2025	23.19567	69.53168	BR	Dark brown to black colored, coarse grained metasomatized ferruginous sandstone with abundant angular to sub-rounded quartz grains and numerous rock fragments, all tightly cemented by iron oxides, primarily hematite. The specimen is hard and dense, with a distinctly granular texture and glossy surface due to iron-rich mineralization. The matrix displays globular and nodular iron accumulations.	Bhuj Formation
63	109037	GSPL-Bhuj-269/01/2025	23.19634	69.53186	BR	Redish brwon to black coloured fine to medium grained metasomatized ferruginous sandstone, composed of angular to sub-rounded quartz grains, subordinate euhedral feldspar?, and occasional muscovite flakes (possibly detrital), all embedded in a hematite- and magnetite-rich matrix/cement.	Bhuj Formation
64	109038	GSPL-Bhuj-263/01/2025	23.19368	69.53232	BR	Whitish sandstone composed of quartz grains, black minerals ??	Bhuj Formation
65	109039	GSPL-Bhuj-270/01/2025	23.21025	69.52410	BR	Metasomatized sandstone	Bhuj Formation
66	109040	GSPL-Bhuj-270/01/2025	23.21025	69.52410	BR	Highly ferruginous red sandstone	Bhuj Formation
67	109041	GSPL-Bhuj-270/01/2025	23.21025	69.52410	BR	White siltstone (very fine grained), overlain by ferruginous and metasomatized sandstone	Bhuj Formation

Table Continued..

Annexure-XX

Sl No.	Sample ID	Al_2O_3	BaO	CaO	Cr_2O_3	Fe_2O_3	K_2O	MgO	MnO	Na_2O	P_2O_5	TiO_2	SiO_2	LOI	S
53	109026	NA	NA	NA	NA	NA	NA	NA	NA	NA	NA	NA	NA	NA	NA
54	109027	NA	NA	NA	NA	NA	NA	NA	NA	NA	NA	NA	NA	NA	NA
55	109028	NA	NA	NA	NA	NA	NA	NA	NA	NA	NA	NA	NA	NA	NA
56	109029	NA	NA	NA	NA	NA	NA	NA	NA	NA	NA	NA	NA	NA	NA
57	109031	NA	NA	NA	NA	NA	NA	NA	NA	NA	NA	NA	NA	NA	NA
58	109032	NA	NA	NA	NA	NA	NA	NA	NA	NA	NA	NA	NA	NA	NA
59	109033	NA	NA	NA	NA	NA	NA	NA	NA	NA	NA	NA	NA	NA	NA
60	109034	NA	NA	NA	NA	NA	NA	NA	NA	NA	NA	NA	NA	NA	NA
61	109035	NA	NA	NA	NA	NA	NA	NA	NA	NA	NA	NA	NA	NA	NA
62	109036	NA	NA	NA	NA	NA	NA	NA	NA	NA	NA	NA	NA	NA	NA
63	109037	NA	NA	NA	NA	NA	NA	NA	NA	NA	NA	NA	NA	NA	NA
64	109038	NA	NA	NA	NA	NA	NA	NA	NA	NA	NA	NA	NA	NA	NA
65	109039	NA	NA	NA	NA	NA	NA	NA	NA	NA	NA	NA	NA	NA	NA
66	109040	NA	NA	NA	NA	NA	NA	NA	NA	NA	NA	NA	NA	NA	NA
67	109041	NA	NA	NA	NA	NA	NA	NA	NA	NA	NA	NA	NA	NA	NA

Sl No.	Sample ID	Location No.	Latitude	Longitude	Sample Type	Sample Description	Stratigraphy
68	109042	GSPL-Bhuj-271/01/2025	23.19749	69.52979	BR	Dark reddish brown colored, fine to medium grained, highly altered ferruginous sandstone, composed of angular to sub-rounded quartz grains and possible subordinate euhedral feldspar, all embedded in a dense hematite-rich matrix/cement. The rock exhibits a gritty texture and compact structure, indicating significant iron oxide impregnation and alteration. Occasional magnetite may also be present in the cement or as accessory grains, contributing to the blackish patches within the matrix. Growth of authigenic feldspar, and silicification are common feature of the sandstone.	Bhuj Formation
69	109043	GSPL-Bhuj-273/01/2025	23.20362	69.52684	BR	Very dark brown to black colored, fine to medium grained metsomatized ferruginous sandstone, composed of angular to sub-rounded quartz grains with possible subordinate feldspar, all embedded in a dense hematite- or magnetite-rich cement/matrix. The specimen features a compact, hard structure with a granular surface texture and irregular banding or nodular iron oxide accumulations. Iron impregnation is very strong, giving the rock its blackish appearance	Bhuj Formation
70	109046	GSPL-Bhuj-274/01/2025	23.19181	69.58950	BR	Yellowish ferruginous sandstone fine grained composed abudantly of quartz grains and few muscovite (<1%)	Katrol Formation
71	109047	GSPL-Bhuj-274/01/2025	23.19181	69.58950	BR	Reddish brown colored, fine to medium grained ferruginous sandstone. The specimen is well cemented and compact, featuring sub rounded to rounded quartz grains with thin reddish hematite rims. The matrix is dominated by iron oxides, mainly hematite, providing the distinctive red coloration. Laminations or bedding may be faintly observed, and the overall texture is gritty and hard. Possibly formed by extensive iron impregnation in a siliciclastic framework.	Katrol Formation
72	109048	GSPL-Bhuj-274/01/2025	23.19180	69.58950	BR	Yellowish ferruginous sandstonemedium to coarse grained composed abudantly of quartz grains and few muscovite (<1%)	Katrol Formation
73	109049	GSPL-Bhuj-276/01/2025	23.20940	69.52536	BR	Dark reddish brown to brown colored, medium to coarse grained ferruginous sandstone exhibiting a rough, granular surface texture. The specimen contains angular to sub rounded quartz grains and possibly subordinate feldspar??, all set in a dense iron oxide-rich matrix, mainly hematite and goethite. Prominent iron oxide crusts and granular patches are visible, causing a locally uneven surface and giving the rock a hard, compact feel. White specks on the surface may represent small quartz grains or crystal inclusions.	Bhuj Formation
74	109050	GSPL-Bhuj-276/01/2025	23.20940	69.52536	BR	Pale yellowish white, fine to medium grained weakly ferruginous sandstone with scattered brown iron oxide staining. The specimen exhibits angular to sub rounded quartz grains as the dominant framework, no visible feldspar, and is loosely cemented by minor limonite/goethite. The rock is friable and porous, with mottled pale and rusty patches resulting from patchy iron oxide impregnation. Surface texture is gritty and irregular, and overall, this fits a description of a weakly ferruginized quartz sandstone.	Bhuj Formation
75	109051	GSPL-Bhuj-277/01/2025	23.20950	69.52221	BR	Very dark brown to black colored, coarse grained ferruginous sandstone with abundant angular to sub rounded quartz grains only, cemented in a dense hematite and goethite rich matrix. The surface is glittery and granular with scattered white quartz grains	Bhuj Formation
76	109052	GSPL-Bhuj-278/01/2025	23.21039	69.52387	BR	Redish brwon to black coloured coarse to medium grained highly metasomatized ferruginous sandstone, composed of angular to sub rounded quartz grains, subordinate euhedral feldspar?, and occasional muscovite flakes (possibly detrital), all embedded in a hematite- and magnetite-rich matrix/cement.Silicidication also observed	Bhuj Formation
77	109058	GSPL-Bhuj-277/01/2025	23.20950	69.52221	BR	White fine grained sandstone	Bhuj Formation
78	109060	GSPL-Bhuj-293/01/2025	23.20096	69.63083	BR	Dark reddish brown to brownish black colored, medium to coarse grained ferruginous sandstone, exhibiting dense, hard, and compact structure due to strong iron oxide cementation. It shows granular texture, with angular to sub rounded quartz grains and possible feldspar, all embedded in a matrix rich in hematite, goethite, and other iron oxides. White specks are observed throughout, likely due to quartz or feldspar grains	Bhuj Formation
79	189111	GSPL-Bhuj-173/11/2024	23.16671	69.64349	BR	Thinly bedded medium to coarse grained redish brown colored sandstone	Bhuj Formation
80	189112	GSPL-Bhuj-174/11/2024	23.16561	69.64349	BR	Thinly bedded medium to coarse grained redish brown colored sandstone	Bhuj Formation

Table Continued..

Annexure-XX

Sl No.	Sample ID	Al_2O_3	BaO	CaO	Cr_2O_3	Fe_2O_3	K_2O	MgO	MnO	Na_2O	P_2O_5	TiO_2	SiO_2	LOI	S
68	109042	NA	NA	NA	NA	NA	NA	NA	NA	NA	NA	NA	NA	NA	NA
69	109043	NA	NA	NA	NA	NA	NA	NA	NA	NA	NA	NA	NA	NA	NA
70	109046	NA	NA	NA	NA	NA	NA	NA	NA	NA	NA	NA	NA	NA	NA
71	109047	NA	NA	NA	NA	NA	NA	NA	NA	NA	NA	NA	NA	NA	NA
72	109048	NA	NA	NA	NA	NA	NA	NA	NA	NA	NA	NA	NA	NA	NA
73	109049	NA	NA	NA	NA	NA	NA	NA	NA	NA	NA	NA	NA	NA	NA
74	109050	NA	NA	NA	NA	NA	NA	NA	NA	NA	NA	NA	NA	NA	NA
75	109051	NA	NA	NA	NA	NA	NA	NA	NA	NA	NA	NA	NA	NA	NA
76	109052	NA	NA	NA	NA	NA	NA	NA	NA	NA	NA	NA	NA	NA	NA
77	109058	NA	NA	NA	NA	NA	NA	NA	NA	NA	NA	NA	NA	NA	NA
78	109060	NA	NA	NA	NA	NA	NA	NA	NA	NA	NA	NA	NA	NA	NA
79	189111	NA	NA	NA	NA	NA	NA	NA	NA	NA	NA	NA	NA	NA	NA
80	189112	NA	NA	NA	NA	NA	NA	NA	NA	NA	NA	NA	NA	NA	NA

Sl No.	Sample ID	Location No.	Latitude	Longitude	Sample Type	Sample Description	Stratigraphy
81	109045	GSPL-Bhuj-274/01/2025	23.19181	69.58950	BR	Grey thick (5cm) Tuffite beds of Katrol unit	Katrol Formation
82	109053	GSPL-Bhuj-279/01/2025	23.22131	69.58954	BR	Sandstone with strong iron impregnation, mainly in layers. A zone of clay (alteration??) is also observed. It could be silicification also	Bhuj Formation
83	109054	GSPL-Bhuj-277/01/2025	23.20950	69.52221	BR	Highly ferruginous (Metasomatized sandstone), possible albite zone??	Bhuj Formation
84	109055	GSPL-Bhuj-280/01/2025	23.20316	69.62894	BR	Metasomatized sandstone	Bhuj Formation
85	109056	GSPL-Bhuj-281/01/2025	23.22556	69.54979	BR	Highly ferrugenous dark red sandstone	Bhuj Formation
86	109057	GSPL-Bhuj-283/01/2025	23.23284	69.52792	BR	Highly ferruginous sandstone, metasomatized at top	Bhuj Formation
87	109061	GSPL-Bhuj-290/02/2025	23.20096	69.63083	BR	Fine grained dark reddish black Tuffite layer?/encrustrations??	Bhuj Formation
88	109062	GSPL-Bhuj-290/02/2025	23.20096	69.63083	BR	Grey Tuffite beds with small circular red inclusions of pellets??	Bhuj Formation
89	109063	GSPL-Bhuj-289/01/2025	23.20370	69.62840	BR	Interbanded white sandstone and ferrugenous layer	Bhuj Formation
90	109064	GSPL-Bhuj-289/01/2025	23.20370	69.62840	BR	White fine-grained sandstone with purple banding	Bhuj Formation
91	109065	GSPL-Bhuj-289/01/2025	23.20370	69.62840	BR	Black Metasomatized sandstone with magnetite	Bhuj Formation
92	109066	GSPL-Bhuj-290/02/2025	23.20096	69.63083	BR	White fine-grained tuffite layers	Bhuj Formation
93	109067	GSPL-Bhuj-292_02_2025	23.20103	69.63058	BR	Metasomatized sandstone with magnetite	Bhuj Formation
94	109068	GSPL-Bhuj-295/02/2025	23.19505	69.57110	BR	White to purplish white light brown coloured sandstone, no grain boundary is clearly visible, clayey matrix/cement	Bhuj Formation
95	109069	GSPL-Bhuj-289/02/2025	23.20370	69.62840	BR	Black metasomatized sandstone with pinkish inclusion/alteration	Bhuj Formation
96	109070	GSPL-Bhuj-289/02/2025	23.20370	69.62840	BR	Black metasomatized sandstone with pinkish inclusion/alteration	Bhuj Formation
97	109071	GSPL-Bhuj-289/02/2025	23.20370	69.62840	BR	Planar cross stratified brownish red to pinkish white coloured, medium to coarse grained sandstone.	Bhuj Formation
98	112451	GSPL-Bhuj-296/07/2025	23.16052	69.68694	BR	Breccia, composed of clasts of ferruginous sandstone embedded in a very coarse to pebbly matrix (very crystal clear quartz, non magnetic black minerals, muscovite). Silicification, hematite coating, and calcareous veinlets are also observed within the sample.	Bhuj Formation
99	112466	GSPL-Bhuj-324/07/2025	23.19268	69.51791	BR	Violitish white to brownish mauve coloured, very light weight altered ferruginous sandstone. Apart from few quartz pebbles no other grains have been identified (no grain boundary is clear) within the sandstone. Porous spaces (pot hole like feature) within the sandstone are filled with clay (fails acid test) and/or hematite. The matrix/cement of the sandstone comprises hematite. The grain contacts does not seems to be sandstone, they are looking like "Y" junction between the grains. The sample has been collected from the contact zone (2.7m thick) of a fault plane. (Surface sample from BH-08)	Bhuj Formation

Table Continued..

Annexure-XX

Sl No.	Sample ID	Al_2O_3	BaO	CaO	Cr_2O_3	Fe_2O_3	K_2O	MgO	MnO	Na_2O	P_2O_5	TiO_2	SiO_2	LOI	S
81	109045	NA	NA	NA	NA	NA	NA	NA	NA	NA	NA	NA	NA	NA	NA
82	109053	NA	NA	NA	NA	NA	NA	NA	NA	NA	NA	NA	NA	NA	NA
83	109054	NA	NA	NA	NA	NA	NA	NA	NA	NA	NA	NA	NA	NA	NA
84	109055	NA	NA	NA	NA	NA	NA	NA	NA	NA	NA	NA	NA	NA	NA
85	109056	NA	NA	NA	NA	NA	NA	NA	NA	NA	NA	NA	NA	NA	NA
86	109057	NA	NA	NA	NA	NA	NA	NA	NA	NA	NA	NA	NA	NA	NA
87	109061	NA	NA	NA	NA	NA	NA	NA	NA	NA	NA	NA	NA	NA	NA
88	109062	NA	NA	NA	NA	NA	NA	NA	NA	NA	NA	NA	NA	NA	NA
89	109063	NA	NA	NA	NA	NA	NA	NA	NA	NA	NA	NA	NA	NA	NA
90	109064	NA	NA	NA	NA	NA	NA	NA	NA	NA	NA	NA	NA	NA	NA
91	109065	NA	NA	NA	NA	NA	NA	NA	NA	NA	NA	NA	NA	NA	NA
92	109066	NA	NA	NA	NA	NA	NA	NA	NA	NA	NA	NA	NA	NA	NA
93	109067	NA	NA	NA	NA	NA	NA	NA	NA	NA	NA	NA	NA	NA	NA
94	109068	NA	NA	NA	NA	NA	NA	NA	NA	NA	NA	NA	NA	NA	NA
95	109069	NA	NA	NA	NA	NA	NA	NA	NA	NA	NA	NA	NA	NA	NA
96	109070	NA	NA	NA	NA	NA	NA	NA	NA	NA	NA	NA	NA	NA	NA
97	109071	NA	NA	NA	NA	NA	NA	NA	NA	NA	NA	NA	NA	NA	NA
98	112451	NA	NA	NA	NA	NA	NA	NA	NA	NA	NA	NA	NA	NA	NA
99	112466	NA	NA	NA	NA	NA	NA	NA	NA	NA	NA	NA	NA	NA	NA

Sl No.	Sample ID	Location No.	Latitude	Longitude	Sample Type	Sample Description	Stratigraphy
100	112492	GSPL-BHUJ 351/07/2025	23.22263	69.59411	BR	Altered highly ferruginous sandstone, occuring as dm scale thin band along the fault plane. It consists of angular to few sub-rounded grains of quartz, very few mica and clasts of hematite embedded in a hematitic matrix/cement. The amount of the framework is ~40%. The rock seems to be a flow along the fault plane and observed only along the fault plane. (Surface sample from BH-06)	Bhuj Formation
101	112493	GSPL-BHUJ 351/07/2025	23.22263	69.59411	BR	Altered ferruginous, pinkish purple coloured sandstone occuring between two fracture zone. It consists of 0.5cm to 16cm long clasts of clay and/ or siltstone (observed as original bed at the other part of the exposure) embedded in a siliceous matrix. The sandstone also comprises angular to rounded, elongated, circular wedge shaped quartz, and muscovite. The grain boundary of the matrix part is not very clear. At very few places feldspar grains are also suspected. Small iron concretion is also observed at places. (Surface sample from BH-06)	Bhuj Formation
102	112493	GSPL_BHUJ _351/07/25	23.22263	69.59411	BR	Altered ferruginous, pinkish purple coloured sandstone occuring between two fracture zone. It consists of 0.5cm to 16cm long clasts of clay and/ or siltstone (observed as original bed at the other part of the exposure) embedded in a siliceous matrix. The sandstone also comprises angular to rounded, elongated, circular wedge shaped quartz, and muscovite. The grain boundary of the matrix part is not very clear. At very few places feldspar grains are also suspected. Small iron concretion is also observed at places. (Surface sample from BH-06)	Bhuj Formation
103	112494	GSPL-BHUJ 351/07/2025	23.22263	69.59411	BR	Breccia occuring along the fault plane. It consists of angular to well-rounded quartz, clay clasts (rectangular, circular, wedge shaped, irregular), small gashes or lens-like structures filled with silica, few book mica (muscovite), well-rounded iron clasts embedded in a hematitic matrix/cement. No magnetite is observed. (Surface sample from BH-06)	Bhuj Formation
104	112495	GSPL-BHUJ 351/07/2025	23.22263	69.59411	BR	Yellowish wite coloured, medium to coarse grained, poorly sorted sandstone. The sandstone comprises of angular to sub rounded grains (moderate to low sphericity) of both grey and white quartz, clay (altered feldspar??) black shale clasts embedded in a silicious to clay matrix. (Surface sample from BH-06)	Bhuj Formation
105	112459	GSPL_BHUJ _313/07/2025	23.20322	69.62856	BR	Metasomatized sandstone with strong iron impregnation (Surface sample from BH-04)	Bhuj Formation
106	112460	GSPL_BHUJ _319/07/2025	23.19757	69.52979	BR	Altered highly ferruginous sandstone. It is medium-grained and composed of angular to rounded quartz grains, euhedral feldspars, and aggregates of mica, all embedded within a hematitic to magnetite-rich matrix or cement. The unit exhibits evidence of flow structures. Additionally, a greenish to greenish-blue hue has been observed along several fracture surfaces. A portion of the powdered rock is attracted to a strong magnet and leaves a a black streak, further indicating a magnetite-rich composition. (Surface sample from BH-07)	Bhuj Formation
107	112461	GSPL_BHUJ _320/07/25	23.20134	69.53626	BR	Blackish red coloured (with purplish tinch) altered ferruginous sandstone, composed of angular to rounded quartz, euhedral feldspar, muscovite (possibly detritus), embedded in a hematitic and magnetite-rich matrix/cement. The rock powder is attracted by strong magnet. Fracture filled with calcrete. (Surface sample from BH-07)	Bhuj Formation
108	112462	GSPL_BHUJ _321/07/25	23.20306	69.53573	BR	Blackish red coloured sandstone, (altered, but did not turn to Metasomatized) separated by yellowish occur coloured shale/clay. Thin veinlets of black materials (very few parts of the powder of the material are attracted by magnet, cherry red streak), are observed to be cross cutting the sandstone. The sandstone is medium to coarse grained and consists of angular to rounded quartz (detritus), muscovite (detritus), biotite (??), weathered sub-rounded feldspar embedded in a mostly hematite and poorly magnetite-rich matrix/cement. Secondary fluid (silvery pinkish blue, golden, varigated colour) along few fractures are also observed. (Surface sample from BH-07)	Bhuj Formation
109	112463	GSPL_BHUJ _322/07/25	23.19357	69.51865	BR	Yellow ocher coloured quartz arenite, composed of sub rounded to very well rounded quartz grains, embedded in a siliceous matrix/cement. (Surface sample from BH-08)	Bhuj Formation
110	112464	GSPL_BHUJ _322/07/25	23.19357	69.51865	BR	Black colour highly altered ferruginous sandstone, composed of angular to sub-rounded quartz, euhedral feldspar, mica embedded in a hematitic to magnetite matrix/cement. (Surface sample from BH-08)	Bhuj Formation

Table Continued..

Annexure-XX

Sl No.	Sample ID	Al_2O_3	BaO	CaO	Cr_2O_3	Fe_2O_3	K_2O	MgO	MnO	Na_2O	P_2O_5	TiO_2	SiO_2	LOI	S
100	112492	NA	NA	NA	NA	NA	NA	NA	NA	NA	NA	NA	NA	NA	NA
101	112493	NA	NA	NA	NA	NA	NA	NA	NA	NA	NA	NA	NA	NA	NA
102	112493	NA	NA	NA	NA	NA	NA	NA	NA	NA	NA	NA	NA	NA	NA
103	112494	NA	NA	NA	NA	NA	NA	NA	NA	NA	NA	NA	NA	NA	NA
104	112495	NA	NA	NA	NA	NA	NA	NA	NA	NA	NA	NA	NA	NA	NA
105	112459	NA	NA	NA	NA	NA	NA	NA	NA	NA	NA	NA	NA	NA	NA
106	112460	NA	NA	NA	NA	NA	NA	NA	NA	NA	NA	NA	NA	NA	NA
107	112461	NA	NA	NA	NA	NA	NA	NA	NA	NA	NA	NA	NA	NA	NA
108	112462	NA	NA	NA	NA	NA	NA	NA	NA	NA	NA	NA	NA	NA	NA
109	112463	NA	NA	NA	NA	NA	NA	NA	NA	NA	NA	NA	NA	NA	NA
110	112464	NA	NA	NA	NA	NA	NA	NA	NA	NA	NA	NA	NA	NA	NA

Sl No.	Sample ID	Location No.	Latitude	Longitude	Sample Type	Sample Description	Stratigraphy
111	112478	GSPL_BHUJ _336/07/2025	23.17271	69.62487	BR	Medium to coarse grained quartzose sandstone with sub-rounded grains having moderate to high sphericity. The sandstone consist of mostly quartz (>98%), very few hematite grains, magnetite and white transparent crystals embedded in a silicified(?) matrix/cement. Iron impregnation has been observed as flow paths [thin veinlets (?)], cross cutting the sandstone. This veinlets are very hard and consists also of quartz, hematite (streak white, black minerals are difficult to get the streak, rarely blackish brown, non-magnetite).	Bhuj Formation
112	112479	GSPL_BHUJ _337/07/2025	23.17199	69.62476	BR	Metasomatized sandstone	Bhuj Formation
113	112480	GSPL_BHUJ _338/07/2025	23.17020	69.62394	BR	Metasomatized sandstone, carbonate as secondary solution and fluid activity is also observed	Bhuj Formation
114	112481	GSPL_BHUJ _338/07/2025	23.17020	69.62394	BR	Metasomatized sandstone, carbonate as secondary solution and fluid activity is also observed	Bhuj Formation
115	112484	GSPL_BHUJ _344/07/2025	23.19073	69.69641	BR	Medium to coarse grained ferruginous weathered sandstone Iron concretion present , angular to rounded grains	Bhuj Formation
116	112488	GSPL_BHUJ _348/07/25	23.19432	69.58188	BR	Sandstone is composed of both clean and detritus quartz, ranging in size from medium to very coarse, angular to sub-rounded embedded in a hematitic to silicic(??) matrix/ cement. The clean semi transparent quartz grains are more angular and surrounded by hematite rims. The sandstones seems to be brecciated at places, specifically where the iron veins are in cross cutting relationship with the sandstone A thin carbonate vein is also observed at an angle to the bedding of the sandstone. (Surface sample from BH-05)	Bhuj Formation
117	112496	GSPL_BHUJ _353/07/25	23.22200	69.59442	BR	Blackish red coloured medium to fine grained sandstone, occuring along the fault plane. This has been observed as dm scale unit, along few of the bedding planes where high amount of ferrugination and alteration making it very hard than the depositional sandstone. It consists of ~30-40% framework of angular to sub angular quartz, muscovite embedded in a hematitic to magnetite (in less amount, part of the rock powder is attracted by magnet) matrix. (Surface sample from BH-06)	Bhuj Formation
118	112498	GSPL_BHUJ _ 358/07/25	23.19465	69.58041	BR	The sandstone is composed of both clean and detritus quartz, ranging in size from coarse to very coarse, angular to sub-rounded, both biotite and muscovite, varigated colour minerals (bornite??), few magnetite grains embedded in a hematitic to silicic(??) matrix/ cement. The clean semi transparent quartz grains are more angular and surrounded by hematite rims. The sandstones seems to be brecciated at places, specifically where the iron veins are in cross cutting relationship with the sandstone. The dust of the rock attracted by magnet. Cluster of 2-3 quartz grains, surrounded by magnetite are occuring as the breccia clast. There is a fine grained variety of dark blackish brown colour rock with lots of very small grains of euhedral feldspar. (Surface sample from BH-05)	Bhuj Formation

Table Continued..

Annexure-XX

Sl No.	Sample ID	Al_2O_3	BaO	CaO	Cr_2O_3	Fe_2O_3	K_2O	MgO	MnO	Na_2O	P_2O_5	TiO_2	SiO_2	LOI	S
111	112478	NA	NA	NA	NA	NA	NA	NA	NA	NA	NA	NA	NA	NA	NA
112	112479	NA	NA	NA	NA	NA	NA	NA	NA	NA	NA	NA	NA	NA	NA
113	112480	NA	NA	NA	NA	NA	NA	NA	NA	NA	NA	NA	NA	NA	NA
114	112481	NA	NA	NA	NA	NA	NA	NA	NA	NA	NA	NA	NA	NA	NA
115	112484	NA	NA	NA	NA	NA	NA	NA	NA	NA	NA	NA	NA	NA	NA
116	112488	NA	NA	NA	NA	NA	NA	NA	NA	NA	NA	NA	NA	NA	NA
117	112496	NA	NA	NA	NA	NA	NA	NA	NA	NA	NA	NA	NA	NA	NA
118	112498	NA	NA	NA	NA	NA	NA	NA	NA	NA	NA	NA	NA	NA	NA

Sl No.	Sample ID	Location No.	Latitude	Longitude	Sample Type	Sample Description	Stratigraphy
119	107550	GSPL-Bhuj-162/06/24	23.22384	69.524377	Fragment of river transported detrital	During sieving, a large (~2.5cm) elongated crystal characterized by white, transparent nature has been found. Diamond pen is giving only a faint line, does not scratch properly.	Bhuj Formation
120	107554	GSPL-Bhuj-164/06/24	23.22097	69.590355	Bulk Sample	Slope wash samples containing broken fragments of bed rock. Bulk sample of (-) 2mm fraction, collected from 4 point locations over a stretch of 15m on the creeks of Basalt intrusion. Consists of coarse grained, angular to sub-angular clasts of basalt, quartz, magnetite in decreasing order of abundance	Bhuj Formation
121	107556	GSPL-Bhuj-165/06/24	23.2211	69.589842	Scree deposit	Scree deposits feature very fine-grained white clasts, possibly with some concretions embedded in fine cement. The clasts are anhedral, subangular to angular, and exhibit worm-like structures.	Bhuj Formation

Table Continued..

Annexure-XX

Sl No.	Sample ID	Al_2O_3	BaO	CaO	Cr_2O_3	Fe_2O_3	K_2O	MgO	MnO	Na_2O	P_2O_5	TiO_2	SiO_2	LOI	S
119	107550	0.351	<0.01	0.028	<0.01	1.338	<0.01	0.071	0.039	0.072	0.015	0.029	96.7810236	0.65463835	<0.05
120	107554	13.791	0.042	7.696	<0.01	12.123	0.834	4.864	0.154	1.357	0.211	1.299	42.7676735	14.0897256	0.08
121	107556	13.201	<0.01	6.247	<0.01	5.278	0.631	1.147	0.108	0.161	2.544	0.952	44.5867251	23.0152366	1.436

Annexure-XXI: ICPMS Analysis BR

Sl No.	Sample ID	Location No.	Latitude	Longitude	Sample Type	Li	Be	Sc	V	Ga	Ge	Se	Rb	Sr	Y	Zr	Nb	Mo
1	105567	GSPL-Bhuj-113/03/24	23.16009	69.72324	BR	14.9	1.3	14.2	255.9	11.0	<0.5	2.6	29.3	1106.9	29.9	131.3	13.1	0.6
2	107476	GSPL-Bhuj-120/06/24	23.18878	69.59946	BR	39.2	1.9	25.0	180.4	10.5	<0.5	0.5	36.9	113.4	26.4	70.2	8.7	1.8
3	107510	GSPL-Bhuj-136/06/24	23.16082	69.72329	BR	3.9	0.6	9.8	109.0	3.2	<0.5	<0.5	11.3	171.9	22.3	1.2	<0.5	1.7
4	107516	GSPL-Bhuj-137/06/24	23.16410	69.72726	BR	16.5	<0.5	4.1	30.5	5.7	<0.5	<0.5	37.4	163.0	5.9	13.0	<0.5	2.7
5	107518	GSPL-Bhuj-137/06/24	23.16410	69.72726	BR	9.2	1.4	13.3	135.8	6.6	<0.5	2.4	19.2	168.4	82.7	4.5	2.8	1.1
6	107541	GSPL-Bhuj-155/06/24	23.22405	69.49290	BR	23.4	4.1	5.9	69.1	10.6	0.6	2.8	52.1	234.1	32.8	179.3	16.0	7.6
7	107542	GSPL-Bhuj-157/06/24	23.23155	69.48264	BR	1.5	<0.5	2.7	26.6	2.5	<0.5	<0.5	12.9	48.9	7.4	121.8	1.9	1.1
8	107543	GSPL-Bhuj-158/06/24	23.25237	69.74468	BR	7.4	2.2	13.4	181.8	23.9	<0.5	<0.5	65.7	951.1	29.1	266.3	70.2	3.6
9	107546	GSPL-Bhuj-159/06/24	23.19947	69.51124	BR	3.6	2.0	2.8	51.8	4.1	<0.5	0.5	4.9	19.8	18.2	38.8	4.5	2.7
10	107551	GSPL-Bhuj-163/06/24	23.22384	69.52438	BR	8.8	<0.5	4.0	48.2	3.2	<0.5	<0.5	6.1	17.6	8.6	64.1	1.3	2.5
11	107561	GSPL-Bhuj-167/06/24	23.18286	69.63318	BR	13.3	0.7	9.6	153.3	7.7	<0.5	<0.5	33.1	415.0	10.8	150.0	1.6	2.2
12	107555	GSPL-Bhuj-165/06/24	23.22110	69.58984	BR	8.0	2.6	5.4	53.0	4.2	<0.5	<0.5	1.7	39.2	10.0	32.0	3.1	4.7
13	107565	GSPL-Bhuj-155/06/24	23.22420	69.49274	BR	6.3	2.9	2.7	21.1	5.3	<0.5	1.0	33.1	197.9	46.4	16.0	1.9	5.4
14	107566	GSPL-Bhuj-156/06/24	23.22796	69.50385	BR	4.6	0.6	1.0	14.8	1.8	<0.5	1.6	9.1	21.1	29.0	12.6	<0.5	3.5
15	107567	GSPL-Bhuj-156/06/24	23.22796	69.50385	BR	3.4	1.2	1.3	13.9	1.2	<0.5	<0.5	6.0	13.4	4.5	12.5	<0.5	5.2
16	107568	GSPL-Bhuj-157/06/24	23.22907	69.47871	BR	2.3	0.6	4.3	41.6	4.0	<0.5	<0.5	19.5	191.6	11.4	113.2	3.3	1.4
17	107569	GSPL-Bhuj-157/06/24	23.22907	69.47871	BR	5.3	1.7	6.5	36.0	4.1	<0.5	<0.5	19.1	114.8	20.0	205.3	10.2	1.4
18	107570	GSPL-Bhuj-157/06/24	23.22907	69.47871	BR	6.8	<0.5	4.0	38.4	4.5	<0.5	<0.5	10.7	43.8	5.7	50.5	0.9	2.0
19	107571	GSPL-Bhuj-157/06/24	23.22907	69.47871	BR	9.2	1.8	11.0	99.8	9.4	<0.5	0.7	36.1	79.9	14.7	178.9	10.1	2.2
20	107572	GSPL-Bhuj-136/06/24	23.16082	69.72329	BR	2.4	<0.5	5.6	60.4	2.3	<0.5	<0.5	7.8	122.2	4.9	14.2	0.5	1.5

Sl No.	Sample ID	Location No.	Latitude	Longitude	Sample Type	Li	Be	Sc	V	Ga	Ge	Se	Rb	Sr	Y	Zr	Nb	Mo
21	107573	GSPL-Bhuj-136/06/24	23.16118	69.72477	BR	9.3	1.4	12.6	212.4	5.6	<0.5	1.9	14.8	206.3	44.0	20.4	4.3	2.3
22	107574	GSPL-Bhuj-136/06/24	23.16118	69.72477	BR	11.8	1.9	23.5	274.9	7.3	<0.5	1.0	21.7	152.5	25.0	87.3	5.6	2.3
23	107575	GSPL-Bhuj-168/08/24	23.14830	69.72647	BR	16.9	2.0	11.6	132.5	14.0	<0.5	0.7	36.1	77.4	36.2	127.4	10.0	4.5
24	107576	GSPL-Bhuj-159/06/24	23.19947	69.51124	BR	15.5	0.9	3.8	35.2	8.9	<0.5	<0.5	12.9	22.3	7.6	65.9	2.9	1.7
25	107577	GSPL-Bhuj-159/06/24	23.19947	69.51124	BR	7.0	<0.5	2.5	12.0	2.5	<0.5	<0.5	7.3	22.7	5.4	22.3	<0.5	2.6
26	107578	GSPL-Bhuj-159/06/24	23.19947	69.51124	BR	5.3	1.6	3.3	24.2	4.5	<0.5	<0.5	6.6	23.9	15.8	74.7	5.3	1.5
27	107579	GSPL-Bhuj-91/01/24	23.15070	69.58000	BR	42.2	0.9	21.5	116.2	13.7	<0.5	<0.5	71.3	202.6	28.8	146.1	12.2	1.3
28	107580	GSPL-Bhuj-91/01/24	23.15070	69.58000	BR	45.2	1.3	18.4	89.4	15.2	<0.5	<0.5	72.5	172.5	29.2	108.7	8.3	1.7
29	107581	GSPL-Bhuj-91/01/24	23.15070	69.58000	BR	33.5	0.7	20.5	71.4	10.0	<0.5	<0.5	65.6	265.4	28.8	85.7	5.2	1.6
30	107582	GSPL-Bhuj-91/01/24	23.15070	69.58000	BR	24.9	0.6	8.2	38.0	8.4	<0.5	<0.5	59.8	316.9	16.4	102.4	4.6	1.1
31	107511	GSPL-Bhuj-136/06/24	23.16082	69.72329	BR	9.1	1.0	10.6	168.8	5.5	<0.5	0.5	17.5	197.8	31.0	6.4	3.7	1.6
32	107535	GSPL-Bhuj-147/06/24	23.17128	69.69256	BR	67.5655	1.4372	14.51	114.3363	17.33	<0.5	1.51	89.52	238.26	13.695	152.03	15.384	<0.5
33	107536	GSPL-Bhuj-150/06/24	23.16548	69.73697	BR	7.21229	<0.5	2.561	55.21829	4.637	<0.5	0.65	22.66	60.92	6.2372	131.38	2.7391	0.6553
34	107559	GSPL-Bhuj-147/06/24	23.18286	69.63318	BR	27.7	0.8	6.0	63.4	10.4	<0.5	<0.5	39.1	127.6	13.7	287.5	13.7	0.7
35	107562	GSPL-Bhuj-150/06/24	23.18286	69.63318	BR	29.5	1.3	7.2	90.1	13.6	<0.5	0.9	50.4	101.4	14.0	316.1	16.4	1.1
36	107563	GSPL-Bhuj-162/06/24	23.18286	69.63318	BR	18.0	0.6	6.6	55.5	7.6	<0.5	0.5	35.3	122.8	14.3	339.4	12.5	1.8
37	105622	GSPL-Bhuj-91/01/24	23.15070	69.58000	BR	79.2	2.4	59.3	143.1	27.5	1.7	14.9	60.3	768.8	505.4	201.2	11.7	1.2
38	109059	GSPL/Bhuj/294/01/2025	23.18957	69.54486	BR	5.50584	0.7559	1.986	13.6212	3.522	0.5	1.3	14.04	48.7	2.5617	37.106	3.4059	0.6544
39	109006	GSPL_BHUJ_249/12/2024	23.19444	69.59791	BR	92.8	<0.5	1.5	283.4	29.2	1.0	1.0	<0.5	182.8	7.7	96.5	1.3	1.1
40	109007	GSPL_BHUJ_249/12/2024	23.19444	69.59791	BR	<0.5	<0.5	<0.5	178.7	23.7	<0.5	<0.5	<0.5	309.7	<0.5	19.5	1.5	<0.5
41	109009	GSPL_BHUJ_250/12/2024	23.19514	69.59717	BR	66.1	<0.5	1.8	143.9	19.6	1.0	1.4	<0.5	211.0	2.5	93.7	1.8	<0.5
42	109011	GSPL_BHUJ_250/12/2024	23.19514	69.59717	BR	276.3	<0.5	1.4	275.0	28.9	0.9	<0.5	<0.5	96.2	4.8	103.5	2.1	1.3

Sl No.	Sample ID	Location No.	Latitude	Longitude	Sample Type	Li	Be	Sc	V	Ga	Ge	Se	Rb	Sr	Y	Zr	Nb	Mo
43	109015	GSPL_BHUJ_252/12/2024	23.27065	69.80465	BR	64.4	<0.5	1.6	45.2	11.8	1.2	1.0	<0.5	27.5	2.7	212.0	2.3	<0.5
44	109016	GSPL_BHUJ_252/12/2024	23.27065	69.80465	BR	<0.5	<0.5	1.0	95.9	24.8	0.8	<0.5	<0.5	56.4	1.3	155.5	2.4	0.7
45	109017	GSPL_BHUJ_253/12/2024	23.19629	69.59651	BR	<0.5	<0.5	<0.5	51.8	6.2	<0.5	<0.5	<0.5	147.5	0.7	150.2	1.4	<0.5
46	109018	GSPL_BHUJ_254/12/2024	23.19570	69.53396	BR	<0.5	<0.5	0.8	29.8	14.1	<0.5	1	<0.5	30.8	1.2	45.2	2.2	<0.5
47	109019	GSPL_BHUJ_254/12/2024	23.19570	69.53396	BR	<0.5	<0.5	<0.5	16.7	3.3	<0.5	<0.5	<0.5	25.1	<0.5	39.7	2.6	<0.5
48	109020	GSPL_BHUJ_254/12/2024	23.19570	69.53396	BR	110.3	<0.5	<0.5	9.0	1.7	<0.5	<0.5	<0.5	26.8	<0.5	36.8	2.0	<0.5
49	109021	GSPL_Bhuj_255/12/2024	23.21766	69.59088	BR	7.9786	2.3575	9.074	60.25327	2.057	0.5	0.5	8.585	21.23	11.365	16.652	2.9911	1.326
50	109022	GSPL_Bhuj_256/12/2024	23.17550	69.61667	BR	6.63199	1.772	12.58	212.489	5.392	0.5	1.96	19.24	174.8	45.143	314.41	14.632	0.6382
51	109023	GSPL_Bhuj_258/12/2024	23.22364	69.59188	BR	6.75526	1.5852	6.253	34.13121	2.443	0.5	1.93	0.5	9.2724	8.0225	24.062	0.8416	4.554
52	109024	GSPL_Bhuj_259/12/2024	23.22338	69.59037	BR	12.9119	0.8661	2.385	22.03369	3.581	0.5	1.53	0.5	42.096	6.7493	72.572	6.614	2.0023
53	109026	GSPL/Bhuj/261/01/2025	23.19690	69.72526	BR	11.683	0.5	3.224	39.13025	2.409	0.5	1.53	11.07	493.3	5.062	20.485	2.3235	0.5
54	109027	GSPL/Bhuj/262/01/2025	23.19785	69.52827	BR	15.1424	0.5	4.257	33.42028	4.437	0.5	0.5	18.99	30.176	4.3613	49.884	3.6291	0.5
55	109028	GSPL_Bhuj_263/01/2025	23.19885	69.53037	BR	10.6259	1.8047	7.225	58.30664	4.375	0.5	0.5	14.7	221.35	8.0413	60.206	3.6903	0.7374
56	109029	GSPL_Bhuj_263/01/2025	23.19885	69.53037	BR	10.1192	0.6006	2.484	52.43818	3.825	0.5	1.65	4.002	136.32	9.3626	64.245	3.7974	1.0345
57	109031	GSPL/Bhuj/264/01/2025	23.20869	69.52542	BR	23.007	1.6286	13.23	256.6337	21.69	0.5	1.17	44.41	69.174	16.17	182.39	18.041	2.5102
58	109032	GSPL_Bhuj_265/01/2025	23.19520	69.53281	BR	5.40839	0.7762	1.269	6.043053	1.777	0.5	0.5	10.15	16.144	4.3448	20.948	0.5149	1.2825
59	109033	GSPL_Bhuj_265/01/2025	23.19520	69.53281	BR	6.2127	0.6281	1.475	7.830051	2.554	0.5	1.96	11.84	58.266	3.8895	31.816	3.0762	0.5562
60	109034	GSPL_Bhuj_266/01/2025	23.19549	69.53124	BR	5.77004	0.6868	2.118	13.99263	2.754	0.5	0.6	14.45	46.381	5.0211	31.547	3.4263	0.8677
61	109035	GSPL/Bhuj/267/01/2025	23.19638	69.53115	BR	9.80469	1.6096	4.717	41.93509	7.829	0.5	0.89	22.36	54.328	11.969	100.31	9.191	0.8107
62	109036	GSPL/Bhuj/268/01/2025	23.19567	69.53168	BR	5.9061	0.6087	0.5	4.639902	1.859	0.5	1.54	17.21	43.555	2.8197	22.607	0.6572	0.6837
63	109037	GSPL_Bhuj_269/01/2025	23.19634	69.53186	BR	5.60253	0.5707	0.926	6.833954	2.283	0.5	1.16	15.56	38.589	3.1627	30.002	3.3532	1.3339
64	109038	GSPL/Bhuj/263/01/2025	23.19368	69.53232	BR	30.6424	1.6773	11.62	72.59361	23.66	0.5	2.1	55.4	66.287	21.325	206.75	22.714	0.7219

Sl No.	Sample ID	Location No.	Latitude	Longitude	Sample Type	Li	Be	Sc	V	Ga	Ge	Se	Rb	Sr	Y	Zr	Nb	Mo
65	109039	GSPL_Bhuj_270/01/2025	23.21025	69.52410	BR	9.4977	0.7897	2.913	10.73551	2.611	0.5	1.77	6.444	17.97	5.5448	44.948	4.0946	0.872
66	109040	GSPL/Bhuj/270/01/2025	23.21025	69.52410	BR	13.386	3.2233	14.86	113.4014	8.63	0.5	1.91	16.82	80.706	26.095	127.92	8.8244	1.3818
67	109041	GSPL_Bhuj_270/01/2025	23.21025	69.52410	BR	35.4948	2.2356	15.18	92.67057	26.52	0.5	2.62	66.62	45.273	36.429	243.8	23.821	0.6573
68	109042	GSPL/Bhuj/271/01/2025	23.19749	69.52979	BR	6.40129	0.6965	1.127	9.263774	2.303	0.5	0.91	12.15	22.794	4.5756	25.02	1.7183	0.6928
69	109043	GSPL/Bhuj/273/01/2025	23.20362	69.52684	BR	6.28921	0.7377	3.266	29.28731	3.542	0.5	1.35	17.89	48.807	11.513	179.72	23.627	0.7681
70	109046	GSPL_Bhuj_274/01/2025	23.19181	69.58950	BR	27.9903	2.4405	31.98	234.2531	10.53	0.5	3.96	31.27	178.76	109.84	114.22	7.7097	4.4469
71	109047	GSPL/Bhuj/274/01/2025	23.19181	69.58950	BR	6.77892	0.5	3.147	34.46561	3.718	0.5	1.6	29.21	305.46	8.9796	136.05	7.5399	0.6694
72	109048	GSPL/Bhuj/274/01/2025	23.19180	69.58950	BR	6.78524	0.7168	5.006	77.646	4.285	0.5	2.78	25.56	364.87	16.068	248.7	11.023	0.9801
73	109049	GSPL_Bhuj_276/01/2025	23.20940	69.52536	BR	6.93634	0.5	3.025	3.970763	1.663	0.5	1	9.92	22.822	4.2486	22.962	0.5569	0.9333
74	109050	GSPL/Bhuj/276/01/2025	23.20940	69.52536	BR	14.0865	0.5	0.609	7.055211	1.975	0.5	0.98	5.542	12.405	3.8197	33.815	0.5	0.7542
75	109051	GSPL_Bhuj_ 277/01/2025	23.20950	69.52221	BR	6.79997	0.954	2.053	15.88523	2.715	0.5	1.47	12.59	55.575	11.61	56.802	6.551	1.7138
76	109052	GSPL_Bhuj_ 278/01/2025	23.21039	69.52387	BR	8.17131	0.5341	1.94	8.012665	1.838	0.5	0.5	10.82	29.378	3.8217	23.187	0.7829	0.6941
77	109058	GSPL_Bhuj_277/01/2025	23.20950	69.52221	BR	27.1847	1.3888	10.66	48.72197	16.86	0.5	0.5	56.6	98.169	21.744	207.1	18.026	0.5
78	109060	GSPL_Bhuj_293/01/2025	23.20096	69.63083	BR	5.63492	0.7122	1.515	9.34263	2.773	0.5	1.38	14.77	43.105	3.291	29.343	1.4612	0.5
79	189111	GSPL-Bhuj-173/11/2024	23.16671	69.64349	BR	17.7849	1.9337	5.12	16.79839	14.27	0.5	3.03	62.39	1242.7	23.063	82.198	3.8867	0.5
80	189112	GSPL-Bhuj-174/11/2024	23.16561	69.64349	BR	62.1474	1.6206	19.75	122.4402	19.47	0.5	2.54	86.58	145.66	21.003	132.33	9.3531	0.9363
81	109045	GSPL_Bhuj_274/01/2025	23.19181	69.58950	BR	41.53	<0.5	8.45	47	6.60	<0.5	<0.5	23.21	236	16.70	250	8.78	1.52
82	109053	GSPL_Bhuj_279/01/2025	23.22131	69.58954	BR	24.96	<0.5	11.59	58	20.43	<0.5	<0.5	18.47	76	22.69	199	16.89	3.74
83	109054	GSPL_Bhuj_277/01/2025	23.20950	69.52221	BR	7.89	0.96	3.00	23	3.39	<0.5	<0.5	1.52	21	5.36	31	1.66	5.50
84	109055	GSPL_Bhuj_280/01/2025	23.20316	69.62894	BR	7.23	<0.5	3.57	17	3.72	<0.5	0.84	9.80	24	6.99	29	<0.5	1.34
85	109056	GSPL_Bhuj_281/01/2025	23.22556	69.54979	BR	34.63	4.51	30.46	422	29.49	<0.5	1.30	16.14	556	65.87	145	10.98	1.76
86	109057	GSPL_Bhuj_283/01/2025	23.23284	69.52792	BR	6.01	0.96	3.45	89	7.54	<0.5	<0.5	13.98	56	14.47	156	5.23	<0.5

Sl No.	Sample ID	Location No.	Latitude	Longitude	Sample Type	Li	Be	Sc	V	Ga	Ge	Se	Rb	Sr	Y	Zr	Nb	Mo
87	109061	GSPL_Bhuj_290/02/2025	23.20096	69.63083	BR	19.20	0.93	11.25	86	14.22	<0.5	1.96	21.37	286	66.07	52	2.90	2.70
88	109062	GSPL_Bhuj_290/02/2025	23.20096	69.63083	BR	20.59	0.82	7.46	60	8.67	<0.5	2.82	31.66	189	18.70	56	3.36	<0.5
89	109063	GSPL_Bhuj_289/01/2025	23.20370	69.62840	BR	8.67	<0.5	1.76	19	6.68	<0.5	<0.5	1.03	8	6.18	75	2.15	<0.5
90	109064	GSPL_Bhuj_289/01/2025	23.20370	69.62840	BR	19.32	0.69	20.52	113	30.30	<0.5	1.34	5.51	21	36.39	446	28.03	1.50
91	109065	GSPL_Bhuj_289/01/2025	23.20370	69.62840	BR	4.48	2.99	5.84	119	5.01	<0.5	<0.5	0.84	8	7.90	34	1.34	2.10
92	109066	GSPL_Bhuj_290/02/2025	23.20096	69.63083	BR	22.56	0.99	11.93	50	13.25	<0.5	0.78	31.10	315	56.59	37	3.72	0.69
93	109067	GSPL_Bhuj_292_02_2025	23.20103	69.63058	BR	5.73	<0.5	2.56	13	5.56	<0.5	<0.5	15.15	42	3.76	35	1.55	0.92
94	109068	GSPL_Bhuj_295/02/2025	23.19505	69.57110	BR	23.50	2.78	87.86	518	25.48	<0.5	1.66	<0.5	58	62.77	134	5.78	1.28
95	109069	GSPL_Bhuj_289/02/2025	23.20370	69.62840	BR	2.90	3.96	9.52	266	7.62	<0.5	6.83	0.62	14	15.58	78	1.49	6.10
96	109070	GSPL_Bhuj_289/02/2025	23.20370	69.62840	BR	2.45	0.54	2.16	17	6.10	<0.5	<0.5	13.73	38	4.14	38	2.11	1.12
97	109071	GSPL_Bhuj_289/02/2025	23.20370	69.62840	BR	12.26	1.34	3.03	33	9.66	<0.5	<0.5	1.87	26	8.00	73	5.11	<0.5
98	112451	GSPL_BHUJ_296/07/2025	23.16052	69.68694	BR	9.35	1.35	20.40	153.53	15.13	0.23	1.81	16.26	256.54	54.23	72.51	18.71	0.78
99	112466	GSPL_BHUJ_324/07/2025	23.19268	69.51791	BR	47.90	2.61	84.36	519.61	44.62	0.26	0.77	<0.1	70.47	43.55	112.71	66.80	6.13
100	112492	GSPL-BHUJ 351/07/2025	23.22263	69.59411	BR	12.95	2.09	9.34	234.09	19.47	0.38	<0.1	1.65	36.24	9.22	74.83	19.06	3.56
101	112493	GSPL-BHUJ 351/07/2025	23.22263	69.59411	BR	22.93	0.62	3.76	40.12	5.23	0.14	<0.1	30.36	153.95	6.96	79.75	20.27	0.51
102	112493	GSPL_BHUJ _351/07/25	23.22263	69.59411	BR	11.98	0.53	4.30	48.31	6.69	<0.1	<0.1	<0.1	247.74	7.94	114.12	9.96	0.67
103	112494	GSPL-BHUJ 351/07/2025	23.22263	69.59411	BR	66.65	3.82	64.10	633.40	38.83	0.45	<0.1	17.40	173.49	19.62	276.82	116.43	1.60
104	112495	GSPL-BHUJ 351/07/2025	23.22263	69.59411	BR	49.11	1.01	4.84	55.50	8.13	0.10	<0.1	98.77	75.74	6.70	88.41	22.05	0.78
105	112459	GSPL_BHUJ _313/07/2025	23.20322	69.62856	BR	4.99	9.44	4.62	24.30	28.82	0.83	<0.1	<0.1	13.01	14.86	43.01	6.32	1.37
106	112460	GSPL_BHUJ _319/07/2025	23.19757	69.52979	BR	5.20	0.92	1.83	15.42	28.33	0.91	0.11	4.63	34.94	5.41	48.35	7.67	0.33
107	112461	GSPL_BHUJ _320/07/25	23.20134	69.53626	BR	5.40	0.88	2.90	16.24	14.38	0.48	1.21	12.86	25.01	3.67	60.86	9.33	0.70
108	112462	GSPL_BHUJ _321/07/25	23.20306	69.53573	BR	8.48	2.59	7.95	57.42	34.89	0.93	<0.1	22.31	70.73	21.16	234.67	8.46	1.10

Sl No.	Sample ID	Location No.	Latitude	Longitude	Sample Type	Li	Be	Sc	V	Ga	Ge	Se	Rb	Sr	Y	Zr	Nb	Mo
109	112463	GSPL_BHUJ _322/07/25	23.19357	69.51865	BR	8.54	0.33	1.57	15.18	4.95	<0.1	0.66	16.72	24.86	3.70	67.29	24.94	0.72
110	112464	GSPL_BHUJ _322/07/25	23.19357	69.51865	BR	6.01	0.63	2.90	21.64	13.14	0.40	<0.1	9.12	50.39	5.38	68.77	11.92	1.06
111	112478	GSPL_BHUJ _336/07/2025	23.17271	69.62487	BR	3.79	1.19	4.64	71.93	17.15	0.36	3.13	16.35	123.02	11.74	107.45	9.24	1.92
112	112479	GSPL_BHUJ _337/07/2025	23.17199	69.62476	BR	4.67	1.49	5.04	57.84	20.13	0.33	<0.1	17.03	197.01	9.32	100.98	5.21	3.92
113	112480	GSPL_BHUJ _338/07/2025	23.17020	69.62394	BR	4.33	1.71	7.15	63.81	25.08	0.34	4.92	16.49	144.02	14.03	128.14	3.88	1.09
114	112481	GSPL_BHUJ _338/07/2025	23.17020	69.62394	BR	5.12	1.65	3.88	44.72	20.64	0.53	5.96	17.67	130.50	13.58	122.54	7.30	0.61
115	112484	GSPL_BHUJ _344/07/2025	23.19073	69.69641	BR	8.51	1.70	8.70	165.91	41.35	1.20	1.01	<0.1	233.96	44.42	81.43	3.73	1.77
116	112488	GSPL_BHUJ _348/07/25	23.19432	69.58188	BR	7.21	3.94	9.27	113.26	17.13	0.54	1.65	2.16	54.69	15.49	70.26	6.94	3.39
117	112496	GSPL_BHUJ _353/07/25	23.22200	69.59442	BR	6.15	6.64	15.05	535.34	35.70	0.94	<0.1	<0.1	49.98	39.86	262.71	10.93	5.73
118	112498	GSPL_BHUJ _ 358/07/25	23.19465	69.58041	BR	6.26	4.47	12.53	36.29	25.98	0.92	<0.1	<0.1	29.92	11.87	47.89	7.90	7.77
119	107550	GSPL-Bhuj-162/06/24	23.2238383	69.5243767	Fragment of river transported detrital	<0.5	<0.5	<0.5	0.9742	0.647	<0.5	<0.5	<0.5	1.8897	<0.5	<0.5	<0.5	13.434
120	107554	GSPL-Bhuj-164/06/24	23.2209667	69.590355	Bulk Sample	8.23821	0.5281	34.03	274.0224	15.62	<0.5	0.92	31.67	341.83	25.531	124.37	19.684	1.4344
121	107556	GSPL-Bhuj-165/06/24	23.221095	69.5898417	Scree deposit	47.5302	2.0404	41.41	191.7366	29.06	<0.5	1.18	2.658	291.97	20.221	189.8	15.542	<0.5

Table Continued..

Annexure-XXI

Sl No.	Sample ID	Cd	In	Cr	Co	Ni	Cu	Zn	Sn	Sb	Te	Cs	Ba	La	Ce	Pr	Nd	Sm	Eu
1	105567	<0.5	<0.5	NA	NA	NA	NA	NA	1.4	2.1	<0.5	0.7	NA	78.2	186.5	19.5	70.4	12.7	1.9
2	107476	<0.5	<0.5	77.9	39.3	80.1	28.5	199.9	1.4	0.9	<0.5	2.4	220.3	20.5	50.9	5.9	24.3	5.5	1.4
3	107510	<0.5	<0.5	34.3	76.7	10.7	2.2	61.3	0.5	<0.5	<0.5	<0.5	126.9	22.2	65.0	6.6	26.2	5.4	1.3
4	107516	<0.5	<0.5	13.9	135.3	28.9	4.8	16.9	1.1	0.5	<0.5	1.1	306.9	21.6	48.4	4.3	15.1	2.5	0.6
5	107518	<0.5	<0.5	44.9	31.8	28.0	11.5	64.6	2.2	0.6	<0.5	0.7	168.5	38.5	138.2	14.0	61.2	14.1	3.7
6	107541	1.1	<0.5	57.3	239.8	254.7	18.6	376.9	22.1	17.7	<0.5	1.2	748.8	52.3	110.8	12.4	49.8	9.3	1.6
7	107542	<0.5	<0.5	40.7	39.7	5.7	2.3	12.6	0.5	<0.5	<0.5	<0.5	127.7	22.6	47.9	5.1	18.2	3.2	<0.5
8	107543	<0.5	<0.5	70.9	67.9	92.3	32.0	161.0	3.0	<0.5	<0.5	1.0	810.6	45.0	95.7	11.8	48.9	9.9	3.5
9	107546	<0.5	<0.5	29.8	51.6	41.8	5.1	91.2	<0.5	<0.5	<0.5	<0.5	98.2	20.3	42.6	4.7	17.5	3.3	0.7
10	107551	<0.5	<0.5	36.0	119.6	6.7	1.4	10.9	0.9	<0.5	<0.5	<0.5	87.2	15.6	33.0	3.6	12.8	2.4	<0.5
11	107561	<0.5	<0.5	78.9	123.2	41.3	8.4	63.4	1.1	<0.5	<0.5	0.7	1485.2	29.9	80.6	8.1	29.1	5.0	1.3
12	107555	<0.5	<0.5	48.1	100.5	81.1	16.4	99.1	0.9	<0.5	<0.5	<0.5	78.0	16.4	33.2	3.7	13.4	2.6	<0.5
13	107565	<0.5	<0.5	24.2	254.4	128.2	6.2	180.7	0.7	<0.5	<0.5	<0.5	1460.8	22.5	59.7	7.6	36.4	9.7	3.9
14	107566	<0.5	<0.5	36.6	209.7	95.7	3.2	381.5	0.6	<0.5	<0.5	<0.5	158.3	3.9	14.0	1.9	9.7	3.1	1.4
15	107567	<0.5	<0.5	32.9	62.7	15.0	20.8	144.5	<0.5	<0.5	<0.5	<0.5	123.2	3.2	5.6	1.1	4.4	1.0	<0.5
16	107568	<0.5	<0.5	54.9	43.9	7.1	4.5	50.4	0.7	<0.5	<0.5	<0.5	235.3	27.9	62.3	5.8	20.7	3.6	0.6
17	107569	<0.5	<0.5	55.4	66.7	51.7	5.7	55.8	1.6	<0.5	<0.5	<0.5	221.1	32.0	67.3	7.6	30.0	6.3	1.1
18	107570	<0.5	<0.5	34.0	82.0	14.0	6.9	16.0	0.6	<0.5	<0.5	0.7	66.2	13.2	28.5	3.1	11.8	2.1	<0.5
19	107571	<0.5	<0.5	85.1	56.0	27.9	9.0	131.4	1.4	<0.5	<0.5	1.1	431.1	48.9	99.9	11.0	39.5	7.1	0.9
20	107572	<0.5	<0.5	40.4	40.4	11.8	2.4	79.2	0.6	<0.5	<0.5	<0.5	248.5	10.7	26.4	2.4	8.1	1.4	<0.5

Sl No.	Sample ID	Cd	In	Cr	Co	Ni	Cu	Zn	Sn	Sb	Te	Cs	Ba	La	Ce	Pr	Nd	Sm	Eu
21	107573	<0.5	<0.5	57.2	45.4	27.2	5.1	46.9	0.9	<0.5	<0.5	0.9	126.3	34.0	95.8	10.3	42.6	9.3	2.3
22	107574	<0.5	<0.5	82.1	74.0	67.6	15.3	92.0	1.3	0.5	<0.5	1.0	197.0	22.4	49.9	6.2	24.5	5.1	1.2
23	107575	<0.5	<0.5	91.9	103.6	113.6	16.1	223.8	1.9	<0.5	<0.5	1.2	453.6	39.0	84.4	9.6	36.7	7.9	1.8
24	107576	<0.5	<0.5	50.3	71.1	11.7	5.6	16.1	1.0	<0.5	<0.5	<0.5	119.4	17.0	34.2	3.7	13.2	2.4	0.5
25	107577	<0.5	<0.5	28.2	105.0	21.2	4.0	37.0	1.1	<0.5	<0.5	<0.5	251.4	6.5	12.9	1.5	5.6	1.1	<0.5
26	107578	<0.5	<0.5	42.4	43.6	47.3	3.8	119.0	0.6	<0.5	<0.5	<0.5	146.0	20.3	42.9	4.8	18.2	3.4	0.7
27	107579	<0.5	<0.5	99.6	53.4	47.9	17.3	119.0	2.4	<0.5	<0.5	2.2	591.4	26.0	54.8	6.5	25.9	5.3	1.5
28	107580	<0.5	<0.5	71.1	79.2	39.0	17.0	142.1	2.9	0.5	<0.5	2.8	541.2	30.3	64.3	7.6	29.6	6.2	1.6
29	107581	<0.5	<0.5	74.5	51.9	41.0	16.5	76.0	2.3	<0.5	<0.5	1.4	583.8	17.8	39.5	5.0	20.6	4.9	1.4
30	107582	<0.5	<0.5	60.3	51.4	17.0	16.5	56.1	2.2	<0.5	<0.5	1.2	602.2	20.5	43.4	4.9	18.7	3.6	0.9
31	107511	<0.5	<0.5	55.2	54.7	19.9	6.1	59.0	1.2	<0.5	<0.5	0.8	151.0	26.3	67.8	7.0	27.9	5.8	1.5
32	107535	<0.5	<0.5	96.047	18.56162	31.532	25.462	79.9937	2.2045	0.52639	<0.5	5.2936	305.236	29.9043	66.22395	7.3226	27.603	5.333	1.07178
33	107536	<0.5	<0.5	53.771	43.61363	<0.5	0.9486	<0.5	<0.5	<0.5	<0.5	<0.5	290.826	20.5093	51.97248	5.2925	19.429	3.356	0.5889
34	107559	<0.5	<0.5	83.9	47.1	<0.5	5.0	17.9	1.6	1.2	<0.5	1.5	261.2	27.7	61.7	6.4	23.2	4.2	0.7
35	107562	<0.5	<0.5	102.9	57.5	<0.5	8.4	32.7	3.3	<0.5	<0.5	2.4	276.1	31.4	67.5	7.2	25.7	4.3	0.7
36	107563	<0.5	<0.5	84.9	77.9	2.6	3.9	40.4	1.8	<0.5	<0.5	0.8	394.7	29.5	66.1	7.1	25.7	4.7	0.7
37	105622	<0.5	<0.5	NA	NA	NA	NA	NA	2.8	1.0	<0.5	4.2	NA	143.0	407.5	51.4	229.4	59.0	16.2
38	109059	0.5	0.5	21.693	28.89584	21.917	2.4359	31.2322	0.5	0.5	0.5	0.5	146.298	3.07793	6.319241	0.7078	2.66899	0.562	0.5
39	109006	0.7	<0.5	99.8	22.9	62.4	48.3	53.6	2.2	2.4	<0.5	21.9	348.3	19.4	37.9	4.5	18.4	5.0	<0.5
40	109007	<0.5	<0.5	78.5	11.0	43.9	40.3	119.0	2.0	1.7	<0.5	2.1	318.2	2.0	4.3	<0.5	1.3	<0.5	<0.5
41	109009	<0.5	<0.5	76.4	15.5	41.1	32.8	38.8	2.0	3.0	<0.5	24.5	303.2	7.2	17.1	1.8	7.6	2.2	6.5
42	109011	1.9	<0.5	104.4	23.2	64.2	51.6	66.3	3.1	2.0	<0.5	31.6	473.2	12.4	30.1	3.5	14.9	4.2	1.2

Sl No.	Sample ID	Cd	In	Cr	Co	Ni	Cu	Zn	Sn	Sb	Te	Cs	Ba	La	Ce	Pr	Nd	Sm	Eu
43	109015	<0.5	<0.5	33.0	7.0	12.0	3.9	17.9	1.4	3.5	<0.5	27.0	250.2	11.6	26.0	2.9	10.4	2.5	4.3
44	109016	<0.5	<0.5	90.9	12.4	24.6	4.6	27.2	4.0	1.6	<0.5	1.3	135.3	10.7	22.2	2.1	7.1	1.2	<0.5
45	109017	<0.5	<0.5	70.5	9.8	26.4	8.4	55.4	1.8	1.9	<0.5	3.0	558.7	6.6	13.4	1.5	5.8	1.2	<0.5
46	109018	0.7	<0.5	85.2	14.7	27.2	2	28.3	2.6	1.7	<0.5	11	1152.2	8.8	16.8	2	7.8	1.7	<0.5
47	109019	<0.5	<0.5	64.1	4.6	15.1	3.6	17.3	1.7	1.6	<0.5	4.6	369.6	3.6	7.2	0.5	2.8	<0.5	<0.5
48	109020	<0.5	<0.5	72.7	2.8	7.3	2.3	13.8	1.9	1.7	<0.5	4.2	317.7	1.9	4.4	<0.5	1.4	<0.5	<0.5
49	109021	0.5	0.5	46.015	48.06103	100.44	15.713	144.776	0.5	0.5	0.5	0.5	96.9007	8.42749	35.09081	3.7174	14.8145	3.257	0.81298
50	109022	0.5	0.5	90.457	59.29279	86.009	13.783	185.873	0.5	0.5	0.5	0.5	990.226	48.5292	119.2235	12.356	46.9815	10.36	2.17036
51	109023	0.5	0.5	30.492	64.53105	92.202	20.04	153.087	0.5	0.5	0.5	0.5	30.912	4.55421	10.13166	1.217	4.95126	1.282	0.5
52	109024	0.5	0.5	28.046	50.15073	51.908	11.219	60.8962	0.5	0.5	0.5	0.5	224.712	25.8957	53.89249	5.8026	20.3531	3.522	0.5
53	109026	0.5	0.5	33.349	13.08098	8.1126	7.0836	7.83168	0.5	0.58378	0.5	0.5	65.9733	6.20051	12.0677	1.467	5.4329	1.108	0.5
54	109027	0.5	0.5	26.677	33.61063	10.769	8.8236	2.93157	0.5	0.5	0.5	0.5	185.882	7.52141	15.64311	1.7686	6.22409	1.174	0.5
55	109028	0.5	0.5	48.156	25.97512	9.8677	5.7557	130.918	0.5	0.5	0.5	0.5	1251.65	15.4523	34.16446	3.5608	12.3558	2.373	0.73319
56	109029	0.5	0.5	58.66	31.82192	4.093	3.7887	20.0473	0.5	0.5	0.5	0.5	255.341	16.9548	40.87144	4.3645	16.9417	3.611	0.81264
57	109031	0.5	0.5	123.75	4.467877	9.1518	34.759	26.108	0.5	0.5	0.5	3.4315	163.295	33.31	62.23289	6.6909	23.3314	4.424	0.81175
58	109032	0.5	0.5	43.14	52.25101	11.873	4.228	40.4189	0.5	0.5	0.5	0.5	104.809	3.59208	8.426715	0.9916	3.75336	0.838	0.5
59	109033	0.5	0.5	39.374	20.90128	7.6768	2.9023	36.2343	0.5	0.5	0.5	0.5	5738.94	6.29218	13.44412	1.5405	5.59906	1.16	1.49852
60	109034	0.5	0.5	33.779	28.96333	13.291	2.238	16.621	0.5	0.5	0.5	0.5	218.102	7.04291	15.35704	1.6826	6.18134	1.202	0.5
61	109035	0.5	0.5	44.611	21.22665	21.611	7.0054	20.6096	0.5	0.5	0.5	0.5	430.95	22.5165	49.31977	5.4038	19.5699	3.719	0.86651
62	109036	0.5	0.5	63.262	29.46588	8.9111	1.207	2.42536	1.1232	0.5	0.5	0.5	166.831	4.36336	8.87255	1.0052	3.58117	0.724	0.5
63	109037	0.5	0.5	28.572	69.92897	5.9018	1.614	4.43167	0.5	0.50426	0.5	0.5	139.897	6.56484	13.82128	1.5735	5.61931	1.033	0.5
64	109038	0.5	0.5	78.226	4.043535	12.281	16.267	9.80826	4.8242	0.5	0.5	2.8989	231.923	45.7573	101.0545	11.287	40.8409	7.767	1.39547

Sl No.	Sample ID	Cd	In	Cr	Co	Ni	Cu	Zn	Sn	Sb	Te	Cs	Ba	La	Ce	Pr	Nd	Sm	Eu
65	109039	0.5	0.5	16.444	40.69617	15.743	2.1585	33.3714	0.5	0.60079	0.5	0.5	103.392	11.1791	24.56941	2.7824	9.82279	1.747	0.5
66	109040	0.5	0.5	52.885	55.63994	82.446	21.637	280.396	0.5	0.57294	0.5	0.5697	454.238	21.0467	43.71246	4.8616	17.7136	3.642	0.77096
67	109041	0.5	0.5	46.759	8.525303	14.931	24.302	24.1629	0.5	0.5	0.5	5.4956	151.593	58.6125	134.0597	14.119	50.9862	10.04	2.16491
68	109042	0.5	0.5	41.974	39.00717	7.8571	2.5495	8.95168	0.5	0.56879	0.5	0.5	593.431	4.24872	9.774258	1.1271	4.1944	0.895	0.5
69	109043	0.5	0.5	38.493	30.06967	21.79	4.7169	23.9096	0.5	0.5	0.5	0.5	256.311	28.7318	60.02714	6.4543	22.4393	4.006	0.55704
70	109046	0.5	0.5	56.74	13.00825	105.29	44.579	157.132	0.5	3.42184	0.5	2.0794	103.91	56.7953	167.3693	18.372	79.0998	20.54	4.60918
71	109047	0.5	0.5	27.412	10.31611	8.5644	3.9402	31.8441	0.5	0.73666	0.5	0.5	229.731	18.7577	43.21737	4.4678	16.2912	3.205	0.5
72	109048	0.5	0.5	42.338	15.10523	22.237	9.1084	37.341	0.5	0.5	0.5	0.554	208.635	24.9854	54.57758	5.6803	20.5357	4.148	0.60409
73	109049	0.5	0.5	37.969	44.26216	23.683	2.1464	40.3915	0.5	0.5914	0.5	0.5	100.707	3.72419	8.161355	0.9406	3.48159	0.708	0.5
74	109050	0.5	0.5	14.058	44.19832	6.6812	3.1221	14.2313	1.2086	0.5	0.5	0.5	72.9804	5.06026	10.20513	1.1781	4.42984	0.942	0.5
75	109051	0.5	0.5	44.128	29.897	14.959	9.0826	64.6304	0.5	0.5	0.5	0.5	329.916	14.7482	33.96888	3.6151	13.1208	2.551	0.65884
76	109052	0.5	0.5	18.911	30.52514	26.137	8.147	22.4366	0.5	0.5	0.5	0.5	134.783	3.72458	8.170383	0.9397	3.50474	0.747	0.5
77	109058	0.5	0.5	6.4724	4.844942	5.9344	14.354	8.39165	3.1098	0.5	0.5	1.8576	375.795	50.7734	114.9924	12.952	46.5753	8.778	1.60184
78	109060	0.5	0.5	20.586	25.68195	15.107	1.9187	14.6103	0.5	0.5	0.5	0.5	175.107	5.49084	11.06806	1.1794	4.20146	0.847	0.5
79	189111	0.5	0.5	16.712	3.275616	4.315	10.184	20.0819	3.5026	0.5	0.5	4.1743	5094.89	50.2535	78.69131	10.602	38.1952	7.13	2.22298
80	189112	0.5	0.5	81.112	26.31564	98.323	62.837	117.795	0.5	0.57829	0.5	6.0712	200.641	19.9947	45.40624	5.0723	19.5365	4.381	0.9275
81	109045	<0.5	<0.5	131	3.84	11	8	24	<0.5	<0.5	<0.5	<0.5	203	45.10	96.47	11.56	43.72	7.53	0.94
82	109053	<0.5	<0.5	149	3.52	17	26	17	35.41	0.91	<0.5	0.67	244	43.73	82.30	9.64	32.55	5.60	1.26
83	109054	<0.5	<0.5	306	22.07	106	11	98	<0.5	<0.5	<0.5	<0.5	37	7.32	14.63	1.54	5.67	0.90	<0.5
84	109055	<0.5	<0.5	131	18.86	46	10	78	<0.5	<0.5	<0.5	<0.5	138	4.81	10.51	1.33	6.39	1.23	0.51
85	109056	<0.5	<0.5	203	115.63	86	13	128	<0.5	<0.5	<0.5	1.02	2215	79.93	221.08	23.72	85.61	19.03	7.23
86	109057	<0.5	<0.5	263	25.44	60	<5	141	<0.5	<0.5	<0.5	<0.5	198	19.52	33.75	5.35	23.75	3.87	1.03

Sl No.	Sample ID	Cd	In	Cr	Co	Ni	Cu	Zn	Sn	Sb	Te	Cs	Ba	La	Ce	Pr	Nd	Sm	Eu
87	109061	<0.5	<0.5	29	7.82	26	7	49	18.65	<0.5	<0.5	1.47	63	39.88	124.17	14.75	68.18	14.07	3.86
88	109062	<0.5	<0.5	44	6.44	16	11	35	<0.5	<0.5	<0.5	2.25	68	16.50	52.07	5.47	21.70	4.63	1.01
89	109063	<0.5	<0.5	60	4.55	10	9	16	<0.5	<0.5	<0.5	<0.5	27	28.02	55.26	6.59	25.27	3.79	<0.5
90	109064	<0.5	<0.5	233	9.06	28	18	36	<0.5	<0.5	<0.5	<0.5	135	150.95	303.47	35.22	119.76	24.65	1.95
91	109065	<0.5	<0.5	183	7.15	29	<5	91	<0.5	<0.5	<0.5	<0.5	24	8.10	13.49	1.73	7.93	2.21	0.63
92	109066	<0.5	<0.5	21	7.70	21	13	34	<0.5	<0.5	<0.5	2.21	90	42.26	129.17	14.88	61.87	12.66	3.17
93	109067	<0.5	<0.5	336	12.90	24	<5	21	<0.5	<0.5	<0.5	<0.5	217	6.11	13.81	1.51	5.63	0.99	<0.5
94	109068	<0.5	<0.5	272	30.21	121	40	384	<0.5	<0.5	<0.5	<0.5	227	7.13	23.89	3.73	17.22	5.19	2.42
95	109069	<0.5	<0.5	280	13.16	62	13	136	<0.5	<0.5	<0.5	<0.5	28	5.89	11.97	2.06	12.43	3.86	1.57
96	109070	<0.5	<0.5	137	7.27	16	<5	15	<0.5	<0.5	<0.5	<0.5	152	7.63	16.38	1.85	6.70	1.16	<0.5
97	109071	<0.5	<0.5	112	7.91	11	<5	11	1.63	<0.5	<0.5	<0.5	67	13.56	29.82	3.22	12.01	2.10	<0.5
98	112451	2.82	6.98	100.00	14.63	47.31	4.90	98.66	28.12	4.86	NA	<0.1	559.59	35.11	81.28	22.28	15.59	11.40	2.44
99	112466	4.59	12.88	281.09	60.14	127.89	264.56	148.79	86.05	12.31	NA	2.57	226.37	4.68	0.14	31.69	55.67	7.87	2.48
100	112492	3.70	9.47	175.35	7.16	40.61	10.13	81.95	52.84	8.46	NA	<0.1	28.00	11.89	18.28	24.96	15.89	5.81	1.04
101	112493	1.70	1.90	157.50	6.10	3.06	4.12	19.93	58.20	0.30	NA	13.48	38.28	20.59	37.41	3.58	16.89	2.36	0.49
102	112493	1.40	1.24	178.92	5.06	5.97	6.66	24.52	69.53	3.13	NA	10.26	61.84	21.72	45.32	3.84	19.96	2.90	0.59
103	112494	3.32	11.13	165.54	21.21	64.34	83.76	84.60	48.41	7.33	NA	33.55	64.87	39.00	92.92	26.62	97.03	11.41	3.83
104	112495	1.27	1.19	1779.13	10.60	14.44	27.47	16.52	672.29	10.74	NA	27.75	45.32	37.07	83.24	8.60	18.38	5.11	1.29
105	112459	4.12	14.64	119.14	9.34	32.07	5.80	166.15	18.06	11.51	NA	<0.1	30.63	4.71	6.84	28.20	7.61	8.30	1.58
106	112460	4.50	15.46	146.21	9.89	19.05	0.72	29.64	51.19	12.48	NA	<0.1	222.78	5.87	9.43	29.34	7.36	6.55	0.43
107	112461	2.52	6.90	164.71	8.94	17.82	0.54	31.19	56.40	7.11	NA	1.63	114.48	5.34	11.47	13.95	7.44	2.75	0.40
108	112462	4.44	15.37	147.36	30.18	54.12	7.75	124.65	27.55	10.55	NA	14.69	391.94	47.60	105.75	34.23	47.74	13.70	1.14

Sl No.	Sample ID	Cd	In	Cr	Co	Ni	Cu	Zn	Sn	Sb	Te	Cs	Ba	La	Ce	Pr	Nd	Sm	Eu
109	112463	1.43	0.38	450.74	6.69	11.52	3.38	27.17	181.35	4.33	NA	2.56	125.01	6.82	15.23	2.05	7.89	0.62	0.27
110	112464	2.62	7.07	209.64	17.50	32.75	5.02	71.76	75.37	6.60	NA	4.56	190.93	9.39	16.43	14.07	11.05	3.81	0.41
111	112478	3.37	7.91	175.71	47.62	115.80	7.37	147.77	61.33	8.35	NA	2.34	571.22	16.54	32.81	17.35	17.46	5.19	0.51
112	112479	3.35	10.88	95.99	97.22	148.48	2.38	160.44	31.45	8.92	NA	2.96	833.14	18.08	39.35	23.43	16.68	6.98	0.60
113	112480	4.83	13.49	83.09	154.50	207.14	2.87	342.06	26.66	10.15	NA	2.72	974.95	20.54	41.92	28.40	20.19	8.10	0.59
114	112481	4.03	10.82	144.55	206.86	271.30	3.79	352.34	50.61	9.90	NA	3.05	965.34	18.19	47.80	24.28	18.64	6.96	0.50
115	112484	4.88	20.30	58.97	13.32	31.55	5.71	70.62	<0.1	13.66	NA	5.53	169.26	46.91	108.35	46.29	45.82	18.74	2.59
116	112488	3.38	8.78	118.7	120.73	207.48	168.55	263.11	39.54	7.89	NA	1.92	897.19	8.2	14.21	16.26	9.65	4.01	0.83
117	112496	4.26	15.20	166.12	69.21	66.37	134.39	105.36	49.02	11.11	NA	27.34	54.56	52.28	99.21	38.86	95.85	30.10	7.19
118	112498	3.35	11.52	136.97	34.20	179.13	47.67	143.27	46.34	9.66	NA	1.10	80.33	23.43	57.99	26.86	20.56	7.08	0.73
119	107550	<0.5	<0.5	63.038	1084.767	<0.5	<0.5	<0.5	<0.5	3.93191	<0.5	<0.5	44.6991	<0.5	<0.5	<0.5	<0.5	<0.5	<0.5
120	107554	<0.5	<0.5	89.739	42.61144	48.327	151	93.5379	1.0106	<0.5	<0.5	1.0127	493.716	19.2435	41.22857	4.8134	19.596	4.366	1.32799
121	107556	<0.5	<0.5	154.59	71.87372	2.9732	13.437	16.7672	1.9253	1.54828	<0.5	<0.5	708.097	16.6614	39.49684	4.7054	18.9976	4.151	1.06529

Table Continued..

Annexure-XXI

Sl No.	Sample ID	Gd	Tb	Dy	Ho	Er	Tm	Yb	Lu	Hf	Ta	W	Tl	Pb	Bi	Th	U	P	Ti	B	Ag	Al
1	105567	10.1	1.4	6.6	1.2	3.2	<0.5	2.8	<0.5	3.5	0.8	NA	0.9	NA	<0.5	32.5	2.4	NA	NA	NA	NA	NA
2	107476	7.0	0.9	5.6	1.1	3.1	<0.5	2.8	<0.5	2.6	0.9	NA	<0.5	25.5	<0.5	11.8	2.7	NA	NA	NA	NA	NA
3	107510	6.4	0.9	5.1	1.0	2.7	<0.5	2.6	<0.5	<0.5	<0.5	NA	<0.5	13.0	<0.5	3.2	0.9	NA	NA	NA	NA	NA
4	107516	2.6	<0.5	1.3	<0.5	0.7	<0.5	0.7	<0.5	0.6	<0.5	NA	<0.5	43.8	<0.5	3.7	0.7	NA	NA	NA	NA	NA
5	107518	19.1	2.5	14.9	2.9	7.4	0.9	5.2	0.6	<0.5	<0.5	NA	<0.5	20.7	<0.5	5.6	3.5	NA	NA	NA	NA	NA
6	107541	10.2	1.2	6.1	1.1	3.0	<0.5	2.6	<0.5	6.0	3.3	NA	1.4	124.8	<0.5	28.6	4.3	NA	NA	NA	NA	NA
7	107542	3.4	<0.5	1.7	<0.5	0.9	<0.5	1.0	<0.5	5.2	<0.5	NA	<0.5	7.3	<0.5	14.7	1.8	NA	NA	NA	NA	NA
8	107543	11.1	1.3	6.9	1.2	2.9	<0.5	2.3	<0.5	9.0	5.8	NA	<0.5	6.1	<0.5	7.0	1.4	NA	NA	NA	NA	NA
9	107546	4.0	<0.5	2.4	0.5	1.3	<0.5	1.0	<0.5	1.7	<0.5	NA	<0.5	72.6	<0.5	13.1	1.8	NA	NA	NA	NA	NA
10	107551	2.6	<0.5	2.0	<0.5	1.0	<0.5	1.1	<0.5	2.7	<0.5	NA	<0.5	19.2	<0.5	11.3	1.3	NA	NA	NA	NA	NA
11	107561	4.9	<0.5	2.6	<0.5	1.4	<0.5	1.5	<0.5	5.7	<0.5	NA	<0.5	26.1	<0.5	11.8	1.8	NA	NA	NA	NA	NA
12	107555	3.1	<0.5	2.2	<0.5	1.1	<0.5	1.1	<0.5	1.3	<0.5	NA	<0.5	42.5	<0.5	13.3	2.8	NA	NA	NA	NA	NA
13	107565	13.5	1.6	8.3	1.5	3.4	<0.5	2.1	<0.5	0.5	<0.5	NA	3.3	11.6	<0.5	8.3	2.6	NA	NA	NA	NA	NA
14	107566	5.1	0.9	6.0	1.3	3.9	0.6	3.8	0.5	0.6	<0.5	NA	<0.5	13.0	<0.5	2.4	3.0	NA	NA	NA	NA	NA
15	107567	1.1	<0.5	0.8	<0.5	<0.5	<0.5	<0.5	<0.5	0.6	<0.5	NA	<0.5	7.8	<0.5	2.2	2.9	NA	NA	NA	NA	NA
16	107568	4.0	<0.5	2.5	<0.5	1.4	<0.5	1.6	<0.5	3.3	<0.5	NA	<0.5	8.8	<0.5	14.3	2.3	NA	NA	NA	NA	NA
17	107569	7.3	0.9	5.2	1.0	2.5	<0.5	2.4	<0.5	7.6	0.8	NA	<0.5	14.5	<0.5	20.5	2.5	NA	NA	NA	NA	NA
18	107570	2.2	<0.5	1.3	<0.5	0.6	<0.5	0.7	<0.5	2.1	<0.5	NA	<0.5	13.3	<0.5	7.9	1.1	NA	NA	NA	NA	NA
19	107571	7.2	0.8	3.7	0.7	1.9	<0.5	1.8	<0.5	6.7	0.8	NA	<0.5	22.9	<0.5	31.0	3.4	NA	NA	NA	NA	NA
20	107572	1.6	<0.5	1.1	<0.5	0.7	<0.5	0.7	<0.5	0.7	<0.5	NA	<0.5	12.0	<0.5	4.8	<0.5	NA	NA	NA	NA	NA

Sl No.	Sample ID	Gd	Tb	Dy	Ho	Er	Tm	Yb	Lu	Hf	Ta	W	Tl	Pb	Bi	Th	U	P	Ti	B	Ag	Al
21	107573	11.7	1.5	8.5	1.7	4.4	0.6	3.6	<0.5	<0.5	<0.5	NA	<0.5	13.4	<0.5	5.4	2.0	NA	NA	NA	NA	NA
22	107574	5.9	0.8	5.0	1.0	2.8	<0.5	2.8	<0.5	3.0	<0.5	NA	0.8	41.0	<0.5	7.5	2.4	NA	NA	NA	NA	NA
23	107575	9.3	1.3	7.4	1.5	4.1	0.6	4.3	0.6	4.9	0.6	NA	0.6	28.9	<0.5	20.1	4.4	NA	NA	NA	NA	NA
24	107576	2.6	<0.5	1.6	<0.5	0.9	<0.5	0.9	<0.5	2.6	<0.5	NA	<0.5	19.0	<0.5	9.9	3.4	NA	NA	NA	NA	NA
25	107577	1.4	<0.5	1.0	<0.5	0.6	<0.5	0.6	<0.5	1.0	<0.5	NA	6.8	11.9	<0.5	3.8	1.1	NA	NA	NA	NA	NA
26	107578	3.8	<0.5	2.5	0.5	1.4	<0.5	1.3	<0.5	2.7	<0.5	NA	1.5	13.7	<0.5	12.4	1.9	NA	NA	NA	NA	NA
27	107579	6.4	0.9	5.7	1.1	3.3	<0.5	3.1	<0.5	6.0	0.9	NA	1.0	26.0	<0.5	11.4	2.4	NA	NA	NA	NA	NA
28	107580	7.2	1.0	6.0	1.2	3.3	<0.5	3.1	<0.5	4.0	0.6	NA	0.9	31.2	<0.5	13.4	2.1	NA	NA	NA	NA	NA
29	107581	5.9	0.9	5.5	1.2	3.2	<0.5	2.8	<0.5	3.2	<0.5	NA	<0.5	21.5	<0.5	8.0	1.5	NA	NA	NA	NA	NA
30	107582	4.1	0.5	3.1	0.6	1.7	<0.5	1.6	<0.5	3.7	<0.5	NA	<0.5	20.7	<0.5	9.0	1.5	NA	NA	NA	NA	NA
31	107511	7.4	1.0	5.8	1.1	3.1	<0.5	2.7	<0.5	<0.5	<0.5	NA	<0.5	10.2	<0.5	6.1	1.4	NA	NA	NA	NA	NA
32	107535	4.12301	0.58054	3.17952	0.5752	1.5856	<0.5	1.6	<0.5	4.1888	0.94	NA	0.746	24.9376	<0.5	14.536	2.3406	NA	NA	NA	NA	NA
33	107536	2.40701	<0.5	1.56675	<0.5	0.6602	<0.5	0.7	<0.5	3.4319	<0.5	NA	<0.5	8.60927	<0.5	7.6803	1.1061	NA	NA	NA	NA	NA
34	107559	3.2	<0.5	2.7	0.5	1.6	<0.5	1.7	<0.5	8.1	0.8	NA	0.6	13.0	<0.5	14.8	2.3	NA	NA	NA	NA	NA
35	107562	3.2	<0.5	2.7	0.5	1.6	<0.5	1.8	<0.5	8.8	1.0	NA	0.6	13.4	<0.5	18.6	2.5	NA	NA	NA	NA	NA
36	107563	3.6	0.5	2.9	0.6	1.7	<0.5	1.9	<0.5	9.1	0.6	NA	0.5	13.7	<0.5	17.8	2.5	NA	NA	NA	NA	NA
37	105622	81.1	14.3	75.0	14.9	36.5	4.2	21.5	2.8	4.3	0.9	NA	0.5	NA	<0.5	12.5	5.5	NA	NA	NA	NA	NA
38	109059	0.5	0.5	0.5	0.5	0.5	0.5	0.5	0.5	1.0151	0.5	111	0.8203	177.608	0.5	1.8776	1.0307	NA	NA	NA	NA	NA
39	109006	7.2	1.6	11.2	2.5	6.9	0.9	4.5	0.6	1.8	1.4	1.5	<0.5	32.8	<0.5	2.1	3.3	NA	NA	NA	NA	NA
40	109007	<0.5	<0.5	<0.5	<0.5	<0.5	<0.5	<0.5	<0.5	1.7	<0.5	1.3	<0.5	58.6	<0.5	2.3	<0.5	NA	NA	NA	NA	NA
41	109009	2.9	0.7	5.0	1.1	3.4	0.5	2.8	<0.5	1.5	1.8	1.7	<0.5	20.2	<0.5	1.9	2.4	NA	NA	NA	NA	NA
42	109011	5.4	1.0	7.0	1.5	3.9	<0.5	2.5	<0.5	2.0	1.8	1.4	<0.5	54.4	0.6	2.6	3.2	NA	NA	NA	NA	NA

Sl No.	Sample ID	Gd	Tb	Dy	Ho	Er	Tm	Yb	Lu	Hf	Ta	W	Tl	Pb	Bi	Th	U	P	Ti	B	Ag	Al
43	109015	2.8	0.5	3.5	0.8	2.2	<0.5	1.8	<0.5	3.0	1.6	1.4	<0.5	20.7	<0.5	3.7	3.1	NA	NA	NA	NA	NA
44	109016	1.2	<0.5	2.2	0.5	1.8	<0.5	2.2	<0.5	3.6	1.6	1.3	<0.5	43.6	<0.5	7.2	1.2	NA	NA	NA	NA	NA
45	109017	1.2	<0.5	1.9	<0.5	1.1	<0.5	0.9	<0.5	3.0	1.0	1.4	<0.5	22.1	<0.5	3.8	<0.5	NA	NA	NA	NA	NA
46	109018	1.7	<0.5	2.4	0.5	1.6	<0.5	1.4	<0.5	3.6	1.5	1.3	<0.5	22.4	<0.5	5.4	1.2	NA	NA	NA	NA	NA
47	109019	0.6	<0.5	1	<0.5	0.7	<0.5	0.7	<0.5	1.9	0.7	1.2	<0.5	10.3	<0.5	2.3	<0.5	NA	NA	NA	NA	NA
48	109020	<0.5	<0.5	0.5	<0.5	<0.5	<0.5	<0.5	<0.5	1.7	<0.5	1.4	<0.5	13.0	<0.5	1.8	<0.5	NA	NA	NA	NA	NA
49	109021	2.97958	0.5	2.37455	0.5	1.119	0.5	1.08	0.5	0.5	0.5	44.3	0.5	10.5211	0.5	2.5782	2.6616	NA	NA	NA	NA	NA
50	109022	10.32	1.51343	7.3667	1.2497	2.7895	0.5	2.11	0.5	8.1915	0.79	8.83	0.8563	6.41007	0.5	19.332	3.3199	NA	NA	NA	NA	NA
51	109023	1.31917	0.5	1.22162	0.5	0.6147	0.5	0.52	0.5	0.6766	0.5	41	0.5	1.6138	0.5	2.4028	4.8983	NA	NA	NA	NA	NA
52	109024	2.72981	0.5	1.39623	0.5	0.5853	0.5	0.56	0.5	1.8768	0.5	51.6	0.5	8.09218	0.5	14.449	2.8676	NA	NA	NA	NA	NA
53	109026	1.01074	0.5	0.80021	0.5	0.5	0.5	0.5	0.5	0.541	0.5	16.4	0.5	3.79599	0.5	2.2298	0.7077	NA	NA	NA	NA	NA
54	109027	0.99749	0.5	0.75012	0.5	0.5	0.5	0.5	0.5	1.3085	0.5	38.1	0.5	3.504	0.5	4.3368	0.6041	NA	NA	NA	NA	NA
55	109028	2.05392	0.5	1.57596	0.5	0.7905	0.5	0.77	0.5	1.6679	0.5	40.1	0.5	17.4797	0.5	5.0004	1.1268	NA	NA	NA	NA	NA
56	109029	2.97211	0.5	1.86796	0.5	0.7337	0.5	0.62	0.5	1.8236	0.5	56.5	0.5	13.0063	0.5	6.2714	1.0601	NA	NA	NA	NA	NA
57	109031	3.59919	0.53052	2.81165	0.5548	1.5279	0.5	1.6	0.5	4.9396	1.32	5.67	0.5	16.9077	0.5	14.76	2.8919	NA	NA	NA	NA	NA
58	109032	0.79506	0.5	0.805	0.5	0.5	0.5	0.5	0.5	0.5909	0.5	79.5	0.5	11.5924	0.5	1.2975	0.5479	NA	NA	NA	NA	NA
59	109033	0.99511	0.5	0.80075	0.5	0.5	0.5	0.5	0.5	0.8972	0.5	35.9	0.5	8.70897	0.5	3.4155	0.9205	NA	NA	NA	NA	NA
60	109034	1.06532	0.5	0.86301	0.5	0.5	0.5	0.5	0.5	0.9186	0.5	44.1	0.6768	9.69885	0.5	3.1884	0.7283	NA	NA	NA	NA	NA
61	109035	3.11136	0.5	2.25028	0.5	1.1406	0.5	1.2	0.5	2.6458	0.52	15.4	1.109	10.2898	0.5	11.274	2.8514	NA	NA	NA	NA	NA
62	109036	0.65982	0.5	0.51349	0.5	0.5	0.5	0.5	0.5	0.6957	0.5	50.4	0.5	3.30056	0.5	1.9721	0.5594	NA	NA	NA	NA	NA
63	109037	0.84051	0.5	0.54957	0.5	0.5	0.5	0.5	0.5	0.8258	0.5	72.3	0.5	2.01264	0.5	3.4269	0.9183	NA	NA	NA	NA	NA
64	109038	6.04529	0.8391	4.10417	0.759	2.0137	0.5	2.01	0.5	5.9788	1.84	5.97	0.5	17.0201	0.5	18.373	3.4221	NA	NA	NA	NA	NA

Sl No.	Sample ID	Gd	Tb	Dy	Ho	Er	Tm	Yb	Lu	Hf	Ta	W	Tl	Pb	Bi	Th	U	P	Ti	B	Ag	Al
65	109039	1.49647	0.5	1.0141	0.5	0.5147	0.5	0.5	0.5	1.338	0.5	68	0.5	19.122	0.5	6.8404	0.9046	NA	NA	NA	NA	NA
66	109040	3.67331	0.61677	3.7198	0.7763	2.151	0.5	2.14	0.5	3.5542	0.5	11.5	0.5	28.0353	0.5	11.985	2.855	NA	NA	NA	NA	NA
67	109041	8.74819	1.32827	7.03512	1.3463	3.557	0.622	3.52	0.5	7.0079	1.39	6.97	0.5	23.5424	0.5	21.447	4.515	NA	NA	NA	NA	NA
68	109042	0.82915	0.5	0.79897	0.5	0.5	0.5	0.51	0.5	0.7722	0.5	69.7	0.5	5.99683	0.5	1.9711	0.6273	NA	NA	NA	NA	NA
69	109043	3.29105	0.5	2.12112	0.5	1.1102	0.5	1.17	0.5	5.1855	0.99	34.4	1.7067	11.7713	0.5	17.319	2.29	NA	NA	NA	NA	NA
70	109046	20.3615	3.24695	19.6676	3.3355	7.1267	0.984	5.48	0.6	2.7975	0.64	6.24	0.6979	23.0596	0.5	8.4459	5.0209	NA	NA	NA	NA	NA
71	109047	2.45261	0.5	1.80037	0.5	0.7549	0.5	0.89	0.5	3.9315	0.5	50.5	0.5	12.7935	0.5	9.5468	1.9077	NA	NA	NA	NA	NA
72	109048	3.36294	0.5	2.73533	0.5001	1.2752	0.5	1.51	0.5	6.7243	0.66	48.4	0.5	17.0077	0.5	12.88	2.7032	NA	NA	NA	NA	NA
73	109049	0.70516	0.5	0.64594	0.5	0.5	0.5	0.5	0.5	0.6822	0.5	46	0.5	11.9538	0.5	1.6513	0.6125	NA	NA	NA	NA	NA
74	109050	0.80727	0.5	0.71537	0.5	0.5	0.5	0.5	0.5	1.0478	0.5	205	0.5	10.4243	0.5	2.8522	0.8056	NA	NA	NA	NA	NA
75	109051	2.3399	0.5	1.7044	0.5	0.8849	0.5	0.82	0.5	1.6511	0.5	42.5	0.5	12.6247	0.5	8.0627	7.6572	NA	NA	NA	NA	NA
76	109052	0.71299	0.5	0.62917	0.5	0.5	0.5	0.5	0.5	0.7096	0.5	48.9	0.8228	7.01002	0.5	1.7896	1.6507	NA	NA	NA	NA	NA
77	109058	6.93594	0.94598	4.54936	0.791	2.0126	0.5	1.9	0.5	5.7371	0.9	7.69	0.5	18.13	0.5	16.478	3.0751	NA	NA	NA	NA	NA
78	109060	0.68531	0.5	0.55803	0.5	0.5	0.5	0.5	0.5	0.8878	0.5	113	0.8871	5.74016	0.5	2.8999	0.6035	NA	NA	NA	NA	NA
79	189111	5.54123	0.68659	3.82484	0.6667	1.6889	0.5	1.89	0.5	2.6708	0.6	24.8	0.5682	53.5293	0.5	9.0923	1.8501	NA	NA	NA	NA	NA
80	189112	3.64374	0.56514	3.68628	0.7181	1.9147	0.5	2.32	0.5	3.7369	0.92	30.4	0.5	18.8084	0.5	7.2363	1.5709	NA	NA	NA	NA	NA
81	109045	10.96	0.73	3.59	0.56	2.13	<0.5	1.75	<0.5	3.18	<0.5	<0.5	<0.5	10	<0.5	14.10	2.98	262	4694	<5	<1	13281
82	109053	8.33	0.65	4.02	0.75	3.06	<0.5	2.68	<0.5	5.49	2.33	20.15	<0.5	10	<0.5	11.19	4.51	329	5162	<5	<1	82357
83	109054	1.51	<0.5	0.81	<0.5	<0.5	<0.5	<0.5	<0.5	<0.5	<0.5	<0.5	<0.5	9	<0.5	2.19	4.49	938	678	<5	<1	11014
84	109055	1.99	<0.5	1.59	<0.5	1.16	<0.5	1.20	<0.5	<0.5	<0.5	<0.5	<0.5	9	<0.5	1.22	0.87	239	388	<5	<1	12926
85	109056	26.09	2.84	14.87	2.85	8.40	0.84	7.66	1.13	1.92	0.86	<0.5	0.70	25	<0.5	17.42	9.14	1947	3302	<5	<1	55864
86	109057	5.89	<0.5	2.37	<0.5	1.50	<0.5	0.93	<0.5	1.10	<0.5	<0.5	1.59	8	<0.5	3.53	1.71	294	2855	<5	<1	13852

Sl No.	Sample ID	Gd	Tb	Dy	Ho	Er	Tm	Yb	Lu	Hf	Ta	W	Tl	Pb	Bi	Th	U	P	Ti	B	Ag	Al
87	109061	21.98	2.35	11.88	2.26	6.87	<0.5	3.57	<0.5	0.53	<0.5	<0.5	<0.5	17	<0.5	1.58	1.35	5283	1490	<5	<1	22847
88	109062	6.47	0.53	3.38	0.53	1.86	<0.5	1.21	<0.5	<0.5	<0.5	<0.5	<0.5	<5	<0.5	2.38	1.01	1523	1979	<5	<1	27498
89	109063	5.81	<0.5	1.32	<0.5	0.61	<0.5	<0.5	<0.5	0.64	<0.5	<0.5	<0.5	<5	<0.5	8.48	1.29	125	1823	<5	<1	24378
90	109064	29.01	2.54	8.44	1.48	4.96	<0.5	3.69	<0.5	7.85	2.24	1.76	<0.5	31	<0.5	55.72	7.96	358	10878	<5	<1	95542
91	109065	2.84	<0.5	2.38	<0.5	1.46	<0.5	1.67	<0.5	<0.5	<0.5	<0.5	<0.5	87	<0.5	2.98	2.02	981	658	<5	<1	13751
92	109066	18.29	2.01	10.57	1.99	5.71	<0.5	3.80	<0.5	<0.5	<0.5	<0.5	<0.5	5	<0.5	2.88	2.15	3744	1801	<5	<1	26326
93	109067	1.44	<0.5	0.63	<0.5	<0.5	<0.5	<0.5	<0.5	<0.5	<0.5	<0.5	0.65	8	<0.5	2.28	1.08	602	604	<5	<1	11104
94	109068	7.71	1.57	11.92	2.97	10.33	1.28	12.49	2.24	1.64	0.57	<0.5	<0.5	7	<0.5	1.74	1.32	566	7938	<5	<1	117671
95	109069	5.00	0.67	4.28	0.79	2.60	<0.5	1.92	<0.5	<0.5	<0.5	<0.5	<0.5	227	<0.5	2.14	3.25	1030	501	<5	<1	15194
96	109070	1.53	<0.5	0.68	<0.5	<0.5	<0.5	<0.5	<0.5	<0.5	<0.5	<0.5	<0.5	13	<0.5	2.73	1.29	374	1029	<5	<1	10375
97	109071	3.14	<0.5	1.35	<0.5	0.79	<0.5	0.61	<0.5	1.48	<0.5	<0.5	<0.5	10	<0.5	2.85	1.03	116	2465	<5	<1	44603
98	112451	11.19	2.45	9.43	1.27	3.50	0.12	2.54	0.23	3.30	2.15	0.23	<0.05	27.82	0.48	22.10	17.46	NA	NA	NA	NA	NA
99	112466	17.71	6.13	8.04	1.03	5.04	0.16	4.57	0.46	2.82	5.27	0.23	1.18	4.56	1.44	44.40	41.28	NA	NA	NA	NA	NA
100	112492	12.52	2.47	1.61	<0.1	1.16	0.16	1.69	0.32	1.82	3.65	0.24	<0.05	23.38	0.23	34.99	30.97	NA	NA	NA	NA	NA
101	112493	1.07	0.28	1.34	0.15	1.09	0.17	0.45	0.01	2.39	0.98	<0.1	0.46	3.83	<0.1	2.80	<0.1	NA	NA	NA	NA	NA
102	112493	1.31	0.67	2.13	<0.1	1.29	0.10	0.56	0.02	2.85	0.93	0.43	1.88	5.07	<0.1	3.38	<0.1	NA	NA	NA	NA	NA
103	112494	13.19	6.55	4.97	0.29	5.58	0.16	2.57	0.30	5.95	5.48	0.31	<0.05	11.50	0.26	31.94	15.62	NA	NA	NA	NA	NA
104	112495	1.93	0.66	1.93	0.17	1.23	0.17	0.47	0.02	1.75	3.55	0.19	2.12	7.82	0.96	2.90	<0.1	NA	NA	NA	NA	NA
105	112459	18.96	1.47	6.89	1.52	1.84	<0.1	4.97	0.39	0.92	3.20	1.16	1.64	34.04	7.15	45.81	42.36	NA	NA	NA	NA	NA
106	112460	18.20	1.38	1.27	0.28	0.40	0.10	2.21	0.36	1.60	3.44	0.19	1.89	6.50	4.65	46.14	45.06	NA	NA	NA	NA	NA
107	112461	8.82	0.78	0.40	<0.1	0.36	0.10	1.23	0.17	1.90	1.76	0.38	1.32	3.78	1.45	23.06	19.21	NA	NA	NA	NA	NA
108	112462	20.39	2.33	4.34	<0.1	1.91	<0.1	2.86	0.37	6.95	4.35	0.93	0.98	12.19	2.01	52.41	38.64	NA	NA	NA	NA	NA

Sl No.	Sample ID	Gd	Tb	Dy	Ho	Er	Tm	Yb	Lu	Hf	Ta	W	Tl	Pb	Bi	Th	U	P	Ti	B	Ag	Al
109	112463	1.08	0.32	0.67	<0.1	0.52	0.10	0.31	0.02	2.03	0.98	0.48	1.61	1.35	<0.1	2.79	0.31	NA	NA	NA	NA	NA
110	112464	8.50	1.00	1.37	<0.1	0.88	0.10	1.19	0.16	1.96	2.05	0.55	2.13	7.53	<0.1	21.65	15.99	NA	NA	NA	NA	NA
111	112478	10.94	1.17	4.87	0.40	0.75	0.10	1.64	0.20	4.63	3.06	1.34	5.98	4.97	1.25	27.32	20.27	NA	NA	NA	NA	NA
112	112479	14.15	1.42	7.08	0.51	0.87	0.10	1.85	0.27	5.26	3.91	1.54	10.82	4.84	1.20	35.50	28.13	NA	NA	NA	NA	NA
113	112480	17.63	1.75	9.34	0.73	1.11	<0.1	2.36	0.33	6.22	4.27	2.45	11.65	7.71	1.46	43.82	37.57	NA	NA	NA	NA	NA
114	112481	14.82	1.49	9.97	0.49	0.91	0.10	2.08	0.28	6.17	4.13	2.14	15.75	7.94	1.94	36.60	30.74	NA	NA	NA	NA	NA
115	112484	27.16	2.31	7.77	<0.1	2.24	<0.1	3.96	0.47	2.35	5.09	1.03	0.92	29.25	3.11	58.81	58.50	NA	NA	NA	NA	NA
116	112488	10.7	1.05	2.51	0.6	1.07	<0.1	1.77	0.19	4.9	2.76	1.87	<0.05	12.09	1.26	26.78	21.77	NA	NA	NA	NA	NA
117	112496	24.81	3.15	20.18	<0.1	4.58	<0.1	6.86	0.41	6.74	6.04	1.77	0.58	21.14	1.55	53.45	34.18	NA	NA	NA	NA	NA
118	112498	15.63	1.21	1.92	0.66	0.57	<0.1	2.10	0.30	1.13	3.16	1.11	0.32	39.82	3.29	38.12	35.29	NA	NA	NA	NA	NA
119	107550	<0.5	<0.5	<0.5	<0.5	<0.5	<0.5	<0.5	<0.5	<0.5	<0.5	NA	<0.5	<0.5	<0.5	<0.5	<0.5	NA	NA	NA	NA	NA
120	107554	4.52054	0.75108	4.65695	0.9495	2.6721	<0.5	2.45	<0.5	3.0234	1.16	NA	<0.5	2.27981	<0.5	3.4342	0.6976	NA	NA	NA	NA	NA
121	107556	4.52338	0.69401	3.98376	0.771	2.0622	<0.5	1.58	<0.5	5.0476	0.93	NA	<0.5	7.82542	<0.5	4.8073	4.7227	NA	NA	NA	NA	NA

Table Continued..

Annexure-XXI

Sl No.	Sample ID	Ca	Fe	K	Mg	Mn	Na	HREEY	LREE	TREEY
1	105567	NA	NA	NA	NA	NA	NA	72.4	367.3	439.7
2	107476	NA	NA	NA	NA	NA	NA	74.3	107.2	181.5
3	107510	NA	NA	NA	NA	NA	NA	53.1	125.4	178.5
4	107516	NA	NA	NA	NA	NA	NA	18.0	91.9	109.9
5	107518	NA	NA	NA	NA	NA	NA	153.3	265.9	419.2
6	107541	NA	NA	NA	NA	NA	NA	65.7	234.5	300.2
7	107542	NA	NA	NA	NA	NA	NA	19.7	97.1	116.7
8	107543	NA	NA	NA	NA	NA	NA	72.7	211.2	283.9
9	107546	NA	NA	NA	NA	NA	NA	32.4	88.3	120.7
10	107551	NA	NA	NA	NA	NA	NA	21.8	67.4	89.1
11	107561	NA	NA	NA	NA	NA	NA	34.0	152.7	186.8
12	107555	NA	NA	NA	NA	NA	NA	25.4	69.3	94.7
13	107565	NA	NA	NA	NA	NA	NA	84.3	135.9	220.2
14	107566	NA	NA	NA	NA	NA	NA	53.5	32.6	86.2
15	107567	NA	NA	NA	NA	NA	NA	11.1	15.3	26.4
16	107568	NA	NA	NA	NA	NA	NA	27.7	120.4	148.0
17	107569	NA	NA	NA	NA	NA	NA	48.0	143.2	191.1
18	107570	NA	NA	NA	NA	NA	NA	17.0	58.7	75.6
19	107571	NA	NA	NA	NA	NA	NA	43.6	206.3	250.0
20	107572	NA	NA	NA	NA	NA	NA	17.1	48.9	66.1
21	107573	NA	NA	NA	NA	NA	NA	91.3	192.0	283.3
22	107574	NA	NA	NA	NA	NA	NA	69.1	108.1	177.1
23	107575	NA	NA	NA	NA	NA	NA	78.6	177.6	256.2
24	107576	NA	NA	NA	NA	NA	NA	19.8	70.5	90.3

Sl No.	Sample ID	Ca	Fe	K	Mg	Mn	Na	HREEY	LREE	TREEY
25	107577	NA	NA	NA	NA	NA	NA	14.0	27.6	41.6
26	107578	NA	NA	NA	NA	NA	NA	30.7	89.5	120.2
27	107579	NA	NA	NA	NA	NA	NA	73.1	118.6	191.7
28	107580	NA	NA	NA	NA	NA	NA	72.0	138.0	210.0
29	107581	NA	NA	NA	NA	NA	NA	71.1	87.8	158.9
30	107582	NA	NA	NA	NA	NA	NA	38.2	91.2	129.4
31	107511	NA	NA	NA	NA	NA	NA	65.3	134.8	200.1
32	107535	NA	NA	NA	NA	NA	NA	41.9	136.4	178.3
33	107536	NA	NA	NA	NA	NA	NA	16.7	100.6	117.3
34	107559	NA	NA	NA	NA	NA	NA	31.6	123.2	154.8
35	107562	NA	NA	NA	NA	NA	NA	33.3	136.1	169.4
36	107563	NA	NA	NA	NA	NA	NA	33.8	133.1	166.9
37	105622	NA	NA	NA	NA	NA	NA	831.4	890.4	1721.8
38	109059	NA	NA	NA	NA	NA	NA	9.0	13.3	22.4
39	109006	NA	NA	NA	NA	NA	NA	45.2	85.3	130.4
40	109007	NA	NA	NA	NA	NA	NA	5.5	8.6	14.1
41	109009	NA	NA	NA	NA	NA	NA	27.7	35.9	63.6
42	109011	NA	NA	NA	NA	NA	NA	29.7	65.2	94.8
43	109015	NA	NA	NA	NA	NA	NA	21.3	53.4	74.7
44	109016	NA	NA	NA	NA	NA	NA	12.3	43.2	55.5
45	109017	NA	NA	NA	NA	NA	NA	8.9	28.4	37.3
46	109018	NA	NA	NA	NA	NA	NA	11.6	37.1	48.7
47	109019	NA	NA	NA	NA	NA	NA	6.5	14.6	21.1
48	109020	NA	NA	NA	NA	NA	NA	5.5	8.7	14.2
49	109021	NA	NA	NA	NA	NA	NA	30.8	65.3	96.1
50	109022	NA	NA	NA	NA	NA	NA	86.2	237.5	323.7

Sl No.	Sample ID	Ca	Fe	K	Mg	Mn	Na	HREEY	LREE	TREEY
51	109023	NA	NA	NA	NA	NA	NA	20.5	22.1	42.6
52	109024	NA	NA	NA	NA	NA	NA	16.9	109.5	126.4
53	109026	NA	NA	NA	NA	NA	NA	13.6	26.3	39.9
54	109027	NA	NA	NA	NA	NA	NA	13.9	32.3	46.2
55	109028	NA	NA	NA	NA	NA	NA	23.2	67.9	91.1
56	109029	NA	NA	NA	NA	NA	NA	20.9	82.7	103.6
57	109031	NA	NA	NA	NA	NA	NA	41.8	130.0	171.8
58	109032	NA	NA	NA	NA	NA	NA	10.7	17.6	28.3
59	109033	NA	NA	NA	NA	NA	NA	11.7	28.0	39.7
60	109034	NA	NA	NA	NA	NA	NA	12.6	31.5	44.0
61	109035	NA	NA	NA	NA	NA	NA	27.3	100.5	127.8
62	109036	NA	NA	NA	NA	NA	NA	8.0	18.5	26.5
63	109037	NA	NA	NA	NA	NA	NA	9.0	28.6	37.6
64	109038	NA	NA	NA	NA	NA	NA	51.1	206.7	257.8
65	109039	NA	NA	NA	NA	NA	NA	14.5	50.1	64.6
66	109040	NA	NA	NA	NA	NA	NA	55.8	91.0	146.8
67	109041	NA	NA	NA	NA	NA	NA	80.4	267.8	348.2
68	109042	NA	NA	NA	NA	NA	NA	10.8	20.2	31.1
69	109043	NA	NA	NA	NA	NA	NA	25.0	121.7	146.7
70	109046	NA	NA	NA	NA	NA	NA	207.2	342.2	549.4
71	109047	NA	NA	NA	NA	NA	NA	20.5	85.9	106.5
72	109048	NA	NA	NA	NA	NA	NA	32.6	109.9	142.5
73	109049	NA	NA	NA	NA	NA	NA	12.1	17.0	29.1
74	109050	NA	NA	NA	NA	NA	NA	9.5	21.8	31.3
75	109051	NA	NA	NA	NA	NA	NA	22.1	68.0	90.1
76	109052	NA	NA	NA	NA	NA	NA	10.6	17.1	27.7

Sl No.	Sample ID	Ca	Fe	K	Mg	Mn	Na	HREEY	LREE	TREEY
77	109058	NA	NA	NA	NA	NA	NA	52.1	234.1	286.2
78	109060	NA	NA	NA	NA	NA	NA	9.5	22.8	32.3
79	189111	NA	NA	NA	NA	NA	NA	45.7	184.9	230.6
80	189112	NA	NA	NA	NA	NA	NA	55.5	94.4	149.9
81	109045	122974	34517	8012	19354	539	1073	46.8	204.4	251.2
82	109053	593	7205	3431	1474	<100	6196	56.0	173.8	229.9
83	109054	2876	153484	309	1147	366	593	14.2	30.1	44.2
84	109055	442	110884	2896	879	1040	290	19.0	24.3	43.3
85	109056	1869	309920	2899	1269	3239	941	168.2	429.4	597.6
86	109057	4932	184991	5782	1153	3102	315	31.7	86.2	117.9
87	109061	58552	353004	4298	28054	3386	2457	131.1	261.1	392.2
88	109062	249223	53699	6052	7371	1007	1114	42.2	100.4	142.5
89	109063	590	6301	334	193	<100	123	18.7	118.9	137.6
90	109064	730	8819	1049	855	<100	3876	110.0	634.0	744.0
91	109065	353	240583	186	101	<100	173	24.7	33.5	58.2
92	109066	262072	27264	5672	4075	2880	1758	115.1	260.8	375.9
93	109067	6525	195647	4562	955	2617	342	11.9	28.0	39.9
94	109068	1489	244839	<100	700	189	442	203.6	57.2	260.7
95	109069	628	310852	165	169	<100	175	42.9	36.2	79.1
96	109070	6412	221866	4099	1326	2687	293	12.0	33.7	45.7
97	109071	6757	4376	425	271	130	295	19.4	60.7	80.1
98	112451	NA	NA	NA	NA	NA	NA	107.8	165.7	273.5
99	112466	NA	NA	NA	NA	NA	NA	173.5	100.1	273.6
100	112492	NA	NA	NA	NA	NA	NA	39.6	76.8	116.5
101	112493	NA	NA	NA	NA	NA	NA	15.8	80.8	96.6
102	112493	NA	NA	NA	NA	NA	NA	19.0	93.7	112.8

Sl No.	Sample ID	Ca	Fe	K	Mg	Mn	Na	HREEY	LREE	TREEY
103	112494	NA	NA	NA	NA	NA	NA	121.2	267.0	388.1
104	112495	NA	NA	NA	NA	NA	NA	19.4	152.4	171.8
105	112459	NA	NA	NA	NA	NA	NA	57.2	55.7	112.9
106	112460	NA	NA	NA	NA	NA	NA	31.9	58.6	90.4
107	112461	NA	NA	NA	NA	NA	NA	18.9	41.0	59.9
108	112462	NA	NA	NA	NA	NA	NA	62.7	249.0	311.7
109	112463	NA	NA	NA	NA	NA	NA	8.7	32.6	41.3
110	112464	NA	NA	NA	NA	NA	NA	22.0	54.8	76.7
111	112478	NA	NA	NA	NA	NA	NA	37.0	89.4	126.3
112	112479	NA	NA	NA	NA	NA	NA	41.2	104.5	145.7
113	112480	NA	NA	NA	NA	NA	NA	55.1	119.2	174.3
114	112481	NA	NA	NA	NA	NA	NA	48.1	115.9	164.0
115	112484	NA	NA	NA	NA	NA	NA	99.8	266.1	365.9
116	112488	NA	NA	NA	NA	NA	NA	43.6	52.3	95.9
117	112496	NA	NA	NA	NA	NA	NA	122.3	316.3	438.6
118	112498	NA	NA	NA	NA	NA	NA	47.6	135.9	183.5
119	107550	NA	NA	NA	NA	NA	NA	5.5	2.5	8.0
120	107554	NA	NA	NA	NA	NA	NA	77.9	89.2	167.1
121	107556	NA	NA	NA	NA	NA	NA	77.3	84.0	161.3

Annexure-XXII: Details of VES Survey

Date: 08/12/2024		VES-01				
Latitude	23.193428		Longitude	69.60356		
S.N	Current Electrode Spacing (AB/2)	Potential Electrode Spacing (MN)	Resistance (ohm)	K value	Aparent Resistivity (Rho_a)	
1	2.5	1	0.309	18.846	5.823	-2.5
2	5	1	0.097	77.73975	7.541	-5
3	10	1	0.043	313.3148	13.473	-10
4	20	1	0.015	1255.615	18.834	-20
5	25	1	0.01	1962.34	19.623	-25
6	30	1	0.007	2826.115	19.783	-30
7	35	1	0.005	3846.94	19.235	-35
8	40	1	0.004	5024.815	20.099	-40
9	45	1	0.003	6359.74	19.079	-45
10	50	1	0.003	7851.715	23.555	-50
11	60	1	0.002	11306.81	22.614	-60
12	70	1	0.001	15390.11	15.390	-70
13	80	1	0.001	20101.61	20.102	-80
14	90	1	0.001	25441.31	25.441	-90
15	100	1	0.001	31409.21	31.409	-100

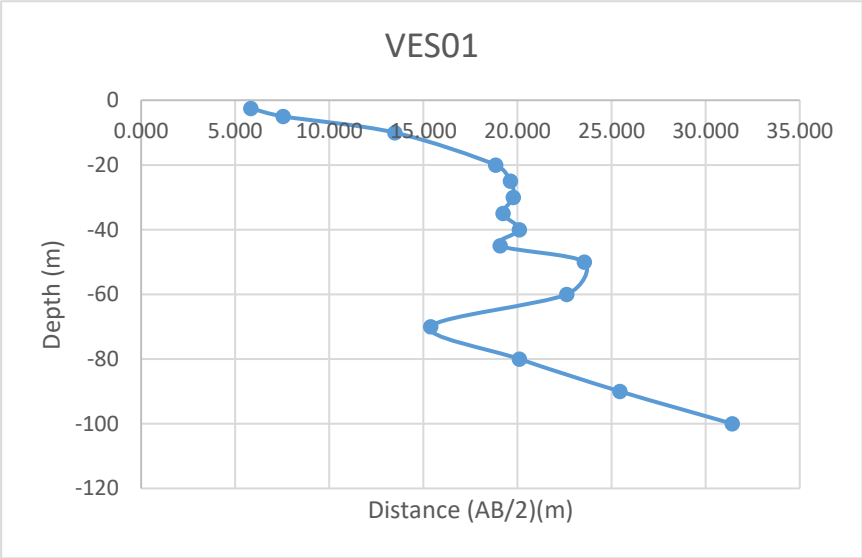

Annexure-XXII: Details of VES Survey

Date: 08/12/2024		VES-02				
Latitude	23.19747		Longitude	69.605817		
S.N	Current Electrode Spacing (AB/2)	Potential Electrode Spacing (MN)	Resistance (ohm)	K value	Aparent Resistivity (Rho_a)	
1	2.5	1	10.52	18.846	198.260	-2.5
2	5	1	0.594	77.73975	46.177	-5
3	10	1	0.046	313.3148	14.412	-10
4	15	1	0.018	705.9398	12.707	-15
5	20	1	0.011	1255.615	13.812	-20
7	30	1	0.005	2826.115	14.131	-25
8	35	1	0.004	3846.94	15.388	-30
9	40	1	0.003	5024.815	15.074	-35
10	45	1	0.003	6359.74	19.079	-40
11	50	1	0.002	7851.715	15.703	-45
12	60	1	0.002	11306.81	22.614	-50
13	70	1	0.001	15390.11	15.390	-60
14	80	1	0.001	20101.61	20.102	-70
15	90	1	0.001	25441.31	25.441	-80
16	100	1	0.0003	31409.21	9.423	-90
17	110	1	0.0003	38005.31	11.402	-100

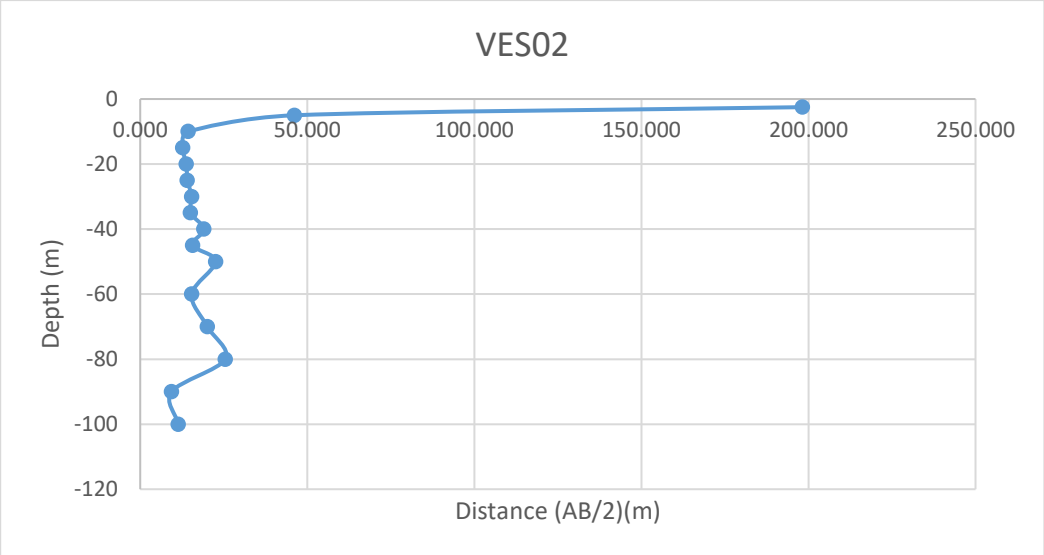

Annexure-XXII: Details of VES Survey

Date: 09/12/2024		VES-03				
Latitude	23.20402		Longitude	69.542003		
S.N	**Current Electrode Spacing (AB/2)**	**Potential Electrode Spacing (MN)**	**Resistance (Ohm)**	**K value**	**Aparent Resistivity (Rho_a)**	
1	2.5	1	18.3	18.846	344.882	-2.5
2	5	1	5.51	77.73975	428.346	-5
3	10	1	1.37	313.31475	429.241	-10
4	15	1	0.535	705.93975	377.678	-15
5	20	1	0.261	1255.61475	327.715	-20
6	25	1	0.152	1962.33975	298.276	-25
7	30	1	0.094	2826.11475	265.655	-30
8	35	1	0.059	3846.93975	226.969	-35
9	40	1	0.035	5024.81475	175.869	-40
10	45	1	0.025	6359.73975	158.993	-45
11	50	1	0.018	7851.71475	141.331	-50
12	60	1	0.01	11306.8148	113.068	-60
13	70	1	0.00674	15390.1148	103.729	-70
14	80	1	0.00445	20101.6148	89.452	-80
15	90	1	0.0034	25441.3148	86.500	-90
16	100	1	0.0028	31409.2148	87.946	-100

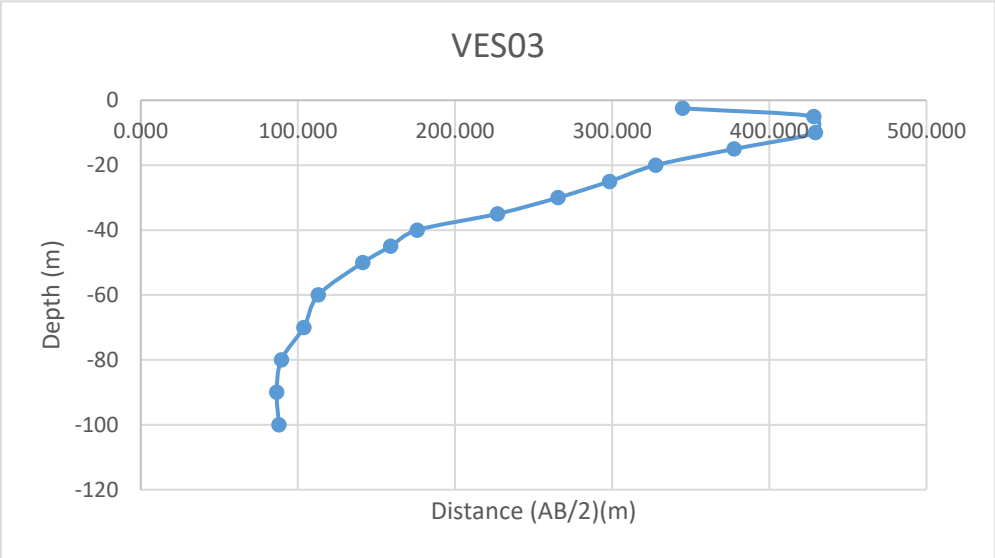

Annexure-XXII: Details of VES Survey

Date: 09/12/2024		VES-04				
Latitude	23.19582		Longitude	69.534385		
S.N	Current Electrode Spacing (AB/2)	Potential Electrode Spacing (MN)	Resistance (Ohm)	K value	Aparent Resistivity (Rho_a)	
1	2.5	1	15.8	18.846	297.767	-2.5
2	5	1	3.85	77.73975	299.298	-5
3	10	1	1.39	313.3148	435.508	-10
4	15	1	0.653	705.9398	460.979	-15
5	20	1	0.352	1255.615	441.976	-20
6	25	1	0.18	1962.34	353.221	-25
7	30	1	0.1	2826.115	282.611	-30
8	35	1	0.066	3846.94	253.898	-35
9	40	1	0.042	5024.815	211.042	-40
10	45	1	0.0307	6359.74	195.244	-45
11	50	1	0.022	7851.715	172.738	-50
12	60	1	0.0121	11306.81	136.812	-60
13	70	1	0.0075	15390.11	115.426	-70
14	80	1	0.00551	20101.61	110.760	-80
15	90	1	0.00351	25441.31	89.299	-90
16	100	1	0.00314	31409.21	98.625	-100

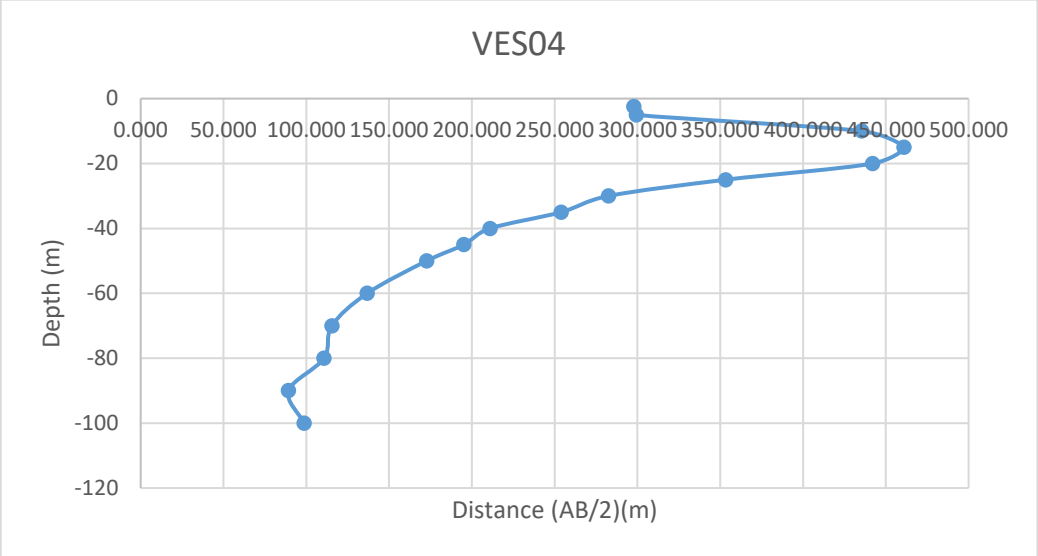

Annexure-XXII: Details of VES Survey

Date: 10/12/2024		VES-05				
Latitude	23.150393		Longitude	69.578688		
S.N	Current Electrode Spacing (AB/2)	Potential Electrode Spacing (MN)	Resistance (Ohm)	K value	Aparent Resistivity (Rho_a)	
1	2.5	1	0.268	18.846	5.051	-2.5
2	5	1	0.082	77.73975	6.375	-5
3	10	1	0.023	313.3148	7.206	-10
4	15	1	0.012	705.9398	8.471	-15
5	20	1	0.0071	1255.615	8.915	-20
6	25	1	0.00455	1962.34	8.929	-25
7	30	1	0.003	2826.115	8.478	-30
8	35	1	0.0022	3846.94	8.463	-35
9	40	1	0.00165	5024.815	8.291	-40
10	45	1	0.0013	6359.74	8.268	-45
11	50	1	0.00105	7851.715	8.244	-50
12	60	1	0.0006	11306.81	6.784	-60
13	70	1	0.0006	15390.11	9.234	-70
14	80	1	0.00045	20101.61	9.046	-80
15	90	1	0.0003	25441.31	7.632	-90
16	100	1	0.0003	31409.21	9.423	-100
17	110	1	0.0002	38005.31	7.601	-110

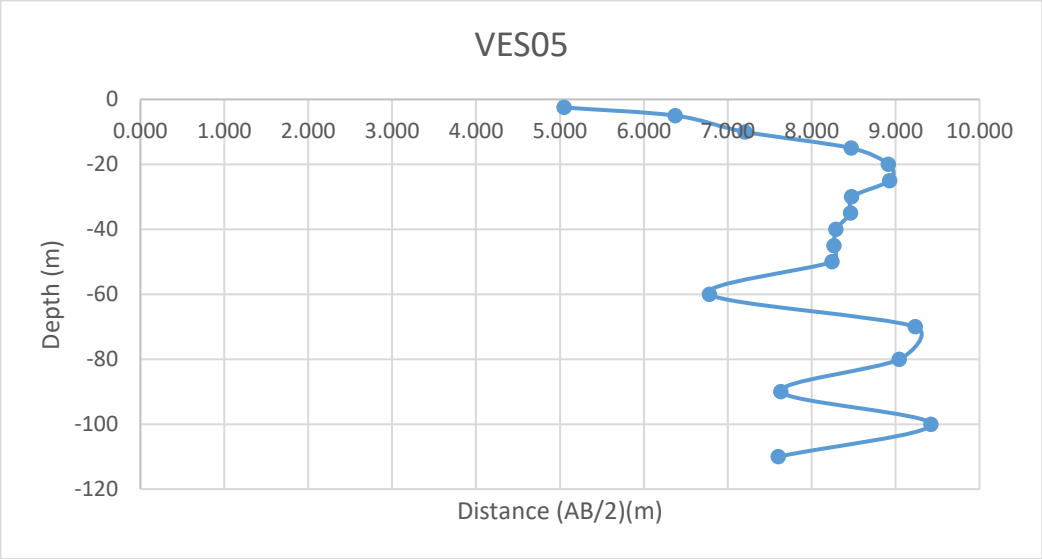

Annexure-XXII: Details of VES Survey

Date: 10/12/2024			VES-06			
Latitude	23.202988		Longitude	69.536828		
S.N	Current Electrode Spacing (AB/2)	Potential Electrode Spacing (MN)	Resistance (Ohm)	K value	Aparent Resistivity (Rho_a)	
1	2.5	1	17.05	18.846	321.324	-2.5
2	5	1	4.64	77.73975	360.712	-5
3	10	1	1.38	313.3148	432.374	-10
4	15	1	0.59	705.9398	416.504	-15
5	20	1	0.307	1255.615	385.474	-20
6	25	1	0.166	1962.34	325.748	-25
7	30	1	0.097	2826.115	274.133	-30
8	35	1	0.0625	3846.94	240.434	-35
9	40	1	0.039	5024.815	195.968	-40
10	45	1	0.028	6359.74	178.073	-45
11	50	1	0.02	7851.715	157.034	-50
12	60	1	0.011	11306.81	124.375	-60
13	70	1	0.0071	15390.11	109.270	-70
14	80	1	0.0049	20101.61	98.498	-80
15	90	1	0.0034	25441.31	86.500	-90
16	100	1	0.00297	31409.21	93.285	-100

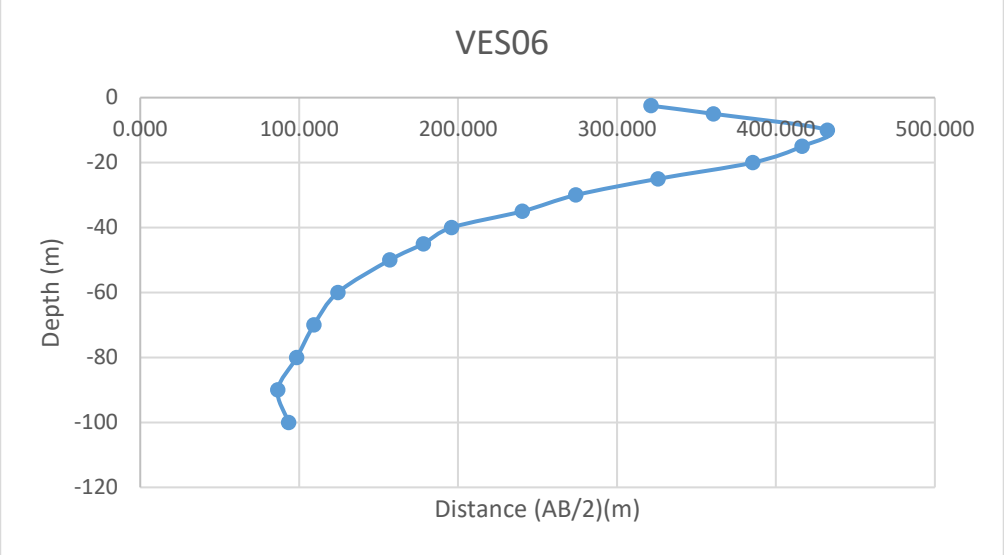

Annexure-XXII: Details of VES Survey

Date: 11/12/2024		VES-07				
Latitude	23.196351		Longitude	69.602342		
S.N	Current Electrode Spacing (AB/2)	Potential Electrode Spacing (MN)	Resistance (Ohm)	K value	Aparent Resistivity (Rho_a)	
1	2.5	1	11.52	18.846	217.106	-2.5
2	5	1	1.501	77.73975	116.687	-5
3	10	1	0.25	313.3148	78.329	-10
4	15	1	0.05	705.9398	35.297	-15
5	20	1	0.024	1255.615	30.135	-20
6	25	1	0.014	1962.34	27.473	-25
7	30	1	0.00605	2826.115	17.098	-30
8	35	1	0.0045	3846.94	17.311	-35
9	40	1	0.003	5024.815	15.074	-40
10	45	1	0.0022	6359.74	13.991	-45
11	50	1	0.00301	7851.715	23.634	-50
12	60	1	0.0028	11306.81	31.659	-60
13	70	1	0.0024	15390.11	36.936	-70
14	80	1	0.00187	20101.61	37.590	-80
15	90	1	0.00155	25441.31	39.434	-90
16	100	1	0.00147	31409.21	46.172	-100

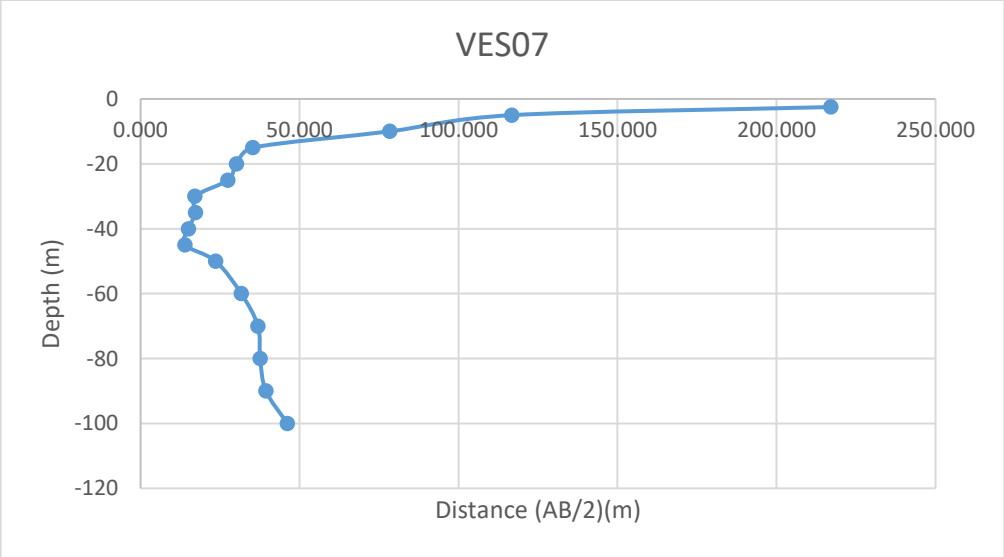

Annexure-XXII: Details of VES Survey

Date: 11/12/2024			VES-08			
Latitude	23.199071		Longitude	69.537331		
S.N	Current Electrode Spacing (AB/2)	Potential Electrode Spacing (MN)	Resistance (Ohm)	K value	Aparent Resistivity (Rho_a)	
1	2.5	1	15.415	18.846	290.511	-2.5
2	5	1	4.243	77.73975	329.850	-5
3	10	1	1.375	313.3148	430.808	-10
4	15	1	0.615	705.9398	434.153	-15
5	20	1	0.327	1255.615	410.586	-20
6	25	1	0.173	1962.34	339.485	-25
7	30	1	0.097	2826.115	274.133	-30
8	35	1	0.064	3846.94	246.204	-35
9	40	1	0.04	5024.815	200.993	-40
10	45	1	0.027	6359.74	171.713	-45
11	50	1	0.021	7851.715	164.886	-50
12	60	1	0.01	11306.81	113.068	-60
13	70	1	0.0073	15390.11	112.348	-70
14	80	1	0.0052	20101.61	104.528	-80
15	90	1	0.0035	25441.31	89.045	-90
16	100	1	0.0027	31409.21	84.805	-100

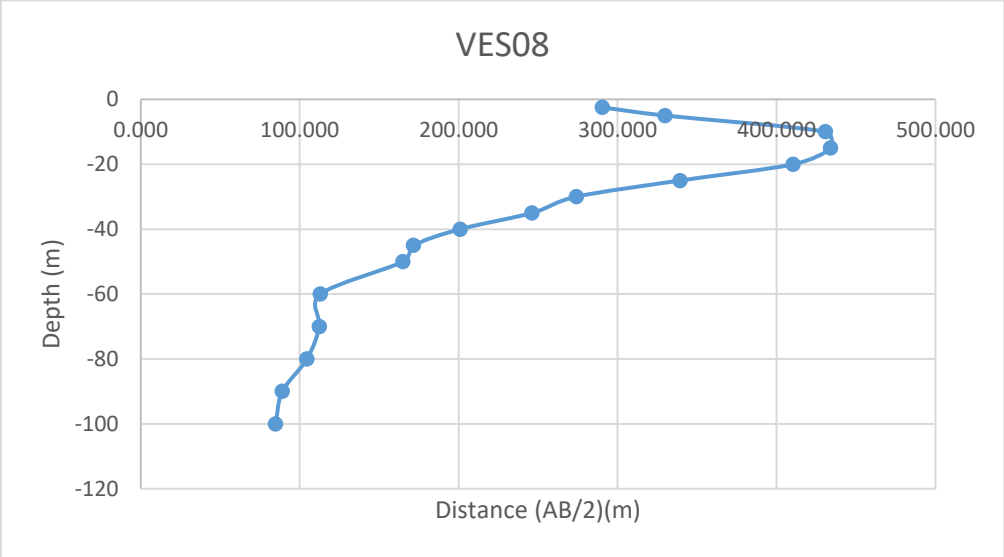

Annexure-XXII: Details of VES Survey

Date: 13/12/2024			VES-09			
Latitude	23.226267		Longitude	69.545123		
S.N	Current Electrode Spacing (AB/2)	Potential Electrode Spacing (MN)	Resistance (Ohm)	K value	Aparent Resistivity (Rho_a)	
1	2.5	1	1.7	18.846	32.038	-2.5
2	5	1	0.258	77.73975	20.057	-5
3	10	1	0.076	313.3148	23.812	-10
4	15	1	0.037	705.9398	26.120	-15
5	20	1	0.0225	1255.615	28.251	-20
6	25	1	0.0152	1962.34	29.828	-25
7	30	1	0.01135	2826.115	32.076	-30
8	35	1	0.0089	3846.94	34.238	-35
9	40	1	0.00745	5024.815	37.435	-40
10	45	1	0.00625	6359.74	39.748	-45
11	50	1	0.00535	7851.715	42.007	-50
12	60	1	0.00395	11306.81	44.662	-60
13	70	1	0.00315	15390.11	48.479	-70
14	80	1	0.00245	20101.61	49.249	-80
15	90	1	0.00205	25441.31	52.155	-90
16	100	1	0.00175	31409.21	54.966	-100
17	110	1	0.00155	38005.31	58.908	-110

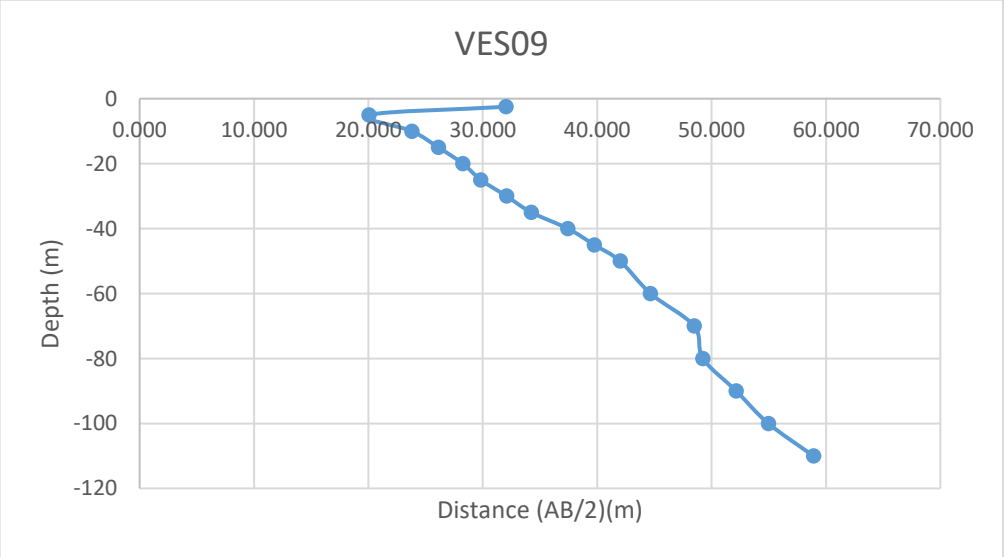

Annexure-XXII: Details of VES Survey

Date: 13/12/2024			VES-10			
Latitude	23.227017		Longitude	69.541275		
S.N	Current Electrode Spacing (AB/2)	Potential Electrode Spacing (MN)	Resistance (Ohm)	K value	Aparent Resistivity (Rho_a)	
1	2.5	1	1.24	18.846	23.369	-2.5
2	5	1	0.185	77.73975	14.382	-5
3	10	1	0.0508	313.3148	15.916	-10
4	15	1	0.0254	705.9398	17.931	-15
5	20	1	0.0169	1255.615	21.220	-20
6	25	1	0.0125	1962.34	24.529	-25
7	30	1	0.00985	2826.115	27.837	-30
8	35	1	0.008	3846.94	30.776	-35
9	40	1	0.0066	5024.815	33.164	-40
10	45	1	0.0055	6359.74	34.979	-45
11	50	1	0.00475	7851.715	37.296	-50
12	60	1	0.0036	11306.81	40.705	-60
13	70	1	0.00275	15390.11	42.323	-70
14	80	1	0.00235	20101.61	47.239	-80
15	90	1	0.00195	25441.31	49.611	-90
16	100	1	0.00165	31409.21	51.825	-100

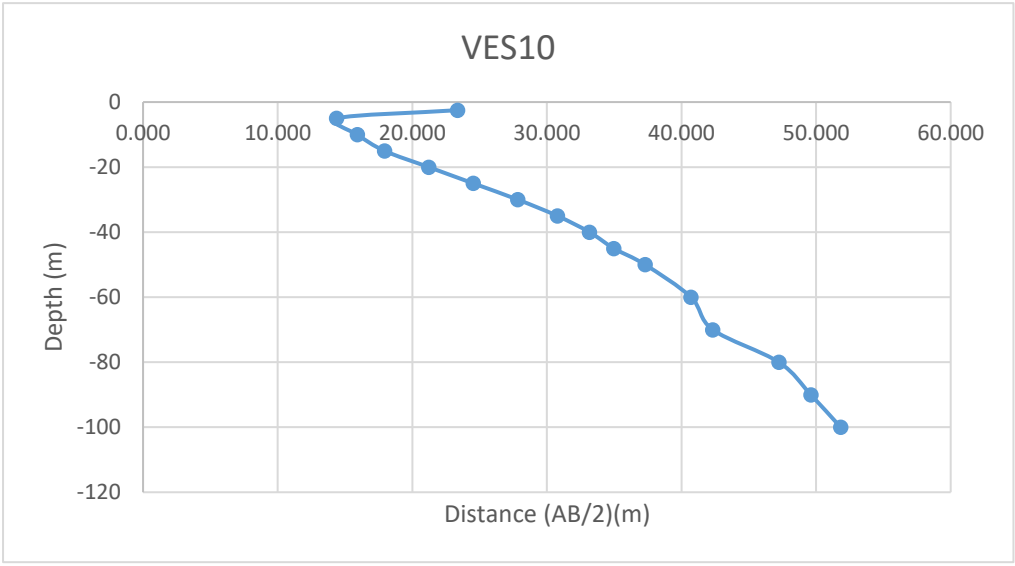

Annexure-XXII: Details of VES Survey

Date: 14/12/2024		VES-11				
Latitude	23.227848		Longitude	69.539537		
S.N	Current Electrode Spacing (AB/2)	Potential Electrode Spacing (MN)	Resistance (Ohm)	K value	Aparent Resistivity (Rho_a)	
1	2.5	1	6.77	18.846	127.587	-2.5
2	5	1	1.81	77.73975	140.709	-5
3	10	1	0.49	313.3148	153.524	-10
4	15	1	0.193	705.9398	136.246	-15
5	20	1	0.0925	1255.615	116.144	-20
6	25	1	0.0524	1962.34	102.827	-25
7	30	1	0.0329	2826.115	92.979	-30
8	35	1	0.0221	3846.94	85.017	-35
9	40	1	0.0163	5024.815	81.904	-40
10	45	1	0.0124	6359.74	78.861	-45
11	50	1	0.01082	7851.715	84.956	-50
12	60	1	0.00892	11306.81	100.857	-60
13	70	1	0.00853	15390.11	131.278	-70
14	80	1	0.00661	20101.61	132.872	-80
15	90	1	0.00531	25441.31	135.093	-90
16	100	1	0.00853	31409.21	267.921	-100

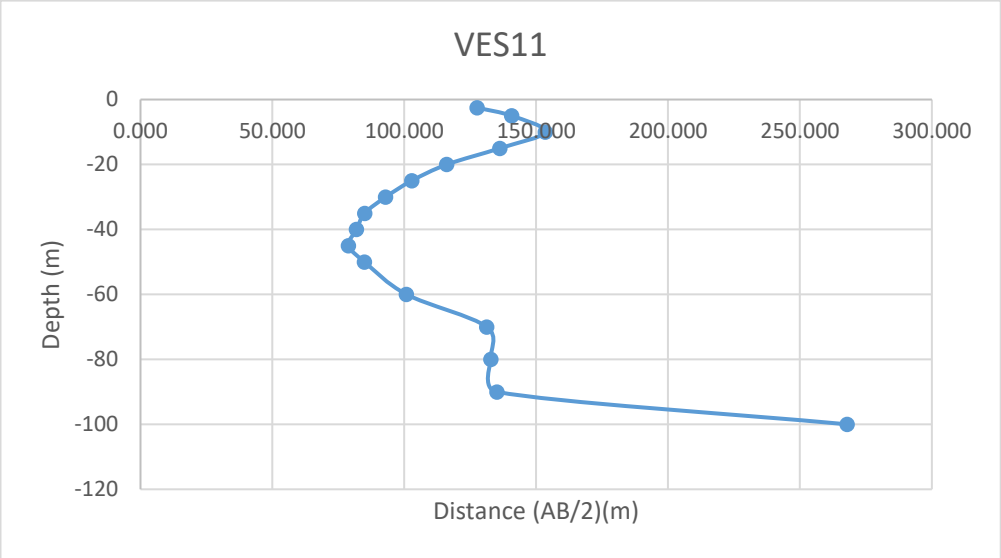

Annexure-XXII: Details of VES Survey

Date: 14/12/2024		VES-12				
Latitude	23.227387		Longitude	69.537865		
S.N	Current Electrode Spacing (AB/2)	Potential Electrode Spacing (MN)	Resistance (Ohm)	K value	Aparent Resistivity (Rho_a)	
1	2.5	1	26.5	18.846	499.419	-2.5
2	5	1	5.21	77.73975	405.024	-5
3	10	1	0.752	313.3148	235.613	-10
4	15	1	0.167	705.9398	117.892	-15
5	20	1	0.0666	1255.615	83.624	-20
6	25	1	0.0384	1962.34	75.354	-25
7	30	1	0.0274	2826.115	77.436	-30
8	35	1	0.0183	3846.94	70.399	-35
9	40	1	0.022	5024.815	110.546	-40
10	45	1	0.01154	6359.74	73.391	-45
11	50	1	0.00972	7851.715	76.319	-50
12	60	1	0.00721	11306.81	81.522	-60
13	70	1	0.00562	15390.11	86.492	-70
14	80	1	0.00358	20101.61	71.964	-80
15	90	1	0.00465	25441.31	118.302	-90
16	100	1	0.00097	31409.21	30.467	-100
17	110	1	0.00228	38005.31	86.652	-110
18	120	1	0.0025	45229.61	113.074	-120

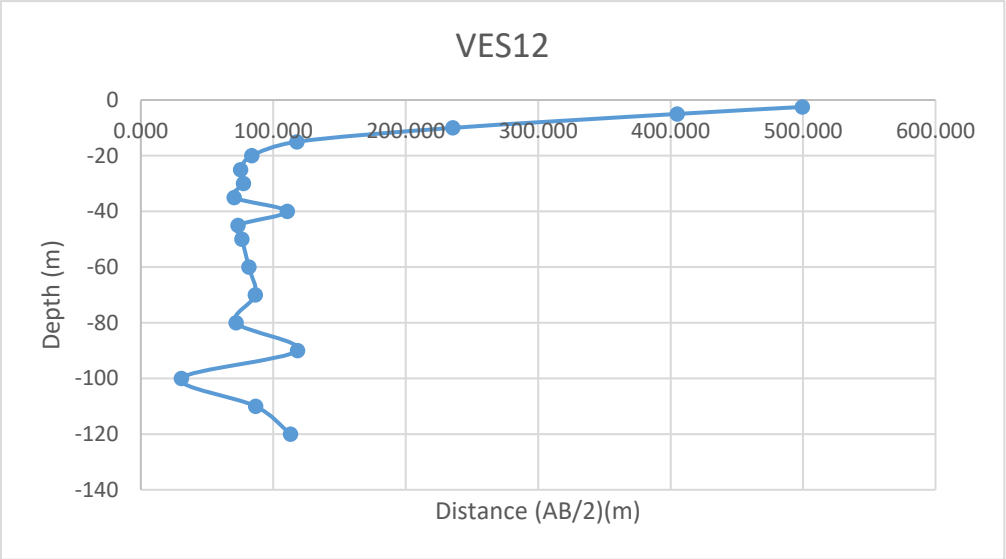

Annexure-XXII: Details of VES Survey

Date: 14/12/2024		VES-13				
Latitude	23.227107		Longitude	69.543019		
S.N	Current Electrode Spacing (AB/2)	Potential Electrode Spacing (MN)	Resistance (Ohm)	K value	Aparent Resistivity (Rho_a)	
1	2.5	1	1.43	18.846	26.950	-2.5
2	5	1	0.221	77.73975	17.180	-5
3	10	1	0.0633	313.3148	19.833	-10
4	15	1	0.0312	705.9398	22.025	-15
5	20	1	0.0195	1255.615	24.484	-20
6	25	1	0.0138	1962.34	27.080	-25
7	30	1	0.0106	2826.115	29.957	-30
8	35	1	0.0084	3846.94	32.314	-35
9	40	1	0.00702	5024.815	35.274	-40
10	45	1	0.00587	6359.74	37.332	-45
11	50	1	0.00505	7851.715	39.651	-50
12	60	1	0.00378	11306.81	42.740	-60
13	70	1	0.0029	15390.11	44.631	-70
14	80	1	0.0024	20101.61	48.244	-80
15	90	1	0.002	25441.31	50.883	-90
16	100	1	0.0017	31409.21	53.396	-100

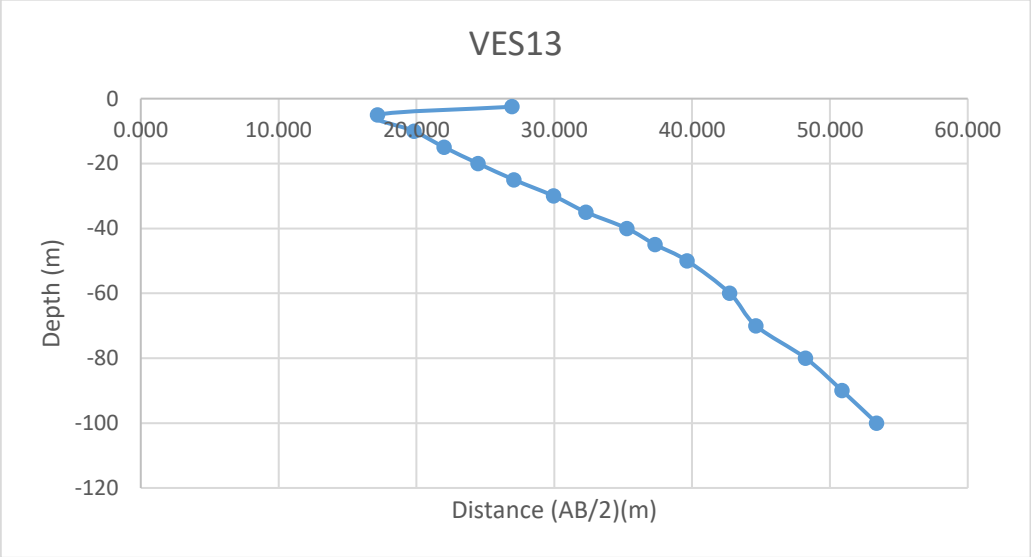

Annexure-XXII: Details of VES Survey

Date: 15/12/2024			VES-14			
Latitude	23.226833		Longitude	69.536295		
S.N	Current Electrode Spacing (AB/2)	Potential Electrode Spacing (MN)	Resistance (Ohm)	K value	Aparent Resistivity (Rho_a)	
1	2.5	1	10.68	18.846	201.275	-2.5
2	5	1	1.12	77.73975	87.069	-5
3	10	1	0.114	313.3148	35.718	-10
4	15	1	0.0429	705.9398	30.285	-15
5	20	1	0.0252	1255.615	31.641	-20
6	25	1	0.017	1962.34	33.360	-25
7	30	1	0.0126	2826.115	35.609	-30
8	35	1	0.0099	3846.94	38.085	-35
9	40	1	0.00795	5024.815	39.947	-40
10	45	1	0.00665	6359.74	42.292	-45
11	50	1	0.0058	7851.715	45.540	-50
12	60	1	0.0044	11306.81	49.750	-60
13	70	1	0.00355	15390.11	54.635	-70
14	80	1	0.003	20101.61	60.305	-80
15	90	1	0.0025	25441.31	63.603	-90
16	100	1	0.00208	31409.21	65.331	-100
17	110	1	0.0018	38005.31	68.410	

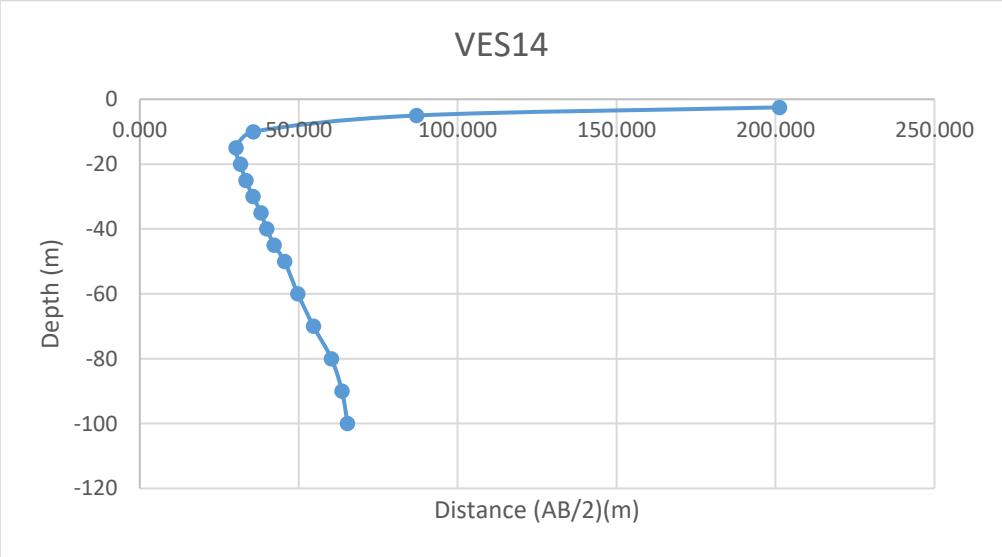

Annexure-XXII: Details of VES Survey

Date: 15/12/2024		VES-15				
Latitude	23.22737		Longitude	69.534817		
S.N	Current Electrode Spacing (AB/2)	Potential Electrode Spacing (MN)	Resistance (Ohm)	K value	Aparent Resistivity (Rho_a)	
1	2.5	1	12.24	18.846	230.675	-2.5
2	5	1	1.324	77.73975	102.927	-5
3	10	1	0.1645	313.3148	51.540	-10
4	15	1	0.0687	705.9398	48.498	-15
5	20	1	0.0414	1255.615	51.982	-20
6	25	1	0.0283	1962.34	55.534	-25
7	30	1	0.0216	2826.115	61.044	-30
8	35	1	0.0173	3846.94	66.552	-35
9	40	1	0.0142	5024.815	71.352	-40
10	45	1	0.0121	6359.74	76.953	-45
11	50	1	0.0106	7851.715	83.228	-50
12	60	1	0.00806	11306.81	91.133	-60
13	70	1	0.00656	15390.11	100.959	-70
14	80	1	0.00534	20101.61	107.343	-80
15	90	1	0.0043	25441.31	109.398	-90
16	100	1	0.00377	31409.21	118.413	-100

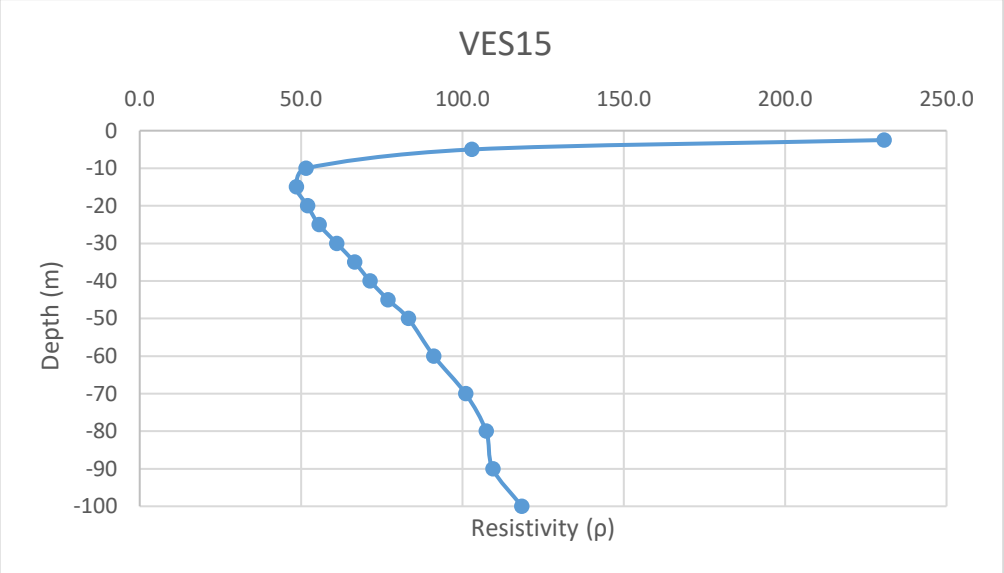

Annexure-XXII: Details of VES Survey

Date: 15/12/2024			VES-16			
Latitude	23.227005		Longitude	69.532597		
S.N	Current Electrode Spacing (AB/2)	Potential Electrode Spacing (MN)	Resistance (Ohm)	K value	Aparent Resistivity (Rho_a)	
1	2.5	1	1.56	18.846	29.400	-2.5
2	5	1	0.204	77.73975	15.859	-5
3	10	1	0.0505	313.3148	15.822	-10
4	15	1	0.0258	705.9398	18.213	-15
5	20	1	0.0162	1255.615	20.341	-20
6	25	1	0.01137	1962.34	22.312	-25
7	30	1	0.00904	2826.115	25.548	-30
8	35	1	0.0074	3846.94	28.467	-35
9	40	1	0.00625	5024.815	31.405	-40
10	45	1	0.00545	6359.74	34.661	-45
11	50	1	0.0048	7851.715	37.688	-50
12	60	1	0.00367	11306.81	41.496	-60
13	70	1	0.003	15390.11	46.170	-70
14	80	1	0.00234	20101.61	47.038	-80
15	90	1	0.00183	25441.31	46.558	-90
16	100	1	0.00167	31409.21	52.453	-100

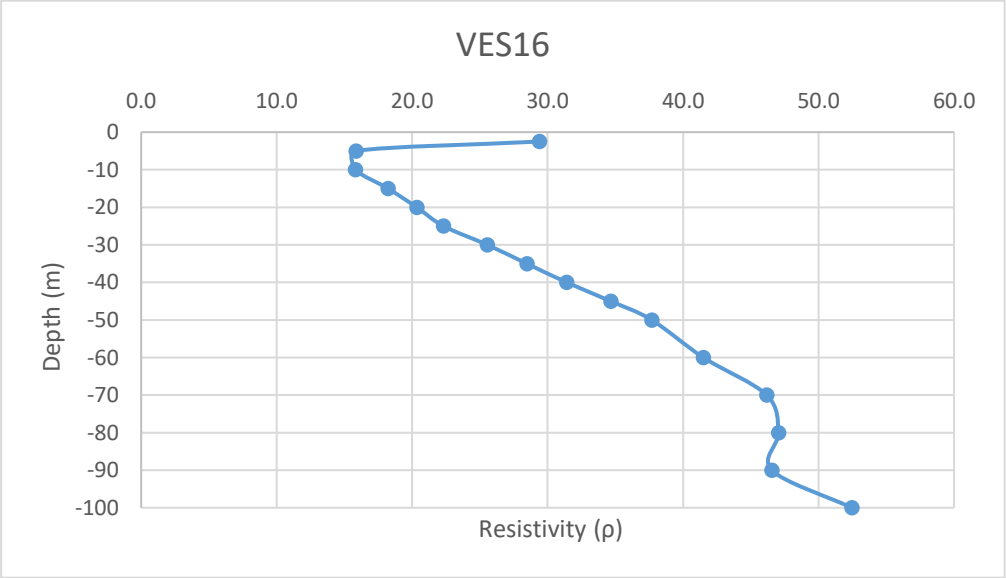

Annexure-XXII: Details of VES Survey

Date: 16/12/2024			VES-17			
Latitude	23.192655		Longitude	69.52488		
S.N	Current Electrode Spacing (AB/2)	Potential Electrode Spacing (MN)	Resistance (Ohm)	K value	Aparent Resistivity (Rho_a)	
1	2.5	1	22.3	18.846	420.266	-2.5
2	5	1	6.7	77.73975	520.856	-5
3	10	1	1.49	313.3148	466.839	-10
4	15	1	0.553	705.9398	390.385	-15
5	20	1	0.243	1255.615	305.114	-20
6	25	1	0.133	1962.34	260.991	-25
7	30	1	0.082	2826.115	231.741	-30
8	35	1	0.0554	3846.94	213.120	-35
9	40	1	0.0392	5024.815	196.973	-40
10	45	1	0.0296	6359.74	188.248	-45
11	50	1	0.0235	7851.715	184.515	-50
12	60	1	0.0165	11306.81	186.562	-60
13	70	1	0.0123	15390.11	189.298	-70
14	80	1	0.0094	20101.61	188.955	-80
15	90	1	0.00765	25441.31	194.626	-90
16	100	1	0.00617	31409.21	193.795	-100

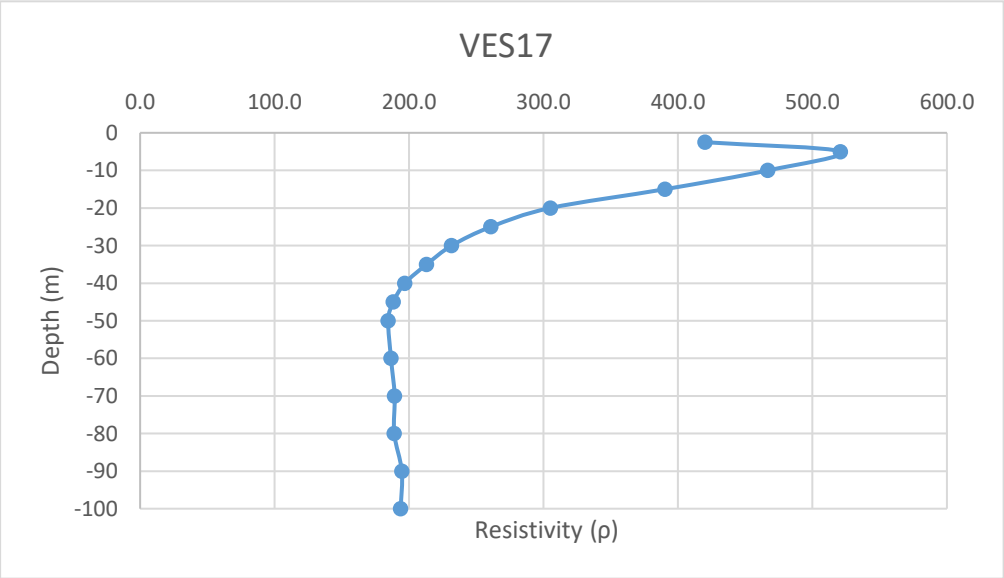

Annexure-XXII: Details of VES Survey

Date: 16/12/2024		VES-18				
Latitude	23.19668		Longitude	69.523086		
S.N	Current Electrode Spacing (AB/2)	Potential Electrode Spacing (MN)	Resistance (Ohm)	K value	Aparent Resistivity (Rho_a)	
1	2.5	1	3.64	18.846	68.599	-2.5
2	5	1	0.848	77.73975	65.923	-5
3	10	1	0.14	313.3148	43.864	-10
4	15	1	0.071	705.9398	50.122	-15
5	20	1	0.0454	1255.615	57.005	-20
6	25	1	0.0332	1962.34	65.150	-25
7	30	1	0.0256	2826.115	72.349	-30
8	35	1	0.0204	3846.94	78.478	-35
9	40	1	0.0165	5024.815	82.909	-40
10	45	1	0.0139	6359.74	88.400	-45
11	50	1	0.01165	7851.715	91.472	-50
12	60	1	0.00822	11306.81	92.942	-60
13	70	1	0.006	15390.11	92.341	-70
14	80	1	0.00481	20101.61	96.689	-80
15	90	1	0.00395	25441.31	100.493	-90
16	100	1	0.0035	31409.21	109.932	-100

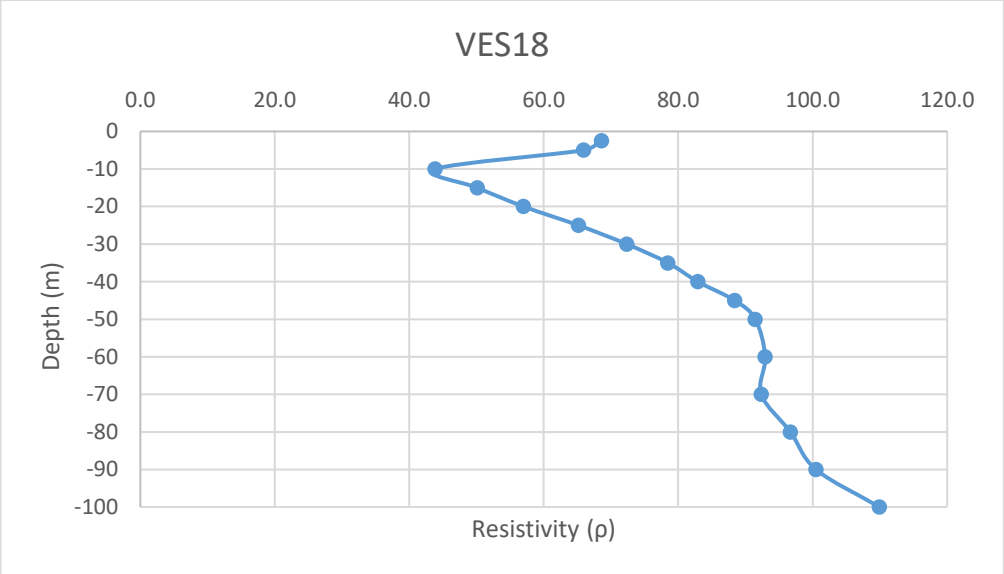

Annexure-XXII: Details of VES Survey

Date: 17/12/2024			VES-19			
Latitude	23.19467		Longitude	69.520368		
S.N	Current Electrode Spacing (AB/2)	Potential Electrode Spacing (MN)	Resistance (Ohm)	K value	Aparent Resistivity (Rho_a)	
1	2.5	1	3.41	18.846	64.265	-2.5
2	5	1	0.441	77.73975	34.283	-5
3	10	1	0.145	313.3148	45.431	-10
4	15	1	0.075	705.9398	52.945	-15
5	20	1	0.0481	1255.615	60.395	-20
6	25	1	0.034	1962.34	66.720	-25
7	30	1	0.0256	2826.115	72.349	-30
8	35	1	0.0188	3846.94	72.322	-35
9	40	1	0.0141	5024.815	70.850	-40
10	45	1	0.0109	6359.74	69.321	-45
11	50	1	0.00899	7851.715	70.587	-50
12	60	1	0.00653	11306.81	73.834	-60
13	70	1	0.00513	15390.11	78.951	-70
14	80	1	0.00424	20101.61	85.231	-80
15	90	1	0.00356	25441.31	90.571	-90
16	100	1	0.0031	31409.21	97.369	-100

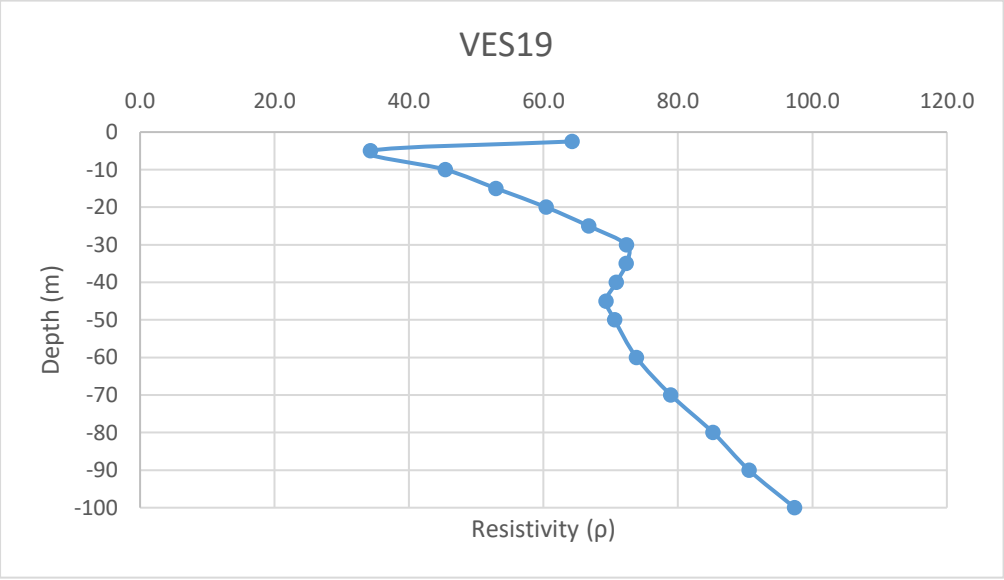

Annexure-XXII: Details of VES Survey

Date: 18/12/2024			VES-20			
Latitude	23.194345		Longitude	69.525985		
S.N	Current Electrode Spacing (AB/2)	Potential Electrode Spacing (MN)	Resistance (Ohm)	K value	Aparent Resistivity (Rho_a)	
1	2.5	1	12.9	18.846	243.113	-2.5
2	5	1	2.31	77.73975	179.579	-5
3	10	1	0.703	313.3148	220.260	-10
4	15	1	0.255	705.9398	180.015	-15
5	20	1	0.126	1255.615	158.207	-20
6	25	1	0.078	1962.34	153.063	-25
7	30	1	0.0531	2826.115	150.067	-30
8	35	1	0.0408	3846.94	156.955	-35
9	40	1	0.0349	5024.815	175.366	-40
10	45	1	0.0302	6359.74	192.064	-45
11	50	1	0.0258	7851.715	202.574	-50
12	60	1	0.0195	11306.81	220.483	-60
13	70	1	0.0152	15390.11	233.930	-70
14	80	1	0.0124	20101.61	249.260	-80
15	90	1	0.01048	25441.31	266.625	-90
16	100	1	0.00909	31409.21	285.510	-100

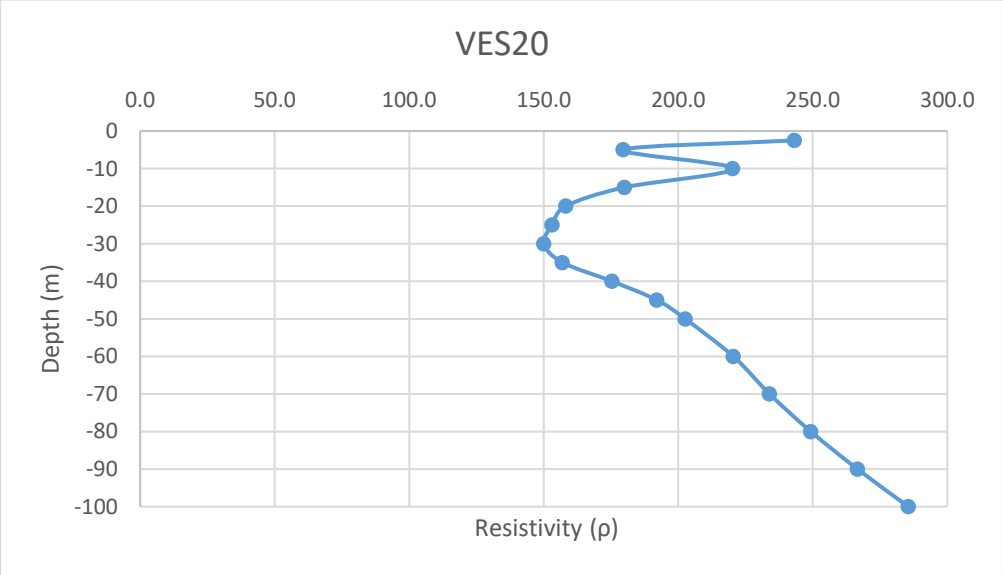

Annexure-XXII: Details of VES Survey

Date: 18/12/2024			VES-21			
Latitude	23.18955		Longitude	69.523838		
S.N	Current Electrode Spacing (AB/2)	Potential Electrode Spacing (MN)	Resistance (Ohm)	K value	Aparent Resistivity (Rho_a)	
1	2.5	1	23.9	18.846	450.419	-2.5
2	5	1	5.23	77.73975	406.579	-5
3	10	1	1.166	313.3148	365.325	-10
4	15	1	0.448	705.9398	316.261	-15
5	20	1	0.215	1255.615	269.957	-20
6	25	1	0.129	1962.34	253.142	-25
7	30	1	0.089	2826.115	251.524	-30
8	35	1	0.0659	3846.94	253.513	-35
9	40	1	0.0511	5024.815	256.768	-40
10	45	1	0.041	6359.74	260.749	-45
11	50	1	0.0335	7851.715	263.032	-50
12	60	1	0.0241	11306.81	272.494	-60
13	70	1	0.0189	15390.11	290.873	-70
14	80	1	0.0156	20101.61	313.585	-80
15	90	1	0.0129	25441.31	328.193	-90
16	100	1	0.01105	31409.21	347.072	-100

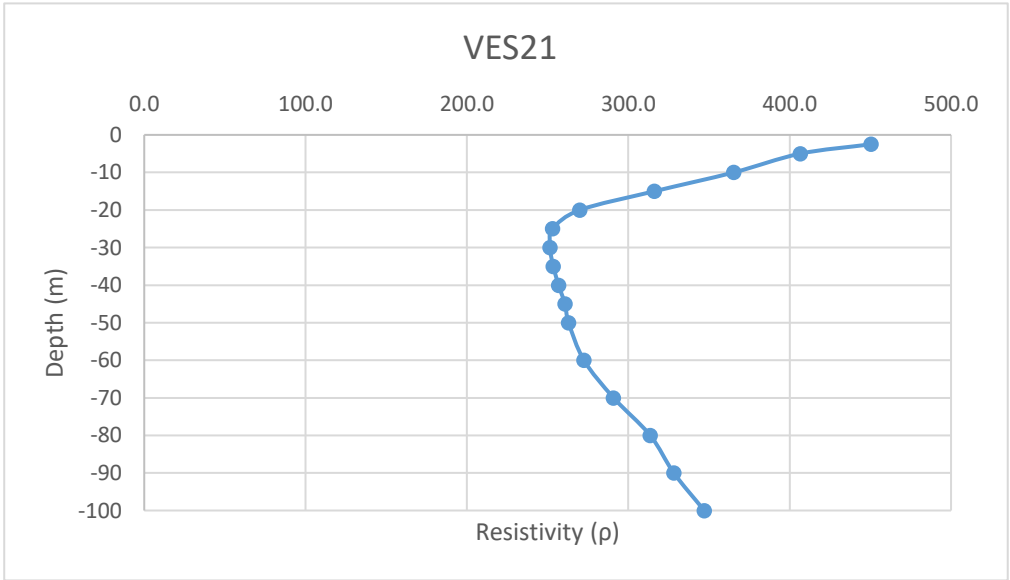

Annexure-XXII: Details of VES Survey

Date: 19/12/2024			VES-22			
Latitude	23.201008		Longitude	69.538357		
S.N	Current Electrode Spacing (AB/2)	Potential Electrode Spacing (MN)	Resistance (Ohm)	K value	Aparent Resistivity (Rho_a)	
1	2.5	1	8.38	18.846	157.929	-2.5
2	5	1	1.29	77.73975	100.284	-5
3	10	1	0.256	313.3148	80.209	-10
4	15	1	0.1	705.9398	70.594	-15
5	20	1	0.056	1255.615	70.314	-20
6	25	1	0.0339	1962.34	66.523	-25
7	30	1	0.0218	2826.115	61.609	-30
8	35	1	0.0162	3846.94	62.320	-35
9	40	1	0.0125	5024.815	62.810	-40
10	45	1	0.01	6359.74	63.597	-45
11	50	1	0.00852	7851.715	66.897	-50
12	60	1	0.00641	11306.81	72.477	-60
13	70	1	0.0051	15390.11	78.490	-70
14	80	1	0.00422	20101.61	84.829	-80
15	90	1	0.00356	25441.31	90.571	-90
16	100	1	0.00276	31409.21	86.689	-100

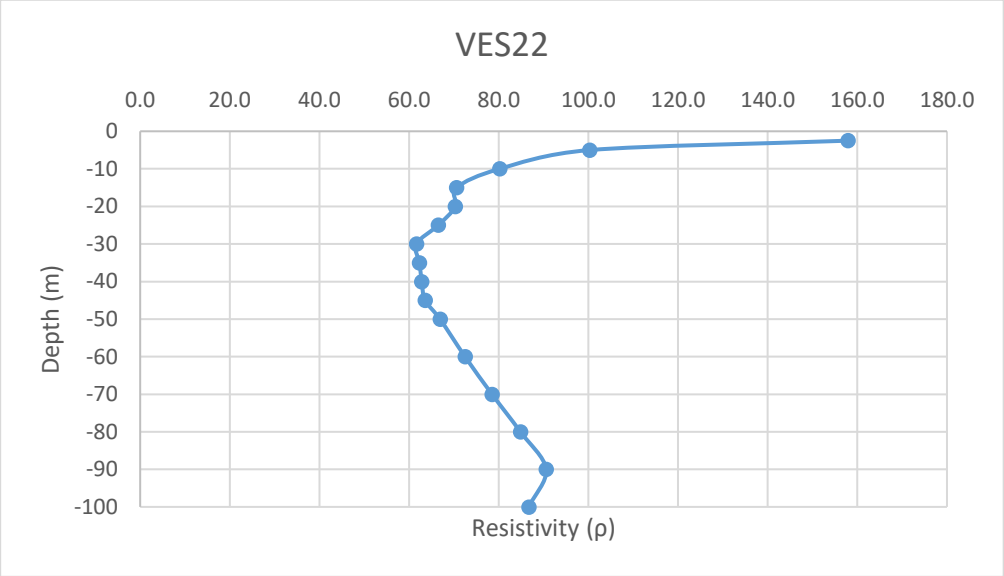

Annexure-XXII: Details of VES Survey

Date: 19/12/2024		VES-23				
Latitude	23.189378		Longitude	69.533657		
S.N	Current Electrode Spacing (AB/2)	Potential Electrode Spacing (MN)	Resistance (Ohm)	K value	Aparent Resistivity (Rho_a)	
1	2.5	1	7.31	18.846	137.764	-2.5
2	5	1	1.161	77.73975	90.256	-5
3	10	1	0.401	313.3148	125.639	-10
4	15	1	0.176	705.9398	124.245	-15
5	20	1	0.096	1255.615	120.539	-20
6	25	1	0.0555	1962.34	108.910	-25
7	30	1	0.037	2826.115	104.566	-30
8	35	1	0.025	3846.94	96.173	-35
9	40	1	0.0185	5024.815	92.959	-40
10	45	1	0.0139	6359.74	88.400	-45
11	50	1	0.01105	7851.715	86.761	-50
12	60	1	0.00771	11306.81	87.176	-60
13	70	1	0.00575	15390.11	88.493	-70
14	80	1	0.00435	20101.61	87.442	-80
15	90	1	0.00345	25441.31	87.773	-90
16	100	1	0.0028	31409.21	87.946	-100

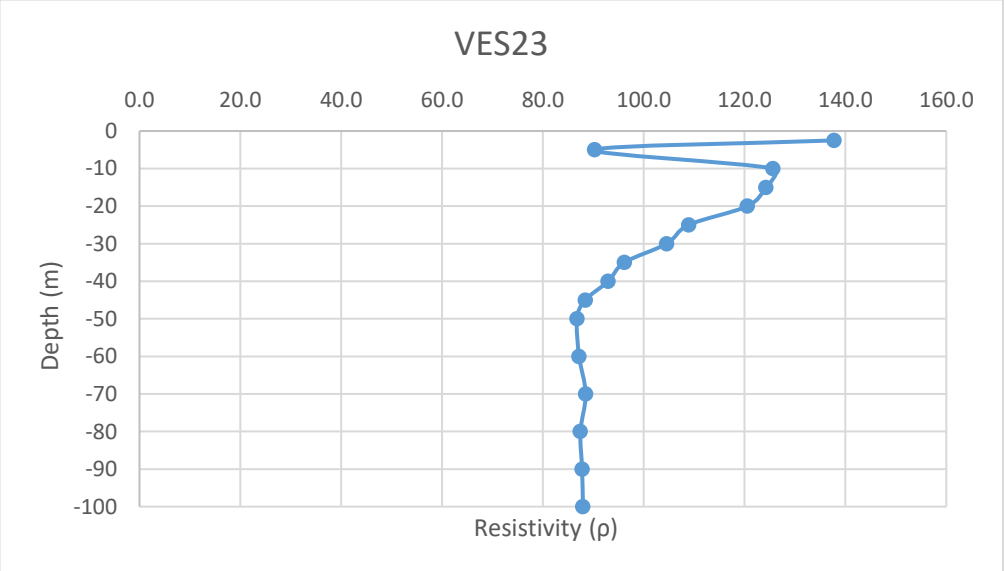

Annexure-XXII: Details of VES Survey

Date: 19/12/2024			VES-24			
Latitude	23.188665		Longitude	69.529407		
S.N	Current Electrode Spacing (AB/2)	Potential Electrode Spacing (MN)	Resistance (Ohm)	K value	Aparent Resistivity (Rho_a)	
1	2.5	1	23.3	18.846	439.112	-2.5
2	5	1	8.88	77.73975	690.329	-5
3	10	1	2.67	313.3148	836.550	-10
4	15	1	1.29	705.9398	910.662	-15
5	20	1	0.658	1255.615	826.195	-20
6	25	1	0.369	1962.34	724.103	-25
7	30	1	0.205	2826.115	579.354	-30
8	35	1	0.126	3846.94	484.714	-35
9	40	1	0.078	5024.815	391.936	-40
10	45	1	0.05	6359.74	317.987	-45
11	50	1	0.0359	7851.715	281.877	-50
12	60	1	0.0204	11306.81	230.659	-60
13	70	1	0.0147	15390.11	226.235	-70
14	80	1	0.01029	20101.61	206.846	-80
15	90	1	0.00805	25441.31	204.803	-90
16	100	1	0.00686	31409.21	215.467	-100
17	110	1	0.0055	38005.31	209.029	-110

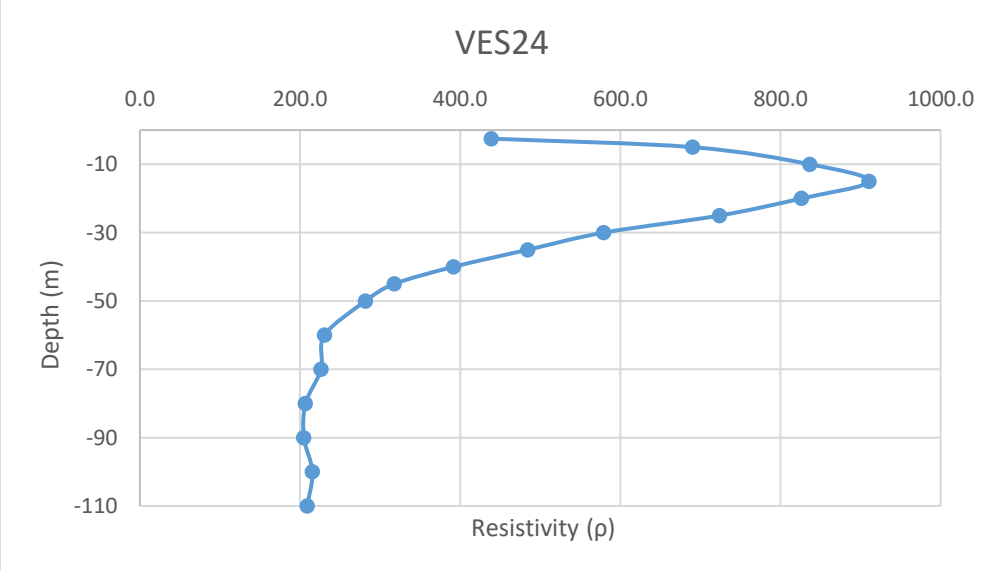

Annexure-XXII: Details of VES Survey

Date: 20/12/2024			VES-25			
Latitude	23.183453		Longitude	69.539355		
S.N	Current Electrode Spacing (AB/2)	Potential Electrode Spacing (MN)	Resistance (Ohm)	K value	Aparent Resistivity (Rho_a)	
1	2.5	1	23.9	18.846	450.419	-2.5
2	5	1	7.1	77.73975	551.952	-5
3	10	1	1.51	313.3148	473.105	-10
4	15	1	0.417	705.9398	294.377	-15
5	20	1	0.178	1255.615	223.499	-20
6	25	1	0.086	1962.34	168.761	-25
7	30	1	0.05	2826.115	141.306	-30
8	35	1	0.033	3846.94	126.949	-35
9	40	1	0.0233	5024.815	117.078	-40
10	45	1	0.017	6359.74	108.116	-45
11	50	1	0.0129	7851.715	101.287	-50
12	60	1	0.00795	11306.81	89.889	-60
13	70	1	0.0051	15390.11	78.490	-70
14	80	1	0.00355	20101.61	71.361	-80
15	90	1	0.0026	25441.31	66.147	-90
16	100	1	0.00215	31409.21	67.530	-100
17	110	1	0.00165	38005.31	62.709	-110

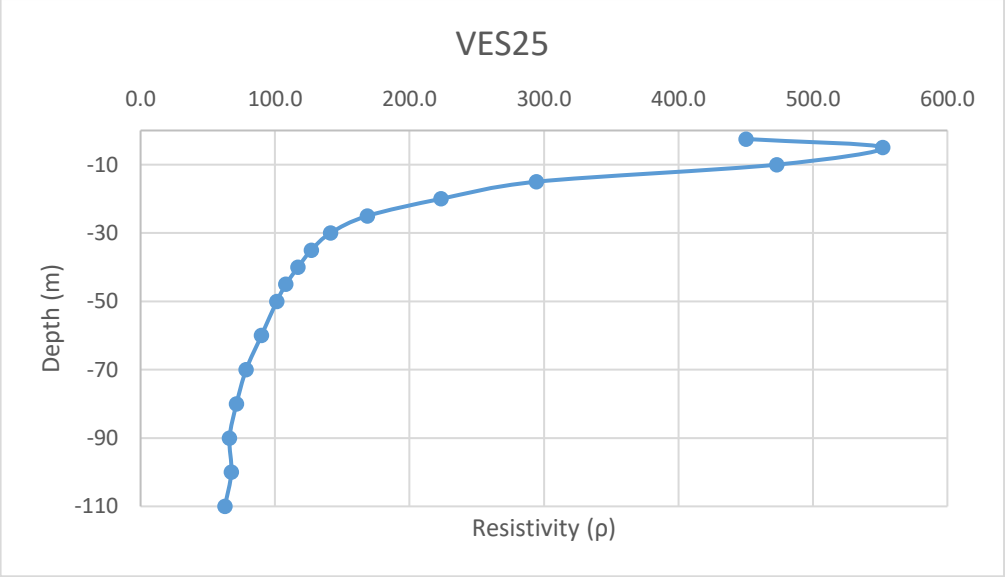

Annexure-XXII: Details of VES Survey

Date: 20/12/2024			VES-26			
Latitude	23.18212		Longitude	69.541245		
S.N	Current Electrode Spacing (AB/2)	Potential Electrode Spacing (MN)	Resistance (Ohm)	K value	Aparent Resistivity (Rho_a)	
1	2.5	1	0.276	18.846	5.201	-2.5
2	5	1	0.044	77.73975	3.421	-5
3	10	1	0.01	313.3148	3.133	-10
4	15	1	0.0048	705.9398	3.389	-15
5	20	1	0.00302	1255.615	3.792	-20
6	25	1	0.0021	1962.34	4.121	-25
7	30	1	0.0016	2826.115	4.522	-30
8	35	1	0.0013	3846.94	5.001	-35
9	40	1	0.00105	5024.815	5.276	-40
10	45	1	0.00095	6359.74	6.042	-45
11	50	1	0.00085	7851.715	6.674	-50
12	60	1	0.000649	11306.81	7.338	-60
13	70	1	0.000499	15390.11	7.680	-70
14	80	1	0.000379	20101.61	7.619	-80
15	90	1	0.000319	25441.31	8.116	-90
16	100	1	0.000224	31409.21	7.036	-100
17	110	1	0.00015	38005.31	5.701	-110

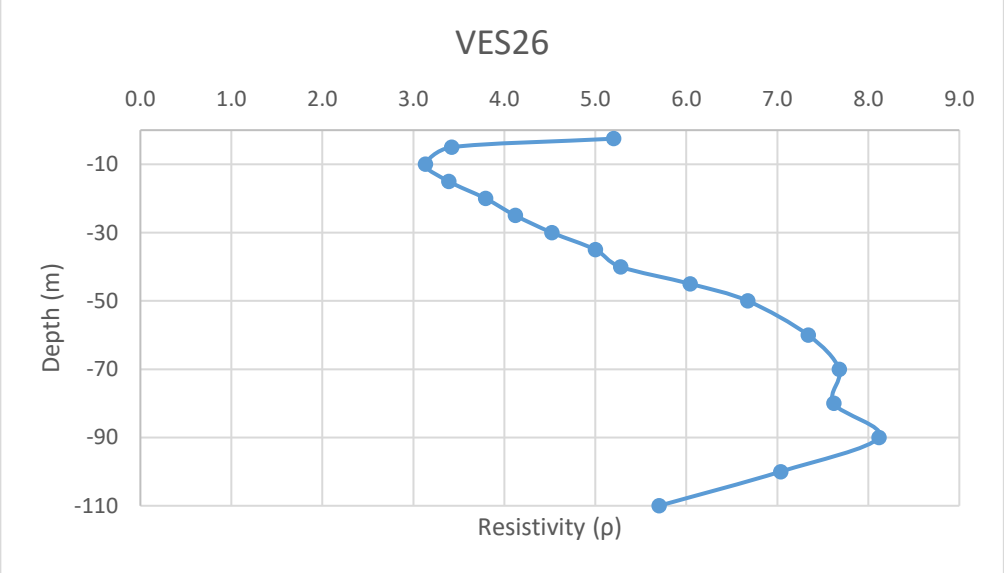

Annexure-XXII: Details of VES Survey

Date: 21/12/2024			VES-27			
Latitude	23.191677		Longitude	69.639958		
S.N	Current Electrode Spacing (AB/2)	Potential Electrode Spacing (MN)	Resistance (Ohm)	K value	Aparent Resistivity (Rho_a)	
1	2.5	1	42.6	18.846	802.840	-2.5
2	5	1	5.58	77.73975	433.788	-5
3	10	1	0.126	313.3148	39.478	-10
4	15	1	0.011	705.9398	7.765	-15
5	20	1	0.00401	1255.615	5.035	-20
6	25	1	0.00264	1962.34	5.181	-25
7	30	1	0.00193	2826.115	5.454	-30
8	35	1	0.00157	3846.94	6.040	-35
9	40	1	0.00142	5024.815	7.135	-40
10	45	1	0.0012	6359.74	7.632	-45
11	50	1	0.0011	7851.715	8.637	-50
12	60	1	0.001	11306.81	11.307	-60
13	70	1	0.00071	15390.11	10.927	-70
14	80	1	0.00064	20101.61	12.865	-80
15	90	1	0.0006	25441.31	15.265	-90
16	100	1	0.0004	31409.21	12.564	-100

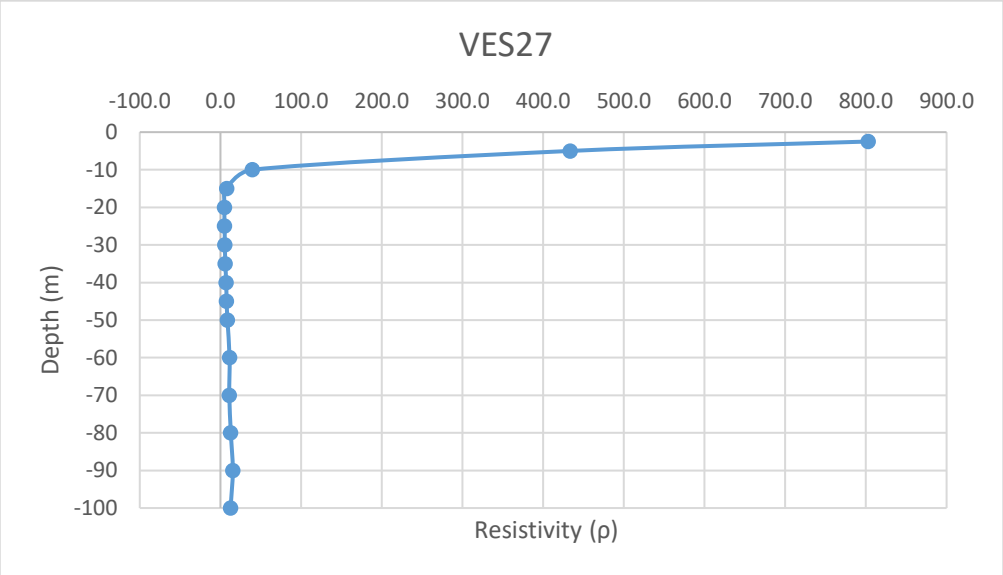

Annexure-XXII: Details of VES Survey

Date: 21/12/2024			VES-28			
Latitude	23.18919		Longitude	69.640363		
S.N	Current Electrode Spacing (AB/2)	Potential Electrode Spacing (MN)	Resistance (Ohm)	K value	Aparent Resistivity (Rho_a)	
1	2.5	1	39.7	18.846	748.186	-2.5
2	5	1	5.26	77.73975	408.911	-5
3	10	1	0.254	313.3148	79.582	-10
4	15	1	0.023	705.9398	16.237	-15
5	20	1	0.00471	1255.615	5.914	-20
6	25	1	0.0026	1962.34	5.102	-25
7	30	1	0.0017	2826.115	4.804	-30
8	35	1	0.0013	3846.94	5.001	-35
9	40	1	0.001	5024.815	5.025	-40
10	45	1	0.001	6359.74	6.360	-45
11	50	1	0.0009	7851.715	7.067	-50
12	60	1	0.00064	11306.81	7.236	-60
13	70	1	0.0004	15390.11	6.156	-70
14	80	1	0.00035	20101.61	7.036	-80
15	90	1	0.0002	25441.31	5.088	-90
16	100	1	0.00014	31409.21	4.397	-100
17	110	1	0.00021	38005.31	7.981	-110

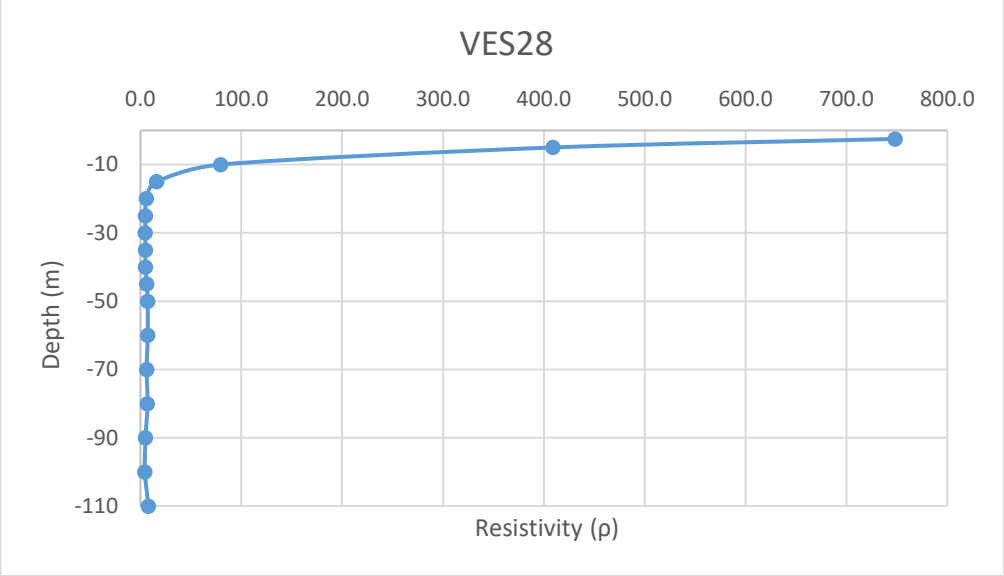

Annexure-XXII: Details of VES Survey

Date: 23/12/2024		VES-29				
Latitude	23.160278		Longitude	69.624822		
S.N	Current Electrode Spacing (AB/2)	Potential Electrode Spacing (MN)	Resistance (Ohm)	K value	Aparent Resistivity (Rho_a)	
1	2.5	1	15.3	18.846	288.344	-2.5
2	5	1	1.8	77.73975	139.932	-5
3	10	1	0.209	313.3148	65.483	-10
4	15	1	0.102	705.9398	72.006	-15
5	20	1	0.0719	1255.615	90.279	-20
6	25	1	0.0457	1962.34	89.679	-25
7	30	1	0.0322	2826.115	91.001	-30
8	35	1	0.0219	3846.94	84.248	-35
9	40	1	0.0164	5024.815	82.407	-40
10	45	1	0.0121	6359.74	76.953	-45
11	50	1	0.0095	7851.715	74.591	-50
12	60	1	0.0059	11306.81	66.710	-60
13	70	1	0.00428	15390.11	65.870	-70
14	80	1	0.00337	20101.61	67.742	-80
15	90	1	0.00255	25441.31	64.875	-90
16	100	1	0.002	31409.21	62.818	-100

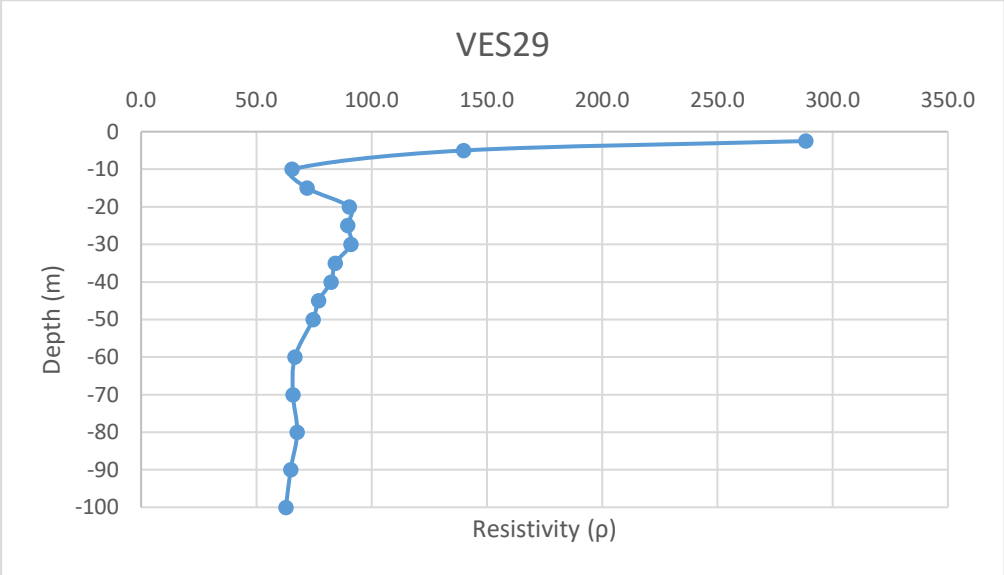

Annexure-XXII: Details of VES Survey

Date: 23/12/2024		VES-30				
Latitude	23.160548		Longitude	69.623283		
S.N	Current Electrode Spacing (AB/2)	Potential Electrode Spacing (MN)	Resistance (Ohm)	K value	Aparent Resistivity (Rho_a)	
1	2.5	1	8.505	18.846	160.285	-2.5
2	5	1	0.978	77.73975	76.029	-5
3	10	1	0.12525	313.3148	39.243	-10
4	15	1	0.06175	705.9398	43.592	-15
5	20	1	0.0432	1255.615	54.243	-20
6	25	1	0.0276	1962.34	54.161	-25
7	30	1	0.019325	2826.115	54.615	-30
8	35	1	0.013425	3846.94	51.645	-35
9	40	1	0.01025	5024.815	51.504	-40
10	45	1	0.00768	6359.74	48.843	-45
11	50	1	0.00615	7851.715	48.288	-50
12	60	1	0.00386	11306.81	43.644	-60
13	70	1	0.002765	15390.11	42.554	-70
14	80	1	0.002185	20101.61	43.922	-80
15	90	1	0.001675	25441.31	42.614	-90
16	100	1	0.001287	31409.21	40.424	-100

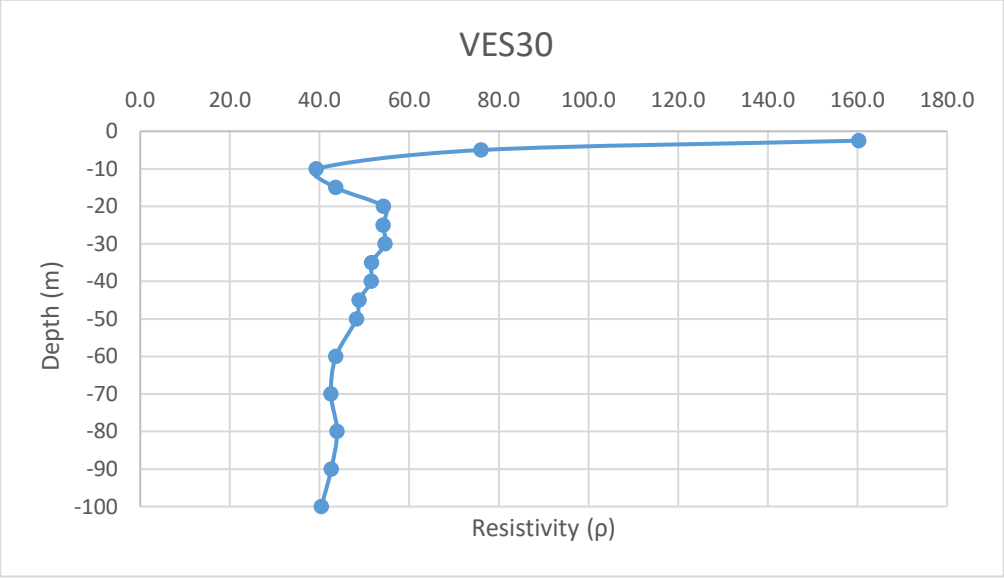

Annexure-XXII: Details of VES Survey

Date: 23/12/2024			VES-31			
Latitude	23.161342		Longitude	69.617467		
S.N	Current Electrode Spacing (AB/2)	Potential Electrode Spacing (MN)	Resistance (Ohm)	K value	Aparent Resistivity (Rho_a)	
1	2.5	1	1.71	18.846	32.227	-2.5
2	5	1	0.156	77.73975	12.127	-5
3	10	1	0.0415	313.3148	13.003	-10
4	15	1	0.0215	705.9398	15.178	-15
5	20	1	0.0145	1255.615	18.206	-20
6	25	1	0.0095	1962.34	18.642	-25
7	30	1	0.00645	2826.115	18.228	-30
8	35	1	0.00495	3846.94	19.042	-35
9	40	1	0.00411	5024.815	20.652	-40
10	45	1	0.00326	6359.74	20.733	-45
11	50	1	0.0028	7851.715	21.985	-50
12	60	1	0.00182	11306.81	20.578	-60
13	70	1	0.00125	15390.11	19.238	-70
14	80	1	0.001	20101.61	20.102	-80
15	90	1	0.0008	25441.31	20.353	-90
16	100	1	0.000574	31409.21	18.029	-100

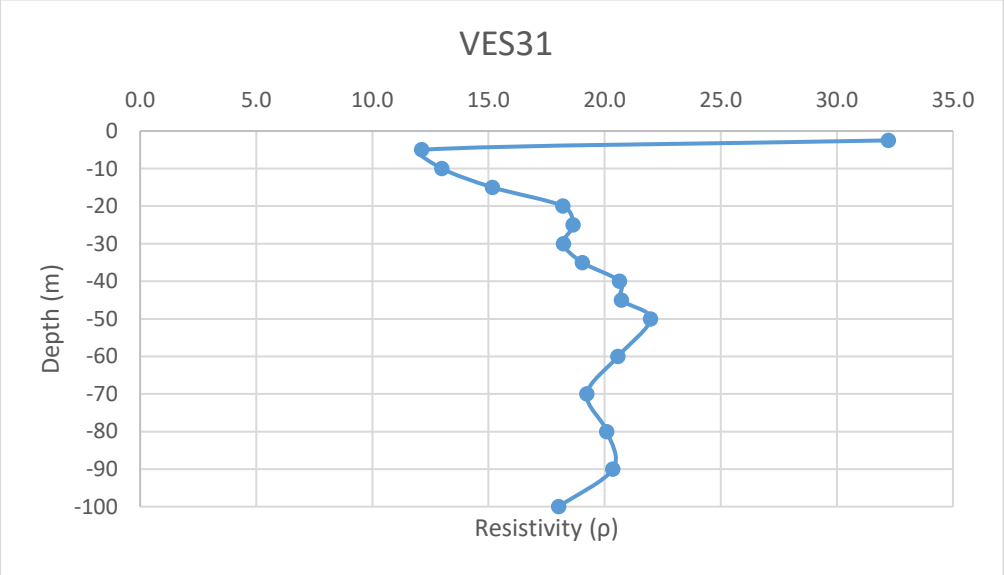

Annexure-XXII: Details of VES Survey

Date: 23/12/2024			VES-32			
Latitude	23.16032		Longitude	69.629115		
S.N	Current Electrode Spacing (AB/2)	Potential Electrode Spacing (MN)	Resistance (Ohm)	K value	Aparent Resistivity (Rho_a)	
1	2.5	1	2.78	18.846	52.392	-2.5
2	5	1	0.299	77.73975	23.244	-5
3	10	1	0.098	313.3148	30.705	-10
4	15	1	0.035	705.9398	24.708	-15
5	20	1	0.02	1255.615	25.112	-20
6	25	1	0.013	1962.34	25.510	-25
7	30	1	0.01076	2826.115	30.409	-30
8	35	1	0.00685	3846.94	26.352	-35
9	40	1	0.00553	5024.815	27.787	-40
10	45	1	0.0047	6359.74	29.891	-45
11	50	1	0.00387	7851.715	30.386	-50
12	60	1	0.00285	11306.81	32.224	-60
13	70	1	0.0023	15390.11	35.397	-70
14	80	1	0.00185	20101.61	37.188	-80
15	90	1	0.0015	25441.31	38.162	-90
16	100	1	0.00124	31409.21	38.947	-100

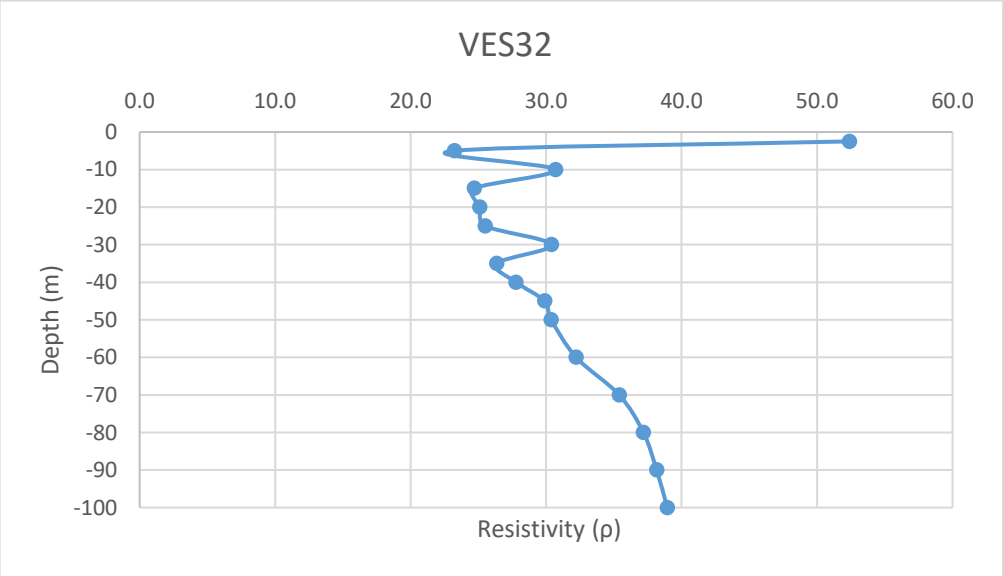

Annexure-XXII: Details of VES Survey

Date: 24/12/2024		VES-33				
Latitude	23.16149		Longitude	69.627327		
S.N	Current Electrode Spacing (AB/2)	Potential Electrode Spacing (MN)	Resistance (Ohm)	K value	Aparent Resistivity (Rho_a)	
1	2.5	1	9.04	18.846	170.368	-2.5
2	5	1	1.049	77.73975	81.549	-5
3	10	1	0.153	313.3148	47.937	-10
4	15	1	0.0685	705.9398	48.357	-15
5	20	1	0.0459	1255.615	57.633	-20
6	25	1	0.0293	1962.34	57.497	-25
7	30	1	0.0214	2826.115	60.479	-30
8	35	1	0.0143	3846.94	55.011	-35
9	40	1	0.0109	5024.815	54.770	-40
10	45	1	0.0084	6359.74	53.422	-45
11	50	1	0.0066	7851.715	51.821	-50
12	60	1	0.00437	11306.81	49.411	-60
13	70	1	0.00329	15390.11	50.633	-70
14	80	1	0.00261	20101.61	52.465	-80
15	90	1	0.00202	25441.31	51.391	-90
16	100	1	0.00162	31409.21	50.883	-100

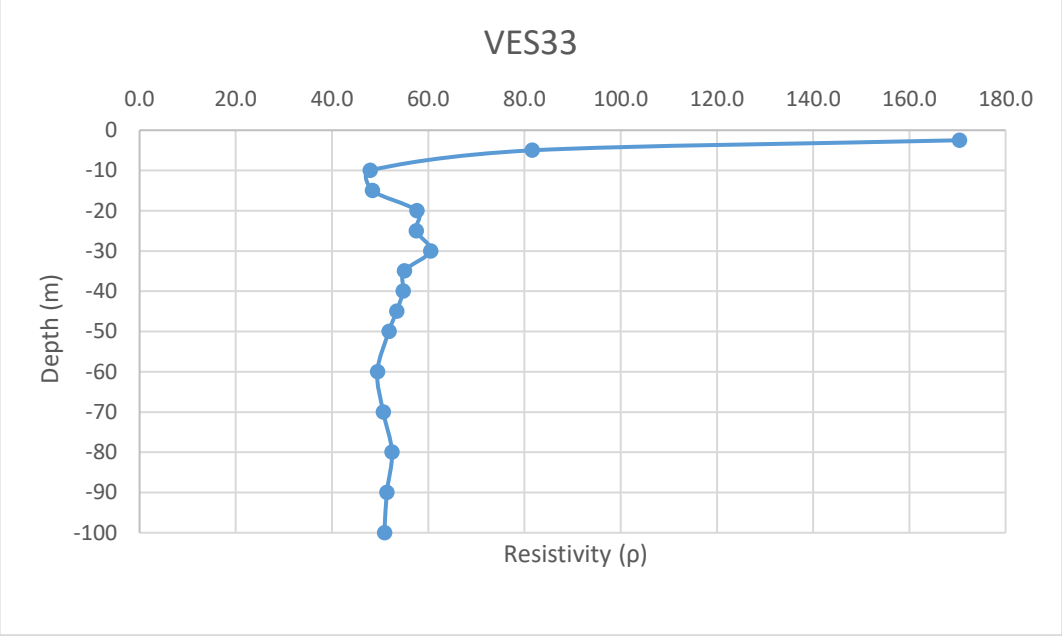

Annexure-XXII: Details of VES Survey

Date: 24/12/2024			VES-34			
Latitude	23.15397		Longitude	69.648108		
S.N	Current Electrode Spacing (AB/2)	Potential Electrode Spacing (MN)	Resistance (Ohm)	K value	Aparent Resistivity (Rho_a)	
1	2.5	1	26.5	18.846	499.419	-2.5
2	5	1	3.11	77.73975	241.771	-5
3	10	1	0.373	313.3148	116.866	-10
4	15	1	0.189	705.9398	133.423	-15
5	20	1	0.121	1255.615	151.929	-20
6	25	1	0.086	1962.34	168.761	-25
7	30	1	0.0635	2826.115	179.458	-30
8	35	1	0.0465	3846.94	178.883	-35
9	40	1	0.0356	5024.815	178.883	-40
10	45	1	0.028	6359.74	178.073	-45
11	50	1	0.0233	7851.715	182.945	-50
12	60	1	0.015	11306.81	169.602	-60
13	70	1	0.01172	15390.11	180.372	-70
14	80	1	0.00693	20101.61	139.304	-80
15	90	1	0.00451	25441.31	114.740	-90
16	100	1	0.0036	31409.21	113.073	-100

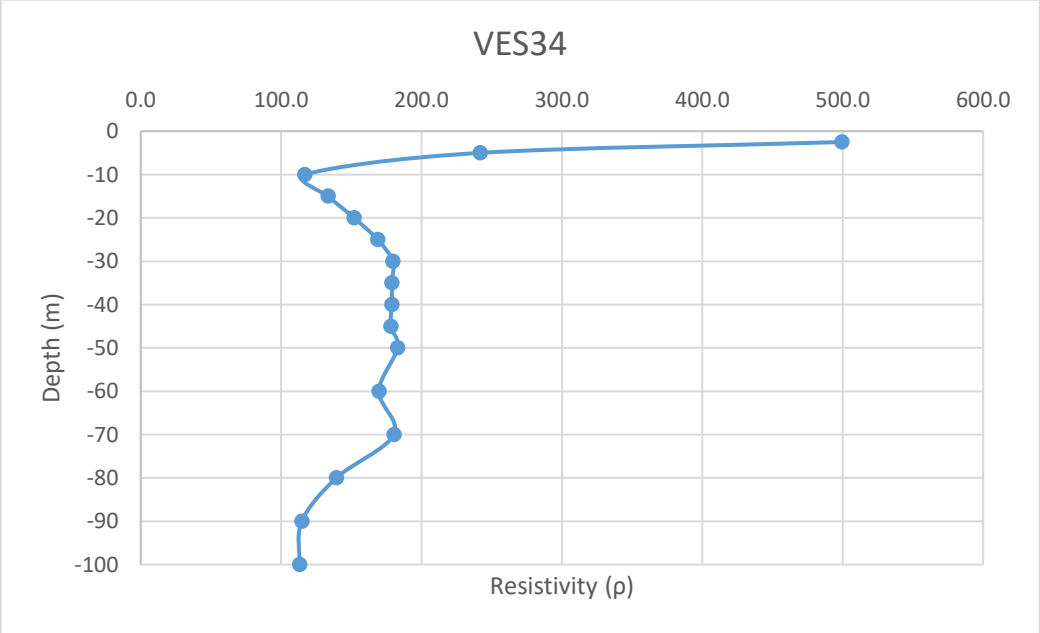

Annexure-XXII: Details of VES Survey

Date: 24/12/2024			VES-35			
Latitude	23.151287		Longitude	69.650398		
S.N	Current Electrode Spacing (AB/2)	Potential Electrode Spacing (MN)	Resistance (Ohm)	K value	Aparent Resistivity (Rho_a)	
1	2.5	1	17.6	18.846	331.690	-2.5
2	5	1	6.35	77.73975	493.647	-5
3	10	1	1.66	313.3148	520.102	-10
4	15	1	0.655	705.9398	462.391	-15
5	20	1	0.317	1255.615	398.030	-20
6	25	1	0.178	1962.34	349.296	-25
7	30	1	0.116	2826.115	327.829	-30
8	35	1	0.084	3846.94	323.143	-35
9	40	1	0.0643	5024.815	323.096	-40
10	45	1	0.0505	6359.74	321.167	-45
11	50	1	0.0415	7851.715	325.846	-50
12	60	1	0.0301	11306.81	340.335	-60
13	70	1	0.0204	15390.11	313.958	-70
14	80	1	0.0169	20101.61	339.717	-80
15	90	1	0.01103	25441.31	280.618	-90
16	100	1	0.00712	31409.21	223.634	-100

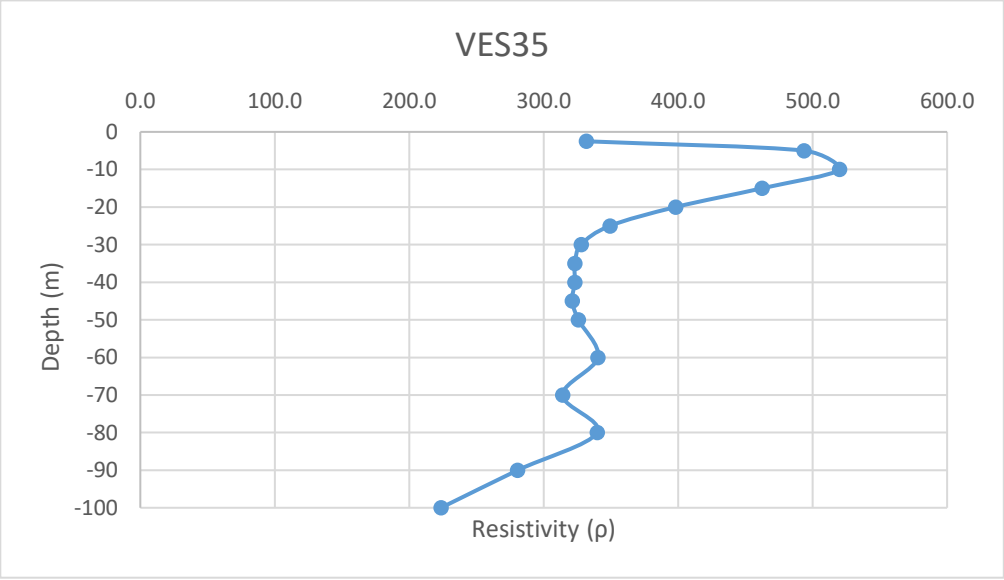

Annexure-XXII: Details of VES Survey

Date: 26/12/2024			VES-36			
Latitude	23.15185		Longitude	69.63702		
S.N	Current Electrode Spacing (AB/2)	Potential Electrode Spacing (MN)	Resistance (Ohm)	K value	Aparent Resistivity (Rho_a)	
1	2.5	1	29.2	18.846	550.303	-2.5
2	5	1	5.55	77.73975	431.456	-5
3	10	1	1.46	313.3148	457.440	-10
4	15	1	0.559	705.9398	394.620	-15
5	20	1	0.248	1255.615	311.392	-20
6	25	1	0.119	1962.34	233.518	-25
7	30	1	0.062	2826.115	175.219	-30
8	35	1	0.0356	3846.94	136.951	-35
9	40	1	0.0215	5024.815	108.034	-40
10	45	1	0.0144	6359.74	91.580	-45
11	50	1	0.01025	7851.715	80.480	-50
12	60	1	0.00605	11306.81	68.406	-60
13	70	1	0.00414	15390.11	63.715	-70
14	80	1	0.00275	20101.61	55.279	-80
15	90	1	0.00205	25441.31	52.155	-90
16	100	1	0.00155	31409.21	48.684	-100

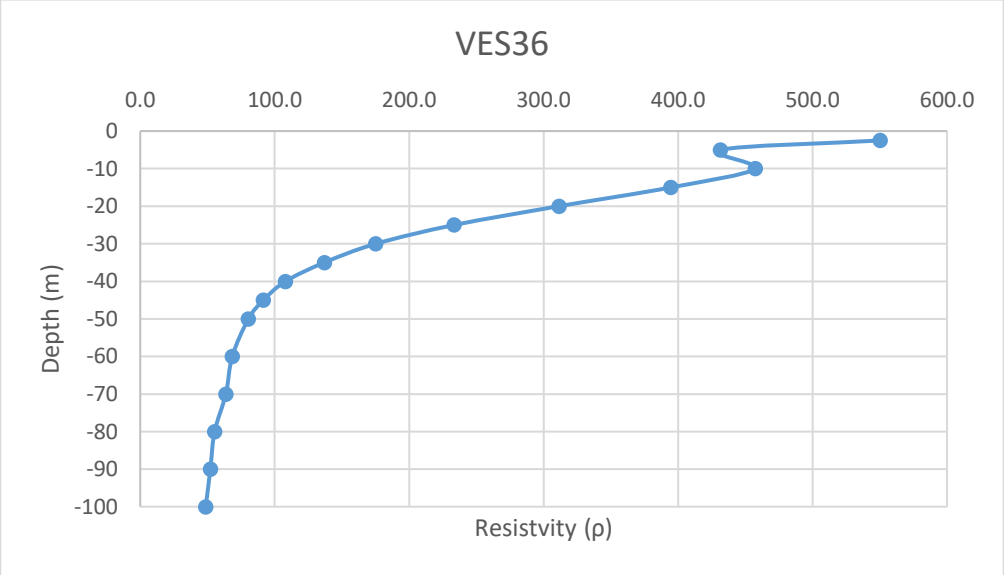

Annexure-XXII: Details of VES Survey

Date: 26/12/2024			VES-37			
Latitude	23.15326		Longitude	69.654052		
S.N	Current Electrode Spacing (AB/2)	Potential Electrode Spacing (MN)	Resistance (Ohm)	K value	Aparent Resistivity (Rho_a)	
1	2.5	1	18.6	18.846	350.536	-2.5
2	5	1	3.16	77.73975	245.658	-5
3	10	1	0.788	313.3148	246.892	-10
4	15	1	0.324	705.9398	228.724	-15
5	20	1	0.167	1255.615	209.688	-20
6	25	1	0.103	1962.34	202.121	-25
7	30	1	0.066	2826.115	186.524	-30
8	35	1	0.0433	3846.94	166.572	-35
9	40	1	0.0318	5024.815	159.789	-40
10	45	1	0.0253	6359.74	160.901	-45
11	50	1	0.0191	7851.715	149.968	-50
12	60	1	0.0132	11306.81	149.250	-60
13	70	1	0.00882	15390.11	135.741	-70
14	80	1	0.00575	20101.61	115.584	-80
15	90	1	0.00445	25441.31	113.214	-90
16	100	1	0.00378	31409.21	118.727	-100
17	110	1	0.0025	38005.31	95.013	-110

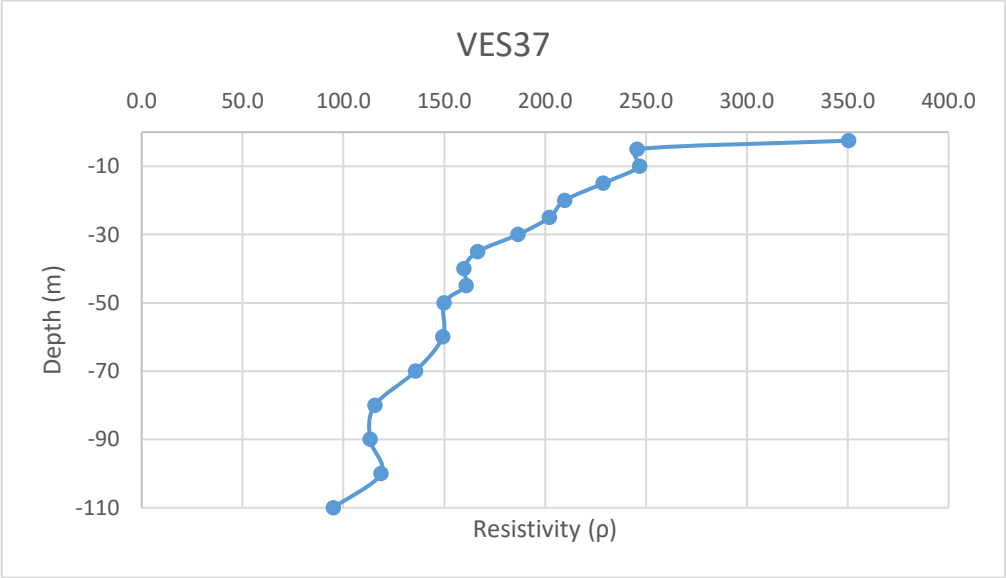

Annexure-XXII: Details of VES Survey

Date: 27/12/2024			VES-38			
Latitude	23.152303		Longitude	69.652243		
S.N	Current Electrode Spacing (AB/2)	Potential Electrode Spacing (MN)	Resistance (Ohm)	K value	Aparent Resistivity (Rho_a)	
1	2.5	1	24.8	18.846	467.381	-2.5
2	5	1	7.67	77.73975	596.264	-5
3	10	1	1.91	313.3148	598.431	-10
4	15	1	0.617	705.9398	435.565	-15
5	20	1	0.284	1255.615	356.595	-20
6	25	1	0.124	1962.34	243.330	-25
7	30	1	0.091	2826.115	257.176	-30
8	35	1	0.0433	3846.94	166.572	-35
9	40	1	0.0318	5024.815	159.789	-40
10	45	1	0.0253	6359.74	160.901	-45
11	50	1	0.0191	7851.715	149.968	-50
12	60	1	0.0132	11306.81	149.250	-60
13	70	1	0.00882	15390.11	135.741	-70
14	80	1	0.00575	20101.61	115.584	-80
15	90	1	0.00445	25441.31	113.214	-90
16	100	1	0.00378	31409.21	118.727	-100

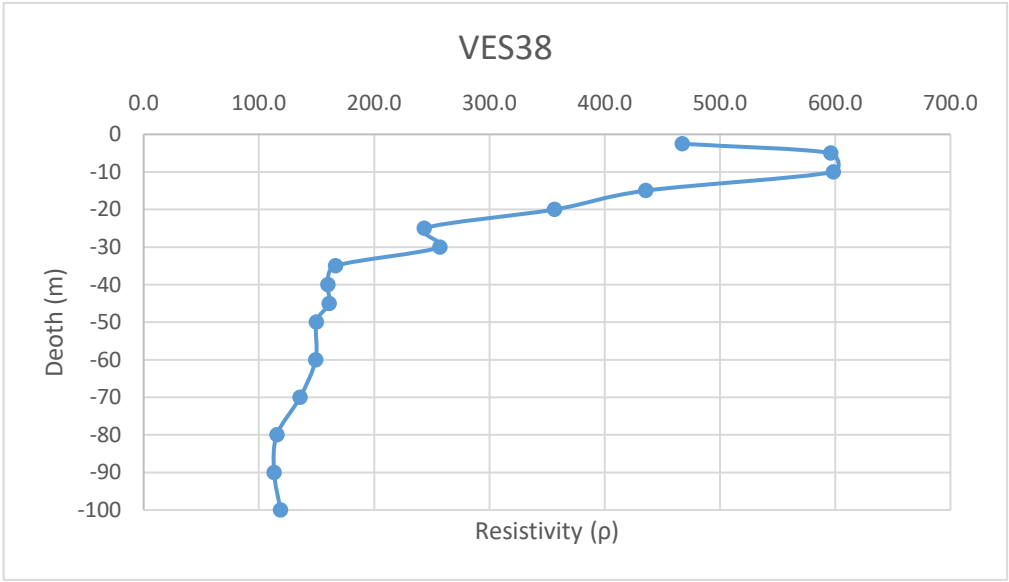

Annexure-XXII: Details of VES Survey

Date: 27/12/2024			VES-39			
Latitude	23.149217		Longitude	69.643638		
S.N	Current Electrode Spacing (AB/2)	Potential Electrode Spacing (MN)	Resistance (Ohm)	K value	Aparent Resistivity (Rho_a)	
1	2.5	1	52.5	18.846	989.415	-2.5
2	5	1	14.2	77.73975	1103.904	-5
3	10	1	3.76	313.3148	1178.063	-10
4	15	1	1.74	705.9398	1228.335	-15
5	20	1	0.927	1255.615	1163.955	-20
6	25	1	0.504	1962.34	989.019	-25
7	30	1	0.258	2826.115	729.138	-30
8	35	1	0.209	3846.94	804.010	-35
9	40	1	0.0982	5024.815	493.437	-40
10	45	1	0.0642	6359.74	408.295	-45
11	50	1	0.0459	7851.715	360.394	-50
12	60	1	0.0274	11306.81	309.807	-60
13	70	1	0.0191	15390.11	293.951	-70
14	80	1	0.00979	20101.61	196.795	-80
15	90	1	0.00976	25441.31	248.307	-90
16	100	1	0.00514	31409.21	161.443	-100

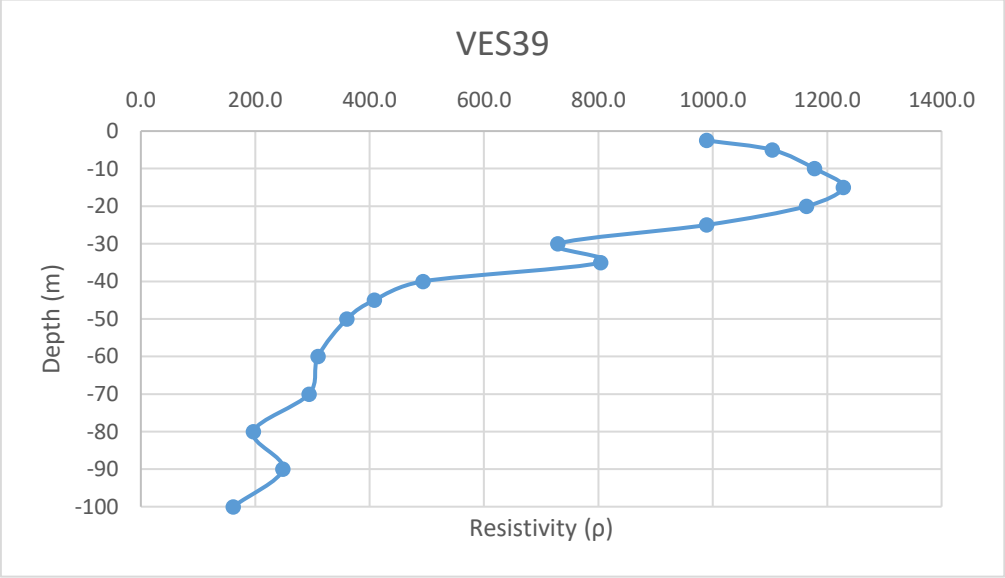

Annexure-XXII: Details of VES Survey

Date: 27/12/2024			VES-40			
Latitude	23.151303		Longitude	69.641313		
S.N	Current Electrode Spacing (AB/2)	Potential Electrode Spacing (MN)	Resistance (Ohm)	K value	Aparent Resistivity (Rho_a)	
1	2.5	1	85.4	18.846	1609.448	-2.5
2	5	1	18.3	77.73975	1422.637	-5
3	10	1	2.69	313.3148	842.817	-10
4	15	1	0.68	705.9398	480.039	-15
5	20	1	0.302	1255.615	379.196	-20
6	25	1	0.161	1962.34	315.937	-25
7	30	1	0.102	2826.115	288.264	-30
8	35	1	0.0644	3846.94	247.743	-35
9	40	1	0.0401	5024.815	201.495	-40
10	45	1	0.0283	6359.74	179.981	-45
11	50	1	0.0221	7851.715	173.523	-50
12	60	1	0.0127	11306.81	143.597	-60
13	70	1	0.00786	15390.11	120.966	-70
14	80	1	0.00501	20101.61	100.709	-80
15	90	1	0.00485	25441.31	123.390	-90
16	100	1	0.00455	31409.21	142.912	-100

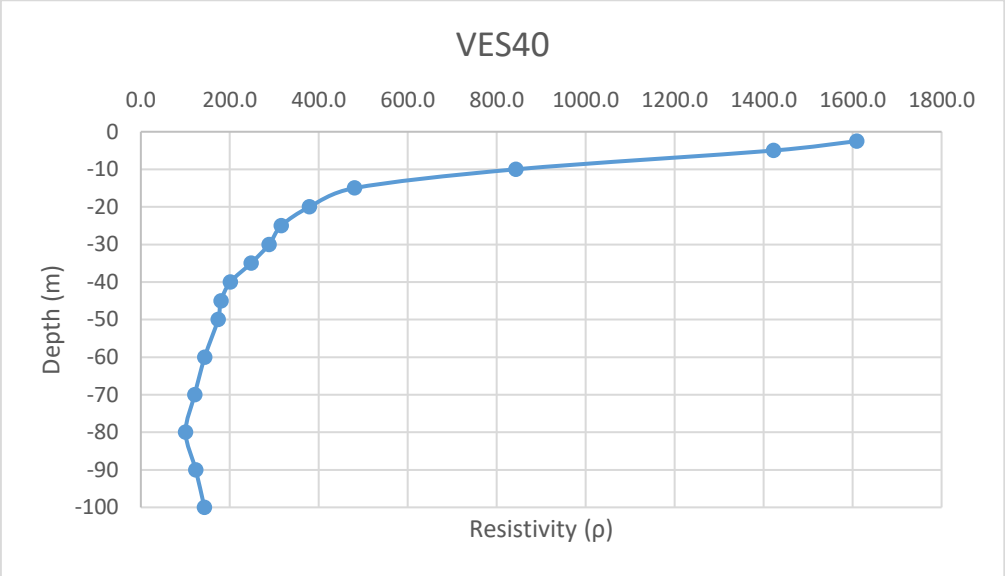

Annexure-XXII: Details of VES Survey

Date: 27/12/2024		VES-41				
Latitude	23.159023		Longitude	69.620378		
S.N	Current Electrode Spacing (AB/2)	Potential Electrode Spacing (MN)	Resistance (Ohm)	K value	Aparent Resistivity (Rho_a)	
1	2.5	1	5.1075	18.846	96.256	-2.5
2	5	1	0.567	77.73975	44.078	-5
3	10	1	0.08337	313.3148	26.121	-10
4	15	1	0.04162	705.9398	29.381	-15
5	20	1	0.02885	1255.615	36.224	-20
6	25	1	0.01855	1962.34	36.401	-25
7	30	1	0.01288	2826.115	36.400	-30
8	35	1	0.009187	3846.94	35.342	-35
9	40	1	0.00718	5024.815	36.078	-40
10	45	1	0.00547	6359.74	34.788	-45
11	50	1	0.00447	7851.715	35.097	-50
12	60	1	0.00284	11306.81	32.111	-60
13	70	1	0.002008	15390.11	30.896	-70
14	80	1	0.00159	20101.61	31.962	-80
15	90	1	0.00123	25441.31	31.293	-90
16	100	1	0.00093	31409.21	29.211	-100

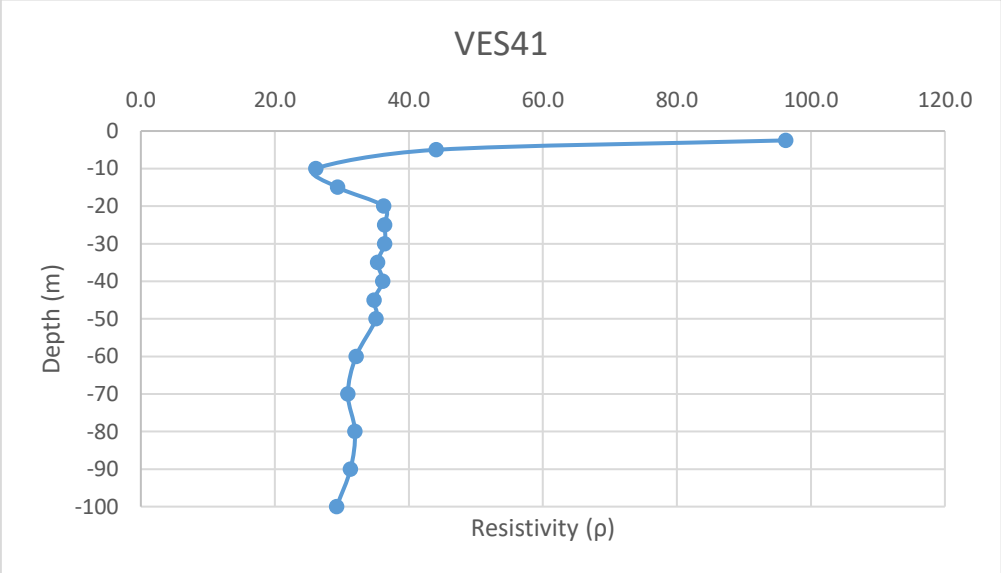

Annexure-XXII: Details of VES Survey

Date: 28/12/2024			VES-42			
Latitude	23.217758		Longitude	69.59535		
S.N	Current Electrode Spacing (AB/2)	Potential Electrode Spacing (MN)	Resistance (Ohm)	K value	Aparent Resistivity (Rho_a)	
1	2.5	1	0.448	18.846	8.443	-2.5
2	5	1	0.12	77.73975	9.329	-5
3	10	1	0.0324	313.3148	10.151	-10
4	15	1	0.0144	705.9398	10.166	-15
5	20	1	0.00901	1255.615	11.313	-20
6	25	1	0.00617	1962.34	12.108	-25
7	30	1	0.0046	2826.115	13.000	-30
8	35	1	0.00352	3846.94	13.541	-35
9	40	1	0.00288	5024.815	14.471	-40
10	45	1	0.0024	6359.74	15.263	-45
11	50	1	0.00208	7851.715	16.332	-50
12	60	1	0.00158	11306.81	17.865	-60
13	70	1	0.00122	15390.11	18.776	-70
14	80	1	0.000998	20101.61	20.061	-80
15	90	1	0.000799	25441.31	20.328	-90
16	100	1	0.00068	31409.21	21.358	-100

15

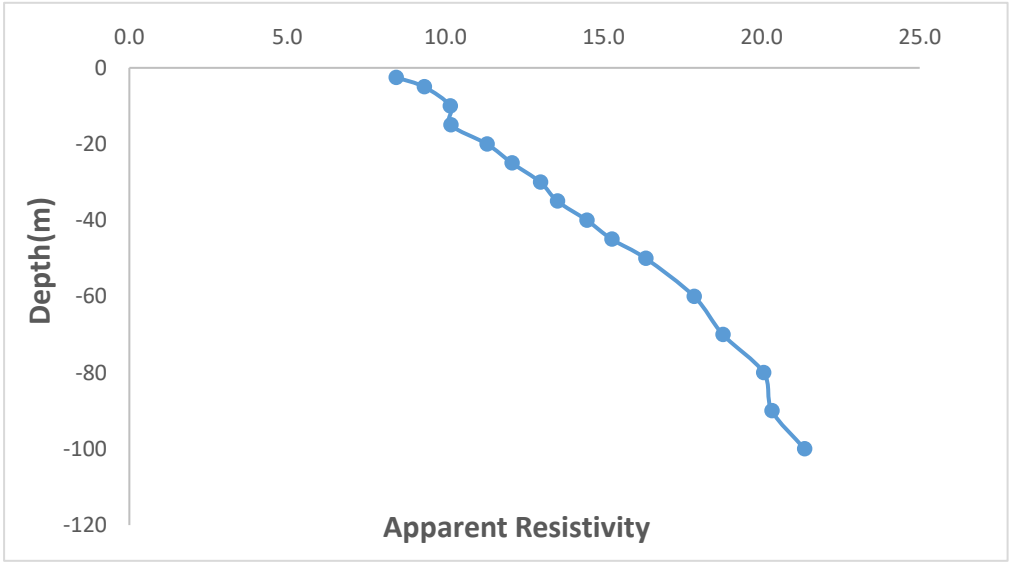

Annexure-XXII: Details of VES Survey

Date: 28/12/2024			VES-43			
Latitude	23.216273		Longitude	69.591057		
S.N	Current Electrode Spacing (AB/2)	Potential Electrode Spacing (MN)	Resistance (Ohm)	K value	Aparent Resistivity (Rho_a)	
1	2.5	1	18.4	18.846	346.766	-2.5
2	5	1	3.27	77.73975	254.209	-5
3	10	1	0.229	313.3148	71.749	-10
4	15	1	0.0631	705.9398	44.545	-15
5	20	1	0.0241	1255.615	30.260	-20
6	25	1	0.0122	1962.34	23.941	-25
7	30	1	0.00792	2826.115	22.383	-30
8	35	1	0.00636	3846.94	24.467	-35
9	40	1	0.00531	5024.815	26.682	-40
10	45	1	0.00461	6359.74	29.318	-45
11	50	1	0.0039	7851.715	30.622	-50
12	60	1	0.00278	11306.81	31.433	-60
13	70	1	0.0022	15390.11	33.858	-70
14	80	1	0.002	20101.61	40.203	-80
15	90	1	0.00125	25441.31	31.802	-90
16	100	1	0.0013	31409.21	40.832	-100
					31.565	

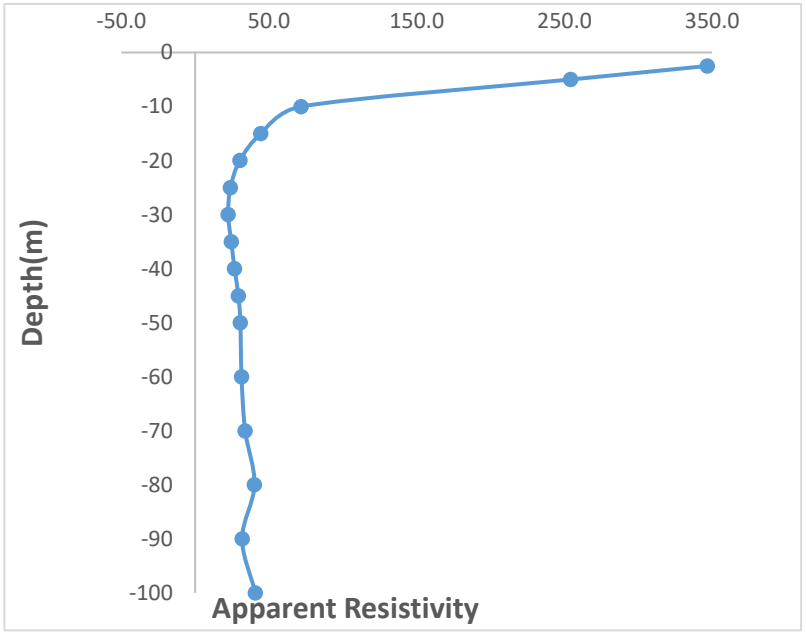

Annexure-XXII: Details of VES Survey

Date: 28/12/2024			VES-44			
Latitude	23.2193		Longitude	69.589518		
S.N	Current Electrode Spacing (AB/2)	Potential Electrode Spacing (MN)	Resistance (Ohm)	K value	Aparent Resistivity (Rho_a)	
1	2.5	1	1.76	18.846	33.169	-2.5
2	5	1	0.192	77.73975	14.926	-5
3	10	1	0.049	313.3148	15.352	-10
4	15	1	0.0204	705.9398	14.401	-15
5	20	1	0.00939	1255.615	11.790	-20
6	25	1	0.00587	1962.34	11.519	-25
7	30	1	0.00417	2826.115	11.785	-30
8	35	1	0.0031	3846.94	11.926	-35
9	40	1	0.0025	5024.815	12.562	-40
10	45	1	0.00198	6359.74	12.592	-45
11	50	1	0.00162	7851.715	12.720	-50
12	60	1	0.0011	11306.81	12.437	-60
13	70	1	0.0008	15390.11	12.312	-70
14	80	1	0.000659	20101.61	13.247	-80
15	90	1	0.000519	25441.31	13.204	-90
16	100	1	0.000416	31409.21	13.066	-100

14

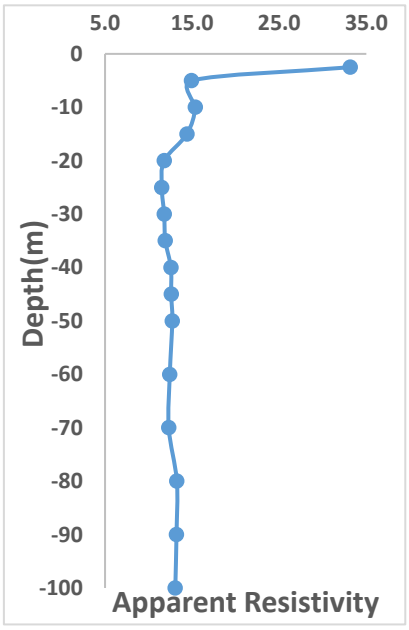

Annexure-XXII: Details of VES Survey

Date: 28/12/2024			VES-45			
Latitude	23.23.215603		Longitude	69.593498		
S.N	Current Electrode Spacing (AB/2)	Potential Electrode Spacing (MN)	Resistance (Ohm)	K value	Aparent Resistivity (Rho_a)	
1	2.5	1	0.732	18.846	13.795	-2.5
2	5	1	0.176	77.73975	13.682	-5
3	10	1	0.034	313.3148	10.653	-10
4	15	1	0.014	705.9398	9.883	-15
5	20	1	0.00799	1255.615	10.032	-20
6	25	1	0.00536	1962.34	10.518	-25
7	30	1	0.00402	2826.115	11.361	-30
8	35	1	0.00321	3846.94	12.349	-35
9	40	1	0.00266	5024.815	13.366	-40
10	45	1	0.00228	6359.74	14.500	-45
11	50	1	0.00194	7851.715	15.232	-50
12	60	1	0.00155	11306.81	17.526	-60
13	70	1	0.00125	15390.11	19.238	-70
14	80	1	0.001032	20101.61	20.745	-80
15	90	1	0.000873	25441.31	22.210	-90
16	100	1	0.00075	31409.21	23.557	-100
					14.915	

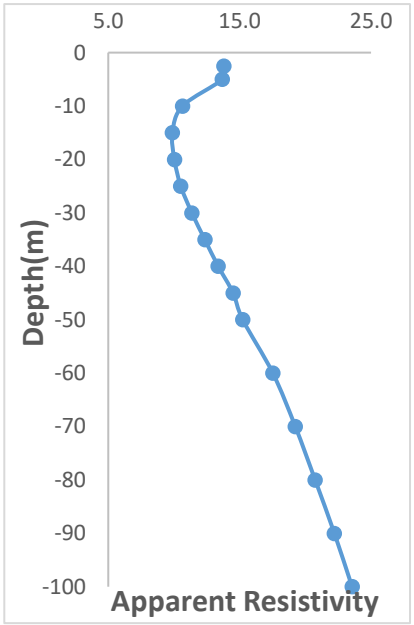

Annexure-XXII: Details of VES Survey

Date: 29/12/2024			VES-46			
Latitude	23.219557		Longitude	69.581838		
S.N	Current Electrode Spacing (AB/2)	Potential Electrode Spacing (MN)	Resistance (Ohm)	K value	Aparent Resistivity (Rho_a)	
1	2.5	1	0.978	18.846	18.431	-2.5
2	5	1	0.416	77.73975	32.340	-5
3	10	1	0.122	313.3148	38.224	-10
4	15	1	0.0495	705.9398	34.944	-15
5	20	1	0.0246	1255.615	30.888	-20
6	25	1	0.0149	1962.34	29.239	-25
7	30	1	0.00979	2826.115	27.668	-30
8	35	1	0.00709	3846.94	27.275	-35
9	40	1	0.00599	5024.815	30.099	-40
10	45	1	0.00427	6359.74	27.156	-45
11	50	1	0.00343	7851.715	26.931	-50
12	60	1	0.00243	11306.81	27.476	-60
13	70	1	0.0015	15390.11	23.085	-70
14	80	1	0.00085	20101.61	17.086	-80
15	90	1	0.00075	25441.31	19.081	-90
16	100	1	0.000624	31409.21	19.599	-100

27

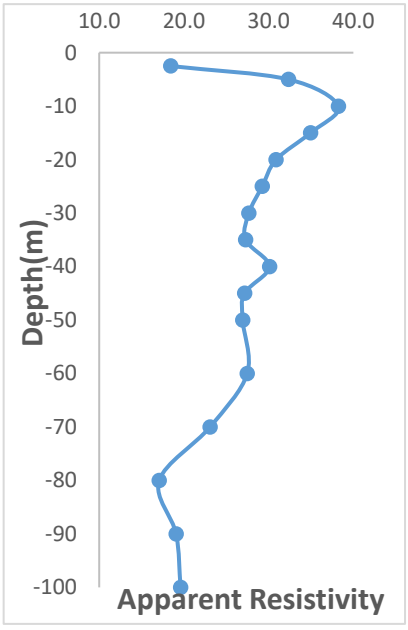

Annexure-XXII: Details of VES Survey

Date: 29/12/2024			VES-47			
Latitude	23.225807		Longitude	69.583925		
S.N	Current Electrode Spacing (AB/2)	Potential Electrode Spacing (MN)	Resistance (Ohm)	K value	Aparent Resistivity (Rho_a)	
1	2.5	1	12.3	18.846	231.806	-2.5
2	5	1	1.49	77.73975	115.832	-5
3	10	1	0.159	313.3148	49.817	-10
4	15	1	0.0587	705.9398	41.439	-15
5	20	1	0.0319	1255.615	40.054	-20
6	25	1	0.0212	1962.34	41.602	-25
7	30	1	0.0148	2826.115	41.826	-30
8	35	1	0.00955	3846.94	36.738	-35
9	40	1	0.0077	5024.815	38.691	-40
10	45	1	0.00625	6359.74	39.748	-45
11	50	1	0.0051	7851.715	40.044	-50
12	60	1	0.00382	11306.81	43.192	-60
13	70	1	0.0031	15390.11	47.709	-70
14	80	1	0.00258	20101.61	51.862	-80
15	90	1	0.0022	25441.31	55.971	-90
16	100	1	0.00192	31409.21	60.306	-100
				Avg.	44.929	

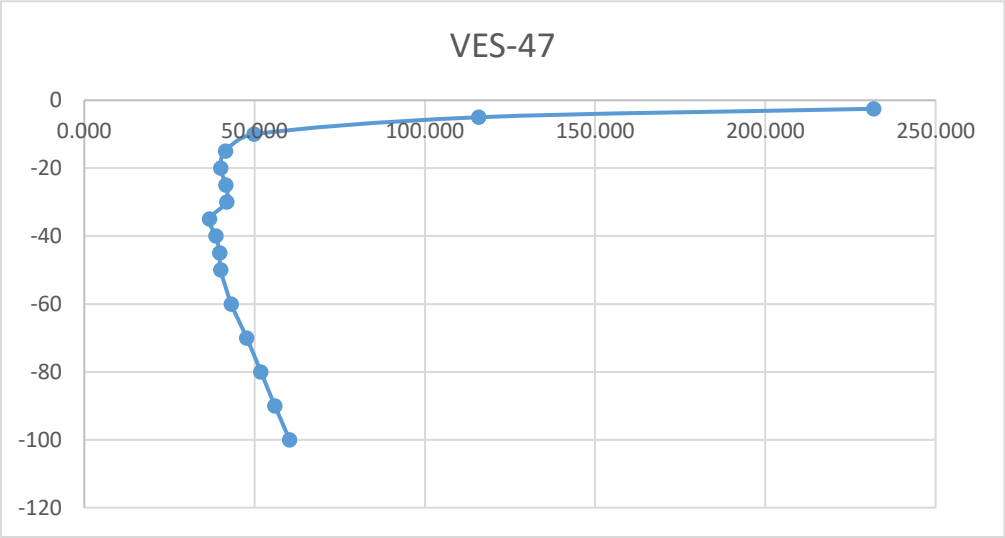

Annexure-XXII: Details of VES Survey

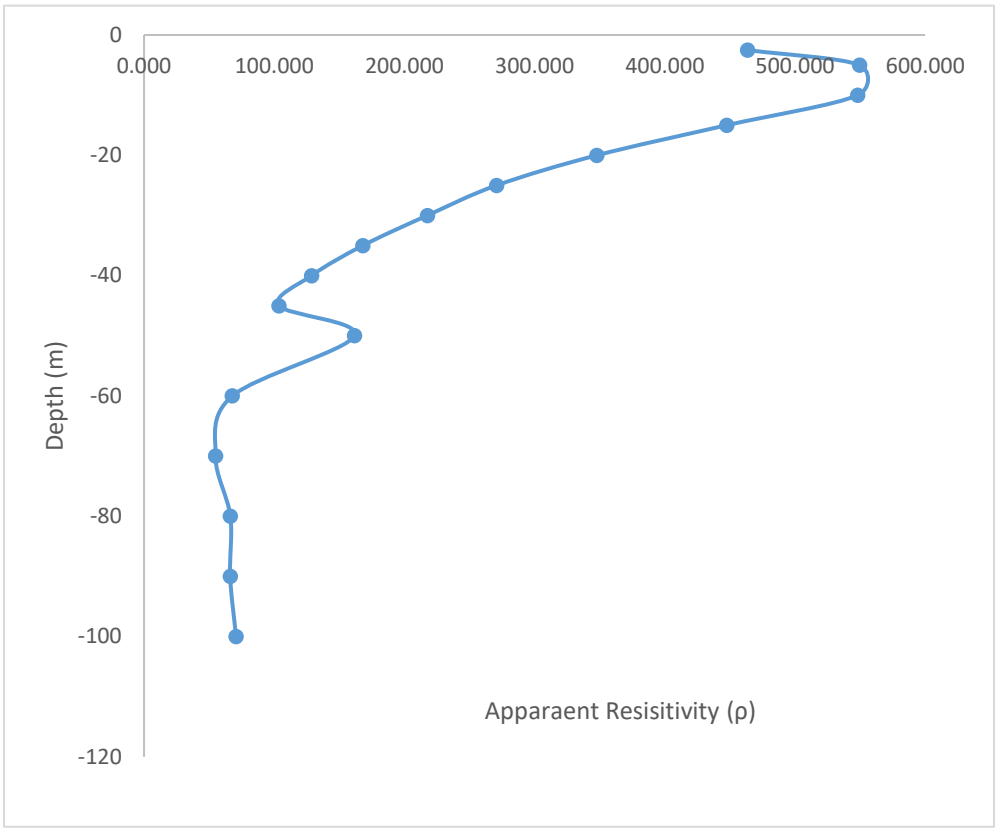

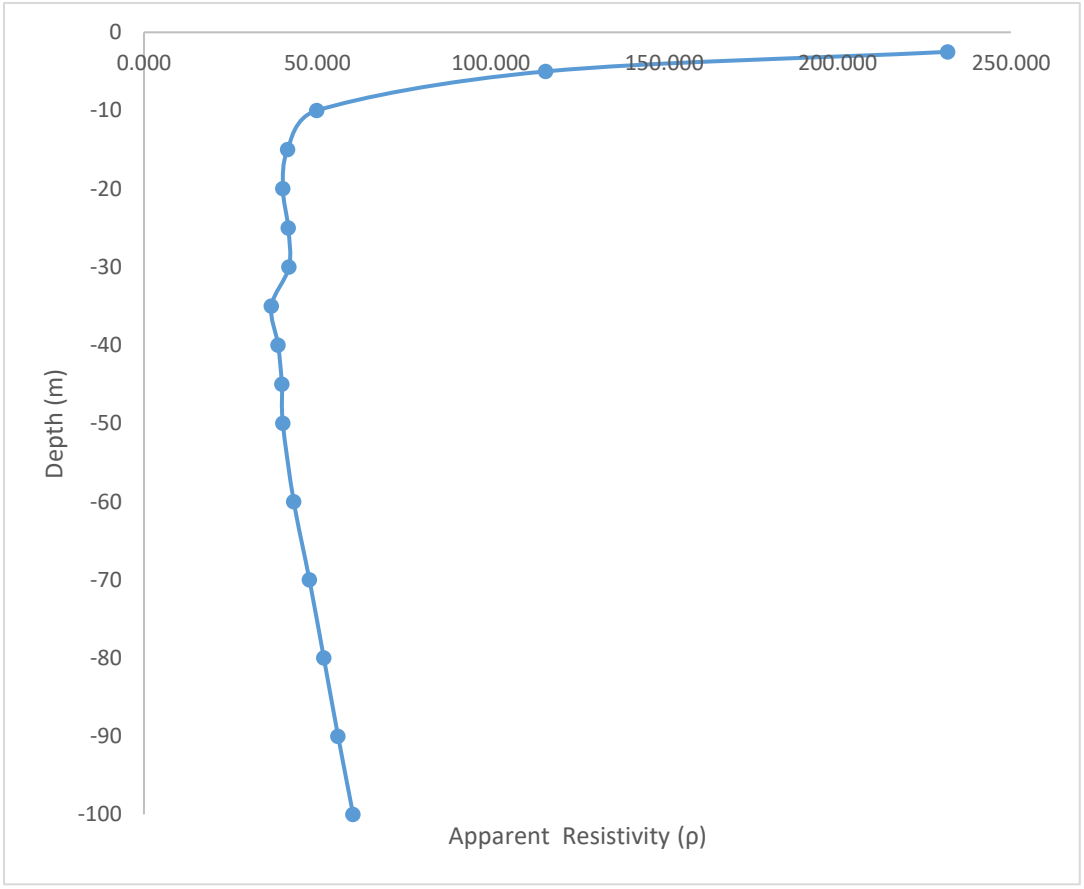

Annexure-XXII: Details of VES Survey

Annexure-XXII: Details of VES Survey

Annexure-XXII: Details of VES Survey

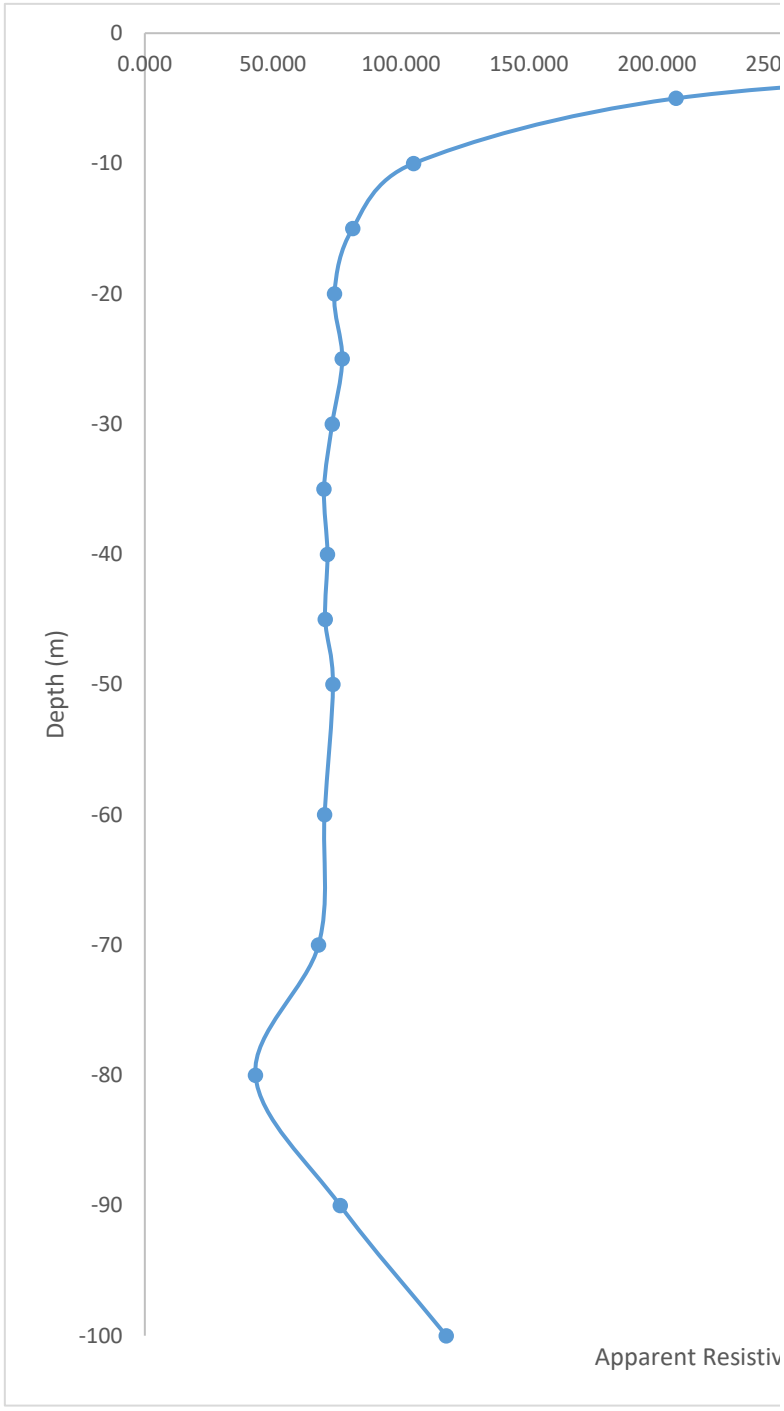


.000
300.000
350.000
400.000
450.000
ity (ρ)

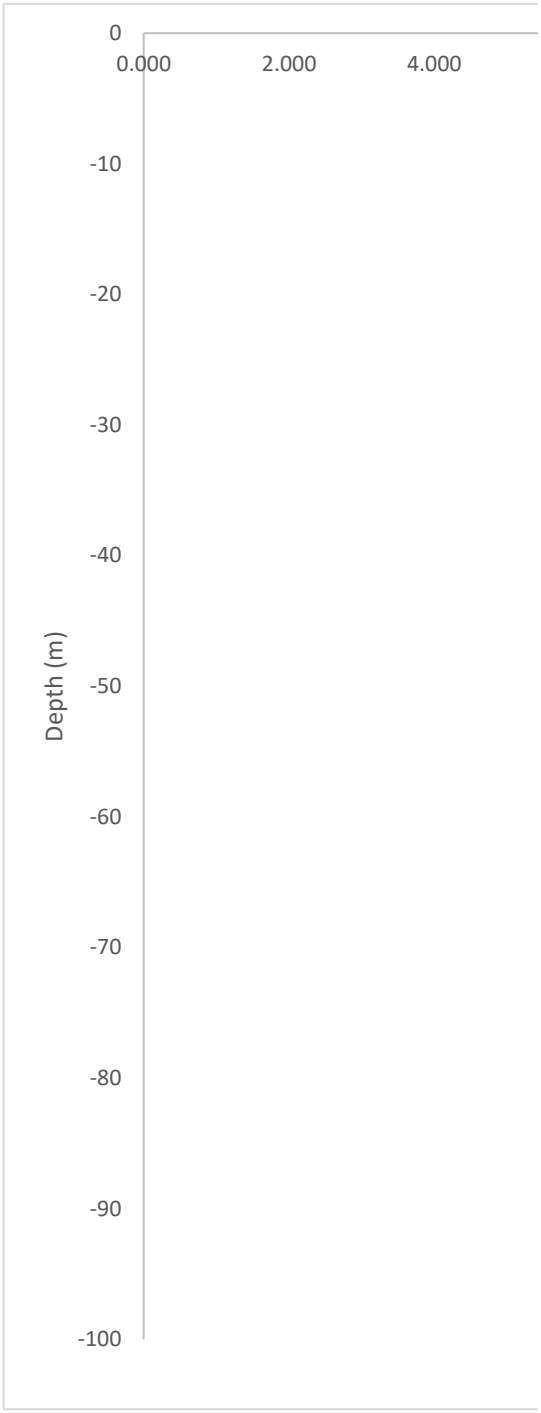
0
0.000
2.000
4.000
-10
-20
-30
-40
Depth (m)
-50
-60
-70
-80
-90
-100

Annexure-XXII: Details of VES Survey

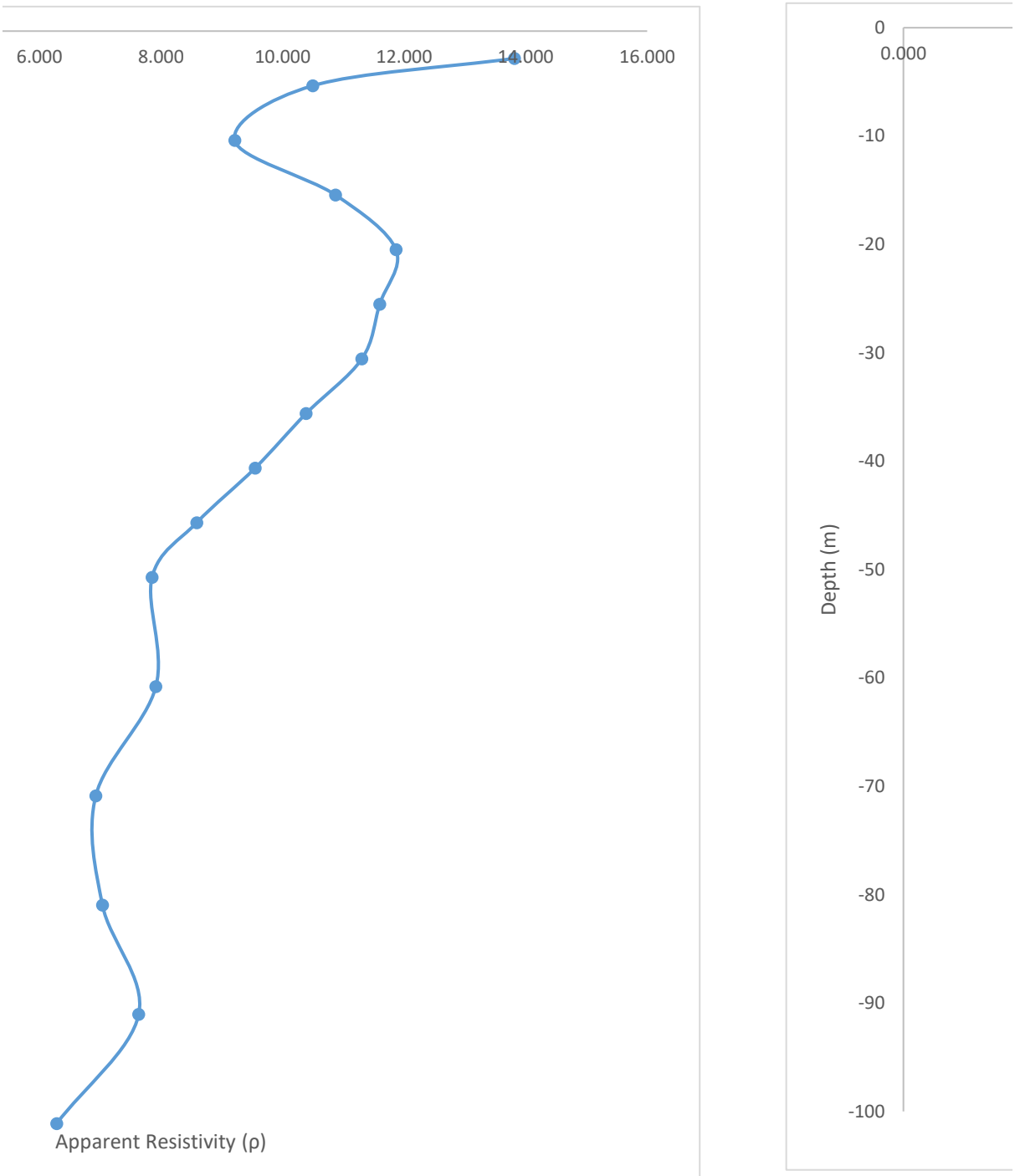

Annexure-XXII: Details of VES Survey

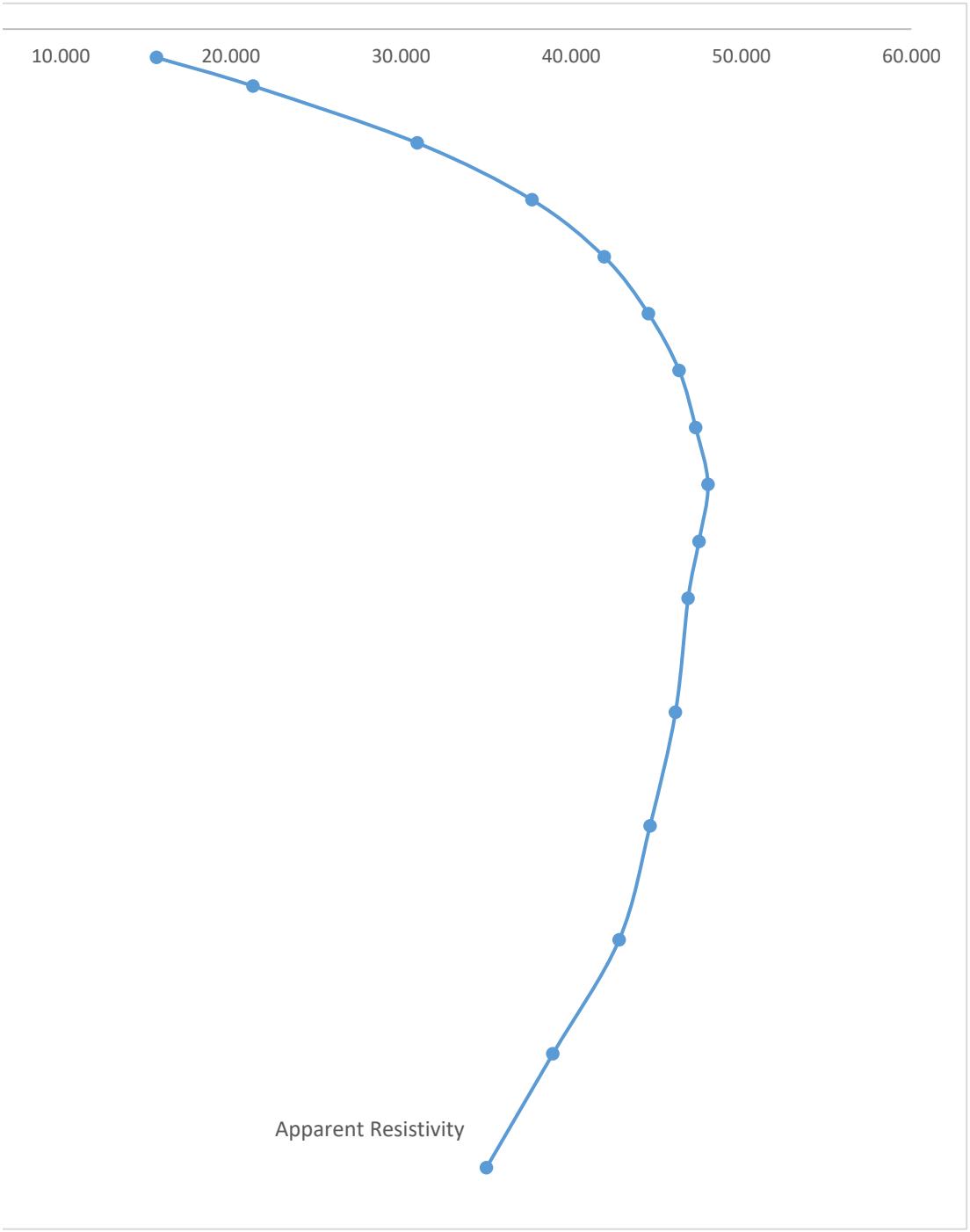

Annexure-XXII: Details of VES Survey

Date: 29/12/2024			VES-48			
Latitude	23.226007		Longitude	69.58217		
S.N	Current Electrode Spacing (AB/2)	Potential Electrode Spacing (MN)	Resistance (Ohm)	K value	Aparent Resistivity (Rho_a)	
1	2.5	1	24.6	18.846	463.612	-2.5
2	5	1	7.07	77.73975	549.620	-5
3	10	1	1.75	313.3148	548.301	-10
4	15	1	0.634	705.9398	447.566	-15
5	20	1	0.277	1255.615	347.805	-20
6	25	1	0.138	1962.34	270.803	-25
7	30	1	0.077	2826.115	217.611	-30
8	35	1	0.0437	3846.94	168.111	-35
9	40	1	0.0256	5024.815	128.635	-40
10	45	1	0.0163	6359.74	103.664	-45
11	50	1	0.0206	7851.715	161.745	-50
12	60	1	0.006	11306.81	67.841	-60
13	70	1	0.00357	15390.11	54.943	-70
14	80	1	0.0033	20101.61	66.335	-80
15	90	1	0.0026	25441.31	66.147	-90
16	100	1	0.00225	31409.21	70.671	-100
			0	AVG	233.338	

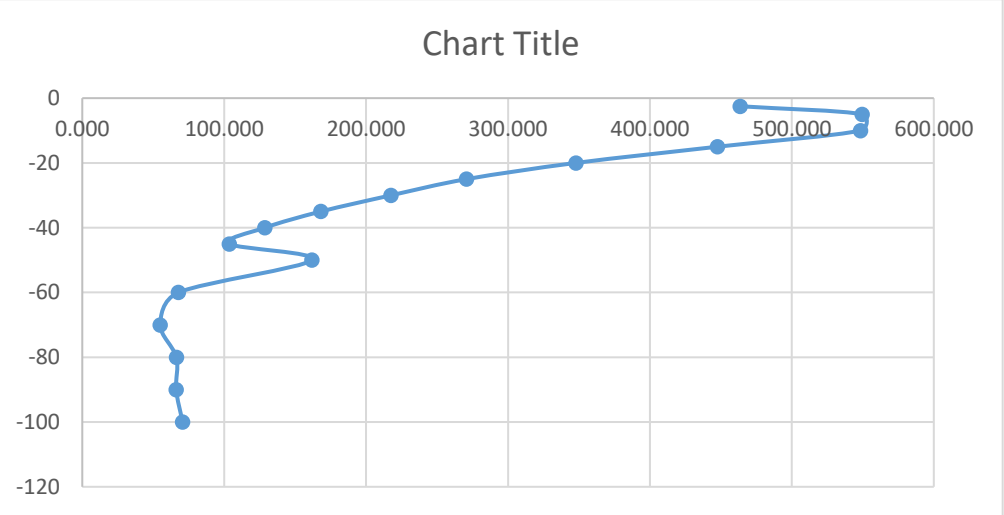

Annexure-XXII: Details of VES Survey

Date: 29/12/2024			VES-49			
Latitude	23.22376		Longitude	69.592273		
S.N	Current Electrode Spacing (AB/2)	Potential Electrode Spacing (MN)	Resistance (Ohm)	K value	Aparent Resistivity (Rho_a)	
1	2.5	1	0.733	18.846	13.814	-2.5
2	5	1	0.135	77.73975	10.495	-5
3	10	1	0.0294	313.3148	9.211	-10
4	15	1	0.0154	705.9398	10.871	-15
5	20	1	0.00945	1255.615	11.866	-20
6	25	1	0.00591	1962.34	11.597	-25
7	30	1	0.004	2826.115	11.304	-30
8	35	1	0.0027	3846.94	10.387	-35
9	40	1	0.0019	5024.815	9.547	-40
10	45	1	0.00135	6359.74	8.586	-45
11	50	1	0.001	7851.715	7.852	-50
12	60	1	0.0007	11306.81	7.915	-60
13	70	1	0.00045	15390.11	6.926	-70
14	80	1	0.00035	20101.61	7.036	-80
15	90	1	0.0003	25441.31	7.632	-90
16	100	1	0.0002	31409.21	6.282	-100
				Avg.	9.458	

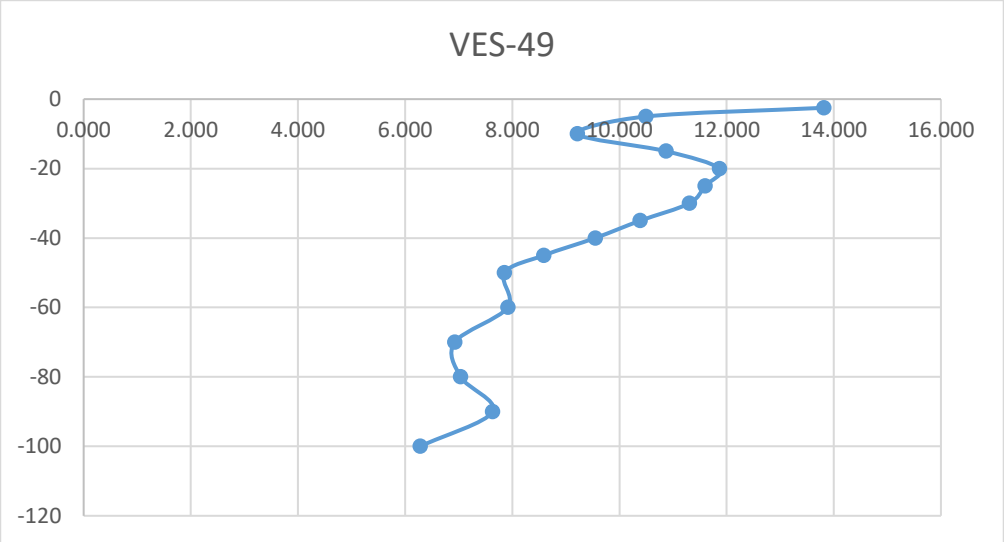

Annexure-XXII: Details of VES Survey

Date: 30/12/2024		VES-50			
Latitude	23.2274		Longitude	69.595728	
S.N	Current Electrode Spacing (AB/2)	Potential Electrode Spacing (MN)	Resistance (Ohm)	K value	Aparent Resistivity (Rho_a)
1	2.5	1	33	18.846	621.918
2	5	1	2.96	77.73975	230.110
3	10	1	0.401	313.3148	125.639
4	15	1	0.154	705.9398	108.715
5	20	1	0.0818	1255.615	102.709
6	25	1	0.0458	1962.34	89.875
7	30	1	0.0294	2826.115	83.088
8	35	1	0.0192	3846.94	73.861
9	40	1	0.0135	5024.815	67.835
10	45	1	0.00888	6359.74	56.474
11	50	1	0.00631	7851.715	49.544
12	60	1	0.00381	11306.81	43.079
13	70	1	0.00412	15390.11	63.407
14	80	1	0.00375	20101.61	75.381
15	90	1	0.00287	25441.31	73.017
16	100	1	0.00334	31409.21	104.907

Annexure-XXII: Details of VES Survey

Date: 30/12/2024			VES-51			
Latitude	23.223395		Longitude	69.590183		
S.N	Current Electrode Spacing (AB/2)	Potential Electrode Spacing (MN)	Resistance (Ohm)	K value	Aparent Resistivity (Rho_a)	
1	2.5	1	20.5	18.846	386.343	-2.5
2	5	1	2.67	77.73975	207.565	-5
3	10	1	0.335	313.3148	104.960	-10
4	15	1	0.115	705.9398	81.183	-15
5	20	1	0.059	1255.615	74.081	-20
6	25	1	0.0393	1962.34	77.120	-25
7	30	1	0.0259	2826.115	73.196	-30
8	35	1	0.0182	3846.94	70.014	-35
9	40	1	0.0142	5024.815	71.352	-40
10	45	1	0.01108	6359.74	70.466	-45
11	50	1	0.00936	7851.715	73.492	-50
12	60	1	0.00621	11306.81	70.215	-60
13	70	1	0.00441	15390.11	67.870	-70
14	80	1	0.00215	20101.61	43.218	-80
15	90	1	0.003	25441.31	76.324	-90
16	100	1	0.00375	31409.21	117.785	-100
				AVG	74.332	

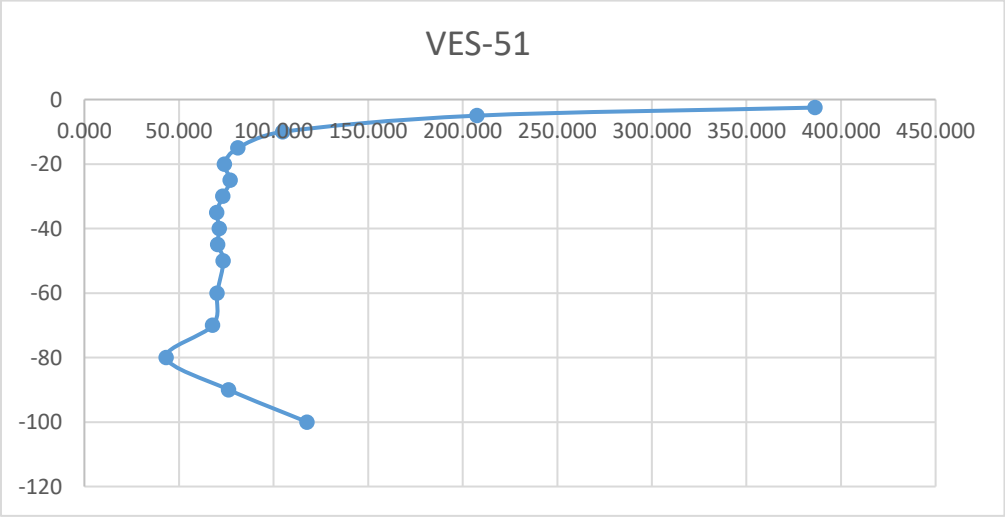

Annexure-XXII: Details of VES Survey

Date: 2/01/2025			VES-52			
Latitude	23.223413		Longitude	69.597242		
S.N	Current Electrode Spacing (AB/2)	Potential Electrode Spacing (MN)	Resistance (Ohm)	K value	Aparent Resistivity (Rho_a)	
1	2.5	1	0.829	18.846	15.623	-2.5
2	5	1	0.274	77.73975	21.301	-5
3	10	1	0.0988	313.3148	30.955	-10
4	15	1	0.0534	705.9398	37.697	-15
5	20	1	0.0334	1255.615	41.938	-20
6	25	1	0.0227	1962.34	44.545	-25
7	30	1	0.0164	2826.115	46.348	-30
8	35	1	0.0123	3846.94	47.317	-35
9	40	1	0.00956	5024.815	48.037	-40
10	45	1	0.00747	6359.74	47.507	-45
11	50	1	0.00597	7851.715	46.875	-50
12	60	1	0.00408	11306.81	46.132	-60
13	70	1	0.0029	15390.11	44.631	-70
14	80	1	0.00213	20101.61	42.816	-80
15	90	1	0.00153	25441.31	38.925	-90
16	100	1	0.001115	31409.21	35.021	-100
				AVG.	**39.729**	

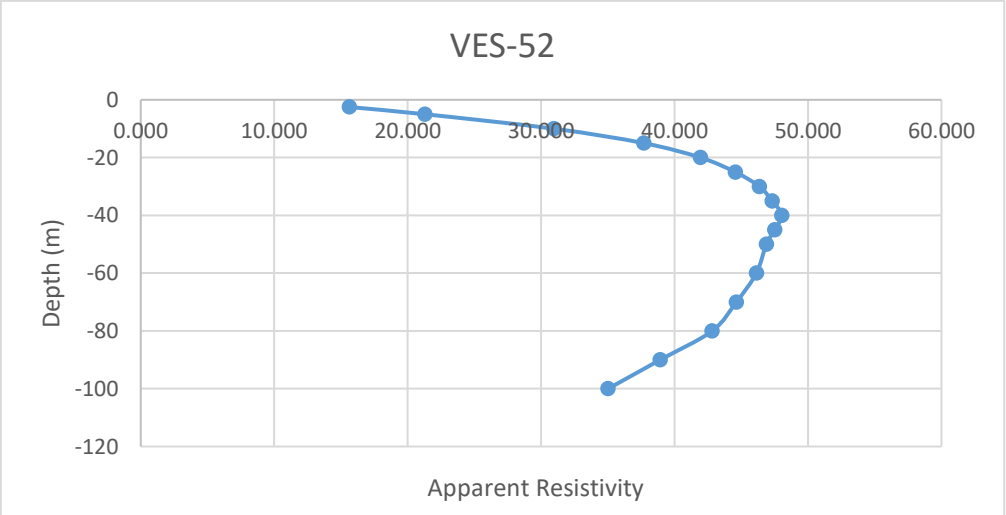

Annexure-XXII: Details of VES Survey

Date: 2/01/2025		VES-53				
Latitude	23.228645		Longitude	69.588767		
S.N	Current Electrode Spacing (AB/2)	Potential Electrode Spacing (MN)	Resistance (Ohm)	K value	Aparent Resistivity (Rho_a)	
1	2.5	1	7.07	18.846	133.241	-2.5
2	5	1	1.94	77.73975	150.815	-5
3	10	1	0.387	313.3148	121.253	-10
4	15	1	0.129	705.9398	91.066	-15
5	20	1	0.0695	1255.615	87.265	-20
6	25	1	0.0449	1962.34	88.109	-25
7	30	1	0.0331	2826.115	93.544	-30
8	35	1	0.0252	3846.94	96.943	-35
9	40	1	0.0185	5024.815	92.959	-40
10	45	1	0.0152	6359.74	96.668	-45
11	50	1	0.014	7851.715	109.924	-50
12	60	1	0.01042	11306.81	117.817	-60
13	70	1	0.00779	15390.11	119.889	-70
14	80	1	0.00607	20101.61	122.017	-80
15	90	1	0.00531	25441.31	135.093	-90
16	100	1	0.00421	31409.21	132.233	-100

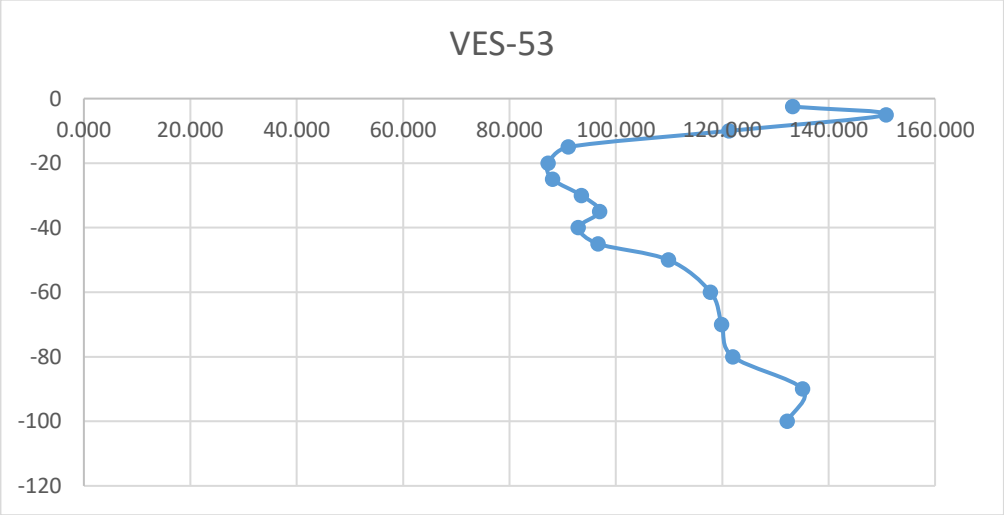

Annexure-XXII: Details of VES Survey

Date: 2/01/2025			VES-54			
Latitude	23.22955		Longitude	69.585748		
S.N	Current Electrode Spacing (AB/2)	Potential Electrode Spacing (MN)	Resistance (Ohm)	K value	Aparent Resistivity (Rho_a)	
1	2.5	1	9.03	18.846	170.179	-2.5
2	5	1	2.07	77.73975	160.921	-5
3	10	1	0.156	313.3148	48.877	-10
4	15	1	0.0326	705.9398	23.014	-15
5	20	1	0.0203	1255.615	25.489	-20
6	25	1	0.0149	1962.34	29.239	-25
7	30	1	0.01186	2826.115	33.518	-30
8	35	1	0.01015	3846.94	39.046	-35
9	40	1	0.00929	5024.815	46.681	-40
10	45	1	0.00802	6359.74	51.005	-45
11	50	1	0.00685	7851.715	53.784	-50
12	60	1	0.00541	11306.81	61.170	-60
13	70	1	0.00451	15390.11	69.409	-70
14	80	1	0.00391	20101.61	78.597	-80
15	90	1	0.00358	25441.31	91.080	-90
16	100	1	0.00318	31409.21	99.881	-100

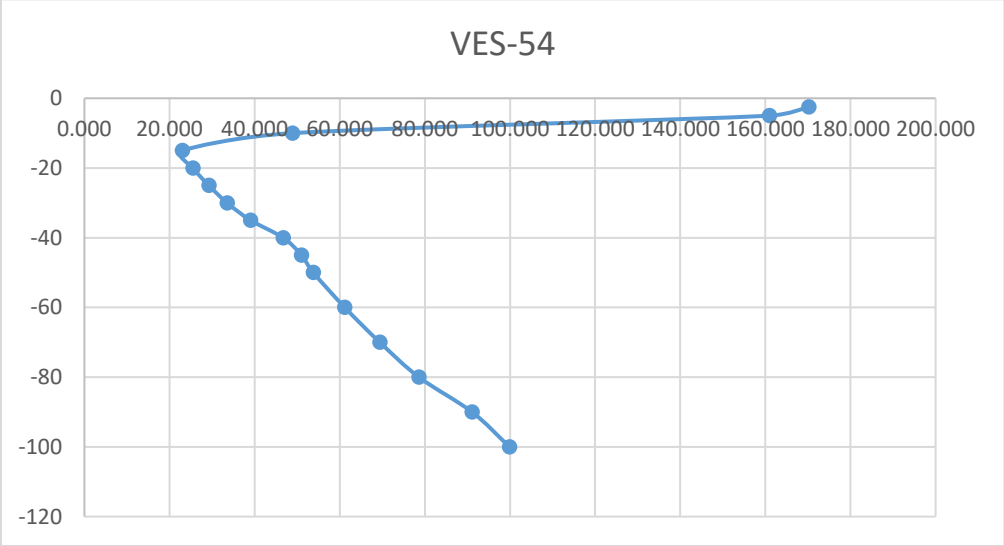

Annexure-XXII: Details of VES Survey

Date: 3/01/2025		VES-55				
Latitude	23.200252		Longitude	69.724585		
S.N	Current Electrode Spacing (AB/2)	Potential Electrode Spacing (MN)	Resistance (Ohm)	K value	Aparent Resistivity (Rho_a)	
1	2.5	1	8.56	18.846	161.322	-2.5
2	5	1	1.53	77.73975	118.942	-5
3	10	1	0.239	313.3148	74.882	-10
4	15	1	0.0791	705.9398	55.840	-15
5	20	1	0.038	1255.615	47.713	-20
6	25	1	0.0255	1962.34	50.040	-25
7	30	1	0.0161	2826.115	45.500	-30
8	35	1	0.011	3846.94	42.316	-35
9	40	1	0.00805	5024.815	40.450	-40
10	45	1	0.00617	6359.74	39.240	-45
11	50	1	0.00515	7851.715	40.436	-50
12	60	1	0.0034	11306.81	38.443	-60
13	70	1	0.00232	15390.11	35.705	-70
14	80	1	0.00177	20101.61	35.580	-80
15	90	1	0.00128	25441.31	32.565	-90
16	100	1	0.000948	31409.21	29.776	-100

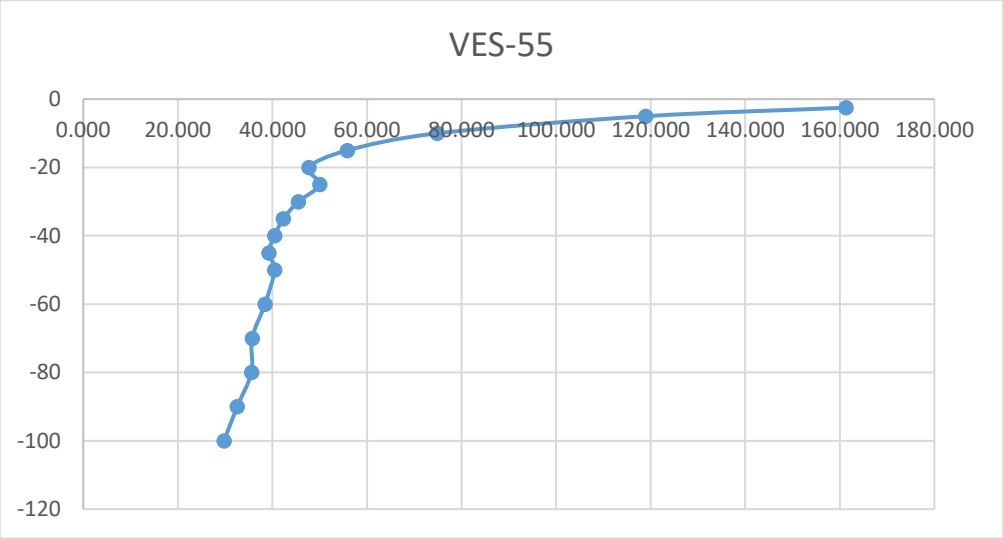

Annexure-XXII: Details of VES Survey

Date: 3/01/2025			VES-56			
Latitude	23.20084		Longitude	69.725847		
S.N	Current Electrode Spacing (AB/2)	Potential Electrode Spacing (MN)	Resistance (Ohm)	K value	Aparent Resistivity (Rho_a)	
1	2.5	1	1.59	18.846	29.965	-2.5
2	5	1	0.459	77.73975	35.683	-5
3	10	1	0.141	313.3148	44.177	-10
4	15	1	0.0606	705.9398	42.780	-15
5	20	1	0.0395	1255.615	49.597	-20
6	25	1	0.0246	1962.34	48.274	-25
7	30	1	0.0166	2826.115	46.914	-30
8	35	1	0.01155	3846.94	44.432	-35
9	40	1	0.00851	5024.815	42.761	-40
10	45	1	0.00641	6359.74	40.766	-45
11	50	1	0.00476	7851.715	37.374	-50
12	60	1	0.00308	11306.81	34.825	-60
13	70	1	0.00208	15390.11	32.011	-70
14	80	1	0.00146	20101.61	29.348	-80
15	90	1	0.001065	25441.31	27.095	-90
16	100	1	0.000773	31409.21	24.279	-100

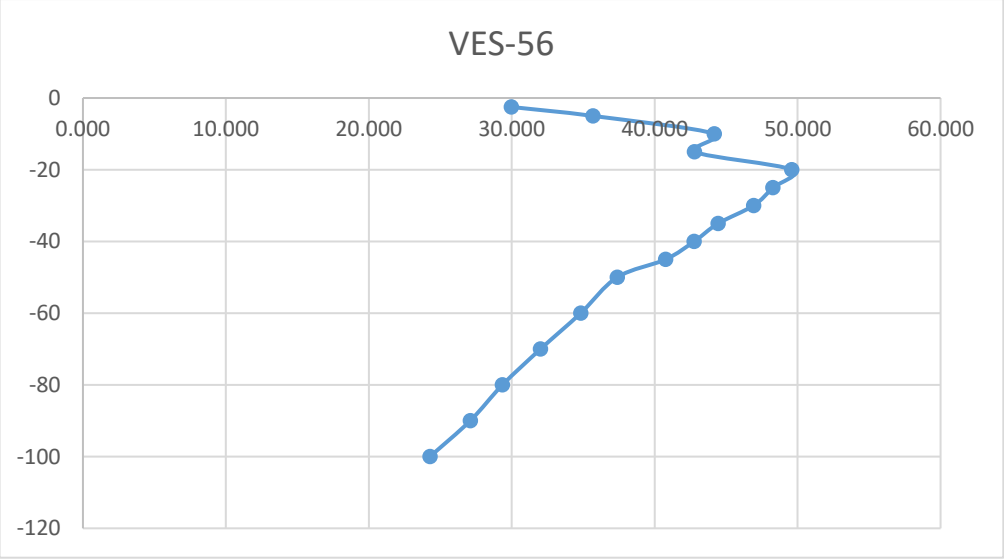

Annexure-XXII: Details of VES Survey

Date: 3/01/2025			VES-57			
Latitude	23.192723		Longitude	69.724655		
S.N	Current Electrode Spacing (AB/2)	Potential Electrode Spacing (MN)	Resistance (Ohm)	K value	Aparent Resistivity (Rho_a)	
1	2.5	1	15.7	18.846	295.882	-2.5
2	5	1	1.171	77.73975	91.033	-5
3	10	1	0.192	313.3148	60.156	-10
4	15	1	0.0537	705.9398	37.909	-15
5	20	1	0.0242	1255.615	30.386	-20
6	25	1	0.0131	1962.34	25.707	-25
7	30	1	0.00862	2826.115	24.361	-30
8	35	1	0.00658	3846.94	25.313	-35
9	40	1	0.00551	5024.815	27.687	-40
10	45	1	0.00477	6359.74	30.336	-45
11	50	1	0.00411	7851.715	32.271	-50
12	60	1	0.0034	11306.81	38.443	-60
13	70	1	0.0024	15390.11	36.936	-70
14	80	1	0.00271	20101.61	54.475	-80
15	90	1	0.0018	25441.31	45.794	-90
16	100	1	0.00155	31409.21	48.684	-100

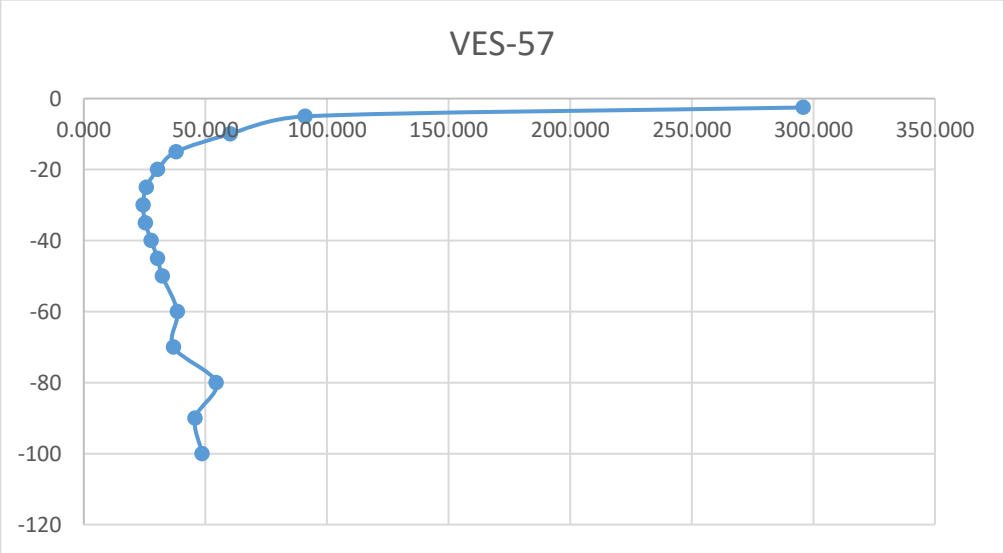

Annexure-XXII: Details of VES Survey

Date: 4/01/2025			VES-58			
Latitude	23.201562		Longitude	69.711313		
S.N	Current Electrode Spacing (AB/2)	Potential Electrode Spacing (MN)	Resistance (Ohm)	K value	Aparent Resistivity (Rho_a)	
1	2.5	1	9.89	18.846	186.387	-2.5
2	5	1	1.96	77.73975	152.370	-5
3	10	1	0.259	313.3148	81.149	-10
4	15	1	0.0839	705.9398	59.228	-15
5	20	1	0.0469	1255.615	58.888	-20
6	25	1	0.0272	1962.34	53.376	-25
7	30	1	0.0178	2826.115	50.305	-30
8	35	1	0.0127	3846.94	48.856	-35
9	40	1	0.00979	5024.815	49.193	-40
10	45	1	0.00735	6359.74	46.744	-45
11	50	1	0.00625	7851.715	49.073	-50
12	60	1	0.00559	11306.81	63.205	-60
13	70	1	0.0043	15390.11	66.177	-70
14	80	1	0.0033	20101.61	66.335	-80
15	90	1	0.00295	25441.31	75.052	-90
16	100	1	0.00232	31409.21	72.869	-100

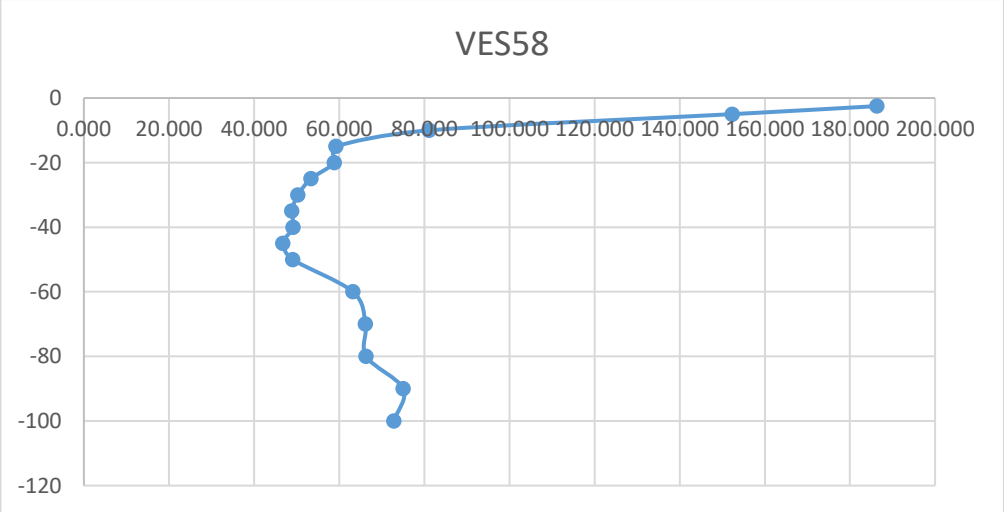

Annexure-XXII: Details of VES Survey

Date: 4/01/2025			VES-59			
Latitude	23.199938		Longitude	69.71292		
S.N	Current Electrode Spacing (AB/2)	Potential Electrode Spacing (MN)	Resistance (Ohm)	K value	Aparent Resistivity (Rho_a)	
1	2.5	1	24	18.846	452.304	-2.5
2	5	1	0.734	77.73975	57.061	-5
3	10	1	0.146	313.3148	45.744	-10
4	15	1	0.0579	705.9398	40.874	-15
5	20	1	0.0327	1255.615	41.059	-20
6	25	1	0.0193	1962.34	37.873	-25
7	30	1	0.0126	2826.115	35.609	-30
8	35	1	0.01103	3846.94	42.432	-35
9	40	1	0.00571	5024.815	28.692	-40
10	45	1	0.00414	6359.74	26.329	-45
11	50	1	0.00387	7851.715	30.386	-50
12	60	1	0.00207	11306.81	23.405	-60
13	70	1	0.0018	15390.11	27.702	-70
14	80	1	0.0015	20101.61	30.152	-80
15	90	1	0.0011	25441.31	27.985	-90
16	100	1	0.0009	31409.21	28.268	-100

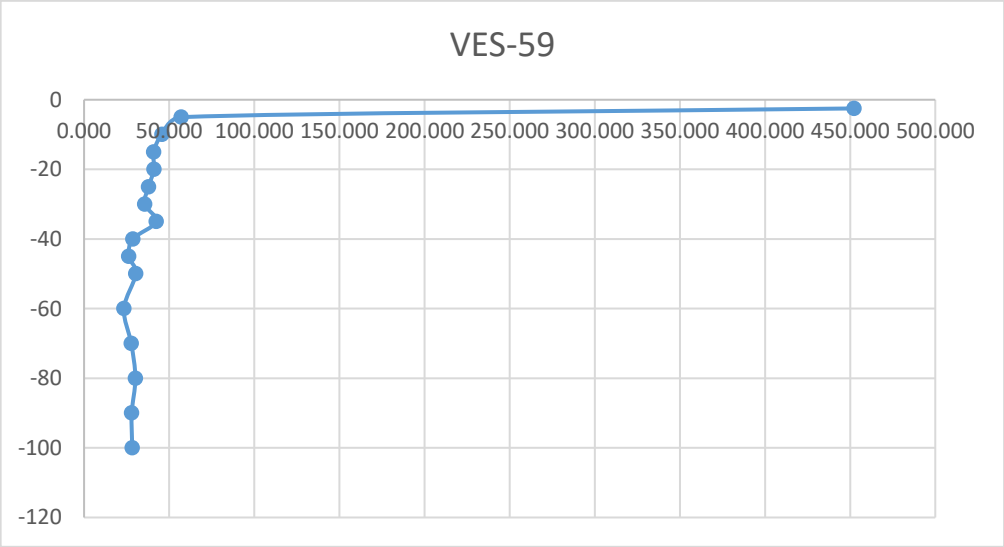

Annexure-XXII: Details of VES Survey

Date: 4/01/2025			VES-60			
Latitude	23.204407		Longitude	69.715118		
S.N	Current Electrode Spacing (AB/2)	Potential Electrode Spacing (MN)	Resistance (Ohm)	K value	Aparent Resistivity (Rho_a)	
1	2.5	1	15	18.846	282.690	-2.5
2	5	1	4.49	77.73975	349.051	-5
3	10	1	1.112	313.3148	348.406	-10
4	15	1	0.487	705.9398	343.793	-15
5	20	1	0.259	1255.615	325.204	-20
6	25	1	0.155	1962.34	304.163	-25
7	30	1	0.0967	2826.115	273.285	-30
8	35	1	0.0639	3846.94	245.819	-35
9	40	1	0.0431	5024.815	216.570	-40
10	45	1	0.0296	6359.74	188.248	-45
11	50	1	0.0215	7851.715	168.812	-50
12	60	1	0.01175	11306.81	132.855	-60
13	70	1	0.00677	15390.11	104.191	-70
14	80	1	0.0041	20101.61	82.417	-80
15	90	1	0.0029	25441.31	73.780	-90
16	100	1	0.0021	31409.21	65.959	-100

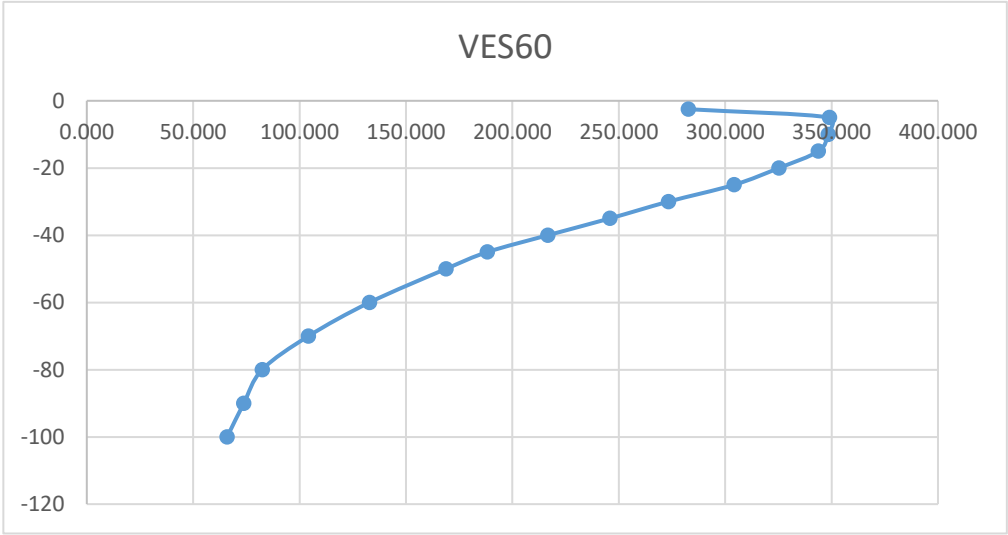

Annexure-XXII: Details of VES Survey

Date: 5/01/2025			VES-61			
Latitude	23.191305		Longitude	69.687983		
S.N	Current Electrode Spacing (AB/2)	Potential Electrode Spacing (MN)	Resistance (Ohm)	K value	Aparent Resistivity (Rho_a)	
1	2.5	1	21	18.846	395.766	-2.5
2	5	1	5.78	77.73975	449.336	-5
3	10	1	0.982	313.3148	307.675	-10
4	15	1	0.226	705.9398	159.542	-15
5	20	1	0.0593	1255.615	74.458	-20
6	25	1	0.0176	1962.34	34.537	-25
7	30	1	0.0068	2826.115	19.218	-30
8	35	1	0.00355	3846.94	13.657	-35
9	40	1	0.0024	5024.815	12.060	-40
10	45	1	0.0019	6359.74	12.084	-45
11	50	1	0.0016	7851.715	12.563	-50
12	60	1	0.00114	11306.81	12.890	-60
13	70	1	0.001	15390.11	15.390	-70
14	80	1	0.0009	20101.61	18.091	-80
15	90	1	0.00065	25441.31	16.537	-90
16	100	1	0.00057	31409.21	17.903	-100

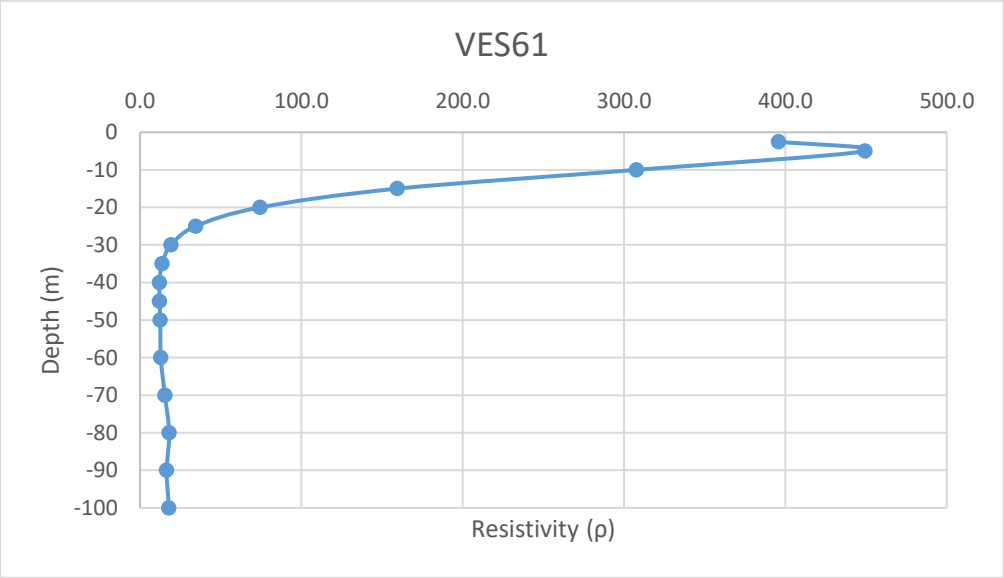

Annexure-XXII: Details of VES Survey

Date: 5/01/2025		VES-62				
Latitude	23.192497		Longitude	69.685387		
S.N	Current Electrode Spacing (AB/2)	Potential Electrode Spacing (MN)	Resistance (Ohm)	K value	Aparent Resistivity (Rho_a)	
1	2.5	1	16.7	18.846	314.728	-2.5
2	5	1	3.95	77.73975	307.072	-5
3	10	1	0.472	313.3148	147.885	-10
4	15	1	0.0686	705.9398	48.427	-15
5	20	1	0.0137	1255.615	17.202	-20
6	25	1	0.0048	1962.34	9.419	-25
7	30	1	0.00265	2826.115	7.489	-30
8	35	1	0.0019	3846.94	7.309	-35
9	40	1	0.0015	5024.815	7.537	-40
10	45	1	0.00125	6359.74	7.950	-45
11	50	1	0.0011	7851.715	8.637	-50
12	60	1	0.00095	11306.81	10.741	-60
13	70	1	0.00075	15390.11	11.543	-70
14	80	1	0.00045	20101.61	9.046	-80
15	90	1	0.00035	25441.31	8.904	-90
16	100	1	0.00035	31409.21	10.993	-100

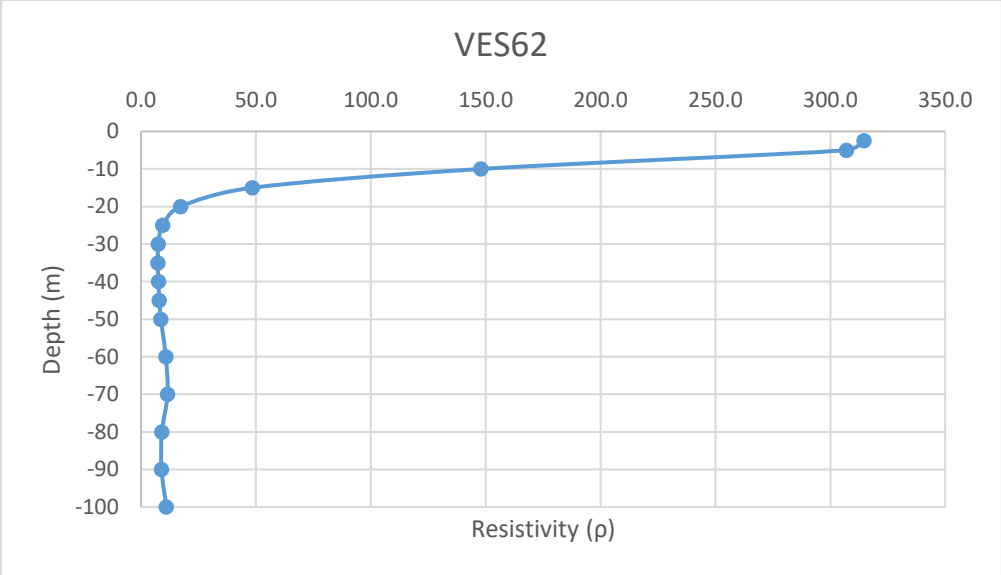

Annexure-XXII: Details of VES Survey

Date: 6/01/2025			VES-63			
Latitude	23.190205		Longitude	69.691063		
S.N	Current Electrode Spacing (AB/2)	Potential Electrode Spacing (MN)	Resistance (Ohm)	K value	Aparent Resistivity (Rho_a)	
1	2.5	1	0.621	18.846	11.703	-2.5
2	5	1	0.072	77.73975	5.597	-5
3	10	1	0.0169	313.3148	5.295	-10
4	15	1	0.00835	705.9398	5.895	-15
5	20	1	0.00461	1255.615	5.788	-20
6	25	1	0.003	1962.34	5.887	-25
7	30	1	0.0022	2826.115	6.217	-30
8	35	1	0.00165	3846.94	6.347	-35
9	40	1	0.00128	5024.815	6.432	-40
10	45	1	0.0011	6359.74	6.996	-45
11	50	1	0.000924	7851.715	7.255	-50
12	60	1	0.00065	11306.81	7.349	-60
13	70	1	0.00045	15390.11	6.926	-70
14	80	1	0.00035	20101.61	7.036	-80
15	90	1	0.000299	25441.31	7.607	-90
16	100	1	0.000249	31409.21	7.821	-100

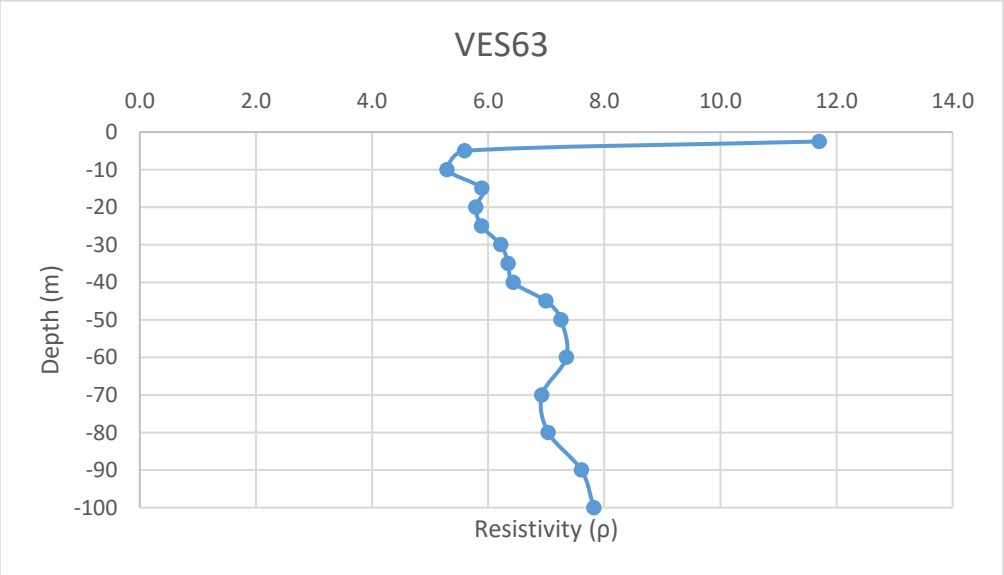

Annexure-XXII: Details of VES Survey

Date: 6/01/2025			VES-64			
Latitude	23.198922		Longitude	69.65412		
S.N	Current Electrode Spacing (AB/2)	Potential Electrode Spacing (MN)	Resistance (Ohm)	K value	Aparent Resistivity (Rho_a)	
1	2.5	1	27.5	18.846	518.265	-2.5
2	5	1	6.23	77.73975	484.319	-5
3	10	1	1.37	313.3148	429.241	-10
4	15	1	0.561	705.9398	396.032	-15
5	20	1	0.291	1255.615	365.384	-20
6	25	1	0.176	1962.34	345.372	-25
7	30	1	0.118	2826.115	333.482	-30
8	35	1	0.087	3846.94	334.684	-35
9	40	1	0.066	5024.815	331.638	-40
10	45	1	0.051	6359.74	324.347	-45
11	50	1	0.0401	7851.715	314.854	-50
12	60	1	0.0249	11306.81	281.540	-60
13	70	1	0.0157	15390.11	241.625	-70
14	80	1	0.0108	20101.61	217.097	-80
15	90	1	0.00755	25441.31	192.082	-90
16	100	1	0.00625	31409.21	196.308	-100

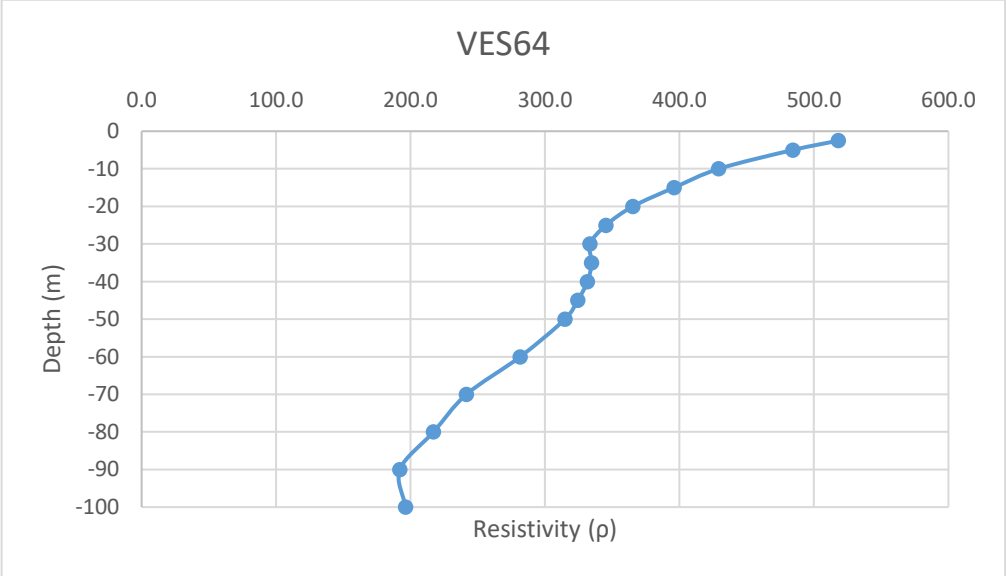

Annexure-XXII: Details of VES Survey

Date: 6/01/2025			VES-65			
Latitude	23.195315		Longitude	69.639257		
S.N	Current Electrode Spacing (AB/2)	Potential Electrode Spacing (MN)	Resistance (Ohm)	K value	Aparent Resistivity (Rho_a)	
1	2.5	1	39.1	18.846	736.879	-2.5
2	5	1	6.44	77.73975	500.644	-5
3	10	1	0.319	313.3148	99.947	-10
4	15	1	0.028	705.9398	19.766	-15
5	20	1	0.00729	1255.615	9.153	-20
6	25	1	0.00414	1962.34	8.124	-25
7	30	1	0.0029	2826.115	8.196	-30
8	35	1	0.0022	3846.94	8.463	-35
9	40	1	0.00171	5024.815	8.592	-40
10	45	1	0.0014	6359.74	8.904	-45
11	50	1	0.00115	7851.715	9.029	-50
12	60	1	0.00085	11306.81	9.611	-60
13	70	1	0.00065	15390.11	10.004	-70
14	80	1	0.0005	20101.61	10.051	-80
15	90	1	0.00057	25441.31	14.502	-90
16	100	1	0.0003	31409.21	9.423	-100

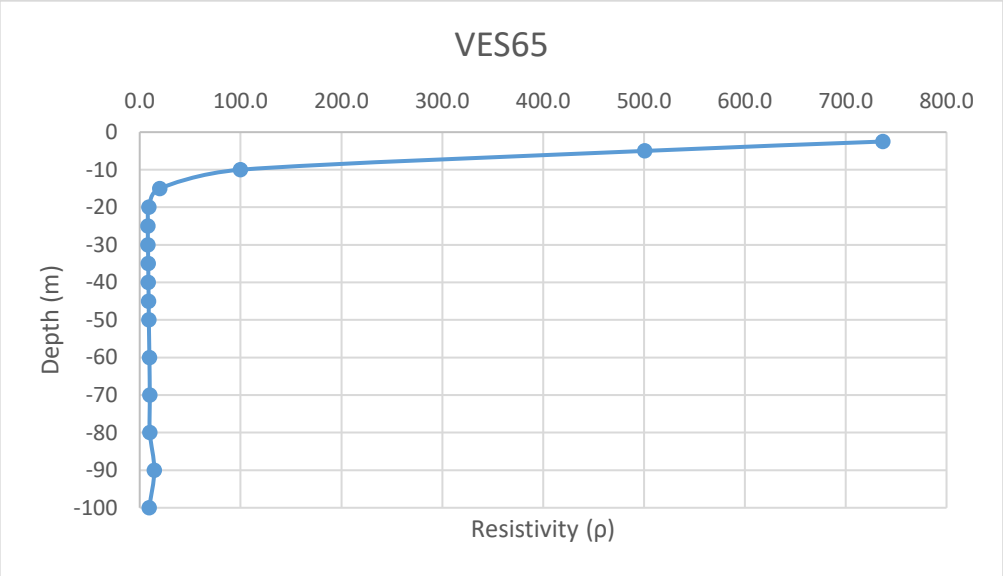

Annexure-XXII: Details of VES Survey

Date: 7/01/2025			VES-66			
Latitude	23.192312		Longitude	69.644915		
S.N	Current Electrode Spacing (AB/2)	Potential Electrode Spacing (MN)	Resistance (Ohm)	K value	Aparent Resistivity (Rho_a)	
1	2.5	1	0.397	18.846	7.482	-2.5
2	5	1	0.0442	77.73975	3.436	-5
3	10	1	0.00719	313.3148	2.253	-10
4	15	1	0.0035	705.9398	2.471	-15
5	20	1	0.00248	1255.615	3.114	-20
6	25	1	0.00172	1962.34	3.375	-25
7	30	1	0.00121	2826.115	3.420	-30
8	35	1	0.0009	3846.94	3.462	-35
9	40	1	0.0011	5024.815	5.527	-40
10	45	1	0.000636	6359.74	4.045	-45
11	50	1	0.000548	7851.715	4.303	-50
12	60	1	0.00043	11306.81	4.862	-60
13	70	1	0.00034	15390.11	5.233	-70
14	80	1	0.00028	20101.61	5.628	-80
15	90	1	0.00023	25441.31	5.852	-90
16	100	1	0.000219	31409.21	6.879	-100

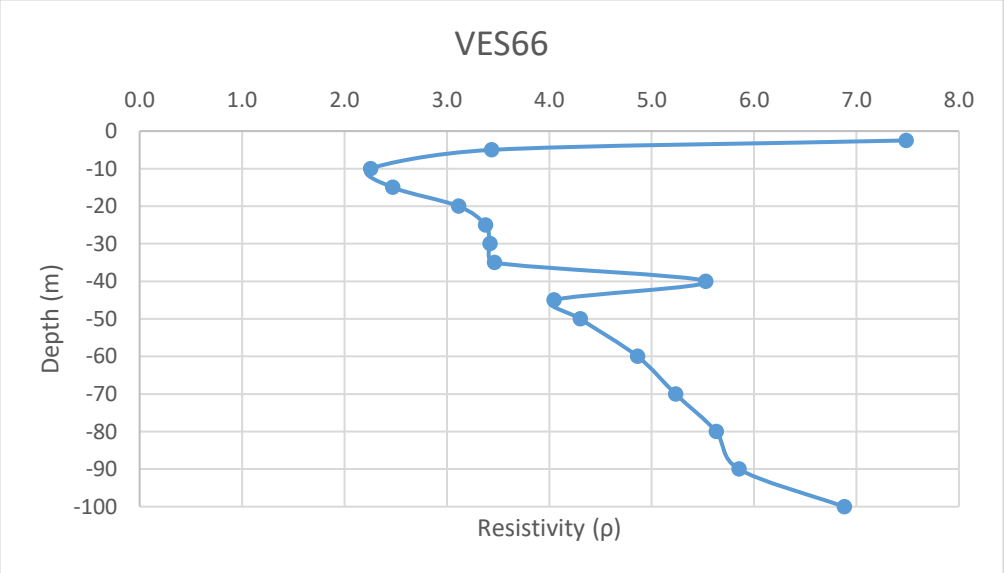

Annexure-XXII: Details of VES Survey

Date: 7/01/2025			VES-67			
Latitude	23.190657		Longitude	69.641957		
S.N	Current Electrode Spacing (AB/2)	Potential Electrode Spacing (MN)	Resistance (Ohm)	K value	Aparent Resistivity (Rho_a)	
1	2.5	1	34.7	18.846	653.956	-2.5
2	5	1	3.1	77.73975	240.993	-5
3	10	1	0.0675	313.3148	21.149	-10
4	15	1	0.00762	705.9398	5.379	-15
5	20	1	0.00531	1255.615	6.667	-20
6	25	1	0.0045	1962.34	8.831	-25
7	30	1	0.00375	2826.115	10.598	-30
8	35	1	0.00271	3846.94	10.425	-35
9	40	1	0.0027	5024.815	13.567	-40
10	45	1	0.0028	6359.74	17.807	-45
11	50	1	0.00401	7851.715	31.485	-50
12	60	1	0.00401	11306.81	45.340	-60
13	70	1	0.0017	15390.11	26.163	-70
14	80	1	0.000257	20101.61	5.166	-80
15	90	1	0.00214	25441.31	54.444	-90
16	100	1	0.00424	31409.21	133.175	-100

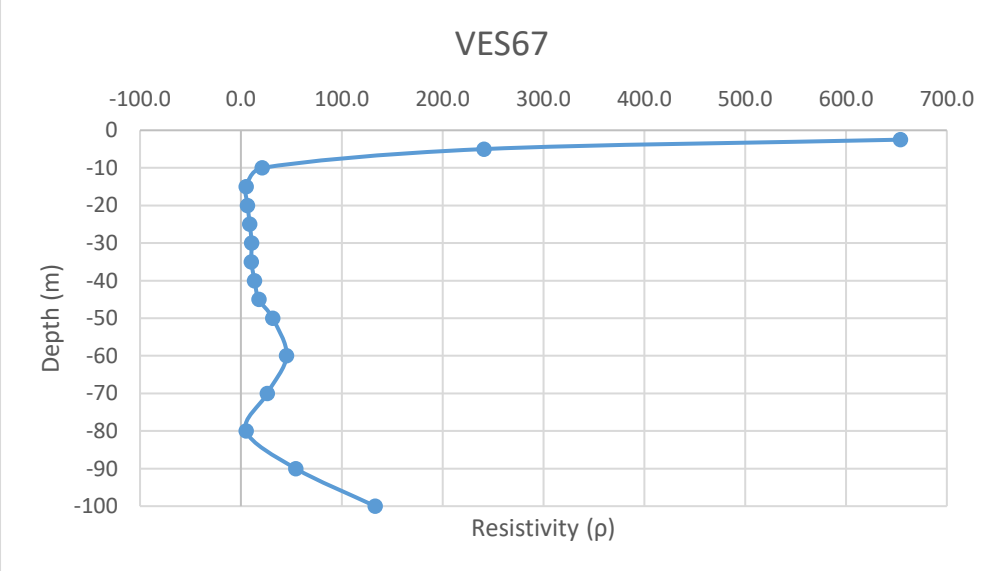

Annexure-XXII: Details of VES Survey

Date: 7/01/2025			VES-68			
Latitude	23.199983		Longitude	69.637427		
S.N	Current Electrode Spacing (AB/2)	Potential Electrode Spacing (MN)	Resistance (Ohm)	K value	Aparent Resistivity (Rho_a)	
1	2.5	1	0.105	18.846	1.979	-2.5
2	5	1	0.0234	77.73975	1.819	-5
3	10	1	0.00613	313.3148	1.921	-10
4	15	1	0.00317	705.9398	2.238	-15
5	20	1	0.00192	1255.615	2.411	-20
6	25	1	0.00135	1962.34	2.649	-25
7	30	1	0.001015	2826.115	2.869	-30
8	35	1	0.000782	3846.94	3.008	-35
9	40	1	0.000632	5024.815	3.176	-40
10	45	1	0.000539	6359.74	3.428	-45
11	50	1	0.000449	7851.715	3.525	-50
12	60	1	0.000319	11306.81	3.607	-60
13	70	1	0.000259	15390.11	3.986	-70
14	80	1	0.0002	20101.61	4.020	-80
15	90	1	0.000199	25441.31	5.063	-90
16	100	1	0.00014	31409.21	4.397	-100

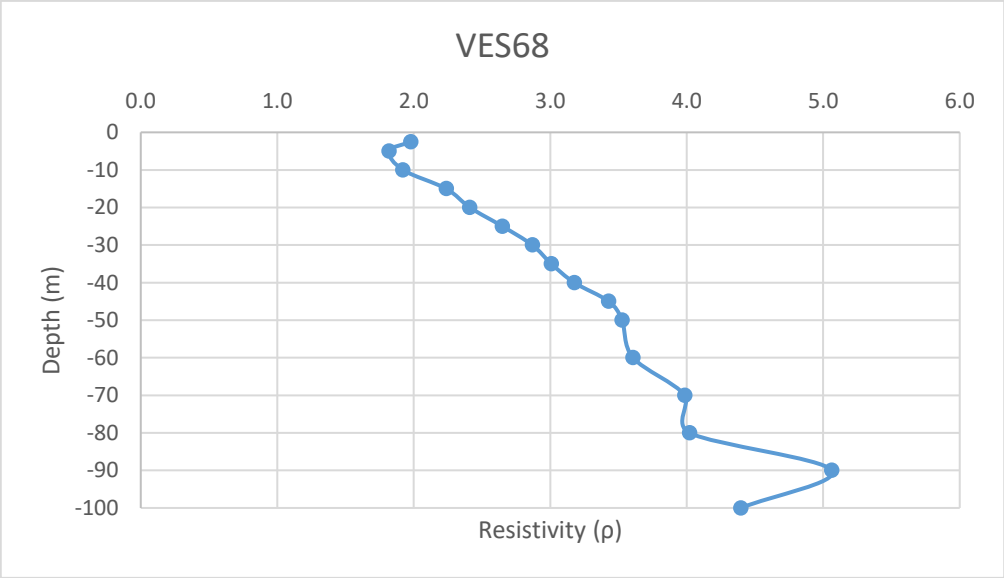

Annexure-XXII: Details of VES Survey

Date: 7/01/2025			VES-69			
Latitude	23.188338		Longitude	69.641693		
S.N	Current Electrode Spacing (AB/2)	Potential Electrode Spacing (MN)	Resistance (Ohm)	K value	Aparent Resistivity (Rho_a)	
1	2.5	1	1.78	18.846	33.546	-2.5
2	5	1	0.083	77.73975	6.452	-5
3	10	1	0.00775	313.3148	2.428	-10
4	15	1	0.00385	705.9398	2.718	-15
5	20	1	0.00251	1255.615	3.152	-20
6	25	1	0.00183	1962.34	3.591	-25
7	30	1	0.00138	2826.115	3.900	-30
8	35	1	0.00116	3846.94	4.462	-35
9	40	1	0.00095	5024.815	4.774	-40
10	45	1	0.000756	6359.74	4.808	-45
11	50	1	0.000639	7851.715	5.017	-50
12	60	1	0.000459	11306.81	5.190	-60
13	70	1	0.0004	15390.11	6.156	-70
14	80	1	0.00035	20101.61	7.036	-80
15	90	1	0.000249	25441.31	6.335	-90
16	100	1	0.000219	31409.21	6.879	-100

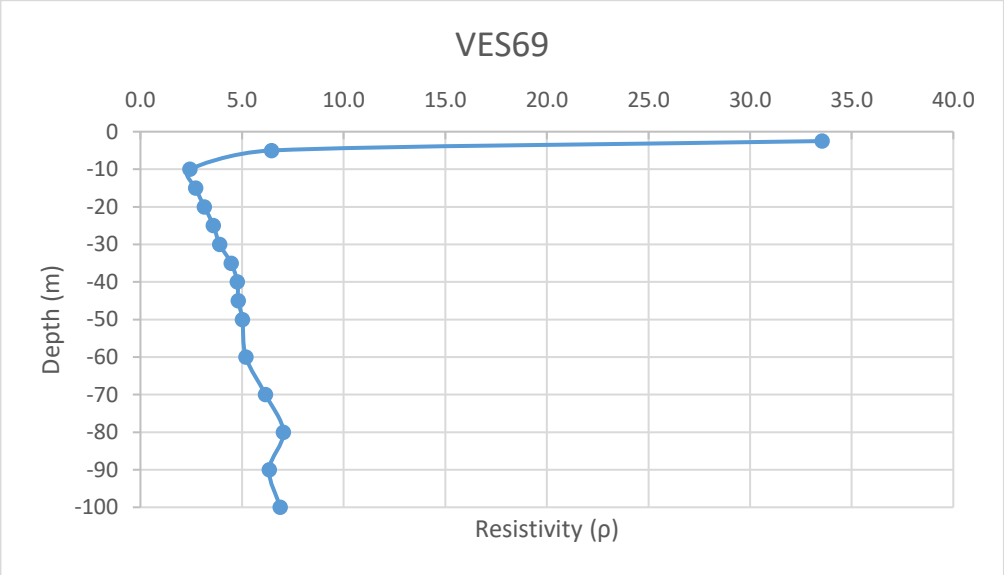

Annexure-XXII: Details of VES Survey

Date: 8/01/2025			VES-70			
Latitude	23.18534		Longitude	69.63876		
S.N	Current Electrode Spacing (AB/2)	Potential Electrode Spacing (MN)	Resistance (Ohm)	K value	Aparent Resistivity (Rho_a)	
1	2.5	1	62.3	18.846	1174.106	-2.5
2	5	1	8.03	77.73975	624.250	-5
3	10	1	0.561	313.3148	175.770	-10
4	15	1	0.0723	705.9398	51.039	-15
5	20	1	0.0389	1255.615	48.843	-20
6	25	1	0.01107	1962.34	21.723	-25
7	30	1	0.00637	2826.115	18.002	-30
8	35	1	0.00471	3846.94	18.119	-35
9	40	1	0.00425	5024.815	21.355	-40
10	45	1	0.0035	6359.74	22.259	-45
11	50	1	0.0026	7851.715	20.414	-50
12	60	1	0.00178	11306.81	20.126	-60
13	70	1	0.00157	15390.11	24.162	-70
14	80	1	0.002	20101.61	40.203	-80
15	90	1	0.0013	25441.31	33.074	-90
16	100	1	0.00064	31409.21	20.102	-100

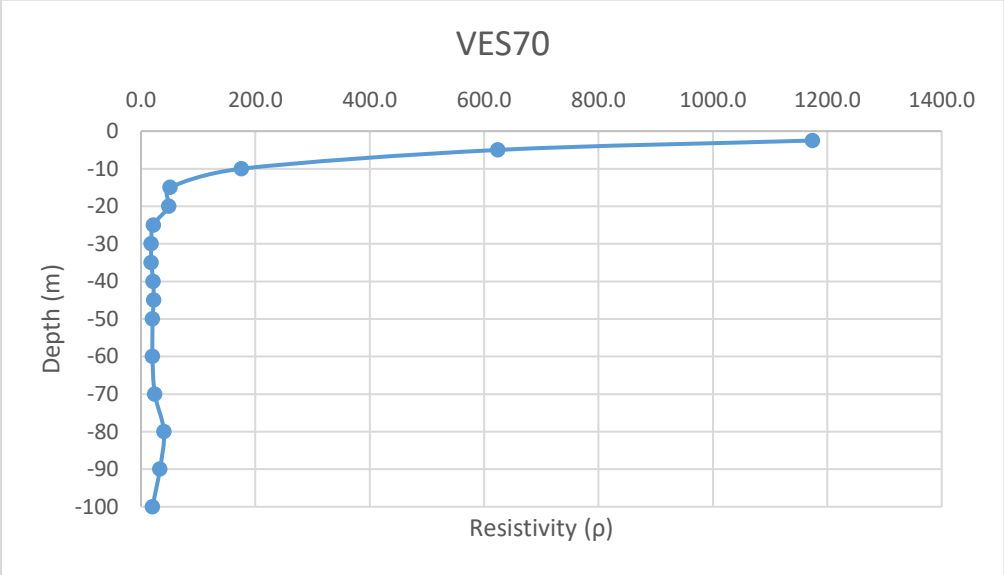

Annexure-XXII: Details of VES Survey

Date: 8/01/2025			VES-71			
Latitude	23.17588		Longitude	69.631278		
S.N	Current Electrode Spacing (AB/2)	Potential Electrode Spacing (MN)	Resistance (Ohm)	K value	Aparent Resistivity (Rho_a)	
1	2.5	1	2.73	18.846	51.450	-2.5
2	5	1	0.291	77.73975	22.622	-5
3	10	1	0.049	313.3148	15.352	-10
4	15	1	0.0246	705.9398	17.366	-15
5	20	1	0.0171	1255.615	21.471	-20
6	25	1	0.0127	1962.34	24.922	-25
7	30	1	0.00945	2826.115	26.707	-30
8	35	1	0.00685	3846.94	26.352	-35
9	40	1	0.00543	5024.815	27.285	-40
10	45	1	0.00437	6359.74	27.792	-45
11	50	1	0.00391	7851.715	30.700	-50
12	60	1	0.00275	11306.81	31.094	-60
13	70	1	0.00202	15390.11	31.088	-70
14	80	1	0.0016	20101.61	32.163	-80
15	90	1	0.00121	25441.31	30.784	-90
16	100	1	0.001	31409.21	31.409	-100

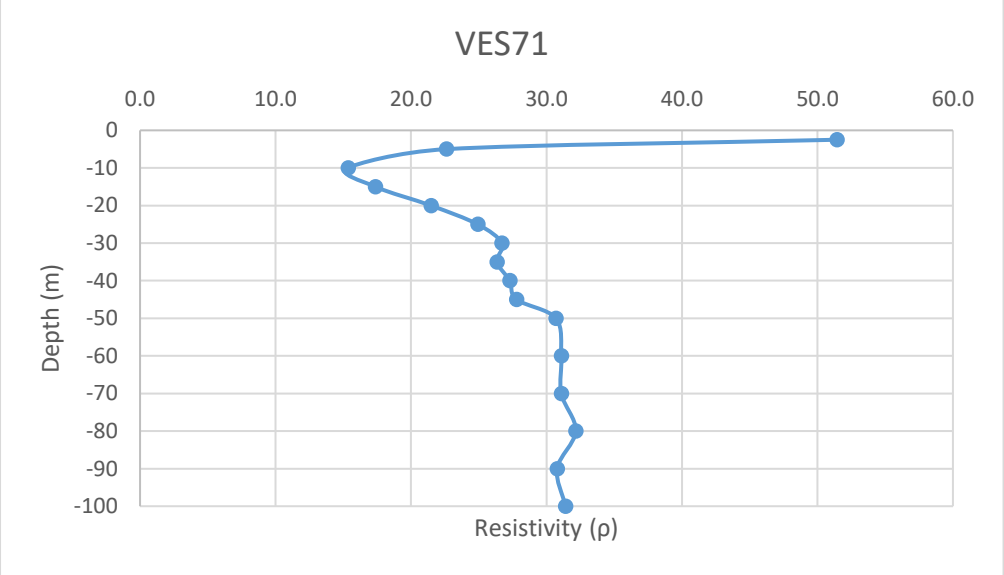

Annexure-XXII: Details of VES Survey

Date: 8/01/2025			VES-72			
Latitude	23.18063		Longitude	69.634735		
S.N	Current Electrode Spacing (AB/2)	Potential Electrode Spacing (MN)	Resistance (Ohm)	K value	Aparent Resistivity (Rho_a)	
1	2.5	1	32.515	18.846	612.778	-2.5
2	5	1	4.1605	77.73975	323.436	-5
3	10	1	0.305	313.3148	95.561	-10
4	15	1	0.048	705.9398	33.885	-15
5	20	1	0.028	1255.615	35.157	-20
6	25	1	0.011	1962.34	21.586	-25
7	30	1	0.00791	2826.115	22.355	-30
8	35	1	0.00578	3846.94	22.235	-35
9	40	1	0.00484	5024.815	24.320	-40
10	45	1	0.00393	6359.74	24.994	-45
11	50	1	0.00325	7851.715	25.518	-50
12	60	1	0.00226	11306.81	25.553	-60
13	70	1	0.00179	15390.11	27.548	-70
14	80	1	0.0018	20101.61	36.183	-80
15	90	1	0.0012	25441.31	30.530	-90
16	100	1	0.0008	31409.21	25.127	-100

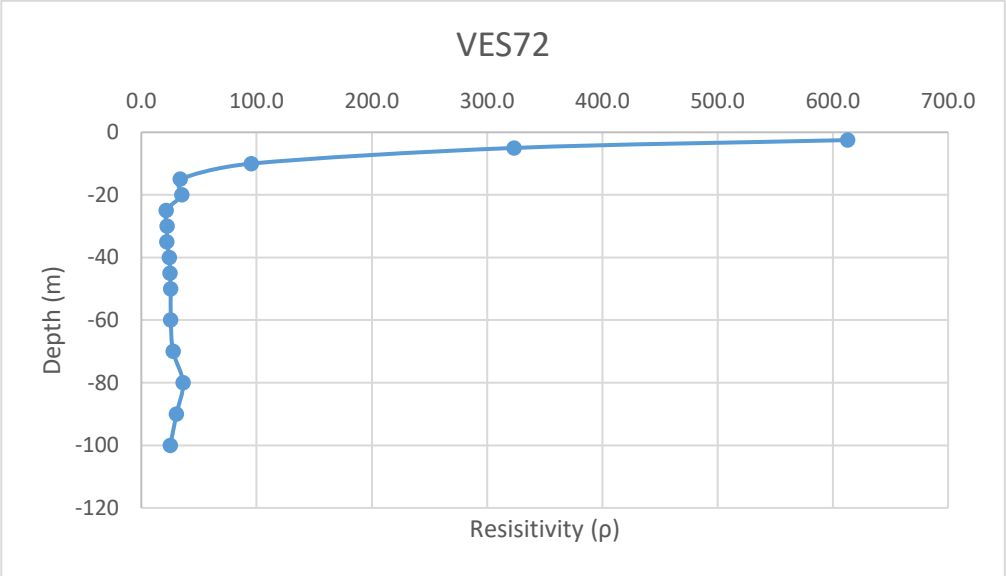

Annexure-XXII: Details of VES Survey

Date: 8/01/2025			VES-73			
Latitude	23.183595		Longitude	69.598063		
S.N	Current Electrode Spacing (AB/2)	Potential Electrode Spacing (MN)	Resistance (Ohm)	K value	Aparent Resistivity (Rho_a)	
1	2.5	1	10.27	18.846	193.548	-2.5
2	5	1	2.87	77.73975	223.113	-5
3	10	1	0.489	313.3148	153.211	-10
4	15	1	0.105	705.9398	74.124	-15
5	20	1	0.036	1255.615	45.202	-20
6	25	1	0.0123	1962.34	24.137	-25
7	30	1	0.00502	2826.115	14.187	-30
8	35	1	0.00287	3846.94	11.041	-35
9	40	1	0.00195	5024.815	9.798	-40
10	45	1	0.00142	6359.74	9.031	-45
11	50	1	0.001148	7851.715	9.014	-50
12	60	1	0.0009	11306.81	10.176	-60
13	70	1	0.0007	15390.11	10.773	-70
14	80	1	0.0065	20101.61	130.660	-80
15	90	1	0.00045	25441.31	11.449	-90
16	100	1	0.0004	31409.21	12.564	-100

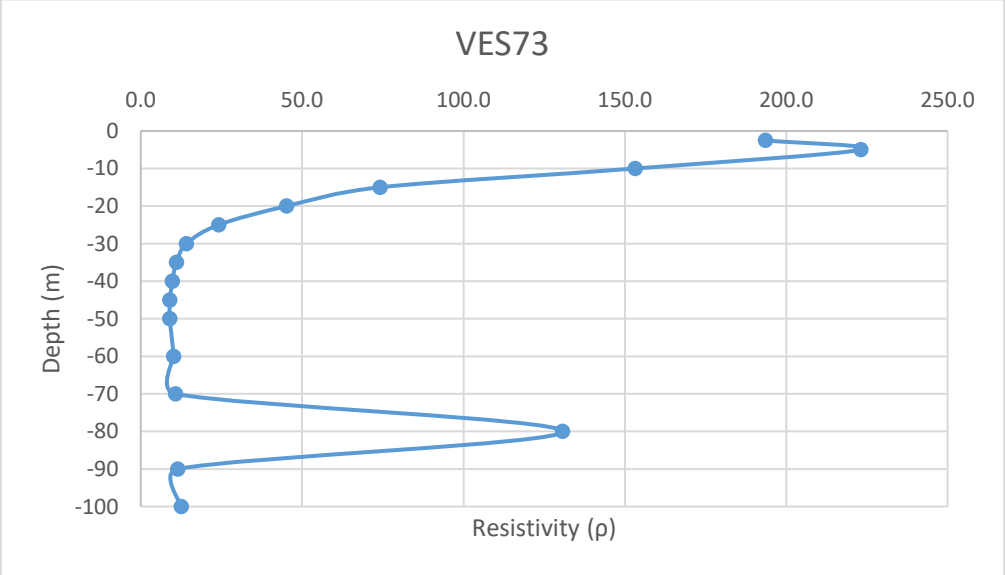

Annexure-XXII: Details of VES Survey

Date: 9/01/2025			VES-74			
Latitude	23.12047		Longitude	69.36272		
S.N	Current Electrode Spacing (AB/2)	Potential Electrode Spacing (MN)	Resistance (Ohm)	K value	Aparent Resistivity (Rho_a)	
1	2.5	1	3.56	18.846	67.092	-2.5
2	5	1	0.483	77.73975	37.548	-5
3	10	1	0.0927	313.3148	29.044	-10
4	15	1	0.0411	705.9398	29.014	-15
5	20	1	0.0226	1255.615	28.377	-20
6	25	1	0.0146	1962.34	28.650	-25
7	30	1	0.00959	2826.115	27.102	-30
8	35	1	0.00637	3846.94	24.505	-35
9	40	1	0.00475	5024.815	23.868	-40
10	45	1	0.00354	6359.74	22.513	-45
11	50	1	0.0028	7851.715	21.985	-50
12	60	1	0.00178	11306.81	20.126	-60
13	70	1	0.0013	15390.11	20.007	-70
14	80	1	0.000932	20101.61	18.735	-80
15	90	1	0.000719	25441.31	18.292	-90
16	100	1	0.000519	31409.21	16.301	-100

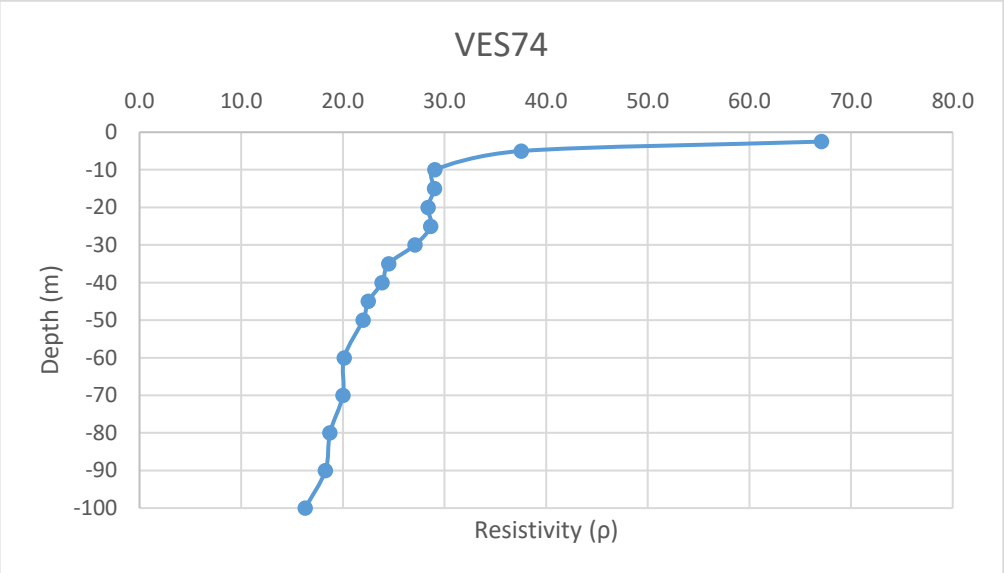

Annexure-XXII: Details of VES Survey

Date: 9/01/2025			VES-75			
Latitude	23.11073		Longitude	69.35216		
S.N	Current Electrode Spacing (AB/2)	Potential Electrode Spacing (MN)	Resistance (Ohm)	K value	Aparent Resistivity (Rho_a)	
1	2.5	1	32.9	18.846	620.033	-2.5
2	5	1	7.77	77.73975	604.038	-5
3	10	1	2.06	313.3148	645.428	-10
4	15	1	0.73	705.9398	515.336	-15
5	20	1	0.257	1255.615	322.693	-20
6	25	1	0.09	1962.34	176.611	-25
7	30	1	0.0328	2826.115	92.697	-30
8	35	1	0.0149	3846.94	57.319	-35
9	40	1	0.00729	5024.815	36.631	-40
10	45	1	0.00378	6359.74	24.040	-45
11	50	1	0.00214	7851.715	16.803	-50
12	60	1	0.00105	11306.81	11.872	-60
13	70	1	0.00117	15390.11	18.006	-70
14	80	1	0.001	20101.61	20.102	-80
15	90	1	0.00171	25441.31	43.505	-90
16	100	1	0.0007	31409.21	21.986	-100
				Bottom	27.807	
				Top	425.262	

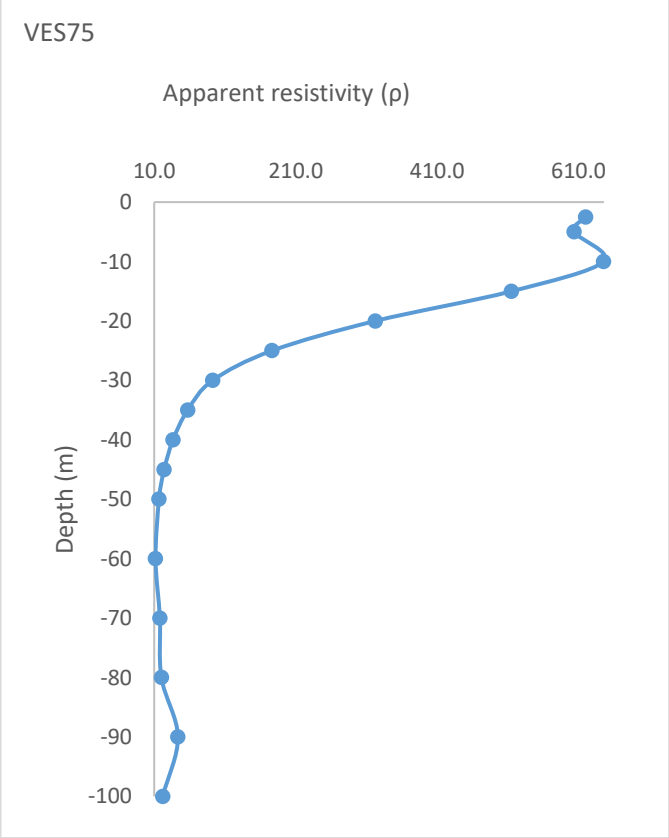

Annexure-XXII: Details of VES Survey

Date: 9/01/2025			VES-76			
Latitude	23.11315		Longitude	69.35206		
S.N	Current Electrode Spacing (AB/2)	Potential Electrode Spacing (MN)	Resistance (Ohm)	K value	Aparent Resistivity (Rho_a)	
1	2.5	1	1.189	18.846	22.408	-2.5
2	5	1	0.153	77.73975	11.894	-5
3	10	1	0.0301	313.3148	9.431	-10
4	15	1	0.01013	705.9398	7.151	-15
5	20	1	0.00561	1255.615	7.044	-20
6	25	1	0.004	1962.34	7.849	-25
7	30	1	0.0028	2826.115	7.913	-30
8	35	1	0.0021	3846.94	8.079	-35
9	40	1	0.0016	5024.815	8.040	-40
10	45	1	0.00127	6359.74	8.077	-45
11	50	1	0.001049	7851.715	8.236	-50
12	60	1	0.000773	11306.81	8.740	-60
13	70	1	0.000598	15390.11	9.203	-70
14	80	1	0.000524	20101.61	10.533	-80
15	90	1	0.000474	25441.31	12.059	-90
16	100	1	0.00045	31409.21	14.134	-100
					10.050	

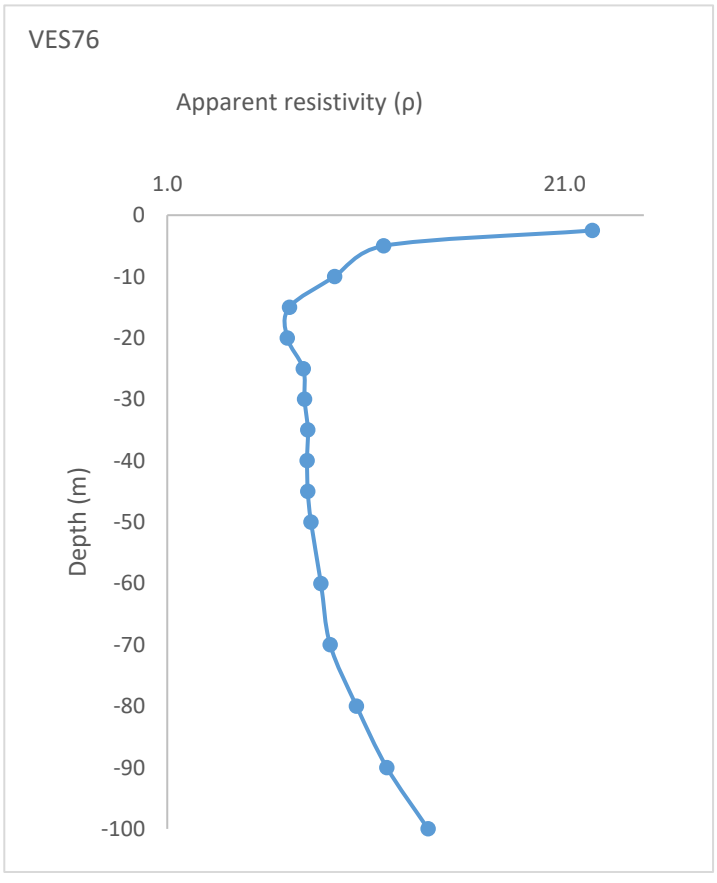

Annexure-XXII: Details of VES Survey

Date: 9/01/2025			VES-77			
Latitude	23.11178		Longitude	69.35176		
S.N	**Current Electrode Spacing (AB/2)**	**Potential Electrode Spacing (MN)**	**Resistance (Ohm)**	**K value**	**Aparent Resistivity (Rho_a)**	
1	2.5	1	17.044	18.846	321.211	-2.5
2	5	1	3.961	77.73975	307.927	-5
3	10	1	1.045	313.3148	327.414	-10
4	15	1	0.37	705.9398	261.198	-15
5	20	1	0.131	1255.615	164.486	-20
6	25	1	0.047	1962.34	92.230	-25
7	30	1	0.017	2826.115	48.044	-30
8	35	1	0.008	3846.94	30.776	-35
9	40	1	0.00444	5024.815	22.310	-40
10	45	1	0.00252	6359.74	16.027	-45
11	50	1	0.00159	7851.715	12.484	-50
12	60	1	0.000912	11306.81	10.306	-60
13	70	1	0.000884	15390.11	13.605	-70
14	80	1	0.000762	20101.61	15.317	-80
15	90	1	0.001092	25441.31	27.782	-90
16	100	1	0.000575	31409.21	18.060	-100
				Bottom	21.471	
				Top	245.744	

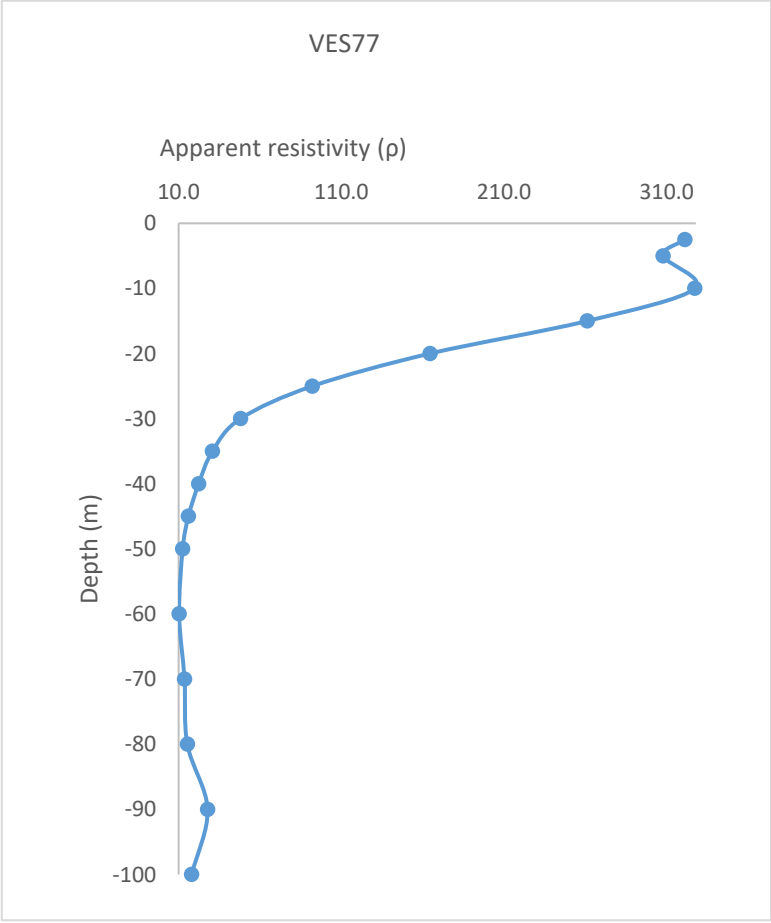

Annexure-XXII: Details of VES Survey

Date: 10/01/2025		VES-78				
Latitude	23.12131		Longitude	69.35235		
S.N	Current Electrode Spacing (AB/2)	Potential Electrode Spacing (MN)	Resistance (Ohm)	K value	Aparent Resistivity (Rho_a)	
1	2.5	1	6.48	18.846	122.122	-2.5
2	5	1	2.36	77.73975	183.466	-5
3	10	1	0.679	313.3148	212.741	-10
4	15	1	0.277	705.9398	195.545	-15
5	20	1	0.129	1255.615	161.974	-20
6	25	1	0.0612	1962.34	120.095	-25
7	30	1	0.031	2826.115	87.610	-30
8	35	1	0.0155	3846.94	59.628	-35
9	40	1	0.00739	5024.815	37.133	-40
10	45	1	0.00348	6359.74	22.132	-45
11	50	1	0.00178	7851.715	13.976	-50
12	60	1	0.000882	11306.81	9.973	-60
13	70	1	0.000539	15390.11	8.295	-70
14	80	1	0.000399	20101.61	8.021	-80
15	90	1	0.000299	25441.31	7.607	-90
16	100	1	0.000259	31409.21	8.135	-100

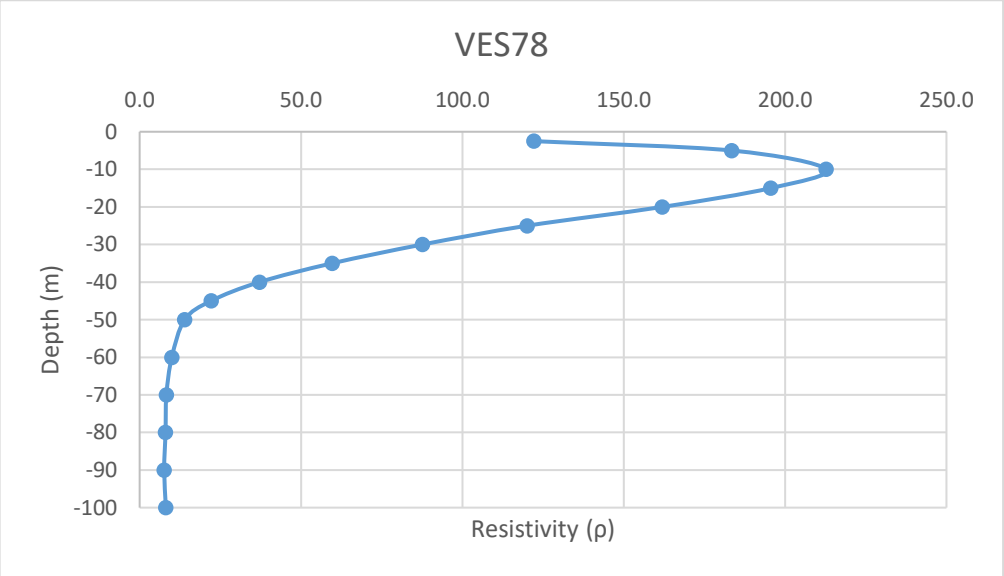

Annexure-XXII: Details of VES Survey

Date: 10/01/2025			VES-79			
Latitude	23.11451		Longitude	69.35304		
S.N	Current Electrode Spacing (AB/2)	Potential Electrode Spacing (MN)	Resistance (Ohm)	K value	Aparent Resistivity (Rho_a)	
1	2.5	1	5.22	18.846	98.376	-2.5
2	5	1	0.871	77.73975	67.711	-5
3	10	1	0.205	313.3148	64.230	-10
4	15	1	0.094	705.9398	66.358	-15
5	20	1	0.0454	1255.615	57.005	-20
6	25	1	0.0239	1962.34	46.900	-25
7	30	1	0.0137	2826.115	38.718	-30
8	35	1	0.0083	3846.94	31.930	-35
9	40	1	0.0053	5024.815	26.632	-40
10	45	1	0.0037	6359.74	23.531	-45
11	50	1	0.00295	7851.715	23.163	-50
12	60	1	0.002	11306.81	22.614	-60
13	70	1	0.00142	15390.11	21.854	-70
14	80	1	0.00085	20101.61	17.086	-80
15	90	1	0.000649	25441.31	16.511	-90
16	100	1	0.0006	31409.21	18.846	-100

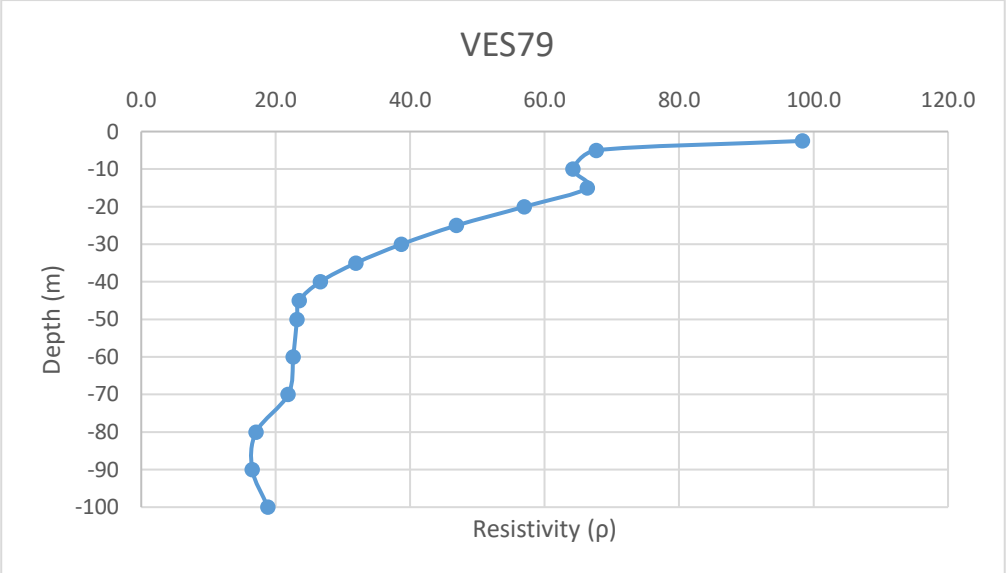

Annexure-XXII: Details of VES Survey

Date: 10/01/2025		VES-80				
Latitude	23.12119		Longitude	69.3458		
S.N	Current Electrode Spacing (AB/2)	Potential Electrode Spacing (MN)	Resistance (Ohm)	K value	Aparent Resistivity (Rho_a)	
1	2.5	1	32.8	18.846	618.149	-2.5
2	5	1	2.35	77.73975	182.688	-5
3	10	1	0.178	313.3148	55.770	-10
4	15	1	0.0834	705.9398	58.875	-15
5	20	1	0.0534	1255.615	67.050	-20
6	25	1	0.0367	1962.34	72.018	-25
7	30	1	0.0249	2826.115	70.370	-30
8	35	1	0.0204	3846.94	78.478	-35
9	40	1	0.0183	5024.815	91.954	-40
10	45	1	0.0159	6359.74	101.120	-45
11	50	1	0.0142	7851.715	111.494	-50
12	60	1	0.01012	11306.81	114.425	-60
13	70	1	0.00671	15390.11	103.268	-70
14	80	1	0.0022	20101.61	44.224	-80
15	90	1	0.00125	25441.31	31.802	-90
16	100	1	0.00024	31409.21	7.538	-100

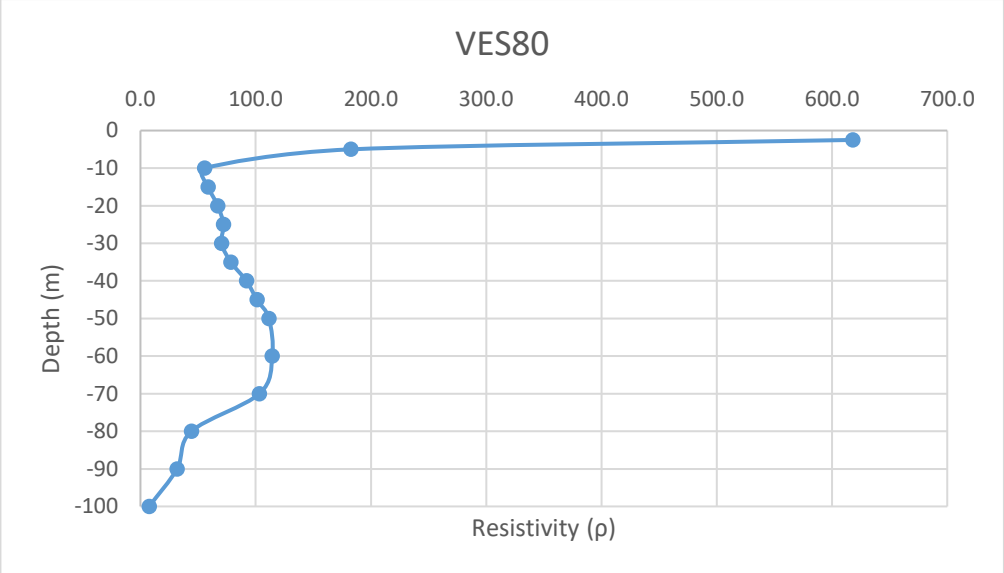

Annexure-XXII: Details of VES Survey

Date: 10/01/2025		VES-81				
Latitude	23.12067		Longitude	69.35123		
S.N	Current Electrode Spacing (AB/2)	Potential Electrode Spacing (MN)	Resistance (Ohm)	K value	Aparent Resistivity (Rho_a)	
1	2.5	1	19.64	18.846	370.135	-2.5
2	5	1	2.365	77.73975	183.855	-5
3	10	1	0.428	313.3148	134.099	-10
4	15	1	0.18	705.9398	127.069	-15
5	20	1	0.091	1255.615	114.261	-20
6	25	1	0.048	1962.34	94.192	-25
7	30	1	0.027	2826.115	76.305	-30
8	35	1	0.017	3846.94	65.398	-35
9	40	1	0.012	5024.815	60.298	-40
10	45	1	0.00969	6359.74	61.626	-45
11	50	1	0.00799	7851.715	62.735	-50
12	60	1	0.0055	11306.81	62.187	-60
13	70	1	0.0036	15390.11	55.404	-70
14	80	1	0.0013	20101.61	26.122	-80
15	90	1	0.000774	25441.31	19.692	-90
16	100	1	0.000249	31409.21	7.821	-100

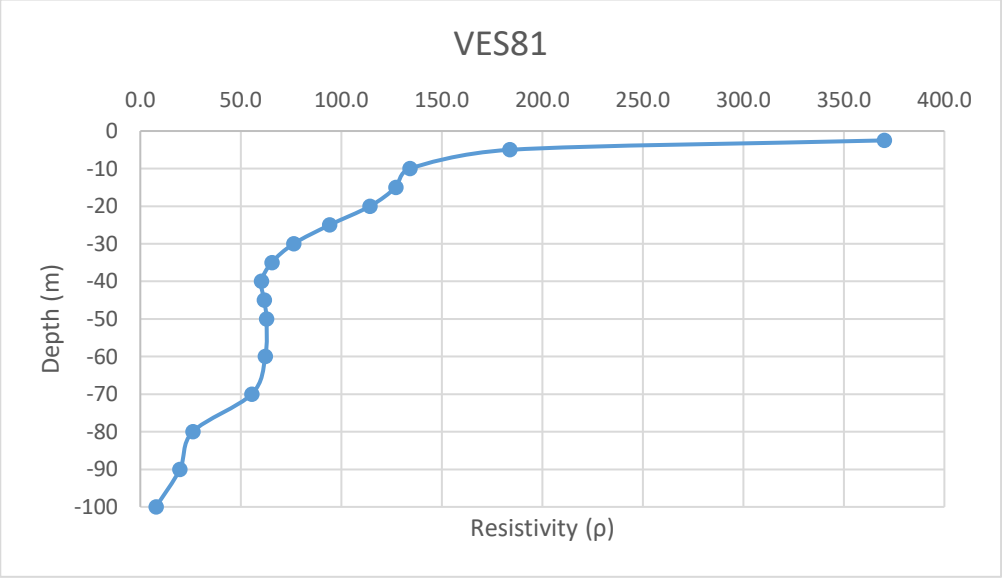

Annexure-XXII: Details of VES Survey

Date: 11/01/2025		VES-82				
Latitude	23.12067		Longitude	69.35123		
S.N	Current Electrode Spacing (AB/2)	Potential Electrode Spacing (MN)	Resistance (Ohm)	K value	Aparent Resistivity (Rho_a)	
1	2.5	1	7.48	18.846	140.968	-2.5
2	5	1	1.25	77.73975	97.175	-5
3	10	1	0.289	313.3148	90.548	-10
4	15	1	0.122	705.9398	86.125	-15
5	20	1	0.0657	1255.615	82.494	-20
6	25	1	0.0404	1962.34	79.279	-25
7	30	1	0.0266	2826.115	75.175	-30
8	35	1	0.0183	3846.94	70.399	-35
9	40	1	0.0134	5024.815	67.333	-40
10	45	1	0.01002	6359.74	63.725	-45
11	50	1	0.00782	7851.715	61.400	-50
12	60	1	0.00493	11306.81	55.743	-60
13	70	1	0.00357	15390.11	54.943	-70
14	80	1	0.0026	20101.61	52.264	-80
15	90	1	0.00183	25441.31	46.558	-90
16	100	1	0.00137	31409.21	43.031	-100
					60.895	

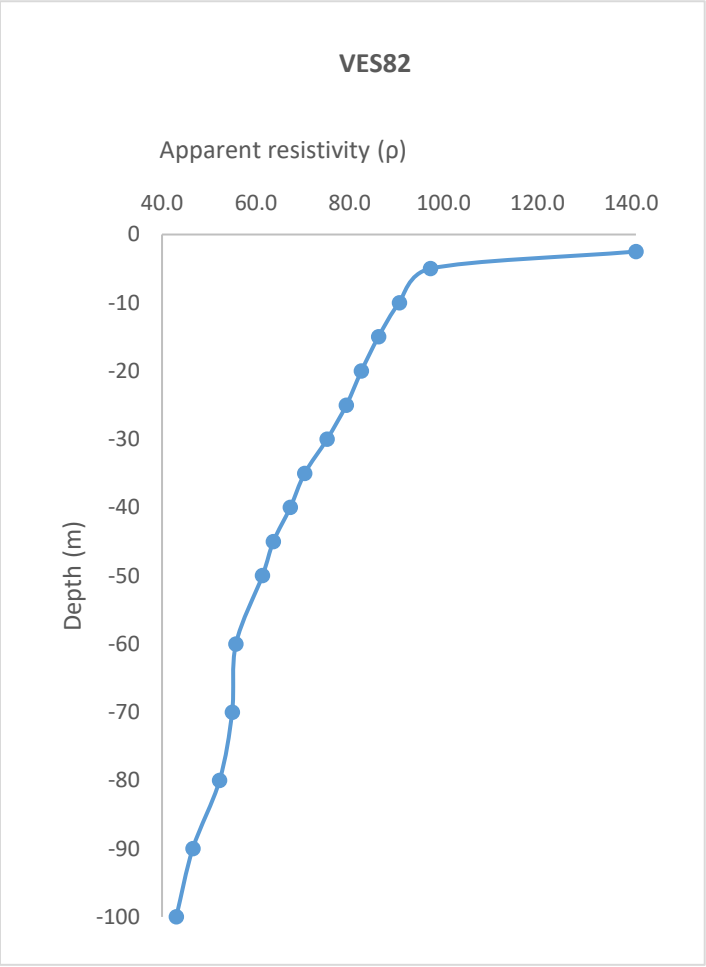

Annexure-XXII: Details of VES Survey

Date: 11/01/2025		VES-83				
Latitude	23.12067		Longitude	69.35123		
S.N	Current Electrode Spacing (AB/2)	Potential Electrode Spacing (MN)	Resistance (Ohm)	K value	Aparent Resistivity (Rho_a)	
1	2.5	1	7.68	18.846	144.737	-2.5
2	5	1	2.21	77.73975	171.805	-5
3	10	1	0.493	313.3148	154.464	-10
4	15	1	0.179	705.9398	126.363	-15
5	20	1	0.0796	1255.615	99.947	-20
6	25	1	0.0422	1962.34	82.811	-25
7	30	1	0.0271	2826.115	76.588	-30
8	35	1	0.0189	3846.94	72.707	-35
9	40	1	0.0139	5024.815	69.845	-40
10	45	1	0.0129	6359.74	82.041	-45
11	50	1	0.00844	7851.715	66.268	-50
12	60	1	0.0056	11306.81	63.318	-60
13	70	1	0.0039	15390.11	60.021	-70
14	80	1	0.0029	20101.61	58.295	-80
15	90	1	0.0023	25441.31	58.515	-90
16	100	1	0.0019	31409.21	59.678	-100
					66.728	

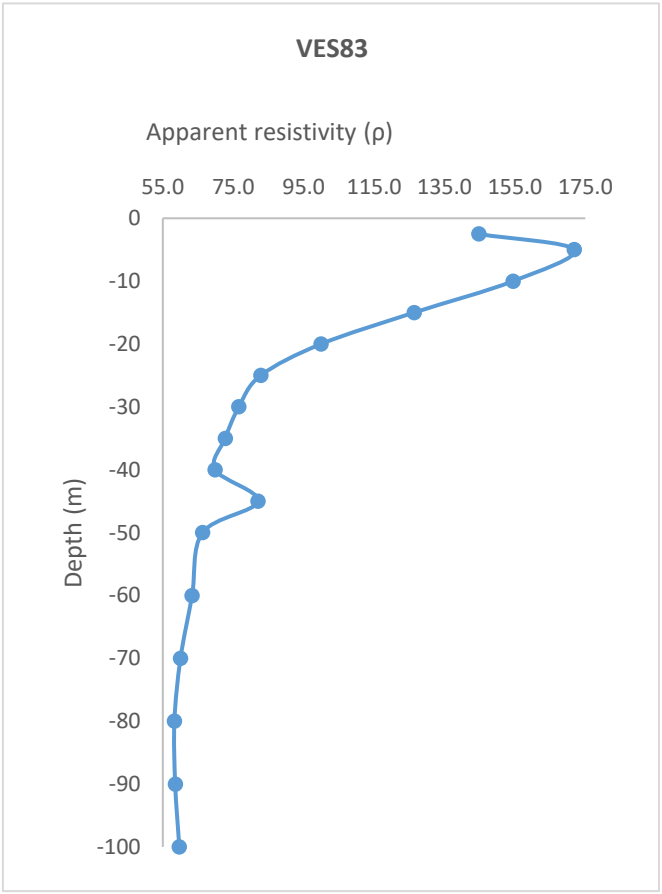

Annexure-XXII: Details of VES Survey

Date: 11/01/2025			VES-84			
Latitude	23.12067		Longitude	69.35123		
S.N	Current Electrode Spacing (AB/2)	Potential Electrode Spacing (MN)	Resistance (Ohm)	K value	Aparent Resistivity (Rho_a)	
1	2.5	1	38	18.846	716.148	-2.5
2	5	1	11.06	77.73975	859.802	-5
3	10	1	2.81	313.3148	880.414	-10
4	15	1	1.128	705.9398	796.300	-15
5	20	1	0.533	1255.615	669.243	-20
6	25	1	0.318	1962.34	624.024	-25
7	30	1	0.209	2826.115	590.658	-30
8	35	1	0.142	3846.94	546.265	-35
9	40	1	0.1	5024.815	502.481	-40
10	45	1	0.0749	6359.74	476.345	-45
11	50	1	0.0536	7851.715	420.852	-50
12	60	1	0.0335	11306.81	378.778	-60
13	70	1	0.237	15390.11	3647.457	-70
14	80	1	0.0154	20101.61	309.565	-80
15	90	1	0.01072	25441.31	272.731	-90
16	100	1	0.00792	31409.21	248.761	-100

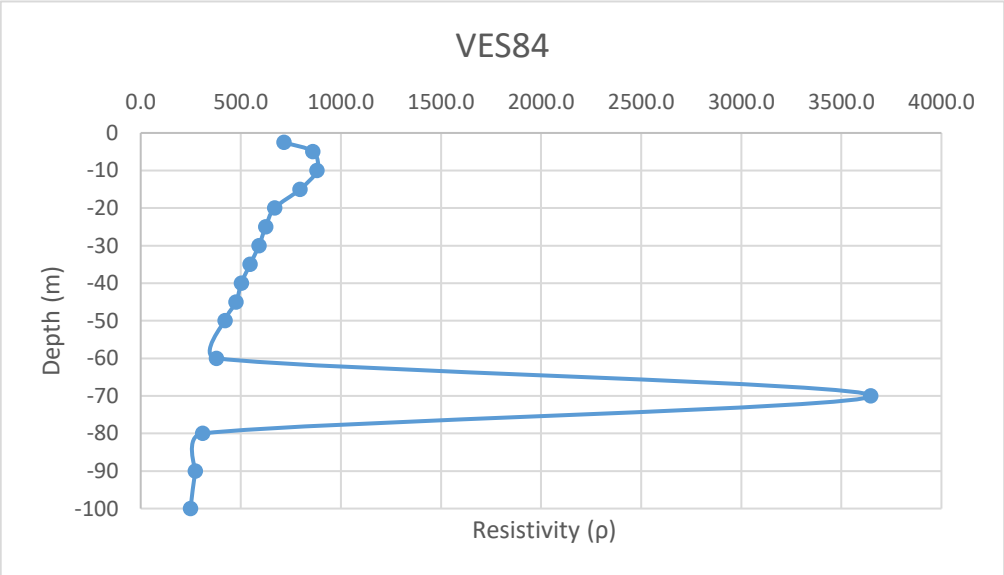

Annexure-XXII: Details of VES Survey

Date: 11/01/2025			VES-85			
Latitude	23.12067		Longitude	69.35123		
S.N	Current Electrode Spacing (AB/2)	Potential Electrode Spacing (MN)	Resistance (Ohm)	K value	Aparent Resistivity (Rho_a)	
1	2.5	1	3.44	18.846	64.830	-2.5
2	5	1	0.608	77.73975	47.266	-5
3	10	1	0.179	313.3148	56.083	-10
4	15	1	0.0586	705.9398	41.368	-15
5	20	1	0.0294	1255.615	36.915	-20
6	25	1	0.0179	1962.34	35.126	-25
7	30	1	0.0124	2826.115	35.044	-30
8	35	1	0.0096	3846.94	36.931	-35
9	40	1	0.00779	5024.815	39.143	-40
10	45	1	0.00671	6359.74	42.674	-45
11	50	1	0.00571	7851.715	44.833	-50
12	60	1	0.0045	11306.81	50.881	-60
13	70	1	0.00355	15390.11	54.635	-70
14	80	1	0.003	20101.61	60.305	-80
15	90	1	0.00264	25441.31	67.165	-90
16	100	1	0.00227	31409.21	71.299	-100

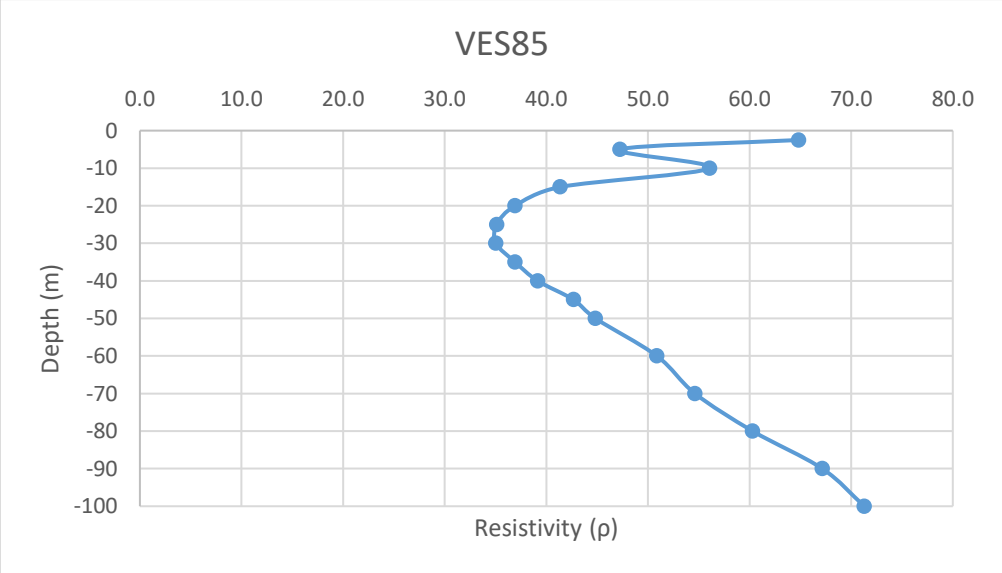

Annexure-XXII: Details of VES Survey

Date: 12/01/2025			VES-86			
Latitude	23.188983		Longitude	69.572268		
S.N	Current Electrode Spacing (AB/2)	Potential Electrode Spacing (MN)	Resistance (Ohm)	K value	Aparent Resistivity (Rho_a)	
1	2.5	1	3.26	18.846	61.438	-2.5
2	5	1	1.139	77.73975	88.546	-5
3	10	1	0.453	313.3148	141.932	-10
4	15	1	0.231	705.9398	163.072	-15
5	20	1	0.116	1255.615	145.651	-20
6	25	1	0.064	1962.34	125.590	-25
7	30	1	0.00419	2826.115	11.841	-30
8	35	1	0.0267	3846.94	102.713	-35
9	40	1	0.0179	5024.815	89.944	-40
10	45	1	0.01191	6359.74	75.745	-45
11	50	1	0.00845	7851.715	66.347	-50
12	60	1	0.00527	11306.81	59.587	-60
13	70	1	0.00372	15390.11	57.251	-70
14	80	1	0.00292	20101.61	58.697	-80
15	90	1	0.0024	25441.31	61.059	-90
16	100	1	0.002	31409.21	62.818	-100

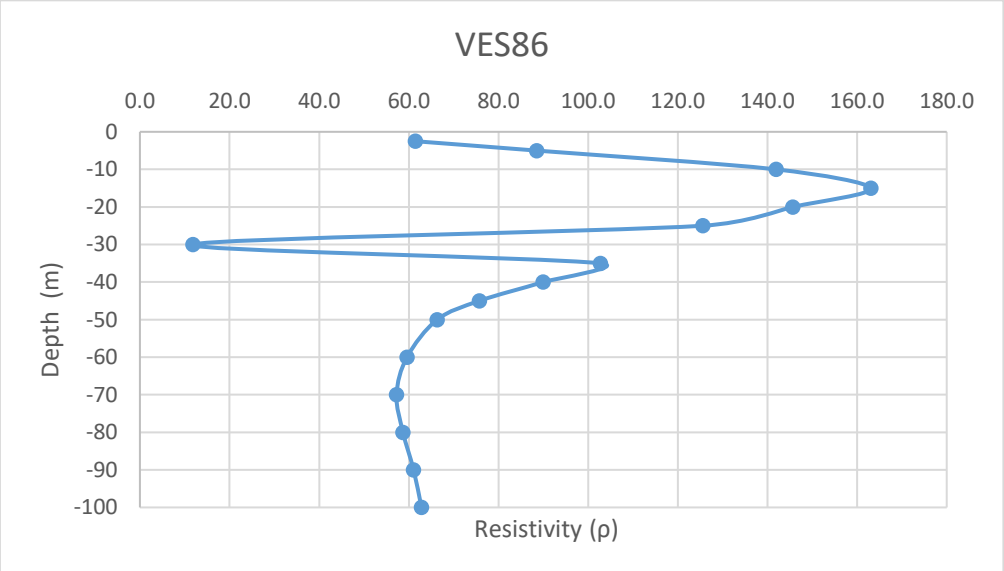

Annexure-XXII: Details of VES Survey

Date: 12/01/2025			VES-87			
Latitude	23.186043		Longitude	69.572503		
S.N	Current Electrode Spacing (AB/2)	Potential Electrode Spacing (MN)	Resistance (Ohm)	K value	Aparent Resistivity (Rho_a)	
1	2.5	1	5.02	18.846	94.607	-2.5
2	5	1	0.233	77.73975	18.113	-5
3	10	1	0.0238	313.3148	7.457	-10
4	15	1	0.01135	705.9398	8.012	-15
5	20	1	0.00635	1255.615	7.973	-20
6	25	1	0.00441	1962.34	8.654	-25
7	30	1	0.00335	2826.115	9.467	-30
8	35	1	0.0027	3846.94	10.387	-35
9	40	1	0.0021	5024.815	10.552	-40
10	45	1	0.00175	6359.74	11.130	-45
11	50	1	0.00145	7851.715	11.385	-50
12	60	1	0.001049	11306.81	11.861	-60
13	70	1	0.000824	15390.11	12.681	-70
14	80	1	0.0007	20101.61	14.071	-80
15	90	1	0.00071	25441.31	18.063	-90
16	100	1	0.00045	31409.21	14.134	-100

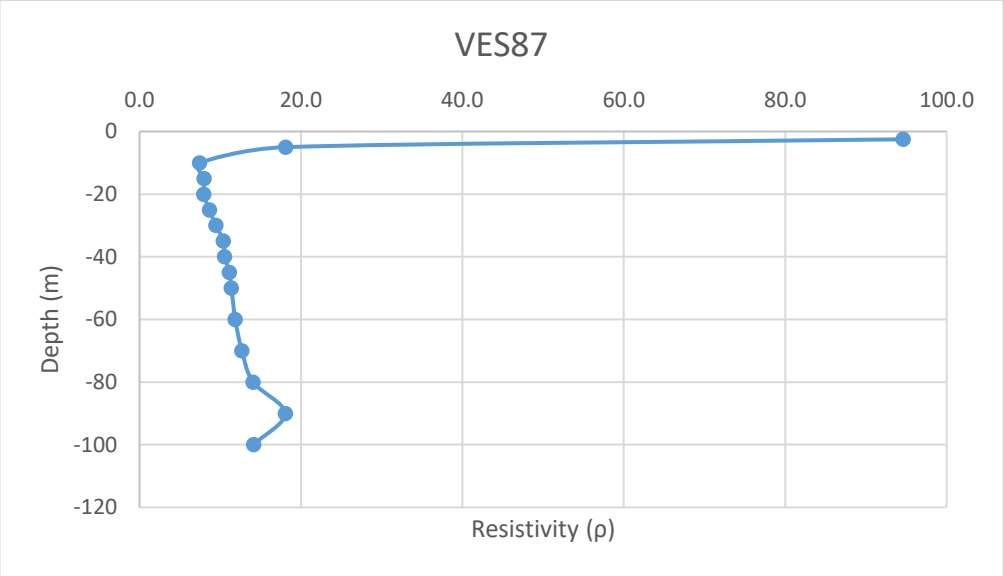

Annexure-XXII: Details of VES Survey

Date: 12/01/2025			VES-88			
Latitude	23.181772		Longitude	69.566574		
S.N	Current Electrode Spacing (AB/2)	Potential Electrode Spacing (MN)	Resistance (Ohm)	K value	Aparent Resistivity (Rho_a)	
1	2.5	1	36.1	18.846	680.341	-2.5
2	5	1	7.06	77.73975	548.843	-5
3	10	1	0.935	313.3148	292.949	-10
4	15	1	0.18	705.9398	127.069	-15
5	20	1	0.043	1255.615	53.991	-20
6	25	1	0.0134	1962.34	26.295	-25
7	30	1	0.00631	2826.115	17.833	-30
8	35	1	0.00489	3846.94	18.812	-35
9	40	1	0.00278	5024.815	13.969	-40
10	45	1	0.00215	6359.74	13.673	-45
11	50	1	0.00178	7851.715	13.976	-50
12	60	1	0.00135	11306.81	15.264	-60
13	70	1	0.00105	15390.11	16.160	-70
14	80	1	0.00075	20101.61	15.076	-80
15	90	1	0.0007	25441.31	17.809	-90
16	100	1	0.00055	31409.21	17.275	-100

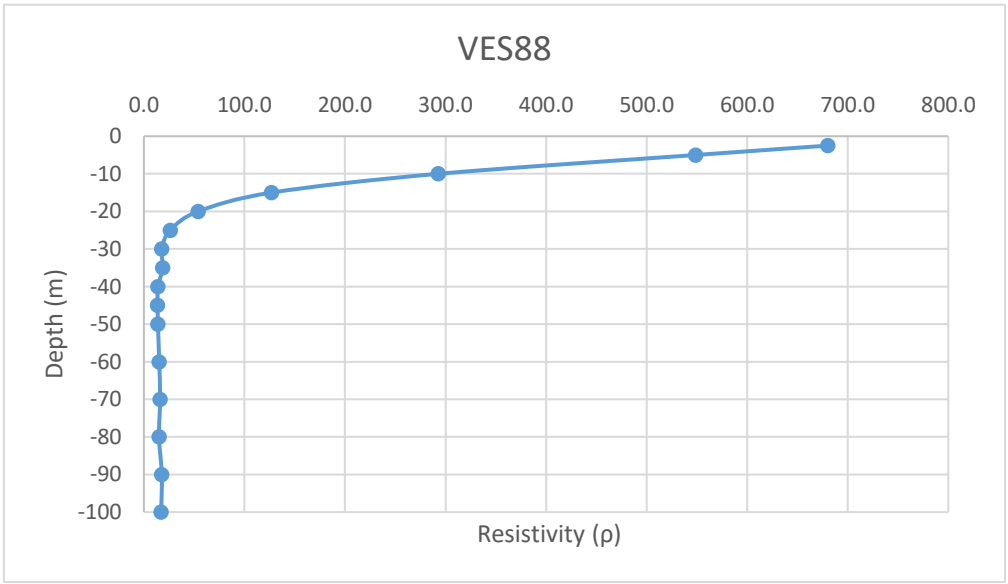

Annexure-XXII: Details of VES Survey

Date: 13/01/2025			VES-89			
Latitude	23.202805		Longitude	69.572888		
S.N	Current Electrode Spacing (AB/2)	Potential Electrode Spacing (MN)	Resistance (Ohm)	K value	Aparent Resistivity (Rho_a)	
1	2.5	1	1.83	18.846	34.488	-2.5
2	5	1	0.529	77.73975	41.124	-5
3	10	1	0.145	313.3148	45.431	-10
4	15	1	0.0608	705.9398	42.921	-15
5	20	1	0.0305	1255.615	38.296	-20
6	25	1	0.0171	1962.34	33.556	-25
7	30	1	0.01096	2826.115	30.974	-30
8	35	1	0.00772	3846.94	29.698	-35
9	40	1	0.00556	5024.815	27.938	-40
10	45	1	0.00396	6359.74	25.185	-45
11	50	1	0.00296	7851.715	23.241	-50
12	60	1	0.0018	11306.81	20.352	-60
13	70	1	0.00122	15390.11	18.776	-70
14	80	1	0.00091	20101.61	18.292	-80
15	90	1	0.00072	25441.31	18.318	-90
16	100	1	0.00061	31409.21	19.160	-100

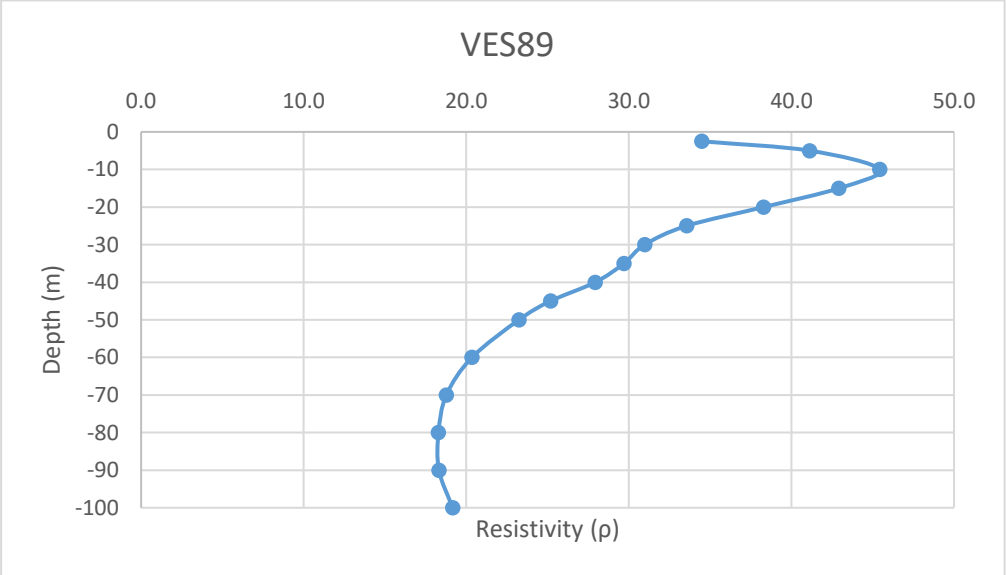

Annexure-XXII: Details of VES Survey

Date: 13/01/2025			VES-90			
Latitude	23.199693		Longitude	69.572128		
S.N	Current Electrode Spacing (AB/2)	Potential Electrode Spacing (MN)	Resistance (Ohm)	K value	Aparent Resistivity (Rho_a)	
1	2.5	1	4.65	18.846	87.634	-2.5
2	5	1	0.889	77.73975	69.111	-5
3	10	1	0.217	313.3148	67.989	-10
4	15	1	0.091	705.9398	64.241	-15
5	20	1	0.048	1255.615	60.270	-20
6	25	1	0.028	1962.34	54.946	-25
7	30	1	0.018	2826.115	50.870	-30
8	35	1	0.013	3846.94	50.010	-35
9	40	1	0.00948	5024.815	47.635	-40
10	45	1	0.00699	6359.74	44.455	-45
11	50	1	0.00539	7851.715	42.321	-50
12	60	1	0.00336	11306.81	37.991	-60
13	70	1	0.00239	15390.11	36.782	-70
14	80	1	0.00175	20101.61	35.178	-80
15	90	1	0.00127	25441.31	32.310	-90
16	100	1	0.00099	31409.21	31.095	-100
					87.634	
					31.095	

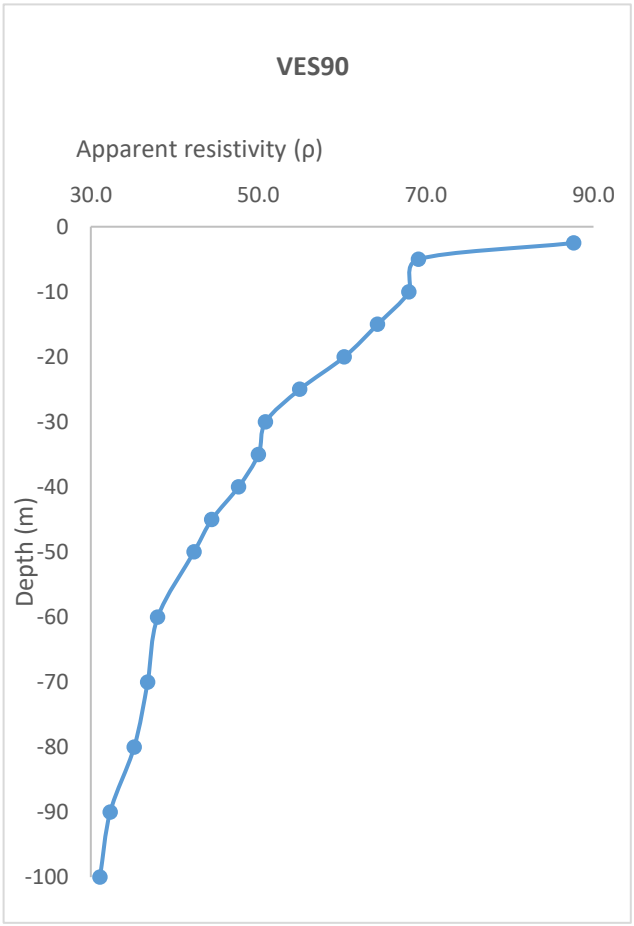

Annexure-XXII: Details of VES Survey

Date: 13/01/2025			VES-91			
Latitude	23.20516		Longitude	69.579963		
S.N	Current Electrode Spacing (AB/2)	Potential Electrode Spacing (MN)	Resistance (Ohm)	K value	Aparent Resistivity (Rho_a)	
1	2.5	1	0.845	18.846	15.925	-2.5
2	5	1	0.327	77.73975	25.421	-5
3	10	1	0.111	313.3148	34.778	-10
4	15	1	0.051	705.9398	36.003	-15
5	20	1	0.0266	1255.615	33.399	-20
6	25	1	0.0155	1962.34	30.416	-25
7	30	1	0.00929	2826.115	26.255	-30
8	35	1	0.00551	3846.94	21.197	-35
9	40	1	0.00376	5024.815	18.893	-40
10	45	1	0.00262	6359.74	16.663	-45
11	50	1	0.00192	7851.715	15.075	-50
12	60	1	0.00115	11306.81	13.003	-60
13	70	1	0.000774	15390.11	11.912	-70
14	80	1	0.00055	20101.61	11.056	-80
15	90	1	0.0004	25441.31	10.177	-90
16	100	1	0.00035	31409.21	10.993	-100

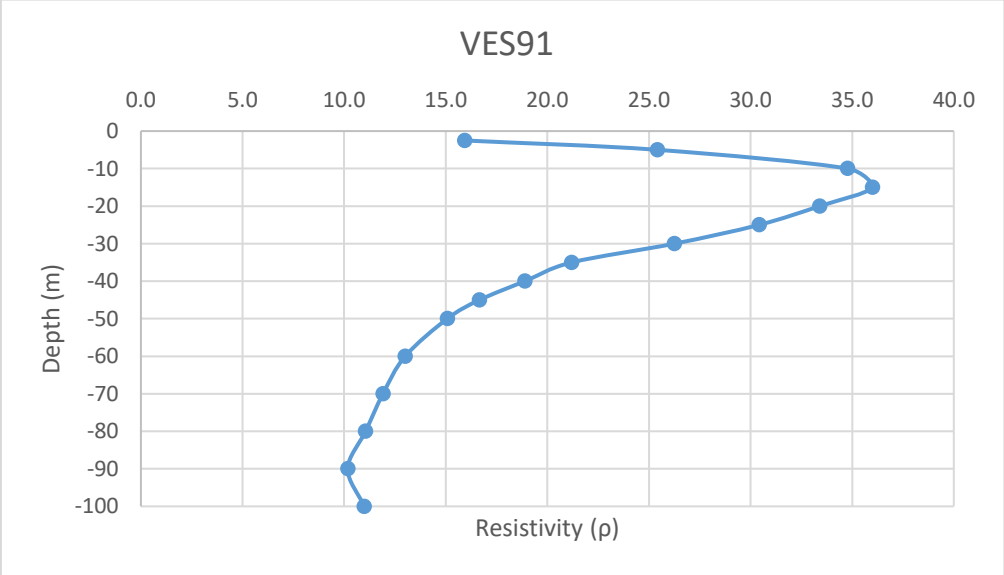

Annexure-XXII: Details of VES Survey

Date: 15/01/2025			VES-92			
Latitude	23.189567		Longitude	69.544863		
S.N	Current Electrode Spacing (AB/2)	Potential Electrode Spacing (MN)	Resistance (Ohm)	K value	Aparent Resistivity (Rho_a)	
1	2.5	1	18.9	18.846	356.189	-2.5
2	5	1	6.24	77.73975	485.096	-5
3	10	1	1.88	313.3148	589.032	-10
4	15	1	0.881	705.9398	621.933	-15
5	20	1	0.472	1255.615	592.650	-20
6	25	1	0.299	1962.34	586.740	-25
7	30	1	0.191	2826.115	539.788	-30
8	35	1	0.129	3846.94	496.255	-35
9	40	1	0.093	5024.815	467.308	-40
10	45	1	0.069	6359.74	438.822	-45
11	50	1	0.0556	7851.715	436.555	-50
12	60	1	0.0362	11306.81	409.307	-60
13	70	1	0.0242	15390.11	372.441	-70
14	80	1	0.0166	20101.61	333.687	-80
15	90	1	0.01173	25441.31	298.427	-90
16	100	1	0.00907	31409.21	284.882	-100

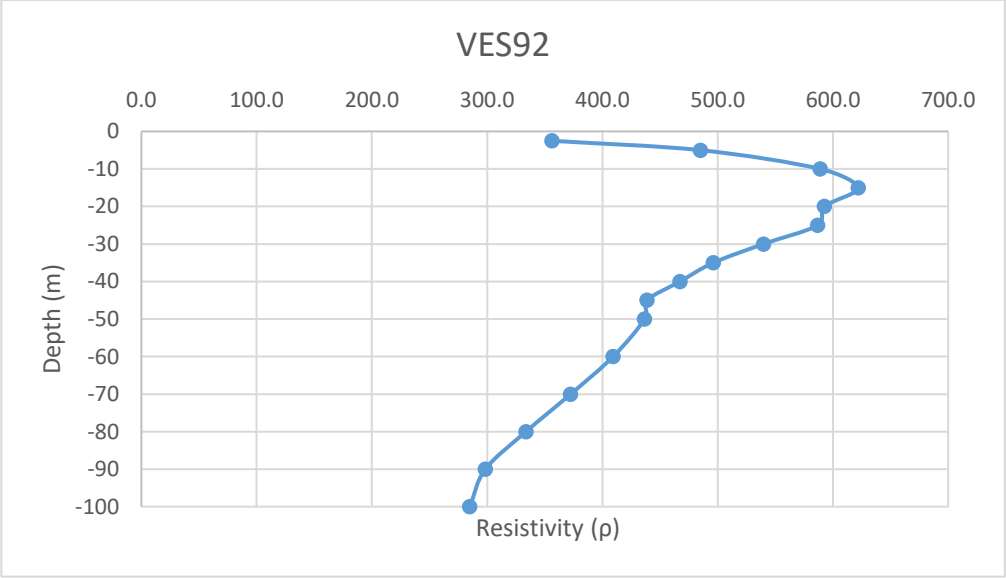

Annexure-XXII: Details of VES Survey

Date: 15/01/2025			VES-93			
Latitude	23.184323		Longitude	69.544988		
S.N	Current Electrode Spacing (AB/2)	Potential Electrode Spacing (MN)	Resistance (Ohm)	K value	Aparent Resistivity (Rho_a)	
1	2.5	1	19.7	18.846	371.266	-2.5
2	5	1	6.37	77.73975	495.202	-5
3	10	1	1.65	313.3148	516.969	-10
4	15	1	0.69	705.9398	487.098	-15
5	20	1	0.374	1255.615	469.600	-20
6	25	1	0.226	1962.34	443.489	-25
7	30	1	0.158	2826.115	446.526	-30
8	35	1	0.117	3846.94	450.092	-35
9	40	1	0.091	5024.815	457.258	-40
10	45	1	0.0716	6359.74	455.357	-45
11	50	1	0.0584	7851.715	458.540	-50
12	60	1	0.0384	11306.81	434.182	-60
13	70	1	0.0257	15390.11	395.526	-70
14	80	1	0.0159	20101.61	319.616	-80
15	90	1	0.01108	25441.31	281.890	-90
16	100	1	0.00944	31409.21	296.503	-100

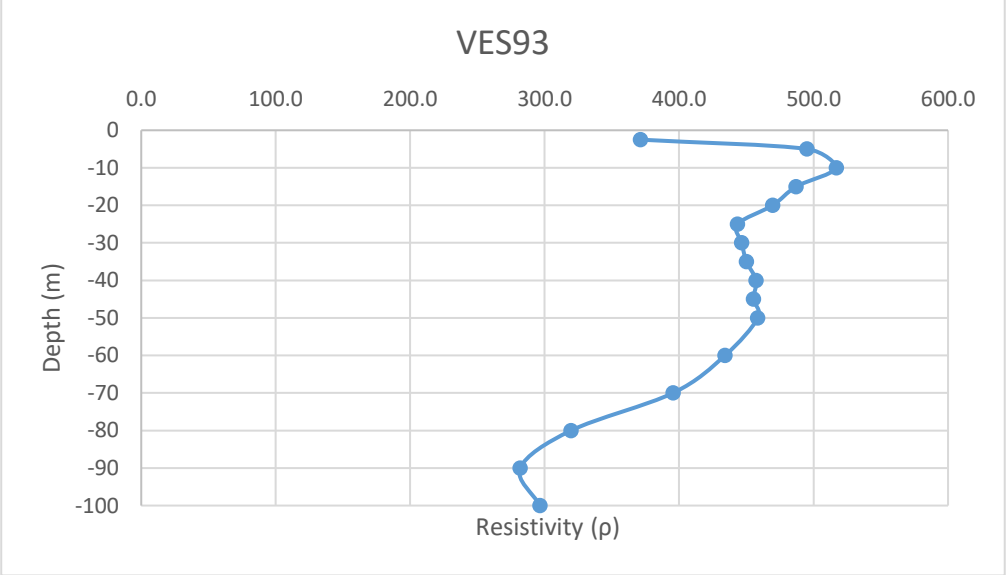

Annexure-XXII: Details of VES Survey

Date: 15/01/2025			VES-94			
Latitude	23.180388		Longitude	69.54081		
S.N	Current Electrode Spacing (AB/2)	Potential Electrode Spacing (MN)	Resistance (Ohm)	K value	Aparent Resistivity (Rho_a)	
1	2.5	1	0.5605	18.846	10.563	-2.5
2	5	1	0.1855	77.73975	14.421	-5
3	10	1	0.0605	313.3148	18.956	-10
4	15	1	0.0279	705.9398	19.696	-15
5	20	1	0.01481	1255.615	18.596	-20
6	25	1	0.0088	1962.34	17.269	-25
7	30	1	0.005445	2826.115	15.388	-30
8	35	1	0.003405	3846.94	13.099	-35
9	40	1	0.002405	5024.815	12.085	-40
10	45	1	0.001785	6359.74	11.352	-45
11	50	1	0.001385	7851.715	10.875	-50
12	60	1	0.0009	11306.81	10.170	-60
13	70	1	0.000637	15390.11	9.796	-70
14	80	1	0.000465	20101.61	9.337	-80
15	90	1	0.00036	25441.31	9.146	-90
16	100	1	0.000287	31409.21	9.014	-100

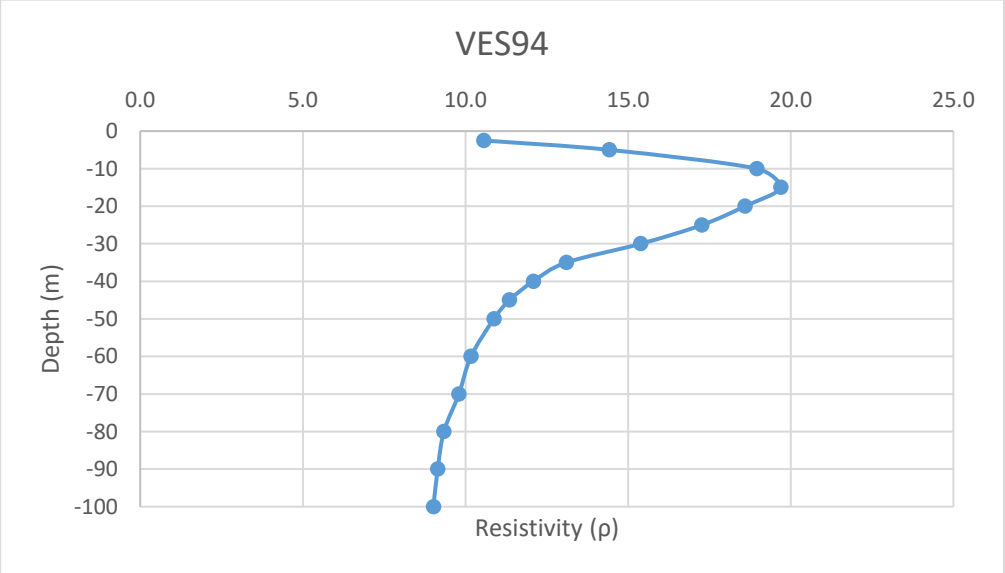

Annexure-XXII: Details of VES Survey

Date: 15/01/2025			VES-95			
Latitude	23.178147		Longitude	69.538322		
S.N	Current Electrode Spacing (AB/2)	Potential Electrode Spacing (MN)	Resistance (Ohm)	K value	Aparent Resistivity (Rho_a)	
1	2.5	1	3.88	18.846	73.122	-2.5
2	5	1	1.019	77.73975	79.217	-5
3	10	1	0.223	313.3148	69.869	-10
4	15	1	0.064	705.9398	45.180	-15
5	20	1	0.026	1255.615	32.646	-20
6	25	1	0.01047	1962.34	20.546	-25
7	30	1	0.00599	2826.115	16.928	-30
8	35	1	0.00405	3846.94	15.580	-35
9	40	1	0.00302	5024.815	15.175	-40
10	45	1	0.00235	6359.74	14.945	-45
11	50	1	0.00176	7851.715	13.819	-50
12	60	1	0.00122	11306.81	13.794	-60
13	70	1	0.000882	15390.11	13.574	-70
14	80	1	0.000639	20101.61	12.845	-80
15	90	1	0.000499	25441.31	12.695	-90
16	100	1	0.000439	31409.21	13.789	-100

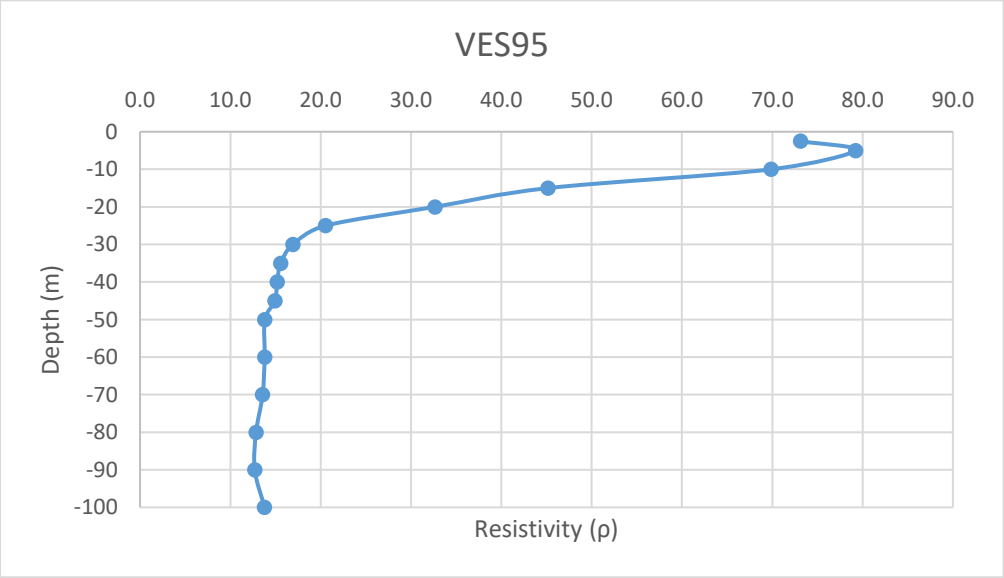

Annexure-XXII: Details of VES Survey

Date: 16/01/2025			VES-96			
Latitude	23.191095		Longitude	69.556115		
S.N	Current Electrode Spacing (AB/2)	Potential Electrode Spacing (MN)	Resistance (Ohm)	K value	Aparent Resistivity (Rho_a)	
1	2.5	1	10.44	18.846	196.752	-2.5
2	5	1	2.43	77.73975	188.908	-5
3	10	1	0.529	313.3148	165.744	-10
4	15	1	0.174	705.9398	122.834	-15
5	20	1	0.0786	1255.615	98.691	-20
6	25	1	0.0403	1962.34	79.082	-25
7	30	1	0.0253	2826.115	71.501	-30
8	35	1	0.0176	3846.94	67.706	-35
9	40	1	0.0131	5024.815	65.825	-40
10	45	1	0.00979	6359.74	62.262	-45
11	50	1	0.00761	7851.715	59.752	-50
12	60	1	0.00515	11306.81	58.230	-60
13	70	1	0.00376	15390.11	57.867	-70
14	80	1	0.00306	20101.61	61.511	-80
15	90	1	0.0026	25441.31	66.147	-90
16	100	1	0.00216	31409.21	67.844	-100

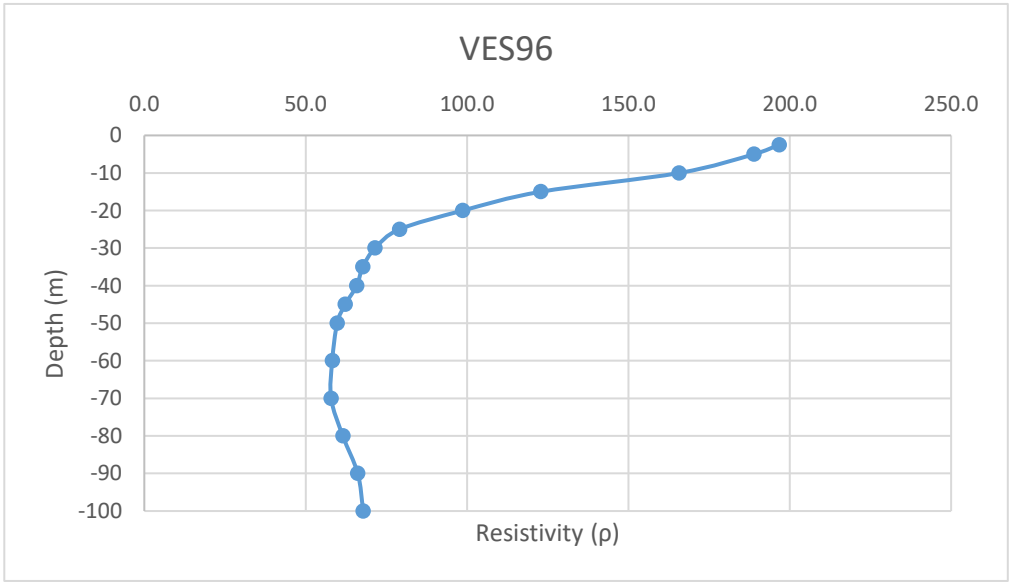

Annexure-XXII: Details of VES Survey

Date: 16/01/2025			VES-97			
Latitude	23.187733		Longitude	69.543253		
S.N	Current Electrode Spacing (AB/2)	Potential Electrode Spacing (MN)	Resistance (Ohm)	K value	Aparent Resistivity (Rho_a)	
1	2.5	1	19.3	18.846	363.728	-2.5
2	5	1	6.305	77.73975	490.149	-5
3	10	1	1.765	313.3148	553.001	-10
4	15	1	0.7855	705.9398	554.516	-15
5	20	1	0.423	1255.615	531.125	-20
6	25	1	0.2625	1962.34	515.114	-25
7	30	1	0.1745	2826.115	493.157	-30
8	35	1	0.123	3846.94	473.174	-35
9	40	1	0.092	5024.815	462.283	-40
10	45	1	0.0703	6359.74	447.090	-45
11	50	1	0.057	7851.715	447.548	-50
12	60	1	0.0373	11306.81	421.744	-60
13	70	1	0.02495	15390.11	383.983	-70
14	80	1	0.01625	20101.61	326.651	-80
15	90	1	0.011405	25441.31	290.158	-90
16	100	1	0.009255	31409.21	290.692	-100

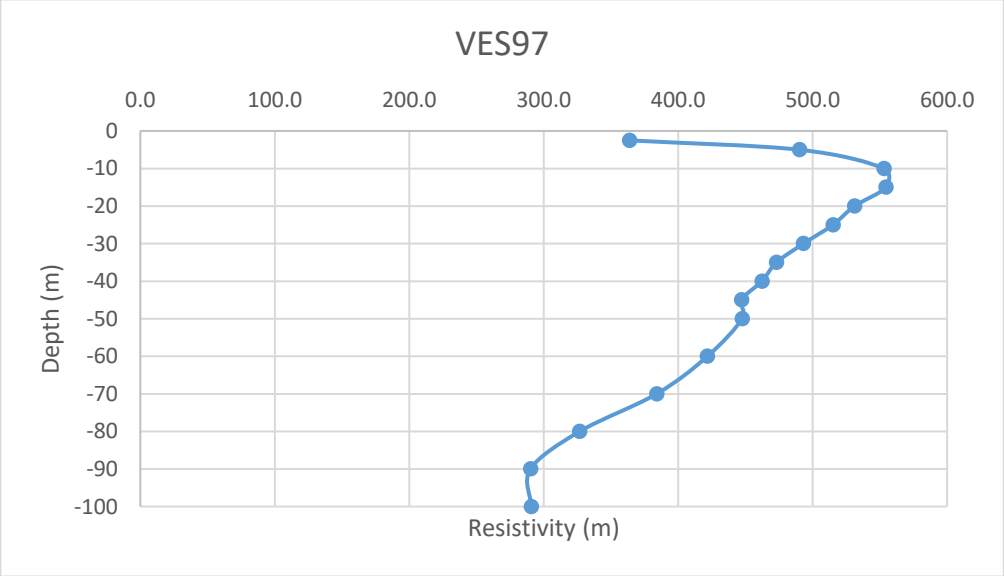

Annexure-XXII: Details of VES Survey

Date: 17/01/2025			VES-98			
Latitude	23.21596009		Longitude	69.53231161		
S.N	Current Electrode Spacing (AB/2)	Potential Electrode Spacing (MN)	Resistance (Ohm)	K value	Aparent Resistivity (Rho_a)	
1	2.5	1	46.2	18.846	870.685	-2.5
2	5	1	13.2	77.73975	1026.165	-5
3	10	1	3.34	313.3148	1046.471	-10
4	15	1	1.56	705.9398	1101.266	-15
5	20	1	0.666	1255.615	836.239	-20
6	25	1	0.36	1962.34	706.442	-25
7	30	1	0.222	2826.115	627.397	-30
8	35	1	0.134	3846.94	515.490	-35
9	40	1	0.0847	5024.815	425.602	-40
10	45	1	0.0565	6359.74	359.325	-45
11	50	1	0.0443	7851.715	347.831	-50
12	60	1	0.0279	11306.81	315.460	-60
13	70	1	0.0201	15390.11	309.341	-70
14	80	1	0.0137	20101.61	275.392	-80
15	90	1	0.0064	25441.31	162.824	-90
16	100	1	0.00111	31409.21	34.864	-100

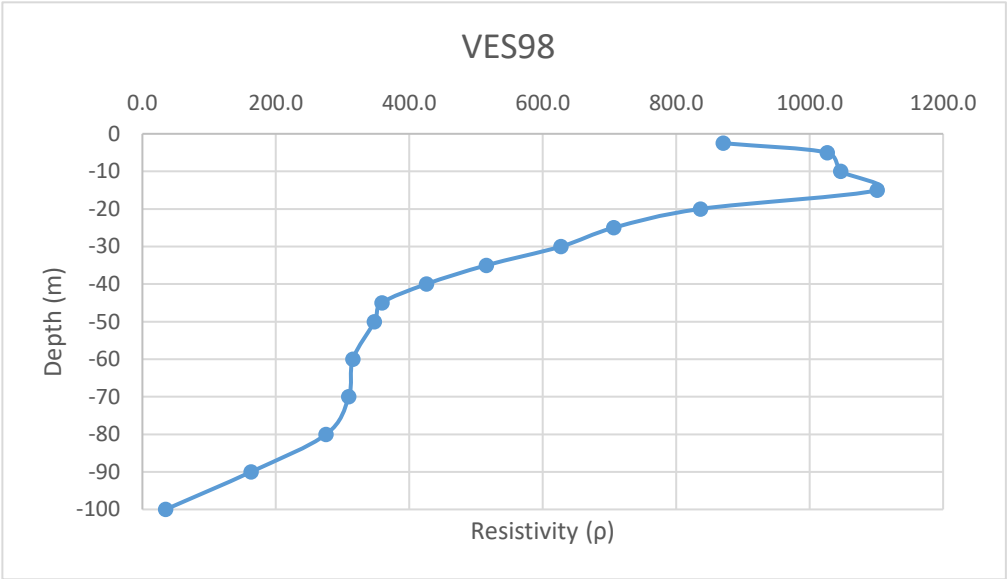

Annexure-XXII: Details of VES Survey

Date: 17/01/2025			VES-99			
Latitude	23.21502568		Longitude	69.53026941		
S.N	Current Electrode Spacing (AB/2)	Potential Electrode Spacing (MN)	Resistance (Ohm)	K value	Aparent Resistivity (Rho_a)	
1	2.5	1	31.2	18.846	587.995	-2.5
2	5	1	6.39	77.73975	496.757	-5
3	10	1	1.37	313.3148	429.241	-10
4	15	1	0.586	705.9398	413.681	-15
5	20	1	0.31	1255.615	389.241	-20
6	25	1	0.177	1962.34	347.334	-25
7	30	1	0.0987	2826.115	278.938	-30
8	35	1	0.0602	3846.94	231.586	-35
9	40	1	0.0401	5024.815	201.495	-40
10	45	1	0.0267	6359.74	169.805	-45
11	50	1	0.0196	7851.715	153.894	-50
12	60	1	0.00979	11306.81	110.694	-60
13	70	1	0.00586	15390.11	90.186	-70
14	80	1	0.00358	20101.61	71.964	-80
15	90	1	0.00097	25441.31	24.678	-90
16	100	1	0.00269	31409.21	84.491	-100

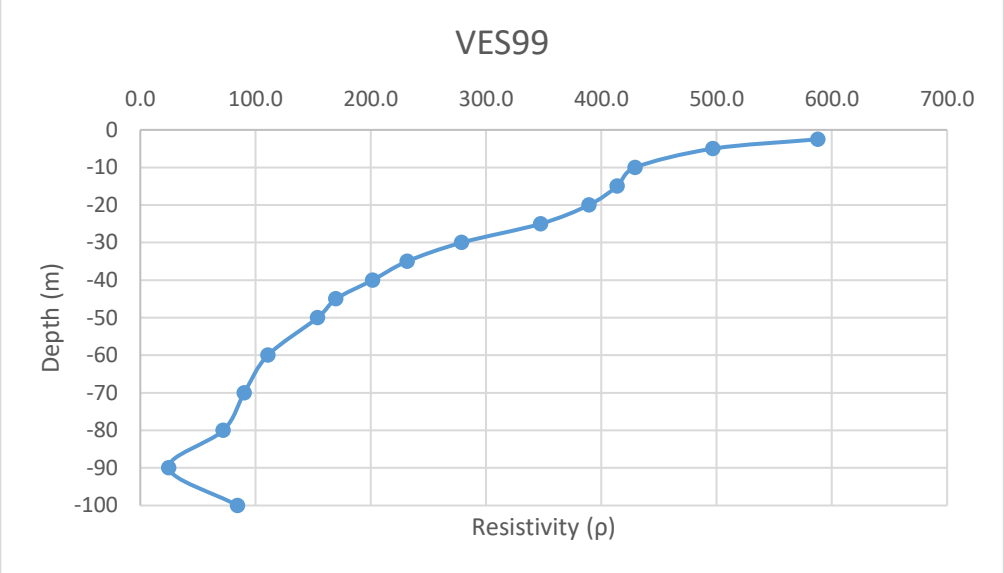

Annexure-XXII: Details of VES Survey

Date: 17/01/2025			VES-100			
Latitude	23.21923217		Longitude	69.52883294		
S.N	Current Electrode Spacing (AB/2)	Potential Electrode Spacing (MN)	Resistance (Ohm)	K value	Aparent Resistivity (Rho_a)	
1	2.5	1	4.82	18.846	90.838	-2.5
2	5	1	1.41	77.73975	109.613	-5
3	10	1	0.477	313.3148	149.451	-10
4	15	1	0.204	705.9398	144.012	-15
5	20	1	0.115	1255.615	144.396	-20
6	25	1	0.0716	1962.34	140.504	-25
7	30	1	0.0469	2826.115	132.545	-30
8	35	1	0.0331	3846.94	127.334	-35
9	40	1	0.0254	5024.815	127.630	-40
10	45	1	0.0177	6359.74	112.567	-45
11	50	1	0.0134	7851.715	105.213	-50
12	60	1	0.0087	11306.81	98.369	-60
13	70	1	0.0064	15390.11	98.497	-70
14	80	1	0.00485	20101.61	97.493	-80
15	90	1	0.0039	25441.31	99.221	-90
16	100	1	0.00328	31409.21	103.022	-100

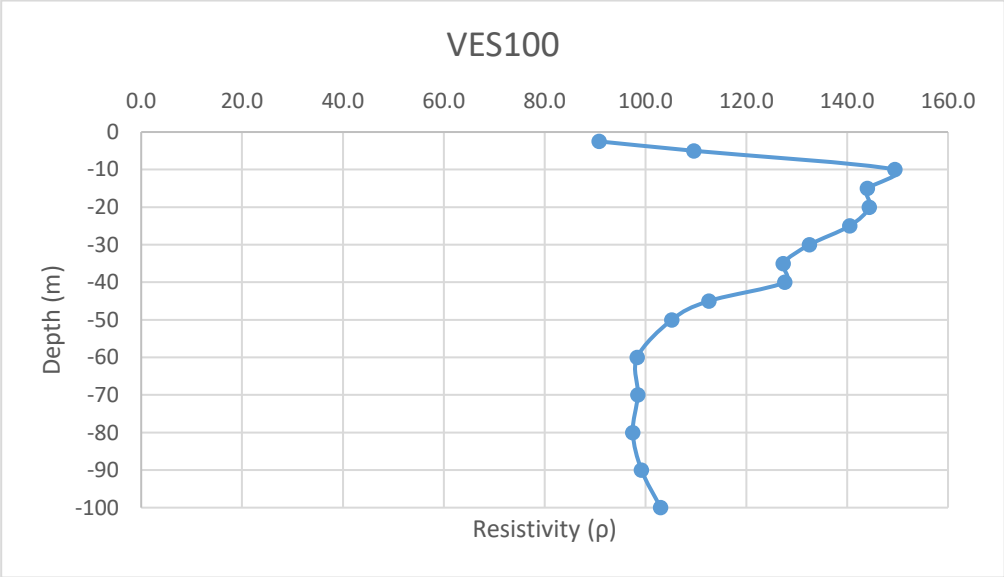

Annexure-XXII: Details of VES Survey

Date: 19/01/2025			VES-101			
Latitude	23.21970236		Longitude	69.52149453		
S.N	Current Electrode Spacing (AB/2)	Potential Electrode Spacing (MN)	Resistance (Ohm)	K value	Aparent Resistivity (Rho_a)	
1	2.5	1	69.4	18.846	1307.912	-2.5
2	5	1	15.5	77.73975	1204.966	-5
3	10	1	2.1	313.3148	657.961	-10
4	15	1	0.669	705.9398	472.274	-15
5	20	1	0.295	1255.615	370.406	-20
6	25	1	0.165	1962.34	323.786	-25
7	30	1	0.108	2826.115	305.220	-30
8	35	1	0.0751	3846.94	288.905	-35
9	40	1	0.0614	5024.815	308.524	-40
10	45	1	0.0362	6359.74	230.223	-45
11	50	1	0.057	7851.715	447.548	-50
12	60	1	0.0167	11306.81	188.824	-60
13	70	1	0.0534	15390.11	821.832	-70
14	80	1	0.0163	20101.61	327.656	-80
15	90	1	0.0139	25441.31	353.634	-90
16	100	1	0.00701	31409.21	220.179	-100

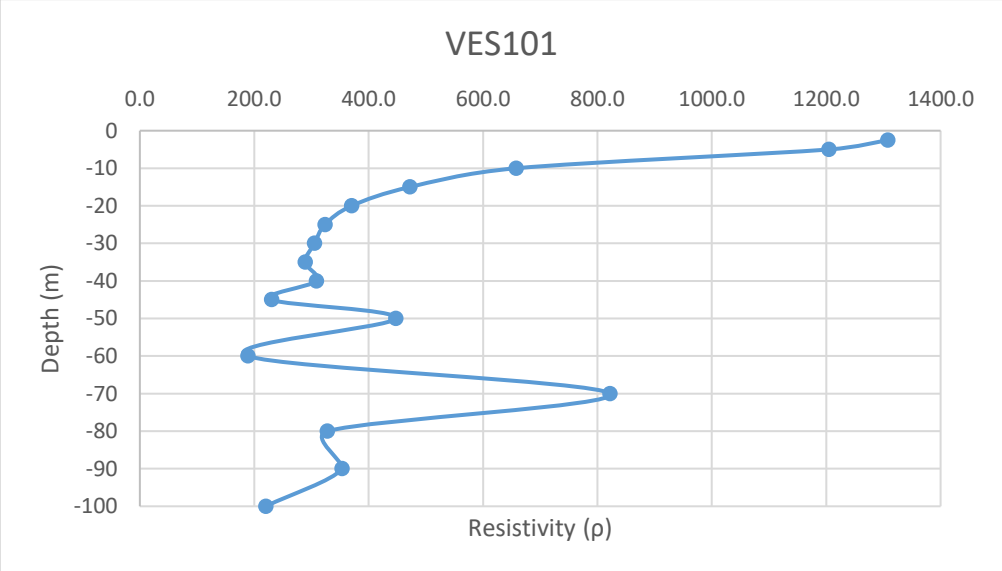

Annexure-XXII: Details of VES Survey

Date: 19/01/2025			VES-102			
Latitude	23.22098203		Longitude	69.52570236		
S.N	Current Electrode Spacing (AB/2)	Potential Electrode Spacing (MN)	Resistance (Ohm)	K value	Aparent Resistivity (Rho_a)	
1	2.5	1	9.87	18.846	186.010	-2.5
2	5	1	1.85	77.73975	143.819	-5
3	10	1	0.307	313.3148	96.188	-10
4	15	1	0.107	705.9398	75.536	-15
5	20	1	0.0578	1255.615	72.575	-20
6	25	1	0.0389	1962.34	76.335	-25
7	30	1	0.0269	2826.115	76.022	-30
8	35	1	0.0201	3846.94	77.323	-35
9	40	1	0.0157	5024.815	78.890	-40
10	45	1	0.0124	6359.74	78.861	-45
11	50	1	0.00988	7851.715	77.575	-50
12	60	1	0.007	11306.81	79.148	-60
13	70	1	0.00531	15390.11	81.722	-70
14	80	1	0.00491	20101.61	98.699	-80
15	90	1	0.00401	25441.31	102.020	-90
16	100	1	0.00284	31409.21	89.202	-100

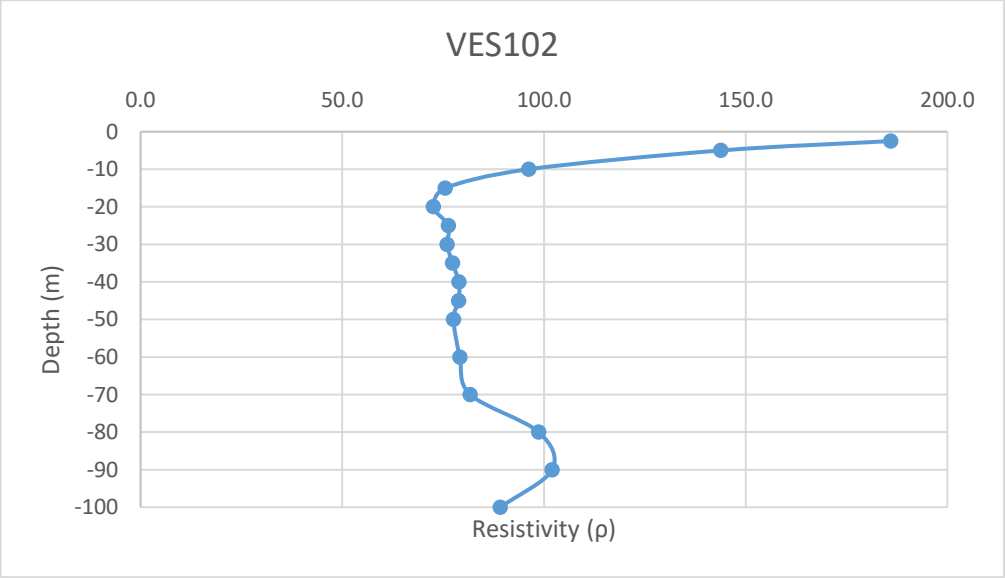

Annexure-XXII: Details of VES Survey

Date: 19/01/2025			VES-103			
Latitude	23.21692845		Longitude	69.52676531		
S.N	Current Electrode Spacing (AB/2)	Potential Electrode Spacing (MN)	Resistance (Ohm)	K value	Aparent Resistivity (Rho_a)	
1	2.5	1	2.66	18.846	50.130	-2.5
2	5	1	0.45	77.73975	34.983	-5
3	10	1	0.109	313.3148	34.151	-10
4	15	1	0.0584	705.9398	41.227	-15
5	20	1	0.0317	1255.615	39.803	-20
6	25	1	0.0212	1962.34	41.602	-25
7	30	1	0.015	2826.115	42.392	-30
8	35	1	0.01174	3846.94	45.163	-35
9	40	1	0.00978	5024.815	49.143	-40
10	45	1	0.00729	6359.74	46.363	-45
11	50	1	0.00593	7851.715	46.561	-50
12	60	1	0.00375	11306.81	42.401	-60
13	70	1	0.00305	15390.11	46.940	-70
14	80	1	0.00215	20101.61	43.218	-80
15	90	1	0.0015	25441.31	38.162	-90
16	100	1	0.00125	31409.21	39.262	-100

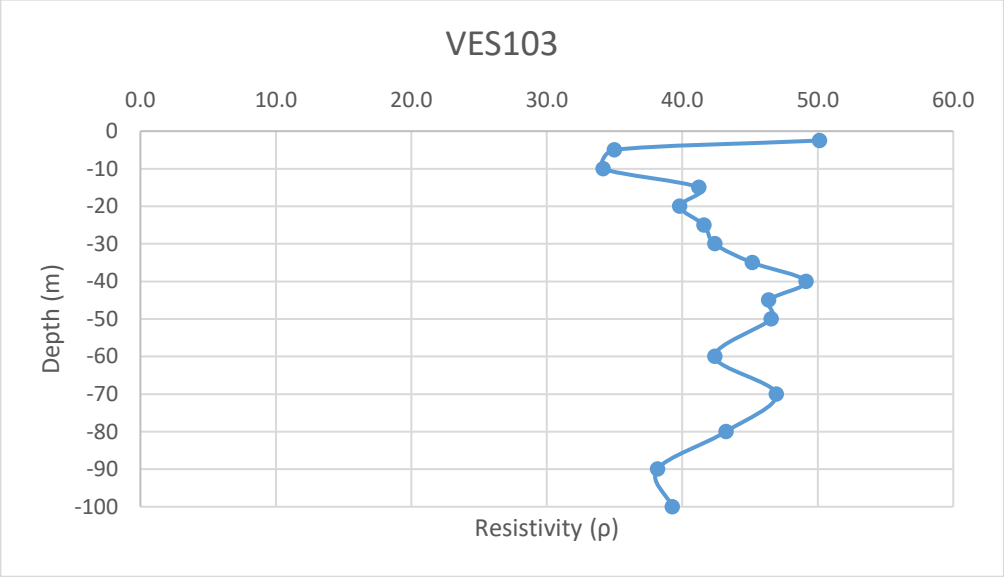

Annexure-XXII: Details of VES Survey

Date: 20/01/2025			VES-104			
Latitude	23.17318643		Longitude	69.57770589		
S.N	Current Electrode Spacing (AB/2)	Potential Electrode Spacing (MN)	Resistance (Ohm)	K value	Aparent Resistivity (Rho_a)	
1	2.5	1	3.22	18.846	60.684	-2.5
2	5	1	0.352	77.73975	27.364	-5
3	10	1	0.0399	313.3148	12.501	-10
4	15	1	0.01113	705.9398	7.857	-15
5	20	1	0.00463	1255.615	5.813	-20
6	25	1	0.00275	1962.34	5.396	-25
7	30	1	0.00145	2826.115	4.098	-30
8	35	1	0.0014	3846.94	5.386	-35
9	40	1	0.001098	5024.815	5.517	-40
10	45	1	0.00085	6359.74	5.406	-45
11	50	1	0.0006	7851.715	4.711	-50
12	60	1	0.000479	11306.81	5.416	-60
13	70	1	0.000382	15390.11	5.879	-70
14	80	1	0.000266	20101.61	5.347	-80
15	90	1	0.000224	25441.31	5.699	-90
16	100	1	0.000199	31409.21	6.250	-100

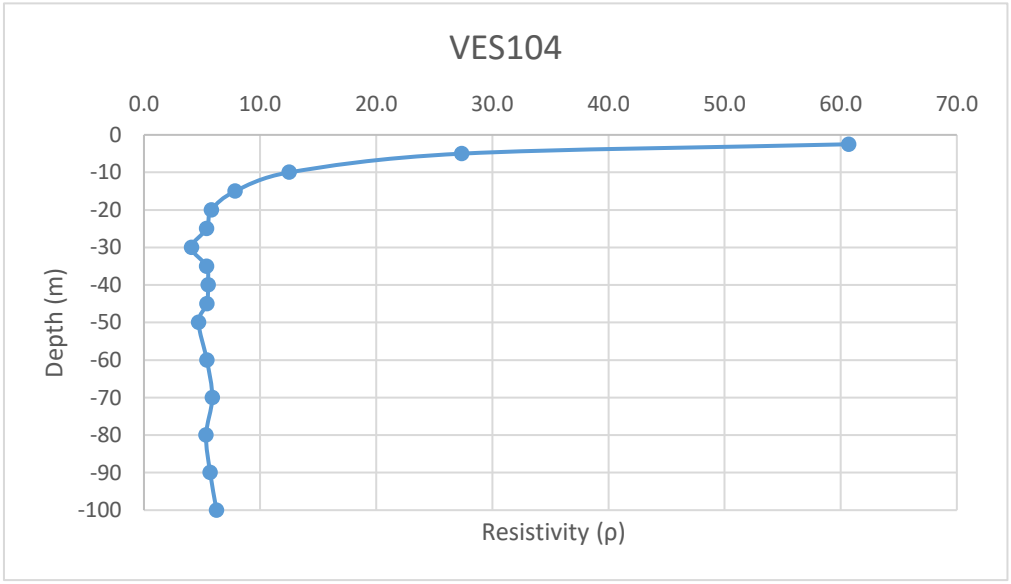

Annexure-XXII: Details of VES Survey

Date: 20/01/2025			VES-105			
Latitude	23.18436824		Longitude	69.55244505		
S.N	Current Electrode Spacing (AB/2)	Potential Electrode Spacing (MN)	Resistance (Ohm)	K value	Aparent Resistivity (Rho_a)	
1	2.5	1	34.3	18.846	646.418	-2.5
2	5	1	4.14	77.73975	321.843	-5
3	10	1	0.62	313.3148	194.255	-10
4	15	1	0.33	705.9398	232.960	-15
5	20	1	0.21	1255.615	263.679	-20
6	25	1	0.138	1962.34	270.803	-25
7	30	1	0.0913	2826.115	258.024	-30
8	35	1	0.0644	3846.94	247.743	-35
9	40	1	0.0438	5024.815	220.087	-40
10	45	1	0.0319	6359.74	202.876	-45
11	50	1	0.0254	7851.715	199.434	-50
12	60	1	0.0162	11306.81	183.170	-60
13	70	1	0.01022	15390.11	157.287	-70
14	80	1	0.00657	20101.61	132.068	-80
15	90	1	0.00551	25441.31	140.182	-90
16	100	1	0.00335	31409.21	105.221	-100

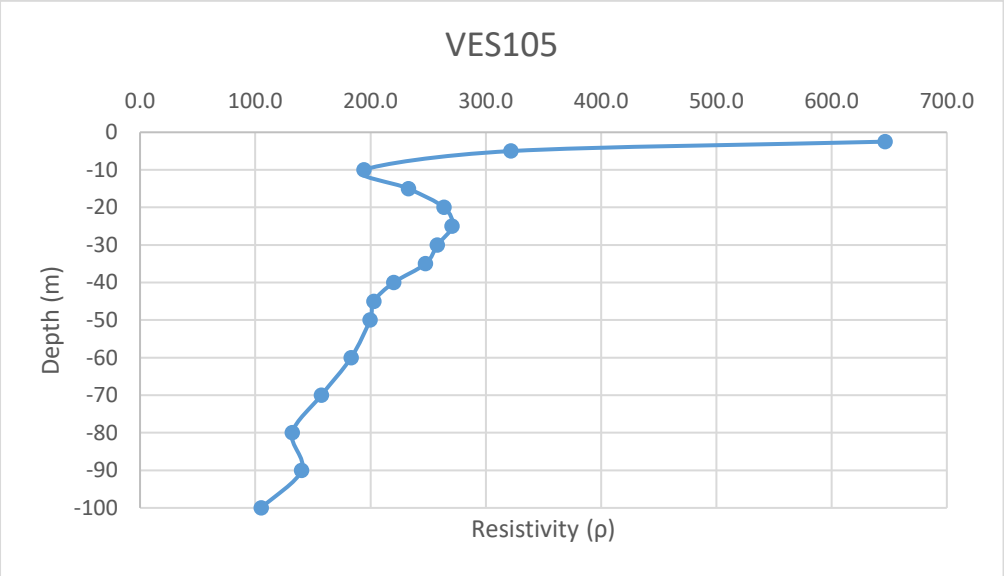

Annexure-XXII: Details of VES Survey

Date: 21/01/2025			VES-106			
Latitude	23.180598		Longitude	69.56102		
S.N	Current Electrode Spacing (AB/2)	Potential Electrode Spacing (MN)	Resistance (Ohm)	K value	Aparent Resistivity (Rho_a)	
1	2.5	1	7.26	18.846	136.822	-2.5
2	5	1	1.92	77.73975	149.260	-5
3	10	1	0.257	313.3148	80.522	-10
4	15	1	0.0534	705.9398	37.697	-15
5	20	1	0.0162	1255.615	20.341	-20
6	25	1	0.00785	1962.34	15.404	-25
7	30	1	0.00481	2826.115	13.594	-30
8	35	1	0.0033	3846.94	12.695	-35
9	40	1	0.00234	5024.815	11.758	-40
10	45	1	0.00176	6359.74	11.193	-45
11	50	1	0.00142	7851.715	11.149	-50
12	60	1	0.001058	11306.81	11.963	-60
13	70	1	0.000874	15390.11	13.451	-70
14	80	1	0.00075	20101.61	15.076	-80
15	90	1	0.00055	25441.31	13.993	-90
16	100	1	0.0004	31409.21	12.564	-100

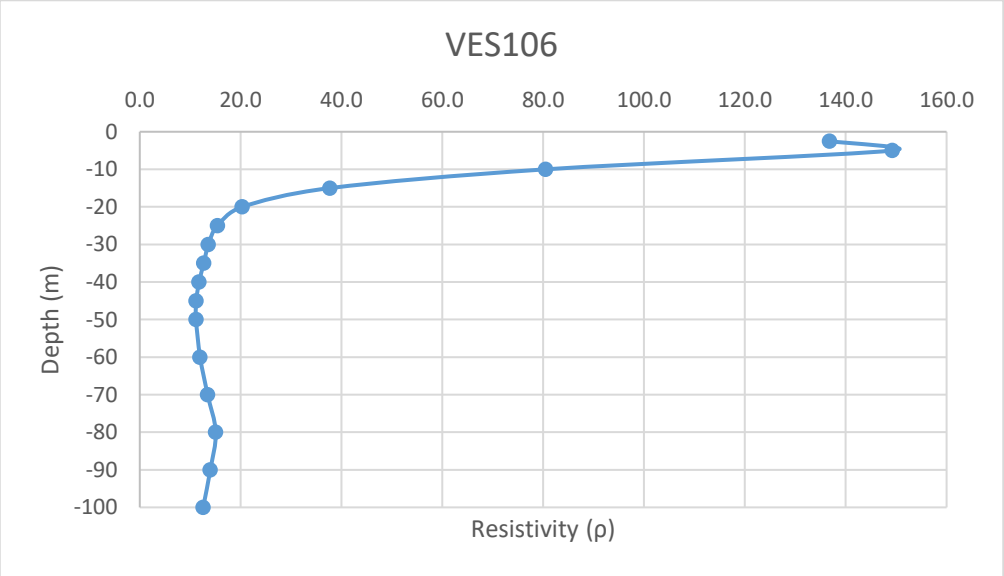

Annexure-XXII: Details of VES Survey

Date: 21/01/2025			VES-107			
Latitude	23.1662383		Longitude	69.55058974		
S.N	Current Electrode Spacing (AB/2)	Potential Electrode Spacing (MN)	Resistance (Ohm)	K value	Aparent Resistivity (Rho_a)	
1	2.5	1	2.95	18.846	55.596	-2.5
2	5	1	0.413	77.73975	32.107	-5
3	10	1	0.0524	313.3148	16.418	-10
4	15	1	0.0144	705.9398	10.166	-15
5	20	1	0.00807	1255.615	10.133	-20
6	25	1	0.00576	1962.34	11.303	-25
7	30	1	0.00455	2826.115	12.859	-30
8	35	1	0.00375	3846.94	14.426	-35
9	40	1	0.00328	5024.815	16.481	-40
10	45	1	0.00295	6359.74	18.761	-45
11	50	1	0.00273	7851.715	21.435	-50
12	60	1	0.00236	11306.81	26.684	-60
13	70	1	0.00217	15390.11	33.397	-70
14	80	1	0.00195	20101.61	39.198	-80
15	90	1	0.00177	25441.31	45.031	-90
16	100	1	0.00162	31409.21	50.883	-100

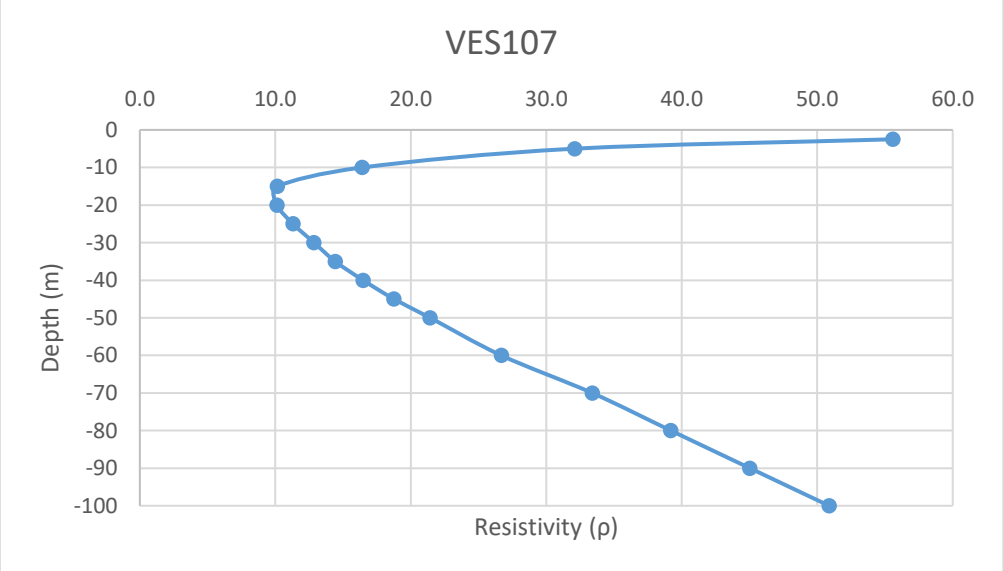

Annexure-XXII: Details of VES Survey

Date: 21/01/2025			VES-108			
Latitude	23.1675255		Longitude	69.55304016		
S.N	Current Electrode Spacing (AB/2)	Potential Electrode Spacing (MN)	Resistance (Ohm)	K value	Aparent Resistivity (Rho_a)	
1	2.5	1	8.9	18.846	167.729	-2.5
2	5	1	0.363	77.73975	28.220	-5
3	10	1	0.0352	313.3148	11.029	-10
4	15	1	0.0129	705.9398	9.107	-15
5	20	1	0.01166	1255.615	14.640	-20
6	25	1	0.00561	1962.34	11.009	-25
7	30	1	0.00538	2826.115	15.204	-30
8	35	1	0.00321	3846.94	12.349	-35
9	40	1	0.00275	5024.815	13.818	-40
10	45	1	0.00245	6359.74	15.581	-45
11	50	1	0.0021	7851.715	16.489	-50
12	60	1	0.00175	11306.81	19.787	-60
13	70	1	0.00144	15390.11	22.162	-70
14	80	1	0.00147	20101.61	29.549	-80
15	90	1	0.001098	25441.31	27.935	-90
16	100	1	0.000974	31409.21	30.593	-100

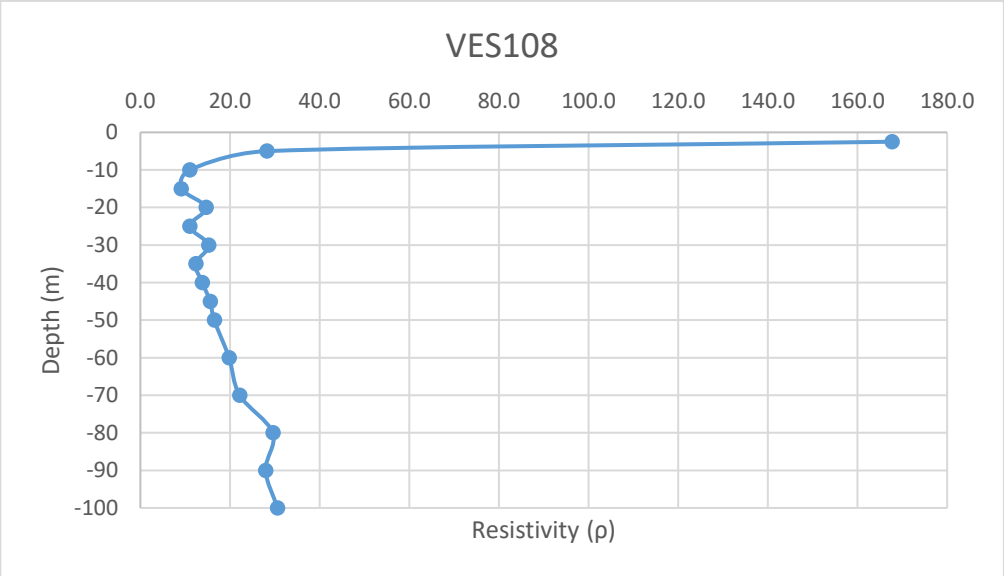

Annexure-XXII: Details of VES Survey

Date: 21/01/2025			VES-109			
Latitude	23.16452312		Longitude	69.55417751		
S.N	Current Electrode Spacing (AB/2)	Potential Electrode Spacing (MN)	Resistance (Ohm)	K value	Aparent Resistivity (Rho_a)	
1	2.5	1	19.2	18.846	361.843	-2.5
2	5	1	1.88	77.73975	146.151	-5
3	10	1	0.0324	313.3148	10.151	-10
4	15	1	0.0252	705.9398	17.790	-15
5	20	1	0.0196	1255.615	24.610	-20
6	25	1	0.0134	1962.34	26.295	-25
7	30	1	0.01076	2826.115	30.409	-30
8	35	1	0.00769	3846.94	29.583	-35
9	40	1	0.0066	5024.815	33.164	-40
10	45	1	0.00471	6359.74	29.954	-45
11	50	1	0.00418	7851.715	32.820	-50
12	60	1	0.00271	11306.81	30.641	-60
13	70	1	0.00177	15390.11	27.241	-70
14	80	1	0.00146	20101.61	29.348	-80
15	90	1	0.00107	25441.31	27.222	-90
16	100	1	0.00098	31409.21	30.781	-100

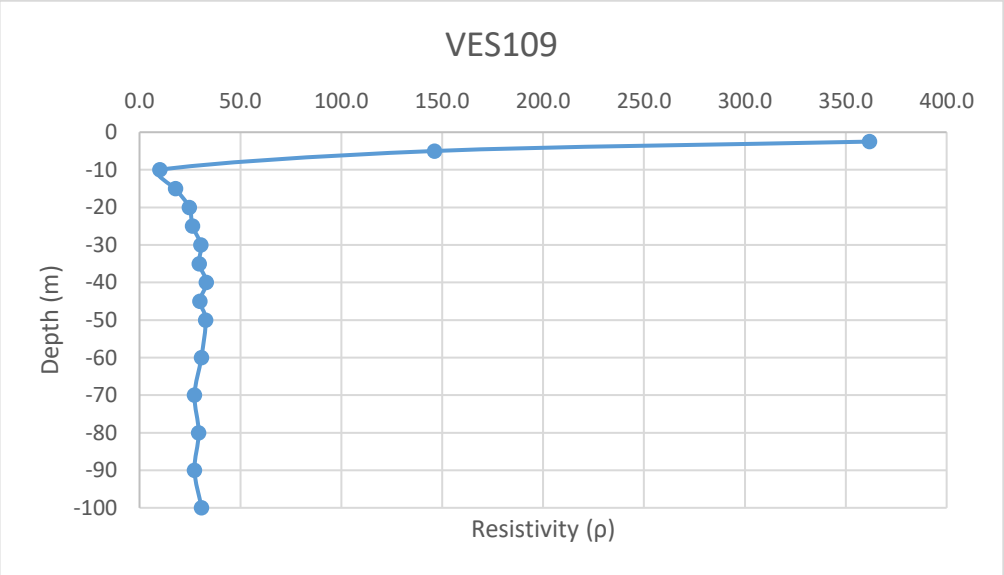

Annexure-XXII: Details of VES Survey

Date: 22/01/2025			VES-110			
Latitude	23.16309		Longitude	69.57008		
S.N	Current Electrode Spacing (AB/2)	Potential Electrode Spacing (MN)	Resistance (Ohm)	K value	Aparent Resistivity (Rho_a)	
1	2.5	1	0.601	18.846	11.326	-2.5
2	5	1	0.0949	77.73975	7.378	-5
3	10	1	0.0138	313.3148	4.324	-10
4	15	1	0.00767	705.9398	5.415	-15
5	20	1	0.00515	1255.615	6.466	-20
6	25	1	0.00344	1962.34	6.750	-25
7	30	1	0.00258	2826.115	7.291	-30
8	35	1	0.00202	3846.94	7.771	-35
9	40	1	0.00167	5024.815	8.391	-40
10	45	1	0.0014	6359.74	8.904	-45
11	50	1	0.00114	7851.715	8.951	-50
12	60	1	0.00087	11306.81	9.837	-60
13	70	1	0.00069	15390.11	10.619	-70
14	80	1	0.000536	20101.61	10.774	-80
15	90	1	0.000416	25441.31	10.584	-90
16	100	1	0.0004	31409.21	12.564	-100

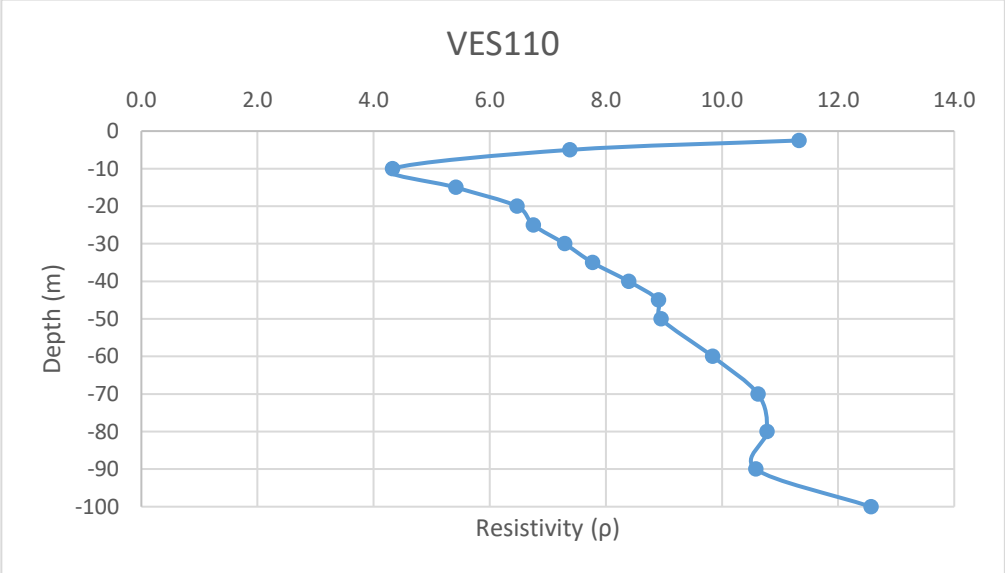

Annexure-XXII: Details of VES Survey

Date: 22/01/2025			VES-111			
Latitude	23.162065		Longitude	69.5596		
S.N	Current Electrode Spacing (AB/2)	Potential Electrode Spacing (MN)	Resistance (Ohm)	K value	Aparent Resistivity (Rho_a)	
1	2.5	1	1.22	18.846	22.992	-2.5
2	5	1	0.28	77.73975	21.767	-5
3	10	1	0.0704	313.3148	22.057	-10
4	15	1	0.0342	705.9398	24.143	-15
5	20	1	0.0182	1255.615	22.852	-20
6	25	1	0.01047	1962.34	20.546	-25
7	30	1	0.00681	2826.115	19.246	-30
8	35	1	0.00485	3846.94	18.658	-35
9	40	1	0.00358	5024.815	17.989	-40
10	45	1	0.0027	6359.74	17.171	-45
11	50	1	0.00196	7851.715	15.389	-50
12	60	1	0.001198	11306.81	13.546	-60
13	70	1	0.0008	15390.11	12.312	-70
14	80	1	0.000599	20101.61	12.041	-80
15	90	1	0.000439	25441.31	11.169	-90
16	100	1	0.000374	31409.21	11.747	-100

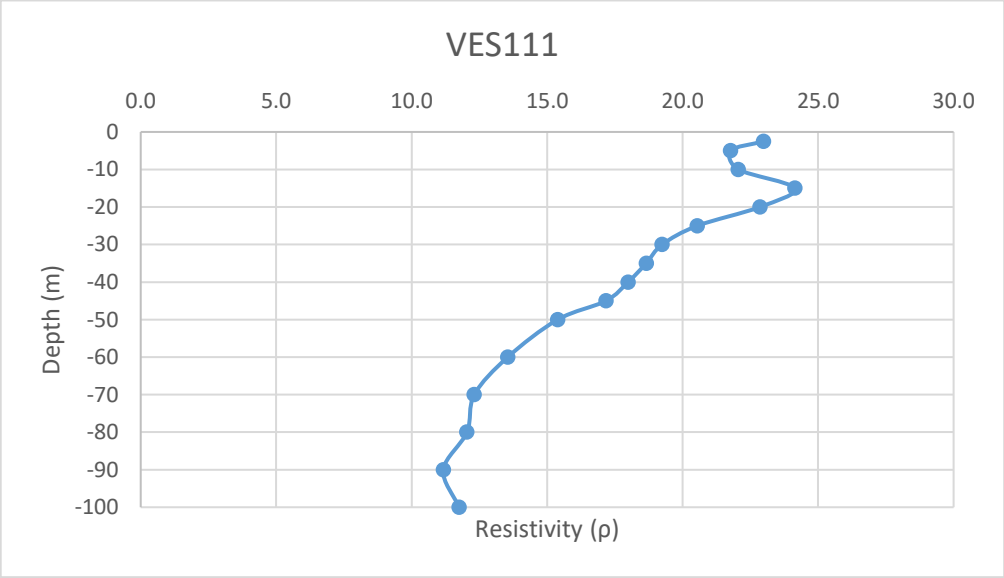

Annexure-XXII: Details of VES Survey

Date: 22/01/2025		VES-112				
Latitude	23		Longitude	69		
S.N	Current Electrode Spacing (AB/2)	Potential Electrode Spacing (MN)	Resistance (Ohm)	K value	Aparent Resistivity (Rho_a)	
1	2.5	1	10.21	18.846	192.418	-2.5
2	5	1	1.08	77.73975	83.959	-5
3	10	1	0.0514	313.3148	16.104	-10
4	15	1	0.0297	705.9398	20.966	-15
5	20	1	0.0189	1255.615	23.731	-20
6	25	1	0.0119	1962.34	23.352	-25
7	30	1	0.00878	2826.115	24.813	-30
8	35	1	0.00627	3846.94	24.120	-35
9	40	1	0.00509	5024.815	25.576	-40
10	45	1	0.0037	6359.74	23.531	-45
11	50	1	0.00307	7851.715	24.105	-50
12	60	1	0.00195	11306.81	22.048	-60
13	70	1	0.00128	15390.11	19.699	-70
14	80	1	0.00102	20101.61	20.504	-80
15	90	1	0.000754	25441.31	19.183	-90
16	100	1	0.000677	31409.21	21.264	-100

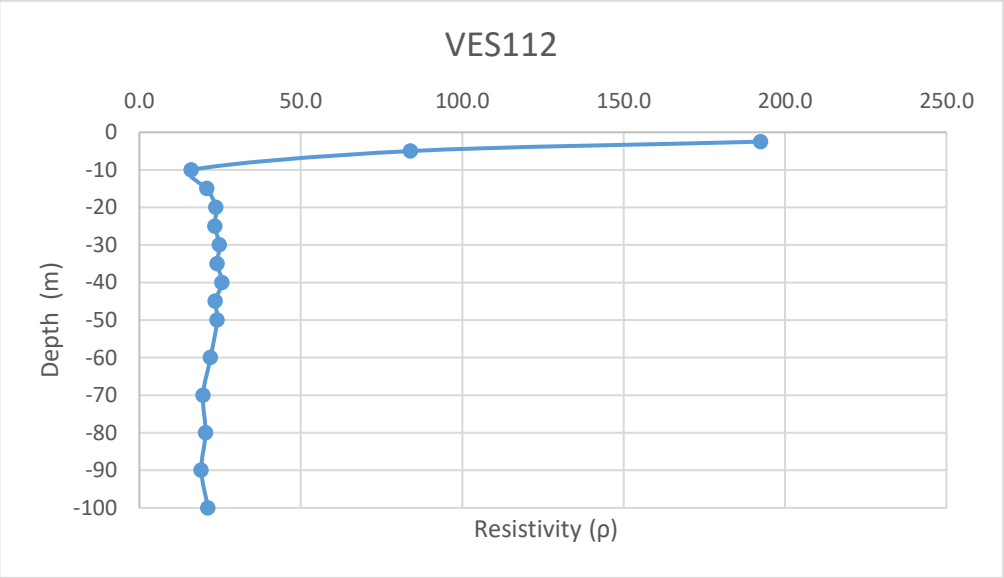

Annexure-XXII: Details of VES Survey

Date: 22/01/2025			VES-113			
Latitude	23.162065		Longitude	69.5596		
S.N	Current Electrode Spacing (AB/2)	Potential Electrode Spacing (MN)	Resistance (Ohm)	K value	Aparent Resistivity (Rho_a)	
1	2.5	1	0.91	18.846	17.150	-2.5
2	5	1	0.187	77.73975	14.537	-5
3	10	1	0.042	313.3148	13.159	-10
4	15	1	0.02	705.9398	14.119	-15
5	20	1	0.011	1255.615	13.812	-20
6	25	1	0.00695	1962.34	13.638	-25
7	30	1	0.00469	2826.115	13.254	-30
8	35	1	0.00343	3846.94	13.195	-35
9	40	1	0.00262	5024.815	13.165	-40
10	45	1	0.00205	6359.74	13.037	-45
11	50	1	0.00155	7851.715	12.170	-50
12	60	1	0.00103	11306.81	11.646	-60
13	70	1	0.000745	15390.11	11.466	-70
14	80	1	0.000568	20101.61	11.418	-80
15	90	1	0.000428	25441.31	10.889	-90
16	100	1	0.000387	31409.21	12.155	-100

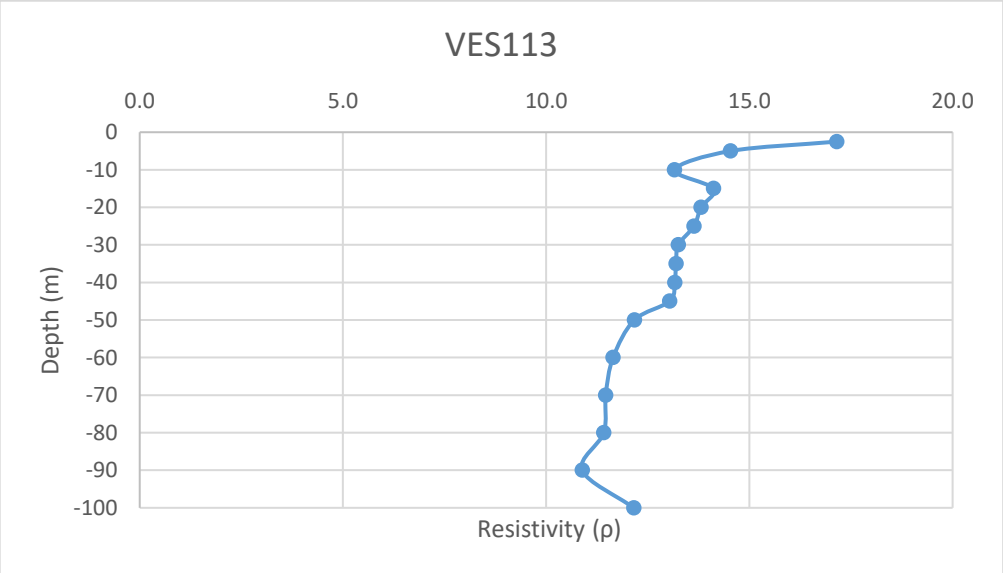

Annexure-XXII: Details of VES Survey

Date: 23/01/2025			VES-114			
Latitude	23.15560167		Longitude	69.55255667		
S.N	Current Electrode Spacing (AB/2)	Potential Electrode Spacing (MN)	Resistance (Ohm)	K value	Aparent Resistivity (Rho_a)	
1	2.5	1	13.9	18.846	261.959	-2.5
2	5	1	0.695	77.73975	54.029	-5
3	10	1	0.0276	313.3148	8.647	-10
4	15	1	0.0087	705.9398	6.142	-15
5	20	1	0.0048	1255.615	6.027	-20
6	25	1	0.00315	1962.34	6.181	-25
7	30	1	0.0021	2826.115	5.935	-30
8	35	1	0.00155	3846.94	5.963	-35
9	40	1	0.0011	5024.815	5.527	-40
10	45	1	0.00085	6359.74	5.406	-45
11	50	1	0.0006	7851.715	4.711	-50
12	60	1	0.00045	11306.81	5.088	-60
13	70	1	0.00035	15390.11	5.387	-70
14	80	1	0.0003	20101.61	6.030	-80
15	90	1	0.0002	25441.31	5.088	-90
16	100	1	0.0001	31409.21	3.141	-100

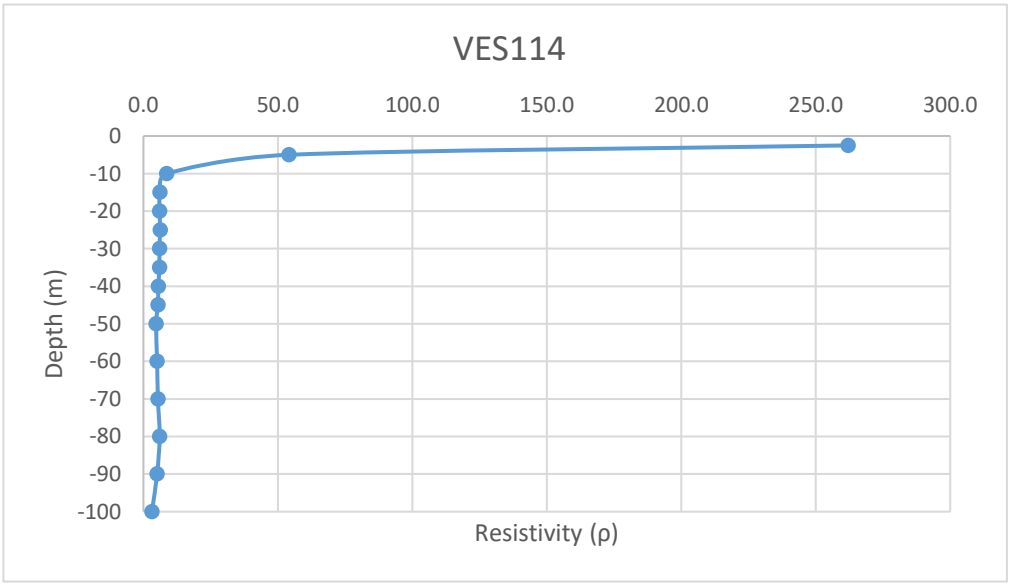

Annexure-XXII: Details of VES Survey

Date: 23/01/2025			VES-115			
Latitude	23.15837163		Longitude	69.55717594		
S.N	Current Electrode Spacing (AB/2)	Potential Electrode Spacing (MN)	Resistance (Ohm)	K value	Aparent Resistivity (Rho_a)	
1	2.5	1	0.706	18.846	13.305	-2.5
2	5	1	0.144	77.73975	11.195	-5
3	10	1	0.0302	313.3148	9.462	-10
4	15	1	0.01164	705.9398	8.217	-15
5	20	1	0.00573	1255.615	7.195	-20
6	25	1	0.00352	1962.34	6.907	-25
7	30	1	0.00235	2826.115	6.641	-30
8	35	1	0.00167	3846.94	6.424	-35
9	40	1	0.00125	5024.815	6.281	-40
10	45	1	0.000978	6359.74	6.220	-45
11	50	1	0.00075	7851.715	5.889	-50
12	60	1	0.000549	11306.81	6.207	-60
13	70	1	0.000411	15390.11	6.325	-70
14	80	1	0.000299	20101.61	6.010	-80
15	90	1	0.000259	25441.31	6.589	-90
16	100	1	0.0002	31409.21	6.282	-100

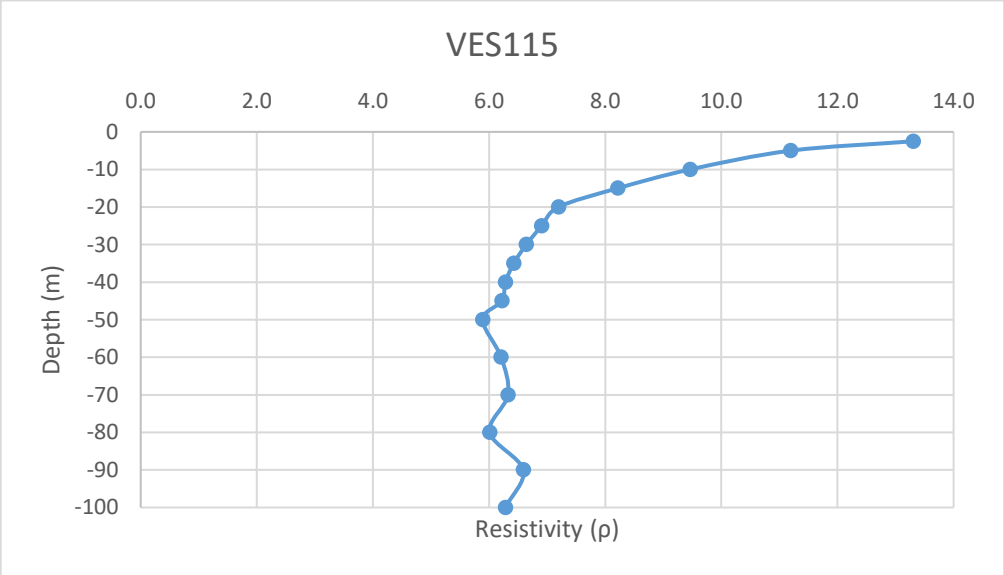

Annexure-XXII: Details of VES Survey

Date: 23/01/2025			VES-116			
Latitude	23.158633		Longitude	69.55718		
S.N	Current Electrode Spacing (AB/2)	Potential Electrode Spacing (MN)	Resistance (Ohm)	K value	Aparent Resistivity (Rho_a)	
1	2.5	1	0.736	18.846	13.871	-2.5
2	5	1	0.198	77.73975	15.392	-5
3	10	1	0.0339	313.3148	10.621	-10
4	15	1	0.0102	705.9398	7.201	-15
5	20	1	0.0065	1255.615	8.161	-20
6	25	1	0.00545	1962.34	10.695	-25
7	30	1	0.00415	2826.115	11.728	-30
8	35	1	0.00315	3846.94	12.118	-35
9	40	1	0.0023	5024.815	11.557	-40
10	45	1	0.0019	6359.74	12.084	-45
11	50	1	0.00145	7851.715	11.385	-50
12	60	1	0.0015	11306.81	16.960	-60
13	70	1	0.0007	15390.11	10.773	-70
14	80	1	0.0006	20101.61	12.061	-80
15	90	1	0.00045	25441.31	11.449	-90
16	100	1	0.0001	31409.21	3.141	-100

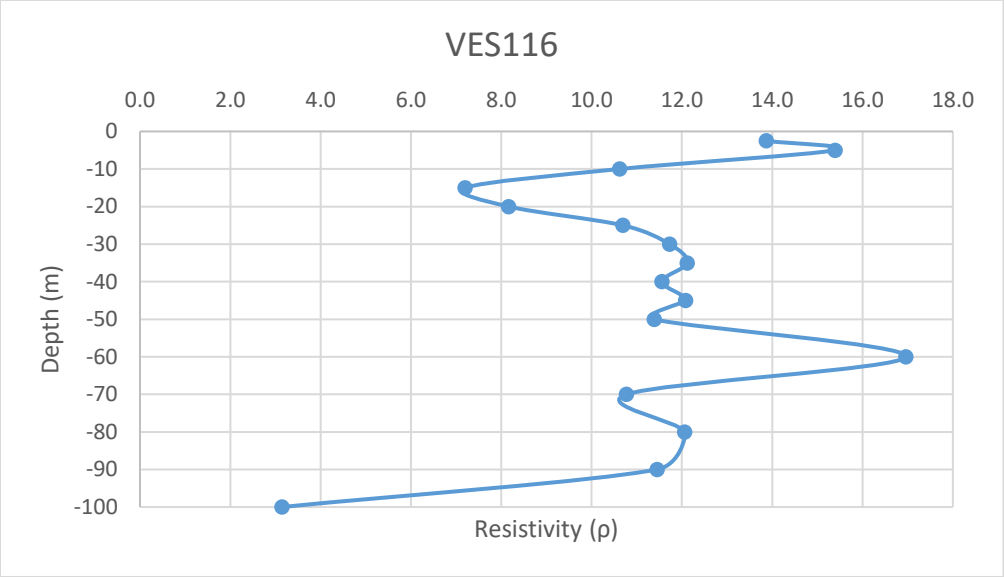

Annexure-XXII: Details of VES Survey

Date: 23/01/2025			VES-117			
Latitude	23.15797667		Longitude	69.55368167		
S.N	Current Electrode Spacing (AB/2)	Potential Electrode Spacing (MN)	Resistance (Ohm)	K value	Aparent Resistivity (Rho_a)	
1	2.5	1	0.514	18.846	9.687	-2.5
2	5	1	0.159	77.73975	12.361	-5
3	10	1	0.0385	313.3148	12.063	-10
4	15	1	0.0165	705.9398	11.648	-15
5	20	1	0.00767	1255.615	9.631	-20
6	25	1	0.00459	1962.34	9.007	-25
7	30	1	0.00272	2826.115	7.687	-30
8	35	1	0.00183	3846.94	7.040	-35
9	40	1	0.000178	5024.815	0.894	-40
10	45	1	0.000874	6359.74	5.558	-45
11	50	1	0.000714	7851.715	5.606	-50
12	60	1	0.000499	11306.81	5.642	-60
13	70	1	0.000339	15390.11	5.217	-70
14	80	1	0.000279	20101.61	5.608	-80
15	90	1	0.000219	25441.31	5.572	-90
16	100	1	0.000179	31409.21	5.622	-100

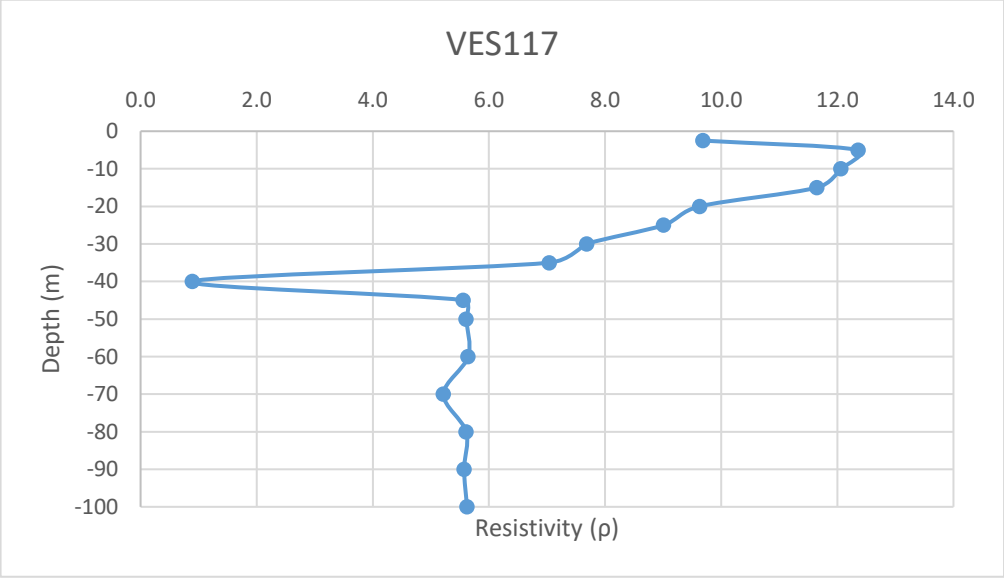

Annexure-XXII: Details of VES Survey

Date: 24/01/2025			VES-118			
Latitude	23.15797667		Longitude	69.55368167		
S.N	Current Electrode Spacing (AB/2)	Potential Electrode Spacing (MN)	Resistance (Ohm)	K value	Aparent Resistivity (Rho_a)	
1	2.5	1	4.65	18.846	87.634	-2.5
2	5	1	0.9605	77.73975	74.669	-5
3	10	1	0.162	313.3148	50.757	-10
4	15	1	0.083	705.9398	58.593	-15
5	20	1	0.042	1255.615	52.736	-20
6	25	1	0.0285	1962.34	55.927	-25
7	30	1	0.0155	2826.115	43.805	-30
8	35	1	0.0105	3846.94	40.393	-35
9	40	1	0.0062	5024.815	31.154	-40
10	45	1	0.00405	6359.74	25.757	-45
11	50	1	0.0023	7851.715	18.059	-50
12	60	1	0.00175	11306.81	19.787	-60
13	70	1	0.000585	15390.11	9.003	-70
14	80	1	0.00044	20101.61	8.845	-80
15	90	1	0.000316	25441.31	8.027	-90
16	100	1	0.00022	31409.21	6.910	-100

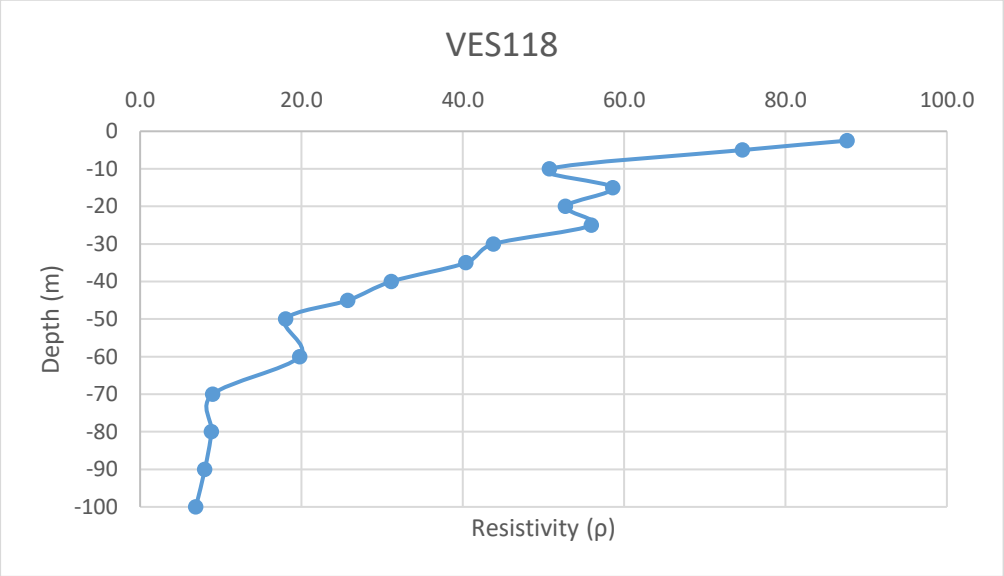

Annexure-XXII: Details of VES Survey

Date: 24/01/2025			VES-119			
Latitude	23.205273		Longitude	69.511762		
S.N	Current Electrode Spacing (AB/2)	Potential Electrode Spacing (MN)	Resistance (Ohm)	K value	Aparent Resistivity (Rho_a)	
1	2.5	1	3	18.846	56.538	-2.5
2	5	1	0.421	77.73975	32.728	-5
3	10	1	0.114	313.3148	35.718	-10
4	15	1	0.054	705.9398	38.121	-15
5	20	1	0.03	1255.615	37.668	-20
6	25	1	0.025	1962.34	49.059	-25
7	30	1	0.011	2826.115	31.087	-30
8	35	1	0.01	3846.94	38.469	-35
9	40	1	0.0073	5024.815	36.681	-40
10	45	1	0.0041	6359.74	26.075	-45
11	50	1	0.0015	7851.715	11.778	-50
12	60	1	0.0014	11306.81	15.830	-60
13	70	1	0.00056	15390.11	8.618	-70
14	80	1	0.00045	20101.61	9.046	-80
15	90	1	0.00032	25441.31	8.141	-90
16	100	1	0.00022	31409.21	6.910	-100

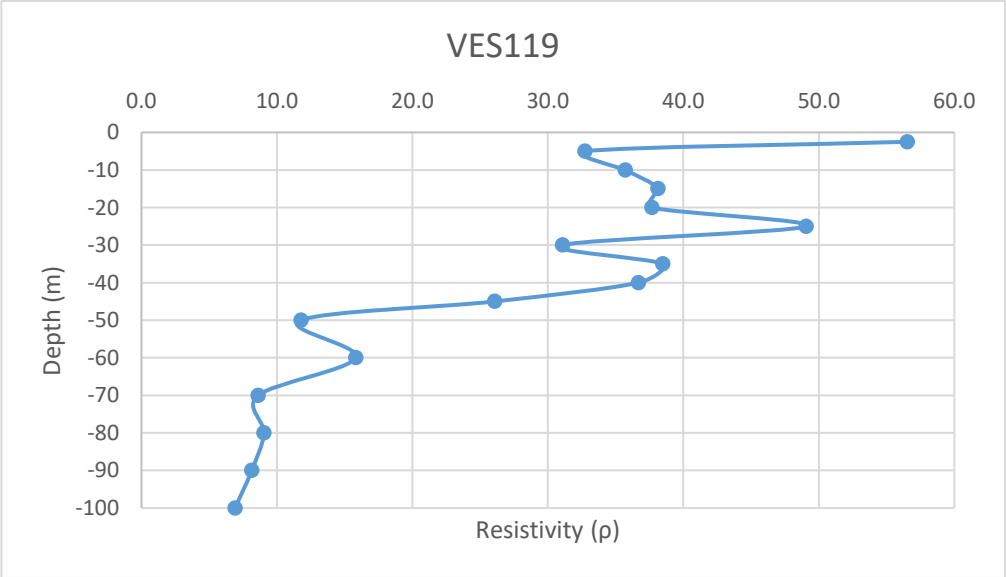

Annexure-XXII: Details of VES Survey

Date: 24/01/2025			VES-120			
Latitude	23.19991463		Longitude	69.6681842		
S.N	Current Electrode Spacing (AB/2)	Potential Electrode Spacing (MN)	Resistance (Ohm)	K value	Aparent Resistivity (Rho_a)	
1	2.5	1	1.32	18.846	24.877	-2.5
2	5	1	0.326	77.73975	25.343	-5
3	10	1	0.075	313.3148	23.499	-10
4	15	1	0.0353	705.9398	24.920	-15
5	20	1	0.0198	1255.615	24.861	-20
6	25	1	0.0122	1962.34	23.941	-25
7	30	1	0.00804	2826.115	22.722	-30
8	35	1	0.00573	3846.94	22.043	-35
9	40	1	0.00446	5024.815	22.411	-40
10	45	1	0.00361	6359.74	22.959	-45
11	50	1	0.00308	7851.715	24.183	-50
12	60	1	0.00233	11306.81	26.345	-60
13	70	1	0.00185	15390.11	28.472	-70
14	80	1	0.00155	20101.61	31.158	-80
15	90	1	0.0015	25441.31	38.162	-90
16	100	1	0.00117	31409.21	36.749	-100

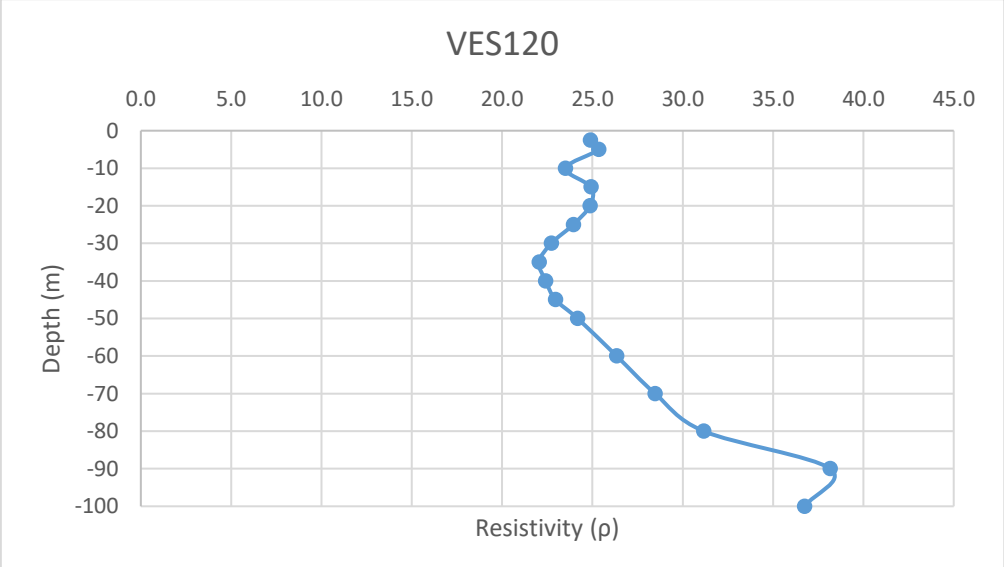

Annexure-XXII: Details of VES Survey

Date: 24/01/2025			VES-121			
Latitude	23.20283056		Longitude	69.66557737		
S.N	Current Electrode Spacing (AB/2)	Potential Electrode Spacing (MN)	Resistance (Ohm)	K value	Aparent Resistivity (Rho_a)	
1	2.5	1	43.4	18.846	817.916	-2.5
2	5	1	6.61	77.73975	513.860	-5
3	10	1	1.156	313.3148	362.192	-10
4	15	1	0.408	705.9398	288.023	-15
5	20	1	0.186	1255.615	233.544	-20
6	25	1	0.101	1962.34	198.196	-25
7	30	1	0.0768	2826.115	217.046	-30
8	35	1	0.0626	3846.94	240.818	-35
9	40	1	0.0433	5024.815	217.574	-40
10	45	1	0.0323	6359.74	205.420	-45
11	50	1	0.0289	7851.715	226.915	-50
12	60	1	0.0206	11306.81	232.920	-60
13	70	1	0.0176	15390.11	270.866	-70
14	80	1	0.0134	20101.61	269.362	-80
15	90	1	0.0196	25441.31	498.650	-90
16	100	1	0.00618	31409.21	194.109	-100

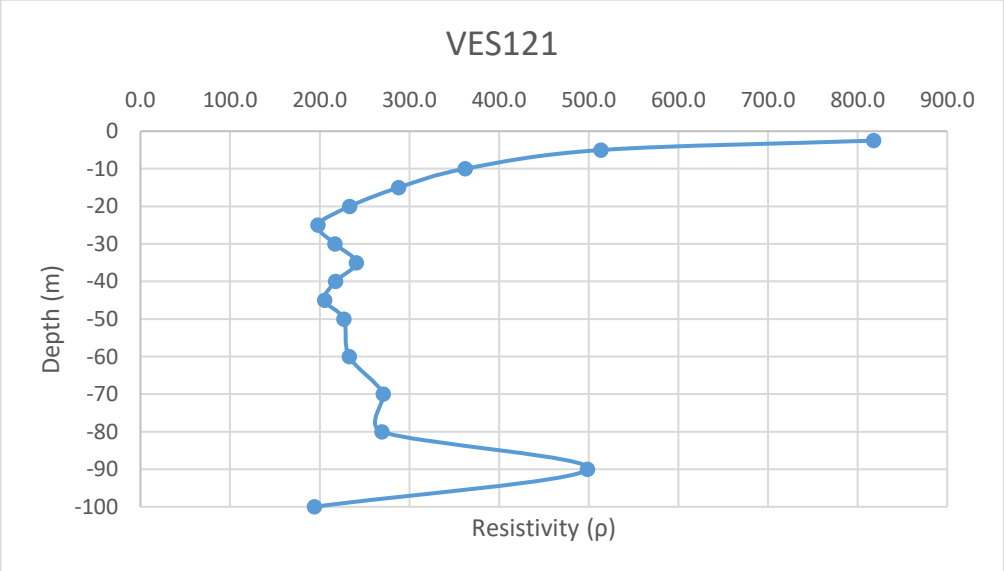

Annexure-XXII: Details of VES Survey

Date: 24/01/2025			VES-122			
Latitude	23.199424		Longitude	69.509573		
S.N	Current Electrode Spacing (AB/2)	Potential Electrode Spacing (MN)	Resistance (Ohm)	K value	Aparent Resistivity (Rho_a)	
1	2.5	1	6.3	18.846	118.730	-2.5
2	5	1	1.5	77.73975	116.610	-5
3	10	1	0.21	313.3148	65.796	-10
4	15	1	0.112	705.9398	79.065	-15
5	20	1	0.054	1255.615	67.803	-20
6	25	1	0.032	1962.34	62.795	-25
7	30	1	0.02	2826.115	56.522	-30
8	35	1	0.011	3846.94	42.316	-35
9	40	1	0.0051	5024.815	25.627	-40
10	45	1	0.004	6359.74	25.439	-45
11	50	1	0.0031	7851.715	24.340	-50
12	60	1	0.0021	11306.81	23.744	-60
13	70	1	0.00061	15390.11	9.388	-70
14	80	1	0.00043	20101.61	8.644	-80
15	90	1	0.000311	25441.31	7.912	-90
16	100	1	0.00022	31409.21	6.910	-100

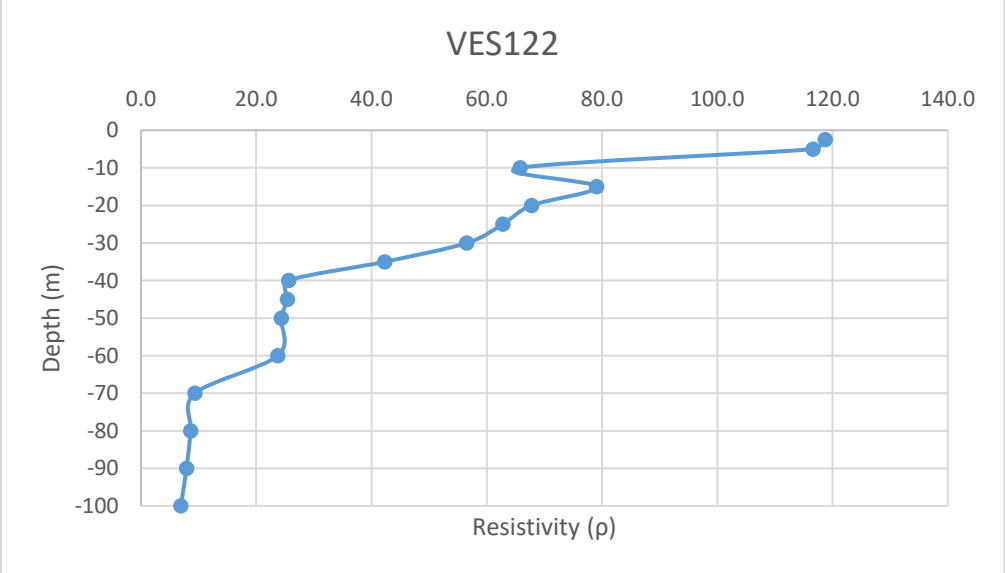

Annexure-XXII: Details of VES Survey

Date: 24/01/2025		VES-123				
Latitude	23.20439508		Longitude	69.67192071		
S.N	Current Electrode Spacing (AB/2)	Potential Electrode Spacing (MN)	Resistance (Ohm)	K value	Aparent Resistivity (Rho_a)	
1	2.5	1	1.46	18.846	27.515	-2.5
2	5	1	0.861	77.73975	66.934	-5
3	10	1	0.367	313.3148	114.987	-10
4	15	1	0.169	705.9398	119.304	-15
5	20	1	0.0843	1255.615	105.848	-20
6	25	1	0.0454	1962.34	89.090	-25
7	30	1	0.0305	2826.115	86.196	-30
8	35	1	0.0214	3846.94	82.325	-35
9	40	1	0.0148	5024.815	74.367	-40
10	45	1	0.013	6359.74	82.677	-45
11	50	1	0.00978	7851.715	76.790	-50
12	60	1	0.00602	11306.81	68.067	-60
13	70	1	0.0041	15390.11	63.099	-70
14	80	1	0.00315	20101.61	63.320	-80
15	90	1	0.00236	25441.31	60.042	-90
16	100	1	0.00166	31409.21	52.139	-100

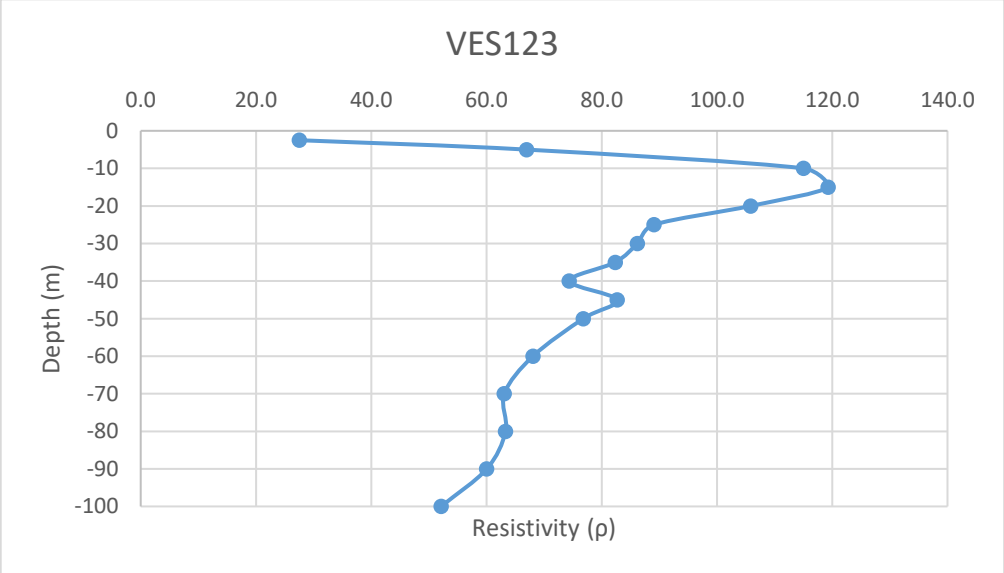

Annexure-XXII: Details of VES Survey

Date: 25/01/2025			VES-124			
Latitude	23.19799		Longitude	69.50809667		
S.N	Current Electrode Spacing (AB/2)	Potential Electrode Spacing (MN)	Resistance (Ohm)	K value	Aparent Resistivity (Rho_a)	
1	2.5	1	18.5	18.846	348.651	-2.5
2	5	1	6.12	77.73975	475.767	-5
3	10	1	1.58	313.3148	495.037	-10
4	15	1	0.564	705.9398	398.150	-15
5	20	1	0.302	1255.615	379.196	-20
6	25	1	0.162	1962.34	317.899	-25
7	30	1	0.0923	2826.115	260.850	-30
8	35	1	0.0598	3846.94	230.047	-35
9	40	1	0.04	5024.815	200.993	-40
10	45	1	0.0268	6359.74	170.441	-45
11	50	1	0.0188	7851.715	147.612	-50
12	60	1	0.01103	11306.81	124.714	-60
13	70	1	0.00737	15390.11	113.425	-70
14	80	1	0.00501	20101.61	100.709	-80
15	90	1	0.00357	25441.31	90.825	-90
16	100	1	0.00243	31409.21	76.324	-100

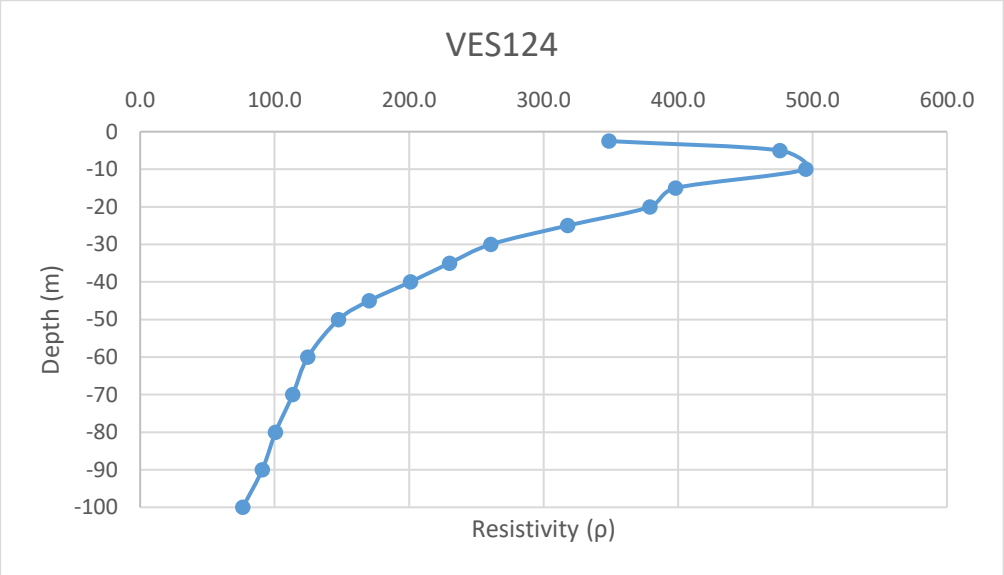

Annexure-XXII: Details of VES Survey

Date: 25/01/2025			VES-125			
Latitude	23.18872333		Longitude	69.51212167		
S.N	Current Electrode Spacing (AB/2)	Potential Electrode Spacing (MN)	Resistance (Ohm)	K value	Aparent Resistivity (Rho_a)	
1	2.5	1	2.46	18.846	46.361	-2.5
2	5	1	0.215	77.73975	16.714	-5
3	10	1	0.0201	313.3148	6.298	-10
4	15	1	0.00789	705.9398	5.570	-15
5	20	1	0.00469	1255.615	5.889	-20
6	25	1	0.00334	1962.34	6.554	-25
7	30	1	0.00265	2826.115	7.489	-30
8	35	1	0.00202	3846.94	7.771	-35
9	40	1	0.00152	5024.815	7.638	-40
10	45	1	0.001198	6359.74	7.619	-45
11	50	1	0.000938	7851.715	7.365	-50
12	60	1	0.000649	11306.81	7.338	-60
13	70	1	0.000474	15390.11	7.295	-70
14	80	1	0.00025	20101.61	5.025	-80
15	90	1	0.0002	25441.31	5.088	-90
16	100	1	0.0001	31409.21	3.141	-100

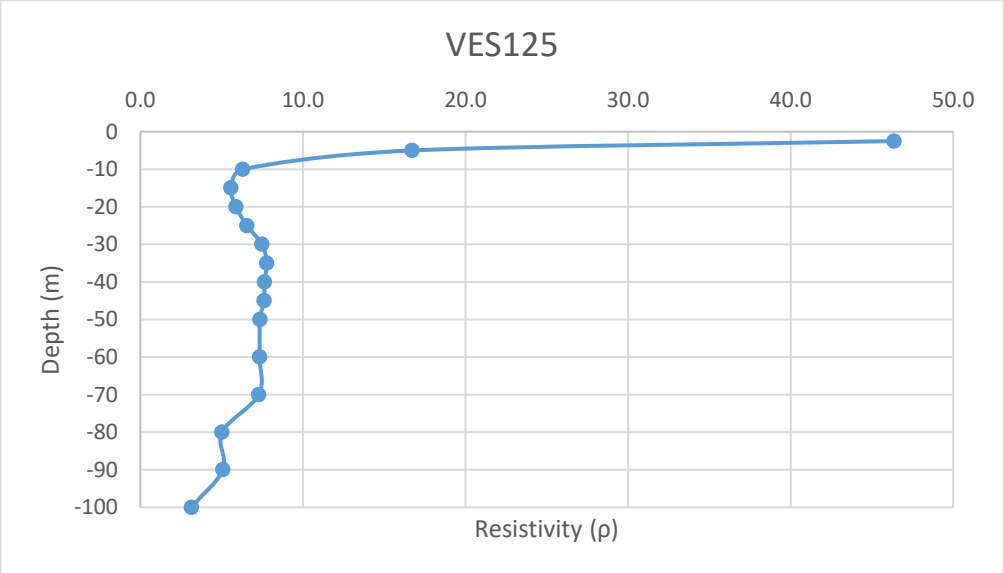

Annexure-XXII: Details of VES Survey

Date: 25/01/2025			VES-126			
Latitude	23.18815667		Longitude	69.50238333		
S.N	Current Electrode Spacing (AB/2)	Potential Electrode Spacing (MN)	Resistance (Ohm)	K value	Aparent Resistivity (Rho_a)	
1	2.5	1	0.107	18.846	2.017	-2.5
2	5	1	0.0307	77.73975	2.387	-5
3	10	1	0.00548	313.3148	1.717	-10
4	15	1	0.00278	705.9398	1.963	-15
5	20	1	0.00188	1255.615	2.361	-20
6	25	1	0.0015	1962.34	2.944	-25
7	30	1	0.0012	2826.115	3.391	-30
8	35	1	0.0008	3846.94	3.078	-35
9	40	1	0.00075	5024.815	3.769	-40
10	45	1	0.0007	6359.74	4.452	-45
11	50	1	0.00042	7851.715	3.298	-50
12	60	1	0.0003	11306.81	3.392	-60
13	70	1	0.00024	15390.11	3.694	-70
14	80	1	0.00033	20101.61	6.634	-80
15	90	1	0.0003	25441.31	7.632	-90
16	100	1	0.0003	31409.21	9.423	-100

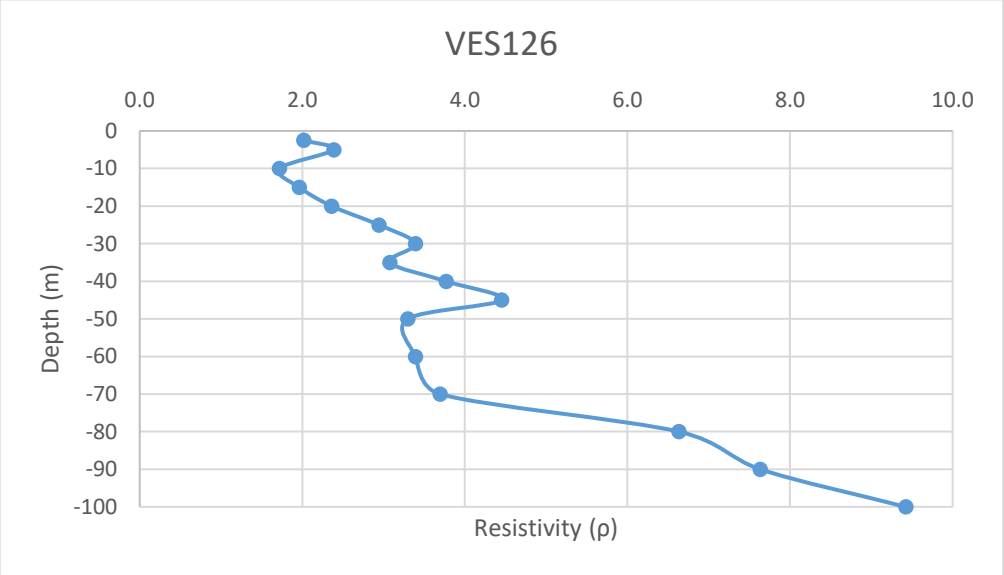

Annexure-XXII: Details of VES Survey

Date: 27/01/2025			VES-127			
Latitude	23.14594167		Longitude	69.54946833		
S.N	Current Electrode Spacing (AB/2)	Potential Electrode Spacing (MN)	Resistance (Ohm)	K value	Aparent Resistivity (Rho_a)	
1	2.5	1	2.28	18.846	42.969	-2.5
2	5	1	0.302	77.73975	23.477	-5
3	10	1	0.0395	313.3148	12.376	-10
4	15	1	0.0156	705.9398	11.013	-15
5	20	1	0.00936	1255.615	11.753	-20
6	25	1	0.00635	1962.34	12.461	-25
7	30	1	0.00457	2826.115	12.915	-30
8	35	1	0.0035	3846.94	13.464	-35
9	40	1	0.00275	5024.815	13.818	-40
10	45	1	0.0025	6359.74	15.899	-45
11	50	1	0.002	7851.715	15.703	-50
12	60	1	0.0013	11306.81	14.699	-60
13	70	1	0.00114	15390.11	17.545	-70
14	80	1	0.0008	20101.61	16.081	-80
15	90	1	0.0007	25441.31	17.809	-90
16	100	1	0.000649	31409.21	20.385	-100

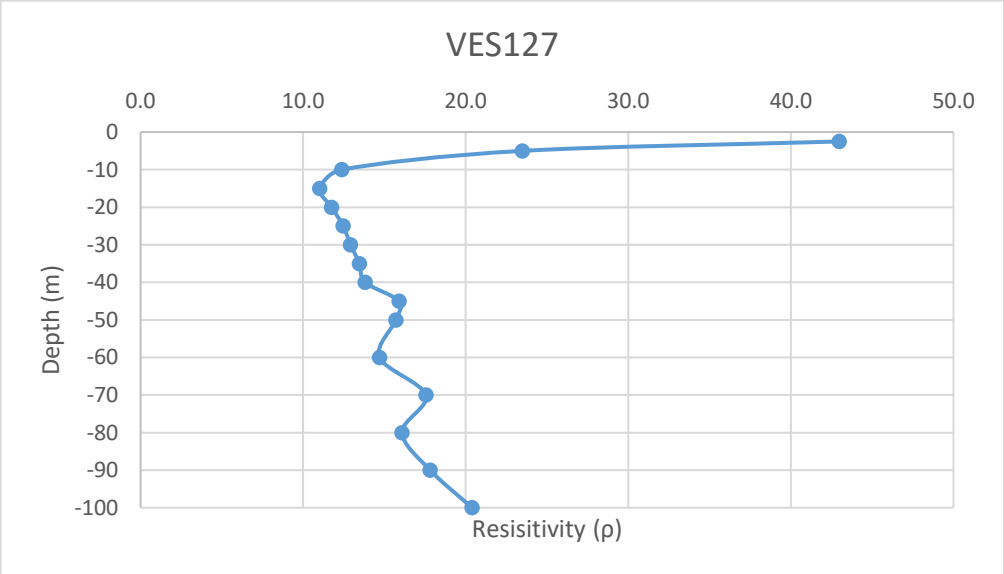

Annexure-XXII: Details of VES Survey

Date: 27/01/2025			VES-128			
Latitude	23.15205167		Longitude	69.55105833		
S.N	Current Electrode Spacing (AB/2)	Potential Electrode Spacing (MN)	Resistance (Ohm)	K value	Aparent Resistivity (Rho_a)	
1	2.5	1	1.25	18.846	23.558	-2.5
2	5	1	0.207	77.73975	16.092	-5
3	10	1	0.0334	313.3148	10.465	-10
4	15	1	0.0154	705.9398	10.871	-15
5	20	1	0.01	1255.615	12.556	-20
6	25	1	0.00755	1962.34	14.816	-25
7	30	1	0.0051	2826.115	14.413	-30
8	35	1	0.0037	3846.94	14.234	-35
9	40	1	0.0028	5024.815	14.069	-40
10	45	1	0.0022	6359.74	13.991	-45
11	50	1	0.00165	7851.715	12.955	-50
12	60	1	0.001058	11306.81	11.963	-60
13	70	1	0.000849	15390.11	13.066	-70
14	80	1	0.000674	20101.61	13.548	-80
15	90	1	0.000516	25441.31	13.128	-90
16	100	1	0.000479	31409.21	15.045	-100

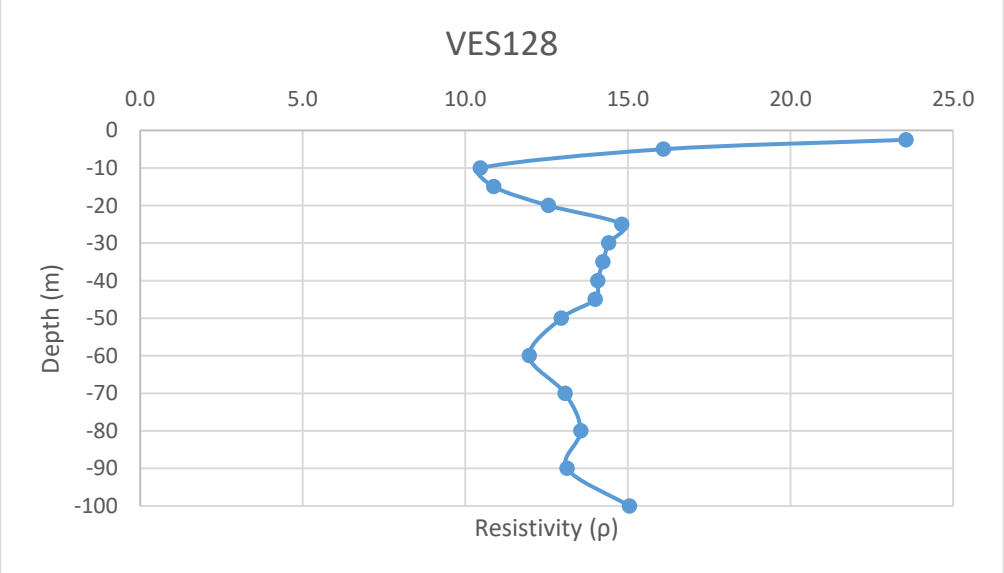

Annexure-XXII: Details of VES Survey

Date: 27/01/2025			VES-129			
Latitude	23.14906667		Longitude	69.54405833		
S.N	Current Electrode Spacing (AB/2)	Potential Electrode Spacing (MN)	Resistance (Ohm)	K value	Aparent Resistivity (Rho_a)	
1	2.5	1	0.305	18.846	5.748	-2.5
2	5	1	0.0895	77.73975	6.958	-5
3	10	1	0.0221	313.3148	6.924	-10
4	15	1	0.01115	705.9398	7.871	-15
5	20	1	0.00574	1255.615	7.207	-20
6	25	1	0.00385	1962.34	7.555	-25
7	30	1	0.0025	2826.115	7.065	-30
8	35	1	0.00191	3846.94	7.348	-35
9	40	1	0.00152	5024.815	7.638	-40
10	45	1	0.0012	6359.74	7.632	-45
11	50	1	0.000824	7851.715	6.470	-50
12	60	1	0.0007	11306.81	7.915	-60
13	70	1	0.000519	15390.11	7.987	-70
14	80	1	0.000349	20101.61	7.015	-80
15	90	1	0.000279	25441.31	7.098	-90
16	100	1	0.000239	31409.21	7.507	-100

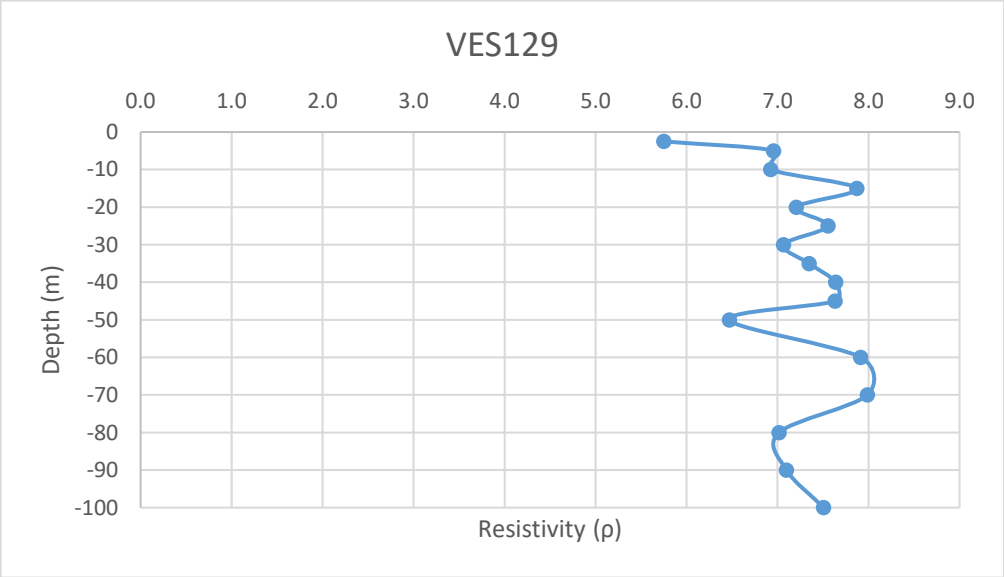

Annexure-XXII: Details of VES Survey

Date: 27/01/2025			VES-130			
Latitude	23.148835		Longitude	69.53840667		
S.N	Current Electrode Spacing (AB/2)	Potential Electrode Spacing (MN)	Resistance (Ohm)	K value	Aparent Resistivity (Rho_a)	
1	2.5	1	0.915	18.846	17.244	-2.5
2	5	1	0.263	77.73975	20.446	-5
3	10	1	0.0661	313.3148	20.710	-10
4	15	1	0.0266	705.9398	18.778	-15
5	20	1	0.016	1255.615	20.090	-20
6	25	1	0.00985	1962.34	19.329	-25
7	30	1	0.0044	2826.115	12.435	-30
8	35	1	0.00335	3846.94	12.887	-35
9	40	1	0.00256	5024.815	12.864	-40
10	45	1	0.00193	6359.74	12.274	-45
11	50	1	0.0015	7851.715	11.778	-50
12	60	1	0.000849	11306.81	9.599	-60
13	70	1	0.000659	15390.11	10.142	-70
14	80	1	0.000459	20101.61	9.227	-80
15	90	1	0.000349	25441.31	8.879	-90
16	100	1	0.000299	31409.21	9.391	-100

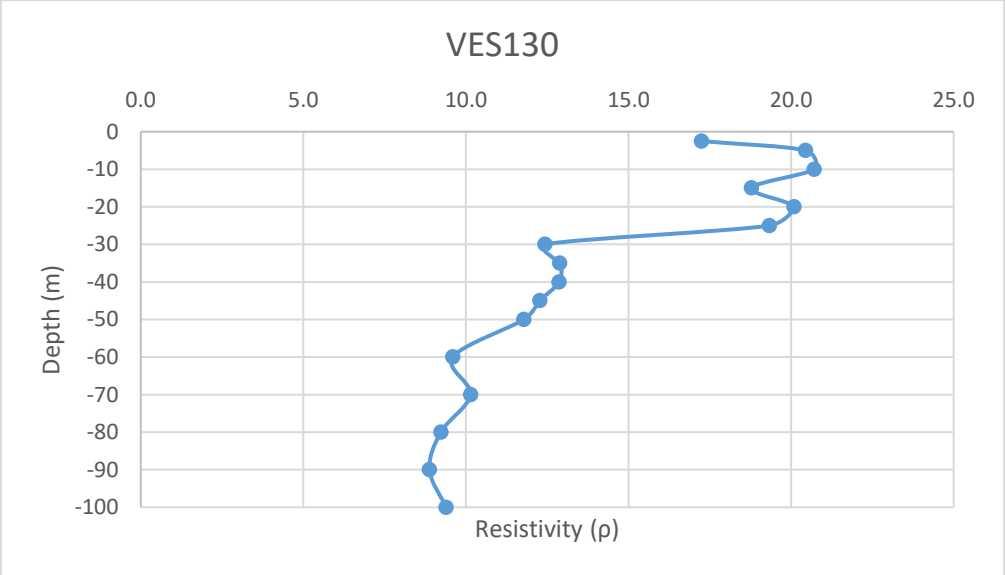

Annexure-XXII: Details of VES Survey

Date: 28/01/2025		VES-131				
Latitude	23.14778333		Longitude	69.53186		
S.N	Current Electrode Spacing (AB/2)	Potential Electrode Spacing (MN)	Resistance (Ohm)	K value	Aparent Resistivity (Rho_a)	
1	2.5	1	2.17	18.846	40.896	-2.5
2	5	1	0.436	77.73975	33.895	-5
3	10	1	0.0648	313.3148	20.303	-10
4	15	1	0.0151	705.9398	10.660	-15
5	20	1	0.00959	1255.615	12.041	-20
6	25	1	0.00577	1962.34	11.323	-25
7	30	1	0.00425	2826.115	12.011	-30
8	35	1	0.0033	3846.94	12.695	-35
9	40	1	0.0024	5024.815	12.060	-40
10	45	1	0.00175	6359.74	11.130	-45
11	50	1	0.0015	7851.715	11.778	-50
12	60	1	0.001018	11306.81	11.510	-60
13	70	1	0.000619	15390.11	9.526	-70
14	80	1	0.000499	20101.61	10.031	-80
15	90	1	0.000374	25441.31	9.515	-90
16	100	1	0.000319	31409.21	10.020	-100

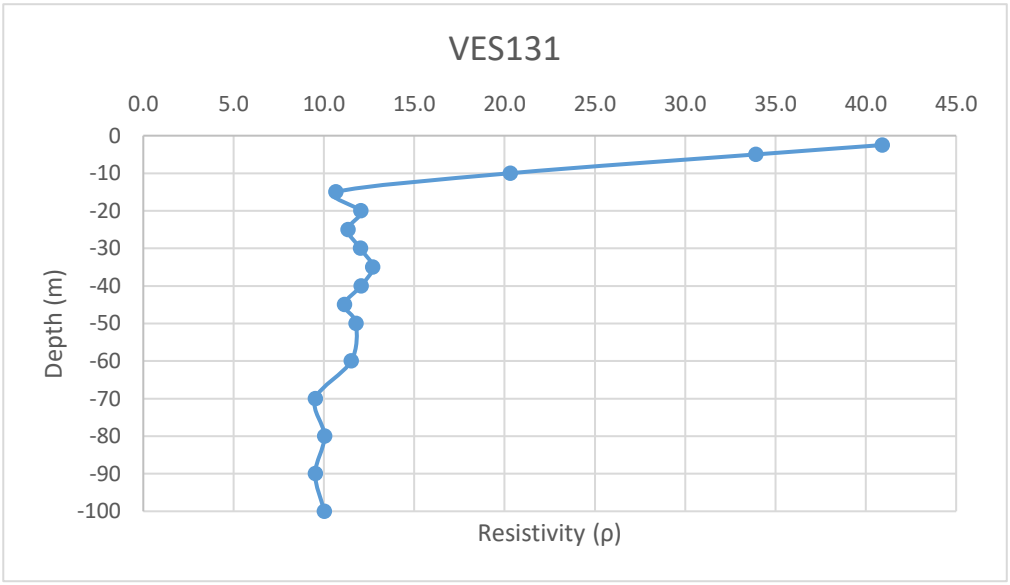

Annexure-XXII: Details of VES Survey

Date: 28/01/2025			VES-132			
Latitude	23.14776333		Longitude	69.52747167		
S.N	Current Electrode Spacing (AB/2)	Potential Electrode Spacing (MN)	Resistance (Ohm)	K value	Aparent Resistivity (Rho_a)	
1	2.5	1	0.771	18.846	14.530	-2.5
2	5	1	0.112	77.73975	8.707	-5
3	10	1	0.0242	313.3148	7.582	-10
4	15	1	0.01059	705.9398	7.476	-15
5	20	1	0.0061	1255.615	7.659	-20
6	25	1	0.00422	1962.34	8.281	-25
7	30	1	0.0029	2826.115	8.196	-30
8	35	1	0.0021	3846.94	8.079	-35
9	40	1	0.00175	5024.815	8.793	-40
10	45	1	0.00135	6359.74	8.586	-45
11	50	1	0.001082	7851.715	8.496	-50
12	60	1	0.000815	11306.81	9.215	-60
13	70	1	0.000732	15390.11	11.266	-70
14	80	1	0.000582	20101.61	11.699	-80
15	90	1	0.000466	25441.31	11.856	-90
16	100	1	0.000399	31409.21	12.532	-100

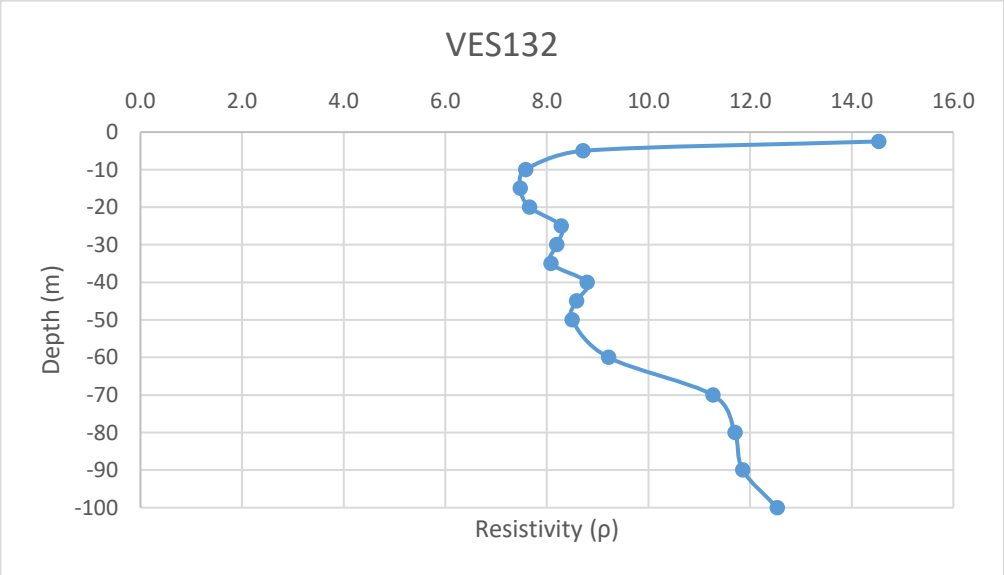

Annexure-XXII: Details of VES Survey

Date: 30/01/2025			VES-133			
Latitude	23.20631899		Longitude	69.70239264		
S.N	Current Electrode Spacing (AB/2)	Potential Electrode Spacing (MN)	Resistance (Ohm)	K value	Aparent Resistivity (Rho_a)	
1	2.5	1	59.3	18.846	1117.568	-2.5
2	5	1	17.2	77.73975	1337.124	-5
3	10	1	4.43	313.3148	1387.984	-10
4	15	1	1.86	705.9398	1313.048	-15
5	20	1	0.875	1255.615	1098.663	-20
6	25	1	0.41	1962.34	804.559	-25
7	30	1	0.257	2826.115	726.311	-30
8	35	1	0.198	3846.94	761.694	-35
9	40	1	0.135	5024.815	678.350	-40
10	45	1	0.0937	6359.74	595.908	-45
11	50	1	0.063	7851.715	494.658	-50
12	60	1	0.0341	11306.81	385.562	-60
13	70	1	0.0196	15390.11	301.646	-70
14	80	1	0.00965	20101.61	193.981	-80
15	90	1	0.00637	25441.31	162.061	-90
16	100	1	0.00383	31409.21	120.297	-100

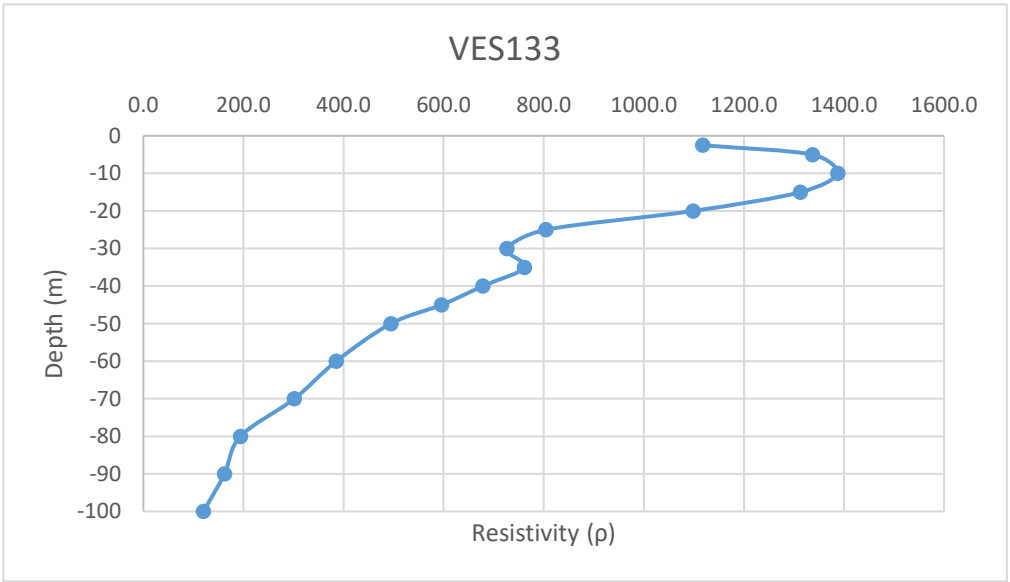

Annexure-XXII: Details of VES Survey

Date: 30/01/2025			VES-134			
Latitude	23.20045162		Longitude	69.70092699		
S.N	Current Electrode Spacing (AB/2)	Potential Electrode Spacing (MN)	Resistance (Ohm)	K value	Aparent Resistivity (Rho_a)	
1	2.5	1	0.513	18.846	9.668	-2.5
2	5	1	0.0336	77.73975	2.612	-5
3	10	1	0.0085	313.3148	2.663	-10
4	15	1	0.00385	705.9398	2.718	-15
5	20	1	0.00271	1255.615	3.403	-20
6	25	1	0.002	1962.34	3.925	-25
7	30	1	0.0014	2826.115	3.957	-30
8	35	1	0.0011	3846.94	4.232	-35
9	40	1	0.0008	5024.815	4.020	-40
10	45	1	0.0005	6359.74	3.180	-45
11	50	1	0.00055	7851.715	4.318	-50
12	60	1	0.00065	11306.81	7.349	-60
13	70	1	0.0004	15390.11	6.156	-70
14	80	1	0.00075	20101.61	15.076	-80
15	90	1	0.00025	25441.31	6.360	-90
16	100	1	0.0002	31409.21	6.282	-100

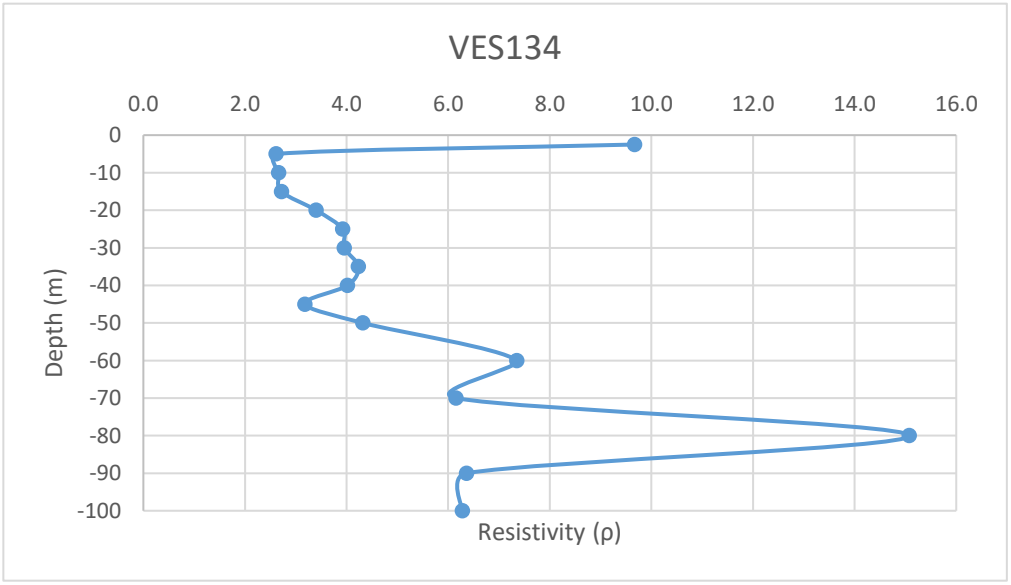

Annexure-XXII: Details of VES Survey

Date: 30/01/2025			VES-135			
Latitude	23.19885732		Longitude	69.69989661		
S.N	Current Electrode Spacing (AB/2)	Potential Electrode Spacing (MN)	Resistance (Ohm)	K value	Aparent Resistivity (Rho_a)	
1	2.5	1	0.279	18.846	5.258	-2.5
2	5	1	0.0665	77.73975	5.170	-5
3	10	1	0.0155	313.3148	4.856	-10
4	15	1	0.00751	705.9398	5.302	-15
5	20	1	0.00435	1255.615	5.462	-20
6	25	1	0.00268	1962.34	5.259	-25
7	30	1	0.00192	2826.115	5.426	-30
8	35	1	0.0015	3846.94	5.770	-35
9	40	1	0.001148	5024.815	5.768	-40
10	45	1	0.000958	6359.74	6.093	-45
11	50	1	0.000799	7851.715	6.274	-50
12	60	1	0.000579	11306.81	6.547	-60
13	70	1	0.000474	15390.11	7.295	-70
14	80	1	0.000373	20101.61	7.498	-80
15	90	1	0.0003	25441.31	7.632	-90
16	100	1	0.00028	31409.21	8.795	-100

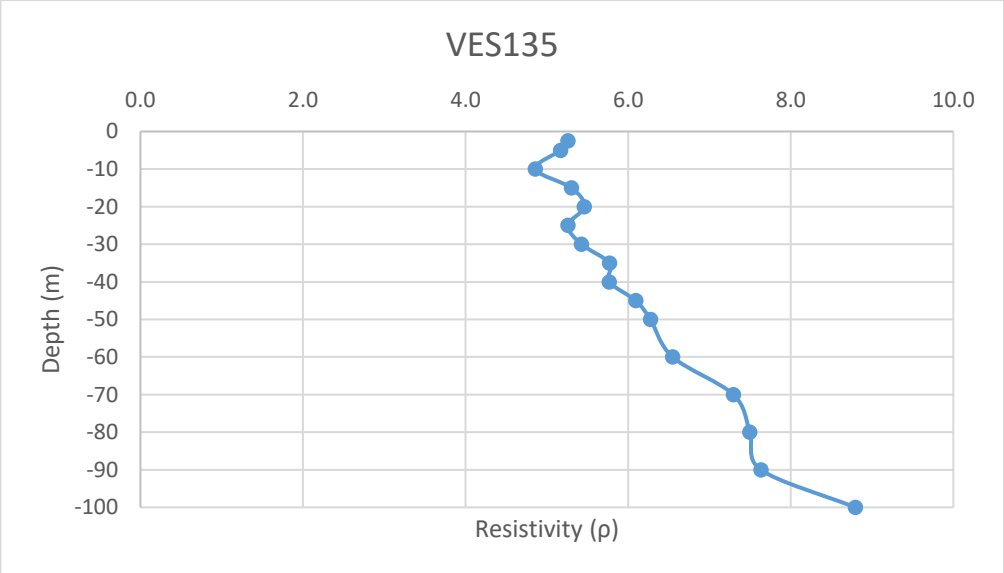

Annexure-XXII: Details of VES Survey

Date: 30/01/2025			VES-136			
Latitude	23.20415417		Longitude	69.70058394		
S.N	Current Electrode Spacing (AB/2)	Potential Electrode Spacing (MN)	Resistance (Ohm)	K value	Aparent Resistivity (Rho_a)	
1	2.5	1	5.2	18.846	97.999	-2.5
2	5	1	0.9968	77.73975	77.491	-5
3	10	1	0.133	313.3148	41.671	-10
4	15	1	0.0439	705.9398	30.991	-15
5	20	1	0.0248	1255.615	31.139	-20
6	25	1	0.0146	1962.34	28.650	-25
7	30	1	0.0096	2826.115	27.131	-30
8	35	1	0.0069	3846.94	26.544	-35
9	40	1	0.005295	5024.815	26.606	-40
10	45	1	0.003925	6359.74	24.962	-45
11	50	1	0.0034	7851.715	26.696	-50
12	60	1	0.00312	11306.81	35.277	-60
13	70	1	0.00235	15390.11	36.167	-70
14	80	1	0.002	20101.61	40.203	-80
15	90	1	0.0016	25441.31	40.706	-90
16	100	1	0.00126	31409.21	39.576	-100

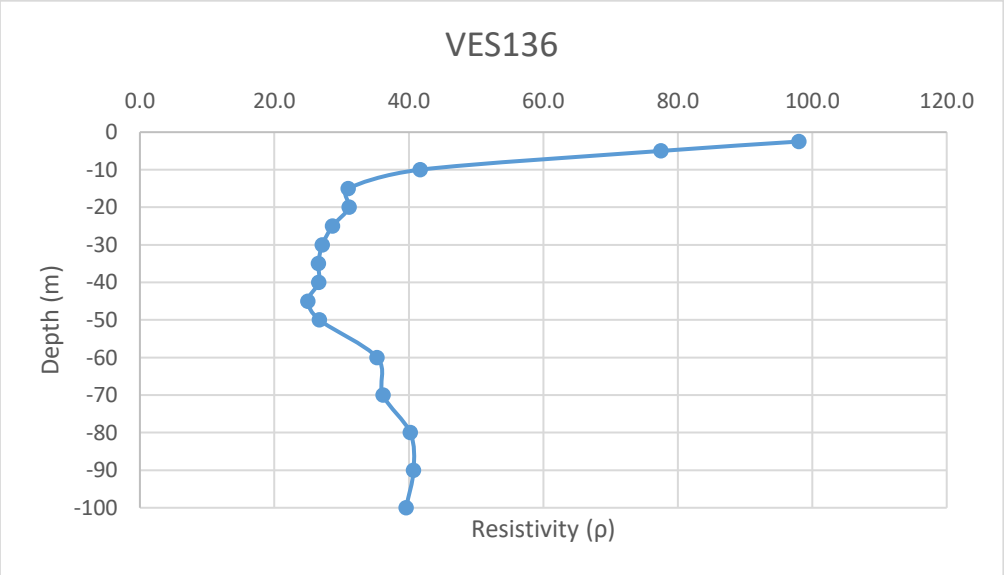

Annexure-XXII: Details of VES Survey

Date: 02/02/2025			VES-137			
Latitude	23.209317		Longitude	69.61069		
S.N	Current Electrode Spacing (AB/2)	Potential Electrode Spacing (MN)	Resistance (Ohm)	K value	Aparent Resistivity (Rho_a)	
1	2.5	1	6	18.846	113.076	-2.5
2	5	1	1.49	77.73975	115.832	-5
3	10	1	0.162	313.3148	50.757	-10
4	15	1	0.041	705.9398	28.944	-15
5	20	1	0.0177	1255.615	22.224	-20
6	25	1	0.00907	1962.34	17.798	-25
7	30	1	0.00564	2826.115	15.939	-30
8	35	1	0.00385	3846.94	14.811	-35
9	40	1	0.00293	5024.815	14.723	-40
10	45	1	0.0023	6359.74	14.627	-45
11	50	1	0.0018	7851.715	14.133	-50
12	60	1	0.0011	11306.81	12.437	-60
13	70	1	0.00085	15390.11	13.082	-70
14	80	1	0.00065	20101.61	13.066	-80
15	90	1	0.00045	25441.31	11.449	-90
16	100	1	0.00045	31409.21	14.134	-100

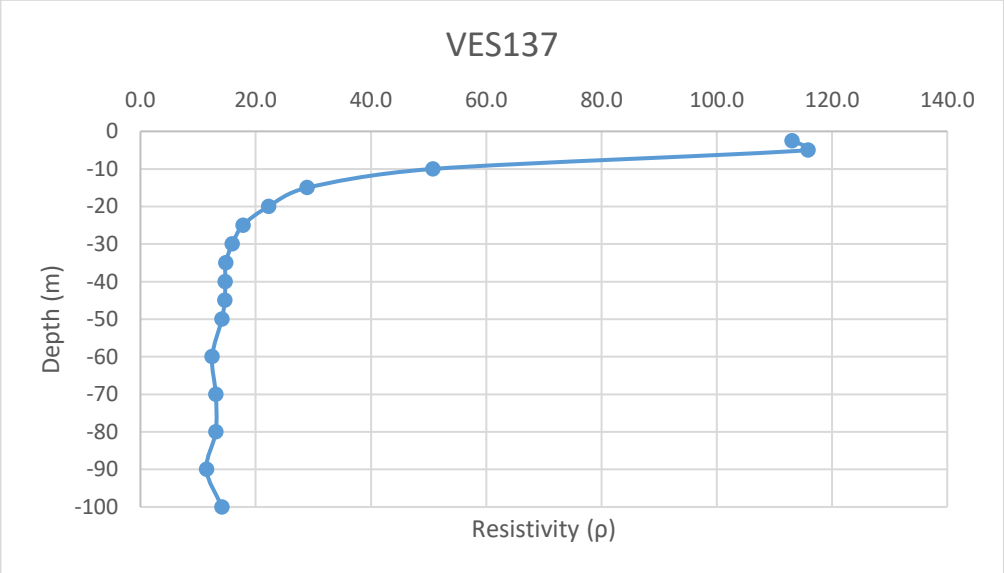

Annexure-XXII: Details of VES Survey

Date: 02/02/2025			VES-138			
Latitude	23.209527		Longitude	69.612557		
S.N	Current Electrode Spacing (AB/2)	Potential Electrode Spacing (MN)	Resistance (Ohm)	K value	Aparent Resistivity (Rho_a)	
1	2.5	1	1.4	18.846	26.384	-2.5
2	5	1	0.344	77.73975	26.742	-5
3	10	1	0.074	313.3148	23.185	-10
4	15	1	0.0316	705.9398	22.308	-15
5	20	1	0.0167	1255.615	20.969	-20
6	25	1	0.00955	1962.34	18.740	-25
7	30	1	0.00615	2826.115	17.381	-30
8	35	1	0.00395	3846.94	15.195	-35
9	40	1	0.00245	5024.815	12.311	-40
10	45	1	0.00185	6359.74	11.766	-45
11	50	1	0.0014	7851.715	10.992	-50
12	60	1	0.00085	11306.81	9.611	-60
13	70	1	0.00065	15390.11	10.004	-70
14	80	1	0.000419	20101.61	8.423	-80
15	90	1	0.000359	25441.31	9.133	-90
16	100	1	0.000349	31409.21	10.962	-100

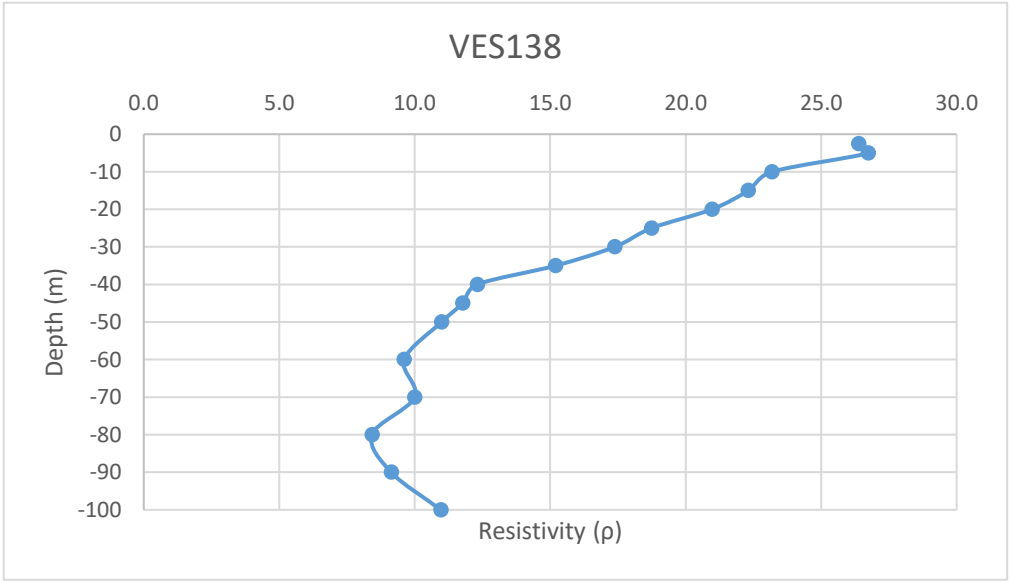

Annexure-XXII: Details of VES Survey

Date: 02/02/2025		VES-139				
Latitude	23.206417		Longitude	69.610282		
S.N	Current Electrode Spacing (AB/2)	Potential Electrode Spacing (MN)	Resistance (Ohm)	K value	Aparent Resistivity (Rho_a)	
1	2.5	1	0.713	18.846	13.437	-2.5
2	5	1	0.187	77.73975	14.537	-5
3	10	1	0.052	313.3148	16.292	-10
4	15	1	0.027	705.9398	19.060	-15
5	20	1	0.0156	1255.615	19.588	-20
6	25	1	0.01014	1962.34	19.898	-25
7	30	1	0.00653	2826.115	18.455	-30
8	35	1	0.00508	3846.94	19.542	-35
9	40	1	0.00416	5024.815	20.903	-40
10	45	1	0.00336	6359.74	21.369	-45
11	50	1	0.00256	7851.715	20.100	-50
12	60	1	0.00175	11306.81	19.787	-60
13	70	1	0.00138	15390.11	21.238	-70
14	80	1	0.001198	20101.61	24.082	-80
15	90	1	0.00101	25441.31	25.696	-90
16	100	1	0.00085	31409.21	26.698	-100
					20.043	

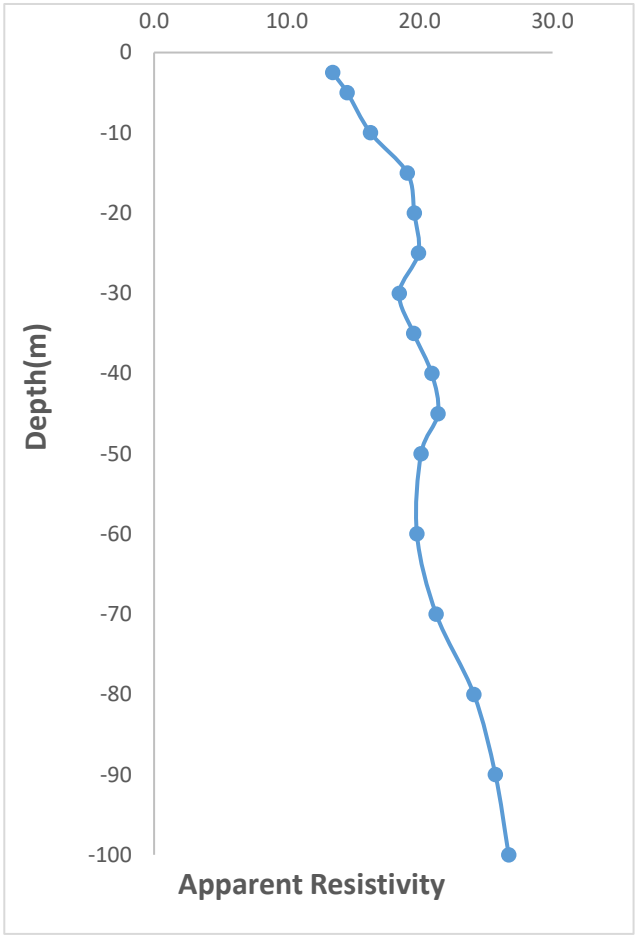

Annexure-XXII: Details of VES Survey

Date: 02/02/2025			VES-140			
Latitude	23.204875		Longitude	69.627738		
S.N	Current Electrode Spacing (AB/2)	Potential Electrode Spacing (MN)	Resistance (Ohm)	K value	Aparent Resistivity (Rho_a)	
1	2.5	1	1.58	18.846	29.777	-2.5
2	5	1	0.654	77.73975	50.842	-5
3	10	1	0.21	313.3148	65.796	-10
4	15	1	0.0947	705.9398	66.852	-15
5	20	1	0.07	1255.615	87.893	-20
6	25	1	0.0514	1962.34	100.864	-25
7	30	1	0.0306	2826.115	86.479	-30
8	35	1	0.0206	3846.94	79.247	-35
9	40	1	0.0161	5024.815	80.900	-40
10	45	1	0.0124	6359.74	78.861	-45
11	50	1	0.00982	7851.715	77.104	-50
12	60	1	0.00702	11306.81	79.374	-60
13	70	1	0.00602	15390.11	92.648	-70
14	80	1	0.00481	20101.61	96.689	-80
15	90	1	0.00387	25441.31	98.458	-90
16	100	1	0.00335	31409.21	105.221	-100
					79.813	

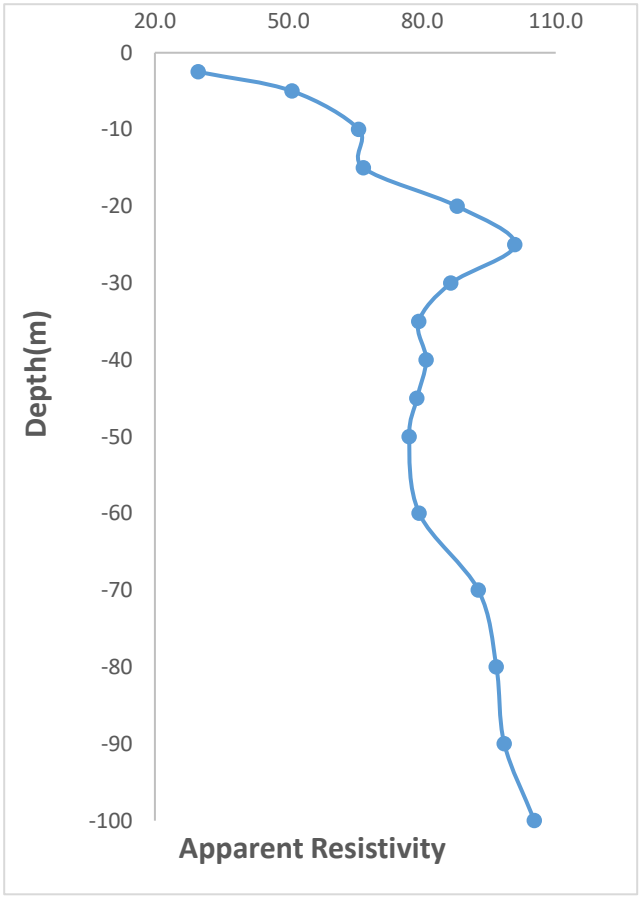

Annexure-XXII: Details of VES Survey

Date: 5/02/2025			VES-141			
Latitude	23.21483		Longitude	69.624894		
S.N	Current Electrode Spacing (AB/2)	Potential Electrode Spacing (MN)	Resistance (Ohm)	K value	Aparent Resistivity (Rho_a)	
1	2.5	1	2.4	18.846	45.230	-2.5
2	5	1	0.783	77.73975	60.870	-5
3	10	1	0.25	313.3148	78.329	-10
4	15	1	0.112	705.9398	79.065	-15
5	20	1	0.0527	1255.615	66.171	-20
6	25	1	0.0267	1962.34	52.394	-25
7	30	1	0.0138	2826.115	39.000	-30
8	35	1	0.00875	3846.94	33.661	-35
9	40	1	0.00604	5024.815	30.350	-40
10	45	1	0.0046	6359.74	29.255	-45
11	50	1	0.00345	7851.715	27.088	-50
12	60	1	0.00235	11306.81	26.571	-60
13	70	1	0.00155	15390.11	23.855	-70
14	80	1	0.0011	20101.61	22.112	-80
15	90	1	0.00095	25441.31	24.169	-90
16	100	1	0.0009	31409.21	28.268	-100

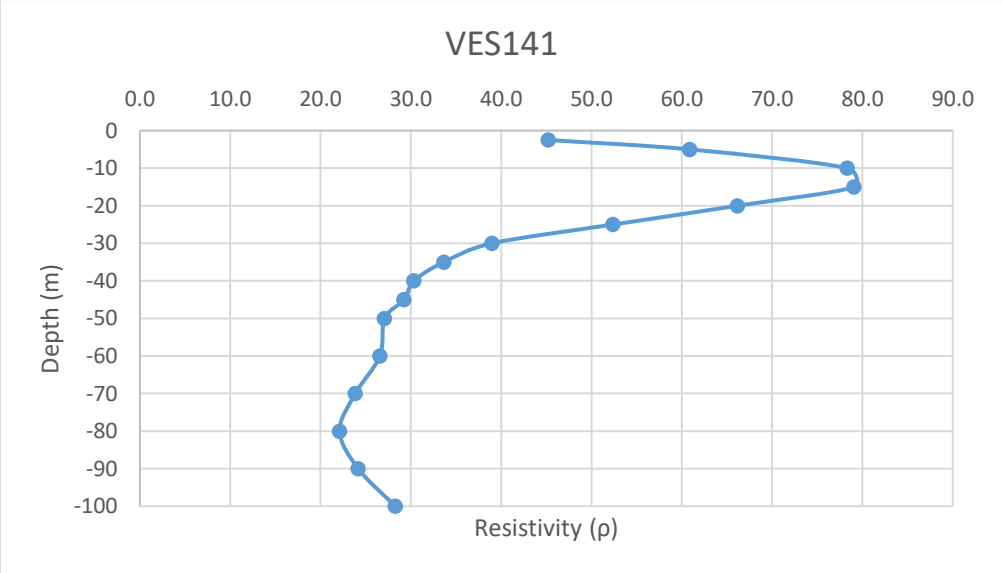

Annexure-XXII: Details of VES Survey

Date: 5/02/2025			VES-142			
Latitude	23.208429		Longitude	69.624837		
S.N	Current Electrode Spacing (AB/2)	Potential Electrode Spacing (MN)	Resistance (Ohm)	K value	Aparent Resistivity (Rho_a)	
1	2.5	1	2	18.846	37.692	-2.5
2	5	1	0.473	77.73975	36.771	-5
3	10	1	0.0927	313.3148	29.044	-10
4	15	1	0.0363	705.9398	25.626	-15
5	20	1	0.0199	1255.615	24.987	-20
6	25	1	0.0129	1962.34	25.314	-25
7	30	1	0.00865	2826.115	24.446	-30
8	35	1	0.00603	3846.94	23.197	-35
9	40	1	0.00477	5024.815	23.968	-40
10	45	1	0.00347	6359.74	22.068	-45
11	50	1	0.003	7851.715	23.555	-50
12	60	1	0.002052	11306.81	23.202	-60
13	70	1	0.0014	15390.11	21.546	-70
14	80	1	0.001018	20101.61	20.463	-80
15	90	1	0.000759	25441.31	19.310	-90
16	100	1	0.000599	31409.21	18.814	-100

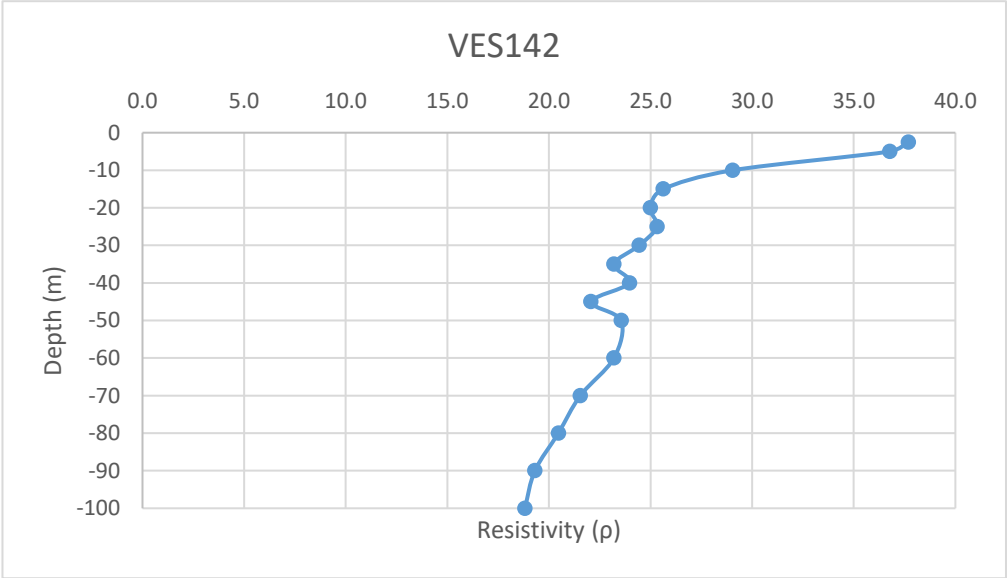

Annexure-XXII: Details of VES Survey

Date: 5/02/2025			VES-143			
Latitude	23.205897		Longitude	69.623316		
S.N	Current Electrode Spacing (AB/2)	Potential Electrode Spacing (MN)	Resistance (Ohm)	K value	Aparent Resistivity (Rho_a)	
1	2.5	1	0.882	18.846	16.622	-2.5
2	5	1	0.231	77.73975	17.958	-5
3	10	1	0.066	313.3148	20.679	-10
4	15	1	0.029	705.9398	20.472	-15
5	20	1	0.015	1255.615	18.834	-20
6	25	1	0.0092	1962.34	18.054	-25
7	30	1	0.00652	2826.115	18.426	-30
8	35	1	0.0044	3846.94	16.927	-35
9	40	1	0.0033	5024.815	16.582	-40
10	45	1	0.00257	6359.74	16.345	-45
11	50	1	0.00196	7851.715	15.389	-50
12	60	1	0.00135	11306.81	15.264	-60
13	70	1	0.00085	15390.11	13.082	-70
14	80	1	0.0006	20101.61	12.061	-80
15	90	1	0.00055	25441.31	13.993	-90
16	100	1	0.00025	31409.21	7.852	-100

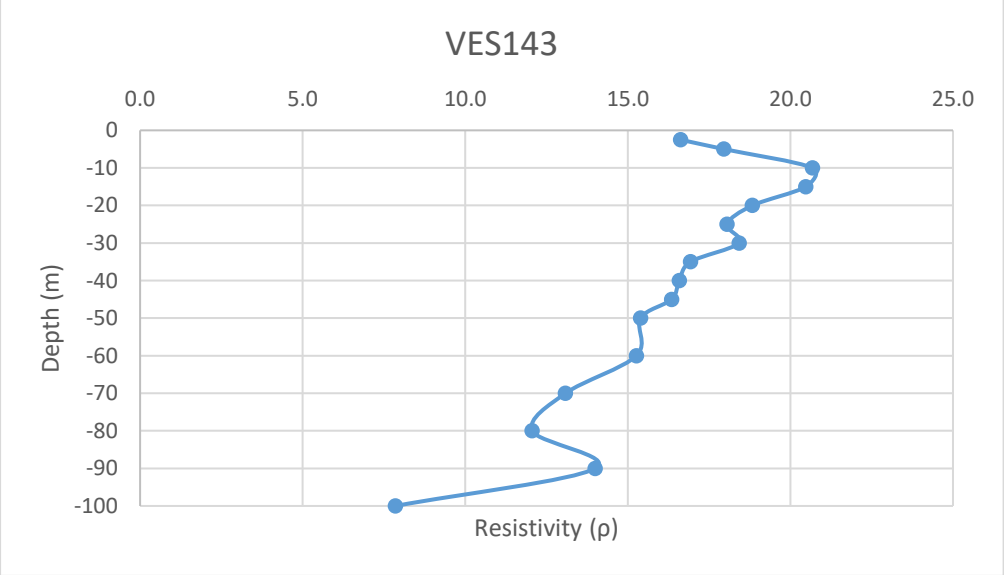

Annexure-XXII: Details of VES Survey

Date: 5/02/2025			VES-144			
Latitude	23.203001		Longitude	69.629145		
S.N	Current Electrode Spacing (AB/2)	Potential Electrode Spacing (MN)	Resistance (Ohm)	K value	Aparent Resistivity (Rho_a)	
1	2.5	1	23.7	18.846	446.650	-2.5
2	5	1	5.44	77.73975	422.904	-5
3	10	1	1.3	313.3148	407.309	-10
4	15	1	0.468	705.9398	330.380	-15
5	20	1	0.185	1255.615	232.289	-20
6	25	1	0.107	1962.34	209.970	-25
7	30	1	0.0636	2826.115	179.741	-30
8	35	1	0.0486	3846.94	186.961	-35
9	40	1	0.0298	5024.815	149.739	-40
10	45	1	0.0233	6359.74	148.182	-45
11	50	1	0.0213	7851.715	167.242	-50
12	60	1	0.0175	11306.81	197.869	-60
13	70	1	0.0127	15390.11	195.454	-70
14	80	1	0.00538	20101.61	108.147	-80
15	90	1	0.00244	25441.31	62.077	-90
16	100	1	0.002	31409.21	62.818	-100

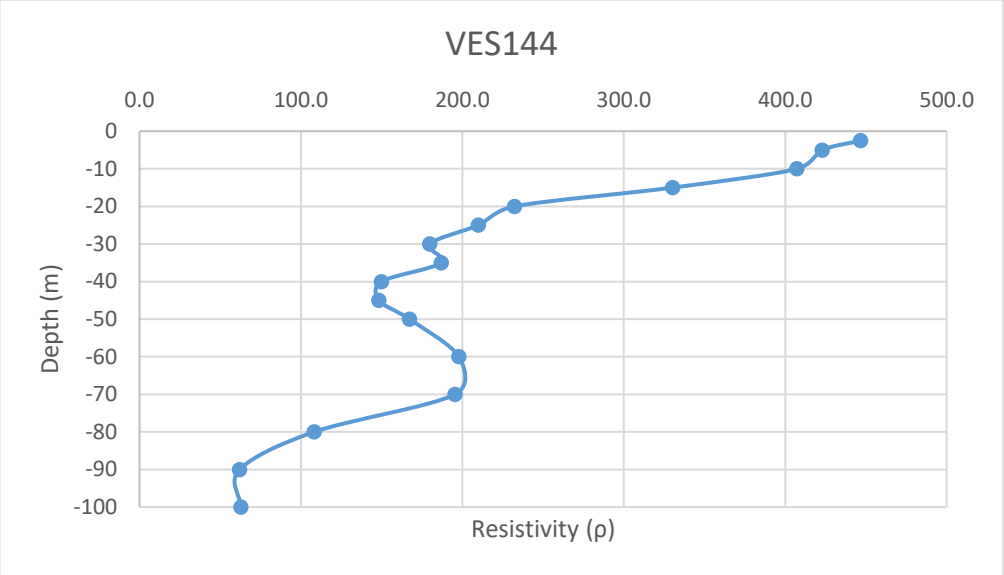

Annexure-XXII: Details of VES Survey

Date: 09/02/2025			VES-145			
Latitude	23.19858822		Longitude	69.63224144		
S.N	Current Electrode Spacing (AB/2)	Potential Electrode Spacing (MN)	Resistance (Ohm)	K value	Aparent Resistivity (Rho_a)	
1	2.5	1	2.26	18.846	42.592	-2.5
2	5	1	0.466	77.73975	36.227	-5
3	10	1	0.0625	313.3148	19.582	-10
4	15	1	0.0165	705.9398	11.648	-15
5	20	1	0.0064	1255.615	8.036	-20
6	25	1	0.00345	1962.34	6.770	-25
7	30	1	0.0019	2826.115	5.370	-30
8	35	1	0.0013	3846.94	5.001	-35
9	40	1	0.00095	5024.815	4.774	-40
10	45	1	0.0007	6359.74	4.452	-45
11	50	1	0.0006	7851.715	4.711	-50
12	60	1	0.0004	11306.81	4.523	-60
13	70	1	0.00025	15390.11	3.848	-70
14	80	1	0.0002	20101.61	4.020	-80
15	90	1	0.0001	25441.31	2.544	-90
16	100	1	0.00011	31409.21	3.455	-100

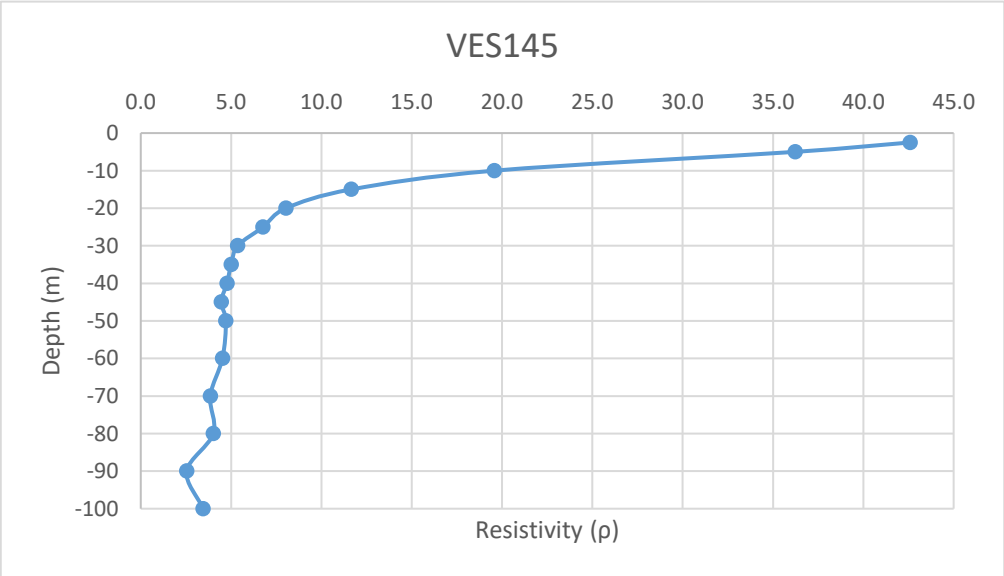

Annexure-XXII: Details of VES Survey

Date: 09/02/2025			VES-146			
Latitude	23.20237107		Longitude	69.63202611		
S.N	Current Electrode Spacing (AB/2)	Potential Electrode Spacing (MN)	Resistance (Ohm)	K value	Aparent Resistivity (Rho_a)	
1	2.5	1	8.25	18.846	155.480	-2.5
2	5	1	2.86	77.73975	222.336	-5
3	10	1	0.829	313.3148	259.738	-10
4	15	1	0.338	705.9398	238.608	-15
5	20	1	0.158	1255.615	198.387	-20
6	25	1	0.0822	1962.34	161.304	-25
7	30	1	0.0468	2826.115	132.262	-30
8	35	1	0.0288	3846.94	110.792	-35
9	40	1	0.0153	5024.815	76.880	-40
10	45	1	0.01009	6359.74	64.170	-45
11	50	1	0.00807	7851.715	63.363	-50
12	60	1	0.00454	11306.81	51.333	-60
13	70	1	0.00201	15390.11	30.934	-70
14	80	1	0.00252	20101.61	50.656	-80
15	90	1	0.00151	25441.31	38.416	-90
16	100	1	0.0005	31409.21	15.705	-100

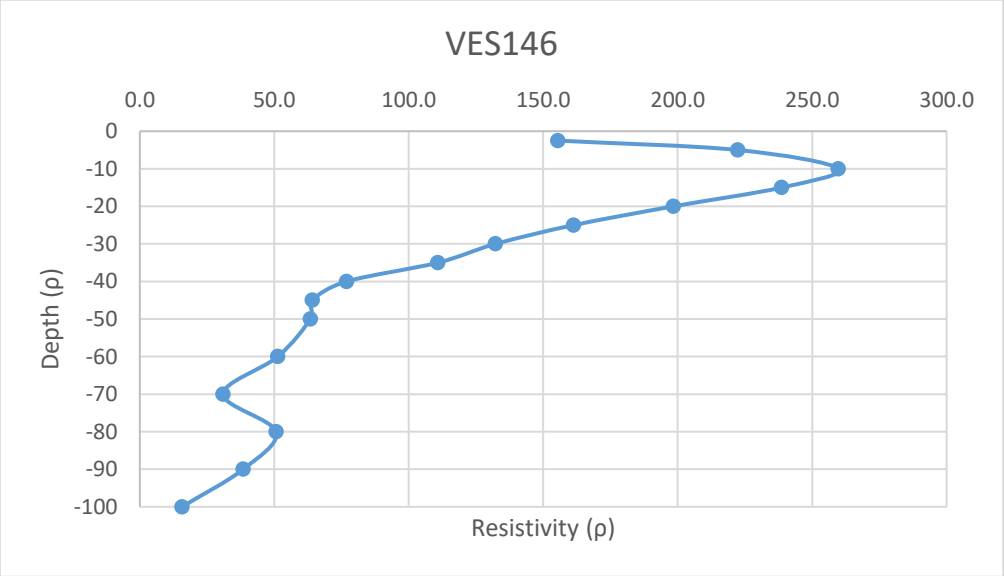

Annexure-XXII: Details of VES Survey

Date: 09/02/2025			VES-147			
Latitude	23.18997		Longitude	69.550302		
S.N	Current Electrode Spacing (AB/2)	Potential Electrode Spacing (MN)	Resistance (Ohm)	K value	Aparent Resistivity (Rho_a)	
1	2.5	1	13.4	18.846	252.536	-2.5
2	5	1	1.7	77.73975	132.158	-5
3	10	1	0.259	313.3148	81.149	-10
4	15	1	0.1	705.9398	70.594	-15
5	20	1	0.0535	1255.615	67.175	-20
6	25	1	0.0322	1962.34	63.187	-25
7	30	1	0.0198	2826.115	55.957	-30
8	35	1	0.0128	3846.94	49.241	-35
9	40	1	0.00904	5024.815	45.424	-40
10	45	1	0.00628	6359.74	39.939	-45
11	50	1	0.00452	7851.715	35.490	-50
12	60	1	0.00251	11306.81	28.380	-60
13	70	1	0.0015	15390.11	23.085	-70
14	80	1	0.00075	20101.61	15.076	-80
15	90	1	0.0005	25441.31	12.721	-90
16	100	1	0.0001	31409.21	3.141	-100

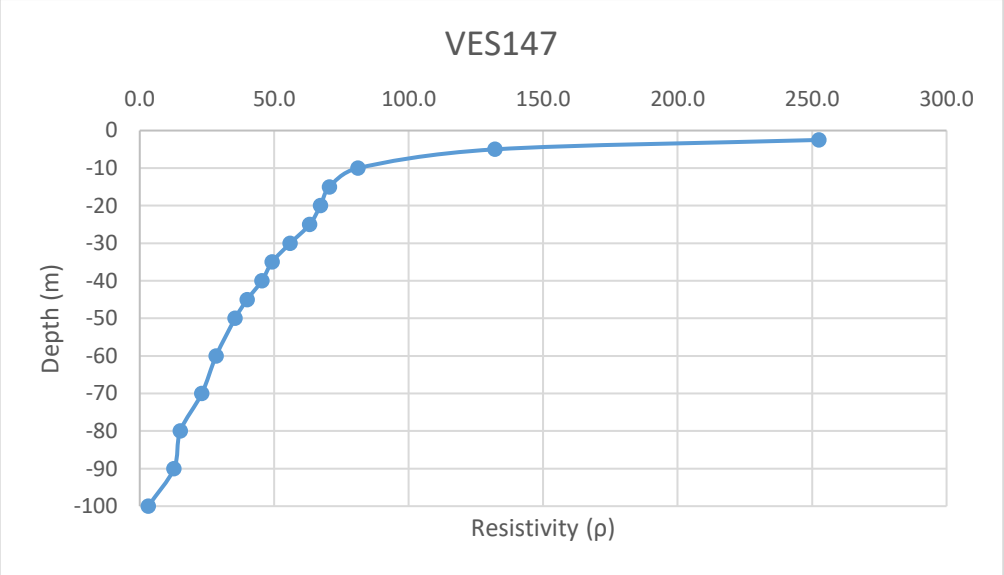

Annexure-XXII: Details of VES Survey

Date: 09/02/2025			VES-148			
Latitude	23.196402		Longitude	69.55389		
S.N	Current Electrode Spacing (AB/2)	Potential Electrode Spacing (MN)	Resistance (Ohm)	K value	Aparent Resistivity (Rho_a)	
1	2.5	1	3.88	18.846	73.122	-2.5
2	5	1	1.98	77.73975	153.925	-5
3	10	1	0.498	313.3148	156.031	-10
4	15	1	0.21	705.9398	148.247	-15
5	20	1	0.121	1255.615	151.929	-20
6	25	1	0.0737	1962.34	144.624	-25
7	30	1	0.0404	2826.115	114.175	-30
8	35	1	0.0303	3846.94	116.562	-35
9	40	1	0.0207	5024.815	104.014	-40
10	45	1	0.0141	6359.74	89.672	-45
11	50	1	0.01109	7851.715	87.076	-50
12	60	1	0.00706	11306.81	79.826	-60
13	70	1	0.00403	15390.11	62.022	-70
14	80	1	0.00302	20101.61	60.707	-80
15	90	1	0.00252	25441.31	64.112	-90
16	100	1	0.00136	31409.21	42.717	-100

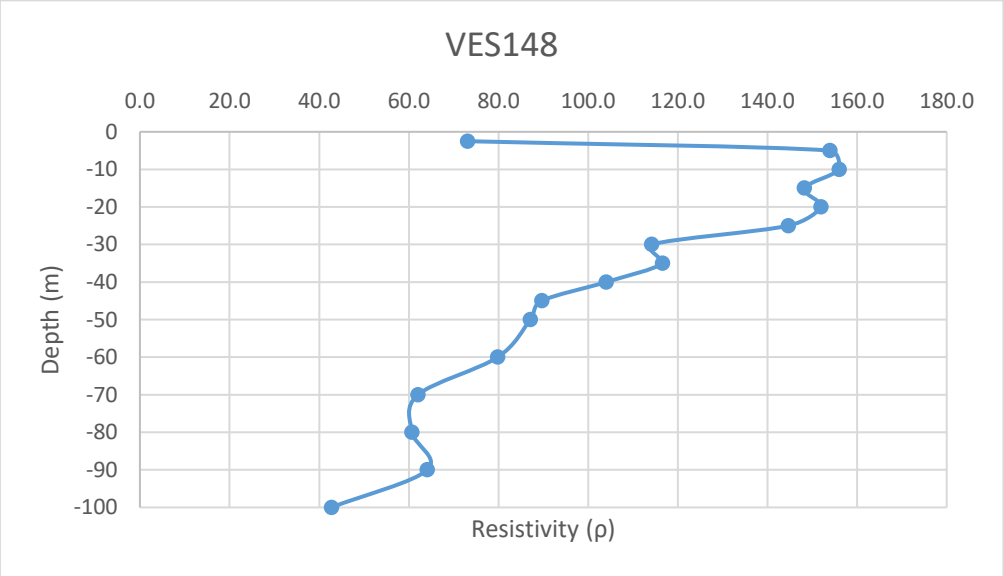

Annexure-XXII: Details of VES Survey

Date: 11/02/2025			VES-149			
Latitude	23.19693088		Longitude	69.52718766		
S.N	Current Electrode Spacing (AB/2)	Potential Electrode Spacing (MN)	Resistance (Ohm)	K value	Aparent Resistivity (Rho_a)	
1	2.5	1	25	18.846	471.150	-2.5
2	5	1	7.93	77.73975	616.476	-5
3	10	1	2.02	313.3148	632.896	-10
4	15	1	0.808	705.9398	570.399	-15
5	20	1	0.403	1255.615	506.013	-20
6	25	1	0.229	1962.34	449.376	-25
7	30	1	0.146	2826.115	412.613	-30
8	35	1	0.0974	3846.94	374.692	-35
9	40	1	0.0717	5024.815	360.279	-40
10	45	1	0.0546	6359.74	347.242	-45
11	50	1	0.0427	7851.715	335.268	-50
12	60	1	0.0273	11306.81	308.676	-60
13	70	1	0.0222	15390.11	341.661	-70
14	80	1	0.0162	20101.61	325.646	-80
15	90	1	0.0145	25441.31	368.899	-90
16	100	1	0.0123	31409.21	386.333	-100

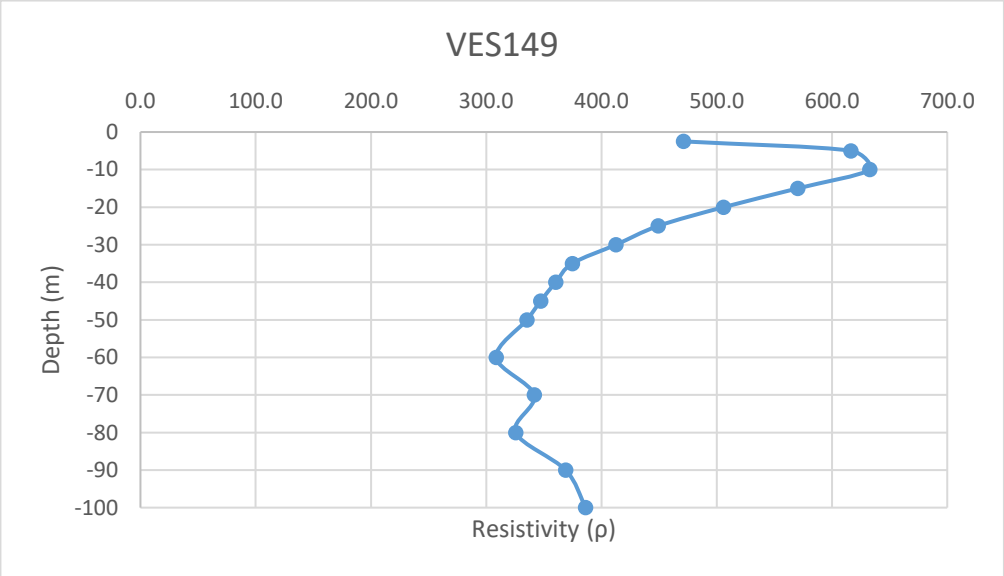

Annexure-XXII: Details of VES Survey

Date: 11/02/2025			VES-150			
Latitude	23.20115959		Longitude	69.5284314		
S.N	Current Electrode Spacing (AB/2)	Potential Electrode Spacing (MN)	Resistance (Ohm)	K value	Aparent Resistivity (Rho_a)	
1	2.5	1	14.1	18.846	265.729	-2.5
2	5	1	5.05	77.73975	392.586	-5
3	10	1	1.48	313.3148	463.706	-10
4	15	1	1.11	705.9398	783.593	-15
5	20	1	0.371	1255.615	465.833	-20
6	25	1	0.195	1962.34	382.656	-25
7	30	1	0.118	2826.115	333.482	-30
8	35	1	0.0757	3846.94	291.213	-35
9	40	1	0.0529	5024.815	265.813	-40
10	45	1	0.0342	6359.74	217.503	-45
11	50	1	0.0231	7851.715	181.375	-50
12	60	1	0.0111	11306.81	125.506	-60
13	70	1	0.00768	15390.11	118.196	-70
14	80	1	0.00341	20101.61	68.547	-80
15	90	1	0.00256	25441.31	65.130	-90
16	100	1	0.00231	31409.21	72.555	-100

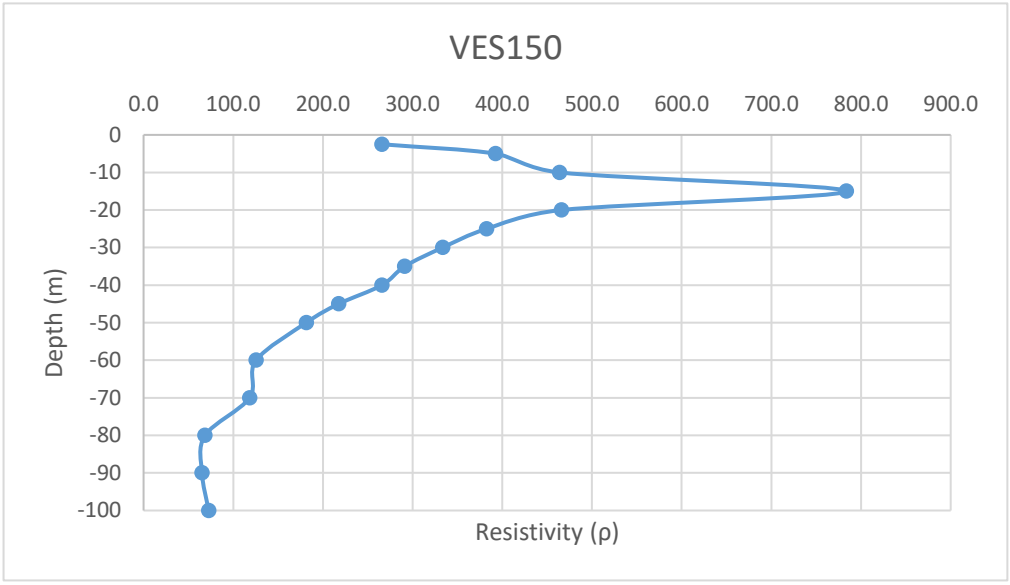

Annexure-XXII: Details of VES Survey

Date: 11/02/2025		VES-151				
Latitude	23.19972041		Longitude	69.51790638		
S.N	Current Electrode Spacing (AB/2)	Potential Electrode Spacing (MN)	Resistance (Ohm)	K value	Aparent Resistivity (Rho_a)	
1	2.5	1	24.4	18.846	459.842	-2.5
2	5	1	3.46	77.73975	268.980	-5
3	10	1	0.389	313.3148	121.879	-10
4	15	1	0.124	705.9398	87.537	-15
5	20	1	0.0811	1255.615	101.830	-20
6	25	1	0.0675	1962.34	132.458	-25
7	30	1	0.0572	2826.115	161.654	-30
8	35	1	0.0529	3846.94	203.503	-35
9	40	1	0.0348	5024.815	174.864	-40
10	45	1	0.0316	6359.74	200.968	-45
11	50	1	0.0231	7851.715	181.375	-50
12	60	1	0.0111	11306.81	125.506	-60
13	70	1	0.01087	15390.11	167.291	-70
14	80	1	0.00597	20101.61	120.007	-80
15	90	1	0.00512	25441.31	130.260	-90
16	100	1	0.00302	31409.21	94.856	-100

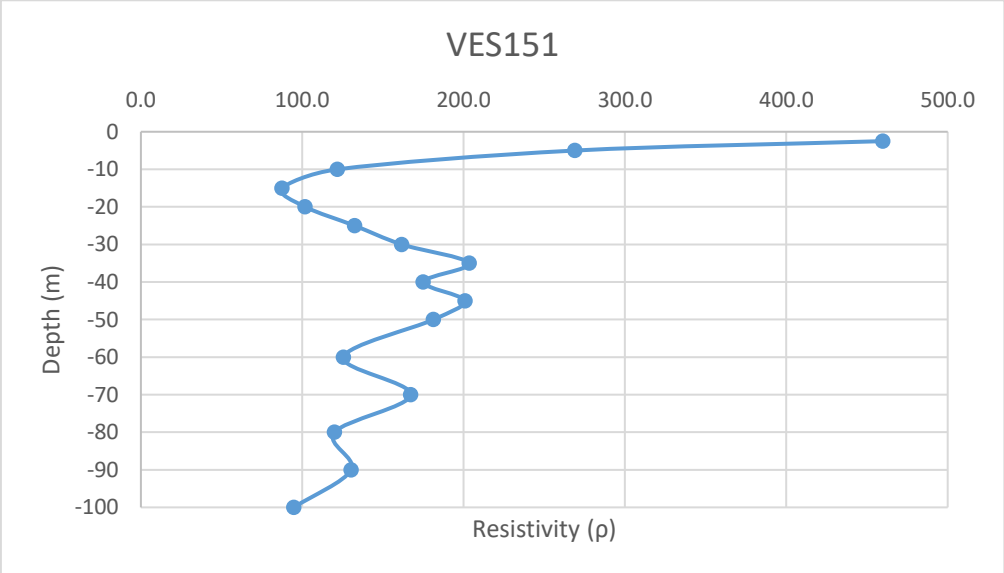

Annexure-XXII: Details of VES Survey

Date: 12/02/2025			VES-152			
Latitude	23.20311416		Longitude	69.5263199		
S.N	Current Electrode Spacing (AB/2)	Potential Electrode Spacing (MN)	Resistance (Ohm)	K value	Aparent Resistivity (Rho_a)	
1	2.5	1	19.8	18.846	373.151	-2.5
2	5	1	2.81	77.73975	218.449	-5
3	10	1	0.631	313.3148	197.702	-10
4	15	1	0.239	705.9398	168.720	-15
5	20	1	0.128	1255.615	160.719	-20
6	25	1	0.0767	1962.34	150.511	-25
7	30	1	0.0484	2826.115	136.784	-30
8	35	1	0.0333	3846.94	128.103	-35
9	40	1	0.0435	5024.815	218.579	-40
10	45	1	0.0179	6359.74	113.839	-45
11	50	1	0.0171	7851.715	134.264	-50
12	60	1	0.0111	11306.81	125.506	-60
13	70	1	0.00683	15390.11	105.114	-70
14	80	1	0.00597	20101.61	120.007	-80
15	90	1	0.00768	25441.31	195.389	-90
16	100	1	0.00426	31409.21	133.803	-100

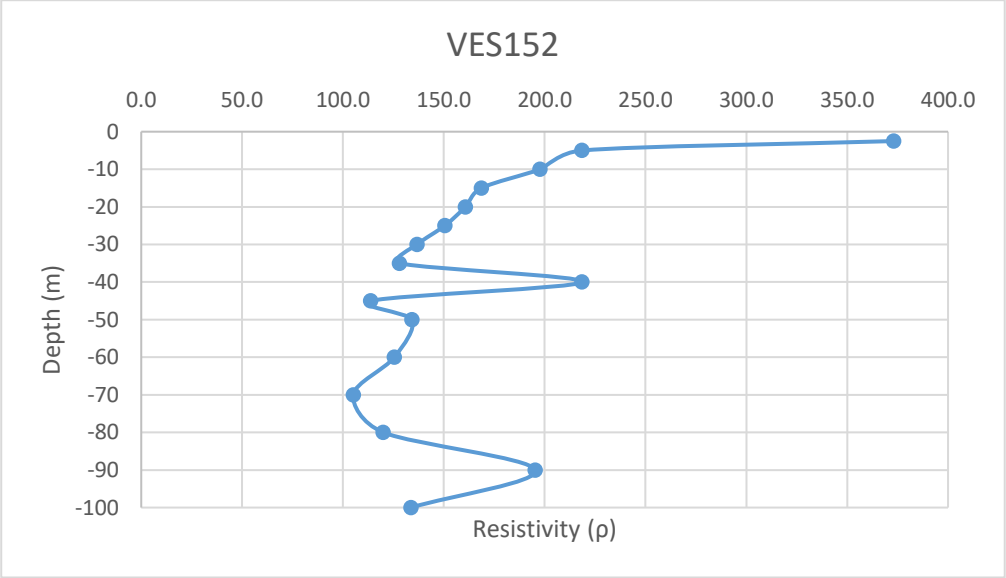

Annexure-XXII: Details of VES Survey

Date: 12/02/2025			VES-153			
Latitude	23.20117158		Longitude	69.52125169		
S.N	Current Electrode Spacing (AB/2)	Potential Electrode Spacing (MN)	Resistance (Ohm)	K value	Aparent Resistivity (Rho_a)	
1	2.5	1	6.23	18.846	117.411	-2.5
2	5	1	1.39	77.73975	108.058	-5
3	10	1	0.384	313.3148	120.313	-10
4	15	1	0.149	705.9398	105.185	-15
5	20	1	0.0767	1255.615	96.306	-20
6	25	1	0.0456	1962.34	89.483	-25
7	30	1	0.0266	2826.115	75.175	-30
8	35	1	0.0196	3846.94	75.400	-35
9	40	1	0.0145	5024.815	72.860	-40
10	45	1	0.0128	6359.74	81.405	-45
11	50	1	0.00768	7851.715	60.301	-50
12	60	1	0.00597	11306.81	67.502	-60
13	70	1	0.00426	15390.11	65.562	-70
14	80	1	0.00419	20101.61	84.226	-80
15	90	1	0.0017	25441.31	43.250	-90
16	100	1	0.00085	31409.21	26.698	-100

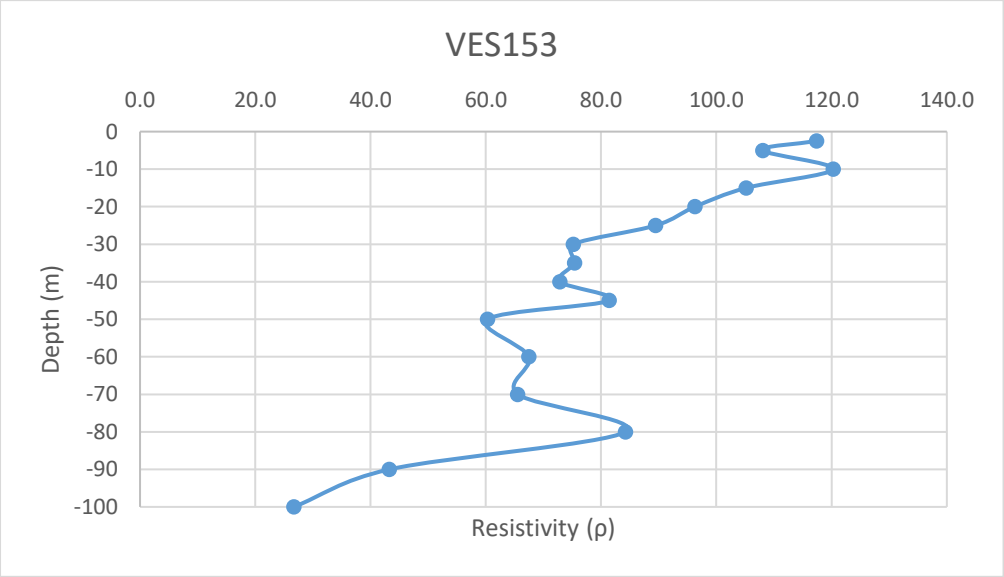

Annexure-XXII: Details of VES Survey

Date: 12/02/2025			VES-154			
Latitude	23.19379326		Longitude	69.50798694		
S.N	Current Electrode Spacing (AB/2)	Potential Electrode Spacing (MN)	Resistance (Ohm)	K value	Aparent Resistivity (Rho_a)	
1	2.5	1	3.07	18.846	57.857	-2.5
2	5	1	0.86	77.73975	66.856	-5
3	10	1	0.279	313.3148	87.415	-10
4	15	1	0.123	705.9398	86.831	-15
5	20	1	0.0665	1255.615	83.498	-20
6	25	1	0.0418	1962.34	82.026	-25
7	30	1	0.0265	2826.115	74.892	-30
8	35	1	0.0179	3846.94	68.860	-35
9	40	1	0.0128	5024.815	64.318	-40
10	45	1	0.01195	6359.74	75.999	-45
11	50	1	0.00768	7851.715	60.301	-50
12	60	1	0.00683	11306.81	77.226	-60
13	70	1	0.00426	15390.11	65.562	-70
14	80	1	0.00341	20101.61	68.547	-80
15	90	1	0.0017	25441.31	43.250	-90
16	100	1	0.00256	31409.21	80.408	-100

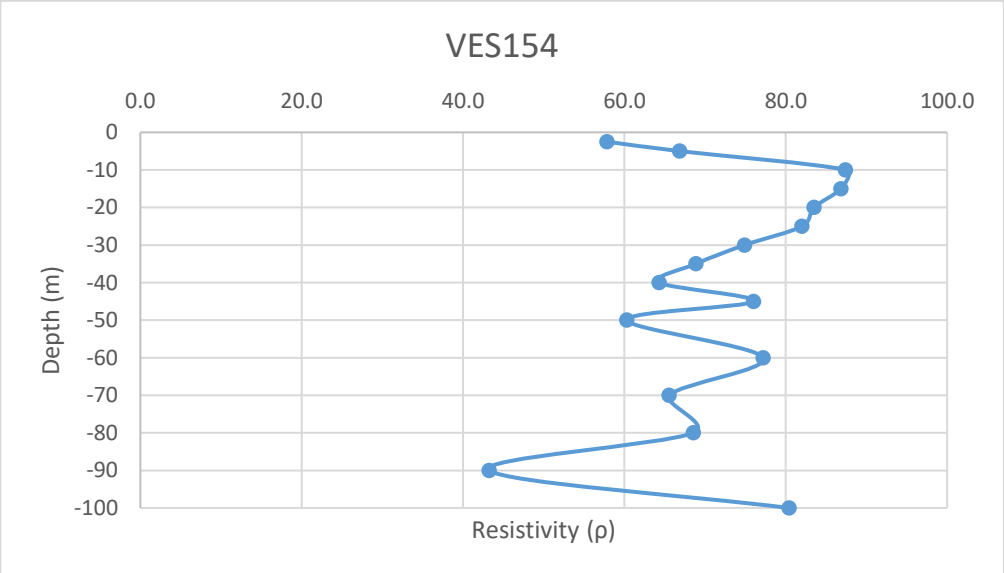

Annexure-XXII: Details of VES Survey

Date: 14/02/2025			VES-155			
Latitude	23.209098		Longitude	69.508466		
S.N	Current Electrode Spacing (AB/2)	Potential Electrode Spacing (MN)	Resistance (Ohm)	K value	Aparent Resistivity (Rho_a)	
1	2.5	1	6.96	18.846	131.168	-2.5
2	5	1	2.41	77.73975	187.353	-5
3	10	1	0.742	313.3148	232.480	-10
4	15	1	0.315	705.9398	222.371	-15
5	20	1	0.167	1255.615	209.688	-20
6	25	1	0.113	1962.34	221.744	-25
7	30	1	0.0787	2826.115	222.415	-30
8	35	1	0.0572	3846.94	220.045	-35
9	40	1	0.0427	5024.815	214.560	-40
10	45	1	0.0367	6359.74	233.402	-45
11	50	1	0.0299	7851.715	234.766	-50
12	60	1	0.0196	11306.81	221.614	-60
13	70	1	0.0128	15390.11	196.993	-70
14	80	1	0.00987	20101.61	198.403	-80
15	90	1	0.00683	25441.31	173.764	-90
16	100	1	0.00426	31409.21	133.803	-100

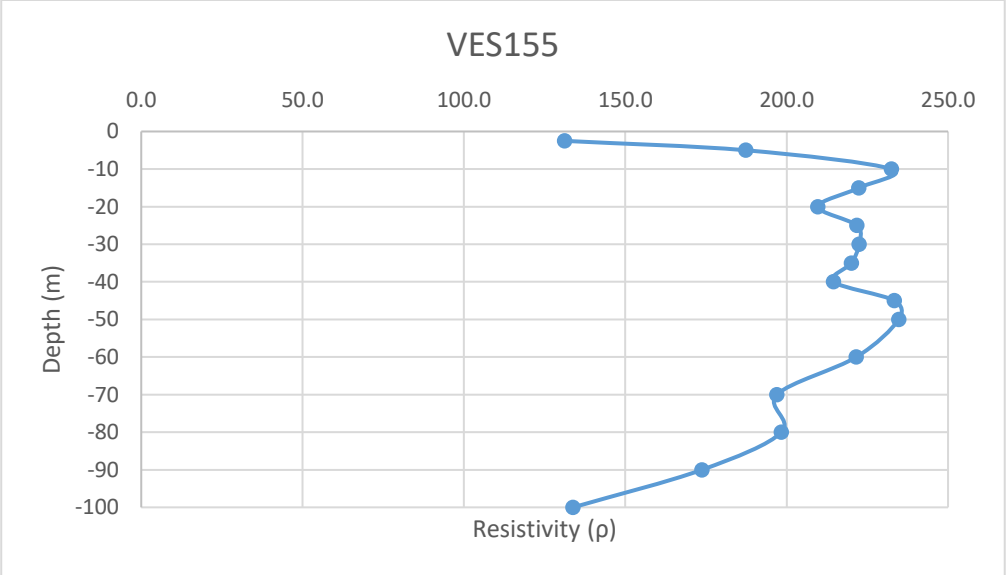

Annexure-XXII: Details of VES Survey

Date: 14/02/2025			VES-156			
Latitude	23.211035		Longitude	69.509153		
S.N	Current Electrode Spacing (AB/2)	Potential Electrode Spacing (MN)	Resistance (Ohm)	K value	Aparent Resistivity (Rho_a)	
1	2.5	1	1.41	18.846	26.573	-2.5
2	5	1	0.342	77.73975	26.587	-5
3	10	1	0.0916	313.3148	28.700	-10
4	15	1	0.041	705.9398	28.944	-15
5	20	1	0.0265	1255.615	33.274	-20
6	25	1	0.0205	1962.34	40.228	-25
7	30	1	0.0137	2826.115	38.718	-30
8	35	1	0.00939	3846.94	36.123	-35
9	40	1	0.00683	5024.815	34.319	-40
10	45	1	0.00512	6359.74	32.562	-45
11	50	1	0.00426	7851.715	33.448	-50
12	60	1	0.00256	11306.81	28.945	-60
13	70	1	0.00185	15390.11	28.472	-70
14	80	1	0.00151	20101.61	30.353	-80
15	90	1	0.0005	25441.31	12.721	-90
16	100	1	0.0004	31409.21	12.564	-100

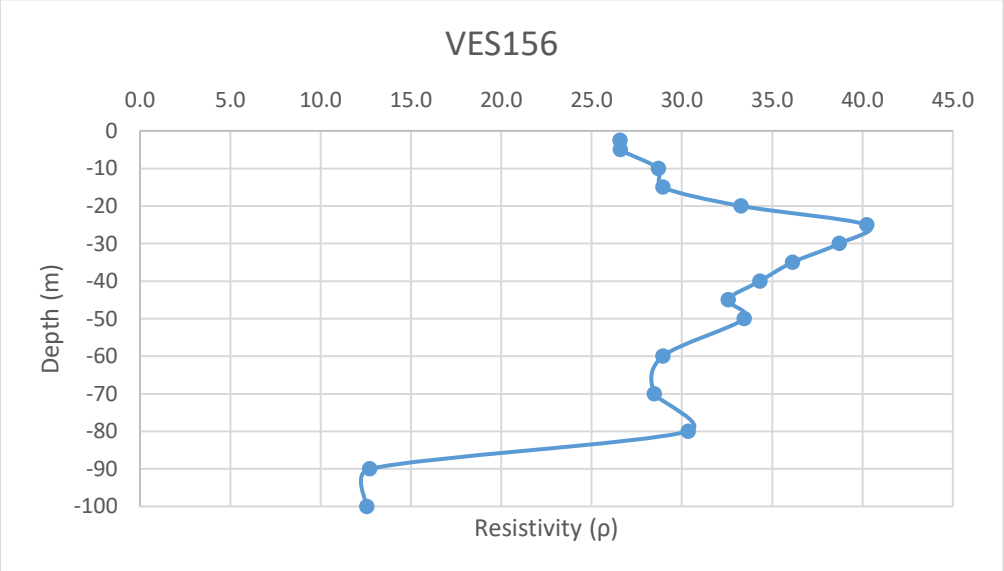

Annexure-XXII: Details of VES Survey

Date: 14/02/2025			VES-157			
Latitude	23.208086		Longitude	69.510714		
S.N	Current Electrode Spacing (AB/2)	Potential Electrode Spacing (MN)	Resistance (Ohm)	K value	Aparent Resistivity (Rho_a)	
1	2.5	1	20.8	18.846	391.997	-2.5
2	5	1	1.3	77.73975	101.062	-5
3	10	1	0.0837	313.3148	26.224	-10
4	15	1	0.0399	705.9398	28.167	-15
5	20	1	0.0242	1255.615	30.386	-20
6	25	1	0.0222	1962.34	43.564	-25
7	30	1	0.0137	2826.115	38.718	-30
8	35	1	0.00939	3846.94	36.123	-35
9	40	1	0.00853	5024.815	42.862	-40
10	45	1	0.00683	6359.74	43.437	-45
11	50	1	0.00512	7851.715	40.201	-50
12	60	1	0.00419	11306.81	47.376	-60
13	70	1	0.00303	15390.11	46.632	-70
14	80	1	0.00149	20101.61	29.951	-80
15	90	1	0.0011	25441.31	27.985	-90
16	100	1	0.0008	31409.21	25.127	-100

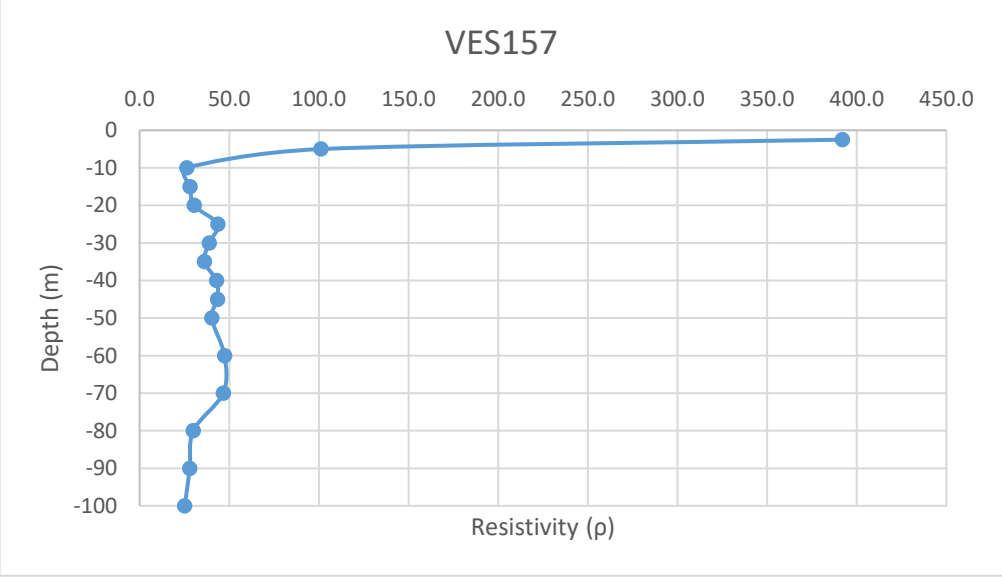

Annexure-XXII: Details of VES Survey

Date: 16/02/2025			VES-158			
Latitude	23.2014272		Longitude	69.51262903		
S.N	Current Electrode Spacing (AB/2)	Potential Electrode Spacing (MN)	Resistance (Ohm)	K value	Aparent Resistivity (Rho_a)	
1	2.5	1	14.5	18.846	273.267	-2.5
2	5	1	4.67	77.73975	363.045	-5
3	10	1	0.769	313.3148	240.939	-10
4	15	1	0.196	705.9398	138.364	-15
5	20	1	0.0806	1255.615	101.203	-20
6	25	1	0.0479	1962.34	93.996	-25
7	30	1	0.0332	2826.115	93.827	-30
8	35	1	0.0273	3846.94	105.021	-35
9	40	1	0.0222	5024.815	111.551	-40
10	45	1	0.0196	6359.74	124.651	-45
11	50	1	0.0145	7851.715	113.850	-50
12	60	1	0.0137	11306.81	154.903	-60
13	70	1	0.0111	15390.11	170.830	-70
14	80	1	0.01024	20101.61	205.841	-80
15	90	1	0.00768	25441.31	195.389	-90
16	100	1	0.00597	31409.21	187.513	-100

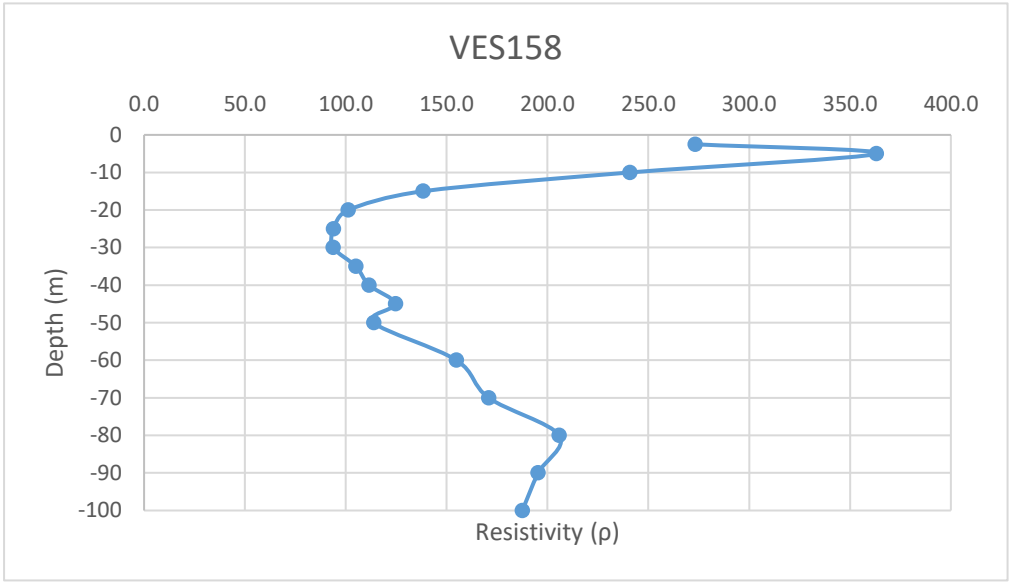

Annexure-XXII: Details of VES Survey

Date: 16/02/2025			VES-159			
Latitude	23.20272306		Longitude	69.51447288		
S.N	Current Electrode Spacing (AB/2)	Potential Electrode Spacing (MN)	Resistance (Ohm)	K value	Aparent Resistivity (Rho_a)	
1	2.5	1	5.7	18.846	107.422	-2.5
2	5	1	0.881	77.73975	68.489	-5
3	10	1	0.125	313.3148	39.164	-10
4	15	1	0.0418	705.9398	29.508	-15
5	20	1	0.0231	1255.615	29.005	-20
6	25	1	0.0171	1962.34	33.556	-25
7	30	1	0.0128	2826.115	36.174	-30
8	35	1	0.00939	3846.94	36.123	-35
9	40	1	0.00683	5024.815	34.319	-40
10	45	1	0.00512	6359.74	32.562	-45
11	50	1	0.00426	7851.715	33.448	-50
12	60	1	0.00256	11306.81	28.945	-60
13	70	1	0.00176	15390.11	27.087	-70
14	80	1	0.00256	20101.61	51.460	-80
15	90	1	0.0017	25441.31	43.250	-90
16	100	1	0.00256	31409.21	80.408	-100

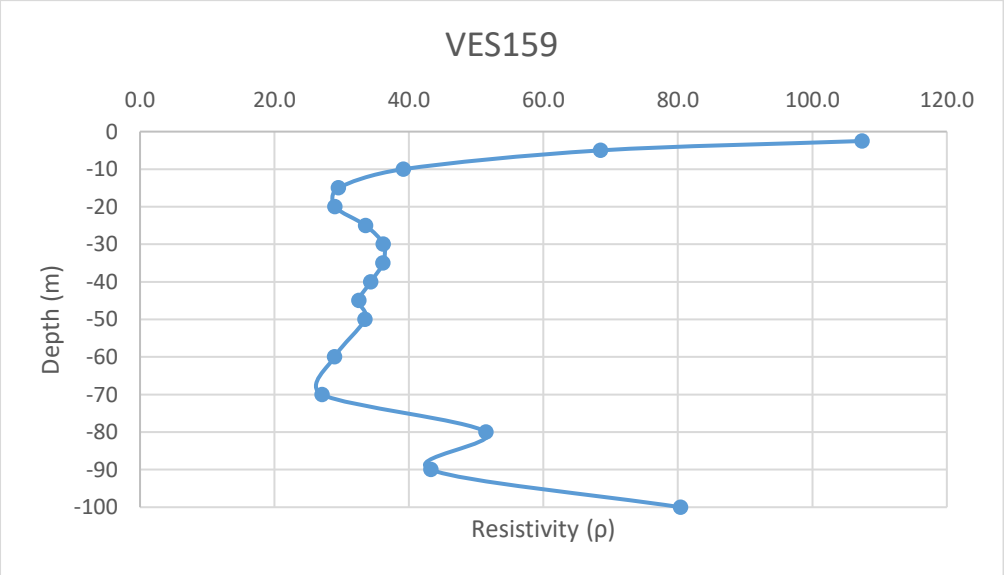

Annexure-XXII: Details of VES Survey

Date: 16/02/2025			VES-160			
Latitude	23.20220715		Longitude	69.51787164		
S.N	Current Electrode Spacing (AB/2)	Potential Electrode Spacing (MN)	Resistance (Ohm)	K value	Aparent Resistivity (Rho_a)	
1	2.5	1	4.31	18.846	81.226	-2.5
2	5	1	1.61	77.73975	125.161	-5
3	10	1	0.198	313.3148	62.036	-10
4	15	1	0.0637	705.9398	44.968	-15
5	20	1	0.0222	1255.615	27.875	-20
6	25	1	0.0111	1962.34	21.782	-25
7	30	1	0.00768	2826.115	21.705	-30
8	35	1	0.00341	3846.94	13.118	-35
9	40	1	0.00426	5024.815	21.406	-40
10	45	1	0.00341	6359.74	21.687	-45
11	50	1	0.0017	7851.715	13.348	-50
12	60	1	0.00085	11306.81	9.611	-60
13	70	1	0.0008	15390.11	12.312	-70
14	80	1	0.00085	20101.61	17.086	-80
15	90	1	0.001	25441.31	25.441	-90
16	100	1	0.0009	31409.21	28.268	-100

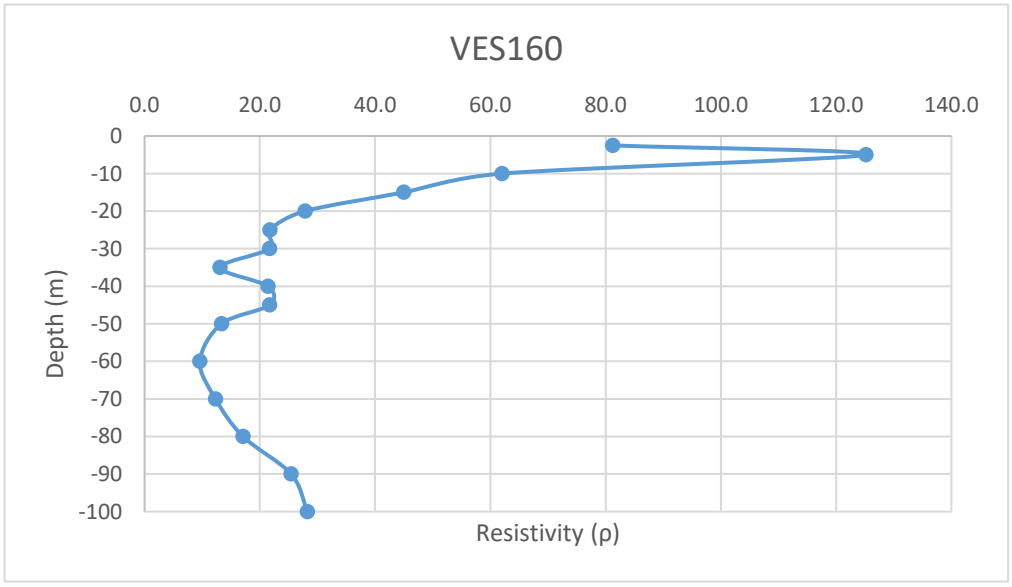

Annexure-XXII: Details of VES Survey

Date: 16/02/2025			VES-161			
Latitude	23.1954137		Longitude	69.50248273		
S.N	Current Electrode Spacing (AB/2)	Potential Electrode Spacing (MN)	Resistance (Ohm)	K value	Aparent Resistivity (Rho_a)	
1	2.5	1	9.62	18.846	181.299	-2.5
2	5	1	2.49	77.73975	193.572	-5
3	10	1	0.561	313.3148	175.770	-10
4	15	1	0.237	705.9398	167.308	-15
5	20	1	0.103	1255.615	129.328	-20
6	25	1	0.0605	1962.34	118.722	-25
7	30	1	0.0394	2826.115	111.349	-30
8	35	1	0.0409	3846.94	157.340	-35
9	40	1	0.0293	5024.815	147.227	-40
10	45	1	0.0489	6359.74	310.991	-45
11	50	1	0.0267	7851.715	209.641	-50
12	60	1	0.0217	11306.81	245.358	-60
13	70	1	0.01691	15390.11	260.247	-70
14	80	1	0.0148	20101.61	297.504	-80
15	90	1	0.0116	25441.31	295.119	-90
16	100	1	0.0083	31409.21	260.696	-100

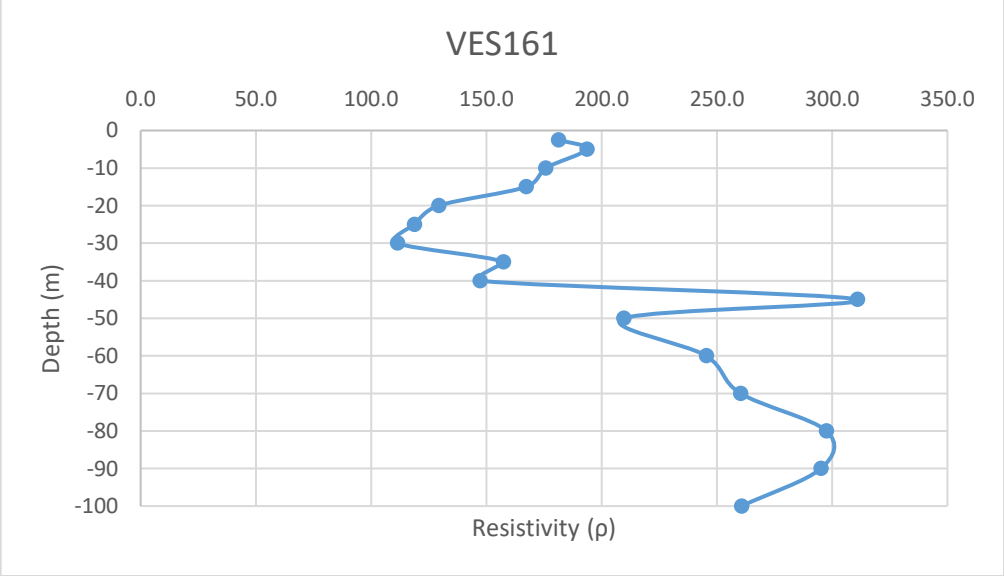

Annexure-XXII: Details of VES Survey

Date: 17/02/2025			VES-162			
Latitude	23.1954137		Longitude	69.50248273		
S.N	Current Electrode Spacing (AB/2)	Potential Electrode Spacing (MN)	Resistance (Ohm)	K value	Aparent Resistivity (Rho_a)	
1	2.5	1	5.44	18.846	102.522	-2.5
2	5	1	1.145	77.73975	89.012	-5
3	10	1	0.302	313.3148	94.621	-10
4	15	1	0.147	705.9398	103.773	-15
5	20	1	0.0883	1255.615	110.871	-20
6	25	1	0.0565	1962.34	110.872	-25
7	30	1	0.0388	2826.115	109.653	-30
8	35	1	0.0267	3846.94	102.713	-35
9	40	1	0.0202	5024.815	101.501	-40
10	45	1	0.0156	6359.74	99.212	-45
11	50	1	0.0126	7851.715	98.932	-50
12	60	1	0.00857	11306.81	96.899	-60
13	70	1	0.00655	15390.11	100.805	-70
14	80	1	0.00504	20101.61	101.312	-80
15	90	1	0.00403	25441.31	102.528	-90
16	100	1	0.00313	31409.21	98.311	-100

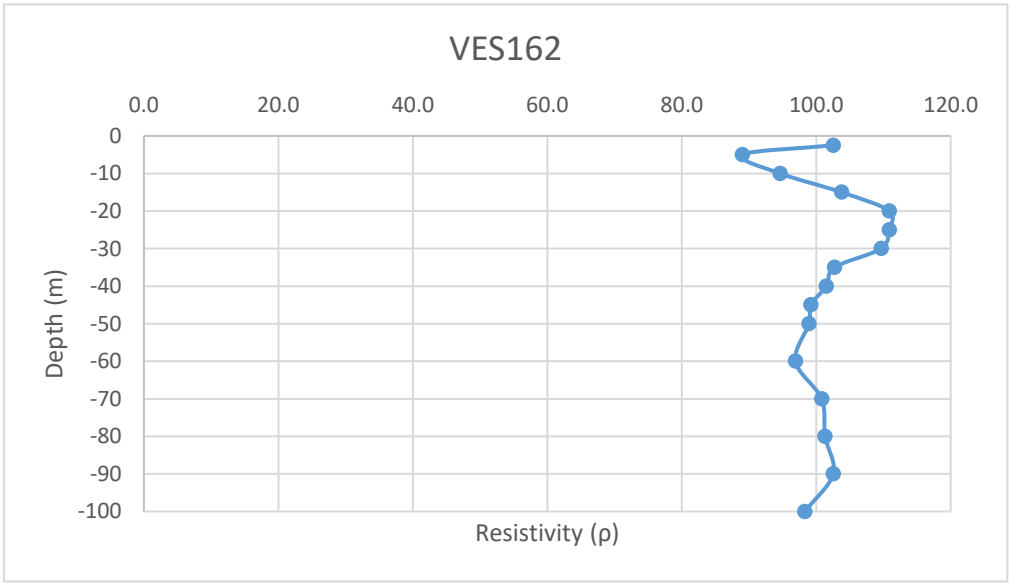

Annexure-XXII: Details of VES Survey

Date: 17/02/2025			VES-163			
Latitude	23.21766313		Longitude	69.53862282		
S.N	Current Electrode Spacing (AB/2)	Potential Electrode Spacing (MN)	Resistance (Ohm)	K value	Aparent Resistivity (Rho_a)	
1	2.5	1	8.86	18.846	166.976	-2.5
2	5	1	1.88	77.73975	146.151	-5
3	10	1	0.363	313.3148	113.733	-10
4	15	1	0.19	705.9398	134.129	-15
5	20	1	0.108	1255.615	135.606	-20
6	25	1	0.0737	1962.34	144.624	-25
7	30	1	0.0499	2826.115	141.023	-30
8	35	1	0.0353	3846.94	135.797	-35
9	40	1	0.0262	5024.815	131.650	-40
10	45	1	0.0197	6359.74	125.287	-45
11	50	1	0.0156	7851.715	122.487	-50
12	60	1	0.01059	11306.81	119.739	-60
13	70	1	0.00504	15390.11	77.566	-70
14	80	1	0.00353	20101.61	70.959	-80
15	90	1	0.00201	25441.31	51.137	-90
16	100	1	0.001	31409.21	31.409	-100

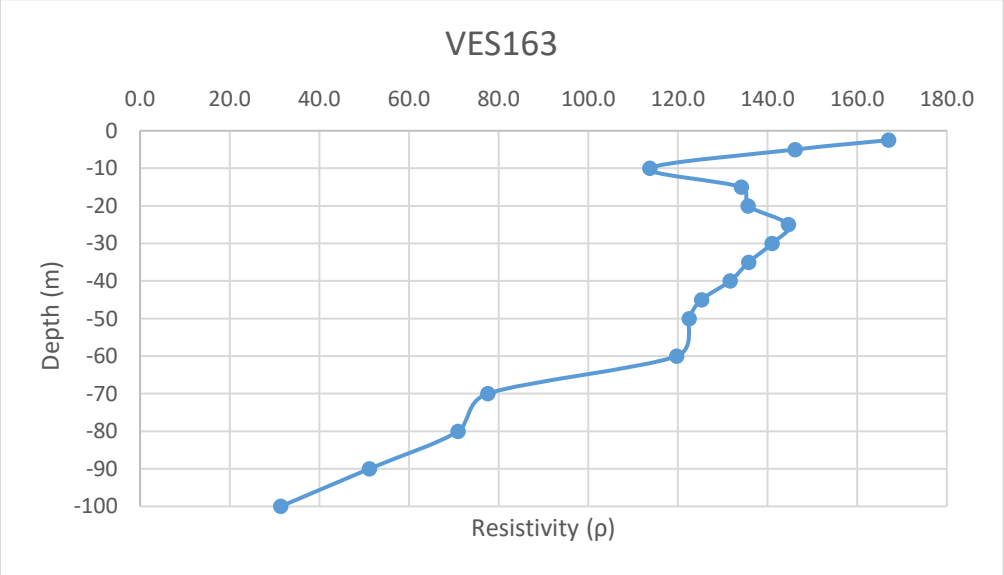

Annexure-XXII: Details of VES Survey

Date: 17/02/2025			VES-164			
Latitude	23.21903294		Longitude	69.5417436		
S.N	Current Electrode Spacing (AB/2)	Potential Electrode Spacing (MN)	Resistance (Ohm)	K value	Aparent Resistivity (Rho_a)	
1	2.5	1	2.23	18.846	42.027	-2.5
2	5	1	0.444	77.73975	34.516	-5
3	10	1	0.117	313.3148	36.658	-10
4	15	1	0.0721	705.9398	50.898	-15
5	20	1	0.0494	1255.615	62.027	-20
6	25	1	0.0368	1962.34	72.214	-25
7	30	1	0.0303	2826.115	85.631	-30
8	35	1	0.0257	3846.94	98.866	-35
9	40	1	0.0212	5024.815	106.526	-40
10	45	1	0.0177	6359.74	112.567	-45
11	50	1	0.0151	7851.715	118.561	-50
12	60	1	0.0116	11306.81	131.159	-60
13	70	1	0.00908	15390.11	139.742	-70
14	80	1	0.00554	20101.61	111.363	-80
15	90	1	0.00454	25441.31	115.504	-90
16	100	1	0.00302	31409.21	94.856	-100

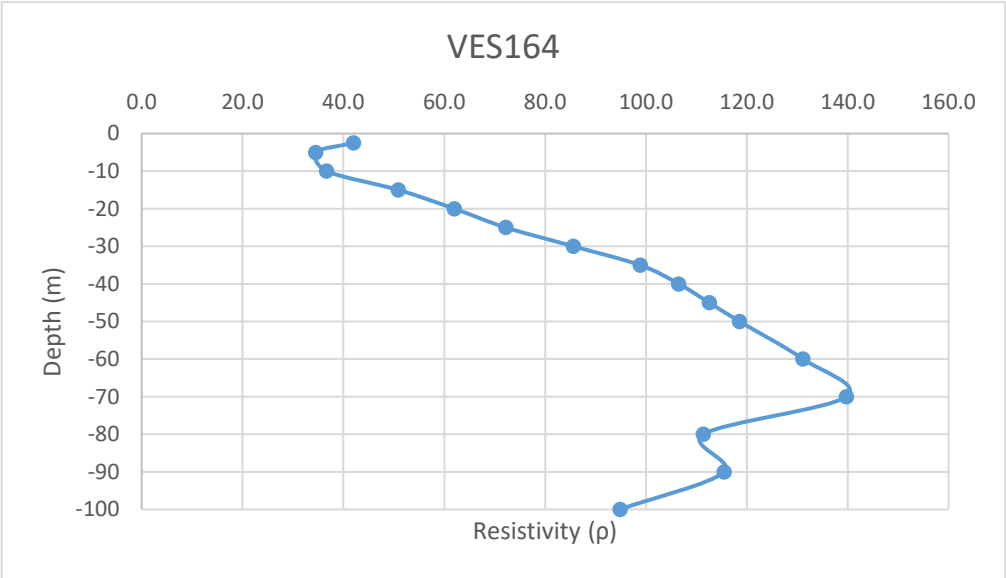

Annexure-XXII: Details of VES Survey

Date: 17/02/2025			VES-165			
Latitude	23.21567517		Longitude	69.53706967		
S.N	Current Electrode Spacing (AB/2)	Potential Electrode Spacing (MN)	Resistance (Ohm)	K value	Aparent Resistivity (Rho_a)	
1	2.5	1	12.5	18.846	235.575	-2.5
2	5	1	2.18	77.73975	169.473	-5
3	10	1	0.497	313.3148	155.717	-10
4	15	1	0.19	705.9398	134.129	-15
5	20	1	0.0933	1255.615	117.149	-20
6	25	1	0.0595	1962.34	116.759	-25
7	30	1	0.0409	2826.115	115.588	-30
8	35	1	0.0252	3846.94	96.943	-35
9	40	1	0.0166	5024.815	83.412	-40
10	45	1	0.00958	6359.74	60.926	-45
11	50	1	0.00655	7851.715	51.429	-50
12	60	1	0.00554	11306.81	62.640	-60
13	70	1	0.00341	15390.11	52.480	-70
14	80	1	0.00239	20101.61	48.043	-80
15	90	1	0.00212	25441.31	53.936	-90
16	100	1	0.00153	31409.21	48.056	-100

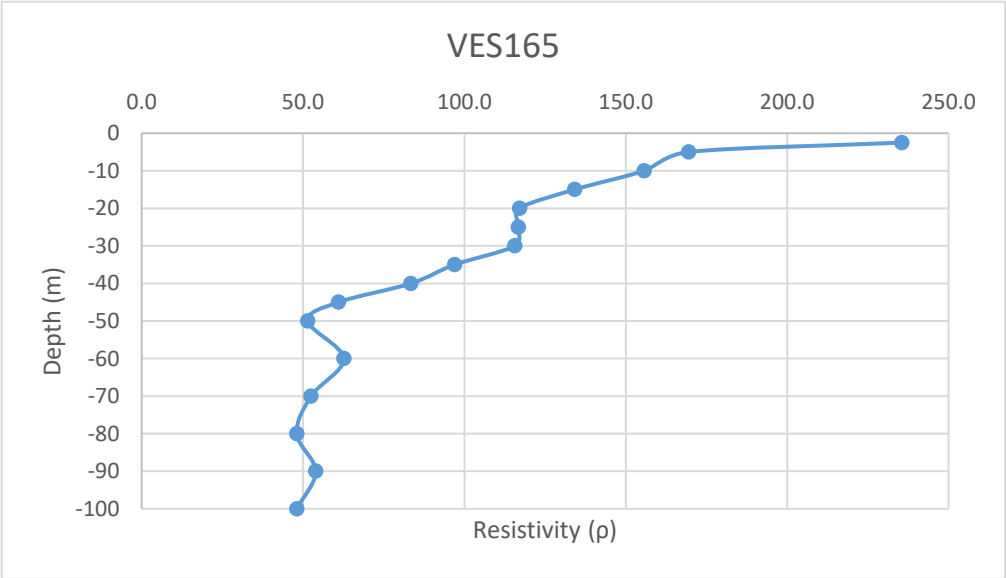

Annexure-XXII: Details of VES Survey

Date: 18/02/2025			VES-166			
Latitude	23.211803		Longitude	69.729438		
S.N	Current Electrode Spacing (AB/2)	Potential Electrode Spacing (MN)	Resistance (Ohm)	K value	Aparent Resistivity (Rho_a)	
1	2.5	1	1.033	18.846	19.468	-2.5
2	5	1	0.35	77.73975	27.209	-5
3	10	1	0.127	313.3148	39.791	-10
4	15	1	0.0616	705.9398	43.486	-15
5	20	1	0.0363	1255.615	45.579	-20
6	25	1	0.0242	1962.34	47.489	-25
7	30	1	0.0187	2826.115	52.848	-30
8	35	1	0.0136	3846.94	52.318	-35
9	40	1	0.01059	5024.815	53.213	-40
10	45	1	0.00857	6359.74	54.503	-45
11	50	1	0.00756	7851.715	59.359	-50
12	60	1	0.00605	11306.81	68.406	-60
13	70	1	0.00504	15390.11	77.566	-70
14	80	1	0.00353	20101.61	70.959	-80
15	90	1	0.00252	25441.31	64.112	-90
16	100	1	0.001	31409.21	31.409	-100

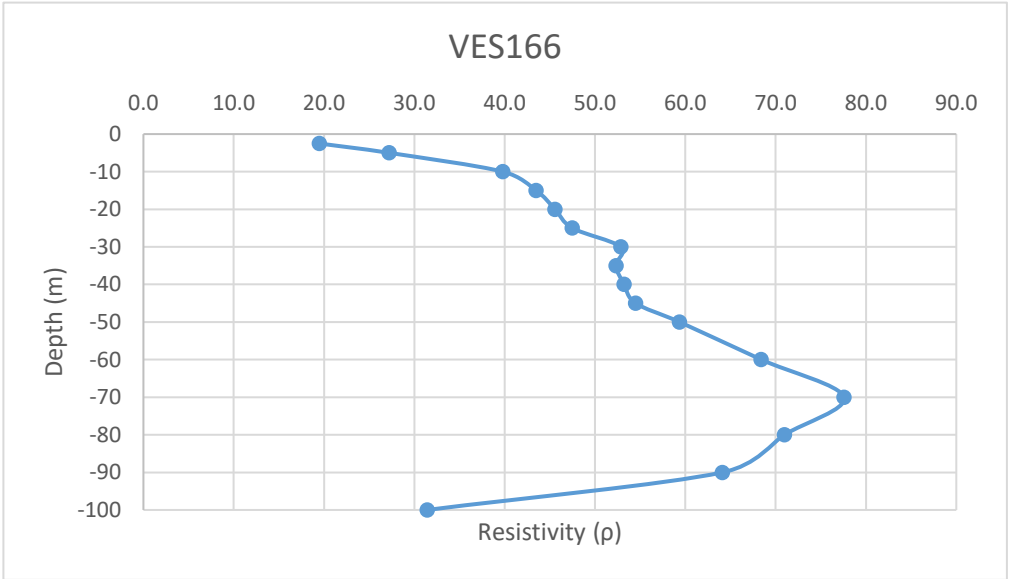

Annexure-XXII: Details of VES Survey

Date: 18/02/2025			VES-167			
Latitude	23.206686		Longitude	69.72762		
S.N	Current Electrode Spacing (AB/2)	Potential Electrode Spacing (MN)	Resistance (Ohm)	K value	Aparent Resistivity (Rho_a)	
1	2.5	1	1.23	18.846	23.181	-2.5
2	5	1	0.355	77.73975	27.598	-5
3	10	1	0.095	313.3148	29.765	-10
4	15	1	0.034	705.9398	24.002	-15
5	20	1	0.0187	1255.615	23.480	-20
6	25	1	0.0117	1962.34	22.959	-25
7	30	1	0.00706	2826.115	19.952	-30
8	35	1	0.00504	3846.94	19.389	-35
9	40	1	0.00252	5024.815	12.663	-40
10	45	1	0.00195	6359.74	12.401	-45
11	50	1	0.00151	7851.715	11.856	-50
12	60	1	0.00151	11306.81	17.073	-60
13	70	1	0.00147	15390.11	16.088	-70
14	80	1	0.001	20101.61	20.102	-80
15	90	1	0.00075	25441.31	19.081	-90
16	100	1	0.00075	31409.21	23.557	-100

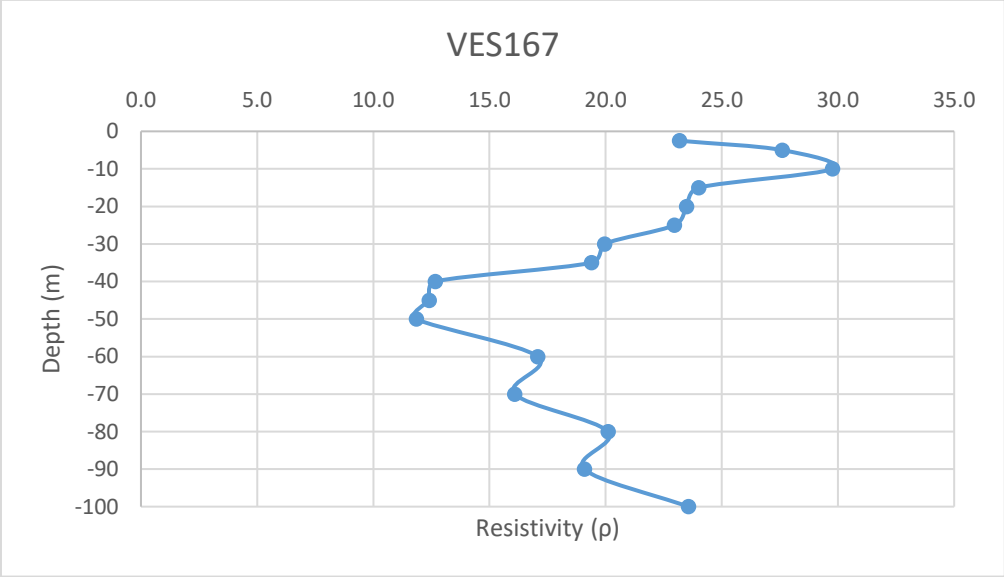

Annexure-XXII: Details of VES Survey

Date: 18/02/2025			VES-168			
Latitude	23.204107		Longitude	69.727828		
S.N	Current Electrode Spacing (AB/2)	Potential Electrode Spacing (MN)	Resistance (Ohm)	K value	Aparent Resistivity (Rho_a)	
1	2.5	1	1.88	18.846	35.430	-2.5
2	5	1	0.316	77.73975	24.566	-5
3	10	1	0.076	313.3148	23.812	-10
4	15	1	0.031	705.9398	21.884	-15
5	20	1	0.0161	1255.615	20.215	-20
6	25	1	0.00979	1962.34	19.211	-25
7	30	1	0.00678	2826.115	19.161	-30
8	35	1	0.00452	3846.94	17.388	-35
9	40	1	0.00301	5024.815	15.125	-40
10	45	1	0.00226	6359.74	14.373	-45
11	50	1	0.00182	7851.715	14.290	-50
12	60	1	0.00125	11306.81	14.134	-60
13	70	1	0.001	15390.11	15.390	-70
14	80	1	0.0005	20101.61	10.051	-80
15	90	1	0.00025	25441.31	6.360	-90
16	100	1	0.0002	31409.21	6.282	-100

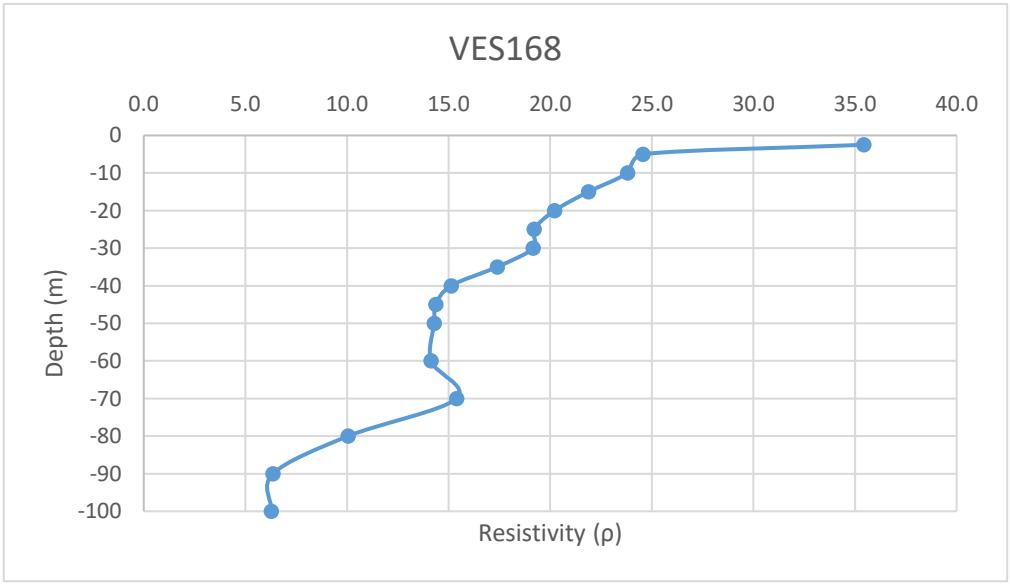

Annexure-XXII: Details of VES Survey

Date: 18/02/2025			VES-169			
Latitude	23.201985		Longitude	69.727916		
S.N	Current Electrode Spacing (AB/2)	Potential Electrode Spacing (MN)	Resistance (Ohm)	K value	Aparent Resistivity (Rho_a)	
1	2.5	1	5.56	18.846	104.784	-2.5
2	5	1	1.122	77.73975	87.224	-5
3	10	1	0.213	313.3148	66.736	-10
4	15	1	0.0831	705.9398	58.664	-15
5	20	1	0.0445	1255.615	55.875	-20
6	25	1	0.0266	1962.34	52.198	-25
7	30	1	0.0168	2826.115	47.479	-30
8	35	1	0.0113	3846.94	43.470	-35
9	40	1	0.00829	5024.815	41.656	-40
10	45	1	0.00603	6359.74	38.349	-45
11	50	1	0.00403	7851.715	31.642	-50
12	60	1	0.00353	11306.81	39.913	-60
13	70	1	0.00201	15390.11	30.934	-70
14	80	1	0.00125	20101.61	25.127	-80
15	90	1	0.00075	25441.31	19.081	-90
16	100	1	0.001	31409.21	31.409	-100

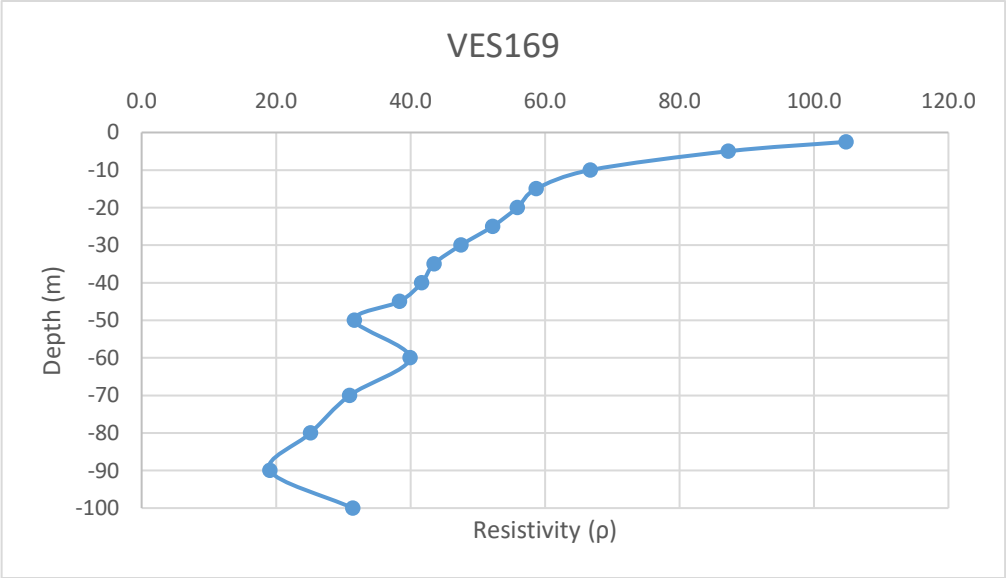

Annexure-XXII: Details of VES Survey

Date: 19/02/2025			VES-170			
Latitude	23.210796		Longitude	69.717637		
S.N	Current Electrode Spacing (AB/2)	Potential Electrode Spacing (MN)	Resistance (Ohm)	K value	Aparent Resistivity (Rho_a)	
1	2.5	1	2.54	18.846	47.869	-2.5
2	5	1	0.2	77.73975	15.548	-5
3	10	1	0.0338	313.3148	10.590	-10
4	15	1	0.0166	705.9398	11.719	-15
5	20	1	0.01009	1255.615	12.669	-20
6	25	1	0.00704	1962.34	13.815	-25
7	30	1	0.00504	2826.115	14.244	-30
8	35	1	0.00406	3846.94	15.619	-35
9	40	1	0.00353	5024.815	17.738	-40
10	45	1	0.00252	6359.74	16.027	-45
11	50	1	0.00252	7851.715	19.786	-50
12	60	1	0.00201	11306.81	22.727	-60
13	70	1	0.001	15390.11	15.390	-70
14	80	1	0.0005	20101.61	10.051	-80
15	90	1	0.001	25441.31	25.441	-90
16	100	1	0.00085	31409.21	26.698	-100

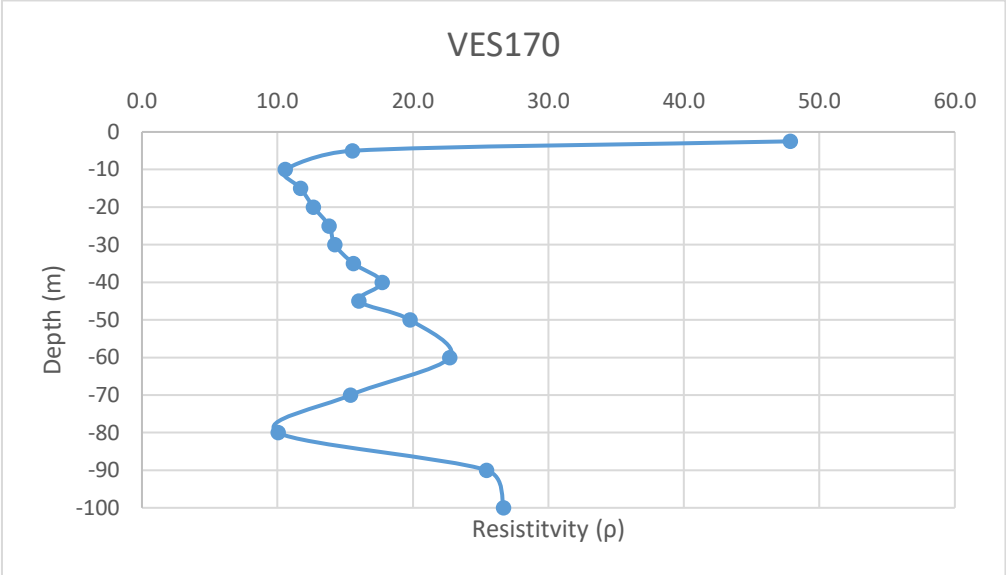

Annexure-XXII: Details of VES Survey

Date: 19/02/2025			VES-171			
Latitude	23.20795027		Longitude	69.71783709		
S.N	Current Electrode Spacing (AB/2)	Potential Electrode Spacing (MN)	Resistance (Ohm)	K value	Aparent Resistivity (Rho_a)	
1	2.5	1	7.84	18.846	147.753	-2.5
2	5	1	1.117	77.73975	86.835	-5
3	10	1	0.13	313.3148	40.731	-10
4	15	1	0.0453	705.9398	31.979	-15
5	20	1	0.0213	1255.615	26.745	-20
6	25	1	0.0128	1962.34	25.118	-25
7	30	1	0.00853	2826.115	24.107	-30
8	35	1	0.00597	3846.94	22.966	-35
9	40	1	0.00426	5024.815	21.406	-40
10	45	1	0.00426	6359.74	27.092	-45
11	50	1	0.0017	7851.715	13.348	-50
12	60	1	0.00201	11306.81	22.727	-60
13	70	1	0.001	15390.11	15.390	-70
14	80	1	0.001	20101.61	20.102	-80
15	90	1	0.0008	25441.31	20.353	-90
16	100	1	0.0005	31409.21	15.705	-100

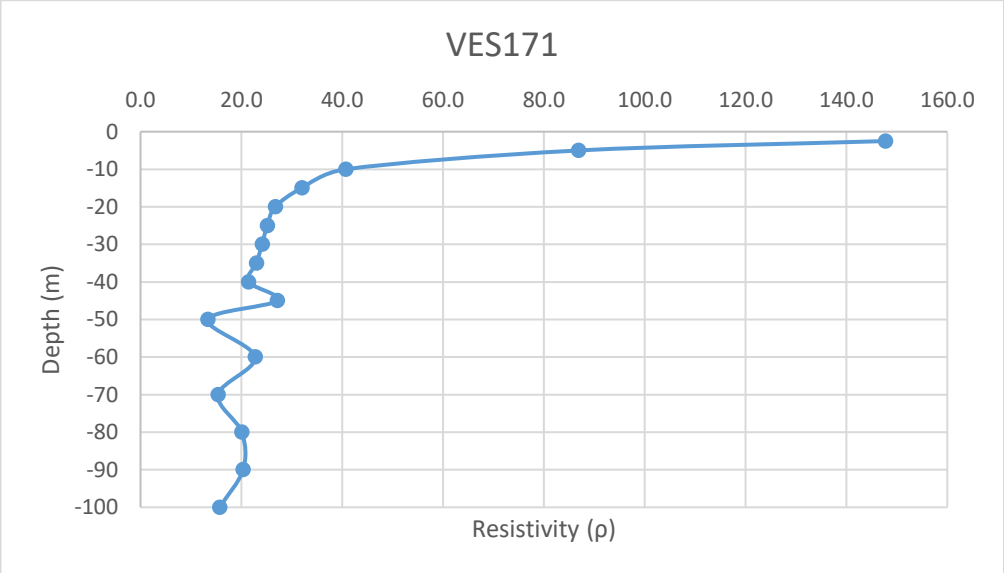

Annexure-XXII: Details of VES Survey

Date: 19/02/2025			VES-172			
Latitude	23.20539187		Longitude	69.71728474		
S.N	Current Electrode Spacing (AB/2)	Potential Electrode Spacing (MN)	Resistance (Ohm)	K value	Aparent Resistivity (Rho_a)	
1	2.5	1	8.77	18.846	165.279	-2.5
2	5	1	2.08	77.73975	161.699	-5
3	10	1	0.4	313.3148	125.326	-10
4	15	1	0.126	705.9398	88.948	-15
5	20	1	0.0558	1255.615	70.063	-20
6	25	1	0.0309	1962.34	60.636	-25
7	30	1	0.0178	2826.115	50.305	-30
8	35	1	0.01155	3846.94	44.432	-35
9	40	1	0.00753	5024.815	37.837	-40
10	45	1	0.00552	6359.74	35.106	-45
11	50	1	0.00376	7851.715	29.522	-50
12	60	1	0.00276	11306.81	31.207	-60
13	70	1	0.00201	15390.11	30.934	-70
14	80	1	0.0015	20101.61	30.152	-80
15	90	1	0.00125	25441.31	31.802	-90
16	100	1	0.001	31409.21	31.409	-100

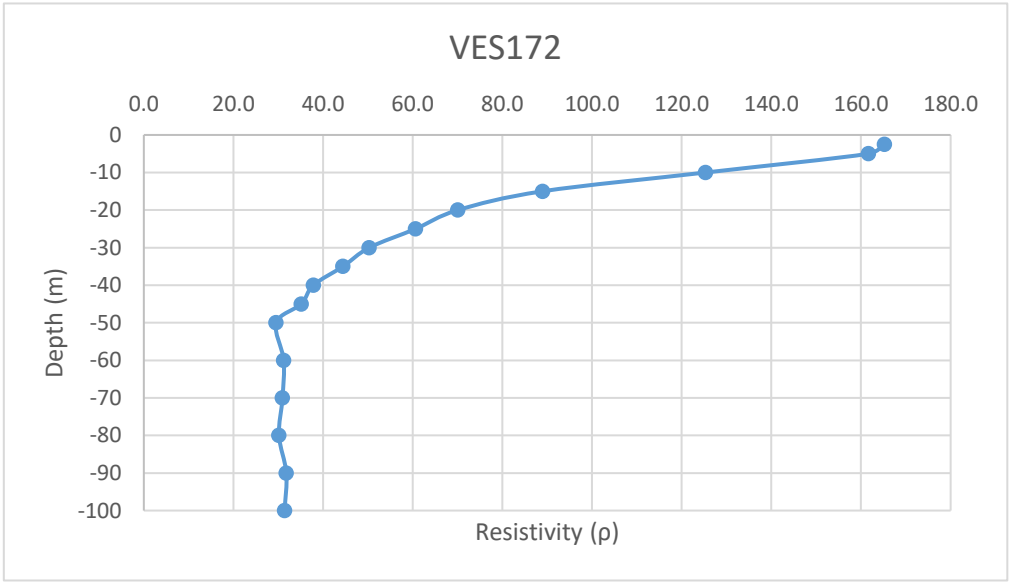

Annexure-XXII: Details of VES Survey

Date: 19/02/2025			VES-173			
Latitude	23.20016845		Longitude	69.7182184		
S.N	Current Electrode Spacing (AB/2)	Potential Electrode Spacing (MN)	Resistance (Ohm)	K value	Aparent Resistivity (Rho_a)	
1	2.5	1	13.9	18.846	261.959	-2.5
2	5	1	1.96	77.73975	152.370	-5
3	10	1	0.47	313.3148	147.258	-10
4	15	1	0.168	705.9398	118.598	-15
5	20	1	0.059	1255.615	74.081	-20
6	25	1	0.0283	1962.34	55.534	-25
7	30	1	0.0166	2826.115	46.914	-30
8	35	1	0.01109	3846.94	42.663	-35
9	40	1	0.00857	5024.815	43.063	-40
10	45	1	0.00605	6359.74	38.476	-45
11	50	1	0.00554	7851.715	43.498	-50
12	60	1	0.00397	11306.81	44.888	-60
13	70	1	0.00302	15390.11	46.478	-70
14	80	1	0.00154	20101.61	30.956	-80
15	90	1	0.0005	25441.31	12.721	-90
16	100	1	0.0005	31409.21	15.705	-100

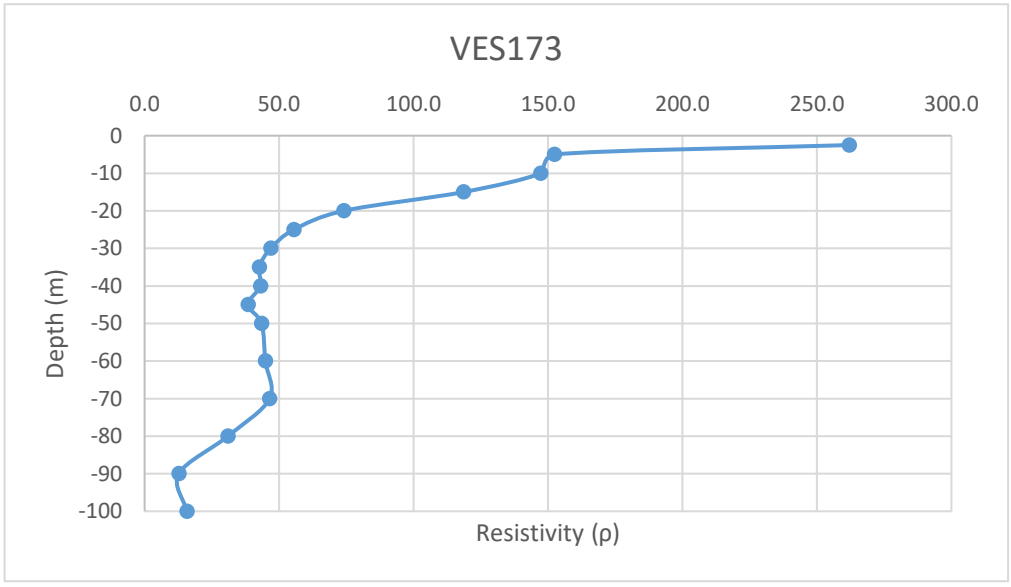

Annexure-XXII: Details of VES Survey

Date: 20/02/2025			VES-174			
Latitude	23.21385933		Longitude	69.70423208		
S.N	Current Electrode Spacing (AB/2)	Potential Electrode Spacing (MN)	Resistance (Ohm)	K value	Aparent Resistivity (Rho_a)	
1	2.5	1	9.73	18.846	183.372	-2.5
2	5	1	3.9	77.73975	303.185	-5
3	10	1	1.24	313.3148	388.510	-10
4	15	1	0.598	705.9398	422.152	-15
5	20	1	0.351	1255.615	440.721	-20
6	25	1	0.207	1962.34	406.204	-25
7	30	1	0.136	2826.115	384.352	-30
8	35	1	0.0883	3846.94	339.685	-35
9	40	1	0.0555	5024.815	278.877	-40
10	45	1	0.0404	6359.74	256.933	-45
11	50	1	0.0279	7851.715	219.063	-50
12	60	1	0.0151	11306.81	170.733	-60
13	70	1	0.00929	15390.11	142.974	-70
14	80	1	0.00552	20101.61	110.961	-80
15	90	1	0.00326	25441.31	82.939	-90
16	100	1	0.00201	31409.21	63.133	-100

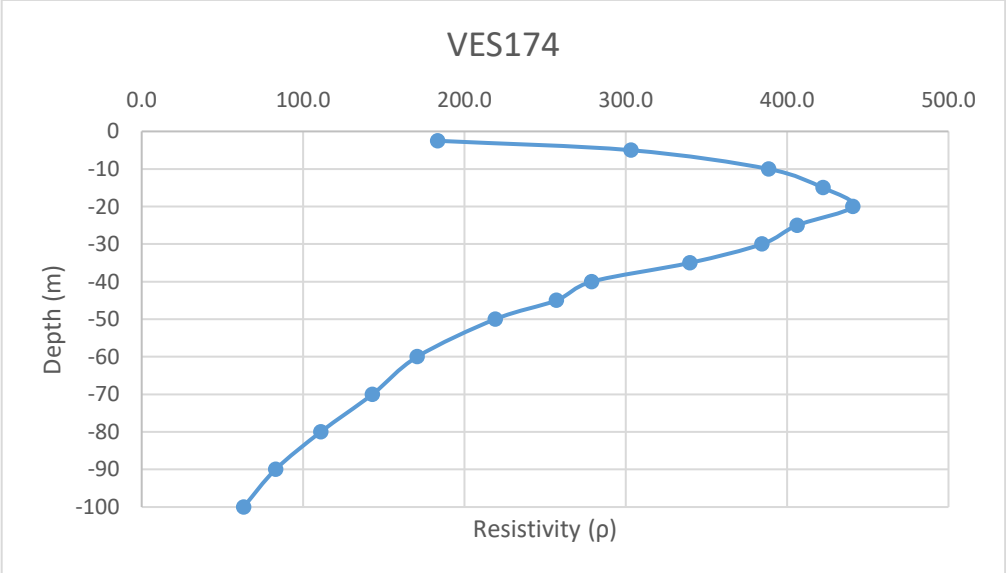

Annexure-XXII: Details of VES Survey

Date: 20/02/2025			VES-175			
Latitude	23.21101007		Longitude	69.70315048		
S.N	Current Electrode Spacing (AB/2)	Potential Electrode Spacing (MN)	Resistance (Ohm)	K value	Aparent Resistivity (Rho_a)	
1	2.5	1	4.27	18.846	80.472	-2.5
2	5	1	1.117	77.73975	86.835	-5
3	10	1	0.215	313.3148	67.363	-10
4	15	1	0.0651	705.9398	45.957	-15
5	20	1	0.0359	1255.615	45.077	-20
6	25	1	0.0226	1962.34	44.349	-25
7	30	1	0.0161	2826.115	45.500	-30
8	35	1	0.01005	3846.94	38.662	-35
9	40	1	0.00678	5024.815	34.068	-40
10	45	1	0.00478	6359.74	30.400	-45
11	50	1	0.00427	7851.715	33.527	-50
12	60	1	0.00251	11306.81	28.380	-60
13	70	1	0.00226	15390.11	34.782	-70
14	80	1	0.001	20101.61	20.102	-80
15	90	1	0.00075	25441.31	19.081	-90
16	100	1	0.0005	31409.21	15.705	-100

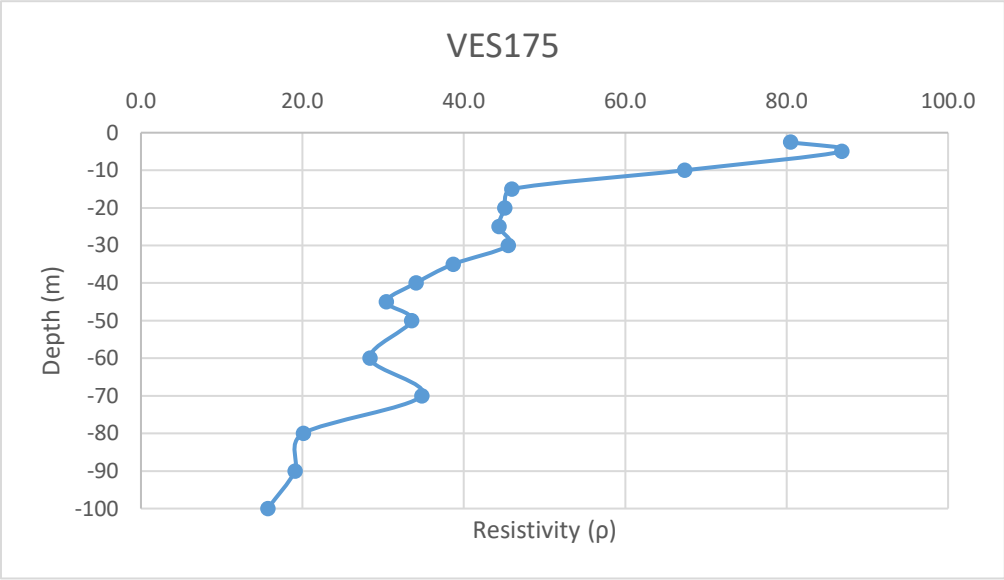

Annexure-XXII: Details of VES Survey

Date: 20/02/2025			VES-176			
Latitude	23.20916295		Longitude	69.70315517		
S.N	Current Electrode Spacing (AB/2)	Potential Electrode Spacing (MN)	Resistance (Ohm)	K value	Aparent Resistivity (Rho_a)	
1	2.5	1	2.4	18.846	45.230	-2.5
2	5	1	0.602	77.73975	46.799	-5
3	10	1	0.19	313.3148	59.530	-10
4	15	1	0.0862	705.9398	60.852	-15
5	20	1	0.0423	1255.615	53.113	-20
6	25	1	0.0246	1962.34	48.274	-25
7	30	1	0.0153	2826.115	43.240	-30
8	35	1	0.00954	3846.94	36.700	-35
9	40	1	0.00728	5024.815	36.581	-40
10	45	1	0.00552	6359.74	35.106	-45
11	50	1	0.00402	7851.715	31.564	-50
12	60	1	0.00226	11306.81	25.553	-60
13	70	1	0.00175	15390.11	26.933	-70
14	80	1	0.0015	20101.61	30.152	-80
15	90	1	0.00075	25441.31	19.081	-90
16	100	1	0.0005	31409.21	15.705	-100

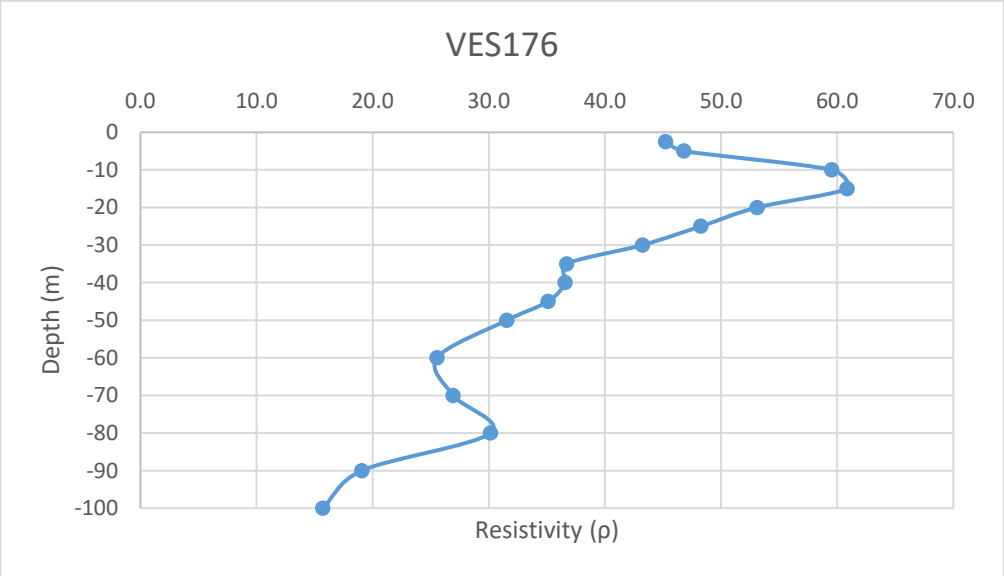

Annexure-XXII: Details of VES Survey

Date: 20/02/2025			VES-177			
Latitude	23.21236566		Longitude	69.70634291		
S.N	Current Electrode Spacing (AB/2)	Potential Electrode Spacing (MN)	Resistance (Ohm)	K value	Aparent Resistivity (Rho_a)	
1	2.5	1	0.438	18.846	8.255	-2.5
2	5	1	0.168	77.73975	13.060	-5
3	10	1	0.06	313.3148	18.799	-10
4	15	1	0.0294	705.9398	20.755	-15
5	20	1	0.0158	1255.615	19.839	-20
6	25	1	0.01005	1962.34	19.722	-25
7	30	1	0.00605	2826.115	17.098	-30
8	35	1	0.00403	3846.94	15.503	-35
9	40	1	0.00302	5024.815	15.175	-40
10	45	1	0.00201	6359.74	12.783	-45
11	50	1	0.001	7851.715	7.852	-50
12	60	1	0.00085	11306.81	9.611	-60
13	70	1	0.0005	15390.11	7.695	-70
14	80	1	0.001	20101.61	20.102	-80
15	90	1	0.00075	25441.31	19.081	-90
16	100	1	0.0005	31409.21	15.705	-100

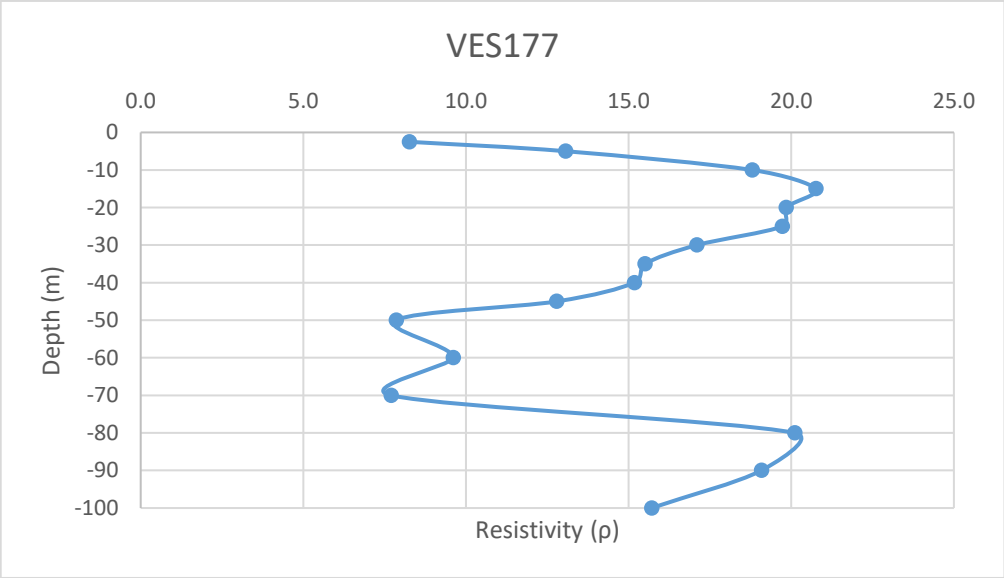

Annexure-XXII: Details of VES Survey

Date: 21/02/2025			VES-179			
Latitude	23.214917		Longitude	69.740521		
S.N	Current Electrode Spacing (AB/2)	Potential Electrode Spacing (MN)	Resistance (Ohm)	K value	Aparent Resistivity (Rho_a)	
1	2.5	1	34.8	18.846	655.841	-2.5
2	5	1	4.02	77.73975	312.514	-5
3	10	1	0.523	313.3148	163.864	-10
4	15	1	0.175	705.9398	123.539	-15
5	20	1	0.1085	1255.615	136.234	-20
6	25	1	0.0737	1962.34	144.624	-25
7	30	1	0.0555	2826.115	156.849	-30
8	35	1	0.0383	3846.94	147.338	-35
9	40	1	0.0318	5024.815	159.789	-40
10	45	1	0.0222	6359.74	141.186	-45
11	50	1	0.0232	7851.715	182.160	-50
12	60	1	0.0172	11306.81	194.477	-60
13	70	1	0.00655	15390.11	100.805	-70
14	80	1	0.00958	20101.61	192.573	-80
15	90	1	0.00807	25441.31	205.311	-90
16	100	1	0.00857	31409.21	269.177	-100

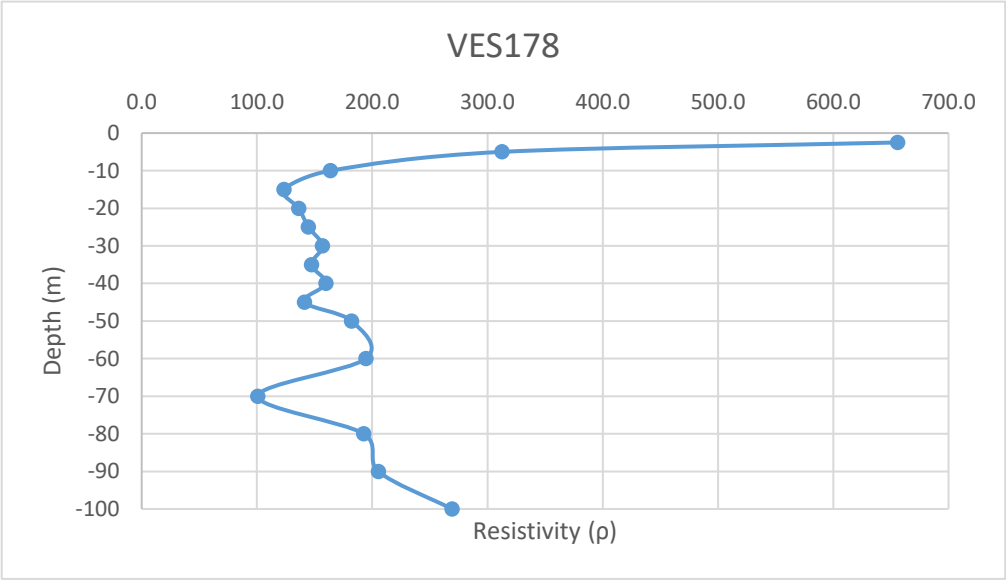

Annexure-XXII: Details of VES Survey

Date: 21/02/2025			VES-178			
Latitude	23.207436		Longitude	69.74137		
S.N	Current Electrode Spacing (AB/2)	Potential Electrode Spacing (MN)	Resistance (Ohm)	K value	Aparent Resistivity (Rho_a)	
1	2.5	1	1.193	18.846	22.483	-2.5
2	5	1	0.332	77.73975	25.810	-5
3	10	1	0.0754	313.3148	23.624	-10
4	15	1	0.0374	705.9398	26.402	-15
5	20	1	0.0231	1255.615	29.005	-20
6	25	1	0.0141	1962.34	27.669	-25
7	30	1	0.01005	2826.115	28.402	-30
8	35	1	0.00703	3846.94	27.044	-35
9	40	1	0.00527	5024.815	26.481	-40
10	45	1	0.00427	6359.74	27.156	-45
11	50	1	0.00376	7851.715	29.522	-50
12	60	1	0.00251	11306.81	28.380	-60
13	70	1	0.00175	15390.11	26.933	-70
14	80	1	0.00125	20101.61	25.127	-80
15	90	1	0.0005	25441.31	12.721	-90
16	100	1	0.00025	31409.21	7.852	-100

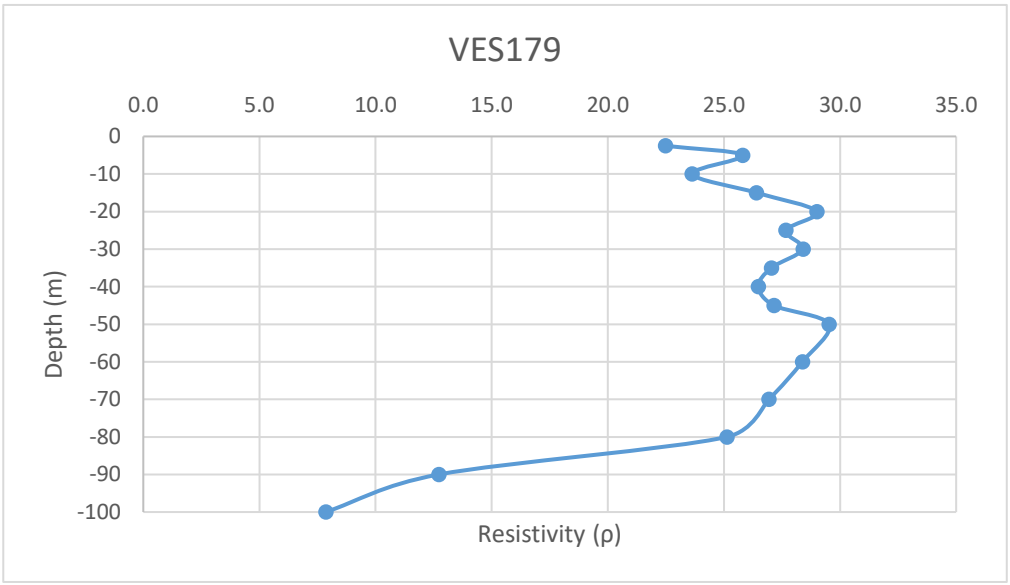

Annexure-XXII: Details of VES Survey

Date: 21/02/2025			VES-180			
Latitude	23.204369		Longitude	69.740116		
S.N	Current Electrode Spacing (AB/2)	Potential Electrode Spacing (MN)	Resistance (Ohm)	K value	Aparent Resistivity (Rho_a)	
1	2.5	1	11.02	18.846	207.683	-2.5
2	5	1	1.68	77.73975	130.603	-5
3	10	1	0.401	313.3148	125.639	-10
4	15	1	0.155	705.9398	109.421	-15
5	20	1	0.079	1255.615	99.194	-20
6	25	1	0.046	1962.34	90.268	-25
7	30	1	0.0248	2826.115	70.088	-30
8	35	1	0.0154	3846.94	59.243	-35
9	40	1	0.00939	5024.815	47.183	-40
10	45	1	0.00512	6359.74	32.562	-45
11	50	1	0.00341	7851.715	26.774	-50
12	60	1	0.00353	11306.81	39.913	-60
13	70	1	0.00151	15390.11	23.239	-70
14	80	1	0.00125	20101.61	25.127	-80
15	90	1	0.00085	25441.31	21.625	-90
16	100	1	0.001	31409.21	31.409	-100

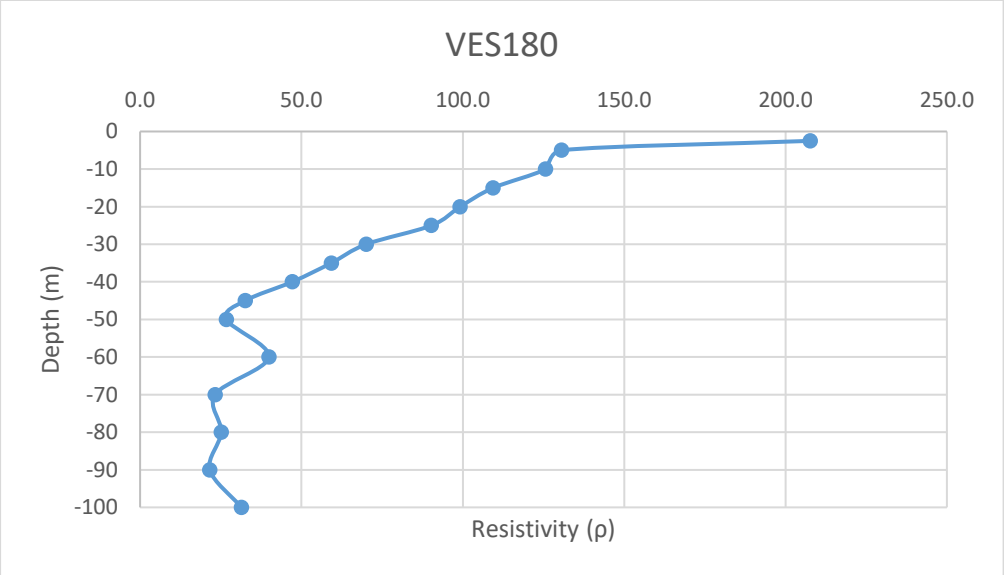

Annexure-XXII: Details of VES Survey

Date: 21/02/2025			VES-181			
Latitude	23.201134		Longitude	69.739191		
S.N	Current Electrode Spacing (AB/2)	Potential Electrode Spacing (MN)	Resistance (Ohm)	K value	Aparent Resistivity (Rho_a)	
1	2.5	1	4.73	18.846	89.142	-2.5
2	5	1	0.742	77.73975	57.683	-5
3	10	1	0.112	313.3148	35.091	-10
4	15	1	0.0383	705.9398	27.037	-15
5	20	1	0.0232	1255.615	29.130	-20
6	25	1	0.0161	1962.34	31.594	-25
7	30	1	0.01109	2826.115	31.342	-30
8	35	1	0.00756	3846.94	29.083	-35
9	40	1	0.00302	5024.815	15.175	-40
10	45	1	0.00252	6359.74	16.027	-45
11	50	1	0.00201	7851.715	15.782	-50
12	60	1	0.0017	11306.81	19.222	-60
13	70	1	0.00125	15390.11	19.238	-70
14	80	1	0.001	20101.61	20.102	-80
15	90	1	0.00075	25441.31	19.081	-90
16	100	1	0.0005	31409.21	15.705	-100

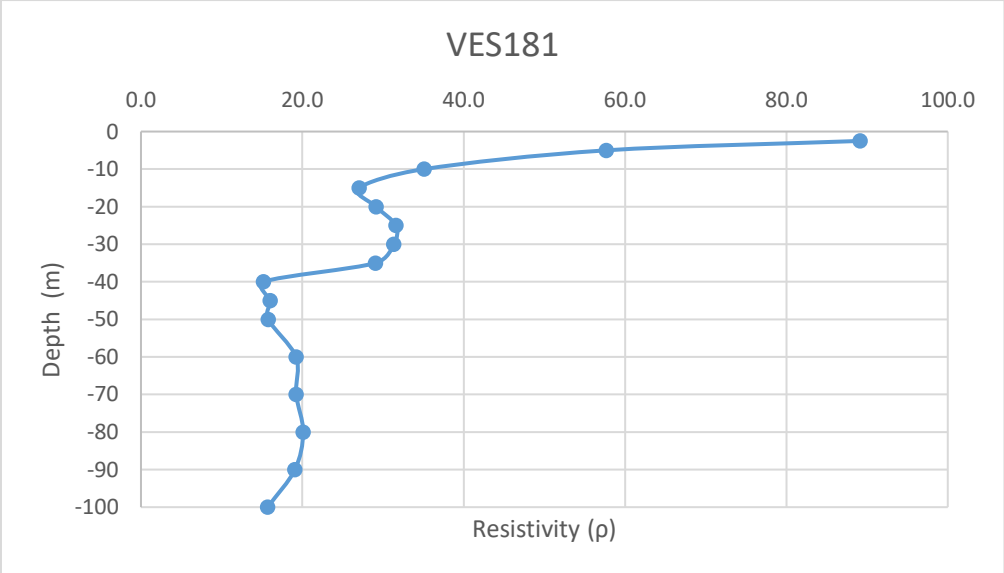

Annexure-XXII: Details of VES Survey

Date: 22/02/2025			VES-182			
Latitude	23.210622		Longitude	69.74031		
S.N	Current Electrode Spacing (AB/2)	Potential Electrode Spacing (MN)	Resistance (Ohm)	K value	Aparent Resistivity (Rho_a)	
1	2.5	1	46.6	18.846	878.224	-2.5
2	5	1	5.16	77.73975	401.137	-5
3	10	1	0.726	313.3148	227.467	-10
4	15	1	0.192	705.9398	135.540	-15
5	20	1	0.073	1255.615	91.660	-20
6	25	1	0.0418	1962.34	82.026	-25
7	30	1	0.0256	2826.115	72.349	-30
8	35	1	0.0213	3846.94	81.940	-35
9	40	1	0.0171	5024.815	85.924	-40
10	45	1	0.01195	6359.74	75.999	-45
11	50	1	0.01195	7851.715	93.828	-50
12	60	1	0.00853	11306.81	96.447	-60
13	70	1	0.00512	15390.11	78.797	-70
14	80	1	0.00683	20101.61	137.294	-80
15	90	1	0.00426	25441.31	108.380	-90
16	100	1	0.00341	31409.21	107.105	-100

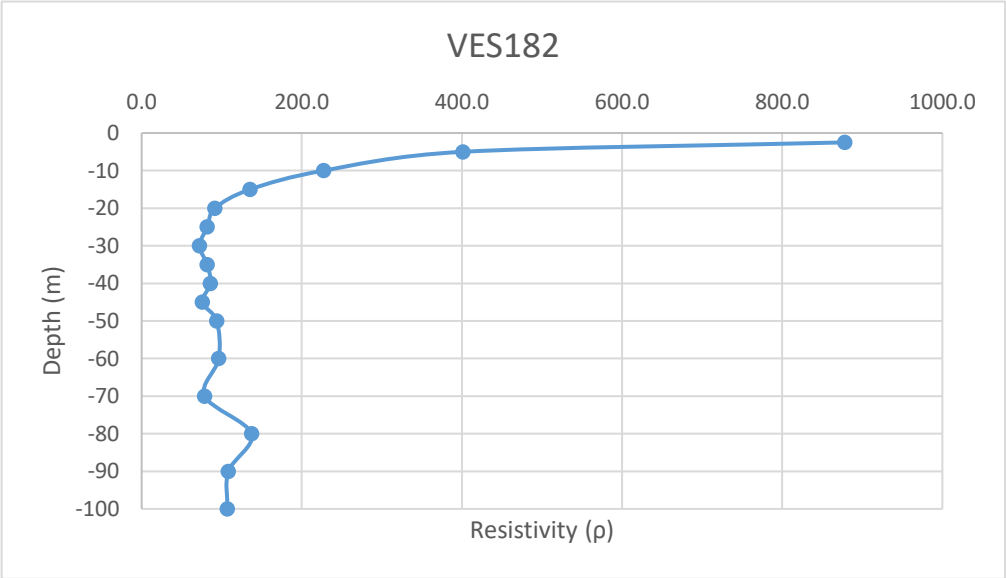

Annexure-XXII: Details of VES Survey

Date: 22/02/2025			VES-183			
Latitude	23.206344		Longitude	69.738319		
S.N	Current Electrode Spacing (AB/2)	Potential Electrode Spacing (MN)	Resistance (Ohm)	K value	Aparent Resistivity (Rho_a)	
1	2.5	1	0.762	18.846	14.361	-2.5
2	5	1	0.183	77.73975	14.226	-5
3	10	1	0.043	313.3148	13.473	-10
4	15	1	0.0209	705.9398	14.754	-15
5	20	1	0.0121	1255.615	15.193	-20
6	25	1	0.00655	1962.34	12.853	-25
7	30	1	0.00605	2826.115	17.098	-30
8	35	1	0.00454	3846.94	17.465	-35
9	40	1	0.00304	5024.815	15.275	-40
10	45	1	0.00252	6359.74	16.027	-45
11	50	1	0.00201	7851.715	15.782	-50
12	60	1	0.00151	11306.81	17.073	-60
13	70	1	0.00175	15390.11	26.933	-70
14	80	1	0.00125	20101.61	25.127	-80
15	90	1	0.00075	25441.31	19.081	-90
16	100	1	0.0005	31409.21	15.705	-100

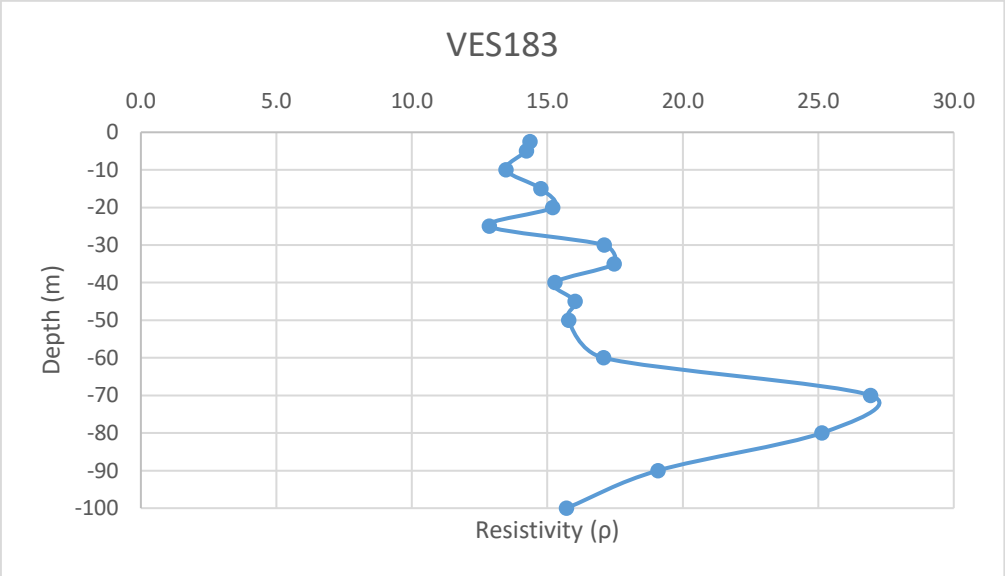

Annexure-XXII: Details of VES Survey

Date: 22/02/2025			VES-184			
Latitude	23.203445		Longitude	69.736828		
S.N	Current Electrode Spacing (AB/2)	Potential Electrode Spacing (MN)	Resistance (Ohm)	K value	Aparent Resistivity (Rho_a)	
1	2.5	1	4.91	18.846	92.534	-2.5
2	5	1	0.914	77.73975	71.054	-5
3	10	1	0.284	313.3148	88.981	-10
4	15	1	0.129	705.9398	91.066	-15
5	20	1	0.0686	1255.615	86.135	-20
6	25	1	0.0429	1962.34	84.184	-25
7	30	1	0.0277	2826.115	78.283	-30
8	35	1	0.0217	3846.94	83.479	-35
9	40	1	0.0141	5024.815	70.850	-40
10	45	1	0.01009	6359.74	64.170	-45
11	50	1	0.00807	7851.715	63.363	-50
12	60	1	0.00454	11306.81	51.333	-60
13	70	1	0.00252	15390.11	38.783	-70
14	80	1	0.00201	20101.61	40.404	-80
15	90	1	0.00301	25441.31	76.578	-90
16	100	1	0.00226	31409.21	70.985	-100

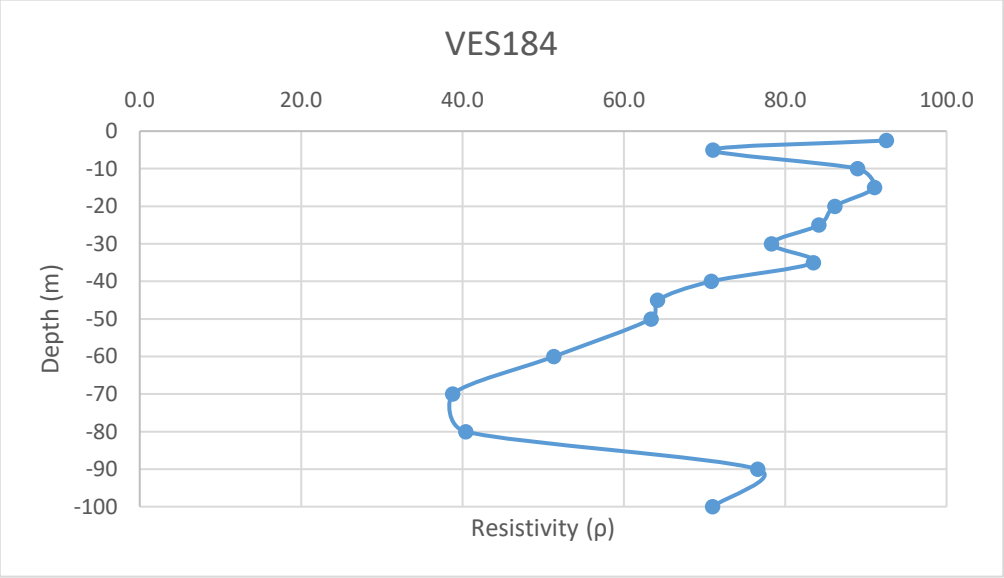

Annexure-XXII: Details of VES Survey

Date: 22/02/2025		VES-185				
Latitude	23.208949		Longitude	69.72922		
S.N	Current Electrode Spacing (AB/2)	Potential Electrode Spacing (MN)	Resistance (Ohm)	K value	Aparent Resistivity (Rho_a)	
1	2.5	1	1.047	18.846	19.732	-2.5
2	5	1	0.188	77.73975	14.615	-5
3	10	1	0.0319	313.3148	9.995	-10
4	15	1	0.0138	705.9398	9.742	-15
5	20	1	0.00753	1255.615	9.455	-20
6	25	1	0.00427	1962.34	8.379	-25
7	30	1	0.00301	2826.115	8.507	-30
8	35	1	0.00201	3846.94	7.732	-35
9	40	1	0.00175	5024.815	8.793	-40
10	45	1	0.0015	6359.74	9.540	-45
11	50	1	0.00125	7851.715	9.815	-50
12	60	1	0.0005	11306.81	5.653	-60
13	70	1	0.00125	15390.11	19.238	-70
14	80	1	0.00085	20101.61	17.086	-80
15	90	1	0.0005	25441.31	12.721	-90
16	100	1	0.0005	31409.21	15.705	-100

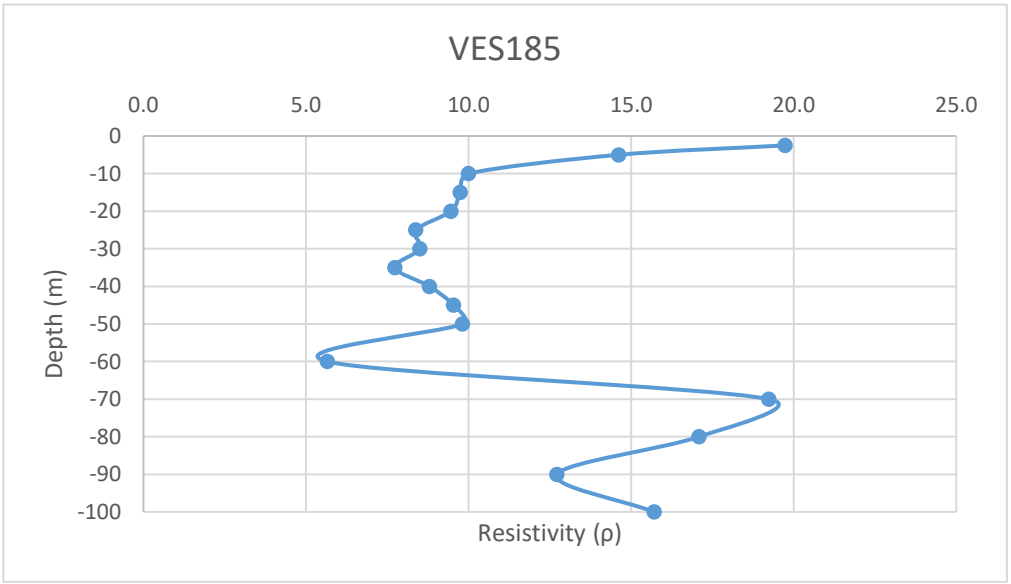

Annexure-XXII: Details of VES Survey

Date: 23/02/2025			VES-186			
Latitude	23.21143052		Longitude	69.67229787		
S.N	Current Electrode Spacing (AB/2)	Potential Electrode Spacing (MN)	Resistance (Ohm)	K value	Aparent Resistivity (Rho_a)	
1	2.5	1	1.08	18.846	20.354	-2.5
2	5	1	0.305	77.73975	23.711	-5
3	10	1	0.126	313.3148	39.478	-10
4	15	1	0.0646	705.9398	45.604	-15
5	20	1	0.0359	1255.615	45.077	-20
6	25	1	0.0224	1962.34	43.956	-25
7	30	1	0.0141	2826.115	39.848	-30
8	35	1	0.00929	3846.94	35.738	-35
9	40	1	0.00628	5024.815	31.556	-40
10	45	1	0.00452	6359.74	28.746	-45
11	50	1	0.00376	7851.715	29.522	-50
12	60	1	0.00226	11306.81	25.553	-60
13	70	1	0.0015	15390.11	23.085	-70
14	80	1	0.00125	20101.61	25.127	-80
15	90	1	0.00075	25441.31	19.081	-90
16	100	1	0.0005	31409.21	15.705	-100

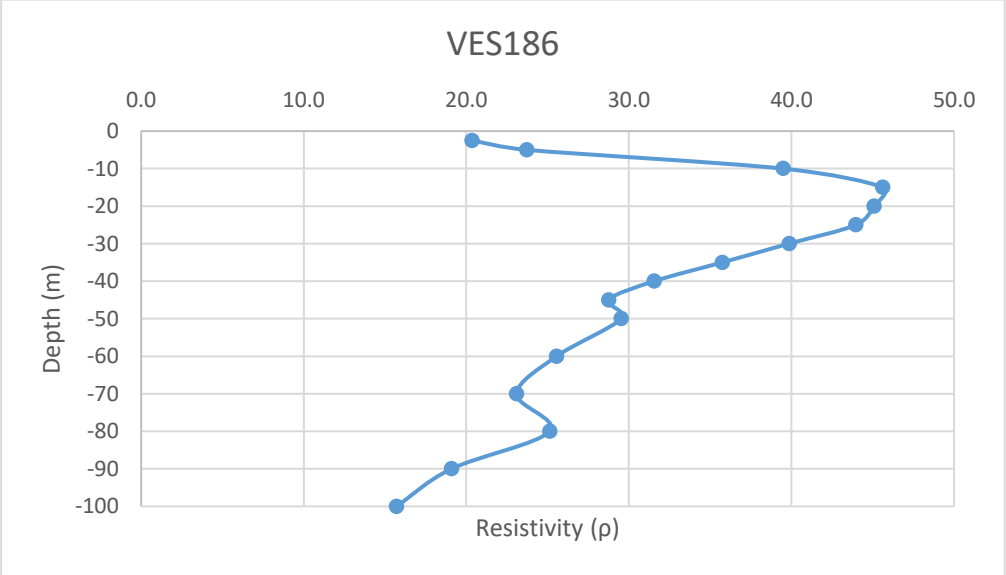

Annexure-XXII: Details of VES Survey

Date: 23/02/2025			VES-187			
Latitude	23.20963669		Longitude	69.67259253		
S.N	Current Electrode Spacing (AB/2)	Potential Electrode Spacing (MN)	Resistance (Ohm)	K value	Aparent Resistivity (Rho_a)	
1	2.5	1	1.78	18.846	33.546	-2.5
2	5	1	0.466	77.73975	36.227	-5
3	10	1	0.171	313.3148	53.577	-10
4	15	1	0.0971	705.9398	68.547	-15
5	20	1	0.0583	1255.615	73.202	-20
6	25	1	0.0362	1962.34	71.037	-25
7	30	1	0.0231	2826.115	65.283	-30
8	35	1	0.0143	3846.94	55.011	-35
9	40	1	0.00979	5024.815	49.193	-40
10	45	1	0.00678	6359.74	43.119	-45
11	50	1	0.00628	7851.715	49.309	-50
12	60	1	0.00351	11306.81	39.687	-60
13	70	1	0.00201	15390.11	30.934	-70
14	80	1	0.0015	20101.61	30.152	-80
15	90	1	0.001	25441.31	25.441	-90
16	100	1	0.0005	31409.21	15.705	-100

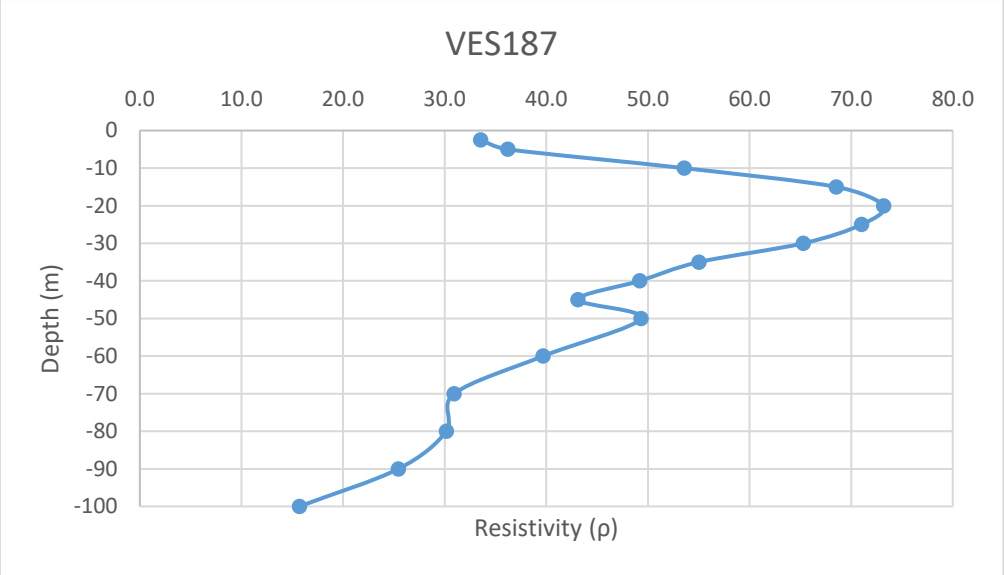

Annexure-XXII: Details of VES Survey

Date: 23/02/2025			VES-188			
Latitude	23.20797246		Longitude	69.67302383		
S.N	Current Electrode Spacing (AB/2)	Potential Electrode Spacing (MN)	Resistance (Ohm)	K value	Aparent Resistivity (Rho_a)	
1	2.5	1	1.3	18.846	24.500	-2.5
2	5	1	0.477	77.73975	37.082	-5
3	10	1	0.119	313.3148	37.284	-10
4	15	1	0.0492	705.9398	34.732	-15
5	20	1	0.0291	1255.615	36.538	-20
6	25	1	0.0181	1962.34	35.518	-25
7	30	1	0.0131	2826.115	37.022	-30
8	35	1	0.00854	3846.94	32.853	-35
9	40	1	0.00655	5024.815	32.913	-40
10	45	1	0.00454	6359.74	28.873	-45
11	50	1	0.00403	7851.715	31.642	-50
12	60	1	0.00201	11306.81	22.727	-60
13	70	1	0.00151	15390.11	23.239	-70
14	80	1	0.001	20101.61	20.102	-80
15	90	1	0.00075	25441.31	19.081	-90
16	100	1	0.0005	31409.21	15.705	-100

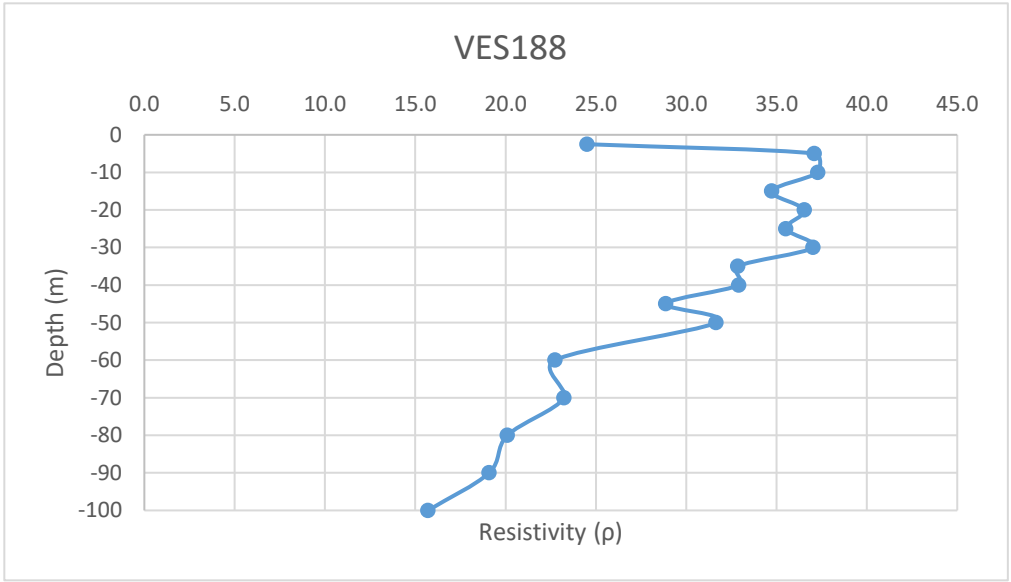

Annexure-XXII: Details of VES Survey

Date: 23/02/2025			VES-189			
Latitude	23.20604745		Longitude	69.67334788		
S.N	Current Electrode Spacing (AB/2)	Potential Electrode Spacing (MN)	Resistance (Ohm)	K value	Aparent Resistivity (Rho_a)	
1	2.5	1	1.31	18.846	24.688	-2.5
2	5	1	0.344	77.73975	26.742	-5
3	10	1	0.115	313.3148	36.031	-10
4	15	1	0.0632	705.9398	44.615	-15
5	20	1	0.0393	1255.615	49.346	-20
7	30	1	0.0179	2826.115	50.587	-30
8	35	1	0.0137	3846.94	52.703	-35
9	40	1	0.0111	5024.815	55.775	-40
10	45	1	0.01024	6359.74	65.124	-45
11	50	1	0.00853	7851.715	66.975	-50
12	60	1	0.00512	11306.81	57.891	-60
13	70	1	0.00256	15390.11	39.399	-70
14	80	1	0.0017	20101.61	34.173	-80
15	90	1	0.00085	25441.31	21.625	-90
16	100	1	0.001	31409.21	31.409	-100

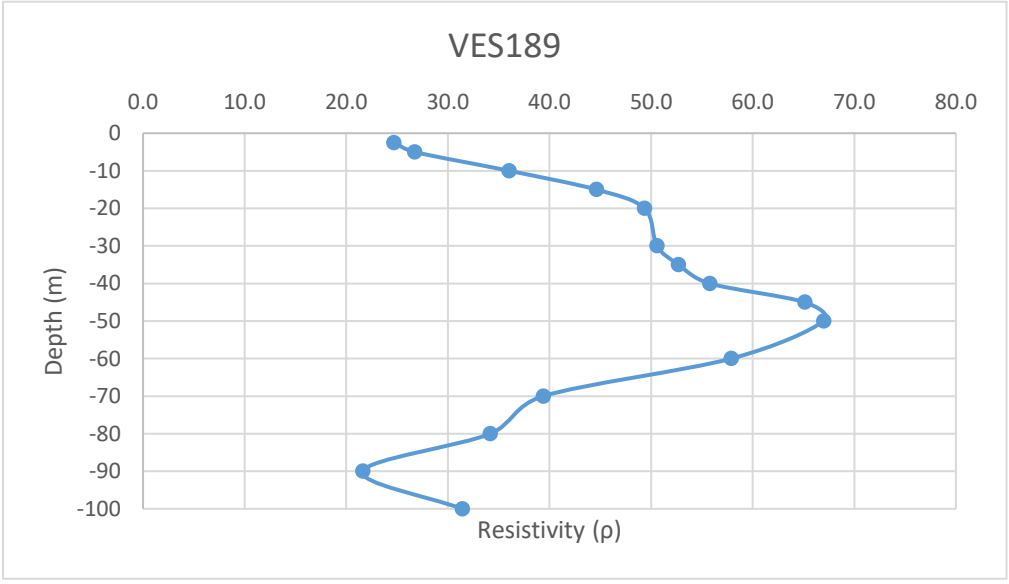

Annexure-XXII: Details of VES Survey

Date: 24/02/2025			VES-190			
Latitude	23.20797246		Longitude	69.67302383		
S.N	Current Electrode Spacing (AB/2)	Potential Electrode Spacing (MN)	Resistance (Ohm)	K value	Aparent Resistivity (Rho_a)	
1	2.5	1	8.53	18.846	160.756	-2.5
2	5	1	2.2	77.73975	171.027	-5
3	10	1	0.811	313.3148	254.098	-10
6	25	1	0.165	1962.34	323.786	-25
7	30	1	0.112	2826.115	316.525	-30
8	35	1	0.0768	3846.94	295.445	-35
9	40	1	0.0525	5024.815	263.803	-40
10	45	1	0.0401	6359.74	255.026	-45
11	50	1	0.0299	7851.715	234.766	-50
12	60	1	0.0205	11306.81	231.790	-60
13	70	1	0.01195	15390.11	183.912	-70
14	80	1	0.00853	20101.61	171.467	-80
15	90	1	0.00768	25441.31	195.389	-90
16	100	1	0.00553	31409.21	173.693	-100

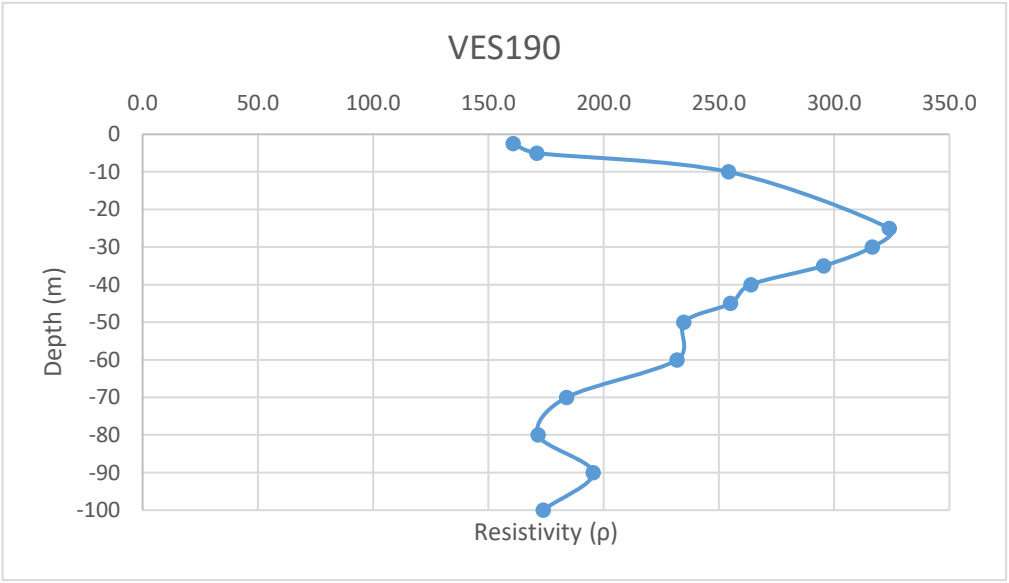

Annexure-XXII: Details of VES Survey

Date: 24/02/2025			VES-191			
Latitude	23.20797246		Longitude	69.67302383		
S.N	Current Electrode Spacing (AB/2)	Potential Electrode Spacing (MN)	Resistance (Ohm)	K value	Aparent Resistivity (Rho_a)	
1	2.5	1	25	18.846	471.150	-2.5
2	5	1	6.4	77.73975	497.534	-5
3	10	1	1.69	313.3148	529.502	-10
4	15	1	0.617	705.9398	435.565	-15
5	20	1	0.329	1255.615	413.097	-20
6	25	1	0.2	1962.34	392.468	-25
7	30	1	0.126	2826.115	356.090	-30
8	35	1	0.0821	3846.94	315.834	-35
9	40	1	0.0581	5024.815	291.942	-40
11	50	1	0.035	7851.715	274.810	-50
12	60	1	0.0196	11306.81	221.614	-60
13	70	1	0.00939	15390.11	144.513	-70
14	80	1	0.00768	20101.61	154.380	-80
15	90	1	0.00532	25441.31	135.348	-90
16	100	1	0.00337	31409.21	105.849	-100

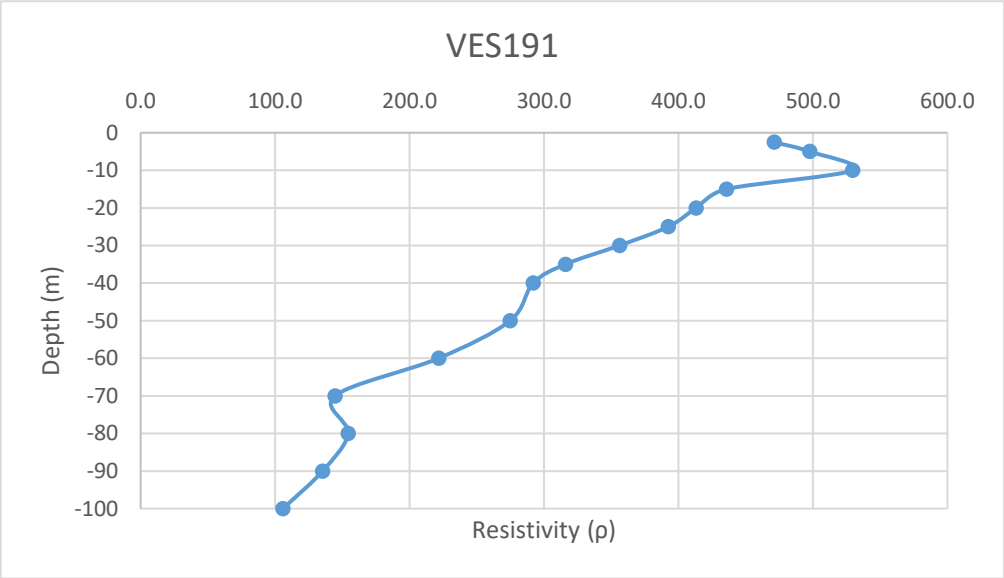

Annexure-XXII: Details of VES Survey

Date: 24/02/2025			VES-192			
Latitude	23.20797246		Longitude	69.67302383		
S.N	Current Electrode Spacing (AB/2)	Potential Electrode Spacing (MN)	Resistance (Ohm)	K value	Aparent Resistivity (Rho_a)	
1	2.5	1	1.48	18.846	27.892	-2.5
2	5	1	0.214	77.73975	16.636	-5
4	15	1	0.0256	705.9398	18.072	-15
5	20	1	0.0162	1255.615	20.341	-20
6	25	1	0.01024	1962.34	20.094	-25
7	30	1	0.00597	2826.115	16.872	-30
8	35	1	0.00426	3846.94	16.388	-35
9	40	1	0.00341	5024.815	17.135	-40
10	45	1	0.00341	6359.74	21.687	-45
11	50	1	0.0017	7851.715	13.348	-50
12	60	1	0.00201	11306.81	22.727	-60
13	70	1	0.0015	15390.11	23.085	-70
14	80	1	0.00125	20101.61	25.127	-80
15	90	1	0.001	25441.31	25.441	-90
16	100	1	0.0005	31409.21	15.705	-100

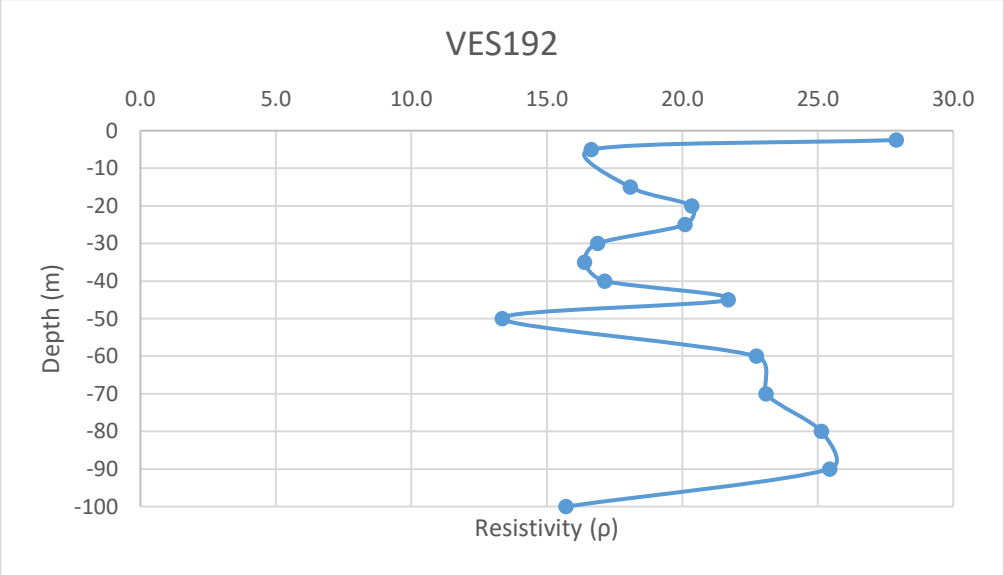

Annexure-XXII: Details of VES Survey

Date: 3/03/2025		VES-193				
Latitude	23.2202056		Longitude	69.69888484		
S.N	Current Electrode Spacing (AB/2)	Potential Electrode Spacing (MN)	Resistance (Ohm)	K value	Aparent Resistivity (Rho_a)	
1	2.5	1	3.23	18.846	60.873	-2.5
2	5	1	0.897	77.73975	69.733	-5
3	10	1	0.228	313.3148	71.436	-10
4	15	1	0.0947	705.9398	66.852	-15
5	20	1	0.0518	1255.615	65.041	-20
6	25	1	0.0304	1962.34	59.655	-25
7	30	1	0.0181	2826.115	51.153	-30
8	35	1	0.01105	3846.94	42.509	-35
9	40	1	0.00728	5024.815	36.581	-40
10	45	1	0.00502	6359.74	31.926	-45
11	50	1	0.00402	7851.715	31.564	-50
12	60	1	0.00251	11306.81	28.380	-60
13	70	1	0.00175	15390.11	26.933	-70
14	80	1	0.0015	20101.61	30.152	-80
15	90	1	0.00075	25441.31	19.081	-90
16	100	1	0.0005	31409.21	15.705	-100

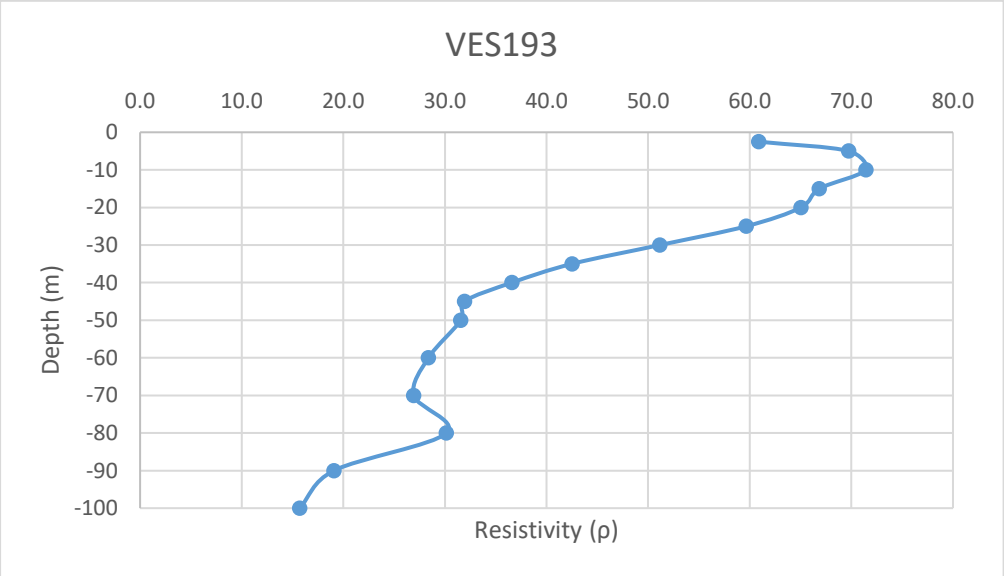

Annexure-XXII: Details of VES Survey

Date: 3/03/2025			VES-194			
Latitude	23.21697751		Longitude	69.6975673		
S.N	Current Electrode Spacing (AB/2)	Potential Electrode Spacing (MN)	Resistance (Ohm)	K value	Aparent Resistivity (Rho_a)	
1	2.5	1	4.8	18.846	90.461	-2.5
2	5	1	0.939	77.73975	72.998	-5
3	10	1	0.193	313.3148	60.470	-10
4	15	1	0.0851	705.9398	60.075	-15
5	20	1	0.0472	1255.615	59.265	-20
6	25	1	0.0289	1962.34	56.712	-25
7	30	1	0.0196	2826.115	55.392	-30
8	35	1	0.0141	3846.94	54.242	-35
9	40	1	0.01005	5024.815	50.499	-40
10	45	1	0.00778	6359.74	49.479	-45
11	50	1	0.00527	7851.715	41.379	-50
12	60	1	0.00427	11306.81	48.280	-60
13	70	1	0.00226	15390.11	34.782	-70
14	80	1	0.0015	20101.61	30.152	-80
15	90	1	0.00125	25441.31	31.802	-90
16	100	1	0.00075	31409.21	23.557	-100

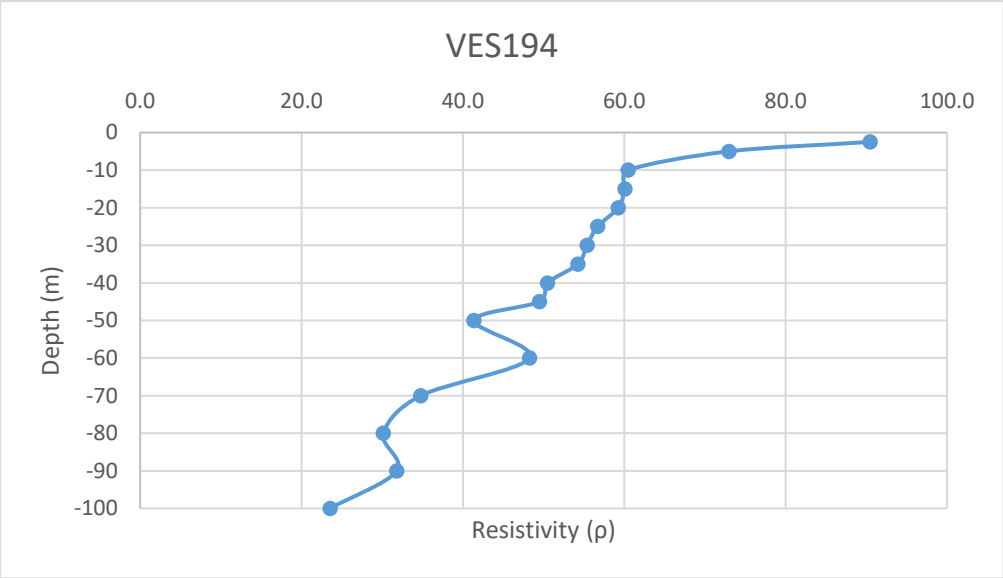

Annexure-XXII: Details of VES Survey

Date: 3/03/2025			VES-195			
Latitude	23.21492396		Longitude	69.69651372		
S.N	Current Electrode Spacing (AB/2)	Potential Electrode Spacing (MN)	Resistance (Ohm)	K value	Aparent Resistivity (Rho_a)	
1	2.5	1	2.19	18.846	41.273	-2.5
2	5	1	0.822	77.73975	63.902	-5
3	10	1	0.246	313.3148	77.075	-10
4	15	1	0.0956	705.9398	67.488	-15
5	20	1	0.0407	1255.615	51.104	-20
6	25	1	0.0211	1962.34	41.405	-25
7	30	1	0.0118	2826.115	33.348	-30
8	35	1	0.00804	3846.94	30.929	-35
9	40	1	0.00603	5024.815	30.300	-40
10	45	1	0.00527	6359.74	33.516	-45
11	50	1	0.00452	7851.715	35.490	-50
12	60	1	0.00301	11306.81	34.034	-60
13	70	1	0.00201	15390.11	30.934	-70
14	80	1	0.0015	20101.61	30.152	-80
15	90	1	0.00125	25441.31	31.802	-90
16	100	1	0.00075	31409.21	23.557	-100

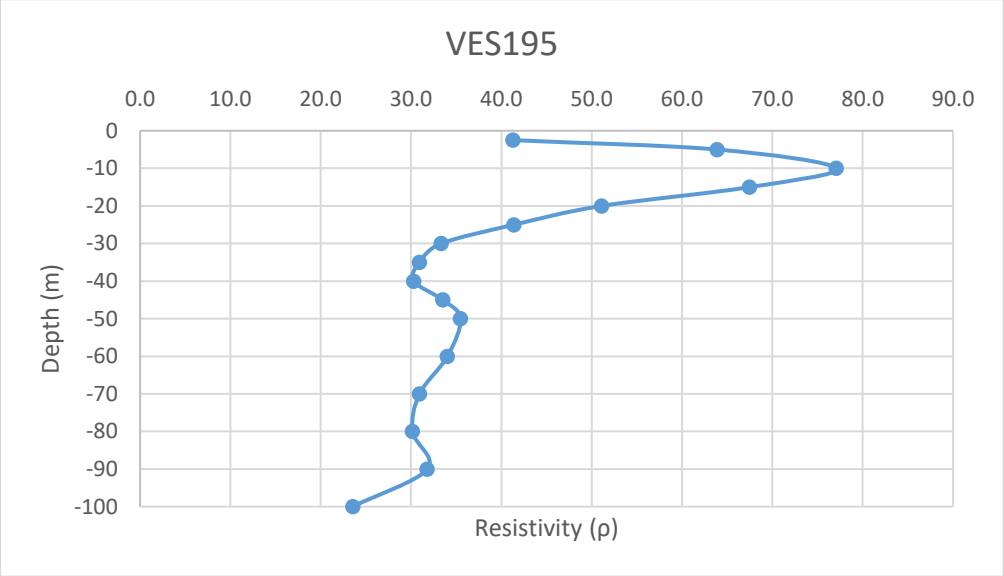

Annexure-XXII: Details of VES Survey

Date: 3/03/2025			VES-196			
Latitude	23.21352057		Longitude	69.69906017		
S.N	Current Electrode Spacing (AB/2)	Potential Electrode Spacing (MN)	Resistance (Ohm)	K value	Aparent Resistivity (Rho_a)	
1	2.5	1	4.32	18.846	81.415	-2.5
2	5	1	1.076	77.73975	83.648	-5
3	10	1	0.341	313.3148	106.840	-10
4	15	1	0.124	705.9398	87.537	-15
5	20	1	0.0681	1255.615	85.507	-20
6	25	1	0.0427	1962.34	83.792	-25
7	30	1	0.0256	2826.115	72.349	-30
8	35	1	0.0173	3846.94	66.552	-35
9	40	1	0.0126	5024.815	63.313	-40
10	45	1	0.00904	6359.74	57.492	-45
11	50	1	0.00653	7851.715	51.272	-50
12	60	1	0.00427	11306.81	48.280	-60
13	70	1	0.00226	15390.11	34.782	-70
14	80	1	0.00175	20101.61	35.178	-80
15	90	1	0.001	25441.31	25.441	-90
16	100	1	0.0005	31409.21	15.705	-100

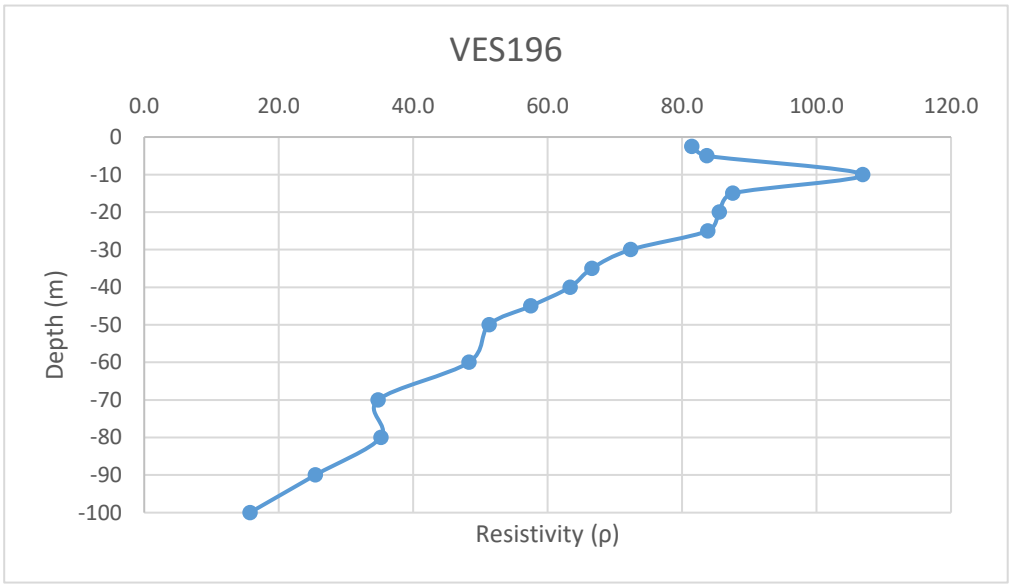

Annexure-XXII: Details of VES Survey

Date: 4/03/2025			VES-197			
Latitude	23.22512268		Longitude	69.6979366		
S.N	Current Electrode Spacing (AB/2)	Potential Electrode Spacing (MN)	Resistance (Ohm)	K value	Aparent Resistivity (Rho_a)	
1	2.5	1	1.87	18.846	35.242	-2.5
2	5	1	0.386	77.73975	30.008	-5
3	10	1	0.101	313.3148	31.645	-10
4	15	1	0.0558	705.9398	39.391	-15
5	20	1	0.0369	1255.615	46.332	-20
6	25	1	0.0271	1962.34	53.179	-25
7	30	1	0.0201	2826.115	56.805	-30
8	35	1	0.0153	3846.94	58.858	-35
9	40	1	0.0121	5024.815	60.800	-40
10	45	1	0.0103	6359.74	65.505	-45
11	50	1	0.00753	7851.715	59.123	-50
12	60	1	0.00502	11306.81	56.760	-60
13	70	1	0.00402	15390.11	61.868	-70
14	80	1	0.00251	20101.61	50.455	-80
15	90	1	0.00201	25441.31	51.137	-90
16	100	1	0.00125	31409.21	39.262	-100

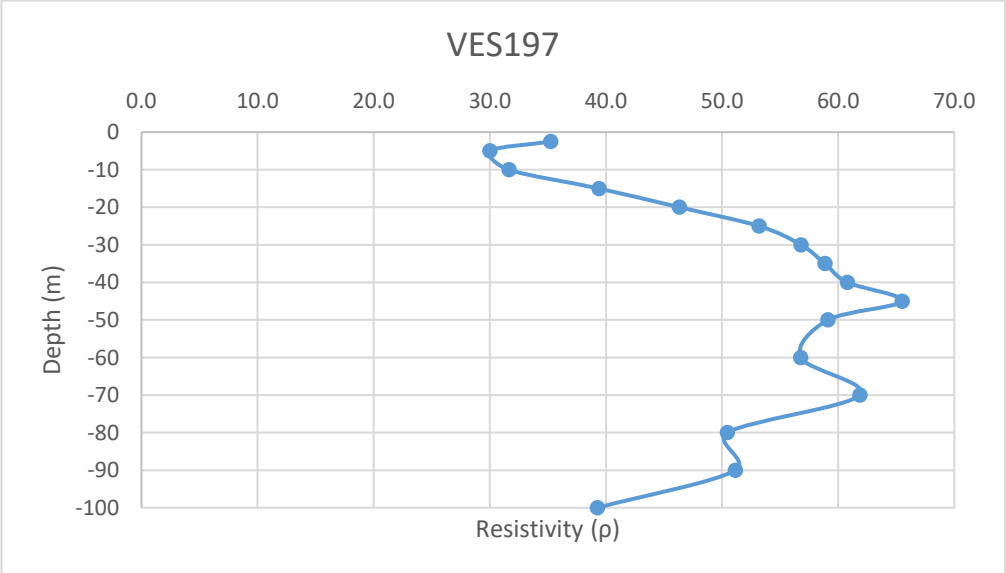

Annexure-XXII: Details of VES Survey

Date: 4/03/2025			VES-198			
Latitude	23.22298074		Longitude	69.69946337		
S.N	Current Electrode Spacing (AB/2)	Potential Electrode Spacing (MN)	Resistance (Ohm)	K value	Aparent Resistivity (Rho_a)	
1	2.5	1	6.33	18.846	119.295	-2.5
2	5	1	1.51	77.73975	117.387	-5
3	10	1	0.243	313.3148	76.135	-10
4	15	1	0.0845	705.9398	59.652	-15
5	20	1	0.0447	1255.615	56.126	-20
6	25	1	0.0264	1962.34	51.806	-25
7	30	1	0.0173	2826.115	48.892	-30
8	35	1	0.0128	3846.94	49.241	-35
9	40	1	0.00979	5024.815	49.193	-40
10	45	1	0.00829	6359.74	52.722	-45
11	50	1	0.00628	7851.715	49.309	-50
12	60	1	0.00412	11306.81	46.584	-60
13	70	1	0.00351	15390.11	54.019	-70
14	80	1	0.00251	20101.61	50.455	-80
15	90	1	0.00175	25441.31	44.522	-90
16	100	1	0.001	31409.21	31.409	-100

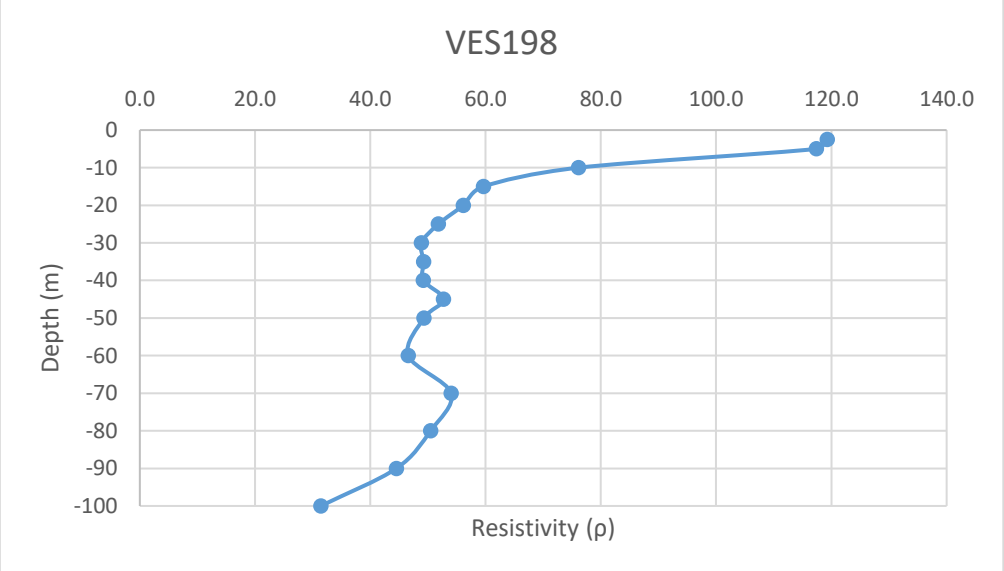

Annexure-XXII: Details of VES Survey

Date: 4/03/2025			VES-199			
Latitude	23.22239797		Longitude	69.6977513		
S.N	Current Electrode Spacing (AB/2)	Potential Electrode Spacing (MN)	Resistance (Ohm)	K value	Aparent Resistivity (Rho_a)	
1	2.5	1	7.9	18.846	148.883	-2.5
2	5	1	1.43	77.73975	111.168	-5
3	10	1	0.239	313.3148	74.882	-10
4	15	1	0.0792	705.9398	55.910	-15
5	20	1	0.0332	1255.615	41.686	-20
6	25	1	0.0153	1962.34	30.024	-25
7	30	1	0.00904	2826.115	25.548	-30
8	35	1	0.00552	3846.94	21.235	-35
9	40	1	0.00402	5024.815	20.200	-40
10	45	1	0.00301	6359.74	19.143	-45
11	50	1	0.00351	7851.715	27.560	-50
12	60	1	0.00226	11306.81	25.553	-60
13	70	1	0.00175	15390.11	26.933	-70
14	80	1	0.00175	20101.61	35.178	-80
15	90	1	0.0015	25441.31	38.162	-90
16	100	1	0.0005	31409.21	15.705	-100

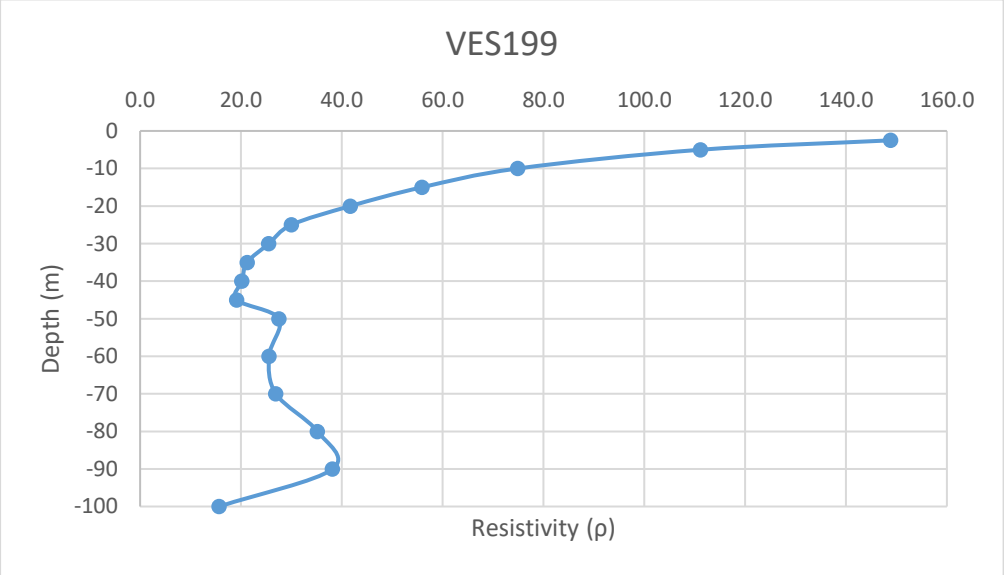

Annexure-XXII: Details of VES Survey

Date: 4/03/2025			VES-200			
Latitude	23.2199043		Longitude	69.70096768		
S.N	Current Electrode Spacing (AB/2)	Potential Electrode Spacing (MN)	Resistance (Ohm)	K value	Aparent Resistivity (Rho_a)	
1	2.5	1	1.59	18.846	29.965	-2.5
2	5	1	0.541	77.73975	42.057	-5
3	10	1	0.17	313.3148	53.264	-10
4	15	1	0.0781	705.9398	55.134	-15
5	20	1	0.0455	1255.615	57.130	-20
6	25	1	0.0266	1962.34	52.198	-25
7	30	1	0.0171	2826.115	48.327	-30
8	35	1	0.01055	3846.94	40.585	-35
9	40	1	0.00778	5024.815	39.093	-40
10	45	1	0.00502	6359.74	31.926	-45
11	50	1	0.00452	7851.715	35.490	-50
12	60	1	0.00276	11306.81	31.207	-60
13	70	1	0.00175	15390.11	26.933	-70
14	80	1	0.00125	20101.61	25.127	-80
15	90	1	0.001	25441.31	25.441	-90
16	100	1	0.0005	31409.21	15.705	-100

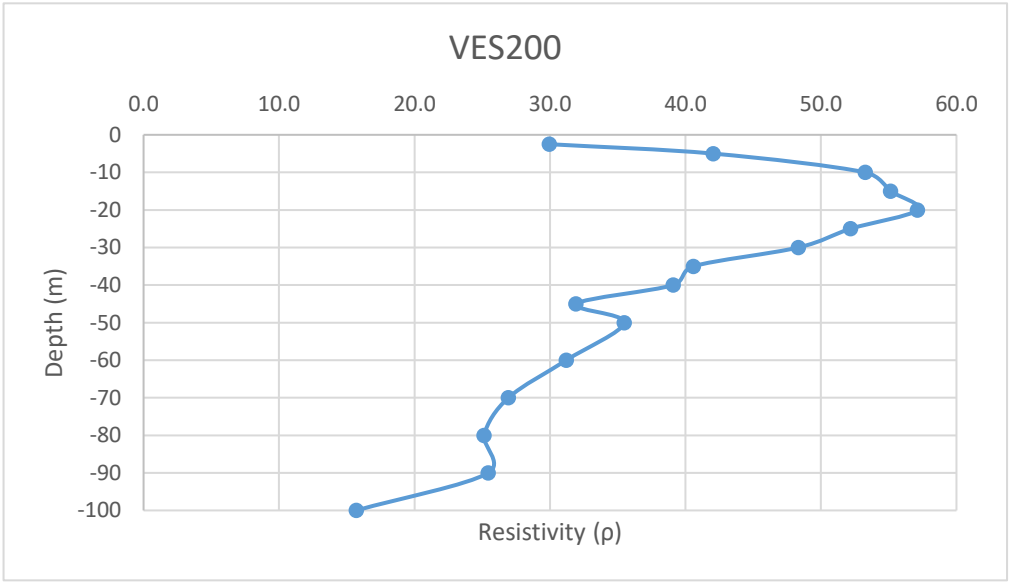

Annexure-XXII: Details of VES Survey

Date: 7/03/2025			VES-201			
Latitude	23.2199043		Longitude	69.70096768		
S.N	Current Electrode Spacing (AB/2)	Potential Electrode Spacing (MN)	Resistance (Ohm)	K value	Aparent Resistivity (Rho_a)	
1	2.5	1	0.84	18.846	15.831	-2.5
2	5	1	0.099	77.73975	7.696	-5
3	10	1	0.0309	313.3148	9.681	-10
4	15	1	0.0151	705.9398	10.660	-15
5	20	1	0.00879	1255.615	11.037	-20
6	25	1	0.00527	1962.34	10.342	-25
7	30	1	0.00351	2826.115	9.920	-30
8	35	1	0.00226	3846.94	8.694	-35
9	40	1	0.0015	5024.815	7.537	-40
10	45	1	0.00125	6359.74	7.950	-45
11	50	1	0.00075	7851.715	5.889	-50
12	60	1	0.0005	11306.81	5.653	-60
13	70	1	0.00075	15390.11	11.543	-70
14	80	1	0.0005	20101.61	10.051	-80
15	90	1	0.00025	25441.31	6.360	-90
16	100	1	0.00025	31409.21	7.852	-100

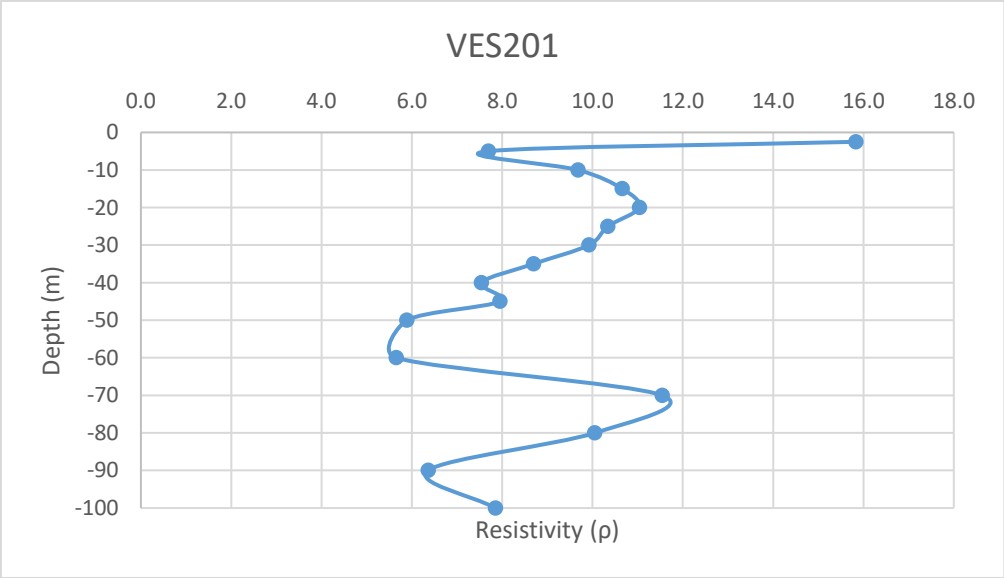

Annexure-XXII: Details of VES Survey

Date: 7/03/2025			VES-202			
Latitude	23.2199043		Longitude	69.70096768		
S.N	Current Electrode Spacing (AB/2)	Potential Electrode Spacing (MN)	Resistance (Ohm)	K value	Aparent Resistivity (Rho_a)	
1	2.5	1	1.172	18.846	22.088	-2.5
2	5	1	0.203	77.73975	15.781	-5
3	10	1	0.0448	313.3148	14.037	-10
4	15	1	0.0173	705.9398	12.213	-15
5	20	1	0.00872	1255.615	10.949	-20
6	25	1	0.00531	1962.34	10.420	-25
7	30	1	0.00371	2826.115	10.485	-30
8	35	1	0.0025	3846.94	9.617	-35
9	40	1	0.0019	5024.815	9.547	-40
10	45	1	0.0014	6359.74	8.904	-45
11	50	1	0.00125	7851.715	9.815	-50
12	60	1	0.0005	11306.81	5.653	-60
13	70	1	0.0003	15390.11	4.617	-70
14	80	1	0.0002	20101.61	4.020	-80
15	90	1	0.0002	25441.31	5.088	-90
16	100	1	0.0002	31409.21	6.282	-100

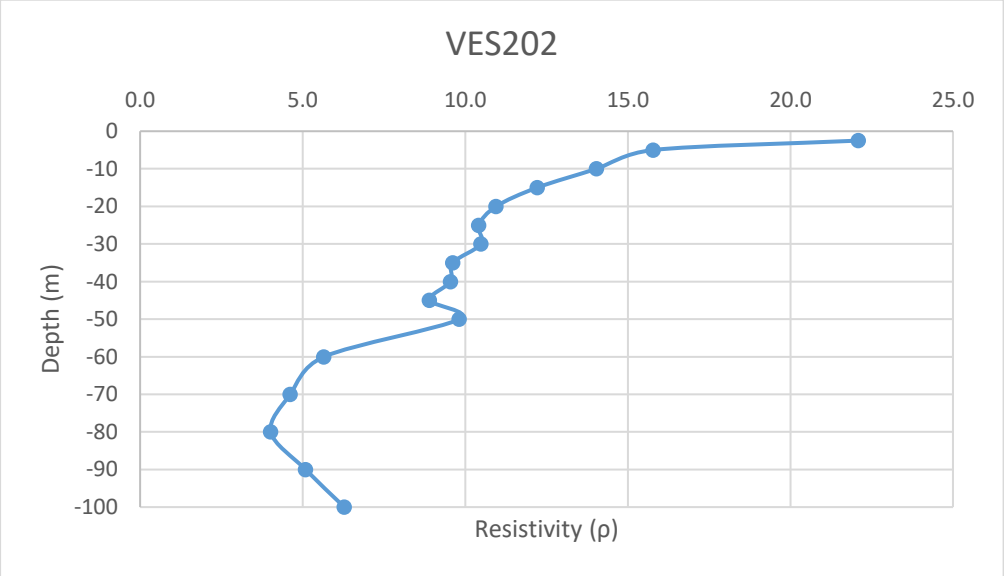

Annexure-XXII: Details of VES Survey

Date: 7/03/2025			VES-203			
Latitude	23.2199043		Longitude	69.70096768		
S.N	Current Electrode Spacing (AB/2)	Potential Electrode Spacing (MN)	Resistance (Ohm)	K value	Aparent Resistivity (Rho_a)	
1	2.5	1	9.2	18.846	173.383	-2.5
2	5	1	1.015	77.73975	78.906	-5
3	10	1	0.0429	313.3148	13.441	-10
4	15	1	0.00792	705.9398	5.591	-15
5	20	1	0.00431	1255.615	5.412	-20
6	25	1	0.0029	1962.34	5.691	-25
7	30	1	0.0017	2826.115	4.804	-30
8	35	1	0.0011	3846.94	4.232	-35
9	40	1	0.0007	5024.815	3.517	-40
10	45	1	0.0013	6359.74	8.268	-45
11	50	1	0.0007	7851.715	5.496	-50
12	60	1	0.0004	11306.81	4.523	-60
13	70	1	0.0003	15390.11	4.617	-70
14	80	1	0.00025	20101.61	5.025	-80
15	90	1	0.0002	25441.31	5.088	-90
16	100	1	0.0001	31409.21	3.141	-100

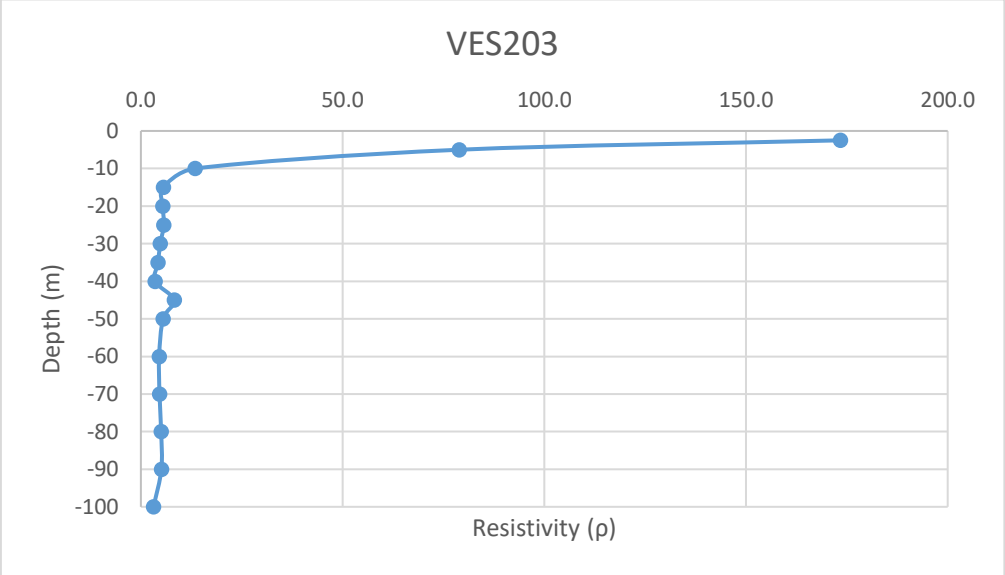

Annexure-XXII: Details of VES Survey

Date: 7/03/2025			VES-204			
Latitude	23.2199043		Longitude	69.70096768		
S.N	Current Electrode Spacing (AB/2)	Potential Electrode Spacing (MN)	Resistance (Ohm)	K value	Aparent Resistivity (Rho_a)	
1	2.5	1	2.33	18.846	43.911	-2.5
2	5	1	0.456	77.73975	35.449	-5
3	10	1	0.0688	313.3148	21.556	-10
4	15	1	0.0254	705.9398	17.931	-15
5	20	1	0.0121	1255.615	15.193	-20
6	25	1	0.00603	1962.34	11.833	-25
7	30	1	0.00402	2826.115	11.361	-30
8	35	1	0.00201	3846.94	7.732	-35
9	40	1	0.00175	5024.815	8.793	-40
10	45	1	0.0015	6359.74	9.540	-45
11	50	1	0.001	7851.715	7.852	-50
12	60	1	0.00075	11306.81	8.480	-60
13	70	1	0.0007	15390.11	10.773	-70
14	80	1	0.0004	20101.61	8.041	-80
15	90	1	0.00025	25441.31	6.360	-90
16	100	1	0.0002	31409.21	6.282	-100

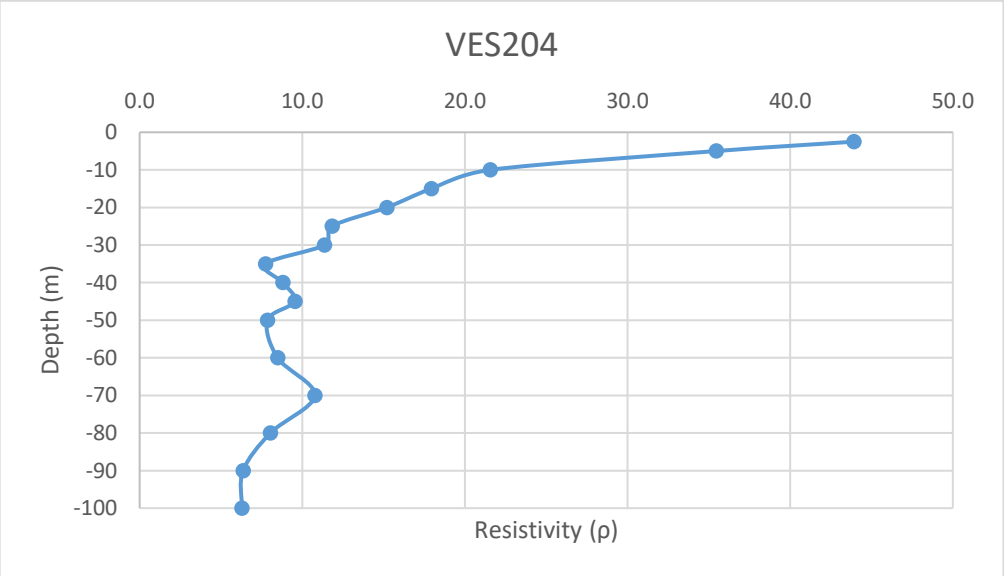

Annexure-XXII: Details of VES Survey

Date: 8/03/2025			VES-205			
Latitude	23.2199043		Longitude	69.70096768		
S.N	Current Electrode Spacing (AB/2)	Potential Electrode Spacing (MN)	Resistance (Ohm)	K value	Aparent Resistivity (Rho_a)	
1	2.5	1	0.365	18.846	6.879	-2.5
2	5	1	0.1078	77.73975	8.380	-5
3	10	1	0.0273	313.3148	8.553	-10
4	15	1	0.01072	705.9398	7.568	-15
5	20	1	0.00531	1255.615	6.667	-20
6	25	1	0.0035	1962.34	6.868	-25
7	30	1	0.0024	2826.115	6.783	-30
8	35	1	0.0019	3846.94	7.309	-35
9	40	1	0.0015	5024.815	7.537	-40
10	45	1	0.0011	6359.74	6.996	-45
11	50	1	0.0008	7851.715	6.281	-50
12	60	1	0.0006	11306.81	6.784	-60
13	70	1	0.0004	15390.11	6.156	-70
14	80	1	0.0003	20101.61	6.030	-80
15	90	1	0.0002	25441.31	5.088	-90
16	100	1	0.0001	31409.21	3.141	-100

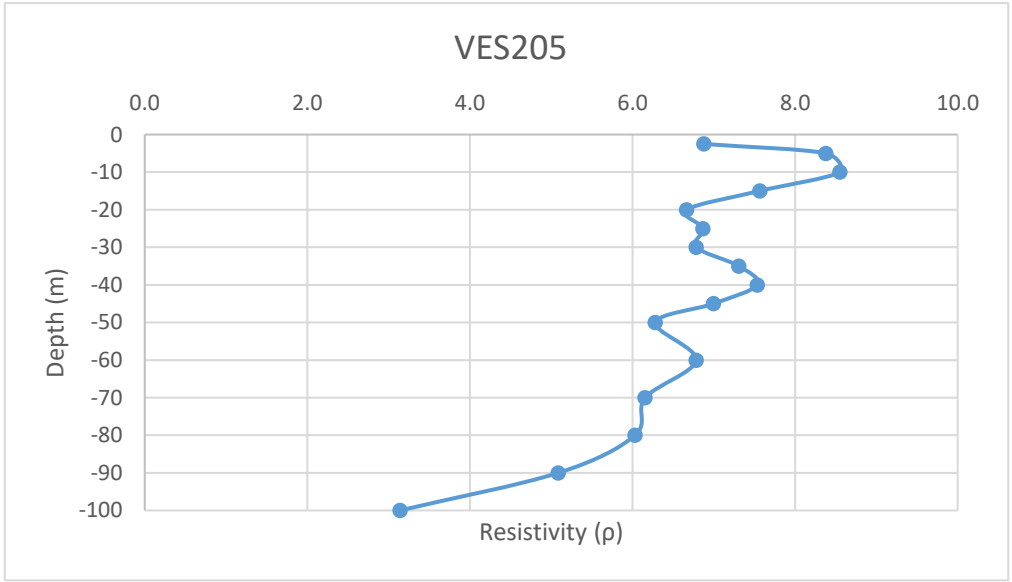

Annexure-XXII: Details of VES Survey

Date: 8/03/2025			VES-206			
Latitude	23.2199043		Longitude	69.70096768		
S.N	Current Electrode Spacing (AB/2)	Potential Electrode Spacing (MN)	Resistance (Ohm)	K value	Aparent Resistivity (Rho_a)	
1	2.5	1	51.9	18.846	978.107	-2.5
2	5	1	3.45	77.73975	268.202	-5
3	10	1	0.615	313.3148	192.689	-10
4	15	1	0.191	705.9398	134.834	-15
5	20	1	0.0681	1255.615	85.507	-20
6	25	1	0.0367	1962.34	72.018	-25
7	30	1	0.0269	2826.115	76.022	-30
8	35	1	0.0204	3846.94	78.478	-35
9	40	1	0.0163	5024.815	81.904	-40
10	45	1	0.0143	6359.74	90.944	-45
11	50	1	0.0126	7851.715	98.932	-50
12	60	1	0.0133	11306.81	150.381	-60
13	70	1	0.01055	15390.11	162.366	-70
14	80	1	0.00929	20101.61	186.744	-80
15	90	1	0.00958	25441.31	243.728	-90
16	100	1	0.00403	31409.21	126.579	-100

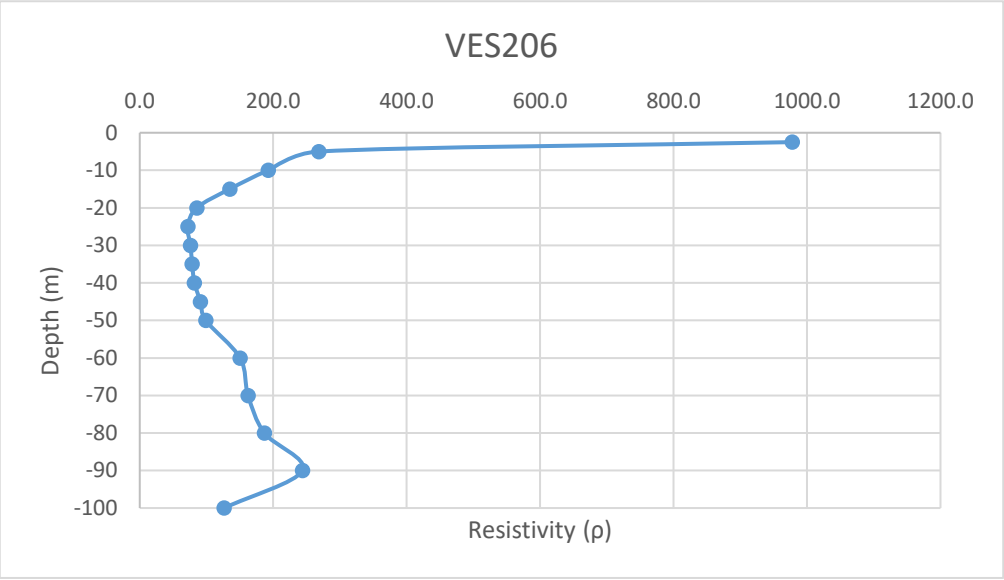

Annexure-XXII: Details of VES Survey

Date: 8/03/2025			VES-207			
Latitude	23.2199043		Longitude	69.70096768		
S.N	Current Electrode Spacing (AB/2)	Potential Electrode Spacing (MN)	Resistance (Ohm)	K value	Aparent Resistivity (Rho_a)	
1	2.5	1	11.89	18.846	224.079	-2.5
2	5	1	2.84	77.73975	220.781	-5
3	10	1	0.426	313.3148	133.472	-10
4	15	1	0.101	705.9398	71.300	-15
5	20	1	0.0364	1255.615	45.704	-20
6	25	1	0.0186	1962.34	36.500	-25
7	30	1	0.01155	2826.115	32.642	-30
8	35	1	0.00804	3846.94	30.929	-35
9	40	1	0.00554	5024.815	27.837	-40
10	45	1	0.00353	6359.74	22.450	-45
11	50	1	0.00403	7851.715	31.642	-50
12	60	1	0.00302	11306.81	34.147	-60
13	70	1	0.00256	15390.11	39.399	-70
14	80	1	0.00201	20101.61	40.404	-80
15	90	1	0.00151	25441.31	38.416	-90
16	100	1	0.00101	31409.21	31.723	-100

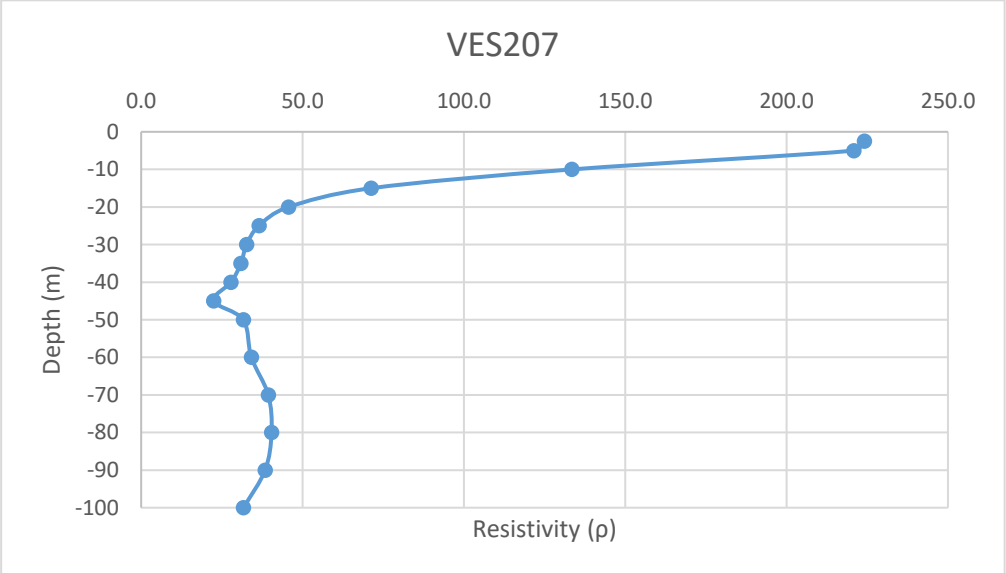

Annexure-XXII: Details of VES Survey

Date: 9/03/2025			VES-208			
Latitude	23.15913979		Longitude	69.71741773		
S.N	Current Electrode Spacing (AB/2)	Potential Electrode Spacing (MN)	Resistance (Ohm)	K value	Aparent Resistivity (Rho_a)	
1	2.5	1	2.2	18.846	41.461	-2.5
2	5	1	0.664	77.73975	51.619	-5
3	10	1	0.273	313.3148	85.535	-10
4	15	1	0.152	705.9398	107.303	-15
5	20	1	0.0709	1255.615	89.023	-20
6	25	1	0.0388	1962.34	76.139	-25
7	30	1	0.0166	2826.115	46.914	-30
8	35	1	0.00858	3846.94	33.007	-35
9	40	1	0.00631	5024.815	31.707	-40
10	45	1	0.00471	6359.74	29.954	-45
11	50	1	0.00257	7851.715	20.179	-50
12	60	1	0.00202	11306.81	22.840	-60
13	70	1	0.00153	15390.11	23.547	-70
14	80	1	0.00137	20101.61	27.539	-80

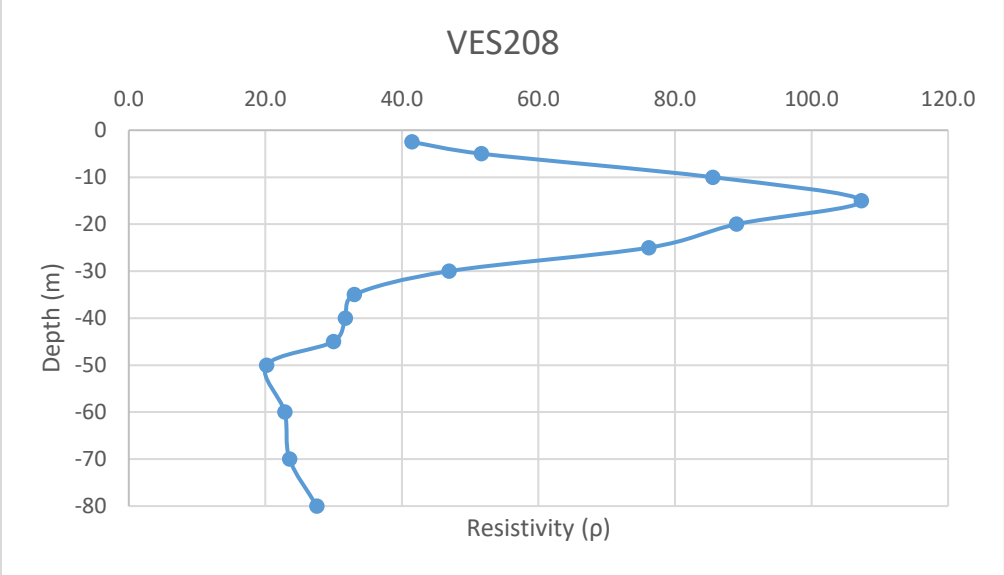

Annexure-XXII: Details of VES Survey

Date: 9/03/2025			VES-209			
Latitude	23.15936167		Longitude	69.7191356		
S.N	Current Electrode Spacing (AB/2)	Potential Electrode Spacing (MN)	Resistance (Ohm)	K value	Aparent Resistivity (Rho_a)	
1	2.5	1	8.59	18.846	161.887	-2.5
2	5	1	2.97	77.73975	230.887	-5
3	10	1	1.058	313.3148	331.487	-10
4	15	1	0.308	705.9398	217.429	-15
5	20	1	0.147	1255.615	184.575	-20
6	25	1	0.0567	1962.34	111.265	-25
7	30	1	0.0227	2826.115	64.153	-30
8	35	1	0.0156	3846.94	60.012	-35
9	40	1	0.0116	5024.815	58.288	-40
10	45	1	0.00908	6359.74	57.746	-45
11	50	1	0.00756	7851.715	59.359	-50
12	60	1	0.00554	11306.81	62.640	-60
13	70	1	0.00403	15390.11	62.022	-70
14	80	1	0.00252	20101.61	50.656	-80
15	90	1	0.00353	25441.31	89.808	-90
16	100	1	0.00175	31409.21	54.966	-100

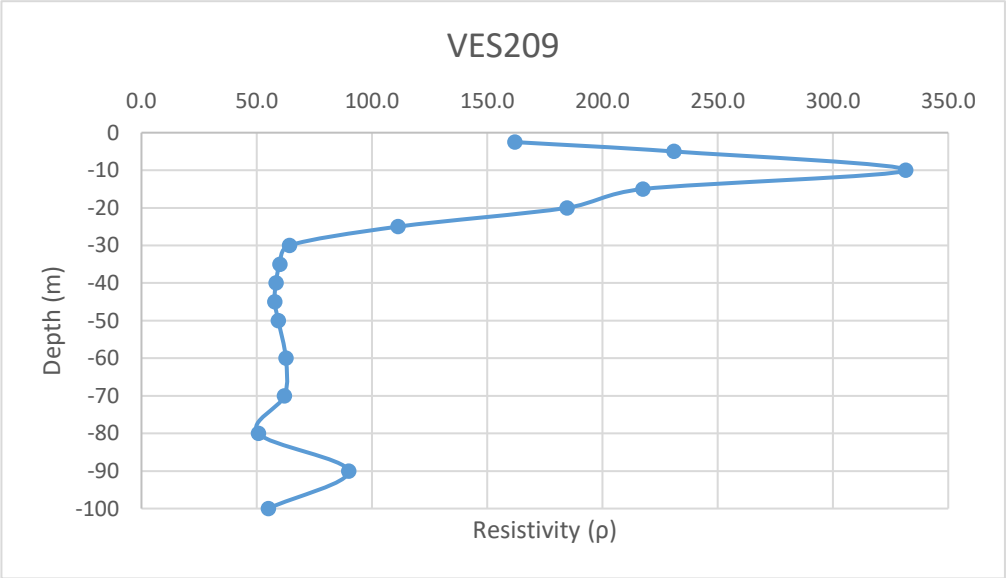

Annexure-XXII: Details of VES Survey

Date: 9/03/2025			VES-210			
Latitude	23.16102203		Longitude	69.7236299		
S.N	Current Electrode Spacing (AB/2)	Potential Electrode Spacing (MN)	Resistance (Ohm)	K value	Aparent Resistivity (Rho_a)	
1	2.5	1	0.644	18.846	12.137	-2.5
2	5	1	0.0976	77.73975	7.587	-5
3	10	1	0.0277	313.3148	8.679	-10
4	15	1	0.0161	705.9398	11.366	-15
5	20	1	0.00957	1255.615	12.016	-20
6	25	1	0.00706	1962.34	13.854	-25
7	30	1	0.00454	2826.115	12.831	-30
8	35	1	0.00353	3846.94	13.580	-35
9	40	1	0.00226	5024.815	11.356	-40
10	45	1	0.00175	6359.74	11.130	-45
11	50	1	0.0015	7851.715	11.778	-50
12	60	1	0.0005	11306.81	5.653	-60
13	70	1	0.00201	15390.11	30.934	-70
14	80	1	0.00085	20101.61	17.086	-80

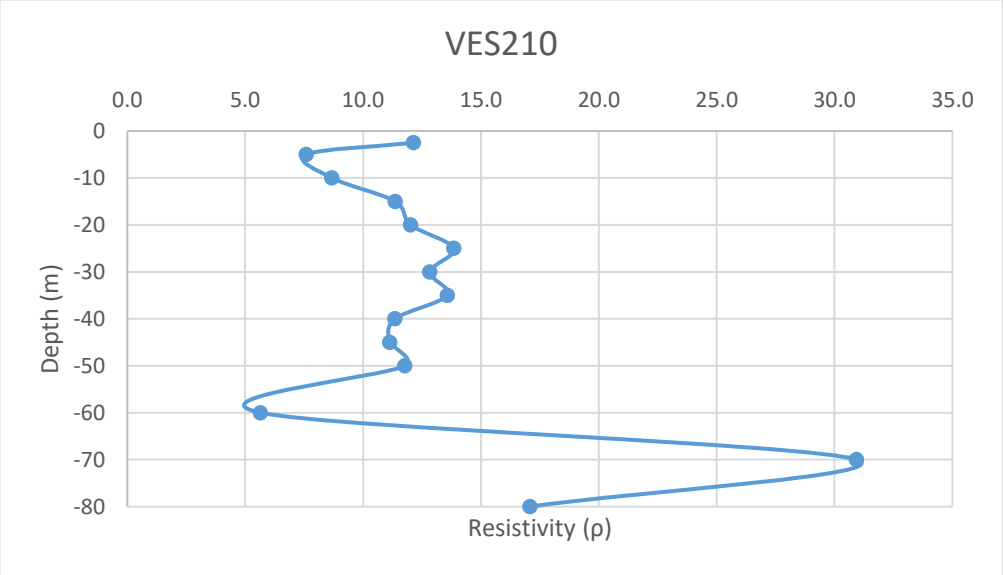

Annexure-XXIII: XRF Analysis of Check Samples

Sl No.	Sample ID	Latitude	Longitude	Sample Type	Lab	Al2O3	BaO	CaO	Cr2O3	Fe2O3	K2O	MgO	MnO	Na2O	P2O5	TiO2	SiO2	LOI	SO3	V2O5
1	105494	23.1507	69.58	BR	Shiva	6.99	<0.05	15.99	<0.05	34.79	0.62	2.22	0.12	<0.08	9.62	0.48	16.38	12.22	0.34	<0.05
					BV	8.8	0.02	11.97	0.02	34.44	0.74	2.16	0.16	0.19	7.64	0.52	20.13	12.27	0.4	NA
2	105405	23.215	69.590	BR	Shiva	24.46	<0.05	0.09	<0.05	0.74	0.46	0.25	<0.05	0.56	0.08	1.39	62.05	9.67	0.12	<0.05
					BV	23.79	0.03	0.06	0.03	0.7	0.49	0.19	0.02	0.41	0.1	1.34	62.74	9.42	0.07	NA
3	105409	23.207	69.645	BR	Shiva	5.91	<0.05	0.37	<0.05	60.81	0.57	0.07	0.10	<0.08	0.17	0.54	25.34	5.63	0.30	<0.05
					BV	1.61	0.03	0.03	0.01	22.11	0.61	0.05	0.05	0.09	0.04	0.33	71.69	2.8	0.39	NA
4	105429	23.240	69.585	BR	Shiva	14.46	<0.05	0.20	<0.05	0.86	1.41	0.43	<0.05	0.83	0.09	1.13	73.77	6.15	0.53	<0.05
					BV	14.89	0.03	0.23	0.02	0.69	1.33	0.53	0.03	0.99	0.08	1.11	72.12	6.8	0.7	NA
5	109056	23.203828	69.628518	Borehole	Shiva	14.88	<0.05	<0.05	0.07	9.77	0.33	0.12	<0.05	<0.08	0.06	1.07	66.36	6.94	0.07	<0.05
					BV	19.27	<0.05	0.08	<0.05	9.23	0.33	0.15	<0.05	0.15	0.05	1.06	62.09	7.05	<0.05	NA
6	109081	23.150838	69.578518	Borehole	Shiva	21.53	<0.05	0.31	<0.05	4.36	2.09	0.87	<0.05	0.23	0.12	1.30	53.54	14.51	0.97	<0.05
					BV	22.80	<0.05	0.26	0.05	5.11	1.91	0.77	<0.05	0.31	0.11	1.20	51.61	13.54	2.06	NA
7	109082	23.150838	69.578518	Borehole	Shiva	7.79	<0.05	7.34	<0.05	30.13	0.68	4.05	<0.05	<0.08	3.49	0.46	18.94	25.99	0.97	<0.05
					BV	13.58	<0.05	4.90	<0.05	22.25	0.97	3.94	0.12	0.27	2.11	0.62	27.47	22.49	1.13	NA
8	109128	23.1562908	69.7070139	Borehole	Shiva	10.05	0.06	4.44	<0.05	3.26	2.24	2.02	<0.05	0.12	0.05	0.75	67.24	9.55	0.06	<0.05
					BV	9.94	0.06	3.99	<0.05	3.24	2.20	1.93	0.06	0.20	0.05	0.77	68.40	8.75	<0.05	NA
9	109132	23.1562908	69.7070139	Borehole	Shiva	10.69	<0.05	13	<0.05	15.58	0.99	1.96	0.05	0.11	7.82	0.69	30.55	18.07	0.35	<0.05
					BV	14.02	<0.05	9.29	<0.05	19.25	0.86	2.55	0.14	0.28	5.30	0.57	27.33	19.65	0.27	NA
10	112151	23.1562908	69.7070139	Borehole	Shiva	10.97	<0.05	7.06	<0.05	4.06	1.97	1.75	<0.05	<0.08	<0.05	0.58	58.24	12.54	2.56	<0.05
					BV	13.66	<0.05	5.17	<0.05	4.38	1.84	1.48	<0.05	0.17	0.06	0.63	59.40	9.80	3.11	NA
11	109091	23.150838	69.578518	Borehole	Shiva	5.68	<0.05	4.29	<0.05	40.1	0.51	3.51	<0.05	<0.08	0.45	0.33	14.05	29.53	1.38	<0.05
					BV	9.06	<0.05	3.69	<0.05	33.65	0.72	3.67	0.14	0.23	0.38	0.44	19.76	26.13	1.65	NA
12	113002	23.197537	69.529703	Borehole	Shiva	3.73	<0.05	0.05	0.08	9.19	0.81	<0.05	<0.05	0.08	<0.05	0.45	83.32	2.06	0.09	<0.05
					BV	4.46	<0.05	<0.05	<0.05	6.78	0.76	<0.05	0.09	0.18	<0.05	0.34	85.63	1.39	<0.05	NA
13	113062	23.1562908	69.7070139	Borehole	Shiva	7.99	<0.05	3.76	<0.05	32.66	0.8	2.93	<0.05	<0.08	0.45	0.55	23.61	25.76	1.21	<0.05
					BV	10.73	<0.05	3.98	<0.05	30.06	0.84	3.11	0.15	0.17	0.45	0.59	25.17	23.51	1.16	NA
14	109150	23.1562908	69.7070139	Borehole	Shiva	0.66	<0.05	36.86	<0.05	1.53	<0.05	0.72	<0.05	<0.08	1.34	0.11	0.28	57.91	0.21	0.15
					BV	9.72	0.00	24.04	0.05	6.52	0.55	1.22	0.06	0.26	1.00	0.25	14.99	40.12	1.13	NA

Annexure-XXIV ICPMS Check Samples

Sl No.	Sample ID	Latitude	Longitude	Sample Type	Lab	Li	Be	B	Sc	V	Cr	Co	Ni	Cu	Zn	Ga	Ge	Se	Rb
1	107451	23.1992	69.7056	BR	Shiva	10.9	2.3	<5	12.5			28				6.4	<0.5	4.6	22.2
					BV	22.7	2.1	NA	15.1	211.1	NA	NA	NA	NA	NA	8.3	<0.5	3.7	23
2	107452	23.1901	69.7231	BR	Shiva	13.3	<0.5	<5	0.8			9.6				7.3	<0.5	<0.5	43.4
					BV	19.8	<0.5	NA	2.1	15.1	NA	NA	NA	NA	NA	7.9	<0.5	0.7	43.2
3	107453	23.2067	69.6464	BR	Shiva	5.9	1.5	<5	10.2			26.5				13.2	<0.5	<0.5	13.3
					BV	10.9	2.7	NA	11.1	390.9	NA	NA	NA	NA	NA	14.4	0.8	1.2	13.5
4	107454	23.1966	69.7455	BR	Shiva	5.6	1.2	<5	9.8			31.8				5.3	<0.5	<0.5	13.5
					BV	15.9	1.6	NA	12.4	255.7	NA	NA	NA	NA	NA	7.6	<0.5	3.3	14.1
5	107455	23.1507	69.5800	BR	Shiva	20.8	2.7	<5	51.3			7.1				12	<0.5	3.5	38.8
					BV	38.6	2.7	NA	54.4	295.5	NA	NA	NA	NA	NA	16.1	<0.5	10.1	38.6
6	107456	23.1601	69.7232	BR	Shiva	7.7	0.8	<5	10.2			10.2				6.4	<0.5	<0.5	24.7
					BV	14.9	1.3	NA	14.2	255.9	NA	NA	NA	NA	NA	11	<0.5	2.6	29.3
7	107457	23.1518	69.5778	BR	Shiva	65.8	0.8	<5	17.4			15				28	<0.5	<0.5	101.9
					BV	13.7	2.9	NA	21.9	182.8	NA	NA	NA	NA	NA	33.8	<0.5	1.8	116.8
8	107458	23.1518	69.5778	BR	Shiva	71.2	3.2	<5	14.4			17.3				30.2	<0.5	<0.5	107.9
					BV	3.6	0.7	NA	4.4	37.6	NA	NA	NA	NA	NA	8.5	<0.5	<0.5	29.8
9	107459	23.1518	69.5778	BR	Shiva	65	1.5	<5	16.3			17.5				27.5	<0.5	<0.5	100
					BV	13	2.4	NA	21.4	157.9	NA	NA	NA	NA	NA	32	<0.5	2.1	113.4
10	107460	23.1523	69.7433	SS	Shiva	8.7	<0.5	<5	2			4.6				4.6	<0.5	<0.5	16.4
					BV	9.2	2.4	NA	51	582	495.4	32	63.2	43.1	220.9	42.8	19	5.7	9
11	107461	23.1508	69.6239	SS	Shiva	6.3	<0.5	<5	15.2			7.5				10.8	0.6	1.3	52.5
					BV	13.5	0.7	NA	27.4	109.8	NA	NA	NA	NA	NA	18.3	1.6	6.7	52.4
12	107462	23.2212	69.5899	BR	Shiva	4.7	1.5	<5	6.8			48.5				3.9	<0.5	<0.6	0.9
					BV	9.1	1.7	NA	9.2	44.6	NA	NA	NA	NA	NA	4.8	<0.5	1.3	0.9
13	107463	23.1507	69.5800	SS	Shiva	31.6	1.1	<5	50.6			11.6				18.7	0.6	8.8	58.9
					BV	79.2	2.4	NA	59.3	143.1	NA	NA	NA	NA	NA	27.5	1.7	14.9	60.3
14	107464	23.1440	69.6452	BR	Shiva	6.9	<0.5	<5	2.1			18.7				5.2	<0.5	<0.6	3.1
					BV	11.7	<0.5	NA	4	52.3	NA	NA	NA	NA	NA	7.4	<0.5	1.7	3.1
15	107465	23.2212	69.5899	BR	Shiva	47.4	2	<5	51.8			19.3				32.5	<0.5	<0.6	<0.5
					BV	79.7	2.3	NA	60.1	252.3	NA	NA	NA	NA	NA	37.6	<0.5	1.3	<0.5
16	107466	23.1829	69.5639	BR	Shiva	27.3	1	<5	11.6			7.1				21.5	<0.5	<0.6	39.3
					BV	57.3	2	NA	16	102.2	NA	NA	NA	NA	NA	26.5	<0.5	2.4	41.8
17	105494	23.1507	69.5800	BR	Shiva	25.4	2.0	<5	46.0			6.9	55	15	48	8.7	<5	2.6	34.9
					BV	38.6	2.7	54.4	295.5	16.1	NA	NA	NA	NA	NA	<0.5	10.1	38.6	521.5
18	105405	23.2153	69.5900	BR	Shiva	32.9	2.0	<5	18.5			8.7	30	50	56	27.1	<5	<5	21.8
					BV	56.7	3	27.1	146.8	40	NA	NA	NA	NA	NA	<0.5	2.1	23.5	131.1

Sl No.	Sample ID	Latitude	Longitude	Sample Type	Lab	Li	Be	B	Sc	V	Cr	Co	Ni	Cu	Zn	Ga	Ge	Se	Rb
19	105409	23.2070	69.6450	BR	Shiva	10.1	1.1	<5	4.2			14.5	22	<5	40	7.1	<5	<5	18.1
					BV	6	1	3.2	31	3.6	NA	NA	NA	NA	NA	<0.5	1.6	14.6	43.3
20	105429	23.2404	69.5847	BR	Shiva	24.9	0.9	<5	7.8			2.0	11	<5	14	16.1	<5	<5	55.7
					BV	51.4	1.4	12	84.2	23	NA	NA	NA	NA	NA	<0.5	1.4	58	138.6
21	108975	23.2041	69.5421	Bedrock (Pitting-A)	Shiva	15.2	1.3	<5	5.6	35	133	13.0	54	12	56	6.2	<0.5	<0.5	12.0
					BV	415	<0.5		1.3	46	91.3	13.6	28.6	3.3	78.1	7.7	1.8	0.7	<0.5
22	108979	23.2041	69.5421	Bedrock (Pitting-A)	Shiva	9.1	0.7	<5	4.4	37	139	2.9	6	14	31	8.2	<0.5	<0.5	12.3
					BV	20.2	<0.5		<0.5	51.2	81.9	14.5	50.4	6.2	62.8	8.7	2	<0.5	<0.5
23	108983	23.1946	69.5977	Bedrock (Pitting-1)	Shiva	51.0	1.6	<5	22.1	203	85	12.1	34	30	45	12.5	<0.5	<0.5	41.8
					BV	84.7	<0.5		1.4	214.5	104	14.1	37.8	24.1	42	25.7	1	<0.5	<0.5
24	108984	23.1946	69.5977	Bedrock (Pitting-1)	Shiva	43.8	1.5	<5	31.9	269	119	20.1	61	35	56	12.0	<0.5	<0.5	39.1
					BV	243.7	<0.5		1.1	274.2	110.3	20.4	62.1	45.3	53.5	26	1.4	0.7	<0.5
25	108985	23.1947	69.5976	Bedrock (Pitting-2)	Shiva	40.4	1.6	<5	28.0	234	77	17.1	49	30	57	10.5	<0.5	<0.5	35.8
					BV	108.5	<0.5		1.8	246.3	96.3	15.6	58	26	46.8	25.1	1.7	1	<0.5
26	108986	23.1947	69.5976	Bedrock (Pitting-2)	Shiva	44.1	1.7	<5	25.4	261	97	25.8	63	62	84	14.6	<0.5	<0.5	24.8
					BV	156	<0.5		2	270.9	105.2	24.2	66.4	49.9	76.7	26.3	1.5	0.8	<0.5
27	108987	23.1949	69.5975	Bedrock (Pitting-3)	Shiva	52.0	1.6	<5	28.6	261	97	12.1	40	24	128	13.6	<0.5	<0.5	45.4
					BV	<0.5	<0.5		<0.5	255.8	102.5	15.8	45.6	29.2	70.8	27.4	<0.5	<0.5	<0.5
28	108988	23.1949	69.5975	Bedrock (Pitting-3)	Shiva	13.2	<0.5	<5	3.1	26	302	4.3	10	7	53	4.8	<0.5	<0.5	37.3
					BV	304.9	<0.5		1.4	26.4	67.7	7.8	12.3	6.7	47.7	3.3	1	0.8	<0.5
29	108989	23.1949	69.5975	Bedrock (Pitting-3)	Shiva	89.9	1.5	<5	12.8	225	121	15.0	50	47	98	21.4	<0.5	<0.5	68.5
					BV	157.6	<0.5		2.1	195.9	116.5	18.1	54.4	46	78.2	23.2	1.6	1.1	<0.5
30	109017	23.1963	69.5965	BR	Shiva	16.64	0.55	<5	7.59	37	137	5.27	15	49	47	6.19	<0.5	0.73	42.05
					BV	<0.5	<0.5		<0.5	51.8	70.5	9.8	26.4	8.4	55.4	6.2	<0.5	<0.5	<0.5
31	109018	23.1957	69.5340	BR	Shiva	4.49	0.60	<5	1.03	18	279	9.55	15	<5	13	3.41	<0.5	<0.5	15.83
					BV	<0.5	<0.5		0.8	29.8	85.2	14.7	27.2	2	28.3	14.1	<0.5	1	<0.5
32	109019A	23.1957	69.5340	BR	Shiva	7.78	<0.5	<5	<0.5	10	86	1.71	5	<5	<5	3.26	<0.5	<0.5	16.93
					BV	<0.5	<0.5		<0.5	16.7	64.1	4.6	15.1	3.6	17.3	3.3	<0.5	<0.5	<0.5
33	109020	23.1957	69.5340	BR	Shiva	5.70	<0.5	<5	<0.5	<5	135	1.15	<5	<5	<5	2.24	<0.5	<0.5	13.26
					BV	110.3	<0.5		<0.5	9	72.7	2.8	7.3	2.3	13.8	1.7	<0.5	<0.5	<0.5

Table Continued..

Annexure- XXIV

Sl No.	Sample ID	Sample Type	Lab	Sr	Y	Zr	Nb	Mo	Cd	In_	Sn	Sb	Te	Cs	Ba	La	Ce	Pr	Nd	Sm
1	107451	BR	Shiva	NA	65	NA	9.7	0.6	<0.5	<0.5	<0.5	0.6	<0.5	1.3		47.1	131.2	17.2	87.3	21
			BV	287.1	77.2	57.5	4.9	1.2	0.6	<0.5	<0.5	<0.5	0.8	1.4	NA	37.7	147.6	17.5	79.7	20.3
2	107452	BR	Shiva	NA	3.5	NA	6	<0.5	<0.5	<0.5	<0.5	<0.5	<0.5	<0.5		13.7	21.8	2.6	11.2	2.2
			BV	118.9	3.3	16.9	1.1	0.7	<0.5	<0.5	<0.5	<0.5	<0.5	<0.5	NA	11.6	24	2.6	9.6	1.8
3	107453	BR	Shiva	NA	18	NA	13.1	4.4	<0.5	<0.5	<0.5	<0.5	<0.5	1		23.9	39.5	5.1	22.2	5
			BV	61.6	18.3	113.3	11.4	4.8	<0.5	<0.5	1.9	4.2	<0.5	1.1	NA	18.6	41.3	5	18.1	4.6
4	107454	BR	Shiva	NA	43.5	NA	3.9	1.3	<0.5	<0.5	<0.5	<0.5	<0.5	0.9		38.4	81.6	10.3	49	10.7
			BV	520.8	45.8	43.4	3.1	1.5	<0.5	<0.5	<0.5	<0.5	<0.5	1	NA	36.9	102.2	11.5	44.6	10.5
5	107455	BR	Shiva	NA	291	NA	8.7	0.7	<0.5	<0.5	<0.5	<0.5	<0.5	2.7		92.3	195.4	27.1	142	36.5
			BV	521.5	289.4	158.2	8.2	1	<0.5	<0.5	1.6	<0.5	<0.5	2.9	NA	87.7	242.1	30.8	131.6	35.5
6	107456	BR	Shiva	NA	24.2	NA	12.9	1.1	<0.5	<0.5	<0.5	<0.5	<0.5	0.5		71	128.7	15.1	63.2	10.9
			BV	1106.9	29.9	131.3	13.1	0.6	<0.5	<0.5	1.4	2.1	<0.5	0.7	NA	78.2	186.5	19.5	70.4	12.7
7	107457	BR	Shiva	NA	29.1	NA	25.5	1.3	<0.5	<0.5	<0.5	0.8	<0.5	7		57.6	90.9	11.4	47.7	9
			BV	257.5	34.1	175	22.2	1.4	<0.5	<0.5	4.6	1.7	<0.5	8.2	NA	58.5	119.1	13.8	50.2	9.7
8	107458	BR	Shiva	NA	23	NA	31.2	1.1	<0.5	<0.5	<0.5	<0.5	<0.5	7.5		61.4	95.7	12.2	50.1	9.3
			BV	57.4	6.8	47.4	5.6	<0.5	<0.5	<0.5	0.9	<0.5	<0.5	2	NA	15.1	31	3.5	12.5	2.3
9	107459	BR	Shiva	NA	27.4	NA	50.2	1.2	<0.5	<0.5	<0.5	<0.5	<0.5	6.4		57.7	88.9	11.4	47	9
			BV	410.4	33.6	185.4	22.4	1.2	<0.5	<0.5	4.3	1.8	<0.5	7.2	NA	59.8	119.8	13.6	49.5	9.5
10	107460	SS	Shiva	NA	8.1	NA	7.5	<0.5	<0.5	<0.5	<0.5	0.6	<0.5	<0.5		35.3	54.2	6.7	27.7	4.5
			BV	136	260	2082	270.3	4.2	1.9	<0.5	16.8	1.1	<0.5	<0.5	569	1578	3162	362	1238	209
11	107461	SS	Shiva	NA	76.2	NA	37.1	<0.5	1	<0.5	<0.5	0.5	<0.5	1.3		362.3	559.5	68.2	282.6	47.1
			BV	138.5	90.7	2435	46.5	0.8	0.5	<0.5	3	2	<0.5	1.3	NA	253.8	506.8	58.4	206.1	36.7
12	107462	BR	Shiva	NA	8	NA	8	9.3	<0.5	<0.5	<0.5	3	<0.5	<0.5		11.7	18.3	2.4	10.5	1.9
			BV	35.9	8.9	38.7	3.4	11.1	<0.5	<0.5	<0.5	<0.5	<0.5	<0.5	NA	11.4	23.3	2.7	9.3	2
13	107463	SS	Shiva	NA	489.3	NA	13.3	2.2	<0.5	<0.5	<0.5	7.3	<0.5	4.3		165.7	347.4	49.8	263.6	65.7
			BV	768.8	505.4	201.2	11.7	1.2	<0.5	<0.5	2.8	1	<0.5	4.2	NA	143	407.5	51.4	229.4	59
14	107464	BR	Shiva	NA	11.2	NA	6.5	0.5	<0.5	<0.5	<0.5	<0.5	<0.5	<0.5		61.7	94.9	12	48.9	8.2
			BV	52.1	11.7	168.3	14.4	0.8	<0.5	<0.5	0.9	<0.5	<0.5	<0.5	NA	59	119.1	13.4	44.8	8
15	107465	BR	Shiva	NA	31.2	NA	24	1	<0.5	<0.5	<0.5	37.7	<0.5	<0.5		31.2	52.4	7.3	33.6	7
			BV	448	32.2	172.7	15.6	0.8	<0.5	<0.5	1.1	0.6	<0.5	<0.5	NA	30	66	8.2	31.4	7
16	107466	BR	Shiva	NA	18.4	NA	19	1.3	<0.5	<0.5	<0.5	2.1	<0.5	4.3		46	61.1	8.2	34	6.2
			BV	66.6	21.6	160	19.1	14.9	<0.5	<0.5	3.4	<0.5	<0.5	4.7	NA	45.7	79.7	9.5	31.9	6.2
17	105494	BR	Shiva	502	290.4	8.1	0.9	<0.5	<0.5	<0.5	<0.5	<0.5	<0.5	2.6		79.7	203.3	24.6	113.2	27.2
			BV	289.4	158.2	8.2	1	<0.5	<0.5	1.6	<0.5	<0.5	2.9	87.7	NA	242.1	30.8	131.6	35.5	10
18	105405	BR	Shiva	72	27.2	25.3	<0.5	<0.5	<0.5	<0.5	<0.5	<0.5	<0.5	0.9		69.7	149.8	16.9	58.9	9.0
			BV	23.6	190.3	24.3	0.8	<0.5	<0.5	4.4	0.6	<0.5	1.1	130.9	NA	290.9	34.2	106.1	14.6	2.7
19	105409	BR	Shiva	60	14.3	8.9	2.4	<0.5	<0.5	<0.5	<0.5	<0.5	<0.5	0.9		24.5	50.4	6.0	22.9	4.2
			BV	5.9	18.5	5.1	1.1	<0.5	<0.5	<0.5	<0.5	<0.5	<0.5	19.4	NA	39.6	4.3	14.8	2.7	<0.5

Sl No.	Sample ID	Sample Type	Lab	Sr	Y	Zr	Nb	Mo	Cd	In_	Sn	Sb	Te	Cs	Ba	La	Ce	Pr	Nd	Sm
20	105429	BR	Shiva	127	19.0	17.6	<0.5	<0.5	<0.5	<0.5	<0.5	<0.5	<0.5	3.2		42.9	99.4	10.9	41.6	7.5
			BV	19.2	271.8	19.1	0.7	<0.5	<0.5	2.9	<0.5	<0.5	4.1	44.5	NA	100.2	10.7	36.2	7.1	1.4
21	108975	Bedrock (Pitting-A)	Shiva	61	12.0	69	7.6	0.9	<0.5	<0.5	<0.5	<0.5	<0.5	<0.5	130	59.0	103.0	10.8	36.8	5.5
			BV	37.3	1.2	92.6	1.2	<0.5	<0.5	<0.5	6.5	2.3	<0.5	86.6	424.9	10.5	21.4	2.1	8.2	1.9
22	108979	Bedrock (Pitting-A)	Shiva	16	13.9	160	17.1	0.6	<0.5	<0.5	<0.5	<0.5	<0.5	<0.5	91	73.0	147.0	16.5	61.3	9.8
			BV	48.3	0.7	133.3	2.7	<0.5	<0.5	<0.5	2.8	1.8	<0.5	4.5	258.9	10.4	17.3	2	7.8	1.3
23	108983	Bedrock (Pitting-1)	Shiva	191	56.0	99	13.8	1.1	<0.5	<0.5	<0.5	0.6	<0.5	2.9	112	46.8	126.0	12.7	53.0	10.6
			BV	164.3	0.9	91.6	2.6	0.5	<0.5	<0.5	7.4	1.9	<0.5	6.5	282	29.4	51.7	5.1	13.9	2.1
24	108984	Bedrock (Pitting-1)	Shiva	106	34.4	93	10.6	2.2	<0.5	<0.5	<0.5	<0.5	<0.5	2.6	107	25.5	62.5	6.4	26.1	5.4
			BV	107.4	3.2	106.6	3.1	0.9	<0.5	<0.5	1.7	2.5	<0.5	26.7	260.2	11.3	29.3	3.1	13.1	3.5
25	108985	Bedrock (Pitting-2)	Shiva	157	51.1	96	9.0	2.0	<0.5	<0.5	<0.5	0.6	<0.5	2.4	111	34.5	86.1	9.0	37.3	7.8
			BV	166.6	2.2	87.4	2.4	1.6	<0.5	<0.5	2.2	2.1	<0.5	28.5	304.9	7	17.6	1.8	7.4	1.9
26	108986	Bedrock (Pitting-2)	Shiva	68	34.9	107	11.3	1.9	<0.5	<0.5	<0.5	<0.5	0.9	2.3	121	21.1	59.2	6.5	27.6	6.2
			BV	70.4	2.5	111.4	1.9	1.3	0.5	<0.5	3.3	2	<0.5	34.7	334.1	8.4	19.6	1.9	8.1	2
27	108987	Bedrock (Pitting-3)	Shiva	120	62.3	103	11.7	1.4	<0.5	<0.5	<0.5	<0.5	<0.5	3.0	107	42.4	122.6	13.6	59.7	12.9
			BV	91.7	0.8	106.7	2.3	0.8	<0.5	<0.5	2.4	1.7	<0.5	9	696.7	9.6	18.6	2	7.7	1.3
28	108988	Bedrock (Pitting-3)	Shiva	186	10.6	68	7.7	<0.5	<0.5	<0.5	<0.5	<0.5	<0.5	0.8	234	27.4	56.2	6.4	23.4	4.1
			BV	166.1	2.3	74.2	1.7	<0.5	<0.5	<0.5	2.1	1.7	<0.5	45.5	383.1	13.5	27.9	3.1	11.9	2.9
29	108989	Bedrock (Pitting-3)	Shiva	74	21.1	147	18.0	1.9	<0.5	<0.5	<0.5	<0.5	<0.5	4.3	157	25.1	61.2	6.6	26.4	5.5
			BV	75.4	4.3	136.2	2	0.6	1.6	<0.5	7.5	5.5	<0.5	22.7	302.4	10.1	22	2.5	11.3	3
30	109017	BR	Shiva	237	21.80	69	5.45	<0.5	<0.5	<0.5	<0.5	<0.5	3.60	0.86	426	20.16	41.75	4.89	18.89	3.83
			BV	147.5	0.7	150.2	1.4	<0.5	<0.5	<0.5	1.8	1.9	<0.5	3	558.7	6.6	13.4	1.5	5.8	1.2
31	109018	BR	Shiva	39	5.67	38	<0.5	<0.5	<0.5	<0.5	<0.5	2.17	23.34	<0.5	223	10.41	21.87	2.46	9.19	1.67
			BV	30.8	1.2	45.2	2.2	<0.5	0.7	<0.5	2.6	1.7	<0.5	11	1152	8.8	16.8	2	7.8	1.7
32	109019A	BR	Shiva	16	3.22	29	<0.5	<0.5	<0.5	<0.5	<0.5	<0.5	<0.5	<0.5	114	5.90	11.70	1.32	5.01	0.93
			BV	25.1	<0.5	39.7	2.6	<0.5	<0.5	<0.5	1.7	1.6	<0.5	4.6	369.6	3.6	7.2	0.5	2.8	<0.5
33	109020	BR	Shiva	18	2.09	29	<0.5	<0.5	<0.5	<0.5	<0.5	<0.5	5.98	<0.5	121	5.99	11.74	1.29	4.74	0.80
			BV	26.8	<0.5	36.8	2	<0.5	<0.5	<0.5	1.9	1.7	<0.5	4.2	317.7	1.9	4.4	<0.5	1.4	<0.5

Table Continued..

Annexure- XXIV

Sl No.	Sample ID	Sample Type	Lab	Eu	Gd	Tb	Dy	Ho	Er	Tm	Yb	Lu	Hf	Ta	W	Tl	Bi	Pb	Th	U
1	107451	BR	Shiva	4.5	20.5	2.9	15.8	2.5	6.6	0.8	4.4	0.6	0.5	2.9	6.8	<0.5	<0.5		44.3	1.9
			BV	5.2	20.9	3.1	18.2	2.9	6.7	0.9	5.1	0.7	1.7	<0.5	NA	<0.5	<0.5	NA	10.2	2
2	107452	BR	Shiva	0.8	1.9	<0.5	1	<0.5	<0.5	<0.5	<0.5	<0.5	0.8	1.8	49.7	<0.5	<0.5		18.3	<0.5
			BV	0.8	1.4	<0.5	0.9	<0.5	<0.5	<0.5	<0.5	<0.5	0.7	<0.5	NA	<0.5	<0.5	NA	2.2	<0.5
3	107453	BR	Shiva	1.1	4.7	0.7	4.5	0.8	2.5	<0.5	2.4	<0.5	1	2.5	16.1	<0.5	<0.5		22.9	9.2
			BV	1.3	4.7	0.8	4.9	0.9	2.8	<0.5	2.7	<0.5	3.3	0.9	NA	<0.5	<0.5	NA	23.2	10.1
4	107454	BR	Shiva	2.4	10.7	1.6	9.5	1.6	5.1	0.6	4.2	0.6	0.7	0.9	9.1	<0.5	0.6		11.8	1.3
			BV	2.6	10.9	1.7	9.8	1.8	5	0.7	4.1	0.6	1.1	<0.5	NA	<0.5	<0.5	NA	13.5	1.3
5	107455	BR	Shiva	9.2	46.8	7.3	46.8	8.4	22.7	2.5	14.1	1.8	1.9	2.7	4.9	<0.5	<0.5		11.1	4.3
			BV	10	50.8	8.1	49	9.7	24.2	2.8	14.2	1.9	3	0.6	NA	<0.5	<0.5	NA	10.3	4.3
6	107456	BR	Shiva	1.6	9.6	1.1	5.9	1	3	<0.5	2.5	<0.5	0.5	1.2	1	<0.5	<0.5		28.9	2
			BV	1.9	10.1	1.4	6.6	1.2	3.2	<0.5	2.8	<0.5	3.5	0.8	NA	0.9	<0.5	NA	32.5	2.4
7	107457	BR	Shiva	1.9	8.4	1.1	6.5	1.1	3.5	<0.5	3.2	<0.5	2.5	6.3	4.1	<0.5	0.5		24.5	2.9
			BV	2.1	8.6	1.3	6.9	1.4	3.7	0.5	3.5	0.5	4.8	1.5	NA	0.8	1.4	NA	21.3	3.4
8	107458	BR	Shiva	1.8	8.1	1	5.6	0.9	3	<0.5	2.9	<0.5	2.6	8.7	3.8	<0.5	<0.5		25.4	3.1
			BV	<0.5	2	<0.5	1.5	<0.5	0.8	<0.5	0.8	<0.5	1.2	<0.5	NA	<0.5	<0.5	NA	5.7	0.8
9	107459	BR	Shiva	1.8	8.1	1.1	6.3	1.1	3.3	<0.5	3	<0.5	2.1	6.6	3.7	0.5	0.7		20.9	2.8
			BV	2	8.4	1.3	6.8	1.3	3.7	0.6	3.4	0.5	5.2	1.6	NA	1.3	0.5	NA	21.2	3.2
10	107460	SS	Shiva	<0.5	4.1	<0.5	2	<0.5	1	<0.5	0.8	<0.5	0.6	0.9	<0.5	<0.5	<0.5		16.3	1.5
			BV	9.1	173.6	16	60.4	9.3	22.4	2.6	16	2.4	55	16	8	<0.5	0.6	199	961	66.41944
11	107461	SS	Shiva	2.7	40	4.2	19.2	3	8.9	1.1	8.2	1.2	13.9	7.3	4.9	<0.5	<0.5		176.2	18
			BV	2.8	29	4.2	18.4	3.4	9.6	1.5	10.5	1.6	68.6	3.3	NA	0.6	<0.5	NA	138.2	19.8
12	107462	BR	Shiva	<0.5	2.2	<0.5	1.7	<0.5	1	<0.5	0.9	<0.5	<0.5	0.9	211	<0.5	<0.5		6.2	7
			BV	<0.5	2.2	<0.5	1.9	<0.5	1	<0.5	0.9	<0.5	1.1	<0.5	NA	<0.5	<0.5	NA	6.1	7
13	107463	SS	Shiva	16.6	85.5	13.3	84.5	15.2	41.1	4.4	23.9	3.1	1.7	2.1	19.7	0.5	0.5		13.5	5.8
			BV	16.2	81.1	14.3	75	14.9	36.5	4.2	21.5	2.8	4.3	0.9	NA	0.5	<0.5	NA	12.5	5.5
14	107464	BR	Shiva	0.7	6.8	0.7	3.2	<0.5	1.4	<0.5	1.2	<0.5	1.2	1.7	111	<0.5	<0.5		34.1	2.8
			BV	0.8	5.9	0.7	3.1	0.5	1.4	<0.5	1.2	<0.5	4.7	0.8	NA	<0.5	<0.5	NA	44.1	2.8
15	107465	BR	Shiva	2.1	8.3	1.2	7	1.3	3.7	<0.5	2.4	<0.5	2.4	7.2	16.9	<0.5	<0.5		5.6	4.4
			BV	2.1	8.7	1.3	7.4	1.4	3.7	<0.5	2.4	<0.5	4.2	1	NA	<0.5	<0.5	NA	4.4	4.3
16	107466	BR	Shiva	1.2	5.4	0.7	4	0.7	2.3	<0.5	2.1	<0.5	2.3	3.5	13.6	<0.5	<0.5		17.4	4
			BV	1.3	5.5	0.8	4.6	0.9	2.6	<0.5	2.3	<0.5	4.3	1.3	NA	<0.5	<0.5	NA	21.8	3.9
17	105494	BR	Shiva	8.0	41.2	6.6	42.6	8.7	22.9	2.7	15.5	2.2	4.5	0.8	1.2	0.5	<5	17	8.3	4.9
			BV	50.8	8.1	49	9.7	24.2	2.8	14.2	1.9	3	0.6	<0.5		<0.5	10.3	NA	4.3	NA
18	105405	BR	Shiva	1.9	7.8	1.2	6.3	1.2	3.5	0.6	3.7	0.6	6.8	2.1	2.7	<5	<5	32	23.7	5.8
			BV	9.2	1.2	6.3	1.1	3.3	0.5	3.2	<0.5	5.2	1.8	<0.5		<0.5	34.5	NA	5	NA
19	105409	BR	Shiva	0.8	4.2	0.6	3.2	0.6	1.8	<0.5	1.7	<0.5	4.6	0.8	0.7	<5	<5	31	13.2	3.1
			BV	2.3	<0.5	1.5	<0.5	0.8	<0.5	0.6	<0.5	0.6	<0.5	<0.5		<0.5	13.5	NA	1	NA

Sl No.	Sample ID	Sample Type	Lab	Eu	Gd	Tb	Dy	Ho	Er	Tm	Yb	Lu	Hf	Ta	W	Tl	Bi	Pb	Th	U
20	105429	BR	Shiva	1.6	6.4	0.9	4.3	0.9	2.4	<0.5	2.5	<0.5	9.4	1.7	1.8	<5	<5	17	19.2	3.7
			BV	5.7	0.8	4.2	0.8	2.3	<0.5	2.1	<0.5	7	1.3	<0.5	NA	<0.5	20.5	NA	2.7	NA
21	108975	Bedrock (Pitting-A)	Shiva	1.2	4.9	0.6	2.8	0.5	1.6	<0.5	1.3	<0.5	1.6	0.5	0.5	<0.5	<0.5	60	15.7	2.2
			BV	21.5	1.5	<0.5	2.7	0.6	2	<0.5	2	<0.5	3.6	3.6	1.3	<0.5	1.4	45.8	4.1	1.3
22	108979	Bedrock (Pitting-A)	Shiva	0.8	7.5	0.8	3.6	0.6	1.6	<0.5	1.4	<0.5	4.0	0.8	0.7	<0.5	<0.5	33	38.5	3.9
			BV	<0.5	1.2	<0.5	1.6	<0.5	1	<0.5	0.9	<0.5	3.2	1.9	1.1	<0.5	<0.5	71.6	6.5	1.2
23	108983	Bedrock (Pitting-1)	Shiva	2.6	12.4	1.6	9.7	1.7	4.8	0.6	3.5	0.5	3.7	1.0	1.4	<0.5	<0.5	29	11.3	6.3
			BV	<0.5	1.7	<0.5	1.7	<0.5	1.2	<0.5	1.2	<0.5	3.5	3.7	1.1	<0.5	0.7	32.1	6.5	2
24	108984	Bedrock (Pitting-1)	Shiva	1.3	6.3	0.9	6.0	1.2	3.6	0.5	3.6	0.5	2.8	0.9	1.2	<0.5	<0.5	22	8.8	3.9
			BV	<0.5	4.6	0.9	5.8	1.2	3.3	<0.5	2.2	<0.5	1.5	1.8	1.3	<0.5	<0.5	24.1	2.1	3.3
25	108985	Bedrock (Pitting-2)	Shiva	1.9	9.2	1.5	8.4	1.7	4.6	0.6	4.2	0.5	3.0	0.9	1.0	<0.5	<0.5	26	8.1	5.4
			BV	<0.5	2.4	0.6	4.2	1	3	<0.5	2.7	<0.5	1.8	1.8	1.4	<0.5	0.5	58.9	2	1.9
26	108986	Bedrock (Pitting-2)	Shiva	1.6	7.3	1.1	6.4	1.4	4.1	0.6	3.9	0.6	3.5	1.0	1.3	<0.5	<0.5	25	8.1	4.2
			BV	3	2.7	0.6	4.4	1	3.1	<0.5	2.9	<0.5	2.1	2.1	1.6	<0.5	0.6	29.5	2.5	2.3
27	108987	Bedrock (Pitting-3)	Shiva	3.4	15.6	2.2	11.8	2.2	5.9	0.7	4.6	0.6	3.4	1.1	1.4	<0.5	<0.5	23	10.4	5.8
			BV	0.9	1.7	<0.5	1.5	<0.5	0.9	<0.5	0.7	<0.5	2.9	1.1	1.2	<0.5	<0.5	26.7	7.5	0.7
28	108988	Bedrock (Pitting-3)	Shiva	0.6	3.5	<0.5	2.3	<0.5	1.0	<0.5	0.9	<0.5	1.2	0.6	0.6	<0.5	<0.5	10	11.7	1.8
			BV	2.7	2.7	0.5	3.8	0.8	2.6	<0.5	2.3	<0.5	3.6	2.8	1.3	<0.5	0.7	12.8	5.2	2.4
29	108989	Bedrock (Pitting-3)	Shiva	1.5	5.4	0.8	5.6	1.2	3.5	<0.5	3.3	<0.5	5.2	1.5	2.0	<0.5	<0.5	30	12.4	4.0
			BV	0.5	4.1	0.8	6.1	1.4	4.1	0.6	3.2	0.6	1.6	1.5	1.4	<0.5	3.9	30.7	1.4	3
30	109017	BR	Shiva	0.89	4.17	0.54	3.37	0.76	2.03	<0.5	1.70	<0.5	1.32	<0.5	0.97	<0.5	<0.5	22	4.96	1.50
			BV	<0.5	1.2	<0.5	1.9	<0.5	1.1	<0.5	0.9	<0.5	3	1	1.4	<0.5	<0.5	22.1	3.8	<0.5
31	109018	BR	Shiva	<0.5	1.67	<0.5	1.10	<0.5	0.61	<0.5	0.61	<0.5	<0.5	<0.5	<0.5	<0.5	<0.5	27	3.84	1.08
			BV	<0.5	1.7	<0.5	2.4	0.5	1.6	<0.5	1.4	<0.5	3.6	1.5	1.3	<0.5	<0.5	22.4	5.4	1.2
32	109019A	BR	Shiva	<0.5	0.95	<0.5	0.56	<0.5	<0.5	<0.5	<0.5	<0.5	<0.5	<0.5	<0.5	<0.5	<0.5	5	<0.5	1.73
			BV	<0.5	0.6	<0.5	1	<0.5	0.7	<0.5	0.7	<0.5	1.9	0.7	1.2	<0.5	<0.5	10.3	2.3	<0.5
33	109020	BR	Shiva	<0.5	0.79	<0.5	<0.5	<0.5	<0.5	<0.5	<0.5	<0.5	0.59	<0.5	<0.5	<0.5	<0.5	8	1.93	<0.5
			BV	<0.5	<0.5	<0.5	0.5	<0.5	<0.5	<0.5	<0.5	<0.5	1.7	<0.5	1.4	<0.5	<0.5	13	1.8	<0.5

Annexure-XXV: Details of Pit Locations

SL. No.	Pit No.	Longitude	Latitude	Dimensions (m x m x m)	Length	Breadth	Height	Volume cu m	Lithology
1	GSPL-Bhuj-Pit-1	69.597735	23.19462	2.1*1.9*2.1	2.1	1.9	2.1	8.4	Shale dominated heterolith with target layer
2	GSPL-Bhuj-Pit-2	69.59762	23.19473	2.1*2.0*2.1	2.1	2.0	2.1	8.8	Shale dominated heterolith with target layer
3	GSPL-Bhuj-Pit-3	69.59751	23.19494	2.5 *1.8*2.1	2.5	1.8	2.1	9.5	Shale dominated heterolith with target layer and ferrugenous sandstone
4	GSPL-Bhuj-Pit-4	69.597185	23.19514	2.1*1.9*2.05	2.1	1.9	2.1	8.2	shale dominated heterolith target layer
5	GSPL-Bhuj-Pit-5	69.597015	23.19578	2.03*1.84*2.1	2.0	1.8	2.1	7.8	Soil (No Hard Rock)
6	GSPL-Bhuj-Pit-6	69.599842	23.19593	2.2*2.35 *2.1	2.2	2.4	2.1	10.9	Soil (No Hard Rock)
7	GSPL-Bhuj-Pit-7	69.599842	23.19593	2.2*2.35 *2.1	2.2	2.4	2.1	10.9	shale and fine grained sandstone with gypsum layers
8	GSPL-Bhuj-Pit-8	69.600232	23.19618	2.1*1.55*2.05	2.1	1.6	2.1	6.7	Highly ferrugenous sandstone
9	GSPL-Bhuj-Pit-9	69.602013	23.19591	2.05*2*2.2	2.1	2.0	2.2	9.0	shale heterolith layer and ferrugenous sandstone
10	GSPL-Bhuj-Pit 10	69.542105	23.2041	5.05*2.2*1.8	5.1	2.2	1.8	20.0	Highly ferrugenous sandstone
11	GSPL-Bhuj-Pit-11	69.511425	23.20576	2.7*2.4*2.25	2.7	2.4	2.3	14.6	Ferruginous Sandstone with Metasomatised effect
12	GSPL-Bhuj-Pit 12	69.570621	23.19563	2.5*2.05*2.2	2.5	2.1	2.2	11.3	Sandstone
13	GSPL-Bhuj-Pit 13	69.576929	23.1958	2.4*2.1*2.6	2.4	2.1	2.6	13.1	Metasomatised Sandstone
14	GSPL-Bhuj-Pit 14	69.559587	23.19652	2.35*2.1*2.3	2.4	2.1	2.3	11.4	Sandstone
15	GSPL-Bhuj-Pit 15	69.583281	23.20324	2.4*2.15*2.3	2.4	2.2	2.3	11.9	Ferruginous Sandstone
16	GSPL-Bhuj-Pit 16	69.619407	23.19994	2.5*2.1*2.2	2.5	2.1	2.2	11.6	Ferruginous Sandstone
17	GSPL-Bhuj-Pit 17	69.62646	23.20633	2.55*2.1*2.15	2.6	2.1	2.2	11.5	Sandstone
18	GSPL-Bhuj-Pit 18	69.653808	23.20694	2.4*2.15*2.3	2.4	2.2	2.3	11.9	Medium Grained Sandstone
19	GSPL-Bhuj-Pit 19	69.543692	23.189	2.6*2.1*1.5	2.6	2.1	1.5	8.2	Ferruginous Sandstone
20	GSPL-Bhuj-Pit 20	69.619266	23.20083	2.25*2.05*2.2	2.3	2.1	2.2	10.1	Sandstone
								215.5	

Annexure-XXVI ICPMS Analysis of Pit Samples

S.N.	Sample ID	Location	Latitude	Longitude	Type	Host Lithology	Sample Description	Formation	Li	Be	Sc	V	Cr	Co	Ni	Cu	Zn
1	109045	GSPL/Bhuj/274/01/2025	23.19181	69.58950	Bedrock/Pit Sample	Tuffite bed	NA	Katrol Formation	41.53	<0.5	8.45	47	131	3.84	11	8	24
2	109053	GSPL/Bhuj/279/01/2025	23.22131	69.58954	Bedrock/Pit Sample	Metasomatized ferruginized sandstone	Highly ferruginous, metasomatized sandstone	Bhuj Formation	24.96	<0.5	11.59	58	149	3.52	17	26	17
3	109054	GSPL/Bhuj/277/01/2025	23.209516	69.52222	Bedrock/Pit Sample	Metasomatized ferruginized sandstone	Metasomatized ferruginized sandstone	Bhuj Formation	7.89	0.96	3.00	23	306	22.07	106	11	98
4	109055	GSPL/Bhuj/280/01/2025	23.203158	69.628937	Bedrock/Pit Sample	Highly ferruginous sandstone	Highly ferruginous sandstone	Bhuj Formation	7.23	<0.5	3.57	17	131	18.86	46	10	78
5	109056	GSPL/Bhuj/281/01/2025	23.225561	69.549791	Bedrock/Pit Sample	Metasomatized ferruginized sandstone	Metasomatized ferruginized sandstone	Bhuj Formation	34.63	4.51	30.46	422	203	115.63	86	13	128
6	109057	GSPL/Bhuj/283/01/2025	23.232838	69.527921	Bedrock/Pit Sample	Shale dominated heterolith	Shale part of the heterolith	Bhuj Formation	6.01	0.96	3.45	89	263	25.44	60	<5	141
7	109061	GSPL/Bhuj/290/02/2025	23.200964	69.63083	Bedrock/Pit Sample	Red ferrugenous layer/pellet	Ferrugenous nodules	Bhuj Formation	19.20	0.93	11.25	86	29	7.82	26	7	49
8	109062	GSPL/Bhuj/290/02/2025	23.200964	69.63083	Bedrock/Pit Sample	Weakly ferruginous and ferruginized sandstone	Interlaminated white and Red Sandstone	Bhuj Formation	20.59	0.82	7.46	60	44	6.44	16	11	35
9	109063	GSPL/Bhuj/289/01/2025	23.2037	69.6284	Bedrock/Pit Sample	Ferruginized sandstone	White fine sandstone with purple banding near KHF	Bhuj Formation	8.67	<0.5	1.76	19	60	4.55	10	9	16
10	109064	GSPL/Bhuj/289/01/2025	23.2037	69.6284	Bedrock/Pit Sample	Metasomatized ferruginized sandstone	Highly ferruginous, metasomatized sandstone	Bhuj Formation	19.32	0.69	20.52	113	233	9.06	28	18	36

S.N.	Sample ID	Location	Latitude	Longitude	Type	Host Lithology	Sample Description	Formation	Li	Be	Sc	V	Cr	Co	Ni	Cu	Zn
11	109064	GSPL/Bhuj/289/01/2025	23.2037	69.6284	Bedrock/Pit Sample	Ferruginized sandstone	White fine sandstone with purple banding near KHF	Bhuj Formation	17.12	0.72	19.26	115	240	9.13	28	20	39
12	109065	GSPL/Bhuj/289/01/2025	23.2037	69.6284	Bedrock/Pit Sample	Metasomatized ferruginized sandstone	Black metasomatized ferruginized sandstone with magnetite	Bhuj Formation	4.48	2.99	5.84	119	183	7.15	29	<5	91
13	109066	GSPL/Bhuj/290/02/2025	23.200964	69.63083	Bedrock/Pit Sample	Shale dominated heterolith	Whitsh suspected tuffitet bed	Bhuj Formation	22.56	0.99	11.93	50	21	7.70	21	13	34
14	109067	GSPL/Bhuj/292/02/2025	23.196989	69.530206	Bedrock/Pit Sample	Metasomatized ferruginized sandstone	metasomatized ferruginized sandstone with magnetite	Bhuj Formation	5.73	<0.5	2.56	13	336	12.90	24	<5	21
15	109068	GSPL/Bhuj/295/02/2025	23.20259	69.519599	Bedrock/Pit Sample	Sandstone	White fine grained sandstone	Bhuj Formation	23.50	2.78	87.86	518	272	30.21	121	40	384
16	109069	GSPL/Bhuj/289/02/2025	23.2037	69.6284	Bedrock/Pit Sample	Metasomatized ferruginized sandstone	metasomatized ferruginized with ferric nodules	Bhuj Formation	2.90	3.96	9.52	266	280	13.16	62	13	136
17	109070	GSPL/Bhuj/255/12/2024	23.196778	69.531259	Bedrock/Pit Sample	Metasomatized ferruginized sandstone	Metasomatized sandstone with lots of feldspar laths	Bhuj Formation	2.45	0.54	2.16	17	137	7.27	16	<5	15
18	109071	GSPL/Bhuj/289/02/2025	23.2037	69.6284	Bedrock/Pit Sample	Metasomatized ferruginized sandstone interlayerd with ferruginized sandstone	Metasomatized sandstone underlain and interlayered with ferruginous sandstone	Bhuj Formation	12.26	1.34	3.03	33	112	7.91	11	<5	11
19	109080	GSPL/Bhuj/Pit-17	23.206453	69.626627	Bedrock/Pit Sample	Ferruginized sandstone	Ferruginized sandstone	Bhuj Formation	4.98	<0.5	4.32	54	212	4.72	20	<5	45
20	109081	GSPL/Bhuj/Pit-16	23.19992	69.61941	Bedrock/Pit Sample	Shale dominated TuffiteLayer with ferruginous frequently		Chari Formation	18.70	1.42	20.40	259	79	28.57	150	32	236

Table Continued..

Annexure-XXVI

S.N.	Sample ID	Ga	Ge	Se	Rb	Sr	Y	Zr	Nb	Mo	Cd	In	Sn	Sb	Te	Cs	Ba	La	Ce	Pr	Nd
1	109045	6.60	<0.5	<0.5	23.21	236	16.70	250	8.78	1.52	<0.5	<0.5	<0.5	<0.5	<0.5	<0.5	203	45.10	96.47	11.56	43.72
2	109053	20.43	<0.5	<0.5	18.47	76	22.69	199	16.89	3.74	<0.5	<0.5	35.41	0.91	<0.5	0.67	244	43.73	82.30	9.64	32.55
3	109054	3.39	<0.5	<0.5	1.52	21	5.36	31	1.66	5.50	<0.5	<0.5	<0.5	<0.5	<0.5	<0.5	37	7.32	14.63	1.54	5.67
4	109055	3.72	<0.5	0.84	9.80	24	6.99	29	<0.5	1.34	<0.5	<0.5	<0.5	<0.5	<0.5	<0.5	138	4.81	10.51	1.33	6.39
5	109056	29.49	<0.5	1.30	16.14	556	65.87	145	10.98	1.76	<0.5	<0.5	<0.5	<0.5	<0.5	1.02	2215	79.93	221.08	23.72	85.61
6	109057	7.54	<0.5	<0.5	13.98	56	14.47	156	5.23	<0.5	<0.5	<0.5	<0.5	<0.5	<0.5	<0.5	198	19.52	33.75	5.35	23.75
7	109061	14.22	<0.5	1.96	21.37	286	66.07	52	2.90	2.70	<0.5	<0.5	18.65	<0.5	<0.5	1.47	63	39.88	124.17	14.75	68.18
8	109062	8.67	<0.5	2.82	31.66	189	18.70	56	3.36	<0.5	<0.5	<0.5	<0.5	<0.5	<0.5	2.25	68	16.50	52.07	5.47	21.70
9	109063	6.68	<0.5	<0.5	1.03	8	6.18	75	2.15	<0.5	<0.5	<0.5	<0.5	<0.5	<0.5	<0.5	27	28.02	55.26	6.59	25.27
10	109064	30.30	<0.5	1.34	5.51	21	36.39	446	28.03	1.50	<0.5	<0.5	<0.5	<0.5	<0.5	<0.5	135	150.95	303.47	35.22	119.76
11	109064	30.33	<0.5	1.00	5.10	21	35.25	437	28.38	1.35	<0.5	<0.5	<0.5	<0.5	<0.5	<0.5	134	147.10	301.46	34.90	117.63
12	109065	5.01	<0.5	<0.5	0.84	8	7.90	34	1.34	2.10	<0.5	<0.5	<0.5	<0.5	<0.5	<0.5	24	8.10	13.49	1.73	7.93
13	109066	13.25	<0.5	0.78	31.10	315	56.59	37	3.72	0.69	<0.5	<0.5	<0.5	<0.5	<0.5	2.21	90	42.26	129.17	14.88	61.87
14	109067	5.56	<0.5	<0.5	15.15	42	3.76	35	1.55	0.92	<0.5	<0.5	<0.5	<0.5	<0.5	<0.5	217	6.11	13.81	1.51	5.63
15	109068	25.48	<0.5	1.66	<0.5	58	62.77	134	5.78	1.28	<0.5	<0.5	<0.5	<0.5	<0.5	<0.5	227	7.13	23.89	3.73	17.22
16	109069	7.62	<0.5	6.83	0.62	14	15.58	78	1.49	6.10	<0.5	<0.5	<0.5	<0.5	<0.5	<0.5	28	5.89	11.97	2.06	12.43
17	109070	6.10	<0.5	<0.5	13.73	38	4.14	38	2.11	1.12	<0.5	<0.5	<0.5	<0.5	<0.5	<0.5	152	7.63	16.38	1.85	6.70
18	109071	9.66	<0.5	<0.5	1.87	26	8.00	73	5.11	<0.5	<0.5	<0.5	1.63	<0.5	<0.5	<0.5	67	13.56	29.82	3.22	12.01
19	109080	9.40	<0.5	0.87	4.58	291	9.20	113	5.63	2.01	<0.5	<0.5	32.30	<0.5	<0.5	<0.5	77	22.42	45.21	5.53	22.83
20	109081	12.74	<0.5	2.51	40.73	425	80.05	106	5.09	1.70	<0.5	<0.5	<0.5	<0.5	<0.5	2.84	171	25.74	68.04	9.67	41.71

Table Continued..

Annexure-XXVI

S.N.	Sample ID	Sm	Eu	Gd	Tb	Dy	Ho	Er	Tm	Yb	Lu	Hf	Ta	W	Tl	Pb	Bi	Th	U	B
1	109045	7.53	0.94	10.96	0.73	3.59	0.56	2.13	<0.5	1.75	<0.5	3.18	<0.5	<0.5	<0.5	10	<0.5	14.10	2.98	<5
2	109053	5.60	1.26	8.33	0.65	4.02	0.75	3.06	<0.5	2.68	<0.5	5.49	2.33	20.15	<0.5	10	<0.5	11.19	4.51	<5
3	109054	0.90	<0.5	1.51	<0.5	0.81	<0.5	<0.5	<0.5	<0.5	<0.5	<0.5	<0.5	<0.5	<0.5	9	<0.5	2.19	4.49	<5
4	109055	1.23	0.51	1.99	<0.5	1.59	<0.5	1.16	<0.5	1.20	<0.5	<0.5	<0.5	<0.5	<0.5	9	<0.5	1.22	0.87	<5
5	109056	19.03	7.23	26.09	2.84	14.87	2.85	8.40	0.84	7.66	1.13	1.92	0.86	<0.5	0.70	25	<0.5	17.42	9.14	<5
6	109057	3.87	1.03	5.89	<0.5	2.37	<0.5	1.50	<0.5	0.93	<0.5	1.10	<0.5	<0.5	1.59	8	<0.5	3.53	1.71	<5
7	109061	14.07	3.86	21.98	2.35	11.88	2.26	6.87	<0.5	3.57	<0.5	0.53	<0.5	<0.5	<0.5	17	<0.5	1.58	1.35	<5
8	109062	4.63	1.01	6.47	0.53	3.38	0.53	1.86	<0.5	1.21	<0.5	<0.5	<0.5	<0.5	<0.5	<5	<0.5	2.38	1.01	<5
9	109063	3.79	<0.5	5.81	<0.5	1.32	<0.5	0.61	<0.5	<0.5	<0.5	0.64	<0.5	<0.5	<0.5	<5	<0.5	8.48	1.29	<5
10	109064	24.65	1.95	29.01	2.54	8.44	1.48	4.96	<0.5	3.69	<0.5	7.85	2.24	1.76	<0.5	31	<0.5	55.72	7.96	<5
11	109064	22.05	1.47	28.59	2.04	8.36	1.33	4.52	<0.5	3.49	<0.5	7.47	2.48	1.51	<0.5	33	<0.5	51.47	8.02	<5
12	109065	2.21	0.63	2.84	<0.5	2.38	<0.5	1.46	<0.5	1.67	<0.5	<0.5	<0.5	<0.5	<0.5	87	<0.5	2.98	2.02	<5
13	109066	12.66	3.17	18.29	2.01	10.57	1.99	5.71	<0.5	3.80	<0.5	<0.5	<0.5	<0.5	<0.5	5	<0.5	2.88	2.15	<5
14	109067	0.99	<0.5	1.44	<0.5	0.63	<0.5	<0.5	<0.5	<0.5	<0.5	<0.5	<0.5	<0.5	0.65	8	<0.5	2.28	1.08	<5
15	109068	5.19	2.42	7.71	1.57	11.92	2.97	10.33	1.28	12.49	2.24	1.64	0.57	<0.5	<0.5	7	<0.5	1.74	1.32	<5
16	109069	3.86	1.57	5.00	0.67	4.28	0.79	2.60	<0.5	1.92	<0.5	<0.5	<0.5	<0.5	<0.5	227	<0.5	2.14	3.25	<5
17	109070	1.16	<0.5	1.53	<0.5	0.68	<0.5	<0.5	<0.5	<0.5	<0.5	<0.5	<0.5	<0.5	<0.5	13	<0.5	2.73	1.29	<5
18	109071	2.10	<0.5	3.14	<0.5	1.35	<0.5	0.79	<0.5	0.61	<0.5	1.48	<0.5	<0.5	<0.5	10	<0.5	2.85	1.03	<5
19	109080	3.40	0.53	5.50	<0.5	1.78	<0.5	1.27	<0.5	1.02	<0.5	1.61	<0.5	2.95	<0.5	17	<0.5	6.89	2.19	<5
20	109081	11.00	2.71	14.94	2.33	13.11	2.70	7.56	0.72	5.86	0.92	1.22	<0.5	<0.5	<0.5	44	<0.5	4.00	3.15	<5

Table Continued..

Annexure-XXVI

S.N.	Sample ID	Ag	Al	Ca	Fe	K	Mg	Mn	Na	P	S	Ti	HREE	LREE	TREE
1	109045	<1	13281	122974	34517	8012	19354	539	1073	0	356	4694	45.8	204.4	250.17
2	109053	<1	82357	593	7205	3431	1474	<100	6196	329	182	5162	55.0	173.8	228.87
3	109054	<1	11014	2876	153484	309	1147	366	593	938	239	678	10.7	30.1	40.74
4	109055	<1	12926	442	110884	2896	879	1040	290	239	380	388	17.0	24.3	41.28
5	109056	<1	55864	1869	309920	2899	1269	3239	941	1947	199	3302	168.2	429.4	597.60
6	109057	<1	13852	4932	184991	5782	1153	3102	315	294	279	2855	29.7	86.2	115.90
7	109061	<1	22847	58552	353004	4298	28054	3386	2457	5283	1118	1490	130.1	261.1	391.16
8	109062	<1	27498	249223	53699	6052	7371	1007	1114	1523	304	1979	41.2	100.4	141.52
9	109063	<1	24378	590	6301	334	193	<100	123	125	<100	1823	15.7	118.9	134.62
10	109064	<1	95542	730	8819	1049	855	<100	3876	358	381	10878	109.0	634.0	743.02
11	109064	<1	96116	733	8894	1040	860	<100	3844	264	379	10601	104.3	623.1	727.45
12	109065	<1	13751	353	240583	186	101	<100	173	981	<100	658	22.7	33.5	56.18
13	109066	<1	26326	262072	27264	5672	4075	2880	1758	3744	686	1801	114.1	260.8	374.87
14	109067	<1	11104	6525	195647	4562	955	2617	342	602	1001	604	8.4	28.0	36.44
15	109068	<1	117671	1489	244839	<100	700	189	442	566	591	7938	203.6	57.2	260.73
16	109069	<1	15194	628	310852	165	169	<100	175	1030	112	501	41.9	36.2	78.14
17	109070	<1	10375	6412	221866	4099	1326	2687	293	374	494	1029	8.5	33.7	42.23
18	109071	<1	44603	6757	4376	425	271	130	295	116	<100	2465	16.9	60.7	77.65
19	109080	<1	31283	16534	14974	1079	1490	<100	124	107	<100	5594	23.6	99.4	123.03
20	109081	<1	44515	7703	345849	8396	8236	748	3701	3559	1551	2613	151.3	156.2	307.47

S.N.	Sample ID	Location No.	Latitude	Longitude	Type	Host Lithology	Sample Description	Formation
21	109082	GSPL/Bhuj/Pit-16	23.19992	69.61941	Bedrock/Pit Sample	Shale dominated TuffiteLayer with ferruginous frequently		Chari Formation
22	109082	GSPL/Bhuj/Pit-16	23.19992	69.61941	Bedrock/Pit Sample	Shale dominated TuffiteLayer with ferruginous frequently		Chari Formation
23	109083	GSPL/Bhuj/Pit-16	23.19992	69.61941	Bedrock/Pit Sample	Shale dominated TuffiteLayer with ferruginous frequently		Chari Formation
24	109084	GSPL/Bhuj/Pit-20	23.200808	69.61931	Bedrock/Pit Sample	Ferruginized sandstone	Ferruginized sandstone	Bhuj Formation
25	109085	GSPL/Bhuj/Pit-20	23.200808	69.61931	Bedrock/Pit Sample	Ferruginized sandstone	Ferruginized sandstone	Bhuj Formation
26	109086	GSPL/Bhuj/Pit-11	23.20085	69.61935	Bedrock/Pit Sample	Ferruginized sandstone	Ferruginized sandstone	Bhuj Formation
27	109087	GSPL/Bhuj/Pit-11	23.20085	69.61935	Bedrock/Pit Sample	Ferruginized sandstone	Ferruginized sandstone	Bhuj Formation
28	109088	GSPL/Bhuj/Pit-11	23.20085	69.61935	Bedrock/Pit Sample	Ferruginized sandstone	Ferruginized sandstone	Bhuj Formation
29	109089	GSPL/Bhuj/Pit-11	23.20085	69.61935	Bedrock/Pit Sample	Ferruginized sandstone	Ferruginized sandstone	Bhuj Formation
30	109090	GSPL/Bhuj/Pit-12	23.19567	69.57062	Bedrock/Pit Sample	Sandstone	Sandstone	Bhuj Formation
31	109091	GSPL/Bhuj/Pit-13	23.195766	69.576966	Bedrock/Pit Sample	Shale dominated heterolith	Shale dominated layer	Bhuj Formation
32	109092	GSPL/Bhuj/Pit-13	23.195766	69.576966	Bedrock/Pit Sample	Shale dominated heterolith	Shale dominated layer	Bhuj Formation
33	109092	GSPL/Bhuj/Pit-13	23.195766	69.576966	Bedrock/Pit Sample	Shale dominated heterolith	Shale dominated layer	Bhuj Formation
34	109093	GSPL/Bhuj/Pit-13	23.195766	69.576966	Bedrock/Pit Sample	Shale dominated heterolith	Shale dominated layer	Bhuj Formation
35	109094	GSPL/Bhuj/Pit-15	23.20324	69.58328	Bedrock/Pit Sample	Weakly ferruginous Sandstone	Weakly ferruginous Sandstone	Bhuj Formation
36	109095	GSPL/Bhuj/Pit-19	23.18900	69.54369	Bedrock/Pit Sample	Sandstone	White sandstone	Bhuj Formation
37	108975	GSPL_BHUJ_244/11/2024	23.204067	69.542105	Bedrock/Pit Sample	Ferruginized sandstone	Ferruginous sandstone with 10cm nodules collected from the depth of 88cm from the surface across the katrol hill fault	Bhuj Formation
38	108979	GSPL_BHUJ_244/11/2024	23.204067	69.542105	Bedrock/Pit Sample	Ferruginized sandstone	Ferruginous nodules collected from the depth of 94cm interval of the fourth sample across the katrol hill fault	Bhuj Formation
39	108983	GSPL_BHUJ_247/12/2024	23.194618	69.597735	Bedrock/Pit Sample	Shale dominated heterolith with Tuffite layer	Tuffite layer of 3 cm thickness from a depth of 110cm	Katrol Formation
40	108984	GSPL_BHUJ_247/12/2024	23.194618	69.597735	Bedrock/Pit Sample	Shale dominated heterolith with Tuffite layer	Tuffite layer of 3 cm from the depth of 87cm	Katrol Formation

S.N.	Sample ID	Location No.	Latitude	Longitude	Type	Host Lithology	Sample Description	Formation
41	108985	GSPL_BHUJ_2 47/12/2024	23.194728	69.59762	Bedrock/Pit Sample	Shale dominated heterolith with Tuffite layer	Tuffite layer of 3cm from shale layer from the depth of 46 cm	Katrol Formation
42	108986	GSPL_BHUJ_2 47/12/2024	23.194728	69.59762	Bedrock/Pit Sample	Shale dominated heterolith with Tuffite layer	Tuffite layer of 2cm from shale layer from 73 cm depth	Katrol Formation
43	108987	GSPL_BHUJ_2 47/12/2024	23.194943	69.59751	Bedrock/Pit Sample	Shale dominated heterolith with Tuffite layer and ferrugenous sandstone	Tuffite bed of 3cm from shale layer from the depth of 138 cm depth	Katrol Formation
44	108988	GSPL_BHUJ_2 47/12/2024	23.194943	69.59751	Bedrock/Pit Sample	Ferrugenous sandstone from Shale dominated heterolith	Ferruginous sandstone of 12 cm from the depth 123 cm	Katrol Formation
45	108989	GSPL_BHUJ_2 47/12/2024	23.194943	69.59751	Bedrock/Pit Sample	Shale dominated heterolith with Tuffite layer and ferrugenous sandstone	NA	Katrol Formation
46	108990	GSPL_BHUJ_2 47/12/2024	23.195137	69.597185	Bedrock/Pit Sample	Shale dominated heterolith with Tuffite layer	Tuffite layer of 2cm from the depth of 153 cm	Katrol Formation
47	108991	GSPL_BHUJ_2 47/12/2024	23.195137	69.597185	Bedrock/Pit Sample	Shale dominated heterolith with ferruginized tuffite layer	Nodular type ferruginous layer from the depth of 20cm	Katrol Formation
48	108992	GSPL_BHUJ_2 48/12/2024	23.195927	69.599842	Bedrock/Pit Sample	Shale and fine grained sandstone with tuffite and gypsum layers	Tuffite layer with shale and sandstone from the depth of 220 cm	Katrol Formation
49	108993	GSPL_BHUJ_2 48/12/2024	23.195927	69.599842	Bedrock/Pit Sample	Shale and fine grained sandstone with tuffite and gypsum layers	Tuffite layer with shale from the depth of 180cm	Katrol Formation
50	108998	GSPL_BHUJ_2 48/12/2024	23.196183	69.600232	Bedrock/Pit Sample	Shale dominated heterolith with Tuffite layer	Tuffite layer of 3cm from shale layer from the depth of 46 cm	Chari Formation
51	108999	GSPL_BHUJ_2 48/12/2024	23.195907	69.602013	Bedrock/Pit Sample	Shale and ferruginous sandstone with tuffite layer	Tuffite bed with shale and sandstones of 35cm from the depth of 172cm	Katrol Formation
52	109000	GSPL_BHUJ_2 48/12/2024	23.195907	69.602013	Bedrock/Pit Sample	Shale and ferruginous sandstone with tuffite layer	Thick tuffite bed of 3 cm from the 169 cm depth	Katrol Formation
53	109004	GSPL_BHUJ_2 48/12/2024	23.195907	69.602013	Bedrock/Pit Sample	Highly ferruginous sandstone,ferruginous sandstone with gypsum and silica of 40cm sample spread, from the depth of 1.55 cm		Katrol Formation

Table Continued..

Annexure-XXVI

S.N.	Sample ID	Li	Be	Sc	V	Cr	Co	Ni	Cu	Zn	Ga	Ge	Se	Rb	Sr	Y	Zr	Nb
21	109082	70.67	<0.5	15.57	175	125	9.12	61	43	81	28.28	<0.5	<0.5	117.02	98	26.28	167	18.95
22	109082	70.73	<0.5	14.13	168	130	9.73	60	46	81	27.06	<0.5	<0.5	112.32	93	25.73	173	18.38
23	109083	73.27	1.14	17.10	189	121	17.55	67	43	94	27.65	<0.5	1.10	126.58	101	41.29	162	18.51
24	109084	11.54	0.57	23.77	225	71	26.71	91	24	180	9.79	<0.5	1.29	25.24	158	32.00	79	3.89
25	109085	4.92	<0.5	3.40	49	68	4.60	19	19	33	4.13	<0.5	<0.5	18.23	692	8.13	41	1.70
26	109086	7.25	<0.5	10.85	82	153	29.22	53	<5	150	16.20	<0.5	<0.5	27.44	171	32.47	248	10.37
27	109087	6.21	0.71	14.17	238	243	30.27	68	8	127	9.50	<0.5	<0.5	11.62	101	24.24	255	23.36
28	109088	7.06	<0.5	4.27	83	164	9.14	26	<5	42	7.20	<0.5	<0.5	15.64	59	13.14	167	8.00
29	109089	22.37	1.89	14.58	101	206	6.63	33	62	47	24.09	<0.5	<0.5	40.58	149	32.33	263	21.66
30	109090	7.77	<0.5	1.09	16	93	2.27	12	<5	15	3.87	<0.5	<0.5	15.82	46	2.88	38	2.09
31	109091	9.86	2.78	9.04	163	89	10.35	42	32	232	16.86	<0.5	<0.5	36.34	85	19.19	159	10.28
32	109092	12.06	1.29	13.74	171	229	6.60	26	32	136	14.98	<0.5	<0.5	29.09	86	15.32	140	10.11
33	109092	11.43	1.56	13.18	169	236	6.36	25	34	132	14.69	<0.5	<0.5	28.94	86	14.36	139	9.79
34	109093	21.66	2.47	19.51	105	230	4.34	22	51	25	30.37	<0.5	0.91	47.24	146	28.26	179	19.32
35	109094	14.64	<0.5	2.94	22	233	4.81	28	<5	24	6.50	<0.5	<0.5	4.69	12	4.75	61	4.59
36	109095	5.27	2.74	1.02	15	126	1.01	6	<5	11	4.17	<0.5	<0.5	15.81	21	2.01	34	1.57
37	108975	415.01	<0.5	1.27	46	91	13.55	29	3	78	7.67	1.84	0.67	<0.5	37	1.22	93	1.22

S.N.	Sample ID	Li	Be	Sc	V	Cr	Co	Ni	Cu	Zn	Ga	Ge	Se	Rb	Sr	Y	Zr	Nb
38	108979	20.2	<0.5	<0.5	51.2	81.9	14.5	50.4	6.2	62.8	8.7	2.0	<0.5	<0.5	48.3	0.7	133.3	2.7
39	108983	84.7	<0.5	1.4	214.5	104.0	14.1	37.8	24.1	42.0	25.7	1.0	<0.5	<0.5	164.3	0.9	91.6	2.6
40	108984	243.7	<0.5	1.1	274.2	110.3	20.4	62.1	45.3	53.5	26.0	1.4	0.7	<0.5	107.4	3.2	106.6	3.1
41	108985	108.5	<0.5	1.8	246.3	96.3	15.6	58.0	26.0	46.8	25.1	1.7	1.0	<0.5	166.6	2.2	87.4	2.4
42	108986	156.0	<0.5	2.0	270.9	105.2	24.2	66.4	49.9	76.7	26.3	1.5	0.8	<0.5	70.4	2.5	111.4	1.9
43	108987	<0.5	<0.5	<0.5	255.8	102.5	15.8	45.6	29.2	70.8	27.4	<0.5	<0.5	<0.5	91.7	0.8	106.7	2.3
44	108988	304.9	<0.5	1.4	26.4	67.7	7.8	12.3	6.7	47.7	3.3	1.0	0.8	<0.5	166.1	2.3	74.2	1.7
45	108989	157.6	<0.5	2.1	195.9	116.5	18.1	54.4	46.0	78.2	23.2	1.6	1.1	<0.5	75.4	4.3	136.2	2.0
46	108990	345.0	<0.5	3.0	206.7	89.6	25.5	67.4	32.8	57.7	26.4	2.0	0.8	<0.5	81.3	4.3	98.4	1.8
47	108991	90.3	<0.5	1.8	175.8	69.9	27.5	92.1	25.4	114.3	27.1	1.8	0.9	<0.5	122.9	3.0	76.5	2.4
48	108992	12.6	<0.5	1.1	168.2	51.2	13.3	27.5	2.5	56.2	20.8	2.2	1.4	<0.5	179.4	3.5	32.6	1.5
49	108993	<0.5	<0.5	0.7	171.0	101.0	18.3	39.6	28.2	81.9	20.2	1.4	0.7	<0.5	92.3	2.5	147.9	1.9
50	108998	434.0	<0.5	1.9	147.0	46.4	16.4	31.0	4.4	54.7	21.0	2.0	0.8	<0.5	287.4	1.0	17.6	1.3
51	108999	56.3	<0.5	1.3	188.8	112.3	23.9	47.7	36.7	92.9	22.4	2.1	1.1	<0.5	140.2	12.5	144.4	1.2
52	109000	36.1	<0.5	1.6	138.8	45.9	13.7	43.8	10.5	85.3	25.2	1.6	0.6	<0.5	215.3	14.3	39.0	1.1
53	109004	<0.5	<0.5	<0.5	115.7	49.4	18.6	48.0	35.8	76.8	17.7	1.5	0.8	<0.5	264.0	3.3	28.2	2.9

Table Continued..

Annexure-XXVI

S.N.	Sample ID	Mo	Cd	In	Sn	Sb	Te	Cs	Ba	La	Ce	Pr	Nd	Sm	Eu	Gd	Tb	Dy	Ho	Er	Tm	Yb
21	109082	0.80	<0.5	<0.5	<0.5	<0.5	<0.5	7.44	257	44.93	89.61	11.55	43.62	7.86	1.98	10.83	0.98	5.01	1.01	3.55	<0.5	3.06
22	109082	0.71	<0.5	<0.5	<0.5	<0.5	<0.5	7.63	264	42.12	88.25	11.30	41.78	7.54	1.86	10.71	0.90	5.04	0.95	3.33	<0.5	2.82
23	109083	1.16	<0.5	<0.5	<0.5	<0.5	<0.5	8.93	263	47.33	103.31	13.43	46.47	10.03	2.20	12.58	1.39	7.82	1.53	4.52	<0.5	4.18
24	109084	0.97	<0.5	<0.5	<0.5	<0.5	<0.5	1.60	132	16.57	39.62	5.11	20.77	5.07	1.20	6.70	0.75	4.76	0.92	2.84	<0.5	2.34
25	109085	<0.5	<0.5	<0.5	<0.5	<0.5	<0.5	0.62	143	10.29	21.38	2.67	10.93	1.96	<0.5	2.90	<0.5	1.38	<0.5	0.87	<0.5	0.67
26	109086	1.94	<0.5	<0.5	4.91	<0.5	<0.5	0.62	811	50.37	113.81	13.38	45.11	9.17	2.33	11.89	1.03	5.88	1.09	3.60	<0.5	3.55
27	109087	1.29	<0.5	<0.5	8.08	<0.5	<0.5	<0.5	393	61.79	136.82	16.00	55.66	10.66	1.48	14.30	1.13	5.16	0.81	2.72	<0.5	2.37
28	109088	0.63	<0.5	<0.5	22.03	<0.5	<0.5	0.94	261	22.60	50.20	6.80	27.29	5.10	1.16	6.86	<0.5	2.81	<0.5	1.64	<0.5	1.56
29	109089	2.65	<0.5	<0.5	12.09	<0.5	<0.5	2.79	608	53.21	114.35	13.26	44.98	8.83	2.18	11.95	1.11	6.02	1.19	4.00	<0.5	3.81
30	109090	<0.5	<0.5	<0.5	<0.5	<0.5	<0.5	<0.5	123	7.68	14.74	1.84	6.13	1.06	<0.5	1.44	<0.5	0.53	<0.5	<0.5	<0.5	<0.5
31	109091	2.50	<0.5	<0.5	6.36	<0.5	<0.5	3.14	243	32.47	52.96	8.18	31.64	5.85	1.32	7.83	0.67	3.97	0.69	2.52	<0.5	2.26
32	109092	4.91	<0.5	<0.5	45.26	<0.5	<0.5	2.02	2483	30.33	57.03	7.55	25.05	5.06	3.69	6.80	0.61	3.44	<0.5	1.87	<0.5	1.88
33	109092	4.47	<0.5	<0.5	43.21	<0.5	<0.5	1.93	2482	29.52	56.10	7.15	25.25	4.95	3.71	6.73	0.55	3.20	<0.5	1.89	<0.5	1.87
34	109093	1.50	<0.5	<0.5	<0.5	<0.5	<0.5	4.92	9454	55.45	118.31	14.85	54.97	11.97	13.35	15.26	1.44	7.60	1.27	3.96	<0.5	3.33
35	109094	0.51	<0.5	<0.5	<0.5	<0.5	<0.5	<0.5	51	12.08	23.30	2.77	9.21	1.79	<0.5	2.25	<0.5	0.84	<0.5	<0.5	<0.5	<0.5
36	109095	<0.5	<0.5	<0.5	<0.5	<0.5	<0.5	<0.5	129	5.55	10.46	1.14	4.08	0.66	<0.5	0.91	<0.5	<0.5	<0.5	<0.5	<0.5	<0.5
37	108975	<0.5	<0.5	<0.5	6.54	2.33	<0.5	86.62	425	10.52	21.45	2.14	8.20	1.86	21.46	1.53	<0.5	2.67	0.59	1.96	<0.5	2.02

S.N.	Sample ID	Mo	Cd	In	Sn	Sb	Te	Cs	Ba	La	Ce	Pr	Nd	Sm	Eu	Gd	Tb	Dy	Ho	Er	Tm	Yb
38	108979	<0.5	<0.5	<0.5	2.8	1.8	<0.5	4.5	258.9	10.4	17.3	2.0	7.8	1.3	<0.5	1.2	<0.5	1.6	<0.5	1.0	<0.5	0.9
39	108983	0.5	<0.5	<0.5	7.4	1.9	<0.5	6.5	282.0	29.4	51.7	5.1	13.9	2.1	<0.5	1.7	<0.5	1.7	<0.5	1.2	<0.5	1.2
40	108984	0.9	<0.5	<0.5	1.7	2.5	<0.5	26.7	260.2	11.3	29.3	3.1	13.1	3.5	<0.5	4.6	0.9	5.8	1.2	3.3	<0.5	2.2
41	108985	1.6	<0.5	<0.5	2.2	2.1	<0.5	28.5	304.9	7.0	17.6	1.8	7.4	1.9	<0.5	2.4	0.6	4.2	1.0	3.0	<0.5	2.7
42	108986	1.3	0.5	<0.5	3.3	2.0	<0.5	34.7	334.1	8.4	19.6	1.9	8.1	2.0	3.0	2.7	0.6	4.4	1.0	3.1	<0.5	2.9
43	108987	0.8	<0.5	<0.5	2.4	1.7	<0.5	9.0	696.7	9.6	18.6	2.0	7.7	1.3	0.9	1.7	<0.5	1.5	<0.5	0.9	<0.5	0.7
44	108988	<0.5	<0.5	<0.5	2.1	1.7	<0.5	45.5	383.1	13.5	27.9	3.1	11.9	2.9	2.7	2.7	0.5	3.8	0.8	2.6	<0.5	2.3
45	108989	0.6	1.6	<0.5	7.5	5.5	<0.5	22.7	302.4	10.1	22.0	2.5	11.3	3.0	0.5	4.1	0.8	6.1	1.4	4.1	0.6	3.2
46	108990	1.5	<0.5	<0.5	1.5	1.6	<0.5	28.3	259.1	14.7	34.6	4.2	18.4	5.1	<0.5	6.8	0.7	4.7	1.0	2.9	<0.5	2.2
47	108991	1.1	0.7	<0.5	2.4	2.0	<0.5	27.1	365.3	10.5	22.2	2.7	13.0	3.9	5.6	4.3	0.7	4.2	0.9	2.3	<0.5	1.8
48	108992	<0.5	0.6	<0.5	1.2	2.2	<0.5	19.5	318.7	9.5	21.3	2.6	10.9	3.6	2.7	4.2	1.0	6.5	1.4	3.6	<0.5	2.4
49	108993	0.6	<0.5	<0.5	1.4	1.9	<0.5	14.0	159.0	9.9	28.1	3.1	12.3	3.5	3.1	3.9	0.9	5.7	1.2	3.4	<0.5	2.7
50	108998	<0.5	<0.5	<0.5	7.2	2.4	<0.5	118.6	452.3	11.0	23.7	2.1	7.1	1.6	3.2	1.4	<0.5	2.0	<0.5	1.4	<0.5	1.5
51	108999	0.6	<0.5	<0.5	1.6	1.6	<0.5	20.2	288.1	22.2	70.1	9.2	43.5	14.6	23.9	20.0	4.0	26.3	5.2	12.7	1.5	6.4
52	109000	<0.5	0.6	<0.5	2.4	1.8	<0.5	17.2	158.4	24.8	72.0	9.6	44.4	13.8	3.8	18.9	3.6	24.4	5.0	12.6	1.5	6.6
53	109004	<0.5	<0.5	<0.5	1.6	1.9	<0.5	9.9	312.8	10.5	29.8	3.2	15.1	4.2	<0.5	5.6	1.3	8.8	1.8	4.8	0.6	3.3

Table Continued..

Annexure-XXVI

S.N.	Sample ID	Lu	Hf	Ta	W	Tl	Pb	Bi	Th	U	B	Ag	Al	Ca	Fe	K	Mg	Mn	Na	P	S	Ti	HREE	LREE	TREE
21	109082	<0.5	2.67	1.64	0.66	<0.5	10	<0.5	10.35	3.02	<5	<1	103724	3175	32115	19960	8063	169	4305	537	1850	6229	68.3	197.6	265.83
22	109082	<0.5	2.30	1.68	0.52	<0.5	12	<0.5	10.22	2.89	<5	<1	102524	3104	32192	19782	7955	166	4294	533	1845	6265	65.5	191.0	256.46
23	109083	0.57	2.41	1.86	3.89	<0.5	13	<0.5	10.85	3.22	<5	<1	101715	9616	46111	18873	7913	214	4740	615	8117	6165	93.2	220.6	313.76
24	109084	<0.5	<0.5	<0.5	<0.5	<0.5	25	<0.5	2.74	2.17	<5	<1	36077	21210	366641	4925	10461	1533	8459	3638	1129	1931	75.3	87.1	162.41
25	109085	<0.5	<0.5	<0.5	<0.5	<0.5	6	<0.5	2.21	1.36	<5	<1	15163	198395	30845	5564	5034	323	2124	654	487	1312	17.4	47.2	64.59
26	109086	<0.5	4.04	0.77	<0.5	1.92	10	<0.5	15.92	5.94	<5	<1	18996	2300	238958	6203	1297	6567	1027	966	255	4560	72.7	231.8	304.53
27	109087	<0.5	2.77	1.82	2.31	<0.5	23	<0.5	23.04	3.28	<5	<1	16792	827	86176	3063	496	938	383	842	374	14308	66.4	280.9	347.31
28	109088	<0.5	1.75	<0.5	<0.5	<0.5	9	<0.5	6.59	1.86	<5	<1	18228	2718	32495	3876	475	500	289	446	<100	3393	31.4	112.0	143.45
29	109089	<0.5	6.24	1.86	1.25	<0.5	15	<0.5	15.84	5.44	<5	<1	92080	1752	18605	7896	1228	<100	507	705	<100	7118	77.2	234.6	311.82
30	109090	<0.5	0.86	<0.5	<0.5	<0.5	10	<0.5	1.91	0.63	<5	<1	18084	246	12755	4685	293	<100	248	139	<100	678	5.9	31.5	37.40
31	109091	<0.5	2.95	0.56	<0.5	<0.5	34	<0.5	8.76	4.57	<5	<1	56764	3989	241657	7206	1408	124	534	575	592	3705	47.5	131.1	178.59
32	109092	<0.5	3.08	<0.5	0.56	<0.5	28	<0.5	9.88	7.68	<5	<1	56703	4476	134815	7220	1152	116	1302	453	1367	4158	47.4	125.0	172.37
33	109092	<0.5	3.66	<0.5	0.51	<0.5	28	<0.5	9.92	7.24	<5	<1	56307	4469	132129	7133	1119	115	1317	425	1379	4117	45.5	123.0	168.46
34	109093	<0.5	2.74	1.62	1.40	<0.5	23	<0.5	12.03	3.93	<5	<1	128036	744	8137	8808	1874	<100	4121	361	2781	6693	94.0	255.6	349.54
35	109094	<0.5	0.55	<0.5	<0.5	<0.5	<5	<0.5	4.91	1.08	<5	<1	28787	306	9545	799	494	<100	100	<100	<100	2008	10.8	49.1	59.93
36	109095	<0.5	<0.5	<0.5	1.43	<0.5	<5	<0.5	1.28	0.57	<5	<1	20940	4558	4822	4668	225	<100	250	<100	<100	864	3.9	21.9	25.84
37	108975	<0.5	3.56	3.61	1.34	<0.5	46	1.39	4.05	1.33	NA	NA	NA	NA	NA	NA	NA	NA	NA	NA	NA	NA	32.7	44.2	76.89
38	108979	<0.5	3.2	1.9	1.1	<0.5	71.6	<0.5	6.5	1.2	NA	NA	NA	NA	NA	NA	NA	NA	NA	NA	NA	NA	5.4	38.8	44.17
39	108983	<0.5	3.5	3.7	1.1	<0.5	32.1	0.7	6.5	2.0	NA	NA	NA	NA	NA	NA	NA	NA	NA	NA	NA	NA	8.1	102.2	110.30
40	108984	<0.5	1.5	1.8	1.3	<0.5	24.1	<0.5	2.1	3.3	NA	NA	NA	NA	NA	NA	NA	NA	NA	NA	NA	NA	22.3	60.3	82.59
41	108985	<0.5	1.8	1.8	1.4	<0.5	58.9	0.5	2.0	1.9	NA	NA	NA	NA	NA	NA	NA	NA	NA	NA	NA	NA	17.9	35.7	53.62

S.N.	Sample ID	Lu	Hf	Ta	W	Tl	Pb	Bi	Th	U	B	Ag	Al	Ca	Fe	K	Mg	Mn	Na	P	S	Ti	HREE	LREE	TREE
42	108986	<0.5	2.1	2.1	1.6	<0.5	29.5	0.6	2.5	2.3	NA	NA	NA	NA	NA	NA	NA	NA	NA	NA	NA	NA	22.2	40.0	62.14
43	108987	<0.5	2.9	1.1	1.2	<0.5	26.7	<0.5	7.5	0.7	NA	NA	NA	NA	NA	NA	NA	NA	NA	NA	NA	NA	6.4	39.1	45.53
44	108988	<0.5	3.6	2.8	1.3	<0.5	12.8	0.7	5.2	2.4	NA	NA	NA	NA	NA	NA	NA	NA	NA	NA	NA	NA	19.2	59.3	78.52
45	108989	0.6	1.6	1.5	1.4	<0.5	30.7	3.9	1.4	3.0	NA	NA	NA	NA	NA	NA	NA	NA	NA	NA	NA	NA	28.0	49.0	76.97
46	108990	<0.5	3.5	2.0	1.5	<0.5	21.3	0.5	3.7	4.5	NA	NA	NA	NA	NA	NA	NA	NA	NA	NA	NA	NA	25.6	77.0	102.55
47	108991	<0.5	2.2	1.8	1.3	<0.5	27.9	0.5	2.0	2.6	NA	NA	NA	NA	NA	NA	NA	NA	NA	NA	NA	NA	24.6	52.3	76.98
48	108992	<0.5	1.4	1.7	1.3	<0.5	23.3	<0.5	1.1	2.7	NA	NA	NA	NA	NA	NA	NA	NA	NA	NA	NA	NA	26.4	48.0	74.31
49	108993	<0.5	0.9	0.7	1.3	<0.5	24.6	<0.5	1.3	<0.5	NA	NA	NA	NA	NA	NA	NA	NA	NA	NA	NA	NA	24.0	56.9	80.91
50	108998	<0.5	4.4	3.4	1.7	<0.5	22.2	1.3	4.2	1.2	NA	NA	NA	NA	NA	NA	NA	NA	NA	NA	NA	NA	12.3	45.5	57.82
51	108999	0.8	0.9	1.1	1.3	0.7	23.3	0.5	0.7	2.4	NA	NA	NA	NA	NA	NA	NA	NA	NA	NA	NA	NA	114.5	159.5	274.01
52	109000	0.8	0.9	1.0	1.3	<0.5	18.3	<0.5	0.8	3.0	NA	NA	NA	NA	NA	NA	NA	NA	NA	NA	NA	NA	93.2	164.6	257.77
53	109004	<0.5	0.8	0.7	1.2	<0.5	17.8	<0.5	0.9	<0.5	NA	NA	NA	NA	NA	NA	NA	NA	NA	NA	NA	NA	29.5	62.8	92.35

Annexure-XXVII-A Details of Core-log of BH-01

Title of the project:	**Reconnaissance Survey for REE Exploration in Bhuj Clay Prospect Block, Kachchh District, Gujarat**
Item no. along with Spill over item No.	NA
Field Season:	**2025**
Borehole No	**GSPL_BHUJ_BH-01**
Location	**Bhuj, Gujarat**
Latitude	**23.15087**
Longitude	**69.57877**
Angle	**Vertical**
Collar RL	**188m**
Date of commencement	**16.06.2025**
Date of closing	**24.07.2025**
Unit No.	**Geovale/ Drill Unit- 1**
Total Depth	**151.00 m**

Box No.	Depth (m) From	Depth (m) To	Run Length (m)	Core recovery (m)	Core recovery (%)	Core loss (%)	RQD (m)	RQD (%)	Litho from (m)	Litho To (m)	Litho Rec. (m)	Litho Ext. (m)	Lithology
CB1	0.00	1.50	1.50	0.80	53.33	46.67	0.00	0.00	0.00	1.50	0.80	1.50	Top Soil
CB1	1.50	3.00	1.50	0.90	60.00	40.00	0.00	0.00	1.50	2.75	0.80	1.25	Top Soil
									2.75	3.00	0.10	0.25	Weathered rock
CB1	3.00	4.50	1.50	1.00	66.67	33.33		0.00	3.00	3.50	0.33	0.50	Weathered rock
									3.50	4.50	0.67	1.00	Sandstone dominated heterolith
CB1 & CB2	4.50	6.00	1.50	1.40	93.33	6.67	0.73	48.67	4.50	4.90	0.35	0.40	Sandstone dominated heterolith
									4.90	6.00	1.05	1.10	Shale dominated heterolith
CB2	6.00	7.50	1.50	1.46	97.33	2.67	0.79	52.66	6.00	7.50	1.46	1.50	Shale dominated heterolith
CB2	7.50	9.00	1.50	1.47	98.00	2.00	1.51	100.60	7.50	7.54	0.04	0.04	Shale dominated heterolith
									7.54	7.98	0.43	0.44	Sandstone dominated heterolith
									7.98	8.50	0.51	0.52	Shale dominated heterolith
									8.50	9.00	0.49	0.50	Sandstone dominated heterolith
CB2 & CB3	9.00	10.50	1.50	1.48	98.67	1.33	0.90	60.00	9.00	10.50	1.48	1.50	Shale dominated heterolith
CB3	10.50	12.00	1.50	1.41	94.00	6.00	0.92	61.50	10.50	12.00	1.41	1.50	Shale dominated heterolith
CB3	12.00	13.50	1.50	1.45	96.67	3.33	1.20	80.10	12.00	12.28	0.27	0.28	Shale dominated heterolith
									12.28	13.23	0.92	0.95	Sandstone dominated heterolith
									13.23	13.50	0.26	0.27	Shale dominated heterolith
CB3	13.50	15.00	1.50	1.44	96.00	4.00	0.47	31.33	13.50	15.00	1.44	1.50	Shale dominated heterolith
CB4	15.00	16.50	1.50	1.49	99.33	0.67	1.13	75.33	15.00	16.50	1.49	1.50	Shale dominated heterolith
CB4	16.50	18.00	1.50	1.50	100.00	0.00	1.15	76.66	16.50	18.00	1.50	1.50	Shale dominated heterolith
CB4	18.00	19.50	1.50	1.48	98.67	1.33	0.86	57.33	18.00	19.50	1.48	1.50	Shale dominated heterolith
CB4 & CB5	19.50	21.00	1.50	1.50	100.00	0.00	0.95	63.33	19.50	20.00	0.50	0.50	Shale dominated heterolith
									20.00	21.00	1.00	1.00	Sandstone dominated heterolith
CB5	21.00	22.50	1.50	1.48	98.67	1.33	0.80	53.33	21.00	22.50	1.48	1.50	Sandstone dominated heterolith
CB5	22.50	24.00	1.50	1.50	100.00	0.00	1.31	87.33	22.50	24.00	1.50	1.50	Sandstone dominated heterolith
CB5	24.00	25.50	1.50	1.43	95.33	4.67	0.61	40.66	24.00	25.30	1.24	1.30	Sandstone dominated heterolith
									25.30	25.50	0.19	0.20	Sandstone
CB6	25.50	27.00	1.50	1.39	92.67	7.33	0.79	52.66	25.50	26.00	0.46	0.50	Sandstone
									26.00	27.00	0.93	1.00	Shale dominated heterolith
CB6	27.00	28.50	1.50	1.47	98.00	2.00	0.30	20.00	27.00	27.20	0.20	0.20	Shale dominated heterolith
									27.20	27.52	0.31	0.32	Sandstone
									27.52	28.47	0.93	0.95	Shale
									28.47	28.50	0.03	0.03	Sandstone
CB6	28.50	30.00	1.50	1.50	100.00	0.00	0.33	22.00	28.50	28.97	0.47	0.47	Shale
									28.97	30.00	1.03	1.03	Shale
CB7	30.00	31.50	1.50	1.49	99.00	1.00	0.44	29.33	30.00	30.13	0.13	0.13	Sandstone
									30.13	31.30	1.16	1.17	Shale dominated heterolith
									31.30	31.50	0.20	0.20	Shale
CB7	31.50	33.00	1.50	1.44	96.00	4.00	0.56	37.33	31.50	32.47	0.93	0.97	Shale
									32.47	33.00	0.51	0.53	Sandstone
CB7	33.00	34.50	1.50	1.50	100.00	0.00	0.79	52.66	33.00	34.32	1.32	1.32	Shale
									34.32	34.50	0.18	0.18	Shale dominated heterolith
CB7	34.50	35.00	0.50	0.50	100.00	0.00	0.28	56.00	34.50	35.00	0.50	0.50	Shale dominated heterolith
CB8	35.00	36.50	1.50	1.46	97.33	2.67	0.28	18.66	35.00	35.33	0.31	0.33	Shale dominated heterolith
									35.33	36.50	1.15	1.17	Shale
CB8	36.50	38.00	1.50	1.47	98.00	2.00	1.13	75.20	36.50	37.26	0.74	0.76	Sandstone

Box No.	Depth (m) From	Depth (m) To	Run Length (m)	Core recovery (m)	Core recovery (%)	Core loss (%)	RQD (m)	RQD (%)	Litho from (m)	Litho To (m)	Litho Rec. (m)	Litho Ext. (m)	Lithology
									37.26	37.83	0.56	0.57	Shale
									37.83	38.00	0.17	0.17	Shale dominated heterolith
CB8	38.00	39.50	1.50	1.48	98.67	1.33	0.65	43.33	38.00	39.50	1.48	1.50	Shale dominated heterolith
CB8 & CB9	39.50	41.00	1.50	1.46	97.33	2.67	0.47	31.33	39.50	41.00	1.46	1.50	Shale dominated heterolith
CB9	41.00	42.50	1.50	1.45	96.67	3.33	0.68	45.00	41.00	41.26	0.26	0.26	Shale dominated heterolith
									41.26	42.31	1.00	1.05	Sandstone dominated heterolith
									42.31	42.50	0.19	0.19	Shale
CB9	42.50	44.00	1.50	1.47	98.00	2.00	0.73	48.66	42.50	44.00	1.47	1.50	Shale
CB9	44.00	45.50	1.50	1.47	98.00	2.00	0.66	44.00	44.00	44.86	0.84	0.86	Shale
									44.86	45.50	0.63	0.64	Sandstone
CB10	45.50	47.00	1.50	1.50	100.00	0.00	1.03	68.66	45.50	46.88	1.38	1.38	Shale dominated heterolith
									46.88	47.00	0.12	0.12	Sandstone
CB10	47.00	48.50	1.50	1.49	99.33	0.67	1.03	68.66	47.00	48.36	1.35	1.36	Sandstone
									48.36	48.50	0.14	0.14	Shale
CB10	48.50	50.00	1.50	1.49	99.33	0.67	0.85	56.66	48.50	49.92	1.41	1.42	Shale
									49.92	50.00	0.08	0.08	Sandstone
CB11	50.00	51.50	1.50	1.46	97.33	2.67	0.62	41.33	50.00	50.16	0.16	0.16	Sandstone
									50.16	50.84	0.64	0.68	Shale
									50.84	51.38	0.54	0.54	Sandstone
									51.38	51.50	0.12	0.12	Sandstone dominated heterolith
CB11	51.50	53.00	1.50	1.48	98.67	1.33	0.91	60.66	51.50	52.26	0.75	0.76	Sandstone dominated heterolith
									52.26	53.00	0.73	0.74	Shale dominated heterolith
CB11	53.00	54.50	1.50	1.44	96.00	4.00	0.89	59.33	53.00	54.50	1.44	1.50	Shale dominated heterolith
CB11 & CB12	54.50	56.00	1.50	1.48	98.67	1.33	0.63	42.00	54.50	55.95	1.43	1.45	Shale dominated heterolith
									55.95	56.00	0.05	0.05	Sandstone
CB12	56.00	57.50	1.50	1.49	99.33	0.67	0.21	14.00	56.00	56.70	0.70	0.70	Sandstone
									56.70	57.11	0.40	0.41	Shale
									57.11	57.50	0.39	0.39	Sandstone
CB12	57.50	59.00	1.50	1.50	100.00	0.00	0.12	8.00	57.50	58.80	1.30	1.30	Shale dominated heterolith
									58.80	59.00	0.20	0.20	Shale
CB12 & CB13	59.00	60.50	1.50	1.45	96.67	3.33	0.35	23.33	59.00	60.50	1.45	1.50	Shale
CB13	60.50	62.00	1.50	1.47	98.00	2.00	0.76	50.66	60.50	60.63	0.12	0.13	Shale
									60.63	62.00	1.35	1.37	Shale- Sandstone heterolith
CB13	62.00	63.50	1.50	1.46	97.33	2.67	0.84	56.00	62.00	63.50	1.46	1.50	Shale- Sandstone heterolith
CB13	63.50	65.00	1.50	1.47	98.00	2.00	0.90	60.00	63.50	65.00	1.47	1.50	Shale- Sandstone heterolith
CB14	65.00	66.50	1.50	1.44	96.00	4.00	0.97	64.66	65.00	65.50	0.48	0.50	Shale- Sandstone heterolith
									65.50	66.50	0.96	1.00	Sandstone
CB14	66.50	68.00	1.50	1.47	98.00	2.00	1.18	78.66	66.50	68.00	1.47	1.50	Sandstone
CB14	68.00	69.50	1.50	1.46	97.33	2.67	1.10	73.33	68.00	69.50	1.46	1.50	Sandstone
CB14 & CB15	69.50	71.00	1.50	1.49	99.33	0.67	0.71	47.33	69.50	69.90	0.40	0.40	Sandstone
									69.90	71.00	1.09	1.10	Shale dominated heterolith
CB15	71.00	72.50	1.50	1.47	98.00	2.00	0.63	42.00	71.00	71.47	0.46	0.47	Shale dominated heterolith
									71.47	72.50	1.01	1.03	Sandstone
CB15	72.50	74.00	1.50	1.45	96.67	3.33	0.70	46.66	72.50	74.00	1.45	1.50	Sandstone
CB15	74.00	75.50	1.50	1.47	98.00	2.00	0.87	58.00	74.00	75.50	1.47	1.50	Sandstone
CB16	75.50	77.00	1.50	1.45	96.67	3.33	1.27	84.66	75.50	77.00	1.45	1.50	Sandstone
CB16	77.00	78.50	1.50	1.41	94.00	6.00	0.73	48.66	77.00	78.50	1.41	1.50	Sandstone
CB16	78.50	80.00	1.50	1.50	100.00	0.00	1.28	85.33	78.50	80.00	1.50	1.50	Sandstone
CB17	80.00	81.50	1.50	1.43	95.33	4.67	1.23	82.00	80.00	81.50	1.43	1.50	Sandstone dominated hetrolith
CB17	81.50	83.00	1.50	1.50	100.00	0.00	1.11	74.00	81.50	83.00	1.50	1.50	Sandstone dominated hetrolith
CB17	83.00	84.50	1.50	1.40	93.33	6.67	1.37	91.33	83.00	84.50	1.40	1.50	Sandstone dominated hetrolith
CB17 & CB18	84.50	86.00	1.50	1.45	96.67	3.33	1.11	74.00	84.50	86.00	1.45	1.50	Sandstone dominated hetrolith
CB18	86.00	87.50	1.50	1.47	98.00	2.00	1.22	81.33	86.00	87.50	1.47	1.50	Sandstone dominated hetrolith
CB18	87.50	89.00	1.50	1.43	95.33	4.67	1.23	82.00	87.50	89.00	1.43	1.50	Sandstone dominated hetrolith
CB18 & CB19	89.00	90.50	1.50	1.41	94.00	6.00	1.17	78.00	89.00	90.50	1.41	1.50	Sandstone dominated hetrolith
CB19	90.50	92.00	1.50	1.47	98.00	2.00	1.02	68.00	90.50	92.00	1.47	1.50	Sandstone dominated hetrolith
CB19	92.00	93.50	1.50	1.47	98.00	2.00	1.12	74.66	92.00	93.50	1.47	1.50	Sandstone dominated hetrolith
CB19	93.50	95.00	1.50	1.48	98.67	1.33	0.72	48.00	93.50	95.00	1.48	1.50	Sandstone dominated hetrolith
CB20	95.00	96.50	1.50	1.44	96.00	4.00	0.69	46.00	95.00	96.50	1.44	1.50	Sandstone dominated hetrolith
CB20	96.50	98.00	1.50	1.49	99.33	0.67	0.97	64.66	96.50	98.00	1.49	1.50	Sandstone dominated hetrolith
CB20	98.00	99.50	1.50	1.45	96.67	3.33	0.79	52.66	98.00	99.50	1.45	1.50	Sandstone dominated hetrolith
	99.50	101.00	1.50	1.40	93.33	6.67	0.33	22.00	99.50	100.00	0.47	0.50	Sandstone dominated hetrolith

Box No.	Depth (m) From	Depth (m) To	Run Length (m)	Core recovery (m)	Core recovery (%)	Core loss (%)	RQD (m)	RQD (%)	Litho from (m)	Litho To (m)	Litho Rec. (m)	Litho Ext. (m)	Lithology
CB20 & CB21									100.00	101.00	0.93	1.00	Shale dominated hetrolith
CB21	101.00	102.50	1.50	1.34	89.33	10.67	0.00	0.00	101.00	102.50	1.34	1.50	Shale dominated hetrolith
CB21	102.50	104.00	1.50	1.44	96.00	4.00	0.82	54.66	102.50	103.42	0.88	0.92	Shale dominated hetrolith
									103.42	104.00	0.56	0.58	Sandstone dominated hetrolith
CB21& CB22	104.00	105.50	1.50	1.46	97.33	2.67	0.79	52.66	104.00	105.50	1.46	1.50	Sandstone dominated hetrolith
CB22	105.50	107.00	1.50	1.43	95.33	4.67	1.02	68.00	105.50	107.00	1.43	1.50	Sandstone dominated hetrolith
CB22	107.00	108.50	1.50	1.49	99.33	0.67	0.54	36.00	107.00	107.30	0.30	0.30	Sandstone dominated hetrolith
									107.30	108.50	1.19	1.20	Sandstone
CB22	108.50	110.00	1.50	1.37	91.33	8.67	0.31	20.66	108.50	109.68	1.08	1.18	Sandstone
									109.68	110.00	0.29	0.32	Shale Sandstone hetrolith
CB23	110.00	111.50	1.50	1.48	98.67	1.33	0.41	27.33	110.00	111.20	1.18	1.20	Shale Sandstone hetrolith
									111.20	111.50	0.30	0.30	Sandstone
CB23	111.50	113.00	1.50	1.21	80.67	19.33	0.54	36.00	111.50	113.00	1.21	1.50	Sandstone
CB23	113.00	114.50	1.50	1.49	99.33	0.67	0.00	0.00	113.00	114.50	1.49	1.50	Sandstone
CB23& CB24	114.50	116.00	1.50	1.10	73.33	26.67	0.00	0.00	114.50	114.70	0.15	0.20	Sandstone
									114.70	116.00	0.95	1.30	Sandstone dominated hetrolith
CB 24	116.00	117.50	1.50	1.44	96.00	4.00	0.00	0.00	116.00	117.50	1.44	1.50	Sandstone dominated hetrolith
CB 24	117.50	119.00	1.50	1.28	85.33	14.67	0.13	8.67	117.50	119.00	1.28	1.50	Sandstone dominated hetrolith
CB24	119.00	120.50	1.50	1.37	91.33	8.67	0.24	16.00	119.00	120.00	0.91	1.00	Sandstone dominated hetrolith
									120.00	120.50	0.46	0.50	Sandstone
CB25	120.50	122.00	1.50	1.40	93.33	6.67	0.00	0.00	120.50	122.00	1.40	1.50	Sandstone
CB25	122.00	123.50	1.50	1.20	80.00	20.00	0.00	0.00	122.00	123.50	1.20	1.50	Sandstone
CB25	123.50	125.00	1.50	1.31	87.33	12.67	0.24	16.00	123.50	125.00	1.31	1.50	Sandstone
CB25 & CB26	125.00	126.50	1.50	1.41	94.00	6.00	0.56	37.33	125.00	126.50	1.41	1.50	Sandstone
CB26	126.50	128.00	1.50	1.16	77.33	22.67	0.15	10.00	126.50	127.70	1.16	1.20	Sandstone
									127.70	128.00		0.30	Shale dominated hetrolith
CB26	128.00	129.50	1.50	1.35	90.00	10.00	0.56	37.33	128.00	129.50	1.35	1.50	Shale dominated hetrolith
CB26	129.50	131.00	1.50	1.50	100.00	0.00	0.65	43.33	129.50	131.00	1.50	1.50	Shale dominated hetrolith
CB26 & CB27	131.00	132.50	1.50	1.39	92.67	7.33	0.27	18.00	131.00	132.50	1.39	1.50	Shale dominated hetrolith
CB 27	132.50	134.00	1.50	1.30	86.67	13.33	0.44	29.33	132.50	134.00	1.30	1.50	Shale dominated hetrolith
CB 27	134.00	135.50	1.50	1.35	90.00	10.00	0.11	7.33	134.00	135.50	1.35	1.50	Shale dominated hetrolith
CB 27	135.50	137.00	1.50	1.40	93.33	6.67	0.26	17.33	135.50	135.58	0.08	0.08	Shale dominated hetrolith
									135.58	137.00	1.32	1.42	Shale- Sandstone heterolith
CB28	137.00	138.50	1.50	1.42	94.67	5.33	0.47	31.33	137.00	138.50	1.42	1.50	Shale- Sandstone heterolith
CB28	138.50	140.00	1.50	1.36	90.67	9.33	0.36	24.00	138.50	140.00	1.36	1.50	Shale- Sandstone heterolith
CB28	140.00	141.50	1.50	1.50	100.00	0.00	0.31	20.67	140.00	140.60	0.60	0.60	Shale- Sandstone heterolith
									140.60	141.50	0.90	0.90	Shale dominated hetrolith
CB28 & CB29	141.50	143.00	1.50	1.25	83.33	16.67	0.44	29.33	141.50	143.00	1.25	1.50	Shale dominated hetrolith
CB29	143.00	144.50	1.50	1.33	88.67	11.33	0.51	34.00	143.00	144.50	1.33	1.50	Shale dominated hetrolith
CB29	144.50	146.00	1.50	1.40	93.33	6.67	0.37	24.67	144.50	146.00	1.40	1.50	Shale dominated hetrolith
CB29 & CB30	146.00	147.50	1.50	1.44	96.00	4.00	0.37	24.67	146.00	147.30	1.24	1.30	Shale dominated hetrolith
									147.30	147.50	0.20	0.20	Sandstone dominated hetrolith
CB 30	147.50	149.00	1.50	1.40	93.33	6.67	0.38	25.33	147.50	149.00	1.40	1.50	Sandstone dominated hetrolith
CB 30	149.00	150.00	1.50	0.90	60.00	40.00	0.13	8.67	149.00	150.00	0.90	1.00	Sandstone dominated hetrolith
CB 30	150.00	151.00	1.50	1.00	66.67	33.33	0.40	26.67	150.00	151.00	1.00	1.00	Sandstone dominated hetrolith

Annexure-XXVII-B Details of Core-log of BH-02

Title of the project:	**Reconnaissance Survey for REE Exploration in Bhuj Clay Prospect Block, Kachchh District, Gujarat**
Item no. along with Spill over item No.	NA
Field Season:	**2025**
Borehole No	**GSPL_BHUJ_BH-02**
Location	**Bhuj, Gujarat**
Angle	**Vertical**
Latitude	**23.15934**
Longitude	**69.71902**
Collar RL	**132 m**
Date of commencement	**21.07.2025**
Date of closing	**29.07.2025**
Unit No.	**Geovale/ Drill Unit- 2**
Total Depth	**170.00 m**

Box No.	Depth (m)From	Depth (m)To	Run Length (m)	Core recovery (m)	Core recovery (%)	Core loss(%)	RQD (m)	RQD (%)	Litho from (m)	Litho To (m)	Litho Rec. (m)	Litho Ext. (m)	Lithology
CB-1	0.00	1.00	1.00	0.8	80.00	20.00	0	0	0.00	1.00	0.80	1.00	Soil
CB-1	1.00	2.00	1.00	0.95	95.00	5.00	0	0	1.00	2.00	0.95	1.00	Ferruginous sandstone
CB-1	2.00	3.00	1.00	0.95	95.00	5.00	0.11	11.00	2.00	3.00	0.95	1.00	Ferruginous sandstone
CB-1	3.00	4.00	1.00	0.93	93.00	7.00	0.23	23.00	3.00	3.20	0.13	0.20	Ferruginous sandstone
									3.20	4.00	0.80	0.80	Sandstone dominated heterolith
CB-2	4.00	5.00	1.00	0.97	97.00	3.00	0.34	34.00	4.00	5.00	0.97	1.00	Sandstone dominated heterolith
CB-2	5.00	8.00	3.00	3.00	100.00	0.00	1.80	60.00	5.00	8.00	3.00	3.00	Sandstone dominated heterolith
CB-3	8.00	11.00	3.00	3.00	100.00	0.00	1.71	57.00	8.00	11.00	3.00	3.00	Sandstone dominated heterolith
CB-3 & CB-4	11.00	14.00	3.00	2.97	99.00	1.00	2.00	66.67	11.00	14.00	2.97	3.00	Sandstone dominated heterolith
CB-4 & CB-5	14.00	17.00	3.00	2.94	98.00	2.00	1.57	52.33	14.00	15.28	1.24	1.28	Sandstone dominated heterolith
									15.28	15.84	0.56	0.56	Sandstone
									15.84	17.00	1.14	1.16	Breccia
CB-5	17.00	20.00	3.00	2.83	94.33	5.67	1.62	54.00	17.00	17.50	0.40	0.50	Breccia
									17.50	19.00	1.47	1.50	Fossiliferous sandstone
									19.00	20.00	0.96	1.00	Sandstone
CB-6	20.00	23.00	3.00	2.98	99.33	0.67	1.61	53.67	20.00	21.35	1.33	1.35	Sandstone
									21.35	23.00	1.65	1.65	Fossiliferous sandstone
CB-6 & CB-7	23.00	26.00	3.00	3.00	100.00	0.00	2.36	78.67	23.00	26.00	3.00	3.00	Fossiliferous sandstone
CB-7 & CB-8	26.00	29.00	3.00	2.98	99.33	0.67	2.36	78.67	26.00	26.08	0.07	0.08	Fossiliferous sandstone
									26.08	27.21	1.12	1.13	Breccia
									27.21	29.00	1.79	1.79	Sandstone dominated Hetrolith
CB-8	29.00	32.00	3.00	2.98	99.33	0.67	2.29	76.33	29.00	30.39	1.39	1.39	Sandstone dominated Hetrolith
									30.39	31.59	1.18	1.20	Sandstone

Box No.	Depth (m)From	Depth (m)To	Run Length (m)	Core recovery (m)	Core recovery (%)	Core loss(%)	RQD (m)	RQD (%)	Litho from (m)	Litho To (m)	Litho Rec. (m)	Litho Ext. (m)	Lithology
									31.59	32.00	0.41	0.41	Shale
CB-9	32.00	35.00	3.00	3.00	100.00	0.00	2.39	79.67	32.00	32.34	0.34	0.34	Shale
									32.34	35.00	2.66	2.66	Shale dominated heterolith
CB-9 & CB-10	35.00	38.00	3.00	3.00	100.00	0.00	2.41	80.33	35.00	37.00	2.00	2.00	Shale dominated heterolith
									37.00	38.00	1.00	1.00	Sandstone dominated heterolith
CB-10 & CB-11	38.00	41.00	3.00	2.96	98.67	1.33	2.68	89.33	38.00	41.00	2.96	3.00	Sandstone dominated heterolith
CB11	41.00	44.00	3.00	2.99	99.67	0.33	2.73	91.00	41.00	42.00	1.00	1.00	Sandstone dominated heterolith
									42.00	42.50	0.49	0.50	Sandstone
									42.50	44.00	1.50	1.50	Sandstone dominated heterolith
CB-12	44.00	47.00	3.00	3.00	100.00	0.00	1.90	63.33	44.00	47.00	3.00	3.00	Sandstone dominated heterolith
CB-12 & CB-13	47.00	50.00	3.00	3.00	100.00	0.00	3.19	106.33	47.00	48.00	1.00	1.00	Sandstone dominated heterolith
									48.00	50.00	2.00	2.00	Shale- Sandstone heterolith
CB-13 & CB-14	50.00	53.00	3.00	2.98	99.33	0.67	2.28	76.00	50.00	53.00	2.98	3.00	Shale- Sandstone heterolith
CB-14	53.00	56.00	3.00	2.95	98.33	1.67	2.61	87.00	53.00	53.67	0.63	0.67	Shale- Sandstone heterolith
									53.67	53.89	0.21	0.22	Sandstone
									53.89	56.00	2.11	2.11	Sandstone dominated heterolith
CB-15	56.00	59.00	3.00	2.96	98.67	1.33	2.31	77.00	56.00	56.54	0.50	0.54	Sandstone dominated heterolith
									56.54	59.00	2.46	2.46	Shale- Sandstone heterolith
CB-15 & CB-16	59.00	62.00	3.00	2.97	99.00	1.00	1.77	59.00	59.00	60.49	1.48	1.49	Shale- Sandstone heterolith
									60.49	62.00	1.49	1.51	Fossiliferous sandstone
CB-16 & CB-17	62.00	65.00	3.00	3.00	100.00	0.00	2.55	85.00	62.00	65.00	3.00	3.00	Fossiliferous sandstone
CB-17	65.00	68.00	3.00	3.00	100.00	0.00	2.50	83.33	65.00	68.00	3.00	3.00	Fossiliferous sandstone
CB-18	68.00	71.00	3.00	2.96	98.67	1.33	2.66	88.67	68.00	71.00	2.96	3.00	Sandstone
CB-18 & CB-19	71.00	74.00	3.00	3.00	100.00	0.00	1.59	53.00	71.00	74.00	3.00	3.00	Sandstone dominated heterolith
CB-19 & CB-20	74.00	77.00	3.00	3.00	100.00	0.00	2.73	91.00	74.00	77.00	3.00	3.00	Sandstone dominated heterolith
CB-20	77.00	80.00	3.00	3.00	100.00	0.00	1.94	64.67	77.00	80.00	3.00	3.00	Sandstone dominated heterolith
CB-21	80.00	83.00	3.00	2.98	99.33	0.67	1.93	64.33	80.00	80.93	0.91	0.93	Sandstone dominated heterolith
									80.93	83.00	2.07	2.07	Fossiliferous sandstone

Box No.	Depth (m)From	Depth (m)To	Run Length (m)	Core recovery (m)	Core recovery (%)	Core loss(%)	RQD (m)	RQD (%)	Litho from (m)	Litho To (m)	Litho Rec. (m)	Litho Ext. (m)	Lithology
CB-21 & CB-22	83.00	86.00	3.00	2.96	98.67	1.33	2.42	80.67	83.00	86.00	2.96	3.00	Fossiliferous sandstone
CB-22 & CB-23	86.00	89.00	3.00	2.94	98.00	2.00	1.90	63.33	86.00	86.70	0.68	0.70	Fossiliferous sandstone
									86.70	89.00	2.26	2.30	Sandstone dominated heterolith
CB-23	89.00	92.00	3.00	3.00	100.00	0.00	1.80	60.00	89.00	89.84	0.84	0.84	Sandstone dominated heterolith
									89.84	90.83	0.99	0.99	Sandstone
									90.83	92.00	1.17	1.17	Sandstone dominated heterolith
CB-24	92.00	95.00	3.00	2.98	99.33	0.67	2.13	71.00	92.00	95.00	2.98	3.00	Sandstone dominated heterolith
CB-24 & CB-25	95.00	98.00	3.00	2.96	98.67	1.33	2.31	77.00	95.00	98.00	2.96	3.00	Sandstone dominated heterolith
CB-25 & CB-26	98.00	101.00	3.00	3.00	100.00	0.00	1.91	63.67	98.00	101.00	3.00	3.00	Sandstone dominated heterolith
CB-26	101.00	104.00	3.00	3.00	100.00	0.00	2.57	85.67	101.00	104.00	3.00	3.00	Sandstone dominated heterolith
CB-27	104.00	107.00	3.00	3.00	100.00	0.00	2.09	69.67	104.00	107.00	3.00	3.00	Sandstone dominated heterolith
CB-27 & CB-28	107.00	110.00	3.00	3.00	100.00	0.00	1.94	64.67	107.00	107.35	0.35	0.35	Sandstone dominated heterolith
									107.35	110.00	2.65	2.65	Shale Sandstone hetrolith
CB-28 & CB-29	110.00	113.00	3.00	3.00	100.00	0.00	2.23	74.33	110.00	112.00	2.00	2.00	Shale Sandstone hetrolith
									112.00	113.00	1.00	1.00	Sandstone dominated heterolith
CB-29	113.00	116.00	3.00	3.00	100.00	0.00	2.04	68.00	113.00	116.00	3.00	3.00	Sandstone dominated heterolith
CB-30	116.00	119.00	3.00	3.00	100.00	0.00	1.95	65.00	116.00	119.00	3.00	3.00	Sandstone dominated heterolith
CB-30 & CB-31	119.00	122.00	3.00	3.00	100.00	0.00	2.21	73.67	119.00	122.00	3.00	3.00	Sandstone dominated heterolith
CB-31 & CB-32	122.00	125.00	3.00	3.00	100.00	0.00	1.87	62.33	122.00	125.00	3.00	3.00	Sandstone dominated heterolith
CB-32	125.00	128.00	3.00	3.00	100.00	0.00	2.42	80.67	125.00	126.45	1.45	1.45	Sandstone dominated heterolith
									126.45	128.00	1.55	1.55	Shale Sandstone hetrolith
CB-33	128.00	131.00	3.00	3.00	100.00	0.00	2.01	67.00	128.00	131.00	3.00	3.00	Shale Sandstone hetrolith
CB-33 & CB-34	131.00	134.00	3.00	3.00	100.00	0.00	2.19	73.00	131.00	134.00	3.00	3.00	Shale Sandstone hetrolith
CB-34 & CB-35	134.00	137.00	3.00	3.00	100.00	0.00	2.20	73.33	134.00	137.00	3.00	3.00	Shale Sandstone hetrolith

Box No.	Depth (m)From	Depth (m)To	Run Length (m)	Core recovery (m)	Core recovery (%)	Core loss(%)	RQD (m)	RQD (%)	Litho from (m)	Litho To (m)	Litho Rec. (m)	Litho Ext. (m)	Lithology
CB-35	137.00	140.00	3.00	2.99	99.67	0.33	1.49	49.67	137.00	140.00	2.99	3.00	Shale Sandstone hetrolith
CB-36	140.00	143.00	3.00	2.99	99.67	0.33	2.14	71.33	140.00	143.00	2.99	3.00	Shale Sandstone hetrolith
CB-36 & CB-37	143.00	146.00	3.00	3.00	100.00	0.00	1.92	64.00	143.00	143.35	0.35	0.35	Shale Sandstone hetrolith
									143.35	146.00	2.65	2.65	Sandstone dominated heterolith
CB-37 & CB-38	146.00	149.00	3.00	2.97	99.00	1.00	2.36	78.67	146.00	149.00	2.97	3.00	Sandstone dominated heterolith
CB-38	149.00	152.00	3.00	2.97	99.00	1.00	2.27	75.67	149.00	150.76	1.73	1.76	Sandstone dominated heterolith
									150.76	152.00	1.24	1.24	Shale dominated heterolith
CB-39	152.00	155.00	3.00	2.97	99.00	1.00	2.18	72.67	152.00	153.40	1.37	1.40	Shale dominated heterolith
									153.40	155.00	1.60	1.60	Sandstone dominated heterolith
CB-39 & CB-40	155.00	158.00	3.00	3.00	100.00	0.00	2.41	80.33	155.00	155.21	0.21	0.21	Sandstone dominated heterolith
CB-40 & CB-41	158.00	161.00	3.00	3.00	100.00	0.00	2.40	80.00	155.21	159.27	4.06	4.06	Shale Sandstone hetrolith
									159.27	160.07	0.80	0.80	Sandstone
									160.07	161.00	0.93	0.93	Shale Sandstone hetrolith
CB-41	161.00	164.00	3.00	3.00	100.00	0.00	2.22	74.00	161.00	164.00	3.00	3.00	Shale Sandstone hetrolith
CB-41 & CB-42	164.00	167.00	3.00	2.97	99.00	1.00	2.24	74.67	164.00	166.53	2.50	2.53	Shale Sandstone hetrolith
									166.53	167.00	0.47	0.47	Shale dominated heterolith
CB-42 & CB-43	167.00	170.00	3.00	3.00	100.00	0.00	1.15	38.33	167.00	170.00	3.00	3.00	Shale dominated heterolith

Annexure-XXVII-C Details of Core-log of BH-03

Title of the project:	**Reconnaissance Survey for REE Exploration in Bhuj Clay Prospect Block, Kachchh District, Gujarat**
Item no. along with Spill over item No.	NA
Field Season:	**2025**
Borehole No	**GSPL_BHUJ_BH-03**
Location:	**Bhuj, Gujarat**
Latitude	**23.20397**
Longitude	**69.62844**
Angle	**Angle 45° ; Azimuth 170°**
Collar RL	**122m**
Date of commencement	**26.07.2025**
Date of closing	**28.07.2025**
Unit No.	**Geovale/ Drill Unit- 1**
Total Depth	**16.00 m**

Box No.	Depth (m) From	Depth (m) To	Run Length (m)	Core recovery (m)	Core recovery (%)	Core loss (%)	RQD (m)	RQD (%)	Litho from (m)	Litho To (m)	Litho Rec. (m)	Litho Ext. (m)	Lithology
CB-1	0.00	1.00	1.00	0.80	80.00	20.00	0.00	0.00	0.00	1.00	0.80	1.00	Sludge, yellowish white , medium to coarse grained sandstone
CB-1	1.00	2.00	1.00	0.80	80.00	20.00	0.00	0.00	1.00	2.00	0.80	1.00	Sludge, yellowish white , medium to coarse grained sandstone
CB-1	2.00	3.00	1.00	0.80	80.00	20.00	0.00	0.00	2.00	3.00	0.80	1.00	Sludge,White, medium to coarse grained sandstone
CB-1	3.00	4.00	1.00	0.80	80.00	20.00	0.00	0.00	3.00	4.00	0.80	1.00	Sludge,White, medium to coarse grained sandstone
CB-2	4.00	5.00	1.00	0.80	80.00	20.00	0.00	0.00	4.00	5.00	0.80	1.00	Sludge,White, medium to fine grained sandstone
CB-2	5.00	6.00	1.00	0.80	80.00	20.00	0.00	0.00	5.00	6.00	0.80	1.00	Sludge,White, medium to fine grained sandstone
CB-2	6.00	7.00	1.00	0.80	80.00	20.00	0.00	0.00	6.00	7.00	0.80	1.00	Sludge,White, medium to fine grained sandstone
CB-2	7.00	8.00	1.00	0.80	80.00	20.00	0.00	0.00	7.00	8.00	0.80	1.00	Sludge,White, medium to fine grained sandstone
CB-3	8.00	9.00	1.00	0.80	80.00	20.00	0.00	0.00	8.00	9.00	0.80	1.00	Sludge of sandstone with differential ferruginization
CB-3	9.00	10.00	1.00	0.80	80.00	20.00	0.00	0.00	9.00	10.00	0.80	1.00	Sludge of sandstone with differential ferruginization
CB-3	10.00	11.00	1.00	0.80	80.00	20.00	0.00	0.00	10.00	11.00	0.80	1.00	Sludge of sandstone with differential ferruginization
CB-3	11.00	12.00	1.00	0.80	80.00	20.00	0.00	0.00	11.00	12.00	0.80	1.00	Sludge of sandstone with differential ferruginization
CB-4	12.00	13.00	1.00	0.80	80.00	20.00	0.00	0.00	12.00	13.00	0.80	1.00	Sludge,White, medium to very fine grained sandstone
CB-4	13.00	14.00	1.00	0.80	80.00	20.00	0.00	0.00	13.00	14.00	0.80	1.00	Sludge,White, medium to very fine grained sandstone
CB-4	14.00	15.00	1.00	0.80	80.00	20.00	0.00	0.00	14.00	15.00	0.80	1.00	Sludge of sandstone with differential ferruginization
CB-4	15.00	16.00	1.00	0.80	80.00	20.00	0.00	0.00	15.00	16.00	0.80	1.00	Sludge of sandstone with differential ferruginization

Annexure-XXVII-D Details of Core-log of BH-04

Title of the project:	**Reconnaissance Survey for REE Exploration in Bhuj Clay Prospect Block, Kachchh District, Gujarat**
Item no. along with Spill over item No.	NA
Field Season:	**2025**
Borehole No	**GSPL_BHUJ_BH-04**
Location	**Bhuj, Gujarat**
Latitude	**23.20400**
Longitude	**69.62840**
Angle	**Angle 45° ; Azimuth 170°**
Collar RL	**122m**
Date of commencement	**31.07.2025**
Date of closing	**05.08.2025**
Unit No.	**Geovale/ Drill Unit- 1**
Total Depth	**51.00 m**

Box No.	Depth (m) From	Depth (m) To	Run Length (m)	Core recovery (m)	Core recovery (%)	Core loss (%)	RQD (m)	RQD (%)	Litho from (m)	Litho To (m)	Litho Rec. (m)	Litho Ext. (m)	Lithology
CB-1	0.00	1.00	1.00	0.80	80.00	20.00	0	0.00	0.00	1.00	0.80	1.00	Sludge of yellowish brown coloured ferruginized sandstone
CB-1	1.00	2.00	1.00	0.80	80.00	20.00	0	0.00	1.00	2.00	0.80	1.00	Sludge of yellowish brown coloured ferruginized sandstone
CB-1	2.00	3.00	1.00	0.80	80.00	20.00	0	0.00	2.00	3.00	0.80	1.00	Sludge of yellowish brown coloured ferruginized sandstone
CB-1	3.00	4.00	1.00	0.80	80.00	20.00	0	0.00	3.00	4.00	0.80	1.00	Sludge of sandstone with differential ferruginization
CB-2	4.00	5.00	1.00	0.80	80.00	20.00	0	0.00	4.00	5.00	0.80	1.00	Sludge of sandstone with differential ferruginization
CB-2	5.00	6.00	1.00	0.80	80.00	20.00	0	0.00	5.00	6.00	0.80	1.00	Sludge of sandstone with differential ferruginization
CB-2	6.00	7.00	1.00	0.80	80.00	20.00	0	0.00	6.00	7.00	0.80	1.00	Sludge of sandstone with differential ferruginization
CB-2	7.00	8.00	1.00	0.80	80.00	20.00	0	0.00	7.00	8.00	0.80	1.00	Sludge of sandstone with differential ferruginization
CB-3	8.00	9.00	1.00	0.80	80.00	20.00	0	0.00	8.00	9.00	0.80	1.00	Sludge of mica bearing ferruginized sandstone
CB-3	9.00	10.00	1.00	0.80	80.00	20.00	0	0.00	9.00	10.00	0.80	1.00	Sludge of sandstone with differential ferruginization
CB-3	10.00	11.00	1.00	0.80	80.00	20.00	0	0.00	10.00	11.00	0.80	1.00	Sludge of sandstone with differential ferruginization
CB-3	11.00	12.00	1.00	0.70	70.00	30.00	0.14	14.00	11.00	11.26	0.10	0.26	Sludge of sandstone with differential ferruginization
									11.26	12.00	0.60	0.74	Sandstone dominated heterolith
CB-4	12.00	13.50	1.50	1.30	86.67	13.33	0.15	10.00	12.00	13.50	1.30	1.50	Sandstone dominated heterolith
CB-4	13.50	15.00	1.50	1.30	86.67	13.33	0.61	40.67	13.50	15.00	1.30	1.50	Sandstone with differential ferruginization
CB-4 & 5	15.00	16.50	1.50	1.35	90.00	10.00	0.14	9.33	15.00	16.50	1.35	1.50	Sandstone with differential ferruginization
CB-5	16.50	18.00	1.50	1.40	93.33	6.67	0.62	41.33	16.50	18.00	1.40	1.50	Sandstone with differential ferruginization
CB-5	18.00	19.50	1.50	1.30	86.67	13.33	0	0.00	18.00	19.50	1.30	1.50	Sludge of yellowish brown coloured ferruginized sandstone
CB-5	19.50	21.00	1.50	1.30	86.67	13.33	0	0.00	19.50	21.00	1.30	1.50	Sludge of yellowish brown coloured ferruginized sandstone
CB-6	21.00	22.50	1.50	1.30	86.67	13.33	0	0.00	21.00	22.50	1.30	1.50	Sludge of yellowish brown coloured ferruginized sandstone
CB-6	22.50	24.00	1.50	1.28	85.33	14.67	0	0.00	22.50	23.91	1.20	1.41	Sludge of yellowish brown coloured ferruginized sandstone
									23.91	24.00	0.08	0.09	Yellowish brown coloured ferruginized sandstone
CB-7	24.00	25.50	1.50	1.07	71.33	28.67	0	0.00	24.00	25.50	1.07	1.50	Yellowish brown coloured ferruginized sandstone
CB-7	25.50	27.00	1.50	1.16	77.33	22.67	0	0.00	25.50	27.00	1.16	1.50	Yellowish brown coloured ferruginized sandstone

Box No.	Depth (m) From	Depth (m) To	Run Length (m)	Core recovery (m)	Core recovery (%)	Core loss (%)	RQD (m)	RQD (%)	Litho from (m)	Litho To (m)	Litho Rec. (m)	Litho Ext. (m)	Lithology
CB-7	27.00	28.50	1.50	1.15	76.67	23.33	0.12	8.00	27.00	27.96	0.85	0.96	Yellowish brown coloured ferruginized sandstone
									27.96	28.50	0.30	0.54	Mica bearing ferruginized sandstone
CB-7 & 8	28.50	30.00	1.50	1.40	93.33	6.67	0	0.00	28.50	30.00	1.40	1.50	Mica bearing ferruginized sandstone
CB-8	30.00	31.50	1.50	0.60	40.00	60.00	0.12	8.00	30.00	31.00	0.10	1.00	Mica bearing ferruginized sandstone
CB-8									31.00	31.50	0.50	0.50	Sandstone with differential ferruginization
CB-8	31.50	33.00	1.50	1.40	93.33	6.67	0	0.00	31.50	33.00	1.40	1.50	Sandstone with differential ferruginization
8 CB- & 9	33.00	34.50	1.50	1.30	86.67	13.33	0	0.00	33.00	33.31	0.24	0.31	Sandstone with differential ferruginization
									33.31	34.50	1.06	1.19	Shale-sandstone heterolith
CB-9	34.50	36.00	1.50	1.40	93.33	6.67	0.44	29.33	34.50	36.00	1.40	1.50	Shale-sandstone heterolith
CB-9	36.00	37.50	1.50	1.15	76.67	23.33	0	0.00	36.00	36.87	0.67	0.87	Shale-sandstone heterolith
									36.87	37.50	0.48	0.63	Shale-sandstone heterolith
CB-9 & 10	37.50	39.00	1.50	0.82	54.67	45.33	0.25	16.67	37.50	39.00	0.82	1.50	Shale-sandstone heterolith
CB-10	39.00	40.50	1.50	1.30	86.67	13.33	0	0.00	39.00	40.00	1.00	1.00	Sandstone with differential ferruginization
									40.00	40.50	0.30	0.50	Mica bearing metasomatized sandstone
CB-10 & 11	40.50	42.00	1.50	0.08	5.33	94.67	0	0.00	40.50	42.00	0.08	1.50	Mica bearing metasomatized sandstone
CB-11	42.00	43.50	1.50	1.30	86.67	13.33	0.1	6.67	42.00	43.50	1.30	1.50	Mica bearing metasomatized sandstone
CB-11	43.50	45.00	1.50	1.00	66.67	33.33	0.25	16.67	43.50	44.13	0.50	0.63	Mica bearing metasomatized sandstone
									44.13	45.00	0.50	0.87	Mica bearing metasomatized sandstone
CB-11 & 12	45.00	46.50	1.50	1.10	73.33	26.67	0.49	32.67	45.00	45.50	0.37	0.50	Mica bearing metasomatized sandstone
									45.50	46.50	0.73	1.00	Breccia
CB-12	46.50	48.00	1.50	1.30	86.67	13.33	0.35	23.33	46.50	48.00	1.30	1.50	Breccia
CB-12	48.00	49.50	1.50	1.35	90.00	10.00	0.54	36.00	48.00	48.50	0.45	0.50	Mica bearing metasomatized sandstone
									48.50	49.50	0.90	1.00	Shale
CB-13	49.50	51.00	1.50	1.40	93.33	6.67	0	0.00	49.50	50.36	0.80	0.86	Shale
									50.36	51.00	0.60	0.64	Highly ferruginized metasomatized sandstone

Annexure-XXVII-E Details of Core-log of BH-05

Title of the project:	Reconnaissance Survey for REE Exploration in Bhuj Clay Prospect Block, Kachchh District, Gujarat
Item no. along with Spill over item No.	NA
Field Season:	**2025**
Borehole No	**GSPL_BHUJ_BH-05**
Location	**Bhuj, Gujarat**
Latitude	**23.19484**
Longitude	**69.58049**
Angle	**Vertical**
Collar RL	**133m**
Date of commencement	**02.08.2025**
Date of closing	**07.08.2025**
Unit No.	**Geovale/ Drill Unit- 2**
Total Depth	**62.00**

Box No.	Depth (m) From	Depth (m) To	Run Length (m)	Total core recovery (m)	Core recovery (%)	Core loss (%)	RQD (m)	RQD (%)	Litho from (m)	Litho To (m)	Litho Rec. (m)	Litho Ext. (m)	Lithology
CB-1	0.00	1.00	1.00	0.82	82.00	18.00	0.00	0.00	0.00	0.43	0.42	0.43	Highly ferruginized metasomatized sandstone
									0.43	1.00	0.40	0.57	Highly ferruginized metasomatized sandstone
CB-1	1.00	2.00	1.00	0.80	80.00	20.00	0.00	0.00	1.00	2.00	0.80	1.00	Sludge of mica bearing ferruginized sandstone
CB-1	2.00	3.00	1.00	0.80	80.00	20.00	0.00	0.00	2.00	3.00	0.80	1.00	Sludge of mica bearing ferruginized sandstone
CB-1	3.00	4.00	1.00	0.80	80.00	20.00	0.00	0.00	3.00	4.00	0.80	1.00	Sludge of mica bearing ferruginized sandstone
CB-2	4.00	5.00	1.00	0.80	80.00	20.00	0.00	0.00	4.00	5.00	0.80	1.00	Sludge of mica bearing ferruginized sandstone
CB-2	5.00	6.00	1.00	0.80	80.00	20.00	0.00	0.00	5.00	6.00	0.80	1.00	Sludge of mica bearing ferruginized sandstone
CB-2	6.00	7.00	1.00	0.80	80.00	20.00	0.00	0.00	6.00	7.00	0.80	1.00	Sludge of mica bearing ferruginized sandstone
CB-2	7.00	8.00	1.00	0.80	80.00	20.00	0.00	0.00	7.00	8.00	0.80	1.00	Sludge of mica bearing ferruginized sandstone
CB-3	8.00	9.00	1.00	0.80	80.00	20.00	0.00	0.00	8.00	9.00	0.80	1.00	Sandstone with differential ferruginization
CB-3	9.00	10.00	1.00	0.80	80.00	20.00	0.00	0.00	9.00	10.00	0.80	1.00	Sandstone with differential ferruginization
CB-3	10.00	11.00	1.00	0.80	80.00	20.00	0.00	0.00	10.00	11.00	0.80	1.00	Sandstone with differential ferruginization
CB-3	11.00	12.00	1.00	0.70	70.00	30.00	0.00	0.00	11.00	12.00	0.70	1.00	Sandstone with differential ferruginization
CB-4	12.00	13.00	1.00	0.80	80.00	20.00	0.00	0.00	12.00	13.00	0.80	1.00	Sandstone with differential ferruginization
CB-4	13.00	14.00	1.00	0.80	80.00	20.00	0.00	0.00	13.00	14.00	0.80	1.00	Sandstone with differential ferruginization
CB-4	14.00	15.00	1.00	0.80	80.00	20.00	0.00	0.00	14.00	15.00	0.80	1.00	Sludge of yellowish brown coloured ferruginized sandstone
CB-4	15.00	16.00	1.00	0.80	80.00	20.00	0.00	0.00	15.00	16.00	0.80	1.00	Sludge of yellowish brown coloured ferruginized sandstone
CB-5	16.00	17.00	1.00	0.80	80.00	20.00	0.00	0.00	16.00	17.00	0.80	1.00	Sandstone with differential ferruginization
CB-5	17.00	18.00	1.00	0.70	70.00	30.00	0.00	0.00	17.00	18.00	0.70	1.00	Sandstone with differential ferruginization
CB-5	18.00	19.00	1.00	0.80	80.00	20.00	0.00	0.00	18.00	19.00	0.80	1.00	Sandstone with differential ferruginization
CB-5	19.00	20.00	1.00	0.80	80.00	20.00	0.00	0.00	19.00	20.00	0.80	1.00	Sandstone with differential ferruginization
CB-6	20.00	21.00	1.00	0.80	80.00	20.00	0.00	0.00	20.00	21.00	0.80	1.00	Sandstone with differential ferruginization
CB-6	21.00	22.00	1.00	0.80	80.00	20.00	0.00	0.00	21.00	22.00	0.80	1.00	Sandstone with differential ferruginization
CB-6	22.00	23.00	1.00	0.80	80.00	20.00	0.00	0.00	22.00	23.00	0.80	1.00	Sludge of yellowish brown coloured ferruginized sandstone
CB-6	23.00	24.00	1.00	0.80	80.00	20.00	0.00	0.00	23.00	24.00	0.80	1.00	Sludge of yellowish brown coloured ferruginized sandstone

Box No.	Depth (m) From	Depth (m) To	Run Length (m)	Total core recovery (m)	Core recovery (%)	Core loss (%)	RQD (m)	RQD (%)	Litho from (m)	Litho To (m)	Litho Rec. (m)	Litho Ext. (m)	Lithology
CB-7	24.00	25.00	1.00	0.80	80.00	20.00	0.00	0.00	24.00	25.00	0.80	1.00	Sludge of yellowish brown coloured ferruginized sandstone
CB-7	25.00	26.00	1.00	0.80	80.00	20.00	0.00	0.00	25.00	26.00	0.80	1.00	Sludge of yellowish brown coloured ferruginized sandstone
CB-7	26.00	27.00	1.00	0.80	80.00	20.00	0.00	0.00	26.00	27.00	0.80	1.00	Sludge of yellowish brown coloured ferruginized sandstone
CB-7	27.00	28.00	1.00	0.85	85.00	15.00	0.00	0.00	27.00	28.00	0.85	1.00	Sludge of yellowish brown coloured ferruginized sandstone
CB-8	28.00	29.00	1.00	0.70	70.00	30.00	0.00	0.00	28.00	28.38	0.20	0.38	Sludge of yellowish brown coloured ferruginized sandstone
									28.38	29.00	0.50	0.62	Sludge of mica bearing ferruginized sandstone
CB-8	29.00	30.00	1.00	0.80	80.00	20.00	0.00	0.00	29.00	30.00	0.80	1.00	Sludge of mica bearing ferruginized sandstone
CB-8	30.00	31.00	1.00	0.80	80.00	20.00	0.00	0.00	30.00	31.00	0.80	1.00	Sludge of mica bearing ferruginized sandstone
CB-8	31.00	32.00	1.00	0.80	80.00	20.00	0.00	0.00	31.00	32.00	0.80	1.00	Sludge of sandstone with differential ferruginization
CB-9	32.00	33.00	1.00	0.80	80.00	20.00	0.00	0.00	32.00	33.00	0.80	1.00	Sludge of mica bearing ferruginized sandstone
CB-9	33.00	34.00	1.00	0.80	80.00	20.00	0.00	0.00	33.00	34.00	0.80	1.00	Sludge of mica bearing ferruginized sandstone
CB-9	34.00	35.00	1.00	0.80	80.00	20.00	0.00	0.00	34.00	35.00	0.80	1.00	Sludge of yellowish brown coloured ferruginized sandstone
CB-9	35.00	36.00	1.00	0.80	80.00	20.00	0.00	0.00	35.00	36.00	0.80	1.00	Sludge of yellowish brown coloured ferruginized sandstone
CB-10	36.00	37.00	1.00	0.80	80.00	20.00	0.00	0.00	36.00	37.00	0.80	1.00	Sludge of yellowish brown coloured ferruginized sandstone
CB-10	37.00	38.00	1.00	0.80	80.00	20.00	0.00	0.00	37.00	38.00	0.80	1.00	Sludge of yellowish brown coloured ferruginized sandstone
CB-10	38.00	39.00	1.00	0.80	80.00	20.00	0.00	0.00	38.00	39.00	0.80	1.00	Sludge of yellowish brown coloured ferruginized sandstone
CB-10	39.00	40.00	1.00	0.80	80.00	20.00	0.00	0.00	39.00	40.00	0.80	1.00	Sludge of yellowish brown coloured ferruginized sandstone
CB-11	40.00	40.50	0.50	0.45	90.00	10.00	0.00	0.00	40.00	40.15	0.10	0.15	Sludge of yellowish brown coloured ferruginized sandstone
									40.15	40.50	0.35	0.35	Sandstone with differential ferruginization
CB-11	40.50	42.00	1.50	1.45	96.67	3.33	0.81	54.00	40.50	42.00	1.45	1.50	Sandstone with differential ferruginization
CB-11	42.00	43.50	1.50	1.10	73.33	26.67	0.13	8.67	42.00	43.50	1.10	1.50	Sandstone with differential ferruginization
CB-11 & CB-12	43.50	45.00	1.50	1.10	73.33	26.67	0.00	0.00	43.50	44.50	0.70	1.00	Sandstone with differential ferruginization
									44.50	45.00	0.40	0.50	Sandstone with differential ferruginization
CB-12	45.00	46.50	1.50	1.30	86.67	13.33	0.00	0.00	45.00	46.50	1.30	1.50	Mica bearing metasomatized sandstone
CB-12	46.50	48.00	1.50	1.20	80.00	20.00	0.00	0.00	46.50	47.75	1.10	1.25	Mica bearing metasomatized sandstone
									47.75	48.00	0.10	0.25	Sandstone with differential ferruginization
CB-13	48.00	49.50	1.50	0.61	40.67	59.33	0.15	10.00	48.00	49.50	0.61	1.50	Sandstone with differential ferruginization
CB-13	49.50	51.00	1.50	0.68	45.33	54.67	0.37	24.67	49.50	51.00	0.68	1.50	Sandstone with differential ferruginization
CB-13 & CB-14	51.00	52.50	1.50	1.00	66.67	33.33	0.13	8.67	51.00	51.75	0.70	0.75	Sandstone with differential ferruginization
									51.75	52.50	0.30	0.75	Sandstone with differential ferruginization
CB-14	52.50	54.00	1.50	0.70	46.67	53.33	0.00	0.00	52.50	54.00	0.70	1.50	Sandstone dominated heterolith
CB-14	54.00	55.50	1.50	1.20	80.00	20.00	0.41	27.33	54.00	55.50	1.20	1.50	Sandstone dominated heterolith
CB-14 & CB-15	55.50	57.00	1.50	1.47	98.00	2.00	0.18	12.00	55.50	57.00	1.47	1.50	Sandstone dominated heterolith
CB-15	57.00	58.50	1.50	1.35	90.00	10.00	0.48	32.00	57.00	58.50	1.35	1.50	Sandstone dominated heterolith

Box No.	Depth (m) From	Depth (m) To	Run Length (m)	Total core recovery (m)	Core recovery (%)	Core loss (%)	RQD (m)	RQD (%)	Litho from (m)	Litho To (m)	Litho Rec. (m)	Litho Ext. (m)	Lithology
CB-15	58.50	60.00	1.50	1.48	98.67	1.33	0.44	29.33	58.50	58.90	0.40	0.40	Sandstone dominated heterolith
									58.90	60.00	1.08	1.10	Breccia
CB-16	60.00	61.50	1.50	0.71	47.33	52.67	0.14	9.33	60.00	61.50	0.71	1.50	Breccia
CB-16	61.50	62.00	1.50	0.17	11.33	88.67	0.00	0.00	61.50	62.00	0.17	0.50	Breccia

Annexure-XXVII-F Details of Core-log of BH-06

Title of the project:	**Reconnaissance Survey for REE Exploration in Bhuj Clay Prospect Block, Kachchh District, Gujarat**
Item no. along with Spill over item No.	NA
Field Season:	**2025**
Borehole No	**GSPL_BHUJ_BH-06**
Location:	**Bhuj, Gujarat**
Latitude	**23.22258**
Longitude	**69.59413**
Angle	**Vertical**
Collar RL	**126m**
Date of commencement	**09.08.2025**
Date of closing	**17.08.2025**
Unit No.	**Geovale/ Drill Unit- 1**
Total Depth	**48.50 m**

Box No.	Depth (m) From	Depth (m) To	Run Length (m)	Core recovery (m)	Core recovery (%)	Core loss (%)	RQD (m)	RQD (%)	Litho from (m)	Litho To (m)	Litho Rec. (m)	Litho Ext. (m)	Lithology
CB-1	0.00	1.00	1.00	0.70	70.00	30.00	0.00	0.00	0.00	1.00	0.70	1.00	Ferrugiized breccia
CB-1	1.00	2.00	1.00	1.01	101.00	-1.00	0.12	12.00	1.00	1.90	0.80	0.90	Ferrugiized breccia
									1.90	2.00	0.21	0.10	Sandstone
CB-1	2.00	3.50	1.50	1.10	73.33	26.67	0.21	14.00	2.00	3.50	1.10	1.50	Sandstone
CB-1 & CB-2	3.50	5.00	1.50	1.35	90.00	10.00	0.72	48.00	3.50	5.00	1.35	1.50	Sandstone
CB-2	5.00	6.50	1.50	0.50	33.33	66.67	0.28	18.67	5.00	6.50	0.50	1.50	Sandstone
CB-2	6.50	8.00	1.50	0.30	20.00	80.00	0.00	0.00	6.50	8.00	0.30	1.50	Sandstone
CB-3	8.00	9.50	1.50	0.15	10.00	90.00	0.00	0.00	8.00	9.50	0.15	1.50	Sandstone
CB-3	9.50	11.00	1.50	1.40	1.40	98.60	0.00	0.00	9.50	11.00	1.40	1.50	Sandstone
CB-3 & CB-4	11.00	12.50	1.50	1.30	86.67	13.33	0.00	0.00	11.00	12.50	1.30	1.50	Sandstone
CB-4	12.50	14.00	1.50	1.00	66.67	33.33	0.00	0.00	12.50	13.46	0.80	0.96	Sandstone
									13.46	14.00	0.20	0.54	Mica bearing metasomatized sandstone
CB-4	14.00	15.50	1.50	0.20	13.33	86.67	0.00	0.00	14.00	15.50	0.20	1.50	Mica bearing metasomatized sandstone
CB-4 & CB-5	15.50	17.00	1.50	1.35	90.00	10.00	0.00	0.00	15.50	17.00	1.35	1.50	Mica bearing metasomatized sandstone
CB-5	17.00	18.50	1.50	0.78	52.00	48.00	0.00	0.00	17.00	17.50	0.26	0.50	Mica bearing metasomatized sandstone
									17.50	18.50	0.52	1.00	Shale
CB-5	18.50	20.00	1.50	1.45	96.67	3.33	0.35	23.33	18.50	20.00	1.45	1.50	Sandstone with differential ferruginization
CB-6	20.00	21.50	1.50	1.20	80.00	20.00	0.10	6.67	20.00	21.50	1.20	1.50	Sandstone with differential ferruginization
CB-6	21.50	23.00	1.50	0.45	30.00	70.00	0.00	0.00	21.50	23.00	0.45	1.50	Mica bearing ferruginized sandstone
CB-6 & CB-7	23.00	24.50	1.50	0.50	33.33	66.67	0.00	0.00	23.00	24.50	0.50	1.50	Mica bearing ferruginized sandstone
CB-7	24.50	26.00	1.50	0.70	46.67	53.33	0.00	0.00	24.50	25.00	0.40	0.50	Mica bearing ferruginized sandstone
									25.00	26.00	0.30	1.00	Sandstone with differential ferruginization
CB-7	26.00	27.50	1.50	0.80	53.33	46.67	0.00	0.00	26.00	26.55	0.30	0.55	Sandstone with differential ferruginization
									26.55	27.50	0.50	0.95	Sandstone
CB-7 & CB-8	27.50	29.00	1.50	1.40	93.33	6.67	0.32	21.33	27.50	27.94	0.40	0.44	Sandstone
									27.94	29.00	1.00	1.06	Mica bearing ferruginized sandstone
CB-8	29.00	30.50	1.50	1.35	90.00	10.00	0.20	13.33	29.00	30.18	1.10	1.18	Mica bearing ferruginized sandstone
									30.18	30.50	0.25	0.32	Sandstone with differential ferruginization
CB-8	30.50	32.00	1.50	0.95	63.33	36.67	0.00	0.00	30.50	31.00	0.35	0.50	Sandstone with differential ferruginization

Box No.	Depth (m) From	Depth (m) To	Run Length (m)	Core recovery (m)	Core recovery (%)	Core loss (%)	RQD (m)	RQD (%)	Litho from (m)	Litho To (m)	Litho Rec. (m)	Litho Ext. (m)	Lithology
									31.00	32.00	0.60	1.00	Sandstone with differential ferruginization
CB-9	32.00	33.50	1.50	1.10	73.33	26.67	0.24	16.00	32.00	33.50	1.10	1.50	Sandstone with differential ferruginization
CB-9	33.50	35.00	1.50	1.30	86.67	13.33	0.00	0.00	33.50	33.70	0.10	0.20	Sandstone with differential ferruginization
									33.70	35.00	1.20	1.30	Yellowish brown coloured ferruginized sandstone
CB-9 & CB-10	35.00	36.50	1.50	1.30	86.67	13.33	0.00	0.00	35.00	36.50	1.30	1.50	Yellowish brown coloured ferruginized sandstone
CB-10	36.50	38.00	1.50	1.30	86.67	13.33	0.00	0.00	36.50	37.00	0.30	0.50	Yellowish brown coloured ferruginized sandstone
									37.00	38.00	1.00	1.00	Sandstone with differential ferruginization
CB-10	38.00	39.50	1.50	1.40	93.33	6.67	0.00	0.00	38.00	39.50	1.40	1.50	Sandstone with differential ferruginization
CB-10 & CB-11	39.50	41.00	1.50	1.32	88.00	12.00	0.00	0.00	39.50	41.00	1.32	1.50	Mica bearing ferruginized sandstone
CB-11	41.00	42.50	1.50	1.30	86.67	13.33	0.00	0.00	41.00	41.23	0.20	0.23	Mica bearing ferruginized sandstone
									41.23	42.50	1.10	1.27	Sandstone with differential ferruginization
CB-11	42.50	44.00	1.50	1.30	86.67	13.33	0.00	0.00	42.50	44.00	1.30	1.50	Sandstone with differential ferruginization
CB-12	44.00	45.50	1.50	1.40	93.33	6.67	0.56	37.33	44.00	45.23	1.20	1.23	Sandstone with differential ferruginization
									45.23	45.50	0.20	0.27	Sandstone with differential ferruginization
CB-12	45.50	47.00	1.50	1.35	90.00	10.00	0.40	26.67	45.50	47.00	1.35	1.50	Sandstone with differential ferruginization
CB-12 & CB-13	47.00	48.50	1.50	1.45	96.67	3.33	0.49	32.67	47.00	48.00	1.00	1.00	Ferruginous sandstone
									48.00	48.50	0.45	0.50	Yellowish brown coloured ferruginized sandstone

Annexure-XXVII-G Details of Core-log of BH-07

Title of the project:	**Reconnaissance Survey for REE Exploration in Bhuj Clay Prospect Block, Kachchh District, Gujarat**
Item no. along with Spill over item No.	NA
Field Season:	**2025**
Borehole No	**GSPL_BHUJ_BH-07**
Location	**Bhuj, Gujarat**
Latitude	**23.19754**
Longitude	**69.52970**
Angle	**Vertical**
Collar RL	**178m**
Date of commencement	**09.08.2025**
Date of closing	**12.08.2025**
Unit No.	**Geovale/ Drill Unit-2**
Total Depth	**55.00 m**

Box No.	Depth (m) From	Depth (m) To	Run Length (m)	Core recovery (m)	Core recovery (%)	Core loss (%)	RQD (m)	RQD (%)	Litho from (m)	Litho To (m)	Litho Rec. (m)	Litho Ext. (m)	Lithology
CB-1	0.00	1.00	1.00	0.80	80.00	20.00	0.00	0.00	0.00	1.00	0.80	1.00	Loose sand (Quarternary sediment)
CB-1	1.00	2.00	1.00	0.98	98.00	2.00	0.39	39.00	1.00	2.00	0.98	1.00	Highly ferruginized metasomatized sandstone
CB-1	2.00	3.50	1.50	1.31	87.33	12.67	0.00	0.00	2.00	2.17	0.11	0.17	Highly ferruginized metasomatized sandstone
									2.17	3.50	1.20	1.33	Sandstone with differential ferruginization
CB-1 & 2	3.50	5.00	1.50	1.30	86.67	13.33	0.00	0.00	3.50	5.00	1.30	1.50	Sandstone with differential ferruginization
CB-2	5.00	6.50	1.50	1.40	93.33	6.67	0.38	18.00	5.00	5.30	0.20	0.30	Sandstone with differential ferruginization
									5.30	5.85	0.55	0.55	Highly ferruginized metasomatized sandstone
									5.85	6.50	0.65	0.65	Mica bearing ferruginized sandstone
CB-2	6.50	8.00	1.50	1.14	76.00	24.00	0.00	0.00	6.50	8.00	1.14	1.50	Mica bearing ferruginized sandstone
CB-3	8.00	9.50	1.50	1.20	80.00	20.00	0.00	0.00	8.00	9.50	1.20	1.50	Sludge of yellowish brown coloured ferruginized sandstone
CB-3	9.50	11.00	1.50	1.30	86.67	13.33	0.00	0.00	9.50	11.00	1.30	1.50	Sludge of yellowish brown coloured ferruginized sandstone
CB-3 & 4	11.00	12.50	1.50	1.20	80.00	20.00	0.00	0.00	11.00	12.50	1.20	1.50	Sludge of yellowish brown coloured ferruginized sandstone
CB-4	12.50	14.00	1.50	1.20	80.00	20.00	0.00	0.00	12.50	14.00	1.20	1.50	Sludge of sandstone with differential ferruginization
CB-4	14.00	15.50	1.50	1.30	86.67	13.33	0.00	0.00	14.00	15.50	1.30	1.50	Sludge of sandstone with differential ferruginization
CB-4 & 5	15.50	17.00	1.50	1.00	66.67	33.33	0.00	0.00	15.50	15.70	0.10	0.20	Sludge of sandstone with differential ferruginization
									15.70	16.30	0.60	0.60	Mica bearing ferruginized sandstone
									16.30	17.00	0.30	0.70	Sludge of sandstone with differential ferruginization
CB-5	17.00	18.50	1.50	1.20	80.00	20.00	0.00	0.00	17.00	18.50	1.20	1.50	Sludge of sandstone with differential ferruginization
CB-5	18.50	20.00	1.50	1.20	80.00	20.00	0.00	0.00	18.50	20.00	1.20	1.50	Sludge of sandstone with differential ferruginization
CB-6	20.00	21.00	1.00	0.80	80.00	20.00	0.00	0.00	20.00	21.00	0.80	1.00	Sludge of sandstone with differential ferruginization
CB-6	21.00	22.50	1.50	1.30	86.67	13.33	0.00	0.00	21.00	22.50	1.30	1.50	Sludge of sandstone with differential ferruginization
CB-6	22.50	24.00	1.50	1.20	80.00	20.00	0.00	0.00	22.50	24.00	1.20	1.50	Sludge of sandstone with differential ferruginization
CB-7	24.00	25.50	1.50	1.00	66.67	33.33	0.13	8.67	24.00	24.50	0.30	0.50	Alternating ferruginous sandstone and mica bearing metasomatized sandstone
									24.50	25.50	0.70	1.00	Alternating ferruginous sandstone and mica bearing metasomatized sandstone

Box No.	Depth (m) From	Depth (m) To	Run Length (m)	Core recovery (m)	Core recovery (%)	Core loss (%)	RQD (m)	RQD (%)	Litho from (m)	Litho To (m)	Litho Rec. (m)	Litho Ext. (m)	Lithology
CB-7	25.50	27.00	1.50	1.40	93.33	6.67	0.51	34.00	25.50	27.00	1.40	1.50	Alternating ferruginous sandstone and mica bearing metasomatized sandstone
CB-7 & 8	27.00	28.50	1.50	1.35	90.00	10.00	0.21	14.00	27.00	28.40	1.30	1.40	Alternating ferruginous sandstone and mica bearing metasomatized sandstone
									28.40	28.50	0.05	0.10	Sludge of yellowish brown coloured ferruginized sandstone
CB-8	28.50	30.00	1.50	1.35	90.00	10.00	0.24	16.00	28.50	29.44	0.80	0.94	Sludge of yellowish brown coloured ferruginized sandstone
									29.44	30.00	0.55	0.56	Mica bearing ferruginized sandstone
CB-8	30.00	31.50	1.50	0.80	53.33	46.67	0.35	23.33	30.00	31.50	0.80	1.50	Mica bearing ferruginized sandstone
CB-8 & 9	31.50	33.00	1.50	1.10	73.33	26.67	0.00	0.00	31.50	32.00	0.30	0.50	Sludge of sandstone with differential ferruginization
									32.00	33.00	0.80	1.00	Sludge of sandstone with differential ferruginization
CB-9	33.00	34.50	1.50	1.20	80.00	20.00	0.00	0.00	33.00	34.50	1.20	1.50	Sludge of sandstone with differential ferruginization
CB-9	34.50	36.00	1.50	1.10	73.33	26.67	0.00	0.00	34.50	36.00	1.10	1.50	Sludge of sandstone with differential ferruginization
CB-10	36.00	37.50	1.50	1.20	80.00	20.00	0.00	0.00	36.00	37.50	1.20	1.50	Sludge of sandstone with differential ferruginization
CB-10	37.50	39.00	1.50	1.10	73.33	26.67	0.00	0.00	37.50	39.00	1.10	1.50	Sludge of sandstone with differential ferruginization
CB-10 & 11	39.00	40.50	1.50	1.20	80.00	20.00	0.00	0.00	39.00	40.50	1.20	1.50	Sludge of yellowish brown coloured ferruginized sandstone
CB-11	40.50	42.00	1.50	1.30	86.67	13.33	0.00	0.00	40.50	42.00	1.30	1.50	Sludge of yellowish brown coloured ferruginized sandstone
CB-11	42.00	43.50	1.50	1.20	80.00	20.00	0.00	0.00	42.00	43.50	1.20	1.50	Sludge of yellowish brown coloured ferruginized sandstone
CB-11 & 12	43.50	45.00	1.50	1.10	73.33	26.67	0.00	0.00	43.50	45.00	1.10	1.50	Sludge of yellowish brown coloured ferruginized sandstone
CB-12	45.00	46.50	1.50	1.10	73.33	26.67	0.00	0.00	45.00	46.50	1.10	1.50	Sludge of yellowish brown coloured ferruginized sandstone
CB-12	46.50	48.00	1.50	1.20	80.00	20.00	0.00	0.00	46.50	48.00	1.20	1.50	Sludge of yellowish brown coloured ferruginized sandstone
CB-13	48.00	49.50	1.50	1.10	73.33	26.67	0.00	0.00	48.00	49.50	1.10	1.50	Sludge of yellowish brown coloured ferruginized sandstone
CB-13	49.50	50.00	0.50	0.30	60.00	40.00	0.00	0.00	49.50	50.00	0.30	0.50	Sludge of yellowish brown coloured ferruginized sandstone
CB-13	50.00	51.50	1.50	1.20	80.00	20.00	0.00	0.00	50.00	51.50	1.20	1.50	Sludge of yellowish brown coloured ferruginized sandstone
CB-13 & 14	51.50	52.50	1.00	0.80	80.00	20.00	0.00	0.00	51.50	52.50	0.80	1.00	Sludge of yellowish brown coloured ferruginized sandstone
CB-14	52.50	54.00	1.50	1.30	86.67	13.33	0.00	0.00	52.50	54.00	1.30	1.50	Sludge of yellowish brown coloured ferruginized sandstone
CB-14	54.00	55.00	1.00	0.80	80.00	20.00	0.00	0.00	54.00	55.00	0.80	1.00	Sludge of yellowish brown coloured ferruginized sandstone

Annexure-XXVII-H Details of Core-log of BH-08

Title of the project:	Reconnaissance Survey for REE Exploration in Bhuj Clay Prospect Block, Kachchh District, Gujarat
Item no. along with Spill over item No.	NA
Field Season:	2025
Borehole No	GSPL_BHUJ_BH-08
Location	Bhuj, Gujarat
Latitude	23.19347
Longitude	69.51839
Angle	Vertical
Collar RL	138m
Date of commencement	15.08.2025
Date of closing	22.08.2025
Unit No.	Geovale/ Drill Unit- 2
Total Depth	50.00 m

Box No.	Depth (m) From	Depth (m) To	Run Length (m)	Core recovery (m)	Core recovery (%)	Core loss (%)	RQD (m)	RQD (%)	Litho from (m)	Litho To (m)	Litho Rec. (m)	Litho Ext. (m)	Lithology
CB-1	0.00	1.50	1.50	1.00	66.67	33.33	0.00	0.00	0.00	0.63	0.50	0.63	Sludge of mica bearing ferruginized sandstone
									0.63	1.50	0.50	0.87	Sludge of yellowish brown coloured ferruginized sandstone
CB-1	1.50	3.00	1.50	1.30	86.67	13.33	0.00	0.00	1.50	3.00	1.30	1.50	Sludge of yellowish brown coloured ferruginized sandstone
CB-1 & CB-2	3.00	4.50	1.50	1.20	80.00	20.00	0.00	0.00	3.00	4.50	1.20	1.50	Sludge of yellowish brown coloured ferruginized sandstone
CB-2	4.50	6.00	1.50	0.90	60.00	40.00	0.00	0.00	4.50	6.00	0.90	1.50	Mica bearing ferruginized sandstone
CB-2	6.00	7.50	1.50	1.10	73.33	26.67	0.00	0.00	6.00	7.50	1.10	1.50	Mica bearing ferruginized sandstone
CB-2 & CB-3	7.50	9.00	1.50	1.10	73.33	26.67	0.00	0.00	7.50	9.00	1.10	1.50	Sludge of yellowish brown coloured ferruginized sandstone
CB-3	9.00	10.50	1.50	1.49	99.33	0.67	0.23	15.33	9.00	9.54	0.54	0.54	Mica bearing ferruginized sandstone
									9.54	10.50	0.95	0.96	Mica bearing metasomatized sandstone
CB-3	10.50	12.00	1.50	1.45	96.67	3.33	0.14	9.33	10.50	11.50	0.97	1.00	Mica bearing metasomatized sandstone
									11.50	12.00	0.48	0.50	Metasomatized shale sandstone hetrolith
CB-4	12.00	13.50	1.50	1.49	99.33	0.67	0.14	9.33	12.00	12.39	0.39	0.39	Metasomatized shale sandstone hetrolith
									12.39	13.50	1.10	1.11	Mica bearing ferruginized sandstone
CB-4	13.50	15.00	1.50	0.85	56.67	43.33	0.00	0.00	13.50	14.33	0.20	0.83	Mica bearing ferruginized sandstone
									14.33	15.00	0.65	0.67	Mica bearing metasomatized sandstone
CB-4 & CB-5	15.00	16.50	1.50	1.20	80.00	20.00	0.10	6.67	15.00	15.40	0.32	0.40	Mica bearing metasomatized sandstone
									15.40	16.50	0.88	1.10	Mica bearing metasomatized sandstone
CB-5	16.50	18.00	1.50	1.48	98.67	1.33	0.42	28.00	16.50	18.00	1.48	1.50	Metasomatized shale sandstone hetrolith
CB-5	18.00	19.50	1.50	1.44	96.00	4.00	0.44	29.33	18.00	19.50	1.44	1.50	Metasomatized shale sandstone hetrolith
CB-5 & CB-6	19.50	21.00	1.50	1.46	97.33	2.67	0.43	28.67	19.50	21.00	1.46	1.50	Metasomatized shale sandstone hetrolith
CB-6	21.00	22.50	1.50	1.24	82.67	17.33	0.00	0.00	21.00	21.25	0.24	0.25	Metasomatized shale sandstone hetrolith
									21.25	22.50	1.00	1.25	Sludge of sandstone with differential ferruginization
CB-6	22.50	24.00	1.50	1.20	80.00	20.00	0.00	0.00	22.50	24.00	1.20	1.50	Sludge of sandstone with differential ferruginization
CB-7	24.00	25.50	1.50	1.10	73.33	26.67	0.00	0.00	24.00	25.50	1.10	1.50	Sludge of sandstone with differential ferruginization
CB-7	25.50	27.00	1.50	1.10	73.33	26.67	0.00	0.00	25.50	27.00	1.10	1.50	Sludge of sandstone with differential ferruginization

Box No.	Depth (m) From	Depth (m) To	Run Length (m)	Core recovery (m)	Core recovery (%)	Core loss (%)	RQD (m)	RQD (%)	Litho from (m)	Litho To (m)	Litho Rec. (m)	Litho Ext. (m)	Lithology
CB-7 & CB-8	27.00	28.50	1.50	1.20	80.00	20.00	0.00	0.00	27.00	28.50	1.20	1.50	Sludge of mica bearing ferruginized sandstone
CB-8	28.50	30.00	1.50	1.30	86.67	13.33	0.00	0.00	28.50	30.00	1.30	1.50	Sludge of mica bearing ferruginized sandstone
CB-8	30.00	31.50	1.50	1.20	80.00	20.00	0.00	0.00	30.00	31.50	1.20	1.50	Sludge of mica bearing ferruginized sandstone
CB-8 & CB-9	31.50	33.00	1.50	1.10	73.33	26.67	0.00	0.00	31.50	33.00	1.10	1.50	Sludge of mica bearing ferruginized sandstone
CB-9	33.00	34.50	1.50	1.20	80.00	20.00	0.00	0.00	33.00	34.50	1.20	1.50	Sludge of yellowish brown coloured ferruginized sandstone
CB-9	34.50	36.00	1.50	1.10	73.33	26.67	0.00	0.00	34.50	36.00	1.10	1.50	Sludge of yellowish brown coloured ferruginized sandstone
CB-10	36.00	37.50	1.50	1.10	73.33	26.67	0.00	0.00	36.00	37.50	1.10	1.50	Sludge of yellowish brown coloured ferruginized sandstone
CB-10	37.50	39.00	1.50	1.30	86.67	13.33	0.00	0.00	37.50	39.00	1.30	1.50	Sludge of yellowish brown coloured ferruginized sandstone
CB-10 & CB-11	39.00	40.50	1.50	1.10	73.33	26.67	0.00	0.00	39.00	40.50	1.10	1.50	Sludge of yellowish brown coloured ferruginized sandstone
CB-11	40.50	42.00	1.50	1.10	73.33	26.67	0.00	0.00	40.50	42.00	1.10	1.50	Sludge of yellowish brown coloured ferruginized sandstone
CB-11	42.00	43.50	1.50	1.10	73.33	26.67	0.00	0.00	42.00	42.45	0.30	0.45	Sludge of yellowish brown coloured ferruginized sandstone
									42.45	43.50	0.80	1.05	Metasomatized shale sandstone hetrolith
CB-11 & CB-12	43.50	45.00	1.50	0.95	63.33	36.67	0.00	0.00	43.50	43.92	0.15	0.42	Metasomatized shale sandstone hetrolith
									43.92	45.00	0.80	1.08	Sludge of yellowish brown coloured ferruginized sandstone
CB-12	45.00	46.50	1.50	1.20	80.00	20.00	0.00	0.00	45.00	46.50	1.20	1.50	Sludge of yellowish brown coloured ferruginized sandstone
CB-12	46.50	48.00	1.50	1.25	83.33	16.67	0.10	6.67	46.50	47.00	0.30	0.50	Sludge of yellowish brown coloured ferruginized sandstone
									47.00	48.00	0.95	1.00	Mica bearing metasomatized sandstone
CB-13	48.00	49.50	1.50	1.40	93.33	6.67	0.31	20.67	48.00	49.50	1.40	1.50	Mica bearing metasomatized sandstone
CB-13	49.50	51.00	1.50	0.47	31.33	68.67	0.00	0.00	49.50	50.00	0.47	0.50	Mica bearing metasomatized sandstone

Annexure-XXVIII: Petrographic study of borehole samples

Sr No.	Sample ID	Latitude	Longitude	Sample (hand specimen) Description	Stratigraphy	Depth (m)	Thin Section Description	Name of the rock according to petrography
1	109054	23.150866	69.578768	Variegated colour shows	Katrol Formation	74.88	Fine-grained rock composed of quartz and biotite, with opaques including magnetite and goethite. Evidence of iron-rich solutions is present, with biotite partially to fully replaced by iron oxides, producing elongated opaque minerals.	Ferruginous sandstone
2	109068	23.150866	69.578768	Sandstone	Katrol Formation	65.96 to 66.00	Fine- to medium-grained tuffite composed of alternating clast-rich and clay-rich layers. The rock contains disseminated magnetite and pyrite as ore minerals, indicating deposition from volcaniclastic and sedimentary processes with subsequent iron and sulfur enrichment.	Tuffite in Sandstone
3	109072	23.150866	69.578768	Sandstone	Katrol Formation	67.88 to 67.92	Fine-grained lapilli-bearing tuffaceous sandstone composed of fragmented quartz, feldspar, and mica set in a fine-grained matrix. The rock contains abundant pyrite, is cemented by carbonates, and includes fossil fragments, indicating volcaniclastic input in a marine sedimentary environment.	Volcanoclatic Sandstone
4	109073	23.150866	69.578768	Sandstone	Katrol Formation	68.20 to 68 to 27	Medium- to fine-grained feldspathic sandstone composed of quartz, feldspar, and mica, with disseminated pyrite and magnetite indicating minor iron enrichment	Sandstone
5	109074	23.150866	69.578768	Sandstone	Katrol Formation	68.46 to 68.49	Intercalated mudstone and tuffite with a mud-rich matrix containing angular quartz, feldspar, and mica. The rock is very fine-grained and includes magnetite and pyrite as accessory minerals	Tuffite in Sandstone
6	109080	23.150866	69.578768	Sandstone	Katrol Formation	72.88 to 72.92	Fine-grained tuffite composed of fragmented quartz, feldspar, and mica, with abundant carbonate pellets, iron oxides, and disseminated pyrite, indicating volcaniclastic deposition with diagenetic iron and carbonate enrichment.	Tuffite

Sr No.	Sample ID	Latitude	Longitude	Sample (hand specimen) Description	Stratigraphy	Depth (m)	Thin Section Description	Name of the rock according to petrography
7	109081	23.150866	69.578768	Sandstone	Katrol Formation	74.87 to 74.89	Tuffite with a clayey matrix showing clay alteration, containing angular quartz grains of medium to fine grain size, indicating volcaniclastic material altered under low-grade diagenetic conditions.	Tuffite
8	109082	23.150866	69.578768	Sandstone	Katrol Formation	75.24 to 75.31	Fine-grained tuffite composed of quartz, feldspar, and mica, with layered patches of sandstone. The rock contains iron oxides, carbonate pellets, and disseminated magnetite and pyrite, reflecting volcaniclastic-sedimentary deposition with iron and carbonate enrichment.	Tuffite
9	109083	23.150866	69.578768	Sandstone	Katrol Formation	75.66 to 75.71	Interlayered sandstone with clast-rich and clast-poor layers, containing sub-rounded to sub-angular quartz grains and carbonate pellets, indicating varying energy conditions during sediment deposition.	Interlayered sandstone
10	109085	23.150866	69.578768	Sandstone	Katrol Formation	77.10 to 77.14	Fine- to medium-grained sandstone intercalated with a fossil-bearing carbonate layer. The sandstone consists mainly of quartz, feldspar, and mica, with very little matrix, giving it a clean framework-supported texture. Accessory ore minerals include magnetite and pyrite, indicating diagenetic sulfide and oxide mineralization	Sandstone
11	109086	23.150866	69.578768	Sandstone	Katrol Formation	77.40 to 77.47	Fine-grained tuffite composed of quartz, feldspar, and mica, with fragmented quartz grains, abundant carbonate pellets, and iron oxides. Magnetite and pyrite are present as accessory minerals, indicating volcaniclastic deposition with iron and carbonate enrichment	Tuffite
12	109092	23.150866	69.578768	sandstone dominated heterolith	Katrol Formation	89.84 to 89. 89	Fine-grained impure mudstone containing fragmented quartz, feldspar, and mica, with minor carbonate, and trace amounts of magnetite and pyrite, indicating clastic deposition with limited diagenetic mineralization.	Mudstone/tuffite

Sr No.	Sample ID	Latitude	Longitude	Sample (hand specimen) Description	Stratigraphy	Depth (m)	Thin Section Description	Name of the rock according to petrography
13	109124	23.194827	69.580497	Contact beween changes in lithology iron impregmation	Bhuj Formation	58.85 to 58.90	Clay matrix–supported rock containing fragmented quartz grains that range from angular to rounded. Accessory phases include magnetite, iron oxides, and scattered carbonate pellets, indicating volcaniclastic input with early diagenetic carbonate and iron enrichment	Tuffite
14	109125	23.194827	69.580497	Pyrite , clast of Conglomerate/Breccia	Bhuj Formation	59.04 to 59.10	Fine-grained sediment with quartz and mica as major components, containing scattered coarser angular quartz grains and fragments of tuffaceous rock. The coarse grains are dispersed within a fine-grained clayey matrix, giving a mixed texture. Magnetite is present as an accessory opaque phase, reflecting volcaniclastic input and early diagenetic mineralization Suspected orthoamphibol opaque phase showing brown reflection, isotropic in nature	Tuffite
15	109126	23.194827	69.580497	Black spots smelling gun powder(Shale dominated heteolith)	Bhuj Formation	52.43 to 52.53	Fine-grained tuffaceous sediment, transitional to siltstone, with needle-shaped quartz, broken quartz clasts, feldspar, and muscovite set in a very dark, clay-rich matrix. Carbonaceous matter is present, along with accessory magnetite and pyrite, indicating volcanic input deposited under reducing conditions Monazite present Glauconitic mica	Tuffaceous siltstone
16	109129	23.15934	69.71902	Sandstone	Katrol Formation	3.60 to 3.68	Fine-grained tuffaceous sandstone dominated by angular quartz with subordinate feldspar and muscovite. The rock is matrix-supported with only a small amount of fine-grained matrix, in which wispy, flow-aligned mica flakes are evident. Clay is present as part of the groundmass. Accessory magnetite occurs as scattered opaques	Tuffaceous sandstone

Sr No.	Sample ID	Latitude	Longitude	Sample (hand specimen) Description	Stratigraphy	Depth (m)	Thin Section Description	Name of the rock according to petrography
17	109133	23.15934	69.71902	sandstone dominated heterolith	Katrol Formation	07.17 to 07.22	Rock composed of broken fragments of quartz and feldspar set in a fine-grained matrix, with disrupted carbonate material and fossil fragments present. Accessory opaque minerals include magnetite and pyrite	Sandstone
18	112203	23.150866	69.578768	Suspected target layers (Gypsum there)	Katrol Formation	6.71 to 6.80	The groundmass is a glassy mass, likely devitrified volcanic glass with patches of carbonate or apatite. Needle-shaped and embayed quartz grains are dispersed within this glassy matrix, suggesting volcanic resorption and rapid deposition. Fossil fragments are also present, indicating background marine conditions during volcanic ash input. Overall, this sample represents quiet-water shale sedimentation intermittently influenced by volcanic activity, with poor primary porosity and limited reservoir potential except where volcanic glass dissolution may create secondary porosity.	Tuffite
19	112204	23.150866	69.578768	Suspected target layers	Katrol Formation	14.35 to 14.44	This slide shows a glass-rich tuffite with abundant volcanic glass fragments in a fine matrix. Black to brown flaky or thread-like minerals are scattered throughout, likely altered volcanic shards or micaceous phases	Tuffite
20	112205	23.150866	69.578768	Suspected target layers	Katrol Formation	13.63 to 13.69	The thin section shows distinct lamination defined by alternating layers: lapilli-rich bands with pellet-like grains and layers enriched in quartz and feldspar fragments. Fossil fragments are present, adding biogenic input. Possible carbonate peloids are also observed, suggesting some allochemical contribution. The overall texture reflects well-preserved primary lamination with volcanic and bioclastic influence, characteristic of a tuffaceous heterolithic facies.	Tuffaceous laminated sandstone

Sr No.	Sample ID	Latitude	Longitude	Sample (hand specimen) Description	Stratigraphy	Depth (m)	Thin Section Description	Name of the rock according to petrography
21	112207	23.150866	69.578768	Suspected target layers	Katrol Formation	13.07 to 13.10	This thin section displays a glass-rich vitric tuff with angular quartz clasts, likely of volcanic origin, set within a glassy to extremely fine-grained apatite-rich matrix. The groundmass also contains scattered feldspar grains and muscovite flakes. The overall texture is matrix-supported, with volcanic glass dominating and framework grains floating within, typical of primary pyroclastic deposition.	Tuffite
22	112208	23.150866	69.578768	Suspected target layers	Katrol Formation	11.76 to 11.81	This thin section shows a crystal-rich tuffite characterized by alternating layers of volcanic glass and crystal fragments. The crystal component is dominated by quartz, feldspar, and mica, forming distinct bands interbedded with glassy layers, reflecting rhythmic pyroclastic deposition with variable crystal content.	Tuffite
23	112209	23.150866	69.578768	Suspected target layers	Katrol Formation	16.87 to 16.89	Glass-rich tuffite with a very thin crystal-rich layer containing abundant opaques (pyrite), set within a glassy/fine-grained matrix. Quartz, feldspar, and mica crystals occur as scattered angular grains, while pyrite is concentrated along the thin layering.	Tuffite
24	112210	23.150866	69.578768	Suspected target layers	Katrol Formation	18.23 to 18.32	Target layer composed of quartz, feldspar, muscovite, and apatite within a highly altered matrix, containing opaque magnetite, framboidal pyrite, and fluorapatite	Tuffite
25	112213	23.150866	69.578768	Target layer & Transition of target layer	Katrol Formation	18.83 to 18.88	The thin section shows alternations of coarser and finer clast-rich layers. The finer-grained layers are dominated by volcanic glass and muddy matrix containing volcanic quartz grains, some of which are elongated and display embayed margins, indicative of magmatic resorption. In contrast, the coarser layers are crystal-rich, comprising abundant quartz, feldspar, and lithic fragments, with carbonate cement acting as a binding phase	Tuffite

Sr No.	Sample ID	Latitude	Longitude	Sample (hand specimen) Description	Stratigraphy	Depth (m)	Thin Section Description	Name of the rock according to petrography
26	112214	23.150866	69.578768	Target layer & Transition of target layer	Katrol Formation	19.68 to 19.75	The thin section exhibits well-defined lamination marked by alternating coarse- and fine-grained layers. The finer laminae are composed of a dark, fine-grained matrix, while the coarser laminae contain abundant volcanic quartz grains and mica flakes dispersed within the groundmass	Laminated tuffite
27	112217	23.150866	69.578768	Target layer suspected	Katrol Formation	24.98 to 25.00	The thin section displays a crudely laminated, very fine-grained sandstone interlayered with silt-sized clasts of quartz, mica, and minor feldspar. The detrital grains appear scattered and floating within a carbonate-rich cement, giving the rock a matrix-supported texture with weak lamination	Calcareous fine-grained sandstone
28	112219	23.150866	69.578768	Target layer suspected	Katrol Formation	27.05 to 27.08	The thin section represents a massive siltstone, composed predominantly of silt-sized clasts of quartz, feldspar (including K-feldspar), and mica. These detrital grains are dispersed and appear to be floating within a carbonate mud (micrite) matrix, indicating a matrix-supported texture	Calcareous siltstone
29	112220	23.150866	69.578768	Lapilli patches with shale layer	Katrol Formation	27.39 to 27.43	The rock is a fine-grained volcaniclastic sandstone characterized by scattered rounded to sub-rounded lapilli set within a dark, glass- and matrix-rich groundmass. Framework grains include elongate and embayed quartz, feldspar, and minor mica, while the finer matrix hosts opaque phases and alteration products. Locally, lensoid organic-like structures are present, possibly representing fossil or plant remains.	Lapilli tuffaceous sandstone

Sr No.	Sample ID	Latitude	Longitude	Sample (hand specimen) Description	Stratigraphy	Depth (m)	Thin Section Description	Name of the rock according to petrography
30	112222	23.150866	69.578768	Target layer suspected	Katrol Formation	28.22 to 28.25	a fine-grained volcaniclastic unit, characterized by needle-like and triangular quartz and feldspar grains dispersed within a dense, mud-supported groundmass. The matrix is dominantly composed of apatite and carbonate micrite, imparting a compact, massive texture. The floating nature of the detrital grains within the fine micritic groundmass suggests rapid settling from suspension and early diagenetic cementation.	Tuffaceous mudstone
31	112225	23.150866	69.578768	Target layer & Transition of target layer	Katrol Formation	33.50 to 33.56	a compact volcaniclastic layer, with very fine, needle-like and triangular quartz and feldspar grains dispersed in a dense groundmass. The matrix is rich in apatite and carbonate mud, suggesting a chemically precipitated support. The grains appear floating within the fine-grained cement, indicating rapid deposition followed by early lithification.	Tuffite
32	112226	23.150866	69.578768	suspected pyrite	Katrol Formation	34.93 to 35.00	Fine-grained sandstone with carbonate cement hosting dispersed quartz and feldspar grains; many detrital quartz fragments are broken/angulose. Opaque sulfide specks within the cement suggest pyrite (locally possibly pyrrhotite). Minor secondary phases include zeolite filling micro-pores/veins. Overall texture is matrix- to cement-supported with low primary porosity; sulfide and zeolitic infill indicate diagenetic alteration of a volcaniclastic-influenced sandstone	Tuffaceous calcareous sandstone

Sr No.	Sample ID	Latitude	Longitude	Sample (hand specimen) Description	Stratigraphy	Depth (m)	Thin Section Description	Name of the rock according to petrography
33	112229	23.150866	69.578768	Target layer consisting of a very fine-grained groundmass dominated by apatite/carbonate mud, within which needle-like and triangular quartz and feldspar crystals are dispersed. Occasional fossil fragments are present, along with isolated quartz grains, indicating deposition in a volcaniclastic–carbonate setting with minor bioclastic input	Katrol Formation	36.40 to 36.48	Target layer consisting of a very fine-grained groundmass dominated by apatite/carbonate mud, within which needle-like and triangular quartz and feldspar crystals are dispersed. Occasional fossil fragments are present, along with isolated quartz grains, indicating deposition in a volcaniclastic–carbonate setting with minor bioclastic input	Tuffite
34	112234	23.150866	69.578768	Sandstone	Katrol Formation	45.58 to 45.60	Medium- to coarse-grained sandstone composed of ~80% framework grains dominated by mixed quartz and feldspar, showing relatively good sorting. The matrix is largely replaced by carbonate with subordinate very fine-grained clayey material, while the cement is predominantly carbonate, including peloidal forms. Diagenetic pyrite developed under reducing conditions is present, along with magnetite and additional pyrite phases. Gold mineralization is suspected	Sandstone
35	112235	23.150866	69.578768	Target layer & Transition of target layer	Katrol Formation	45.95 to 50.00	Target layer characterized by alternating laminae of coarse clastic material containing mud clasts and finer muddy layers	Tuffite
36	112243	23.150866	69.578768	Sandstone with target layer	Katrol Formation	51.65 to 51.67	Medium- to fine-grained sandstone from the target layer, composed primarily of quartz and feldspar. The framework grains are supported by a fine matrix/cement. Apetite present	Sandstone

Sr No.	Sample ID	Latitude	Longitude	Sample (hand specimen) Description	Stratigraphy	Depth (m)	Thin Section Description	Name of the rock according to petrography
37	112244	23.150866	69.578768	Target layer suspected	Katrol Formation	53.65 to 53.67	Extremely fine-grained vitric tuff, dominated by volcanic glass with scattered quartz, feldspar, and minor mica. The groundmass is exceedingly fine and indistinct, with goethite alteration products disseminated throughout. Fossil fragments are also present	Tuffite
38	112248	23.150866	69.578768	NA	Katrol Formation	57.34 to 57.38	Medium- to coarse-grained sandstone composed of >80% quartz and feldspar, with subordinate volcanic glass and mica. Accessory opaques include magnetite, pyrite, and goethite. Diagenetic iron oxides and pyrite occur in alternating concentric ring-like layers	Sandstone
39	112249	23.150866	69.578768	Sandstone with mud layer	Katrol Formation	57.57 to 57. 63	Sandstone containing scattered lapilli clasts set within a framework of quartz and albite grains. The target layer shows clear volcanic input, with the lapilli fragments embedded in the sandstone matrix	Sandstone
40	112250	23.150866	69.578768	Sandstone with suspected pyrite	Katrol Formation	58.45 to 58.50	Medium-grained sandstone characterized by framboidal pyrite and patches of felted pyrite masses disseminated within the framework, indicating diagenetic sulfide mineralization under strongly reducing conditions.	Sandstone

Annexure-XXIX: XRF Analysis of BH Samples

Sl No.	Sample ID	Location Number	Latitude	Longitude	Depth (m)	Sample Description	Host Lithology
1	109056	GSPL-Bhuj-BH04	23.20383	69.628518	44.35	Pinkish to yellowish brown coloured, medium to fine grained, ferruginous metasomatized sandstone, composed of quartz (>95%), muscovite(1-2%), black mineral (non magnetic, pyrolusite??), biotite in decreasing order of abundance. Occurence of mica mainly observed at purpulsih to brownish part of the sample. Iron imprgnation occur as thin layers (veinlets??). The layers are red to blackish brown in colour and very fine grained. Suspected clay alteration is also observed.	Mica bearing meta-somatized sandstone
2	109065	GSPL Bhuj BH01	23.15084	69.578518	63.33	Suspected tuffite layer	Shale-Sandstone heterolith
3	109066	GSPL Bhuj BH01	23.15084	69.578518	63.69	Very thick tuffite layers are observed within the shale, specifically, where the grain size of the shale is clay. Yellowish white coloured, medium grained sandstone composed of quartz, mica (1-2%), black colour mineral with dull luster (possibly tourmaline) and infrequently very small iron concretion	Shale-Sandstone heterolith
4	109076	GSPL Bhuj BH01	23.15084	69.578518	70.1	Suspected fine to medium grained, greyish coloured tuffite layer composed predominantly of clay material, with a relatively higher proportion of sandy material (mainly quartz) and minor glass shards.	Shale dominated heterolith
5	109081	GSPL Bhuj BH01	23.15084	69.578518	74.87	Suspected fine to medium grained, greyish coloured tuffite layer composed predominantly of clay material, with a relatively higher proportion of sandy material (mainly quartz) and minor glass shards.	Sandstone
6	109082	GSPL Bhuj BH01	23.15084	69.578518	75.24	the suspected tuffite layers are fine grained clay. However, silty material is also observed in few of them. Near the suspected tuffite layer, the unit become more fine grained and shalley, where the tuffite layers are more clayey.	Sandstone
7	109084	GSPL Bhuj BH01	23.15084	69.578518	76.61	Suspected fine to medium grained, greyish white coloured tuffite layer composed of clay material, with a relatively higher proportion of sandy material (mainly quartz) and minor glass shards.	Sandstone
8	109086	GSPL Bhuj BH01	23.15084	69.578518	77.4	Shale dominating heterolith composed of dark grey to black shale alternating with sand layers (mm scale). The tuffite layer is composed of mostly clay materials.	Shale dominated heterolith
9	109091	GSPL Bhuj BH01	23.15084	69.578518	86.72	Abundance of shale layrer are increasing with depth along with 0.5 to 4 cm thick tuffite layers and lenses coming from 85m. From 80.23m to 81m and between 86.9 m to 87.73 m , 91.40m to 91.50m, 92.60m to 92.75 m , 94.15 m to 94.25 m occurence of pyrite (chalcopyrite?), malachite?, bornite?? specifically within the shale clast mm thin blue lines are also observed within this part of the succesion. Very small circular and elleptical lapilli? are observed at diffferents. The tuffite layers are medium to very fine grain with some black glass shards.	Sandstone dominated heterolith
10	109097	GSPL Bhuj BH01	23.15084	69.578518	100.05	Suspected tuffite layers, fine grained greyish coloured, predominantly composed of clay material with few black elongated minerals, glass shards?	Shale dominated hetrolith
11	109100	GSPL Bhuj BH01	23.15084	69.578518	110.61	Suspected tuffite layer minor mixed with shale unit greyish to relatively light brown in colour, very fine grained predominantly composed of clay material with few black coloured elongated minerals (possible glass shrads??), minor quartz grains and noticeable thin venlets (may be secondary) filled with carbonate are also observed within the layers.	Shale Sandstone hetrolith
12	109101	GSPL Bhuj BH01	23.15084	69.578518	112.58	Suspected tuffite layer greyish to relatively brownish in colour, very fine grained predominantly composed of clay material with few black coloured elongated minerals (possible glass shrads??), minor quartz grains and noticeable thin venlets (may be secondary) filled with carbonate are also observed within the layers.	Sandstone

Table Continued..

Annexure-XXIX

Sl No.	Sample ID	Al_2O_3	BaO	CaO	Cr_2O_3	Fe_2O_3	K_2O	MgO	MnO	Na_2O	P_2O_5	SiO_2	SO_3	TiO_2	LOI
1	109056	19.27	0.05	0.08	0.05	9.23	0.33	0.15	0.05	0.15	0.05	62.09	0.05	1.06	7.05
2	109065	13.14	0.05	1.91	0.05	23.65	1.30	2.79	0.12	0.21	0.36	34.03	1.30	0.68	20.43
3	109066	9.97	0.05	7.64	0.05	24.46	0.89	3.75	0.14	0.26	4.03	25.75	1.08	0.53	21.44
4	109076	19.31	0.05	1.55	0.05	16.29	1.47	2.67	0.11	0.32	0.15	36.82	0.30	0.89	19.83
5	109081	22.80	0.05	0.26	0.05	5.11	1.91	0.77	0.05	0.31	0.11	51.61	2.06	1.20	13.54
6	109082	13.58	0.05	4.90	0.05	22.25	0.97	3.94	0.12	0.27	2.11	27.47	1.13	0.62	22.49
7	109084	20.10	0.05	0.53	0.05	6.37	2.02	1.02	0.05	0.26	0.09	52.78	3.35	0.89	12.36
8	109086	3.34	0.56	44.88	0.05	0.67	0.29	0.90	0.06	0.16	0.17	11.82	0.40	0.06	36.55
9	109091	9.06	0.05	3.69	0.05	33.65	0.72	3.67	0.14	0.23	0.38	19.76	1.65	0.44	26.13
10	109097	15.37	0.05	2.16	0.05	21.89	1.26	2.09	0.12	0.36	0.20	35.14	0.53	0.74	20.08
11	109100	12.13	0.05	2.08	0.05	30.52	1.03	1.75	0.15	0.31	0.18	27.33	0.32	0.63	23.30
12	109101	7.89	0.05	6.91	0.05	32.51	0.71	3.14	0.19	0.31	3.04	19.53	0.10	0.45	25.13

Sl No.	Sample ID	Location Number	Latitude	Longitude	Depth (m)	Sample Description	Host Lithology
13	109102	GSPL Bhuj BH01	23.15084	69.578518	117.1	Sandstone with pyrite patches	Sandstone
14	109104	GSPL Bhuj BH01	23.15084	69.578518	118	Suspected tuffite layer Greyish to light brown in colour, fine to medium grained, predominantly composed of clay material. However, sand sized quartz grains, a few black elongated minerals (possibly glass shards) are also observed.	Sandstone dominated hetrolith
15	109107	GSPL Bhuj BH01	23.15084	69.578518	130.86	Suspected tuffite layer mixed with shale unit relatively dark grey to brownish in colour, fine to medium grained, predominantly composed of clay material. However, sand sized quartz grains, a few black elongated minerals (possibly glass shards) are also observed.	Shale dominated hetrolith
16	109125	GSPL Bhuj BH05	23.19484	69.580492	59.07 to 59.13	Seldom occurrence of pyrite within the clast of breccia. Grey coloured breccia, consist of elliptical to elongated, rectangular shaped clasts of blackish grey and bluish grey coloured shale, embedded in a quartzose and clay matrix/cement. The clasts are angular to sub-angular with low sphericity. The matrix consists of subangular quartz, hematite and clay.	Breccia
17	109128	GSPL Bhuj BH02	23.15629	69.7070139	2.90	Sandstone composed mainly of sand sized mineral grains. Grains are medium to fine, moderately sorted, and consist mostly of quartz with muscovite and biotite. The reddish brown colour indicates iron oxide as the cementing material. Cherry red streak hematite is present in iron concretions.	Ferruginous sandstone
18	109132	GSPL Bhuj BH02	23.15629	69.7070139	11.07	Fine grained Tuffite layer composed predominantly of clay rich material with disseminated? fine grained black minerals possible glass shards. Distinct grey to dark grey lamination is present at bottom. No ferruginisation observed.	Sandstone dominated heterolith
19	109134	GSPL Bhuj BH02	23.15629	69.7070139	7.45	Tuffite layer composed of predominantley clay materials with fine quartz grains, and ocassional very fine grained black minerals, no ferrugination observed	Sandstone dominated heterolith
20	109137	GSPL Bhuj BH02	23.15629	69.7070139	15.25	Suspected Tuffite layer ?, fine grained, gray to light gray argillaceous siltstone, compact and massive in appearance. composed of predominantley clay materials.Minor soft sediment deformation or compaction features are present and composed of medium quartz grains. Sand part is also included within the sandstone.	Sandstone dominated heterolith
21	109140	GSPL Bhuj BH02	23.15629	69.7070139	18.16	Fossiliferous sandstone, fine to medium grained, with a light grey to greyish white coloration, locally displaying brownish or rusty patches due to iron oxide staining composed of mostly quartz, fossils, shale clast, obsidian?, mica , malachite.	Fossiliferous sandstone
22	109141	GSPL Bhuj BH02	23.15629	69.7070139	17.24	Breccia composed of angular to sub angular clasts embedded in a fine grained clayey to silty matrix. Clasts include quartz grains, dark grey shale (tabular and occasionally laminated), fossil fragments and imprints, rock fragments and muscovite. Scattered greenish malachite grains are observed at multiple stratigraphic levels, indicating copper mineralization. clay rich Tuffite layers or lenses were noted, with carbonate filled fractures.	Breccia
23	109142	GSPL Bhuj BH02	23.15629	69.7070139	23.96	Medium to fine grained, light gray sandstone, moderately compacted and fairly well sorted, with slight ferruginous staining in the matrix, composed predominantly of sub angular to sub rounded quartz grains, fossils and its imprints A localized black, angular patch is present, interpreted as a carbonaceous fragment ?	Fossiliferous sandstone
24	109143	GSPL Bhuj BH02	23.15629	69.7070139	26.00	Fine to medium grained Tuffite layer?? with a uniform, light brown to buff coloration and a smooth, compact texture.Composed of clay materal along with quartz, and abundant amount of accicular, irregylar shaped black material (glass shards??). Mineralized burrow fill is also observed within the sample.The burrows are infilled with carbonate.	Fossiliferous sandstone
25	109144	GSPL Bhuj BH02	23.15629	69.7070139	25.85	Fossiliferous sandstone, light gray, medium grained, siliceous matrix with scattered white calcareous patches and visible fossil fragments. Prominent fossil material occurs as dark, elongate stringers and nodules, which are well preserved and distributed subparallel to bedding.The rock exhibits moderate sorting and rounding, with cementing largely of silica and occasional calcareous materials(effervescence obserced).	Fossiliferous sandstone
26	109145	GSPL Bhuj BH02	23.15629	69.7070139	27.04	Breccia composed of angular to sub angular clasts embedded in a fine to medium grained, grey to brownish grey matrix. Clasts include quartz grains, dark grey shale (tabular and occasionally laminated), fossil fragments and imprints, rock fragments and muscovite. Scattered greenish malachite grains are observed at multiple stratigraphic levels, indicating copper mineralization (write if it is within the sample)	Breccia

Table Continued..

Annexure-XXIX

Sl No.	Sample ID	Al_2O_3	BaO	CaO	Cr_2O_3	Fe_2O_3	K_2O	MgO	MnO	Na_2O	P_2O_5	SiO_2	SO_3	TiO_2	LOI
13	109102	19.61	0.05	3.43	0.05	10.77	0.39	3.23	0.32	1.50	0.12	43.79	0.05	0.83	15.61
14	109104	10.99	0.05	4.24	0.05	30.06	0.99	2.42	0.18	0.33	1.28	26.46	0.22	0.63	22.15
15	109107	17.75	0.05	1.62	0.05	18.88	1.42	1.82	0.14	0.45	0.15	37.42	0.52	0.85	18.87
16	109125	11.00	0.05	20.75	0.05	5.71	1.10	1.77	0.08	0.69	0.11	36.83	0.05	0.71	20.96
17	109128	9.94	0.06	3.99	0.05	3.24	2.20	1.93	0.06	0.20	0.05	68.40	0.05	0.77	8.75
18	109132	14.02	0.05	9.29	0.05	19.25	0.86	2.55	0.14	0.28	5.30	27.33	0.27	0.57	19.65
19	109134	9.71	0.05	18.61	0.05	15.94	0.80	1.72	0.11	0.28	11.91	23.20	0.35	0.48	16.43
20	109137	10.60	0.05	2.49	0.05	30.11	0.82	3.58	0.15	0.11	0.20	25.35	0.69	0.57	24.76
21	109140	1.31	0.05	28.66	0.05	5.52	0.20	0.71	0.05	0.05	0.19	37.71	0.05	0.05	25.50
22	109141	14.45	0.05	2.21	0.05	11.27	1.01	0.80	0.05	0.11	0.25	51.10	3.53	1.02	13.79
23	109142	5.49	0.05	17.37	0.05	26.84	0.40	4.23	0.06	0.12	0.45	11.63	0.68	0.20	32.21
24	109143	8.03	0.05	11.44	0.05	24.38	0.74	3.44	0.06	0.14	0.32	24.04	0.86	0.40	25.95
25	109144	6.54	0.05	10.10	0.05	29.39	0.67	3.09	0.09	0.27	0.97	21.27	0.99	0.42	25.90
26	109145	7.24	0.05	8.65	0.06	17.31	0.67	1.73	0.10	0.12	0.64	44.17	0.43	0.45	18.25

Sl No.	Sample ID	Location Number	Latitude	Longitude	Depth (m)	Sample Description	Host Lithology
27	109146	GSPL Bhuj BH02	23.15629	69.7070139	27.28	Tuffite layer, predominantly composed of clay material .However sand sized quartz grains are also observed with few black elongated minerals and thin venlets (may be secondary) filled with carbonate are observed. The Tuffite layers are medium to very fine grained. Slight ferrugination observed.	Sandstone dominated heterolith
28	109148	GSPL Bhuj BH05	23.19484	69.580492	55.58 to 55.63	Sand dominated hetrolith, characterized by dm to cm scale sandstones, separated by mm thin black shale layers. The sandstone is grey in colour, medium to fine grained, moderate to well sorted. Often the grains are angular to sub rounded with moderate sphericity. The shales are dark grey to blackish grey in colour & consist of clay materials with minor muscovite and biotite. Thin hair like jet black materials are also observed within the shale, pyrolusite?? (black streak, feebly magnetic). The jet black part is also observed within the sandstone , and are smelling gum powders.	Sandstone dominated heterolith characterized by thick sanstone layers separated by mm thin shale layers
29	109150	GSPL Bhuj BH02	23.15629	69.7070139	31.21	Fine to medium grained greyish white coloured sandstone composed of quartz (95%), biotite, muscovite, in a decreasing order of abundance. Patchy appearance and soft sediment deformation is common.	Sandstone
30	112151	GSPL Bhuj BH02	23.15629	69.7070139	30.73	Fine to medium grained greyish white coloured sandstone composed of quartz (95%), biotite, muscovite, in a decreasing order of abundance and Within the sandstone, a localized elongated streak of dark, metallic material is observed along the broken surface, a few centimeters in extent. The feature emits a distinct sulfur like odor when exposed, suggesting pyritic concentration with carbonaceous matter.	Sandstone
31	112154	GSPL Bhuj BH02	23.15629	69.7070139	35.46	Tuffite layer, fine grained predominantly composed of clay rich material and within this, a few elongated black streaks are observed, possibly representing glass shards. Minor white veinlets, interpreted as calcium carbonate, are also present. Ferrugination of the Tuffite layer is observed.	Shale dominated heterolith
32	112158	GSPL Bhuj BH02	23.15629	69.7070139	42.05	Tuffite layer, fine grained predominantly composed of clay material , few black elongated minerals, glass shards? Carbonate ?and also few coars quartz grains.	Sandstone
33	112172	GSPL Bhuj BH07	23.19754	69.529703	1.97 to 2.00	Brownish red to black coloured altered ferruginous sandstone, comprising coarse to fine grained quartz, quartz aggregates, hematite, magnetite, euhedral alkali feldspars, muscovite, bluish quartz, seldom occurence of native Cu embedded in a hematite-magnetite ground mass. The grains are predominantly angular to sub angular with low sphericity, sharp crystal phase boundaries are also observed.The quartz aggregates are consist of 3/4 quartz crystals, surrounded by & embedded in dark black (possibly magnetite) groundmass.Alterations are observed in layers & the euhedral feldspars mostly grow along the boundaries. Native Cu, bluish to green (malachite??) staining is also observed within the sample.	Highly ferruginized metasomatized sandstone
34	112194	GSPL Bhuj BH02	23.15629	69.7070139	18	Fossiliferous sandstone, fine to medium grained, with a light grey to greyish white coloration, locally displaying brownish or rusty patches due to iron oxide staining composed of mostly quartz, fossils, shale clast, obsidian?, mica , malachite. The	Fossiliferous sandstone (composite sample)
35	112195	GSPL Bhuj BH02	23.15629	69.7070139	2	This Sandstone rock composed primarily of sand-sized mineral particles. The grains appear to be moderately sorted medium to fine. Mostly quartz and Muscovite-Biotite. In this core, the reddish-brown color suggests the presence of iron oxide as a cementing agent	Ferruginous sandstone (composite sample)
36	112196	GSPL Bhuj BH02	23.15629	69.7070139	26.08	breccia composed of angular to sub-angular clasts embedded in a fine- to medium-grained, grey to brownish-grey matrix. Clasts include quartz grains, dark grey shale (tabular and occasionally laminated), fossil fragments and imprints, rock fragments and muscovite. Scattered greenish malachite grains are observed at multiple stratigraphic levels, indicating copper mineralization.	Breccia (composite sample)

Table Continued..

Annexure-XXIX

Sl No.	Sample ID	Al_2O_3	BaO	CaO	Cr_2O_3	Fe_2O_3	K_2O	MgO	MnO	Na_2O	P_2O_5	SiO_2	SO_3	TiO_2	LOI
27	109146	4.15	0.05	10.31	0.05	37.38	0.38	3.31	0.12	0.19	3.71	12.50	1.04	0.28	26.50
28	109148	17.35	0.22	0.07	0.05	0.67	0.28	0.10	0.05	0.14	0.36	69.07	0.35	0.90	9.90
29	109150	9.72	0.00	24.04	0.05	6.52	0.55	1.22	0.06	0.26	1.00	14.99	1.13	0.25	40.12
30	112151	13.66	0.05	5.17	0.05	4.38	1.84	1.48	0.05	0.17	0.06	59.40	3.11	0.63	9.80
31	112154	6.52	0.05	3.60	0.05	39.05	0.55	3.11	0.13	0.16	0.53	18.67	0.56	0.38	26.58
32	112158	4.61	0.05	5.61	0.05	32.65	0.57	3.31	0.11	0.15	0.36	27.08	0.32	0.39	24.75
33	112172	1.27	0.05	0.05	0.05	30.62	0.50	0.05	0.21	0.05	0.05	64.23	0.11	0.11	2.35
34	112194	2.15	0.05	16.89	0.05	9.01	0.26	1.73	0.05	0.07	0.41	49.51	0.05	0.08	19.43
35	112195	9.38	0.06	4.27	0.05	4.77	2.09	1.33	0.06	0.17	0.06	68.06	0.05	0.93	8.25
36	112196	12.92	0.05	5.25	0.05	12.82	1.10	1.46	0.05	0.14	0.34	47.86	2.61	0.81	14.43

Sl No.	Sample ID	Location Number	Latitude	Longitude	Depth (m)	Sample Description	Host Lithology
37	112208	GSPL-Bhuj-BH01	23.15084	69.578518	11.76	Suspected tuffite layers ,The tuffite layer is composed of silt to clay material (mineral cannot be identified) with amorphous shaped thin, often elongated black coluered glass shards with concoidal fracture. Rarely, these shards give cherry red colour streak	Shale dominated heterolith
38	112216	GSPL-Bhuj-BH01	23.15084	69.578518	21.89	Suspected tuffite layer is brownish in colour,(ferruginous ?) fine to medium grained, mainly composed of silt to clay material (minerals cannot be identified), with few amorphous, thin, and often elongated black coloured glass shards and notably, milky white grains have also been observed, which are likely weathered quartz grains ?	Sandstone dominated heterolith
39	112217	GSPL Bhuj BH01	23.15084	69.578518	24.98	Suspected very fine to fine grained, greyish to light brown coloured tuffite layer composed predominantly of clay material, with a relatively higher proportion of sandy material (mainly quartz) and minor glass shards.	Sandstone dominated heterolith
40	112219	GSPL Bhuj BH01	23.15084	69.578518	27.05	Suspected tuffite layer is brownish in colour,(ferruginous ?) fine to medium grained, mainly composed of silt to clay material (minerals cannot be identified), with amorphous, thin, and often elongated black coloured glass shards and notably, milky white grains have also been observed, which are likely weathered quartz grains ?	Shale dominated heterolith
41	112220	GSPL Bhuj BH01	23.15084	69.578518	27.39	Greyish white colour, medium grained, very well sorted, sandstone unit, composed of quartz, muscovite (1%), approximately 1 to 2% jet black colour mineral. The quartz grains are moderately round with low spheresity.(Sandstone lappilli patches with shale layer)	Sandstone
42	112222	GSPL Bhuj BH01	23.15084	69.578518	28.22	Brownish to reddish ferruginous tuffite lenses within a shale unit. These lenses are mainly composed of silt to clay material (minerals cannot be identified), and may contain minor milky white quartz grains. The ferruginous nature of the lens indicates iron enrichment, which imparts the distinctive reddish coloration. Additionally, the boundary between the lens and the surrounding shale is sharp, and the lens is lenticular	Shale
43	112224	GSPL Bhuj BH01	23.15084	69.578518	31.57	Alternate shale unit and tuffite layer is composed of clay material (mineral cannot be identified) with relatively less amount of amorphous shaped thin, often elongated black coloured glass shards.	Shale
44	112225	GSPL Bhuj BH01	23.15084	69.578518	33.5	Suspected very fine grained tuffite layer is composed of clay material (mineral cannot be identified), amorphous shaped thin, often elongated black coloured glass shards.	Sandstone
45	112235	GSPL Bhuj BH01	23.15084	69.578518	45.95	The tuffite layer is composed of clay material (mineral cannot be identified) with very less amount of amorphous shaped thin, often elongated black coloured glass shards observed	Shale dominated heterolith
46	112242	GSPL Bhuj BH01	23.15084	69.578518	51.38	Transition layer with shale,Grey to greyish white coloured, medium grained quartz arenite.	Sandstone dominated heterolith
47	112245	GSPL Bhuj BH01	23.15084	69.578518	54.64	The tuffite layer is composed of clay material (silty at places) with very less amount of amorphous shaped thin, often elongated black coloured glass shards observed.	Shale dominated heterolith
48	112248	GSPL Bhuj BH01	23.15084	69.578518	56.34	Yellowish white coloured, medium to fine grained sandstone composed of quartz, black colour mineral with dull luster (possibly tourmaline) and small iron concretion. The sandstone is well sorted with well-rounded grain, high sphericity.Small lens filled with pyrite is also observed very near to this hematite occurrence at 56.36m	Sandstone
49	112459	GSPL BHUJ 313/07/2025	23.20322	69.62856	0	Blackish red coloured metasomatized sandstone with strong iron impregnation and comprising very coarse to coarse grained quartz, quartz aggregates, hematite, muscovite, embedded in a hematitic-magnetite rich ground mass. The grains are predominantly angular to sub angular with low sphericity.The quartz aggregates are consist of 3/4 quartz crystals, surrounded by & embedded in dark black (possibly magnetite) groundmass. Almost each grain is surrounded by hematite rim.	Highly ferruginized metasomatized sandstone
50	112462	GSPL BHUJ 321/07/25	23.20306	69.53573	0	Blackish red coloured sandstone, (altered, but did not turn to jhama) separated by yellowish occur coloured shale/clay. Thin veinlets of black materials (very few parts of the powder of the material are attracted by magnet, cherry red streak), are observed to be cross cutting the sandstone. The sandstone is medium to coarse grained and consists of angular to rounded quartz (detritus), muscovite (detritus), biotite (??), weathered sub-rounded feldspar embedded in a mostly hematite and poorly magnetite-rich matrix/cement. Secondary fluid (silvery pinkish blue, golden, varigated colour) along few fractures are also observed.	Ferruginous sandstone

Table Continued..

Annexure-XXIX

Sl No.	Sample ID	Al_2O_3	BaO	CaO	Cr_2O_3	Fe_2O_3	K_2O	MgO	MnO	Na_2O	P_2O_5	SiO_2	SO_3	TiO_2	LOI
37	112208	18.61	0.05	1.77	0.05	11.67	1.62	1.82	0.08	0.29	0.12	46.09	0.55	0.98	16.10
38	112216	15.72	0.05	1.62	0.21	7.53	1.68	1.26	0.05	0.25	0.11	57.05	0.91	1.07	12.16
39	112217	12.02	0.05	3.22	0.05	24.18	1.03	3.72	0.12	0.24	0.18	31.17	0.68	0.68	22.68
40	112219	9.66	0.05	3.21	0.08	33.93	0.68	3.49	0.12	0.20	0.85	21.62	0.14	0.52	25.46
41	112220	4.66	0.05	2.43	0.13	3.02	1.19	0.71	0.05	0.10	0.06	80.80	1.29	1.22	3.94
42	112222	8.89	0.09	3.71	0.05	35.37	0.56	4.44	0.15	0.19	0.88	17.09	0.15	0.43	27.84
43	112224	10.40	0.05	2.31	0.06	28.51	0.97	3.11	0.12	0.20	0.33	29.53	0.34	0.68	23.06
44	112225	10.99	0.05	8.45	0.05	25.49	0.78	2.82	0.10	0.34	4.62	23.31	0.49	0.53	21.97
45	112235	13.35	0.05	4.35	0.05	21.02	1.19	2.82	0.10	0.23	2.02	33.11	0.15	0.77	20.35
46	112242	11.37	0.05	2.26	0.05	21.38	1.13	3.16	0.11	0.19	0.42	37.87	0.81	0.74	20.15
47	112245	8.45	0.05	3.03	0.05	32.87	0.73	4.50	0.17	0.18	0.67	21.43	0.80	0.49	26.34
48	112248	6.14	0.05	0.97	0.08	5.48	1.65	0.72	0.06	0.17	0.13	76.09	1.77	1.56	4.73
49	112459	1.57	0.05	0.06	0.05	34.54	0.05	0.05	0.05	0.05	0.57	58.22	0.05	0.05	4.94
50	112462	6.01	0.05	0.22	0.05	35.59	1.08	0.14	0.20	0.22	0.13	49.40	0.17	0.79	5.98

Sl No.	Sample ID	Location Number	Latitude	Longitude	Depth (m)	Sample Description	Host Lithology
51	112466	GSPL BHUJ 324/07/2025	23.19268	69.51791	0	Violitish white to brownish mauve coloured, very light weight altered ferruginous sandstone. Apart from few quartz pebbles no other grains have been identified (no grain boundary is clear) within the sandstone. Porous spaces (pot hole like feature) within the sandstone are filled with clay (fails acid test) and/or hematite. The matrix/cement of the sandstone comprises hematite. The grain contacts does not seems to be sandstone, they are looking like "Y" junction between the grains. The sample has been collected from the contact zone (2.7m thick) of a fault plane.	Metasomatized shale sandstone hetrolith
52	112488	GSPL BHUJ 348/07/25	23.19432	69.58188	0	Sandstone is composed of both clean and detritus quartz, ranging in size from medium to very coarse, angular to sub-rounded and very few muscovite (1%) embedded in a hematitic to silicic(??) matrix/ cement. Small pods of clay is also observed (clay alteration??). The clean semi transparent quartz grains are more angular and surrounded by hematite rims. The sandstones seems to be brecciated at places, specifically where the iron veins are in cross cutting relationship with the sandstone A thin carbonate vein is also observed at an angle to the bedding of the sandstone .	Mica bearing metasomatized sandstone cross cutting by hematite and carbonate veins (~150m EES of BH 05 location)
53	112494	GSPL BHUJ 353/07/25	23.22200	69.59442	0	Breccia occuring along the fault plane. It consists of angular to well-rounded quartz, clay clasts (rectangular, circular, wedge shaped, irregular), small gashes or lens-like structures filled with silica, few book mica (muscovite), well-rounded iron clasts embedded in a hematitic matrix/cement. No magnetite is observed.	Breccia
54	112496	GSPL BHUJ 353/07/25	23.22200	69.59442	0	Blackish red coloured medium to fine grained sandstone, occuring along the fault plane. This has been observed as dm scale unit, along few of the bedding planes where high amount of ferrugination and alteration making it very hard than the depositional sandstone. It consists of ~30-40% framework of angular to sub angular quartz, muscovite embedded in a hematitic to magnetite (in less amount, part of the rock powder is attracted by magnet) matrix.	Altered highly ferruginous sandstone
55	112498	GSPL BHUJ 358/07/25	23.19465	69.58041	0	The sandstone is composed of both clean and detritus quartz, ranging in size from coarse to very coarse, angular to sub-rounded, both biotite and muscovite, varigated colour minerals (bornite??), few magnetite grains embedded in a hematitic to silicic(??) matrix/ cement. The clean semi transparent quartz grains are more angular and surrounded by hematite rims. The sandstones seems to be brecciated at places, specifically where the iron veins are in cross cutting relationship with the sandstone. The dust of the rock attracted by magnet. Cluster of 2-3 quartz grains, surrounded by magnetite are occuring as the breccia clast. There is a fine grained variety of dark blackish brown colour rock with lots of very small grains of euhedral feldspar.	Highly ferruginized metasomatized sandstone with seldom grain of suspected bornite, Surface sample of BH05
56	113002	GSPL Bhuj BH07	23.19754	69.529703	31.10 to 31.20	Reddish brown to blackish brown coloured, medium to fine grained, moderately sorted ferruginous sandstone. The sandstone is highly ferruginous & consists of angular to sub angular quartz (each grain is stained), very few feldspar, magnetite, seldom occurrence of mica in a decreasing order of abundance. Thin laminae of silicification is observed at places.	Mica bearing ferruginized sandstone
57	113007	GSPL Bhuj BH06	23.22258	69.594128	23.69 to 23.76	Reddish white to reddish-purple coloured, well sorted medium to very fine grained ferruginous sandstone with rounded to sub rounded grains. It consists of quartz and muscovite (~1%). Ferrugination generally occurs in layers within the sample. Grainsize alteration (medium and fine to very fine) is also a characterestic feature of the sample.	Mica bearing ferruginized sandstone
58	113038	GSPL Bhuj BH08	23.19347	69.518388	11.46 to 11.48	Yellowish brown coloured medium to fine grained, moderate to well sorted, metasomatized ferruginous sandstone. The sandstone comprises sub-rounded to rounded grains of quartz with high sphericity (97-98%) & ~ 1% mica (muscovite, and biotite) embedded in a ferruginous to magnetite and/or clay cement/matrix. Silicification is also observed.	Mica bearing metasomatized sandstone

Table Continued..

Annexure-XXIX

Sl No.	Sample ID	Al_2O_3	BaO	CaO	Cr_2O_3	Fe_2O_3	K_2O	MgO	MnO	Na_2O	P_2O_5	SiO_2	SO_3	TiO_2	LOI
51	112466	23.11	0.05	0.14	0.06	34.56	0.01	0.01	0.58	0.06	0.04	28.04	0.04	1.35	11.79
52	112488	2.78	0.06	2.07	0.05	19.44	0.05	0.13	0.09	0.05	0.27	69.79	0.05	0.21	4.79
53	112494	19.47	0.05	0.42	0.05	22.98	0.05	0.14	0.05	0.22	0.13	45.70	0.05	2.21	8.35
54	112496	3.54	0.05	0.19	0.05	34.19	0.05	0.05	0.07	0.18	0.10	56.86	0.05	1.04	3.58
55	112498	1.77	0.05	0.23	0.05	28.68	0.05	0.05	0.05	0.05	0.34	64.14	0.05	0.09	4.58
56	113002	4.46	0.05	0.05	0.05	6.78	0.76	0.05	0.09	0.18	0.05	85.63	0.05	0.34	1.39
57	113007	20.88	0.05	0.07	0.05	1.87	0.88	0.31	0.05	0.18	0.08	67.92	0.05	1.06	6.16
58	113038	10.89	0.05	0.05	0.06	4.63	1.23	0.07	0.05	0.19	0.05	78.98	0.05	0.60	2.92

Sl No.	Sample ID	Location Number	Latitude	Longitude	Depth (m)	Sample Description	Host Lithology
59	113051	GSPL Bhuj BH02	23.15629	69.7070139	46.60	Fine grained, brownish gray suspected Tuffite layer ? with subtle ferruginous staining that imparts a light brown tint. The grains are fine to silt sized, giving the interval a homogeneous and compact appearance.	Shale Sandstone hetrolith
60	113052	GSPL Bhuj BH02	23.15629	69.7070139	49.30	Very fine grained, brownish gray suspected Tuffite layer ? with ferruginous staining that imparts a light brown tint. The grains are very fine to silt sized, giving the interval a homogeneous and compact appearance. Few irregular, jet black mineral (glass shards??) are observed.	Shale Sandstone hetrolith
61	113053	GSPL Bhuj BH02	23.15629	69.7070139	52.12	Brownish gray suspected Tuffite layer ? with subtle ferruginous staining that imparts a light brown tint and are predominantly composed of clay material.	Shale Sandstone hetrolith
62	113054	GSPL Bhuj BH02	23.15629	69.7070139	52.91	Very fine grained, brownish gray suspected Tuffite layer ? with subtle ferruginous staining that imparts a light brown tint and are predominantly composed of clay material with few black coloured elongated minerals (possible glass shrads??).	Shale Sandstone hetrolith
63	113055	GSPL Bhuj BH02	23.15629	69.7070139	55.04	Fine to medium grained brownish gray suspected Tuffite layer with subtle ferruginous staining imparting a light brown tint; predominantly clay rich with medium quartz grains and a few black elongated mineral inclusions (possible glass shards). A localized dark black streak, a few centimeters in extent, occurs along the broken surface, emitting a sulfur like odor on exposure, suggesting pyritic concentration with carbonaceous matter.	Sandstone dominated heterolith
64	113056	GSPL Bhuj BH02	23.15629	69.7070139	53.88	Fine to medium grained brownish gray suspected Tuffite layer with subtle ferruginous staining imparting a light brown tint; predominantly clay rich with medium quartz grains and a few black angular mineral inclusions (possible glass shards).	Sandstone dominated heterolith
65	113057	GSPL Bhuj BH02	23.15629	69.7070139	56.85	Fine to medium grained brownish gray suspected Tuffite layer with subtle ferruginous staining imparting a light brown tint; predominantly clay rich with medium quartz grains and a few black angular mineral inclusions (possible glass shards). Minor white veinlets, interpreted as calcium carbonate, are also present.	Sandstone dominated heterolith
66	113058	GSPL Bhuj BH04	23.20383	69.628518	13.00	Greyish white sandstone layers separated by mm to cm thin dark grey to blackish grey coloured shale. The sandstone is medium to fine grained and dominantly composed of quartz.	Sandstone dominated heterolith
67	113059	GSPL Bhuj BH04	23.20383	69.628518	15.99	Medium to coarse grained yellowish white sandstone, composed predominantly of quartz with muscovite, biotite (more in ferruginous part) set in a clayey to siliceous matrix/cement.Ferruginous staining is observed in layers, forming boudin like structure within the sample. Overall, it represents a quartz-rich, partly ferruginized sandstone with variable grain size and minor accessory minerals.	Sandstone with differential ferruginization
68	113062	GSPL Bhuj BH02	23.15629	69.7070139	56.85	Fine to medium grained brownish suspected Tuffite layer with subtle ferruginous staining imparting a dark brown tint; predominantly clay rich.	Shale Sandstone hetrolith
69	113063	GSPL Bhuj BH02	23.15629	69.7070139	59.44	Fine to medium grained brownish suspected Tuffite layer with subtle ferruginous staining imparting a dark brown tint; surface is moderately gritty with scattered dark mineral specks and few muscovite.	Shale Sandstone hetrolith
70	113064	GSPL Bhuj BH02	23.15629	69.7070139	60.45	Ferruginous Tuffite layer, fine grained predominantly composed of clay rich material and within this, a few elongated black streaks are observed, possibly representing glass shards	Shale Sandstone hetrolith
71	113065	GSPL Bhuj BH02	23.15629	69.7070139	63.48	Greyish sandstone; fine medium grained; quartz dominant with muscovite, shale clasts, fossils; greenish yellow to black elongated lath shaped components, possibly carbonaceous, sulfur odor, smelling gun powder	Fossiliferous sandstone
72	113066	GSPL Bhuj BH02	23.15629	69.7070139	65.25	Dark brownish grey coloured, medium to coarse grained sandstone composed dominantly of coarse quartz grains, with minor dark mineral fragments and patches that impart a slight sulphur (greenish-grey) odour. The sample exhibits a gritty, porous texture, and does not display obvious bedding or veinlets.	Fossiliferous sandstone
73	113067	GSPL Bhuj BH02	23.15629	69.7070139	67.79	Ferruginous Tuffite lens within light brown to grey sandstone. The suspected Tuffite lens is fine to medium grained, with prominent concentric banding, patchy color zonation, and evidence of soft-sediment deformation. White calcite veinlets traverse the matrix, localized darker regions suggest minor ferruginous staining. A few elongated black inclusions, possibly glass shards, are also observed. The texture is smooth and consolidated, with well preserved structure.	Fossiliferous sandstone

Table Continued..

Annexure-XXIX

Sl No.	Sample ID	Al_2O_3	BaO	CaO	Cr_2O_3	Fe_2O_3	K_2O	MgO	MnO	Na_2O	P_2O_5	SiO_2	SO_3	TiO_2	LOI
59	113051	6.60	0.05	3.58	0.05	41.01	0.48	3.46	0.18	0.18	0.56	14.87	0.28	0.35	28.35
60	113052	7.23	0.05	5.60	0.05	37.39	0.53	3.50	0.19	0.19	2.10	15.60	0.44	0.36	26.83
61	113053	9.92	0.05	3.04	0.05	34.34	0.70	3.38	0.15	0.16	0.34	20.51	0.37	0.48	26.48
62	113054	6.19	0.05	8.16	0.05	36.39	0.49	3.20	0.13	0.20	3.54	14.90	0.41	0.31	25.93
63	113055	9.33	0.05	10.87	0.05	19.18	0.89	2.40	0.06	0.16	0.21	32.62	1.00	0.55	22.42
64	113056	6.39	0.05	6.92	0.05	35.51	0.50	3.41	0.11	0.19	0.44	17.89	0.58	0.37	27.53
65	113057	3.54	0.05	11.25	0.05	37.50	0.35	3.07	0.09	0.14	0.81	12.65	0.30	0.20	30.04
66	113058	26.74	0.05	0.08	0.05	1.12	0.53	0.16	0.05	0.08	0.06	59.56	0.05	1.36	9.68
67	113059	15.97	0.05	0.07	0.06	1.25	0.16	0.05	0.05	0.05	0.05	74.87	0.05	1.22	5.59
68	113062	10.86	0.05	3.91	0.05	29.78	0.84	2.92	0.15	0.20	0.45	25.40	1.14	0.58	23.51
69	113063	5.88	0.05	3.63	0.05	43.85	0.46	3.11	0.17	0.15	0.41	12.90	0.11	0.30	28.88
70	113064	9.08	0.05	3.16	0.05	37.89	0.56	3.67	0.18	0.20	0.31	16.16	0.15	0.37	27.91
71	113065	13.58	0.05	2.40	0.05	4.17	1.31	0.78	0.05	0.28	0.06	65.84	3.56	0.87	7.00
72	113066	5.96	0.05	4.58	0.05	2.73	0.73	1.25	0.05	0.08	0.05	75.43	1.35	0.37	7.14
73	113067	5.69	0.05	7.95	0.05	20.90	0.75	2.49	0.09	0.15	1.05	40.75	1.04	0.48	18.26

Sl No.	Sample ID	Location Number	Latitude	Longitude	Depth (m)	Sample Description	Host Lithology
74	113068	GSPL Bhuj BH02	23.15629	69.7070139	69.67	Greyish sandstone; fine medium grained; quartz dominant with muscovite, shale clasts, fossils and black patch components, possibly carbonaceous, sulfur odor.	sandstone
75	113069	GSPL Bhuj BH02	23.15629	69.7070139	70.56	Greyish sandstone; fine medium grained; quartz dominant with muscovite, shale clasts, fossils and black lath shaped components, possibly carbonaceous, sulfur odor.	sandstone
76	113070	GSPL Bhuj BH02	23.15629	69.7070139	71.64	Fine to very fine grained sandstone beds interbedded with thin laminae and lenses of grey shale. The sandstone units are light grey to whitish,fine to medium grained, composed primarily of quartz, muscovite, shale clast and few iron concretions. A noticeable small patch of clay or mud unit is also observed, representing localized alteration or a mineral filled cavity.	Sandstone dominated heterolith
77	113071	GSPL Bhuj BH02	23.15629	69.7070139	71.77	Tuffite layer composed of clay material	Sandstone dominated heterolith
78	113072	GSPL Bhuj BH02	23.15629	69.7070139	74.03	Tuffite layers and or lenses composed primarily of clay material and fractures infilled with black mineral glass shards?? and bottom part few cm is hetrolith part with soft sediment deformation.	Sandstone dominated heterolith
79	113073	GSPL Bhuj BH02	23.15629	69.7070139	75.33	Fine to medium grained brownish suspected tuffite layer with subtle ferruginous staining imparting a dark brown tint.	Sandstone dominated heterolith
80	113140	GSPL Bhuj BH06	23.22258	69.594128	15.50 to 17.50	The unit received as both core and sludge, from 13.46m to 14 m and from 15 to 15.86m and 16.85-17m core has been recieved where as the rest part is recieved as sludge. The core is of ferruginous sandstone, medium to fine grained and comprises both angular to sub-rounded transparent (crystal clear) & detritus quartz, clay, white sandstone clasts (remnanet of the parent rock??), magnetite, very few euhedral feldspar (??), very few mica (mainly at the high ferruginized part) embedded in ferruginous cement/matrix. Voids filled with carbonates (acid test positve) also observed at places. From 15.26 m to 15.86m the amount of ferrugination increases abruptly in such a way that it seems to be a zoned alteration. The grainsize decreases at this depth. At 15.63m secondary verigated colour alteration is observed along thin veinletts and pyrite occurs within the groove area (blue material gives blue streak). The sludge is yellowish white to white in colour, poorly sorted, coarse to fine grained (grain size decreases with depth), and consists predpominantly of angular to sub angular grains with low sphericity. The sludge is mineralogically comprises quartz (>95%), white transparent crystals, hematite, few magnetite (mainly observed within the grooves of quartz grains) & rock fragments in a decreasing order of abundance.	Mica bearing metasomatized sandstone
81	113151	GSPL Bhuj BH05	23.19484	69.580492	51.75m to 52.75m	Sand dominated hetrolith, characterized by dm to cm scale sandstones, separated by mm thin shale layers. Thickness of shale increases to tens of cm at a particular depth. The sandstone is greyish white in colour, medium to fine grained, moderate to well sorted. Often the grains are angular to sub rounded with moderate sphericity. The shales are dark grey to blackish grey in colour & consist of clay materials with minor muscovite and biotite. Milimeter to cm scale thin, jet black materials are also observed within the shale, pyrolusite?? (black streak, feebly magnetic). The jet black part is also observed within the sandstone , and are smelling gun powders. At 52.3m the unit is completely dark grey & more shaly and this darker parts are also smelling gun powder. At places soft sediment deformations is also observed.	Sandstone dominated heterolith
82	113152	GSPL Bhuj BH05	23.19484	69.580492	55m to 56m	Sand dominated hetrolith, characterized by dm to cm scale sandstones, separated by mm thin shale layers. The sandstone is greyish white in colour, medium to fine grained, moderate to well sorted. Often the grains are angular to sub rounded with moderate sphericity. The shales are dark grey to blackish grey in colour & consist of clay materials with minor muscovite and biotite. Milimeter to cm scale thin, jet black materials are also observed within the shale, pyrolusite?? (black streak, feebly magnetic). The jet black part is also observed within the sandstone , and are smelling gun powders. This jet black material occurence intensity is higher in the sample.	Sandstone dominated heterolith

Table Continued..

Annexure-XXIX

Sl No.	Sample ID	Al_2O_3	BaO	CaO	Cr_2O_3	Fe_2O_3	K_2O	MgO	MnO	Na_2O	P_2O_5	SiO_2	SO_3	TiO_2	LOI
74	113068	13.28	0.05	1.48	0.07	3.10	1.48	0.58	0.05	0.17	0.13	69.32	1.75	0.91	7.31
75	113069	11.64	0.05	1.46	0.05	3.75	1.54	0.61	0.05	0.16	0.07	69.34	2.90	0.87	7.18
76	113070	12.34	0.05	1.19	0.05	3.38	1.67	0.46	0.05	0.17	0.05	69.55	2.58	0.86	7.23
77	113071	12.33	0.05	2.09	0.05	15.46	1.55	1.73	0.09	0.17	0.16	48.80	1.30	0.88	15.02
78	113072	11.72	0.05	2.66	0.05	24.78	1.10	3.34	0.14	0.20	0.23	32.22	1.02	0.67	21.64
79	113073	14.84	0.05	2.07	0.05	7.96	1.67	1.13	0.05	0.19	0.11	58.03	1.42	0.97	11.21
80	113140	2.86	0.05	0.39	0.05	1.03	0.05	0.05	0.05	0.05	0.05	93.11	0.05	0.46	1.60
81	113151	20.17	0.05	0.07	0.05	0.60	0.41	0.09	0.05	0.09	0.05	68.54	0.06	1.23	8.16
82	113152	16.36	0.05	0.05	0.05	0.56	0.29	0.06	0.05	0.08	0.07	73.74	0.24	1.12	6.88

Sl No.	Sample ID	Location Number	Latitude	Longitude	Depth (m)	Sample Description	Host Lithology
83	113153	GSPL Bhuj BH05	23.19484	69.580492	59m to 60m	Grey coloured breccia, consist of elliptical to elongated, rectangular shaped clasts of white to bluish grey and blackish grey coloured shale, silicified (??) sandstone, quartzose sandstone (more rounded clasts) embedded in a quartzose and clay matrix/cement. The clasts are angular to sub-angular with low sphericity. The matrix consists of subangular quartz, hematite and clay. Seldom occurrence of pyrite is observed at 59.07 m. The contact between the previous lithology of the breccia is marked by iron impregnation.	Breccia
84	113154	GSPL Bhuj BH04	23.20383	69.628518	35 to 36	The unit occur as alternate appearance of 1-1.5m thick shale and sandstone. The shale is greysish white to buff in colour, very fine grained and ferruginous in nature at different stratigraphic levels. The sandstone is fine to very fine grained, reddish brown to buff in colour and ferruginous in nature. It composed mainly of quartz (with possible minor feldspar?) and subordinate muscovite and biotite. The thickness of the sand unit increases at depth. Sludge of the sandstone is recieved at the last 50cm of the unit. The rock shows pronounced ferruginous staining throughout the unit. Strong colouration in shades of reddish brown, dark brown and goethite colour is also observed to be occured in alternate layers at different part of the unit (are these veinlets of hematite-goethite??)	Shale-sandstone heterolith
85	113155	GSPL Bhuj BH07	23.19754	69.529703	15.50 to 16.30	Brownish red to yellow ochre coloured ferruginous sandstone with grain size varying from v. coarse to fine, poorly sorted, grains are ranging between sub angular to sub rounded to moderate to high sphericity. The degree of ferruginisation varies with grain size, the higher the grain size, the higher the ferruginisation. The sandstone comprises quartz (>95%), hematite, biotite, few platy white transparent crystals, magnetite in a decreasing order of abundance embedded in a ferruginous matrix/cement. Occurence of euhedral feldspars (possibly) with sharp crystal boundaries and areas with green (malachite??) staining is observed at the highest ferruginous zone.	Altered Ferruginous Sandstone
86	113156	GSPL Bhuj BH08	23.19347	69.518388	42.96 m to 43.80m	Alternate occurrence of ferruginous sandstone and shale/siltstone. The sandstone is highly ferruginous and consists of medium to fine grained, moderate to well sorted, sub-angular to sub-rounded grains of quartz (97–98%), very few muscovite, biotite, hematite clasts, magnetite embedded in a ferruginous matrix/cement. The muscovites are abundant at the areas of high ferruginisation/alteration whereas it is scarce and/or unavailable at the non-ferruginous part of the sandstone from 43.5–43.92m. Degree of ferrugination is different at different places. Thin veinlets of hematite is also observed at different parts. Shale clast is also observed within the sandstone. Silicification (??) binding the quartz framework grains is also observed. The shale is grey in colour & observed to be planar parallel to wavy parallel laminated at places, the shale comp., cannot be identified.	Metasomatized shale sandstone hetrolith
87	113351	GSPL Bhuj BH08	23.19347	69.518388	17.77 to 17.83	The shale/siltstone is grey in colour, & very fine grained with no mineral identification.	Metasomatized shale sandstone hetrolith
88	113356	GSPL Bhuj BH08	23.19347	69.518388	48.11 to 48.16	Highly ferruginous, metasomatized medium to coarse grained brownish black coloured sandstone with moderate to poor sorting & consists of sub-rounded to rounded grains of quartz, embedded in a clay (??) matrix/cement. Occurrence of ~2% muscovite & biotite is observed at these ferruginous parts.	Mica bearing metasomatized sandstone
89	113359	GSPL Bhuj BH01	23.15084	69.578518	100.55	Suspected very fine grained greyish coloured tuffite layer within the shale unit,composed of clay	Shale dominated hetrolith
90	113360	GSPL Bhuj BH01	23.15084	69.578518	59.81	Dark grey to black, fine grained, compact shale, exhibiting subconchoidal fracture and earthy luster, and no clear bedding or lamination.	Black Shale
91	113364	GSPL Bhuj BH01	23.15084	69.578518	59	Composite sample of 1m , Greyish to dark grey coloured, very fine grained shale with suspected tuffite layers.	Shale (composite sample)

Table Continued..

Annexure-XXIX

Sl No.	Sample ID	Al_2O_3	BaO	CaO	Cr_2O_3	Fe_2O_3	K_2O	MgO	MnO	Na_2O	P_2O_5	SiO_2	SO_3	TiO_2	LOI
83	113153	17.57	0.35	0.07	0.05	0.94	0.23	0.06	0.05	0.08	0.63	70.09	1.06	1.64	6.72
84	113154	22.62	0.07	0.07	0.05	1.68	0.41	0.12	0.05	0.09	0.05	64.67	0.05	1.33	8.34
85	113155	10.30	0.05	0.05	0.05	5.48	1.49	0.05	0.05	0.14	0.05	77.18	0.05	0.95	3.85
86	113156	11.37	0.56	0.05	0.05	15.73	0.49	0.05	0.05	0.06	0.11	62.44	0.41	2.35	5.75
87	113351	23.87	0.05	0.07	0.05	1.67	1.13	0.26	0.05	0.09	0.05	62.67	0.05	1.27	8.42
88	113356	2.27	0.05	0.05	0.06	11.74	0.17	0.05	0.05	0.05	0.05	83.81	0.05	0.12	1.43
89	113359	27.02	0.05	0.34	0.05	2.98	1.96	0.86	0.05	0.46	0.11	51.44	0.30	1.28	12.80
90	113360	24.52	0.05	0.27	0.05	2.68	2.02	0.73	0.05	0.27	0.08	56.74	0.28	1.26	10.67
91	113364	21.31	0.05	0.73	0.05	5.52	1.70	1.20	0.05	0.29	0.10	49.06	0.41	1.09	18.29

Sl No.	Sample ID	Location Number	Latitude	Longitude	Depth (m)	Sample Description	Host Lithology
92	113365	GSPL Bhuj BH07	23.19754	69.529703	26.01 to 26.07	Reddish brown to dark brown coloured, medium to fine grained metasomatised ferruginous sandstone. The fine grained sandstone is metasomatised with iron impregnation and consists angular to sub angular grains of quartz, lots of muscovite, hematite, magnetite (in the darker area) in a decreasing order of abundance. The more the metasomatism the amount of muscovite increases. Silicification of the metasomatised part also observed. This part is more metasomatised than the previous sample (112173).	Alternating ferruginous sandstone and mica bearing metasomatized sandstone
93	113374	GSPL Bhuj BH06	23.22258	69.594128	15.63 to 15.71	Medium to fine grained ferruginized sandstone, comprises both angular to sub-rounded transparent (crystal clear) & detritus quartz, clay, white sandstone clasts (remnanet of the parent rock??), magnetite, very few euhedral feldspar (??), very few mica (mainly at the high ferruginized part) embedded in ferruginous cement/matrix. Voids filled with carbonates (acid test positve) also observed at places. From 15.26 m to 15.86m the amount of ferrugination increases abruptly in such a way that it seems to be a zoned alteration. Secondary verigated colour alteration is observed along thin veinletts and pyrite occurs within the groove area (blue material gives blue streak).	Mica bearing metasomatized sandstone
94	113382	GSPL Bhuj BH01	23.15084	69.578518	133.92	The shale-dominated heterolith comprises dark grey to black shale with millimetre to 2.5 centimetre-scale sand layers.Sandstone layers are fine to medium grained and greyish white in colour composed of quartz (95%), muscovite, biotite, magnetite in decreasimg order of abundance.	Shale dominated hetrolith
95	113394	GSPL Bhuj BH08	23.19347	69.518388	10m to 11m	Yellowish brown coloured medium to fine grained moderate to well sorted altered ferruginous sandstone. The sandstone comprises sub-rounded to rounded grains of quartz with high sphericity (97-98%) & ≈ 2% mica (muscovite, and biotite) embedded in a ferruginous to magnetite & clay (??) cement/matrix.The degree of ferrugination is different at different stratigraphic levels, varying in colour from yellow ochre to yellowish brown to brown to reddish brown to dark brown. The higher the ferrugination the higher the amount of mica (lots of figure taken). Ripple cross lamination & planar parallel lamination is observed. Silicification is also observed at dif stratigraphic levels.[This is probably the fault zone/very near to the fault zone, as from ~15m water loss started]	Mica bearing metasomatized sandstone
96	113395	GSPL Bhuj BH08	23.19347	69.518388	11.50 to 12.39	Brownish red to mauve coloured altered shale - sandstone heterolith. The unit comprises thick ferruginous sandstone interspersed by clay. Apart from few quartz pebbles no other grains have been identified (no grain boundary is clear) within the sandstone. Porous spaces (pot hole like feature, pit surface) within the sandstone are filled with clay (fails acid test) and/or hematite. The matrix/cement of the sandstone comprises hematite, & magnetite (less in amount, magnetic mineral with black streak). Silicification is also observed at different stratigraphic level. The clay part is mainly showing the mauve colour.	Metasomatized shale sandstone hetrolith
97	113396	GSPL Bhuj BH08	23.19347	69.518388	15.40 to 16.50	Reddish Yellow to reddish brown coloured, altered ferruginous sandstone unit. The sandstone is medium to fine grained, moderate to well sorted with sub-rounded to rounded grains of high sphericity. The sandstone comprises quartz (>95%), muscovite and biotite (mica 1–2%), very minor amount of magnetite in a decreasing order of abundance. A greyish black steel shiny mineral (steel grey texture, prismatic elongated) is also observed at places. Degree of ferrugination is different at different parts. The higher the ferruginisation the higher the amount of biotite.	Mica bearing metasomatized sandstone
98	113397	GSPL Bhuj BH08	23.19347	69.518388	18.50 to 19.50	Shale/siltstone-sst heterolith, occuring as alternate layers of shale/siltstone and ferruginous sandstone. However, shale as irregular layers, intercalating within the sandstone is also observed at places. The sandstone is highly ferruginous medium to fine grained and comprises quartz (>95%), muscovite and biotite (mica 1–2%), very minor amount of magnetite in a decreasing order of abundance. The matrix is hematitic and iron impregnation follows the internal structure of the sandstone. Degree of ferrugination is different at different parts. The higher the ferruginisation the higher the amount of mica. Both silicification and clay concentration is also observed. The shale/siltstone is grey in colour, & consists of quartz, muscovite & biotite. The shale is generally unaltered. From 18m onwards, the amount/thickness of shale/siltstone increases, upto 20.5m. The shale is planar parallel to wavy parallel laminated.	Metasomatized shale sandstone hetrolith
99	113398	GSPL Bhuj BH07	23.19754	69.529703	24.50 to 25.50	White to reddish brown coloured, medium to fine grained altered sandstone. The fine grained sandstone is altered with iron impregnation at different stratigraphic levels with different order of alteration. The unaltered part of the sandstone is medium to fine grained, white in colour and consist of quartz, very very few muscovite embedded in a clay matrix cement. Whereas the altered part consists angular to sub angular grains of quartz,	Altered Sandstone

Sl No.	Sample ID	Location Number	Latitude	Longitude	Depth (m)	Sample Description	Host Lithology
						lots of muscovite, hematite, magnetite & altered feldspar, in a decreasing order of abundance. The more the alteration the amount of muscovite increases. Silicification of the altered part also observed. The colour of alteration varies from yellow, ochres to reddish brown to purple to blackish red.	
100	113399	GSPL Bhuj BH06	23.22258	69.594128	17.50 to 18.46	Reddish white to greyish white shale. Very fine grained, no minerals can be identified. Ferrugination of different order is observed at different stratigraphic levels. The ferrugination decreases with depth.	Shale

Table Continued..

Annexure-XXIX

Sl No.	Sample ID	Al_2O_3	BaO	CaO	Cr_2O_3	Fe_2O_3	K_2O	MgO	MnO	Na_2O	P_2O_5	SiO_2	SO_3	TiO_2	LOI
92	113365	8.23	0.05	0.06	0.05	29.25	1.27	0.12	0.33	0.08	0.11	53.28	0.05	0.68	6.47
93	113374	2.99	0.05	0.05	0.05	7.97	0.05	0.05	0.05	0.05	0.06	86.09	0.05	0.23	2.13
94	113382	23.08	0.05	0.71	0.05	5.61	2.18	1.26	0.05	0.56	0.11	52.23	0.15	1.19	12.38
95	113394	17.01	0.08	0.06	0.05	8.52	2.82	0.05	0.10	0.16	0.05	63.68	0.05	1.34	5.64
96	113395	29.78	0.05	0.15	0.07	19.53	0.05	0.16	0.31	0.05	0.08	34.81	0.05	1.79	12.78
97	113396	16.71	0.05	0.06	0.05	4.49	1.72	0.11	0.05	0.10	0.06	69.24	0.05	1.13	5.83
98	113397	21.46	0.05	0.06	0.05	6.48	1.24	0.13	0.05	0.12	0.06	61.07	0.05	1.17	7.72
99	113398	14.79	0.05	0.05	0.05	3.85	2.01	0.06	0.08	0.11	0.05	72.29	0.05	1.33	4.74
100	113399	24.63	0.05	0.18	0.05	1.42	0.78	0.22	0.05	0.07	0.17	61.84	0.05	1.33	8.88

Annexure-XXX a: ICPMS Analysis of BH01

Sl No.	Sample Number	Depth	Sample Description	Host Lithology	Li	Be	Sc	V
1	112203	6.71	Suspected tuffite layers (Gypsum there),	Shale dominated heterolith	50.93	2.30	32.28	236.51
2	112208	11.76	Suspected tuffite layers ,The tuffite layer is composed of silt to clay material (mineral cannot be identified) with amorphous shaped thin, often elongated black coluered glass shards with concoidal fracture. Rarely, these shards give cherry red colour streak	Shale dominated heterolith	76.22	1.97	23.02	151.01
3	112207	12.07	Suspected tuffite layers , The tuffite layer is composed of silt to clay material (mineral cannot be identified) with amorphous shaped thin, often elongated black coluered glass shards with concoidal fracture. Rarely, these shards give cherry red colour streak	Shale dominated heterolith	65.53	2.04	27.52	197.11
4	112205	12.63	Ferruginous brownish to grayish zones with faint lamination are observed, where the tuffite layers are relatively more sandy, composed of medium to fine grained quartz within a silt to clay matrix, and the overall texture appears compact with slight colour variations	Shale dominated heterolith	51.29	2.00	25.32	160.72
5	112206	12.88	Suspected tuffite layer mixed with shale units and appears ferruginous brownish in colour. It is fine to medium grained, mainly composed of silt to clay material (minerals cannot be identified), containing amorphous, thin, and often elongated black coloured glass shards, with minor quartz grains also present.	Shale dominated heterolith	52.97	2.03	23.75	170.58
6	112204	14.41	Suspected tuffite layer is brownish in colour,(ferruginous ?) fine to medium grained, mainly composed of silt to clay material (minerals cannot be identified), with amorphous, thin, and often elongated black coloured glass shards, and shale units are also present in between.	Shale dominated heterolith	51.25	2.25	35.63	276.65

Sl No.	Sample Number	Depth	Sample Description	Host Lithology	Li	Be	Sc	V
7	112209	16.87	Suspected tuffite layer is brownish in colour,(ferruginous ?) fine to medium grained, mainly composed of silt to clay material (minerals cannot be identified), with amorphous, thin, and often elongated black coloured glass shards, and shale units are also present in between.	Shale dominated heterolith	34.95	1.91	24.16	202.84
8	112210	18.23	Suspected tuffite layer mixed with sand units and appears brownish in colour. It is fine to medium grained, mainly composed of silt to clay material (minerals cannot be identified), containing amorphous, thin, and often elongated black coloured glass shards, with minor quartz grains also present. Notably, milky white grains have also been observed, which are likely weathered quartz grains ?	Shale dominated heterolith	60.66	2.03	22.45	170.24
9	112212	18.51	Suspected tuffite layer is brownish in colour,(ferruginous ?) fine to medium grained, mainly composed of silt to clay material (minerals cannot be identified), with amorphous, thin, and often elongated black coloured glass shards.	Shale dominated heterolith	31.36	1.54	24.45	207.67
10	112213	18.83	Suspected tuffite layer mixed with sand units and appears brownish in colour. It is fine to medium grained, mainly composed of silt to clay material (minerals cannot be identified). Milky white grains, probably feldspar or weathered quartz, can be observed. Notably, within the tuffite layer, load cast structures are seen, indicating soft sediment deformation.	Shale dominated heterolith	55.32	1.95	18.45	173.11
11	112216	21.89	Suspected tuffite layer is brownish in colour,(ferruginous ?) fine to medium grained, mainly composed of silt to clay material (minerals cannot be identified), with few amorphous, thin, and often elongated black coloured glass shards and notably, milky white grains have also been observed, which are likely weathered quartz grains ?	Sandstone dominated heterolith	73.77	1.80	15.25	121.76
12	112217	24.98	Suspected very fine to fine grained, greyish to light brown coloured tuffite layer composed predominantly of clay material, with a relatively higher proportion of sandy material (mainly quartz) and minor glass shards.	Sandstone dominated heterolith	49.84	1.99	21.37	218.40

Sl No.	Sample Number	Depth	Sample Description	Host Lithology	Li	Be	Sc	V
13	112219	27.05	Suspected tuffite layer is brownish in colour,(ferruginous ?) fine to medium grained, mainly composed of silt to clay material (minerals cannot be identified), with amorphous, thin, and often elongated black coloured glass shards and notably, milky white grains have also been observed, which are likely weathered quartz grains ?	Shale dominated heterolith	46.46	1.76	19.91	167.17
14	112220	27.39	Greyish white colour, medium grained, very well sorted, sandstone unit, composed of quartz, muscovite (<1%), approximately 1 to 2% jet black colour mineral. The quartz grains are moderately round with low spheresity.(Sandstone lappilli patches with shale layer)	Sandstone	10.25	0.31	7.56	53.01
15	112222	28.22	Brownish to reddish ferruginous tuffite lenses within a shale unit. These lenses are mainly composed of silt to clay material (minerals cannot be identified), and may contain minor milky white quartz grains. The ferruginous nature of the lens indicates iron enrichment, which imparts the distinctive reddish coloration. Additionally, the boundary between the lens and the surrounding shale is sharp, and the lens is lenticular	Shale	44.39	1.76	27.90	211.83
16	112224	31.57	Alternate shale unit and tuffite layer is composed of clay material (mineral cannot be identified) with relatively less amount of amorphous shaped thin, often elongated black coloured glass shards.	Shale	54.35	1.91	19.95	173.33
17	112225	33.5	Suspected very fine grained tuffite layer is composed of clay material (mineral cannot be identified), amorphous shaped thin, often elongated black coloured glass shards.	Sandstone	45.13	2.21	26.87	137.09
18	112226	34.94	Suspected tuffite layer is composed of clay to silt material (mineral cannot be identified), with relatively less amount of amorphous shaped thin, often elongated black coloured glass shards and small iron concretions. This layer is interbedded with sandstone units.	Shale dominated heterolith	36.76	0.99	11.38	76.61

Sl No.	Sample Number	Depth	Sample Description	Host Lithology	Li	Be	Sc	V
19	112230	37.64	The tuffite layer is composed of clay material (mineral cannot be identified)	Shale	86.55	2.37	23.49	179.43
20	112232	39.75	The tuffite layer is composed of clay material (mineral cannot be identified) with relatively very less amount of amorphous shaped thin, often elongated black coloured glass shards.	Shale dominated heterolith	74.86	2.23	20.41	162.62
21	112233	43.5	Suspected tuffite layer is composed of clay to silt material (mineral cannot be identified), with relatively less amount of amorphous shaped thin, often elongated black coloured glass shards and small iron concretions.	Shale	69.49	2.30	20.28	156.99
22	112234	45.58	Yellowish white coloured, medium to fine grained sandstone composed of quartz, biotite, muscovite, black colour mineral with dull luster (possibly tourmaline) and small iron concretion. The sandstone is well sorted with well-rounded to very well rounded grain, moderate to high sphericity	Sandstone	15.53	0.39	6.41	41.58
23	112235	45.95	The tuffite layer is composed of clay material (mineral cannot be identified) with very less amount of amorphous shaped thin, often elongated black coloured glass shards observed	Shale dominated heterolith	73.80	2.29	24.71	127.45
24	112236	47.01	The sample is a fine grained sedimentary rock, primarily composed of quartz grains. Its colour is light grey with prominent, irregular black units interbedded throughout, which resemble mud or shale laminae. Within these black streaks, a few elongated shiny surfaces appear, likely representing glass shards, The structure is characterized by well-developed horizontal lamination and wavy layering;	Sandstone	34.72	0.92	7.82	66.07

Sl No.	Sample Number	Depth	Sample Description	Host Lithology	Li	Be	Sc	V
25	112239	48.8	present Black colour Mineral	Sandstone	17.95	0.47	5.04	41.06
26	112240	49.84	The tuffite layer is composed of silt and clay material (mineral cannot be identified). the tuffite layers are more sandy.	Shale	108.16	2.38	14.69	126.77
27	112241	50.18	Transition Layer with Suspected Traget layer, Grey to greyish white coloured, medium grained quartz arenite.	Shale	71.30	2.30	18.20	171.08
28	112242	51.38	Transition layer with shale,Grey to greyish white coloured, medium grained quartz arenite.	Sandstone dominated heterolith	43.19	1.93	17.23	150.74
29	112244	53.65	The tuffite layer is composed of clay material (silty at places) with very less amount of amorphous shaped thin, often elongated black coloured glass shards observed.	Shale dominated heterolith	48.34	2.37	27.79	211.41
30	112245	54.64	The tuffite layer is composed of clay material (silty at places) with very less amount of amorphous shaped thin, often elongated black coloured glass shards observed.	Shale dominated heterolith	45.73	1.92	20.08	159.12

Sl No.	Sample Number	Depth	Sample Description	Host Lithology	Li	Be	Sc	V
31	112247	56.18	Yellowish white coloured, medium to fine grained sandstone composed of quartz, black colour mineral with dull luster (possibly tourmaline) and small iron concretion. The sandstone is well sorted with well-rounded grain, high sphericity	Sandstone	0.59	<0.1	0.16	1.61
32	112248	56.34	Yellowish white coloured, medium to fine grained sandstone composed of quartz, black colour mineral with dull luster (possibly tourmaline) and small iron concretion. The sandstone is well sorted with well-rounded grain, high sphericity.Small lens filled with pyrite is also observed very near to this hematite occurrence at 56.36m	Sandstone	16.59	0.58	8.65	81.90
33	112250	58.45	Shale dominated heterolith composed of black shale interrupted by 3 to 6 cm thick sandstone units. The shale is black, very fine grained with small lenticular elongated amorphous shaped sand layers mainly filled with clean quartz.Some amorphous lenses of sulfide (pyrite/chalcopyrite?), sometimes within small rounded iron concretion.	Shale dominated heterolith	28.34	0.89	25.98	99.16
34	113364	59	Composite sample of 1m , Greyish to dark grey coloured, very fine grained shale with suspected tuffite layers.	Shale (composite sample)	95.38	2.41	16.03	141.08
35	113360	59.81	Dark grey to black, fine grained, compact shale, exhibiting subconchoidal fracture and earthy luster, and no clear bedding or lamination.	Black Shale	107.94	2.35	13.72	127.80
36	109065	63.33	Suspected tuffite layer	Shale- Sandstone heterolith	69.90	2.17	20.72	151.35

Sl No.	Sample Number	Depth	Sample Description	Host Lithology	Li	Be	Sc	V
37	109066	63.69	Very thick tuffite layers are observed within the shale, specifically, where the grain size of the shale is clay. Yellowish white coloured, medium grained sandstone composed of quartz, mica (1-2%), black colour mineral with dull luster (possibly tourmaline) and infrequently very small iron concretion	Shale- Sandstone heterolith	49.19	2.44	28.11	113.80
38	109067	65.04	Suspected tuffite layers are observed within the shale	Shale Sandstone heterolith	36.14	2.60	23.97	171.19
39	109069	66.09	Suspected fine to medium grained, greyish coloured tuffite layer composed predominantly of clay material, with a relatively higher proportion of sandy material (mainly quartz) and minor glass shards.	Sandstone	80.73	2.30	12.43	121.98
40	112211	67.88	lapilli tuff,Lapilli (long axis ranging between 0.3 to 3.5 cm) of different sizes are observed mainly within the dark grey coloured sandstone. The lamination is generally observed to be laping these lapilli. 66.5-68m, patches and/or elongated continuous layers of yellowish green material (smelling gun powder) is observed, almost always associated with glass (??), either occuring as scattered grains or within the sulphide(??) layers	Sandstone	114.73	2.81	13.62	138.44
41	109072	67.88	The sandstone is medium to fine grained with colour variation from yellowish white to dark grey. The rock is composed of quartz, muscovite, biotite, black colour mineral with dull luster (possibly tourmaline), possibly tourmaline and small iron concretions are observed at few places. Lapilli (long axis ranging between 0.3 to 3.5 cm) of different sizes are observed mainly within the dark grey coloured sandstone. The lamination is generally observed to be laping these lapilli. 66.5-68m, patches and/or elongated continuous layers of yellowish green material (smelling gun powder) is observed, almost always associated with glass (??), either occuring as scattered grains or within the sulphide(??) layers.	Sandstone	89.41	2.16	12.31	104.90
42	109074	68.46	the suspected tuffite layers are fine grain with relatively sandier material, mainly quartz and very less amount of glass shards. Petrographic samples are sent to confirm the suspected tuffite layer (?) .	Sandstone	80.65	2.72	21.52	152.17

Sl No.	Sample Number	Depth	Sample Description	Host Lithology	Li	Be	Sc	V
43	109075	69.65	Suspected fine to medium grained, greyish coloured tuffite layer composed predominantly of clay material, with a relatively higher proportion of sandy material (mainly quartz) and glass shards.	Sandstone	80.23	2.52	15.52	128.77
44	109076	70.1	Suspected fine to medium grained, greyish coloured tuffite layer composed predominantly of clay material, with a relatively higher proportion of sandy material (mainly quartz) and minor glass shards.	Shale dominated heterolith	82.70	3.43	30.29	189.22
45	109079	71.73	Suspected fine to medium grained, greyish coloured tuffite layer composed predominantly of clay material, with a relatively higher proportion of sandy material (mainly quartz) and glass shards.	Sandstone	78.65	2.47	17.94	138.44
46	109080	72.88	Suspected fine to medium grained, greyish coloured tuffite layer composed predominantly of clay material, with a relatively higher proportion of sandy material (mainly quartz) and minor glass shards. Noticeable iron stains? appear locally as isolated brownish spots within the layer.	Sandstone	33.74	2.09	20.89	134.63
47	109081	74.87	Suspected fine to medium grained, greyish coloured tuffite layer composed predominantly of clay material, with a relatively higher proportion of sandy material (mainly quartz) and minor glass shards.	Sandstone	110.75	3.13	13.28	140.56
48	109082	75.24	the suspected tuffite layers are fine grained clay. However, silty material is also observed in few of them. Near the suspected tuffite layer, the unit become more fine grained and shalley, where the tuffite layers are more clayey.	Sandstone	74.27	2.78	22.26	142.52

Sl No.	Sample Number	Depth	Sample Description	Host Lithology	Li	Be	Sc	V
49	109084	76.61	Suspected fine to medium grained, greyish white coloured tuffite layer composed of clay material, with a relatively higher proportion of sandy material (mainly quartz) and minor glass shards.	Sandstone	64.22	2.11	15.66	119.07
50	109086	77.4	Shale dominating heterolith composed of dark grey to black shale alternating with sand layers (mm scale). The tuffite layer is composed of mostly clay materials.	Shale dominated heterolith	13.20	0.67	9.17	178.46
51	109087	79.76	Suspected fine to medium grained, greyish white coloured tuffite layer composed predominantly of clay material, with a relatively higher proportion of sandy material (mainly quartz) and minor glass shards.	Sandstone	57.91	1.77	14.21	125.36
52	109088	80.24	Greyish white coloured medium to fine grained sandstone composed of quartz, muscovite,elongated shale clast with size varying from 0.3 to 1.5 cm embedded in clayey matrix and mostly composed of white coloured clean quartz and muscovite , small iron concretions at different stratigraphic levels .	Sandstone dominated hetrolith	43.82	1.34	11.85	102.52
53	109090	85.75	Suspected tuffite layer relatively brownish in colour, fine to medium grained, predominantly composed of clay material. However, sand sized quartz grains, a few black elongated minerals (possibly glass shards) are also observed.	Sandstone dominated hetrolith	31.74	2.19	15.32	132.58
54	109091	86.72	Abundance of shale layrer are increasing with depth along with 0.5 to 4 cm thick tuffite layers and lenses coming from 85m. From 80.23m to 81m and between 86.9 m to 87.73 m , 91.40m to 91.50m, 92.60m to 92.75 m , 94.15 m to 94.25 m occurence of pyrite (chalcopyrite?), malachite?, bornite?? specifically within the shale clast mm thin blue lines are also observed within this part of the succesion. Very small circular and elleptical lapilli? are observed at diffferents. The tuffite layers are medium to very fine grain with some black glass shards.	Sandstone dominated heterolith	46.63	2.16	19.22	164.28

Sl No.	Sample Number	Depth	Sample Description	Host Lithology	Li	Be	Sc	V
55	109094	92.04	The tuffite layers are medium to very fine grain with some black glass shards	Sandstone dominated heterolith	81.19	2.17	17.82	135.32
56	109096	96.95	The tuffite layers are medium to very fine grain with some black glass shards	Sandstone dominated heterolith	69.59	2.39	27.88	181.58
57	109097	100.05	Suspected tuffite layers, fine grained greyish coloured, predominantly composed of clay material with few black elongated minerals, glass shards?	Shale dominated hetrolith	57.80	2.46	26.20	178.74
58	113359	100.55	Suspected very fine grained greyish coloured tuffite layer within the shale unit,composed of clay	Shale dominated hetrolith	106.64	2.63	13.92	135.38
59	109098	105.96	Suspected tuffite layers, fine grained greyish coloured, predominantly composed of clay material with few black elongated minerals, glass shards?	Sandstone dominated hetrolith	23.46	1.62	22.25	159.42
60	109099	106.76	Suspected tuffite layers, fine grained greyish coloured, predominantly composed of clay material with few black elongated minerals, glass shards? and noticeable thin venlets (may be secondary) filled with carbonate are also observed within the layers.	Sandstone dominated hetrolith	57.82	2.02	17.76	135.01

Sl No.	Sample Number	Depth	Sample Description	Host Lithology	Li	Be	Sc	V
61	109100	110.61	Suspected tuffite layer minor mixed with shale unit greyish to relatively light brown in colour, very fine grained predominantly composed of clay material with few black coloured elongated minerals (possible glass shrads??), minor quartz grains and noticeable thin venlets (may be secondary) filled with carbonate are also observed within the layers.	Shale Sandstone hetrolith	50.60	2.08	20.41	143.36
62	109101	112.58	Suspected tuffite layer greyish to relatively brownish in colour, very fine grained predominantly composed of clay material with few black coloured elongated minerals (possible glass shrads??), minor quartz grains and noticeable thin venlets (may be secondary) filled with carbonate are also observed within the layers.	Sandstone	36.72	2.51	30.95	203.48
63	109102	117.1	Sandstone with pyrite patches	Sandstone	8.69	0.34	7.11	36.96
64	109104	118	Suspected tuffite layer Greyish to light brown in colour, fine to medium grained, predominantly composed of clay material. However, sand sized quartz grains, a few black elongated minerals (possibly glass shards) are also observed.	Sandstone dominated hetrolith	50.93	2.63	35.02	218.46
65	109105	126.6	Suspected tuffite layer relatively brownish in colour, fine to medium grained, predominantly composed of clay material. However, sand sized quartz grains, a few black elongated minerals (possibly glass shards) are also observed.	Sandstone	56.94	2.40	21.83	159.69
66	109106	127.36	Dark grey to yellowish white, medium to coarse grained sandstone composed of quartz, muscovite, biotite, and black coloured minerals with dull lustre, possibly pyroxene, showing dark grey streak and near 90° cleavage.	Sandstone	45.50	1.44	7.87	70.94

Sl No.	Sample Number	Depth	Sample Description	Host Lithology	Li	Be	Sc	V
67	109107	130.86	Suspected tuffite layer mixed with shale unit relatively dark grey to brownish in colour, fine to medium grained, predominantly composed of clay material. However, sand sized quartz grains, a few black elongated minerals (possibly glass shards) are also observed.	Shale dominated hetrolith	75.65	2.40	27.52	178.34
68	113382	133.92	The shale-dominated heterolith comprises dark grey to black shale with millimetre to 2.5 centimetre-scale sand layers.Sandstone layers are fine to medium grained and greyish white in colour composed of quartz (95%), muscovite, biotite, magnetite in decreasimg order of abundance.	Shale dominated hetrolith	107.64	2.25	17.32	131.24
69	109108	137.28	suspected tuffite layers and or lenses composed predominantly of clay material observed.	Shale- Sandstone heterolith	67.27	2.25	25.87	181.59
70	109110	138.14	Suspected tuffite layer greyish in colour, fine to medium grained, predominantly composed of clay material. However, sand sized quartz grains, a few black elongated minerals (possibly glass shards) are also observed.	Shale- Sandstone heterolith	89.29	2.40	18.54	142.01
71	109114	139.07	Suspected tuffite layer, very fine grained greyish white predominantly composed of clay material	Shale- Sandstone heterolith	64.55	2.51	25.76	194.78
72	109116	141.88	Suspected tuffite layer, fine to medium grained greyish coloured predominantly composed of clay material with few black coloured elongated minerals (possible glass shrads??)	Shale dominated hetrolith	67.76	2.02	18.40	155.77

Sl No.	Sample Number	Depth	Sample Description	Host Lithology	Li	Be	Sc	V
73	109118	146.88	Suspected tuffite layers greyish to relatively brownish in colour, very fine grained predominantly composed of clay material with few black coloured elongated minerals (possible glass shrads??) and thin venlets (may be secondary) filled with carbonate are also observed within the layers.	Shale dominated hetrolith	36.77	1.78	23.35	191.01
74	109120	149.26	Suspected tuffite layers greyish to relatively brownish in colour, very fine grained predominantly composed of clay material with few black coloured elongated minerals (possible glass shrads??), minor quartz grains and thin venlets (may be secondary) filled with carbonate are also observed within the layers.	Sandstone dominated hetrolith	75.16	2.42	22.67	211.86
75	109121	150.37	uspected tuffite layer brownish in colour, fine to medium grained, predominantly composed of clay material. However, sand sized quartz grains, a few black elongated minerals (possibly glass shards), and thin veinlets, likely of secondary origin and filled with carbonate, are also observed.	Sandstone dominated hetrolith	44.03	1.86	17.29	189.49

Table Continued..

Annexure-XXXa

Sl No.	Sample Number	Cr	Mn	Co	Ni	Cu	Zn	Ga	Ge	Se	Rb	Sr	Y	Zr	Nb
1	112203	147.61	-	8.53	27.93	15.57	62.95	14.94	0.23	1.94	51.00	1118.62	25.21	91.15	8.94
2	112208	174.48	-	15.03	50.05	32.30	90.82	23.63	0.14	5.47	81.65	226.50	30.49	138.83	15.68
3	112207	197.56	-	11.02	35.70	21.47	62.22	19.04	0.14	3.76	65.45	306.60	27.90	97.04	10.82
4	112205	202.91	-	8.85	28.42	25.58	90.08	18.03	0.13	2.04	66.54	233.32	27.79	140.08	11.93
5	112206	168.64	-	10.70	30.59	18.28	48.49	16.28	0.18	3.49	51.54	258.37	26.30	99.26	9.90
6	112204	150.31	-	8.78	28.83	17.96	56.01	15.09	0.21	2.39	48.75	185.20	30.03	87.35	8.55

Sl No.	Sample Number	Cr	Mn	Co	Ni	Cu	Zn	Ga	Ge	Se	Rb	Sr	Y	Zr	Nb
7	112209	168.06	-	5.58	19.40	11.04	28.55	9.15	0.24	2.45	30.30	194.16	19.10	61.57	5.38
8	112210	116.83	-	11.38	35.45	24.67	66.96	19.55	0.15	3.45	72.01	142.76	23.05	127.84	12.75
9	112212	156.60	-	5.43	19.88	8.39	54.15	8.84	0.20	3.07	30.95	191.43	17.81	67.66	5.45
10	112213	150.81	-	10.25	33.25	19.88	69.14	17.20	0.13	3.42	71.40	225.07	17.73	128.67	11.27
11	112216	1355.48	-	21.22	39.10	24.51	58.66	21.23	0.23	<0.1	107.52	212.54	22.98	237.04	49.94
12	112217	145.48	766.43	14.82	28.33	15.93	55.04	28.47	0.93	1.37	51.25	298.27	16.45	106.14	31.34

Sl No.	Sample Number	Cr	Mn	Co	Ni	Cu	Zn	Ga	Ge	Se	Rb	Sr	Y	Zr	Nb
13	112219	357.32	-	9.97	18.38	8.47	28.30	29.47	0.44	<0.1	33.73	353.99	60.06	84.12	24.35
14	112220	974.16	-	18.03	12.61	40.81	35.83	6.23	0.14	<0.1	52.12	111.78	18.63	376.97	62.19
15	112222	169.29	-	7.68	15.79	7.98	28.49	30.68	0.45	<0.1	26.48	514.49	71.08	72.15	20.09
16	112224	265.35	-	12.15	25.06	12.69	39.47	28.28	0.45	<0.1	58.22	177.03	22.47	126.39	32.10
17	112225	77.42	629.35	12.51	21.55	12.81	46.66	26.37	0.82	0.90	38.70	366.04	87.58	20.15	19.12
18	112226	210.24	170.21	16.79	28.05	17.69	80.51	14.08	0.21	1.18	59.52	156.17	17.66	167.81	44.74

Sl No.	Sample Number	Cr	Mn	Co	Ni	Cu	Zn	Ga	Ge	Se	Rb	Sr	Y	Zr	Nb
19	112230	202.36	-	18.47	34.74	23.55	127.78	26.66	0.25	<0.1	101.88	198.08	19.10	137.20	46.23
20	112232	152.69	-	14.91	32.75	19.25	83.53	26.64	0.30	<0.1	82.01	186.07	37.55	115.39	38.45
21	112233	112.67	440.25	21.76	36.89	26.87	88.91	27.84	0.12	<0.1	81.76	239.22	24.16	159.12	27.30
22	112234	279.06	-	11.40	12.05	11.16	53.08	6.93	0.10	<0.1	73.90	88.93	15.17	263.78	36.84
23	112235	121.21	-	14.30	30.93	19.87	68.01	26.77	0.30	1.98	85.11	213.85	87.77	126.32	37.86
24	112236	211.76	138.81	16.75	29.39	15.88	87.14	14.70	0.21	0.74	72.31	141.72	11.53	130.15	43.25

Sl No.	Sample Number	Cr	Mn	Co	Ni	Cu	Zn	Ga	Ge	Se	Rb	Sr	Y	Zr	Nb
25	112239	769.25	-	8.41	10.94	11.25	25.12	8.18	0.17	<0.1	61.02	140.47	12.38	175.19	29.55
26	112240	163.11	-	22.48	42.65	31.63	71.63	27.05	0.17	<0.1	126.85	198.30	22.75	177.53	57.43
27	112241	126.40	491.74	21.36	35.50	24.02	80.93	29.13	0.69	0.27	69.50	271.66	24.96	161.67	28.11
28	112242	122.59	702.53	17.64	28.23	16.13	69.81	27.62	0.97	1.32	49.40	348.50	42.01	125.18	28.12
29	112244	227.63	-	9.24	19.34	8.38	37.29	30.53	0.46	0.20	37.72	153.87	18.45	75.94	22.55
30	112245	144.82	-	11.07	20.55	8.58	72.73	28.21	0.38	<0.1	39.87	322.16	48.07	84.38	23.69

Sl No.	Sample Number	Cr	Mn	Co	Ni	Cu	Zn	Ga	Ge	Se	Rb	Sr	Y	Zr	Nb
31	112247	7.33	-	0.45	0.46	0.96	1.56	0.26	<0.1	<0.1	2.30	3.56	0.41	7.15	1.55
32	112248	386.14	-	21.94	16.66	58.84	52.83	9.15	0.14	<0.1	65.72	298.91	23.26	409.40	80.35
33	112250	252.61	-	12.99	32.65	11.44	45.38	12.66	0.15	<0.1	67.02	148.42	23.04	180.14	33.28
34	113364	112.69	-	24.38	53.33	37.57	124.30	32.09	0.27	<0.1	105.52	151.90	20.30	191.97	7.57
35	113360	154.22	-	60.17	58.58	39.58	107.64	31.44	0.22	<0.1	109.64	140.98	18.93	188.95	10.35
36	109065	318.73	-	16.12	34.40	16.85	68.17	28.48	0.37	<0.1	78.56	203.17	26.19	113.72	33.71

Sl No.	Sample Number	Cr	Mn	Co	Ni	Cu	Zn	Ga	Ge	Se	Rb	Sr	Y	Zr	Nb
37	109066	120.71	-	10.27	22.82	11.42	62.74	23.62	0.27	<0.1	60.91	274.64	106.31	33.28	25.55
38	109067	67.28	1207.09	13.14	26.91	6.19	61.63	34.49	1.32	0.86	20.98	221.81	27.44	59.45	15.13
39	109069	171.79	178.87	31.18	59.70	29.62	121.86	27.09	0.19	1.38	93.94	216.82	20.22	188.53	40.61
40	112211	422.14	-	23.68	71.99	36.82	204.62	35.50	0.16	3.49	109.95	217.67	20.96	176.66	19.78
41	109072	202.62	-	20.67	41.14	26.37	99.00	22.68	0.17	<0.1	141.42	177.69	19.37	166.82	51.00
42	109074	207.86	-	14.57	30.65	15.23	54.99	28.36	0.37	0.15	142.31	251.21	22.76	110.94	34.65

Sl No.	Sample Number	Cr	Mn	Co	Ni	Cu	Zn	Ga	Ge	Se	Rb	Sr	Y	Zr	Nb
43	109075	132.95	280.27	28.61	55.16	31.87	228.64	27.34	0.21	0.57	85.39	252.26	23.57	150.52	31.40
44	109076	126.20	754.62	24.73	49.23	29.28	81.41	32.48	0.49	0.53	82.17	201.60	30.59	117.25	29.37
45	109079	121.79	365.10	23.71	44.13	30.92	118.51	27.66	<0.1	<0.1	85.32	225.96	24.46	143.52	29.47
46	109080	99.16	970.63	10.57	19.36	5.66	47.59	34.26	1.68	<0.1	21.34	204.26	20.00	57.41	20.89
47	109081	231.18	141.92	32.21	62.07	40.30	134.99	32.09	0.41	1.28	104.42	186.55	20.20	168.46	50.76
48	109082	112.22	-	14.78	34.03	16.45	117.86	27.58	0.31	<0.1	59.13	209.79	95.69	102.87	31.01

Sl No.	Sample Number	Cr	Mn	Co	Ni	Cu	Zn	Ga	Ge	Se	Rb	Sr	Y	Zr	Nb
49	109084	219.32	202.96	23.14	48.30	29.56	93.33	24.96	0.11	0.57	90.11	144.69	24.19	145.81	46.93
50	109086	167.90	37.06	10.30	7.83	12.60	14.88	16.47	<0.1	10.36	<0.1	674.00	22.58	133.08	54.59
51	109087	199.52	263.00	21.25	44.65	20.00	95.21	21.89	0.26	1.49	77.35	207.94	20.42	197.90	42.91
52	109088	204.92	233.17	19.86	34.96	15.58	114.33	17.41	0.21	1.41	72.28	196.12	18.95	301.59	44.44
53	109090	76.58	916.75	9.62	20.29	3.02	53.96	31.33	1.54	0.90	24.27	208.15	16.12	78.46	16.74
54	109091	97.35	-	11.98	30.25	12.34	57.37	29.10	0.53	<0.1	31.44	188.10	16.87	87.72	21.68

Sl No.	Sample Number	Cr	Mn	Co	Ni	Cu	Zn	Ga	Ge	Se	Rb	Sr	Y	Zr	Nb
55	109094	121.03	-	15.94	35.23	19.77	57.13	29.50	0.38	<0.1	80.47	195.25	20.25	107.93	36.94
56	109096	142.07	-	12.56	25.99	18.47	65.08	27.82	0.30	<0.1	79.76	172.17	30.69	112.44	35.24
57	109097	143.97	870.40	16.35	28.62	35.72	73.99	29.31	0.70	1.15	60.87	184.63	27.92	112.62	29.23
58	113359	136.47	-	29.43	73.00	48.56	106.08	35.50	0.09	1.91	112.92	226.42	20.56	183.31	9.69
59	109098	89.76	1273.81	7.02	9.89	1.74	24.32	34.72	1.32	<0.1	<0.1	145.62	21.62	51.39	17.98
60	109099	161.13	764.35	20.87	42.25	20.19	86.13	30.07	0.56	0.26	67.53	150.64	22.73	124.83	34.56

Sl No.	Sample Number	Cr	Mn	Co	Ni	Cu	Zn	Ga	Ge	Se	Rb	Sr	Y	Zr	Nb
61	109100	99.75	986.42	15.46	26.60	12.20	65.12	32.53	1.25	0.95	35.85	141.76	24.63	97.65	23.03
62	109101	90.83	1277.12	11.56	18.52	11.33	36.39	30.48	1.31	0.33	27.92	228.06	76.75	33.99	20.64
63	109102	762.77	-	12.18	12.69	18.26	44.30	7.02	0.15	0.90	55.62	146.33	18.57	224.80	47.63
64	109104	116.44	1147.86	15.38	28.00	7.90	57.19	32.41	1.10	<0.1	47.25	169.50	93.53	111.19	29.69
65	109105	130.60	928.48	20.77	38.50	18.20	62.47	33.46	1.39	0.84	53.00	128.02	26.08	105.06	29.16
66	109106	421.72	173.61	18.98	33.88	28.06	65.99	16.80	0.23	0.49	76.94	221.79	9.89	116.88	85.67

Sl No.	Sample Number	Cr	Mn	Co	Ni	Cu	Zn	Ga	Ge	Se	Rb	Sr	Y	Zr	Nb
67	109107	157.09	881.49	21.23	39.88	26.10	84.54	31.21	0.58	0.33	73.93	182.38	35.65	122.62	34.57
68	113382	171.64	336.06	27.73	60.58	37.16	133.08	29.08	<0.1	<0.1	119.07	220.01	28.26	180.18	50.41
69	109108	130.06	-	11.51	24.75	13.56	39.67	28.99	0.45	0.25	77.93	181.00	25.14	93.05	28.15
70	109110	192.46	347.31	24.01	47.80	30.74	92.69	28.42	0.26	1.11	98.01	202.00	24.53	167.79	42.01
71	109114	184.04	652.79	16.54	32.11	19.78	57.04	31.23	1.00	2.13	59.54	222.91	26.07	114.38	38.37
72	109116	158.19	757.93	20.29	35.50	22.93	330.59	27.64	0.48	0.19	74.34	159.97	27.36	156.48	34.80

Sl No.	Sample Number	Cr	Mn	Co	Ni	Cu	Zn	Ga	Ge	Se	Rb	Sr	Y	Zr	Nb
73	109118	136.10	1250.98	11.83	19.26	7.87	52.88	28.17	0.98	0.26	28.94	176.55	22.25	118.56	26.31
74	109120	154.36	585.45	20.82	36.61	25.86	73.44	29.56	0.45	<0.1	79.52	177.05	31.80	143.26	34.67
75	109121	147.85	803.01	11.28	21.75	9.02	42.48	32.03	1.60	0.67	29.19	205.74	20.53	92.34	30.29

Table Continued..

Annexure-XXXa

Sl No.	Sample Number	Mo	Ag	Cd	In	Sn	Sb	Te	Cs	Ba	La	Ce	Pr	Nd	Sm
1	112203	0.34	<0.1	<0.05	0.03	1.62	0.32	<0.1	3.58	964.64	25.14	54.02	6.16	23.42	5.26
2	112208	0.65	0.84	<0.05	0.06	3.38	2.59	<0.1	5.38	313.43	41.56	88.19	10.09	38.01	8.30
3	112207	0.35	0.12	<0.05	0.03	2.33	0.56	0.18	5.04	207.44	27.69	61.54	6.89	26.46	5.90
4	112205	0.33	<0.1	<0.05	0.04	2.50	0.64	<0.1	4.10	238.70	27.57	63.00	7.16	27.22	6.53
5	112206	0.28	<0.1	<0.05	0.03	1.98	0.66	<0.1	3.53	195.50	27.31	58.60	6.62	24.88	5.73
6	112204	0.27	<0.1	<0.05	0.03	1.88	0.83	<0.1	3.65	155.44	23.04	51.48	5.86	22.98	5.43

Sl No.	Sample Number	Mo	Ag	Cd	In	Sn	Sb	Te	Cs	Ba	La	Ce	Pr	Nd	Sm
7	112209	0.28	0.46	<0.05	<0.01	1.00	0.76	<0.1	2.33	109.71	16.09	34.57	3.95	14.89	3.57
8	112210	0.41	0.44	<0.05	0.03	2.61	3.05	<0.1	5.19	205.50	28.94	60.98	7.20	27.25	6.29
9	112212	0.16	<0.1	<0.05	<0.01	1.10	2.01	<0.1	2.15	123.33	15.66	34.79	3.93	15.52	3.57
10	112213	0.19	0.11	<0.05	0.04	2.32	<0.1	0.14	5.05	198.72	25.59	56.78	6.41	23.43	5.22
11	112216	0.78	-	1.89	3.81	490.38	7.05	-	<0.1	227.55	39.49	89.51	13.75	41.61	7.31
12	112217	0.84	0.55	1.17	0.18	25.43	7.19	16.28	4.80	169.39	25.48	51.34	32.59	30.93	8.77

Sl No.	Sample Number	Mo	Ag	Cd	In	Sn	Sb	Te	Cs	Ba	La	Ce	Pr	Nd	Sm
13	112219	0.21	-	3.65	13.19	109.59	11.43	-	10.84	143.78	33.51	87.25	41.37	20.29	19.24
14	112220	0.69	-	1.55	2.31	358.76	5.20	-	14.09	238.29	50.13	121.46	13.82	51.83	7.52
15	112222	0.35	-	4.08	13.80	45.84	11.89	-	26.98	833.09	35.27	108.84	43.58	16.74	25.31
16	112224	0.38	-	3.89	11.26	81.13	7.65	-	14.01	144.28	26.95	48.70	33.60	26.75	10.92
17	112225	0.19	0.19	1.27	0.19	12.65	7.84	18.97	3.70	159.35	41.33	106.99	43.80	53.04	16.85
18	112226	0.86	0.54	<0.05	0.03	42.76	1.61	4.43	5.36	329.09	28.82	72.18	6.56	34.88	5.00

Sl No.	Sample Number	Mo	Ag	Cd	In	Sn	Sb	Te	Cs	Ba	La	Ce	Pr	Nd	Sm
19	112230	2.39	-	2.80	8.20	62.08	4.36	-	32.38	185.59	34.09	68.58	22.00	38.53	8.67
20	112232	0.19	-	3.02	9.43	45.31	7.82	-	4.70	153.90	30.23	61.69	22.72	32.04	11.20
21	112233	0.58	0.61	0.64	0.09	22.98	3.46	10.53	7.54	263.54	33.41	76.53	17.90	46.34	8.42
22	112234	0.41	-	1.41	2.81	100.66	0.25	-	19.08	392.98	36.78	86.54	4.72	30.70	5.42
23	112235	0.96	-	3.08	9.20	30.17	6.61	-	22.33	163.37	51.36	124.11	32.00	31.55	16.84
24	112236	0.59	0.50	<0.05	0.03	45.21	0.23	3.63	4.49	503.44	25.22	59.40	7.14	29.85	4.15

Sl No.	Sample Number	Mo	Ag	Cd	In	Sn	Sb	Te	Cs	Ba	La	Ce	Pr	Nd	Sm
25	112239	0.75	-	1.65	2.48	276.03	6.09	-	12.28	280.19	32.41	69.66	9.02	24.62	4.95
26	112240	0.94	-	1.89	3.96	52.59	3.35	-	<0.1	258.84	38.50	82.35	10.58	47.86	7.98
27	112241	0.74	0.63	0.79	0.13	25.26	4.68	12.62	6.73	293.04	35.42	81.70	25.02	46.96	10.30
28	112242	0.55	0.42	0.98	0.15	22.76	6.46	15.03	4.96	281.04	30.85	79.13	30.99	47.55	13.59
29	112244	<0.1	-	4.07	13.67	71.17	9.17	-	12.64	108.22	21.21	34.33	37.92	18.79	10.07
30	112245	0.10	-	3.99	12.80	42.10	9.10	-	<0.1	184.25	31.75	76.71	38.67	19.74	18.85

Sl No.	Sample Number	Mo	Ag	Cd	In	Sn	Sb	Te	Cs	Ba	La	Ce	Pr	Nd	Sm
31	112247	<0.1	-	<0.05	0.07	2.68	<0.1	-	<0.1	0.65	1.33	3.17	0.15	1.29	0.20
32	112248	1.08	-	1.79	3.47	141.58	3.93	-	48.00	390.49	83.70	198.10	18.59	66.95	12.72
33	112250	1.36	-	1.95	4.43	86.77	3.82	-	9.69	320.03	28.48	56.42	9.97	27.73	5.55
34	113364	1.46	1.8	1.74	3.56	40.86	5.10	-	27.46	290.47	39.77	89.83	8.26	43.64	6.96
35	113360	1.42	1.78	1.31	2.70	58.77	2.92	5.52	27.57	330.21	46.45	101.35	7.66	51.30	7.43
36	109065	0.54	-	3.47	9.63	103.03	6.87	-	16.84	255.50	31.24	60.69	27.02	28.09	11.22

Sl No.	Sample Number	Mo	Ag	Cd	In	Sn	Sb	Te	Cs	Ba	La	Ce	Pr	Nd	Sm
37	109066	0.40	-	3.43	10.09	29.93	7.75	-	30.31	159.83	47.80	104.43	35.76	21.29	18.33
38	109067	0.11	0.75	2.23	0.28	11.41	9.63	25.13	2.30	142.63	20.82	47.71	53.87	29.69	13.67
39	109069	1.19	0.68	0.08	0.04	35.93	3.57	4.93	7.95	488.65	48.70	120.46	10.42	56.58	8.58
40	112211	0.65	0.17	<0.05	0.08	4.24	1.65	<0.1	7.31	414.50	52.07	114.81	12.29	44.90	9.30
41	109072	0.99	-	1.45	3.47	71.29	2.94	-	23.49	441.26	46.24	97.70	9.23	42.50	8.10
42	109074	0.38	-	3.37	10.16	64.70	9.63	-	3.05	313.72	34.63	66.17	27.03	28.87	9.74

Sl No.	Sample Number	Mo	Ag	Cd	In	Sn	Sb	Te	Cs	Ba	La	Ce	Pr	Nd	Sm
43	109075	1.15	0.60	0.25	0.05	28.51	2.33	7.85	7.82	426.61	44.53	105.07	14.07	56.38	8.77
44	109076	0.83	0.39	0.73	0.12	24.81	4.17	12.16	6.40	252.55	40.18	88.41	27.30	49.48	10.32
45	109079	0.81	0.56	0.29	0.06	25.83	2.91	7.06	6.98	381.44	41.91	99.22	14.56	51.29	9.05
46	109080	0.22	0.44	2.03	0.29	17.19	10.37	24.73	2.11	193.50	17.05	30.13	52.89	21.83	11.04
47	109081	1.43	0.58	<0.05	0.04	46.97	3.48	6.26	9.26	300.41	47.95	117.80	13.20	60.33	8.94
48	109082	0.50	-	3.35	9.63	31.10	6.07	-	13.76	166.27	51.85	115.86	33.40	25.84	19.34

Sl No.	Sample Number	Mo	Ag	Cd	In	Sn	Sb	Te	Cs	Ba	La	Ce	Pr	Nd	Sm
49	109084	1.33	0.55	0.21	0.05	43.25	3.61	6.95	6.47	387.29	39.34	88.57	12.55	45.40	7.74
50	109086	2.22	0.45	1.88	1.48	17.88	<0.1	<0.1	4.83	3344.63	85.61	250.25	21.99	103.55	20.85
51	109087	1.06	0.82	0.13	0.06	40.01	3.36	7.34	6.53	375.99	38.89	88.68	14.85	45.19	7.74
52	109088	0.59	1.07	<0.05	0.04	38.88	2.09	6.87	6.95	413.53	44.37	110.07	14.69	52.62	8.00
53	109090	<0.1	0.53	1.93	0.27	12.81	9.39	23.61	2.05	176.41	16.49	27.72	49.39	20.69	10.67
54	109091	1.38	-	4.54	13.89	24.93	9.38	-	25.02	167.32	21.57	30.77	37.98	18.07	9.96

Sl No.	Sample Number	Mo	Ag	Cd	In	Sn	Sb	Te	Cs	Ba	La	Ce	Pr	Nd	Sm
55	109094	0.93	-	3.25	9.12	34.26	9.31	-	4.15	219.61	32.45	54.25	23.61	30.78	8.99
56	109096	0.88	-	3.38	9.06	40.55	7.74	-	6.93	223.21	30.84	54.13	27.29	29.37	10.04
57	109097	1.06	0.68	1.14	0.16	26.30	5.62	14.27	5.08	260.13	32.03	65.72	31.62	37.89	9.94
58	113359	1.97	1.73	1.34	2.67	52.67	3.00	-	29.57	375.43	59.22	125.83	9.03	61.54	9.33
59	109098	<0.1	0.42	2.28	0.31	14.74	12.69	26.61	1.34	115.81	11.77	28.82	56.22	19.68	11.49
60	109099	1.16	0.59	0.76	0.15	29.43	6.65	14.23	5.28	337.61	35.27	71.46	29.22	42.08	10.18

Sl No.	Sample Number	Mo	Ag	Cd	In	Sn	Sb	Te	Cs	Ba	La	Ce	Pr	Nd	Sm
61	109100	0.69	0.62	1.69	0.22	17.45	6.92	19.31	4.22	227.32	30.00	57.56	40.18	36.20	11.08
62	109101	0.53	0.33	1.49	0.24	15.51	8.86	21.66	3.13	167.94	30.69	64.00	49.78	38.85	14.38
63	109102	0.73	-	1.51	2.40	280.88	4.67	-	16.26	417.24	49.15	108.88	9.63	39.69	7.45
64	109104	0.76	0.67	1.50	0.21	19.45	8.37	18.08	4.07	190.13	43.56	132.21	49.01	77.48	24.14
65	109105	0.78	0.55	1.43	0.20	22.60	7.92	18.36	4.71	234.07	26.31	46.72	38.49	34.04	10.23
66	109106	1.03	0.58	0.07	0.03	82.02	1.45	3.18	4.37	530.70	35.13	79.99	6.78	36.45	4.74

Sl No.	Sample Number	Mo	Ag	Cd	In	Sn	Sb	Te	Cs	Ba	La	Ce	Pr	Nd	Sm
67	109107	1.16	0.45	0.69	0.15	29.67	5.79	12.82	5.98	279.67	39.06	82.30	27.74	47.84	11.01
68	113382	1.16	0.64	2.03	3.03	19.36	<0.1	2.14	8.04	442.42	47.93	115.59	12.46	50.48	8.78
69	109108	0.24	-	3.64	11.59	31.94	8.55	-	25.83	166.38	25.76	40.11	30.14	23.46	10.19
70	109110	1.39	0.68	0.39	0.07	37.37	2.82	8.31	7.17	402.82	41.55	92.36	16.31	47.94	8.48
71	109114	0.83	0.53	1.13	0.15	32.26	8.40	15.66	5.09	254.72	30.55	61.00	31.10	36.76	10.56
72	109116	0.60	0.68	1.49	0.12	27.46	3.92	12.13	6.21	232.42	34.75	77.81	24.79	44.82	10.12

Sl No.	Sample Number	Mo	Ag	Cd	In	Sn	Sb	Te	Cs	Ba	La	Ce	Pr	Nd	Sm
73	109118	0.17	0.87	1.50	0.21	22.71	7.75	19.49	3.19	194.10	23.18	47.56	39.72	31.14	10.51
74	109120	1.23	0.56	0.70	0.11	29.98	5.04	11.85	6.76	227.69	36.08	81.86	22.42	49.04	10.82
75	109121	0.19	0.53	1.40	0.24	23.90	9.13	20.78	3.34	156.89	22.96	43.07	46.71	28.14	10.58

Table Continued..

Annexure-XXXa

Sl No.	Sample Number	Eu	Gd	Tb	Dy	Ho	Er	Tm	Yb	Lu	Hf	Ta	W	Tl	Pb	Bi	Th	U	HREEY	LREE	TREEY
1	112203	1.22	4.94	0.75	4.85	0.99	2.91	0.42	2.63	0.41	2.48	0.67	1.15	<0.05	8.82	0.18	9.30	1.49	76.61	114.01	190.62
2	112208	1.79	7.36	1.08	6.46	1.27	3.65	0.54	3.18	0.47	4.09	1.28	1.83	0.26	17.35	0.30	16.08	2.69	79.31	186.15	265.46
3	112207	1.37	5.66	0.87	5.43	1.13	3.38	0.50	2.99	0.48	2.83	0.82	1.41	<0.05	20.16	0.23	10.63	1.77	77.22	128.47	205.69
4	112205	1.47	6.22	0.93	5.64	1.11	3.16	0.46	2.83	0.43	4.07	0.89	1.35	<0.05	10.62	0.20	11.84	1.99	75.37	131.48	206.84
5	112206	1.23	5.03	0.77	4.86	1.01	3.05	0.46	2.76	0.43	2.77	0.72	1.17	<0.05	8.82	0.19	9.76	1.63	69.64	123.13	192.77
6	112204	1.27	5.36	0.87	5.61	1.17	3.52	0.52	3.31	0.53	2.41	0.64	1.16	<0.05	8.13	0.18	8.59	1.41	87.81	108.80	196.61

Sl No.	Sample Number	Eu	Gd	Tb	Dy	Ho	Er	Tm	Yb	Lu	Hf	Ta	W	Tl	Pb	Bi	Th	U	HREEY	LREE	TREEY
7	112209	0.85	3.27	0.55	3.62	0.75	2.28	0.34	2.13	0.33	1.57	0.44	0.83	<0.05	6.59	0.13	5.85	0.90	57.38	73.07	130.44
8	112210	1.38	5.44	0.82	4.79	1.00	2.92	0.42	2.69	0.41	3.77	1.02	1.46	<0.05	12.80	0.26	12.48	2.00	65.37	130.65	196.02
9	112212	0.82	3.52	0.57	3.48	0.74	2.23	0.33	2.00	0.32	1.82	0.41	0.80	<0.05	6.26	0.11	6.23	0.95	56.26	73.47	129.73
10	112213	1.07	4.22	0.64	4.03	0.77	2.36	0.34	2.23	0.34	3.63	0.88	1.36	0.26	10.14	0.23	11.48	1.83	52.16	117.43	169.59
11	112216	1.59	5.53	2.43	4.45	<0.1	3.24	0.16	1.79	0.12	5.47	2.80	0.30	0.92	13.77	<0.1	13.13	1.39	57.65	191.67	249.32
12	112217	1.41	3.51	0.85	3.09	0.36	2.09	<0.1	3.08	0.77	2.35	3.24	1.23	1.08	19.55	1.22	100.51	22.58	53.08	149.11	202.19

Sl No.	Sample Number	Eu	Gd	Tb	Dy	Ho	Er	Tm	Yb	Lu	Hf	Ta	W	Tl	Pb	Bi	Th	U	HREEY	LREE	TREEY
13	112219	3.65	20.74	5.15	12.24	1.67	3.48	0.14	2.92	0.42	2.18	3.75	<0.1	<0.05	10.93	1.55	44.70	41.85	130.39	201.66	332.06
14	112220	0.78	3.55	1.99	4.47	<0.1	3.49	0.25	1.23	0.06	9.25	2.13	0.31	1.16	11.62	<0.1	10.32	<0.1	42.11	244.76	286.87
15	112222	5.02	23.53	4.60	16.88	2.12	4.12	0.11	3.41	0.45	3.80	4.20	<0.1	<0.05	10.42	<0.1	48.13	48.72	159.22	229.75	388.97
16	112224	1.84	15.34	3.79	4.53	<0.1	2.37	0.16	2.27	0.37	3.09	2.91	0.18	<0.05	13.38	<0.1	38.49	32.73	73.19	146.92	220.11
17	112225	3.16	15.28	1.04	13.19	3.22	4.74	<0.1	5.09	0.89	0.21	2.37	0.61	0.60	18.60	1.78	104.24	25.95	161.16	262.01	423.17
18	112226	1.11	4.21	0.57	3.58	0.44	2.30	<0.1	1.63	0.15	4.93	1.13	<0.1	0.75	25.76	<0.1	<0.1	0.67	43.13	147.44	190.57

Sl No.	Sample Number	Eu	Gd	Tb	Dy	Ho	Er	Tm	Yb	Lu	Hf	Ta	W	Tl	Pb	Bi	Th	U	HREEY	LREE	TREEY
19	112230	1.69	9.82	3.55	3.44	<0.1	2.86	0.15	2.03	0.23	3.79	3.20	0.43	<0.05	12.87	<0.1	25.67	14.24	66.46	171.86	238.33
20	112232	2.37	12.80	3.96	7.73	<0.1	3.25	0.12	2.36	0.28	2.85	2.63	0.34	<0.05	15.77	<0.1	29.59	24.37	90.93	157.87	248.81
21	112233	1.69	6.20	0.77	4.89	<0.1	2.86	<0.1	2.80	0.46	4.51	2.09	1.49	0.78	23.59	<0.1	51.00	8.37	64.32	182.60	246.92
22	112234	0.78	2.45	1.05	3.63	<0.1	2.28	0.22	0.97	0.04	7.91	0.76	0.17	0.42	15.68	<0.1	6.55	<0.1	33.09	164.16	197.25
23	112235	3.70	15.34	3.85	14.72	2.00	5.32	0.15	3.46	0.30	2.92	2.00	0.19	2.29	15.18	0.22	29.11	19.93	161.31	255.86	417.17
24	112236	0.92	3.01	0.49	2.21	<0.1	1.75	<0.1	1.20	0.13	4.72	0.98	0.60	0.27	22.05	<0.1	<0.1	0.55	29.26	125.76	155.02

Sl No.	Sample Number	Eu	Gd	Tb	Dy	Ho	Er	Tm	Yb	Lu	Hf	Ta	W	Tl	Pb	Bi	Th	U	HREEY	LREE	TREEY
25	112239	0.79	3.41	1.39	2.53	<0.1	1.89	0.19	0.86	0.06	4.54	1.40	0.19	0.53	9.35	0.91	8.48	<0.1	28.64	140.66	169.30
26	112240	1.78	5.84	3.05	5.13	<0.1	3.55	0.16	1.61	0.13	4.79	1.85	0.31	<0.05	14.83	<0.1	13.73	2.35	58.78	187.27	246.06
27	112241	1.94	7.39	0.90	5.35	<0.1	2.84	<0.1	2.86	0.57	4.68	2.84	1.37	0.20	26.04	<0.1	71.33	12.77	65.21	199.40	264.61
28	112242	2.67	12.01	0.97	9.20	<0.1	3.06	<0.1	3.13	0.71	3.19	2.94	<0.1	0.88	23.74	1.03	90.22	19.19	91.18	202.11	293.30
29	112244	1.57	17.89	4.07	2.68	<0.1	1.88	0.15	2.60	0.44	1.95	4.18	0.18	<0.05	13.67	2.96	46.37	52.15	77.63	122.31	199.94
30	112245	3.54	20.61	4.72	10.97	1.57	3.10	0.10	2.69	0.42	2.65	3.88	0.16	<0.05	10.50	0.84	43.68	44.23	115.87	185.73	301.60

Sl No.	Sample Number	Eu	Gd	Tb	Dy	Ho	Er	Tm	Yb	Lu	Hf	Ta	W	Tl	Pb	Bi	Th	U	HREEY	LREE	TREEY
31	112247	<0.1	<0.1	<0.1	0.10	<0.1	<0.1	<0.1	<0.1	<0.1	0.21	<0.1	<0.1	<0.05	0.38	<0.1	0.21	<0.1	1.47	6.14	7.61
32	112248	1.23	5.75	2.87	4.93	0.15	4.40	0.21	1.59	0.10	10.15	1.63	0.26	1.86	40.50	<0.1	16.45	<0.1	53.13	380.06	433.20
33	112250	1.14	5.39	1.67	4.31	0.50	2.62	0.21	1.68	0.13	4.92	1.52	0.23	<0.05	20.27	<0.1	13.46	4.91	66.67	128.16	194.83
34	113364	1.73	5.20	1.64	4.84	0.54	2.46	0.10	1.72	0.09	5.98	2.04	1.97	2.92	12.59	<0.1	12.26	1.78	54.65	188.46	243.11
35	113360	1.75	3.59	1.53	4.85	0.52	2.65	0.10	1.48	0.05	6.00	1.76	2.61	0.79	18.92	<0.1	8.47	<0.1	49.17	214.19	263.36
36	109065	2.00	13.65	3.20	5.34	0.58	2.67	0.13	2.24	0.31	3.28	2.75	0.34	0.59	13.20	0.69	33.19	27.23	77.03	158.26	235.29

Sl No.	Sample Number	Eu	Gd	Tb	Dy	Ho	Er	Tm	Yb	Lu	Hf	Ta	W	Tl	Pb	Bi	Th	U	HREEY	LREE	TREEY
37	109066	3.82	17.52	4.21	16.25	2.62	5.45	0.11	4.20	0.36	0.67	2.81	0.26	1.61	9.35	<0.1	32.90	29.01	188.95	227.62	416.57
38	109067	1.87	6.45	1.02	5.53	<0.1	2.07	<0.1	3.96	1.24	1.28	4.05	0.18	0.15	21.97	3.83	172.11	43.83	73.75	165.76	239.52
39	109069	1.68	6.15	0.69	4.24	<0.1	2.90	<0.1	2.00	0.19	6.19	1.61	2.17	1.37	33.04	<0.1	14.24	1.02	50.70	244.74	295.44
40	112211	1.85	7.05	0.90	4.93	0.92	2.58	0.35	2.28	0.32	5.24	1.51	2.20	<0.05	22.82	0.39	22.01	3.25	55.75	233.38	289.13
41	109072	1.59	4.13	2.43	4.36	<0.1	3.12	0.15	1.37	0.08	5.51	1.22	0.16	1.90	19.50	<0.1	9.96	<0.1	49.01	203.77	252.78
42	109074	1.56	12.66	3.37	3.89	0.40	2.53	0.14	2.32	0.31	3.88	4.14	0.32	0.23	12.99	0.46	32.12	27.12	71.46	166.44	237.90

Sl No.	Sample Number	Eu	Gd	Tb	Dy	Ho	Er	Tm	Yb	Lu	Hf	Ta	W	Tl	Pb	Bi	Th	U	HREEY	LREE	TREEY
43	109075	1.83	6.22	0.85	4.71	0.62	2.98	<0.1	2.39	0.27	4.72	1.81	2.16	2.93	30.29	<0.1	22.85	2.59	59.06	228.82	287.88
44	109076	1.98	6.93	0.92	5.70	<0.1	3.06	<0.1	3.59	0.59	3.37	2.73	<0.1	0.78	26.16	<0.1	68.81	12.29	83.86	215.69	299.55
45	109079	1.86	6.98	0.71	4.95	0.95	2.93	<0.1	2.56	0.31	4.59	1.88	0.68	1.26	28.52	<0.1	28.58	3.51	63.75	216.03	279.78
46	109080	1.12	2.94	0.98	3.18	0.54	1.64	<0.1	3.83	1.25	1.64	4.14	<0.1	0.83	19.65	1.72	173.21	44.10	56.47	132.94	189.42
47	109081	1.83	6.46	0.73	4.24	0.18	3.13	<0.1	2.20	0.23	4.88	1.84	2.72	6.59	31.35	<0.1	17.62	1.29	52.58	248.22	300.80
48	109082	4.09	16.71	4.14	15.49	2.18	5.33	<0.1	3.83	0.32	2.15	3.19	0.44	0.25	11.80	0.17	30.69	23.90	170.14	246.28	416.43

Sl No.	Sample Number	Eu	Gd	Tb	Dy	Ho	Er	Tm	Yb	Lu	Hf	Ta	W	Tl	Pb	Bi	Th	U	HREEY	LREE	TREEY
49	109084	1.58	5.87	0.73	4.68	0.84	2.96	<0.1	2.41	0.27	4.60	1.66	<0.1	0.31	26.68	<0.1	22.31	2.79	59.30	193.60	252.90
50	109086	4.73	15.96	2.40	7.27	0.85	2.50	<0.1	1.70	0.03	13.07	1.67	0.78	0.26	39.25	<0.1	<0.1	<0.1	67.29	482.25	549.53
51	109087	1.53	6.08	0.70	4.11	0.62	2.66	<0.1	2.15	0.27	5.99	1.64	1.00	0.96	21.14	<0.1	21.49	3.03	52.86	195.35	248.21
52	109088	1.26	5.16	0.69	3.91	0.21	2.69	<0.1	2.16	0.25	8.78	1.60	<0.1	0.33	20.89	<0.1	22.04	2.17	47.24	229.75	276.99
53	109090	1.05	3.14	0.91	2.80	0.24	1.36	<0.1	3.16	1.14	1.79	3.92	0.13	0.34	17.36	1.19	157.39	40.32	45.35	124.96	170.31
54	109091	1.18	17.17	3.81	2.81	<0.1	1.71	<0.1	2.30	0.42	2.25	3.16	0.21	<0.05	70.81	0.34	44.79	46.98	65.69	118.35	184.05

Sl No.	Sample Number	Eu	Gd	Tb	Dy	Ho	Er	Tm	Yb	Lu	Hf	Ta	W	Tl	Pb	Bi	Th	U	HREEY	LREE	TREEY
55	109094	1.45	12.58	3.37	3.73	0.48	2.54	0.16	2.15	0.31	3.21	3.44	0.34	<0.05	25.22	<0.1	32.61	26.20	64.84	150.08	214.93
56	109096	1.74	12.64	3.20	5.15	0.55	3.07	0.12	2.75	0.31	3.25	3.06	0.21	<0.05	17.92	1.10	30.88	24.82	88.10	151.68	239.78
57	109097	1.73	5.80	0.94	4.83	<0.1	2.82	<0.1	3.51	0.74	3.03	3.12	0.80	0.37	22.54	1.12	91.14	19.61	74.69	177.20	251.89
58	113359	2.07	4.16	1.96	5.55	0.56	2.75	0.09	1.52	0.05	6.24	1.87	2.30	0.40	17.23	<0.1	9.24	0.17	53.19	264.95	318.14
59	109098	1.17	3.08	1.00	3.30	0.27	1.39	<0.1	4.12	1.37	1.09	4.17	<0.1	0.90	20.16	2.50	194.09	48.73	59.68	127.98	187.66
60	109099	1.51	4.91	0.90	4.18	0.56	2.34	<0.1	3.10	0.69	3.88	2.61	<0.1	0.13	21.07	1.30	88.11	17.45	58.77	188.21	246.97

Sl No.	Sample Number	Eu	Gd	Tb	Dy	Ho	Er	Tm	Yb	Lu	Hf	Ta	W	Tl	Pb	Bi	Th	U	HREEY	LREE	TREEY
61	109100	1.47	5.07	0.99	4.31	0.36	2.20	<0.1	3.62	0.96	2.63	3.23	<0.1	1.06	22.26	2.06	131.65	29.84	64.12	175.02	239.14
62	109101	2.49	10.02	1.04	9.43	2.11	3.83	<0.1	5.64	1.10	0.80	3.84	<0.1	0.61	18.99	2.51	135.22	33.63	143.45	197.70	341.15
63	109102	0.83	3.18	1.83	3.91	<0.1	2.86	0.22	1.07	0.05	6.13	1.64	0.17	<0.05	8.91	0.38	8.10	<0.1	39.72	214.80	254.52
64	109104	4.92	21.41	1.14	16.20	<0.1	4.84	<0.1	5.64	1.00	2.55	3.68	<0.1	0.78	21.72	0.52	123.58	27.89	183.90	326.40	510.31
65	109105	1.52	4.55	0.98	4.57	0.58	2.58	<0.1	3.78	0.93	2.58	3.42	<0.1	0.27	21.05	1.79	123.96	26.87	67.50	155.79	223.30
66	109106	0.94	3.48	0.44	2.11	0.18	1.90	<0.1	1.09	0.12	4.19	1.30	<0.1	1.92	28.00	<0.1	<0.1	0.45	28.13	163.09	191.22

Sl No.	Sample Number	Eu	Gd	Tb	Dy	Ho	Er	Tm	Yb	Lu	Hf	Ta	W	Tl	Pb	Bi	Th	U	HREEY	LREE	TREEY
67	109107	2.09	7.18	0.95	6.47	1.11	3.38	<0.1	3.95	0.66	3.24	2.79	<0.1	0.17	26.86	0.27	79.02	15.32	89.05	207.95	297.00
68	113382	1.78	7.36	2.44	5.78	0.94	3.22	<0.1	2.51	0.05	5.17	1.89	2.07	0.97	<0.1	<0.1	17.07	1.53	69.76	235.24	305.00
69	109108	1.58	15.91	3.47	4.44	0.70	2.39	0.15	2.68	0.39	2.17	3.60	0.25	<0.05	12.65	1.65	40.44	41.46	82.72	129.66	212.38
70	109110	1.66	6.34	0.83	4.67	0.36	3.14	<0.1	2.69	0.34	5.19	2.11	<0.1	0.83	27.57	<0.1	34.31	4.36	63.20	206.64	269.83
71	109114	1.77	5.32	0.94	4.64	0.60	2.70	<0.1	3.60	0.77	3.14	2.96	<0.1	0.32	20.14	0.97	99.03	21.30	72.27	169.97	242.24
72	109116	1.86	6.88	0.86	5.22	0.24	3.00	<0.1	2.95	0.55	4.10	2.32	2.17	1.18	26.30	<0.1	64.52	11.62	67.41	192.29	259.71

Sl No.	Sample Number	Eu	Gd	Tb	Dy	Ho	Er	Tm	Yb	Lu	Hf	Ta	W	Tl	Pb	Bi	Th	U	HREEY	LREE	TREEY
73	109118	1.48	4.93	0.88	3.91	0.41	1.95	<0.1	3.44	0.93	2.62	3.81	<0.1	0.77	20.47	0.20	123.87	29.20	63.62	152.11	215.73
74	109120	2.24	7.71	0.92	6.04	1.00	3.00	<0.1	3.27	0.53	3.63	2.67	0.28	1.49	23.17	<0.1	60.83	10.16	79.28	200.22	279.50
75	109121	1.34	3.42	0.95	3.25	0.20	1.74	<0.1	3.59	1.07	1.96	3.77	<0.1	0.46	20.77	<0.1	145.92	34.62	53.49	151.46	204.95

Annexure-XXX b: ICPMS Analysis of BH02

Sl No.	Sample No.	Depth	Sample Description	Host lithology	Li	Be	Sc	V
1	112451	0.00	Breccia, very coarse-grained, containing quartz and muscovite.	Breccia	9.35	1.35	20.40	153.53
2	112478	0.00	Highly ferruginous altered sandstone (black part)	Jhama Sandstone	3.79	1.19	4.64	71.93
3	112479	0.00	Highly ferruginous altered sandstone (black part)	Jhama sandstone	4.67	1.49	5.04	57.84
4	112480	0.00	Highly ferruginous altered sandstone (black part)	Jhama sandstone	4.33	1.71	7.15	63.81
5	112481	0.00	Highly ferruginous altered sandstone (black part)	Jhama sandstone	5.12	1.65	3.88	44.72
6	112484	0.00	Medium to coarse grained ferruginous weathered sandstone Iron concretion present , angular to rounded grains	ferruginous weathered sandstone	8.51	1.70	8.70	165.91

Sl No.	Sample No.	Depth	Sample Description	Host lithology	Li	Be	Sc	V
7	112195	2	This Sandstone rock composed primarily of sand-sized mineral particles. The grains appear to be moderately sorted medium to fine. Mostly quartz and Muscovite-Biotite. In this core, the reddish-brown color suggests the presence of iron oxide as a cementing agent	Ferruginous sandstone (composite sample)	26.19	0.84	10.25	84.69
8	109128	2.90	Sandstone composed mainly of sand sized mineral grains. Grains are medium to fine, moderately sorted, and consist mostly of quartz with muscovite and biotite. The reddish brown colour indicates iron oxide as the cementing material. Cherry red streak hematite is present in iron concretions.	Ferruginous sandstone	26.29	0.75	7.81	55.81
9	109134	7.45	Tuffite layer composed of predominantley clay materials with fine quartz grains, and ocassional very fine grained black minerals, no ferrugination observed	Sandstone dominated heterolith	39.11	2.88	25.53	113.81
10	109132	11.07	Fine grained Tuffite layer composed predominantly of clay rich material with disseminated? fine grained black minerals possible glass shards. Distinct grey to dark grey lamination is present at bottom. No ferruginisation observed.	Sandstone dominated heterolith	50.93	2.63	25.50	152.56
11	109137	15.25	Suspected Tuffite layer ?, fine grained, gray to light gray argillaceous siltstone, compact and massive in appearance. composed of predominantley clay materials.Minor soft sediment deformation or compaction features are present and composed of medium quartz grains. Sand part is also included within the sandstone.	Sandstone dominated heterolith	55.72	2.59	23.24	179.36

Sl No.	Sample No.	Depth	Sample Description	Host lithology	Li	Be	Sc	V
12	109141	17.24	Breccia composed of angular to sub angular clasts embedded in a fine grained clayey to silty matrix. Clasts include quartz grains, dark grey shale (tabular and occasionally laminated), fossil fragments and imprints, rock fragments and muscovite. Scattered greenish malachite grains are observed at multiple stratigraphic levels, indicating copper mineralization. clay rich Tuffite layers or lenses were noted, with carbonate filled fractures.	Breccia	52.78	2.00	12.37	177.25
13	112194	18	Fossiliferous sandstone, fine to medium grained, with a light grey to greyish white coloration, locally displaying brownish or rusty patches due to iron oxide staining composed of mostly quartz, fossils, shale clast, obsidian?, mica , malachite. The	Fossiliferous sandstone (composite sample)	5.49	0.67	4.61	129.32
14	109140	18.16	Fossiliferous sandstone, fine to medium grained, with a light grey to greyish white coloration, locally displaying brownish or rusty patches due to iron oxide staining composed of mostly quartz, fossils, shale clast, obsidian?, mica , malachite.	Fossiliferous sandstone	3.57	0.28	1.71	46.18
15	109142	23.96	Medium to fine grained, light gray sandstone, moderately compacted and fairly well sorted, with slight ferruginous staining in the matrix, composed predominantly of sub angular to sub rounded quartz grains, fossils and its imprints A localized black, angular patch is present, interpreted as a carbonaceous fragment ?	Fossiliferous sandstone	13.22	1.46	8.76	193.21

Sl No.	Sample No.	Depth	Sample Description	Host lithology	Li	Be	Sc	V
16	109144	25.85	Fossiliferous sandstone, light gray, medium grained, siliceous matrix with scattered white calcareous patches and visible fossil fragments. Prominent fossil material occurs as dark, elongate stringers and nodules, which are well preserved and distributed subparallel to bedding.The rock exhibits moderate sorting and rounding, with cementing largely of silica and occasional calcareous materials(effervescence obserced).	Fossiliferous sandstone	23.81	1.99	21.15	245.51
17	109143	26.00	Fine to medium grained Tuffite layer?? with a uniform, light brown to buff coloration and a smooth, compact texture.Composed of clay materal along with quartz, and abundant amount of accicular, irregylar shaped black material (glass shards??). Mineralized burrow fill is also observed within the sample.The burrows are infilled with carbonate.	Fossiliferous sandstone	24.57	1.67	17.19	186.75
18	112196	26.08	breccia composed of angular to sub-angular clasts embedded in a fine- to medium-grained, grey to brownish-grey matrix. Clasts include quartz grains, dark grey shale (tabular and occasionally laminated), fossil fragments and imprints, rock fragments and muscovite. Scattered greenish malachite grains are observed at multiple stratigraphic levels, indicating copper mineralization.	Breccia (composite sample)	42.79	1.80	13.94	203.75
19	109145	27.04	Breccia composed of angular to sub angular clasts embedded in a fine to medium grained, grey to brownish grey matrix. Clasts include quartz grains, dark grey shale (tabular and occasionally laminated), fossil fragments and imprints, rock fragments and muscovite. Scattered greenish malachite grains are observed at multiple stratigraphic levels, indicating copper mineralization (write if it is within the sample)	Breccia	22.59	1.60	27.22	234.83
20	109146	27.28	Tuffite layer, predominantly composed of clay material .However sand sized quartz grains are also observed with few black elongated minerals and thin venlets (may be secondary) filled with carbonate are observed. The Tuffite layers are medium to very fine grained. Slight ferrugination observed.	Sandstone dominated heterolith	23.25	1.87	18.65	203.54

Sl No.	Sample No.	Depth	Sample Description	Host lithology	Li	Be	Sc	V
21	112151	30.73	Fine to medium grained greyish white coloured sandstone composed of quartz (95%), biotite, muscovite, in a decreasing order of abundance and Within the sandstone, a localized elongated streak of dark, metallic material is observed along the broken surface, a few centimeters in extent. The feature emits a distinct sulfur like odor when exposed, suggesting pyritic concentration with carbonaceous matter.	Sandstone	47.80	1.16	7.83	86.03
22	109150	31.21	Fine to medium grained greyish white coloured sandstone composed of quartz (95%), biotite, muscovite, in a decreasing order of abundance. Patchy appearance and soft sediment deformation is common.	Sandstone	6.01	0.99	23.54	579.53
23	112154	35.46	Tuffite layer, fine grained predominantly composed of clay rich material and within this, a few elongated black streaks are observed, possibly representing glass shards. Minor white veinlets, interpreted as calcium carbonate, are also present. Ferrugination of the Tuffite layer is observed.	Shale dominated heterolith	34.63	1.91	13.72	133.60
24	112158	42.05	Tuffite layer, fine grained predominantly composed of clay material , few black elongated minerals, glass shards? Carbonate ?and also few coars quartz grains.	Sandstone	18.75	1.17	8.36	146.73
25	113051	46.60	Fine grained, brownish gray suspected Tuffite layer ? with subtle ferruginous staining that imparts a light brown tint. The grains are fine to silt sized, giving the interval a homogeneous and compact appearance.	Shale Sandstone hetrolith	24.34	3.41	14.47	184.15

Sl No.	Sample No.	Depth	Sample Description	Host lithology	Li	Be	Sc	V
26	113052	49.30	Very fine grained, brownish gray suspected Tuffite layer ? with ferruginous staining that imparts a light brown tint. The grains are very fine to silt sized, giving the interval a homogeneous and compact appearance. Few irregular, jet black mineral (glass shards??) are observed.	Shale Sandstone hetrolith	27.53	3.41	26.51	165.91
27	113053	52.12	Brownish gray suspected Tuffite layer ? with subtle ferruginous staining that imparts a light brown tint and are predominantly composed of clay material.	Shale Sandstone hetrolith	28.98	2.28	13.85	212.19
28	113054	52.91	Very fine grained, brownish gray suspected Tuffite layer ? with subtle ferruginous staining that imparts a light brown tint and are predominantly composed of clay material with few black coloured elongated minerals (possible glass shrads??).	Shale Sandstone hetrolith	26.70	0.00	22.79	179.63
29	113056	53.88	Fine to medium grained brownish gray suspected Tuffite layer with subtle ferruginous staining imparting a light brown tint; predominantly clay rich with medium quartz grains and a few black angular mineral inclusions (possible glass shards).	Sandstone dominated heterolith	27.75	1.15	8.12	230.94
30	113055	55.04	Fine to medium grained brownish gray suspected Tuffite layer with subtle ferruginous staining imparting a light brown tint; predominantly clay rich with medium quartz grains and a few black elongated mineral inclusions (possible glass shards). A localized dark black streak, a few centimeters in extent, occurs along the broken surface, emitting a sulfur like odor on exposure, suggesting pyritic concentration with carbonaceous matter.	Sandstone dominated heterolith	26.73	3.44	10.78	191.95

Sl No.	Sample No.	Depth	Sample Description	Host lithology	Li	Be	Sc	V
31	113057	56.85	Fine to medium grained brownish gray suspected Tuffite layer with subtle ferruginous staining imparting a light brown tint; predominantly clay rich with medium quartz grains and a few black angular mineral inclusions (possible glass shards). Minor white veinlets, interpreted as calcium carbonate, are also present.	Sandstone dominated heterolith	29.33	3.40	8.85	222.71
32	113062	56.85	Fine to medium grained brownish suspected Tuffite layer with subtle ferruginous staining imparting a dark brown tint; predominantly clay rich.	Shale Sandstone hetrolith	51.36	1.13	4.10	69.16
33	113063	59.44	Fine to medium grained brownish suspected Tuffite layer with subtle ferruginous staining imparting a dark brown tint; surface is moderately gritty with scattered dark mineral specks and few muscovite.	Shale Sandstone hetrolith	25.14	1.15	6.44	136.13
34	113064	60.45	Ferruginous Tuffite layer, fine grained predominantly composed of clay rich material and within this, a few elongated black streaks are observed, possibly representing glass shards	Shale Sandstone hetrolith	25.17	2.28	17.44	150.04
35	113065	63.48	Greyish sandstone; fine medium grained; quartz dominant with muscovite, shale clasts, fossils; greenish yellow to black elongated lath shaped components, possibly carbonaceous, sulfur odor, smelling gun powder	Fossiliferous sandstone	28.12	2.27	13.17	155.32
36	113066	65.25	Dark brownish grey coloured, medium to coarse grained sandstone composed dominantly of coarse quartz grains, with minor dark mineral fragments and patches that impart a slight sulphur (greenish-grey) odour. The sample exhibits a gritty, porous texture, and does not display obvious bedding or veinlets.	Fossiliferous sandstone	27.29	2.29	23.33	156.83

Sl No.	Sample No.	Depth	Sample Description	Host lithology	Li	Be	Sc	V
37	113067	67.79	Ferruginous Tuffite lens within light brown to grey sandstone. The suspected Tuffite lens is fine to medium grained, with prominent concentric banding, patchy color zonation, and evidence of soft-sediment deformation. White calcite veinlets traverse the matrix, localized darker regions suggest minor ferruginous staining. A few elongated black inclusions, possibly glass shards, are also observed. The texture is smooth and consolidated, with well preserved structure.	Fossiliferous sandstone	27.84	3.44	4.60	104.68
38	113068	69.67	Greyish sandstone; fine medium grained; quartz dominant with muscovite, shale clasts, fossils and black patch components, possibly carbonaceous, sulfur odor.	sandstone	56.11	1.30	8.25	92.47
39	113069	70.56	Greyish sandstone; fine medium grained; quartz dominant with muscovite, shale clasts, fossils and black lath shaped components, possibly carbonaceous, sulfur odor.	sandstone	50.80	1.30	9.59	97.89
40	113070	71.64	Fine to very fine grained sandstone beds interbedded with thin laminae and lenses of grey shale. The sandstone units are light grey to whitish,fine to medium grained, composed primarily of quartz, muscovite, shale clast and few iron concretions. A noticeable small patch of clay or mud unit is also observed, representing localized alteration or a mineral filled cavity.	Sandstone dominated heterolith	53.56	1.12	12.87	79.64
41	113071	71.77	Tuffite layer composed of clay material	Sandstone dominated heterolith	56.93	1.68	24.41	166.78
42	113072	74.03	Tuffite layers and or lenses composed primarily of clay material and fractures infilled with black mineral glass shards?? and bottom part few cm is hetrolith part with soft sediment deformation.	Sandstone dominated heterolith	58.70	1.89	23.34	215.63

Sl No.	Sample No.	Depth	Sample Description	Host lithology	Li	Be	Sc	V
43	113073	75.33	Fine to medium grained brownish suspected tuffite layer with subtle ferruginous staining imparting a dark brown tint.	Sandstone dominated heterolith	66.08	1.58	14.36	124.79
44	113074	76.03	Fine to medium grained brownish suspected tuffite layer with subtle ferruginous staining imparting a dark brown tint.	Sandstone dominated heterolith	34.23	1.92	25.59	270.21
45	113075	87.55	Fine to medium grained brownish suspected tuffite layer with subtle ferruginous staining composed primarily of clay material and fractures infilled with black mineral glass shards?? and bottom part few cm is hetrolith part with soft sediment deformation.	Sandstone dominated heterolith	31.90	1.75	22.15	249.64
46	113076	89.20	Fine to medium grained greyish suspected tuffite layers and or lenses composed primarily of clay material and fractures infilled with black mineral glass shards?? and bottom part few cm is hetrolith part with soft sediment deformation.	Sandstone dominated heterolith	50.22	1.91	18.77	205.84
47	113079	92.11	Tuffite layers and or lenses composed primarily of clay material and fractures infilled with black mineral glass shards?? and bottom part few cm is hetrolith part with soft sediment deformation.	Sandstone dominated heterolith	34.96	1.70	25.72	301.82
48	113080	92.45	Tuffite layers and or lenses composed primarily of clay material and fractures infilled with black mineral glass shards?? and bottom part few cm is hetrolith part	Sandstone dominated heterolith	38.13	1.70	22.28	264.51

Sl No.	Sample No.	Depth	Sample Description	Host lithology	Li	Be	Sc	V
49	113078	94.17	Fine to medium grained brownish suspected tuffite layer with subtle ferruginous staining composed primarily of clay material and fractures infilled with black mineral glass shards?? and bottom part few cm is hetrolith part with soft sediment deformation.	Sandstone dominated heterolith	49.37	1.74	22.32	269.30
50	113077	95.55	Fine to medium grained brownish suspected tuffite layer with subtle ferruginous staining composed primarily of clay material and fractures infilled with black mineral glass shards?? and bottom part few cm is hetrolith part with soft sediment deformation.	Sandstone dominated heterolith	25.03	1.51	20.19	233.51
51	113081	96.25	Tuffite layers and or lenses composed primarily of clay material and fractures infilled with black mineral glass shards?? and bottom part few cm is hetrolith part	Sandstone dominated heterolith	26.97	1.51	19.30	237.42
52	113082	97.29	Tuffite layers and or lenses composed primarily of clay material and fractures infilled with black mineral glass shards?? and bottom part few cm is hetrolith part	Sandstone dominated heterolith	49.92	1.94	23.62	221.68
53	113083	98.25	Tuffite layers and or lenses composed primarily of clay material and fractures infilled with black mineral glass shards?? and bottom part few cm is hetrolith part	Sandstone dominated heterolith	49.82	1.53	19.94	145.42
54	113084	99.39	Tuffite layers and or lenses fine to medium grain composed primarily of clay material and fractures infilled with black mineral glass shards?? and bottom part few cm is hetrolith part	Sandstone dominated heterolith	48.64	1.86	23.55	250.18

Sl No.	Sample No.	Depth	Sample Description	Host lithology	Li	Be	Sc	V
55	113085	100.16	Tuffite layers and or lenses composed primarily of clay material and fractures infilled with black mineral glass shards?? and bottom part few cm is hetrolith part with soft sediment deformation.	Sandstone dominated heterolith	19.59	1.48	19.32	246.22
56	113086	101.61	Tuffite layer composed of clay material	Sandstone dominated heterolith	30.19	1.84	27.46	309.64
57	113087	103.28	Tuffite layer composed of clay material	Sandstone dominated heterolith	64.08	2.22	24.08	247.25
58	113088	106.52	Ferruginous Tuffite layer, fine grained predominantly composed of clay rich material and within this, a few elongated black streaks are observed, possibly representing glass shards, minor white veinlets, interpreted as calcium carbonate, are also present.	Sandstone dominated heterolith	37.20	1.98	21.70	216.76
59	113089	107.12	Ferruginous Tuffite layer, fine grained predominantly composed of clay rich material and within this, a few elongated black streaks are observed, possibly representing glass shards.	Sandstone dominated heterolith	21.72	1.58	21.59	216.88
60	113090	108.27	Ferruginous Tuffite layer, fine to medium grained predominantly composed of clay rich material and within this, a few elongated black streaks are observed, possibly representing glass shards.	Shale Sandstone hetrolith	35.28	1.98	31.61	297.82
61	113092	109.44	Suspected Tuffite lense in between the soft sediment deformation part	Shale Sandstone hetrolith	58.52	2.15	21.44	181.83
62	113091	109.76	Fine to medium grained Tuffite layer predominantly composed of clay rich material	Shale Sandstone hetrolith	50.81	2.25	26.51	276.79
63	113093	111.52	Tuffite lense fine grain mainly composed of clay materials with fractures filled with carbonate and black coloured minerals.	Shale Sandstone hetrolith	64.25	1.82	15.56	121.10
64	113094	112.24	Ferruginous Tuffite layer, fine to medium grained predominantly composed of clay rich material and within this, a few elongated black streaks are observed, possibly representing glass shards.	Shale Sandstone hetrolith	44.54	1.95	27.41	211.07

Sl No.	Sample No.	Depth	Sample Description	Host lithology	Li	Be	Sc	V
65	113097	113.96	Tuffite layers are mostly fine to medium grained composed of clay materias,quartz, black elongated minerals.	Sandstone dominated heterolith	66.79	2.45	23.27	243.07
66	113095	114.36	Tuffite layers are mostly fine to medium grained composed of clay materias,quartz, black elongated minerals.	Sandstone dominated heterolith	76.44	2.57	24.61	217.78
67	113096	115.18	Tuffite layers are mostly fine to medium grained composed of clay materias,quartz, black elongated minerals.	Sandstone dominated heterolith	73.47	2.43	24.15	197.65
68	113100	116.64	Tuffite layers are mostly fine to medium grained composed of clay materias,quartz, black elongated minerals.	Sandstone dominated heterolith	59.83	2.25	25.99	250.50
69	113008	119.00	Tuffite layers and or lenses composed primarily of clay material and soft sediment deformation , top part is hetrolith part.	Sandstone dominated heterolith	42.83	1.95	28.45	286.81
70	113009	122.30	Tuffite layers and or lenses composed primarily of clay material and soft sediment deformation , top part is hetrolith part.	Sandstone dominated heterolith	49.80	2.23	26.25	303.62
71	113010	122.64	Tuffite layer mainly composed of clay materials (some lenses are fine grained) with fractures in some lenses or layers filled with carbonate and black coloured minerals.	Sandstone dominated heterolith	29.88	1.77	25.35	245.72
72	113011	123.21	Tuffite layers are mostly fine to medium grained composed of clay materias,quartz, black elongated minerals.	Sandstone dominated heterolith	58.49	2.36	29.19	265.20
73	113098	124.56	Tuffite layers are mostly fine to medium grained composed of clay materias,quartz, black elongated minerals.	Sandstone dominated heterolith	46.58	2.03	25.05	268.62
74	113099	126.42	Tuffite layers are mostly fine to medium grained composed of clay materias,quartz, black elongated minerals.	Sandstone dominated heterolith	40.76	1.99	35.52	272.72

Sl No.	Sample No.	Depth	Sample Description	Host lithology	Li	Be	Sc	V
75	113361	126.45	composite sample of Shale Sandstone hetrolith	Shale Sandstone hetrolith (composite sample)	73.90	2.13	15.31	136.22
76	113012	129.53	Tuffite layer mainly composed of clay materials and black coloured minerals.	Shale Sandstone hetrolith	51.46	2.27	30.66	286.54
77	113013	131.77	Tuffite layer composed of clay materials and black coloured minerals.	Shale Sandstone hetrolith	54.85	1.91	22.17	194.60
78	113014	133.58	Tuffite layer composed of clay materials and black coloured minerals, with hetrolith part at bottom	Shale Sandstone hetrolith	57.72	2.32	31.65	296.48
79	113016	135.52	Tuffite layer composed of clay materials and black coloured minerals.	Shale Sandstone hetrolith	60.03	2.22	27.05	251.66
80	113015	135.93	Tuffite layer composed of clay materials and black coloured minerals.	Shale Sandstone hetrolith	60.92	2.24	25.94	254.55
81	113017	137.21	Tuffite layer composed of clay materials and black coloured minerals.	Shale Sandstone hetrolith	66.86	2.44	28.37	230.32
82	113018	137.82	Tuffite layer composed of clay materials and black coloured minerals.	Shale Sandstone hetrolith	71.86	2.55	28.21	288.76
83	113019	139.46	Tuffite layer composed of clay materials and black coloured minerals.	Shale Sandstone hetrolith	60.49	2.41	26.64	274.05
84	113020	140.29	Tuffite layer composed of clay materials and black coloured minerals.	Shale Sandstone hetrolith	33.33	1.66	20.30	193.52
85	113021	143.13	Tuffite layer composed of clay materials and black coloured minerals.	Shale Sandstone hetrolith	56.41	2.19	32.53	283.09
86	113022	146.00	Tuffite layers/ lenses are mostly fine to medium grained composed of clay materials,quartz, black elongated minerals.	Sandstone dominated heterolith	67.55	2.28	24.61	223.25
87	113023	147.97	Tuffite layers/ lenses are mostly fine to medium grained composed of clay materials,quartz, black elongated minerals.	Sandstone dominated heterolith	62.83	2.23	37.59	188.49

Sl No.	Sample No.	Depth	Sample Description	Host lithology	Li	Be	Sc	V
88	113024	149.54	Tuffite layers/ lenses are mostly fine to medium grained composed of clay materials,quartz, black elongated minerals.	Sandstone dominated heterolith	64.16	2.32	26.63	252.70
89	113025	151.14	Tuffite layers/ lenses are mostly fine to medium grained composed of clay materials,quartz, black elongated minerals.	Shale dominated heterolith	57.29	1.98	25.03	212.64
90	113363	153.40	composite sample of Sandstone dominated hetrolith	Sandstone dominated heterolith (composite sample)	70.76	1.99	15.23	132.49
91	113026	154.64	Tuffite layers/ lenses are mostly fine to medium grained composed of clay materials,quartz, black elongated minerals.	Sandstone dominated heterolith	54.99	2.08	33.15	211.96
92	113027	157.19	Tuffite layers/ lenses are mostly fine to medium grained composed of clay materials,quartz, black elongated minerals.	Shale Sandstone hetrolith	63.02	2.32	27.50	244.98
93	113028	159.19	Tuffite layers/ lenses are mostly fine to medium grained composed of clay materials,quartz, black elongated minerals.	Shale Sandstone hetrolith	55.09	2.52	31.03	361.12
94	113030	161.37	Tuffite layer mainly composed of clay materials	Shale Sandstone hetrolith	31.03	1.75	27.90	262.86
95	113362	162.00	composite sample of Shale Sandstone hetrolith	Shale Sandstone hetrolith (composite sample)	89.09	2.23	15.20	136.71
96	113031	163.72	Tuffite layer mainly composed of clay materials. No ferrugination observed.	Shale Sandstone hetrolith	38.31	2.00	35.58	314.96
97	113029	164.14	Tuffite layer and ferruginous at edges mainly composed of clay materials with fractures filled with carbonates	Shale Sandstone hetrolith	35.04	1.64	25.14	199.30
98	113032	169.94	Tuffite layer mainly composed of clay materials	Shale dominated heterolith	59.85	2.25	30.09	241.06

Table Continued..

Annexure-XXXb

Sl No.	Sample No.	Cr	Mn	Co	Ni	Cu	Zn	Ga	Ge	Se	Rb	Sr	Y	Zr	Nb
1	112451	100.00	-	14.63	47.31	4.90	98.66	15.13	0.23	1.81	16.26	256.54	54.23	72.51	18.71
2	112478	175.71	-	47.62	115.80	7.37	147.77	17.15	0.36	3.13	16.35	123.02	11.74	107.45	9.24
3	112479	95.99	-	97.22	148.48	2.38	160.44	20.13	0.33	0.10	17.03	197.01	9.32	100.98	5.21
4	112480	83.09	-	154.50	207.14	2.87	342.06	25.08	0.34	4.92	16.49	144.02	14.03	128.14	3.88
5	112481	144.55	-	206.86	271.30	3.79	352.34	20.64	0.53	5.96	17.67	130.50	13.58	122.54	7.30
6	112484	58.97	-	13.32	31.55	5.71	70.62	41.35	1.20	1.01	0.10	233.96	44.42	81.43	3.73
7	112195	121.34	360.19	17.10	31.59	7.41	92.23	12.97	0.10	1.16	50.64	146.09	16.46	247.38	27.71
8	109128	182.84	-	14.42	29.91	8.14	97.96	10.37	0.14	0.10	71.58	148.35	13.59	189.20	37.95
9	109134	84.47	-	8.22	20.68	11.14	58.45	19.66	0.23	0.10	33.87	579.75	270.22	9.54	15.05

Sl No.	Sample No.	Cr	Mn	Co	Ni	Cu	Zn	Ga	Ge	Se	Rb	Sr	Y	Zr	Nb
10	109132	99.72	-	13.13	30.34	15.45	156.94	26.19	0.23	0.20	46.43	296.03	178.39	34.15	30.14
11	109137	103.63	-	13.09	34.23	11.05	62.12	31.13	0.38	0.10	63.23	148.73	24.66	103.33	28.32
12	109141	157.02	-	42.79	141.45	25.32	92.72	23.83	0.26	0.11	69.58	252.57	26.10	170.23	54.56
13	112194	94.57	235.26	4.08	11.35	1.51	69.50	7.83	0.10	0.85	0.10	148.72	15.65	31.22	19.20
14	109140	102.32	-	1.03	2.85	0.10	23.26	3.99	0.10	0.83	0.10	140.42	5.07	23.51	2.29
15	109142	91.75	-	5.17	12.18	0.10	73.67	20.37	0.42	0.10	0.10	223.55	20.20	72.53	10.19
16	109144	119.11	-	9.44	23.85	2.77	99.79	24.99	0.35	0.10	15.03	232.49	44.37	115.22	20.78
17	109143	93.25	-	9.52	23.65	5.46	61.65	19.99	0.38	0.90	20.47	194.54	21.77	98.10	20.42
18	112196	137.72	306.40	20.23	38.39	16.81	118.30	21.58	0.12	0.26	47.02	201.44	23.75	166.93	31.78
19	109145	254.20	-	11.36	21.82	5.73	102.19	18.23	0.26	0.10	38.15	232.83	42.69	127.48	22.74

Sl No.	Sample No.	Cr	Mn	Co	Ni	Cu	Zn	Ga	Ge	Se	Rb	Sr	Y	Zr	Nb
20	109146	82.49	-	7.05	17.74	1.46	93.95	28.07	0.42	0.31	4.70	246.02	317.27	21.86	12.97
21	112151	139.91	-	12.89	25.96	15.14	49.40	15.72	0.14	0.10	90.46	171.28	10.76	131.92	33.82
22	112150	203.68	-	15.87	44.49	5.75	73.72	16.55	0.12	0.10	4.59	168.59	124.51	59.28	12.57
23	112154	84.00	-	7.71	16.44	0.80	34.21	27.90	0.58	0.10	12.21	176.46	17.65	101.67	17.65
24	112158	86.54	-	6.04	9.25	0.10	24.47	22.28	0.46	0.84	6.55	162.68	11.59	162.30	17.90
25	113051	69.31	-	4.01	16.29	0.10	46.47	6.10	0.10	0.10	86.71	148.64	27.05	74.18	6.48
26	113052	54.86	-	4.33	20.78	0.10	60.06	9.73	1.67	27.36	33.50	185.95	72.32	99.67	6.02
27	113053	115.24	-	7.24	16.07	0.10	69.87	7.25	2.23	25.81	69.19	156.83	21.46	82.53	8.63
28	113054	54.51	-	2.73	16.89	0.10	43.52	16.32	1.76	0.10	91.36	207.73	69.84	19.62	6.85
29	113056	110.91	-	2.85	1.94	0.10	30.39	0.10	3.54	0.10	0.10	198.11	17.22	125.05	4.62

Sl No.	Sample No.	Cr	Mn	Co	Ni	Cu	Zn	Ga	Ge	Se	Rb	Sr	Y	Zr	Nb
30	113055	142.70	-	7.45	16.80	0.10	155.23	13.48	0.88	0.10	31.91	255.57	20.71	181.88	10.48
31	113057	71.95	-	3.11	2.79	0.10	61.65	6.40	1.65	0.10	37.56	292.65	11.24	73.55	2.04
32	113062	139.42	-	6.50	7.23	0.10	121.59	5.58	1.03	0.10	0.10	125.94	5.23	70.73	4.00
33	113063	76.94	-	4.08	21.94	0.10	53.28	9.26	0.90	0.10	105.53	419.47	30.46	19.75	6.32
34	113064	127.25	-	7.26	27.90	0.10	98.44	38.22	1.84	0.10	0.10	73.89	22.19	179.98	14.67
35	113065	210.17	-	3.11	27.39	0.10	51.32	16.56	0.10	0.10	0.10	34.40	21.53	224.13	17.40
36	113066	142.74	-	23.84	61.58	33.64	288.15	20.17	2.18	49.27	0.10	95.93	27.44	188.71	16.07
37	113067	131.40	-	6.51	26.30	0.10	120.45	20.61	1.61	0.10	0.10	28.07	7.13	86.20	4.92
38	113068	332.20	-	15.24	27.08	19.82	53.81	14.23	0.15	0.10	69.60	446.22	12.18	222.14	71.36
39	113069	158.65	-	16.23	32.09	18.11	62.56	14.94	0.20	0.10	70.15	171.53	14.28	223.85	36.03

Sl No.	Sample No.	Cr	Mn	Co	Ni	Cu	Zn	Ga	Ge	Se	Rb	Sr	Y	Zr	Nb
40	113070	209.85	-	16.45	33.55	18.47	115.65	13.35	0.20	0.10	65.93	116.09	16.31	223.30	46.72
41	113071	143.77	-	15.59	24.79	18.02	68.62	20.34	0.57	0.10	64.61	141.92	23.89	204.28	34.24
42	113072	96.93	-	13.31	26.35	14.89	80.91	25.64	0.61	0.10	54.04	157.72	22.35	142.06	22.99
43	113073	112.93	-	16.38	28.06	19.48	201.71	18.57	0.15	0.40	70.34	158.12	19.10	223.94	27.99
44	113074	83.76	-	8.92	15.45	5.52	28.27	30.96	0.96	0.10	28.22	208.38	23.97	94.86	17.96
45	113075	83.53	-	10.13	19.73	10.30	39.02	26.03	0.76	0.10	38.22	162.73	26.52	114.54	19.54
46	113076	92.40	-	12.52	26.38	16.12	50.79	25.57	0.69	0.11	58.89	161.65	26.83	126.09	22.83
47	113079	86.47	-	8.51	16.86	6.73	26.38	29.60	1.04	0.10	31.33	173.79	20.46	102.40	18.88
48	113080	85.18	-	9.26	17.61	7.71	28.78	28.64	0.84	0.10	35.51	194.30	22.31	106.14	19.51
49	113078	117.70	-	6.97	11.75	4.21	22.96	30.77	1.03	0.13	19.01	171.35	13.60	74.29	23.87

Sl No.	Sample No.	Cr	Mn	Co	Ni	Cu	Zn	Ga	Ge	Se	Rb	Sr	Y	Zr	Nb
50	113077	83.18	-	8.68	15.57	7.17	192.27	26.89	0.95	0.10	30.39	180.60	16.86	70.99	17.85
51	113081	83.73	-	8.71	16.93	7.46	36.11	26.24	1.04	0.10	30.85	182.85	18.38	48.94	19.95
52	113082	89.11	-	12.16	23.25	15.99	45.89	24.92	0.62	0.10	58.50	156.37	54.59	32.78	24.63
53	113083	99.16	-	14.33	25.71	19.22	111.89	19.04	0.47	0.10	67.85	193.66	21.43	181.92	25.76
54	113084	109.14	-	11.72	22.70	14.62	33.17	27.00	0.63	1.15	53.34	163.08	18.56	120.43	25.31
55	113085	77.06	-	6.51	9.70	4.42	20.11	31.79	1.13	0.10	18.54	190.16	13.02	82.12	14.67
56	113086	105.78	-	8.79	15.72	8.98	28.08	27.80	0.97	0.10	34.02	159.81	31.93	117.80	24.78
57	113087	111.61	-	14.53	29.94	19.07	38.23	27.97	0.57	0.10	66.59	165.18	22.64	125.79	25.50
58	113088	92.52	-	9.71	19.11	11.96	933.67	29.42	0.91	1.19	37.53	193.10	17.94	90.95	21.09
59	113089	82.42	-	5.95	9.28	2.73	19.54	32.69	1.15	0.10	13.52	214.93	15.45	71.87	18.01

Sl No.	Sample No.	Cr	Mn	Co	Ni	Cu	Zn	Ga	Ge	Se	Rb	Sr	Y	Zr	Nb
60	113090	114.76	-	8.00	18.07	7.35	37.26	29.62	0.84	0.10	28.97	159.03	22.64	116.07	5.93
61	113092	184.02	-	16.61	38.27	19.52	131.06	26.89	0.51	0.10	74.25	173.91	22.88	155.94	10.72
62	113091	138.36	-	12.01	29.41	16.43	44.36	29.48	0.75	0.10	52.92	170.81	21.55	142.20	7.42
63	113093	147.84	-	15.50	36.44	24.06	67.68	22.46	0.23	0.10	81.72	228.41	19.66	152.36	8.47
64	113094	145.44	-	11.55	28.14	13.27	237.48	26.38	0.61	0.10	49.42	196.56	21.58	113.26	7.87
65	113097	117.40	-	13.90	31.02	24.33	79.24	28.64	0.54	0.39	74.14	181.76	27.84	150.91	6.63
66	113095	140.69	-	14.76	34.05	27.98	73.90	29.97	0.43	0.10	83.95	169.37	23.52	145.94	8.15
67	113096	117.45	-	15.91	37.26	27.20	58.67	28.04	0.33	0.10	87.86	206.88	25.52	154.86	7.12
68	113100	106.85	-	13.48	30.76	19.75	62.29	28.48	0.57	0.58	69.40	168.52	27.52	149.70	6.52
69	113008	103.15	-	8.86	19.38	10.38	36.23	29.42	0.82	0.10	37.34	174.83	20.42	116.22	5.55

Sl No.	Sample No.	Cr	Mn	Co	Ni	Cu	Zn	Ga	Ge	Se	Rb	Sr	Y	Zr	Nb
70	113009	118.97	-	11.43	25.38	14.26	46.36	29.98	0.71	0.10	49.20	165.25	27.80	137.30	7.11
71	113010	81.41	-	5.73	12.03	2.33	24.22	35.92	1.21	0.10	12.89	195.47	17.60	62.10	4.01
72	113011	136.80	-	14.27	32.93	19.63	68.94	28.50	0.59	0.10	64.13	154.64	24.12	136.87	8.24
73	113098	109.51	-	11.46	25.54	13.85	59.15	27.90	0.63	0.10	50.57	156.50	21.59	135.93	5.40
74	113099	114.50	-	12.17	27.95	13.48	43.78	26.22	0.68	0.10	41.76	179.46	102.76	161.19	7.21
75	113361	101.78	-	21.74	46.85	28.31	93.74	30.32	0.27	3.13	94.23	172.59	20.35	185.18	6.59
76	113012	106.84	-	12.70	28.27	16.97	46.61	28.70	0.72	0.10	61.70	139.31	28.17	138.67	6.30
77	113013	137.64	-	14.63	31.49	19.55	56.37	24.48	0.52	0.10	68.44	164.92	23.94	181.70	8.38
78	113014	116.47	-	12.95	29.29	18.62	47.21	30.59	0.66	0.10	68.63	149.49	33.11	134.04	7.47
79	113016	100.15	-	13.75	31.87	21.99	63.47	29.91	0.61	0.10	71.88	154.94	59.79	146.75	6.59

Sl No.	Sample No.	Cr	Mn	Co	Ni	Cu	Zn	Ga	Ge	Se	Rb	Sr	Y	Zr	Nb
80	113015	133.22	-	13.21	30.49	20.37	66.90	28.73	0.61	0.41	67.63	165.36	22.90	126.92	8.07
81	113017	110.37	-	14.92	34.27	23.56	72.74	29.95	0.64	0.10	74.91	157.84	30.19	125.23	6.59
82	113018	144.08	-	15.73	35.83	23.94	50.32	31.18	0.65	1.61	81.54	157.85	25.70	137.54	8.98
83	113019	124.10	-	13.74	29.92	34.25	137.20	30.50	0.61	0.10	75.44	142.33	29.47	154.62	7.85
84	113020	80.44	-	6.32	12.27	3.54	24.00	35.88	1.28	0.28	16.46	190.36	16.52	65.56	4.24
85	113021	104.21	-	12.36	28.03	18.02	49.18	30.00	0.64	0.10	58.70	173.55	143.20	154.33	7.00
86	113022	128.17	-	16.56	36.42	25.03	64.24	28.42	0.49	0.10	86.59	167.35	27.02	188.34	8.21
87	113023	112.88	-	14.72	33.15	24.11	86.11	25.78	0.38	0.81	77.66	243.31	258.22	196.99	8.70
88	113024	109.24	-	15.44	34.93	22.55	52.41	30.45	0.56	0.90	75.23	149.20	37.42	141.36	6.26
89	113025	110.52	-	14.02	31.21	18.67	60.69	28.41	0.57	0.61	64.51	173.52	23.84	125.21	7.05

Sl No.	Sample No.	Cr	Mn	Co	Ni	Cu	Zn	Ga	Ge	Se	Rb	Sr	Y	Zr	Nb
90	113363	99.14	-	21.34	44.17	28.44	88.28	28.92	0.14	3.20	97.42	169.26	21.99	184.41	7.27
91	113026	92.56	-	12.94	29.30	19.55	92.73	25.84	0.53	0.10	65.73	223.39	118.41	197.81	6.11
92	113027	112.91	-	15.44	34.28	20.64	58.91	29.24	0.57	0.10	68.80	161.24	34.56	142.29	6.61
93	113028	145.42	-	12.41	38.42	16.47	42.97	32.69	0.71	0.10	49.60	140.37	24.99	157.62	8.09
94	113030	84.69	-	6.88	13.82	4.42	55.05	33.73	1.12	0.10	20.47	161.30	18.18	80.43	4.40
95	113362	105.96	-	23.98	50.20	32.71	94.03	31.18	0.30	0.48	105.45	182.81	23.65	196.47	7.03
96	113031	120.27	-	10.31	20.11	11.20	78.47	30.26	0.72	0.10	36.76	201.06	135.08	154.14	7.56
97	113029	89.22	-	8.24	21.46	8.70	549.56	29.70	1.10	0.10	32.05	202.21	18.51	95.35	5.01
98	113032	118.43	-	14.58	33.17	20.92	55.16	29.55	0.53	0.10	67.15	162.78	32.14	130.77	6.70

Table Continued..

Annexure-XXXb

Sl No.	Sample No.	Mo	Ag	Cd	In	Sn	Sb	Te	Cs	Ba	La	Ce	Pr	Nd	Sm
1	112451	0.78	-	2.82	6.98	28.12	4.86	13.49	0.10	559.59	35.11	81.28	22.28	15.59	11.40
2	112478	1.92	2.13	3.37	7.91	61.33	8.35	11.65	2.34	571.22	16.54	32.81	17.35	17.46	5.19
3	112479	3.92	2.43	3.35	10.88	31.45	8.92	15.51	2.96	833.14	18.08	39.35	23.43	16.68	6.98
4	112480	1.09	3.40	4.83	13.49	26.66	10.15	19.71	2.72	974.95	20.54	41.92	28.40	20.19	8.10
5	112481	0.61	3.43	4.03	10.82	50.61	9.90	15.93	3.05	965.34	18.19	47.80	24.28	18.64	6.96
6	112484	1.77	1.89	4.88	20.30	0.10	13.66	30.44	5.53	169.26	46.91	108.35	46.29	45.82	18.74
7	112195	0.67	0.89	0.19	0.05	27.21	2.68	5.84	6.19	537.58	44.03	109.54	10.64	51.23	7.65
8	109128	0.56	-	2.16	2.76	63.59	2.25	-	17.61	497.54	41.42	87.73	6.42	31.62	6.39
9	109134	0.44	-	2.73	7.79	20.95	4.68	-	105.57	154.58	120.54	257.41	42.41	12.54	33.56

Sl No.	Sample No.	Mo	Ag	Cd	In	Sn	Sb	Te	Cs	Ba	La	Ce	Pr	Nd	Sm
10	109132	0.20	-	3.27	8.78	24.15	7.22	-	56.65	141.21	92.73	242.23	48.99	25.12	36.66
11	109137	0.28	-	4.12	12.21	27.04	9.10	-	6.67	153.41	29.03	51.23	35.70	23.60	10.82
12	109141	3.18	-	2.32	5.88	49.87	4.82	-	28.39	310.18	70.69	158.14	19.82	45.47	11.97
13	112194	0.10	0.12	0.40	0.06	19.94	2.65	9.48	0.15	67.92	20.54	70.82	19.58	29.30	8.61
14	109140	0.18	-	1.76	3.48	34.51	1.71	-	0.10	34.35	12.07	18.18	13.06	1.91	2.03
15	109142	0.16	-	4.03	12.22	23.37	8.42	-	47.83	149.52	30.05	74.99	37.43	8.50	12.78
16	109144	0.29	-	4.05	12.43	29.91	8.18	-	24.29	104.09	41.58	109.78	43.35	17.31	18.46
17	109143	0.61	-	3.71	8.71	23.29	5.99	-	31.56	113.91	31.49	72.20	32.50	17.01	11.20
18	112196	1.04	0.60	0.18	0.10	26.98	4.80	11.30	6.31	206.91	42.66	116.08	24.43	53.56	10.33
19	109145	0.14	-	3.12	6.98	82.09	5.82	-	63.47	112.39	47.62	128.82	31.28	18.95	17.93

Sl No.	Sample No.	Mo	Ag	Cd	In	Sn	Sb	Te	Cs	Ba	La	Ce	Pr	Nd	Sm
20	109146	0.11	-	3.98	14.28	19.10	12.12	-	83.37	64.60	75.44	281.46	72.70	10.81	62.83
21	112151	1.08	-	1.56	3.06	48.52	4.85	-	5.26	312.47	24.87	49.16	5.45	28.18	3.50
22	112150	3.63	-	2.01	4.66	68.97	4.37	-	67.40	106.09	26.03	97.25	21.43	10.47	24.31
23	112154	0.18	-	4.65	15.61	16.90	11.73	-	7.28	108.62	22.33	39.52	43.59	14.71	11.81
24	112158	0.10	-	4.38	13.38	19.67	9.70	-	26.33	109.39	21.72	45.20	34.85	14.92	10.04
25	113051	0.21	0.05	2.11	0.10	3.53	27.25	-	0.58	85.43	12.81	43.99	4.92	18.47	4.38
26	113052	0.01	0.27	1.19	0.36	0.10	28.43	-	4.32	105.38	33.06	74.06	9.03	35.76	9.07
27	113053	0.48	1.06	2.46	0.54	0.99	27.97	-	4.68	103.27	19.28	52.82	5.21	18.14	3.76
28	113054	0.00	0.05	1.15	0.10	0.10	25.70	-	0.10	96.60	46.18	112.61	12.30	45.21	10.64
29	113056	0.70	0.50	1.32	0.33	2.50	32.57	-	1.45	84.48	16.36	51.62	4.26	13.74	2.54

Sl No.	Sample No.	Mo	Ag	Cd	In	Sn	Sb	Te	Cs	Ba	La	Ce	Pr	Nd	Sm
30	113055	0.30	0.94	1.15	0.10	2.63	23.81	-	4.08	116.92	37.05	85.20	8.58	30.07	6.16
31	113057	0.22	8.50	2.32	0.10	1.19	29.54	-	0.10	76.07	14.88	48.95	5.09	17.86	3.45
32	113062	0.30	0.32	0.87	0.10	1.67	27.63	-	0.10	114.03	10.86	29.61	1.79	10.79	0.54
33	113063	0.10	0.05	1.41	0.19	1.87	28.39	-	0.10	142.79	37.47	96.76	9.09	34.49	7.86
34	113064	1.23	0.05	1.39	0.06	7.47	28.74	-	0.10	146.09	86.90	156.22	13.19	40.16	4.09
35	113065	0.10	0.05	0.77	0.43	7.14	33.25	-	0.10	74.75	63.81	118.02	13.73	50.52	7.50
36	113066	3.32	0.05	0.55	0.30	3.67	31.94	-	1.56	2710.53	54.24	100.26	11.54	39.63	6.11
37	113067	1.76	0.05	1.45	0.04	1.89	24.06	-	0.10	59.12	18.85	35.99	2.51	14.07	2.13
38	113068	0.93	0.78	1.31	2.49	128.39	2.10	-	23.82	244.66	45.38	121.17	1.78	49.44	7.58
39	113069	1.05	0.76	1.69	2.67	58.04	2.01	-	22.92	239.28	32.52	78.70	1.38	36.34	5.58

Sl No.	Sample No.	Mo	Ag	Cd	In	Sn	Sb	Te	Cs	Ba	La	Ce	Pr	Nd	Sm
40	113070	1.24	0.74	1.67	2.22	78.82	2.88	-	23.09	312.19	31.00	72.97	1.27	33.30	5.91
41	113071	0.35	0.62	2.29	7.33	45.35	5.52	-	21.98	276.03	33.53	71.67	3.31	34.63	8.22
42	113072	0.47	0.62	2.98	12.20	25.01	6.37	-	16.33	182.00	26.92	52.18	4.83	29.87	8.61
43	113073	0.70	0.68	2.23	3.87	36.99	3.82	-	25.33	292.78	39.14	87.67	2.18	42.78	7.70
44	113074	0.21	0.56	3.53	18.39	18.85	10.28	-	9.51	104.66	18.70	39.73	7.18	23.97	11.39
45	113075	0.27	0.54	3.94	15.19	19.69	9.87	-	12.79	127.78	21.96	49.35	6.09	30.26	12.85
46	113076	0.59	0.55	3.30	11.80	26.85	6.43	-	16.93	150.78	25.72	52.71	4.94	32.61	11.83
47	113079	0.10	0.50	3.91	16.98	19.10	9.18	-	10.21	111.94	17.44	32.78	6.92	21.40	10.96
48	113080	0.30	0.54	4.17	15.94	22.46	7.86	-	10.32	126.78	20.53	41.02	6.66	26.65	10.82
49	113078	0.22	0.48	4.46	19.47	30.29	10.95	-	7.30	101.60	12.20	22.86	7.35	15.90	9.20

Sl No.	Sample No.	Mo	Ag	Cd	In	Sn	Sb	Te	Cs	Ba	La	Ce	Pr	Nd	Sm
50	113077	0.17	0.35	4.30	16.26	20.78	8.21	-	10.49	134.35	18.21	31.30	5.98	22.03	9.05
51	113081	0.39	0.38	4.24	16.44	21.45	8.93	-	11.06	145.39	19.16	35.37	6.31	22.83	9.74
52	113082	0.39	0.05	3.22	10.91	20.38	5.42	-	18.79	171.89	36.06	90.61	5.28	56.72	18.91
53	113083	0.71	0.66	2.38	5.99	31.16	2.42	-	21.44	248.13	33.21	72.02	2.84	38.73	7.92
54	113084	0.26	0.53	3.46	14.17	30.73	6.21	-	15.14	154.18	22.87	41.82	5.29	26.17	9.34
55	113085	0.10	0.67	4.95	19.64	18.59	11.92	-	7.16	105.20	13.73	27.69	7.62	16.03	10.19
56	113086	0.31	0.47	4.17	16.63	26.12	9.54	-	11.22	119.95	21.23	52.02	6.88	31.59	15.53
57	113087	0.41	0.54	3.50	11.41	30.37	6.66	-	18.03	163.22	25.21	46.48	4.82	28.39	8.63
58	113088	0.36	0.49	5.87	16.17	22.24	8.92	-	11.79	167.84	19.93	33.38	6.31	20.91	9.68
59	113089	0.23	0.58	5.11	20.72	18.49	11.30	-	5.82	103.92	13.03	29.61	7.94	17.13	10.64

Sl No.	Sample No.	Mo	Ag	Cd	In	Sn	Sb	Te	Cs	Ba	La	Ce	Pr	Nd	Sm
60	113090	0.41	1.44	3.56	14.59	28.34	9.15	-	8.26	125.62	17.83	35.32	32.65	23.79	9.24
61	113092	0.98	1.46	2.49	7.54	54.69	8.08	-	18.64	259.64	31.94	59.81	14.92	39.99	7.36
62	113091	0.69	1.47	2.88	12.02	36.51	9.49	-	13.73	175.18	23.56	42.67	26.20	31.65	8.46
63	113093	1.05	1.20	1.84	4.89	47.76	5.62	-	17.92	312.38	34.69	73.06	12.03	40.28	6.88
64	113094	0.78	1.33	2.99	10.37	40.91	8.16	-	11.62	235.91	24.04	43.29	23.46	29.69	7.35
65	113097	0.96	1.35	2.52	8.30	34.29	7.84	-	17.57	206.74	30.23	59.88	20.62	41.27	8.84
66	113095	1.05	1.41	2.21	7.56	42.74	7.15	-	20.53	220.94	30.86	58.90	17.60	38.95	7.70
67	113096	0.99	1.29	2.03	6.69	35.45	5.59	-	21.60	240.32	34.71	69.33	16.62	42.46	8.81
68	113100	0.73	1.40	2.91	9.22	28.93	7.00	-	16.31	210.36	26.85	52.98	21.58	36.07	9.05
69	113008	0.52	1.12	3.55	13.96	23.74	9.18	-	11.02	158.59	21.64	39.17	31.04	27.17	9.89

Sl No.	Sample No.	Mo	Ag	Cd	In	Sn	Sb	Te	Cs	Ba	La	Ce	Pr	Nd	Sm
70	113009	0.48	1.60	3.35	11.84	30.67	10.61	-	13.04	172.95	24.74	47.74	27.69	33.14	11.01
71	113010	0.13	1.36	4.49	18.78	16.07	13.65	-	4.72	96.43	12.80	28.13	41.49	19.21	10.51
72	113011	0.95	1.52	2.68	9.10	39.84	8.59	-	15.28	205.44	28.24	54.87	22.56	34.73	8.21
73	113098	0.62	1.44	3.19	11.35	28.11	7.44	-	11.71	171.52	23.14	43.32	25.00	29.25	8.32
74	113099	0.34	1.12	2.67	10.60	27.65	7.92	-	12.79	189.36	35.61	110.48	26.44	72.57	24.02
75	113361	1.43	1.74	1.97	4.42	34.75	5.81	-	22.75	305.99	39.82	84.80	10.26	44.63	7.83
76	113012	0.60	1.76	2.80	10.57	27.47	8.05	-	15.15	173.10	24.93	46.88	25.46	32.68	10.37
77	113013	0.77	1.73	2.42	7.04	43.41	6.69	-	17.45	235.38	32.04	64.21	17.83	40.18	7.92
78	113014	0.44	1.36	2.88	10.84	30.44	9.02	-	15.22	184.21	25.68	49.04	24.52	35.18	10.36
79	113016	0.76	1.31	3.12	9.60	26.70	8.75	-	16.96	194.91	30.25	73.69	24.64	55.36	17.19

Sl No.	Sample No.	Mo	Ag	Cd	In	Sn	Sb	Te	Cs	Ba	La	Ce	Pr	Nd	Sm
80	113015	0.70	1.35	2.81	9.62	39.98	7.66	-	15.96	198.52	27.71	52.55	23.18	34.17	8.61
81	113017	0.81	1.21	2.73	8.57	30.99	7.83	-	17.32	202.32	30.54	61.15	20.88	38.96	9.67
82	113018	1.08	1.36	2.96	8.79	41.96	9.52	-	18.00	199.07	30.48	59.30	22.41	37.66	9.35
83	113019	0.92	5.01	2.91	9.41	33.10	9.92	-	17.34	248.05	27.23	53.91	22.02	37.24	9.56
84	113020	0.42	1.36	4.62	18.33	16.40	11.98	-	5.81	109.55	14.16	27.15	40.43	20.13	10.53
85	113021	0.84	1.02	3.04	10.69	25.15	8.19	-	15.29	187.16	47.72	142.33	29.87	88.30	27.84
86	113022	0.94	1.65	2.44	7.21	38.98	6.36	-	21.11	258.92	38.00	79.92	18.77	47.53	9.46
87	113023	1.08	1.78	2.11	5.98	31.69	5.20	-	20.23	233.17	96.08	260.12	27.01	120.47	30.13
88	113024	0.88	1.76	2.72	9.81	29.97	9.34	-	17.95	192.87	33.79	69.97	23.03	45.89	11.19
89	113025	0.78	1.96	2.82	9.90	31.17	8.45	-	16.54	213.58	28.56	54.70	22.93	35.51	9.04

Sl No.	Sample No.	Mo	Ag	Cd	In	Sn	Sb	Te	Cs	Ba	La	Ce	Pr	Nd	Sm
90	113363	1.42	1.36	1.73	3.75	34.36	4.34	-	22.95	290.94	39.71	85.63	10.81	44.64	7.15
91	113026	0.98	1.56	2.58	7.38	23.93	6.85	-	16.85	210.06	67.33	168.69	24.42	83.47	20.02
92	113027	0.97	1.86	2.59	8.90	32.90	8.65	-	17.84	225.85	32.07	64.66	21.04	43.28	9.66
93	113028	6.38	2.40	2.92	12.31	40.56	9.58	-	13.28	159.00	25.51	47.31	28.31	31.09	9.44
94	113030	0.42	1.40	4.50	16.90	18.51	12.94	-	6.59	114.17	11.24	20.11	36.93	17.52	8.64
95	113362	1.56	1.79	1.57	3.50	37.60	4.38	-	25.39	310.78	45.21	96.85	9.78	50.47	8.21
96	113031	0.53	0.94	3.48	13.19	28.74	10.67	-	12.32	169.47	40.03	122.07	35.81	77.12	25.32
97	113029	0.44	1.48	4.61	13.77	20.80	10.90	-	9.67	132.80	20.21	39.08	30.07	24.01	9.24
98	113032	0.96	1.37	2.56	8.69	33.47	9.31	-	17.24	190.49	28.30	56.63	22.63	36.99	8.98

Table Continued..

Annexure-XXXb

Sl No.	Sample No.	Eu	Gd	Tb	Dy	Ho	Er	Tm	Yb	Lu	Hf	Ta	W	Tl	Pb	Bi	Th	U	HREEY	LREE	TREEY	HREEY/LREE
1	112451	2.44	11.19	2.45	9.43	1.27	3.50	0.12	2.54	0.23	3.30	2.15	0.23	0.05	27.82	0.48	22.10	17.46	107.80	165.66	273.45	0.65
2	112478	0.51	10.94	1.17	4.87	0.40	0.75	0.10	1.64	0.20	4.63	3.06	1.34	5.98	4.97	1.25	27.32	20.27	36.96	89.35	126.31	0.41
3	112479	0.60	14.15	1.42	7.08	0.51	0.87	0.10	1.85	0.27	5.26	3.91	1.54	10.82	4.84	1.20	35.50	28.13	41.21	104.52	145.73	0.39
4	112480	0.59	17.63	1.75	9.34	0.73	1.11	0.10	2.36	0.33	6.22	4.27	2.45	11.65	7.71	1.46	43.82	37.57	55.12	119.15	174.27	0.46
5	112481	0.50	14.82	1.49	9.97	0.49	0.91	0.10	2.08	0.28	6.17	4.13	2.14	15.75	7.94	1.94	36.60	30.74	48.10	115.87	163.97	0.42
6	112484	2.59	27.16	2.31	7.77	0.10	2.24	0.10	3.96	0.47	2.35	5.09	1.03	0.92	29.25	3.11	58.81	58.50	99.81	266.11	365.92	0.38
7	112195	1.07	5.95	0.63	3.50	0.41	2.64	0.20	1.65	0.20	7.96	1.38	3.21	0.93	24.48	0.10	17.84	1.36	42.97	223.09	266.06	0.19
8	109128	0.96	3.18	1.17	2.88	0.47	2.28	0.19	0.89	0.05	6.55	0.94	0.32	0.05	13.69	0.50	8.08	0.10	33.48	173.59	207.07	0.19
9	109134	8.11	21.99	4.75	37.43	4.47	###	0.19	6.21	0.29	0.94	1.40	0.10	0.05	9.29	0.10	21.13	14.44	389.69	466.46	856.15	0.84

Sl No.	Sample No.	Eu	Gd	Tb	Dy	Ho	Er	Tm	Yb	Lu	Hf	Ta	W	Tl	Pb	Bi	Th	U	HREEY	LREE	TREEY	HREEY/LREE
10	109132	8.56	22.95	4.95	31.19	4.34	8.42	0.21	4.93	0.32	0.94	2.53	0.26	0.05	10.63	0.10	27.31	18.08	289.75	445.73	735.48	0.65
11	109137	1.67	15.99	3.59	4.27	0.10	2.32	0.14	2.56	0.39	2.96	4.04	0.17	0.77	11.98	1.28	40.20	40.80	78.93	150.38	229.31	0.52
12	109141	1.98	8.29	3.10	5.04	0.59	3.61	0.16	2.19	0.18	5.34	2.20	0.30	1.29	103.10	0.10	21.60	6.39	63.61	306.10	369.71	0.21
13	112194	1.66	6.32	0.29	3.71	0.55	1.43	0.10	1.59	0.30	0.78	1.36	0.96	1.37	23.61	0.10	20.67	6.85	36.21	148.85	185.07	0.24
14	109140	0.43	2.96	0.51	0.82	0.10	0.47	0.20	0.47	0.06	0.91	1.07	0.10	0.21	4.16	0.57	7.58	4.58	12.80	47.25	60.05	0.27
15	109142	2.00	15.03	2.80	4.12	0.62	1.52	0.16	2.03	0.35	1.78	3.12	0.26	0.05	12.54	0.81	36.39	39.67	57.59	163.75	221.34	0.35
16	109144	3.47	18.27	3.46	9.25	1.33	3.12	0.16	2.98	0.39	3.14	3.58	0.21	0.65	16.23	1.21	40.34	40.94	107.95	230.48	338.43	0.47
17	109143	1.82	13.62	2.77	4.40	0.10	2.17	0.16	2.19	0.33	2.55	3.41	0.11	0.05	12.75	0.56	33.14	30.89	66.52	164.40	230.93	0.40
18	112196	2.03	6.53	0.78	4.78	0.69	2.80	0.30	2.85	0.46	4.62	2.61	2.06	0.52	32.87	0.10	53.22	8.86	58.90	247.06	305.95	0.24
19	109145	3.69	12.96	2.71	10.08	1.21	3.42	0.13	2.87	0.25	3.25	2.70	0.10	0.38	17.48	0.10	26.17	18.02	107.23	244.60	351.83	0.44

Sl No.	Sample No.	Eu	Gd	Tb	Dy	Ho	Er	Tm	Yb	Lu	Hf	Ta	W	Tl	Pb	Bi	Th	U	HREEY	LREE	TREEY	HREEY/LREE
20	109146	14.16	41.24	8.58	59.61	8.51	###	0.37	8.04	0.56	1.10	3.95	0.10	0.05	9.93	0.26	49.20	53.96	491.38	503.24	994.62	0.98
21	112151	0.89	2.96	1.36	2.00	0.25	2.01	0.15	1.00	0.07	4.15	1.11	0.12	1.43	12.77	0.10	7.75	0.10	29.28	111.16	140.45	0.26
22	112150	7.87	13.67	3.15	26.63	2.19	6.48	0.21	4.09	0.14	0.74	2.28	0.12	0.05	11.90	0.10	9.66	5.21	212.49	179.50	391.99	1.18
23	112154	1.24	19.72	3.73	2.68	0.43	1.54	0.13	2.27	0.48	2.31	3.83	0.10	0.05	9.96	0.10	51.01	59.10	63.58	131.96	195.54	0.48
24	112158	1.15	16.50	3.14	1.34	0.10	1.41	0.14	1.90	0.40	3.55	2.87	0.10	0.05	9.31	0.10	43.17	46.24	46.03	126.73	172.76	0.36
25	113051	1.31	5.48	0.84	4.01	0.87	3.84	0.48	2.63	0.40	1.47	2.61	1.67	0.06	2.38	0.07	4.71	0.85	61.38	84.57	145.96	0.73
26	113052	1.74	11.49	1.71	10.10	2.31	5.88	1.06	3.68	0.86	1.79	2.67	0.76	0.07	5.43	0.08	5.87	1.11	137.68	160.97	298.66	0.86
27	113053	1.68	6.03	0.49	4.66	0.97	2.96	0.79	2.09	0.47	2.06	3.26	1.83	0.05	4.47	0.12	7.32	1.09	55.44	99.21	154.65	0.56
28	113054	3.15	16.94	1.91	13.33	2.37	8.23	0.99	5.48	0.64	0.64	1.26	1.53	0.06	1.04	0.06	5.02	1.79	145.67	226.93	372.60	0.64
29	113056	0.51	3.01	0.70	3.71	0.91	1.92	0.13	2.76	0.36	2.28	0.53	1.46	0.06	3.83	0.04	6.67	1.08	39.35	88.53	127.88	0.44

Sl No.	Sample No.	Eu	Gd	Tb	Dy	Ho	Er	Tm	Yb	Lu	Hf	Ta	W	Tl	Pb	Bi	Th	U	HREEY	LREE	TREEY	HREEY/LREE
30	113055	1.39	4.64	0.77	4.81	0.74	2.66	0.34	2.81	0.47	3.58	3.18	1.99	0.06	5.71	0.06	10.99	1.73	50.12	167.05	217.17	0.30
31	113057	0.10	2.92	0.21	1.81	0.50	2.50	0.12	1.22	0.16	1.91	0.11	0.71	0.07	8.66	0.07	4.91	0.48	29.64	90.23	119.87	0.33
32	113062	0.11	1.05	0.31	0.78	0.46	0.47	0.10	0.87	0.10	2.54	0.30	0.83	0.06	3.64	0.10	7.07	1.00	13.59	53.59	67.18	0.25
33	113063	2.01	14.26	1.29	7.83	1.52	5.38	0.79	2.86	0.28	1.41	0.10	0.91	0.10	2.55	0.10	6.83	1.27	73.13	185.68	258.80	0.39
34	113064	1.08	5.85	0.84	3.59	0.73	5.15	0.44	3.48	0.39	5.32	1.15	2.38	0.05	18.54	0.16	20.35	4.49	61.19	300.57	361.76	0.20
35	113065	1.15	5.71	1.09	5.82	1.22	3.57	0.60	4.18	0.50	5.27	1.03	2.13	0.06	22.22	0.10	28.67	3.92	58.54	253.58	312.12	0.23
36	113066	2.01	6.64	0.92	5.72	1.00	5.77	0.64	4.58	0.43	5.39	0.96	2.40	0.06	31.84	0.10	17.68	11.02	78.46	211.77	290.23	0.37
37	113067	0.44	3.16	0.31	0.96	0.35	1.60	0.14	2.42	0.10	3.41	0.32	4.77	0.06	13.99	0.10	8.92	2.38	21.20	73.56	94.75	0.29
38	113068	1.33	3.12	1.08	3.14	0.47	0.80	0.11	0.98	0.05	5.77	1.48	1.40	2.64	16.81	0.10	7.71	0.11	31.52	225.35	256.87	0.14
39	113069	1.15	3.52	1.15	3.29	0.45	0.95	0.11	1.10	0.06	5.93	1.43	1.79	1.53	17.77	0.10	8.99	0.45	35.66	154.52	190.18	0.23

Sl No.	Sample No.	Eu	Gd	Tb	Dy	Ho	Er	Tm	Yb	Lu	Hf	Ta	W	Tl	Pb	Bi	Th	U	HREEY	LREE	TREEY	HREEY/LREE
40	113070	1.16	3.36	0.94	3.87	0.32	0.88	0.11	1.16	0.05	6.05	1.39	2.04	2.18	23.47	0.10	7.93	0.32	41.03	144.45	185.48	0.28
41	113071	1.58	9.63	1.53	4.85	0.81	1.14	0.11	2.21	0.20	5.23	2.63	1.77	2.94	22.35	0.10	22.70	8.48	70.36	151.36	221.71	0.46
42	113072	1.75	14.46	1.60	4.81	0.86	0.93	0.10	2.27	0.30	3.49	3.68	1.82	1.44	24.86	0.10	32.98	17.96	72.78	122.41	195.19	0.59
43	113073	1.49	5.93	1.16	4.06	0.10	1.03	0.11	1.49	0.11	6.05	1.72	2.75	0.10	25.38	0.10	14.17	2.18	48.95	179.47	228.42	0.27
44	113074	2.01	19.94	1.75	4.58	0.99	0.77	0.10	2.83	0.44	1.97	4.81	1.18	0.05	19.97	1.44	47.73	31.28	82.98	100.97	183.94	0.82
45	113075	2.24	18.41	1.68	5.61	1.01	0.92	0.10	2.57	0.37	2.20	3.82	2.20	0.97	25.54	1.00	39.77	24.06	81.58	120.51	202.09	0.68
46	113076	2.44	15.18	1.69	6.09	0.10	0.98	0.10	2.17	0.29	2.77	3.24	1.93	0.43	20.42	0.87	32.10	16.51	74.65	127.81	202.46	0.58
47	113079	2.06	20.12	1.67	3.75	0.93	0.71	0.10	2.66	0.42	2.15	4.89	0.87	0.60	16.81	3.65	45.19	29.10	78.61	89.50	168.11	0.88
48	113080	2.12	18.28	1.76	4.58	0.90	0.79	0.10	2.55	0.40	2.13	4.09	1.21	2.78	17.41	0.60	43.20	27.50	76.07	105.68	181.76	0.72
49	113078	1.50	21.16	1.71	2.80	0.82	0.54	0.10	2.58	0.46	1.55	4.80	0.32	2.03	22.31	2.95	48.92	32.08	67.59	67.51	135.10	1.00

Sl No.	Sample No.	Eu	Gd	Tb	Dy	Ho	Er	Tm	Yb	Lu	Hf	Ta	W	Tl	Pb	Bi	Th	U	HREEY	LREE	TREEY	HREEY/LREE
50	113077	1.60	17.87	1.68	3.18	0.66	0.66	0.10	2.29	0.38	1.62	4.12	2.48	1.71	17.97	1.63	40.94	24.96	65.47	86.57	152.04	0.76
51	113081	1.81	17.20	1.74	3.94	0.80	0.71	0.10	2.43	0.38	1.10	4.01	1.25	1.94	24.24	1.29	41.37	26.15	66.79	93.41	160.20	0.72
52	113082	4.02	16.90	1.93	11.76	1.69	1.40	0.10	2.78	0.28	0.67	3.09	1.73	2.56	16.33	1.04	29.44	14.95	119.08	207.58	326.66	0.57
53	113083	1.62	8.25	1.22	4.88	0.65	1.05	0.11	1.75	0.15	4.91	2.37	1.88	2.92	16.35	0.10	18.21	6.04	61.05	154.72	215.77	0.39
54	113084	1.68	15.53	1.65	3.28	0.10	0.81	0.10	2.29	0.33	2.65	3.81	0.96	2.44	16.95	0.38	35.14	20.42	67.88	105.49	173.37	0.64
55	113085	1.45	20.55	1.71	2.09	0.10	0.64	0.10	2.53	0.47	1.66	4.30	0.43	0.43	14.46	2.98	50.21	34.56	61.99	75.26	137.25	0.82
56	113086	2.83	20.77	1.75	6.92	0.39	0.88	0.10	2.87	0.41	1.61	4.16	1.43	1.59	13.23	2.29	42.52	28.23	96.32	127.25	223.57	0.76
57	113087	1.92	14.08	1.63	4.45	0.56	0.91	0.10	2.31	0.29	2.88	3.48	1.78	1.92	19.48	0.10	31.07	16.87	72.96	113.53	186.50	0.64
58	113088	1.53	17.14	1.66	3.21	0.10	0.68	0.10	2.49	0.39	2.50	3.73	7.23	0.05	20.12	1.30	41.23	27.08	66.95	90.21	157.16	0.74
59	113089	1.44	21.73	1.75	2.78	0.10	0.57	0.10	2.68	0.50	1.52	4.70	0.97	2.30	15.65	3.35	51.86	37.23	68.70	78.35	147.05	0.88

Sl No.	Sample No.	Eu	Gd	Tb	Dy	Ho	Er	Tm	Yb	Lu	Hf	Ta	W	Tl	Pb	Bi	Th	U	HREEY	LREE	TREEY	HREEY/LREE
60	113090	1.95	19.43	1.89	4.39	0.97	1.99	0.12	2.95	0.32	2.51	4.34	0.77	0.25	36.23	2.89	44.75	34.89	88.26	118.83	207.09	0.74
61	113092	1.58	10.45	1.83	4.65	0.10	2.46	0.12	2.21	0.17	4.59	2.72	1.53	0.81	30.74	0.10	24.53	10.32	67.89	154.02	221.91	0.44
62	113091	2.02	15.47	1.92	4.02	0.10	2.05	0.11	2.55	0.25	3.52	3.98	1.41	1.59	33.54	0.85	35.91	23.92	76.55	132.54	209.09	0.58
63	113093	1.59	6.81	1.32	4.63	0.10	2.30	0.12	1.61	0.10	4.89	2.22	1.31	0.05	33.08	0.10	15.88	4.36	53.80	166.94	220.74	0.32
64	113094	1.73	14.06	1.77	4.46	0.10	1.94	0.11	2.45	0.23	3.23	3.40	1.82	1.46	35.61	0.10	32.61	21.20	75.84	127.83	203.67	0.59
65	113097	2.21	12.46	1.93	6.15	0.87	2.85	0.12	2.37	0.19	4.09	3.03	1.36	0.87	31.21	1.16	27.53	14.94	80.26	160.84	241.10	0.50
66	113095	1.91	10.30	1.78	5.13	0.10	2.46	0.11	2.26	0.16	4.09	2.97	1.64	1.07	33.55	0.10	24.22	11.06	72.34	154.01	226.35	0.47
67	113096	1.99	9.73	1.70	5.66	0.68	2.70	0.11	2.25	0.15	4.67	2.67	1.31	0.77	31.54	0.10	22.03	8.73	74.64	171.93	246.57	0.43
68	113100	2.19	12.99	1.90	6.06	0.94	2.38	0.11	2.43	0.20	4.02	3.63	1.55	1.10	39.11	0.10	28.42	16.49	82.71	146.53	229.24	0.56
69	113008	1.99	18.07	1.90	4.35	0.79	1.93	0.11	2.72	0.29	2.79	4.30	0.73	1.26	31.56	1.35	40.81	31.47	81.02	128.91	209.93	0.63

Sl No.	Sample No.	Eu	Gd	Tb	Dy	Ho	Er	Tm	Yb	Lu	Hf	Ta	W	Tl	Pb	Bi	Th	U	HREEY	LREE	TREEY	HREEY/LREE
70	113009	2.40	15.70	1.90	5.93	1.07	2.62	0.11	2.77	0.26	3.44	3.67	0.82	0.59	31.26	1.21	36.28	25.25	86.81	144.32	231.13	0.60
71	113010	1.53	24.02	2.07	3.47	0.10	1.44	0.12	3.01	0.39	1.60	4.98	0.57	0.62	31.10	3.31	54.23	46.92	79.10	112.14	191.24	0.71
72	113011	2.01	13.05	1.77	5.16	0.88	2.51	0.12	2.55	0.21	3.93	3.27	1.53	0.80	30.36	0.85	29.33	17.92	81.57	148.61	230.18	0.55
73	113098	1.87	14.79	1.77	4.58	0.80	1.95	0.12	2.41	0.24	3.26	3.74	0.86	0.59	35.60	0.10	33.59	22.78	75.17	129.03	204.20	0.58
74	113099	5.61	21.56	2.23	22.13	3.02	5.11	0.12	4.36	0.26	3.64	3.75	0.56	0.83	34.03	0.32	32.85	22.43	202.68	269.12	471.80	0.75
75	113361	1.74	6.57	1.81	4.82	0.50	2.45	0.10	1.86	0.11	5.94	2.31	1.76	0.05	11.59	0.10	15.21	3.03	55.62	187.34	242.96	0.30
76	113012	2.21	15.19	1.90	6.03	1.13	2.81	0.11	2.86	0.24	3.44	3.77	1.36	3.61	31.17	0.84	33.49	22.70	91.31	140.32	231.63	0.65
77	113013	1.86	10.17	1.69	5.33	0.76	2.68	0.12	2.23	0.16	4.94	3.01	1.62	0.56	33.24	0.10	22.67	10.66	71.11	162.18	233.29	0.44
78	113014	2.54	15.19	1.96	7.32	1.22	2.98	0.12	2.94	0.23	3.57	4.01	1.36	2.17	31.05	1.50	32.13	21.27	99.26	144.78	244.04	0.69
79	113016	4.06	17.42	2.11	14.84	1.94	3.74	0.12	3.08	0.22	3.86	3.40	1.38	1.68	31.53	0.51	29.65	17.94	134.37	201.13	335.50	0.67

Sl No.	Sample No.	Eu	Gd	Tb	Dy	Ho	Er	Tm	Yb	Lu	Hf	Ta	W	Tl	Pb	Bi	Th	U	HREEY	LREE	TREEY	HREEY/LREE
80	113015	1.96	13.57	1.86	4.98	0.89	2.31	0.12	2.48	0.22	3.59	3.24	1.08	1.62	31.99	0.95	30.38	18.85	77.23	146.22	223.45	0.53
81	113017	2.19	12.72	1.82	6.63	1.11	2.66	0.12	2.59	0.20	3.52	2.79	1.14	3.24	29.24	0.67	27.12	15.41	88.60	161.20	249.80	0.55
82	113018	2.15	12.93	1.87	5.47	1.00	2.67	0.11	2.60	0.20	3.92	3.54	1.61	2.51	34.46	0.10	28.92	16.79	82.91	159.20	242.11	0.52
83	113019	2.37	13.33	1.90	6.80	1.03	2.65	0.12	2.69	0.21	4.55	3.32	1.97	0.43	77.02	0.56	28.72	17.39	87.21	149.96	237.17	0.58
84	113020	1.37	23.76	2.05	2.90	0.10	1.45	0.12	2.76	0.39	1.79	4.68	0.80	0.06	32.18	1.97	53.49	45.63	71.72	112.40	184.12	0.64
85	113021	6.86	24.23	2.51	31.04	2.93	6.30	0.14	4.53	0.26	3.39	3.50	1.04	1.74	34.99	0.26	31.66	20.63	254.53	336.06	590.59	0.76
86	113022	2.05	10.76	1.52	5.95	0.81	2.91	0.12	2.49	0.17	5.49	2.94	1.09	1.19	35.40	0.10	24.02	11.35	78.41	193.68	272.09	0.40
87	113023	7.83	21.75	2.53	0.17	5.90	9.71	0.17	6.16	0.19	4.34	2.57	1.52	3.65	35.24	0.10	19.30	8.00	350.22	533.81	884.03	0.66
88	113024	2.60	14.00	1.95	1.88	1.11	2.97	0.12	2.67	0.21	3.69	3.75	1.60	2.16	40.45	0.54	29.52	17.33	91.56	183.87	275.43	0.50
89	113025	1.79	13.46	1.87	2.97	0.78	2.58	0.12	2.48	0.22	3.65	3.35	1.21	0.05	35.96	0.55	30.72	18.72	75.14	150.74	225.88	0.50

Sl No.	Sample No.	Eu	Gd	Tb	Dy	Ho	Er	Tm	Yb	Lu	Hf	Ta	W	Tl	Pb	Bi	Th	U	HREEY	LREE	TREEY	HREEY/LREE
90	113363	1.82	5.99	1.76	5.35	0.10	2.47	0.10	1.82	0.10	5.68	2.34	1.75	1.71	10.59	0.10	13.58	2.93	56.73	187.94	244.67	0.30
91	113026	4.85	16.42	1.98	0.10	0.35	5.29	0.13	3.97	0.19	4.17	3.09	1.45	0.60	30.54	0.11	23.45	12.07	184.84	363.93	548.77	0.51
92	113027	2.42	12.90	1.87	0.10	0.96	2.89	0.12	2.63	0.19	3.91	3.46	1.26	1.16	31.25	0.10	27.52	15.57	86.14	170.71	256.85	0.50
93	113028	2.33	16.70	1.90	0.10	0.83	2.10	0.11	2.77	0.27	3.46	3.97	0.86	0.05	32.40	1.48	38.11	27.56	83.13	141.66	224.79	0.59
94	113030	1.42	21.79	1.95	43.13	1.06	1.55	0.12	2.91	0.36	2.01	4.44	1.11	1.57	31.20	1.32	50.16	41.55	120.37	94.44	214.81	1.27
95	113362	1.95	5.33	1.87	5.70	0.54	2.71	0.10	1.79	0.08	6.29	1.99	1.99	1.71	11.57	0.10	11.81	1.47	58.92	210.52	269.44	0.28
96	113031	5.98	25.66	2.45	7.78	3.81	5.67	0.13	4.94	0.31	3.14	4.00	1.38	1.23	29.36	0.10	39.96	29.23	227.39	300.35	527.74	0.76
97	113029	1.65	18.22	1.84	0.10	0.74	1.75	0.12	2.48	0.29	2.50	4.28	3.88	1.19	32.37	2.28	41.31	32.40	70.84	122.61	193.45	0.58
98	113032	2.12	13.67	1.89	7.74	1.00	2.81	0.11	2.76	0.21	3.83	2.92	1.14	5.03	34.66	1.53	30.05	18.22	94.54	153.53	248.07	0.62

Annexure-XXXd: ICPMS Analysis of BH04

Sl No.	Sample No.	Depth	Sample Description	Host lithology	Li	Be	Sc	V	Cr	Co	Ni	Cu	Zn	Ga	Ge	Se	Rb	Sr	Y	Zr	Nb	Mo
1.00	112459	0.00	Blackish red coloured metasomatized sandstone with strong iron impregnation and comprising very coarse to coarse grained quartz, quartz aggregates, hematite, muscovite, embedded in a hematitic-magnetite rich ground mass. The grains are predominantly angular to sub angular with low sphericity.The quartz aggregates are consist of 3/4 quartz crystals, surrounded by & embedded in dark black (possibly magnetite) groundmass. Almost each grain is surrounded by hematite rim.	Highly ferruginized metasomatized sandstone	4.99	9.44	4.62	24.30	119.14	9.34	32.07	5.80	166.15	28.82	0.83	<0.1	<0.1	13.01	14.86	43.01	6.32	1.37
2.00	113058	13.00	Greyish white sandstone layers separated by mm to cm thin dark grey to blackish grey coloured shale. The sandstone is medium to fine grained and dominantly composed of quartz.	Sandstone dominated heterolith	25.17	2.28	17.44	150.04	127.25	7.26	27.90	<0.1	98.44	38.22	1.84	<0.1	<0.1	73.89	22.19	179.98	14.67	1.23
3.00	113059	15.99	Medium to coarse grained yellowish white sandstone, composed predominantly of quartz with muscovite, biotite (more in ferruginous part) set in a clayey to siliceous matrix/cement.Ferruginous staining is observed in layers, forming boudin like structure within the sample. Overall, it represents a quartz-rich, partly ferruginized sandstone with variable	Sandstone with differential ferruginization	28.12	2.27	13.17	155.32	210.17	3.11	27.39	<0.1	51.32	16.56	<0.1	<0.1	<0.1	34.40	21.53	224.13	17.40	<0.1

Sl No.	Sample No.	Depth	Sample Description	Host lithology	Li	Be	Sc	V	Cr	Co	Ni	Cu	Zn	Ga	Ge	Se	Rb	Sr	Y	Zr	Nb	Mo
			grain size and minor accessory minerals.																			
4.00	113393	27.79	Yellowish brown to brownish white coloured, medium to coare grained, moderate to well sorted, ferruginous quartzose sandstone. The ferruginization occurs either as through or in layers, following the statification.	Yellowish brown coloured ferruginized sandstone	23.71	0.13	5.00	39.21	56.62	1.63	6.54	<0.1	12.55	9.42	0.07	1.24	3.09	8.88	6.99	76.11	5.87	31.33
5.00	109055	32.34	Purplish white, very coarse to coarse grained sandstone, predominantly composed of quartz (98-99%) embedded in a siliceous to clayey matrix/cement. Ferruginization is observed mainly occuring in layers.	Sandstone with differential ferruginization	17.74	0.93	5.38	34.86	145.41	3.90	8.56	<0.1	35.47	11.07	<0.1	0.50	2.09	14.29	10.91	153.00	10.00	0.19
6.00	113392	34.28	Buff coloured very fine grained, ferruginous shale	Shale-sandstone heterolith	56.32	3.47	24.94	140.58	155.40	3.61	20.51	<0.1	35.77	35.41	0.14	4.48	34.20	100.44	37.37	180.19	22.42	13.03
7.00	113060	35.50	Fine to very fine grained reddish brown coloured ferruginous sandstone, composed mainly of quartz (with possible minor feldspar?) and subordinate muscovite and biotite. The rock shows pronounced ferruginous staining throughout the sample. Strong colouration in shades of reddish brown, dark brown and goethite colour is observed to be occured in alternate layers at one part of the samples (are these veinlets of hematite-goethite??)	Shale-sandstone heterolith	27.29	2.29	23.33	156.83	142.74	23.84	61.58	33.64	288.15	20.17	2.18	49.27	<0.1	95.93	27.44	188.71	16.07	3.32
8.00	109056	44.35	Pinkish to yellowish brown coloured, medium to fine grained, ferruginous metasomatized sandstone,	Mica bearing metasomatized sandstone	36.17	2.61	14.62	105.79	183.21	14.70	38.91	10.83	228.40	23.30	0.16	6.64	19.17	51.43	21.50	247.75	15.49	3.14

Sl No.	Sample No.	Depth	Sample Description	Host lithology	Li	Be	Sc	V	Cr	Co	Ni	Cu	Zn	Ga	Ge	Se	Rb	Sr	Y	Zr	Nb	Mo
			composed of quartz (>95%), muscovite(1-2%), black mineral (non magnetic, pyrolusite??), biotite in decreasing order of abundance. Occurence of mica mainly observed at purpulsih to brownish part of the sample. Iron imprgnation occur as thin layers (veinlets??). The layers are red to blackish brown in colour and very fine grained. Suspected clay alteration is also observed.																			
9.00	109057	48.26	Purplish to yellowish brown coloured, coarse to medium grained, ferruginous sandstone , composed of quartz (>95%), muscovite(1-2%), black mineral (non magnetic), biotite in decreasing order of abundance . Silicification observed at various stratigraphic levels. Biotite occurence is mainly observed at purpulsih to brownish part.	Mica bearing metasomatized sandstone	15.20	2.33	5.97	60.27	196.32	8.91	24.27	<0.1	213.68	8.56	<0.1	2.08	9.14	29.70	10.38	99.17	6.11	1.06
10.00	113391	49.71	Grey to blackish grey, very fine grained shale. Internally the shale is plane parallel laminated. Very tiny crystals of black, non magnetic mineral is also observed	Shale	9.21	3.08	9.26	110.94	89.52	25.13	22.27	<0.1	403.31	5.32	0.19	2.11	6.21	38.77	19.66	48.99	4.40	35.69
11.00	113061	50.37	Brownish red to black coloured highly ferruginous sandstone, comprising coarse to fine grained quartz, quartz aggregates, hematite, muscovite, embedded in a hematitic-magnetite rich ground mass. The grains are predominantly angular to	Highly ferruginized metasomatized sandstone	27.84	3.44	4.60	104.68	131.40	6.51	26.30	<0.1	120.45	20.61	1.61	<0.1	<0.1	28.07	7.13	86.20	4.92	1.76

Sl No.	Sample No.	Depth	Sample Description	Host lithology	Li	Be	Sc	V	Cr	Co	Ni	Cu	Zn	Ga	Ge	Se	Rb	Sr	Y	Zr	Nb	Mo
			sub angular with low sphericity.The quartz aggregates are consist of 3/4 quartz crystals, surrounded by & embedded in dark black (possibly magnetite) groundmass. The surface displays uneven granular characteristics and locally vesicular or pitted zones, suggestive of secondary alteration processes. Iron impregnation occur in different shades of red, and blackish red.																			
12.00	112199	25.00 to 26.01	The unit is characterized by yellowish brown coloured medium to coare grained, moderate to well sorted ferruginous quartzose sandstone. The ferruginization occurs either as through or in layers, following the statification.	Yellowish brown coloured ferruginized sandstone	18.57	1.17	6.96	52.70	164.92	18.73	23.94	44.72	52.77	29.03	0.27	2.17	51.18	67.91	28.06	171.79	33.23	2.54
13.00	112198	36.00 to 36.88	The unit occur as alternate appearance of 1-1.5m thick shale and sandstone. The shale is greysish white to buff in colour, very fine grained and ferruginous in nature at different stratigraphic levels. The sandstone is fine to very fine grained, reddish brown to buff in colour and ferruginous in nature. It composed mainly of quartz (with possible minor feldspar?) and subordinate muscovite and biotite. The thickness of the sand unit increases at depth. Sludge of the sandstone is recieved at the last 50cm of the unit. The rock shows	Shale-sandstone heterolith	53.82	3.24	17.45	147.61	131.60	9.95	8.76	16.58	24.88	13.31	<0.1	1.37	<0.1	36.22	18.75	128.49	36.47	0.69

Sl No.	Sample No.	Depth	Sample Description	Host lithology	Li	Be	Sc	V	Cr	Co	Ni	Cu	Zn	Ga	Ge	Se	Rb	Sr	Y	Zr	Nb	Mo
			pronounced ferruginous staining throughout the unit. Strong colouration in shades of reddish brown, dark brown and goethite colour is also observed to be occured in alternate layers at different part of the unit (are these veinlets of hematite-goethite??)																			
14.00	113154	35m to 36m	The unit occur as alternate appearance of 1-1.5m thick shale and sandstone. The shale is greysish white to buff in colour, very fine grained and ferruginous in nature at different stratigraphic levels. The sandstone is fine to very fine grained, reddish brown to buff in colour and ferruginous in nature. It composed mainly of quartz (with possible minor feldspar?) and subordinate muscovite and biotite. The thickness of the sand unit increases at depth. Sludge of the sandstone is recieved at the last 50cm of the unit. The rock shows pronounced ferruginous staining throughout the unit. Strong colouration in shades of reddish brown, dark brown and goethite colour is also observed to be occured in alternate layers at different part of the unit (are these veinlets of hematite-goethite??)	Shale-sandstone heterolith	49.47	3.92	20.25	113.46	118.73	6.56	43.24	6.96	78.79	26.30	0.19	6.96	22.62	71.25	29.69	223.97	14.93	4.60

Table Continued..

Annexure-XXXd

Sl No.	Sample No.	Cd	In	Sn	Sb	Cs	Ba	La	Ce	Pr	Nd	Sm	Eu	Gd	Tb	Dy	Ho	Er	Tm	Yb	Lu	Hf
1.00	112459	4.12	14.64	18.06	11.51	<0.1	30.63	4.71	6.84	28.20	7.61	8.30	1.58	18.96	1.47	6.89	1.52	1.84	<0.1	4.97	0.39	0.92
2.00	113058	1.39	0.06	7.47	28.74	<0.1	146.09	86.90	156.22	13.19	40.16	4.09	1.08	5.85	0.84	3.59	0.73	5.15	0.44	3.48	0.39	5.32
3.00	113059	0.77	0.43	7.14	33.25	<0.1	74.75	63.81	118.02	13.73	50.52	7.50	1.15	5.71	1.09	5.82	1.22	3.57	0.60	4.18	0.50	5.27
4.00	113393	0.34	<0.01	0.89	<0.1	<0.1	34.16	15.65	30.98	3.51	12.84	2.41	0.56	2.03	0.25	1.47	0.32	0.81	0.14	0.82	0.14	1.87
5.00	109055	<0.05	0.02	0.73	<0.1	<0.1	31.70	32.89	65.90	7.39	26.23	5.11	0.68	3.72	0.46	2.30	0.42	1.18	0.17	1.11	0.16	4.64
6.00	113392	0.29	<0.01	3.43	1.00	4.24	145.54	85.20	170.23	18.86	69.72	13.27	2.91	11.21	1.64	7.80	1.43	3.95	0.52	3.30	0.46	4.43
7.00	113060	0.55	0.30	3.67	31.94	1.56	2710.53	54.24	100.26	11.54	39.63	6.11	2.01	6.64	0.92	5.72	1.00	5.77	0.64	4.58	0.43	5.39
8.00	109056	0.10	0.06	2.46	<0.1	1.64	233.27	48.34	96.38	10.92	39.02	8.21	1.27	6.10	0.84	4.77	0.91	2.71	0.39	2.54	0.38	7.01
9.00	109057	<0.05	0.02	0.70	<0.1	0.82	169.96	24.12	49.29	5.54	19.74	4.07	0.57	3.02	0.44	2.23	0.43	1.21	0.19	1.14	0.17	2.89
10.00	113391	0.65	<0.01	0.17	2.03	<0.1	187.63	22.77	53.47	5.68	21.98	4.61	1.21	4.90	0.74	4.20	0.79	2.25	0.32	2.02	0.28	1.30
11.00	113061	1.45	0.04	1.89	24.06	<0.1	59.12	18.85	35.99	2.51	14.07	2.13	0.44	3.16	0.31	0.96	0.35	1.60	0.14	2.42	<0.1	3.41
12.00	112199	<0.05	0.02	30.71	2.82	8.92	1448.63	47.30	105.13	6.95	57.88	7.61	1.96	6.74	0.90	5.59	1.10	3.50	<0.6	2.49	0.13	9.32
13.00	112198	<0.05	0.01	37.47	1.64	6.28	63.03	35.72	90.99	6.45	44.95	6.95	1.74	6.54	0.49	4.23	0.51	2.36	<0.7	1.48	0.07	3.25
14.00	113154	0.38	<0.01	2.57	<0.1	2.09	659.64	64.63	127.69	13.57	49.73	9.47	2.06	8.66	1.31	6.19	1.18	3.24	0.47	3.01	0.43	5.47

Table Continued..

Annexure-XXXd

Sl No.	Sample No.	Ta	W	Tl	Pb	Bi	Th	U	Ag	Te	Mn	HREEY	LREE	TREEY	HREEY/LREE	THIE
1.00	112459	3.20	1.16	1.64	34.04	7.15	45.81	42.36	-	-	-	57.20	55.66	112.86	1.03	424.74
2.00	113058	1.15	2.38	0.05	18.54	0.16	20.35	4.49	3.58	2.10	-	61.19	300.57	361.76	0.20	699.44
3.00	113059	1.03	2.13	0.06	22.22	<0.1	28.67	3.92	0.89	1.05	-	58.54	253.58	312.12	0.23	617.44
4.00	113393	0.18	0.39	<0.1	8.32	<0.1	6.81	1.47	<0.05	<0.05	261.39	18.52	65.38	83.91	0.28	187.51
5.00	109055	0.49	0.35	<0.05	14.70	<0.1	18.69	2.94	0.15	<0.1	-	26.48	137.53	164.01	0.19	272.95
6.00	113392	1.16	1.85	<0.1	23.36	<0.1	19.75	9.17	<0.05	<0.05	18.13	95.53	357.27	452.80	0.27	727.39
7.00	113060	0.96	2.40	0.06	31.84	<0.1	17.68	11.02	2.51	1.06	-	78.46	211.77	290.23	0.37	890.14
8.00	109056	0.78	0.99	0.42	48.71	0.12	23.70	13.34	<0.1	0.14	-	56.01	202.88	258.89	0.28	672.62
9.00	109057	0.36	1.82	<0.05	13.22	<0.1	13.37	2.82	<0.1	<0.1	-	25.76	102.76	128.52	0.25	436.22
10.00	113391	0.22	0.44	<0.1	8.56	<0.1	5.97	3.30	<0.05	<0.05	3921.63	45.62	108.51	154.12	0.42	734.22
11.00	113061	0.32	4.77	0.06	13.99	<0.1	8.92	2.38	<0.05	3.19	-	21.20	73.56	94.75	0.29	369.95
12.00	112199	1.76	2.86	3.50	38.09	<0.1	<0.1	<0.1	31.27	5.46	31.27	58.02	224.87	282.89	0.26	-
13.00	112198	0.91	<0.1	0.57	28.87	<0.1	<0.1	<0.1	47.38	1.64	47.38	54.33	185.06	239.39	0.29	-
14.00	113154	0.60	0.91	<0.1	19.71	<0.1	20.24	8.19	<0.05	0.12	31.92	76.49	265.09	341.58	0.29	-

Annexure-XXXe: ICPMS Analysis result of BH05

Sl No.	Sample No.	Sample Deptrh	Sample Description	Host lithology	Li	Be	Sc
1	112488	0	Sandstone is composed of both clean and detritus quartz, ranging in size from medium to very coarse, angular to sub-rounded and very few muscovite (<1%) embedded in a hematitic to silicic(??) matrix/ cement. Small pods of clay is also observed (clay alteration??). The clean semi transparent quartz grains are more angular and surrounded by hematite rims. The sandstones seems to be brecciated at places, specifically where the iron veins are in cross cutting relationship with the sandstone A thin carbonate vein is also observed at an angle to the bedding of the sandstone .	Mica bearing metasomatized sandstone cross cutting by hematite and carbonate veins (~150m EES of BH 05 location)	7.21	3.94	9.27
2	112498	0	The sandstone is composed of both clean and detritus quartz, ranging in size from coarse to very coarse, angular to sub-rounded, both biotite and muscovite, varigated colour minerals (bornite??), few magnetite grains embedded in a hematitic to silicic(??) matrix/ cement. The clean semi transparent quartz grains are more angular and surrounded by hematite rims. The sandstones seems to be brecciated at places, specifically where the iron veins are in cross cutting relationship with the sandstone. The dust of the rock attracted by magnet. Cluster of 2-3 quartz grains, surrounded by magnetite are occuring as the breccia clast. There is a fine grained variety of dark blackish brown colour rock with lots of very small grains of euhedral feldspar.	Highly ferruginized metasomatized sandstone with seldom grain of suspected bornite, Surface sample of BH05	6.26	4.47	12.53
3	109058	0-1m	Brownish yellow coloured very coarse to fine grained sands consist of quartz, muscovite, hematite, magnetite and a colourless mineral (platy to needle like appearance, colourless, crystal clear, no streak, easily breakable through scriber) in a decreasing order of abundance. Few rock fragments of altered very highly ferruginous sandstone is also observed. These are poorly sorted, the grains varies from very angular to well rounded and generally with low spherecity. Very fine fragments of magnetite are observed within the group of quartz clasts.	Sludge of highly ferruginized metasomatized sandstone	11.13	1.45	3.02
4	109059	2-3m	Yellowish brown coloured very coarse to fine grained sands consist of quartz, muscovite, hematite, less magnetite and a colourless mineral (platy to needle like appearance, colourless, crystal clear, no streak, easily breakable through scriber) in a decreasing order of abundance. Less rock fragments is observed. The unit is poorly sorted, with grains varying between very angular to well rounded grains, generally with low spherecity. Very fine fragments of magnetite are observed within the groove of quartz clasts.	Sludge of mica bearing ferruginized sandstone	11.03	0.64	1.76

Sl No.	Sample No.	Sample Deptrh	Sample Description	Host lithology	Li	Be	Sc
5	109060	6-8m	Dark brown coloured very coarse to fine grained sands consist of quartz (99%), muscovite, hematite, less magnetite and a colourless mineral (platy to needle like appearance, colourless, crystal clear, no streak, easily breakable through scriber) in a decreasing order of abundance. Less rock fragments is observed. The sludge is well sorted with sub rounded to well rounded grains, generally with moderate spherecity. Very fine fragments of magnetite are observed within the grooves of quartz clasts and also few grains of xenotime is suspected.	Sludge of mica bearing ferruginized sandstone	12.72	0.62	2.67
6	109061	14-16m	Brownish white to yellowish brown coloured, medium to fine-grained, moderately sorted sludge with predominantly sub-rounded to rounded grains with moderate to high sphericity. The sludge comprises >90% quartz, feldspar (weathered ??, clayey), apatite (rare??, (platy to needle like appearance, colourless, crystal clear, no streak, easily breakable through scriber), rock fragments, hematite fragments and <1% magnetite in a decreasing order of abundance .The apatite (??) crystals are angular to sub-angular with low sphericity. Magnetite grains & magnetite engraved within the grooves of the quartz is also observed.	Sludge of yellowish brown coloured ferruginized sandstone	10.93	0.36	1.54
7	113383	40.39 to 40.49	Grey coloured medium to coarse grained sandstone, characterized by sub-angular to sub-rounded grains of quartz, rock fragments, and magnetite embedded in a clay-rich matrix/cement. Reddish-brown ferruginous to purplish alteration is observed at different stratigraphic levels, suggesting variable intensity of alteration. Pebble sized clasts of grey shale and white siltstone/claystone (carbonate/marl??).	Sandstone with differential ferruginization	12.89	0.78	9.93
8	113385	40.58 to 40.67	Grey coloured medium to coarse grained sandstone, characterized by sub-angular to sub-rounded grains of quartz, rock fragments, Reddish-brown ferruginous to purplish alteration is observed. Pebble sized clasts of grey shale and white siltstone/claystone (carbonate/marl??) are also present within the unit. Between 40.50 m and 40.75 m, abundant clay clasts par ??/ (argillic alteration).	Sandstone with differential ferruginization	45.14	1.82	18.10

Sl No.	Sample No.	Sample Deptrh	Sample Description	Host lithology	Li	Be	Sc
9	113386	42.50 to 42.56	Grey coloured medium to coarse grained sandstone, characterized by sub-angular to sub-rounded grains of quartz, rock fragments, and magnetite embedded in a clay-rich matrix/cement. Reddish-brown ferruginous to purplish alteration is observed. Pebble sized clasts of grey shale and white siltstone/claystone (carbonate/marl??)	Sandstone with differential ferruginization	13.20	0.67	9.17
10	113384	49.10 to 49.13	The sandstone core is ferruginous alteration. Composed of muscovite & white transparent crystals. However coarser quartz grains, few clasts of hematite are also observed	Sandstone with differential ferruginization	17.66	0.71	9.99
11	109126	52.43 to 52.5	Dark grey to blackish grey, very fine grained, moderate to well sorted siltstone/shale with sub rounded grains and moderate sphericity. The sample is more shaly. The shales are dark grey to blackish grey in colour & consist of clay materials with minor muscovite and biotite. The blackish grey part of the shale are smelling gun powders.	Sandstone dominated heterolith characterized by thick sanstone layers separated by mm thin shale layers	20.12	4.51	14.85
12	109127	55.38 to 55.44	Sample of grey coloured, medium to fine grained, moderate to well sorted sandstone, separated by mm to cm thin black shale layers. Often the grains of the sandstone are angular to sub rounded with moderate sphericity. The shales are dark grey to blackish grey in colour & consist of clay materials with minor muscovite and biotite. Milimeter to cm scale thin, jet black materials are also observed within the shale, pyrolusite?? (black streak, feebly magnetic). The jet black part is also observed within the sandstone , and are smelling gun powders. An elliptical shale clast of shale is observed, which is full of pyrite/chalcopyrite crystals along the boundary of the clast. At places soft sediment deformations is also observed.	Sandstone dominated heterolith characterized by thick sanstone layers separated by mm thin shale layers	27.11	1.11	5.42
13	109148	55.58 to 55.63	Sand dominated hetrolith, characterized by dm to cm scale sandstones, separated by mm thin black shale layers. The sandstone is grey in colour, medium to fine grained, moderate to well sorted. Often the grains are angular to sub rounded with moderate sphericity. The shales are dark grey to blackish grey in colour & consist of clay materials with minor muscovite and biotite. Thin hair like jet black materials are also observed within the shale, pyrolusite?? (black streak, feebly magnetic). The jet black part is also observed within the sandstone , and are smelling gum powders.	Sandstone dominated heterolith characterized by thick sanstone layers separated by mm thin shale layers	16.46	1.10	11.25

Sl No.	Sample No.	Sample Deptrh	Sample Description	Host lithology	Li	Be	Sc
14	109122	56.60 to 56.67	Single layer of black gun powder smelling material within the mm to cm thin shale layers, separating the dm scale sandstone.	Sandstone dominated heterolith characterized by thick sanstone layers separated by mm thin shale layers	23.81	6.70	8.41
15	109123	58.37 to 58.41	Sand dominated hetrolith, characterized by dm to cm scale sandstones are separated by mm thin shale layers. The sandstone is grey in colour, medium to fine grained, moderate to well sorted. Often the grains are angular to sub rounded with moderate sphericity. The shales are dark grey to blackish grey in colour & consist of clay materials with minor muscovite and biotite. The gun powder smell of this sample is very low	Sandstone dominated heterolith characterized by thick sanstone layers separated by mm thin shale layers	27.33	5.68	4.57
16	109124	58.9 to 58.95	The contact beween the breccia and the sandstone dominated heterolith marked by iron impregnation. The breccia is grey in colour and consist of elliptical to elongated shaped clasts of white to bluish grey coloured shale embedded in a quartzose and clay matrix/cement. The clasts are angular to sub-angular with low sphericity. The matrix consists of subangular quartz, hematite and clay.	Breccia	12.68	0.00	17.74
17	109125	59.07 to 59.13	Seldom occurrence of pyrite within the clast of breccia. Grey coloured breccia, consist of elliptical to elongated, rectangular shaped clasts of blackish grey and bluish grey coloured shale, embedded in a quartzose and clay matrix/cement. The clasts are angular to sub-angular with low sphericity. The matrix consists of subangular quartz, hematite and clay.	Breccia	14.92	3.41	2.16
18	113358	59.32 to 59.41	Grey coloured breccia, consist of elliptical to elongated rectangular shaped clasts of white to bluish grey and blackish grey coloured shale, silicified (??), sandstone, quartzose sandstone (more rounded clasts) embedded in a quartzose and clay matrix/cement. The clasts are angular to sub-angular with low sphericity. The matrix consists of subangular quartz, hematite and clay	Breccia	16.59	0.87	10.26
19	113151	51.75m to 52.75m	Sand dominated hetrolith, characterized by dm to cm scale sandstones, separated by mm thin shale layers. Thickness of shale increases to tens of cm at a particular depth. The sandstone is greyish white in colour, medium to fine grained, moderate to well sorted. Often the grains are angular to sub rounded with moderate sphericity. The shales are dark grey to blackish grey in colour & consist of clay materials with minor muscovite and biotite. Milimeter to cm scale thin, jet black materials are also observed within the shale, pyrolusite??	Sandstone dominated heterolith	29.15	0.47	18.22

Sl No.	Sample No.	Sample Deptrh	Sample Description	Host lithology	Li	Be	Sc
			(black streak, feebly magnetic). The jet black part is also observed within the sandstone , and are smelling gun powders. At 52.3m the unit is completely dark grey & more shaly and this darker parts are also smelling gun powder. At places soft sediment deformations is also observed.				
20	113152	55m to 56m	Sand dominated hetrolith, characterized by dm to cm scale sandstones, separated by mm thin shale layers. The sandstone is greyish white in colour, medium to fine grained, moderate to well sorted. Often the grains are angular to sub rounded with moderate sphericity. The shales are dark grey to blackish grey in colour & consist of clay materials with minor muscovite and biotite. Milimeter to cm scale thin, jet black materials are also observed within the shale, pyrolusite?? (black streak, feebly magnetic). The jet black part is also observed within the sandstone , and are smelling gun powders. This jet black material occurence intensity is higher in the sample.	Sandstone dominated heterolith	29.10	0.46	13.06
21	113153	59m to 60m	Grey coloured breccia, consist of elliptical to elongated, rectangular shaped clasts of white to bluish grey and blackish grey coloured shale, silicified (??) sandstone, quartzose sandstone (more rounded clasts) embedded in a quartzose and clay matrix/cement. The clasts are angular to sub-angular with low sphericity. The matrix consists of subangular quartz, hematite and clay.Seldom occurrence of pyrite is observed at 59.07 m. The contact between the previous lithology of the breccia is marked by iron impregnation.	Breccia	20.86	<0.1	10.68
22	112197	57.00 to 58.00	Sand dominated hetrolith, characterized by dm to cm scale sandstones, separated by mm thin shale layers. The sandstone is greyish white in colour, medium to fine grained, moderate to well sorted. Often the grains are angular to sub rounded with moderate sphericity. The shales are dark grey to blackish grey in colour & consist of clay materials with minor muscovite and biotite. Milimeter to cm scale thin, jet black materials are also observed within the shale, pyrolusite?? (black streak, feebly magnetic). The jet black part is also observed within the sandstone , and are smelling gun powders	Sandstone dominated heterolith	26.23	1.49	13.68

Table Continued..

Annexure-XXXe

Sl No.	Sample No.	V	Cr	Co	Ni	Cu	Zn	Ga	Ge
1	112488	113.26	118.7	120.73	207.48	168.55	263.11	17.13	0.54
2	112498	36.29	137.0	34.20	179.13	47.67	143.27	25.98	0.92
3	109058	23.96	155.02	26.20	59.44	57.64	98.27	2.78	<0.1
4	109059	12.16	181.66	15.57	23.81	6.75	36.99	2.14	<0.1
5	109060	22.58	158.11	7.47	19.84	9.87	38.97	3.53	<0.1
6	109061	9.94	198.07	5.26	15.32	13.75	27.27	2.34	<0.1
7	113383	102.65	217.13	10.96	10.61	33.38	13.40	13.99	<0.1
8	113385	154.83	149.55	27.21	31.09	54.88	25.38	41.38	<0.1
9	113386	178.46	167.90	10.30	7.83	12.60	14.88	16.47	<0.1
10	113384	75.74	257.26	11.25	9.79	12.72	35.91	13.85	<0.1
11	109126	112.59	<0.1	7.05	25.32	391.61	13.44	32.68	1.18

Sl No.	Sample No.	V	Cr	Co	Ni	Cu	Zn	Ga	Ge
12	109127	57.04	71.51	289.76	732.03	10.93	34.69	34.92	1.30
13	109148	106.91	45.00	33.08	36.10	<0.1	187.28	15.27	1.08
14	109122	56.46	43.14	21.88	30.70	<0.1	90.06	16.86	0.11
15	109123	102.24	177.14	24.54	28.03	<0.1	96.30	30.93	0.09
16	109124	245.69	122.60	4.81	16.27	<0.1	10.16	19.90	0.53
17	109125	81.85	77.76	77.92	85.07	<0.1	26.57	22.33	0.61
18	113358	114.35	217.16	60.17	63.03	44.48	51.59	21.83	0.39
19	113151	85.36	110.05	2.13	21.31	63.98	13.75	23.67	0.11
20	113152	75.45	92.90	26.36	30.12	16.27	86.01	18.48	0.08
21	113153	96.79	156.45	103.34	130.90	45.66	86.94	21.46	0.23
22	112197	90.42	113.76	36.83	30.79	27.12	147.41	20.80	0.34

Table Continued..

Annexure-XXXe

Sl No.	Sample No.	Se	Rb	Sr	Y	Zr	Nb	Mo	Cd	In
1	112488	1.65	2.16	54.69	15.49	70.26	6.94	3.39	3.38	8.78
2	112498	<0.1	<0.1	29.92	11.87	47.89	7.9	7.77	3.35	11.52
3	109058	0.72	2.64	13.14	4.02	41.37	2.41	0.45	<0.05	<0.01
4	109059	0.58	0.78	6.01	3.10	50.93	2.85	0.48	<0.05	<0.01
5	109060	0.73	2.68	13.29	4.15	64.15	5.80	0.34	<0.05	<0.01
6	109061	0.28	0.60	5.35	3.39	69.28	3.24	0.25	<0.05	<0.01
7	113383	0.94	<0.1	685.08	24.00	136.23	70.66	2.05	1.75	1.08
8	113385	2.31	<0.1	19.73	1.88	138.93	40.63	1.99	1.73	4.08
9	113386	10.36	<0.1	674.00	22.58	133.08	54.59	2.22	1.88	1.48
10	113384	5.64	<0.1	70.90	26.20	380.20	71.60	1.12	1.73	1.21
11	109126	15.29	85.68	72.03	29.12	189.47	19.55	2.28	5.74	0.12

Sl No.	Sample No.	Se	Rb	Sr	Y	Zr	Nb	Mo	Cd	In
12	109127	15.18	<0.1	55.73	24.23	283.00	15.41	2.13	2.80	<0.01
13	109148	0.00	2.67	396.56	24.41	191.09	17.27	0.64	5.21	0.47
14	109122	0.00	<0.1	82.88	26.97	175.91	14.65	0.55	5.26	0.35
15	109123	14.98	<0.1	72.72	28.87	199.96	20.37	1.70	4.38	0.34
16	109124	15.06	77.39	360.59	28.83	155.60	38.49	5.17	3.08	0.13
17	109125	27.99	111.53	410.38	25.55	151.71	38.54	3.09	3.66	0.34
18	113358	1.66	7.51	699.76	25.13	198.63	16.98	4.42	1.45	2.18
19	113151	5.17	18.71	57.57	28.35	234.45	16.35	14.20	0.68	<0.01
20	113152	4.94	12.01	71.23	25.79	255.98	16.55	6.49	0.66	<0.01
21	113153	6.62	11.09	681.13	26.41	149.37	38.46	12.35	0.86	<0.01
22	112197	2.26	19.35	76.83	29.32	209.43	29.23	1.40	0.18	0.02

Table Continued..

Annexure-XXXe

Sl No.	Sample No.	Sn	Sb	Cs	Ba	La	Ce	Pr	Nd	Sm
1	112488	39.54	7.89	1.92	897.19	8.2	14.21	16.26	9.65	4.01
2	112498	46.34	9.66	1.1	80.33	23.43	57.99	26.86	20.56	7.08
3	109058	0.21	<0.1	0.14	56.69	7.92	17.39	1.74	5.97	1.25
4	109059	0.22	<0.1	<0.1	40.23	6.65	13.91	1.49	5.43	1.02
5	109060	0.60	<0.1	0.14	64.37	10.37	21.32	2.31	8.17	1.48
6	109061	0.31	<0.1	<0.1	39.94	8.97	18.51	2.06	7.29	1.38
7	113383	23.23	<0.1	4.24	3142.60	124.39	353.78	29.07	110.04	19.37
8	113385	18.40	1.46	19.73	29.19	0.27	<0.1	<0.1	30.49	0.45
9	113386	17.88	<0.1	4.83	3344.63	85.61	250.25	21.99	103.55	20.85
10	113384	25.42	0.29	8.53	232.74	60.63	175.94	8.92	56.23	9.01
11	109126	10.49	27.97	5.80	157.29	56.43	111.82	9.73	38.69	5.96

Sl No.	Sample No.	Sn	Sb	Cs	Ba	La	Ce	Pr	Nd	Sm
12	109127	4.19	28.37	1.89	176.18	57.42	115.62	10.84	36.16	2.47
13	109148	4.43	31.18	<0.1	2327.85	101.06	186.72	20.08	67.97	12.56
14	109122	2.18	34.16	<0.1	257.12	58.34	121.57	12.88	43.34	5.72
15	109123	3.35	27.89	<0.1	137.30	58.39	106.56	9.99	36.14	4.05
16	109124	3.84	28.06	<0.1	1505.97	99.17	209.55	18.32	62.85	10.26
17	109125	2.52	31.37	0.15	1620.92	85.75	180.88	15.98	61.66	6.98
18	113358	85.59	1.57	21.86	3176.65	96.05	226.66	13.46	96.12	17.82
19	113151	2.38	<0.1	0.16	118.86	65.19	128.67	13.28	47.27	8.30
20	113152	2.23	0.56	<0.1	303.18	60.51	124.43	12.94	46.56	8.41
21	113153	1.59	<0.1	<0.1	3734.44	108.25	221.79	23.69	89.21	15.63
22	112197	27.65	0.84	8.48	131.87	52.33	128.22	9.47	55.75	7.63

Table Continued..

Annexure-XXXe

Sl No.	Sample No.	Eu	Gd	Tb	Dy	Ho	Er	Tm	Yb	Lu	Hf	Ta
1	112488	0.83	10.7	1.05	2.51	0.6	1.07	<0.1	1.77	0.19	4.9	2.76
2	112498	0.73	15.63	1.21	1.92	0.66	0.57	<0.1	2.1	0.3	1.13	3.16
3	109058	0.20	1.05	0.14	0.83	0.16	0.47	<0.1	0.47	0.08	1.23	0.17
4	109059	0.16	0.81	0.12	0.65	0.13	0.37	<0.1	0.42	0.07	1.51	0.19
5	109060	0.21	1.23	0.16	0.86	0.17	0.51	<0.1	0.52	0.09	1.89	0.35
6	109061	0.14	1.01	0.13	0.74	0.14	0.40	<0.1	0.43	0.07	1.70	0.30
7	113383	4.09	13.99	2.11	7.33	0.60	2.65	0.19	1.61	0.02	12.88	1.63
8	113385	0.38	0.23	4.22	0.59	0.48	3.96	<0.1	0.48	0.01	3.29	2.05
9	113386	4.73	15.96	2.40	7.27	0.85	2.50	<0.1	1.70	0.03	13.07	1.67
10	113384	1.05	6.83	1.43	4.88	0.86	2.90	0.11	2.02	0.02	9.78	1.47
11	109126	0.96	7.52	0.90	5.74	1.60	3.01	0.24	4.17	0.75	3.90	1.37
12	109127	1.61	8.67	0.68	3.81	0.78	2.30	0.68	4.11	0.40	7.22	1.02

Sl No.	Sample No.	Eu	Gd	Tb	Dy	Ho	Er	Tm	Yb	Lu	Hf	Ta
13	109148	5.54	17.77	1.14	6.93	0.95	2.22	0.14	3.76	0.47	3.98	0.88
14	109122	1.18	5.00	0.87	5.20	1.23	1.64	0.51	3.13	0.48	4.30	0.90
15	109123	2.19	5.44	0.80	6.47	1.05	2.36	0.43	5.76	0.67	4.25	1.46
16	109124	2.22	10.59	1.28	7.28	1.16	2.66	0.42	3.76	0.54	4.13	2.35
17	109125	2.72	10.70	1.15	6.02	0.90	1.81	0.13	4.09	0.34	3.15	1.98
18	113358	4.21	5.84	2.20	8.71	<0.1	2.99	0.12	1.32	0.03	17.07	2.05
19	113151	1.33	7.05	1.04	5.49	1.08	3.17	0.44	2.97	0.42	5.57	0.57
20	113152	1.31	7.07	0.96	4.94	0.93	2.83	0.37	2.51	0.36	6.01	0.81
21	113153	3.97	13.32	1.68	6.55	1.06	2.90	0.34	2.30	0.32	3.26	1.64
22	112197	1.44	6.25	0.54	5.34	1.00	3.03	<0.5	2.38	0.10	5.84	1.26

Table Continued..

Annexure-XXXe

Sl No.	Sample No.	W	Tl	Pb	Bi	Th	U	Ag	Te	Mn	HREEY	LREE	TREEY	HREEY/LREE	THIE
1	112488	1.87	<0.05	12.09	1.26	26.78	21.77	1.17	10.48		43.58	52.33	95.91	0.83	863.92
2	112498	1.11	0.32	39.82	3.29	38.12	35.29	1.07	15.21		47.62	135.92	183.54	0.35	723.08
3	109058	9.05	0.52	8.07	<0.1	4.31	1.69	0.19	<0.1		10.54	34.27	44.80	0.31	272.68
4	109059	9.97	0.52	3.04	<0.1	4.48	0.95	0.13	<0.1		7.68	28.52	36.20	0.27	114.72
5	109060	14.11	0.08	7.79	<0.1	7.81	0.99	0.55	<0.1		10.66	43.65	54.31	0.24	142.15
6	109061	**30.47**	0.08	2.72	<0.1	6.14	0.87	0.24	<0.1		8.08	38.21	46.29	0.21	115.25
7	113383	**0.57**	<0.1	79.89	<0.1	<0.1	<0.1	0.37	<0.1	21.33	66.52	636.65	703.17	0.10	867.45
8	113385	**<0.1**	3.14	<0.1	<0.1	<0.1	<0.1	0.52	1.67	12.16	30.33	31.21	61.54	0.97	257.71
9	113386	**0.78**	0.26	39.25	<0.1	<0.1	<0.1	0.45	<0.1	37.06	67.19	482.25	549.43	0.14	679.06
10	113384	**<0.1**	<0.1	26.59	<0.1	4.67	<0.1	1.27	<0.1	44.75	56.29	310.73	367.02	0.18	546.05
11	109126	0.88	0.07	23.24	0.22	20.27	19.33	6.25	3.14	NA	68.88	222.62	291.50	0.31	864.75
12	109127	0.25	0.17	296.45	0.10	25.85	7.60	3.20	4.16	NA	52.69	222.51	275.20	0.24	1165.04

Sl No.	Sample No.	W	Tl	Pb	Bi	Th	U	Ag	Te	Mn	HREEY	LREE	TREEY	HREEY/LREE	THIE
13	109148	0.87	0.08	39.38	<0.1	19.11	8.09	<0.05	<0.05	NA	74.57	388.39	462.97	0.19	782.87
14	109122	0.23	0.11	12.59	0.14	21.48	3.28	<0.05	1.03	NA	54.62	241.86	296.48	0.23	507.70
15	109123	2.10	0.10	11.13	0.12	22.34	5.02	0.90	<0.05	NA	58.62	215.13	273.75	0.27	501.88
16	109124	0.91	0.19	15.43	0.15	19.89	9.17	2.53	1.06	NA	76.48	400.15	476.64	0.19	641.98
17	109125	1.29	0.10	12.15	0.10	18.23	15.85	<0.05	2.11	NA	55.55	351.24	406.79	0.16	660.86
18	113358	1.63	1.75	13.94	<0.1	5.95	<0.1	1.74	5.57	NA	60.91	450.11	511.02	0.14	800.89
19	113151	1.00	0.26	22.79	<0.1	27.65	18.28	<0.05	<0.05	16.23	69.55	262.72	332.27	0.26	NA
20	113152	1.05	0.31	15.50	<0.1	26.79	6.21	<0.05	<0.05	20.20	60.11	252.86	312.97	0.24	NA
21	113153	1.52	0.24	23.28	<0.1	19.66	10.05	<0.05	0.09	18.69	69.54	458.57	528.11	0.15	NA
22	112197	2.19	1.16	23.62	<0.1	<0.1	<0.1	0.66	3.51	27.03	27.03	253.40	280.43	0.11	NA

Annexure-XXXf: ICPMS Analysis result of BH06

Sl No.	Sample No.	Sample Deptrh (m)	Sample Description	Host lithology	Li	Be	Sc	V	Cr	Co	Ni	Cu	Zn	Ga
1	112492	0	Altered highly ferruginous sandstone, occuring as dm scale thin band along the fault plane. It consists of angular to few sub-rounded grains of quartz, very few mica and clasts of hematite embedded in a hematitic matrix/cement. The amount of the framework is ~40%. The rock seems to be a flow along the fault plane and observed only along the fault plane.	Highly ferruginous metasomatized sandstone	12.95	2.09	9.34	234.09	175.35	7.16	40.61	10.13	81.95	19.47
2	112493	0	Altered ferruginous, pinkish purple coloured sandstone occuring between two fracture zone. It consists of 0.5cm to 16cm long clasts of clay and/ or siltstone (observed as original bed at the other part of the exposure) embedded in a siliceous matrix. The sandstone also comprises angular to rounded, elongated, circular wedge shaped quartz, and muscovite. The grain boundary of the matrix part is not very clear. At very few places feldspar grains are also suspected. Small iron concretion is also observed at places.	Mica bearing metasomatized sandstone	22.93	0.62	3.76	40.12	157.50	6.10	3.06	4.12	19.93	5.23
3	112493	0	Altered ferruginous, pinkish purple coloured sandstone occuring between two fracture zone. It consists of 0.5cm to 16cm long clasts of clay and/ or siltstone (observed as original bed at the other part of the exposure) embedded in a siliceous matrix. The sandstone also comprises angular to rounded, elongated, circular wedge shaped quartz, and muscovite. The grain boundary	Mica bearing metasomatized sandstone	11.98	0.53	4.30	48.31	178.92	5.06	5.97	6.66	24.52	6.69

Sl No.	Sample No.	Sample Deptrh (m)	Sample Description	Host lithology	Li	Be	Sc	V	Cr	Co	Ni	Cu	Zn	Ga
			of the matrix part is not very clear. At very few places feldspar grains are also suspected. Small iron concretion is also observed at places.											
4	112494	0	Breccia occuring along the fault plane. It consists of angular to well-rounded quartz, clay clasts (rectangular, circular, wedge shaped, irregular), small gashes or lens-like structures filled with silica, few book mica (muscovite), well-rounded iron clasts embedded in a hematitic matrix/cement. No magnetite is observed.	Ferrugiized breccia	66.65	3.82	64.10	633.40	165.54	21.21	64.34	83.76	84.60	38.83
5	112495	0	Yellowish wite coloured, medium to coarse grained, poorly sorted sandstone. The sandstone comprises of angular to sub rounded grains (moderate to low sphericity) of both grey and white quartz, clay (altered feldspar??) black shale clasts embedded in a silicious to clay matrix.	Sandstone	49.11	1.01	4.84	55.50	1779.13	10.60	14.44	27.47	16.52	8.13
6	112496	0	Blackish red coloured medium to fine grained sandstone, occuring along the fault plane. This has been observed as dm scale unit, along few of the bedding planes where high amount of ferrugination and alteration making it very hard than the depositional sandstone. It consists of ~30-40% framework of angular to sub angular quartz, muscovite embedded in a hematitic to magnetite (in less	Highly ferruginous metasomatized sandstone	6.15	6.64	15.05	535.34	166.12	69.21	66.37	134.39	105.36	35.70

Sl No.	Sample No.	Sample Deptrh (m)	Sample Description	Host lithology	Li	Be	Sc	V	Cr	Co	Ni	Cu	Zn	Ga
			amount, part of the rock powder is attracted by magnet) matrix.											
7	113375	1.77 to 1.83	Breccia comprises of angular to sub-rounded transparent (crystal clear) and detrital quartz, white siltstone clasts, magnetite, and very few euhedral feldspar (?) fragments, all embedded in ferruginous cement/matrix.	Ferrugiized breccia	10.46	0.90	5.38	59.64	294.91	6.82	13.24	30.04	29.69	9.06
8	113376	1.89 to 1.95	Breccia comprises of angular to sub-rounded transparent (crystal clear) and detrital quartz, clay clasts, white siltstone clasts, magnetite, and very few euhedral feldspar (?) fragments, all embedded in ferruginous cement/matrix.Cluster of 2-3 quartz grains, surrounded by magnetite are also occuring as the breccia clast. Voids are locally infilled by silica , with no effervescence observed on acid test.	Ferrugiized breccia	8.22	1.97	9.16	107.58	197.49	8.20	29.26	34.19	63.26	18.09
9	113378	3.79 to 3.85	Medium to coarse grained quartzose sandstone with sub-rounded grains having moderate to high sphericity. The sandstone consist of mostly quartz (>98%), very few hematite grains, magnetite and white transparent crystals embedded in a silicified(?) matrix/cement. Iron impregnation has been observed as flow paths [thin veinlets (?)], cross cutting the sandstone. This veinlets are very hard and consists also of quartz, hematite (streak white, black minerals are	Sandstone	11.25	0.50	3.86	38.59	211.36	11.97	14.25	12.66	32.05	5.80

Sl No.	Sample No.	Sample Deptrh (m)	Sample Description	Host lithology	Li	Be	Sc	V	Cr	Co	Ni	Cu	Zn	Ga
			difficult to get the streak, rarely blackish brown, non-magnetite).											
10	113374	15.63 to 15.71	Medium to fine grained ferruginized sandstone, comprises both angular to sub-rounded transparent (crystal clear) & detritus quartz, clay, white sandstone clasts (remnanet of the parent rock??), magnetite, very few euhedral feldspar (??), very few mica (mainly at the high ferruginized part) embedded in ferruginous cement/matrix. Voids filled with carbonates (acid test positve) also observed at places. From 15.26 m to 15.86m the amount of ferrugination increases abruptly in such a way that it seems to be a zoned alteration. Secondary verigated colour alteration is observed along thin veinletts and pyrite occurs within the groove area (blue material gives blue streak).	Mica bearing metasomatized sandstone	9.27	1.13	8.50	416.58	212.85	33.33	113.82	120.28	188.98	13.64
11	113373	17.85 to 17.9	Very fine grained reddish white shale with iron impregnation patches	Shale	35.74	2.89	22.73	172.60	136.81	17.39	30.97	40.87	68.19	35.70

Sl No.	Sample No.	Sample Deptrh (m)	Sample Description	Host lithology	Li	Be	Sc	V	Cr	Co	Ni	Cu	Zn	Ga
12	113006	22.91 to 22.95	Yellow ocher to yellowish brown coloured, well sorted coarse to medium grained ferruginous sandstone with rounded to sub rounded grains and consists of quartz and muscovite (~1%). The sample has an abrupt change of grain size from the remaining part of the core with relatively higher degree of ferrugination. Silicification is also observed within the sample.	Mica bearing ferruginized sandstone	25.11	4.44	0.91	61.92	113.17	7.33	40.34	<0.1	23.76	10.36
13	113007	23.69 to 23.76	Reddish white to reddish-purple coloured, well sorted medium to very fine grained ferruginous sandstone with rounded to sub rounded grains. It consists of quartz and muscovite (~1%). Ferrugination generally occurs in layers within the sample. Grainsize alteration (medium and fine to very fine) is also a characterestic feature of the sample.	Mica bearing ferruginized sandstone	43.77	2.26	22.99	175.80	33.04	7.16	36.92	14.86	34.57	22.80
14	113357	29.69 to 29.79	Yellow ocher to yellowish brown coloured medium to fine grained, moderately sorted ferruginous sandstone with sub angular to sub rounded grains. The sandstone is composed of quartz (97%), muscovite (1-2%), few magnetite grains embedded in a clayey matrix/cement. Ferrugination varies in different order and in colour from yellow ocher to brownish red.	Mica bearing ferruginized sandstone	22.39	1.47	10.52	99.46	130.77	18.02	32.62	23.18	56.10	20.88
15	113004	29.80 to 29.85	Yellow ocher, coarse to medium grained, moderately sorted ferruginous sandstone with sub angular to sub rounded grains. They are composed of quartz (97%), muscovite (1-2%), few magnetic grains embedded in a clayey matrix/cement. Ferrugination varies in different order and in colour from yellow	Mica bearing ferruginized sandstone	42.88	1.13	11.41	66.92	85.88	6.76	31.14	<0.1	32.71	26.45

Sl No.	Sample No.	Sample Deptrh (m)	Sample Description	Host lithology	Li	Be	Sc	V	Cr	Co	Ni	Cu	Zn	Ga
			ocher to brownish red and occur either in layers or uniform.											
16	113005	30.05 to 30.15	Yellow ocher to yellowish white medium to fine grained, moderate to well sorted ferruginous sandstone with sub angular to sub rounded grains. They are composed of quartz (97%), muscovite (1-2%), few magnetic grains embedded in a clayey matrix/cement. Ferrugination varies in colour from yellow ocher to brownish red uniform ferrugination is observed.	Mica bearing ferruginized sandstone	26.48	<0.1	4.67	40.65	55.72	2.92	21.95	<0.1	10.63	17.55
17	113367	33.29 to 33.35	The sandstone is yellow ochre to yellowish brown in colour, very coarse to coarse grained, poorly sorted and consists of quartz (95-97%), hematite grains, white transparent crystals, very few muscovite embedded in a clay/siliceous material/cement (??). The degree of ferrugination is different at different parts of the unit and occur mainly in layers. Silicification (??) is also observed within the sample.	Sandstone with differential ferruginization	9.69	0.48	2.37	23.93	237.10	5.31	11.97	21.81	41.73	5.35

Sl No.	Sample No.	Sample Deptrh (m)	Sample Description	Host lithology	Li	Be	Sc	V	Cr	Co	Ni	Cu	Zn	Ga
18	113368	40.11 to 40.16	Yellowish ocher to yellowish brown coloured, very coarse to coarse grained, planar cross stratified ferruginous sandstone. The sandstone comprises subangular to subrounded grains of quartz (~97%), hematite, very few muscovite (<1%) and white transparent crystals embedded in a clay matrix/cement. Magnetite are observed to be associated with the quartz grains. Silicification has also observed at different parts of the stratigraphic levels. Different orders of ferruginization is also observed, mainly defining the stratification.Silicification may have reduced grain size ???	Mica bearing ferruginized sandstone	9.48	0.40	2.03	23.41	238.84	4.70	6.65	17.90	16.25	6.21
19	113369	40.62 to 40.70	Yellowish brown coloured, very coarse to extremely coarse grained, planar cross stratified ferruginous sandstone. The sandstone comprises subangular to subrounded grains (with moderate to high sphericity) of quartz (97%), other white transparent crystals (both or translucent), very few hematite (& <1), muscovite & magnetite are observed to be within the quartz grains. Silicification has also observed	Mica bearing ferruginized sandstone	10.16	0.52	2.14	29.66	193.49	5.68	8.87	29.24	19.27	5.24

Sl No.	Sample No.	Sample Deptrh (m)	Sample Description	Host lithology	Li	Be	Sc	V	Cr	Co	Ni	Cu	Zn	Ga
20	113370	44.51 to 44.58	Yellowish brown coloured, very coarse to coarse grained, planar cross-stratified ferruginous sandstone. Grains are sub-angular to sub-rounded and composed predominantly of quartz (~97%), with minor hematite, very few muscovite (<1%), and white transparent crystals embedded in a clay matrix. Magnetite are observed to be associated within the grooves of the quartz grains. Localised silicification is present at different stratigraphic levels and may have reduced grain size at the corresponding stratigraphic level. Weak to moderate ferruginisation in shades of yellowish brown to reddish white to reddish brown and red colour is observed, variably defining stratification.	Mica bearing ferruginized sandstone	10.44	0.46	2.74	24.20	147.35	24.35	6.30	186.38	16.05	5.58
21	113371	47.40 to 47.59	Yellowish white coloured, poorly sorted, medium to coarse grained ferruginous sandstone. The sandstone comprises sub-angular grains of mostly quartz, very few hematite embedded in a siliceous/clay matrix/cement. No internal structure has been observed within the sandstone. Strong ferruginization (brownish red colour) occurs mostly in the form of patch or thin layers.	Sandstone with differential ferruginization	10.01	0.58	5.33	51.27	115.18	12.39	6.22	21.74	24.38	8.24
22	113372	48.36 to 48.46	Yellowish brown to reddish brown coloured, poorly sorted, medium to coarse grained ferruginous sandstone. The sandstone comprises sub-angular grains of mostly quartz, very few hematite embedded in a siliceous/clay matrix/cement. No internal structure has been observed within the sandstone. Ferruginization occurs in different orders, ranging in	Yellowish brown coloured ferruginized sandstone	9.46	0.62	2.73	86.69	188.14	10.69	13.66	67.29	41.49	5.86

Sl No.	Sample No.	Sample Deptrh (m)	Sample Description	Host lithology	Li	Be	Sc	V	Cr	Co	Ni	Cu	Zn	Ga
			shades of brown, red and yellowish brown at different stratigraphic levels. Almost all the quartz grains are stained.											
23	113140	15.50 to 17.50	The unit received as both core and sludge, from 13.46m to 14 m and from 15 to 15.86m and 16.85-17m core has been recieved where as the rest part is recieved as sludge. The core is of ferruginous sandstone, medium to fine grained and comprises both angular to sub-rounded transparent (crystal clear) & detritus quartz, clay, white sandstone clasts (remnanet of the parent rock??), magnetite, very few euhedral feldspar (??), very few mica (mainly at the high ferruginized part) embedded in ferruginous cement/matrix. Voids filled with carbonates (acid test positve) also observed at places. From 15.26 m to 15.86m the amount of ferrugination increases abruptly in such a way that it seems to be a zoned alteration. The grainsize decreases at this depth. At 15.63m secondary verigated colour alteration is observed along thin veinletts and pyrite occurs within the groove area (blue material gives blue streak).The sludge is yellowish white to white in colour, poorly sorted, coarse to fine grained (grain size decreases with depth), and consists predpominantly of angular to sub	Mica bearing metasomatized sandstone	11.29	<0.1	4.06	47.63	106.71	5.66	16.79	12.03	73.52	3.36

Sl No.	Sample No.	Sample Deptrh (m)	Sample Description	Host lithology	Li	Be	Sc	V	Cr	Co	Ni	Cu	Zn	Ga
			angular grains with low sphericity. The sludge is mineralogically comprises quartz (>95%), white transparent crystals, hematite, few magnetite (mainly observed within the grooves of quartz grains) & rock fragments in a decreasing order of abundance.											
24	113399	17.50 to 18.46	Reddish white to greyish white shale. Very fine grained, no minerals can be identified. Ferrugination of different order is observed at different stratigraphic levels. The ferrugination decreases with depth.	Shale	39.10	3.73	21.71	146.70	88.73	5.80	26.18	29.62	66.89	27.19

Table Continued..

Annexure-XXXf

Sl No.	Sample No.	Ge	Se	Rb	Sr	Y	Zr	Nb	Mo	Cd	In	Sn	Sb	Cs
1	112492	0.38	<0.1	1.65	36.24	9.22	74.83	19.06	3.56	3.70	9.47	52.84	8.46	<0.1
2	112493	0.14	<0.1	30.36	153.95	6.96	79.75	20.27	0.51	1.70	1.90	58.20	0.30	13.48
3	112493	<0.1	<0.1	<0.1	247.74	7.94	114.12	9.96	0.67	1.40	1.24	69.53	3.13	10.26
4	112494	0.45	<0.1	17.40	173.49	19.62	276.82	116.43	1.60	3.32	11.13	48.41	7.33	33.55

Sl No.	Sample No.	Ge	Se	Rb	Sr	Y	Zr	Nb	Mo	Cd	In	Sn	Sb	Cs
5	112495	0.10	<0.1	98.77	75.74	6.70	88.41	22.05	0.78	1.27	1.19	672.29	10.74	27.75
6	112496	0.94	<0.1	<0.1	49.98	39.86	262.71	10.93	5.73	4.26	15.20	49.02	11.11	27.34
7	113375	0.13	2.29	6.69	23.82	5.38	102.52	16.93	1.20	1.56	1.46	114.08	3.78	11.10
8	113376	0.52	1.54	3.18	24.93	7.99	89.13	11.07	1.89	2.57	6.81	69.74	7.61	8.97

Sl No.	Sample No.	Ge	Se	Rb	Sr	Y	Zr	Nb	Mo	Cd	In	Sn	Sb	Cs
9	113378	<0.1	0.42	1.23	36.12	6.81	93.61	12.15	1.02	1.28	0.27	82.42	2.56	9.05
10	113374	0.15	5.13	<0.1	45.31	7.08	87.95	12.04	4.20	2.26	3.37	78.83	6.02	3.69
11	113373	0.19	0.33	54.05	83.94	33.02	157.18	10.00	1.70	1.27	2.84	53.54	2.72	30.64
12	113006	1.02	28.48	<0.1	16.06	14.26	220.67	12.41	0.48	1.87	<0.01	5.99	31.50	<0.1

Sl No.	Sample No.	Ge	Se	Rb	Sr	Y	Zr	Nb	Mo	Cd	In	Sn	Sb	Cs
13	113007	<0.1	<0.1	11.15	49.78	38.49	263.94	19.39	<0.1	2.17	0.38	9.60	8.18	3.75
14	113357	0.33	1.17	8.64	89.01	18.52	276.24	9.31	1.73	1.31	1.72	49.24	2.81	35.37
15	113004	0.72	<0.1	<0.1	57.15	11.67	105.04	8.12	4.86	0.97	0.23	2.14	30.02	0.17
16	113005	0.35	<0.1	21.88	54.24	10.35	93.73	6.06	0.61	1.55	<0.01	1.39	26.92	2.37

Sl No.	Sample No.	Ge	Se	Rb	Sr	Y	Zr	Nb	Mo	Cd	In	Sn	Sb	Cs
17	113367	<0.1	3.14	6.20	21.68	4.03	74.38	13.68	1.57	1.49	0.52	93.68	3.90	2.71
18	113368	0.11	1.11	0.21	28.73	3.37	63.79	13.46	0.78	1.29	<0.01	94.73	2.12	3.78
19	113369	0.08	2.54	<0.1	19.81	2.99	54.57	10.99	1.03	1.26	0.25	78.92	3.88	2.16
20	113370	<0.1	<0.1	<0.1	19.40	4.23	79.33	8.29	0.89	1.29	0.35	80.47	2.01	6.73

Sl No.	Sample No.	Ge	Se	Rb	Sr	Y	Zr	Nb	Mo	Cd	In	Sn	Sb	Cs
21	113371	0.12	1.83	0.25	68.16	13.76	247.37	8.14	1.05	1.28	0.96	46.79	2.83	24.42
22	113372	<0.1	1.37	<0.1	20.20	3.74	65.54	10.59	1.91	1.40	0.59	79.60	2.98	4.14
23	113140	<0.01	1.74	0.87	25.14	8.49	102.59	5.62	16.97	0.18	<0.01	0.42	<0.1	<0.1
24	113399	0.21	5.71	44.09	83.61	39.03	148.54	15.42	2.81	0.32	<0.01	2.85	1.15	3.73

Table Continued..

Annexure-XXXf

Sl No.	Sample No.	Ba	La	Ce	Pr	Nd	Sm	Eu	Gd	Tb	Dy	Ho	Er	Tm	Yb
1	112492	28.00	11.89	18.28	24.96	15.89	5.81	1.04	12.52	2.47	1.61	<0.1	1.16	0.16	1.69
2	112493	38.28	20.59	37.41	3.58	16.89	2.36	0.49	1.07	0.28	1.34	0.15	1.09	0.17	0.45
3	112493	61.84	21.72	45.32	3.84	19.96	2.90	0.59	1.31	0.67	2.13	<0.1	1.29	0.10	0.56
4	112494	64.87	39.00	92.92	26.62	97.03	11.41	3.83	13.19	6.55	4.97	0.29	5.58	0.16	2.57
5	112495	45.32	37.07	83.24	8.60	18.38	5.11	1.29	1.93	0.66	1.93	0.17	1.23	0.17	0.47

Sl No.	Sample No.	Ba	La	Ce	Pr	Nd	Sm	Eu	Gd	Tb	Dy	Ho	Er	Tm	Yb
6	112496	54.56	52.28	99.21	38.86	95.85	30.10	7.19	24.81	3.15	20.18	<0.1	4.58	<0.1	6.86
7	113375	49.66	14.16	29.20	3.06	15.85	1.97	0.42	1.94	0.76	1.45	<0.1	0.83	0.10	0.59
8	113376	42.63	14.20	27.58	14.57	17.10	4.81	0.82	9.19	1.17	1.79	0.46	1.01	0.10	1.55
9	113378	53.48	18.85	42.92	2.80	19.73	2.91	0.58	1.27	0.62	1.74	0.27	0.94	0.10	0.43
10	113374	278.95	11.61	23.26	7.89	12.24	3.18	1.75	4.77	0.74	1.37	0.32	0.62	<0.1	1.41

Sl No.	Sample No.	Ba	La	Ce	Pr	Nd	Sm	Eu	Gd	Tb	Dy	Ho	Er	Tm	Yb
11	113373	222.09	64.26	127.85	7.78	56.25	8.15	2.35	3.83	1.97	7.84	0.77	3.10	<0.1	2.09
12	113006	68.58	52.30	87.58	7.24	26.72	5.21	0.41	4.07	0.49	2.62	0.48	1.72	0.22	1.42
13	113007	175.59	75.35	134.72	10.02	46.17	5.13	1.95	6.88	1.36	10.22	1.45	3.65	0.62	5.85
14	113357	290.21	54.19	127.75	7.46	61.13	8.51	1.81	3.52	2.13	5.00	<0.1	2.75	0.11	1.16
15	113004	399.05	30.51	60.68	4.59	17.00	1.61	0.74	6.18	0.43	2.52	0.51	0.99	0.15	0.53

Sl No.	Sample No.	Ba	La	Ce	Pr	Nd	Sm	Eu	Gd	Tb	Dy	Ho	Er	Tm	Yb
16	113005	166.62	38.73	81.00	6.08	26.04	6.10	0.41	6.07	0.86	1.38	0.31	0.79	<0.1	1.52
17	113367	285.14	8.96	19.51	1.88	9.96	1.48	0.18	1.07	0.39	1.16	0.25	0.63	0.10	0.35
18	113368	138.27	8.23	17.26	1.56	9.32	1.61	0.31	0.75	0.33	1.05	0.37	0.47	0.10	0.28
19	113369	67.70	6.71	14.02	1.52	6.97	1.41	0.38	0.93	0.21	0.71	0.21	0.41	0.10	0.29
20	113370	79.12	15.08	34.90	2.28	16.61	2.42	0.21	0.91	0.50	1.24	0.27	0.75	0.10	0.32

Sl No.	Sample No.	Ba	La	Ce	Pr	Nd	Sm	Eu	Gd	Tb	Dy	Ho	Er	Tm	Yb
21	113371	329.42	71.58	172.80	8.38	66.92	9.56	0.93	3.13	1.52	4.21	0.52	2.12	0.11	0.80
22	113372	64.77	9.60	20.52	2.82	9.43	1.07	0.57	1.54	0.40	0.68	0.22	0.49	0.09	0.46
23	113140	73.18	24.44	48.83	5.43	19.21	3.34	0.36	2.79	0.29	1.72	0.32	0.98	0.14	0.89
24	113399	248.23	69.27	138.88	14.57	53.13	10.08	2.27	9.71	1.51	7.65	1.48	4.15	0.60	3.73

Table Continued..

Annexure-XXXf

Sl No.	Sample No.	Lu	Hf	Ta	W	Tl	Pb	Bi	Th	U	Ag	Te	Mn	HREEY	LREE	TREEY	HREEY/LREE	THIE
1	112492	0.32	1.82	3.65	0.24	<0.05	23.38	0.23	34.99	30.97	NA	14.66	NA	39.62	76.83	116.45	0.52	240.75
2	112493	0.01	2.39	0.98	<0.1	0.46	3.83	<0.1	2.80	<0.1	NA	2.23	NA	15.77	80.84	96.60	0.20	113.58
3	112493	0.02	2.85	0.93	0.43	1.88	5.07	<0.1	3.38	<0.1	1.29	1.79	NA	19.01	93.74	112.75	0.20	128.55
4	112494	0.30	5.95	5.48	0.31	<0.05	11.50	0.26	31.94	15.62	NA	22.73	NA	121.17	266.97	388.14	0.45	495.02

Sl No.	Sample No.	Lu	Hf	Ta	W	Tl	Pb	Bi	Th	U	Ag	Te	Mn	HREEY	LREE	TREEY	HREEY/LREE	THIE
5	112495	0.02	1.75	3.55	0.19	2.12	7.82	0.96	2.90	<0.1	NA	1.15	NA	19.42	152.40	171.82	0.13	770.76
6	112496	0.41	6.74	6.04	1.77	0.58	21.14	1.55	53.45	34.18	2.52	23.75	NA	122.29	316.30	438.59	0.39	422.76
7	113375	0.04	2.61	1.12	0.29	<0.05	4.25	<0.1	5.88	0.77	1.05	2.37	NA	16.99	64.24	81.23	0.26	218.12
8	113376	0.17	1.92	2.38	0.68	0.63	9.42	<0.1	23.75	14.52	1.16	10.26	NA	33.41	78.26	111.67	0.43	238.28
9	113378	0.10	2.57	0.93	0.63	2.73	4.95	<0.1	3.04	<0.1	1.14	0.75	NA	16.72	87.21	103.93	0.19	163.12

Sl No.	Sample No.	Lu	Hf	Ta	W	Tl	Pb	Bi	Th	U	Ag	Te	Mn	HREEY	LREE	TREEY	HREEY/LREE	THIE
10	113374	0.09	2.81	2.51	1.17	<0.05	30.07	<0.1	12.09	6.21	1.07	3.82	NA	26.75	58.18	84.93	0.46	535.62
11	113373	0.05	5.00	1.91	2.23	2.90	17.99	<0.1	8.09	<0.1	1.35	5.23	NA	77.85	264.29	342.14	0.29	236.87
12	113006	0.47	4.63	0.64	0.60	0.06	6.81	<0.1	22.21	3.14	1.45	1.03	NA	27.07	179.04	206.11	0.15	119.25
13	113007	0.71	7.46	1.03	3.20	0.09	18.48	<0.1	23.60	6.42	<0.05	1.04	NA	94.17	271.40	365.57	0.35	149.72
14	113357	0.03	7.79	1.86	1.20	1.50	16.72	<0.1	8.33	<0.1	2.31	6.43	NA	45.65	259.04	304.69	0.18	193.83

Sl No.	Sample No.	Lu	Hf	Ta	W	Tl	Pb	Bi	Th	U	Ag	Te	Mn	HREEY	LREE	TREEY	HREEY/LREE	THIE
15	113004	<0.1	4.04	0.47	0.40	0.06	16.44	<0.1	10.60	3.48	<0.05	<0.05	NA	35.23	114.39	149.62	0.31	116.51
16	113005	0.09	1.98	0.20	0.12	0.07	11.75	<0.1	16.78	2.31	<0.05	1.06	NA	26.54	157.94	184.48	0.17	74.23
17	113367	0.02	2.94	0.77	0.68	1.99	15.44	<0.1	3.01	0.21	3.41	0.87	NA	10.55	41.79	52.34	0.25	194.91
18	113368	0.01	1.91	0.82	1.53	0.64	3.14	<0.1	1.98	<0.1	0.95	<0.05	NA	9.07	37.98	47.05	0.24	155.38
19	113369	0.02	1.63	0.63	2.13	1.53	2.26	<0.1	2.34	0.32	0.71	0.39	NA	8.39	30.63	39.02	0.27	155.67

Sl No.	Sample No.	Lu	Hf	Ta	W	Tl	Pb	Bi	Th	U	Ag	Te	Mn	HREEY	LREE	TREEY	HREEY/LREE	THIE
20	113370	0.01	2.29	0.71	0.50	0.58	4.05	<0.1	3.07	<0.1	1.05	<0.05	NA	11.28	71.29	82.57	0.16	304.58
21	113371	0.02	7.82	1.28	0.50	<0.05	8.47	<0.1	11.80	<0.1	1.87	1.86	NA	32.45	329.24	361.69	0.10	120.44
22	113372	0.03	1.87	0.83	1.20	0.46	8.29	<0.1	4.24	1.05	0.78	0.58	NA	10.95	43.44	54.39	0.25	221.10
23	113140	0.13	2.68	0.16	72.88	<0.1	1.37	<0.1	12.62	1.63	2.24	<0.05	62.1483	20.18	101.25	121.43	0.20	114.85
24	113399	0.55	3.92	0.72	1.29	<0.1	24.83	<0.1	22.12	6.23	<0.05	0.08	21.7205	92.40	285.92	378.32	0.32	164.23

Annexure-XXXg: ICPMS of BH07

Sl No.	Sample No.	BH No.	Sample Depth (m)	Sample Description	Host Lithology
1	112460	GSPL BHUJ 319/07 /2025	0	Highly ferruginized metasomatized sandstone. It is medium-grained and composed of angular to rounded quartz grains, euhedral feldspars, and aggregates of mica, all embedded within a hematitic to magnetite-rich matrix or cement. The unit exhibits evidence of flow structures. Additionally, a greenish to greenish-blue hue has been observed along several fracture surfaces. A portion of the powdered rock is attracted to a strong magnet and leaves a a black streak, further indicating a magnetite-rich composition.	Highly ferruginized metasomatized sandstone
2	112461	GSPL BHUJ 320/07 /25	0	Blackish red coloured (with purplish tint) ferruginous sandstone, composed of angular to rounded quartz, euhedral feldspar, muscovite (possibly detritus), embedded in a hematitic and magnetite-rich matrix/cement. The rock powder is attracted by strong magnet. Fracture filled with calcrete.	Mica bearing ferruginized sandstone
3	112462	GSPL BHUJ 321/07 /25	0	Blackish red coloured sandstone, separated by yellowish occur coloured shale/clay. Thin veinlets of black materials (very few parts of the powder of the material are attracted by magnet, cherry red streak), are observed to be cross cutting the sandstone. The sandstone is medium to coarse grained and consists of angular to rounded quartz (detritus), muscovite (detritus), biotite (??), weathered sub-rounded feldspar embedded in a mostly hematite and poorly magnetite-rich matrix/cement. Secondary fluid (silvery pinkish blue, golden, varigated colour) along few fractures are also observed.	Mica bearing ferruginized sandstone
4	112172	GSPL BHUJ BH07	1.97 to 2.00	Brownish red to black coloured altered ferruginous sandstone, comprising coarse to fine grained quartz, quartz aggregates, hematite, magnetite, euhedral alkali feldspars, muscovite, bluish quartz, seldom occurence of native Cu embedded in a hematite-magnetite ground mass. The grains are predominantly angular to sub angular with low sphericity, sharp crystal phase boundaries are also observed.The quartz aggregates are consist of 3/4 quartz crystals, surrounded by & embedded in dark black (possibly magnetite) groundmass.Alterations are observed in layers & the euhedral feldspars mostly grow along the boundaries. Native Cu, bluish to green (malachite??) staining is also observed within the sample.	Highly ferruginized metasomatized sandstone
5	113388	GSPL BHUJ BH07	5.31m to 5.43	Brownish red to black coloured ferruginous sandstone, comprising of coarse to fine grained quartz, quartz aggregates, hematite, magnetite, euhedral alkali feldspars, muscovite, bluish quartz, embedded in a hematite-magnetite rich ground mass. The grains are predominantly angular to sub angular with low sphericity, sharp crystal phase boundaries are also observed.The quartz aggregates are consist of 3/4 quartz crystals, surrounded by & embedded in dark black (possibly magnetite) groundmass.Ferruginization are observed in layers & the euhedral feldspars mostly grow along the boundaries. However, the amount of feldspar decreases with respect to the litho-unit, observed at 1-2.17m depth. Alternating coarse & fine layering is also observed.	Highly ferruginized metasomatized sandstone
6	113389	GSPL BHUJ BH07	7.00m to 7.10m	Reddish brown to yellowish brown coloured ferruginous sandstone comprises of medium to coarse grained, moderate to well sorted, quartz, hematite & few feldspar embedded in a hematitic matrix. Ferrugination of the sandstone differs at different stratigraphic levels, where the ferruginisation is high, it generally occurs as layer. Occurrence of book mica (biotite) along the layers of strong iron impregnation is also observed. Silicification also observed along these layers.	Mica bearing ferruginized sandstone
7	113003	GSPL BHUJ BH07	15.80 to 15.85	Reddish brown to yellowish brown coloured ferruginous sandstone with grain size varying from v. coarse to fine, poorly sorted, grains are ranging between sub angular to sub rounded with moderate to high sphericity. The degree of ferruginization varies with grain size, the higher the grain size, the higher the ferruginization. Planar cross stratification within the core is also observed.The sandstone comprises quartz (>95%), hematite, biotite, few platy white transparent crystals, magnetite in a decreasing order of abundance embedded in a ferruginous matrix/cement. Occurence of euhedral feldspars (with sharp crystal boundaries) and areas with green (malachite??) staining is observed at the highest ferruginous zone.	Mica bearing ferruginized sandstone
8	113390	GSPL BHUJ BH07	16.13 to 16.18	Brownish red to yellow ochre coloured ferruginous sandstone with grain size varying from very coarse to fine, poorly sorted, grains are ranging between sub angular to sub rounded to moderate to high sphericity. The degree of ferruginisation varies with grain size, the higher the grain size, the higher the ferruginisation..The sandstone comprises quartz (>95%), hematite, biotite, few platy white transparent crystals, magnetite in a decreasing order of abundance embedded in a ferruginous matrix/cement. Occurence of euhedral feldspars (possibly) with sharp crystal boundaries and areas with green (malachite??) staining is observed at the highest ferruginous zone.	Mica bearing ferruginized sandstone

Table Continued..

Annexure-XXXg

Sl No.	Sample No.	Li	Be	Sc	V	Cr	Co	Ni	Cu	Zn	Ga	Ge	Se	Rb	Sr	Y	Zr	Nb
1	112460	5.2	0.9	1.8	15.4	146.2	9.9	19.1	0.72	29.6	28.3	0.9	0.1	4.6	34.9	5.4	48.4	7.7
2	112461	5.4	0.9	2.9	16.2	164.7	8.9	17.8	0.54	31.2	14.4	0.5	1.2	12.9	25.0	3.7	60.9	9.3
3	112462	8.5	2.6	8.0	57.4	147.4	30.2	54.1	7.75	124.7	34.9	0.9	<0.1	22.3	70.7	21.2	234.7	8.5
4	112172	29.02	1.19	2.72	22.96	3.92	10.96	45.01	8.32	27.48	6.76	0.89	5.32	18.82	14.68	6.41	24.95	1.60
5	113388	5.64	<0.1	2.26	11.13	67.97	9.57	21.77	<0.1	30.00	1.12	0.10	0.81	10.97	16.48	3.77	21.13	1.47
6	113389	9.84	<0.1	1.61	12.55	111.03	2.23	1.69	<0.1	7.36	2.94	<0.01	1.29	12.03	15.27	2.89	40.76	3.66
7	113003	18.79	3.44	1.90	36.10	132.27	10.80	44.83	<0.1	84.22	6.49	1.75	<0.1	9.77	20.06	6.98	30.38	2.90
8	113390	10.38	<0.1	3.00	26.43	146.27	0.89	1.56	<0.1	10.17	5.45	<0.01	0.90	15.33	30.18	5.89	102.07	8.17

Table Continued..

Annexure-XXXg

Sl No.	Sample No.	Mo	Cd	In	Sn	Sb	Cs	Ba	La	Ce	Pr	Nd	Sm	Eu	Gd	Tb	Dy	Ho	Er
1	112460	0.3	4.5	15.5	51.2	12.5	<0.1	222.8	5.9	9.4	29.3	7.4	6.6	0.4	18.2	1.4	1.3	0.3	0.4
2	112461	0.7	2.5	6.9	56.4	7.1	1.6	114.5	5.3	11.5	14.0	7.4	2.8	0.4	8.8	0.8	0.4	<0.1	0.4
3	112462	1.1	4.4	15.4	27.6	10.6	14.7	391.9	47.6	105.8	34.2	47.7	13.7	1.1	20.4	2.3	4.3	<0.1	1.9
4	112172	<0.1	1.85	<0.01	<0.1	27.11	3.13	132.98	4.96	14.61	1.73	5.78	1.00	0.46	0.93	0.13	0.95	0.21	0.27
5	113388	31.13	0.32	<0.01	<0.01	1.65	<0.1	129.58	6.61	15.77	2.06	7.16	1.51	0.40	1.37	0.13	1.02	0.20	0.56
6	113389	37.39	0.23	<0.01	0.95	0.25	<0.1	115.22	11.96	23.76	2.59	9.29	1.58	0.25	1.33	<0.1	0.80	0.15	0.43
7	113003	2.28	2.94	0.22	1.85	32.29	2.03	153.05	8.21	18.76	2.19	7.00	1.56	0.54	1.48	0.25	0.68	0.23	0.39
8	113390	44.99	0.32	<0.01	0.93	0.49	<0.1	156.64	33.68	70.34	7.19	24.70	3.95	0.41	3.15	0.31	1.59	0.26	0.73

Table Continued..

Annexure-XXXg

Sl No.	Sample No.	Tm	Yb	Lu	Hf	Ta	W	Tl	Pb	Bi	Th	U	Ag	Te	Mn	HREEY	LREE	TREEY	HREEY/LREE
1	112460	0.1	2.2	0.4	1.6	3.4	0.2	1.9	6.5	4.7	46.1	45.1	1.33	20.05	NA	31.87	58.55	90.42	0.54
2	112461	0.1	1.2	0.2	1.9	1.8	0.4	1.3	3.8	1.5	23.1	19.2	1.00	8.69	NA	18.93	40.95	59.88	0.46
3	112462	<0.1	2.9	0.4	7.0	4.4	0.9	1.0	12.2	2.0	52.4	38.6	2.84	22.53	NA	62.65	249.02	311.67	0.25
4	112172	<0.1	0.26	0.12	0.31	0.16	0.52	0.07	7.19	<0.1	2.31	0.88	0.75	<0.05	NA	12.55	28.08	40.64	0.45
5	113388	<0.1	0.57	0.08	0.66	<0.1	0.44	<0.1	7.64	<0.1	3.15	3.24	<0.05	<0.05	1438.37	10.46	33.11	43.57	0.32
6	113389	<0.1	0.43	0.06	1.34	<0.1	0.59	<0.1	4.47	<0.1	6.01	1.24	<0.05	<0.05	209.49	8.14	49.18	57.32	0.17
7	113003	<0.1	0.25	0.08	0.45	<0.1	9.36	0.08	16.49	<0.1	5.63	4.08	4.15	2.13	NA	12.89	37.72	50.61	0.34
8	113390	<0.1	0.66	0.09	2.76	0.26	0.68	<0.1	11.20	<0.1	19.15	1.46	<0.05	<0.05	85.19	16.19	139.85	156.04	0.12

Table Continued..

Annexure-XXXg

SI No.	Sample No.	BH No.	Sample Depth (m)	Sample Description	Host Lithology
9	113001	GSPL BHUJ BH07	24.53 to 24.59	Reddish brown coloured, medium to fine grained ferruginized sandstone. The sandstone consist of quartz, very very few muscovite (<1%) embedded in a clay matrix cement. Silicification is also suspected at places. A consistent ferruginous staining is observed within the sample.	Alternating ferruginous sandstone and mica bearing metasomatized sandstone
10	112173	GSPL BHUJ BH07	24.74 to 24.81	Yellow ocher to reddish brown coloured, medium to fine grained metasomatised ferruginous sandstone. It consists of angular to sub angular grains of quartz, moderate amount of muscovite, hematite, biotite and magnetite in a decreasing order of abundance. Silicification of the metasomatised part also observed. The colour of ferruginization varies from yellow, ochres to reddish brown to dark red.	Alternating ferruginous sandstone and mica bearing metasomatized sandstone
11	113365	GSPL BHUJ BH07	26.01 to 26.07	Reddish brown to dark brown coloured, medium to fine grained metasomatised ferruginous sandstone. The fine grained sandstone is metasomatised with iron impregnation and consists angular to sub angular grains of quartz, lots of muscovite, hematite, magnetite (in the darker area) in a decreasing order of abundance. The more the metasomatism the amount of muscovite increases. Silicification of the metasomatised part also observed. This part is more metasomatised than the previous sample (112173).	Alternating ferruginous sandstone and mica bearing metasomatized sandstone
12	113366	GSPL BHUJ BH07	28.01 to 28.08	Yellow ocher to reddish brown coloured, medium to fine grained metasomatised sandstone. The fine grained sandstone is metasomatised with iron impregnation in thin layers, possibly following the stratification. It consists of angular to sub angular grains of quartz, lots of muscovite, hematite, magnetite in a decreasing order of abundance. The more the metasomatism the amount of muscovite increases.	Alternating ferruginous sandstone and mica bearing metasomatized sandstone

Table Continued..

Annexure-XXXg

SI No.	Sample No.	BH No.	Sample Depth (m)	Sample Description	Host Lithology
13	113387	GSPL BHUJ BH07	29.59 m to 29.69m	Brown to reddish brown coloured, fine to medium grained, moderately sorted ferruginous sandstone . The sandstone shows distinct horizontal laminations and gradational colour bands from pale brownish yellow at the base to dark brown at the top. Grain composition includes angular to sub angular quartz grains stained by iron oxides, limited feldspar content, trace magnetite, and rare mica flakes in decreasing order of abundance. Presence of ferruginous cement and oxidized zones is indicated by the strong reddish hue and textural variation throughout the unit.	Mica bearing ferruginized sandstone
14	113002	GSPL BHUJ BH07	31.10 to 31.20	Reddish brown to blackish brown coloured, medium to fine grained, moderately sorted ferruginous sandstone. The sandstone is highly ferruginous & consists of angular to sub angular quartz (each grain is stained), very few feldspar, magnetite, seldom occurrence of mica in a decreasing order of abundance. Thin laminae of silicification is observed at places.	Mica bearing ferruginized sandstone
15	113155	GSPL_BHUJ_BH07	15.50 to 16.30	Reddish brown to yellowish brown coloured ferruginous sandstone with grain size varying from v. coarse to fine, poorly sorted, grains are ranging between sub angular to sub rounded with moderate to high sphericity. The degree of ferruginization varies with grain size, the higher the grain size, the higher the ferruginization. Planar cross stratification within the core is also observed.The sandstone comprises quartz (>95%), hematite, biotite, few platy white transparent crystals, magnetite in a decreasing order of abundance embedded in a ferruginous matrix/cement. Occurence of euhedral feldspars (with sharp crystal boundaries) and areas with green (malachite??) staining is observed at the highest ferruginous zone.	Mica bearing ferruginized sandstone
16	113398	GSPL_BHUJ_BH07	24.50 to 25.50	White to dark brown coloured, alternating occurence of ferruginous and mica bearing metasomatized sandstone with different degree of ferrugination and metasomatism. ~60-70% of the sample consists of the mica bearing metasomatized sandstone.	Alternating ferruginous sandstone and mica bearing metasomatized sandstone
17	113379	GSPL_BHUJ_BH07	30.50 to 31.50	Reddish brown to blackish brown coloured, medium to fine grained, moderately sorted ferruginous sandstone.The sandstone is highly ferruginous & consists of angular to sub angular quartz (each grain is stained), very few feldspar, magnetite, seldom occurrence of mica in a decreasing order of abundance. Thin laminae of silicification is observed at places.The sludge is similar as previous with less amount of magnetite, few altered feldspar and brownish white in colour, moderate sorting & angular to sub angular grains with low sphericity. Silicification in thin laminae is also observed.	Mica bearing ferruginized sandstone

Table Continued..

Annexure-XXXg

Sl No.	Sample No.	Li	Be	Sc	V	Cr	Co	Ni	Cu	Zn	Ga	Ge	Se	Rb	Sr	Y	Zr	Nb
9	113001	32.59	3.42	6.31	24.86	211.09	9.31	28.44	<0.1	21.47	10.95	0.90	29.38	<0.1	30.95	9.89	141.10	10.85
10	112173	31.50	5.67	12.95	79.88	<0.1	13.90	38.73	<0.1	55.98	15.83	0.27	14.92	18.30	59.81	20.94	257.82	8.00
11	113365	10.60	2.70	12.15	84.95	93.67	21.91	34.85	9.24	108.09	32.53	0.66	<0.1	33.91	81.76	25.64	222.08	5.94
12	113366	17.15	1.14	9.30	123.61	138.30	13.47	14.50	17.90	42.25	25.68	0.48	<0.1	40.68	63.72	17.59	345.94	8.80
13	113387	21.91	0.81	9.25	93.40	131.43	3.50	14.39	<0.1	38.18	17.13	<0.01	3.60	36.82	89.37	16.00	242.46	14.41
14	113002	28.15	<0.1	2.41	15.93	15.77	6.92	20.72	<0.1	12.19	3.93	<0.1	<0.1	27.83	33.10	4.18	66.08	4.59

Table Continued..

Annexure-XXXg

Sl No.	Sample No.	Li	Be	Sc	V	Cr	Co	Ni	Cu	Zn	Ga	Ge	Se	Rb	Sr	Y	Zr	Nb
15	113155	17.78	0.28	6.55	48.72	92.75	4.47	17.40	<0.1	95.47	11.84	0.09	2.43	37.77	58.01	12.75	160.71	9.16
16	113398	25.47	1.31	13.33	83.66	76.51	7.56	25.84	<0.1	39.74	20.68	0.19	7.12	55.88	68.11	25.08	378.32	13.01
17	113379	7.77	0.39	2.26	17.22	128.22	11.82	10.28	12.78	19.11	6.97	<0.1	0.37	18.26	53.54	4.48	79.30	26.79

Table Continued..

Annexure-XXXg

Sl No.	Sample No.	Mo	Cd	In	Sn	Sb	Cs	Ba	La	Ce	Pr	Nd	Sm	Eu	Gd	Tb	Dy	Ho	Er
9	113001	2.74	3.47	0.03	8.61	25.37	<0.1	269.99	33.03	77.35	7.05	25.39	2.42	0.14	2.69	0.34	2.31	0.60	0.92
10	112173	4.50	1.73	<0.01	<0.1	37.80	1.34	457.81	75.79	177.94	14.00	59.16	12.70	0.84	6.36	0.93	7.44	1.21	2.49
11	113365	2.17	5.05	12.39	24.47	10.11	12.47	463.82	42.33	102.01	28.85	43.63	12.25	1.61	17.42	2.00	6.84	<0.1	2.14
12	113366	2.21	2.17	4.88	48.15	5.16	24.80	510.92	49.38	101.80	13.36	50.00	7.96	1.01	7.51	1.66	4.15	0.39	2.30
13	113387	17.83	0.21	<0.01	1.91	1.70	0.93	436.70	69.52	138.37	14.22	50.30	8.44	1.12	6.88	0.83	3.74	0.65	1.85
14	113002	<0.1	0.67	<0.01	5.02	27.43	<0.1	210.83	13.07	30.67	2.84	11.91	0.49	0.39	0.57	0.40	1.29	0.23	0.38

Table Continued..

Annexure-XXXg

Sl No.	Sample No.	Mo	Cd	In	Sn	Sb	Cs	Ba	La	Ce	Pr	Nd	Sm	Eu	Gd	Tb	Dy	Ho	Er
15	113155	133.61	1.07	<0.01	1.68	<0.1	<0.1	336.04	54.03	112.65	11.60	40.71	6.94	0.77	5.45	0.65	3.06	0.52	1.41
16	113398	13.94	0.61	<0.01	1.91	3.33	0.66	483.14	100.99	210.14	22.15	78.71	13.64	1.50	10.55	1.32	5.80	0.98	2.72
17	113379	1.05	0.25	0.04	29.00	1.68	1.75	276.67	16.39	40.29	5.66	18.90	2.87	0.33	1.69	0.31	1.06	<0.1	0.64

Table Continued..

Annexure-XXXg

Sl No.	Sample No.	Tm	Yb	Lu	Hf	Ta	W	Tl	Pb	Bi	Th	U	Ag	Te	Mn	HREEY	LREE	TREEY	HREEY/LREE
9	113001	<0.1	0.96	0.25	5.00	0.51	0.86	0.14	8.97	<0.1	18.66	2.06	1.39	1.06		24.51	145.25	169.76	0.17
10	112173	0.44	4.49	0.34	6.24	0.79	0.88	0.13	21.61	<0.1	31.27	5.08	1.52	1.05		58.42	339.59	398.00	0.17
11	113365	<0.1	3.36	0.32	6.58	3.78	1.18	2.19	18.59	<0.1	43.28	30.81	2.44	18.51		71.68	229.07	300.75	0.31
12	113366	0.10	1.76	0.13	9.85	2.25	1.42	0.44	19.78	<0.1	21.98	5.18	14.92	10.99		45.90	222.50	268.40	0.21
13	113387	0.25	1.73	0.25	6.16	0.60	0.97	<0.1	20.63	<0.1	37.21	4.01	<0.05	<0.05	92.26	42.54	280.85	323.39	0.15
14	113002	<0.1	0.49	0.02	1.17	0.14	2.52	0.07	5.25	<0.1	8.00	1.04	<0.05	3.16		10.47	58.98	69.46	0.18

Table Continued..

Annexure-XXXg

Sl No.	Sample No.	Tm	Yb	Lu	Hf	Ta	W	Tl	Pb	Bi	Th	U	Ag	Te	Mn	HREEY	LREE	TREEY	HREEY/LREE
15	113155	0.20	1.38	0.20	4.45	0.37	1.92	0.63	33.71	<0.1	32.98	3.67	<0.05	<0.05	156.27	32.94	225.93	258.87	0.15
16	113398	0.38	2.64	0.38	8.82	0.59	1.00	0.75	27.26	<0.1	55.50	6.15	<0.05	<0.05	564.39	32.94	225.93	258.87	0.15
17	113379	<0.8	0.66	0.18	2.83	0.79	1.65	1.41	21.30	<0.1	8.21	3.11	0.33	3.24	575.82	64.69	425.63	490.32	0.15

Annexure-XXX h: ICPMS Analysis of BH08

Sl No.	Sample No.	Depth	Sample Description	Host lithology	Li	Be	Sc	V	Cr	Co	Ni	Cu
1	**112463**	0	Yellow ocher coloured quartz arenite, composed of sub rounded to very well rounded quartz grains, embedded in a siliceous matrix/cement.	Quartz arenite	8.54	0.33	1.57	15.18	450.74	6.69	11.52	3.38
2	**112464**	0	Black colour highly ferruginous metasomatised sandstone, composed of angular to sub-rounded quartz, euhedral feldspar, mica embedded in a hematitic to magnetite matrix/cement.	Highly ferruginous metasomatised sandstone	6.01	0.63	2.90	21.64	209.64	17.50	32.75	5.02
3	**112466**	0	Violitish white to brownish mauve coloured, very light weight altered ferruginous sandstone. Apart from few quartz pebbles no other grains have been identified (no grain boundary is clear) within the sandstone. Porous spaces (pot hole like feature) within the sandstone are filled with clay (fails acid test) and/or hematite. The matrix/cement of the sandstone comprises hematite. The grain contacts does not seems to be sandstone, they are looking like "Y" junction between the grains. The sample has been collected from the contact zone (2.7m thick) of a fault plane.	Metasomatized shale sandstone hetrolith	47.90	2.61	84.36	519.61	281.09	60.14	127.89	264.56

Sl No.	Sample No.	Depth	Sample Description	Host lithology	Li	Be	Sc	V	Cr	Co	Ni	Cu
4	113033	6.64 to 6.70	Medium to fine grained, moderately sorted ferruginous sandstone with sub-angular to sub-rounded grains of moderate to high sphericity. It comprises quartz (>97%), hematite grains, & few clay clast (may also be altered feldspar), magnetite (??) in a decreasing order of abundance.Muscovite is also observed within the clay clast. The ferrugination colour varies from yellow ochre to pinkish red to brownish black to purple.Silicification is also observed.	Mica bearing ferruginized sandstone	9.50	0.53	2.83	24.47	388.82	7.58	13.39	10.29
5	**113034**	6.80 to 6.86	Medium to fine grained, moderately sorted ferruginous sandstone with sub-angular to sub-rounded grains of moderate to high sphericity. It comprises quartz (>97%), hematite grains, & few clay clast (may also be altered feldspar), magnetite (??) in a decreasing order of abundance.Muscovite is also observed within the clay clast. The ferrugination colour varies from yellow ochre to pinkish red to brownish black to purple.Silicification is also observed.	Mica bearing ferruginized sandstone	7.33	2.42	3.63	16.23	299.32	11.79	37.59	4.75

Sl No.	Sample No.	Depth	Sample Description	Host lithology	Li	Be	Sc	V	Cr	Co	Ni	Cu
6	**113036**	9.69 to 9.74	Yellowish brown coloured medium to fine grained, moderate to well sorted, metasomatized ferruginous sandstone. The sandstone comprises sub-rounded to rounded grains of quartz with high sphericity (97-98%) & ~ 1% mica (muscovite, and biotite) embedded in a ferruginous to magnetite and/or clay cement/matrix. Ripple cross lamination & planar parallel lamination is observed. Silicification is also observed.	Mica bearing metasomatized sandstone	11.14	0.89	5.07	43.77	206.83	12.78	30.83	17.35
7	**113037**	9.89 to 9.96	Brownish red coloured medium to fine grained, moderate to well sorted, metasomatized ferruginous sandstone. The sandstone comprises sub-rounded to rounded grains of quartz with high sphericity (97-98%) & ~ 1-2% mica (muscovite, and biotite) embedded in a ferruginous to magnetite and/or clay cement/matrix. Ripple cross lamination & planar parallel lamination is observed. Silicification is also observed. The higher the ferrugination the higher the amount of mica.	Mica bearing metasomatized sandstone	13.53	1.33	8.78	57.40	101.42	22.07	20.90	42.57

Sl No.	Sample No.	Depth	Sample Description	Host lithology	Li	Be	Sc	V	Cr	Co	Ni	Cu
8	**113035**	10.45 to 10.49	Brownish red coloured highly ferruginous fine grained, well sorted, metasomatized sandstone. The sandstone comprises sub-rounded to rounded grains of quartz with high sphericity (97-98%) & ~ 2% mica (muscovite, and biotite) embedded in a ferruginous cement/matrix. The higher the ferrugination the higher the amount of mica. Mostlikely this is very near to fault zone.	Mica bearing metasomatized sandstone	11.70	3.28	11.70	88.98	102.75	48.56	96.50	18.87
9	**113038**	11.46 to 11.48	Yellowish brown coloured medium to fine grained, moderate to well sorted, metasomatized ferruginous sandstone. The sandstone comprises sub-rounded to rounded grains of quartz with high sphericity (97-98%) & ~ 1% mica (muscovite, and biotite) embedded in a ferruginous to magnetite and/or clay cement/matrix. Silicification is also observed.	Mica bearing metasomatized sandstone	50.60	0.83	12.46	91.16	280.74	10.48	13.42	15.36

Sl No.	Sample No.	Depth	Sample Description	Host lithology	Li	Be	Sc	V	Cr	Co	Ni	Cu
10	**113039**	11.49 to 11.53	The sample is at the contact between the altered ferruginous sandstone and shale-sandstone heterolith and comprises breccia, hematite layer and flesh coloured very fine grained (minerals can not be identified) material, occuring one after another, down to the stratigraphic level. The breccia, seems to be the ferruginous altered sandstone with quartz, mica embedded in ferruginous matrix/cement. However the cluster of quartz grains, surrounded by magnetite are occuring as the breccia clast.	Contact between mica bearing metasomatized sandstone and metasomatized shale-sandstone heterolith	70.82	8.71	39.01	425.24	264.11	75.14	152.46	162.42
11	**113040**	11.51 to 11.58	Mauve coloured very fine grained altered sandstone. No grains have been identified (no grain boundary is clear) within the sandstone. Porous spaces (pot hole like feature) within the sandstone are filled with white clay (fails acid test). The matrix/cement of the sandstone comprises hematite, & magnetite (less in amount, magnetic mineral with black streak). Different order of ferrugination is observed.	Metasomatized shale sandstone hetrolith	149.40	2.66	78.49	738.51	505.11	31.25	33.64	187.74

Sl No.	Sample No.	Depth	Sample Description	Host lithology	Li	Be	Sc	V	Cr	Co	Ni	Cu
12	**113041**	11.67 to 11.73	Brownish mauve coloured very fine grained altered sandstone. No grains have been identified (no grain boundary is clear) within the sandstone. Porous spaces (pot hole like feature) within the sandstone are filled with white clay (fails acid test) and hematite. The matrix/cement of the sandstone comprises hematite, & magnetite (less in amount, magnetic mineral with black streak). Higher order of ferrugination is observed than the previous sample. Silicification is also observed within the sample. It appears like baking effect within the sample.	Metasomatized shale sandstone hetrolith	28.04	2.56	82.70	652.21	289.92	55.29	139.26	409.03
13	**113042**	11.78 to 11.83	Brownish mauve coloured very fine grained altered sandstone. No grains have been identified (no grain boundary is clear) within the sandstone. Porous spaces (pot hole like feature) within the sandstone are filled with white clay (fails acid test) and hematite. The matrix/cement of the sandstone comprises hematite, & magnetite (less in amount, magnetic mineral with black streak). Higher order of ferrugination is observed than the previous sample. Silicification is also observed within the sample. It appears like baking effect within the sample.	Metasomatized shale sandstone hetrolith	43.23	2.23	109.26	568.61	452.01	95.07	204.71	271.08

Sl No.	Sample No.	Depth	Sample Description	Host lithology	Li	Be	Sc	V	Cr	Co	Ni	Cu
14	**113043**	11.87 to 11.96	Brownish red to mauve coloured altered sandstone. Apart from few quartz pebbles no other grains have been identified (no grain boundary is clear) within the sandstone. Porous spaces (pot hole like feature) within the sandstone are filled with clay (fails acid test) and/or hematite. The matrix/cement of the sandstone comprises hematite, & magnetite (less in amount, magnetic mineral with black streak). The sample has a violetish tinch. Does not seems to be sandstone, looking like "Y" junction between the grains.	Metasomatized shale sandstone hetrolith	33.29	2.65	81.37	656.05	356.61	77.85	174.45	409.18
15	**113044**	12.31 to 12.35	Mauve to violitish white coloured very fine grained clay sample. No mineral can be identified within the sample	Metasomatized shale sandstone hetrolith	57.78	2.62	66.29	691.87	525.51	20.42	19.78	91.19
16	**113045**	12.77 to 12.83	Yellowish brown coloured very coarse to gritty sandstone.The sandstone is poorly sorted & contains very coarse to gritty, sub-angular to sub-rounded grains of low sphericity. It comprises >99% quartz; few white transparent crystals, very few muscovite and magnetite, embedded in a clay (no effervescence) cement or matrix. Magnetite content is very low.	Mica bearing ferruginized sandstone	9.70	0.40	3.80	19.64	371.60	17.03	15.20	105.81

Sl No.	Sample No.	Depth	Sample Description	Host lithology	Li	Be	Sc	V	Cr	Co	Ni	Cu
17	**113046**	13.51 to 13.59	Yellowish brown coloured very coarse to gritty sandstone.The sandstone is poorly sorted & contains very coarse to gritty grains, with sub-angular to sub-rounded grains with low sphericity & comprises >99% quartz; few white transparent crystals, very few muscovite and magnetite, embedded in a clay (no effervescence) cement or matrix. Magnetite content is very low.	Mica bearing ferruginized sandstone	11.02	0.43	2.27	17.39	353.93	22.24	8.17	175.01
18	**113049**	14.33 to 14.38	Dark brown to brownish red coloured, medium to fine grained moderate to well sorted altered ferruginous sandstone. The sandstone comprises sub-rounded to rounded grains of quartz with high sphericity (97-98%) & ~1% mica (muscovite, and biotite) embedded in a ferruginous to magnetite & clay (??) cement/matrix. Silicification is also observed.	Mica bearing metasomatized sandstone	10.63	0.83	7.48	57.96	195.38	23.50	25.68	68.92

Sl No.	Sample No.	Depth	Sample Description	Host lithology	Li	Be	Sc	V	Cr	Co	Ni	Cu
19	**113380**	15.19 to 15.24	Dark brown to brownish red coloured, medium to coarse grained moderate to well sorted altered ferruginous sandstone. The sandstone comprises sub-rounded to rounded grains of quartz with high sphericity (97-98%) & ≈ 1-2% mica (muscovite, and biotite) embedded in a ferruginous to magnetite & clay (??) cement/matrix.The degree of ferrugination is different at different stratigraphic levels, varying in colour from yellow ochre to yellowish brown to brown to reddish brown to dark brown. The higher the ferrugination the higher the amount of mica (lots of figure taken). Ripple cross lamination & planar parallel lamination is observed. Silicification is also observed at dif stratigraphic levels.	Mica bearing metasomatized sandstone	21.50	1.13	11.08	93.98	188.06	11.81	23.56	8.53

Sl No.	Sample No.	Depth	Sample Description	Host lithology	Li	Be	Sc	V	Cr	Co	Ni	Cu
20	**113381**	15.37 to 15.46	Dark brown to brownish red coloured, medium to coarse grained moderate to well sorted altered ferruginous sandstone. The sandstone comprises sub-rounded to rounded grains of quartz with high sphericity (97-98%) & ≈ 1-2% mica (muscovite, and biotite) embedded in a ferruginous to magnetite & clay (??) cement/matrix.The degree of ferrugination is different at different stratigraphic levels, varying in colour from yellow ochre to yellowish brown to brown to reddish brown to dark brown. The higher the ferrugination the higher the amount of mica (lots of figure taken). Ripple cross lamination & planar parallel lamination is observed. Silicification is also observed at dif stratigraphic levels.	Mica bearing metasomatized sandstone	25.87	1.66	13.07	130.26	126.05	32.23	25.26	24.91
21	**113047**	15.44 to 15.50	Reddish Yellow to reddish brown coloured, altered ferruginous sandstone. The sandstone is medium to fine grained, moderate to well sorted with sub-rounded to rounded grains with high sphericity. The sandstone comprises quartz (>95%), muscovite and biotite (mica 1–2%), very minor amount of magnetite in a decreasing order of abundance. A greyish black steel shiny mineral (steel grey texture, prismatic elongated) is also observed at places. Degree of ferruginisation is different at different parts. The	Mica bearing metasomatized sandstone	20.44	1.56	10.44	128.49	152.77	11.81	21.59	33.62

Sl No.	Sample No.	Depth	Sample Description	Host lithology	Li	Be	Sc	V	Cr	Co	Ni	Cu
			higher the ferruginisation the higher the amount of biotite									
22	**113048**	15.91 to 15.95	Reddish brown coloured, altered ferruginous sandstone unit. The sandstone is medium to fine grained, moderate to well sorted with sub-rounded to rounded grains with high sphericity. The sandstone comprises quartz (>95%), muscovite and biotite (mica 1–2%), very minor amount of magnetite in a decreasing order of abundance. Degree of ferrugination is different at different parts. The higher the ferruginisation the higher the amount of biotite	Mica bearing metasomatized sandstone	14.93	2.47	12.34	93.95	155.75	18.21	50.87	55.84
23	**113050**	17.09 to 17.14	Reddish brown coloured, altered ferruginous sandstone and seems to be occur as breccia (insitu brecciation) where cluster of quartz grains, surrounded by magnetite are occuring as the breccia clast, embedded in a ferruginous matrix. The sandstone is coarse to very coarse grained, poorly sorted with angular grains.	Metasomatized shale sandstone hetrolith	8.46	1.76	5.17	27.67	204.40	20.30	46.61	15.56
24	**113351**	17.77 to 17.83	The shale/siltstone is grey in colour, & very fine grained with no mineral identification.	Metasomatized shale sandstone hetrolith	46.41	2.22	16.08	103.31	137.34	14.94	24.00	32.97

Sl No.	Sample No.	Depth	Sample Description	Host lithology	Li	Be	Sc	V	Cr	Co	Ni	Cu
25	**113352**	20.89 to 20.96	The sandstone is highly ferruginous, brownish red in colour and medium to fine grained and comprises quartz (>95%), muscovite and biotite (mica 1–2%), very minor amount of magnetite in a decreasing order of abundance. The matrix is ferruginous and iron impregnation observed following the internal structure of the sandstone. The higher the ferruginisation the higher the amount of mica. Both silicification and clay concentration is also observed. Irregular clay clast (very few amount) is also observed.	Metasomatized shale sandstone hetrolith	7.77	1.57	7.57	57.02	121.84	25.70	47.89	14.06
26	**113353**	43.44 to 43.50	The sandstone is highly ferruginous and consists of medium to fine grained, moderate to well sorted, sub-angular to sub-rounded grains of quartz (97–98%), very few muscovite, biotite, hematite clasts, magnetite embedded in a ferruginous matrix/cement. The muscovites are abundant at the areas of high ferruginisation/alteration. Degree of ferrugination is different at different places. Thin veinlets of hematite is also observed at different parts. Silicification (??) binding the quartz framework grains is also observed.	Metasomatized shale sandstone hetrolith	13.57	9.87	18.07	85.82	110.21	82.88	270.65	101.33

Sl No.	Sample No.	Depth	Sample Description	Host lithology	Li	Be	Sc	V	Cr	Co	Ni	Cu
27	**113354**	47.22 to 47.25	Medium to coarse grained yellow ochre coloured sandstone with moderate to poor sorting & consists of sub-rounded to rounded grains of quartz, embedded in a clay (??) matrix/cement. This part of the sample is less ferruginous and metasomatized	Mica bearing metasomatized sandstone	14.05	0.84	5.60	45.27	211.34	17.62	16.31	52.11
28	**113355**	47.31 to 47.38	Medium to coarse grained brownish red colouredmetasomatized sandstone with moderate to poor sorting & consists of sub-rounded to rounded grains of quartz, embedded in a clay (??) matrix/cement. The sst is ferruginous in nature where the iron impregnation occurs following the internal structure. Occurrence of ~1% muscovite & biotite is observed at these ferruginous parts.	Mica bearing metasomatized sandstone	11.40	0.71	3.23	25.47	249.97	29.46	16.44	204.10
29	**113377**	47.68 to 47.77	Medium to coarse grained yellow ochre to brownish red to brownish black coloured sandstone with different order of ferruginization at different stratigraphic levels. The sandstone is moderate to poorly sorted & consists of sub-rounded to rounded grains of quartz, embedded in a clay (??) matrix/cement. Occurrence of 1–2% muscovite & biotite is observed at the ferruginous parts. Lapilli (??? clast remnant??) is also observed at 47.7m. Silicification (?) is common within the sandstone.	Mica bearing metasomatized sandstone	9.65	1.09	4.35	36.50	242.64	12.56	19.83	9.11

Sl No.	Sample No.	Depth	Sample Description	Host lithology	Li	Be	Sc	V	Cr	Co	Ni	Cu
30	**113356**	48.11 to 48.16	Highly ferruginous, metasomatized medium to coarse grained brownish black coloured sandstone with moderate to poor sorting & consists of sub-rounded to rounded grains of quartz, embedded in a clay (??) matrix/cement. Occurrence of ~2% muscovite & biotite is observed at these ferruginous parts.	Mica bearing metasomatized sandstone	8.12	0.63	2.99	17.53	305.59	32.42	24.35	224.94
31	**113394**	10m to 11m	Yellowish brown coloured medium to fine grained moderate to well sorted altered ferruginous sandstone. The sandstone comprises sub-rounded to rounded grains of quartz with high sphericity (97-98%) & ≈ 2% mica (muscovite, and biotite) embedded in a ferruginous to magnetite & clay (??) cement/matrix.The degree of ferrugination is different at different stratigraphic levels, varying in colour from yellow ochre to yellowish brown to brown to reddish brown to dark brown. The higher the ferrugination the higher the amount of mica (lots of figure taken). Ripple cross lamination & planar parallel lamination is observed. Silicification is also observed at dif stratigraphic levels.[This is probably the fault zone/very near to the fault zone, as from ~15m water loss started]	Mica bearing metasomatized sandstone	23.45	1.73	12.00	78.12	83.44	19.06	29.26	<0.1

Sl No.	Sample No.	Depth	Sample Description	Host lithology	Li	Be	Sc	V	Cr	Co	Ni	Cu
32	**113395**	11.50 to 12.39	Brownish red to mauve coloured altered shale - sandstone heterolith. The unit comprises thick ferruginous sandstone interspersed by clay. Apart from few quartz pebbles no other grains have been identified (no grain boundary is clear) within the sandstone. Porous spaces (pot hole like feature, pit surface) within the sandstone are filled with clay (fails acid test) and/or hematite. The matrix/cement of the sandstone comprises hematite, & magnetite (less in amount, magnetic mineral with black streak). Silicification is also observed at different stratigraphic level. The clay part is mainly showing the mauve colour.	Metasomatized shale sandstone hetrolith	65.16	3.13	81.62	670.11	400.72	76.20	129.50	308.67

Sl No.	Sample No.	Depth	Sample Description	Host lithology	Li	Be	Sc	V	Cr	Co	Ni	Cu
33	**113396**	15.40 to 16.50	Reddish Yellow to reddish brown coloured, altered ferruginous sandstone unit. The sandstone is medium to fine grained, moderate to well sorted with sub-rounded to rounded grains of high sphericity. The sandstone comprises quartz (>95%), muscovite and biotite (mica 1–2%), very minor amount of magnetite in a decreasing order of abundance. A greyish black steel shiny mineral (steel grey texture, prismatic elongated) is also observed at places. Degree of ferrugination is different at different parts. The higher the ferruginisation the higher the amount of biotite.	Mica bearing metasomatized sandstone	30.13	1.41	15.60	110.90	103.88	6.47	21.03	0.08

Sl No.	Sample No.	Depth	Sample Description	Host lithology	Li	Be	Sc	V	Cr	Co	Ni	Cu
34	**113397**	18.50 to 19.50	Shale/siltstone-sst heterolith, occuring as alternate layers of shale/siltstone and ferruginous sandstone. However, shale as irregular layers, intercalating within the sandstone is also observed at places. The sandstone is highly ferruginous medium to fine grained and comprises quartz (>95%), muscovite and biotite (mica 1–2%), very minor amount of magnetite in a decreasing order of abundance. The matrix is hematitic and iron impregnation follows the internal structure of the sandstone. Degree of ferrugination is different at different parts. The higher the ferruginisation the higher the amount of mica. Both silicification and clay concentration is also observed. The shale/siltstone is grey in colour, & consists of quartz, muscovite & biotite. The shale is generally unaltered. From 18m onwards, the amount/thickness of shale/siltstone increases, upto 20.5m. The shale is planar parallel to wavy parallel laminated.	Metasomatized shale sandstone hetrolith	35.19	2.26	17.64	79.08	100.72	7.13	26.62	<0.1

Sl No.	Sample No.	Depth	Sample Description	Host lithology	Li	Be	Sc	V	Cr	Co	Ni	Cu
35	**113156**	42.96 m to 43.80m	Alternate occurrence of ferruginous sandstone and shale/siltstone. The sandstone is highly ferruginous and consists of medium to fine grained, moderate to well sorted, sub-angular to sub-rounded grains of quartz (97–98%), very few muscovite, biotite, hematite clasts, magnetite embedded in a ferruginous matrix/cement. The muscovites are abundant at the areas of high ferruginisation/alteration whereas it is scarce and/or unavailable at the non-ferruginous part of the sandstone from 43.5–43.92m. Degree of ferrugination is different at different places. Thin veinlets of hematite is also observed at different parts. Shale clast is also observed within the sandstone. Silicification (??) binding the quartz framework grains is also observed. The shale is grey in colour & observed to be planar parallel to wavy parallel laminated at places, the shale comp., cannot be identified.	Metasomatized shale sandstone hetrolith	19.17	4.01	16.74	106.52	92.14	25.76	63.21	<0.1

Table Continued..

Annexure-XXXh

Sl No.	Sample No.	Zn	Ga	Ge	Se	Rb	Sr	Y	Zr	Nb	Mo	Cd	In
1	**112463**	27.17	4.95	<0.1	0.66	16.72	24.86	3.70	67.29	24.94	0.72	1.43	0.38
2	**112464**	71.76	13.14	0.40	<0.1	9.12	50.39	5.38	68.77	11.92	1.06	2.62	7.07
3	**112466**	148.79	44.62	0.26	0.77	<0.1	70.47	43.55	112.71	66.80	6.13	4.59	12.88
4	113033	24.14	6.77	<0.1	<0.1	12.12	44.93	5.64	79.37	20.61	1.54	1.33	0.89
5	**113034**	143.57	9.79	0.19	0.16	14.23	38.70	9.60	56.18	16.52	0.94	1.97	2.92
6	**113036**	58.77	9.93	0.14	<0.1	18.96	37.17	11.20	143.04	11.52	1.39	1.51	1.73
7	**113037**	86.02	13.10	0.21	<0.1	32.50	64.75	18.05	185.12	7.00	1.15	1.61	2.52
8	**113035**	229.48	41.44	1.08	0.38	16.44	44.33	22.47	119.33	6.33	2.45	5.11	21.08

Sl No.	Sample No.	Zn	Ga	Ge	Se	Rb	Sr	Y	Zr	Nb	Mo	Cd	In
9	**113038**	29.08	12.03	0.14	<0.1	29.95	46.99	54.16	56.91	16.11	1.15	1.46	2.31
10	**113039**	286.67	47.54	0.93	0.58	<0.1	175.96	55.84	92.16	14.50	2.20	4.27	16.80
11	**113040**	27.98	46.21	0.22	1.86	0.19	50.12	8.20	179.64	27.61	1.04	1.10	4.02
12	**113041**	125.75	45.84	0.62	1.43	<0.1	267.75	32.88	151.18	14.14	1.40	3.30	12.43
13	**113042**	85.12	43.33	0.52	<0.1	<0.1	31.42	8.83	148.63	23.38	0.87	2.52	9.39
14	**113043**	165.03	44.43	0.15	<0.1	<0.1	297.51	35.43	125.72	19.34	4.05	3.71	12.53
15	**113044**	20.29	45.21	0.14	0.17	0.90	130.10	8.59	167.92	28.38	0.90	1.12	2.95
16	**113045**	27.95	5.03	<0.1	<0.1	17.48	37.49	3.61	37.99	20.03	0.87	1.24	0.95
17	**113046**	14.52	5.33	<0.1	<0.1	15.34	49.69	5.15	79.51	19.27	0.87	1.07	<0.1

Sl No.	Sample No.	Zn	Ga	Ge	Se	Rb	Sr	Y	Zr	Nb	Mo	Cd	In
18	**113049**	76.35	11.26	0.26	<0.1	18.77	42.56	10.54	113.91	10.30	1.51	1.82	3.66
19	**113380**	21.32	15.79	<0.1	0.39	20.48	165.60	11.60	177.74	48.83	1.07	1.80	0.67
20	**113381**	36.93	27.45	<0.1	0.45	45.37	165.90	14.39	163.49	36.78	2.56	2.33	4.52
21	**113047**	46.82	25.59	0.37	0.93	49.79	101.63	13.76	199.39	9.27	2.75	1.94	5.48
22	**113048**	181.57	25.57	0.61	0.66	32.39	94.86	18.68	169.20	9.06	4.05	2.61	8.81
23	**113050**	255.70	16.33	0.51	<0.1	14.27	70.05	19.77	92.85	11.53	0.65	2.21	7.82
24	**113351**	56.00	29.96	0.25	<0.1	69.16	74.87	18.49	200.70	9.11	1.32	1.25	2.64
25	**113352**	104.41	33.14	1.03	<0.1	14.18	52.24	17.51	221.30	7.38	1.47	3.97	16.64
26	**113353**	909.09	41.73	1.22	<0.1	6.27	55.62	20.74	120.72	6.44	6.72	4.64	20.54

Sl No.	Sample No.	Zn	Ga	Ge	Se	Rb	Sr	Y	Zr	Nb	Mo	Cd	In
27	**113354**	44.69	11.36	<0.1	<0.1	8.24	59.07	9.56	151.06	11.29	1.30	1.24	0.87
28	**113355**	32.24	8.71	0.10	<0.1	5.57	42.33	5.16	71.68	12.04	1.09	1.36	1.41
29	**113377**	32.69	12.55	0.26	2.49	3.60	32.81	6.93	95.46	14.11	1.16	1.95	3.09
30	**113356**	37.59	9.96	0.36	<0.1	1.81	24.80	3.27	50.60	15.99	1.26	1.99	5.03
31	**113394**	84.49	23.81	0.24	7.21	70.82	92.05	27.94	262.32	15.00	28.60	1.01	<0.01
32	**113395**	149.43	29.97	0.22	3.51	0.61	108.39	28.67	138.90	7.55	9.82	0.60	<0.01
33	**113396**	45.49	20.95	0.12	4.94	57.05	92.70	24.06	282.27	14.58	10.48	0.49	<0.01
34	**113397**	85.49	23.50	0.11	4.64	46.35	73.46	26.31	213.95	13.09	10.93	0.62	<0.01
35	**113156**	261.98	22.53	0.38	11.57	16.23	125.21	44.16	556.89	21.49	12.57	0.75	<0.01

Table Continued..

Annexure-XXXh

Sl No.	Sample No.	Sn	Sb	Cs	Ba	La	Ce	Pr	Nd	Sm	Eu	Gd	Tb
1	**112463**	181.35	4.33	2.56	125.01	6.82	15.23	2.05	7.89	0.62	0.27	1.08	0.32
2	**112464**	75.37	6.60	4.56	190.93	9.39	16.43	14.07	11.05	3.81	0.41	8.50	1.00
3	**112466**	86.05	12.31	2.57	226.37	4.68	0.14	31.69	55.67	7.87	2.48	17.71	6.13
4	113033	142.22	4.91	4.81	258.52	11.29	23.12	3.23	13.95	1.72	0.39	1.96	0.45
5	**113034**	112.16	5.78	0.34	183.87	7.80	16.18	7.15	8.32	2.91	0.56	4.83	0.48
6	**113036**	73.77	3.02	17.50	232.63	37.66	84.83	7.68	42.50	5.62	0.62	3.92	1.30

Sl No.	Sample No.	Sn	Sb	Cs	Ba	La	Ce	Pr	Nd	Sm	Eu	Gd	Tb
7	**113037**	36.37	3.19	23.48	384.14	59.99	136.62	10.07	65.03	9.47	1.12	5.68	1.40
8	**113035**	25.27	16.70	10.62	297.52	45.42	80.27	47.92	48.22	16.22	2.03	26.85	2.58
9	**113038**	100.61	2.17	12.13	355.54	38.01	82.41	8.43	38.06	6.64	1.26	4.86	1.22
10	**113039**	77.24	13.74	24.75	450.50	21.83	30.22	36.99	38.26	12.60	3.46	23.47	3.27
11	**113040**	184.44	7.33	61.62	132.45	3.08	1.11	4.73	37.40	1.70	2.91	2.09	3.06
12	**113041**	88.44	12.18	34.79	900.63	21.18	33.51	28.48	53.98	13.51	4.83	18.52	3.67
13	**113042**	150.19	9.95	46.30	66.99	2.43	0.90	18.54	27.96	2.53	2.28	10.95	3.03

Sl No.	Sample No.	Sn	Sb	Cs	Ba	La	Ce	Pr	Nd	Sm	Eu	Gd	Tb
14	**113043**	112.45	11.13	30.64	1149.70	35.01	60.10	28.63	59.62	13.72	5.04	18.08	3.37
15	**113044**	191.84	7.36	56.81	364.11	21.53	27.14	9.50	46.98	3.24	3.46	2.18	3.04
16	**113045**	144.89	4.16	1.26	256.01	6.70	12.56	2.57	7.69	1.32	0.20	1.52	0.30
17	**113046**	152.38	3.10	4.44	293.42	15.29	34.18	2.45	16.22	2.53	0.28	1.09	0.43
18	**113049**	70.85	5.17	12.17	268.90	37.17	82.53	9.38	37.75	6.61	0.59	6.30	1.03
19	**113380**	19.90	0.48	4.42	384.25	44.61	107.94	5.01	33.24	4.00	0.66	2.86	1.08
20	**113381**	16.27	1.57	5.79	446.68	40.07	93.98	9.71	34.24	5.28	0.96	2.85	1.88

Sl No.	Sample No.	Sn	Sb	Cs	Ba	La	Ce	Pr	Nd	Sm	Eu	Gd	Tb
21	**113047**	48.49	6.95	17.44	392.30	44.91	95.05	13.32	45.56	7.26	1.07	7.98	1.53
22	**113048**	46.03	7.74	14.74	364.03	42.25	85.31	21.11	41.95	9.36	1.42	12.18	1.76
23	**113050**	66.32	8.50	5.49	3489.38	22.13	52.00	17.34	28.34	6.84	0.86	11.02	1.26
24	**113351**	50.61	4.41	28.72	395.90	48.57	84.84	5.90	46.68	5.83	1.17	2.55	1.78
25	**113352**	32.37	13.96	21.93	330.59	76.83	167.64	40.80	74.19	17.87	0.81	23.00	2.70
26	**113353**	25.30	13.66	10.17	216.61	25.34	48.31	44.40	37.04	14.80	1.55	26.60	2.48
27	**113354**	80.36	3.30	14.51	302.43	29.84	65.86	5.37	33.51	4.16	0.64	2.47	1.06

Sl No.	Sample No.	Sn	Sb	Cs	Ba	La	Ce	Pr	Nd	Sm	Eu	Gd	Tb
28	**113355**	110.55	4.30	4.56	188.38	12.30	24.06	4.52	13.22	2.50	0.36	2.66	0.45
29	**113377**	89.91	5.97	6.32	174.48	15.95	32.57	7.95	17.18	3.35	0.49	5.05	0.83
30	**113356**	132.75	6.54	0.99	89.91	6.72	12.00	9.52	7.56	1.88	0.28	6.18	0.60
31	**113394**	3.48	<0.1	0.08	695.43	121.44	244.50	25.81	91.86	15.68	1.66	12.10	1.46
32	**113395**	1.21	1.59	<0.1	384.80	13.71	29.90	3.78	15.87	4.19	1.34	5.28	0.95
33	**113396**	2.93	0.58	2.77	389.52	70.08	140.10	14.27	49.81	8.83	1.28	7.20	0.97
34	**113397**	2.26	1.21	3.35	336.07	62.28	125.10	13.33	47.68	8.63	1.46	7.65	1.06
35	**113156**	1.69	<0.1	<0.1	7287.10	181.33	359.59	38.14	136.33	23.44	2.43	18.28	2.26

Table Continued..

Annexure-XXXh

Sl No.	Sample No.	Dy	Ho	Er	Tm	Yb	Lu	Hf	Ta	W	Tl	Pb	Bi	Th	U	Ag	Te	Mn	HREEY	LREE	TREEY	THIE
1	**112463**	0.67	<0.1	0.52	0.10	0.31	0.02	2.03	0.98	0.48	1.61	1.35	<0.1	2.79	0.31	1.03	0.81	-	8.66	32.61	41.27	719.61
2	**112464**	1.37	<0.1	0.88	0.10	1.19	0.16	1.96	2.05	0.55	2.13	7.53	<0.1	21.65	15.99	1.33	10.45	-	21.99	54.75	76.74	493.39
3	**112466**	8.04	1.03	5.04	0.16	4.57	0.46	2.82	5.27	0.23	1.18	4.56	1.44	44.40	41.28	NA	NA	-	173.53	100.05	273.58	1232.20
4	113033	19.71	<0.1	0.78	0.12	0.43	0.03	2.61	1.16	0.77	1.47	30.42	<0.1	4.84	0.83	0.97	1.80	-	32.44	53.31	85.75	627.72
5	**113034**	1.09	0.28	0.53	0.10	0.90	0.10	1.90	1.29	1.86	0.92	13.69	0.34	12.29	7.53	0.84	4.24	-	22.10	42.36	64.46	665.59
6	**113036**	4.08	<0.1	1.80	0.12	0.78	0.05	4.75	1.29	1.27	0.45	31.52	<0.1	11.94	1.18	1.25	5.66	-	29.09	178.29	207.38	443.40
7	**113037**	3.58	<0.1	2.49	0.14	1.16	<0.01	6.45	1.55	0.93	3.36	34.83	<0.1	16.51	1.72	1.37	7.24	-	42.60	281.18	323.78	356.64

Sl No.	Sample No.	Dy	Ho	Er	Tm	Yb	Lu	Hf	Ta	W	Tl	Pb	Bi	Th	U	Ag	Te	Mn	HREEY	LREE	TREEY	THIE
8	**113035**	5.55	1.11	1.99	0.10	3.06	0.44	3.29	5.46	1.74	2.96	54.86	3.91	66.35	50.66	2.12	30.73	-	77.88	238.05	315.93	736.09
9	**113038**	25.35	<0.1	3.60	0.15	3.01	<0.01	2.06	1.43	0.71	<0.05	29.41	<0.1	11.29	1.62	0.46	4.61	-	106.27	173.55	279.82	506.38
10	**113039**	6.31	1.70	4.35	<0.1	4.66	0.38	2.83	5.56	1.58	<0.05	34.45	2.46	51.23	35.36	1.24	26.28	-	142.55	139.90	282.45	1201.69
11	**113040**	1.20	<0.1	3.51	0.14	1.52	<0.01	4.74	4.62	1.06	1.95	21.18	<0.1	5.00	<0.1	1.38	9.91	-	101.32	48.02	149.34	1129.59
12	**113041**	6.18	<0.1	4.28	0.13	3.25	0.26	5.56	5.68	1.50	0.61	32.09	<0.1	36.78	19.98	1.76	22.41	-	156.80	150.66	307.46	1313.89
13	**113042**	5.90	<0.1	3.08	0.13	2.33	0.20	3.00	4.64	0.95	0.37	23.57	<0.1	27.24	13.83	1.54	17.57	-	146.09	52.36	198.45	1429.16
14	**113043**	2.75	<0.1	3.94	<0.1	3.56	0.26	5.87	5.61	1.37	2.00	28.64	<0.1	34.51	20.07	1.75	20.19	-	154.00	197.08	351.08	1477.73

Sl No.	Sample No.	Dy	Ho	Er	Tm	Yb	Lu	Hf	Ta	W	Tl	Pb	Bi	Th	U	Ag	Te	Mn	HREE Y	LREE	TREE Y	THIE
15	**113044**	4.38	0.44	3.45	0.14	1.32	<0.01	5.14	4.53	0.60	1.52	22.97	<0.1	2.97	<0.1	1.40	8.40	-	93.39	108.39	201.78	1021.78
16	**113045**	8.65	<0.1	0.52	0.12	0.34	<0.01	1.73	0.79	1.56	2.65	28.46	<0.1	3.86	1.22	0.36	0.80	-	19.26	30.84	50.10	710.64
17	**113046**	1.68	<0.1	0.75	0.13	0.33	<0.01	2.91	0.81	1.14	<0.05	29.59	<0.1	3.37	<0.1	0.81	0.62	-	12.31	70.67	82.98	741.09
18	**113049**	<0.1	<0.1	1.55	0.13	1.09	<0.01	3.78	1.91	0.91	1.69	43.28	<0.1	18.18	4.56	1.38	6.24	-	29.01	173.44	202.45	511.86
19	**113380**	2.19	<0.1	1.50	<0.1	1.20	0.02	5.24	1.25	0.80	<0.1	<0.1	<0.1	<0.1	<0.1	0.67	<0.1	217.02	32.39	194.80	227.19	343.01
20	**113381**	2.59	<0.1	1.89	<0.1	1.93	0.07	4.96	2.08	1.03	3.31	51.74	<0.1	40.62	5.10	0.69	3.67	1124.48	39.83	183.28	223.10	372.47
21	**113047**	10.11	<0.1	1.87	0.12	1.45	0.12	6.27	2.30	0.97	0.95	50.08	<0.1	21.59	6.69	1.64	9.35	-	48.55	206.10	254.65	407.01

Sl No.	Sample No.	Dy	Ho	Er	Tm	Yb	Lu	Hf	Ta	W	Tl	Pb	Bi	Th	U	Ag	Te	Mn	HREE Y	LREE	TREE Y	THIE
22	**113048**	1.36	<0.1	1.97	0.11	2.15	0.20	5.31	3.21	1.61	2.50	54.04	<0.1	31.52	16.13	1.29	13.81	-	52.27	199.98	252.25	626.41
23	**113050**	<0.1	<0.1	1.58	0.11	1.62	0.17	15.00	2.26	1.71	2.42	50.20	<0.1	25.91	14.82	1.68	10.39	-	41.76	126.65	168.41	698.89
24	**113351**	3.09	0.46	2.73	0.13	1.16	<0.01	6.85	1.63	2.14	1.17	75.62	<0.1	7.92	<0.1	3.41	4.65	-	47.74	191.82	239.56	384.92
25	**113352**	<0.1	<0.1	2.37	0.11	2.28	0.34	7.09	4.88	1.16	0.72	71.80	<0.1	60.28	33.28	1.08	25.05	-	56.89	377.33	434.22	531.22
26	**113353**	<0.1	1.02	1.63	<0.1	2.95	0.41	3.35	4.95	6.14	2.46	58.04	3.14	63.21	44.19	2.41	28.67	-	75.65	169.89	245.54	1670.03
27	**113354**	<0.1	<0.1	1.40	0.13	0.66	<0.01	4.84	1.17	1.42	0.28	27.20	<0.1	7.49	0.13	1.05	2.25	-	21.82	138.74	160.56	451.90
28	**113355**	2.12	0.24	0.60	0.12	0.45	<0.01	2.43	0.95	0.96	2.26	31.78	<0.1	7.10	1.93	0.83	2.04	-	15.49	56.60	72.09	659.91

Sl No.	Sample No.	Dy	Ho	Er	Tm	Yb	Lu	Hf	Ta	W	Tl	Pb	Bi	Th	U	Ag	Te	Mn	HREE Y	LREE	TREE Y	THIE
29	**113377**	1.38	0.30	0.84	0.10	0.90	0.09	2.78	1.52	0.90	1.00	11.51	<0.1	13.58	5.38	1.02	5.55	-	-	-	-	465.08
30	**113356**	3.33	0.44	0.41	0.13	0.64	0.10	1.53	1.38	0.61	1.32	25.99	0.61	15.86	9.59	0.86	6.00	-	18.37	37.68	56.05	803.33
31	**113394**	6.03	1.04	2.77	0.36	2.40	0.35	6.49	0.60	0.84	0.72	26.82	<0.1	69.43	5.02	<0.05	<0.05	663.58	68.11	499.28	567.39	-
32	**113395**	5.69	1.22	3.68	0.57	3.61	0.57	3.35	0.39	0.45	0.08	0.28	<0.1	4.21	4.50	<0.05	<0.05	2210.81	133.20	67.44	200.64	-
33	**113396**	4.87	0.92	2.64	0.39	2.61	0.38	6.70	0.66	1.32	0.09	21.87	<0.1	32.68	5.70	<0.05	<0.05	160.25	60.92	283.09	344.02	-
34	**113397**	5.19	0.99	2.91	0.39	2.57	0.37	5.47	0.66	0.91	0.21	17.93	<0.1	25.89	4.27	<0.05	<0.05	116.37	66.55	257.02	323.57	-
35	**113156**	9.35	1.61	4.41	0.58	3.90	0.58	12.93	1.14	1.00	<0.1	25.34	<0.1	97.37	8.40	<0.05	<0.05	276.45	104.31	738.82	843.13	-

Annexure-XXXi: ICPMS Analysis of Heavies Samples

Sl No.	Sample Number	BH Number	Depth (from) metre	Depth (to) metre	Heavies weight (gm)	Wt% of heavies	Sample Description	Host Lithology	Li	Be	Sc	V
1	112186	GSPL_BHUJ_BH04	4	8	2.94	2.58	Pinkish white coloured, medium to coarse grained, moderate to poorly sorted sludge, comprisies of sub-angular to sub-rounded grains of quartz with subordinate amount of magnetite; muscovite, suspected feldspar (?), biotite, pink quartz, hematite clasts, black-coloured mineral (tourmaline?) and suspected zircon/apatite (??).	Sludge of sandstone with differential ferruginization	11.00	3.03	110.90	627.90
2	112191	GSPL_BHUJ_BH04	19	23	1.46	0.58	Brownish yellow coloured, medium to fine grained, moderately sorted sludge, comprises of quartz with subordinate magnetite; carbonate and clasts of iron concretion. The sludge is strongly attracted by the magnet of a diamond pen.	Sludge of yellowish brown coloured ferruginized sandstone	13.52	4.56	52.37	370.72
3	112187	GSPL_BHUJ_BH04	42	45	1.55	0.13	The unit has been recieved as both sludge and core where the sludge unit is significantly higher than the core unit. The sludge is yellowish brown in colour, moderately sorted, medium to fine grained and consists of quartz with subordinate amount of muscovite and magnetite. The sandstone is medium to fine grained, well to moderately sorted, and composed of >95% quartz, muscovite (1-2%), black minerals??	Mica bearing metasomatized sandstone	7.59	1.51	27.09	248.11

Sl No.	Sample Number	BH Number	Depth (from) metre	Depth (to) metre	Heavies weight (gm)	Wt% of heavies	Sample Description	Host Lithology	Li	Be	Sc	V
							(non magnetic, pyrolusite??) and biotite embedded in a clayey to silicified matrix/cement. Amount of mica increases with ferruginization. The colour of the sandstone varies from pinkish to yellowish brown in colour. Iron imprgnation occur either as uniform stain or as thin layers (veinlets??). The layers are red to blackish brown in colour and very fine grained. Suspected clay alteration is also observed.					
4	112175	GSPL_BHUJ_BH05	12	14	2.58	2.35	Yellowish white to pinkish white coloured, coarse to fine grained, poorly sorted sludge. Grains are generally sub-angular to rounded with moderate to high sphericity.The sludge consists of quartz (97–98%), some cloudy white opaque grains (possibly altered feldspar), hematite, rock fragments, and very very less amount of magnetite. Magnetites are mostly emplaced in the grooves of the quartz grains. Rare occurence of white transparent, elongated, needle shaped crystals are also bserved.	Sandstone with differential ferruginization	6.54	7.10	109.32	555.61
5	112177	GSPL_BHUJ_BH05	19	21	1.12	0.77	Brownish white coloured, medium to fine grained sludge with bimodal size distribution. The larger grains are sub-rounded to well-rounded with high sphericity , whereas the smaller grains are relatively well-sorted, sub-	Sludge of sandstone with differential ferruginization	5.26	8.11	120.59	646.47

Sl No.	Sample Number	BH Number	Depth (from) metre	Depth (to) metre	Heavies weight (gm)	Wt% of heavies	Sample Description	Host Lithology	Li	Be	Sc	V
							angular to sub-rounded. The sludge comprises >90% quartz, feldspar (weathered ??, clayey), apatite (rare??, (platy to needle like appearance, colourless, crystal clear, no streak, easily breakable through scriber), magnetite, rock fragments, and hematite fragments in a decreasing order of abundance . Magnetite grains & magnetite engraved within the grooves of the quartz is also observed.					
6	112161	GSPL_BHUJ_BH07	2.5	4.5	1.88	1.13	Yellowish-white to pinkish white coloured, fine grained moderately to well sorted sludge, comprising predominantly of sub-angular to sub-rounded grains of low sphericity. The sludge consist of quartz, hematite grains, very few muscovite and white transparent crystals in a decreasing order of abundance. Magnetites are observed to be at the groove of the quartz grains. Pink quartz/quartz with pinkish red stain is also observed. Last 7cm we have received core, with similar composition and grain size as the sludge.	Sludge of sandstone with differential ferruginization	5.38	2.69	67.57	629.47
7	112163	GSPL_BHUJ_BH07	13	15	1.33	0.31	Yellowish white to white coloured, medium to fine grained, poorly sorted sludge with angular to sub angular to rounded grains and low to high sphericity of the grains. However,	Sludge of sandstone with differential ferruginization	4.66	4.01	98.99	851.35

Sl No.	Sample Number	BH Number	Depth (from) metre	Depth (to) metre	Heavies weight (gm)	Wt% of heavies	Sample Description	Host Lithology	Li	Be	Sc	V
							angular grains with low sphericity predominates. The sludge consists of quartz (both white translucent and bluish grey) >95%, hematite, white transparent crystals, rare altered feldspar (??), rock fragment in a decreasing order of abundance. Ferruginous staining of different order of the quartz grains are also observed.The last 25 cm we have received with same composition as core.					
8	112165	GSPL_BHUJ_BH07	28.4	29.44	5.54	2.52	Reddish brown to yellowish brown coloured medium to fine grained poorly sorted sludge with bimodal size distribution, predominantly sub-angular to angular grains with low sphericity. The sludge comprises quartz, (both stained and unstained), hematite magnetite, white transparent crystals, few rock fragment of ferruginous sandstone in a decreasing order of abundance.	Sludge of yellowish brown coloured ferruginized sandstone	6.63	3.27	79.83	713.60
9	112168	GSPL_BHUJ_BH07	40	42	1.33	1.33	Brownish white to dark brown coloured, coarse to fine grained, poorly sorted sludge with angular to sub-rounded grains and low sphericity. The sludge comprises quartz (both stained and unstained), rock fragments (ferruginous sst), altered feldspar, hematite, magnetite, white transparent crystals, altered	Sludge of yellowish brown coloured ferruginized sandstone	7.36	4.08	60.01	587.85

Sl No.	Sample Number	BH Number	Depth (from) metre	Depth (to) metre	Heavies weight (gm)	Wt% of heavies	Sample Description	Host Lithology	Li	Be	Sc	V
							feldspar in a decreasing order of abundance. Magnetite in this is higher than the previous sludge. The amount of magnetite increases with depth from 39 m.					
10	112193	GSPL_BHUJ_BH08	24	28	2.83	0.90	Yellowish white coloured, medium to fine grained, poorly sorted sludge with sub-angular to sub-rounded grains of moderate to high sphericity.The sludge comprises quartz (97–98%), white transparent crystals, hematite, magnetite (of negligible quantity) in a decreasing order of abundance. Few quartz grains are observed to be stained to pinkish red.	Sludge of sandstone with differential ferruginization	6.76	4.33	93.02	782.21
11	112190	GSPL_BHUJ_BH08	36	40	1.89	1.15	Yellowish white, medium to fine grained, moderately sorted sludge with subrounded grains, predominantly with high sphericity.The sludge comprises quartz (98–99%), white transparent crystal, very few (<1%) rock fragments of ferruginous sandstone, unidentified black mineral,fine grained hematite, biotite in a decreasing order of abundance. Magnetite High. Some of the quartz grains are stained to yellow, yellowish brown & pinkish red.	Sludge of yellowish brown coloured ferruginized sandstone	5.14	3.67	82.07	699.99

Table Continued..

Annexure-XXXi

Sl No.	Sample Number	Cr	Mn	Co	Ni	Cu	Zn	Ga	Ge	Se	Rb	Sr	Y	Zr	Nb
1	112186	407.88	617.01	149.48	71.13	149.22	352.01	82.07	2.88	7.33	16.80	93.03	793.71	9614.73	487.72
2	112191	312.16	10160.16	177.02	122.60	177.74	3190.35	54.76	1.10	3.93	11.53	540.21	370.89	3192.31	298.66
3	112187	175.83	1491.24	62.94	46.39	89.75	932.32	24.58	0.93	<0.1	4.55	152.00	118.68	1014.50	100.92
4	112175	270.88	332.84	163.24	557.87	1229.63	1118.56	51.15	3.96	9.37	10.56	56.11	307.65	7244.90	194.18
5	112177	314.23	440.73	182.58	712.62	1657.37	1355.75	66.11	2.73	17.31	13.44	59.47	375.01	6495.30	273.54
6	112161	349.71	3017.87	172.93	754.58	2144.17	1847.81	56.18	1.19	24.39	24.41	104.80	270.22	3415.06	268.04

Sl No.	Sample Number	Cr	Mn	Co	Ni	Cu	Zn	Ga	Ge	Se	Rb	Sr	Y	Zr	Nb
7	112163	523.96	2412.22	201.03	797.28	2165.77	1661.63	73.24	2.17	20.31	31.32	90.98	515.63	5214.01	468.15
8	112165	373.96	2608.58	209.68	134.41	299.78	544.15	52.55	2.42	4.18	29.03	349.39	358.45	4860.80	332.03
9	112168	373.18	2056.79	144.22	222.32	582.78	738.83	46.35	2.34	6.01	28.60	162.27	205.20	2974.44	249.70
10	112193	423.79	1721.47	177.68	322.14	1001.73	731.82	69.34	2.16	3.16	24.23	106.78	417.74	4084.84	362.08
11	112190	847.77	2106.11	162.98	525.25	2196.24	1571.02	52.24	3.50	30.77	21.41	86.26	237.65	4422.60	373.24

Table Continued..

Annexure-XXXi

Sl No.	Sample Number	Mo	Ag	Cd	In	Sn	Sb	Te	Cs	Ba	La	Ce	Pr	Nd	Sm
1	112186	13.09	20.30	3.32	16.57	136.88	2.37	168.87	2003.75	493.26	5033.24	10285.66	642.95	2853.88	772.88
2	112191	23.12	13.43	4.35	15.68	99.94	7.36	92.82	1008.38	5997.44	2776.55	5552.30	360.76	1542.94	428.64
3	112187	20.00	12.79	4.04	9.97	55.59	5.16	45.60	223.59	1690.18	555.32	1078.83	80.27	341.42	85.74
4	112175	17.11	34.12	9.81	16.41	96.59	3.42	88.33	409.15	864.62	711.65	1705.76	105.34	556.84	122.46
5	112177	19.20	26.28	9.07	22.48	104.13	2.48	130.31	833.97	794.65	1715.65	3584.03	227.70	1112.83	265.36
6	112161	9.86	56.03	9.93	22.89	106.12	7.64	146.54	925.32	4206.11	1884.81	3793.64	243.70	1189.06	272.19

Sl No.	Sample Number	Mo	Ag	Cd	In	Sn	Sb	Te	Cs	Ba	La	Ce	Pr	Nd	Sm
7	112163	13.13	35.64	8.98	23.84	173.35	10.25	188.70	1692.04	682.24	3807.33	7589.46	478.21	2240.59	562.82
8	112165	10.11	19.90	4.37	20.88	122.56	10.42	171.90	1126.29	17802.23	2171.69	4421.45	257.23	1414.06	329.64
9	112168	17.82	22.11	5.30	22.51	119.53	6.68	95.07	522.28	4599.80	1002.08	2015.28	145.00	672.28	162.38
10	112193	13.49	15.49	6.26	19.31	133.03	8.98	163.90	1356.06	2834.52	3008.60	5925.56	384.41	1793.92	452.61
11	112190	85.36	21.71	5.35	24.12	300.08	13.98	131.08	635.77	489.49	1014.14	2109.80	142.53	760.11	160.82

Table Continued..

Annexure-XXXi

Sl No.	Sample Number	Eu	Gd	Tb	Dy	Ho	Er	Tm	Yb	Lu	Hf	Ta	W	Tl	Pb	Bi	Th	U	HREEY	LREE	TREEY
1	112186	30.25	439.56	11.55	218.16	<0.1	56.65	6.84	32.62	8.48	225.55	25.90	34.55	2.55	597.33	<0.1	883.81	4.69	1708.82	19588.61	21297.43
2	112191	14.82	231.56	5.31	113.86	<0.1	26.71	0.97	17.21	7.26	98.15	14.69	17.19	2.38	375.35	<0.1	618.37	5.47	841.06	10661.19	11502.26
3	112187	4.49	49.48	3.17	28.50	<0.1	11.75	1.11	8.11	4.16	28.29	8.03	11.88	1.98	198.63	<0.1	147.01	4.07	256.63	2141.57	2398.20
4	112175	8.47	84.52	7.75	58.55	<0.1	34.68	3.22	23.67	10.05	153.92	21.53	1549.72	1.57	262.51	<0.1	182.95	1.49	647.97	3202.04	3850.01
5	112177	12.48	162.07	8.96	85.42	<0.1	40.50	3.59	23.97	11.38	146.20	23.98	2665.02	1.48	287.52	<0.1	350.63	2.84	844.06	6905.57	7749.64
6	112161	13.19	162.12	10.95	72.67	<0.1	40.26	5.80	15.35	10.34	91.48	24.08	3180.39	2.87	1413.99	<0.1	475.74	<0.1	668.57	7383.40	8051.98

Sl No.	Sample Number	Eu	Gd	Tb	Dy	Ho	Er	Tm	Yb	Lu	Hf	Ta	W	Tl	Pb	Bi	Th	U	HREEY	LREE	TREEY
7	112163	23.54	321.92	11.77	148.32	<0.1	58.78	7.75	25.81	10.90	138.14	29.61	3396.95	<0.1	864.09	<0.1	857.25	<0.1	1223.50	14678.41	15901.92
8	112165	13.93	185.75	12.75	93.60	<0.1	50.32	7.67	19.30	7.55	161.54	29.56	422.74	<0.1	394.95	<0.1	495.89	<0.1	829.26	8594.06	9423.32
9	112168	9.59	99.17	8.81	50.48	<0.1	34.33	4.53	13.75	8.55	76.31	23.61	1125.46	3.65	357.80	<0.1	262.94	<0.1	494.53	3997.01	4491.54
10	112193	17.12	254.29	10.71	117.21	<0.1	47.46	6.84	19.24	8.07	109.19	25.06	780.30	<0.1	355.92	<0.1	658.52	<0.1	991.80	11565.09	12556.90
11	112190	9.47	109.12	9.51	56.60	<0.1	38.88	5.95	16.43	11.07	95.85	27.12	4484.20	1.83	376.64	0.34	208.39	<0.1	576.85	4187.40	4764.24

Annexure-XXXj: ICPMS of surface samples far from BHs

Sl No.	Sample No.	BH No.		Sample Depth (m)	Sample Description	Host Lithology
1	113469	GSPL_Bhuj_382/09/2025	23.15239833	69.66687333	Unaltered sandstone, fine to medium grain composed of quartz grains with non magntic black colour mineral	Unaltered Sandstone
2	113475	GSPL_Bhuj_390/09/2025	23.189915	69.505605	Highly ferruginous metasomatized sandstone.The rock is fine to medium grained, dark grey to black, and composed dominantly of angular to sub-rounded quartz grains, feldspar, and hematite clasts embedded in a hematitic matrix/cement. black tabular grains of a non-magnetic mineral were also observed.	Highly ferruginous metasomatized sandstone
3	113451	GSPL_Bhuj_361/09/2025	23.208023	69.615335	mica bearing ferruginized sandstone, composed of quartz , muscovite	Mica bearing Ferruginized sandstone
4	113455	GSPL_Bhuj_367/09/2025	23.222636	69.616365	Ferruginous altered sandstone , purpulish to reddish coloured fine to medium grained , mainly composed of quartz , muscovite and silicification??	Mica bearing Ferruginized sandstone
5	113460	GSPL_Bhuj_371/09/2025	23.14249667	69.651635	The exposure represents a highly oxidized ferruginous outcrop with a brecciated to massive texture. The rock is dominated by iron oxides (hematite, goethite, limonite) with patchy development of bluish to greenish metallic stains, suggesting the presence (or former presence) of copper sulphides (bornite/chalcopyrite). Quartz grains are visible	Highly altered ferruginous sandstone
6	113471	GSPL_Bhuj_386/09/2025	23.15302333	69.67406833	Highly ferruginous metasomatized sandstone, composed of angular to subrounded quartz, muscovite, suspected feldspar. Hematite layer are also found.	Highly ferruginous metasomatized sandstone

Table Continued..

Annexure-XXXj

Sl No.	Sample No.	Li	Be	Sc	V	Cr	Co	Ni	Cu	Zn	Ga	Ge	Se	Rb	Sr	Y	Zr	Nb
1	113469	8.89	0.32	2.24	21.41	160.21	4.74	7.44	3.58	21.53	4.15	<0.1	<0.1	<0.1	37.80	4.94	73.96	40.95
2	113475	5.01	0.80	4.31	38.85	128.57	16.11	17.91	<0.1	44.77	20.81	0.11	<0.1	<0.1	44.80	11.32	124.77	34.85
3	113451	8.36	1.79	9.09	218.46	94.25	18.95	41.91	9.21	179.97	36.71	0.22	0.37	<0.1	121.60	22.82	75.77	26.29
4	113455	8.58	1.84	12.97	121.51	144.69	70.95	98.52	3.71	245.17	31.27	0.18	0.31	<0.1	121.22	15.40	78.23	35.61
5	113460	7.48	2.76	6.01	93.48	167.76	53.07	105.70	26.38	224.53	13.63	<0.1	2.55	<0.1	6589.04	34.98	49.70	47.58
6	113471	5.70	0.51	1.41	15.98	151.01	8.65	24.77	0.14	22.11	21.35	<0.1	0.47	<0.1	39.23	3.61	38.93	35.74

Table Continued..

Annexure-XXXj

Sl No.	Sample No.	Mo	Cd	In	Sn	Sb	Cs	Ba	La	Ce	Pr	Nd	Sm	Eu	Gd	Tb	Dy	Ho	Er
1	113469	1.00	1.53	0.66	19.48	0.90	2.15	55.30	14.63	34.31	0.37	15.04	2.04	0.29	1.73	0.50	1.15	0.27	0.87
2	113475	0.75	4.22	13.78	13.21	6.31	4.62	550.33	29.49	72.56	35.19	33.92	9.76	0.50	2.70	3.97	2.53	<0.1	1.65
3	113451	3.23	4.59	20.80	9.94	11.24	0.79	1213.74	28.54	61.09	55.04	30.66	14.58	2.01	5.55	4.35	3.92	<0.1	1.35
4	113455	0.44	4.27	18.94	14.77	9.90	1.20	536.60	19.43	36.69	47.70	18.13	10.16	0.85	2.49	3.71	2.71	0.10	0.95
5	113460	2.68	2.89	6.52	18.64	3.16	0.94	8213.00	45.88	114.02	21.65	51.93	13.83	3.77	11.90	2.20	7.44	1.88	1.74
6	113471	0.54	4.26	14.61	18.16	7.18	0.25	49.97	4.64	6.93	31.17	5.19	6.39	0.15	0.24	2.63	1.34	0.59	0.31

Table Continued..

Annexure-XXXj

Sl No.	Sample No.	Tm	Yb	Lu	Hf	Ta	W	Tl	Pb	Bi	Th	U	Ag	Te	Mn	HREEY	LREE	TREEY	HREEY/LREE
1	113469	<0.1	0.34	0.01	1.92	0.68	<0.1	<0.1	<0.1	<0.1	<0.1	<0.1	0.27	<0.1	77.65	12.34	66.39	78.73	0.19
2	113475	<0.1	2.58	0.20	3.98	3.35	<0.1	0.84	<0.1	0.51	171.27	28.86	0.73	18.42	1934.80	29.76	180.92	210.68	0.16
3	113451	<0.1	4.38	0.29	4.59	4.83	1.27	0.22	13.50	4.65	238.17	49.55	0.80	28.17	452.50	53.77	189.91	243.68	0.28
4	113455	<0.1	3.46	0.26	2.99	4.31	0.80	0.11	<0.1	3.74	207.46	44.70	0.57	25.09	1417.80	42.89	132.11	175.01	0.32
5	113460	<0.1	1.83	0.10	27.22	2.28	0.76	0.56	6.24	<0.1	66.03	10.42	0.26	5.59	769.28	71.84	247.31	319.16	0.29
6	113471	<0.1	1.93	0.20	0.83	3.09	<0.1	0.94	<0.1	4.07	159.33	34.88	0.41	15.82	3092.35	12.41	54.32	66.73	0.23

Annexure-XXXI: Isodynamic Separation samples

Sl. No.	Sample ID	Location no	Latitude	Longitude	Size Range	Isodynamic Separation of BH samples								Total weight
						Isodynamically separated fraction (according to magnetic suseptibility)								
						Ampere	0.3	0.5	0.7	1	1.5	1.7	1.7	1.7
						Tilt	20	20	20	20	20	20	5 (Magnetic)	5 (Non-magnetic)	
1	113101	BH03	23.2039847	69.6284411	- 250 + 40	Weight in grams	0.56	0.47	0.37	0.39	0.52	0.28	49.25	46.04	97.88
						Weight%	0.57	0.48	0.38	0.40	0.53	0.29	50.32	47.04	100.00
2	113106	BH04	23.203828	69.628518	- 250 + 40	Weight in grams	0.68	0.46	0.32	0.29	0.31	0.14	50.69	40.16	93.05
						Weight%	0.73	0.49	0.34	0.31	0.33	0.15	54.48	43.16	100.00
3	113110	BH05	23.19484	69.580492	- 250 + 40	Weight in grams	2.45	0.33	0.52	0.73	0.54	0.54	13.95	77.21	96.27
						Weight%	2.54	0.34	0.54	0.76	0.56	0.56	14.49	80.20	100.00
4	113115	BH07	23.197537	69.529703	- 250 + 40	Weight in grams	2.11	1.69	0.91	1.36	2.03	0.56	39.28	49.77	97.71
						Weight%	2.16	1.73	0.93	1.39	2.08	0.57	40.20	50.94	100.00
5	113116	BH06	23.222575	69.594128	- 250 + 40	Weight in grams	0.98	1.2	0.78	2.68	4.19	2.34	60.17	21.78	94.12
						Weight%	1.04	1.27	0.83	2.85	4.45	2.49	63.93	23.14	100.00
6	113117	BH08	23.193472	69.518388	- 250 + 40	Weight in grams	1.08	1.15	0.9	1.44	1.09	0.49	43.03	48.04	97.22
						Weight%	1.11	1.18	0.93	1.48	1.12	0.50	44.26	49.41	100.00
7	113113	BH05	23.19484	69.580492	- 250 + 40	Weight in grams	0.73	1.06	0.52	0.84	0.71	0.71	54.94	37.2	96.71
						Weight%	0.75	1.10	0.54	0.87	0.73	0.73	56.81	38.47	100.00
8	113111	BH05	23.19484	69.580492	- 250 + 40	Weight in grams	50.36	17.34	6.86	4.71	2.1	15.64	1.04	0.16	98.21
						Weight%	51.28	17.66	6.99	4.80	2.14	15.93	1.06	0.16	100.00
9	113105	BH03	23.2039847	69.6284411	- 250 + 40	Weight in grams	1.57	4.77	1.94	2.69	2.74	1.11	58.29	25.16	98.27
						Weight%	1.60	4.85	1.97	2.74	2.79	1.13	59.32	25.60	100.00
10	113103	BH03	23.2039847	69.6284411	- 250 + 40	Weight in grams	0.37	0.52	0.47	0.47	0.59	0.45	26.31	63.91	93.09
						Weight%	0.40	0.56	0.50	0.50	0.63	0.48	28.26	68.65	100.00
11	113108	BH04	23.203828	69.628518	- 250 + 40	Weight in grams	38.64	7.94	17.3	16.12	9.24	2.09	6.56	0.04	97.93
						Weight%	39.46	8.11	17.67	16.46	9.44	2.13	6.70	0.04	100.00
12	1113120	BH06	23.222575	69.594128	- 250 + 40	Weight in grams	0.83	0.34	0.15	0.23	0.22	0.15	56.24	39.68	97.84
						Weight%	0.85	0.35	0.15	0.24	0.22	0.15	57.48	40.56	100.00
13	113112	BH05	23.19484	69.580492	- 250 + 40	Weight in grams	85.06	10.61	0.65	0.43	0.27	NA	NA	NA	97.02
						Weight%	87.67	10.94	0.67	0.44	0.28	0.00	0.00	0.00	100.00

Table Continued..

Annexure-XXXI

Sl. No.	Sample ID	Location no	Latitude	Longitude	Size Range	Isodynamic Separation of BH samples								Total weight
						Isodynamically separated fraction (according to magnetic suseptibility)								
						Ampere	0.3	0.5	0.7	1	1.5	1.7	1.7	1.7	
						Tilt	20	20	20	20	20	20	5 (Magnetic)	5 (Non-magnetic)	
14	113107	BH04	23.203828	69.628518	- 250 + 40	Weight in grams	1.64	5.13	1.27	3.13	3.01	1.24	49.24	32.56	97.22
						Weight%	1.69	5.28	1.31	3.22	3.10	1.28	50.65	33.49	100.00
15	113114	BH05	23.19484	69.580492	- 250 + 40	Weight in grams	1.44	1.3	1.2	1.72	2.26	1.08	48.85	41.32	99.17
						Weight%	1.45	1.31	1.21	1.73	2.28	1.09	49.26	41.67	100.00
16	113118	BH08	23.193472	69.518388	- 250 + 40	Weight in grams	0.71	0.96	1.27	0.59	0.87	0.44	38	53.31	96.15
						Weight%	0.74	1.00	1.32	0.61	0.90	0.46	39.52	55.44	100.00
17	113119	BH07	23.197537	69.529703	- 250 + 40	Weight in grams	1.02	0.71	0.38	0.41	0.69	0.45	45.34	47.99	96.99
						Weight%	1.05	0.73	0.39	0.42	0.71	0.46	46.75	49.48	100.00
18	105467	GSPL_Bhuj_49/12/23	23.1508	69.6239	<1mm	Weight in grams	1.16	0.759	0.498	0.405	0.396	0.315	0.42	0.331	4.284
						Weight%	27.08	17.72	11.62	9.45	9.24	7.35	9.80	7.73	100.00
19	105485	GSPL_Bhuj_68/01/24	23.1498	69.7271	< 2mm	Weight in grams	0.669	0.412	0.298	0.295	0.314	0.295	0.39	0.354	3.027
						Weight%	22.10	13.61	9.84	9.75	10.37	9.75	12.88	11.69	100.00
20	105464	GSPL_Bhuj_47/12/23	23.1642	69.6306	< 2mm	Weight in grams	0.55	0.394	0.315	0.305	0.294	0.288	0.324	0.317	2.787
						Weight%	19.73	14.14	11.30	10.94	10.55	10.33	11.63	11.37	100.00

Annexure-XXXII: EPMA Analysis Results Of BH Samples

Sl. No.	Sample Number	Data Point	Lat	Long	Sample Type	Host Lithology	Lithology (from thin section)	Minerals	Formation	Depth (m)	Na2O	SiO2	P2O5	Al2O3	MgO	CaO	TiO2	FeO	MnO
1	109125	1 / 1 .	23.195	69.58	Borehole(BH05)	Shale	Fine grained sandstone	Pyrite	Bhuj Formation	59.04 to 59.10	NA	NA	NA	NA	NA	NA	NA	NA	NA
2	109125	2 / 1 .	23.195	69.58	Borehole(BH05)	Shale	Fine grained sandstone	Pyrite	Bhuj Formation	59.04 to 59.11	NA	NA	NA	NA	NA	NA	NA	NA	NA
3	109125	3 / 1 .	23.195	69.58	Borehole(BH05)	Shale	Fine grained sandstone	Fe-cu-zn Sulphide	Bhuj Formation	59.04 to 59.12	NA	NA	NA	NA	NA	NA	NA	NA	NA
4	109125	4 / 1 .	23.195	69.58	Borehole(BH05)	Shale	Fine grained sandstone	Pyrite	Bhuj Formation	59.04 to 59.13	NA	NA	NA	NA	NA	NA	NA	NA	NA
5	109125	5 / 1 .	23.195	69.58	Borehole(BH05)	Shale	Fine grained sandstone	Pyrite	Bhuj Formation	59.04 to 59.14	NA	NA	NA	NA	NA	NA	NA	NA	NA
6	109125	6 / 1 .	23.195	69.58	Borehole(BH05)	Shale	Fine grained sandstone	NA	Bhuj Formation	59.04 to 59.15	NA	NA	NA	NA	NA	NA	NA	NA	NA
7	113033	1 / 1 .	23.223	69.594	Borehole(BH08)	Altered Sanstone	Coarse grained sandstone	Fe-s Pyrhotite	Bhuj Formation	6.64 to 6.70	NA	NA	NA	NA	NA	NA	NA	NA	NA
8	113033	2 / 1 .	23.223	69.594	Borehole(BH08)	Altered Sanstone	Coarse grained sandstone	Pyrhotite	Bhuj Formation	6.64 to 6.71	NA	NA	NA	NA	NA	NA	NA	NA	NA
9	113033	3 / 1 .	23.223	69.594	Borehole(BH08)	Altered Sanstone	Coarse grained sandstone	Pyrhotite	Bhuj Formation	6.64 to 6.72	NA	NA	NA	NA	NA	NA	NA	NA	NA
10	113036	4 / 1 .	23.223	69.594	Borehole(BH08)	Altered Sanstone	Medium grained sandstone	Cuprite(Cu-Oxide)	Bhuj Formation	9.69 to 9.74	NA	NA	NA	NA	NA	NA	NA	NA	NA
11	113036	5 / 1 .	23.223	69.594	Borehole(BH08)	Altered Sanstone	Medium grained sandstone	Cu-Co-Fe	Bhuj Formation	9.69 to 9.75	NA	NA	NA	NA	NA	NA	NA	NA	NA
12	113060	1 / 1 .	23.204	69.628	Borehole(BH04)	Sandstone	Interlayered Sandstone	Monazite	Bhuj Formation	35.47 to 35.52	0	1.6	27.29	0	0	0.43	0.01	0.2	0
13	113060	2 / 1 .	23.204	69.628	Borehole(BH04)	Sandstone	Interlayered Sandstone	Monazite	Bhuj Formation	35.47 to 35.53	0	0.47	29.4	0	0	0.19	0	0.27	0
14	113060	3 / 1 .	23.204	69.628	Borehole(BH04)	Sandstone	Interlayered Sandstone	Zircon	Bhuj Formation	35.47 to 35.54	0	31.25	0.65	0.02	0	0.03	0	0.48	0.04

Table Continued..

Annexure-XXXII

Sl. No.	Sample Number	UO2	PbO	ThO2	ZrO2	Ce2O3	La2O3	Sm2O3	Nd2O3	Eu2O3	Gd2O3	Er2O3	Yb2O3	Ho2O3	Y2O3	Ta2O5	Dy2O3	Pr2O3	BaO	Nb2O5
1	109125	NA	NA	NA	NA	NA	NA	NA	NA	NA	NA	NA	NA	NA	NA	NA	NA	NA	NA	NA
2	109125	NA	NA	NA	NA	NA	NA	NA	NA	NA	NA	NA	NA	NA	NA	NA	NA	NA	NA	NA
3	109125	NA	NA	NA	NA	NA	NA	NA	NA	NA	NA	NA	NA	NA	NA	NA	NA	NA	NA	NA
4	109125	NA	NA	NA	NA	NA	NA	NA	NA	NA	NA	NA	NA	NA	NA	NA	NA	NA	NA	NA
5	109125	NA	NA	NA	NA	NA	NA	NA	NA	NA	NA	NA	NA	NA	NA	NA	NA	NA	NA	NA
6	109125	NA	NA	NA	NA	NA	NA	NA	NA	NA	NA	NA	NA	NA	NA	NA	NA	NA	NA	NA
7	113033	NA	NA	NA	NA	NA	NA	NA	NA	NA	NA	NA	NA	NA	NA	NA	NA	NA	NA	NA
8	113033	NA	NA	NA	NA	NA	NA	NA	NA	NA	NA	NA	NA	NA	NA	NA	NA	NA	NA	NA
9	113033	NA	NA	NA	NA	NA	NA	NA	NA	NA	NA	NA	NA	NA	NA	NA	NA	NA	NA	NA
10	113036	NA	NA	NA	NA	NA	NA	NA	NA	NA	NA	NA	NA	NA	NA	NA	NA	NA	NA	NA
11	113036	NA	NA	NA	NA	NA	NA	NA	NA	NA	NA	NA	NA	NA	NA	NA	NA	NA	NA	NA
12	113060	0.22	0.17	7.8	0	30.42	14.79	0.99	11.06	0.54	0.28	0.09	0	0	0.11	0	0.02	3.57	0.01	0
13	113060	0.1	0.04	1.44	0	32.56	15.29	1.34	13.01	0.68	0.44	0.03	0.02	0	0.16	0	0	4.07	0	0
14	113060	0.07	0	0	65.48	0	0.04	0	0.01	0	0	0.07	0.01	0.06	0.11	0	0	0	0	0

Table Continued..

Annexure-XXXII

Sl. No.	Sample Number	SrO	S	Fe	Co	Ni	Zn	As	Sb	Ag	Mo	Pb	Bi	Te	Ba	Ta	Au	Sr	Cu	Total
1	109125	NA	52.49	46.21	0.05	0	0	0.03	0	0	0	0	0.01	0	0	0	0.15	0	0.03	98.96
2	109125	NA	51.42	45.61	0.06	0.02	0.02	0.02	0	0	0	0	0.09	0	0	0	0	0	0.03	97.27
3	109125	NA	32.7	3.45	0.03	0.03	56.59	0.02	0	0	0	0	0.02	0.03	0	0	0	0	6.18	99.05
4	109125	NA	50.26	45.12	0.08	0	0	0.07	0	0	0.07	0	0.12	0	0	0	0	0	0	95.71
5	109125	NA	52.7	45.46	0	0.13	0.16	0.09	0	0	0	0	0	0	0	0	0	0	0.09	98.63
6	109125	NA	32.93	6.17	0.13	0.68	46.45	0.02	0.01	0.15	0.05	0	0	0.02	0.01	0	0	0	9.3	95.93
7	113033	NA	38.38	59.33	0.09	0.42	0	0.1	0	0.02	0	0	0.05	0	0	0	0	0	0.03	98.43
8	113033	NA	39.02	58.61	0.14	0.22	0	0	0	0.01	0	0	0	0	0	0	0	0	0.01	98
9	113033	NA	38.83	58.96	0.1	0.29	0	0.11	0	0.01	0	0	0.1	0	0	0	0	0	0.03	98.43
10	113036	NA	0.18	2.15	4.76	0.05	0.09	0	0	0	0	0.12	0	0	0	0	0	0	57.89	65.23
11	113036	NA	0.29	0.42	1.23	0.04	0.14	0	0	0	0	0.09	0	0	0.08	0	0	0	85.43	87.72
12	113060	0	NA	NA	NA	NA	NA	NA	NA	NA	NA	NA	NA	NA	NA	NA	NA	NA	NA	99.62
13	113060	0	NA	NA	NA	NA	NA	NA	NA	NA	NA	NA	NA	NA	NA	NA	NA	NA	NA	99.5
14	113060	0	NA	NA	NA	NA	NA	NA	NA	NA	NA	NA	NA	NA	NA	NA	NA	NA	NA	98.3